Sadržaj

1 MOLBA

Naučnom veću Instituta za fiziku u Beogradu

Beograd, 18. januar 2017.

PREDMET: Molba za pokretanje postupka za sticanje zvanja viši naučni saradnik

Molim Naučno veće Instituta za fiziku da u skladu sa Pravilnikom o postupku i načinu vrednovanja i kvantitativnom iskazivanju naučno-istraživačkih rezultata istraživača pokrene postupak za moj izbor u zvanje viši naučni saradnik.

U prilogu dostavljam:
– mišljenje rukovodioca projekta sa predlogom članova komisije,
– kratku biografiju,
– pregled naučne aktivnosti,
– elemente za kvalitativnu ocenu naučnog doprinosa,
– elemente za kvantitativnu ocenu naučnog doprinosa,
– spisak objavljenih radova i njihove kopije,
– spisak javnih nota ATLAS kolaboracije sa ključnim doprinosom,
– spisak internih nota ATLAS kolaboracije sa ključnim doprinosom,
– spisak indikativnih prezentacija na sastancima ATLAS kolaboracije,
– podatke o citiranosti radova (spisak citata bez autocitata),
– fotokopiju rešenja o prethodnom izboru u zvanje naučni saradnik,
– dodatke.

S poštovanjem,

dr Nenad Vranješ,
naučni saradnik

2 MIŠLJENJE RUKOVODIOCA PROJEKTA SA PREDLOGOM ČLANOVA KOMISIJE

18. јануар 2017.

Научно веће Института за физику

Предмет: Мишљење руководиоца пројекта за избор др Ненада Врањеша у звање виши научни сарадник

Поштовани,

Др Ненад Врањеш запослен је у Лабораторији за физику високих енергија Института за физику у Београду од 2005. године. Ангажован је на пројекту основних истраживања Министарства просвете, науке и технолошког развоја 171004 под називом "АТЛАС експеримент и физика честица на ЛХЦ енергијама" у оквиру ког руководи пројектним задатком испитивања особина стандардног модела физике честица. Провео је три године у лабораторији CEA-Saclay у Француској у оквиру међународне сарадње, која је успешно настављена по његовом повратку на Институт. Члан је међународне колаборације АТЛАС на истоименом експерименту на Великом сударачу хадрона у ЦЕРН–у. Руководилац је једне докторске дисертације у изради (Александра Димитриевска), а био је руководилац мастер рада (Милена Бајић).

С обзиром да испуњава све услове предвиђене Правилником за изборе у научно–истраживачка звања, велико ми је задовољство да подржим захтев др Ненада Врањеша за покретање поступка за избор у звање виши научни сарадник.

За чланове комисије за избор др Ненада Врањеша у звање виши научни сарадник предлажем следећи састав:

1. Академик проф. др Ђорђе Шијачки, научни саветник, Институт за физику, и редовни члан САНУ;
2. др Лидија Живковић, научни саветник, Институт за физику;
3. др Магдалена Ђорђевић, научни саветник, Институт за физику;
4. проф. др Петар Аџић, редовни професор Физичког факултета;

Руководилац пројекта 171004,

др Лидија Живковић
Научни саветник

3 KRATKA BIOGRAFIJA

Nenad Vranješ je rođen 1980. u Beogradu, gde je završio osnovnu školu i gimnaziju. Studije fizike na Fizičkom fakultetu upisao je 1999, a diplomirao je 1. jula 2004. na smeru teorijska i eksperimentalna fizika sa srednjom ocenom 9.44 i ocenom 10 na diplomskom ispitu. Na istom fakultetu 2004. godine upisao je postdiplomske studije na smeru Nuklearna fizika i fizika elementarnih čestica. Položio je sve predviđene ispite sa srednjom ocenom 10, a magistarski rad pod nazivom "Mogućnosti ATLAS detektora za merenje produkcije parova W bozona na Velikom hadronskom kolajderu" odbranio je oktobra 2007. Doktorirao je na Fizičkom fakultetu Univerziteta u Beogradu 11. novembra 2011. sa temom "Traganje za novim teškim naelektrisanim gradijentnim bozonima na ATLAS detektoru (A Search for New Heavy Charged Gauge Bosons at ATLAS)". Doktorska disertacija je realizovana u okviru Sporazuma o zajedničkom mentorstvu nad doktorskim disertacijama izmedju Univerziteta u Beogradu i Nacionalnog i Kapodistrijskog univerziteta u Atini.

Dr Nenad Vranješ radi od 2004. u Laboratoriji za fiziku visokih energija Instituta za fiziku, najpre kao stipendista Ministarstva za nauku, a zatim kao istraživač pripravnik od marta 2005. U zvanje istraživač saradnik izabran je decembra 2008, a u zvanje naučni saradnik izabran je 18. jula 2012. Bio je angažovan na projektima osnovnih istraživanja br. 101488 "Eksperimenti sa elektron-pozitron, proton-proton i jezgro-jezgro sudarima na visokim energijama", potom na projektu br. 141037 "Precizna merenja parametara Standardnog modela i traganje za novim česticama na ATLAS eksperimentu", a od 1. januara 2011. angažovan na projektu br. 171004 "ATLAS eksperiment i fizika čestica na Velikom hadronskom sudaraču". U periodu 2011-2014. bio je na postdoktorskom usavršavanju u francuskom institutu CEA-Saclay, pritom baziran u CERN-u. U novembru 2014. godine Nenad Vranješ se vratio u Srbiju i trenutno radi kao naučni saradnik u Institutu za fiziku u Beogradu.

4 PREGLED NAUČNE AKTIVNOSTI

Tokom svoje dosadašnje karijere, dr Nenad Vranješ je bio uključen u nekoliko istraživačkih projekata vezanih za eksperiment ATLAS na Velikom sudaraču hadrona (*Large Hadron Collider, LHC*) u CERN-u. Ovi projekti su se odnosili na merenje parametara Standardnog modela (SM), kao i na direktne potrage za novim česticama čije postojanje predviđaju različiti fenomenološki modeli koji predstavljaju proširenje Standardnog modela. Tokom rada na ovim projektima imao je priliku da razmenjuje iskustva sa kolegama širom sveta, pokazuje inicijativu, učestvuje u planiranju budućih istraživačkih aktivnosti, kao i da rukovodi radom mlađih kolega.

Dosadašnji rezultati odnose se na sledeće aktivnosti:

- precizna merenja mase W bozona, mase Higsovog bozona i mase top kvarka i kalibracija impulsa miona na detektoru ATLAS;
- traganje za novim teškim naelektrisanim gradijentnim bozonima;
- apsolutna kalibracija izmerene luminoznosti na detektoru ATLAS.

• Precizna merenja mase W bozona, mase Higsovog bozona i mase top kvarka i kalibracija impulsa miona na detektoru ATLAS

Prva tema istraživanja odnosi se na merenje mase W bozona u *Drell-Yan* produkciji kroz leptonske kanale raspada. Masa W bozona se na hadronskim sudaračima meri koristeći karakteristične opservable kao što su transverzalni impuls leptona i transverzalna masa lepton-neutrino sistema. Na masu W bozona utiču drugi paramatri Standardnog modela: kroz korekcije višeg reda masa W bozona zavisi od mase top kvarka i mase Higsovog bozona, a takođe mogu uticati i korekcije koje potiču od čestica čije postojanje predviđaju teoretski modeli izvan SM. U kontekstu globalnog fita parametara SM, ograničenja na fazni prostor fizike izvan SM su pre svega uslovljena preciznošću poznavanja mase W bozona, pa je poboljšanje preciznosti od ključnog značaja za testiranje konzistentnosti SM. Ovo merenje je izuzetno kompleksno i potrebno je dostići ekstremnu preciznost od 0.01%. U okviru pomenute tematike dr N.Vranješ je radio na kalibraciji impulsa miona, merenju efikasnosti rekonstrukcije i trigerovanja miona, kalibraciji hadronskog uzmaka (nedostajuće transverzalne energije), selekciji događaja od interesa, proceni neodređenosti usled fonskih procesa. Treba napomenuti da je kalibracija impulsa leptona najkritičnija komponenta merenja mase W bozona na hadronskim sudaračima. Takođe, radio je i na merenju karakteristika Z bozona u cilju testiranja izvedenih eksperimentalnih korekcija i teorijskog modelovanja produkcije W bozona, kao i konačnoj ekstrakciji mase W bozona iz postojećih podataka. Kandidat je u saradnji sa drugim kolegom iz CEA-Saclay napisao i celokupni programski okvir za analizu događaja. Preliminarni rezultati dobijeni podacima iz proton-proton sudara prikupljenim tokom 2011. godine objavljeni su u jednoj javnoj noti ATLAS kolaboracije:

ATLAS Collaboration, *Measurement of the $W-$boson mass in pp collisions at $\sqrt{s}$ = 7 TeV with the ATLAS detector*, ATLAS-CONF-2016-113, CERN (2016).

Dobijeni rezultat po preciznosti ± 19 MeV odgovara najpreciznijim rezultatima merenja do danas ostvarenim na eksperimentima CDF i D0 na sudaraču Tevatron, dok je srednja vrednost kompatibilna sa trenutnom svetskom srednjom vrednošću kao i poslednjim teorijskim predviđanjem. Publikovanje konačnih rezultata (iste ili nešto bolje preciznosti) u časopisu očekuje se tokom 2017. Tokom rada na ovoj problematici izučavane su i neodređenosti usled teorijskog modelovanja produkcije i raspada W bozona. Dr. Vranješ je bio zadužen za procenu uticaja eksperimentalnih efekata usled rezolucije leptona i nedostajuće energije. Rezultat je objavljen u sledećoj javnoj noti:

ATLAS Collaboration, *Studies of theoretical uncertainties on the measurement of the mass of the W boson at the LHC*, ATL-PHYS-PUB-2014-015, CERN, (2014).

U okviru ove aktivnosti kalibracija impulsa miona i ograničenje sistematskih neodređenosti koje proizilaze iz toga je od ključnog značaja za postizanje odgovaraće preciznosti merenja. Rekonstrukcija miona u simuliranim događajima je korigovana kako bi se poklopila sa skalom i rezolucijom izmerenim u realnim događajima. U ovu svrhu korišćeni su kalibracioni uzorci dobro izučenih procesa velike statistike: produkcija J/ψ mezona i produkcija Z bozona i njihovi raspadi na parove miona. Analizirani podaci su prikupljeni tokom prve faze rada LHC-a (*Run-I*), 2011. i 2012. Dr Vranješ je bio među prvim iztraživačima koji su koristili J/ψ događaje za kalibraciju impulsa miona na eksperimentu ATLAS. Velika statistika i kinematičke karakteristike ovih događaja omogućavaju korigovanje efekata lokalizovanih u prostoru, što je od ključnog značaja za merenje mase Higsovog bozona u četvoroleptonskom kanalu gde je statistika signala veoma mala. Korekcije su izvedene nezavisno sa mione izmerene u unutrašnjem detektoru i mionskom spektrometru ATLAS detektora, iz fita invarijantih masa dve rezonance, kao i razlike izmerenog impulsa u ova navedena dva podsistema. Eksploatacija razlike izmerenih impulsa omogućila je mapiranje korekcije energetskih gubitaka prolaska miona kroz kalorimetre. Pokazano je da su korekcije energetskih gubitaka približno 1% ukupnih energetskih gubitaka miona prilikom prolaska kroz kalorimetre i neaktivan materijal ispred mionskog spektrometra. Rezultati su kompatibilni sa raspodelom materijala u simulaciji detektora zasnovanoj na GEANT 4 simulacijama. Navedena procedura kalibracije impulsa miona predstavlja značajan napredak u odnosu na prethodne rezultate na eksperimentu u kinematičkom opsegu tranverzalnog impulsa miona vrednosti izmedju 6 GeV i 100 GeV. Svi ovi rezultati su dokumentovani u jednom radu ATLAS kolaboracije objavljenom u vrhunskom međunarodnom časopisu:

Aad, G., ... ,Vranjes N., *et al.* [ATLAS Collaboration], *Measurement of the muon reconstruction performance of the ATLAS detector using 2011 and 2012 LHC proton–proton collision data*, Eur.Phys.J. C74 (2014) no.11, 3130, arXiv:1407.3935 [hep-ex].

N.Vranješ je bio jedan od editora navedene publikacije. Pored ovih aktivnosti radio je na proceni neodređenosti raspodele materijala u unutrašnjem detektoru korišćenjem metoda viešestrukog rasejanja miona, kao i proceni efekata uticaja pozicioniranja detektorskih elemenata na izmereni impuls tragova. Netačan opis pozicije detektorskih elemenata u simulaciji detektora vodi pogrešnom merenju sagite, pa je korigovanje ovog efekta kao i procena povezanih sistematskih neodređenosti veoma značajana za merenje mase W bozona na LHC-u usled različitog uticaja na pozitivno i

negativno naelektrisane mione. Uračunavanje uticaja pogrešnog merenja sagite je od značaja i za merenje preseka Z bozona u zavisnosti od invarijantne mase dileptonskog para, rapiditeta Z bozona i ugla u Kolin-Soper sistemu reference (trostruko diferencijalno merenje preseka za produkciju Z bozona). N. Vranješ učestvuje i u ovoj studiji dokumentovanoj u sledećoj internoj noti:

L. J. Armitage,..., N. Vranjes, et al., *Measurement of the Drell-Yan triple-differential cross-section in pp collisions at* $\sqrt{s}$ *= 8 TeV*, ATL-COM-PHYS-2015-1575

Publikovanje rezultata trostrukog diferencijalnog merenja u časopisu očekuje se tokom ove godine, a dobijeni rezultati imaće uticaj na buduća merenja mase W bozona na LHC-u.

Ostvareni rezultati se nadovezuju na aktivnost pre izbora u prethodno zvanje kada je kandidat radio na izučavanju karakteristika rekonstruisanih miona poređenjem eksperimentalnih podataka sa predviđanjima Monte Karlo simulacija. Sa prvim podacima iz proton-proton sudara na LHC-u sakupljenim tokom 2009. godine ne energiji $\sqrt{s}$ =0.9 TeV i $\sqrt{s}$ =2.36 TeV analizirani su karakteristični spektri miona. Rezultati su prikazani u jednom kolaboracijskom radu:

G. Aad,...,N. Vranjes *et al.* [ATLAS Collaboration], *Performance of the ATLAS Detector using First Collision Data*, JHEP, 1009, 056 (2010) 65p; arXiv:1005.5254 [hep-ex].

Precizno merenje impulsa miona i ograničenje eksperimantalnih neodređenosti je od ključnog značaja za merenje mase Higsovog bozona, merenje jačina sprezanja sa drugim česticama kao i merenje preseka za produkciju Higsovog bozona na LHC-u. Za ove studije analizirani su podaci iz *pp* sudara prikupljeni tokom perioda *Run-I*. Izmerena masa Higsovog bozona u četvoroleptonskom kanalu (4 miona, 4 elektrona i dva miona i dva elektrona) sa relativnom preciznošću 0.3% je zasnovana na unapređenoj impulsnoj skali leptona. Zahvaljujući preciznoj kalibraciji impulsa leptona u konačnom rezultatu mase Higsa dominira statistička neodređenost, dok u drugim merenjima pored statističke od značaja su jedino teorijske neodređenosti. Rezultati su objavljeni u tri rada u vrhunskim časopisima:

- Aad, G., ... ,Vranjes N., *et al.* [ATLAS Collaboration], *Measurement of the Higgs boson mass from the* $H \to \gamma\gamma$ *and* $H \to ZZ^* \to 4\ell$ *channels with the ATLAS detector using 25* fb^{-1} *of pp collision data*, Phys.Rev. D90 (2014) no.5, 052004, arXiv:1406.3827 [hep-ex],

- Aad, G., ... ,Vranjes N., *et al.* [ATLAS Collaboration], *Measurements of Higgs boson production and couplings in the four-lepton channel in pp collisions at center-of-mass energies of 7 and 8 TeV with the ATLAS detector*, Phys.Rev. D91 (2015) no.1, 012006, arXiv:1408.5191 [hep-ex],

- Aad, G., ... ,Vranjes N., *et al.* [ATLAS Collaboration], *Fiducial and differential cross sections of Higgs boson production measured in the four-lepton decay channel in pp collisions at* $\sqrt{s}$*=8 TeV with the ATLAS detector*, Phys.Lett. B738 (2014) 234-253, arXiv:1408.3226 [hep-ex].

U januaru 2016. godine dr N. Vranješ izabran je za člana recenzentskog tima za studiju koja se bavi merenjem mase top kvarka u događajima sa dva leptona korišćenjem podataka iz *pp* sudara

na energiji $\sqrt{s}$ =8 TeV. Dobijeni rezultat predstavlja prvo merenje mase top kvarka ATLAS kolaboracije sa pomenutim podacima. U okviru ATLAS kolaboracije, recenzentski tim zajedno sa autorima ima odgovornost da proizvede i objavi naučnu publikaciju vrhunskog kvaliteta. U poređenju sa prethodnim merenjem mase top kvarka na eksperimentu selekcija događaja je unapređena korišćenjem srednje vrednosti lepton-$b$jet sistema kako bi se uvećao udeo tačno rekonstruisanih događaja i posledično smanjile sistematske neodređenosti. Neodređenost izmerene vrednosti mase top kvarka iznosi 0.84 GeV, dok je kombinovanjem sa prethodnim rezultatim postignuta ukupna neodredjenost 0.7 GeV, odnosno 0.4% relativne preciznosti. Po završetku ove studije rezultati su prezentovani na više vodećih međunarodnih konferencija i objavljeni u prestižnom međunarodnom časopisu:

Aaboud, M., ... ,Vranjes N., *et al.* [ATLAS Collaboration], *Measurement of the top quark mass in the $t\bar{t} \to$ dilepton channel from $\sqrt{s} = 8$ TeV ATLAS data*, Phys.Lett. B761 (2016) 350-371, arXiv:1606.02179 [hep-ex].

Od januara 2017. N.Vranješ je izabran za člana recenzentskog tima za studiju koja se bavi merenjem mase Higsovog bozona u četvoroleptonskom kanalu sa podacima prikupljenim tokom 2015. i 2016. (*Run-II*). Očekivano je poboljšanje preciznosti merenja sobzirom na veću prikupljenu statistiku u odnosu na podatke iz *Run-I*.

Pre izbora u prethodno zvanje, na početku rada LHC-a, N. Vranješ je takođe radio na izučavanju mogućnosti ATLAS detektora za merenje produkcije para W bozona pomoću Monte Karlo simulacija. Detaljno izučavanje ovog procesa omogućava testiranje neabelove gradijentne strukture Standardnog modela i postavljanje granice za trostruka anomalna sprezanja gradijentnih bozona WWZ i $WW\gamma$. Eventualno odstupanje od predviđanja Standardnog modela bi indirektno ukazalo na postojanje novih fenomena na višoj energetskoj skali od direktno dostupne na LHC-u. Određene su karakteristike ATLAS detektora za rekonstrukciju osnovnih objekata (elektrona, miona, džetova i nedostajuće transverzalne energije) koji su karakteristični za leptonski kanal raspada W para i predložen je osnovni skup kinematičkih ograničenja koji omogućava efikasno izdvajanje WW signala od dominantnih fonskih procesa. Rezultati su objavljeni u dve javne note ATLAS kolaboracije i u jednom radu u međunarodnom časopisu:

- K.Bachas,..., Lj. Simic, D.S.Popovic,..., N. Vranjes et al., *Diboson physics studies*, ATL-PHYS-PUB-2009-038; publikovano i u monografiji: Detector, Trigger and Physics", CERN-OPEN-2008-020, ISBN 978-92-9083-321-5, arXiv:0901.0512 [hep-ex], 1852 p. (2008).

- Lj. Simic, I. Mendas, N. Vranjes, D.S.Popović, *Prospects for Measuring Triple Gauge Boson Couplings in WW Production at the LHC*, ATL-PHYS-PUB-2006-011, CERN (2006).

- Lj. Simic, N.Vranjes, D.Reljić, D.Vudragović, D.S.Popović, *WW Production and Triple Gauge Boson Couplings at ATLAS*, Acta Physica Polonica B, 38 525 (2007).

Navedeni rezultati su prikazani i na nekoliko međunarodnih i domaćih konferencija.

• **Traganje za novim teškim gradijentnim bozonima**

Postoji jaka teorijska motivacija da se novi fenomeni, čije postojanje ne predviđa Standardni model, mogu očekivati na TeV energetskoj skali koja se može direktno izučavati na LHC-u. Jedno moguće proširenje Standardnog modela je proširenje njegove gradijentne grupe $SU(3)_c \otimes SU(2)_L \otimes U(1)_Y$, koje u nekim fenomenološkim modelima dovodi do postojanja novih (teških) gradijentnih bozona: naelektrisanih W' i neutralnih Z'. U okviru *Exotics Lepton+X* grupe N. Vranješ je radio na potrazi za W' bozonom koji se raspada na lepton i neutrino. Rezultati su dobijeni analiziranjem podataka iz proton-proton sudara na energiji od $\sqrt{s} = 7$ TeV i $\sqrt{s} = 8$ TeV prikupljenim na eksperimentu ATLAS tokom 2011. i 2012, koji redom odgovaraju integralnoj luminoznosti od 4.7 fb^{-1} i 20.3 fb^{-1}. Osnov za potragu čini model u kome novi gradijentni bozoni imaju ista sprezanja sa fermionima kao W i Z bozoni iz Standardnog modela. Pored navedenog modela, razmatran je još jedan model (W^*) u kome novi naelektrisani gradijentni bozon predstavlja naelektrisanog partnera kiralnog bozona. U radovima u kojima je N. Vranješ dao ključni doprinos ustanovljeno je da je masa W' veća od 3.24 TeV na nivou poverenja 95%, čime je u energetskom domenu dostupnom na LHC-u data značajna potvrda Standardnog modela, i postavljena su nova ograničenja na odgovarajuće alternativne modele fizike elementarnih čestica. U traganju za W^* bozonom postavljena je donja granica na njegovu masu od 3.21 TeV na nivou poverenja 95%. U okviru efektivne teorije polja postavljena su ograničenja na presek za interakciju hipotetičkih čestica tamne materije sa nukleonima, kao i na masenu skalu nove nepoznate interakcije kroz koju bi se parovi čestica tamne materije proizvodili zajedno sa W bozonom koji bi se raspadao leptonski.

Dobijeni rezultati predstavljeni su u dva kolaboracijska rada objavljena u vrhunskim međunarodnim časopisima:

- Aad, G., ... ,Vranjes N., *et al.* [ATLAS Collaboration], *Search for new particles in events with one lepton and missing transverse momentum in pp collisions at* $\sqrt{s}$ *=8 TeV with the ATLAS detector*, JHEP 1409 (2014) 037, arXiv:1407.7494 [hep-ex],

- Aad, G., ... ,Vranjes N., *et al.* [ATLAS Collaboration], *ATLAS search for a heavy gauge boson decaying to a charged lepton and a neutrino in pp collisions at* $\sqrt{s}$*=7 TeV*, Eur.Phys.J. C72 (2012) 2241, arXiv:1209.4446 [hep-ex].

Kao jedan od najkompetentnijih istraživača N.Vranješ je bio editor rada JHEP 1409 (2014) 037. Rezultati pre prethodnog izbora u zvanje, zatim rezultati sa Monte Karlo simulacijama, kao i preliminarni rezultati kolaboracije, objavljeni su u vrhunski međunarodnom časopisima i većem broju javnih nota ATLAS kolaboracije:

- G. Aad,...,N. Vranjes *et al.* [ATLAS Collaboration] , *Search for a heavy gauge boson decaying to a charged lepton and a neutrino in 1 fb*$^{-1}$ *of pp collisions at* $\sqrt{s}$ *= 7 TeV using the ATLAS detector*, Physics Letters B **705**, 28-46 (2011) arXiv:1108.1316 [hep-ex]

- G. Aad,...,N. Vranjes *et al.* [ATLAS Collaboration], *Search for high-mass states with one lepton*

plus missing transverse momentum in proton-proton collisions at $\sqrt{s}$ *= 7 TeV with the ATLAS detector*, Physics Letters B **701**, 50-69 (2011) arXiv:1103.1391 [hep-ex].

- ATLAS Collaboration, *Search for high-mass states with one lepton plus missing transverse momentum in pp collisions at* $\sqrt{s}$ *=8 TeV with the ATLAS detector*, ATLAS-CONF- 2014-017, CERN (2014).

- ATLAS Collaboration, *Search for high-mass states with one muon plus missing transverse momentum in proton-proton collisions at* $\sqrt{s}$*=7 TeV with the ATLAS detector*, ATLAS-CONF-2011-082, CERN (2011).

- ATLAS Collaboration, *Physics potential of* Z' *and* W' *searches with the ATLAS Detector as a function of the LHC center-of-mass energy*, ATL-PHYS-PUB-2011-002, CERN (2011).

- ATLAS Collaboration, *Search for high-mass states with electron plus missing transverse energy using the ATLAS Detector at* $\sqrt{s}$*=7TeV*, ATLAS-CONF-2010-089, CERN (2010).

- ATLAS Collaboration, *ATLAS sensitivity prospects to* W' *and* Z' *at 7 TeV*, ATL-PHYS-PUB-2010-007, CERN (2010).

- D.L.Adams, D.Fassouliotis, C.Kourkoumelis, B.R.Mellado Garcia, M.I.Pedraza Morales, N.Vranjes, S.L.Wu, *Lepton plus missing transverse energy signals at high mass*, ATL-PHYS-PUB-2009-07; publikovano i u monografiji: Detector, Trigger and Physics", CERN-OPEN-2008-020, ISBN 978-92-9083-321-5, arXiv:0901.0512 [hep-ex], 1852 p. (2008).

Rezultati su prikazani i na međunarodnim konferencijama. Na konferenciji "LHC on the March" u Protvinu N. Vranješ je sumirao celokupne rezultate kolaboracije koji se odnose na potrage za novim česticama:

N.Vranjes on behalf of ATLAS Collaboration, Exotic Searches in ATLAS, PoS(IHEP- LHC-2011)021, ATL-PHYS-PROC-2012-040, arXiv:1202.3171[hep-ex], LHC on the March, November 16-18, 2011, Protvino, Moscow region, Russian Federation.

• Apsolutna kalibracija izmerene luminoznosti na detektoru ATLAS

Nakon povratka u Srbiju N. Vranješ je, u cilju jačanja prepoznatljivosti beogradske ATLAS grupe, započeo aktivnost na apsolutnoj kalibraciji izmerene luminoznosti na detektoru ATLAS u okviru grupe za pripremu podataka (*Data Preparation*). Precizno poznavanje integralne luminoznosti je od vitalnog značaja kako za precizna marenja na eksperimentu, tako i za potrage za novim česticama gde je potrebno tačno proceniti nivo fonskih procesa. U svrhu apsolutne kalibracije koriste se podaci iz specijalih sudara protona pri kojima su snopovi protona separisani. Dr Vranješ je radio na analizi podataka prikupljenih na energijama 8 i 13 TeV prikupljenih tokom 2012, 2015. i 2016. Pored merenja vidljivog preseka za dvadesetak algoritama zasnovanih na podacima iz nekoliko luminometera različite tehnologije, analizirane su i različite sistematske

neodređenisti povezane sa ovom procedurom. U podacima iz 2012. re-evaluiran je nivo fona koji potiče od sudara, kao i sistematske neodređenosti vezane za izbor empirijske funkcije koja opisuje presek interakcije u zavisnosti od veličine separacije snopova. Rezultati su deo publikacije:

Aaboud, M., ... ,Vranjes N., *et al.* [ATLAS Collaboration], *Luminosity determination in pp collisions at* $\sqrt{s}$ *= 8 TeV using the ATLAS detector at the LHC*, Eur.Phys.J. C76 (2016) no.12, 653, arXiv:1608.03953 [hep-ex].

Pored ovih studija u 2015. i 2016. učinjen je značajan napor kako bi se uzeli u obzir različiti efekti koji se odnose na neodređenost pozicije protonskog snopa usled elektromagnetnih defleksija i transverzalnih driftova. Pored podataka relevantnih za kalibraciju luminoznosti na ATLAS-u, analizirani su podaci iz sudara sa različitim uglovima sudara snopova i različitim vrednostima emitanse snopova. Dobijeni rezultati su relevantni za planiranje radnih parametara celokupnog LHC-a tokom 2017. i 2018. godine do kraja *Run-II*.

Dr Nenad Vranješ takođe ima značajno iskustvo u rukovođenju radom mlađih kolega. Bio je rukovodilac master rada studentkinje Milene Bajić pod naslovom "Produkcija parova gradijentnih bozona u proton-proton sudarima na $\sqrt{s} = 100$ TeV" odbranjenom na Departmanu za fiziku Prirodno-matematičkog fakulteta Univerziteta u Novom Sadu juna 2015. godine. Koleginica Bajić je sada student doktorskih studija na Institutu Nils Bor u Kopenhagenu, a svoju doktorsku disertaciju radi na eksperimentu ATLAS. U toku svog postdoktorskog usavršavanja u CEA-Saclay, i nakon toga, dr N. Vranješ je pratio rad dvoje studenata na doktorskim studijama Univerziteta Paris-Saclay: Remmie Hanna (doktorirala 2015) i Oleha Kivernyuka (doktorat odbranjen 2016). Mentor je doktorske disertacije Aleksandre Dimitrievske na temi "Measurement of the W boson mass and the calibration of the muon momentum with the ATLAS detector" (*Merenje mase W bozona i kalibracija impulsa miona na detektoru ATLAS*). Odbrana doktorske disertacije na Fizičkom fakulteta Univerziteta u Beogradu planira se u prvoj polovini 2017. godine.

U periodu 2008-2010. godine dr Nenad Vranješ redovno je držao seminare studentima Fizičkog fakulteta u okviru predmeta Fizika elementarnih čestica i Seminar savremene fizike, na eksperimentalnom B smeru. Aktivno je učestvovao u organizaciji izložbe "LHC, Veliki hadronski sudarač" 2008. godine u SANU. Takođe je učestvovao u realizaciji Programa podsticanja aktivnosti naučnih i stručnih društava, u funkciji unapređivanja naučnoistraživačkog rada, promocije i popularizacije nauke: "Veb stranica o Velikom hardonskom kolajderu u CERN-u - popularizacija fizike elementarnih čestica putem interneta". Nekoliko godina učestvovao je u organizaciji međunarodnog Masterclass programa za učenike i nastavnike srednjih škola u Srbiji pod pokroviteljstvom IPPOG (*International Particle Physics Outreach Group*). Učestvovao je i u seminaru za nastavnike fizike u Institutu za fiziku 2015. godine.

5 ELEMENTI ZA KVALITATIVNU OCENU NAUČNOG DOPRINOSA

5.1 Kvalitet naučnih rezultata

Značaj radova u kojima je kandidat dao ključni doprinos odnosi se pre svega na testiranje konzistentnosti Standardnog modela, kroz merenje mase W bozona, Higsovog bozona i mase top kvarka, kao i produkcije i sprezanja Higsovog bozona. Ove teme predstavljaju jedne od ključnih tačaka programa eksperimenta ATLAS, na kome je kandidat angažovan. Merenje mase W bozona na hadronskom sudaraču predstavlja poseban izazov, i prvo je takvo merenje na LHC-u. Po preciznosti merenje je uporedivo sa merenjima na sudaraču Tevatron, gde je eksperimentima bilo potrebno značajno duže vreme za ostvarivanje rezultata sa sličnom preciznošću. Rezultati merenja mase Higsovog bozona i mase top kvarka su relevantni za testiranje konzistentnosti SM i važan korak ka konačnoj preciznosti koja će biti ostvarena u merenju navedenih parametara SM. Rezultati koje je kandidat ostvario u okviru *Muon Combined Performance*, kao i *Luminosity Task Force* grupe su od značaja za celokupni program ATLAS eksperimenta.

Dr Nenad Vranješ je u svom dosadašnjem naučnom radu dao ključni doprinos u dvanaest radova u međunarodnim časopisima sa ISI liste, od čega jedanaest kategorije M21 ili M21a i jedan kategorije M23, kao i u tri rada kategorije M24 (međunarodni časopisi priznati posebnom odlukom MNO). Na međunarodnim skupovima imao je četiri predavanja po pozivu štampana u celini (M31), četiri saopštenja kategorije M33 (štampanih u celini) i dva saopštenja kategorije M34 (štampanih u izvodima), a na nacionalnim skupovima ima dva saopštenja kategorije M63 (štampanih u celini). Kandidat je koautor ukupno 574 rada objavljena u međunarodnim časopisima.

Nakon prethodnog izbora u zvanje, dr Nenad Vranješ je imao ključni doprinos u osam radova u međunarodnim časopisima sa ISI liste. Svi navedeni radovi pripadaju kategoriji M21 ili M21a. Na međunarodnim skupovima imao je dva predavanja po pozivu štampana u celini (M31) i dva saopštenja kategorije M63 (štampana u celini).

Svi radovi su objavljeni u časopisima sa visokim impakt faktorima (>4). Kolaboracijski radovi u kojima je dr N. Vranješ dao ključni doprinos objavljeni su u *Physics Letters B* (najveći IF 6.019), *Physical Review D* (IF 4.864), *European Physical Journal C* (IF 5.247) i *Journal of High Energy Physics* (IF 6.220). Uticajnost ovih radova se vidi po kvalitetu časopisa, kao i po citiranosti.

Prema bazi *Web of Science*, naučni radovi u kojima je dr Nenad Vranješ imao ključni doprinos citirani su preko 200 puta ne računajući autocitate. Prema bazi *inSPIRE* ovi radovi su citirani preko 500 puta ne računajući autocitate. Ukupan h-indeks kandidata prema bazi *WoS* iznosi 52.

Detaljni pregled aktivnosti Dr Nenada Vranješa dat je u opisu naučne aktivnosti. Treba napomenuti da je kandidat prepoznat kao veoma aktivan član ATLAS kolaboracije, sobzirom da je svoje, kao i rezultate u ime celih grupa u kojima je radio, prezentovao preko 100 puta na

sastancima radnih grupa ATLAS kolaboracije. Konkretno, na sastancima *Standard Model radne grupe, Muon Combined Performance, Inner Detector*, kao i *Higgs WG*. Značajne prezentacije bile su date i na radnim sastancima grupe *Luminosity Task Force*.

Kao jedan od najkompetentnijih, i istraživač sa glavnim doprinosom bio je jedan od editora u tri publikacije ATLAS kolaboracije: JHEP 1409 (2014) 037, Eur.Phys.J. C74 (2014) no.11, 313, i ATLAS-CONF-2016-113. Takođe, od strane ATLAS kolaboracije imenovan za editora kapitalne publikacije koja će obuhvatati petogodišnje rezultate prvog merenja mase W bozona. Ova publikacija je u završnoj fazi odobravanja od strane ATLAS kolaboracije.

Takođe, član je ATLAS-ovog recenzentskog tima za studiju merenja mase top kvarka u dileptonskom kanalu raspada u protonskim sudarima na energiji $\sqrt{s} = 8$ TeV, kao i recenzentskog tima za studiju merenja mase Higsovog bozona u četvoroleptonskom kanalu sa podacima na energiji $\sqrt{s} = 13$ TeV prikupljenim tokom 2015. i 2016. godine.

Pored toga, kandidat je učestvovao u organizaciji dvodnevnog W Mass workshop-a održanog u CERN-u https://indico.cern.ch/event/458880/ sa pregledom rezultata grupe, statusom i planovima za nastupajući period.

Više puta je po pozivu prezentovao svoje rezultate i rezultate ATLAS (kao i CMS) kolaboracije na međunarodnim i nacionalnim konferencijama:

- ,,Exotics searches at ATLAS", konferencija ,,LHC on the March", 16-18 novembar, 2011, Protvino, Rusija, https://indico.cern.ch/event/142227/.
- ,,Electroweak tests at the LHC", u ime dve kolaboracije ATLAS i CMS, konferencija ,,26th Rencontres de Blois", 18-23 maj 2014, Blois, Francuska http://blois.in2p3.fr/2014/.
- ,,Challenges in W mass measurements with ATLAS and CMS", u ime dve kolaboracije ATLAS i CMS, The Fourth Annual Large Hadron Collider Physics, LHCP2016, 13-18. jun 2016, Lund, Švedska, http://lhcp2016.hep.lu.se.
- ,,Poslednji rezultati eksperimenta ATLAS", XII Kongresu fizičara Srbije (Vrnjačka Banja 2013), http://www.dfs.rs/kongres/program.htm
- predavanje ,,Muon reconstruction in ATLAS+CMS", LHC France 2013, Annecy 2013, Francuska, https://indico.in2p3.fr/event/6838/.

5.2 Angažovanost u formiranju naučnih kadrova

Kandidat je mentor pri izradi doktorske disertacije Aleksandre Dimitrievske na temi ,,Measurement of the W boson mass and the calibration of the muon momentum with the ATLAS detector" (*Merenje mase W bozona i kalibracija impulsa miona na detektoru ATLAS*). Odbrana ove doktorske disertacije na Fizičkom fakulteta Univerziteta u Beogradu planira se u prvoj polovini 2017. godine.

Takođe, kandidat je bio mentor za izradu master rada studentkinje Milene Bajić pod naslovom ,,Produkcija parova gradijentnih bozona u proton-proton sudarima na $\sqrt{s} = 100$ TeV" odbranjenom na Departmanu za fiziku Prirodno-matematičkog fakulteta Univerziteta u Novom Sadu juna 2015. godine.

U okviru seminara za nastavnike srednjih škola 5. marta 2015. u Institutu za fiziku kandidat je održao predavanje pod nazivom ,,Otkriće Higsovog bozona: šta dalje?".

Nekoliko godina učestvovao je u organizaciji međunarodnog Masterclass programa za učenike i nastavnike srednjih škola u Srbiji pod pokroviteljstvom IPPOG (*International Particle Physics Outreach Group*). Cilj ovog programa je popularizacija fizike čestica i istraživanja u CERN-u.

Od 2008-2010. godine redovno je držao seminare studentima Fizičkog fakulteta u okviru predmeta Fizika elementarnih čestica i Seminar savremene fizike, na istraživačkom smeru, iz tematike fizike čestica na LHC-u i savremenih detektora čestica.

5.3 Normiranje broja koautorskih radova, patenata i tehničkih rešenja

Dr Nenad Vranješ je član ATLAS kolaboracije od 2004. godine. Svi dobijeni rezultati objavljeni su ili prezentirani na konferencijama po pravilima ATLAS kolaboracije formulisanim u dva dokumenta: "*ATLAS Publication Policy* " i "*ATLAS Authorship Policy* ". Za kvantitativnu ocenu naučnog doprinosa računati su samo radovi na kojima kandidat ima istaknuti i originalni doprinos. Ovi radovi su praćeni internim i javnim notama ATLAS kolaboracije navedenim u prilogu.

5.4 Rukovođenje projektima, potprojektima i projektnim zadacima

Kandidat rukovodi projektnim zadatkom ispitivanja osobina Standardnog modela fizike čestica u okviru projekat OI 171004.

5.5 Aktivnost u naučnim i naučno-stručnim društvima

Kandidat je član Saveta Društva fizičara Srbije za naučna istraživanja i visoko obrazovanje, odsek za fiziku jezgra, elementarnih čestica i osnovnih interakcija.

5.6 Uticaj naučnih rezultata

Uticaj naučnih rezultata kandidata naveden je u odeljku 5.1. Pun spisak radova i radova koji ih citiraju je dat u prilogu.

5.7 Konkretan doprinos kandidata u realizaciji radova u naučnim centrima u zemlji i inostranstvu

Kandidat je član međunarodne kolaboracije ATLAS na Velikom sudaraču hadrona u CERN-u od 2004. godine. Kolaboracija danas broji peko 3000 istraživača iz preko 170 naučnih institu-

cija. U togu izrade doktorske disertacije u periodu od 2008-2011. godine aktivno je sarađivao sa ATLAS grupom Nacionalnog i Kapodistrijskog Univerziteta u Atini pod rukovodstvom prof. dr. C. Kourkoumelis koja je bila komentor teze kandidata. Nakon postdoktorskog usavršavanja u francuskom institutu CEA-Saclay 2011-2014, saradnja sa tamošnjom ATLAS grupom se nastavlja kroz rad na projektima merenja mase W bozona i apsolutnoj kalibraciji luminoznosti na ATLAS eksperimentu.

Konkretan doprinos kandidata je demonstriran kroz autorstvo u internim notama kolaboracije koja prate publikacije u časopisima, kroz editorski rad, kroz prezentacije svojih, kao i rezultata celokupnih grupa u okviru kolaboracije, kao i kroz predavanja po pozivu koja je kandidat držao u ime cele kolaboracije na međunarodnim konferencijama. Rezultati ostvareni u okviru *Muon Combined Performance*, kao i *Luminosity Task Force* grupe su od značaja za celokupni program ATLAS eksperimenta, i imaju primenu u velikom broju rezultata koje je objavila kolaboracija u datom periodu.

6 ELEMENTI ZA KVANTITATIVNU OCENU NAUČNOG DOPRINOSA

6.1 Ostvareni rezultati u periodu nakon prethodnog izbora u zvanje

Kategorija	M bodova po radu	Broj radova	Ukupno M bodova
M21a	10	2	20
M21	8	6	48
M31	3.5	2	7
M63	1	2	2

6.2 Poređenje sa minimalnim kvantitativnim uslovima za izbor u zvanje viši naučni saradnik

Minimalan broj M bodova		Ostvareno
Ukupno	50	77
M10+M20+M31+M32+M33+ M41+M42 $\geq$	40	75
M11+M12+M21+M22+ M23 $\geq$	30	48

6.3 Citiranost i h-indeks

Prema bazi *Web of Science*, naučni radovi u kojima je dr Nenad Vranješ imao ključni doprinos citirani su preko 200 puta ne računajući autocitate. Prema bazi *inSPIRE* ovi radovi su citirani preko 500 puta ne računajući autocitate. Ukupan h-indeks kandidata prema bazi *WoS* iznosi 52.

7 SPISAK OBJAVLJENIH RADOVA PO KATEGORIJAMA

7.1 Radovi u međunarodnim časopisima izuzetnih vrednosti (M21a)

7.1.1 Radovi objavljeni nakon prethodnog izbora u zvanje:

1. Aaboud, M., ... ,Vranjes N., *et al.* [ATLAS Collaboration], *Measurement of the top quark mass in the $t\bar{t} \to$ dilepton channel from $\sqrt{s} = 8$ TeV ATLAS data*, Phys.Lett. B761 (2016) 350-371, arXiv:1606.02179 [hep-ex], IF=6.131.

2. Aad, G., ... ,Vranjes N., *et al.* [ATLAS Collaboration], *Fiducial and differential cross sections of Higgs boson production measured in the four-lepton decay channel in pp collisions at $\sqrt{s}$=8 TeV with the ATLAS detector*, Phys.Lett. B738 (2014) 234-253, arXiv:1408.3226 [hep-ex], IF=6.131.

7.2 Radovi u vrhunskim međunarodnim časopisima (M21)

7.2.1 Radovi objavljeni nakon prethodnog izbora u zvanje:

1. Aaboud, M., ... ,Vranjes N., *et al.* [ATLAS Collaboration], *Luminosity determination in pp collisions at $\sqrt{s}$ = 8 TeV using the ATLAS detector at the LHC*, Eur.Phys.J. C76 (2016) no.12, 653, arXiv:1608.03953 [hep-ex], IF=5.084.

2. Aad, G., ... ,Vranjes N., *et al.* [ATLAS Collaboration], *Measurement of the Higgs boson mass from the $H \to \gamma\gamma$ and $H \to ZZ^* \to 4\ell$ channels with the ATLAS detector using 25 fb^{-1} of pp collision data*, Phys.Rev. D90 (2014) no.5, 052004, arXiv:1406.3827 [hep-ex], IF=4.643.

3. Aad, G., ... ,Vranjes N., *et al.* [ATLAS Collaboration], *Measurements of Higgs boson production and couplings in the four-lepton channel in pp collisions at center-of-mass energies of 7 and 8 TeV with the ATLAS detector*, Phys.Rev. D91 (2015) no.1, 012006, arXiv:1408.5191 [hep-ex], IF=4.643.

4. Aad, G., ... ,Vranjes N., *et al.* [ATLAS Collaboration], *Measurement of the muon reconstruction performance of the ATLAS detector using 2011 and 2012 LHC proton–proton collision data*, Eur.Phys.J. C74 (2014) no.11, 3130, arXiv:1407.3935 [hep-ex], IF=5.084.

5. Aad, G., ... ,Vranjes N., *et al.* [ATLAS Collaboration], *Search for new particles in events with one lepton and missing transverse momentum in pp collisions at $\sqrt{s}$ =8 TeV with the ATLAS detector*, JHEP 1409 (2014) 037, arXiv:1407.7494 [hep-ex], IF=6.220.

6. Aad, G., ... ,Vranjes N., *et al.* [ATLAS Collaboration], *ATLAS search for a heavy gauge boson decaying to a charged lepton and a neutrino in pp collisions at $\sqrt{s}$=7 TeV*, Eur.Phys.J. C72 (2012) 2241, arXiv:1209.4446 [hep-ex], IF=5.247.

7.2.2 Radovi objavljeni pre prethodnog izbora u zvanje:

1. Aad, G., ... ,Vranjes N., *et al.* [ATLAS Collaboration], *Search for a heavy gauge boson decaying to a charged lepton and a neutrino in 1 fb^{-1} of pp collisions at $\sqrt{s}$ = 7 TeV using the ATLAS detector*, Phys.Lett. B705 (2011) 28-46, arXiv:1108.1316[hep-ex], IF=4.558.

2. Aad, G., ... ,Vranjes N., *et al.* [ATLAS Collaboration], *Search for high-mass states with one lepton plus missing transverse momentum in proton-proton collisions at* $\sqrt{s} = 7$ *TeV with the ATLAS detector*, Phys.Lett. B701 (2011) 50-69, arXiv:1103.1391[hep-ex], IF=4.558.

3. Aad, G., ... ,Vranjes N., *et al.* [ATLAS Collaboration], *Performance of the ATLAS Detector using First Collision Data*, JHEP, 1009, 056 (2010) 65pp, arXiv:1005.5254 [hep-ex], IF=6.220.

7.3 Radovi u međunarodnim časopisima (M23)

7.3.1 Radovi objavljeni pre prethodnog izbora u zvanje:

1. Lj.Simić, N.Vranješ, D.Reljić, D.Vudragović, D.S.Popović, "WW Production and Triple Gauge Boson Couplings at ATLAS", Acta Physica Polonica B, **38** 525 (2007), IF=0.998.

7.4 Radovi u međunarodnim časopisima verifikovani posebnom odlukom MNO, (M24)

7.4.1 Radovi objavljeni pre prethodnog izbora u zvanje:

1. D.L.Adams, D.Fassouliotis, C.Kourkoumelis, B.R.Mellado Garcia, M.I.Pedraza Morales, N.Vranjes, S.L.Wu, *Lepton plus missing transverse energy signals at high mass*, ATLAS Note, ATL-PHYS-PUB-2009-007, CERN-OPEN-2008-020, CERN, 29p. (2009).

2. K.Bachas,..., Lj. Simic, D.S.Popovic,..., N. Vranjes *et al*, *Diboson physics studies*, ATLAS Note, ATL-PHYS-PUB-2009-038, CERN-OPEN-2008-020, CERN, 37p. (2009).

3. Lj. Simić, I. Mendaš, N. Vranješ, D.S.Popović, *Prospects for Measuring Triple Gauge Boson Couplings in WW Production at the LHC*, ATL-PHYS-PUB-2006-011 (2006)

7.5 Predavanje po pozivu sa međunarodnog skupa štampano u celini (M31)

7.5.1 Nakon prethodnog izbora u zvanje:

1. N.Vranjes on behalf of ATLAS and CMS Collaborations, *Challenges in W mass measurements with ATLAS and CMS*, PoS(LHCP2016)053, ATL-PHYS-PROC-2016-143, The Fourth Annual Large Hadron Collider Physics, LHCP2016, 13-18 June 2016, Lund, Sweden.

2. N.Vranjes on behalf of ATLAS and CMS Collaborations, *Electroweak tests at the LHC*, ATL-PHYS-PROC-2014-139, https://cds.cern.ch/record/1756275/files/ATL-PHYS-PROC-2014-139.pdf, 26th Rencontres de Blois, May 18-23, 2014, Blois, France.

7.5.2 Pre prethodnog izbora u zvanje:

1. N.Vranjes on behalf of ATLAS Collaboration, *Exotic Searches in ATLAS*, PoS(IHEP-LHC-2011)021, ATL-PHYS-PROC-2012-040, arXiv:1202.3171[hep-ex], LHC on the March, November 16-18, 2011, Protvino, Moscow region, Russian Federation.

2. N. Vranjes on behalf of ATLAS Collaboration for the ATLAS Collaboration, *Search for W' in lepton+missing E_T final state with early data at ATLAS*, Proceedings of Science 2008LHC:121, 2008. ATL-PHYS-PROC-2008-085.

7.6 Saopštenja sa međunarodnih skupova štampana u celini (M33)

7.6.1 Pre prethodnog izbora u zvanje:

1. N. Vranjes on behalf of ATLAS Collaboration for the ATLAS Collaboration, *Search for W' in lepton+missing E_T final state with early data at ATLAS*, Proceedings of Science 2008LHC:121, 2008. ATL-PHYS-PROC-2008-085, Physics at LHC - 2008, Split, Croatia, 29 September - 4 October 2008.

2. K.Bachas,...,L.Simic, D. Popovic,..., N.Vranjes *et al. Studies of diboson production with the ATLAS detector*, Nucl.Phys.Proc.Suppl. 177-178:255-257, 2008, Hadron Collider Physics Symposium 2007.

3. N. Vranjes, L. Simic, D. Reljic, D. Vudragovic, D.S. Popovic, *WW production at the LHC in NLO simulations*, American Institute of Physics Conf. Proceedings, **899**, 225, 2007, AIP Conference Proceedings 899, 207-208 (2007), 6th International Conference of the Balkan Physical Union, Istanbul, Turkey, 22-26 Aug 2006.

4. Lj.Simic, N.Vranjes, I.Mendas, D.S.Popovic, *ATLAS Sensitivity to Anomalous WWV Couplings*, American Institute of Physics Conf. Proceedings, **899**, 219, 2007, AIP Conference Proceedings 899, 207-208 (2007), 6th International Conference of the Balkan Physical Union, Istanbul, Turkey, 22-26 Aug 2006.

7.7 Saopštenja sa međunarodnih skupova štampana u izvodima (M34)

7.7.1 Pre prethodnog izbora u zvanje:

1. N. Vranjes, C. Kourkoumelis, D. Fassouliotis, A. Antonaki, D. Popovic, *Searches for new gauge bosons with the ATLAS detector*, XXVIII Workshop on Recent Advances in Particle Physics and Cosmology, 25-28 March 2010, Thessaloniki, Greece.

2. L.Simic, N.Vranjes, D. Popovic, *WW Production and Triple Gauge Boson Couplings at ATLAS*, Published in Abstract book, Marue Curie Workshop 2006 in Croatia and Serbia, Celebrating 150th Anniversary of the birth of Nikola Tesla, ISBN 86-7282-056-8, Publishers: Croatian Academy of Engeneering and Ministry of Science and Environmantal Protection Serbia (2006), Marue Curie Workshop 2006 in Croatia and Serbia, Celebrating Nikola Tesla, 7-11 October 2006.

7.8 Saopštenja sa skupova nacionalnog značaja štampana u celini (M63)

7.8.1 Nakon prethodnog izbora u zvanje:

1. N.Vranješ, *Poslednji rezultati eksperimenta ATLAS*, Društvo fizičara Srbije, XII Kongres fizičara Srbije ISBN 978-86-86169–08-2, 28. april−2. maj 2013, Vrnjačka Banja, Srbija.

2. A.Dimitrievska, N.Vranješ, *Karakteristike rekonstrukcije miona niskog impulsa na ATLAS detektoru*, Društvo fizičara Srbije, XII Kongres fizičara Srbije ISBN 978-86-86169–08-2, 28. april−2. maj 2013, Vrnjačka Banja, Srbija, poster u sekciji 2: Fizika jezgra, elementarnih čestica i osnovnih interakcija.

7.8.2 Pre prethodnog izbora u zvanje:

1. N.Vranješ, Lj. Simić and D.S.Popović, *Prospect for WW Study With Early ATLAS Data*, Journal of Research in Physics, **31**, 82, 2007, FIS2007 - Fundamentalne Interakcije - Srbija 2007, Iriški venac, Novi Sad, Srbija, 26-28. septembar 2007.

2. Lj. Simić, N.Vranješ and D.S.Popović, *Gauge Boson Pair Production and Charged Triple Gauge Boson Couplings at the LHC*, Journal of Research in Physics, **31**, 65, 2007, FIS2007 - Fundamentalne Interakcije - Srbija 2007, Iriški venac, Novi Sad, Srbija, 26-28. septembar 2007.

7.9 Odbranjena doktorska disertacija (M71)

Nenad Vranješ, *Traganje za novim teškim naelektrisanim gradijentnim bozonima na ATLAS detektoru (A Search for New Heavy Charged Gauge Bosons at ATLAS)*, doktorska disertacija, 2011, Fizički fakultet.

7.10 Odbranjen magistarski rad (M72)

Nenad Vranješ, *Mogućnosti ATLAS detektora za merenje produkcije parova W bozona na Velikom hadronskom kolajderu*, Fizički fakultet Univerziteta u Beogradu, 2007.

8 SPISAK JAVNIH NOTA ATLAS KOLABORACIJE SA KLJUČNIM DOPRINOSOM

Dr Nenad Vranješ je nakon prethodnog izbora u zvanje imao značajan doprinos u sledećim javnim notama ATLAS kolaboracije sa međunarodnom recenzijom:

1. ATLAS Collaboration, *Measurement of the $W-$boson mass in pp collisions at $\sqrt{s}$ = 7 TeV with the ATLAS detector*, ATLAS-CONF-2016-113, 85p, CERN (2016), https://cds.cern.ch/record/2238954

2. ATLAS Collaboration, *Studies of theoretical uncertainties on the measurement of the mass of the W boson at the LHC*, ATL-PHYS-PUB-2014-015, 26p, CERN, (2014), https://cds.cern.ch/record/1956455

3. ATLAS Collaboration, *Search for high-mass states with one lepton plus missing transverse momentum in pp collisions at $\sqrt{s}$ =8 TeV with the ATLAS detector*, ATLAS-CONF-2014-017, 22p, CERN (2014), https://cds.cern.ch/record/1692660

4. ATLAS Collaboration, *Preliminary muon performance 2012*, ATLAS-CONF-2013-088, 15p, CERN (2013), https://cds.cern.ch/record/1580207

Pre prethodnog izbora u zvanje.

1. ATLAS Collaboration, *Search for high-mass states with one muon plus missing transverse momentum in proton-proton collisions at $\sqrt{s}$=7 TeV with the ATLAS detector*, ATLAS-CONF-2011-082, 13p, https://cds.cern.ch/record/1356189

2. ATLAS Collaboration, *Physics potential of Z' and W' searches with the ATLAS Detector as a function of the LHC center-of-mass energy*, ATL-PHYS-PUB-2011-002, 7p, https://cds.cern.ch/record/1323860

3. ATLAS Collaboration, *Search for high-mass states with electron plus missing transverse energy using the ATLAS Detector at $\sqrt{s}$=7TeV*, ATLAS-CONF-2010-089, 12p, https://cds.cern.ch/record/1299104

4. ATLAS Collaboration, *ATLAS sensitivity prospects to W' and Z' at 7 TeV*, ATL-PHYS-PUB-2010-007, 18p, https://cds.cern.ch/record/1277012

9 SPISAK INTERNIH NOTA ATLAS KOLABORACIJE SA KLJUČNIM DOPRINOSOM

Navedene interne note preuzete su direktno sa CERN-ovog CDS servera https://cds.cern.ch i demonstriraju naučni doprinos kandidata u okviru kolaboracije nakon prethodnog izbora u zvanje.

1. Nancy Andari, ..., Maarten Boonekamp, ..., Aleksandra Dimitrievska, ..., Matthias Schott, ..., Nenad Vranjes, et al., *Measurement of mW at 7 TeV : Muon momentum corrections and uncertainties*, ATL-COM-PHYS-2014-1433, 46p, https://cds.cern.ch/record/1966962

2. Nancy Andari, ..., Maarten Boonekamp, ..., Aleksandra Dimitrievska, ..., Matthias Schott, ..., Nenad Vranjes, et al., *Measurement of mW with 7 TeV : W boson mass measurement*, ATL-COM-PHYS-2014-1569, 186p, https://cds.cern.ch/record/1976186

3. Nancy Andari, ..., Maarten Boonekamp, ..., Aleksandra Dimitrievska, ..., Matthias Schott, ..., Nenad Vranjes, et al., *Measurement of mW at 7 TeV : Z-based cross check measurements*, ATL-COM-PHYS-2014-1437, 28p, https://cds.cern.ch/record/1966966

4. Nancy Andari, ..., Maarten Boonekamp, ..., Aleksandra Dimitrievska, ..., Matthias Schott, ..., Nenad Vranjes, et al., *Measurement of mW at 7 TeV : Physics modeling*, ATL-COM-PHYS-2014-1436, 137p, https://cds.cern.ch/record/1966965

5. Nancy Andari, ..., Maarten Boonekamp, ..., Aleksandra Dimitrievska, ..., Matthias Schott, ..., Nenad Vranjes, et al., *Measurement of mW at 7 TeV : Reconstruction of the hadronic recoil*, ATL-COM-PHYS-2014-1435, 34p, https://cds.cern.ch/record/1966964

6. Nancy Andari, ..., Maarten Boonekamp, ..., Aleksandra Dimitrievska, ..., Matthias Schott, ..., Nenad Vranjes, et al., *Measurement of mW at 7 TeV : Electron performance corrections and uncertainties*, ATL-COM-PHYS-2014-1434, 59p, https://cds.cern.ch/record/1966963

7. Nancy Andari, ..., Maarten Boonekamp, ..., Aleksandra Dimitrievska, ..., Matthias Schott, ..., Nenad Vranjes, et al., *Measurement of mW at 7 TeV : Muon efficiency corrections and uncertainties*, ATL-COM-PHYS-2015-073, 40p, https://cds.cern.ch/record/1987497

8. Nancy Andari, ..., Maarten Boonekamp, ..., Aleksandra Dimitrievska, ..., Matthias Schott, ..., Nenad Vranjes, et al., *Measurement of mW at 7 TeV : Hadronic recoil corrections*, ATL-COM-PHYS-2015-344, 156p, https://cds.cern.ch/record/2013274

9. L. J. Armitage, S. Glazov, R. Keeler, T. Kwan, D. MacDonell, E. Rizvi, A. Sapronov, N. Vranjes, E. Yatsenko, *Measurement of the Drell-Yan triple-differential cross-section in pp collisions at* $\sqrt{s}$ *= 8 TeV*, ATL-COM-PHYS-2015-1575, 243pp, https://cds.cern.ch/record/2117171

10. S. H. Abidi , ... , N.Vranjes, et al., *Study of the SM-like Higgs particle at 125 GeV properties using production mechanisms specific signatures in the* $H \to ZZ^{(*)} \to \ell^+\ell^-\ell^+\ell^-$ *channel.*, ATL-COM-PHYS-2013-1663, 160p, https://cds.cern.ch/record/1639131

11. S. H. Abidi, ... , N.Vranjes, et al., *Measurement of inclusive and differential fiducial cross-sections of the Higgs boson in the $H \to ZZ \to \ell\ell\ell\ell$ decay channel using 20.3 fb^{-1} of $\sqrt{s}$ =8 TeV pp collision data at the ATLAS detector.*, ATL-COM-PHYS-2014-056, 130p, https://cds.cern.ch/record/1646073?#

12. Amelung, C, ..., Vranjes N, ... et al., *Muon reconstruction performances of the ATLAS detector during Run 1*, ATL-COM-MUON-2014-025, 31p, https://cds.cern.ch/record/1696343?#

13. S. Camarda, ..., N.Vranjes, et al. *Studies of theoretical uncertainties on the measurement of the mass of the W boson at the LHC*, ATL-COM-PHYS-2014-875, 26p, https://cds.cern.ch/record/1744695

14. G. Artoni, M. Corradi, A. Dimitrievska, F. Sforza, N. Vranjes, P. Fleischmann, *Muon momentum scale and resolution corrections evaluated with $Z \to \mu\mu$ and $J/\psi \to \mu\mu$ decays on Run I ATLAS data*, ATL-COM-MUON-2014-001, 60p, https://cds.cern.ch/record/1643495

15. L. Chevalier, A Dimitrievska, N. Vranjes, *Muon performance studies using $J/\psi \to \mu\mu$ at $\sqrt{s}$ = 7 TeV and $\sqrt{s}$ = 8 TeV of pp collisions*, ATL-COM-MUON-2013-022, 66p, https://cds.cern.ch/record/1596789

16. T. Adye,..., A. Dimitrievska,..., N. Vranjes, et al., *Supporting Document for Higgs papers: Higgs mass measurements and uncertainties in 2012*, ATL-COM-PHYS-2012-1774, 138p, https://cds.cern.ch/record/1498240

17. D. L. Adams, ... , N.Vranjes et al. , *Search for high-mass states with one lepton plus missing transverse momentum using the ATLAS detector with 4.7 $fb^{-}1$ of pp collisions at $\sqrt{s}$= 7TeV*, ATL-COM-PHYS-2012-689, 137p, https://cds.cern.ch/record/1451899?

18. D. L. Adams, ... , N.Vranjes et al. *Search for new heavy gauge bosons in the charged lepton plus missing transverse energy final state using pp collisions at $\sqrt{s}$ = 8 TeV in the ATLAS detector*, ATL-COM-PHYS-2012-1771, 83p, https://cds.cern.ch/record/1498078#

10 SPISAK INDIKATIVNIH PREZENTACIJA NA SASTANCIMA ATLAS KOLABORACIJE

Dr Nenad Vranješ ima preko 100 izlaganja na radnim sastancima ATLAS kolaboracije različitog nivoa. Ovde su navedene samo indikativne prezentacije koje su u vezi sa aktivnostima nakon prethodnog izbora u zvanje.

- 16/11/2016,
  Open Presentation of the Measurement of the $W-$boson mass in pp collisions at $\sqrt{s} = 7$ TeV with the ATLAS detector,
  Nenad Vranjes on behalf of W mass analysis team, *Presentation of the analysis*,
  http://indico.cern.ch/event/588125/contributions/2370653/

- 24/11/2016,
  Luminosity Task Force Meeting,
  Nenad Vranjes, Witold Kozanecki *Analysis of the crossing angle scans*,
  http://indico.cern.ch/event/435647/contributions/2383582/

- 19/10/2016,
  Luminosity Task Force Meeting,
  Nenad Vranjes, *Status of the vdM analysis-orbit drifts*,
  indico.cern.ch/event/435642/contributions/2346448/

- 14/09/2016,
  $W-$mass Editorial Board meeting,
  Nenad Vranjes *Summary of final analysis changes*,
  https://indico.cern.ch/event/568969/contributions/2304206/

- 04/05/2016,
  $W-$mass Editorial Board meeting,
  M.Boonekamp, M. Schott, N.Vranjes, *Overview of Analysis Status*,
  https://indico.cern.ch/event/523350/contributions/2158719/

- 25/02/2016,
  Luminosity Task Force Meeting,
  W. Kozanecki, N. Vranjes, *August 2015 vdM analysis: updated results and systematics*,
  https://indico.cern.ch/event/435608/contributions/1934297/

- 24-25/11/2015,
  Nenad Vranjes, Matthias Schott, Maarten Boonekamp, W mass workshop (CERN) :
  https://indico.cern.ch/event/458880/timetable/

- 19/05/2015,
  W mass EdBoard meeting,
  Maarten Boonekamp, Nenad Vranjes, *Introduction and Update of Supporting Documentation* ,
  https://indico.cern.ch/event/394419/timetable/

- 16/04/2015,
  Luminosity Task Force Meeting,
  N.Vranjes, W. Kozanecki, *Systematics in the VdM background-subtraction*,
  https://indico.cern.ch/event/359531/

- 19/09/2014,
  Inner Detector Alignment meeting,
  N.Vranjes, *Studies of the Jpsi and Z sagitta bias from W mass group*,
  https://indico.cern.ch/event/278634/

- 23-25/06/2014,
  W mass Workshop,
  Nenad Vranjes, *Muon discussion summary*,
  https://indico.cern.ch/event/324232/timetable/

- 03/06/2014,
  ATLAS Weekly,
  Nenad Vranjes, *Paper presentations : Muon reconstruction performances of the ATLAS detector during Run 1*,
  https://indico.cern.ch/event/286465/

- 11/04/2014,
  Inner Tracking CP Weekly
  Nenad Vranjes, *Momentum resolution and J/psi*,
  https://indico.cern.ch/event/313693/contributions/1686582/

- 13/02/2014,
  TrackCP + MCP joint meeting during ATLAS week,
  Nenad Vranjes, *Effect of ID angular resolution and material on muon momentum resolution corrections*,
  https://indico.cern.ch/event/301790/contributions/692927/

- 07/02/2014,
  Higgs working group plenary meeting,
  N. Vranjes on behalf of MCP, *Muon Combined Performance Report*,
  https://indico.cern.ch/event/298812/contributions/1659204/

- 19/12/2013,
  ATLAS Higgs working group meeting,
  Nenad Vranjes, *Muon calibration*,
  https://indico.cern.ch/event/288560/contributions/1644307/

- 13/12/2013,
  Wmass WG meeting
  N.Vranjes, *Lepton scale and resolution*,
  https://indico.cern.ch/event/288424/contributions/1644044/

- 03/12/2013,
  ATLAS Weekly,
  N.Vranjes on behalf of MCP,
  Report from the Muon Combined Performance group,
  https://indico.cern.ch/event/286149/

- 27/11/2013,
  MCP weekly meeting,
  Nenad Vranjes, *2011 momentum scales*,
  https://indico.cern.ch/event/285387/contributions/649121/

- 27/11/2013,
  MCP weekly meeting
  G. Artoni, M. Corradi, A. Dimitrievska, N. Orlando, P. Kluit, F. Sforza, N. Vranjes, *Update on MuonMomentumCorrections*,
  https://indico.cern.ch/event/285387/

- 04/10/2013,
  Wmass WG meeting
  N.Vranjes, *Code update*,
  https://indico.cern.ch/event/276524/contributions/1620303/

- 19-21/09/2013, Harward, USA
  Standard Model Workshop
  Nenad Vranjes, *W mass measurement* ,
  https://indico.cern.ch/event/266334/contributions/599684/

- 18/06/2013,
  MCP meeting during the atlas week,
  Laurent Chevalier, Aleksandra Dimitrievska, Nenad Vranjes, *Momentum scale with* $J/\psi \rightarrow \mu\mu$,
  https://indico.cern.ch/event/258263/

- 26/03/2013,
  Muon performance in the Muon Week,
  Laurent Chevalier, Aleksandra Dimitrievska, Nenad Vranjes, *Calorimeter energy loss corrections using* $J/\psi \rightarrow \mu\mu$,
  https://indico.cern.ch/event/242777/contributions/1559020/

- 12/02/2012
  Muon CP + Tracking CP meeting in the PP week
  N.Vranjes, *FSR update*
  https://indico.cern.ch/event/221905/contributions/1526031/

- 11/06/2012 Wmass WG meeting
  N.Vranjes, *Common items, backgrounds, fitting range*,
  https://indico.cern.ch/event/195126/

- 09/01/2012 W' weekly
  N.Vranjes, *W' NNLO cross section calculation*,
  https://indico.cern.ch/event/195126/

- 16/12/2011 Wmass WG meeting
  N.Vranjes, *TSelector skeleton; comments on overall analysis chain*,
  https://indico.cern.ch/event/167255/

11 KOMPLETNA LISTA PUBLIKACIJA

Kompletna lista svih naučnih publikacija ATLAS kolaboracije na kojima je dr Nenada Vranješ koautor dostupna je na sledećem linku:

http://inspirehep.net/author/profile/N.Vranjes.1

12 DODACI

23. децембар 2016

Научно веће Института за физику

Предмет: Потврда руководиоца пројекта поводом избора др Ненада Врањеша у звање виши научни сарадник

Поштовани,

Др Ненад Врањеш запослен је у Лабораторији за физику високих енергија Института за физику у Београду од 2005. године. Ангажован је на пројекту основних истраживања Министарства просвете, науке и технолошког развоја 171004 под називом "АТЛАС експеримент и физика честица на ЛХЦ енергијама" у оквиру ког руководи пројектним задатком под називом "Испитивање особина Стандардног модела физике честица на експерименту АТЛАС". Публикације које се односе на овај пројектни задатак излистане су у годишњим извештајима пројекта 171004 као и у посебном прилогу.

Руководилац пројекта 171004,

др Лидија Живковић
Научни саветник

1 RADOVI OBJAVLJENI U OKVIRU PROJEKTNOG ZADATKA ISPITIVANJE SVOJSTAVA STANDARDNOG MODELA

1. Aaboud, M., ... ,Vranjes N., *et al.* [ATLAS Collaboration], *Measurement of the top quark mass in the $t\bar{t} \to$ dilepton channel from $\sqrt{s} = 8$ TeV ATLAS data*, Phys.Lett. B761 (2016) 350-371, arXiv:1606.02179 [hep-ex], IF=6.131.

2. Aad, G., ... ,Vranjes N., *et al.* [ATLAS Collaboration], *Measurement of the muon reconstruction performance of the ATLAS detector using 2011 and 2012 LHC proton–proton collision data*, Eur.Phys.J. C74 (2014) no.11, 3130, arXiv:1407.3935 [hep-ex], IF=5.084.

3. Aad, G., ... ,Vranjes N., *et al.* [ATLAS Collaboration], *Measurement of the Higgs boson mass from the $H \to \gamma\gamma$ and $H \to ZZ^* \to 4\ell$ channels with the ATLAS detector using 25 fb^{-1} of pp collision data*, Phys.Rev. D90 (2014) no.5, 052004, arXiv:1406.3827 [hep-ex], IF=4.643.

4. Aad, G., ... ,Vranjes N., *et al.* [ATLAS Collaboration], *Measurements of Higgs boson production and couplings in the four-lepton channel in pp collisions at center-of-mass energies of 7 and 8 TeV with the ATLAS detector*, Phys.Rev. D91 (2015) no.1, 012006, arXiv:1408.5191 [hep-ex], IF=4.643.

5. Aad, G., ... ,Vranjes N., *et al.* [ATLAS Collaboration], *Fiducial and differential cross sections of Higgs boson production measured in the four-lepton decay channel in pp collisions at $\sqrt{s}$=8 TeV with the ATLAS detector*, Phys.Lett. B738 (2014) 234-253, arXiv:1408.3226 [hep-ex], IF=6.131.

6. N.Vranjes on behalf of ATLAS and CMS Collaborations, *Challenges in W mass measurements with ATLAS and CMS*, PoS(LHCP2016)053, ATL-PHYS-PROC-2016-143, The Fourth Annual Large Hadron Collider Physics, LHCP2016, 13-18 June 2016, Lund, Sweden.

7. ATLAS Collaboration, *Measurement of the $W-$boson mass in pp collisions at $\sqrt{s} = 7$ TeV with the ATLAS detector*, ATLAS-CONF-2016-113, 85pp, CERN (2016), `https://cds.cern.ch/record/2238954`

8. ATLAS Collaboration, *Studies of theoretical uncertainties on the measurement of the mass of the W boson at the LHC*, ATL-PHYS-PUB-2014-015, 26pp, CERN, (2014), `https://cds.cern.ch/record/1956455`

Република Србија
МИНИСТАРСТВО ПРОСВЕТЕ И НАУКЕ
Комисија за стицање научних звања

Број:06-00-75/835
18.07.2012. године
Б е о г р а д

На основу члана 22. става 2. члана 70. став 5. Закона о научноистраживачкој делатности ("Службени гласник Републике Србије", број 110/05 и 50/06 – исправка и 18/10), члана 2. става 1. и 2. тачке 1 – 4.(прилози) и члана 38. Правилника о поступку и начину вредновања и квантитативном исказивању научноистраживачких резултата истраживача ("Службени гласник Републике Србије", број 38/08) и захтева који је поднео

Институт за физику у Београду

Комисија за стицање научних звања на седници одржаној 18.07.2012. године, донела је

ОДЛУКУ
О СТИЦАЊУ НАУЧНОГ ЗВАЊА

Др Ненад Врањеш
стиче научно звање
Научни сарадник

у области природно-математичких наука - физика

О Б Р А З Л О Ж Е Њ Е

Институт за физику* у *Београду

утврдио је предлог број 374/1 од 03.04.2012. године на седници научног већа Института и поднео захтев Комисији за стицање научних звања број 442/1 од 20.04.2012. године за доношење одлуке о испуњености услова за стицање научног звања ***Научни сарадник***.

Комисија за стицање научних звања је по предходно прибављеном позитивном мишљењу Матичног научног одбора за физику на седници одржаној 18.07.2012. године разматрала захтев и утврдила да именовани испуњава услове из члана 70. став 5. Закона о научноистраживачкој делатности ("Службени гласник Републике Србије", број 110/05 и 50/06 – исправка и 18/10), члана 2. става 1. и 2. тачке 1 – 4.(прилози) и члана 38. Правилника о поступку и начину вредновања и квантитативном исказивању научноистраживачких резултата истраживача ("Службени гласник Републике Србије", број 38/08) за стицање научног звања ***Научни сарадник***, па је одлучила као у изреци ове одлуке.

Доношењем ове одлуке именовани стиче сва права која му на основу ње по закону припадају.

Одлуку доставити подносиоцу захтева, именованом и архиви Министарства просвете и науке у Београду.

ПРЕДСЕДНИК КОМИСИЈЕ
др Станислава Стошић-Грујичић,
научни саветник

МИНИСТАР
Проф. др Жарко Обрадовић

640/12
11. 11. 11.

На основу члана 161. Закона о општем управном поступку («Службени Лист СРЈ» број 33/97 и 31/01) и члана 129. Статута Физичког факултета Универзитета у Београду, по захтеву Ненада Врањеша дипломираног физичара из Београда, дана 11. новембра 2011. године издаје се следећа,

П О Т В Р Д А

Овим се потврђује да је **Ненад Врањеш,** дипломирани физичар из Београда, дана 11. новембра 2011. године, одбранио докторску дисертацију под називом

« ТРАГАЊЕ ЗА НОВИМ ТЕШКИМ НАЕЛЕКТРИСАНИМ ГРАДИЈЕНТНИМ БОЗОНИМА НА АТЛАС ДЕТЕКТОРУ »

пред Комисијом Физичког факултета Универзитета у Београду и тиме испунио све услове за промоцију у ДОКТОРА ФИЗИЧКИХ НАУКА.

Потврда се издаје на лични захтев, а служи ради регулисања права из радног односа и важи до промоције, односно добијања докторске дипломе.

Потврда је ослобођена плаћања таксе.

ДЕКАН ФИЗИЧКОГ ФАКУЛТЕТА

Проф. др Љубиша Зековић

From: **Lydia Roos** lroos@in2p3.fr
Subject: Invitation to give a talk at Blois 2014
Date: 18 March 2014 at 06:50
To: nenad.vranjes@cern.ch
Cc: atlas-speakers-comm@cern.ch

LR

Dear Nenad,

on behalf of the ATLAS Speakers Committee, I would like to invite you to give a (15+5)' ATLAS+CMS talk at Blois 2014, Blois (France), from 18-May-14 to 23-May-14.

The title of the talk is:

Electroweak tests at the LHC (anomalous couplings from diboson production and prospects for m_W at the LHC)

The web site is:

http://blois.in2p3.fr/2014/

The Speakers Committee recommends that you confer with your Institute Representative before replying to this invitation.

Please acknowledge receipt of this invitation in the next three days, and please let me know soon if you can accept this invitation, I do hope you can!

Best regards,
Lydia
(for the ATLAS Speakers Committee)

From: **John Butler** butler@cern.ch
Subject: ATLAS: Invitation to give a talk at LHCP2016
Date: 2 April 2016 at 21:04
To: Nenad Vranjes nenad.vranjes@cern.ch
Cc: atlas-speakers-comm@cern.ch, John Butler butler@cern.ch

JB

Dear Nenad,

on behalf of the ATLAS Speakers Committee, I would like to invite you to give a (15)' talk at LHCP2016, Lund, Sweden, from Monday, June 13, 2016 to Saturday, June 18, 2016.

The title of this LHC talk is

Challenges in or results from W mass measurements with ATLAS and CMS

The web site of the conference is:

https://indico.cern.ch/event/442390/

The Speakers Committee recommends that you confer with your Institute Representative before replying to this invitation.

Please acknowledge receipt of this invitation in the next three days, and please let me know soon if you can accept this invitation. I do hope you can!

Best regards,
John (for the ATLAS Speakers Committee).

From: **Kongres 2013** kongres2013@ff.bg.ac.rs
Subject: Poziv XII Kongres fizicara Srbije - 2
Date: 14 March 2013 at 14:11
To: Nenad.Vranjes@cern.ch

Postovani kolega Vranjes,

Obracamo Vam se u ime Naucnog i Organizacionog komiteta
XII Kongresa fizicara Srbije, koji ce biti odrzan od 28. aprila
do 2. maja 2013. godine u Vrnjackoj Banji.

Sa zadovoljstvom Vas pozivamo da ucestvujete
na Kongresu i odrzite pozivno predavanje pod nazivom
"Poslednji rezultati eksperimenta ATLAS".

Pozivna predavanja (30 minuta, ukljucujuci pitanja i diskusiju)
ce biti organizovana po tematskim sekcijama.
Predavanja ce biti na srpskom jeziku.

Oslobodjeni ste placanja kotizacije, a vasi troskovi smestaja ce biti pokriveni.
Molimo Vas da se registrujete putem sajta: www.dfs.rs/kongres

Molimo Vas da Vas rad (do 10 strana, cirilica) posaljete putem web servisa,
koji se nalazi na adresi http://www.dfs.rs/kongres/radovi.htm ,
gde se nalazi i uzorak (template) u ".doc" formatu.
Ukoliko Vam je lakse, rad mozete napisati latinicom, pa cak i na engleskom.

Umesto rada mozete poslati prosireni abstrakt (2 strane).

Rok za podnosenje radova je 31. mart 2013.

Sve aktivnosti na Kongresu ce biti odrzane u hotelu "Zvezda" u Vrnjackoj Banji.

Vise informacija mozete naci na nasem sajtu:
http://www.dfs.rs/kongres/

Ukoliko imate pitanja slobodno nam se obratite.

S postovanjem,

Prof. Jaroslav Labat
Predsednik Naucnog komiteta
XII Kongresa fizicara Srbije

Dr Ivan Dojcinovic
Predsednik Organizacionog komiteta
XII Kongresa fizicara Srbije

International Workshop

LHC ON THE MARCH

16-18 NOVEMBER 2011,
PROTVINO, RUSSIA

Institute for High Energy Physics
142281, Pobeda-1, Protvino,
Moscow Region, Russian Federation

Fax: +007(4967)744937
Tel.: +007(4967)713847
e-mail: hepft@th1.ihep.su

Dear Professor ***Vranjes*** ,

I have a pleasure to inform you that the International Workshop "**LHC on the March**" is planned to be held in the Institute for High Energy Physics (Protvino, Russia) in 16-18 November, 2011.

I am happy to invite you to participate in the Workshop and to discuss physical problems of mutual interest. We also invite you to give a talk.

Looking forward to hearing from you soon (FAX or e-mail are preferable).

Sincerely yours,

Nikolai Tyurin

Chairman of the Organizing Committee

Citation Report: 556

(from Web of Science Core Collection)

You searched for: **AUTHOR:** (Vranjes, N) ...More

This report reflects citations to source items indexed within Web of Science Core Collection. Perform a Cited Reference Search to include citations to items not indexed within Web of Science Core Collection.

Published Items in Each Year

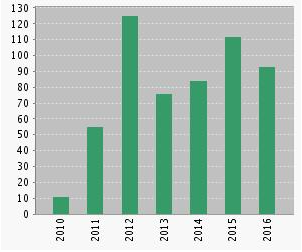

The latest 20 years are displayed.

Citations in Each Year

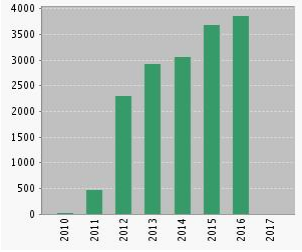

The latest 20 years are displayed.

Results found:	556
Sum of the Times Cited [?] :	16385
Sum of Times Cited without self-citations [?] :	14726
Citing Articles [?] :	8749
Citing Articles without self-citations [?] :	8226
Average Citations per Item [?] :	29.47
h-index [?] :	52

Sort by: Times Cited -- highest to lowest

Page 1 of 56

Use the checkboxes to remove individual items from this Citation Report

or restrict to items published between 2009 and 2017 Go

	2013	2014	2015	2016	2017	Total	Average Citations per Year
	2934	3068	3699	3859	5	16385	2048.12
1. **Observation of a new particle in the search for the Standard Model Higgs boson with the ATLAS detector at the LHC** By: Aad, G.; Abajyan, T.; Abbott, B.; et al. Group Author(s): ATLAS Collaboration PHYSICS LETTERS B Volume: 716 Issue: 1 Pages: 1-29 Published: SEP 17 2012	1045	1019	919	669	3	3793	632.17
2. **The ATLAS Simulation Infrastructure** By: Aad, G.; Abbott, B.; Abdallah, J.; et al. Group Author(s): ATLAS Collaboration EUROPEAN PHYSICAL JOURNAL C Volume: 70 Issue: 3 Pages: 823-874 Published: DEC 2010	73	87	107	92	0	530	66.25
3. **Observation of a Centrality-Dependent Dijet Asymmetry in Lead-Lead Collisions at root s(NN)=2.76 TeV with the ATLAS Detector at the LHC** By: Aad, G.; Abbott, B.; Abdallah, J.; et al. Group Author(s): ATLAS Collaboration PHYSICAL REVIEW LETTERS Volume: 105 Issue: 25 Article Number: 252303 Published: DEC 13 2010	86	62	54	52	0	378	47.25

Citation Report: 9

(from Web of Science Core Collection)

You searched for: **AUTHOR:** (Vranjes, N) ...More

This report reflects citations to source items indexed within Web of Science Core Collection. Perform a Cited Reference Search to include citations to items not indexed within Web of Science Core Collection.

Published Items in Each Year

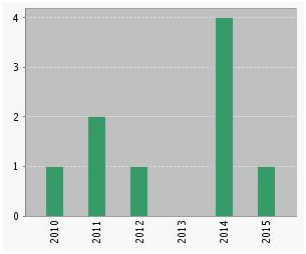

The latest 20 years are displayed.

Citations in Each Year

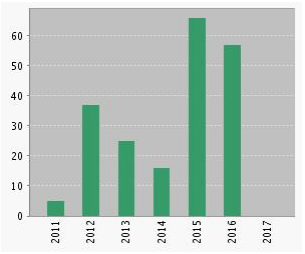

The latest 20 years are displayed.

Results found:	9
Sum of the Times Cited [?] :	206
Sum of Times Cited without self-citations [?] :	201
Citing Articles [?] :	188
Citing Articles without self-citations [?] :	185
Average Citations per Item [?] :	22.89
h-index [?] :	7

Sort by: **Times Cited -- highest to lowest** Page 1 of 1

Use the checkboxes to remove individual items from this Citation Report
or restrict to items published between 2009 and 2017 Go

	2013	2014	2015	2016	2017	Total	Average Citations per Year
	25	16	66	57	0	206	29.43
1. **Search for a heavy gauge boson decaying to a charged lepton and a neutrino in 1 fb(-1) of pp collisions at root s=7 TeV using the ATLAS detector ATLAS Collaboration** By: Aad, G.; Abbott, B.; Abdallah, J.; et al. Group Author(s): ATLAS Collaboration PHYSICS LETTERS B Volume: 705 Issue: 1-2 Pages: 28-46 Published: NOV 3 2011	14	6	5	1	0	52	7.43
2. **Measurements of Higgs boson production and couplings in the four-lepton channel in pp collisions at center-of-mass energies of 7 and 8 TeV with the ATLAS detector** By: Aad, G.; Abbott, B.; Abdallah, J.; et al. Group Author(s): Collaboration, A PHYSICAL REVIEW D Volume: 91 Issue: 1 Article Number: 012006 Published: JAN 16 2015	0	0	14	23	0	37	12.33
3. **Measurement of the Higgs boson mass from the H -> gamma gamma and H -> ZZ* -> 4l channels in pp collisions at center-of-mass energies of 7 and 8 TeV with the ATLAS detector** By: Aad, G.; Abbott, B.; Abdallah, J.; et al. Group Author(s): ATLAS Collaboration	0	1	17	12	0	30	7.50

	PHYSICAL REVIEW D Volume: 90 Issue: 5 Article Number: 052004 Published: SEP 9 2014							
4.	**Fiducial and differential cross sections of Higgs boson production measured in the four-lepton decay channel in pp collisions at root s=8 TeV with the ATLAS detector** By: Aad, G.; Abbott, B.; Abdallah, J.; et al. Group Author(s): ATLAS Collaboration PHYSICS LETTERS B Volume: 738 Pages: 234-253 Published: NOV 10 2014	0	1	15	10	0	26	6.50
5.	**Search for high-mass states with one lepton plus missing transverse momentum in proton-proton collisions root s=7 TeV with the ATLAS detector** By: Aad, G.; Abbott, B.; Abdallah, J.; et al. Group Author(s): ATLAS Collaboration PHYSICS LETTERS B Volume: 701 Issue: 1 Pages: 50-69 Published: JUN 27 2011	5	3	0	0	0	22	3.14
6.	**Search for new particles in events with one lepton and missing transverse momentum in pp collisions at root s=8 TeV with the ATLAS detector** By: Aad, G.; Abbott, B.; Abdallah, J.; et al. Group Author(s): ATLAS Collaboration JOURNAL OF HIGH ENERGY PHYSICS Issue: 9 Article Number: UNSP 037 Published: SEP 5 2014	0	1	11	6	0	18	4.50
7.	**ATLAS search for a heavy gauge boson decaying to a charged lepton and a neutrino in pp collisions at root s=7 TeV** By: Aad, G.; Abajyan, T.; Abbott, B.; et al. Group Author(s): ATLAS Collaboration EUROPEAN PHYSICAL JOURNAL C Volume: 72 Issue: 12 Article Number: 2241 Published: DEC 2012	5	3	3	2	0	13	2.17
8.	**Measurement of the muon reconstruction performance of the ATLAS detector using 2011 and 2012 LHC proton-proton collision data** By: Aad, G.; Abbott, B.; Abdallah, J.; et al. Group Author(s): ATLAS Collaboration EUROPEAN PHYSICAL JOURNAL C Volume: 74 Issue: 11 Article Number: 3130 Published: NOV 26 2014	0	0	1	3	0	4	1.00
9.	**Performance of the ATLAS detector using first collision data** By: Aad, G.; Abat, E.; Abbott, B.; et al. Group Author(s): ATLAS Collaboration JOURNAL OF HIGH ENERGY PHYSICS Issue: 9 Article Number: 056 Published: SEP 2010	1	1	0	0	0	4	0.50

Select Page | Save to Text File

Sort by: Times Cited -- highest to lowest

Page 1 of 1

9 records matched your query of the 17,845,499 in the data limits you selected.

Vranjes, Nenad

2017-01-25 11:27:12

Personal Details (HepNames)

Citations Summary

627 papers found, 626 of them citeable (published or arXiv)

	Citeable papers	Published only
Number of papers analyzed:	626	589
Number of citations:	63793	61678
Citations per paper (average):	101.9	104.7
h_{HEP} index [?]	116	116

Breakdown of papers by citations:

	Citeable papers	Published only
Renowned papers (500+)	13	12
Famous papers (250-499)	23	23
Very well-known papers (100-249)	113	113

	Citeable papers	Published only
Well-known papers (50-99)	152	151
Known papers (10-49)	243	242
Less known papers (1-9)	67	46
Unknown papers (0)	15	2

Click here to view statistics without self-citations or RPP

Warning: The citations count should be interpreted with great care. Read the fine print

Publications Datasets External

Publication Graph

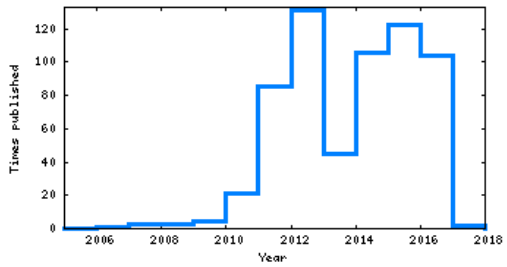

Co-Authors

ATLAS Membership

ions | User: nenadv | Role: Member | Logout

Nenad Vranjes

Member information | Authorship Qualification

Member Information

Last Name	Vranjes	First Name	Nenad
CERN ID	[redacted]	CERN CCID	[redacted]
Last Name (LaTeX)	Vranjes	First Name (LaTeX)	Nenad
Initials (First. Middle.)	N.	Photo permission	no
Comments		Status	ACTIVE ○None ○Retired ○Deceased
INSPIRE Reference	INSPIRE-00225275	Qualification Info	Qualified author on 2005/11/01

Last modification on 2014/10/29 15:20:57 **by** Lucie Aguirre

Update Data

ployment | Thesis | Appointments | Talks and Posters | Papers, CONF and Pub Notes | CDS Documents | OTP Activities | Qualification Projects

Show all records

Employ	Starting Date	End Date	CERN Phone	Institute Phone	CERN Mobile	CERN Office	Email	Profession	Activities	Institute
Edit	2014/11/01	2017/10/31	7XXXX			[redacted]	nenad.vranjes@cern.ch	Physicist	**Physics**: Standard Model, **Combined Performance**: Muon	Belgrade IP

ATLAS Membership

Options | User: nenadv | Role: Member | Logout

Nenad Vranjes

Member Information | Authorship Qualification

Member Information

Last Name	Vranjes	First Name	Nenad
CERN ID	[redacted]	CERN CCID	[redacted]
Last Name (LaTeX)	Vranjes	First Name (LaTeX)	Nenad
Initials (First. Middle.)	N.	Photo permission	no
Comments		Status	ACTIVE ○None ○Retired ○Deceased
INSPIRE Reference	INSPIRE-00225275	Qualification Info	Qualified author on 2005/11/01

Last modification on 2014/10/29 15:20:57 **by** Lucie Aguirre

Update Data

Employment | Thesis | Appointments | Talks and Posters | Papers, CONF and Pub Notes | CDS Documents | OTP Activities | Qualification Projects

Papers

Reference Code	Title	Member Role	Contributions
EXOT-2012-02	LPX Search for W' to lν	Analysis/Editor	
EXOT-2013-10	LPX - Search for W' to lν at 8 TeV	Analysis/Contact Editor	
DAPR-2013-01	2012 Luminosity	Analysis/Editor	
HIGG-2013-12	HSG1 HSG2 HSG7 Higgs Mass	Analysis/Editor	
HIGG-2013-21	HSG2 Main Couplings Paper	Analysis/Editor	
HIGG-2013-22	HSG2 Differential and fiducial	Analysis/Editor	
PERF-2014-05	Muon performance 2012	Analysis/Contact Editor	
STDM-2014-18	W mass measurement 7 TeV	Analysis/Contact Editor	
TOPQ-2016-03	MS dilepton top mass at 8 TeV	Editorial Board	
HIGG-2016-33	HZZ mass 2015+2016	Editorial Board	

Employment | Thesis | Appointments | Talks and Posters | Papers, CONF and Pub Notes | CDS Documents | OTP Activities | Qualification Projects

Papers

Reference Code	Title	Member Role	Contributions
EXOT-2012-02	LPX Search for W' to lv	Analysis/Editor	
EXOT-2013-10	LPX - Search for W' to lv at 8 TeV	Analysis/Contact Editor	
DAPR-2013-01	2012 Luminosity	Analysis/Editor	
HIGG-2013-12	HSG1 HSG2 HSG7 Higgs Mass	Analysis/Editor	
HIGG-2013-21	HSG2 Main Couplings Paper	Analysis/Editor	
HIGG-2013-22	HSG2 Differential and fiducial	Analysis/Editor	
PERF-2014-05	Muon performance 2012	Analysis/Contact Editor	
STDM-2014-18	W mass measurement 7 TeV	Analysis/Contact Editor	
TOPQ-2016-03	MS dilepton top mass at 8 TeV	Editorial Board	
HIGG-2016-33	HZZ mass 2015+2016	Editorial Board	

Conference Notes

Report Number	Title	Member Role	Contributions
ATLAS-CONF-2013-088	Preliminary muon performance 2012	Analysis/Editor	
ATLAS-CONF-2014-017	LPX - Search for W' to lv at 8 TeV	Analysis/Contact Editor	
ATLAS-CONF-2014-044	HSG2 Differential and fiducial	Analysis/Editor	
ATLAS-CONF-2016-113	W mass measurement 7 TeV	Analysis/Contact Editor	

Publication Notes

Temporary Ref Code	Final Reference Code	Title	Member Role	Contributions
PUB-STDM-2014-01	ATL-PHYS-PUB-2014-015	W mass theory uncertainty study	Analysis/Editor	

ATLAS Membership

Options | User: nenadv | Role: Member | Logo

Nenad Vranjes

Member information | Authorship Qualification

Member Information

Last Name	Vranjes	First Name	Nenad
CERN ID	[redacted]	CERN CCID	[redacted]
Last Name (LaTeX)	Vranjes	First Name (LaTeX)	Nenad
Initials (First. Middle.)	N.	Photo permission	no
Comments		Status	ACTIVE ○None ○Retired ○Deceased
INSPIRE Reference	INSPIRE-00225275	Qualification Info	Qualified author on 2005/11/01

Last modification on 2014/10/29 15:20:57 **by** Lucie Aguirre

Update Data

Employment | Thesis | Appointments | Talks and Posters | Papers, CONF and Pub Notes | CDS Documents | OTP Activities | Qualification Projects

1

System	Activity	Task	2009	2010	2011	2012	2013	2014	2015	2016	Total
General Tasks	Computing/Software	Shifts for Tier-0 processing	3.00								3.00
Total			3.00								3.00

Class 1

System	Activity	Task	2009	2010	2011	2012	2013	2014	2015	2016	Total
General Tasks	Computing/Software	Comp@P1 Shifts		3.94	7.87	15.11					26.92
General Tasks	Computing/Software	Tier-0		19.51							19.51
Total				23.45	7.87	15.11					46.43

Class 2

Class 1

System	Activity	Task	2009	2010	2011	2012	2013	2014	2015	2016	Total
General Tasks	Computing/Software	Comp@P1 Shifts		3.94	7.87	15.11					26.92
General Tasks	Computing/Software	Tier-0		19.51							19.51
Total				23.45	7.87	15.11					46.43

Class 2

System	Activity	Task	2009	2010	2011	2012	2013	2014	2015	2016	Total
General Tasks	Data Preparation	Luminosity offline DQ							5.18	1.48	6.66
General Tasks	Data Preparation	Muon Combined DQ Monitoring Shifts				7.00					7.00
Muon	Detector Operation	Muon Data Quality Expert Shifter					2.64				2.64
Muon	Detector Operation	Muon Data Quality Shifter					7.92				7.92
General Tasks	Data Preparation	Offline DQ shifts (DQ-SCR or REMOTE) (Archive)		11.00	31.00						42.00
General Tasks	Computing/Software	Reconstruction Software Shifts			14.00						14.00
General Tasks	Computing/Software	T0/P1 Software Validation Shifts	5.25								5.25
Total			5.25	11.00	45.00	7.00	10.56		5.18	1.48	85.47

Class 3

System	Activity	Task	2009	2010	2011	2012	2013	2014	2015	2016	Total
General Tasks	Data Preparation	Offline Luminosity Measurement							0.32	0.26	0.58
General Tasks	Analysis Support	Performance Studies					0.30	0.10			0.40
General Tasks	Computing/Software	Reconstruction				0.03					0.03
Total						0.03	0.30	0.10	0.32	0.26	1.00

УНИВЕРЗИТЕТ У БЕОГРАДУ

Адреса: Студентски трг 1, 11000 Београд, Република Србија
Тел.: 011 3207400; Факс: 011 2638818; E-mail: officebu@rect.bg.ac.rs

ВЕЋЕ НАУЧНИХ ОБЛАСТИ
ПРИРОДНО-МАТЕМАТИЧКИХ
НАУКА

Београд, 14.11.2016.
02-04 Број 61206-5626/2-16
МЦ

На основу члана члана 47. став 5. тачка. 3. Статута Универзитета у Београду ("Гласник Универзитета у Београду", број 186/15-пречишћени текст и 189/16) и чл. 14. – 21. Правилника о већима научних области на Универзитету у Београду ("Гласник Универзитета у Београду", број 134/07, 150/09, 158/11, 164/11 и 165/11), а на захтев Физичког факултета, број: 313/4 од 01.11.2016. године, Веће научних области природно-математичких наука, на седници одржаној 14.11.2016. године, донело је

О Д Л У К У

ДАЈЕ СЕ САГЛАСНОСТ на предлог теме докторске дисертације АЛЕКСАНДРЕ ДИМИТРИЕВСКЕ, под називом: „Measurement of the W boson mass and the calibration of the muon momentum with the ATLAS detector" (Мерење масе W бозона и калибрација импулса миона на детектору ATLAS).

ПРЕДСЕДНИК ВЕЋА

Проф. др Павле Младеновић

Доставити:
- Факултету
- архиви Универзитета

5. <u>тачка</u>

Усвојен је Извештај Комисије за оцену испуњености услова и оправданост предложене теме за израду докторске дисертације и одређен ментор за:

a) ТИЈАНУ ЂОРЂЕВИЋ, дипломираног физичара, која је пријавила докторску дисертацију под називом: „ТЕОРИЈСКИ МОДЕЛИ ПЛАЗМОНА У ГРАФЕНУ ПРИ ИНТЕРАКЦИЈИ СА НАЕЛЕКТРИСАНИМ ЧЕСТИЦАМА“
Ментор: др Иван Радовић, виши научни сарадник ИНН Винча

b) НЕНАДА ТАДИЋА, дипломираног физичара, који је пријавио докторску дисертацију под називом: „СТРУКТУРНА И ОПТИЧКА КАРАКТЕРИЗАЦИЈА ФОТОКАТАЛИЗАТОРА НА БАЗИ TiO_2 И ZnO ПРАХОВА ДОБИЈЕНИХ ПЛАЗМЕНОМ ЕЛЕКТРОЛИТИЧКОМ ОКСИДАЦИЈОМ“
Ментор: др Стеван Стојадиновић, ванредни професор ФФ

c) АЛЕКСАНДРУ ДИМИТРИЕВСКУ, дипломираног физичара, која је пријавила докторску дисертацију под називом: „MEASUREMENT OF THE W BOSON MASS AND THE CALIBRATION OF THE MUON MOMENTUM WITH THE ATLAS DETECTOR“ (Мерење масе W бозона и калибрација импулса миона на детектору *ATLAS*)
Ментор: др Ненад Врањеш, научни сарадник ИФ

UNIVERZITET U NOVOM SADU
PRIRODNO-MATEMATIČKI
FAKULTET
DEPARTMAN ZA FIZIKU

Produkcija parova gradijentnih bozona u proton-proton sudarima na $\sqrt{s} = 100$ TeV

-master rad-

Autor:
Milena Bajić

Mentori :
dr Nenad Vranješ, Institut za fiziku, Beograd
dr Jovana Nikolov, PMF, Novi Sad

Novi Sad, 2015

Zahvalnica

Ovaj master rad je urađen u Laboratoriji za fiziku visokih energija Instituta za fiziku u Beogradu. Želim da se zahvalim svim saradnicima laboratorije, posebno dr Nenadu Vranješu na prenetom znanju, trudu i vremenu. Takođe i dr Jovani Nikolov sa PMF-a u Novom Sadu za svu podršku tokom izrade master rada.

Milena Bajić

From: **Atlas Analysis Glance** atlas-analysis-glance@cern.ch
Subject: Analysis TOPQ-2016-03 "MS dilepton top mass at 8 TeV" - EdBoard formed
Date: 25 January 2016 at 11:26
To: Thorsten.Kuhl@cern.ch, Tancredi.Carli@cern.ch, nenad.vranjes@cern.ch, Richard.Nisius@cern.ch, andreas.alexander.maier@cern.ch, cortiana@mppmu.mpg.de, frederic.deliot@cern.ch, mark.andrew.owen@cern.ch
Cc: Giacomo.Polesello@cern.ch, d.r.tovey@sheffield.ac.uk, h26@nikhef.nl, kado@lal.in2p3.fr, atlas-TOPQ-MASS-conveners@cern.ch

Dear colleagues,

The EdBoard for:

TOPQ-2016-03
"MS dilepton top mass at 8 TeV"
https://atglance.web.cern.ch/atglance/analysis/detailAnalysis.php?readonly=true&id=7982

is formed now.

Members are:
- Editorial board: Nenad Vranjes (Belgrade IP),Thorsten Kuhl (DESY),Tancredi Carli (CERN)
- Chair: Thorsten Kuhl (DESY)

The supporting documents should be already available at
https://atglance.web.cern.ch/atglance/analysis/detailAnalysis.php?readonly=true&id=7982 (in phase 1)

or directly at:
supporting notes:
https://cds.cern.ch/record/2124214/

Editorial board members can find guidelines for the work on edboards at:

https://twiki.cern.ch/twiki/bin/view/AtlasProtected/EditorialBoardGuidelines

Editorial board members and analysis team: a checklist to follow for the review of your note is stored at:

https://twiki.cern.ch/twiki/bin/view/AtlasProtected/PubComConfCheckList

Please have look at the guidelines also when you worked on edboards recently. We try to keep this page up to date with recent information. We invite the chair to organize a meeting of the edboard with the group conveners and the authors to discuss the analysis and the following draft.
Thank you.

Best wishes
Paul De Jong
(email generated via glance)

PS. For the Group Conveners (if not done already):
Please go in glance and when ready fill the relevant fields under the section Analysis review and production of draft.
Then click on the "Proceed and release of draft" button.
THANKS.

From: **Atlas Analysis Glance** atlas-analysis-glance@cern.ch
Subject: Analysis Paper HIGG-2016-33 'HZZ mass 2015+2016' - Editorial Board Formed
Date: 13 January 2017 at 13:37
To: Fabio.Cerutti@cern.ch, michael.duehrssen@cern.ch, kortner@mppmu.mpg.de, ioannis.nomidis@cern.ch, Gaetano.Barone@cern.ch, Gerald.Eigen@cern.ch, shassani@hep.saclay.cea.fr, nicolaid@hep.saclay.cea.fr, Kirill.Prokofiev@cern.ch, Christos.Anastopoulos@cern.ch, sau.lan.wu@cern.ch, luis.flores.castillo@cern.ch, ryszard@physics.smu.edu, daits@umich.edu, zhaozg@ustc.edu.cn, bzhou@umich.edu, lfayard@lal.in2p3.fr, schaffer@mail.cern.ch, Sandra.Kortner@cern.ch, ckourk@mail.cern.ch, fassoul@mail.cern.ch, thomas.koffas@cern.ch, Reisaburo.Tanaka@cern.ch, gabriella.sciolla@cern.ch, williams@hep.upenn.edu, alexei.maslennikov@cern.ch, stefano.rosati@cern.ch, Rostislav.Konoplich@cern.ch, roberto.di.nardo@cern.ch, eleni.mountricha@cern.ch, sarah.heim@cern.ch, Antonio.Salvucci@cern.ch, Susumu.Oda@cern.ch, Jochen.Meyer@cern.ch, giacomo.artoni@cern.ch, hulin.wang@cern.ch, xiangyang.ju@cern.ch, ludovica.aperio.bella@cern.ch, Joany.Andreina.Manjarres.Ramos@cern.ch, Valerio.Bortolotto@cern.ch, Stylianos.Angelidakis@cern.ch, goblirsc@cern.ch , cyril.becot@cern.ch, justas.zalieckas@cern.ch, bijan.haney@cern.ch, andrea.gabrielli@cern.ch, ddivalen@physics.carleton.ca, gcree@physics.carleton.ca, mcanobre@cern.ch, katharina.maria.ecker@cern.ch, nanlu@umich.edu, karolos.potamianos@cern.ch, giada.mancini@cern.ch, nikita.belyaev@cern.ch, william.axel.leight@cern.ch, xiandong.zhao@cern.ch, syed.haider.abidi@cern.ch, Haonan.lu@cern.ch, zongchang.yang@cern.ch, ppodberezko@gmail.com, hherde@brandeis.edu, denys.denysiuk@cern.ch, antoine.laudrain@cern.ch, ngtszyu@gmail.com, cong.geng@cern.ch, arthur.lesage@cea.fr, lauts.hk@gmail.com, walbrech@mpp.mpg.de, joseph.william.carter@cern.ch, marco.scodeggio@student.unife.it, simona.gargiulo15@gmail.com , pan.bellos@hotmail.com, christian.weber@yale.edu, tdpowell@sheffield.ac.uk, nenad.vranjes@cern.ch, alexandre.glazov@desy.de, montoya@cern.ch
Cc: d.r.tovey@sheffield.ac.uk, Tancredi.Carli@cern.ch, atlas-publication-committee-chair@cern.ch, atlas-higg-hsg2-conveners@cern.ch

Dear colleagues,

The EdBoard for HIGG-2016-33 "HZZ mass 2015+2016" is formed now.

Link: https://glance.cern.ch/atlas/analysis/papers/details.php?id=9923

Members are:

- Editorial board:

  - CARRILLO MONTOYA, German David
  - GLAZOV, Alexandre
  - VRANJES, Nenad

- Chair:

  - GLAZOV, Alexandre

Best wishes,

(Automatic e-mail generated by Stephane Willocq)

This message was automatically generated by Glance (hash d65810ca7dc7c996decad1a2fbf85c43).

Information | Discussion (53) | Files

[redacted] Internal Note

Report number	ATL-COM-PHYS-2012-1771
Title	**Search for new heavy gauge bosons in the charged lepton plus missing transverse energy final state using pp collisions at sqrt{s} = 8 TeV in the ATl detector**
Author(s)	Adams, D L (BNL) ; Becker, M (Mainz) ; Bugge, M K (Oslo) ; Butler, J M (Boston) ; Castaneda-Miranda, E (Wisconsin) ; Degenhardt, J (Pennsylvania) ; Elli (Mainz) ; Fassouliotis, D (Athens) ; Fedin, O (PNPI) ; Klein, U (Liverpool) ; Kretzschmar, J (Liverpool) ; Kourkomelis, C (Athens) ; Long, B A (Boston) ; Ou F (Oslo) ; Schuh, N (Mainz) ; Sedykh, E (PNPI) ; Solovyev, V (PNPI) ; Tsirintanis, N (Athens) ; Wu, S L (Wisconsin) *Hide*
Imprint	04 Dec 2012. - 83 p.
Subject category	Detectors and Experimental Techniques
Accelerator/Facility, Experiment	CERN LHC ; ATLAS
Free keywords	Wprime ; Lepton + MET ; EXOTICS
Abstract	The ATLAS detector is used to search for heavy charged gauge bosons, decaying to a lepton (electron or muon) and neutrino. Results are presented the analysis of pp collisions at a center-of-mass energy of 8 TeV corresponding to an integrated luminosity of 20 fb-1 acquired in 2012.

Email contact: john.mark.butler@cern.ch ; Victor.Solovyev@cern.ch ; ellingha@uni-mainz.de ; Olga.Igonkina@cern.ch ; Nenad.Vranjes@cern.ch ; alaettin.serhan.mete@along528@bu.edu

Being an author of this document, you can Submit a Revised Version or Update the Bibliographic Information or Other actions

[Approved as a Note - Check status]

Record created 2012-12-06, last modified 2014-08-12

Simil

Information | Discussion (10) | Files

[redacted] Internal Note

Report number	ATL-COM-PHYS-2012-689
Title	**Search for high-mass states with one lepton plus missing transverse momentum using the ATLAS detector with 4.7 fb^-1 of pp collisions at root{s}=**
Author(s)	Adams, DL (BNL) ; Amelung, C (Brandeis Univ.) ; Bauer, F (Centre d'Etudes de Saclay) ; Aperio Bella, L (CNRS) ; Bugge, MK (Univ. Oslo) ; Castaneda-Mi (Univ. Wisc.) ; Cerutti, F (INFN) ; Chizhov, M (JINR) ; Degenhardt, J (Univ. Penn.) ; Fassouliotis, D (Univ. Athens) ; Fedin, O (PNPI) ; Francois Giraud, P (Ce d'Etudes de Saclay) ; Heim, S (Univ. Mich. State) ; Kortner, O (MPI) ; Kourkomelis, O (Univ. Athens) ; Kretzschmar, J (Univ. Liverpool) ; Liebig, W (Univ. B Potrap, I (MPI) ; Mal, P (Centre d'Etudes de Saclay) ; Mete, AS (UCI) ; Nunnemann, T (Ludwig Maximilians Universitat Meunchen) ; Pontecorvo, L (INF Saada, F (Univ. Oslo) ; Schernau, M (CNRS) ; Schuh, N (Johannes Gutenberg Universitat Mainz) ; Schroeder, C (Johannes Gutenberg Universitat Mainz) Solovyev, V (PNPI) ; Stahlman, J (Univ. Penn.) ; Thomson, E (Univ. Penn.) ; Tsirintanis, N (Univ. Athens) ; Vranjes, N (Centre d'Etudes de Saclay) ; Viel, S (Willocq, S (Univ. Mass.) ; Wu, SL (Univ. Wisc.) *Hide*
Imprint	26 May 2012. - mult. p.
Subject category	Detectors and Experimental Techniques
Accelerator/Facility, Experiment	CERN LHC ; ATLAS
Free keywords	Exotics ; W Prime ; W Star ; Sequential Standard Model ; EXOTICS
Abstract	The ATLAS detector is used to search for high-mass states, such as heavy charged gauge bosons (W'), decaying to a lepton (electron or muon) plus r transverse momentum. Results are presented based on the analysis of pp collisions at a center-of-mass energy of 7 TeV corresponding to an integra luminosity of 4.7 fb^-1 acquired in 2011. No excess beyond standard model expectations is observed. A W' with standard model couplings is exclud CL for masses below 2.55 TeV and a W* is excluded at 95% CL for masses below 2.41 TeV.

Email contact: james.degenhardt@cern.ch ; dladams@bnl.gov ; wojtek.fedorko@cern.ch ; stelzer-chilton@triumf.ca ; max.klein@desy.de ; Erez.Etzion@cern.ch ; henri.bachacou@cern.ch

[Approved as a Note - Check status]

Record created 2012-05-27, last modified 2012-09-29

Simil

ATLAS NOTE

February 12, 2013

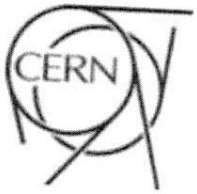

Supporting Document for Higgs papers: Higgs mass measurements and uncertainties in 2012
ATL-COM-PHYS-2012-1774

T. Adye, C. Amelung, C. Anastopoulos, N. Andari, C. Becot, N. Berger, N. Besson, A. Bocci, M. Boonekamp, L. Carminati, J. Catmore, F. Cerutti, L. Chevalier, M. Corradi, T. Cuhadar, M. Delmastro, J.-B. de Vivi, A. Dimitrievska, M. Duehrssen, K. M. Ecker, M. Elsing, M. Escalier, L. Flores Castillo, P. Fleischmann, D. Froidevaux, P. F. Giraud, M. Golbrisch-Kolb, A. Hard, R. Harrington, S. Hassani, L. Iconomidou-Fayard, V. Ippolito, H. Ji, X. Ju, P. Kluit, O. Kortner, S. Kreiss, J. F. Laporte, B. Lenzi, B. Lopez Paredes, N. Lorenzo Martinez, J.-F. Marchand, A. Morley, E. Moyse, R. Nicolaidou, J. Ocariz, A. Ouraou, S. Paganis, K. Peters, E. Petit, L. Pontecorvo, S. Protopapadaki, C. Rangel-Smith, F. Rauscher, S. Rosati, A. Salvucci, A. Salzburger, R. D. Schaffer, K. Selbach, F. Sforza, J. Stahlman, K. Tackmann, F. Tarrade, F. Teischinger, R. Turra, G. Unal, N. Vranjes, F. Wang, M. Xiao, Y. Yamaguchi, H. Yang, S. Zambito

Abstract

This note describes the results from the work done within several performance and physics groups to provide documentation supporting the results presented in the December 2012 Council week on the mass measurements with their uncertainties for the $H \to ZZ^{(*)} \to \ell\ell\ell\ell$ and $H \to \gamma\gamma$ channels.

Information | Discussion (0) | Files

[redacted] Internal Note

Report number	ATL-COM-MUON-2013-022
Title	**Muon performance studies using $J/\psi \to \mu^+\mu^-$ at $\sqrt{s} = 7$ TeV and $\sqrt{s} = 8$ TeV of pp collisions**
Author(s)	Chevalier, L (Saclay-CEA) ; Dimitrievska, A (Institute of Physics, Belgrade) ; Vranjes, N (Saclay-CEA)
Imprint	03 Sep 2013. - mult. p.
Subject category	Detectors and Experimental Techniques
Accelerator/Facility, Experiment	CERN LHC ; ATLAS
Free keywords	muon ; momentum scale ; energy loss ; J/psi
Abstract	The high statistics $J/\psi \to \mu^+\mu^-$ samples are used to study muon reconstruction performance in the low momentum regime. Studying differences between momenta of muons reconstructed in the Inner Detector and Muon Spectrometer extrapolated to the interaction point of the ATLAS detector, allow to derive effective correction to the spectrometer The effect of the corrections is verified on the $Z \to \mu\mu$ events.

Email contact: aleksandra.dimitrievska@cern.ch ; laurent.chavalier@cern.ch ; adimitrievska@ipb.ac.rs ; nenad.vranjes@cern.ch

Being an author of this document, you can Submit a Revised Version or Update the Bibliographic Information or Other actions

Record created 2013-09-03, last modified 2013-09-06

Sim

Information | Discussion (18) | Files

Internal Note

Report number	ATL-COM-MUON-2014-001
Title	**Muon momentum scale and resolution corrections evaluated with Z->mumu 2 and J/psi->mumu decays on Run I ATLAS data**
Author(s)	Artoni, G ; Corradi, M ; Dimitrievska, A ; Sforza, F ; Vranjes, N ; Fleischmann, P
Imprint	17 Jan 2014. - 60 p.
Note	Preliminary version of MCP scale and momentum corrections for 2012 data
Subject category	Detectors and Experimental Techniques
Accelerator/Facility, Experiment	CERN LHC ; ATLAS
Abstract	The differences in the momentum scale and resolution for muons reconstructed in real data and in simulation are studied. The muon momentum in simulated data is corrected a smeared to reproduce the scale and resolution of the data. The corrections are extracted using a MC template fit method on large J/psi->mumu and Z->mumu samples. The correc the associated systematic uncertainties are validated, in the transverse momentum range 7 < pT < 120GeV, by independent analyses using the same samples and, in addition, Upsi >mumu samples.

Email contact: massimo.corradi@bo.infn.it ; niels.van.eldik@cern.ch ; federico.sforza@cern.ch ; nenad.vranjes@cern.ch

Record created 2014-01-17, last modified 2014-05-23

Simi

Information | Discussion (24) | Files

[redacted] Internal Note

Report number	ATL-COM-PHYS-2014-875
Title	**Studies of theoretical uncertainties on the measurement of the mass of the W boson at the LHC**
Author(s)	Camarda, S ; Hanna, R ; Huang, Y ; Glazov, S ; Boonekamp, M ; Vranjes, N ; Blanchard, JB ; Radescu, V ; Strohmer, R ; Schott, M ; Siragusa, G ; Dimitrievska, A ; Karnevskiy, M ; Zimme Andari, N ; Kivernyk, O ; Cuth, J ; Lin, T-H *Hide*
Imprint	21 07 2014. - mult. p.
Subject category	Particle Physics - Experiment
Accelerator/Facility, Experiment	CERN LHC ; ATLAS
Free keywords	wmass ; EWEAK
Abstract	The measurement of the mass of the W boson at the LHC requires control of both theoretical and experimental uncertainties. The extraction of the W-boson mass from the tr momentum spectrum of electrons and muons produced in the leptonic decay of the W boson, is likely to be limited by theoretical uncertainties. Uncertainties arising from the i knowledge of the parton density functions and from the modelling of the low transverse momentum of the W boson are estimated, accounting for the resolution effects of the detector. Emphasis is given to the study of the physical origin of the uncertainties, so as to provide useful information for further reduction of the uncertainties.

Email contact: stefano.camarda@cern.ch ; maarten.boonekamp@cern.ch ; remie.hanna@cern.ch

[Approved as a Note - Check status]
Record created 2014-07-21, last modified 2014-10-20

Si

Information | Discussion (8) | Files

[redacted] Internal Note

Report number	ATL-COM-MUON-2014-025
Title	**Muon reconstruction performances of the ATLAS detector during Run 1**
Author(s)	Amelung, C ; Artoni, G ; Bachas, K ; Bauer, F ; Benekos, N ; Borroni, S ; Catmore, J ; Chevalier, L ; Chiodini, G ; Corradi, M ; Dimitrievska, A ; Fleischmann, P ; Gatti, C ; Giraud, P-F ; M ; Guimares da Costa, J ; Hassani, S ; Ippolito, V ; Kluit, P ; Kortner, O ; Kyriazopoulos, D ; Laporte, J-F ; Leontsinis, S ; Liebig, W ; Lopez Paredas, B ; Matsushita, T ; Morii, M ; Moy Nikolaidou, R ; Orlando, N ; Ouraou, A ; Paganis, E ; Pontecorvo, L ; Poppleton, A ; Price, D ; Salvucci, A ; Sandstroem, R ; Sciolla, G ; Sforza, F ; Solfaroli, E ; Spagnolo, S ; Spearma ; Tolley, E ; Vallecorsa, S ; Van Eldik, N ; Vanadia, M ; Venturini, A ; Vranjes, N ; Zambito, S *Hide*
Imprint	17 Apr 2014. - mult. p.
Note	Draft of Run-1 muon performance paper
Subject category	Detectors and Experimental Techniques
Accelerator/Facility, Experiment	CERN LHC ; ATLAS
Free keywords	Muons ; Efficiency ; Resolution ; FSR
Abstract	This paper presents the performances of the ATLAS muon reconstruction during the LHC Run-1, focusing mainly on data collected in 2012. The measurements of the reconstru efficiency and of the momentum scale and resolutions, based on large reference samples of $J/\psi \to \mu\mu$, $Z \to \mu\mu$ and $\Upsilon \to \mu\mu$ decays, are presented and compared to MC sim Corrections to the simulation imperfections, to be used in physics analysis, are provided. A method for the recovery of final state radiation is also presented.

Email contact: massimo.corradi@bo.infn.it

Record created 2014-04-17, last modified 2014-07-13

Si

Information | Discussion (19) | Files

[redacted] Internal Note

Report number	ATL-COM-PHYS-2014-056
Title	**Measurement of inclusive and differential fiducial cross-sections of the Higgs boson in the H -> ZZ -> llll decay channel using 20.3 fb−1 of sqrt(s)=8 TeV pp collision data at the detector.**
Author(s)	Abidi, S H ; Anastopoulos, C ; Antonelli, M ; Aperio Bella, L ; Artoni, G ; Baker, O K ; Barreiro Guimaraes Da Costa, J P ; Belyaev, N ; Benhar Noccioli, E ; Brendlinger, K ; Calandri, A ; Carrillo Montoya, G ; Catastini, P ; Cerutti, F ; Charfeddine, D ; Chevalier, L ; Cirotto, F ; Clark, A ; Clark, P J ; Conventi, F ; Corradi, M ; Cree, G ; Cuhadar Donszelmann, T ; Dai, T ; Dar Daniells, A ; Dawson, I ; Di Mattia, S ; Di Nardo, R ; DiValentino, D ; Dimitrievska, A ; Edwards, N ; Fassouliotis, D ; Feng, E ; Flores Castillo, L R ; Franklin, M ; Gabrielli, A ; Gao, Y ; G M ; Giagu, S ; Gkougkousis, V ; Goblirsch-Kolb, M ; Gozani, E ; Guillemin, T ; Gustavino, G ; Harrington, R ; Heim, S ; Hoffmann, M ; Hou, S ; Iconomidou-Fayard, L ; Iordanidou, K ; Ip X ; Kaplan, L S ; Koffas, T ; Konoplich, R ; Kortner, O ; Kourkoumelis, C ; Kyriazopoulos, D ; Lagouri, T ; Leonidopoulos, C ; Li, B ; Li, H ; Lopez Paredes, B ; Lu, N ; Mancini, G ; Manso Meyer, J ; Monnier, E ; Mountricha, E ; Mudd, R ; Nicolaidou, R ; Nikolopoulos, K ; Oda, S ; Olivares Pino, SA ; Paganis, E ; Pasztor, G ; Pedersen, L E ; Pilcher, J ; Potamianos, K ; Proko Rescigno, M ; Rosati, S ; Rossi, E ; Rozen, Y ; Salvucci, A ; Sanchez Pineda, A ; Schaffer, A ; Sciolla, G ; Sekula, S ; Selbach, K E ; Sforza, F ; Spearman, W ; Stahlman, J ; Stern, S ; Stroy Sun, S ; Tanaka, R ; Tarrade, F ; Tiouchichine, E ; Tsybychev, D ; Verducci, M ; Vickey, T ; Vranjes, N ; Webster, J ; Whalen, K ; Williams, H ; Wu, Y ; Wu, S L ; Wynne, B ; Xu, L ; Yang, H ; Zhao, Z ; Zhou, B *Hide*
Imprint	03 Feb 2014. - mult. p.
Note	Supporting note for paper.
Subject category	Detectors and Experimental Techniques
Accelerator/Facility, Experiment	CERN LHC ; ATLAS
Free keywords	Higgs ; Differential ; Cross-sections ; Properties ; HIGGS
Abstract	This note decribes the measurement of the inclusive as well as a number of differential cross-sections of the Higgs boson in the H -> ZZ -> llll decay channel. The cross-sectior determined within a fiducial region of the ATLAS detector and corrected for detection efficiency and resolution effects. They are compared to results from different calculations Measurements are performed in bins of the transverse momentum and the rapidity of the four-lepton system, the invariant mass of the two subleading leptons and the decay a cos(theta•) , as well as the number of jets and the transverse momentum of the leading jet. For this analysis, 20.3 fb−1 of pp collision data were used, produced at sqrt(s)=8 TeV mass energy at the LHC and recorded by the ATLAS detector.

Email contact: sarah.heim@cern.ch ; fabio.cerutti@cern.ch ; andrea.gabrielli@cern.ch ; jonathan.mark.stahlman@cern.ch ; fabien.tarrade@cern.ch ; stefano.rosati@cern.ch

[Approved as a Note - Check status]

Record created 2014-02-03, last modified 2014-10-06

S

Internal Note

ort number	ATL-COM-PHYS-2013-1663
e	**Study of the SM-like Higgs particle at 125 GeV properties using production mechanisms specific signatures in the H $\rightarrow ZZ^{(*)} \rightarrow \ell^+\ell^-\ell^+\ell^-$ channel.**
hor(s)	Abidi, S H ; Anastopoulos, C ; Antonelli, M ; Aperio Bella, L ; Artoni, G ; Baker, O K ; Barreiro Guimaraes Da Costa, J P ; Belyaev, N ; Benhar Noccioli, E ; Brendlinger, K ; Calandri, A ; Cao, T ; Carrillo Montoya, G ; Catastini, P ; Cerutti, F ; Charfeddine, D ; Chevalier, L ; Cirotto, F ; Clark, A ; Clark, P J ; Conventi, F ; Corradi, M ; Cree, G ; Cuhadar Donszelmann, T ; Dai, T ; Dandoy, J ; Daniells, A ; Dawson, I ; Di Mattia, S ; Di Nardo, R ; Dimitrievska, A ; Edwards, N ; Fassouliotis, D ; Feng, E ; Flores Castillo, L R ; Franklin, M ; Gao, Y ; Garay Walls, F M ; Giagu, S ; Gkougkou ; Goblirsch-Kolb, M ; Gozani, E ; Guillemin, T ; Gustavino, G ; Harrington, R ; Heim, S ; Hoffmann, M ; Iconomidou-Fayard, L ; Iordanidou, K ; Ippolito, V ; Ju, X ; Koffas, T ; Konoplich, R ; Kor O ; Kourkoumelis, C ; Kyriazopoulos, D ; Lagouri, T ; Leonidopoulos, C ; Lopez Paredes, B ; Mancini, G ; Mansoulie, B ; Monnier, E ; Mountricha, E ; Mudd, R ; Nicolaidou, R ; Nikolopoulos, K Olivares Pino, SA ; Paganis, E ; Pasztor, G ; Pilcher, J ; Potamianos, K ; Prokofiev, K ; Rescigno, M ; Rosati, S ; Rozen, Y ; Salvucci, A ; Schaffer, A ; Sciolla, G ; Sekula, S ; Selbach, K E ; Sforza, F Spearman, W ; Stahlman, J ; Stern, S ; Stroynowski, R ; Tanaka, R ; Tarrade, F ; Tiouchichine, E ; Tsybychev, D ; Verducci, M ; Vickey, T ; Vranjes, N ; Webster, J ; Whalen, K ; Williams, H ; Wynr Xu, L ; Zambito, S ; Zhao, Z ; Zhou, B ; Baker, Keith (**Yale University**) ; Hou, Suen (**Academia Sinica, Taipei**) ; Kaplan, Laser Seymour (**Department of Physics, University of Wisconsin**) ; Li, Bir (**University of Science and Technology of China**) ; Li, Haifeng (**Stony Brook University**) ; Lu, Nan (**University of Michigan, Department of Physics**) ; Meyer, Jochen (**FOM - Institute SAF Nikh and University of Amsterdam/Nikhef**) ; Oda, Susumu (**Kyushu University**) ; Pedersen, Lars Egholm (**Niels Bohr Institute (NBI), University of Copenhagen**) ; Rossi, Elvira (**INFN Napoli and Universita' di Napoli, Dipartimento di Fisica, Napoli**) ; Sun, Siyuan (**Harvard University, Department of Physics**) ; Wu, Yusheng (**University of Michigan, Department of Physics**) ; Wu, Sau La (**Department of Physics, University of Wisconsin**) ; Yang, Haijun (**Shanghai Jiao Tong University**) ; Divalentino, David (**Carleton University (CA)**) ; Sanchez, Arturo (**INFN Napoli and Univers Napoli, Dipartimento di Fisica, Napoli**) *Hide*
rint	20 Dec 2013. - mult. p.
ject category	Detectors and Experimental Techniques
elerator/Facility, eriment	CERN LHC ; ATLAS
keywords	H->ZZ(*)->4l ; H4l supporting note ; HIGGS
tract	H$\rightarrow ZZ^{(*)} \rightarrow$4l supporting documentation: properties using production mechanisms specific signatures.

il contact: roberto.di.nardo@cern.ch ; Giacomo.Artoni@cern.ch ; xiangyang.ju@cern.ch ; R.D.Schaffer@cern.ch ; Rosy.Nicolaidou@cern.ch ; Konstantinos.Nikolopoulos@cern.ch ; Stefano.Rosati@cern. en.Tarrade@cern.ch ; Robert.Duane.Harrington.Jr@cern.ch

roved as a Note - Check status]

ord created 2013-12-20, last modified 2015-03-20

Similar rec

Draft version 1.5

ATLAS NOTE

December 2, 2016

Measurement of the Drell-Yan triple-differential cross-section in pp collisions at $\sqrt{s} = 8$ TeV

L. J. Armitage[1], S. Glazov[2], R. Keeler[3], T. Kwan[3], D. MacDonell[3], E. Rizvi[1], A. Sapronov[4], N. Vranjes[5], E. Yatsenko[2,6]

[1] *Queen Mary, University of London*
[2] *DESY*
[3] *University of Victoria*
[4] *JINR*
[5] *Belgrade IP*
[6] *LAPP*

Abstract

This supporting document details the methods and results of the measurement of the Drell-Yan triple differential cross-section using $Z/\gamma^* \to e^+e^-$ and $Z/\gamma^* \to \mu^+\mu^-$ decays in 20.1 fb^{-1} of ATLAS data recorded in 2012 at a centre-of-mass energy of 8 TeV. Three analyses are presented here: $Z/\gamma^* \to e^+e^-$ and $Z/\gamma^* \to \mu^+\mu^-$ measurements where both leptons are reconstructed in the central region of the detector and a $Z/\gamma^* \to e^+e^-$ measurement where one electron is measured in the central region of the detector and the other in the forward region. The triple differential cross-section is binned in dimensions of dilepton invariant mass $M_{\ell\ell}$, absolute rapidity, $|y_{\ell\ell}|$, and $\cos\theta^*$ where θ^* is the scattering angle in the Collins-Soper reference frame. The measurement provides sensitivity to the parton distribution functions or PDFs of the proton predominantly through the $M_{\ell\ell}$ and $|y_{\ell\ell}|$ dimensions. The data are also sensitive to forward-backward asymmetry, $A_{\rm FB}$, through all three dimensions of interest. Therefore this measurement allows PDF effects to be decorrelated from electroweak effects and the effective weak mixing angle $\sin^2\theta_W^{\rm eff}$ to be determined from the $M_{\ell\ell}$ dependence of $A_{\rm FB}$. The triple differential cross-section results presented here are provided at the born- and dressed-levels. A comparison is made to the predictions of perturbative QCD calculations and various event generators. The extraction of $\sin^2\theta_W^{\rm eff}$ is deferred to a second publication and will not be presented in this support note.

mation | Discussion (13) | Files

Internal Note

ort number	ATL-COM-PHYS-2015-344
	Measurement of m_W at 7 TeV : Hadronic recoil corrections
ıor(s)	Dimitrievska, Aleksandra (Institute of Physics, University of Belgrade) ; Vranjes, Nenad (Institute of Physics, University of Belgrade) ; Schott, Matthias (Institut fuer Physik, Universitaet Mainz) ; Boonekamp, Maarten (Commissariat a l'Energie Atomique (CEA), DSM/IRFU, Centre d'Etudes de Saclay)
int	30 Apr 2015. - mult. p.
ect category	Particle Physics - Experiment
lerator/Facility, riment	CERN LHC ; ATLAS
keywords	EWEAK
act	This note summarizes the studies regarding the calibration of the hadronic recoil in Monte Carlo simulations used for the W boson mass measurement of th 2011 dataset. Spe- cial focus is drawn on the evaluation of systematic uncertainties in the recoil calibration using Z boson events as control samples. Severa approaches are presented and a baseline recommendation is given.

contact: maarten.boonekamp@cern.ch ; matthias.schott@cern.ch ; aleksandra.dimitrievska@cern.ch ; nenad.vranjes@cern.ch
an author of this document, you can Submit a Revised Version or Update the Bibliographic Information or Other actions
d created 2015-04-30, last modified 2016-10-01

Similar records

Draft version 1.2

ATLAS NOTE

September 3, 2016

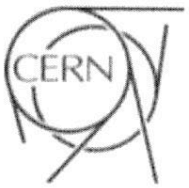

Muon efficiency corrections for the W boson mass measurement in the ATLAS 2011 data-set

Nancy Andari[c], Jean-Baptiste Blanchard[a], Maarten Boonekamp[a], Stefano Camarda[h], Jakub Cuth[b], Aleksandra Dimitrievska[i], Remie Hanna[a], Chris Hays[c], Mikhail Karnevskyi[b], Oleh Kivernyk[a], Jan Kretzschmar[g], Tai-Hua Lin[b], Mikhail Lisovyi[h], James Monk[f], Troels Petersen[f], Matthias Schott[1b], Giovanni Siragusa[d], Raimund Ströhmer[d], Nenad Vranjes[a,i], Christoph Zimmermann[b]

[a] *DSM/IRFU, CEA Saclay, Gif-sur-Yvette, France*
[b] *Mainz*
[c] *Oxford*
[d] *Julius-Maximilians-Universität Würzburg, Germany*
[e] *CERN*
[f] *NBI*
[g] *Liverpool*
[h] *DESY*
[i] *Institute of Physics Belgrade*

Abstract

The muon reconstruction, trigger and isolation-cut efficiency impacts significantly the predicted shape of the lepton p_T in $W \to \mu\nu$ events and plays therefore a crucial role in the W boson mass measurement. A correct modeling of these quantities in Monte Carlo simulations is therefore of high relevance. We reestimate these correction factors as function of lepton p_T, η, ϕ and the projection of the transverse momentum of the lepton onto the hadronic recoil $u_{\parallel}$. We estimate systematic uncertainties that are specifically targeted to a propagation from Z- to W-boson samples, which are based on the same MC generator.

Draft version 1.0

ATLAS NOTE

August 6, 2016

Measurement of m_W with 7 TeV data : Electron experimental corrections and related uncertainties

Nancy Andari[e], Fabrice Balli[a], Nathalie Besson[a], Jean-Baptiste Blanchard[a], Maarten Boonekamp[a], Stefano Camarda[e], Jakub Cuth[b], Aleksandra Dimitrievska[i], Sasha Glazov[h], Remie Hanna[a], Chris Hays[c], Mikhail Karnevskyi[b], Oleh Kivernyk[a], Jan Kretzschmar[g], Tai-Hua Lin[b], Mikhail Lisovyi[h], James Monk[f], Troels Petersen[f], Elzbieta Richter-Was[j], Matthias Schott[b], Giovanni Siragusa[d], Raimund Ströhmer[d], Nenad Vranjes[a,i], Samuel Webb[b], Christoph Zimmermann[b]

[a] *DSM/IRFU, CEA Saclay, Gif-sur-Yvette, France*
[b] *Institut für Physik, Universität Mainz*
[c] *Department of Physics, Oxford University*
[d] *Julius-Maximilians-Universität Würzburg*
[e] *European Laboratory for Particle Physics, CERN*
[f] *Niels Bohr Institute, Copenhagen*
[g] *Department of Physics, Universoty of Liverpool*
[h] *DESY, Hamburg and Zeuthen*
[i] *Institute of Physics, Belgrade*
[j] *Institute of Physics, Jagiellonian University, Krakow*

Abstract

This note describes the electron calibration analysis. The electron pseudo-rapidity range is optimized to obtain the best possible description of the Z boson kinematic distributions, with emphasis in the electron pair invariant mass distribution, and to define dedicated electron energy corrections in order to optimize the W boson mass measurement. The impact of electron trigger, reconstruction and identification efficiency uncertainties is also evaluated.

Draft version 0.1

ATLAS NOTE

December 5, 2014

Measurement of the W boson Mass at $\sqrt{s} = 7\,TeV$: Hadronic Recoil Algorithms

Nancy Andari[c], Jean-Baptiste Blanchard[a], Maarten Boonekamp[a], Stefano Camarda[h], Jakub Cuth[b], Aleksandra Dimitrievska[i], Remie Hanna[a], Chris Hays[c], Mikhail Karnevskyi[b], Oleh Kivernyk[a], Jan Kretzschmar[g], Tai-Hua Lin[b], Mikhail Lisovyi[h], James Monk[f], Troels Petersen[f], Matthias Schott[1b], Giovanni Siragusa[d], Raimund Ströhmer[d], Nenad Vranjes[a,i], Christoph Zimmermann[b]

[a] *DSM/IRFU, CEA Saclay, Gif-sur-Yvette, France*
[b] *Mainz*
[c] *Oxford*
[d] *Julius-Maximilians-Universität Würzburg, Germany*
[e] *CERN*
[f] *NBI*
[g] *Liveprool*
[h] *DESY*
[i] *Institute of Physics Belgrade*

Abstract

In this note we describe various approaches to calculate the hadronic recoil in vector boson events. In particular, we present studies on their performance with respect to high pile-up conditions and their sensitivity to the transverse momentum of the vector boson. The note concludes with a recommendation for a hadronic recoil algorithm to be used in the W boson mass analysis for the 2011 data-set at $\sqrt{s} = 7\,TeV$.

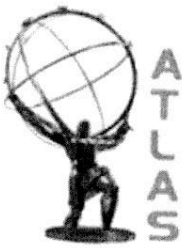

Draft version 1.02

ATLAS NOTE

October 1, 2016

Measurement of m_W with 7 TeV data : Physics Modeling

Nancy Andari[e], Fabrice Balli[a], Nathalie Besson[a], Jean-Baptiste Blanchard[a], Maarten Boonekamp[a], Stefano Camarda[e], Jakub Cuth[b], Aleksandra Dimitrievska[i], Sasha Glazov[h], Remie Hanna[a], Chris Hays[c], Mikhail Karnevskyi[b], Oleh Kivernyk[a], Jan Kretzschmar[g], Tai-Hua Lin[b], Mikhail Lisovyi[h], James Monk[f], Troels Petersen[f], Elzbieta Richter-Was[j], Matthias Schott[b], Giovanni Siragusa[d], Raimund Ströhmer[d], Nenad Vranjes[a,i], Samuel Webb[b], Christoph Zimmermann[b]

[a] *DSM/IRFU, CEA Saclay, Gif-sur-Yvette, France*
[b] *Institut für Physik, Universität Mainz*
[c] *Department of Physics, Oxford University*
[d] *Julius-Maximilians-Universität Würzburg*
[e] *European Laboratory for Particle Physics, CERN*
[f] *Niels Bohr Institute, Copenhagen*
[g] *Department of Physics, Universoty of Liverpool*
[h] *DESY, Hamburg and Zeuthen*
[i] *Institute of Physics, Belgrade*
[j] *Institute of Physics, Jagiellonian University, Krakow*

Information | Discussion (20) | Files

Internal Note

Report number	ATL-COM-PHYS-2014-1437
Title	**Measurement of m_W at 7 TeV : Z-based cross check measurements**
Author(s)	Andari, Nansi (European Laboratory for Particle Physics, CERN) ; Boonekamp, Maarten (Commissariat a l\'Energie Atomique (CEA), DSM/IRFU, Centre de Saclay) ; Blanchard, Jean-Baptiste (Commissariat a l\'Energie Atomique (CEA), DSM/IRFU, Centre d\'Etudes de Saclay) ; Vranjes, Nenad (Institute c University of Belgrade)
Imprint	04 Nov 2014. - mult. p.
Subject category	Particle Physics - Experiment
Accelerator/Facility, Experiment	CERN LHC ; ATLAS
Free keywords	EWEAK
Abstract	This note summarizes an analysis of the Z event sample collected by ATLAS in 2011, and corresponding to 4.5 fb−1 of data. Starting from distributic obtained after nominal experimental corrections, the aim of this note is to illustrate the importance of physics mod- eling corrections in obtaining satisfactory agreement between data and simulation for the kinematic distributions sensitive to the vector boson masses. Comparisons between da simulation are shown after the successive corrections, and Z boson mass fits are performed to check the self-consistency of the experimental and p modeling corrections. Tem- plates fits to mZ are performed using the invariant mass, lepton transverse momentum and lepton-recoil transverse ma distributions. The results based on the transverse momentum distribution are found to agree with the known value of mZ within 12 MeV, the statist accuracy of the fit.

Email contact: maarten.boonekamp@cern.ch ; nansi.andari@cern.ch ; nenad.vranjes@cern.ch ; jean-baptiste.blanchard@cern.ch

Record created 2014-11-04, last modified 2016-08-28

Information | Discussion (40) | Files

[redacted] Internal Note

Report number	ATL-COM-PHYS-2014-1569
Title	**Measurement of m_W with 7~TeV data : W boson mass measurement**
Author(s)	Andari, Nansi (European Laboratory for Particle Physics, CERN) ; Blanchard, Jean-Baptiste (Commissariat a l'Energie Atomique (CEA), DSM/IRFU, Cent d'Etudes de Saclay) ; Boonekamp, Maarten (Commissariat a l'Energie Atomique (CEA), DSM/IRFU, Centre d'Etudes de Saclay) ; Camarda, Stefano (DE Hamburg and Zeuthen) ; Dimitrievska, Aleksandra (Institute of Physics, University of Belgrade) ; Hanna, Remie (Commissariat a l'Energie Atomique (DSM/IRFU, Centre d'Etudes de Saclay) ; Hays, Chris (Department of Physics, Oxford University) ; Karnevskiy, Mikhail (Institut fuer Physik, Universitaet Kivernyk, Oleh (Commissariat a l'Energie Atomique (CEA), DSM/IRFU, Centre d'Etudes de Saclay) ; Schott, Matthias (Institut fuer Physik, Universitaet Siragusa, Giovanni (Julius-Maximilians-University of W\"urzburg) ; Stroehmer, Raimund (Julius-Maximilians-University of W\"urzburg) ; Vranjes, Nena (Institute of Physics, University of Belgrade) ; Webb, Samuel (Institut fuer Physik, Universitaet Mainz) ; Zimmermann, Christoph (Institut fuer Physik, Universitaet Mainz) *Hide*
Imprint	11 Dec 2014. - 35 p.
Subject category	Particle Physics - Experiment
Accelerator/Facility, Experiment	CERN LHC ; ATLAS
Free keywords	EWEAK
Abstract	Temporary abstract. Contents: measurement method; W event selections and corrections; background determination; data/MC control plots after cor blinded fit results and systematics; unblinded measurement.

Email contact: maarten.boonekamp@cern.ch ; oleh.kivernyk@cern.ch ; aleksandra.dimitrievska@cern.ch ; nansi.andari@cern.ch ; matthias.schott@cern.ch

Record created 2014-12-11, last modified 2016-10-01

Back t

Similar

ЗАПИСНИК

са седнице Одељења ДФС за научна истраживања и високо образовање одржане 16.12.2016. на Физичком факултету

Присутни чланови:

Физички факултет: Милан Дамњановић, Татјана Вуковић, Маја Бурић, Милан Кнежевић, Сава Галијаш, Зоран Николић, Срђан Буквић

Институт за физику у Београду: Игор Франовић, Ненад Вранješ, Марко Војиновић, Владимир Срећковић, Ивана Васић, Јелана Маљковић, Сања Тошић, Марина Лекић, Никола Шкоро, Срђан Марјановић, Марко Николић, Милош Радоњић, Михаило Рабасовић

Астрономска опсерваторија: Лука Поповић

Институт за нуклеарне науке „Винча": Ивица Брадарић

Електротехнички факултет: Петар Матавуљ

Природно математички факултет – Косовска Митровица: Бранко Дрљача, Љиљана Гулан

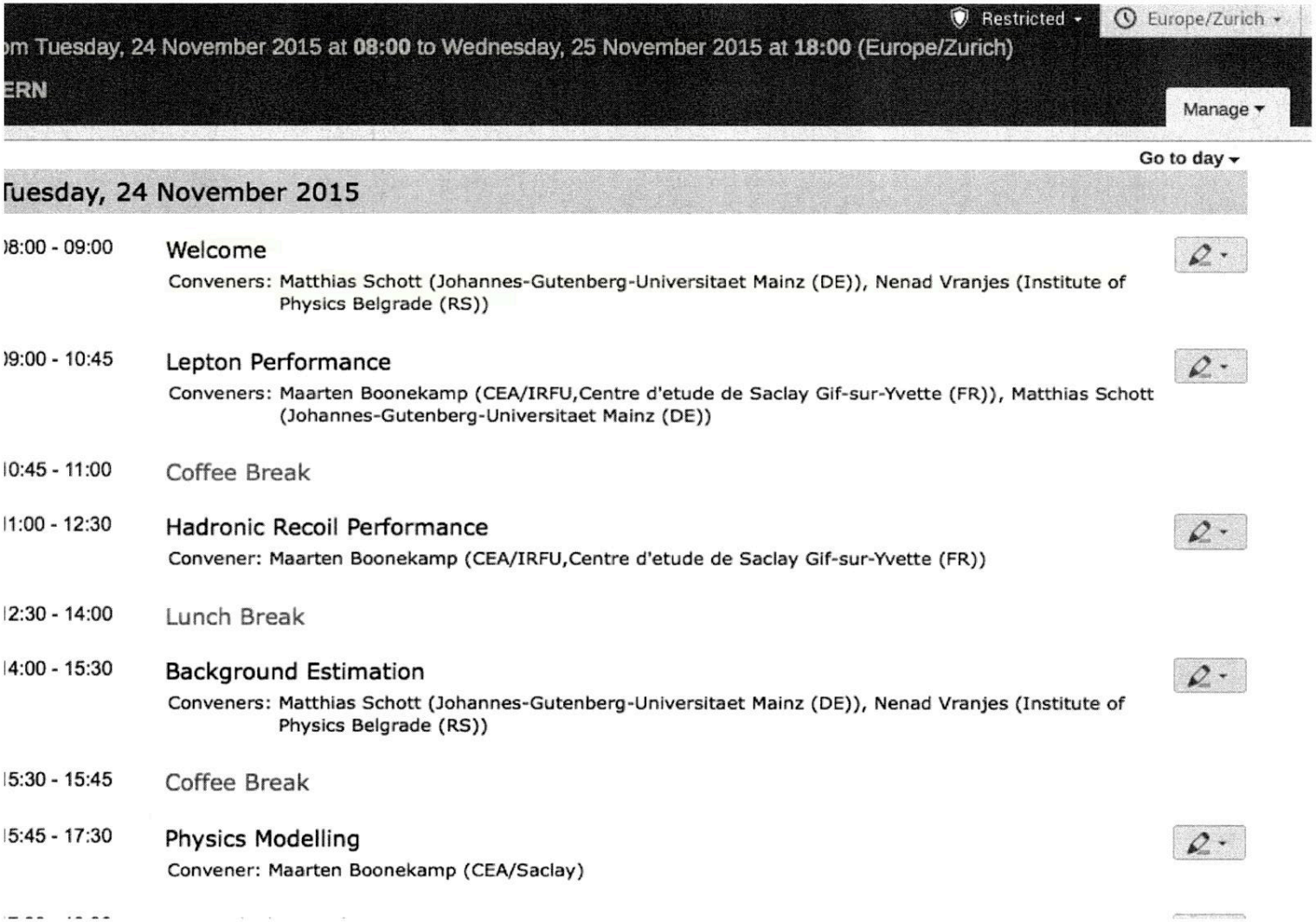
Restricted
Europe/Zurich
om Tuesday, 24 November 2015 at 08:00 to Wednesday, 25 November 2015 at 18:00 (Europe/Zurich)
ERN
Manage
Go to day
Tuesday, 24 November 2015
08:00 - 09:00
Welcome
Conveners: Matthias Schott (Johannes-Gutenberg-Universitaet Mainz (DE)), Nenad Vranjes (Institute of Physics Belgrade (RS))
09:00 - 10:45
Lepton Performance
Conveners: Maarten Boonekamp (CEA/IRFU,Centre d'etude de Saclay Gif-sur-Yvette (FR)), Matthias Schott (Johannes-Gutenberg-Universitaet Mainz (DE))
10:45 - 11:00
Coffee Break
11:00 - 12:30
Hadronic Recoil Performance
Convener: Maarten Boonekamp (CEA/IRFU,Centre d'etude de Saclay Gif-sur-Yvette (FR))
12:30 - 14:00
Lunch Break
14:00 - 15:30
Background Estimation
Conveners: Matthias Schott (Johannes-Gutenberg-Universitaet Mainz (DE)), Nenad Vranjes (Institute of Physics Belgrade (RS))
15:30 - 15:45
Coffee Break
15:45 - 17:30
Physics Modelling
Convener: Maarten Boonekamp (CEA/Saclay)

Програм сталног стручног усавршавања, акредитован од стране МПНТР Србије за школску 2014/15 и 2015/16

Савремена физика у истраживањима, настави и примени

5. и 6. март 2015.

Институт за физику
Прегревица 118, 11080 Београд

Аутори: др Александар Белић и др Мирјана Поповић-Божић

Реализатори: **др Антун Балаж,** др Ненад Вукмировић, Владимир Вељић, **др Радош Гајић,** др Горан Исић, Александар Матковић, **др Брана Јеленковић** , др Сенка Ђук , Немања Лучић; **др Љиљана Симић ,** др Ненад Врањеш, др Лидија Живковић, Петар Бокан, Татјана Јовин, др Марија Врањеш,

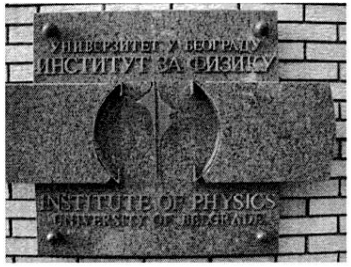

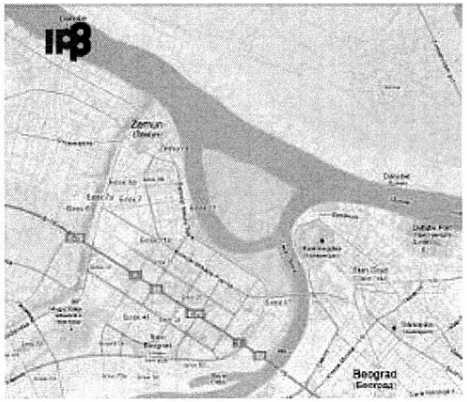

Каталошки број: 592; Компетенције: К1 - Компетенције за ужу стручну област;
Приоритети: 2 - учење да се учи и развијање мотивације за учење, Трајање: два дана; Број бодова: 16
Координатор: М. П. Божић, bozic@ipb.ac.rs, 011 - 3713 127, 065 - 693 9971

PHYSICAL REVIEW D **90,** 052004 (2014)

Measurement of the Higgs boson mass from the $H \to \gamma\gamma$ and $H \to ZZ^* \to 4\ell$ channels in pp collisions at center-of-mass energies of 7 and 8 TeV with the ATLAS detector

G. Aad *et al.*[*]
(ATLAS Collaboration)
(Received 17 June 2014; published 9 September 2014)

An improved measurement of the mass of the Higgs boson is derived from a combined fit to the reconstructed invariant mass spectra of the decay channels $H \to \gamma\gamma$ and $H \to ZZ^* \to 4\ell$. The analysis uses the pp collision data sample recorded by the ATLAS experiment at the CERN Large Hadron Collider at center-of-mass energies of 7 TeV and 8 TeV, corresponding to an integrated luminosity of 25 fb^{-1}. The measured value of the Higgs boson mass is $m_H = 125.36 \pm 0.37(\text{stat}) \pm 0.18(\text{syst})$ GeV. This result is based on improved energy-scale calibrations for photons, electrons, and muons as well as other analysis improvements, and supersedes the previous result from ATLAS. Upper limits on the total width of the Higgs boson are derived from fits to the invariant mass spectra of the $H \to \gamma\gamma$ and $H \to ZZ^* \to 4\ell$ decay channels.

DOI: 10.1103/PhysRevD.90.052004 PACS numbers: 14.80.Bn

I. INTRODUCTION

In 2012, the ATLAS and CMS collaborations published the discovery of a new particle [1,2] in the search for the Standard Model (SM) Higgs boson [3–8] at the CERN Large Hadron Collider (LHC) [9]. In the SM, the Higgs boson mass is not predicted. Its measurement is therefore required for precise calculations of electroweak observables including the production and decay properties of the Higgs boson itself. These calculations are needed to test the coupling structure of the SM Higgs boson, as suggested in Ref. [10] and references therein.

The LHC collaborations have chosen a model-independent approach to measure the Higgs boson mass based on fitting the spectra of the reconstructed invariant masses of the two decay modes $H \to \gamma\gamma$ and $H \to ZZ^* \to 4\ell$.[1] In these two channels the Higgs boson produces a narrow mass peak with a typical experimental resolution of 1.6 GeV to 2 GeV over a smooth background, from which the mass can be extracted without assumptions on the signal production and decay yields. Interference effects are expected between the Higgs boson signal and SM background processes. For the $H \to ZZ^* \to 4\ell$ channel, the impact of this interference on the mass measurement is negligible (< 10 MeV) if the Higgs boson width is close to the SM value [11]. For the $H \to \gamma\gamma$ channel, such effects are larger for widths close to the SM value [12–14], shifting the mass down by a few tens of MeV, but still small compared to the present experimental precision. The interference effects on the mass spectra are neglected in this paper.

Recent measurements of the Higgs boson mass from the ATLAS and CMS collaborations are reported in Refs. [15] and [16]. The ATLAS measurement was based on the same data sample as that analyzed in this paper, corresponding to an integrated luminosity of 4.5 fb^{-1} at $\sqrt{s} = 7$ TeV and of 20.3 fb^{-1} at $\sqrt{s} = 8$ TeV of pp collisions, taken in 2011 and 2012, respectively. The luminosity determination for the 2012 data set has been improved compared to Ref. [15], reaching an accuracy of 2.8% for the 2012 data.

The measurement of the Higgs boson mass is updated in this work with improved analyses of the two channels $H \to \gamma\gamma$ and $H \to ZZ^* \to 4\ell$, as described in Secs. IV and V. The $H \to \gamma\gamma$ channel profits from an improved calibration of the energy measurements of electron and photon candidates, which results in a sizable reduction of the systematic uncertainties on their energy scales. In the $H \to ZZ^* \to 4\ell$ channel both the expected statistical uncertainty and the systematic uncertainty on the mass measurement have been reduced with respect to the previous publication. The improvement of the statistical uncertainty arises primarily from the use of a multivariate discriminant that is designed to increase the separation of the signal from background. The systematic uncertainty reduction comes from both the improved electromagnetic energy calibration and a reduction in the muon momentum scale uncertainty, which was obtained by studying large samples of $Z \to \mu^+\mu^-$ and $J/\psi \to \mu^+\mu^-$ decays.

More information on the general aspects of the $H \to \gamma\gamma$ and $H \to ZZ^* \to 4\ell$ analyses is contained in the concurrent Refs. [17,18], where in particular, the details of the signal and background simulation can be found. The present measurement of the Higgs boson mass relies

[*] Full author list given at the end of the article.

[1] Throughout this paper, the symbol ℓ stands for electron or muon.

strongly upon both the calibration of the energy measurement for electrons and photons described in Ref. [19], and the understanding of the muon momentum scale and resolution presented in Ref. [20].

The ATLAS detector [21] is a multipurpose detector with a forward-backward symmetric cylindrical geometry.[2] At small radii, the inner detector (ID), immersed in a 2 T magnetic field produced by a thin superconducting solenoid located in front of the calorimeter, is made up of fine-granularity pixel and microstrip detectors. These silicon-based detectors cover the pseudorapidity range $|\eta| < 2.5$. A gas-filled straw-tube transition radiation tracker (TRT) complements the silicon tracker at larger radii and also provides electron identification based on transition radiation. The electromagnetic (EM) calorimeter is a lead/liquid-argon sampling calorimeter with accordion geometry. The calorimeter is divided into a barrel section covering $|\eta| < 1.475$ and two end-cap sections covering $1.375 < |\eta| < 3.2$. For $|\eta| < 2.5$ it is divided into three layers in depth, which are finely segmented in η and ϕ. A thin presampler layer, covering $|\eta| < 1.8$, is used to correct for fluctuations in upstream energy losses. Hadronic calorimetry in the region $|\eta| < 1.7$ uses steel absorbers and scintillator tiles as the active medium. Liquid argon calorimetry with copper absorbers is used in the hadronic end-cap calorimeters, which cover the region $1.5 < |\eta| < 3.2$. A forward calorimeter using copper or tungsten absorbers with liquid argon completes the calorimeter coverage up to $|\eta| = 4.9$. The muon spectrometer (MS) measures the deflection of muon tracks with $|\eta| < 2.7$, using three stations of precision drift tubes, with cathode strip chambers in the innermost layer for $|\eta| > 2.0$. The deflection is provided by a toroidal magnetic field with an integral of approximately 3 Tm and 6 Tm in the central and end-cap regions of ATLAS, respectively. The muon spectrometer is also instrumented with separate trigger chambers covering $|\eta| < 2.4$.

The outline of this paper is the following. In Secs. II and III, the improvements in the measurement of the physics objects used for the mass measurement (photons, electrons and muons) are described. In Secs. IV and V a brief description of the analyses used to measure the Higgs boson mass in the $H \to \gamma\gamma$ and $H \to ZZ^* \to 4\ell$ channels is presented, with emphasis on the improvements with respect to the analysis published in Ref. [15]. The statistical procedures used for the measurement of the mass and the contributions of the different systematic uncertainties are discussed in Sec. VI. The results of the combined mass measurement and the compatibility of the individual measurements of the two channels are reported in Sec. VII.

[2]ATLAS uses a right-handed coordinate system with its origin at the nominal interaction point (IP) in the center of the detector and the z axis along the beam pipe. The x axis points from the IP to the center of the LHC ring, and the y axis points upward. Cylindrical coordinates (r, ϕ) are used in the transverse plane, ϕ being the azimuthal angle around the beam pipe. The pseudorapidity is defined in terms of the polar angle θ as $\eta = -\ln \tan(\theta/2)$.

II. PHOTON AND ELECTRON RECONSTRUCTION, ENERGY SCALE CALIBRATION AND SYSTEMATIC UNCERTAINTIES

The calibration strategy for the energy measurement of electrons and photons is described in detail in Ref. [19]. In this section, the definitions of photon and electron objects are given, followed by a description of their energy scale calibration. To achieve the best energy resolution and to minimize systematic uncertainties, the calibration and stability of the calorimeter cell energy measurement are optimized, the relative calibration of the longitudinal layers of the calorimeter is adjusted, and a determination of the amount of material in front of the calorimeter is performed. The global calorimeter energy scale is then determined *in situ* with a large sample of $Z \to e^+e^-$ events, and verified using $J/\psi \to e^+e^-$ and $Z \to \ell^+\ell^-\gamma$ events. The calibration analysis uses a total of 6.6 million $Z \to e^+e^-$ decays, 0.3 million $J/\psi \to e^+e^-$ decays, and 0.2 million radiative Z boson decays. Compared to the previous publication [15], the uncertainties in the calibration are significantly reduced by using data-driven measurements for the intercalibration of the calorimeter layers and for the estimate of the material in front of the calorimeter, as well as by improving the accuracy of the *in situ* calibration with $Z \to e^+e^-$ events [19]. The expected range for transverse energy of photons from $H \to \gamma\gamma$ decays is from 40 GeV to about 100 GeV. The range for electrons from $H \to ZZ^* \to 4\ell$ decays is from 7 GeV to about 50 GeV.

A. Definition of photon and electron objects

Photon and electron candidates are reconstructed from clusters of energy deposited in the EM calorimeter. Candidates without a matching track or reconstructed conversion vertex in the ID are classified as unconverted photon candidates. Candidates with a matching reconstructed conversion vertex or a matching track consistent with originating from a photon conversion are classified as converted photon candidates. Candidates matched to a track consistent with originating from an electron produced in the beam interaction region are kept as electron candidates.

The measurement of the electron or photon energy is based on the energy collected in calorimeter cells in an area of size $\Delta\eta \times \Delta\phi$ of 0.075×0.175 for electrons and converted photons in the barrel, 0.075×0.125 for unconverted photons in the barrel, and 0.125×0.125 for electrons and photons in the end caps. The choice of a different area for electrons and unconverted photons in the barrel is driven by the deflection of charged particles in the magnetic field and

bremsstrahlung in upstream material. A multivariate regression algorithm to calibrate electron and photon energy measurements was developed and optimized using simulation. Corrections are made for the energy deposited in front of the calorimeter (typically between a few % and 20% of the electron energy for 100 GeV energy electrons [21]) and outside of the cluster (around 5%), as well as for the variation of the energy response as a function of the impact point on the calorimeter. The inputs to the energy calibration algorithm are the measured energy per calorimeter layer, including the presampler, η of the cluster, and the local position of the shower within the second-layer cell corresponding to the cluster centroid. In addition, for converted photons, the track transverse momenta and the conversion radius are used as input to the regression algorithm to further improve the energy resolution, especially at low energy. This calibration procedure gives a 10% improvement in the expected mass resolution for $H \to \gamma\gamma$ compared to the calibration used in the previous publication. For electron and photon candidates, the associated tracks are fitted with a Gaussian-sum filter to account for bremsstrahlung energy losses [22]. For $H \to ZZ^* \to 4\ell$ candidates, the resulting momentum measurement is combined with the energy measured in the calorimeter to improve the electron energy measurement, especially at low energy or in the transition region between the barrel and end-cap calorimeters, where the calorimeter and ID have similar resolution.

B. Cell energy calibration and stability

The raw signal from each calorimeter cell is converted into a deposited energy using the electronics calibration of the EM calorimeter [23]. The calibration coefficients are determined periodically using dedicated electronics calibration runs and are stable in time to better than 0.1%. The relative calibration of the different gains used in the readout is investigated by studying the $Z \to e^+e^-$ sample, used for the global energy scale, as a function of the electron energy and categorizing the events according to the electronics gain used for the energy measurement, and small corrections (typically less than a few per mille) are applied. The corrections applied to the few percent of channels operated at non-nominal high voltage values are verified using data. The stability of the calorimeter response for data, both as a function of time and of instantaneous luminosity, is monitored using electrons from W or Z decays and is found to be better than 0.05%.

C. Intercalibration of the different calorimeter layers

Accurate relative intercalibration of the different layers of the EM calorimeter is critical to achieve good linearity of the energy response. The relative calibration of the first two layers of the EM calorimeter, which contain most of the energy deposited by electrons and photons, is performed using muons from Z boson decays by comparing their measured energy loss in data and simulation. The use of muons allows the determination of the intrinsic relative layer calibration, independently of uncertainties on the material in front of the EM calorimeter. Small corrections, around 2% on average, for the relative calibration of the two layers are derived. The uncertainty on the relative calibration of the first two layers of the EM calorimeter varies between 1% and 2% as a function of η and is dominated by the uncertainties on the exact amount of liquid argon traversed by the muons and by the accuracy of the simulation of the cross-talk between calorimeter cells. The relative calibration of the presampler layer is derived from electrons, by comparing the presampler energy in data and simulation as a function of the longitudinal shower development measured in the calorimeter. The accuracy of this calibration, which does not depend on knowledge of the material in front of the presampler, is better than 5%.

D. Determination of the material in front of the EM calorimeter

Accurate knowledge of the material in front of the EM calorimeter is required to properly correct for the energy lost upstream of the calorimeter, which also depends on the nature of the particle (electron, unconverted photon, converted photon) and its energy. The total amount of material in front of the presampler layer varies from two radiation lengths (for $|\eta| < 0.6$) to about five radiation lengths (for $|\eta| \sim 1.7$). The amount of material in front of the calorimeter is verified using collision data by studying the longitudinal development of electromagnetic showers, measured using the first two layers of the calorimeter, which are intercalibrated as described above, without any assumption about the material in front of the calorimeter. The uncertainties given below result from the statistical accuracy of the data and from the uncertainties in the modeling of the longitudinal shower profiles in the calorimeter.

The material between the presampler and the first calorimeter layer is measured using unconverted photons with low energy deposition in the presampler. Comparison of data and simulation shows that this material is well described in the simulation with an accuracy between 0.03 and 0.05 radiation lengths.

The integral of the material in front of the presampler is determined using the difference between electron and unconverted photon longitudinal shower profiles. The accuracy of this measurement is between 0.02 and 0.10 radiation lengths, depending on η. Over most of the calorimeter acceptance, the simulation is found to reproduce the data well, after some improvements in the description of the material in front of the end-cap calorimeter, with the exception of a few small localized regions where differences of up to 0.3 radiation lengths remain. The relative calibration of electron and photon energy measurements also depends on the radial position of detector

material in front of the presampler, which cannot be directly probed using longitudinal shower profiles measured in the calorimeter. The uncertainty on the amount of material in the ID active area is estimated from a comparison between a bottom-up inventory of the ID components and the measured weight of different ID subdetector units [21]. A 5% relative uncertainty, corresponding to 0.02 to 0.10 radiation lengths depending on the detector region, in the amount of material in the ID active area is derived from this comparison. Measurement of the rates of hadronic interactions [24] and of photon conversions with collision data are consistent with (albeit less precise than) this *a priori* knowledge. The determination of the integral of the material in front of the presampler is then used together with knowledge of the material in the ID active area to constrain the material in the detector services beyond the active part of the ID and in the calorimeter cryostats.

E. Global calorimeter energy scale adjustment

The global calorimeter energy scale is determined from $Z \to e^+e^-$ decays by comparing the reconstructed mass distributions in data and simulation. This is done in bins of η of the electrons. The energy scale correction factors are typically of the order of 1%–3% and are consistent with the uncertainties on the initial energy scale derived from test-beam data. The uncertainty in the measurement of these factors from the Z sample is less than 0.1% on average, and up to 0.3% for $|\eta| \sim 1.5$ at the transition region between the barrel and end-cap calorimeters. The uncertainty is significantly reduced compared to Ref. [25], owing to the improved detector description discussed above, to improved simulation, to the intercalibration corrections, and to a larger Z boson decay sample. No variation of the energy scale correction factors with pileup was observed. At the same time, an effective constant term for the calorimeter energy resolution is extracted by adjusting the width of the reconstructed Z mass distribution in simulation to match the distribution in data. This constant term is, on average, 0.7% for $|\eta| < 0.6$, and between 0.7% and 1.5% in the remainder of the calorimeter acceptance, except in the transition region between barrel and end-cap calorimeters where it is 3.5% and at the end of the end-cap acceptance ($|\eta| > 2.3$) where it is 2.5%. This constant term is used to adjust the energy resolution in simulated samples. The extraction of the energy scale and of the effective constant term is done separately for the 7 TeV and 8 TeV data. The effective constant term is about 0.2%–0.3% larger in the 8 TeV data.

F. Systematic uncertainties on the energy scale and cross-checks

The calorimeter energy scale adjustment with Z events determines the scale for electrons with transverse energy (E_{T}) close to that of $Z \to e^+e^-$ events ($E_{\mathrm{T}} \sim 40$ GeV on average). Any systematic uncertainty thus has minimal impact for 40 GeV E_{T} electrons but can lead to residual nonlinearities and differences between the electron, unconverted photon, and converted photon energy scales.

In addition to the uncertainty on the overall energy scale adjustment, the uncertainties affecting the energy measurement of electrons and photons can be classified as follows. The impact of these systematic uncertainties on the photon energy scale is detailed for photons from Higgs boson decays, as the impact of energy scale systematic uncertainties is larger for this decay channel.

(i) Uncertainty on the nonlinearity of the energy measurement at the cell level: this arises mostly from the relative calibration of the different gains used in the calorimeter readout. The uncertainty on the nonlinearity of the cell energy calibration contributes an uncertainty of about 0.1% to the energy scale of photons from Higgs boson decays (up to 1% for $1.5 < |\eta| < 1.7$).

(ii) Uncertainty on the relative calibration of the different calorimeter layers: these contribute an uncertainty of about 0.10% to 0.15% to the energy scale of photons from Higgs boson decays.

(iii) Uncertainty on the amount of material in front of the calorimeter: these contribute between 0.1% and 0.3% as a function of η for unconverted photons from Higgs boson decays. This uncertainty is typically 2 times smaller for converted photons that have an energy loss before the calorimeter closer to that of the Z decay electrons used in the energy scale adjustment.

(iv) Uncertainty in the reconstruction of photon conversions: unconverted and converted photons are calibrated differently to take into account the difference in the energy loss before the calorimeter. Converted photons misidentified as unconverted photons, or vice versa, are typically reconstructed with an energy shifted by 2%. The uncertainty in the modeling of the efficiency to properly classify converted or unconverted photons is a few percent. This translates into an uncertainty on the photon energy scale of 0.02%–0.04% for both the converted and unconverted photons.

(v) Uncertainty in the modeling of the lateral shower shape: differences between data and simulation for the lateral development of electromagnetic showers contribute to the uncertainty on the energy scale if they depend on energy or particle type. These differences are compared for photons and electrons using a sample of radiative Z decays. They are found to be consistent. The resulting uncertainty on the photon energy scale is 0.05%–0.3% depending on η and whether or not the photon converted.

At an E_{T} of about 60 GeV, the total uncertainty on the photon energy scale is between 0.2% and 0.3% for $|\eta| < 1.37$ or $|\eta| > 1.82$; for $1.52 < |\eta| < 1.82$, the uncertainty

is 0.9% and 0.4% for unconverted and converted photons, respectively. The energy dependence of the photon energy scale uncertainty is weak. The uncertainty on the electron energy scale at an E_T of 40 GeV is, on average, 0.04% for $|\eta| < 1.37$, 0.2% for $1.37 < |\eta| < 1.82$ and 0.05% for $|\eta| > 1.82$. At an E_T of about 10 GeV, the electron energy scale uncertainty ranges from 0.4% to 1% for $|\eta| < 1.37$, is about 1.1% for $1.37 < |\eta| < 1.82$, and again 0.4% for $|\eta| > 1.82$. The largest uncertainty for electrons is in the transition region between the barrel and end-cap calorimeters, which is not used for photons. These uncertainties are modeled using 29 independent sources to account for their η dependence, and are almost fully correlated between the 7 TeV and 8 TeV samples. These 29 uncertainty sources are assigned in the following way:

(i) one for the uncertainty in the extraction of the calorimeter energy scale from $Z \to e^+e^-$ events,
(ii) three for the uncertainty on the nonlinearity of the energy measurement at the cell level,
(iii) four for the uncertainty on the ID material in different eta regions,
(iv) six for the uncertainties affecting the relative calibration of the different calorimeter layers covering uncertainties in the muon measurement as well as in the modeling of muon energy loss in the simulation,
(v) ten for the uncertainties affecting the determination of the material after the ID volume and between the presampler and the first calorimeter layer covering uncertainties in the data measurement and in the modeling of longitudinal shower profiles in the simulation,
(vi) three for uncertainties in the modeling of the conversion reconstruction performance in the simulation,
(vii) two for the uncertainties in the modeling of the lateral shower shapes, separating converted and unconverted photons.

An independent verification of the energy scale is performed using samples of $J/\psi \to e^+e^-$ and $Z \to \ell^+\ell^-\gamma$ decays. The latter sample allows, for instance, a direct measurement of the photon energy scale in the low transverse energy range (typically between 7 GeV and 35 GeV). The results are in good agreement with the energy scale determined from the $Z \to e^+e^-$ sample, taking into account the systematic uncertainties discussed above. With the $Z \to \ell^+\ell^-\gamma$ sample, the energy scale of photons with

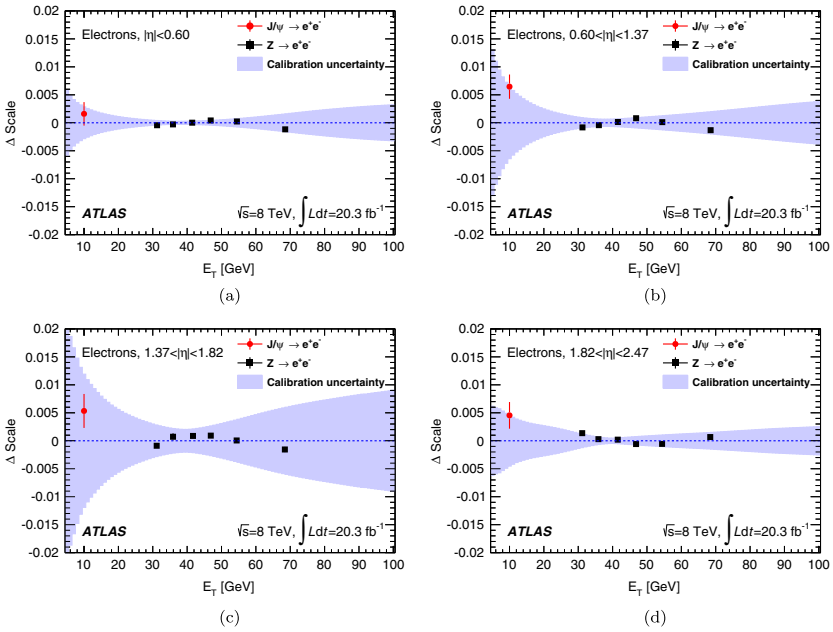

FIG. 1 (color online). Relative scale difference, Δ Scale, between the measured electron energy scale and the nominal energy scale, as a function of E_T using $J/\psi \to e^+e^-$ and $Z \to e^+e^-$ events (points with error bars), for four different η regions: (a) $|\eta| < 0.6$, (b) $0.6 < |\eta| < 1.37$, (c) $1.37 < |\eta| < 1.82$ and (d) $1.82 < |\eta| < 2.37$. The uncertainty on the nominal energy scale for electrons is shown as the shaded area. The error bars include the systematic uncertainties specific to the $J/\psi \to e^+e^-$ measurement.

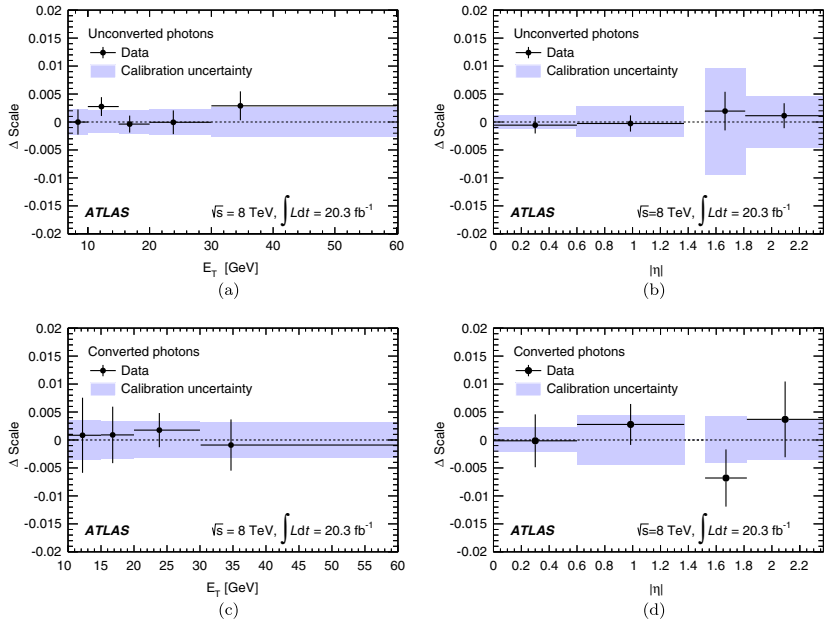

FIG. 2 (color online). Relative scale difference, Δ Scale, between the measured photon energy scale using $Z \to \ell\ell\gamma$ events and the nominal energy scale: (a) as a function of E_{T} for unconverted photons, (b) as a function of η for unconverted photons, (c) as a function of E_{T} for converted photons and (d) as a function of η for converted photons. Photons reconstructed in the transition region between the barrel and end-cap calorimeters are not considered. The $Z \to \ell\ell\gamma$ measurements are the points with error bars. The uncertainty on the nominal energy scale for photons is shown as the shaded area. The error bars include the systematic uncertainties specific to the $Z \to \ell\ell\gamma$ measurement.

transverse energy around 30 GeV is probed with an accuracy of about 0.3%. Figures 1 and 2 summarize the verifications of the electron and photon energy scales from these samples using the 8 TeV data set, after the full calibration procedure is applied. In addition to the $J/\psi \to e^+e^-$ and $Z \to \ell^+\ell^-\gamma$ samples, the nonlinearity in the electron energy scale is also probed by dividing the $Z \to e^+e^-$ sample into bins of electron E_{T}. These figures also show the total systematic uncertainty on the electron and photon energy scales as a function of E_{T} and η. The same verifications are performed using the 7 TeV data set with results consistent within uncertainties.

G. Uncertainties on the calorimeter energy resolution

Systematic uncertainties on the calorimeter energy resolution arise from uncertainties in the modeling of the sampling term and on the measurement of the constant term in Z boson decays, from uncertainties related to the amount of material in front of the calorimeter, which affect electrons and photons differently, and from uncertainty in the modeling of the small contribution to the resolution from fluctuations in the pileup from other proton-proton interactions in the same or neighboring bunch crossings. The uncertainty on the calorimeter energy resolution is typically ∼10% for photons from Higgs boson decays, and varies from 10% to 5% for electrons in the E_{T} range from 10 GeV to 45 GeV.

III. MUON RECONSTRUCTION, MOMENTUM SCALE AND RESOLUTION SYSTEMATIC UNCERTAINTIES

The muon momentum is measured independently by the ID and the MS detector systems. Four types of muon candidates are reconstructed, depending on the available information from the ID, the MS, and the calorimeters. Most muon candidates are identified by matching a reconstructed ID track with either a complete or a partial (local segment) track reconstructed in the MS [20,26]. If a complete MS track is present, the two independent momentum measurements are combined (CB muons); otherwise the momentum is measured using the ID, and the partial MS track serves as identification (segment-tagged muons). The muon reconstruction and identification coverage is extended by using tracks reconstructed in the

forward region ($2.5 < |\eta| < 2.7$) of the MS, which is outside the ID coverage (standalone muons). The parameters of the muon track reconstructed in the MS are expressed at the interaction point by extrapolating the track back to the point of closest approach to the beam line, taking into account the energy loss of the muon in the calorimeters. In the center of the barrel region ($|\eta| < 0.1$), which lacks MS geometrical coverage, ID tracks with transverse momentum $p_{\mathrm{T}} > 15$ GeV are identified as muons if their calorimetric energy deposits are consistent with a minimum ionizing particle (calorimeter-tagged muons). The combination of the track measurements provided by the ID and MS ensures excellent momentum resolution across 3 orders of magnitude, from a few GeV up to a few TeV.

The muon reconstruction in simulation is corrected to match the momentum scale and resolution measured from collision data as described in detail in Ref. [20]. About 6 million $J/\psi \to \mu^+\mu^-$ events[3] and about 9 million $Z \to \mu^+\mu^-$ events were used to extract the corrections to be applied to the simulated data. They consist of scale corrections for the ID and MS, a p_{T}-independent momentum correction for the MS and a p_{T}-dependent smearing correction to be applied to reproduce the resolution observed in data. The corrections for the ID and MS momentum measurements were derived separately. For the momentum of CB muons, the individual corrections from the ID and MS momentum are combined according to their relative weight in the measurement of the combined muon.

To extract the ID corrections, template fits to the $J/\psi \to \mu^+\mu^-$ and $Z \to \mu^+\mu^-$ invariant mass distributions are performed in bins of η and p_{T}. The MS corrections are extracted by fitting the $J/\psi \to \mu^+\mu^-$ and $Z \to \mu^+\mu^-$ invariant mass distributions and the difference between the momentum measured in the ID and MS. The MS corrections are derived in bins of p_{T} and η, and follow the sector granularity of the MS in the azimuthal coordinate ϕ. The systematic uncertainties on the corrections are estimated by varying several ingredients of the fit procedure: the parametrization and the normalization of the backgrounds, the fit ranges, and the parametrization of the resonances and their kinematic distributions. The systematic uncertainties on the resolution are varied independently for the ID and MS, whereas the ID and MS systematic scale uncertainties are treated as fully correlated, hence maximizing the impact of the scale variation on the CB muons.

The major improvement with respect to the previous publication is the use of $J/\psi \to \mu^+\mu^-$ events in addition to the $Z \to \mu^+\mu^-$ sample in the simulation correction procedure. This allows a significant reduction of the momentum scale uncertainty in the low momentum range that is relevant for the $H \to ZZ^* \to 4\ell$ mass measurement. In previous studies, the $J/\psi \to \mu^+\mu^-$ sample was used only for the evaluation of the systematic uncertainties.

The ID momentum scale corrections are below 0.1%. The systematic uncertainties on the ID scale increase with $|\eta|$, starting from 0.02% at $\eta = 0$ and rising to about 0.2% for $|\eta| > 2$. The MS scale corrections vary from −0.4% to +0.3% depending on the η and ϕ regions. The p_{T}-independent momentum correction to the MS measurement takes into account the difference between the muon energy loss in the calorimeters in data and simulation, is of the order of a few tens of MeV and has a negligible impact on the Higgs boson mass measurement. Typical systematic uncertainties on the MS momentum scale range from less than 0.1% to about 0.2%. The systematic uncertainties on the CB momentum scale are 0.04% in the barrel region and increase to about 0.2% for $|\eta| > 2$.

These results were checked by separately fitting the dimuon invariant mass distribution to extract the peak position and the width of the J/ψ, Z and Υ resonances in data and in the simulation, with and without corrections. For this study 17 million J/ψ events were used. The Υ sample, about 5 million events, was not used in the simulation correction procedure and therefore provides an independent validation performed in bins of p_{T}, η and ϕ. Figure 3(a) shows the ratio of the reconstructed dimuon invariant mass for data to the corrected mass in simulation for J/ψ, Υ and Z events as a function of η of the higher-p_{T} muon. Figure 3(b) shows the same ratio as a function of the average transverse momentum, $\langle p_{\mathrm{T}} \rangle$, of the two muons. The error bars on data points show the combined statistical and systematic uncertainties. The systematic uncertainty is extracted by varying the fitted dimuon mass range and, in the case of J/ψ, by taking into account the uncertainty on the background. These studies demonstrate the validity of the corrections and of the associated systematic uncertainties in the range $6 < p_{\mathrm{T}} \lesssim 100$ GeV.

IV. MASS AND WIDTH MEASUREMENT IN THE $H \to \gamma\gamma$ CHANNEL

The $H \to \gamma\gamma$ channel provides good sensitivity to the Higgs boson mass, due to the excellent mass resolution in the diphoton final state, allowing the observation of a narrow mass peak over a smooth background which can be determined directly from data. The EM calorimeter provides a measurement of the photon energy and direction (photon pointing), utilizing its longitudinal segmentation. The typical mass resolution is 1.7 GeV for a 125 GeV Higgs boson mass. The main background is continuum $\gamma\gamma$ production with smaller contributions, of about 20%, from the γ + jet and dijet processes. A more complete

[3]Only J/ψ events with a muon with $p_{\mathrm{T}} > 8$ GeV are used to derive the muon momentum corrections, to avoid any bias in the corrections from nonlinearities in the momentum scale in the low momentum range.

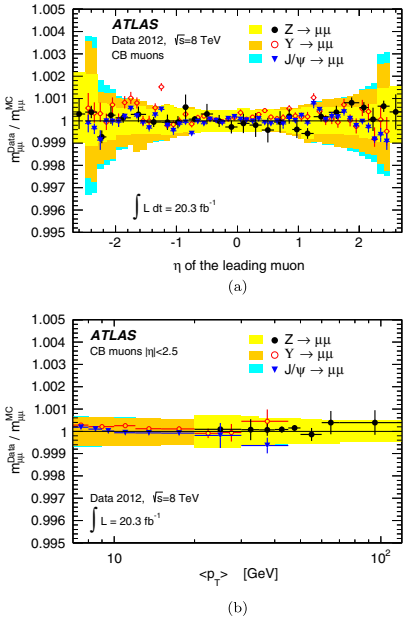

FIG. 3 (color online). Ratio of the reconstructed dimuon invariant mass for data to the corrected mass in simulation for J/ψ, Υ and Z events: (a) as a function of η of the higher-p_{T} muon and (b) as a function of $\langle p_{\mathrm{T}} \rangle$ of the two muons, as defined in the text. The shaded areas show the systematic uncertainty on the simulation corrections for each of the three samples. The error bars on the points show the combined statistical and systematic uncertainties as explained in the text. In (a), the two large $|\eta|$ bins have measurements only from Z events due to trigger limitations above $|\eta| = 2.4$.

description of the selection criteria and background modeling is reported in Ref. [17].

A. Event selection

Events are selected using a diphoton trigger. For the 7 TeV data, an E_{T} threshold of 20 GeV is applied to both photons at the trigger level. For the 8 TeV data, the E_{T} threshold at the trigger level is 35 GeV for the photon with the highest E_{T} and 25 GeV for the photon with the next-highest E_{T}. Loose photon identification cuts are applied at the trigger level, which is more than 99% efficient for events fulfilling the final analysis selection.

Only photon candidates with $|\eta| < 2.37$ are considered, removing the transition region $1.37 < |\eta| < 1.56$ between the barrel and end-cap calorimeters. The calorimeter granularity in the transition region is reduced, and the presence of significant additional inactive material affects the identification capabilities and energy resolution.

Two photons are required to fulfill tight identification criteria that are based primarily on shower shapes in the EM calorimeter [27]. For the 7 TeV data, a neural network discriminant is built from shower shape variables to suppress the contamination from jets misidentified as photon candidates. For the 8 TeV data, a set of cuts optimized for the pileup conditions of the 2012 data taking are applied. The efficiency of the photon identification selection ranges between 85% and 95% as a function of the photon E_{T}.

To further reject background from jets misidentified as photons, the photon candidates are required to be isolated using both the calorimeter isolation and track isolation requirements. The calorimeter isolation is defined as the sum of the E_{T} of clusters of energy deposited in a cone of size $\Delta R = \sqrt{(\Delta\eta)^2 + (\Delta\phi)^2} = 0.4$ around the photon candidate, excluding an area of size $\Delta\eta \times \Delta\phi = 0.125 \times 0.175$ centered on the photon cluster; the expected photon energy deposit outside the excluded area is subtracted. The pileup and underlying event contribution to the calorimeter isolation is subtracted event by event [28]. The calorimeter isolation is required to be smaller than 5.5 GeV for the 7 TeV data and smaller than 6 GeV for the 8 TeV data. The track isolation is defined as the scalar sum of the transverse momenta of the tracks in a cone of $\Delta R = 0.2$ around the photon candidate. The tracks are required to have $p_{\mathrm{T}} > 0.4(1.0)$ GeV, for the 7 (8) TeV data, and to be consistent with originating from the diphoton primary vertex, defined below. In the case of converted photons, the tracks associated with the photon conversion are excluded from the track isolation. The track isolation is required to be smaller than 2.2 GeV for the 7 TeV data and smaller than 2.6 GeV for the 8 TeV data. The efficiency of the isolation requirement is about 95% per photon for both 7 TeV and 8 TeV data.

Identifying which reconstructed primary vertex corresponds to the pp collision that produced the diphoton candidate is important for the mass reconstruction. The correct identification of the tracks coming from the pp collision producing the diphoton candidate is also necessary to avoid pileup contributions to the track isolation. To keep the contribution of the opening angle resolution to the mass resolution significantly smaller than the energy resolution contribution, a position resolution for the primary vertex of about 15 mm in the z direction is sufficient. Better resolution is needed to correctly match tracks to the pp collision vertex of the diphoton candidate. The directions of the photon candidates are measured using the longitudinal and transverse segmentation of the EM calorimeter, with a resolution of about 60 mrad$/\sqrt{E}$, where E is the photon energy in GeV. An estimate of the diphoton primary vertex z position is obtained by combining the average beam-spot position with this photon pointing, which is enhanced by using the tracks from photon conversions with conversion radii before or in the silicon

detectors. This estimate gives a resolution of about 15 mm in the z direction. In order to select the best reconstructed primary vertex, three additional variables are defined for each reconstructed primary vertex: Σp_{T} of the track transverse momenta, Σp_{T}^2, and the azimuthal angle between the combined photon system and the combined system of the tracks in the transverse plane. A neural network discriminant is constructed using the diphoton primary vertex z position estimated by the photon pointing, its uncertainty and this additional track information to select the best primary vertex candidate for the diphoton event. This algorithm selects a primary vertex within ± 15 mm in z of the true production vertex with an efficiency of 93% for the average pileup conditions in the 8 TeV data set. The contribution of the opening angle resolution to the mass resolution is thus negligible.

The diphoton invariant mass $m_{\gamma\gamma}$ is computed using the measured photon energies and their opening angle estimated from the selected primary vertex and the photon impact points in the calorimeter. The transverse energy is required to be $E_{\mathrm{T}} > 0.35 \times m_{\gamma\gamma}$ for the photon with the highest E_{T} and $E_{\mathrm{T}} > 0.25 \times m_{\gamma\gamma}$ for the photon with the second-highest E_{T}. This selection leads to a smoother background distribution in each of the event categories compared to using fixed cuts on E_{T}. The combined signal reconstruction and selection efficiency for the Higgs boson signal at an assumed mass of 125 GeV is around 40%. In total, 94627 (17225) events are selected in the 8 TeV (7 TeV) data set with $105 < m_{\gamma\gamma} < 160$ GeV.

B. Event categorization

To improve the accuracy of the mass measurement, the selected events are separated into ten mutually exclusive categories that have different signal-to-background ratios, different diphoton invariant mass resolutions and different systematic uncertainties. To keep the analysis simple, the categorization is based only on the two photon candidates. The categorization, which is different from the one used in Ref. [17], is optimized to minimize the expected uncertainty on the mass measurement, assuming a Higgs boson signal produced with the predicted SM yield, while also accounting for systematic uncertainties. Events are first separated into two groups, one where both photons are unconverted and the other where at least one photon is converted. The simulation predicts that the energy resolution for unconverted photons is better than the one for converted photons, and energy scale systematic uncertainties are different for converted and unconverted photons. The events are then classified according to the η of the two photons: the central category corresponds to events where both photons are within $|\eta| < 0.75$, the transition category corresponds to events with at least one photon with $1.3 < |\eta| < 1.75$, and the rest category corresponds to all other diphoton events. The central category has the best mass resolution and signal-to-background ratio, as well as the smallest energy scale uncertainties. The transition category suffers from worse energy resolution, due to the larger amount of material in front of the calorimeter, and also from larger systematic uncertainties. Finally, the central and rest categories are each split into a low p_{Tt} (< 70 GeV) and a high p_{Tt} (> 70 GeV) category, where p_{Tt} is the component of the diphoton transverse momentum orthogonal to the diphoton thrust axis in the transverse plane.[4] The high p_{Tt} categories have better signal-to-background ratios and mass resolution, but have smaller yield. This categorization provides a 20% reduction of the expected statistical uncertainty compared to an inclusive measurement.

C. Signal modeling

The signal mass spectrum is modeled by the sum of a Crystal Ball function for the bulk of the events, which have a narrow Gaussian spectrum in the peak and tails toward lower reconstructed mass, and a wide Gaussian distribution to model the far outliers in the mass resolution. The Crystal Ball function is defined as

$$N \cdot \begin{cases} e^{-t^2/2} & \text{if } t > -\alpha_{\mathrm{CB}} \\ \left(\frac{n_{\mathrm{CB}}}{\alpha_{\mathrm{CB}}}\right)^{n_{\mathrm{CB}}} e^{-\alpha_{\mathrm{CB}}^2/2} \left(\frac{n_{\mathrm{CB}}}{\alpha_{\mathrm{CB}}} - \alpha_{\mathrm{CB}} - t\right)^{-n_{\mathrm{CB}}} & \text{otherwise} \end{cases}$$

where $t = (m_{\gamma\gamma} - \mu_{\mathrm{CB}})/\sigma_{\mathrm{CB}}$, N is a normalization parameter, μ_{CB} is the peak of the narrow Gaussian distribution, σ_{CB} represents the Gaussian resolution for the core component, and n_{CB} and α_{CB} parametrize the non-Gaussian tail.

The σ_{CB} parameter varies from 1.2 GeV to 2.1 GeV depending on the category of the event. The overall resolution can be quantified either through its full width at half maximum (FWHM), which varies from 2.8 GeV to 5.3 GeV, or using σ_{eff}, defined as half of the smallest range containing 68% of the signal events, which varies from 1.2 GeV to 2.4 GeV.

The parameters of the Crystal Ball and Gaussian functions, and their dependence on the Higgs boson mass, are fixed by fits to simulation samples at discrete mass values to obtain a smooth signal model depending only on the assumed Higgs boson mass and yield. The accuracy of this procedure is checked by fitting the Higgs boson mass in simulated samples with this signal model and is found to be better than 0.01% of the Higgs boson mass.

D. Background modeling and estimation

The background is obtained directly from a fit to the diphoton mass distribution in the data over the range 105–160 GeV after final selection. The procedure used to select

[4] $p_{\mathrm{Tt}} = |(\boldsymbol{p}_{\mathrm{T}}^{\gamma_1} + \boldsymbol{p}_{\mathrm{T}}^{\gamma_2}) \times \hat{\mathbf{t}}|$, where $\hat{\mathbf{t}} = \frac{\boldsymbol{p}_{\mathrm{T}}^{\gamma_1} - \boldsymbol{p}_{\mathrm{T}}^{\gamma_2}}{|\boldsymbol{p}_{\mathrm{T}}^{\gamma_1} - \boldsymbol{p}_{\mathrm{T}}^{\gamma_2}|}$ is the thrust axis in the transverse plane, and $\boldsymbol{p}_{\mathrm{T}}^{\gamma_1}$, $\boldsymbol{p}_{\mathrm{T}}^{\gamma_2}$ are the transverse momenta of the two photons.

the analytical form of the function describing the background shape is explained in more detail in Ref. [17]. Different analytical functions are evaluated using a large simulated background sample composed of diphoton events, photon + jet events (with one jet misidentified as a photon) and dijet events (with both jets misidentified as photons). Signal-plus-background fits are performed on this background-only sample; thus, the fitted signal yield should be zero if the functional form used describes the background shape well. The functional form retained to describe the background is required to have a spurious fitted signal less than 20% of the expected statistical uncertainty in the data or less than 10% of the expected Standard Model signal yield over a wide range of Higgs boson mass hypotheses. The functional form satisfying these criteria with the smallest number of free parameters is used to describe the background shape in the fit of the data. In the four high p_{Tt} categories, an exponential function in mass is used. In the six other categories, the exponential of a second-order polynomial in mass is used.

Table I summarizes the expected signal rate, mass resolution and background in the ten categories for the 7 TeV and 8 TeV data samples. Small differences in mass resolution arise from the differences in the effective constant term measured with $Z \to e^+e^-$ events and from the lower pileup level in the 7 TeV data.

E. Mass measurement method

The mass spectra for the ten data categories and the two center-of-mass energies are fitted simultaneously assuming the signal-plus-background hypothesis, using an unbinned maximum likelihood fit with background and signal parametrization described in the previous sections. The fitted parameters of interest for the signal are the Higgs boson mass and the signal strength, defined as the yield normalized to the SM prediction, and applied to all production modes. Using separate signal strength modifiers for vector boson fusion and gluon fusion production has a negligible impact on the mass measurement compared to the statistical uncertainty. The parameters describing the background mass distributions for each category and center-of-mass energy are also free in the fit. The systematic uncertainties are described by a set of nuisance parameters in the likelihood. They include uncertainties affecting the signal mass peak position, modeled as Gaussian constraints, uncertainties affecting the signal mass resolution and uncertainties affecting the signal yield.

TABLE I. Summary of the expected number of signal events in the 105–160 GeV mass range n_{sig}, the FWHM of mass resolution, σ_{eff} (half of the smallest range containing 68% of the signal events), number of background events b in the smallest mass window containing 90% of the signal (σ_{eff90}), and the ratio s/b and $s/\sqrt{b}$ with s the expected number of signal events in the window containing 90% of signal events, for the $H \to \gamma\gamma$ channel. b is derived from the fit of the data in the 105–160 GeV mass range. The value of m_H is taken to be 126 GeV and the signal yield is assumed to be the expected Standard Model value. The estimates are shown separately for the 7 TeV and 8 TeV data sets and for the inclusive sample as well as for each of the categories used in the analysis.

Category	n_{sig}	FWHM [GeV]	σ_{eff} [GeV]	b in $\pm\sigma_{\mathrm{eff90}}$	s/b [%]	$s/\sqrt{b}$
$\sqrt{s} = 8$ TeV						
Inclusive	402.	3.69	1.67	10670	3.39	3.50
Unconverted central low p_{Tt}	59.3	3.13	1.35	801	6.66	1.88
Unconverted central high p_{Tt}	7.1	2.81	1.21	26.0	24.6	1.26
Unconverted rest low p_{Tt}	96.2	3.49	1.53	2624	3.30	1.69
Unconverted rest high p_{Tt}	10.4	3.11	1.36	93.9	9.95	0.96
Unconverted transition	26.0	4.24	1.86	910	2.57	0.78
Converted central low p_{Tt}	37.2	3.47	1.52	589	5.69	1.38
Converted central high p_{Tt}	4.5	3.07	1.35	20.9	19.4	0.88
Converted rest low p_{Tt}	107.2	4.23	1.88	3834	2.52	1.56
Converted rest high p_{Tt}	11.9	3.71	1.64	144.2	7.44	0.89
Converted transition	42.1	5.31	2.41	1977	1.92	0.85
$\sqrt{s} = 7$ TeV						
Inclusive	73.9	3.38	1.54	1752	3.80	1.59
Unconverted central low p_{Tt}	10.8	2.89	1.24	128	7.55	0.85
Unconverted central high p_{Tt}	1.2	2.59	1.11	3.7	30.0	0.58
Unconverted rest low p_{Tt}	16.5	3.09	1.35	363	4.08	0.78
Unconverted rest high p_{Tt}	1.8	2.78	1.21	13.6	11.6	0.43
Unconverted transition	4.5	3.65	1.61	125	3.21	0.36
Converted central low p_{Tt}	7.1	3.28	1.44	105	6.06	0.62
Converted central high p_{Tt}	0.8	2.87	1.25	3.5	21.6	0.40
Converted rest low p_{Tt}	21.0	3.93	1.75	695	2.72	0.72
Converted rest high p_{Tt}	2.2	3.43	1.51	24.7	7.98	0.40
Converted transition	8.1	4.81	2.23	365	2.00	0.38

Figure 4 shows the result of the simultaneous fit to the data over all categories. For illustration, all categories are summed together, with a weight given by the signal-to-background (s/b) ratio in each category.

F. Systematic uncertainties

The dominant systematic uncertainties on the mass measurement arise from uncertainties on the photon energy scale. These uncertainties, discussed in Sec. II, are propagated to the diphoton mass measurement in each of the ten categories, by modifying the peak of the Crystal Ball function and the average of the Gaussian function describing the signal mass spectrum. The total uncertainty on the mass measurement from the photon energy scale uncertainties ranges from 0.17% to 0.57% depending on the category. The category with the lowest systematic uncertainty is the low p_{Tt} central converted category, for which the energy scale extrapolation from $Z \to e^+e^-$ events is the smallest.

Systematic uncertainties related to the reconstruction of the diphoton primary vertex are investigated using $Z \to e^+e^-$ events reweighted to match the transverse momentum distribution of the Higgs boson and the η distribution of the decay products. The primary vertex is reconstructed using the same technique as for diphoton events, ignoring the tracks associated with the electrons, and treating them as unconverted photons. When this procedure is applied to simulated samples, the efficiency to reconstruct the primary vertex is the same in $Z \to e^+e^-$ events and $H \to \gamma\gamma$ events [17]. The dielectron invariant mass is then computed in the same way as the diphoton invariant mass. Comparing the results of this procedure in data and simulation leads to an uncertainty of 0.03% on the position of the peak of the reconstructed invariant mass.

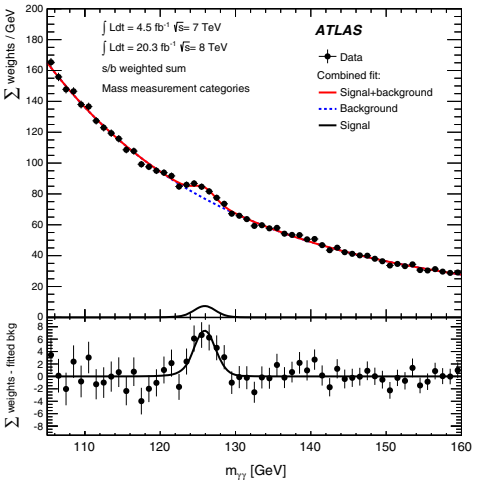

FIG. 4 (color online). Invariant mass distribution in the $H \to \gamma\gamma$ analysis for data (7 TeV and 8 TeV samples combined), showing weighted data points with errors, and the result of the simultaneous fit to all categories. The fitted signal plus background is shown, along with the background-only component of this fit. The different categories are summed together with a weight given by the s/b ratio in each category. The bottom plot shows the difference between the summed weights and the background component of the fit.

Systematic uncertainties related to the modeling of the background are estimated by performing signal-plus-background fits to samples containing large numbers of simulated background events plus the expected signal at various assumed Higgs boson masses. The signal is injected using the same functional form used in the fit, so the fitted Higgs boson mass is sensitive only to the accuracy of the background modeling. The maximum difference between the fitted Higgs boson mass and the input mass over the tested mass range is assigned as a systematic uncertainty on the mass measurement. This uncertainty varies from 0.05% to 0.20% depending on the category. The uncertainties in the different categories are taken as uncorrelated. As a cross-check, to investigate the impact of a background shape in data different than in the large statistics simulated background sample, signal-plus-background pseudo-experiments are generated using a functional form for the background with one more degree of freedom than the nominal background model used in the fit: for the four high p_{Tt} categories, a second-order Bernstein polynomial or the exponential of a second-order polynomial is used; for the six other categories, a third-order Bernstein polynomial is used. The parameters of the functional form used to generate these pseudo-experiments are determined from the data. These pseudo-experiments are then fitted using the nominal background model. This procedure leads to an uncertainty on the mass measurement between 0.01% and 0.05% depending on the category, and smaller than the uncertainties derived from the baseline method using the large sample of simulated background events.

Systematic uncertainties on the diphoton mass resolution due to uncertainties on the energy resolution vary between 9% and 16% depending on the category and have a negligible impact on the mass measurement.

Systematic uncertainties affecting the relative signal yield in each category arise from uncertainties on the photon conversion rate, uncertainties in the proper classification of converted and unconverted photon candidates and uncertainties in the modeling of the transverse momentum of the Higgs boson. These migration systematic uncertainties vary between 3% for the low p_{Tt} categories, dominated by uncertainties on the efficiency for reconstructing photon conversions, and 24% for the gluon fusion production process in the high p_{Tt} categories, dominated by

the uncertainty on the transverse momentum of the Higgs boson. The uncertainty on the transverse momentum of the Higgs boson is estimated by changing the renormalization and factorization scales in the HRes2 [29,30] computation of the Higgs boson transverse momentum distribution as well as the resummation scales associated with t and b quarks. These migration uncertainties have a negligible effect on the mass measurement.

Finally, uncertainties on the predicted overall signal yield are estimated as follows [17]. The uncertainty on the predicted cross section for Higgs boson production is about 10% for the dominant gluon fusion process. The uncertainty on the predicted branching ratio to two photons is 5%. The uncertainty from the photon identification efficiency is derived from studies using several control samples: a sample of radiative Z decays, a sample of $Z \to e^+e^-$ events, where the shower shapes of electrons are corrected to resemble the shower shapes of photons, and a sample of high E_{T} isolated prompt photons. The estimated photon identification uncertainty amounts to 1.0% for the 8 TeV data set, after correcting for small residual differences between simulation and data, and 8.4% for the 7 TeV data set. The uncertainty is larger for the 7 TeV data set because of the stronger correlation of the neural network photon identification with the photon isolation, and because the neural network identification relies more strongly on the correlations between the individual shower shape variables, complicating the measurement and introducing larger uncertainties on the estimate of its performance in data. The uncertainty on the integrated luminosity is 2.8% for the 8 TeV data set and 1.8% for the 7 TeV data set [31]. The uncertainties on the isolation cut efficiency and on the trigger efficiency are less than 1% for both the 7 TeV and 8 TeV data sets. These uncertainties on the overall signal yield also have a negligible effect on the mass measurement.

Table II gives a summary of the systematic uncertainties on the mass measurement for the different categories. For illustration, the 29 sources of uncertainty on the photon energy scale are grouped into seven classes, so the correlations in the uncertainties per class between categories are not 100%.

The total systematic uncertainty on the measured mass is $\pm 0.22\%$, dominated by the uncertainty on the photon energy scale.

G. Result

The measured Higgs boson mass in the $H \to \gamma\gamma$ decay channel is

$$\begin{aligned} m_H &= 125.98 \pm 0.42(\mathrm{stat}) \pm 0.28(\mathrm{syst})\ \mathrm{GeV} \\ &= 125.98 \pm 0.50\ \mathrm{GeV} \end{aligned} \quad (1)$$

where the first error represents the statistical uncertainty and the second the systematic uncertainty. The change in central value compared to the previous result in Ref. [15] of $126.8 \pm 0.2(\mathrm{stat}) \pm 0.7(\mathrm{syst})$ GeV is consistent with the expected change resulting from the updated photon energy scale calibration and its much smaller systematic uncertainty. From the changes in the calibration procedure an average shift of about -0.45 GeV in the measured Higgs boson mass is expected, with an expected statistical spread of about 0.35 GeV from fluctuations in the measured masses of individual events. The average shift between the old and new calibrations is estimated from the distribution of the mass difference of the common events in the mass sidebands outside the signal region.

The mass measurement is performed leaving the overall signal strength free in the fit. The measured signal strength, μ, normalized to the Standard Model expectation is found to be $\mu = 1.29 \pm 0.30$. The most precise results for μ from

TABLE II. Summary of the relative systematic uncertainties (in %) on the $H \to \gamma\gamma$ mass measurement for the different categories described in the text. The first seven rows give the impact of the photon energy scale systematic uncertainties, grouped into seven classes.

	Unconverted					Converted				
	Central		Rest			Central		Rest		
Class	low p_{Tt}	high p_{Tt}	low p_{Tt}	high p_{Tt}	Transition	low p_{Tt}	high p_{Tt}	low p_{Tt}	high p_{Tt}	Transition
$Z \to e^+e^-$ calibration	0.02	0.03	0.04	0.04	0.11	0.02	0.02	0.05	0.05	0.11
LAr cell nonlinearity	0.12	0.19	0.09	0.16	0.39	0.09	0.19	0.06	0.14	0.29
Layer calibration	0.13	0.16	0.11	0.13	0.13	0.07	0.10	0.05	0.07	0.07
ID material	0.06	0.06	0.08	0.08	0.10	0.05	0.05	0.06	0.06	0.06
Other material	0.07	0.08	0.14	0.15	0.35	0.04	0.04	0.07	0.08	0.20
Conversion reconstruction	0.02	0.02	0.03	0.03	0.05	0.03	0.02	0.05	0.04	0.06
Lateral shower shape	0.04	0.04	0.07	0.07	0.06	0.09	0.09	0.18	0.19	0.16
Background modeling	0.10	0.06	0.05	0.11	0.16	0.13	0.06	0.14	0.18	0.20
Vertex measurement					0.03					
Total	0.23	0.28	0.24	0.30	0.59	0.21	0.25	0.27	0.33	0.47

these data are based on an analysis optimized to measure the signal strength [17]. The statistical uncertainties on the mass and signal yield obtained from the data fit are consistent with the expected statistical accuracy in pseudo-experiments generated with this measured signal yield. The average expected statistical uncertainty on the mass for $\mu = 1.3$ is 0.35 GeV and the fraction of pseudo-experiments with a statistical error larger than the one observed in data (0.42 GeV) is about 16%. From these pseudo-experiments, the distribution of fitted masses is compared to the input mass value to verify that the statistical uncertainty from the fit provides 68% coverage. In the previous measurement, the expected statistical uncertainty was about 0.33 GeV for $\mu = 1.55$ and the observed statistical uncertainty (0.24 GeV) was better than expected. The change in expected statistical uncertainty mostly comes from the change in the fitted signal strength, which was slightly larger in the previous measurement, as the statistical uncertainty on the mass measurement is inversely proportional to the signal strength. Changes in the mass resolution and the event categorization also contribute to the change in the expected statistical uncertainty. The increase in the statistical uncertainty between the previous result and this result is consistent with a statistical fluctuation from changes in the measured masses of individual events. Assuming the SM signal yield ($\mu = 1$), the statistical uncertainty on the mass measurement is expected to be 0.45 GeV.

No significant shift in the values of the nuisance parameters associated with the systematic uncertainties is observed in the fit to the data. The result is also stable if a different mass range, 115 GeV to 135 GeV, is used in the fit.

Several cross-checks of the mass measurement are performed, dividing the data into subsamples with different sensitivities to systematic uncertainties. To evaluate the compatibility between the mass measured in a subsample and the combined mass from all other subsamples, a procedure similar to the one used to evaluate the mass compatibility between different channels, described in Sec. VI, is applied. The mass difference Δ_i between the subsample i under test and the combined mass from all other subsamples is added as a parameter in the likelihood, and the value of Δ_i with its uncertainty is extracted from the fit to the data, leaving the combined Higgs boson mass from all other subsamples as a free parameter. With this procedure, the uncertainty on Δ_i correctly accounts for the correlation in systematic uncertainties between the subsample under test and the rest of the data set. The values of Δ_i with their uncertainties are shown in Fig. 5 for three different alternative event categorizations, with three subsamples each: as a function of the conversion status of the two photons, as a function of the number of primary vertices reconstructed in the event and as a function of the photon impact point in the calorimeter (barrel vs end-cap).

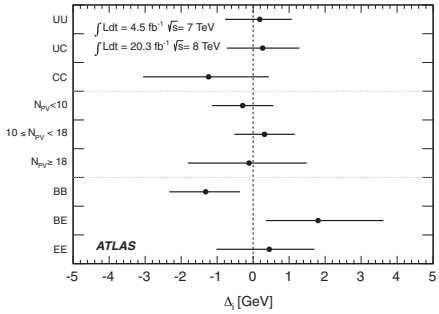

FIG. 5. Difference, Δ_i, between the mass measured in a given $\gamma\gamma$ subsample and the combined $\gamma\gamma$ mass, using three different alternative categorizations to define the subsamples. The top three points show a categorization based on the photon conversion status: UU is the subsample with both photons unconverted, UC the subsample with one converted and one unconverted photon, and CC the subsample with two converted photons. The middle three points show a categorization based on the number of reconstructed primary vertices (N_{PV}) in the event. The bottom three points show a categorization based on the photon impact points on the calorimeter: BB is the subsample with both photons detected in the barrel calorimeter, BE the subsample with one photon in the barrel calorimeter and one photon in the end-cap calorimeter and EE the subsample with both photons in the end-cap calorimeter.

No value of Δ_i inconsistent with zero is found in these checks, or in other categorizations related to the conversion topology, the instantaneous luminosity, the photon isolation and the data taking periods. A similar procedure, fitting simultaneously one Δ_i per subsample, is performed to assess the global consistency of all the different subsamples with a common combined mass. In nine different categorizations, no global inconsistency larger than 1.5σ is observed.

A direct limit on the decay width of the Higgs boson is set from the observed width of the invariant mass peak, under the assumption that there is no interference with background processes. The signal model is extended by convolving the detector resolution with a nonrelativistic Breit-Wigner distribution to model a nonzero decay width. The test statistic used to obtain the limit on the width is a profile likelihood estimator with the width as the main parameter of interest, where the mass and the signal strength of the observed particle are also treated as free parameters. Pseudo-experiments with different assumed widths are performed to estimate the distribution of the test statistic, which does not perfectly follow a χ^2 distribution, and to compute the exclusion level. The observed (expected for $\mu = 1$) 95% confidence level (CL) upper limit on the width is 5.0 (6.2) GeV. For $\mu = 1.3$, the expected upper limit on the width is 4.2 GeV. These limits, properly

calibrated with pseudo-experiments, are about 15% larger than estimates based on a χ^2 distribution of the test statistic.

V. MASS AND WIDTH MEASUREMENT IN THE $H \to ZZ^* \to 4\ell$ CHANNEL

The $H \to ZZ^* \to 4\ell$ channel provides good sensitivity to the measurement of the Higgs properties due to its high signal-to-background ratio, which is about two in the signal mass window 120–130 GeV, and its excellent mass resolution, for each of the four final states: $\mu^+\mu^-\mu^+\mu^-$ (4μ), $e^+e^-\mu^+\mu^-$ ($2e2\mu$), $\mu^+\mu^-e^+e^-$ ($2\mu2e$), and $e^+e^-e^+e^-$ ($4e$), where the first pair is defined to be the one with the dilepton mass closest to the Z boson mass. The typical mass resolution varies from 1.6 GeV for the 4μ final state to 2.2 GeV for the $4e$ final state. For a SM Higgs boson with a mass of about 125 GeV, the dominant background is the $(Z^{(*)}/\gamma^*)(Z^{(*)}/\gamma^*) \to 4\ell$ process, referred to hereafter as ZZ^*. A smaller contribution is expected from the Z + jets and $t\bar{t}$ processes.

Several improvements were introduced in the analysis with respect to Ref. [15]. For the 8 TeV data, the electron identification was changed from a cut-based to a likelihood method, which improves the rejection of light-flavor jets and photon conversions by a factor of 2 for the same signal efficiency [32]. The updated electromagnetic calibration based on multivariate techniques, described in Sec. II, is used for electrons and final-state radiation (FSR) photons. In addition, a new combined fit of the track momentum and cluster energy was introduced. This is applied to electrons with $E_{\mathrm{T}} < 30$ GeV when the track momentum and cluster energy are consistent within their uncertainties, and improves the resolution of the $m_{4\ell}$ invariant mass distribution for the $H \to ZZ^* \to 4e$ and $H \to ZZ^* \to 2\mu2e$ final states by about 4%. Finally, a multivariate discriminant was introduced to separate the signal and ZZ^* background.

The following subsections describe the details of the Higgs mass measurement in the $H \to ZZ^* \to 4\ell$ channel. A more complete discussion of the selection criteria and background determination is reported in Ref. [18].

A. Event selection

Four-lepton events are selected with single-lepton and dilepton triggers. The p_{T} (E_{T}) thresholds for single-muon (single-electron) triggers increased from 18 GeV to 24 GeV (20 GeV to 24 GeV) between the 7 and 8 TeV data sets, due to the increase of the instantaneous luminosity during these two data-taking periods. The dilepton triggers include dimuon, dielectron and mixed electron and muon topologies, and have thresholds starting at 6 GeV (10 GeV) for muons (electrons) for 7 TeV data. For the 8 TeV data, the dilepton trigger thresholds were raised to 13 GeV for the dimuon and to 12 GeV for the dielectron. In addition, for the 8 TeV data, an asymmetric threshold of (8,18) GeV was added for the dimuon trigger. The trigger efficiency for Higgs boson signal events passing the final selection is greater than 97% for the 4μ, $2e2\mu$ and $2\mu2e$ channels and close to 100% for the $4e$ channel.

For the 7 TeV data, electrons are required to satisfy a cut-based selection using tracking and shower profile criteria [33]. The 8 TeV data have an improved electron reconstruction algorithm with higher efficiency, and the likelihood-based electron identification with improved background rejection mentioned above. The four types of muons described in Sec. III are allowed with at most one standalone or calorimeter-tagged muon per event. Muon tracks are required to have a minimum number of hits in the ID, or hits in all muon stations for standalone muons.

Higgs boson candidates are formed by selecting two same-flavor, opposite-sign lepton pairs (a lepton quadruplet) in an event. Each lepton is required to have a longitudinal impact parameter less than 10 mm with respect to the primary vertex, defined as the primary vertex with the largest $\sum p_{\mathrm{T}}^2$, and muons are required to have a transverse impact parameter less than 1 mm to reject cosmic-ray muons. Each muon (electron) must satisfy $p_{\mathrm{T}} > 6$ GeV ($E_{\mathrm{T}} > 7$ GeV) and be measured in the pseudorapidity range $|\eta| < 2.7$ ($|\eta| < 2.47$). The highest p_{T} lepton in the quadruplet must satisfy $p_{\mathrm{T}} > 20$ GeV, and the second (third) lepton in p_{T} order must satisfy $p_{\mathrm{T}} > 15$ GeV ($p_{\mathrm{T}} > 10$ GeV). The leptons are required to be separated from each other by $\Delta R > 0.1$ (0.2) for the same (different) flavor. Each event is required to have the triggering lepton(s) matched to one or two of the selected leptons.

Multiple quadruplets within a single event are possible: for four muons or electrons there are two ways to pair the leptons, and for five or more leptons there are multiple ways to choose the leptons. Quadruplet selection is done separately in each channel: 4μ, $2e2\mu$, $2\mu2e$, $4e$, keeping only a single quadruplet per channel. For each channel, the lepton pair with the mass closest to the Z boson mass is selected as the leading dilepton pair and its invariant mass m_{12} is required to be between 50 GeV and 106 GeV. The second, subleading, pair of each channel is chosen as the pair with its invariant mass m_{34} closest to the Z mass, and also satisfying $m_{\mathrm{min}} < m_{34} < 115$ GeV. Here m_{min} takes the value of 12 GeV for $m_{4\ell} < 140$ GeV, increases linearly between 12 and 50 GeV for $140 < m_{4\ell} < 190$ GeV, and is 50 GeV for $m_{4\ell} > 190$ GeV. Finally, if the event contains a quadruplet passing the selection in more than one channel, the quadruplet from the channel with the highest expected rate is taken; i.e., the first is taken from the order: 4μ, $2e2\mu$, $2\mu2e$, $4e$.

The Z + jets and $t\bar{t}$ background contributions are further reduced by applying impact parameter and track- and calorimeter-based isolation requirements to the leptons. The impact parameter significance, $|d_0|/\sigma_{d_0}$, for all muons (electrons) is required to be less than 3.5 (6.5). The normalized track isolation discriminant, defined as the sum of the transverse momenta of tracks inside a cone

of size $\Delta R = 0.2$ around the lepton, excluding the lepton track, divided by the lepton p_{T}, is required to be smaller than 0.15. The normalized calorimetric isolation is computed from the energy in the electromagnetic and hadronic calorimeters within a cone of $\Delta R < 0.2$ around the lepton, excluding the cells containing the lepton energy. This energy is corrected, event by event, for the ambient energy deposition in the event from pileup as well as for the underlying event, and then divided by the lepton p_{T}. The normalized calorimetric isolation is required to be smaller than 0.2 (0.3) for electrons in the 7 TeV (8 TeV) data, and smaller than 0.3 for muons (0.15 for standalone muons).

The effect of photon emission from FSR on the reconstructed invariant mass is well modeled in the simulation. In addition, some FSR recovery is performed allowing at most one photon to be added per event. Leading dimuon candidates with m_{12} in the range 66–89 GeV, below the Z boson mass, are corrected for collinear FSR by including in the invariant mass any reconstructed photon lying close to one of the muon tracks, as long as the corrected mass $m_{\mu\mu\gamma}$ remains below 100 GeV. In a second step, for events without collinear FSR, noncollinear FSR photons with a significant E_{T} are included for both the leading dimuon and dielectron candidates, an improvement introduced since Ref. [15]. The expected number of events with a collinear or noncollinear FSR correction is 4% and 1%, respectively. Full details are discussed in Ref. [18].

For the 8 TeV data, the combined signal reconstruction and selection efficiency for $m_H = 125$ GeV is 39% for the 4μ channel, 27% for the $2e2\mu/2\mu2e$ channel and 20% for the $4e$ channel.

Finally, a kinematic fit is used to constrain the mass of the leading lepton pair to the Z pole mass within the experimental resolution, including any FSR photon, as in the analysis of Ref. [15]. This improves the $m_{4\ell}$ resolution by about 15%.

B. Background estimation

The ZZ^* background is estimated from simulation and normalized to NLO calculations [34]. The reducible $Z+$ jets and $t\bar{t}$ backgrounds are estimated with data-driven methods, separately for the two final states with subleading muons, $\ell\ell+\mu\mu$, and the two final states with subleading electrons, $\ell\ell+ee$. For the $\ell\ell+\mu\mu$ reducible background, the $Z+$ jets background mostly consists of $Z+b\bar{b}$ events with heavy-flavor semileptonic decays and, to a lesser extent, π/K in-flight decays. The $Z+$ jets and $t\bar{t}$ backgrounds can be distinguished in the m_{12} distribution where the former background peaks at the Z boson mass, and the latter has a broad distribution. Four control regions, with relaxed impact parameter and isolation selection on the subleading muons, are fit simultaneously to extract the different components of the reducible background. The four control regions are defined by the following: at least one subleading muon with inverted impact parameter significance to enhance the heavy-flavor contribution, at least one subleading muon with inverted isolation significance to enhance the π/K in-flight decays, same-sign subleading muons to include all contributions, and finally a leading $e\mu$ pair with either a same-sign or an opposite-sign subleading muon pair, which removes the $Z+$ jets contribution. The fitted yields in the control regions are extrapolated to the signal region using efficiencies obtained from simulation. A small contribution from WZ decays is estimated using simulation.

The electron background contributing to the $\ell\ell+ee$ final states arises mainly from jets misidentified as electrons, occurring in three ways: light-flavor hadrons misidentified as electrons, photon conversions reconstructed as electrons, and nonisolated electrons from heavy-flavor hadronic decays. The electron background is evaluated by three data-driven methods where the selection is relaxed or inverted for one or two of the subleading electrons. The final estimate is obtained using a "$3\ell+X$" control region, and the other methods, which are used as cross-checks, are described in Ref. [18]. The $3\ell+X$ control region requires the three highest p_{T} leptons (3ℓ) to satisfy the full selection, with the third ℓ an electron, and the remaining electron (X) to have the electron identification fully relaxed except for the requirement on the number of hits in the silicon tracker—at least seven silicon hits with at least one in the pixel detector. In addition, the X is required to have the same sign as the other subleading electron to minimize the contribution from the ZZ^* background. The yields of the background components of X are extracted with a fit to the number of hits in the first pixel layer (B layer) and the high-threshold to low-threshold TRT hit ratio. Most photons have no B-layer hit, and the TRT threshold distinguishes between the hadrons misidentified as electrons and the photon-conversion and heavy-flavor electrons. The fitted yields in the control region are extrapolated to the signal region using efficiencies obtained from a large sample of Z bosons produced with a single additional electron candidate satisfying the relaxed selection.

To evaluate the background in the signal region, the $m_{4\ell}$ shape is evaluated using simulated events for the $\ell\ell+\mu\mu$ final states and with data using the $3\ell+X$ method for the $\ell\ell+ee$ final states. The estimates for the ZZ^* and the reducible backgrounds in the $120 < m_{4\ell} < 130$ GeV mass window are provided in Table III.

C. Multivariate discriminant

The multivariate discriminant used to reduce the impact of the ZZ^* background on the fitted mass is based on a boosted decision tree (BDT) [35]. The BDT classifier (BDT_{ZZ^*}) is trained using simulated signal events generated with $m_H = 125$ GeV and simulated ZZ^* background events that pass the event selection and have $115 < m_{4\ell} < 130$ GeV, the mass window that contains over 95% of the signal. The variables used in the training

are the transverse momentum and the pseudorapidity of the four-lepton system, plus a matrix-element-based kinematic discriminant (D_{ZZ^*}) defined as

$$D_{ZZ^*} = \ln\left(\frac{|\mathcal{M}_{\rm sig}|^2}{|\mathcal{M}_{ZZ}|^2}\right), \quad (2)$$

where $\mathcal{M}_{\rm sig}$ and $\mathcal{M}_{ZZ}$ are the matrix elements for the signal and ZZ^* background processes, respectively, computed at leading order using MadGraph [36].

D. Signal and background model

Several methods are used to measure the Higgs boson mass in the $H \to ZZ^* \to 4\ell$ decay channel. The two-dimensional (2D) fit to $m_{4\ell}$ and the BDT_{ZZ^*} output ($O_{\mathrm{BDT}_{ZZ^*}}$) is chosen as the baseline because it has the smallest expected uncertainty among the different methods. The one-dimensional (1D) fit to the $m_{4\ell}$ spectra used for the previous measurement [15] serves as a cross-check. For both the 1D and 2D fits, the signal model is based on simulation distributions that are smoothed using a kernel density estimation method [37]. These distributions are generated at 15 different m_H values in the range $115 < m_H < 130$ GeV and form templates that are parametrized as a function of m_H using B-spline interpolation [38]. These simulation samples at different masses are normalized to the expected SM cross section times branching ratio [10] to derive the expected signal yields after acceptance and selection. For all of the methods, the $m_{4\ell}$ range used for the fit is 110 GeV to 140 GeV.

The signal probability density function (PDF) in the 2D fit is modeled as

$$\begin{aligned}\mathcal{P}(m_{4\ell}, O_{\mathrm{BDT}_{ZZ^*}}|m_H) &= \mathcal{P}(m_{4\ell}|O_{\mathrm{BDT}_{ZZ^*}}, m_H)\mathcal{P}(O_{\mathrm{BDT}_{ZZ^*}}|m_H) \\ &\simeq \left(\sum_{n=1}^{4}\mathcal{P}_n(m_{4\ell}|m_H)\theta_n(O_{\mathrm{BDT}_{ZZ^*}})\right)\mathcal{P}(O_{\mathrm{BDT}_{ZZ^*}}|m_H) \quad (3)\end{aligned}$$

where θ_n defines four equal-sized bins for the value of the BDT_{ZZ^*} output, and $\mathcal{P}_n$ represents the 1D PDF for $m_{4\ell}$ for the signal in the corresponding $O_{\mathrm{BDT}_{ZZ^*}}$ bin. The variation of the $m_{4\ell}$ shape within a single $O_{\mathrm{BDT}_{ZZ^*}}$ bin is found to be negligible, and studies indicate that the binning approximation does not bias the mass measurement. The background model, $\mathcal{P}_{\rm bkg}(m_{4\ell}, O_{\mathrm{BDT}_{ZZ^*}})$, is described using a full 2D PDF that is derived from simulation for the ZZ^* background, and by using data-driven techniques for the reducible background. The 2D template fit method reduces the expected statistical error on the measured mass with respect to the simple fit to the $m_{4\ell}$ spectra (1D method) by about 8%.

Extensive studies were performed in order to validate the signal and background PDFs using a 2D fit to fully simulated signal and background events normalized to the SM expectation. No bias was found between the input and resulting 2D fit values for the Higgs mass and signal strength, tested for different m_H values in the range 120 GeV to 130 GeV. Different values for the parameter used to control the amount of smoothing for both the signal and background PDFs were tested and no biases on the fitted m_H and signal strength were found. An additional check for a possible bias due to a small dependence of the BDT_{ZZ^*} output on m_H for the signal, included in Eq. (3), is performed by fitting a sample of background-only simulated data. No dependence of the likelihood scan on m_H was observed.

In addition to the 2D fit method, described above, and the 1D fit method used in Ref. [15], a third approach is used. This approach combines an analytic description of the signal mass spectra with the BDT_{ZZ^*} output and can be used both for the mass measurement and to provide a direct limit on the width of the Higgs boson. In this method, the signal $m_{4\ell}$ PDF is computed event by event by convolving the estimated detector response for each of the four leptons with the nonrelativistic Breit-Wigner function describing the generated Higgs mass line shape. The advantage of this method is that the typical detector response for each data candidate is taken into account in the signal modeling. This is referred to as the per-event-error method. In this fit the Z mass constraint is not applied. The muon and electron response functions are modeled by the sum of two or three Gaussian distributions, respectively, to provide a better description of the responses. This parametrization is performed in bins of η and $p_{\rm T}$. These response functions are validated with several simulation samples and with data. One validation consists of comparing the Z boson mass distribution measured in collision data with the convolution of the generator-level Z boson resonance with the detector response, constructed using the single-lepton response. The ratio of the two distributions agrees to better than 2% for $Z \to \mu\mu$ and 5% for $Z \to ee$. In addition, the per-event-error model is checked by fitting the four-lepton invariant mass from the Z decay in the $Z \to 4\ell$ process. The fit results are in agreement with the world average values of the Z boson mass and width [39]. The per-event-error fit is used both as a cross-check for the mass measurement and as the baseline method to set an upper limit on the Higgs boson total width Γ_H.

For the mass measurement, the $m_{4\ell}$ (and $O_{\mathrm{BDT}_{ZZ^*}}$) data distributions for eight sets of events, one for each final state for the 7 TeV and 8 TeV data, are simultaneously fitted using an unbinned maximum likelihood assuming the signal and background models described above. The backgrounds are set in the fit to their estimated values, and the associated normalization and shape uncertainties are treated as nuisance parameters, as discussed in Sec. VI.

E. Systematic uncertainties

The main sources of systematic uncertainties on the mass measurement are the electron energy scale and the muon momentum scale. The expected impact of these uncertainties on the mass measurement corresponds to about 60 MeV for both the $4e$ and the 4μ channels, obtained from the 2D fit to simulation. When all the final states are combined together, this translates to an observed $\pm 0.03\%$ uncertainty on m_H for both the electron energy scale and the muon momentum scale.

Systematic uncertainties on the measurement of the inclusive signal rate are also included in the model. The uncertainty on the inclusive signal strength due to the identification and reconstruction efficiency for muons and electrons is $\pm 2\%$. The dominant theory systematic uncertainties arise from QCD scale variations of the $gg \to H$ process ($\pm 7\%$), parton distribution function variations ($\pm 6\%$) and the decay branching ratio ($\pm 4\%$). The uncertainty on the Higgs boson transverse momentum, evaluated as described in Sec. IV F, has a negligible impact on the mass and the inclusive signal rate measurements. The uncertainty on the integrated luminosity is given in Sec. IV F, and it has a negligible impact on the mass measurement.

F. Results

Figure 6(a) shows the $m_{4\ell}$ distribution of the selected candidates for 7 TeV and 8 TeV collision data along with the expected distributions for a signal with a mass of 124.5 GeV and the ZZ^* and reducible backgrounds. The expected signal is normalized to the measured signal strength, given below. Figure 6(b) shows the BDT_{ZZ^*} output versus $m_{4\ell}$ for the selected candidates in the $m_{4\ell}$ range 110–140 GeV. The compatibility of the data with the expectations shown in Fig. 6(b) has been checked using pseudo-experiments generated according to the expected two-dimensional distributions and good agreement has been found. Table III presents the observed and expected number of events for $\sqrt{s} = 7$ TeV and $\sqrt{s} = 8$ TeV, in a mass window of 120–130 GeV, corresponding to about $\pm 2\sigma_{m_{4\ell}}$.

The measured Higgs boson mass in the $H \to ZZ^* \to 4\ell$ decay channel obtained with the baseline 2D method is

$$\begin{aligned} m_H &= 124.51 \pm 0.52(\mathrm{stat}) \pm 0.06(\mathrm{syst})\ \mathrm{GeV} \\ &= 124.51 \pm 0.52\ \mathrm{GeV} \end{aligned} \quad (4)$$

where the first error represents the statistical uncertainty and the second the systematic uncertainty. The systematic uncertainty is obtained from the quadrature subtraction of the fit uncertainty evaluated with and without the systematic uncertainties fixed at their best-fit values. Due to the large difference between the magnitude of the statistical and systematic uncertainties, the numerical precision on the quadrature subtraction is estimated to be of the order of 10 MeV. The measured signal strength for this inclusive selection is $\mu = 1.66^{+0.45}_{-0.38}$, consistent with the SM expectation of 1. The most precise results for μ from these data are

TABLE III. The number of events expected and observed for a $m_H = 125$ GeV hypothesis for the four-lepton final states. The second column shows the number of expected signal events for the full mass range. The other columns show the number of expected signal events, the number of ZZ^* and reducible background events, and the signal-to-background ratio (s/b), together with the numbers of observed events, in a window of $120 < m_{4\ell} < 130$ GeV for 4.5 fb^{-1} at $\sqrt{s} = 7$ TeV and 20.3 fb^{-1} at $\sqrt{s} = 8$ TeV as well as for the combined sample.

Final state	Signal Full mass range	Signal	ZZ^*	$Z+$jets, $t\bar{t}$	s/b	Expected	Observed
$\sqrt{s} = 7$ TeV							
4μ	1.00 ± 0.10	0.91 ± 0.09	0.46 ± 0.02	0.10 ± 0.04	1.7	1.47 ± 0.10	2
$2e2\mu$	0.66 ± 0.06	0.58 ± 0.06	0.32 ± 0.02	0.09 ± 0.03	1.5	0.99 ± 0.07	2
$2\mu 2e$	0.50 ± 0.05	0.44 ± 0.04	0.21 ± 0.01	0.36 ± 0.08	0.8	1.01 ± 0.09	1
$4e$	0.46 ± 0.05	0.39 ± 0.04	0.19 ± 0.01	0.40 ± 0.09	0.7	0.98 ± 0.10	1
Total	2.62 ± 0.26	2.32 ± 0.23	1.17 ± 0.06	0.96 ± 0.18	1.1	4.45 ± 0.30	6
$\sqrt{s} = 8$ TeV							
4μ	5.80 ± 0.57	5.28 ± 0.52	2.36 ± 0.12	0.69 ± 0.13	1.7	8.33 ± 0.6	12
$2e2\mu$	3.92 ± 0.39	3.45 ± 0.34	1.67 ± 0.08	0.60 ± 0.10	1.5	5.72 ± 0.37	7
$2\mu 2e$	3.06 ± 0.31	2.71 ± 0.28	1.17 ± 0.07	0.36 ± 0.08	1.8	4.23 ± 0.30	5
$4e$	2.79 ± 0.29	2.38 ± 0.25	1.03 ± 0.07	0.35 ± 0.07	1.7	3.77 ± 0.27	7
Total	15.6 ± 1.6	13.8 ± 1.4	6.24 ± 0.34	2.00 ± 0.28	1.7	22.1 ± 1.5	31
$\sqrt{s} = 7$ TeV and $\sqrt{s} = 8$ TeV							
4μ	6.80 ± 0.67	6.20 ± 0.61	2.82 ± 0.14	0.79 ± 0.13	1.7	9.81 ± 0.64	14
$2e2\mu$	4.58 ± 0.45	4.04 ± 0.40	1.99 ± 0.10	0.69 ± 0.11	1.5	6.72 ± 0.42	9
$2\mu 2e$	3.56 ± 0.36	3.15 ± 0.32	1.38 ± 0.08	0.72 ± 0.12	1.5	5.24 ± 0.35	6
$4e$	3.25 ± 0.34	2.77 ± 0.29	1.22 ± 0.08	0.76 ± 0.11	1.4	4.75 ± 0.32	8
Total	18.2 ± 1.8	16.2 ± 1.6	7.41 ± 0.40	2.95 ± 0.33	1.6	26.5 ± 1.7	37

based on an analysis optimized to measure the signal strength [18]. The expected statistical uncertainty for the 2D fit with the observed μ value of 1.66 is 0.49 GeV, close to the observed statistical uncertainty. With the improved uncertainties on the electron and muon energy scales, the mass uncertainty given above is predominantly statistical with a nearly negligible contribution from systematic uncertainties. The mass measurement performed with the 1D model gives $m_H = 124.63 \pm 0.54$ GeV, consistent with the 2D result where the expected difference has a root mean square (RMS) of 250 MeV estimated from Monte Carlo pseudo-experiments. These measurements can be compared to the previously reported result [15] of $124.3^{+0.6}_{-0.5}(\text{stat})^{+0.5}_{-0.3}(\text{syst})$ GeV, which was obtained using the 1D model. The difference between the measured values arises primarily from the changes to the channels with electrons—the new calibration and resolution model, the introduction of the combined track momentum and cluster energy fit, and the improved identification, as well as the recovery of noncollinear FSR photons, which affects all channels. In the 120–130 GeV mass window, there are four new events and one missing event as compared to Ref. [15]. Finally, as a third cross-check, the measured mass obtained with the per-event-error method is within 60 MeV of the value found with the 2D method.

Figure 7 shows the scan of the profile likelihood, $-2\ln\Lambda(m_H)$, for the 2D model as a function of the mass of the Higgs boson for the four final states, as well as for all of the channels combined. The signal strength and all the nuisance parameters are profiled (allowed to float to the values that maximize the likelihood) in the scan. The compatibility among the mass measurements from the four final states is estimated to be about 20% using a χ^2 test.

Using the per-event-error method a direct limit on the total width of the Higgs boson of $\Gamma_H < 2.6$ GeV at

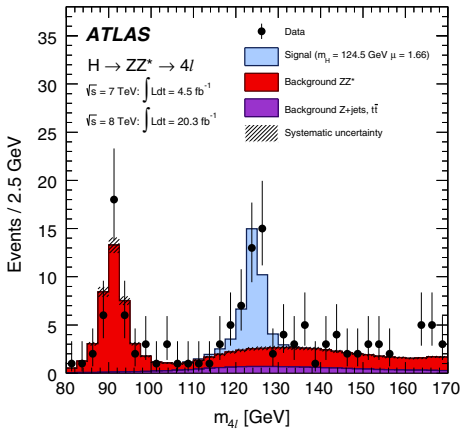

FIG. 6 (color online). (a) Distribution of the four-lepton invariant mass for the selected candidates in the $m_{4\ell}$ range 80–170 GeV for the combined 7 TeV and 8 TeV data samples. Superimposed are the expected distributions of a SM Higgs boson signal for $m_H = 124.5$ GeV normalized to the measured signal strength, as well as the expected ZZ^* and reducible backgrounds. (b) Distribution of the BDT_{ZZ^*} output versus $m_{4\ell}$ for the selected candidates in the 110–140 GeV $m_{4\ell}$ range for the combined 7 TeV and 8 TeV data samples. The expected distribution for a SM Higgs with $m_H = 124.5$ GeV is indicated by the size of the blue boxes, and the total background is indicated by the intensity of the red shading.

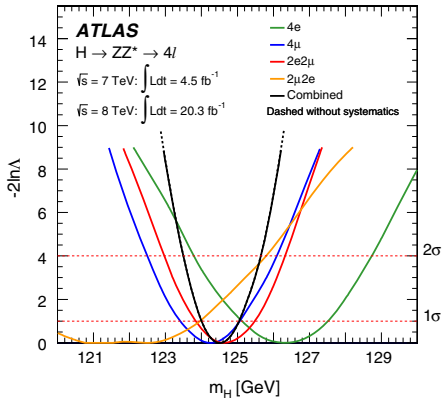

FIG. 7 (color online). The profile likelihood as a function of m_H for the combination of all $H \to ZZ^* \to 4\ell$ channels and for the individual channels for the combined 7 TeV and 8 TeV data samples. The combined result is shown both with (solid line) and without (dashed line) systematic uncertainties, and the two results are almost indistinguishable.

95% CL is obtained. The expected limit is $\Gamma_H < 6.2$ GeV at 95% CL for a signal at the SM rate and $\Gamma_H < 3.5$ GeV at 95% CL for the observed signal rate. The difference between the observed and expected results arises from the higher signal strength observed in the data, as well as from the measured $m_{4\ell}$, $O_{\mathrm{BDT}_{ZZ^*}}$ and mass resolution values for the selected candidate events. These limits are estimated under the asymptotic assumption, described in Sec. VI, and a cross-check with Monte Carlo ensemble tests provides consistent results. The limit on the total width was cross-checked with a 2D fit using signal templates parametrized as a function of the Higgs boson width and found to be in agreement.

VI. STATISTICAL PROCEDURE AND TREATMENT OF SYSTEMATIC UNCERTAINTIES

The statistical treatment of the data is described in Refs. [40–44]. Confidence intervals are based on the profile likelihood ratio $\Lambda(\boldsymbol{\alpha})$ [45]. The latter depends on one or more parameters of interest $\boldsymbol{\alpha}$, such as the Higgs boson mass m_H or production yields normalized to the SM expectation μ, as well as on the nuisance parameters $\boldsymbol{\theta}$:

$$\Lambda(\boldsymbol{\alpha}) = \frac{L(\boldsymbol{\alpha}, \hat{\hat{\boldsymbol{\theta}}}(\boldsymbol{\alpha}))}{L(\hat{\boldsymbol{\alpha}}, \hat{\boldsymbol{\theta}})}. \quad (5)$$

The likelihood functions in the numerator and denominator of the above equation are built using sums of signal and background PDFs in the discriminating variables, such as the $\gamma\gamma$ mass spectra for the $H \to \gamma\gamma$ channel and the $m_{4\ell}$ and BDT_{ZZ^*} output distributions for the $H \to ZZ^* \to 4\ell$ channel. The PDFs are derived from simulation for the signal and from both data and simulation for the background, as described in Secs. IV and V. Likelihood fits to the observed data are carried out for the parameters of interest. The vector $\hat{\boldsymbol{\theta}}$ denotes the unconditional maximum likelihood estimate of the parameter values, and $\hat{\hat{\boldsymbol{\theta}}}$ denotes the conditional maximum likelihood estimate for given fixed values of the parameters of interest $\boldsymbol{\alpha}$. Systematic uncertainties and their correlations [40] are modeled by introducing nuisance parameters $\boldsymbol{\theta}$ described by likelihood functions associated with the estimate of the corresponding effect. The choice of the parameters of interest depends on the test under consideration, with the remaining parameters treated as nuisance parameters, i.e., set to the values that maximize the likelihood function ("profiled") for the given fixed values of the parameters of interest.

For the combined mass measurement, hypothesized values of m_H are tested using the profile likelihood ratio defined in terms of m_H and treating $\mu_{\gamma\gamma}(m_H)$ and $\mu_{4\ell}(m_H)$ as independent nuisance parameters, so as to avoid making any assumptions about the Higgs boson couplings:

$$\Lambda(m_H) = \frac{L(m_H, \hat{\hat{\mu}}_{\gamma\gamma}(m_H), \hat{\hat{\mu}}_{4\ell}(m_H), \hat{\hat{\boldsymbol{\theta}}}(m_H))}{L(\hat{m}_H, \hat{\mu}_{\gamma\gamma}, \hat{\mu}_{4\ell}, \hat{\boldsymbol{\theta}})}. \quad (6)$$

The leading source of systematic uncertainty on the mass measurement comes from the energy and momentum scale uncertainties on the main physics objects used in the two analyses, namely, photons for the $H \to \gamma\gamma$ and muons and electrons for the $H \to ZZ^* \to 4\ell$ final state. They are detailed in Secs. II and III. The correlation between the two measurements stems from common systematic uncertainties and is modeled in the combination by correlating the corresponding nuisance parameters. For the mass measurement this correlation comes mainly from the uncertainty on the energy scale calibration with $Z \to e^+e^-$ events, which affects both the electron and photon energy scale uncertainties. This source of uncertainty is greatly reduced with respect to the previous publication and has a small impact on the total mass uncertainty for both channels. For this reason, the correlation between the two measurements is now almost negligible.

To directly quantify the level of consistency between the measurements of $m_H^{\gamma\gamma}$ and $m_H^{4\ell}$, the profile likelihood used for the mass combination is parametrized as a function of the difference in measured mass values $\Delta m_H = m_H^{\gamma\gamma} - m_H^{4\ell}$, with the common mass m_H profiled in the fit. Specifically, the observable $m_H^{4\ell}$ is fit to the parameter m_H while the observable $m_H^{\gamma\gamma}$ is fit to the parameter $m_H + \Delta m_H$. The two measurements are compatible if the fitted value of Δm_H is compatible with zero. The original model used to combine the two measurements is recovered by fixing the parameter Δm_H to zero.

The signal strengths $\mu_{\gamma\gamma}$ and $\mu_{4\ell}$ are treated as independent nuisance parameters in this approach, as is the common mass m_H. The variation of $-2\ln\Lambda(\Delta m_H)$ between its minimum and the $\Delta m_H = 0$ point is used as an estimate of the compatibility of the two masses, with all other fit parameters profiled to the data. This result relies on the assumption that the statistical observable $-2\ln\Lambda$ behaves as a χ^2 distribution with 1 degree of freedom, referred to as the asymptotic assumption. This result is also cross-checked with Monte Carlo ensemble tests that do not rely on this assumption. All sources of energy and momentum scale systematic uncertainty are treated assuming Gaussian PDFs.

VII. COMBINED MASS MEASUREMENT

The measured masses from the $H \to \gamma\gamma$ and $H \to ZZ^* \to 4\ell$ channels reported in Secs. IV and V are combined following the method described in Sec. VI. For the $H \to ZZ^* \to 4\ell$ channel the 2D method discussed in Sec. V is used. The combined mass measurement is

$$\begin{aligned} m_H &= 125.36 \pm 0.37(\mathrm{stat}) \pm 0.18(\mathrm{syst})\ \mathrm{GeV} \\ &= 125.36 \pm 0.41\ \mathrm{GeV} \end{aligned} \quad (7)$$

where the first error represents the statistical uncertainty and the second the systematic uncertainty. The statistical component is determined by repeating the likelihood scan with all nuisance parameters related to systematic uncertainty fixed to their best-fit value. The systematic component is then derived by subtracting in quadrature the statistical one from the total error. The $-2\ln\Lambda$ value as a function of m_H for the individual $H \to \gamma\gamma$ and $H \to ZZ^* \to 4\ell$ channels and their combination is shown in Fig. 8.

With respect to the previously published value [15] of $m_H = 125.49 \pm 0.24(\text{stat})^{+0.50}_{-0.58}(\text{syst})$ GeV, the observed statistical error has increased. This is due to the increase of the observed statistical error in the $H \to \gamma\gamma$ channel as discussed in Sec. IV G. The systematic uncertainty is significantly reduced thanks to the improvements in the calibration of the photons and electrons and the reduction in the uncertainty on the muon momentum scale, as detailed in Secs. II and III, respectively.

In order to check that the fitted signal yield is not significantly correlated with the measured mass, the profile likelihood ratio as a function of both m_H and the normalized signal yield S, $\Lambda(S, m_H)$ is used. The normalized signal yield is defined as $S = \sigma/\sigma_{\text{SM}}(m_H = 125.36\ \text{GeV})$. It is similar to the signal strength $\mu = \sigma/\sigma_{\text{SM}}(m_H)$, except the m_H dependence of the expected SM cross sections and branching ratios that enter into the denominator, principally for the $H \to ZZ^* \to 4\ell$ channel, is removed by fixing m_H to the combined best-fit mass. Asymptotically, the test statistic $-2\ln\Lambda(S, m_H)$ is distributed as a χ^2 distribution with 2 degrees of freedom. The resulting 68% and 95% CL contours are shown in Fig. 9. No significant correlation between the two fitted variables is observed, confirming the model independence of the mass measurement described in this paper.

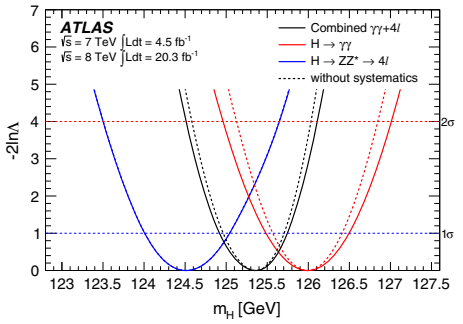

FIG. 8 (color online). Value of $-2\ln\Lambda$ as a function of m_H for the individual $H \to \gamma\gamma$ and $H \to ZZ^* \to 4\ell$ channels and their combination, where the signal strengths $\mu_{\gamma\gamma}$ and $\mu_{4\ell}$ are allowed to vary independently. The dashed lines show the statistical component of the mass measurements. For the $H \to ZZ^* \to 4\ell$ channel, this is indistinguishable from the solid line that includes the systematic uncertainties.

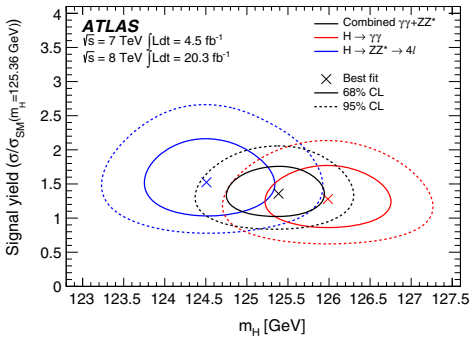

FIG. 9 (color online). Likelihood contours $-2\ln\Lambda(S, m_H)$ as a function of the normalized signal yield $S = \sigma/\sigma_{\text{SM}}(m_H = 125.36\ \text{GeV})$ and m_H for the $H \to \gamma\gamma$ and $H \to ZZ^* \to 4\ell$ channels and their combination, including all systematic uncertainties. For the combined contour, a common normalized signal yield S is used. The markers indicate the maximum likelihood estimates in the corresponding channels.

As a cross-check, the mass combination was repeated by fixing the values of the two signal strengths to the SM expectation $\mu = 1$. The mass measurement only changes by 80 MeV, demonstrating that the combined mass measurement is quite insensitive to the fitted values of the individual channel signal strengths.

The contributions of the main sources of systematic uncertainty to the combined mass measurement are shown in Table IV. In the mass measurement fit, the post-fit values of the most relevant nuisance parameters, which are related to the photon energy scale, do not show significant deviations from their pre-fit input values.

In order to assess the compatibility of the mass measurements from the two channels, a dedicated test statistic that takes into account correlations between the two measurements is used, as described in Sec. VI. A value of

$$\begin{aligned}\Delta m_H &= 1.47 \pm 0.67(\text{stat}) \pm 0.28(\text{syst})\ \text{GeV} \\ &= 1.47 \pm 0.72\ \text{GeV}\end{aligned} \tag{8}$$

is derived. From the value of $-2\ln\Lambda$ at $\Delta m_H = 0$, a compatibility of 4.8%, equivalent to 1.98σ, is estimated under the asymptotic assumption. This probability was cross-checked using Monte Carlo ensemble tests. With this approach a compatibility of 4.9% is obtained, corresponding to 1.97σ.

As an additional cross-check, some of the systematic uncertainties related to the photon energy scale, namely, the inner detector material uncertainty and the uncertainty in the modeling of the photon lateral leakage, were modeled

TABLE IV. Principal systematic uncertainties on the combined mass. Each uncertainty is determined from the change in the 68% CL range for m_H when the corresponding nuisance parameter is removed (fixed to its best-fit value), and it is calculated by subtracting this reduced uncertainty from the original uncertainty in quadrature.

Systematic	Uncertainty on m_H [MeV]
LAr syst on material before presampler (barrel)	70
LAr syst on material after presampler (barrel)	20
LAr cell nonlinearity (layer 2)	60
LAr cell nonlinearity (layer 1)	30
LAr layer calibration (barrel)	50
Lateral shower shape (conv)	50
Lateral shower shape (unconv)	40
Presampler energy scale (barrel)	20
ID material model ($\lvert\eta\rvert < 1.1$)	50
$H \to \gamma\gamma$ background model (unconv rest low $p_{\mathrm{T}t}$)	40
$Z \to ee$ calibration	50
Primary vertex effect on mass scale	20
Muon momentum scale	10
Remaining systematic uncertainties	70
Total	180

using a "boxlike" PDF defined as a double Fermi-Dirac function. This choice is compatible with the fact that for these uncertainties the data do not suggest a preferred value within the systematic error range. In this case the compatibility between the two masses increases to 7.5%, equivalent to 1.8σ. The compatibility between the two measurements increases to 11% (1.6σ) if the two signal strengths are set to the SM value of 1, instead of being treated as free parameters.

With respect to the value published in Ref. [15], the compatibility between the measurements from the individual channels has changed from 2.5σ to 2.0σ.

VIII. CONCLUSIONS

An improved measurement of the mass of the Higgs boson has been derived from a combined fit to the invariant mass spectra of the decay channels $H \to \gamma\gamma$ and $H \to ZZ^* \to 4\ell$. These measurements are based on the pp collision data sample recorded by the ATLAS experiment at the CERN Large Hadron Collider at center-of-mass energies of $\sqrt{s} = 7$ TeV and $\sqrt{s} = 8$ TeV, corresponding to an integrated luminosity of 25 fb^{-1}. As shown in Table V, the measured values of the Higgs boson mass for the $H \to \gamma\gamma$ and $H \to ZZ^* \to 4\ell$ channels are $125.98 \pm 0.42(\mathrm{stat}) \pm 0.28(\mathrm{syst})$ GeV and $124.51 \pm 0.52(\mathrm{stat}) \pm 0.06(\mathrm{syst})$ GeV, respectively. The compatibility between the mass measurements from the two individual channels is at the level of 2.0σ corresponding to a probability of 4.8%.

From the combination of these two channels, the value of $m_H = 125.36 \pm 0.37(\mathrm{stat}) \pm 0.18(\mathrm{syst})$ GeV is obtained.

TABLE V. Summary of Higgs boson mass measurements.

Channel	Mass measurement [GeV]
$H \to \gamma\gamma$	$125.98 \pm 0.42(\mathrm{stat}) \pm 0.28(\mathrm{syst}) = 125.98 \pm 0.50$
$H \to ZZ^* \to 4\ell$	$124.51 \pm 0.52(\mathrm{stat}) \pm 0.06(\mathrm{syst}) = 124.51 \pm 0.52$
Combined	$125.36 \pm 0.37(\mathrm{stat}) \pm 0.18(\mathrm{syst}) = 125.36 \pm 0.41$

These results are based on improved calibrations for photons, electrons and muons and on improved analysis techniques with respect to Ref. [15], and they supersede the previous results.

Upper limits on the total width of the Higgs boson are derived from fits to the mass spectra of the $H \to \gamma\gamma$ and $H \to ZZ^* \to 4\ell$ decay channels, under the assumption that there is no interference with background processes. In the $H \to \gamma\gamma$ channel, a 95% CL limit of 5.0 (6.2) GeV is observed (expected). In the $H \to ZZ^* \to 4\ell$ channel, a 95% CL limit of 2.6 (6.2) GeV is observed (expected).

ACKNOWLEDGMENTS

We thank CERN for the very successful operation of the LHC, as well as the support staff from our institutions without whom ATLAS could not be operated efficiently. We acknowledge the support of ANPCyT, Argentina; YerPhI, Armenia; ARC, Australia; BMWF and FWF, Austria; ANAS, Azerbaijan; SSTC, Belarus; CNPq and FAPESP, Brazil; NSERC, NRC and CFI, Canada; CERN; CONICYT, Chile; CAS, MOST and NSFC, China; COLCIENCIAS, Colombia; MSMT CR, MPO CR and VSC CR, Czech Republic; DNRF, DNSRC and Lundbeck Foundation, Denmark; EPLANET, ERC and NSRF, European Union; IN2P3-CNRS, CEA-DSM/IRFU, France; GNSF, Georgia; BMBF, DFG, HGF, MPG and AvH Foundation, Germany; GSRT and NSRF, Greece; ISF, MINERVA, GIF, I-CORE and Benoziyo Center, Israel; INFN, Italy; MEXT and JSPS, Japan; CNRST, Morocco; FOM and NWO, Netherlands; BRF and RCN, Norway; MNiSW and NCN, Poland; GRICES and FCT, Portugal; MNE/IFA, Romania; MES of Russia and ROSATOM, Russian Federation; JINR; MSTD, Serbia; MSSR, Slovakia; ARRS and MIZŠ, Slovenia; DST/NRF, South Africa; MINECO, Spain; SRC and Wallenberg Foundation, Sweden; SER, SNSF and Cantons of Bern and Geneva, Switzerland; NSC, Taiwan; TAEK, Turkey; STFC, the Royal Society and Leverhulme Trust, United Kingdom; DOE and NSF, United States of America. The crucial computing support from all WLCG partners is acknowledged gratefully, in particular, from CERN and the ATLAS Tier-1 facilities at TRIUMF (Canada), NDGF (Denmark, Norway, Sweden), CC-IN2P3 (France), KIT/GridKA (Germany), INFN-CNAF (Italy), NL-T1 (Netherlands), PIC (Spain), ASGC (Taiwan), RAL (UK) and BNL (USA), and in the Tier-2 facilities worldwide.

[1] ATLAS Collaboration, Phys. Lett. B **716**, 1 (2012).
[2] CMS Collaboration, Phys. Lett. B **716**, 30 (2012).
[3] F. Englert and R. Brout, Phys. Rev. Lett. **13**, 321 (1964).
[4] P. W. Higgs, Phys. Lett. **12**, 132 (1964).
[5] P. W. Higgs, Phys. Rev. Lett. **13**, 508 (1964).
[6] G. S. Guralnik, C. R. Hagen, and T. W. B. Kibble, Phys. Rev. Lett. **13**, 585 (1964).
[7] P. W. Higgs, Phys. Rev. **145**, 1156 (1966).
[8] T. W. B. Kibble, Phys. Rev. **155**, 1554 (1967).
[9] L. Evans and P. Bryant, JINST **3**, S08001 (2008).
[10] LHC Higgs Cross Section Working Group, *Handbook of LHC Higgs Cross Sections: 3. Higgs Properties*, edited by S. Heinemeyer, C. Mariotti, G. Passarino, and R. Tanaka (CERN, Geneva, 2013), p. 404 [arXiv:1307.1347].
[11] N. Kauer and G. Passarino, J. High Energy Phys. 08 (2012) 116.
[12] L. J. Dixon and M. S. Siu, Phys. Rev. Lett. **90**, 252001 (2003).
[13] L. J. Dixon and Y. Li, Phys. Rev. Lett. **111**, 111802 (2013).
[14] S. P. Martin, Phys. Rev. D **86**, 073016 (2012).
[15] ATLAS Collaboration, Phys. Lett. B **726**, 88 (2013).
[16] CMS Collaboration, Phys. Rev. D **89**, 092007 (2014).
[17] ATLAS Collaboration, arXiv:1408.7084.
[18] ATLAS Collaboration, arXiv:1408.5191.
[19] ATLAS Collaboration, arXiv:1407.5063.
[20] ATLAS Collaboration, arXiv:1407.3935.
[21] ATLAS Collaboration, JINST **3**, S08003 (2008).
[22] ATLAS Collaboration, Report No. ATLAS-CONF-2012-047, 2012, http://cds.cern.ch/record/1449796.
[23] H. Abreu *et al.*, JINST **5**, P09003 (2010).
[24] ATLAS Collaboration, JINST **7**, P01013 (2012).
[25] ATLAS Collaboration, Eur. Phys. J. C **72**, 1909 (2012).
[26] ATLAS Collaboration, arXiv:1404.4562.
[27] ATLAS Collaboration, Report No. ATLAS-CONF-2012-123, 2012, http://cds.cern.ch/record/1473426.
[28] M. Cacciari and G. P. Salam, Phys. Lett. B **659**, 119 (2008).
[29] D. de Florian, G. Ferrera, M. Grazzini, and D. Tommasini, J. High Energy Phys. 06 (2012) 132.
[30] M. Grazzini and H. Sargsyan, J. High Energy Phys. 09 (2013) 129.
[31] ATLAS Collaboration, Eur. Phys. J. C **73**, 2518 (2013).
[32] ATLAS Collaboration, Report No. ATLAS-CONF-2014-032, 2014, http://cds.cern.ch/record/1706245.
[33] ATLAS Collaboration, Eur. Phys. J. C **74**, 2941 (2014).
[34] LHC Higgs Cross Section Working Group, edited by S. Dittmaier, C. Mariotti, G. Passarino, and R. Tanaka, Reports No. CERN-2012-002, and No. 10.5170/CERN-2012-002, 2012 arXiv:1201.3084.
[35] A. Hocker *et al.*, *Proc. Sci.*, ACAT2007 (2007) 040 [arXiv:physics/0703039].
[36] J. Alwall, R. Frederix, S. Frixione, V. Hirschi, F. Maltoni, O. Mattelaer, H.-S. Shao, T. Stelzer, P. Torrielli, and M. Zaro, J. High Energy Phys. 07 (2014) 079.
[37] K. S. Cranmer, Comput. Phys. Commun. **136**, 198 (2001).
[38] L. A. Piegl and W. Tiller, *The Nurbs Book*, 2nd ed. (Springer, Berlin Heidelberg, 1997) Chap. B-Spline Basis Function.
[39] S. Schael *et al.* (ALEPH Collaboration, DELPHI Collaboration, L3 Collaboration, OPAL Collaboration, SLD Collaboration, LEP Electroweak Working Group, SLD Electroweak Group, and SLD Heavy Flavour Group), Phys. Rep. **427**, 257 (2006).
[40] ATLAS Collaboration, Phys. Rev. D **86**, 032003 (2012).
[41] ATLAS and CMS Collaborations, Reports No. ATL-PHYS-PUB-2011-011 and No. CERN-CMS-NOTE-2011-005, 2011, http://cds.cern.ch/record/1375842.
[42] L. Moneta *et al.*, *Proc. Sci.*, ACAT2010 (2010) 057 [arXiv:1009.1003].
[43] K. Cranmer *et al.*, Report No. CERN-OPEN-2012-016, 2012 [http://cdsweb.cern.ch/record/1456844].
[44] W. Verkerke and D. P. Kirkby, *The RooFit Toolkit for Data Modeling* eConf C 0303241, MOLT007 (2003) [arXiv:physics/0306116].
[45] G. Cowan, K. Cranmer, E. Gross, and O. Vitells, Eur. Phys. J. C **71**, 1554 (2011).

G. Aad,[84] B. Abbott,[112] J. Abdallah,[152] S. Abdel Khalek,[116] O. Abdinov,[11] R. Aben,[106] B. Abi,[113] S. H. Abidi,[159] M. Abolins,[89] O. S. AbouZeid,[159] H. Abramowicz,[154] H. Abreu,[153] R. Abreu,[30] Y. Abulaiti,[147a,147b] B. S. Acharya,[165a,165b,b] L. Adamczyk,[38a] D. L. Adams,[25] J. Adelman,[177] S. Adomeit,[99] T. Adye,[130] T. Agatonovic-Jovin,[13a] J. A. Aguilar-Saavedra,[125a,125f] M. Agustoni,[17] S. P. Ahlen,[22] F. Ahmadov,[64,c] G. Aielli,[134a,134b] H. Akerstedt,[147a,147b] T. P. A. Åkesson,[80] G. Akimoto,[156] A. V. Akimov,[95] G. L. Alberghi,[20a,20b] J. Albert,[170] S. Albrand,[55] M. J. Alconada Verzini,[70] M. Aleksa,[30] I. N. Aleksandrov,[64] C. Alexa,[26a] G. Alexander,[154] G. Alexandre,[49] T. Alexopoulos,[10] M. Alhroob,[165a,165c] G. Alimonti,[90a] L. Alio,[84] J. Alison,[31] B. M. M. Allbrooke,[18] L. J. Allison,[71] P. P. Allport,[73] J. Almond,[83] A. Aloisio,[103a,103b] A. Alonso,[36] F. Alonso,[70] C. Alpigiani,[75] A. Altheimer,[35] B. Alvarez Gonzalez,[89] M. G. Alviggi,[103a,103b] K. Amako,[65] Y. Amaral Coutinho,[24a] C. Amelung,[23] D. Amidei,[88] S. P. Amor Dos Santos,[125a,125c] A. Amorim,[125a,125b] S. Amoroso,[48] N. Amram,[154] G. Amundsen,[23] C. Anastopoulos,[140] L. S. Ancu,[49] N. Andari,[30] T. Andeen,[35] C. F. Anders,[58b] G. Anders,[30] K. J. Anderson,[31] A. Andreazza,[90a,90b] V. Andrei,[58a] X. S. Anduaga,[70] S. Angelidakis,[9] I. Angelozzi,[106] P. Anger,[44] A. Angerami,[35] F. Anghinolfi,[30] A. V. Anisenkov,[108] N. Anjos,[125a] A. Annovi,[47] A. Antonaki,[9] M. Antonelli,[47] A. Antonov,[97] J. Antos,[145b] F. Anulli,[133a] M. Aoki,[65] L. Aperio Bella,[18] R. Apolle,[119,d] G. Arabidze,[89] I. Aracena,[144] Y. Arai,[65] J. P. Araque,[125a] A. T. H. Arce,[45] J-F. Arguin,[94] S. Argyropoulos,[42] M. Arik,[19a] A. J. Armbruster,[30] O. Arnaez,[30]

V. Arnal,[81] H. Arnold,[48] M. Arratia,[28] O. Arslan,[21] A. Artamonov,[96] G. Artoni,[23] S. Asai,[156] N. Asbah,[42] A. Ashkenazi,[154] B. Åsman,[147a,147b] L. Asquith,[6] K. Assamagan,[25] R. Astalos,[145a] M. Atkinson,[166] N. B. Atlay,[142] B. Auerbach,[6] K. Augsten,[127] M. Aurousseau,[146b] G. Avolio,[30] G. Azuelos,[94,e] Y. Azuma,[156] M. A. Baak,[30] A. Baas,[58a] C. Bacci,[135a,135b] H. Bachacou,[137] K. Bachas,[155] M. Backes,[30] M. Backhaus,[30] J. Backus Mayes,[144] E. Badescu,[26a] P. Bagiacchi,[133a,133b] P. Bagnaia,[133a,133b] Y. Bai,[33a] T. Bain,[35] J. T. Baines,[130] O. K. Baker,[177] P. Balek,[128] F. Balli,[137] E. Banas,[39] Sw. Banerjee,[174] A. A. E. Bannoura,[176] V. Bansal,[170] H. S. Bansil,[18] L. Barak,[173] S. P. Baranov,[95] E. L. Barberio,[87] D. Barberis,[50a,50b] M. Barbero,[84] T. Barillari,[100] M. Barisonzi,[176] T. Barklow,[144] N. Barlow,[28] B. M. Barnett,[130] R. M. Barnett,[15] Z. Barnovska,[5] A. Baroncelli,[135a] G. Barone,[49] A. J. Barr,[119] F. Barreiro,[81] J. Barreiro Guimarães da Costa,[57] R. Bartoldus,[144] A. E. Barton,[71] P. Bartos,[145a] V. Bartsch,[150] A. Bassalat,[116] A. Basye,[166] R. L. Bates,[53] J. R. Batley,[28] M. Battaglia,[138] M. Battistin,[30] F. Bauer,[137] H. S. Bawa,[144,f] M. D. Beattie,[71] T. Beau,[79] P. H. Beauchemin,[162] R. Beccherle,[123a,123b] P. Bechtle,[21] H. P. Beck,[17] K. Becker,[176] S. Becker,[99] M. Beckingham,[171] C. Becot,[116] A. J. Beddall,[19c] A. Beddall,[19c] S. Bedikian,[177] V. A. Bednyakov,[64] C. P. Bee,[149] L. J. Beemster,[106] T. A. Beermann,[176] M. Begel,[25] K. Behr,[119] C. Belanger-Champagne,[86] P. J. Bell,[49] W. H. Bell,[49] G. Bella,[154] L. Bellagamba,[20a] A. Bellerive,[29] M. Bellomo,[85] K. Belotskiy,[97] O. Beltramello,[30] O. Benary,[154] D. Benchekroun,[136a] K. Bendtz,[147a,147b] N. Benekos,[166] Y. Benhammou,[154] E. Benhar Noccioli,[49] J. A. Benitez Garcia,[160b] D. P. Benjamin,[45] J. R. Bensinger,[23] K. Benslama,[131] S. Bentvelsen,[106] D. Berge,[106] E. Bergeaas Kuutmann,[16] N. Berger,[5] F. Berghaus,[170] J. Beringer,[15] C. Bernard,[22] P. Bernat,[77] C. Bernius,[78] F. U. Bernlochner,[170] T. Berry,[76] P. Berta,[128] C. Bertella,[84] G. Bertoli,[147a,147b] F. Bertolucci,[123a,123b] C. Bertsche,[112] D. Bertsche,[112] M. I. Besana,[90a] G. J. Besjes,[105] O. Bessidskaia,[147a,147b] M. F. Bessner,[42] N. Besson,[137] C. Betancourt,[48] S. Bethke,[100] W. Bhimji,[46] R. M. Bianchi,[124] L. Bianchini,[23] M. Bianco,[30] O. Biebel,[99] S. P. Bieniek,[77] K. Bierwagen,[54] J. Biesiada,[15] M. Biglietti,[135a] J. Bilbao De Mendizabal,[49] H. Bilokon,[47] M. Bindi,[54] S. Binet,[116] A. Bingul,[19c] C. Bini,[133a,133b] C. W. Black,[151] J. E. Black,[144] K. M. Black,[22] D. Blackburn,[139] R. E. Blair,[6] J.-B. Blanchard,[137] T. Blazek,[145a] I. Bloch,[42] C. Blocker,[23] W. Blum,[82,a] U. Blumenschein,[54] G. J. Bobbink,[106] V. S. Bobrovnikov,[108] S. S. Bocchetta,[80] A. Bocci,[45] C. Bock,[99] C. R. Boddy,[119] M. Boehler,[48] T. T. Boek,[176] J. A. Bogaerts,[30] A. G. Bogdanchikov,[108] A. Bogouch,[91,a] C. Bohm,[147a] J. Bohm,[126] V. Boisvert,[76] T. Bold,[38a] V. Boldea,[26a] A. S. Boldyrev,[98] M. Bomben,[79] M. Bona,[75] M. Boonekamp,[137] A. Borisov,[129] G. Borissov,[71] M. Borri,[83] S. Borroni,[42] J. Bortfeldt,[99] V. Bortolotto,[135a,135b] K. Bos,[106] D. Boscherini,[20a] M. Bosman,[12] H. Boterenbrood,[106] J. Boudreau,[124] J. Bouffard,[2] E. V. Bouhova-Thacker,[71] D. Boumediene,[34] C. Bourdarios,[116] N. Bousson,[113] S. Boutouil,[136d] A. Boveia,[31] J. Boyd,[30] I. R. Boyko,[64] J. Bracinik,[18] A. Brandt,[8] G. Brandt,[15] O. Brandt,[58a] U. Bratzler,[157] B. Brau,[85] J. E. Brau,[115] H. M. Braun,[176,a] S. F. Brazzale,[165a,165c] B. Brelier,[159] K. Brendlinger,[121] A. J. Brennan,[87] R. Brenner,[167] S. Bressler,[173] K. Bristow,[146c] T. M. Bristow,[46] D. Britton,[53] F. M. Brochu,[28] I. Brock,[21] R. Brock,[89] C. Bromberg,[89] J. Bronner,[100] G. Brooijmans,[35] T. Brooks,[76] W. K. Brooks,[32b] J. Brosamer,[15] E. Brost,[115] J. Brown,[55] P. A. Bruckman de Renstrom,[39] D. Bruncko,[145b] R. Bruneliere,[48] S. Brunet,[60] A. Bruni,[20a] G. Bruni,[20a] M. Bruschi,[20a] L. Bryngemark,[80] T. Buanes,[14] Q. Buat,[143] F. Bucci,[49] P. Buchholz,[142] R. M. Buckingham,[119] A. G. Buckley,[53] S. I. Buda,[26a] I. A. Budagov,[64] F. Buehrer,[48] L. Bugge,[118] M. K. Bugge,[118] O. Bulekov,[97] A. C. Bundock,[73] H. Burckhart,[30] S. Burdin,[73] B. Burghgrave,[107] S. Burke,[130] I. Burmeister,[43] E. Busato,[34] D. Büscher,[48] V. Büscher,[82] P. Bussey,[53] C. P. Buszello,[167] B. Butler,[57] J. M. Butler,[22] A. I. Butt,[3] C. M. Buttar,[53] J. M. Butterworth,[77] P. Butti,[106] W. Buttinger,[28] A. Buzatu,[53] M. Byszewski,[10] S. Cabrera Urbán,[168] D. Caforio,[20a,20b] O. Cakir,[4a] P. Calafiura,[15] A. Calandri,[137] G. Calderini,[79] P. Calfayan,[99] R. Calkins,[107] L. P. Caloba,[24a] D. Calvet,[34] S. Calvet,[34] R. Camacho Toro,[49] S. Camarda,[42] D. Cameron,[118] L. M. Caminada,[15] R. Caminal Armadans,[12] S. Campana,[30] M. Campanelli,[77] A. Campoverde,[149] V. Canale,[103a,103b] A. Canepa,[160a] M. Cano Bret,[75] J. Cantero,[81] R. Cantrill,[125a] T. Cao,[40] M. D. M. Capeans Garrido,[30] I. Caprini,[26a] M. Caprini,[26a] M. Capua,[37a,37b] R. Caputo,[82] R. Cardarelli,[134a] T. Carli,[30] G. Carlino,[103a] L. Carminati,[90a,90b] S. Caron,[105] E. Carquin,[32a] G. D. Carrillo-Montoya,[146c] J. R. Carter,[28] J. Carvalho,[125a,125c] D. Casadei,[77] M. P. Casado,[12] M. Casolino,[12] E. Castaneda-Miranda,[146b] A. Castelli,[106] V. Castillo Gimenez,[168] N. F. Castro,[125a] P. Catastini,[57] A. Catinaccio,[30] J. R. Catmore,[118] A. Cattai,[30] G. Cattani,[134a,134b] S. Caughron,[89] V. Cavaliere,[166] D. Cavalli,[90a] M. Cavalli-Sforza,[12] V. Cavasinni,[123a,123b] F. Ceradini,[135a,135b] B. Cerio,[45] K. Cerny,[128] A. S. Cerqueira,[24b] A. Cerri,[150] L. Cerrito,[75] F. Cerutti,[15] M. Cerv,[30] A. Cervelli,[17] S. A. Cetin,[19b] A. Chafaq,[136a] D. Chakraborty,[107] I. Chalupkova,[128] P. Chang,[166] B. Chapleau,[86] J. D. Chapman,[28] D. Charfeddine,[116] D. G. Charlton,[18] C. C. Chau,[159] C. A. Chavez Barajas,[150] S. Cheatham,[86] A. Chegwidden,[89] S. Chekanov,[6] S. V. Chekulaev,[160a] G. A. Chelkov,[64,g] M. A. Chelstowska,[88] C. Chen,[63] H. Chen,[25] K. Chen,[149] L. Chen,[33d,h] S. Chen,[33c] X. Chen,[146c] Y. Chen,[66] Y. Chen,[35] H. C. Cheng,[88] Y. Cheng,[31] A. Cheplakov,[64] R. Cherkaoui El Moursli,[136e] V. Chernyatin,[25,a] E. Cheu,[7]

L. Chevalier,[137] V. Chiarella,[47] G. Chiefari,[103a,103b] J. T. Childers,[6] A. Chilingarov,[71] G. Chiodini,[72a] A. S. Chisholm,[18] R. T. Chislett,[77] A. Chitan,[26a] M. V. Chizhov,[64] S. Chouridou,[9] B. K. B. Chow,[99] D. Chromek-Burckhart,[30] M. L. Chu,[152] J. Chudoba,[126] J. J. Chwastowski,[39] L. Chytka,[114] G. Ciapetti,[133a,133b] A. K. Ciftci,[4a] R. Ciftci,[4a] D. Cinca,[53] V. Cindro,[74] A. Ciocio,[15] P. Cirkovic,[13b] Z. H. Citron,[173] M. Citterio,[90a] M. Ciubancan,[26a] A. Clark,[49] P. J. Clark,[46] R. N. Clarke,[15] W. Cleland,[124] J. C. Clemens,[84] C. Clement,[147a,147b] Y. Coadou,[84] M. Cobal,[165a,165c] A. Coccaro,[139] J. Cochran,[63] L. Coffey,[23] J. G. Cogan,[144] J. Coggeshall,[166] B. Cole,[35] S. Cole,[107] A. P. Colijn,[106] J. Collot,[55] T. Colombo,[58c] G. Colon,[85] G. Compostella,[100] P. Conde Muiño,[125a,125b] E. Coniavitis,[48] M. C. Conidi,[12] S. H. Connell,[146b] I. A. Connelly,[76] S. M. Consonni,[90a,90b] V. Consorti,[48] S. Constantinescu,[26a] C. Conta,[120a,120b] G. Conti,[57] F. Conventi,[103a,i] M. Cooke,[15] B. D. Cooper,[77] A. M. Cooper-Sarkar,[119] N. J. Cooper-Smith,[76] K. Copic,[15] T. Cornelissen,[176] M. Corradi,[20a] F. Corriveau,[86,j] A. Corso-Radu,[164] A. Cortes-Gonzalez,[12] G. Cortiana,[100] G. Costa,[90a] M. J. Costa,[168] D. Costanzo,[140] D. Côté,[8] G. Cottin,[28] G. Cowan,[76] B. E. Cox,[83] K. Cranmer,[109] G. Cree,[29] S. Crépé-Renaudin,[55] F. Crescioli,[79] W. A. Cribbs,[147a,147b] M. Crispin Ortuzar,[119] M. Cristinziani,[21] V. Croft,[105] G. Crosetti,[37a,37b] C.-M. Cuciuc,[26a] T. Cuhadar Donszelmann,[140] J. Cummings,[177] M. Curatolo,[47] C. Cuthbert,[151] H. Czirr,[142] P. Czodrowski,[3] Z. Czyczula,[177] S. D'Auria,[53] M. D'Onofrio,[73] M. J. Da Cunha Sargedas De Sousa,[125a,125b] C. Da Via,[83] W. Dabrowski,[38a] A. Dafinca,[119] T. Dai,[88] O. Dale,[14] F. Dallaire,[94] C. Dallapiccola,[85] M. Dam,[36] A. C. Daniells,[18] M. Dano Hoffmann,[137] V. Dao,[48] G. Darbo,[50a] S. Darmora,[8] J. A. Dassoulas,[42] A. Dattagupta,[60] W. Davey,[21] C. David,[170] T. Davidek,[128] E. Davies,[119,d] M. Davies,[154] O. Davignon,[79] A. R. Davison,[77] P. Davison,[77] Y. Davygora,[58a] E. Dawe,[143] I. Dawson,[140] R. K. Daya-Ishmukhametova,[85] K. De,[8] R. de Asmundis,[103a] S. De Castro,[20a,20b] S. De Cecco,[79] N. De Groot,[105] P. de Jong,[106] H. De la Torre,[81] F. De Lorenzi,[63] L. De Nooij,[106] D. De Pedis,[133a] A. De Salvo,[133a] U. De Sanctis,[165a,165b] A. De Santo,[150] J. B. De Vivie De Regie,[116] W. J. Dearnaley,[71] R. Debbe,[25] C. Debenedetti,[138] B. Dechenaux,[55] D. V. Dedovich,[64] I. Deigaard,[106] J. Del Peso,[81] T. Del Prete,[123a,123b] F. Deliot,[137] C. M. Delitzsch,[49] M. Deliyergiyev,[74] A. Dell'Acqua,[30] L. Dell'Asta,[22] M. Dell'Orso,[123a,123b] M. Della Pietra,[103a,i] D. della Volpe,[49] M. Delmastro,[5] P. A. Delsart,[55] C. Deluca,[106] S. Demers,[177] M. Demichev,[64] A. Demilly,[79] S. P. Denisov,[129] D. Derendarz,[39] J. E. Derkaoui,[136d] F. Derue,[79] P. Dervan,[73] K. Desch,[21] C. Deterre,[42] P. O. Deviveiros,[106] A. Dewhurst,[130] S. Dhaliwal,[106] A. Di Ciaccio,[134a,134b] L. Di Ciaccio,[5] A. Di Domenico,[133a,133b] C. Di Donato,[103a,103b] A. Di Girolamo,[30] B. Di Girolamo,[30] A. Di Mattia,[153] B. Di Micco,[135a,135b] R. Di Nardo,[47] A. Di Simone,[48] R. Di Sipio,[20a,20b] D. Di Valentino,[29] F. A. Dias,[46] M. A. Diaz,[32a] E. B. Diehl,[88] J. Dietrich,[42] T. A. Dietzsch,[58a] S. Diglio,[84] A. Dimitrievska,[13a] J. Dingfelder,[21] C. Dionisi,[133a,133b] P. Dita,[26a] S. Dita,[26a] F. Dittus,[30] F. Djama,[84] T. Djobava,[51b] M. A. B. do Vale,[24c] A. Do Valle Wemans,[125a,125g] T. K. O. Doan,[5] D. Dobos,[30] C. Doglioni,[49] T. Doherty,[53] T. Dohmae,[156] J. Dolejsi,[128] Z. Dolezal,[128] B. A. Dolgoshein,[97,a] M. Donadelli,[24d] S. Donati,[123a,123b] P. Dondero,[120a,120b] J. Donini,[34] J. Dopke,[130] A. Doria,[103a] M. T. Dova,[70] A. T. Doyle,[53] M. Dris,[10] J. Dubbert,[88] S. Dube,[15] E. Dubreuil,[34] E. Duchovni,[173] G. Duckeck,[99] O. A. Ducu,[26a] D. Duda,[176] A. Dudarev,[30] F. Dudziak,[63] L. Duflot,[116] L. Duguid,[76] M. Dührssen,[30] M. Dunford,[58a] H. Duran Yildiz,[4a] M. Düren,[52] A. Durglishvili,[51b] M. Dwuznik,[38a] M. Dyndal,[38a] J. Ebke,[99] W. Edson,[2] N. C. Edwards,[46] W. Ehrenfeld,[21] T. Eifert,[144] G. Eigen,[14] K. Einsweiler,[15] T. Ekelof,[167] M. El Kacimi,[136c] M. Ellert,[167] S. Elles,[5] F. Ellinghaus,[82] N. Ellis,[30] J. Elmsheuser,[99] M. Elsing,[30] D. Emeliyanov,[130] Y. Enari,[156] O. C. Endner,[82] M. Endo,[117] R. Engelmann,[149] J. Erdmann,[177] A. Ereditato,[17] D. Eriksson,[147a] G. Ernis,[176] J. Ernst,[2] M. Ernst,[25] J. Ernwein,[137] D. Errede,[166] S. Errede,[166] E. Ertel,[82] M. Escalier,[116] H. Esch,[43] C. Escobar,[124] B. Esposito,[47] A. I. Etienvre,[137] E. Etzion,[154] H. Evans,[60] A. Ezhilov,[122] L. Fabbri,[20a,20b] G. Facini,[31] R. M. Fakhrutdinov,[129] S. Falciano,[133a] R. J. Falla,[77] J. Faltova,[128] Y. Fang,[33a] M. Fanti,[90a,90b] A. Farbin,[8] A. Farilla,[135a] T. Farooque,[12] S. Farrell,[15] S. M. Farrington,[171] P. Farthouat,[30] F. Fassi,[136e] P. Fassnacht,[30] D. Fassouliotis,[9] A. Favareto,[50a,50b] L. Fayard,[116] P. Federic,[145a] O. L. Fedin,[122,k] W. Fedorko,[169] M. Fehling-Kaschek,[48] S. Feigl,[30] L. Feligioni,[84] C. Feng,[33d] E. J. Feng,[6] H. Feng,[88] A. B. Fenyuk,[129] S. Fernandez Perez,[30] S. Ferrag,[53] J. Ferrando,[53] A. Ferrari,[167] P. Ferrari,[106] R. Ferrari,[120a] D. E. Ferreira de Lima,[53] A. Ferrer,[168] D. Ferrere,[49] C. Ferretti,[88] A. Ferretto Parodi,[50a,50b] M. Fiascaris,[31] F. Fiedler,[82] A. Filipčič,[74] M. Filipuzzi,[42] F. Filthaut,[105] M. Fincke-Keeler,[170] K. D. Finelli,[151] M. C. N. Fiolhais,[125a,125c] L. Fiorini,[168] A. Firan,[40] A. Fischer,[2] J. Fischer,[176] W. C. Fisher,[89] E. A. Fitzgerald,[23] M. Flechl,[48] I. Fleck,[142] P. Fleischmann,[88] S. Fleischmann,[176] G. T. Fletcher,[140] G. Fletcher,[75] T. Flick,[176] A. Floderus,[80] L. R. Flores Castillo,[174,l] A. C. Florez Bustos,[160b] M. J. Flowerdew,[100] A. Formica,[137] A. Forti,[83] D. Fortin,[160a] D. Fournier,[116] H. Fox,[71] S. Fracchia,[12] P. Francavilla,[79] M. Franchini,[20a,20b] S. Franchino,[30] D. Francis,[30] L. Franconi,[118] M. Franklin,[57] S. Franz,[61] M. Fraternali,[120a,120b] S. T. French,[28] C. Friedrich,[42] F. Friedrich,[44] D. Froidevaux,[30] J. A. Frost,[28] C. Fukunaga,[157] E. Fullana Torregrosa,[82] B. G. Fulsom,[144] J. Fuster,[168] C. Gabaldon,[55] O. Gabizon,[173] A. Gabrielli,[20a,20b]

A. Gabrielli,[133a,133b] S. Gadatsch,[106] S. Gadomski,[49] G. Gagliardi,[50a,50b] P. Gagnon,[60] C. Galea,[105] B. Galhardo,[125a,125c] E. J. Gallas,[119] V. Gallo,[17] B. J. Gallop,[130] P. Gallus,[127] G. Galster,[36] K. K. Gan,[110] J. Gao,[33b,h] Y. S. Gao,[144,f] F. M. Garay Walls,[46] F. Garberson,[177] C. García,[168] J. E. García Navarro,[168] M. Garcia-Sciveres,[15] R. W. Gardner,[31] N. Garelli,[144] V. Garonne,[30] C. Gatti,[47] G. Gaudio,[120a] B. Gaur,[142] L. Gauthier,[94] P. Gauzzi,[133a,133b] I. L. Gavrilenko,[95] C. Gay,[169] G. Gaycken,[21] E. N. Gazis,[10] P. Ge,[33d] Z. Gecse,[169] C. N. P. Gee,[130] D. A. A. Geerts,[106] Ch. Geich-Gimbel,[21] K. Gellerstedt,[147a,147b] C. Gemme,[50a] A. Gemmell,[53] M. H. Genest,[55] S. Gentile,[133a,133b] M. George,[54] S. George,[76] D. Gerbaudo,[164] A. Gershon,[154] H. Ghazlane,[136b] N. Ghodbane,[34] B. Giacobbe,[20a] S. Giagu,[133a,133b] V. Giangiobbe,[12] P. Giannetti,[123a,123b] F. Gianotti,[30] B. Gibbard,[25] S. M. Gibson,[76] M. Gilchriese,[15] T. P. S. Gillam,[28] D. Gillberg,[30] G. Gilles,[34] D. M. Gingrich,[3,e] N. Giokaris,[9] M. P. Giordani,[165a,165c] R. Giordano,[103a,103b] F. M. Giorgi,[20a] F. M. Giorgi,[16] P. F. Giraud,[137] D. Giugni,[90a] C. Giuliani,[48] M. Giulini,[58b] B. K. Gjelsten,[118] S. Gkaitatzis,[155] I. Gkialas,[155,m] L. K. Gladilin,[98] C. Glasman,[81] J. Glatzer,[30] P. C. F. Glaysher,[46] A. Glazov,[42] G. L. Glonti,[64] M. Goblirsch-Kolb,[100] J. R. Goddard,[75] J. Godfrey,[143] J. Godlewski,[30] C. Goeringer,[82] S. Goldfarb,[88] T. Golling,[177] D. Golubkov,[129] A. Gomes,[125a,125b,125d] L. S. Gomez Fajardo,[42] R. Gonçalo,[125a] J. Goncalves Pinto Firmino Da Costa,[137] L. Gonella,[21] S. González de la Hoz,[168] G. Gonzalez Parra,[12] S. Gonzalez-Sevilla,[49] L. Goossens,[30] P. A. Gorbounov,[96] H. A. Gordon,[25] I. Gorelov,[104] B. Gorini,[30] E. Gorini,[72a,72b] A. Gorišek,[74] E. Gornicki,[39] A. T. Goshaw,[6] C. Gössling,[43] M. I. Gostkin,[64] M. Gouighri,[136a] D. Goujdami,[136c] M. P. Goulette,[49] A. G. Goussiou,[139] C. Goy,[5] S. Gozpinar,[23] H. M. X. Grabas,[137] L. Graber,[54] I. Grabowska-Bold,[38a] P. Grafström,[20a,20b] K-J. Grahn,[42] J. Gramling,[49] E. Gramstad,[118] S. Grancagnolo,[16] V. Grassi,[149] V. Gratchev,[122] H. M. Gray,[30] E. Graziani,[135a] O. G. Grebenyuk,[122] Z. D. Greenwood,[78,n] K. Gregersen,[77] I. M. Gregor,[42] P. Grenier,[144] J. Griffiths,[8] A. A. Grillo,[138] K. Grimm,[71] S. Grinstein,[12,o] Ph. Gris,[34] Y. V. Grishkevich,[98] J.-F. Grivaz,[116] J. P. Grohs,[44] A. Grohsjean,[42] E. Gross,[173] J. Grosse-Knetter,[54] G. C. Grossi,[134a,134b] J. Groth-Jensen,[173] Z. J. Grout,[150] L. Guan,[33b] F. Guescini,[49] D. Guest,[177] O. Gueta,[154] C. Guicheney,[34] E. Guido,[50a,50b] T. Guillemin,[116] S. Guindon,[2] U. Gul,[53] C. Gumpert,[44] J. Gunther,[127] J. Guo,[35] S. Gupta,[119] P. Gutierrez,[112] N. G. Gutierrez Ortiz,[53] C. Gutschow,[77] N. Guttman,[154] C. Guyot,[137] C. Gwenlan,[119] C. B. Gwilliam,[73] A. Haas,[109] C. Haber,[15] H. K. Hadavand,[8] N. Haddad,[136e] P. Haefner,[21] S. Hageböck,[21] Z. Hajduk,[39] H. Hakobyan,[178] M. Haleem,[42] D. Hall,[119] G. Halladjian,[89] K. Hamacher,[176] P. Hamal,[114] K. Hamano,[170] M. Hamer,[54] A. Hamilton,[146a] S. Hamilton,[162] G. N. Hamity,[146c] P. G. Hamnett,[42] L. Han,[33b] K. Hanagaki,[117] K. Hanawa,[156] M. Hance,[15] P. Hanke,[58a] R. Hanna,[137] J. B. Hansen,[36] J. D. Hansen,[36] P. H. Hansen,[36] K. Hara,[161] A. S. Hard,[174] T. Harenberg,[176] F. Hariri,[116] S. Harkusha,[91] D. Harper,[88] R. D. Harrington,[46] O. M. Harris,[139] P. F. Harrison,[171] F. Hartjes,[106] M. Hasegawa,[66] S. Hasegawa,[102] Y. Hasegawa,[141] A. Hasib,[112] S. Hassani,[137] S. Haug,[17] M. Hauschild,[30] R. Hauser,[89] M. Havranek,[126] C. M. Hawkes,[18] R. J. Hawkings,[30] A. D. Hawkins,[80] T. Hayashi,[161] D. Hayden,[89] C. P. Hays,[119] H. S. Hayward,[73] S. J. Haywood,[130] S. J. Head,[18] T. Heck,[82] V. Hedberg,[80] L. Heelan,[8] S. Heim,[121] T. Heim,[176] B. Heinemann,[15] L. Heinrich,[109] J. Hejbal,[126] L. Helary,[22] C. Heller,[99] M. Heller,[30] S. Hellman,[147a,147b] D. Hellmich,[21] C. Helsens,[30] J. Henderson,[119] R. C. W. Henderson,[71] Y. Heng,[174] C. Hengler,[42] A. Henrichs,[177] A. M. Henriques Correia,[30] S. Henrot-Versille,[116] C. Hensel,[54] G. H. Herbert,[16] Y. Hernández Jiménez,[168] R. Herrberg-Schubert,[16] G. Herten,[48] R. Hertenberger,[99] L. Hervas,[30] G. G. Hesketh,[77] N. P. Hessey,[106] R. Hickling,[75] E. Higón-Rodriguez,[168] E. Hill,[170] J. C. Hill,[28] K. H. Hiller,[42] S. Hillert,[21] S. J. Hillier,[18] I. Hinchliffe,[15] E. Hines,[121] M. Hirose,[158] D. Hirschbuehl,[176] J. Hobbs,[149] N. Hod,[106] M. C. Hodgkinson,[140] P. Hodgson,[140] A. Hoecker,[30] M. R. Hoeferkamp,[104] F. Hoenig,[99] J. Hoffman,[40] D. Hoffmann,[84] J. I. Hofmann,[58a] M. Hohlfeld,[82] T. R. Holmes,[15] T. M. Hong,[121] L. Hooft van Huysduynen,[109] Y. Horii,[102] J-Y. Hostachy,[55] S. Hou,[152] A. Hoummada,[136a] J. Howard,[119] J. Howarth,[42] M. Hrabovsky,[114] I. Hristova,[16] J. Hrivnac,[116] T. Hryn'ova,[5] C. Hsu,[146c] P. J. Hsu,[82] S.-C. Hsu,[139] D. Hu,[35] X. Hu,[25] Y. Huang,[42] Z. Hubacek,[30] F. Hubaut,[84] F. Huegging,[21] T. B. Huffman,[119] E. W. Hughes,[35] G. Hughes,[71] M. Huhtinen,[30] T. A. Hülsing,[82] M. Hurwitz,[15] N. Huseynov,[64,c] J. Huston,[89] J. Huth,[57] G. Iacobucci,[49] G. Iakovidis,[10] I. Ibragimov,[142] L. Iconomidou-Fayard,[116] E. Ideal,[177] P. Iengo,[103a] O. Igonkina,[106] T. Iizawa,[172] Y. Ikegami,[65] K. Ikematsu,[142] M. Ikeno,[65] Y. Ilchenko,[31,cc] D. Iliadis,[155] N. Ilic,[159] Y. Inamaru,[66] T. Ince,[100] P. Ioannou,[9] M. Iodice,[135a] K. Iordanidou,[9] V. Ippolito,[57] A. Irles Quiles,[168] C. Isaksson,[167] M. Ishino,[67] M. Ishitsuka,[158] R. Ishmukhametov,[110] C. Issever,[119] S. Istin,[19a] J. M. Iturbe Ponce,[83] R. Iuppa,[134a,134b] J. Ivarsson,[80] W. Iwanski,[39] H. Iwasaki,[65] J. M. Izen,[41] V. Izzo,[103a] B. Jackson,[121] M. Jackson,[73] P. Jackson,[1] M. R. Jaekel,[30] V. Jain,[2] K. Jakobs,[48] S. Jakobsen,[30] T. Jakoubek,[126] J. Jakubek,[127] D. O. Jamin,[152] D. K. Jana,[78] E. Jansen,[77] H. Jansen,[30] J. Janssen,[21] M. Janus,[171] G. Jarlskog,[80] N. Javadov,[64,c] T. Javůrek,[48] L. Jeanty,[15] J. Jejelava,[51a,p] G.-Y. Jeng,[151] D. Jennens,[87] P. Jenni,[48,q] J. Jentzsch,[43] C. Jeske,[171] S. Jézéquel,[5] H. Ji,[174] J. Jia,[149] Y. Jiang,[33b] M. Jimenez Belenguer,[42] S. Jin,[33a] A. Jinaru,[26a] O. Jinnouchi,[158] M. D. Joergensen,[36]

K. E. Johansson,[147a,147b] P. Johansson,[140] K. A. Johns,[7] K. Jon-And,[147a,147b] G. Jones,[171] R. W. L. Jones,[71] T. J. Jones,[73] J. Jongmanns,[58a] P. M. Jorge,[125a,125b] K. D. Joshi,[83] J. Jovicevic,[148] X. Ju,[174] C. A. Jung,[43] R. M. Jungst,[30] P. Jussel,[61] A. Juste Rozas,[12,o] M. Kaci,[168] A. Kaczmarska,[39] M. Kado,[116] H. Kagan,[110] M. Kagan,[144] E. Kajomovitz,[45] C. W. Kalderon,[119] S. Kama,[40] A. Kamenshchikov,[129] N. Kanaya,[156] M. Kaneda,[30] S. Kaneti,[28] V. A. Kantserov,[97] J. Kanzaki,[65] B. Kaplan,[109] L. S. Kaplan,[174] A. Kapliy,[31] D. Kar,[53] K. Karakostas,[10] N. Karastathis,[10] M. Karnevskiy,[82] S. N. Karpov,[64] Z. M. Karpova,[64] K. Karthik,[109] V. Kartvelishvili,[71] A. N. Karyukhin,[129] L. Kashif,[174] G. Kasieczka,[58b] R. D. Kass,[110] A. Kastanas,[14] Y. Kataoka,[156] A. Katre,[49] J. Katzy,[42] V. Kaushik,[7] K. Kawagoe,[69] T. Kawamoto,[156] G. Kawamura,[54] S. Kazama,[156] V. F. Kazanin,[108] M. Y. Kazarinov,[64] R. Keeler,[170] R. Kehoe,[40] M. Keil,[54] J. S. Keller,[42] J. J. Kempster,[76] H. Keoshkerian,[5] O. Kepka,[126] B. P. Kerševan,[74] S. Kersten,[176] K. Kessoku,[156] J. Keung,[159] F. Khalil-zada,[11] H. Khandanyan,[147a,147b] A. Khanov,[113] A. Khodinov,[97] A. Khomich,[58a] T. J. Khoo,[28] G. Khoriauli,[21] A. Khoroshilov,[176] V. Khovanskiy,[96] E. Khramov,[64] J. Khubua,[51b] H. Y. Kim,[8] H. Kim,[147a,147b] S. H. Kim,[161] N. Kimura,[172] O. Kind,[16] B. T. King,[73] M. King,[168] R. S. B. King,[119] S. B. King,[169] J. Kirk,[130] A. E. Kiryunin,[100] T. Kishimoto,[66] D. Kisielewska,[38a] F. Kiss,[48] T. Kittelmann,[124] K. Kiuchi,[161] E. Kladiva,[145b] M. Klein,[73] U. Klein,[73] K. Kleinknecht,[82] P. Klimek,[147a,147b] A. Klimentov,[25] R. Klingenberg,[43] J. A. Klinger,[83] T. Klioutchnikova,[30] P. F. Klok,[105] E.-E. Kluge,[58a] P. Kluit,[106] S. Kluth,[100] E. Kneringer,[61] E. B. F. G. Knoops,[84] A. Knue,[53] D. Kobayashi,[158] T. Kobayashi,[156] M. Kobel,[44] M. Kocian,[144] P. Kodys,[128] P. Koevesarki,[21] T. Koffas,[29] E. Koffeman,[106] L. A. Kogan,[119] S. Kohlmann,[176] Z. Kohout,[127] T. Kohriki,[65] T. Koi,[144] H. Kolanoski,[16] I. Koletsou,[5] J. Koll,[89] A. A. Komar,[95,a] Y. Komori,[156] T. Kondo,[65] N. Kondrashova,[42] K. Köneke,[48] A. C. König,[105] S. König,[82] T. Kono,[65,r] R. Konoplich,[109,s] N. Konstantinidis,[77] R. Kopeliansky,[153] S. Koperny,[38a] L. Köpke,[82] A. K. Kopp,[48] K. Korcyl,[39] K. Kordas,[155] A. Korn,[77] A. A. Korol,[108,t] I. Korolkov,[12] E. V. Korolkova,[140] V. A. Korotkov,[129] O. Kortner,[100] S. Kortner,[100] V. V. Kostyukhin,[21] V. M. Kotov,[64] A. Kotwal,[45] C. Kourkoumelis,[9] V. Kouskoura,[155] A. Koutsman,[160a] R. Kowalewski,[170] T. Z. Kowalski,[38a] W. Kozanecki,[137] A. S. Kozhin,[129] V. Kral,[127] V. A. Kramarenko,[98] G. Kramberger,[74] D. Krasnopevtsev,[97] A. Krasznahorkay,[30] J. K. Kraus,[21] A. Kravchenko,[25] S. Kreiss,[109] M. Kretz,[58c] J. Kretzschmar,[73] K. Kreutzfeldt,[52] P. Krieger,[159] K. Kroeninger,[54] H. Kroha,[100] J. Kroll,[121] J. Kroseberg,[21] J. Krstic,[13a] U. Kruchonak,[64] H. Krüger,[21] T. Kruker,[17] N. Krumnack,[63] Z. V. Krumshteyn,[64] A. Kruse,[174] M. C. Kruse,[45] M. Kruskal,[22] T. Kubota,[87] S. Kuday,[4a] S. Kuehn,[48] A. Kugel,[58c] A. Kuhl,[138] T. Kuhl,[42] V. Kukhtin,[64] Y. Kulchitsky,[91] S. Kuleshov,[32b] M. Kuna,[133a,133b] J. Kunkle,[121] A. Kupco,[126] H. Kurashige,[66] Y. A. Kurochkin,[91] R. Kurumida,[66] V. Kus,[126] E. S. Kuwertz,[148] M. Kuze,[158] J. Kvita,[114] A. La Rosa,[49] L. La Rotonda,[37a,37b] C. Lacasta,[168] F. Lacava,[133a,133b] J. Lacey,[29] H. Lacker,[16] D. Lacour,[79] V. R. Lacuesta,[168] E. Ladygin,[64] R. Lafaye,[5] B. Laforge,[79] T. Lagouri,[177] S. Lai,[48] H. Laier,[58a] L. Lambourne,[77] S. Lammers,[60] C. L. Lampen,[7] W. Lampl,[7] E. Lançon,[137] U. Landgraf,[48] M. P. J. Landon,[75] V. S. Lang,[58a] A. J. Lankford,[164] F. Lanni,[25] K. Lantzsch,[30] S. Laplace,[79] C. Lapoire,[21] J. F. Laporte,[137] T. Lari,[90a] M. Lassnig,[30] P. Laurelli,[47] W. Lavrijsen,[15] A. T. Law,[138] P. Laycock,[73] O. Le Dortz,[79] E. Le Guirriec,[84] E. Le Menedeu,[12] T. LeCompte,[6] F. Ledroit-Guillon,[55] C. A. Lee,[152] H. Lee,[106] J. S. H. Lee,[117] S. C. Lee,[152] L. Lee,[177] G. Lefebvre,[79] M. Lefebvre,[170] F. Legger,[99] C. Leggett,[15] A. Lehan,[73] M. Lehmacher,[21] G. Lehmann Miotto,[30] X. Lei,[7] W. A. Leight,[29] A. Leisos,[155] A. G. Leister,[177] M. A. L. Leite,[24d] R. Leitner,[128] D. Lellouch,[173] B. Lemmer,[54] K. J. C. Leney,[77] T. Lenz,[21] G. Lenzen,[176] B. Lenzi,[30] R. Leone,[7] S. Leone,[123a,123b] K. Leonhardt,[44] C. Leonidopoulos,[46] S. Leontsinis,[10] C. Leroy,[94] C. G. Lester,[28] C. M. Lester,[121] M. Levchenko,[122] J. Levêque,[5] D. Levin,[88] L. J. Levinson,[173] M. Levy,[18] A. Lewis,[119] G. H. Lewis,[109] A. M. Leyko,[21] M. Leyton,[41] B. Li,[33b,u] B. Li,[84] H. Li,[149] H. L. Li,[31] L. Li,[45] L. Li,[33e] S. Li,[45] Y. Li,[33c,v] Z. Liang,[138] H. Liao,[34] B. Liberti,[134a] P. Lichard,[30] K. Lie,[166] J. Liebal,[21] W. Liebig,[14] C. Limbach,[21] A. Limosani,[87] S. C. Lin,[152,w] T. H. Lin,[82] F. Linde,[106] B. E. Lindquist,[149] J. T. Linnemann,[89] E. Lipeles,[121] A. Lipniacka,[14] M. Lisovyi,[42] T. M. Liss,[166] D. Lissauer,[25] A. Lister,[169] A. M. Litke,[138] B. Liu,[152] D. Liu,[152] J. B. Liu,[33b] K. Liu,[33b,x] L. Liu,[88] M. Liu,[45] M. Liu,[33b] Y. Liu,[33b] M. Livan,[120a,120b] S. S. A. Livermore,[119] A. Lleres,[55] J. Llorente Merino,[81] S. L. Lloyd,[75] F. Lo Sterzo,[152] E. Lobodzinska,[42] P. Loch,[7] W. S. Lockman,[138] T. Loddenkoetter,[21] F. K. Loebinger,[83] A. E. Loevschall-Jensen,[36] A. Loginov,[177] T. Lohse,[16] K. Lohwasser,[42] M. Lokajicek,[126] V. P. Lombardo,[5] B. A. Long,[22] J. D. Long,[88] R. E. Long,[71] L. Lopes,[125a] D. Lopez Mateos,[57] B. Lopez Paredes,[140] I. Lopez Paz,[12] J. Lorenz,[99] N. Lorenzo Martinez,[60] M. Losada,[163] P. Loscutoff,[15] X. Lou,[41] A. Lounis,[116] J. Love,[6] P. A. Love,[71] A. J. Lowe,[144,f] F. Lu,[33a] N. Lu,[88] H. J. Lubatti,[139] C. Luci,[133a,133b] A. Lucotte,[55] F. Luehring,[60] W. Lukas,[61] L. Luminari,[133a] O. Lundberg,[147a,147b] B. Lund-Jensen,[148] M. Lungwitz,[82] D. Lynn,[25] R. Lysak,[126] E. Lytken,[80] H. Ma,[25] L. L. Ma,[33d] G. Maccarrone,[47] A. Macchiolo,[100] J. Machado Miguens,[125a,125b] D. Macina,[30] D. Madaffari,[84] R. Madar,[48] H. J. Maddocks,[71] W. F. Mader,[44] A. Madsen,[167] M. Maeno,[8] T. Maeno,[25] E. Magradze,[54] K. Mahboubi,[48] J. Mahlstedt,[106] S. Mahmoud,[73] C. Maiani,[137]

C. Maidantchik,[24a] A. A. Maier,[100] A. Maio,[125a,125b,125d] S. Majewski,[115] Y. Makida,[65] N. Makovec,[116] P. Mal,[137,y] B. Malaescu,[79] Pa. Malecki,[39] V. P. Maleev,[122] F. Malek,[55] U. Mallik,[62] D. Malon,[6] C. Malone,[144] S. Maltezos,[10] V. M. Malyshev,[108] S. Malyukov,[30] J. Mamuzic,[13b] B. Mandelli,[30] L. Mandelli,[90a] I. Mandić,[74] R. Mandrysch,[62] J. Maneira,[125a,125b] A. Manfredini,[100] L. Manhaes de Andrade Filho,[24b] J. A. Manjarres Ramos,[160b] A. Mann,[99] P. M. Manning,[138] A. Manousakis-Katsikakis,[9] B. Mansoulie,[137] R. Mantifel,[86] L. Mapelli,[30] L. March,[168] J. F. Marchand,[29] G. Marchiori,[79] M. Marcisovsky,[126] C. P. Marino,[170] M. Marjanovic,[13a] C. N. Marques,[125a] F. Marroquim,[24a] S. P. Marsden,[83] Z. Marshall,[15] L. F. Marti,[17] S. Marti-Garcia,[168] B. Martin,[30] B. Martin,[89] T. A. Martin,[171] V. J. Martin,[46] B. Martin dit Latour,[14] H. Martinez,[137] M. Martinez,[12,o] S. Martin-Haugh,[130] A. C. Martyniuk,[77] M. Marx,[139] F. Marzano,[133a] A. Marzin,[30] L. Masetti,[82] T. Mashimo,[156] R. Mashinistov,[95] J. Masik,[83] A. L. Maslennikov,[108] I. Massa,[20a,20b] L. Massa,[20a,20b] N. Massol,[5] P. Mastrandrea,[149] A. Mastroberardino,[37a,37b] T. Masubuchi,[156] P. Mättig,[176] J. Mattmann,[82] J. Maurer,[26a] S. J. Maxfield,[73] D. A. Maximov,[108,t] R. Mazini,[152] S. M. Mazza,[90a,90b] L. Mazzaferro,[134a,134b] G. Mc Goldrick,[159] S. P. Mc Kee,[88] A. McCarn,[88] R. L. McCarthy,[149] T. G. McCarthy,[29] N. A. McCubbin,[130] K. W. McFarlane,[56,a] J. A. Mcfayden,[77] G. Mchedlidze,[54] S. J. McMahon,[130] R. A. McPherson,[170,j] A. Meade,[85] J. Mechnich,[106] M. Medinnis,[42] S. Meehan,[31] S. Mehlhase,[99] A. Mehta,[73] K. Meier,[58a] C. Meineck,[99] B. Meirose,[80] C. Melachrinos,[31] B. R. Mellado Garcia,[146c] F. Meloni,[17] A. Mengarelli,[20a,20b] S. Menke,[100] E. Meoni,[162] K. M. Mercurio,[57] S. Mergelmeyer,[21] N. Meric,[137] P. Mermod,[49] L. Merola,[103a,103b] C. Meroni,[90a] F. S. Merritt,[31] H. Merritt,[110] A. Messina,[30,z] J. Metcalfe,[25] A. S. Mete,[164] C. Meyer,[82] C. Meyer,[121] J-P. Meyer,[137] J. Meyer,[30] R. P. Middleton,[130] S. Migas,[73] L. Mijović,[21] G. Mikenberg,[173] M. Mikestikova,[126] M. Mikuž,[74] A. Milic,[30] D. W. Miller,[31] C. Mills,[46] A. Milov,[173] D. A. Milstead,[147a,147b] D. Milstein,[173] A. A. Minaenko,[129] I. A. Minashvili,[64] A. I. Mincer,[109] B. Mindur,[38a] M. Mineev,[64] Y. Ming,[174] L. M. Mir,[12] G. Mirabelli,[133a] T. Mitani,[172] J. Mitrevski,[99] V. A. Mitsou,[168] S. Mitsui,[65] A. Miucci,[49] P. S. Miyagawa,[140] J. U. Mjörnmark,[80] T. Moa,[147a,147b] K. Mochizuki,[84] S. Mohapatra,[35] W. Mohr,[48] S. Molander,[147a,147b] R. Moles-Valls,[168] K. Mönig,[42] C. Monini,[55] J. Monk,[36] E. Monnier,[84] J. Montejo Berlingen,[12] F. Monticelli,[70] S. Monzani,[133a,133b] R. W. Moore,[3] A. Moraes,[53] N. Morange,[62] D. Moreno,[82] M. Moreno Llácer,[54] P. Morettini,[50a] M. Morgenstern,[44] M. Morii,[57] S. Moritz,[82] A. K. Morley,[148] G. Mornacchi,[30] J. D. Morris,[75] L. Morvaj,[102] H. G. Moser,[100] M. Mosidze,[51b] J. Moss,[110] K. Motohashi,[158] R. Mount,[144] E. Mountricha,[25] S. V. Mouraviev,[95,a] E. J. W. Moyse,[85] S. Muanza,[84] R. D. Mudd,[18] F. Mueller,[58a] J. Mueller,[124] K. Mueller,[21] T. Mueller,[28] T. Mueller,[82] D. Muenstermann,[49] Y. Munwes,[154] J. A. Murillo Quijada,[18] W. J. Murray,[171,130] H. Musheghyan,[54] E. Musto,[153] A. G. Myagkov,[129,aa] M. Myska,[127] O. Nackenhorst,[54] J. Nadal,[54] K. Nagai,[61] R. Nagai,[158] Y. Nagai,[84] K. Nagano,[65] A. Nagarkar,[110] Y. Nagasaka,[59] M. Nagel,[100] A. M. Nairz,[30] Y. Nakahama,[30] K. Nakamura,[65] T. Nakamura,[156] I. Nakano,[111] H. Namasivayam,[41] G. Nanava,[21] R. Narayan,[58b] T. Nattermann,[21] T. Naumann,[42] G. Navarro,[163] R. Nayyar,[7] H. A. Neal,[88] P. Yu. Nechaeva,[95] T. J. Neep,[83] P. D. Nef,[144] A. Negri,[120a,120b] G. Negri,[30] M. Negrini,[20a] S. Nektarijevic,[49] A. Nelson,[164] T. K. Nelson,[144] S. Nemecek,[126] P. Nemethy,[109] A. A. Nepomuceno,[24a] M. Nessi,[30,bb] M. S. Neubauer,[166] M. Neumann,[176] R. M. Neves,[109] P. Nevski,[25] P. R. Newman,[18] D. H. Nguyen,[6] R. B. Nickerson,[119] R. Nicolaidou,[137] B. Nicquevert,[30] J. Nielsen,[138] N. Nikiforou,[35] A. Nikiforov,[16] V. Nikolaenko,[129,aa] I. Nikolic-Audit,[79] K. Nikolics,[49] K. Nikolopoulos,[18] P. Nilsson,[8] Y. Ninomiya,[156] A. Nisati,[133a] R. Nisius,[100] T. Nobe,[158] L. Nodulman,[6] M. Nomachi,[117] I. Nomidis,[29] S. Norberg,[112] M. Nordberg,[30] O. Novgorodova,[44] S. Nowak,[100] M. Nozaki,[65] L. Nozka,[114] K. Ntekas,[10] G. Nunes Hanninger,[87] T. Nunnemann,[99] E. Nurse,[77] F. Nuti,[87] B. J. O'Brien,[46] F. O'grady,[7] D. C. O'Neil,[143] V. O'Shea,[53] F. G. Oakham,[29,e] H. Oberlack,[100] T. Obermann,[21] J. Ocariz,[79] A. Ochi,[66] M. I. Ochoa,[77] S. Oda,[69] S. Odaka,[65] H. Ogren,[60] A. Oh,[83] S. H. Oh,[45] C. C. Ohm,[15] H. Ohman,[167] W. Okamura,[117] H. Okawa,[25] Y. Okumura,[31] T. Okuyama,[156] A. Olariu,[26a] A. G. Olchevski,[64] S. A. Olivares Pino,[46] D. Oliveira Damazio,[25] E. Oliver Garcia,[168] A. Olszewski,[39] J. Olszowska,[39] A. Onofre,[125a,125e] P. U. E. Onyisi,[31,cc] C. J. Oram,[160a] M. J. Oreglia,[31] Y. Oren,[154] D. Orestano,[135a,135b] N. Orlando,[72a,72b] C. Oropeza Barrera,[53] R. S. Orr,[159] B. Osculati,[50a,50b] R. Ospanov,[121] G. Otero y Garzon,[27] H. Otono,[69] M. Ouchrif,[136d] E. A. Ouellette,[170] F. Ould-Saada,[118] A. Ouraou,[137] K. P. Oussoren,[106] Q. Ouyang,[33a] A. Ovcharova,[15] M. Owen,[83] V. E. Ozcan,[19a] N. Ozturk,[8] K. Pachal,[119] A. Pacheco Pages,[12] C. Padilla Aranda,[12] M. Pagáčová,[48] S. Pagan Griso,[15] E. Paganis,[140] C. Pahl,[100] F. Paige,[25] P. Pais,[85] K. Pajchel,[118] G. Palacino,[160b] S. Palestini,[30] M. Palka,[38b] D. Pallin,[34] A. Palma,[125a,125b] J. D. Palmer,[18] Y. B. Pan,[174] E. Panagiotopoulou,[10] J. G. Panduro Vazquez,[76] P. Pani,[106] N. Panikashvili,[88] S. Panitkin,[25] D. Pantea,[26a] L. Paolozzi,[134a,134b] Th. D. Papadopoulou,[10] K. Papageorgiou,[155,m] A. Paramonov,[6] D. Paredes Hernandez,[34] M. A. Parker,[28] F. Parodi,[50a,50b] J. A. Parsons,[35] U. Parzefall,[48] E. Pasqualucci,[133a] S. Passaggio,[50a] A. Passeri,[135a] F. Pastore,[135a,135b,a] Fr. Pastore,[76] G. Pásztor,[29] S. Pataraia,[176] N. D. Patel,[151] J. R. Pater,[83] S. Patricelli,[103a,103b]

T. Pauly,[30] J. Pearce,[170] M. Pedersen,[118] S. Pedraza Lopez,[168] R. Pedro,[125a,125b] S. V. Peleganchuk,[108] D. Pelikan,[167] H. Peng,[33b] B. Penning,[31] J. Penwell,[60] D. V. Perepelitsa,[25] E. Perez Codina,[160a] M. T. Pérez García-Estañ,[168] V. Perez Reale,[35] L. Perini,[90a,90b] H. Pernegger,[30] R. Perrino,[72a] R. Peschke,[42] V. D. Peshekhonov,[64] K. Peters,[30] R. F. Y. Peters,[83] B. A. Petersen,[30] T. C. Petersen,[36] E. Petit,[42] A. Petridis,[147a,147b] C. Petridou,[155] E. Petrolo,[133a] F. Petrucci,[135a,135b] N. E. Pettersson,[158] R. Pezoa,[32b] P. W. Phillips,[130] G. Piacquadio,[144] E. Pianori,[171] A. Picazio,[49] E. Piccaro,[75] M. Piccinini,[20a,20b] R. Piegaia,[27] D. T. Pignotti,[110] J. E. Pilcher,[31] A. D. Pilkington,[77] J. Pina,[125a,125b,125d] M. Pinamonti,[165a,165c,dd] A. Pinder,[119] J. L. Pinfold,[3] A. Pingel,[36] B. Pinto,[125a] S. Pires,[79] M. Pitt,[173] C. Pizio,[90a,90b] L. Plazak,[145a] M.-A. Pleier,[25] V. Pleskot,[128] E. Plotnikova,[64] P. Plucinski,[147a,147b] S. Poddar,[58a] F. Podlyski,[34] R. Poettgen,[82] L. Poggioli,[116] D. Pohl,[21] M. Pohl,[49] G. Polesello,[120a] A. Policicchio,[37a,37b] R. Polifka,[159] A. Polini,[20a] C. S. Pollard,[45] V. Polychronakos,[25] K. Pommès,[30] L. Pontecorvo,[133a] B. G. Pope,[89] G. A. Popeneciu,[26b] D. S. Popovic,[13a] A. Poppleton,[30] X. Portell Bueso,[12] S. Pospisil,[127] K. Potamianos,[15] I. N. Potrap,[64] C. J. Potter,[150] C. T. Potter,[115] G. Poulard,[30] J. Poveda,[60] V. Pozdnyakov,[64] P. Pralavorio,[84] A. Pranko,[15] S. Prasad,[30] R. Pravahan,[8] S. Prell,[63] D. Price,[83] J. Price,[73] L. E. Price,[6] D. Prieur,[124] M. Primavera,[72a] M. Proissl,[46] K. Prokofiev,[47] F. Prokoshin,[32b] E. Protopapadaki,[137] S. Protopopescu,[25] J. Proudfoot,[6] M. Przybycien,[38a] H. Przysiezniak,[5] E. Ptacek,[115] D. Puddu,[135a,135b] E. Pueschel,[85] D. Puldon,[149] M. Purohit,[25,ee] P. Puzo,[116] J. Qian,[88] G. Qin,[53] Y. Qin,[83] A. Quadt,[54] D. R. Quarrie,[15] W. B. Quayle,[165a,165b] M. Queitsch-Maitland,[83] D. Quilty,[53] A. Qureshi,[160b] V. Radeka,[25] V. Radescu,[42] S. K. Radhakrishnan,[149] P. Radloff,[115] P. Rados,[87] F. Ragusa,[90a,90b] G. Rahal,[179] S. Rajagopalan,[25] M. Rammensee,[30] A. S. Randle-Conde,[40] C. Rangel-Smith,[167] K. Rao,[164] F. Rauscher,[99] T. C. Rave,[48] T. Ravenscroft,[53] M. Raymond,[30] A. L. Read,[118] N. P. Readioff,[73] D. M. Rebuzzi,[120a,120b] A. Redelbach,[175] G. Redlinger,[25] R. Reece,[138] K. Reeves,[41] L. Rehnisch,[16] H. Reisin,[27] M. Relich,[164] C. Rembser,[30] H. Ren,[33a] Z. L. Ren,[152] A. Renaud,[116] M. Rescigno,[133a] S. Resconi,[90a] O. L. Rezanova,[108,t] P. Reznicek,[128] R. Rezvani,[94] R. Richter,[100] M. Ridel,[79] P. Rieck,[16] J. Rieger,[54] M. Rijssenbeek,[149] A. Rimoldi,[120a,120b] M. Rimoldi,[90a,90b] L. Rinaldi,[20a] E. Ritsch,[61] I. Riu,[12] F. Rizatdinova,[113] E. Rizvi,[75] S. H. Robertson,[86,j] A. Robichaud-Veronneau,[86] D. Robinson,[28] J. E. M. Robinson,[83] A. Robson,[53] C. Roda,[123a,123b] L. Rodrigues,[30] S. Roe,[30] O. Røhne,[118] S. Rolli,[162] A. Romaniouk,[97] M. Romano,[20a,20b] E. Romero Adam,[168] N. Rompotis,[139] M. Ronzani,[48] L. Roos,[79] E. Ros,[168] S. Rosati,[133a] K. Rosbach,[49] M. Rose,[76] P. Rose,[138] P. L. Rosendahl,[14] O. Rosenthal,[142] V. Rossetti,[147a,147b] E. Rossi,[103a,103b] L. P. Rossi,[50a] R. Rosten,[139] M. Rotaru,[26a] I. Roth,[173] J. Rothberg,[139] D. Rousseau,[116] C. R. Royon,[137] A. Rozanov,[84] Y. Rozen,[153] X. Ruan,[146c] F. Rubbo,[12] I. Rubinskiy,[42] V. I. Rud,[98] C. Rudolph,[44] M. S. Rudolph,[159] F. Rühr,[48] A. Ruiz-Martinez,[30] Z. Rurikova,[48] N. A. Rusakovich,[64] A. Ruschke,[99] J. P. Rutherfoord,[7] N. Ruthmann,[48] Y. F. Ryabov,[122] M. Rybar,[128] G. Rybkin,[116] N. C. Ryder,[119] A. F. Saavedra,[151] S. Sacerdoti,[27] A. Saddique,[3] I. Sadeh,[154] H. F-W. Sadrozinski,[138] R. Sadykov,[64] F. Safai Tehrani,[133a] H. Sakamoto,[156] Y. Sakurai,[172] G. Salamanna,[135a,135b] A. Salamon,[134a] M. Saleem,[112] D. Salek,[106] P. H. Sales De Bruin,[139] D. Salihagic,[100] A. Salnikov,[144] J. Salt,[168] D. Salvatore,[37a,37b] F. Salvatore,[150] A. Salvucci,[105] A. Salzburger,[30] D. Sampsonidis,[155] A. Sanchez,[103a,103b] J. Sánchez,[168] V. Sanchez Martinez,[168] H. Sandaker,[14] R. L. Sandbach,[75] H. G. Sander,[82] M. P. Sanders,[99] M. Sandhoff,[176] T. Sandoval,[28] C. Sandoval,[163] R. Sandstroem,[100] D. P. C. Sankey,[130] A. Sansoni,[47] C. Santoni,[34] R. Santonico,[134a,134b] H. Santos,[125a] I. Santoyo Castillo,[150] K. Sapp,[124] A. Sapronov,[64] J. G. Saraiva,[125a,125d] B. Sarrazin,[21] G. Sartisohn,[176] O. Sasaki,[65] Y. Sasaki,[156] G. Sauvage,[5,a] E. Sauvan,[5] P. Savard,[159,e] D. O. Savu,[30] C. Sawyer,[119] L. Sawyer,[78,n] D. H. Saxon,[53] J. Saxon,[121] C. Sbarra,[20a] A. Sbrizzi,[3] T. Scanlon,[77] D. A. Scannicchio,[164] M. Scarcella,[151] V. Scarfone,[37a,37b] J. Schaarschmidt,[173] P. Schacht,[100] D. Schaefer,[30] R. Schaefer,[42] S. Schaepe,[21] S. Schaetzel,[58b] U. Schäfer,[82] A. C. Schaffer,[116] D. Schaile,[99] R. D. Schamberger,[149] V. Scharf,[58a] V. A. Schegelsky,[122] D. Scheirich,[128] M. Schernau,[164] M. I. Scherzer,[35] C. Schiavi,[50a,50b] J. Schieck,[99] C. Schillo,[48] M. Schioppa,[37a,37b] S. Schlenker,[30] E. Schmidt,[48] K. Schmieden,[30] C. Schmitt,[82] C. Schmitt,[99] S. Schmitt,[58b] B. Schneider,[17] Y. J. Schnellbach,[73] U. Schnoor,[44] L. Schoeffel,[137] A. Schoening,[58b] B. D. Schoenrock,[89] A. L. S. Schorlemmer,[54] M. Schott,[82] D. Schouten,[160a] J. Schovancova,[25] S. Schramm,[159] M. Schreyer,[175] C. Schroeder,[82] N. Schuh,[82] M. J. Schultens,[21] H.-C. Schultz-Coulon,[58a] H. Schulz,[16] M. Schumacher,[48] B. A. Schumm,[138] Ph. Schune,[137] C. Schwanenberger,[83] A. Schwartzman,[144] Ph. Schwegler,[100] Ph. Schwemling,[137] R. Schwienhorst,[89] J. Schwindling,[137] T. Schwindt,[21] M. Schwoerer,[5] F. G. Sciacca,[17] E. Scifo,[116] G. Sciolla,[23] W. G. Scott,[130] F. Scuri,[123a,123b] F. Scutti,[21] J. Searcy,[88] G. Sedov,[42] E. Sedykh,[122] S. C. Seidel,[104] A. Seiden,[138] F. Seifert,[127] J. M. Seixas,[24a] G. Sekhniaidze,[103a] S. J. Sekula,[40] K. E. Selbach,[46] D. M. Seliverstov,[122,a] G. Sellers,[73] N. Semprini-Cesari,[20a,20b] C. Serfon,[30] L. Serin,[116] L. Serkin,[54] T. Serre,[84] R. Seuster,[160a] H. Severini,[112] T. Sfiligoj,[74] F. Sforza,[100] A. Sfyrla,[30] E. Shabalina,[54] M. Shamim,[115] L. Y. Shan,[33a] R. Shang,[166] J. T. Shank,[22] M. Shapiro,[15] P. B. Shatalov,[96] K. Shaw,[165a,165b] C. Y. Shehu,[150] P. Sherwood,[77]

L. Shi,[152,ff] S. Shimizu,[66] C. O. Shimmin,[164] M. Shimojima,[101] M. Shiyakova,[64] A. Shmeleva,[95] M. J. Shochet,[31] D. Short,[119] S. Shrestha,[63] E. Shulga,[97] M. A. Shupe,[7] S. Shushkevich,[42] P. Sicho,[126] O. Sidiropoulou,[155] D. Sidorov,[113] A. Sidoti,[133a] F. Siegert,[44] Dj. Sijacki,[13a] J. Silva,[125a,125d] Y. Silver,[154] D. Silverstein,[144] S. B. Silverstein,[147a] V. Simak,[127] O. Simard,[5] Lj. Simic,[13a] S. Simion,[116] E. Simioni,[82] B. Simmons,[77] R. Simoniello,[90a,90b] M. Simonyan,[36] P. Sinervo,[159] N. B. Sinev,[115] V. Sipica,[142] G. Siragusa,[175] A. Sircar,[78] A. N. Sisakyan,[64,a] S. Yu. Sivoklokov,[98] J. Sjölin,[147a,147b] T. B. Sjursen,[14] H. P. Skottowe,[57] K. Yu. Skovpen,[108] P. Skubic,[112] M. Slater,[18] T. Slavicek,[127] K. Sliwa,[162] V. Smakhtin,[173] B. H. Smart,[46] L. Smestad,[14] S. Yu. Smirnov,[97] Y. Smirnov,[97] L. N. Smirnova,[98,gg] O. Smirnova,[80] K. M. Smith,[53] M. Smizanska,[71] K. Smolek,[127] A. A. Snesarev,[95] G. Snidero,[75] S. Snyder,[25] R. Sobie,[170,j] F. Socher,[44] A. Soffer,[154] D. A. Soh,[152,ff] C. A. Solans,[30] M. Solar,[127] J. Solc,[127] E. Yu. Soldatov,[97] U. Soldevila,[168] A. A. Solodkov,[129] A. Soloshenko,[64] O. V. Solovyanov,[129] V. Solovyev,[122] P. Sommer,[48] H. Y. Song,[33b] N. Soni,[1] A. Sood,[15] A. Sopczak,[127] B. Sopko,[127] V. Sopko,[127] V. Sorin,[12] M. Sosebee,[8] R. Soualah,[165a,165c] P. Soueid,[94] A. M. Soukharev,[108] D. South,[42] S. Spagnolo,[72a,72b] F. Spanò,[76] W. R. Spearman,[57] F. Spettel,[100] R. Spighi,[20a] G. Spigo,[30] M. Spousta,[128] T. Spreitzer,[159] B. Spurlock,[8] R. D. St. Denis,[53,a] S. Staerz,[44] J. Stahlman,[121] R. Stamen,[58a] E. Stanecka,[39] R. W. Stanek,[6] C. Stanescu,[135a] M. Stanescu-Bellu,[42] M. M. Stanitzki,[42] S. Stapnes,[118] E. A. Starchenko,[129] J. Stark,[55] P. Staroba,[126] P. Starovoitov,[42] R. Staszewski,[39] P. Stavina,[145a,a] P. Steinberg,[25] B. Stelzer,[143] H. J. Stelzer,[30] O. Stelzer-Chilton,[160a] H. Stenzel,[52] S. Stern,[100] G. A. Stewart,[53] J. A. Stillings,[21] M. C. Stockton,[86] M. Stoebe,[86] G. Stoicea,[26a] P. Stolte,[54] S. Stonjek,[100] A. R. Stradling,[8] A. Straessner,[44] M. E. Stramaglia,[17] J. Strandberg,[148] S. Strandberg,[147a,147b] A. Strandlie,[118] E. Strauss,[144] M. Strauss,[112] P. Strizenec,[145b] R. Ströhmer,[175] D. M. Strom,[115] R. Stroynowski,[40] S. A. Stucci,[17] B. Stugu,[14] N. A. Styles,[42] D. Su,[144] J. Su,[124] R. Subramaniam,[78] A. Succurro,[12] Y. Sugaya,[117] C. Suhr,[107] M. Suk,[127] V. V. Sulin,[95] S. Sultansoy,[4c] T. Sumida,[67] S. Sun,[57] X. Sun,[33a] J. E. Sundermann,[48] K. Suruliz,[140] G. Susinno,[37a,37b] M. R. Sutton,[150] Y. Suzuki,[65] M. Svatos,[126] S. Swedish,[169] M. Swiatlowski,[144] I. Sykora,[145a] T. Sykora,[128] D. Ta,[89] C. Taccini,[135a,135b] K. Tackmann,[42] J. Taenzer,[159] A. Taffard,[164] R. Tafirout,[160a] N. Taiblum,[154] H. Takai,[25] R. Takashima,[68] H. Takeda,[66] T. Takeshita,[141] Y. Takubo,[65] M. Talby,[84] A. A. Talyshev,[108,t] J. Y. C. Tam,[175] K. G. Tan,[87] J. Tanaka,[156] R. Tanaka,[116] S. Tanaka,[132] S. Tanaka,[65] A. J. Tanasijczuk,[143] B. B. Tannenwald,[110] N. Tannoury,[21] S. Tapprogge,[82] S. Tarem,[153] F. Tarrade,[29] G. F. Tartarelli,[90a] P. Tas,[128] M. Tasevsky,[126] T. Tashiro,[67] E. Tassi,[37a,37b] A. Tavares Delgado,[125a,125b] Y. Tayalati,[136d] F. E. Taylor,[93] G. N. Taylor,[87] W. Taylor,[160b] F. A. Teischinger,[30] M. Teixeira Dias Castanheira,[75] P. Teixeira-Dias,[76] K. K. Temming,[48] H. Ten Kate,[30] P. K. Teng,[152] J. J. Teoh,[117] S. Terada,[65] K. Terashi,[156] J. Terron,[81] S. Terzo,[100] M. Testa,[47] R. J. Teuscher,[159,j] J. Therhaag,[21] T. Theveneaux-Pelzer,[34] J. P. Thomas,[18] J. Thomas-Wilsker,[76] E. N. Thompson,[35] P. D. Thompson,[18] P. D. Thompson,[159] A. S. Thompson,[53] L. A. Thomsen,[36] E. Thomson,[121] M. Thomson,[28] W. M. Thong,[87] R. P. Thun,[88,a] F. Tian,[35] M. J. Tibbetts,[15] V. O. Tikhomirov,[95,hh] Yu. A. Tikhonov,[108,t] S. Timoshenko,[97] E. Tiouchichine,[84] P. Tipton,[177] S. Tisserant,[84] T. Todorov,[5] S. Todorova-Nova,[128] B. Toggerson,[7] J. Tojo,[69] S. Tokár,[145a] K. Tokushuku,[65] K. Tollefson,[89] L. Tomlinson,[83] M. Tomoto,[102] L. Tompkins,[31] K. Toms,[104] N. D. Topilin,[64] E. Torrence,[115] H. Torres,[143] E. Torró Pastor,[168] J. Toth,[84,ii] F. Touchard,[84] D. R. Tovey,[140] H. L. Tran,[116] T. Trefzger,[175] L. Tremblet,[30] A. Tricoli,[30] I. M. Trigger,[160a] S. Trincaz-Duvoid,[79] M. F. Tripiana,[12] W. Trischuk,[159] B. Trocmé,[55] C. Troncon,[90a] M. Trottier-McDonald,[143] M. Trovatelli,[135a,135b] P. True,[89] M. Trzebinski,[39] A. Trzupek,[39] C. Tsarouchas,[30] J. C-L. Tseng,[119] P. V. Tsiareshka,[91] D. Tsionou,[137] G. Tsipolitis,[10] N. Tsirintanis,[9] S. Tsiskaridze,[12] V. Tsiskaridze,[48] E. G. Tskhadadze,[51a] I. I. Tsukerman,[96] V. Tsulaia,[15] S. Tsuno,[65] D. Tsybychev,[149] A. Tudorache,[26a] V. Tudorache,[26a] A. N. Tuna,[121] S. A. Tupputi,[20a,20b] S. Turchikhin,[98,gg] D. Turecek,[127] I. Turk Cakir,[4d] R. Turra,[90a,90b] P. M. Tuts,[35] A. Tykhonov,[49] M. Tylmad,[147a,147b] M. Tyndel,[130] K. Uchida,[21] I. Ueda,[156] R. Ueno,[29] M. Ughetto,[84] M. Ugland,[14] M. Uhlenbrock,[21] F. Ukegawa,[161] G. Unal,[30] A. Undrus,[25] G. Unel,[164] F. C. Ungaro,[48] Y. Unno,[65] D. Urbaniec,[35] P. Urquijo,[87] G. Usai,[8] A. Usanova,[61] L. Vacavant,[84] V. Vacek,[127] B. Vachon,[86] N. Valencic,[106] S. Valentinetti,[20a,20b] A. Valero,[168] L. Valery,[34] S. Valkar,[128] E. Valladolid Gallego,[168] S. Vallecorsa,[49] J. A. Valls Ferrer,[168] W. Van Den Wollenberg,[106] P. C. Van Der Deijl,[106] R. van der Geer,[106] H. van der Graaf,[106] R. Van Der Leeuw,[106] D. van der Ster,[30] N. van Eldik,[30] P. van Gemmeren,[6] J. Van Nieuwkoop,[143] I. van Vulpen,[106] M. C. van Woerden,[30] M. Vanadia,[133a,133b] W. Vandelli,[30] R. Vanguri,[121] A. Vaniachine,[6] P. Vankov,[42] F. Vannucci,[79] G. Vardanyan,[178] R. Vari,[133a] E. W. Varnes,[7] T. Varol,[85] D. Varouchas,[79] A. Vartapetian,[8] K. E. Varvell,[151] F. Vazeille,[34] T. Vazquez Schroeder,[54] J. Veatch,[7] F. Veloso,[125a,125c] S. Veneziano,[133a] A. Ventura,[72a,72b] D. Ventura,[85] M. Venturi,[170] N. Venturi,[159] A. Venturini,[23] V. Vercesi,[120a] M. Verducci,[133a,133b] W. Verkerke,[106] J. C. Vermeulen,[106] A. Vest,[44] M. C. Vetterli,[143,e] O. Viazlo,[80] I. Vichou,[166] T. Vickey,[146c,jj] O. E. Vickey Boeriu,[146c] G. H. A. Viehhauser,[119] S. Viel,[169] R. Vigne,[30] M. Villa,[20a,20b] M. Villaplana Perez,[90a,90b]

E. Vilucchi,[47] M. G. Vincter,[29] V. B. Vinogradov,[64] J. Virzi,[15] I. Vivarelli,[150] F. Vives Vaque,[3] S. Vlachos,[10] D. Vladoiu,[99] M. Vlasak,[127] A. Vogel,[21] M. Vogel,[32a] P. Vokac,[127] G. Volpi,[123a,123b] M. Volpi,[87] H. von der Schmitt,[100] H. von Radziewski,[48] E. von Toerne,[21] V. Vorobel,[128] K. Vorobev,[97] M. Vos,[168] R. Voss,[30] J. H. Vossebeld,[73] N. Vranjes,[137] M. Vranjes Milosavljevic,[106] V. Vrba,[126] M. Vreeswijk,[106] T. Vu Anh,[48] R. Vuillermet,[30] I. Vukotic,[31] Z. Vykydal,[127] P. Wagner,[21] W. Wagner,[176] H. Wahlberg,[70] S. Wahrmund,[44] J. Wakabayashi,[102] J. Walder,[71] R. Walker,[99] W. Walkowiak,[142] R. Wall,[177] P. Waller,[73] B. Walsh,[177] C. Wang,[152,kk] C. Wang,[45] F. Wang,[174] H. Wang,[15] H. Wang,[40] J. Wang,[42] J. Wang,[33a] K. Wang,[86] R. Wang,[104] S. M. Wang,[152] T. Wang,[21] X. Wang,[177] C. Wanotayaroj,[115] A. Warburton,[86] C. P. Ward,[28] D. R. Wardrope,[77] M. Warsinsky,[48] A. Washbrook,[46] C. Wasicki,[42] P. M. Watkins,[18] A. T. Watson,[18] I. J. Watson,[151] M. F. Watson,[18] G. Watts,[139] S. Watts,[83] B. M. Waugh,[77] S. Webb,[83] M. S. Weber,[17] S. W. Weber,[175] J. S. Webster,[31] A. R. Weidberg,[119] P. Weigell,[100] B. Weinert,[60] J. Weingarten,[54] C. Weiser,[48] H. Weits,[106] P. S. Wells,[30] T. Wenaus,[25] D. Wendland,[16] Z. Weng,[152,ff] T. Wengler,[30] S. Wenig,[30] N. Wermes,[21] M. Werner,[48] P. Werner,[30] M. Wessels,[58a] J. Wetter,[162] K. Whalen,[29] A. White,[8] M. J. White,[1] R. White,[32b] S. White,[123a,123b] D. Whiteson,[164] D. Wicke,[176] F. J. Wickens,[130] W. Wiedenmann,[174] M. Wielers,[130] P. Wienemann,[21] C. Wiglesworth,[36] L. A. M. Wiik-Fuchs,[21] P. A. Wijeratne,[77] A. Wildauer,[100] M. A. Wildt,[42,ll] H. G. Wilkens,[30] J. Z. Will,[99] H. H. Williams,[121] S. Williams,[28] C. Willis,[89] S. Willocq,[85] A. Wilson,[88] J. A. Wilson,[18] I. Wingerter-Seez,[5] F. Winklmeier,[115] B. T. Winter,[21] M. Wittgen,[144] T. Wittig,[43] J. Wittkowski,[99] S. J. Wollstadt,[82] M. W. Wolter,[39] H. Wolters,[125a,125c] B. K. Wosiek,[39] J. Wotschack,[30] M. J. Woudstra,[83] K. W. Wozniak,[39] M. Wright,[53] M. Wu,[55] S. L. Wu,[174] X. Wu,[49] Y. Wu,[88] E. Wulf,[35] T. R. Wyatt,[83] B. M. Wynne,[46] S. Xella,[36] M. Xiao,[137] D. Xu,[33a] L. Xu,[33b,mm] B. Yabsley,[151] S. Yacoob,[146b,nn] R. Yakabe,[66] M. Yamada,[65] H. Yamaguchi,[156] Y. Yamaguchi,[117] A. Yamamoto,[65] K. Yamamoto,[63] S. Yamamoto,[156] T. Yamamura,[156] T. Yamanaka,[156] K. Yamauchi,[102] Y. Yamazaki,[66] Z. Yan,[22] H. Yang,[33e] H. Yang,[174] U. K. Yang,[83] Y. Yang,[110] S. Yanush,[92] L. Yao,[33a] W-M. Yao,[15] Y. Yasu,[65] E. Yatsenko,[42] K. H. Yau Wong,[21] J. Ye,[40] S. Ye,[25] A. L. Yen,[57] E. Yildirim,[42] M. Yilmaz,[4b] R. Yoosoofmiya,[124] K. Yorita,[172] R. Yoshida,[6] K. Yoshihara,[156] C. Young,[144] C. J. S. Young,[30] S. Youssef,[22] D. R. Yu,[15] J. Yu,[8] J. M. Yu,[88] J. Yu,[113] L. Yuan,[66] A. Yurkewicz,[107] I. Yusuff,[28,oo] B. Zabinski,[39] R. Zaidan,[62] A. M. Zaitsev,[129,aa] A. Zaman,[149] S. Zambito,[23] L. Zanello,[133a,133b] D. Zanzi,[100] C. Zeitnitz,[176] M. Zeman,[127] A. Zemla,[38a] K. Zengel,[23] O. Zenin,[129] T. Ženiš,[145a] D. Zerwas,[116] G. Zevi della Porta,[57] D. Zhang,[88] F. Zhang,[174] H. Zhang,[89] J. Zhang,[6] L. Zhang,[152] X. Zhang,[33d] Z. Zhang,[116] Z. Zhao,[33b] A. Zhemchugov,[64] J. Zhong,[119] B. Zhou,[88] L. Zhou,[35] N. Zhou,[164] C. G. Zhu,[33d] H. Zhu,[33a] J. Zhu,[88] Y. Zhu,[33b] X. Zhuang,[33a] K. Zhukov,[95] A. Zibell,[175] D. Zieminska,[60] N. I. Zimine,[64] C. Zimmermann,[82] R. Zimmermann,[21] S. Zimmermann,[21] S. Zimmermann,[48] Z. Zinonos,[54] M. Ziolkowski,[142] G. Zobernig,[174] A. Zoccoli,[20a,20b] M. zur Nedden,[16] G. Zurzolo,[103a,103b] V. Zutshi[107] and L. Zwalinski[30]

(ATLAS Collaboration)

[1]*Department of Physics, University of Adelaide, Adelaide, Australia*
[2]*Physics Department, SUNY Albany, Albany, New York, USA*
[3]*Department of Physics, University of Alberta, Edmonton AB, Canada*
[4a]*Department of Physics, Ankara University, Ankara, Turkey*
[4b]*Department of Physics, Gazi University, Ankara, Turkey*
[4c]*Division of Physics, TOBB University of Economics and Technology, Ankara, Turkey*
[4d]*Turkish Atomic Energy Authority, Ankara, Turkey*
[5]*LAPP, CNRS/IN2P3 and Université de Savoie, Annecy-le-Vieux, France*
[6]*High Energy Physics Division, Argonne National Laboratory, Argonne, Illinois, USA*
[7]*Department of Physics, University of Arizona, Tucson, Arizona, USA*
[8]*Department of Physics, The University of Texas at Arlington, Arlington, Texas, USA*
[9]*Physics Department, University of Athens, Athens, Greece*
[10]*Physics Department, National Technical University of Athens, Zografou, Greece*
[11]*Institute of Physics, Azerbaijan Academy of Sciences, Baku, Azerbaijan*
[12]*Institut de Física d'Altes Energies and Departament de Física de la Universitat Autònoma de Barcelona, Barcelona, Spain*
[13a]*Institute of Physics, University of Belgrade, Belgrade, Serbia*
[13b]*Vinca Institute of Nuclear Sciences, University of Belgrade, Belgrade, Serbia*
[14]*Department for Physics and Technology, University of Bergen, Bergen, Norway*
[15]*Physics Division, Lawrence Berkeley National Laboratory and University of California, Berkeley, California, USA*

[16]Department of Physics, Humboldt University, Berlin, Germany
[17]Albert Einstein Center for Fundamental Physics and Laboratory for High Energy Physics, University of Bern, Bern, Switzerland
[18]School of Physics and Astronomy, University of Birmingham, Birmingham, United Kingdom
[19a]Department of Physics, Bogazici University, Istanbul, Turkey
[19b]Department of Physics, Dogus University, Istanbul, Turkey
[19c]Department of Physics Engineering, Gaziantep University, Gaziantep, Turkey
[20a]INFN Sezione di Bologna, Bologna, Italy
[20b]Dipartimento di Fisica e Astronomia, Università di Bologna, Bologna, Italy
[21]Physikalisches Institut, University of Bonn, Bonn, Germany
[22]Department of Physics, Boston University, Boston, Massachusetts, USA
[23]Department of Physics, Brandeis University, Waltham, Massachusetts, USA
[24a]Universidade Federal do Rio De Janeiro COPPE/EE/IF, Rio de Janeiro, Brazil
[24b]Federal University of Juiz de Fora (UFJF), Juiz de Fora, Brazil
[24c]Federal University of Sao Joao del Rei (UFSJ), Sao Joao del Rei, Brazil
[24d]Instituto de Fisica, Universidade de Sao Paulo, Sao Paulo, Brazil
[25]Physics Department, Brookhaven National Laboratory, Upton, New York, USA
[26a]National Institute of Physics and Nuclear Engineering, Bucharest, Romania
[26b]National Institute for Research and Development of Isotopic and Molecular Technologies, Physics Department, Cluj Napoca, Romania
[26c]University Politehnica Bucharest, Bucharest, Romania
[26d]West University in Timisoara, Timisoara, Romania
[27]Departamento de Física, Universidad de Buenos Aires, Buenos Aires, Argentina
[28]Cavendish Laboratory, University of Cambridge, Cambridge, United Kingdom
[29]Department of Physics, Carleton University, Ottawa ON, Canada
[30]CERN, Geneva, Switzerland
[31]Enrico Fermi Institute, University of Chicago, Chicago, Illinois, USA
[32a]Departamento de Física, Pontificia Universidad Católica de Chile, Santiago, Chile
[32b]Departamento de Física, Universidad Técnica Federico Santa María, Valparaíso, Chile
[33a]Institute of High Energy Physics, Chinese Academy of Sciences, Beijing, China
[33b]Department of Modern Physics, University of Science and Technology of China, Anhui, China
[33c]Department of Physics, Nanjing University, Jiangsu, China
[33d]School of Physics, Shandong University, Shandong, China
[33e]Physics Department, Shanghai Jiao Tong University, Shanghai, China
[34]Laboratoire de Physique Corpusculaire, Clermont Université and Université Blaise Pascal and CNRS/IN2P3, Clermont-Ferrand, France
[35]Nevis Laboratory, Columbia University, Irvington, New York, USA
[36]Niels Bohr Institute, University of Copenhagen, Kobenhavn, Denmark
[37a]INFN Gruppo Collegato di Cosenza, Laboratori Nazionali di Frascati, Italy
[37b]Dipartimento di Fisica, Università della Calabria, Rende, Italy
[38a]AGH University of Science and Technology, Faculty of Physics and Applied Computer Science, Krakow, Poland
[38b]Marian Smoluchowski Institute of Physics, Jagiellonian University, Krakow, Poland
[39]The Henryk Niewodniczanski Institute of Nuclear Physics, Polish Academy of Sciences, Krakow, Poland
[40]Physics Department, Southern Methodist University, Dallas, Texas, USA
[41]Physics Department, University of Texas at Dallas, Richardson, Texas, USA
[42]DESY, Hamburg and Zeuthen, Germany
[43]Institut für Experimentelle Physik IV, Technische Universität Dortmund, Dortmund, Germany
[44]Institut für Kern- und Teilchenphysik, Technische Universität Dresden, Dresden, Germany
[45]Department of Physics, Duke University, Durham, North Carolina, USA
[46]SUPA - School of Physics and Astronomy, University of Edinburgh, Edinburgh, United Kingdom
[47]INFN Laboratori Nazionali di Frascati, Frascati, Italy
[48]Fakultät für Mathematik und Physik, Albert-Ludwigs-Universität, Freiburg, Germany
[49]Section de Physique, Université de Genève, Geneva, Switzerland
[50a]INFN Sezione di Genova, Genova, Italy
[50b]Dipartimento di Fisica, Università di Genova, Genova, Italy
[51a]E. Andronikashvili Institute of Physics, Iv. Javakhishvili Tbilisi State University, Tbilisi, Georgia
[51b]High Energy Physics Institute, Tbilisi State University, Tbilisi, Georgia
[52]II Physikalisches Institut, Justus-Liebig-Universität Giessen, Giessen, Germany
[53]SUPA - School of Physics and Astronomy, University of Glasgow, Glasgow, United Kingdom

[54]*II Physikalisches Institut, Georg-August-Universität, Göttingen, Germany*
[55]*Laboratoire de Physique Subatomique et de Cosmologie, Université Grenoble-Alpes, CNRS/IN2P3, Grenoble, France*
[56]*Department of Physics, Hampton University, Hampton, Virginia, USA*
[57]*Laboratory for Particle Physics and Cosmology, Harvard University, Cambridge, Massachusetts, USA*
[58a]*Kirchhoff-Institut für Physik, Ruprecht-Karls-Universität Heidelberg, Heidelberg, Germany*
[58b]*Physikalisches Institut, Ruprecht-Karls-Universität Heidelberg, Heidelberg, Germany*
[58c]*ZITI Institut für technische Informatik, Ruprecht-Karls-Universität Heidelberg, Mannheim, Germany*
[59]*Faculty of Applied Information Science, Hiroshima Institute of Technology, Hiroshima, Japan*
[60]*Department of Physics, Indiana University, Bloomington, Indiana, USA*
[61]*Institut für Astro- und Teilchenphysik, Leopold-Franzens-Universität, Innsbruck, Austria*
[62]*University of Iowa, Iowa City, Iowa, USA*
[63]*Department of Physics and Astronomy, Iowa State University, Ames, Iowa, USA*
[64]*Joint Institute for Nuclear Research, JINR Dubna, Dubna, Russia*
[65]*KEK, High Energy Accelerator Research Organization, Tsukuba, Japan*
[66]*Graduate School of Science, Kobe University, Kobe, Japan*
[67]*Faculty of Science, Kyoto University, Kyoto, Japan*
[68]*Kyoto University of Education, Kyoto, Japan*
[69]*Department of Physics, Kyushu University, Fukuoka, Japan*
[70]*Instituto de Física La Plata, Universidad Nacional de La Plata and CONICET, La Plata, Argentina*
[71]*Physics Department, Lancaster University, Lancaster, United Kingdom*
[72a]*INFN Sezione di Lecce, Lecce, Italy*
[72b]*Dipartimento di Matematica e Fisica, Università del Salento, Lecce, Italy*
[73]*Oliver Lodge Laboratory, University of Liverpool, Liverpool, United Kingdom*
[74]*Department of Physics, Jožef Stefan Institute and University of Ljubljana, Ljubljana, Slovenia*
[75]*School of Physics and Astronomy, Queen Mary University of London, London, United Kingdom*
[76]*Department of Physics, Royal Holloway University of London, Surrey, United Kingdom*
[77]*Department of Physics and Astronomy, University College London, London, United Kingdom*
[78]*Louisiana Tech University, Ruston, Louisiana, USA*
[79]*Laboratoire de Physique Nucléaire et de Hautes Energies, UPMC and Université Paris-Diderot and CNRS/IN2P3, Paris, France*
[80]*Fysiska institutionen, Lunds universitet, Lund, Sweden*
[81]*Departamento de Fisica Teorica C-15, Universidad Autonoma de Madrid, Madrid, Spain*
[82]*Institut für Physik, Universität Mainz, Mainz, Germany*
[83]*School of Physics and Astronomy, University of Manchester, Manchester, United Kingdom*
[84]*CPPM, Aix-Marseille Université and CNRS/IN2P3, Marseille, France*
[85]*Department of Physics, University of Massachusetts, Amherst, Massachusetts, USA*
[86]*Department of Physics, McGill University, Montreal QC, Canada*
[87]*School of Physics, University of Melbourne, Victoria, Australia*
[88]*Department of Physics, The University of Michigan, Ann Arbor, Michigan, USA*
[89]*Department of Physics and Astronomy, Michigan State University, East Lansing, Michigan, USA*
[90a]*INFN Sezione di Milano, Milano, Italy*
[90b]*Dipartimento di Fisica, Università di Milano, Milano, Italy*
[91]*B. I. Stepanov Institute of Physics, National Academy of Sciences of Belarus, Minsk, Republic of Belarus*
[92]*National Scientific and Educational Centre for Particle and High Energy Physics, Minsk, Republic of Belarus*
[93]*Department of Physics, Massachusetts Institute of Technology, Cambridge, Massachusetts, USA*
[94]*Group of Particle Physics, University of Montreal, Montreal, Québec, Canada*
[95]*P. N. Lebedev Institute of Physics, Academy of Sciences, Moscow, Russia*
[96]*Institute for Theoretical and Experimental Physics (ITEP), Moscow, Russia*
[97]*Moscow Engineering and Physics Institute (MEPhI), Moscow, Russia*
[98]*D. V. Skobeltsyn Institute of Nuclear Physics, M. V. Lomonosov Moscow State University, Moscow, Russia*
[99]*Fakultät für Physik, Ludwig-Maximilians-Universität München, München, Germany*
[100]*Max-Planck-Institut für Physik (Werner-Heisenberg-Institut), München, Germany*
[101]*Nagasaki Institute of Applied Science, Nagasaki, Japan*
[102]*Graduate School of Science and Kobayashi-Maskawa Institute, Nagoya University, Nagoya, Japan*
[103a]*INFN Sezione di Napoli, Napoli, Italy*
[103b]*Dipartimento di Fisica, Università di Napoli, Napoli, Italy*
[104]*Department of Physics and Astronomy, University of New Mexico, Albuquerque, New Mexico, USA*

[105]*Institute for Mathematics, Astrophysics and Particle Physics, Radboud University Nijmegen/Nikhef, Nijmegen, Netherlands*
[106]*Nikhef National Institute for Subatomic Physics and University of Amsterdam, Amsterdam, Netherlands*
[107]*Department of Physics, Northern Illinois University, DeKalb, Illinois, USA*
[108]*Budker Institute of Nuclear Physics, SB RAS, Novosibirsk, Russia*
[109]*Department of Physics, New York University, New York, New York, USA*
[110]*Ohio State University, Columbus, Ohio, USA*
[111]*Faculty of Science, Okayama University, Okayama, Japan*
[112]*Homer L. Dodge Department of Physics and Astronomy, University of Oklahoma, Norman, Oklahoma, USA*
[113]*Department of Physics, Oklahoma State University, Stillwater, Oklahoma, USA*
[114]*Palacký University, RCPTM, Olomouc, Czech Republic*
[115]*Center for High Energy Physics, University of Oregon, Eugene, Oregon, USA*
[116]*LAL, Université Paris-Sud and CNRS/IN2P3, Orsay, France*
[117]*Graduate School of Science, Osaka University, Osaka, Japan*
[118]*Department of Physics, University of Oslo, Oslo, Norway*
[119]*Department of Physics, Oxford University, Oxford, United Kingdom*
[120a]*INFN Sezione di Pavia, Pavia, Italy*
[120b]*Dipartimento di Fisica, Università di Pavia, Pavia, Italy*
[121]*Department of Physics, University of Pennsylvania, Philadelphia, Pennsylvania, USA*
[122]*Petersburg Nuclear Physics Institute, Gatchina, Russia*
[123a]*INFN Sezione di Pisa, Pisa, Italy*
[123b]*Dipartimento di Fisica E. Fermi, Università di Pisa, Pisa, Italy*
[124]*Department of Physics and Astronomy, University of Pittsburgh, Pittsburgh, Pennsylvania, USA*
[125a]*Laboratorio de Instrumentacao e Fisica Experimental de Particulas - LIP, Lisboa, Portugal*
[125b]*Faculdade de Ciências, Universidade de Lisboa, Lisboa, Portugal*
[125c]*Department of Physics, University of Coimbra, Coimbra, Portugal*
[125d]*Centro de Física Nuclear da Universidade de Lisboa, Lisboa, Portugal*
[125e]*Departamento de Fisica, Universidade do Minho, Braga, Portugal*
[125f]*Departamento de Fisica Teorica y del Cosmos and CAFPE, Universidad de Granada, Granada (Spain), Portugal*
[125g]*Dep Fisica and CEFITEC of Faculdade de Ciencias e Tecnologia, Universidade Nova de Lisboa, Caparica, Portugal*
[126]*Institute of Physics, Academy of Sciences of the Czech Republic, Praha, Czech Republic*
[127]*Czech Technical University in Prague, Praha, Czech Republic*
[128]*Faculty of Mathematics and Physics, Charles University in Prague, Praha, Czech Republic*
[129]*State Research Center Institute for High Energy Physics, Protvino, Russia*
[130]*Particle Physics Department, Rutherford Appleton Laboratory, Didcot, United Kingdom*
[131]*Physics Department, University of Regina, Regina, Saskatchewan, Canada*
[132]*Ritsumeikan University, Kusatsu, Shiga, Japan*
[133a]*INFN Sezione di Roma, Roma, Italy*
[133b]*Dipartimento di Fisica, Sapienza Università di Roma, Roma, Italy*
[134a]*INFN Sezione di Roma Tor Vergata, Roma, Italy*
[134b]*Dipartimento di Fisica, Università di Roma Tor Vergata, Roma, Italy*
[135a]*INFN Sezione di Roma Tre, Roma, Italy*
[135b]*Dipartimento di Matematica e Fisica, Università Roma Tre, Roma, Italy*
[136a]*Faculté des Sciences Ain Chock, Réseau Universitaire de Physique des Hautes Energies - Université Hassan II, Casablanca, Morocco*
[136b]*Centre National de l'Energie des Sciences Techniques Nucleaires, Rabat, Morocco*
[136c]*Faculté des Sciences Semlalia, Université Cadi Ayyad, LPHEA-Marrakech, Morocco*
[136d]*Faculté des Sciences, Université Mohamed Premier and LPTPM, Oujda, Morocco*
[136e]*Faculté des sciences, Université Mohammed V-Agdal, Rabat, Morocco*
[137]*DSM/IRFU (Institut de Recherches sur les Lois Fondamentales de l'Univers), CEA Saclay (Commissariat à l'Energie Atomique et aux Energies Alternatives), Gif-sur-Yvette, France*
[138]*Santa Cruz Institute for Particle Physics, University of California Santa Cruz, Santa Cruz, California, USA*
[139]*Department of Physics, University of Washington, Seattle, Washington, USA*
[140]*Department of Physics and Astronomy, University of Sheffield, Sheffield, United Kingdom*
[141]*Department of Physics, Shinshu University, Nagano, Japan*
[142]*Fachbereich Physik, Universität Siegen, Siegen, Germany*

[143]*Department of Physics, Simon Fraser University, Burnaby, British Columbia, Canada*
[144]*SLAC National Accelerator Laboratory, Stanford, California, USA*
[145a]*Faculty of Mathematics, Physics & Informatics, Comenius University, Bratislava, Slovak Republic*
[145b]*Department of Subnuclear Physics, Institute of Experimental Physics of the Slovak Academy of Sciences, Kosice, Slovak Republic*
[146a]*Department of Physics, University of Cape Town, Cape Town, South Africa*
[146b]*Department of Physics, University of Johannesburg, Johannesburg, South Africa*
[146c]*School of Physics, University of the Witwatersrand, Johannesburg, South Africa*
[147a]*Department of Physics, Stockholm University, Stockholm, Sweden*
[147b]*The Oskar Klein Centre, Stockholm, Sweden*
[148]*Physics Department, Royal Institute of Technology, Stockholm, Sweden*
[149]*Departments of Physics & Astronomy and Chemistry, Stony Brook University, Stony Brook, New York, USA*
[150]*Department of Physics and Astronomy, University of Sussex, Brighton, United Kingdom*
[151]*School of Physics, University of Sydney, Sydney, Australia*
[152]*Institute of Physics, Academia Sinica, Taipei, Taiwan*
[153]*Department of Physics, Technion: Israel Institute of Technology, Haifa, Israel*
[154]*Raymond and Beverly Sackler School of Physics and Astronomy, Tel Aviv University, Tel Aviv, Israel*
[155]*Department of Physics, Aristotle University of Thessaloniki, Thessaloniki, Greece*
[156]*International Center for Elementary Particle Physics and Department of Physics, The University of Tokyo, Tokyo, Japan*
[157]*Graduate School of Science and Technology, Tokyo Metropolitan University, Tokyo, Japan*
[158]*Department of Physics, Tokyo Institute of Technology, Tokyo, Japan*
[159]*Department of Physics, University of Toronto, Toronto, Ontario, Canada*
[160a]*TRIUMF, Vancouver, British Columbia, Canada*
[160b]*Department of Physics and Astronomy, York University, Toronto, Ontario, Canada*
[161]*Faculty of Pure and Applied Sciences, University of Tsukuba, Tsukuba, Japan*
[162]*Department of Physics and Astronomy, Tufts University, Medford, Massachusetts, USA*
[163]*Centro de Investigaciones, Universidad Antonio Narino, Bogota, Colombia*
[164]*Department of Physics and Astronomy, University of California Irvine, Irvine, California, USA*
[165a]*INFN Gruppo Collegato di Udine, Sezione di Trieste, Udine, Italy*
[165b]*ICTP, Trieste, Italy*
[165c]*Dipartimento di Chimica, Fisica e Ambiente, Università di Udine, Udine, Italy*
[166]*Department of Physics, University of Illinois, Urbana, Illinois, USA*
[167]*Department of Physics and Astronomy, University of Uppsala, Uppsala, Sweden*
[168]*Instituto de Física Corpuscular (IFIC) and Departamento de Física Atómica, Molecular y Nuclear and Departamento de Ingeniería Electrónica and Instituto de Microelectrónica de Barcelona (IMB-CNM), University of Valencia and CSIC, Valencia, Spain*
[169]*Department of Physics, University of British Columbia, Vancouver, British Columbia, Canada*
[170]*Department of Physics and Astronomy, University of Victoria, Victoria, British Columbia, Canada*
[171]*Department of Physics, University of Warwick, Coventry, United Kingdom*
[172]*Waseda University, Tokyo, Japan*
[173]*Department of Particle Physics, The Weizmann Institute of Science, Rehovot, Israel*
[174]*Department of Physics, University of Wisconsin, Madison, Wisconsin, USA*
[175]*Fakultät für Physik und Astronomie, Julius-Maximilians-Universität, Würzburg, Germany*
[176]*Fachbereich C Physik, Bergische Universität Wuppertal, Wuppertal, Germany*
[177]*Department of Physics, Yale University, New Haven, Connecticut, USA*
[178]*Yerevan Physics Institute, Yerevan, Armenia*
[179]*Centre de Calcul de l'Institut National de Physique Nucléaire et de Physique des Particules (IN2P3), Villeurbanne, France*

[a]Deceased.
[b]Also at Department of Physics, King's College London, London, United Kingdom.
[c]Also at Institute of Physics, Azerbaijan Academy of Sciences, Baku, Azerbaijan.
[d]Also at Particle Physics Department, Rutherford Appleton Laboratory, Didcot, United Kingdom.
[e]Also at TRIUMF, Vancouver BC, Canada.
[f]Also at Department of Physics, California State University, Fresno CA, United States of America.
[g]Also at Tomsk State University, Tomsk, Russia.
[h]Also at CPPM, Aix-Marseille Université and CNRS/IN2P3, Marseille, France.
[i]Also at Università di Napoli Parthenope, Napoli, Italy.

[j]Also at Institute of Particle Physics (IPP), Canada.
[k]Also at Department of Physics, St. Petersburg State Polytechnical University, St. Petersburg, Russia.
[l]Also at Chinese University of Hong Kong, China.
[m]Also at Department of Financial and Management Engineering, University of the Aegean, Chios, Greece.
[n]Also at Louisiana Tech University, Ruston LA, United States of America.
[o]Also at Institucio Catalana de Recerca i Estudis Avancats, ICREA, Barcelona, Spain.
[p]Also at Institute of Theoretical Physics, Ilia State University, Tbilisi, Georgia.
[q]Also at CERN, Geneva, Switzerland.
[r]Also at Ochadai Academic Production, Ochanomizu University, Tokyo, Japan.
[s]Also at Manhattan College, New York NY, United States of America.
[t]Also at Novosibirsk State University, Novosibirsk, Russia.
[u]Also at Institute of Physics, Academia Sinica, Taipei, Taiwan.
[v]Also at LAL, Université Paris-Sud and CNRS/IN2P3, Orsay, France.
[w]Also at Academia Sinica Grid Computing, Institute of Physics, Academia Sinica, Taipei, Taiwan.
[x]Also at Laboratoire de Physique Nucléaire et de Hautes Energies, UPMC and Université Paris-Diderot and CNRS/IN2P3, Paris, France.
[y]Also at School of Physical Sciences, National Institute of Science Education and Research, Bhubaneswar, India.
[z]Also at Dipartimento di Fisica, Sapienza Università di Roma, Roma, Italy.
[aa]Also at Moscow Institute of Physics and Technology State University, Dolgoprudny, Russia.
[bb]Also at Section de Physique, Université de Genève, Geneva, Switzerland.
[cc]Also at Department of Physics, The University of Texas at Austin, Austin TX, United States of America.
[dd]Also at International School for Advanced Studies (SISSA), Trieste, Italy.
[ee]Also at Department of Physics and Astronomy, University of South Carolina, Columbia SC, United States of America.
[ff]Also at School of Physics and Engineering, Sun Yat-sen University, Guangzhou, China.
[gg]Also at Faculty of Physics, M. V. Lomonosov Moscow State University, Moscow, Russia.
[hh]Also at Moscow Engineering and Physics Institute (MEPhI), Moscow, Russia.
[ii]Also at Institute for Particle and Nuclear Physics, Wigner Research Centre for Physics, Budapest, Hungary.
[jj]Also at Department of Physics, Oxford University, Oxford, United Kingdom.
[kk]Also at Department of Physics, Nanjing University, Jiangsu, China.
[ll]Also at Institut für Experimentalphysik, Universität Hamburg, Hamburg, Germany.
[mm]Also at Department of Physics, The University of Michigan, Ann Arbor MI, United States of America.
[nn]Also at Discipline of Physics, University of KwaZulu-Natal, Durban, South Africa.
[oo]Also at University of Malaya, Department of Physics, Kuala Lumpur, Malaysia.

PHYSICAL REVIEW D **91,** 012006 (2015)

Measurements of Higgs boson production and couplings in the four-lepton channel in *pp* collisions at center-of-mass energies of 7 and 8 TeV with the ATLAS detector

G. Aad *et al.*[*]
(ATLAS Collaboration)
(Received 22 August 2014; published 16 January 2015)

The final ATLAS Run 1 measurements of Higgs boson production and couplings in the decay channel $H \to ZZ^* \to \ell^+\ell^-\ell'^+\ell'^-$, where $\ell, \ell' = e$ or μ, are presented. These measurements were performed using pp collision data corresponding to integrated luminosities of 4.5 and 20.3 fb^{-1} at center-of-mass energies of 7 and 8 TeV, respectively, recorded with the ATLAS detector at the LHC. The $H \to ZZ^* \to 4\ell$ signal is observed with a significance of 8.1 standard deviations, with an expectation of 6.2 standard deviations, at $m_H = 125.36$ GeV, the combined ATLAS measurement of the Higgs boson mass from the $H \to \gamma\gamma$ and $H \to ZZ^* \to 4\ell$ channels. The production rate relative to the Standard Model expectation, the signal strength, is measured in four different production categories in the $H \to ZZ^* \to 4\ell$ channel. The measured signal strength, at this mass, and with all categories combined, is $1.44^{+0.40}_{-0.33}$. The signal strength for Higgs boson production in gluon fusion or in association with $t\bar{t}$ or $b\bar{b}$ pairs is found to be $1.7^{+0.5}_{-0.4}$, while the signal strength for vector-boson fusion combined with WH/ZH associated production is found to be $0.3^{+1.6}_{-0.9}$.

DOI: 10.1103/PhysRevD.91.012006 PACS numbers: 14.80.Bn

I. INTRODUCTION

In the Standard Model (SM) the Brout-Englert-Higgs (BEH) mechanism is the source of electroweak symmetry breaking and results in the appearance of a fundamental scalar particle, the Higgs boson [1–3]. The ATLAS and CMS experiments have reported the observation of a particle in the search for the SM Higgs boson [4,5], where the most sensitive channels are $H \to ZZ^* \to 4\ell$, $H \to WW^* \to \ell\nu\ell\nu$ and $H \to \gamma\gamma$. An important step in the confirmation of the new particle as the SM Higgs boson is the measurement of its properties, which are completely defined in the SM once its mass is known. Previous ATLAS studies [6,7] have shown that this particle is consistent with the SM Higgs boson.

The Higgs boson decay to four leptons, $H \to ZZ^* \to 4\ell$, where $\ell = e$ or μ, provides good sensitivity for the measurement of the Higgs boson properties due to its high signal-to-background ratio, which is about 2 for each of the four final states: $\mu^+\mu^-\mu^+\mu^-$ (4μ), $e^+e^-\mu^+\mu^-$ ($2e2\mu$), $\mu^+\mu^-e^+e^-$ ($2\mu2e$), and $e^+e^-e^+e^-$ ($4e$), where the first lepton pair is defined to be the one with the dilepton invariant mass closest to the Z boson mass. The contribution to these final states from $H \to ZZ^*$, $Z^{(*)} \to \tau^+\tau^-$ decays is below the per mille level in the current analysis. The largest background in this search comes from continuum $(Z^{(*)}/\gamma^*)(Z^{(*)}/\gamma^*)$ production, referred to as ZZ^* hereafter. For the four-lepton events with an invariant mass, $m_{4\ell}$, below about 160 GeV, there are also important background contributions from Z + jets and $t\bar{t}$ production with two prompt leptons, where the additional charged lepton candidates arise from decays of hadrons with b- or c-quark content, from photon conversions or from misidentification of jets.

Interference effects are expected between the Higgs boson signal and SM background processes. For the $H \to ZZ^* \to 4\ell$ channel, the impact of this interference on the mass spectrum near the resonance is negligible [8]. This analysis does not account for interference effects in the mass spectra.

In the SM, the inclusive production of the $H \to ZZ^* \to 4\ell$ final state is dominated by the gluon fusion (ggF) Higgs boson production mode, which represents 86% of the total production cross section for $m_H = 125$ GeV at $\sqrt{s} = 8$ TeV. Searching for Higgs boson production in the vector-boson fusion (VBF) and the vector-boson associated production (VH) modes allows further exploration of the coupling structure of the new particle. The corresponding fractions of the production cross section for VBF and VH are predicted to be 7% and 5%, respectively.

This paper presents the final ATLAS Run 1 results of the measurement of the SM Higgs boson production in the $H \to ZZ^* \to 4\ell$ decay mode, where the production is studied both inclusively and with events categorized according to the characteristics of the different production modes. The categorized analysis allows constraints to be placed on possible deviations from the expected couplings of the SM Higgs boson. The data sample used corresponds to an integrated luminosity of 4.5 fb^{-1} at a center-of-mass energy of 7 TeV and 20.3 fb^{-1} at a center-of-mass energy of 8 TeV, collected in the years 2011 and 2012, respectively.

[*] Full author list given at the end of the article.

The method adopted to extract the production rates simultaneously provides a measurement of the Higgs boson mass. The measurement of the Higgs boson mass for this channel, performed in combination with the $H \to \gamma\gamma$ decay mode, is discussed in Ref. [9] and is only covered briefly here. This paper contains a full description of the signal and background simulation, the object reconstruction and identification, the event selection and the background estimations of the $H \to ZZ^* \to 4\ell$ decay mode, providing the details for other Run 1 final results, including the combined mass measurement, reported elsewhere. The corresponding final Run 1 CMS results for the $H \to ZZ^* \to 4\ell$ decay mode have been reported in Ref. [10].

The present analysis improves on the earlier result [6] with the following changes: (a) the electron identification uses a multivariate likelihood instead of a cut-based method, improving the background rejection at a fixed efficiency; (b) the electron transverse energy (E_{T}) measurement has been improved by a refined cluster energy reconstruction in the calorimeter and by combining the electron cluster energy with the track momentum for low-E_{T} electrons; (c) the energy scale for electrons and momentum scale for muons have both been improved; (d) the inclusion of final-state radiation (FSR) off charged leptons has been extended to noncollinear photons; (e) a multivariate discriminant against the ZZ^* background has been introduced to improve the signal-to-background ratio for the ggF production mode; (f) the estimates of the reducible $\ell\ell$ + jets and $t\bar{t}$ background processes have been improved; (g) the sensitivity for different production modes has been improved, both by introducing a new VH category with two jets in the final state and by using multivariate techniques for this category and the VBF category.

The ATLAS detector is briefly described in Sec. II, and the signal and background simulation is presented in Sec. III. The object reconstruction and identification, the event selection and categorization, and the background estimation are presented in Secs. IV, V and VI, respectively. The multivariate discriminants and the signal and background modeling are discussed in Secs. VII and VIII. Finally, the systematic uncertainties and the results are presented in Secs. IX and X.

II. THE ATLAS DETECTOR

The ATLAS detector [11] is a multipurpose particle detector with approximately forward-backward symmetric cylindrical geometry.[1] The inner tracking detector (ID) consists of a silicon pixel detector, which is closest to the interaction point, and a silicon microstrip detector surrounding the pixel detector, both covering $|\eta| < 2.5$, followed by a transition radiation straw-tube tracker (TRT) covering $|\eta| < 2$. The ID is surrounded by a thin superconducting solenoid providing a 2 T axial magnetic field. A highly segmented lead/liquid-argon (LAr) sampling electromagnetic calorimeter measures the energy and the position of electromagnetic showers with $|\eta| < 3.2$. The LAr calorimeter includes a presampler (for $|\eta| < 1.8$) and three sampling layers, longitudinal in shower depth, for $|\eta| < 2.5$. LAr sampling calorimeters are also used to measure hadronic showers in the end-caps ($1.5 < |\eta| < 3.2$) and electromagnetic and hadronic showers in the forward ($3.1 < |\eta| < 4.9$) regions, while an iron/scintillator tile calorimeter measures hadronic showers in the central region ($|\eta| < 1.7$).

The muon spectrometer (MS) surrounds the calorimeters and is designed to detect muons in the pseudorapidity range up to $|\eta| = 2.7$. The MS consists of one barrel ($|\eta| < 1.05$) and two end-cap regions. A system of three large superconducting air-core toroid magnets, each with eight coils, provides a magnetic field with a bending integral of about 2.5 T m in the barrel and up to 6 T m in the end-caps. Monitored drift-tube chambers in both the barrel and end cap regions and cathode strip chambers covering $|\eta| > 2$ are used as precision chambers, whereas resistive plate chambers in the barrel and thin gap chambers in the end caps are used as trigger chambers, covering up to $|\eta| = 2.4$. The chambers are arranged in three layers, so high-p_{T} particles traverse at least three stations with a lever arm of several meters.

A three-level trigger system selects events to be recorded for offline analysis.

III. SIGNAL AND BACKGROUND SIMULATION

The $H \to ZZ^* \to 4\ell$ signal is modeled using the POWHEG-BOX Monte Carlo (MC) event generator [12–16], which provides separate calculations for the ggF and VBF production mechanisms with matrix elements up to next-to-leading order (NLO) in the QCD coupling constant. The description of the Higgs boson transverse momentum (p_{T}) spectrum in the ggF process is reweighted to follow the calculation of Refs. [17,18], which includes QCD corrections up to next-to-next-to-leading order (NNLO) and QCD soft-gluon resummations up to next-to-next-to-leading logarithm (NNLL). The effects of nonzero quark masses are also taken into account [19]. POWHEG-BOX is interfaced to PYTHIA8.1 [20,21] for showering and hadronization, which in turn is interfaced to PHOTOS [22,23] for QED radiative corrections in the final state. PYTHIA8.1 is used to simulate the production of a Higgs boson in association with a W or a Z boson (VH) or with a $t\bar{t}$ pair ($t\bar{t}H$). The production of a Higgs boson in association with a $b\bar{b}$ pair ($b\bar{b}H$) is included in the signal

[1]The ATLAS experiment uses a right-handed coordinate system with its origin at the nominal interaction point (IP) in the center of the detector and the z-axis along the beam pipe. The x-axis points from the IP to the center of the LHC ring, and the y-axis points upward. Cylindrical coordinates (r, ϕ) are used in the transverse plane, ϕ being the azimuthal angle around the beam pipe. The pseudorapidity is defined in terms of the polar angle θ as $\eta = -\ln\tan(\theta/2)$.

yield assuming the same m_H dependence as for the $t\bar{t}H$ process, while the signal efficiency is assumed to be equal to that for ggF production.

The Higgs boson production cross sections and decay branching ratios, as well as their uncertainties, are taken from Refs. [24,25]. The cross sections for the ggF process have been calculated to NLO [26–28] and NNLO [29–31] in QCD. In addition, QCD soft-gluon resummations calculated in the NNLL approximation are applied for the ggF process [32]. NLO electroweak (EW) radiative corrections are also applied [33,34]. These results are compiled in Refs. [35–37] assuming factorization between QCD and EW corrections. For the VBF process, full QCD and EW corrections up to NLO [38–40] and approximate NNLO QCD [41] corrections are used to calculate the cross section. The cross sections for the associated WH/ZH production processes are calculated at NLO [42] and at NNLO [43] in QCD, and NLO EW radiative corrections are applied [44]. The cross section for associated Higgs boson production with a $t\bar{t}$ pair is calculated at NLO in QCD [45–48]. The cross section for the $b\bar{b}H$ process is calculated in the four-flavor scheme at NLO in QCD [49–51] and in the five-flavor scheme at NNLO in QCD [52] and combined via the Santander matching scheme [25,53].

The Higgs boson decay widths for the WW and ZZ four-lepton final states are provided by PROPHECY4F [54,55], which includes the complete NLO QCD + EW corrections and interference effects between identical final-state fermions. The other Higgs boson decay widths, e.g. $\gamma\gamma$, $\tau\tau$, $b\bar{b}$, etc., are obtained with HDECAY [56] and combined with the PROPHECY4F results to obtain the $H \to ZZ^* \to 4\ell$ branching ratios. Table I gives the production cross sections and branching ratios for $H \to ZZ^* \to 4\ell$, which are used to normalize the signal simulation, for several values of m_H.

The QCD scale uncertainties for $m_H = 125$ GeV [24] amount to $+7\%$ and -8% for the ggF process, from $\pm 1\%$ to $\pm 2\%$ for the VBF and associated WH/ZH production processes and $+4\%$ and -9% for the associated $t\bar{t}H$ production process. The uncertainties on the production cross section due to uncertainties on the parton distribution functions (PDF) and the strong coupling constant, α_s, is $\pm 8\%$ for gluon-initiated processes and $\pm 4\%$ for quark-initiated processes, estimated by following the prescription in Ref. [57] and by using the PDF sets of CTEQ [58], MSTW [59] and NNPDF [60]. The PDF uncertainties are assumed to be 100% correlated among processes with identical initial states, regardless of whether they are signal or background [61].

The ZZ^* continuum background is modeled using POWHEG-BOX [62] for quark-antiquark annihilation and GG2ZZ [63] for gluon fusion. The PDF + α_s and QCD scale uncertainties are parametrized as functions of $m_{4\ell}$ as recommended in Ref. [25]. For the ZZ^* background at $m_{4\ell} = 125$ GeV, the quark-initiated (gluon-initiated) processes have a QCD scale uncertainty of $\pm 5\%$ ($\pm 25\%$), and $\pm 4\%$ ($\pm 8\%$) for the PDF and α_s uncertainties, respectively.

The Z + jets production is modeled using ALPGEN [64] and is divided into two sources: Z + light-jets, which includes $Zc\bar{c}$ in the massless c-quark approximation and $Zb\bar{b}$ with $b\bar{b}$ from parton showers, and $Zb\bar{b}$ using matrix-element calculations that take into account the b-quark mass. The MLM [65] matching scheme is used to remove any double counting of identical jets produced via the matrix-element calculation and the parton shower, but this scheme is not implemented for b-jets. Therefore, $b\bar{b}$ pairs with separation $\Delta R \equiv \sqrt{(\Delta\phi)^2 + (\Delta\eta)^2} > 0.4$ between the b-quarks are taken from the matrix-element calculation, whereas for $\Delta R < 0.4$ the parton-shower $b\bar{b}$ pairs are used. In this search the Z + jets background is normalized using control samples from data. For comparison between data and simulation, the NNLO QCD FEWZ [66,67] and NLO QCD MCFM [68,69] cross-section calculations are used to normalize the simulations for inclusive Z boson and $Zb\bar{b}$ production, respectively. The $t\bar{t}$ background is modeled

TABLE I. Calculated SM Higgs boson production cross sections for gluon fusion, vector-boson fusion and associated production with a W or Z boson or with a $b\bar{b}$ or $t\bar{t}$ pair in pp collisions at $\sqrt{s}$ of 7 and 8 TeV [24]. The quoted uncertainties correspond to the total theoretical systematic uncertainties calculated by adding in quadrature the QCD scale and PDF + α_s uncertainties. The decay branching ratio (B) for $H \to 4\ell$ with $\ell = e, \mu$, is reported in the last column [24].

m_H (GeV)	$\sigma(gg \to H)$ (pb)	$\sigma(qq' \to Hqq')$ (pb)	$\sigma(q\bar{q} \to WH)$ (pb)	$\sigma(q\bar{q} \to ZH)$ (pb)	$\sigma(q\bar{q}/gg \to b\bar{b}H/t\bar{t}H)$ (pb)	$B(H \to ZZ^* \to 4\ell)$ (10^{-3})
			$\sqrt{s} = 7$ TeV			
123	15.6 ± 1.6	1.25 ± 0.03	0.61 ± 0.02	0.35 ± 0.01	0.26 ± 0.04	0.103 ± 0.005
125	15.1 ± 1.6	1.22 ± 0.03	0.58 ± 0.02	0.34 ± 0.01	0.24 ± 0.04	0.125 ± 0.005
127	14.7 ± 1.5	1.20 ± 0.03	0.55 ± 0.02	0.32 ± 0.01	0.23 ± 0.03	0.148 ± 0.006
			$\sqrt{s} = 8$ TeV			
123	19.9 ± 2.1	1.61 ± 0.05	0.74 ± 0.02	0.44 ± 0.02	0.35 ± 0.05	0.103 ± 0.005
125	19.3 ± 2.0	1.58 ± 0.04	0.70 ± 0.02	0.42 ± 0.02	0.33 ± 0.05	0.125 ± 0.005
127	18.7 ± 1.9	1.55 ± 0.04	0.67 ± 0.02	0.40 ± 0.02	0.32 ± 0.05	0.148 ± 0.006

using POWHEG-BOX interfaced to PYTHIA8.1 for parton shower and hadronization, PHOTOS for QED radiative corrections and TAUOLA [70,71] for the simulation of τ lepton decays. SHERPA [72] is used for the simulation of WZ production.

Generated events are processed through the ATLAS detector simulation [73] within the GEANT4 framework [74]. Additional pp interactions in the same and nearby bunch crossings (pileup) are included in the simulation. The simulation samples are weighted to reproduce the observed distribution of the mean number of interactions per bunch crossing in the data.

IV. OBJECT RECONSTRUCTION AND IDENTIFICATION

The $H \to ZZ^* \to 4\ell$ channel has a small rate but is a relatively clean final state where the signal-to-background ratio *vis-à-vis* the reducible backgrounds alone, i.e. ignoring the ZZ^* background, is above 6 for the present analysis. Significant effort was made to obtain a high efficiency for the reconstruction and identification of electrons and muons, while keeping the loss due to background rejection as small as possible. In particular, this becomes increasingly difficult for electrons as E_{T} decreases.

Electrons are reconstructed using information from the ID and the electromagnetic calorimeter. For electrons, background discrimination relies on the shower shape information available from the highly segmented LAr EM calorimeter, high-threshold TRT hits, as well as compatibility of the tracking and calorimeter information. Muons are reconstructed as tracks in the ID and MS, and their identification is primarily based on the presence of a matching track or tag in the MS. Finally, jets are reconstructed from clusters of calorimeter cells and calibrated using a dedicated scheme designed to adjust the energy measured in the calorimeter to that of the true jet energy on average.

A. Electron reconstruction and identification

Electron candidates are clusters of energy deposited in the electromagnetic calorimeter associated with ID tracks [75,76]. All candidate electron tracks are fitted using a Gaussian-sum filter [77] (GSF) to account for bremsstrahlung energy losses. The GSF fit brings the candidate electron E/p distribution closer to unity and improves the measured electron direction, resulting in better impact parameter resolution. For the 2012 (8 TeV) data set, the electron reconstruction was modified to allow for large bremsstrahlung energy losses. A second pass was added to the ATLAS track pattern recognition that allows for an electron hypothesis with larger energy loss to be tried after a first pass with a pion hypothesis. Furthermore, the track-to-cluster matching algorithm was improved, for example by incorporating an additional test that extrapolates tracks to the calorimeter using the measured cluster energy rather than the track momentum. These improvements increased the electron reconstruction efficiency on average by 5% for electrons with E_{T} above 15 GeV, with a 7% improvement for E_{T} at 15 GeV, as measured with data [78].

The electron identification is based on criteria that require the longitudinal and transverse shower profiles to be consistent with those expected for electromagnetic showers, the track and cluster positions to match in η and ϕ, and the presence of high-threshold TRT hits. To maintain both large acceptance and good discrimination, the selection is kept "loose" for a large number of discriminating variables; for comparison, the most stringent electron identification would induce an additional 15% reduction in electron efficiency. Compared to the previous measurement [6], the electron identification was improved for the 2012 data set by moving from a cut-based method to a likelihood method. The likelihood allows the inclusion of discriminating variables that are difficult to use with explicit cuts without incurring significant efficiency losses. For example, the GSF fit measures a significant difference between the momenta at the start and end of the electron trajectory for only a fraction of true electrons so that requiring a large difference for all electrons would not be an efficient selection cut. The likelihood improves the rejection of light-flavor jets and photon conversions by a factor of 2 for the same signal efficiency. For the 2011 (7 TeV) data set, the electron reconstruction proceeds as described above, but without the improved pattern recognition and cluster-to-track matching. The electron identification used for the 2011 data set is the same cut-based identification as in the previous measurement [6]. Detailed descriptions of the likelihood identification used for the 2012 data set, the cut-based identification used for the 2011 data set and the corresponding efficiency measurements can be found in Refs. [78,79].

Finally, the electron transverse energy is computed from the cluster energy and the track direction at the interaction point. The cluster energy is the sum of the calibrated energy deposited in the cells in a fixed-size window in $\eta \times \phi$, different for the barrel and end-cap. The cluster energy is corrected for energy lost before the calorimeter, deposited in neighboring cells and beyond the calorimeter. Further corrections for the response dependence are applied as a function of the impact point within the central cluster cell. The cluster energy measurement was improved compared to the previous analysis [6] and is described elsewhere [76]. Several of the steps in the energy calibration were significantly improved including: (a) the addition of a multivariate technique to extract the cluster energy from the energy deposit in simulation, (b) additional corrections for response details not included in the simulation, and (c) equalization of the energy scales of the longitudinal calorimeter layers.

These improvements resulted in a significant reduction in the overall energy scale uncertainty (for example for

$|\eta| < 1.37$ the uncertainty is reduced from 0.4% to 0.04% for electrons of $E_T = 40$ GeV [76]) and have an important impact on the systematic uncertainty of the Higgs boson mass measurement [9]. In addition, a combined fit of the cluster energy and track momentum is applied to electrons with E_T below 30 GeV when the cluster E_T and the track p_T agree within their uncertainties. The combined fit improves the resolution of $m_{4\ell}$ for the $4e$ and $2\mu 2e$ final states by about 4%.

B. Muon reconstruction and identification

Four types of muon candidates are distinguished, depending on how they are reconstructed. Most muon candidates are identified by matching a reconstructed ID track with either a complete or partial track reconstructed in the MS [80,81]. If a complete MS track is present, the two independent momentum measurements are combined (combined muons); otherwise the momentum is measured using the ID, and the partial MS track serves as identification (segment-tagged muons). The muon reconstruction and identification coverage is extended by using tracks reconstructed in the forward region ($2.5 < |\eta| < 2.7$) of the MS, which is outside the ID coverage (standalone muons). In the center of the barrel region ($|\eta| < 0.1$), which lacks MS geometrical coverage, ID tracks with $p_T > 15$ GeV are identified as muons if their calorimetric energy deposition is consistent with a minimum ionizing particle (calorimeter-tagged muons). The inner detector tracks associated with muons that are identified inside the ID acceptance are required to have a minimum number of associated hits in each of the ID subdetectors to ensure good track reconstruction. The muon candidates outside the ID acceptance that are reconstructed only in the MS are required to have hits in each of the three stations they traverse. At most one standalone or calorimeter-tagged muon is used per event.

C. Final-state radiation recovery

The QED process of radiative photon production in Z decays is well modeled by simulation. Some of the FSR photons can be identified in the calorimeter and incorporated into the four-lepton measurement. A dedicated method to include the FSR photons in the reconstruction of Z bosons was developed. This method includes a search for collinear and noncollinear FSR photons, with the collinear search described in Ref. [82]. Collinear photons are only associated with muons[2] ($\Delta R_{\mathrm{cluster},\mu} \leq 0.15$), and noncollinear photons can be associated with either muons or electrons ($\Delta R_{\mathrm{cluster},\ell} > 0.15$).

At most one FSR photon is used per event, with priority given to collinear photons. The probability of having more than one FSR per event with significant energy is negligible. The collinear photons are required to have a transverse energy of $E_T > 1.5$ GeV and a fraction of the total energy deposited in the front sampling layer of the calorimeter greater than 0.1. If more than one collinear photon is found, only the one with the highest E_T is kept. Noncollinear photons must have $E_T > 10$ GeV, be isolated (E_T below 4 GeV within a cone of size $\Delta R = 0.4$, excluding the photon itself), and satisfy strict ("tight") identification criteria [83]. Again, only the highest-E_T noncollinear photon is retained, and only if no collinear photon is found.

The inclusion of a FSR photon in a four-lepton event is discussed below in Sec. VA. The collinear FSR selection recovers 70% of the FSR photons within the selected fiducial region with a purity of about 85%, where misidentified photons come from pileup and muon ionization. The noncollinear FSR selection has an efficiency of approximately 60% and a purity greater than 95% within the fiducial region.

In Fig. 1, the invariant mass distributions are shown for $Z \to \mu^+\mu^-$ candidate events where either a collinear [Fig. 1(a)] or noncollinear [Fig. 1(b)] FSR photon is found. The invariant mass distributions are shown both before and after the addition of the FSR photons, for both data and simulation. Good agreement between data and simulation is observed.

D. Jet reconstruction

Jets are reconstructed using the anti-k_t algorithm [84,85] with a distance parameter $R = 0.4$. The inputs to the reconstruction are three-dimensional clusters of energy [86,87] in the calorimeter, calibrated to the electromagnetic energy scale and corrected for contributions from in-time and out-of-time pileup [88], and the position of the primary interaction vertex (see Sec. V). The algorithm for this clustering suppresses noise by keeping only cells with a significant energy deposit and their neighboring cells. Subsequently, the jets are calibrated to the hadronic energy scale using p_T- and η-dependent correction factors determined from simulation (2011 data set) and from data (2012 data set) [87,89]. The uncertainty on these correction factors is determined from control samples in data. To reduce the number of jet candidates originating from pileup vertices, jets with $p_T < 50$ GeV within the ID acceptance ($|\eta| < 2.4$) are required to have more than 50% (75% for 2011 data) of the summed scalar p_T of the tracks associated with the jet (within $\Delta R = 0.4$ around the jet axis) come from tracks of the primary vertex [90].

V. EVENT SELECTION

The data are subjected to quality requirements: if any relevant detector component is not operating correctly during a period when an event is recorded, the event is

[2]Photons collinear to electrons are included in the calorimeter shower.

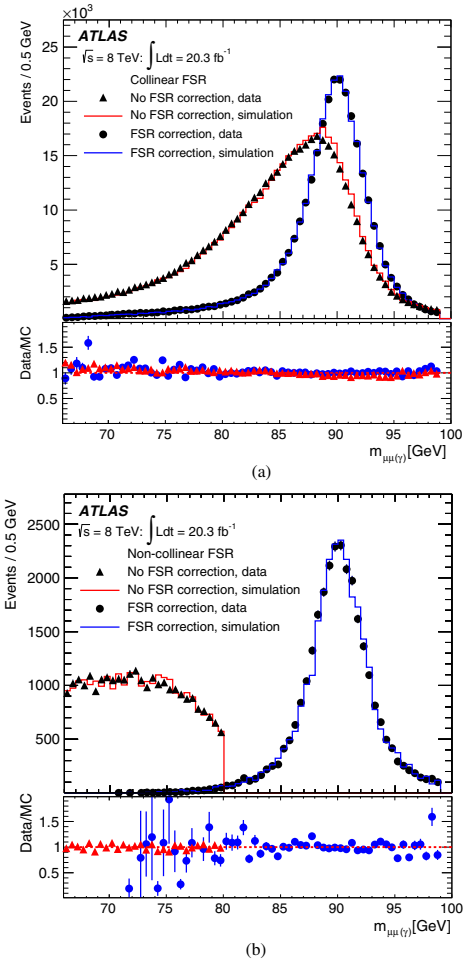

FIG. 1 (color online). (a) The invariant mass distributions of $Z \to \mu^+\mu^-(\gamma)$ events in data before collinear FSR correction (filled triangles) and after collinear FSR correction (filled circles), for events with a collinear FSR photon satisfying the selection criteria as described in Sec. IV C. The prediction of the simulation is shown before correction (red histogram) and after correction (blue histogram). (b) The invariant mass distributions of $Z \to \mu^+\mu^-(\gamma)$ events with a noncollinear FSR photon satisfying the selection criteria as described in Sec. IV C. The prediction of the simulation is shown before correction (red histogram) and after correction (blue histogram).

rejected. Events are required to have at least one vertex with three associated tracks with $p_{\mathrm{T}} > 400$ MeV, and the primary vertex is chosen to be the reconstructed vertex with the largest track $\sum p_{\mathrm{T}}^2$. Identical requirements are applied to all four-lepton final states. For the inclusive analysis, four-lepton events are selected and classified according to their channel: 4μ, $2e2\mu$, $2\mu2e$, $4e$. These events are subsequently categorized according to their production mechanism to provide measurements of each corresponding signal strength.

A. Inclusive analysis

Four-lepton events were selected with single-lepton and dilepton triggers. The p_{T} (E_{T}) thresholds for single-muon (single-electron) triggers increased from 18 to 24 GeV (20 to 24 GeV) between the 7 and 8 TeV data, in order to cope with the increasing instantaneous luminosity. The dilepton trigger thresholds for 7 TeV data are set at 10 GeV p_{T} for muons, 12 GeV E_{T} for electrons and (6, 10) GeV for (muon, electron) mixed-flavor pairs. For the 8 TeV data, the thresholds were raised to 13 GeV for the dimuon trigger, to 12 GeV for the dielectron trigger and (8, 12) GeV for the (muon, electron) trigger; furthermore, a dimuon trigger with different thresholds on the muon p_{T}, 8 and 18 GeV, was added. The trigger efficiency for events passing the final selection is above 97% in the 4μ, $2\mu2e$ and $2e2\mu$ channels and close to 100% in the $4e$ channel for both 7 and 8 TeV data.

Higgs boson candidates are formed by selecting two same-flavor, opposite-sign lepton pairs (a lepton quadruplet) in an event. Each lepton is required to have a longitudinal impact parameter less than 10 mm with respect to the primary vertex, and muons are required to have a transverse impact parameter of less than 1 mm to reject cosmic-ray muons. These selections are not applied to standalone muons that have no ID track. Each electron (muon) must satisfy $E_{\mathrm{T}} > 7$ GeV ($p_{\mathrm{T}} > 6$ GeV) and be measured in the pseudorapidity range $|\eta| < 2.47$ ($|\eta| < 2.7$). The highest-p_{T} lepton in the quadruplet must satisfy $p_{\mathrm{T}} > 20$ GeV, and the second (third) lepton in p_{T} order must satisfy $p_{\mathrm{T}} > 15$ GeV ($p_{\mathrm{T}} > 10$ GeV). Each event is required to have the triggering lepton(s) matched to one or two of the selected leptons.

Multiple quadruplets within a single event are possible: for four muons or four electrons there are two ways to pair the masses, and for five or more leptons there are multiple ways to choose the leptons. Quadruplet selection is done separately in each subchannel: 4μ, $2e2\mu$, $2\mu2e$, $4e$, keeping only a single quadruplet per channel. For each channel, the lepton pair with the mass closest to the Z boson mass is referred to as the leading dilepton and its invariant mass, m_{12}, is required to be between 50 and 106 GeV. The second, subleading, pair of each channel is chosen from the remaining leptons as the pair closest in mass to the Z boson and in the range $m_{\mathrm{min}} < m_{34} < 115$ GeV, where m_{min} is 12 GeV for $m_{4\ell} < 140$ GeV, rises linearly to 50 GeV at $m_{4\ell} = 190$ GeV and then remains at 50 GeV for $m_{4\ell} > 190$ GeV. Finally, if more than one channel has a quadruplet passing the selection, the channel with the highest expected signal rate is kept, i.e. in the order 4μ,

$2e2\mu$, $2\mu2e$, $4e$. The rate of two quadruplets in one event is below the per mille level.

Events with a selected quadruplet are required to have their leptons a distance $\Delta R > 0.1$ from each other if they are of the same flavor and $\Delta R > 0.2$ otherwise. For 4μ and $4e$ events, if an opposite-charge same-flavor dilepton pair is found with $m_{\ell\ell}$ below 5 GeV the event is removed.

The Z + jets and $t\bar{t}$ background contributions are further reduced by applying impact parameter requirements as well as track- and calorimeter-based isolation requirements to the leptons. The transverse impact parameter significance, defined as the impact parameter in the transverse plane divided by its uncertainty, $|d_0|/\sigma_{d_0}$, for all muons (electrons) is required to be lower than 3.5 (6.5). The normalized track isolation discriminant, defined as the sum of the transverse momenta of tracks, inside a cone of size $\Delta R = 0.2$ around the lepton, excluding the lepton track, divided by the lepton p_{T}, is required to be smaller than 0.15.

The relative calorimetric isolation for electrons in the 2012 data set is computed as the sum of the cluster transverse energies E_{T}, in the electromagnetic and hadronic calorimeters, with a reconstructed barycenter inside a cone of size $\Delta R = 0.2$ around the candidate electron cluster, divided by the electron E_{T}. The electron relative calorimetric isolation is required to be smaller than 0.2. The cells within 0.125×0.175 in $\eta \times \phi$ around the electron barycenter are excluded. The pileup and underlying event contribution to the calorimeter isolation is subtracted event by event [91]. The calorimetric isolation of electrons in the 2011 data set is cell based (electromagnetic and hadronic calorimeters) rather than cluster based, and the calorimeter isolation relative to the electron E_{T} requirement is 0.3 instead of 0.2. In the case of muons, the relative calorimetric isolation discriminant is defined as the sum, ΣE_{T}, of the calorimeter cells above 3.4σ, where σ is the quadrature sum of the expected electronic and pileup noise, inside a cone of size $\Delta R < 0.2$ around the muon direction, divided by the muon p_{T}. Muons are required to have a relative calorimetric isolation less than 0.3 (0.15 in the case of stand-alone muons). For both the track- and calorimeter-based isolations any contributions arising from other leptons of the quadruplet are subtracted.

As discussed in Sec. IV C, a search is performed for FSR photons arising from any of the lepton candidates in the final quadruplet, and at most one FSR photon candidate is added to the 4ℓ system. The FSR correction is applied only to the leading dilepton, and priority is given to collinear photons. The correction is applied if $66 < m_{\mu\mu} < 89$ GeV and $m_{\mu\mu\gamma} < 100$ GeV. If the collinear-photon search fails then the noncollinear FSR photon with the highest E_{T} is added, provided it satisfies the following requirements: $m_{\ell\ell} < 81$ GeV and $m_{\ell\ell\gamma} < 100$ GeV. The expected fraction of collinear (noncollinear) corrected events is 4% (1%).

For the 7 TeV data, the combined signal reconstruction and selection efficiency for $m_H = 125$ GeV is 39% for the 4μ channel, 25% for the $2e2\mu/2\mu2e$ channels and 17% for the $4e$ channel. The improvements in the electron reconstruction and identification for the 8 TeV data lead to increases in these efficiencies by 10%–15% for the channels with electrons, bringing their efficiencies to 27% for the $2e2\mu/2\mu2e$ channels and 20% for the $4e$ channel.

After the FSR correction, the lepton four-momenta of the leading dilepton are recomputed by means of a Z-mass-constrained kinematic fit. The fit uses a Breit-Wigner Z line shape and a single Gaussian to model the lepton momentum response function with the Gaussian σ set to the expected resolution for each lepton. The Z-mass constraint improves the $m_{4\ell}$ resolution by about 15%. More complex momentum response functions were compared to the single Gaussian and found to have only minimal improvement for the $m_{4\ell}$ resolution.

Events satisfying the above criteria are considered candidate signal events for the inclusive analysis, defining a signal region independent of the value of $m_{4\ell}$.

B. Event categorization

To measure the rates for the ggF, VBF, and VH production mechanisms, discussed in Sec. III, each $H \to 4\ell$ candidate selected by the criteria described above is assigned to one of four categories (VBF enriched, VH-hadronic enriched, VH-leptonic enriched, or ggF enriched), depending on other event characteristics. A schematic view of the event categorization is shown in Fig. 2.

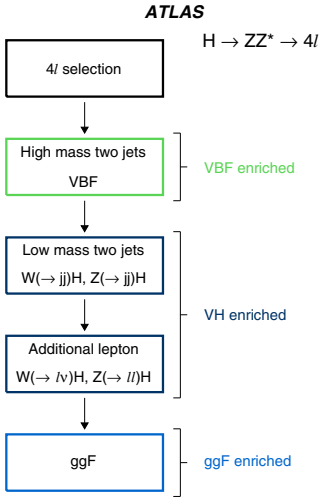

FIG. 2 (color online). Schematic view of the event categorization. Events are required to pass the four-lepton selection, and then they are assigned to one of four categories which are tested sequentially: VBF enriched, VH-hadronic enriched, VH-leptonic enriched, or ggF enriched.

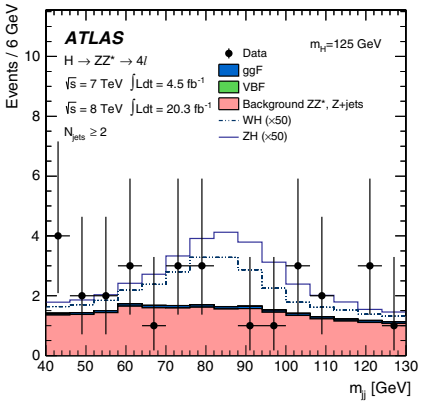

FIG. 3 (color online). Distributions of the dijet invariant mass for the events with at least two jets for the data (filled circles), the expected signal (solid and dot-dot-dashed histograms) and the backgrounds (filled histograms). The WH and ZH hadronic signals are scaled by a factor 50 and the ZH distribution is added on top of the WH distribution.

The VBF enriched category is defined by events with two high-p_{T} jets. The kinematic requirements for jets are $p_{\mathrm{T}} > 25(30)$ GeV for $|\eta| < 2.5$ ($2.5 < |\eta| < 4.5$). If more than two jets fulfill these requirements, the two highest-p_{T} jets are selected as VBF jets. The event is assigned to the VBF enriched category if the invariant mass of the dijet system, m_{jj}, is greater than 130 GeV, leading to a signal efficiency of approximately 55%. This category has a considerable contamination from ggF events, with 54% of the expected events in this category arising from production via gluon fusion.

Events that do not satisfy the VBF enriched criteria are considered for the VH-hadronic enriched category. The same jet-related requirements are applied but with $40 < m_{jj} < 130$ GeV, as presented in Fig. 3. Moreover, the candidate has to fulfill a requirement on the output weight of a specific multivariate discriminant, presented in Sec. VII B. The signal efficiency for requiring two jets is 48% for VH and applying the multivariate discriminant brings the overall signal efficiency to 25%.

Events failing to satisfy the above criteria are next considered for the VH-leptonic enriched category. Events are assigned to this category if there is an extra lepton (e or μ), in addition to the four leptons forming the Higgs boson candidate, with $p_{\mathrm{T}} > 8$ GeV and satisfying the same lepton requirements. The signal efficiency for the extra vector boson for the VH-leptonic enriched category is around 90% (100%) for the W (Z), where the Z has two leptons which can pass the extra lepton selection.

Finally, events that are not assigned to any of the above categories are associated with the ggF enriched category. Table II shows the expected yields for Higgs boson production and ZZ^* background events in each category from each of the production mechanisms, for $m_H = 125$ GeV and 4.5 fb^{-1} at $\sqrt{s} = 7$ TeV and 20.3 fb^{-1} at $\sqrt{s} = 8$ TeV.

VI. Background Estimation

The rate of the ZZ^* background is estimated using simulation normalized to the SM cross section as described in Sec. III, while the rate and composition of the reducible $\ell\ell$ + jets and $t\bar{t}$ background processes are evaluated with data-driven methods. The composition of the reducible backgrounds depends on the flavor of the subleading dilepton pair, and different approaches are taken for the $\ell\ell + \mu\mu$ and the $\ell\ell + ee$ final states. These two cases are discussed in Secs. VI A and VI B, respectively, and the yields for all reducible backgrounds in the signal region are summarized in Tables V and VII. Finally, the small contribution from the WZ reducible background is

TABLE II. The expected number of events in each category (ggF enriched, VBF enriched, VH-hadronic enriched and VH-leptonic enriched), after all analysis criteria are applied, for each signal production mechanism (ggF/$b\bar{b}H/t\bar{t}H$, VBF, VH) at $m_H = 125$ GeV, for 4.5 fb^{-1} at $\sqrt{s} = 7$ TeV and 20.3 fb^{-1} at $\sqrt{s} = 8$ TeV. The requirement $m_{4\ell} > 110$ GeV is applied.

Category	$gg \to H$, $q\bar{q}/gg \to b\bar{b}H/t\bar{t}H$	$qq' \to Hqq'$	$q\bar{q} \to W/ZH$
	$\sqrt{s} = 7$ TeV		
ggF enriched	2.06 ± 0.25	0.114 ± 0.005	0.067 ± 0.003
VBF enriched	0.13 ± 0.04	0.137 ± 0.009	0.015 ± 0.001
VH-hadronic enriched	0.053 ± 0.018	0.007 ± 0.001	0.038 ± 0.002
VH-leptonic enriched	0.005 ± 0.001	0.0007 ± 0.0001	0.023 ± 0.002
	$\sqrt{s} = 8$ TeV		
ggF enriched	12.0 ± 1.4	0.52 ± 0.02	0.37 ± 0.02
VBF enriched	1.2 ± 0.4	0.69 ± 0.05	0.10 ± 0.01
VH-hadronic enriched	0.41 ± 0.14	0.030 ± 0.004	0.21 ± 0.01
VH-leptonic enriched	0.021 ± 0.003	0.0009 ± 0.0002	0.13 ± 0.01

estimated from simulation. The background estimation follows the methods previously described in Refs. [4,92] with several improvements and additional cross-checks.

A. $\ell\ell + \mu\mu$ background

The $\ell\ell + \mu\mu$ reducible background arises from Z + jets and $t\bar{t}$ processes, where the Z + jets contribution has a $Zb\bar{b}$ heavy-flavor quark component in which the heavy-flavor quarks decay semileptonically, and a component arising from Z + light-flavor jets with subsequent π/K in-flight decays. The number of background events from Z + jets and $t\bar{t}$ production is estimated from an unbinned maximum likelihood fit, performed simultaneously to four orthogonal control regions, each of them providing information on one or more of the background components. The fit results are expressed in terms of yields in a reference control region, defined by applying the analysis event selection except for the isolation and impact parameter requirements to the subleading dilepton pair. The reference control region is also used for the validation of the estimates. Finally, the background estimates in the reference control region are extrapolated to the signal region.

The control regions used in the maximum likelihood fit are designed to minimize contamination from the Higgs boson signal and the ZZ^* background. The four control regions are

(a) *Inverted requirement on impact parameter significance.* Candidates are selected following the analysis event selection, but (1) without applying the isolation requirement to the muons of the subleading dilepton and (2) requiring that at least one of the two muons fails the impact parameter significance requirement. As a result, this control region is enriched in $Zb\bar{b}$ and $t\bar{t}$ events.

(b) *Inverted requirement on isolation.* Candidates are selected following the analysis event selection, but requiring that at least one of the muons of the subleading dilepton fails the isolation requirement. As a result, this control region is enriched in Z + light-flavor-jet events (π/K in-flight decays) and $t\bar{t}$ events.

(c) *$e\mu$ leading dilepton ($e\mu + \mu\mu$).* Candidates are selected following the analysis event selection, but requiring the leading dilepton to be an electron-muon pair. Moreover, the isolation and impact parameter requirements are not applied to the muons of the subleading dilepton, which are also allowed to have the same or opposite charge sign. Events containing a Z-boson candidate decaying into e^+e^- or $\mu^+\mu^-$ pairs are removed with a requirement on the mass. This control region is dominated by $t\bar{t}$ events.

(d) *Same-sign subleading dilepton.* The analysis event selection is applied, but for the subleading dilepton neither isolation nor impact parameter significance requirements are applied and the leptons are required to have the same charge sign (SS). This same-sign control region is not dominated by a specific background; all the reducible backgrounds have a significant contribution.

The expected composition for each control region is shown in Table III. The uncertainties on the relative yields between the control regions and the reference control region are introduced in the maximum likelihood fit as nuisance parameters. The residual contribution from ZZ^* and the contribution from WZ production, where—contrary to the Z + jets and $t\bar{t}$ backgrounds—only one of the leptons in the subleading dilepton is expected to be a nonisolated backgroundlike muon, are estimated for each control region from simulation.

In all the control regions, the observable is the mass of the leading dilepton, m_{12}, which peaks at the Z mass for the resonant (Z + jets) component and has a broad distribution for the nonresonant ($t\bar{t}$) component. For the $t\bar{t}$ component the m_{12} distribution is modeled by a second-order Chebyshev polynomial, while for the Z + jets component it is modeled using a convolution of a Breit-Wigner distribution with a Crystal Ball function. The shape parameters are derived from simulation. In the combined fit, the shape parameters are constrained to be the same in each of the control regions, and are allowed to fluctuate within the uncertainties obtained from simulation. The results of the combined fit in the four control regions are shown in Fig. 4, along with the individual background components, while the event yields in the reference control region are summarized in Table IV. As a validation of the fit method, the maximum likelihood fit is applied to the individual control regions yielding estimates compatible to those of the combined fit; these are also summarized in Table IV.

The estimated yields in the reference control region are extrapolated to the signal region by multiplying each

TABLE III. Expected contribution of the $\ell\ell + \mu\mu$ background sources in each of the control regions.

	Control region			
Background	Inverted d_0	Inverted isolation	$e\mu + \mu\mu$	Same-sign
$Zb\bar{b}$	$32.8 \pm 0.5\%$	$26.5 \pm 1.2\%$	$0.3 \pm 1.2\%$	$30.6 \pm 0.7\%$
Z + light-flavor jets	$9.2 \pm 1.3\%$	$39.3 \pm 2.6\%$	$0.0 \pm 0.8\%$	$16.9 \pm 1.6\%$
$t\bar{t}$	$58.0 \pm 0.9\%$	$34.2 \pm 1.6\%$	$99.7 \pm 1.0\%$	$52.5 \pm 1.1\%$

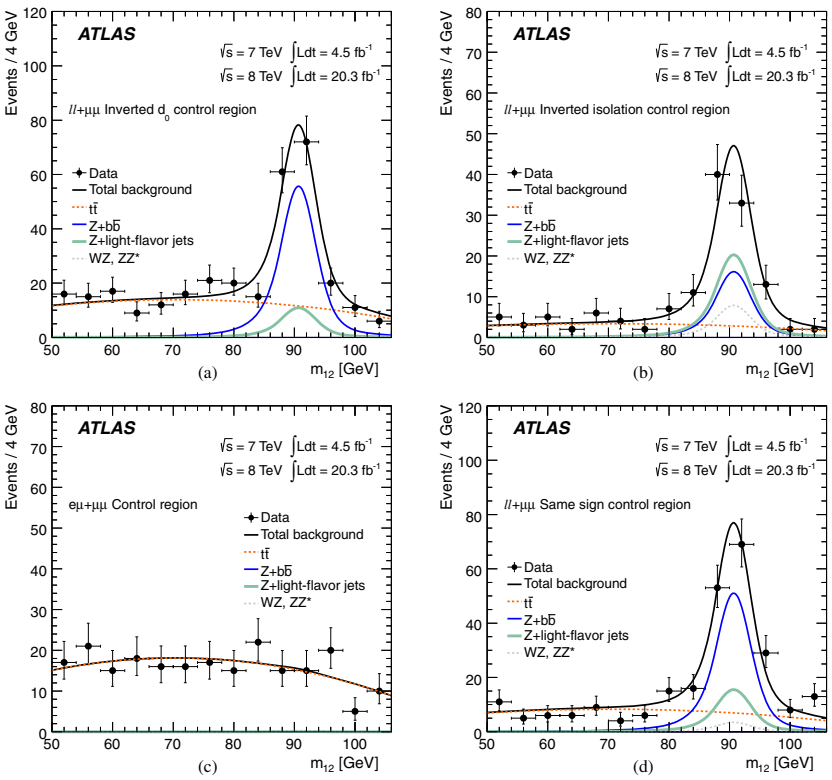

FIG. 4 (color online). The observed m_{12} distributions (filled circles) and the results of the maximum likelihood fit are presented for the four control regions: (a) inverted requirement on impact parameter significance, (b) inverted requirement on isolation, (c) $e\mu$ leading dilepton, where the backgrounds besides $t\bar{t}$ are small and not visible, and (d) same-sign subleading dilepton. The fit results are shown for the total background (black line) as well as the individual components: $Z+$jets decomposed into $Z+b\bar{b}$ (blue line) and $Z+$ light-flavor jets (green line), $t\bar{t}$ (dashed red line), and the combined WZ and ZZ (dashed gray line), where the WZ and ZZ contributions are estimated from simulation.

background component by the probability of satisfying the isolation and impact parameter significance requirements, estimated from the relevant simulated sample. The systematic uncertainty in these transfer factors, stemming mostly from the size of the simulated sample, is 6% for $Zb\bar{b}$, 60% for $Z+$ light-flavor jets and 16% for $t\bar{t}$. Furthermore, these simulation-based efficiencies are validated with data using muons accompanying $Z \to \ell\ell$ candidates, where the leptons composing the Z boson candidate are required to satisfy isolation and impact parameter criteria. Events with four leptons, or with an opposite-sign dimuon with mass less than 5 GeV, are excluded. Based on the data/simulation agreement of the efficiencies in this control region an additional systematic uncertainty of 1.6% is added. Figure 5 shows the relative difference between the ID and MS p_{T} measurements for combined muons for a subset of the $Z+X$ control region where the X represents a single combined muon. The contribution from π/K in-flight decays is clearly visible and well described by the simulation.

The reducible background estimates in the signal region are given in Table V, separately for the $\sqrt{s} = 7$ TeV and 8 TeV data. The uncertainties are separated into statistical and systematic contributions, where in the latter the transfer factor uncertainty and the fit systematic uncertainties are included.

B. $\ell\ell + ee$ background

The background for subleading electron pairs arises from jets misidentified as electrons. The background is classified

TABLE IV. Data-driven $\ell\ell + \mu\mu$ background estimates for the $\sqrt{s} = 7$ TeV and $\sqrt{s} = 8$ TeV data, expressed as yields in the reference control region, for the combined fit and fits to the individual control regions. In the individual control regions only the total Z+jets contribution can be determined, while the $e\mu + \mu\mu$ control region is only sensitive to the $t\bar{t}$ background. The statistical uncertainties are also shown.

Reducible background yields for 4μ and $2e2\mu$ in reference control region				
Control region	$Zb\bar{b}$	Z + light-flavor jets	Total Z + jets	$t\bar{t}$
Combined fit	159 ± 20	49 ± 10	208 ± 22	210 ± 12
Inverted impact parameter			206 ± 18	208 ± 23
Inverted isolation			210 ± 21	201 ± 24
$e\mu + \mu\mu$			–	201 ± 12
Same-sign dilepton			198 ± 20	196 ± 22

into three distinct sources: light-flavor jets (f), photon conversions (γ) and heavy-flavor semileptonic decays (q). These sources are identified exactly in simulated background events. In addition, corresponding data control regions are defined which are enriched in events associated with each of these sources, thus allowing data-driven classification of reconstructed events into matching categories. For the background estimation, two types of control regions are defined:

(i) the first, denoted as $3\ell + X$, in which the identification requirements for the lower-p_{T} electron of the subleading pair are relaxed;

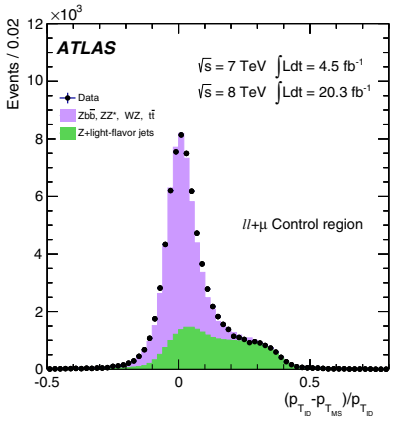

FIG. 5 (color online). The distribution of the difference between the transverse momentum measured in the ID and in the MS normalized to the ID measurement, $(p_{\mathrm{T_{ID}}} - p_{\mathrm{T_{MS}}})/p_{\mathrm{T_{ID}}}$, for combined muons accompanying a $Z \to \ell\ell$ candidate. The data (filled circles) are compared to the background simulation (filled histograms) which has the Z + light-flavor background shown separately to distinguish the contribution from π/K in-flight decays. The additional muon is selected to be a combined muon with $p_{\mathrm{T}} > 6$ GeV, which fulfills the ΔR requirement for the lepton separation of the analysis and in the case of $Z(\to \mu^+\mu^-) + \mu$ final state, the opposite sign pairs are required to have $m_{\mu^+\mu^-} > 5$ GeV to remove J/ψ decays.

(ii) the second, denoted as $\ell\ell + XX$, which comes in two variants: one in which the identification requirements for both electrons of the subleading pair are relaxed, and another in which an inverted selection is applied to the subleading pair.

In both cases, the leading pair satisfies the complete event selection. The final background estimate is obtained from the $3\ell + X$ region, while the estimates from the $\ell\ell + XX$ region are used as cross-checks.

The efficiencies needed to extrapolate the different background sources from the control regions into the signal region are obtained separately for each of the f, γ, q background sources, in p_{T} and η bins, from simulation. These simulation-based efficiencies are corrected to correspond to the efficiency measured in data using a third type of control region, denoted as $Z + X$, enhanced for each X component. The $Z + X$ control region has a leading lepton pair, compatible with the decay of a Z boson, passing the full event selection and an additional object (X) that satisfies the relaxed identification for the specific control region to be extrapolated. The $Z + X$ data sample is significantly larger than the background control data samples. For all of the methods, the extrapolation from the background control region, $3\ell + X$ or $\ell\ell + XX$, to the signal region cannot be done directly with the efficiencies from the $Z + X$ data control region due to differences in the fractions of f, γ, q for the X of the two control regions. In the following, the q contribution in the simulation is increased by a factor of 1.4 to match the data.

1. Background estimation from $3\ell + X$

This method uses the $3\ell + X$ data control region with one loosely identified lepton for normalization. The control region is then fit using templates derived from simulation to determine the composition in terms of the three background sources f, γ, q, and these components are extrapolated individually to the signal region using the efficiency from the $Z + X$ control region.

The background estimation from the $3\ell + X$ region uses data that has quadruplets built as for the full analysis, with the exception that the full selection is applied to only the three highest-p_{T} leptons. Relaxed requirements are applied

TABLE V. Estimates for the $\ell\ell + \mu\mu$ background in the signal region for the full $m_{4\ell}$ mass range for the $\sqrt{s} = 7$ TeV and $\sqrt{s} = 8$ TeV data. The $Z +$ jets and $t\bar{t}$ background estimates are data-driven and the WZ contribution is from simulation. The decomposition of the $Z +$ jets background in terms of the $Zb\bar{b}$ and the $Z +$ light-flavor-jets contributions is also provided.

Background	4μ	$2e2\mu$
	$\sqrt{s} = 7$ TeV	
$Z +$ jets	$0.42 \pm 0.21(\text{stat}) \pm 0.08(\text{syst})$	$0.29 \pm 0.14(\text{stat}) \pm 0.05(\text{syst})$
$t\bar{t}$	$0.081 \pm 0.016(\text{stat}) \pm 0.021(\text{syst})$	$0.056 \pm 0.011(\text{stat}) \pm 0.015(\text{syst})$
WZ expectation	0.08 ± 0.05	0.19 ± 0.10
	$Z +$ jets decomposition	
$Zb\bar{b}$	$0.36 \pm 0.19(\text{stat}) \pm 0.07(\text{syst})$	$0.25 \pm 0.13(\text{stat}) \pm 0.05(\text{syst})$
$Z +$ light-flavor jets	$0.06 \pm 0.08(\text{stat}) \pm 0.04(\text{syst})$	$0.04 \pm 0.06(\text{stat}) \pm 0.02(\text{syst})$
	$\sqrt{s} = 8$ TeV	
$Z +$ jets	$3.11 \pm 0.46(\text{stat}) \pm 0.43(\text{syst})$	$2.58 \pm 0.39(\text{stat}) \pm 0.43(\text{syst})$
$t\bar{t}$	$0.51 \pm 0.03(\text{stat}) \pm 0.09(\text{syst})$	$0.48 \pm 0.03(\text{stat}) \pm 0.08(\text{syst})$
WZ expectation	0.42 ± 0.07	0.44 ± 0.06
	$Z +$ jets decomposition	
$Zb\bar{b}$	$2.30 \pm 0.26(\text{stat}) \pm 0.14(\text{syst})$	$2.01 \pm 0.23(\text{stat}) \pm 0.13(\text{syst})$
$Z +$ light-flavor jets	$0.81 \pm 0.38(\text{stat}) \pm 0.41(\text{syst})$	$0.57 \pm 0.31(\text{stat}) \pm 0.41(\text{syst})$

to the lowest-p_{T} electron: only a track with a minimum number of silicon hits which matches a cluster is required and the electron identification and isolation/impact parameter significance selection criteria are not applied. In addition, the subleading electron pair is required to have the same sign for both charges (SS) to minimize the contribution from the ZZ^* background. A residual ZZ^* component with a magnitude of 5% of the background estimate survives the SS selection, and is subtracted to get the final estimate.

By requiring only a single electron with relaxed selection, the composition of the control region is simplified when compared with the other $\ell\ell + XX$ control regions, and the yields of the different background components can be extracted with a two-dimensional fit. Two variables, the number of hits in the innermost layer of the pixel detector ($n_{\mathrm{hits}}^{\mathrm{B\text{-}layer}}$) and the ratio of the number of high-threshold to low-threshold TRT hits (r_{TRT}),[3] allow the separation of the f, γ and q components, since most photons convert after the innermost pixel layer, and hadrons faking electrons have a lower r_{TRT} compared to conversions and heavy-flavor electrons. Templates for the fit are taken from the $Z + X$ simulation after applying corrections from data.

The results of the fit are shown in Fig. 6, for the $2\mu 2e$ and $4e$ channels combined. The *sPlot* method [93] is used to unfold the contributions from the different background sources as a function of electron p_{T}. The background estimates for the f, γ and q components in the control region, averaged over the $2\mu 2e$ and $4e$ channels, are summarized in Table VI.

To extrapolate the f, γ and q components from the $3\ell + X$ control region to the signal region, the efficiency for the different components to satisfy all selection criteria is obtained from the $Z + X$ simulation. As previously mentioned, the simulation efficiency for each component is corrected by comparing with data using the $Z + X$ control region with an adjusted selection to enrich it for each specific component. For the f component, the simulation efficiency is corrected by a factor between 1.6 and 2.5, rising with increasing p_{T}. The simulation is found to model well the efficiency of the γ component, to within approximately 10%. For the q component, the efficiency is found to be modeled well by simulation, but there is an additional correction, obtained from simulation, to estimate the number of background opposite-sign (OS) events from the number of SS events, which is $\mathrm{OS/SS} \approx 1.7$. The systematic uncertainty is dominated by these simulation efficiency corrections, corresponding to 30%, 20%, 25% uncertainties for f, γ, q, respectively. The extrapolation efficiency and signal yields are also given in Table VI. After removing the residual ZZ^* background ($\approx$5%), the final results for the $2\mu 2e$ and $4e$ reducible backgrounds are given in Table VII.

2. Background estimation from the $\ell\ell + XX$ region using the transfer-factor method

The transfer-factor method starts from the $\ell\ell + XX$ control region in data with two leptons with inverted

[3]A large number of hits above a high signal pulse-height threshold is an indication of the presence of transition radiation, which is more probable for electrons than for pions.

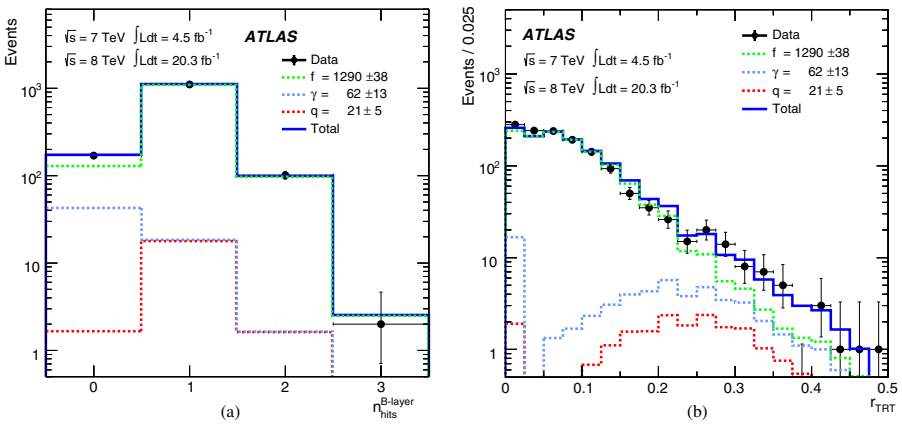

FIG. 6 (color online). The results of a simultaneous fit to (a) $n_{\text{hits}}^{\text{B-layer}}$, the number of hits in the innermost pixel layer, and (b) r_{TRT}, the ratio of the number of high-threshold to low-threshold TRT hits, for the background components in the $3\ell + X$ control region. The fit is performed separately for the $2\mu 2e$ and $4e$ channels and summed together in the present plots. The data are represented by the filled circles. The sources of background electrons are denoted as light-flavor jets faking an electron (f, green dashed histogram), photon conversions (γ, blue dashed histogram) and electrons from heavy-flavor quark semileptonic decays (q, red dashed histogram). The total background is given by the solid blue histogram.

selection requirements. Using the predicted sample composition from simulation, two approaches are taken to obtain transfer factors: one using the $Z + X$ simulation corrected by data, and the other using the $Z + X$ data control region that is enriched to obtain a q component matching that of the $\ell\ell + XX$ control region.

The $\ell\ell + XX$ data control region has relaxed electron likelihood identification on the X pair and requires each X to fail one selection among the full electron identification, isolation and impact parameter significance selections, leading to a sample of around 700 events for each of the $2\mu + XX$ and $2e + XX$ channels. The inverted selection removes most of the ZZ^* background from the control region as well as the Higgs signal. The main challenge is to correctly estimate the extrapolation efficiency, or transfer factor, from the $\ell\ell + XX$ control region to the signal region using the $Z + X$ sample, since the background composition of f, γ and q is different for the $Z + X$ and $\ell\ell + XX$ control regions and each of their extrapolation efficiencies is significantly different.

In order to aid in the understanding of the control region composition and to improve the uncertainty on the estimate of the extrapolation to the signal region, each X is assigned to one of two reconstruction categories: electron-like (E) or

TABLE VI. The fit results for the $3\ell + X$ control region, the extrapolation factors and the signal region yields for the reducible $\ell\ell + ee$ background. The second column gives the fit yield of each component in the $3\ell + X$ control region. The corresponding extrapolation efficiency and signal region yield are in the next two columns. The background values represent the sum of the $2\mu 2e$ and $4e$ channels. The uncertainties are the combination of the statistical and systematic uncertainties.

$2\mu 2e$ and $4e$ Type	Fit yield in control region	Extrapolation factor	Yield in signal region
		$\sqrt{s} = 7$ TeV data	
f	391 ± 29	0.010 ± 0.001	3.9 ± 0.9
γ	19 ± 9	0.10 ± 0.02	2.0 ± 1.0
q	5.1 ± 1.0	0.10 ± 0.03	0.51 ± 0.15
		$\sqrt{s} = 8$ TeV data	
f	894 ± 44	0.0034 ± 0.0004	3.1 ± 1.0
γ	48 ± 15	0.024 ± 0.004	1.1 ± 0.6
q	18.3 ± 3.6	0.10 ± 0.02	1.8 ± 0.5

TABLE VII. Summary of the $\ell\ell + ee$ data-driven background estimates for the $\sqrt{s} = 7$ TeV and $\sqrt{s} = 8$ TeV data for the full $m_{4\ell}$ mass range. OS (SS) stands for opposite-sign (same-sign) lepton pairs. The "†" symbol indicates the estimates used for the background normalization; the other estimates are used as cross-checks. The first uncertainty is statistical, while the second is systematic. The SS data full analysis is limited to the region with $m_{4\ell}$ below 160 GeV to avoid a ZZ contribution; this region contains 70% of the expected background.

Method	$\sqrt{s} = 7$ TeV data	$\sqrt{s} = 8$ TeV data
	$2\mu 2e$	
$3\ell + X^{\dagger}$	$2.9 \pm 0.5 \pm 0.5$	$2.9 \pm 0.3 \pm 0.6$
$\ell\ell + XX$ transfer factor	$2.2 \pm 0.3 \pm 1.1$	$2.5 \pm 0.1 \pm 0.9$
$\ell\ell + XX$ transfer factor b-enriched	$2.8 \pm 0.5 \pm 0.8$	$3.2 \pm 0.2 \pm 0.9$
$\ell\ell + XX$ reco-truth	$2.8 \pm 0.4 \pm 1.0$	$2.9 \pm 0.3 \pm 0.3$
$2\mu 2e$ SS data full analysis	1	2
	$4e$	
$3\ell + X^{\dagger}$	$3.3 \pm 0.5 \pm 0.5$	$2.9 \pm 0.3 \pm 0.5$
$\ell\ell + XX$ transfer factor	$2.0 \pm 0.3 \pm 0.9$	$2.4 \pm 0.1 \pm 0.9$
$\ell\ell + XX$ transfer factor b-enriched	$3.4 \pm 0.9 \pm 0.8$	$2.9 \pm 0.2 \pm 0.8$
$\ell\ell + XX$ reco-truth	$2.6 \pm 0.4 \pm 0.9$	$2.8 \pm 0.3 \pm 0.3$
$4e$ SS data full analysis	2	2

fake-like (F), for both data and simulation. For the E category, a selection is applied to enhance the electron content, and the remaining X's fall into the F category. For the $\ell\ell + XX$ control region, the composition of X in terms of the background source is balanced between fakes (f) and electrons (γ, q) for the E category corresponding to component fractions of 50% f, 20% γ, and 30% q, and is dominated by fakes for the F category with 92% f, 5% γ and 3% q.

The two approaches taken to estimate the background from the $\ell\ell + XX$ data control region differ in the way they estimate the extrapolation to the signal region with $Z + X$ events. Both approaches separate XX into the four reconstruction categories: EE, EF, FE and FF. The first approach uses the $Z + X$ simulation to determine the transfer factors for X in bins of p_{T} and η, where the extrapolation efficiency of each background component of the $\ell\ell + XX$ simulation is combined according to the composition seen in the $\ell\ell + XX$ simulation. In addition, the simulation extrapolation efficiency is corrected to agree with data as previously described in Sec. VI B 1. For the background estimate, the transfer factors are applied to the $\ell\ell + XX$ data control region, accounting for the inverted selection. The result is corrected by subtracting a small residual ZZ^* contribution, and including a WZ contribution that is removed by the inverted selection on the XX; both are estimated with simulation. The background estimate with the transfer-factor method is given in Table VII.

The second approach differs in the manner in which the background composition of the $Z + X$ control region is brought into agreement with the $\ell\ell + XX$ control region. The most important difference lies in the heavy-flavor component fraction, which is three times larger in the $\ell\ell + XX$ control region and has a significantly larger transfer factor than either the f or γ backgrounds. This approach modifies the composition of the $Z + X$ data control region by requiring a b-jet in each event. By tuning the selection of a multivariate b-tagger [94], the q and f composition of the $Z + X$ control region can be brought into agreement with that of the $\ell\ell + XX$ control region to the level of 5%–10%, as seen with simulation. The transfer factors are extracted from the $Z + X$ data control region and applied in bins of p_{T} and η as for the other approach, and the systematic uncertainty is estimated in part by varying the operating point used for the multivariate b-tagger. Finally, the WZ contribution is accounted for with simulation, as previously. The background estimate from the transfer factors based on b-enriched samples is given in Table VII.

3. Reco-truth unfolding method

A third method uses the $\ell\ell + XX$ data control region; however, the two subleading electrons have only the electron identification relaxed and do not have an inverted selection applied as for the transfer-factor method. This control region thus contains all backgrounds, including the ZZ^* background, and the $H \to ZZ^* \to 4\ell$ signal. The extrapolation to the signal region is performed with the $Z + X$ simulation. This method was used as the baseline for previous publications [4,6], but is now superseded by the $3\ell + X$ method, which provides the smallest uncertainties of the data-driven methods. Using the simulation, each of the paired reconstruction categories (EE, EF, FE and FF) of the $\ell\ell + XX$ sample is decomposed into its background origin components (ee, ff, $\gamma\gamma$, qq and the 12 cross combinations), where the e background category is introduced to contain the isolated electrons from ZZ^* and $H \to ZZ^* \to 4\ell$. This 4×16 composition table is summed with efficiency weights, in bins of p_{T} and η, obtained from the $Z + X$ simulation, which is corrected from comparison with data as previously mentioned. To remove the ZZ^* and $H \to ZZ^* \to 4\ell$ contributions from this estimate, the

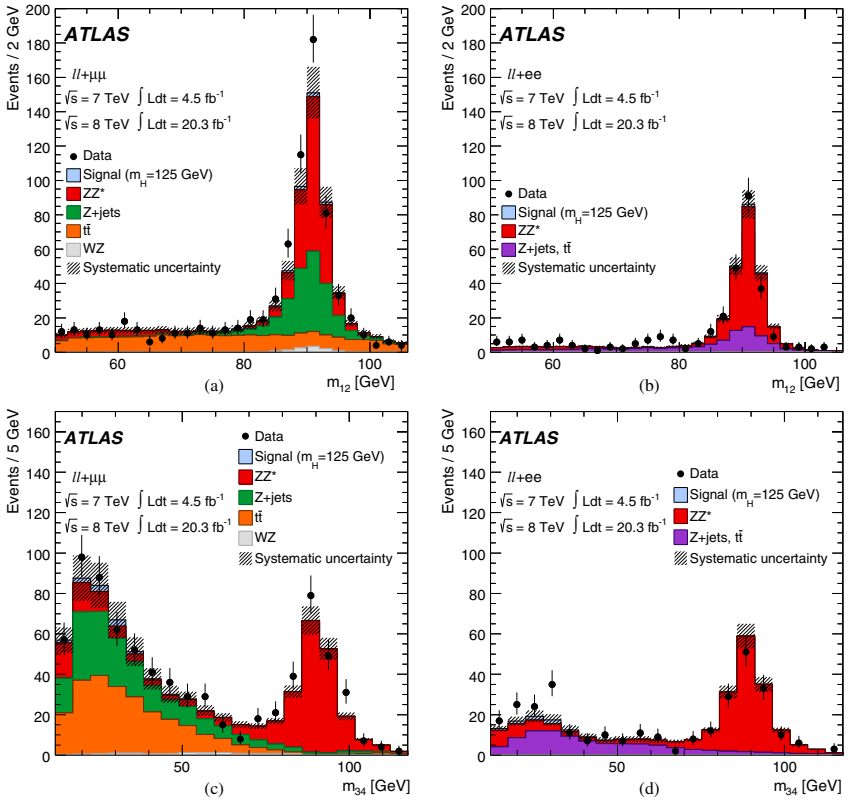

FIG. 7 (color online). Invariant mass distributions of the lepton pairs in the control sample defined by a Z boson candidate and an additional same-flavor lepton pair, including all signal and background contributions, for the $\sqrt{s} = 7$ TeV and $\sqrt{s} = 8$ TeV data sets. The sample is divided according to the flavor of the additional lepton pair. In (a) and (c) the m_{12} and m_{34} distributions are presented for $\ell\ell + \mu^+\mu^-$ events, where $\ell\ell$ is $\mu^+\mu^-$ or e^+e^-. In (b) and (d) the m_{12} and m_{34} distributions are presented for $\ell\ell + e^+e^-$ events. The data are shown as filled circles and the different backgrounds as filled histograms with the total background systematic uncertainty represented by the hatched areas. The kinematic selection of the analysis is applied. Isolation and impact parameter significance requirements are applied to the first lepton pair only. The simulation is normalized to the data-driven background estimates.

background origin category ee is removed from the sum, and an estimated residual of 1.2 ± 0.4 ZZ^* events is subtracted to obtain the final result, which is also given in Table VII.

4. Summary of reducible background estimates for $\ell\ell + ee$

The summary of the reducible backgrounds for the $\ell\ell + ee$ final states is given for the full mass region in Table VII. In addition to the previously discussed methods, the results are presented for the full analysis applied to $\ell\ell + ee$ events in data where the subleading ee pair is required to have the same-sign charge, and $m_{4\ell}$ is required to be below 160 GeV to avoid a ZZ contribution; the region with $m_{4\ell} <$ 160 GeV contains 70% of the expected reducible backgrounds. Although limited in statistical precision, this agrees well with the other estimates.

C. Shape of the reducible background contributions

The $m_{4\ell}$ distributions of the reducible backgrounds are required for the normalization and shape of these backgrounds in the mass fit region, discussed below. The shape of the distribution for the $\ell\ell + \mu\mu$ background is taken from simulation and the uncertainty comes from varying

TABLE VIII. Summary of the background estimates for the data recorded at $\sqrt{s} = 7$ TeV and $\sqrt{s} = 8$ TeV for the full $m_{4\ell}$ mass range. The quoted uncertainties include the combined statistical and systematic components.

Channel	ggF enriched	VBF enriched	VH-hadronic enriched	VH-leptonic enriched
			$\sqrt{s} = 7$ TeV	
$\ell\ell + \mu\mu$	0.98 ± 0.32	0.12 ± 0.08	0.04 ± 0.02	0.004 ± 0.004
$\ell\ell + ee$	5.5 ± 1.2	0.51 ± 0.6	0.20 ± 0.16	0.06 ± 0.11
			$\sqrt{s} = 8$ TeV	
$\ell\ell + \mu\mu$	6.7 ± 1.4	0.6 ± 0.6	0.21 ± 0.13	0.003 ± 0.003
$\ell\ell + ee$	5.1 ± 1.4	0.5 ± 0.6	0.19 ± 0.15	0.06 ± 0.11

the track isolation and impact parameter significance selections. The corresponding distribution for the $\ell\ell + ee$ background comes from the $3\ell + X$ sample, after reweighting with the transfer factor to match the kinematics of the signal region. The uncertainty in the $\ell\ell + ee$ background shape is taken as the difference between the shapes obtained from the control regions of the two other methods: transfer factor and reco-truth. The estimates in the $120 < m_{4\ell} < 130$ GeV mass window are provided in Table XI. Figure 7 presents the m_{12} and m_{34} distributions for the $\ell\ell + \mu\mu$ and $\ell\ell + ee$ control regions where the full selection has been applied except for subleading lepton impact parameter significance and isolation requirements, which are not applied. Good agreement is seen between the data and the sum of the various background estimates. The shape of the background in the $m_{4\ell}$ distribution extrapolated to the signal region can be seen in Fig. 13.

D. Background for categories

For the reducible background, the fraction of background in each category is evaluated using simulation. Applying these fractions to the background estimates from Tables V and VII gives the reducible background estimates per category shown in Table VIII. The systematic uncertainties include the differences observed between the fractions obtained from simulation and those from the reducible background data control regions. The expected ZZ^* background evaluated from simulation for each category is given in Table XII. To obtain the reducible background in the signal region, the shapes of the $m_{4\ell}$ distributions for the reducible backgrounds discussed in Sec. VI C are used.

VII. MULTIVARIATE DISCRIMINANTS

The analysis sensitivity is improved by employing three multivariate discriminants to distinguish between the different classes of four-lepton events: one to separate the Higgs boson signal from the ZZ^* background in the inclusive analysis, and two to separate the VBF- and VH-produced Higgs boson signal from the ggF-produced Higgs boson signal in the VBF enriched and VH-hadronic enriched categories. These discriminants are based on boosted decision trees (BDT) [95].

A. BDT for ZZ^* background rejection

The differences in the kinematics of the $H \to ZZ^* \to 4\ell$ decay and the ZZ^* background are incorporated into a BDT discriminant (BDT_{ZZ^*}). The training is done using fully simulated $H \to ZZ^* \to 4\ell$ signal events, generated with $m_H = 125$ GeV for ggF production, and $qq \to ZZ^*$ background events. Only events satisfying the inclusive event selection requirements and with $115 < m_{4\ell} < 130$ GeV are considered. This range contains 95% of the signal and is asymmetric around 125 GeV to include the residual effects of FSR and bremsstrahlung. The discriminating variables used in the training are the transverse momentum of the four-lepton system ($p_{\mathrm{T}}^{4\ell}$); the pseudorapidity of the four-lepton system ($\eta^{4\ell}$), correlated to the $p_{\mathrm{T}}^{4\ell}$; and a matrix-element-based kinematic discriminant (D_{ZZ^*}). The discriminant D_{ZZ^*} is defined as

$$D_{ZZ^*} = \ln\left(\frac{|\mathcal{M}_{\mathrm{sig}}|^2}{|\mathcal{M}_{ZZ}|^2}\right), \tag{1}$$

where $\mathcal{M}_{\mathrm{sig}}$ corresponds to the matrix element for the signal process, while $\mathcal{M}_{ZZ}$ is the matrix element for the ZZ^* background process. The matrix elements for both signal and background are computed at leading order using MadGraph5 [96]. The matrix element for the signal is evaluated according to the SM hypothesis of a scalar boson with spin-parity $J^P = 0^+$ [7] and under the assumption that $m_H = m_{4\ell}$. Figures 8(a)–8(c) show the distributions of the variables used to train the BDT_{ZZ^*} classifier for the signal and the ZZ^* background. The separation between a SM Higgs signal and the ZZ^* background can be seen in Fig. 8(d).

As discussed in Sec. VIII, the BDT_{ZZ^*} output is exploited in the two-dimensional model built to measure the Higgs boson mass, the inclusive signal strength and the signal strength in the ggF enriched category.

B. BDT for categorization

For event categorization, two separate BDT classifiers were developed to discriminate against ggF production: one for VBF production ($\mathrm{BDT}_{\mathrm{VBF}}$) and another for the vector boson hadronic decays of VH production ($\mathrm{BDT}_{\mathrm{VH}}$). In the first case the BDT output is used as an observable together with $m_{4\ell}$ in a maximum likelihood fit for the VBF category, while in the latter case the BDT output value is used as a

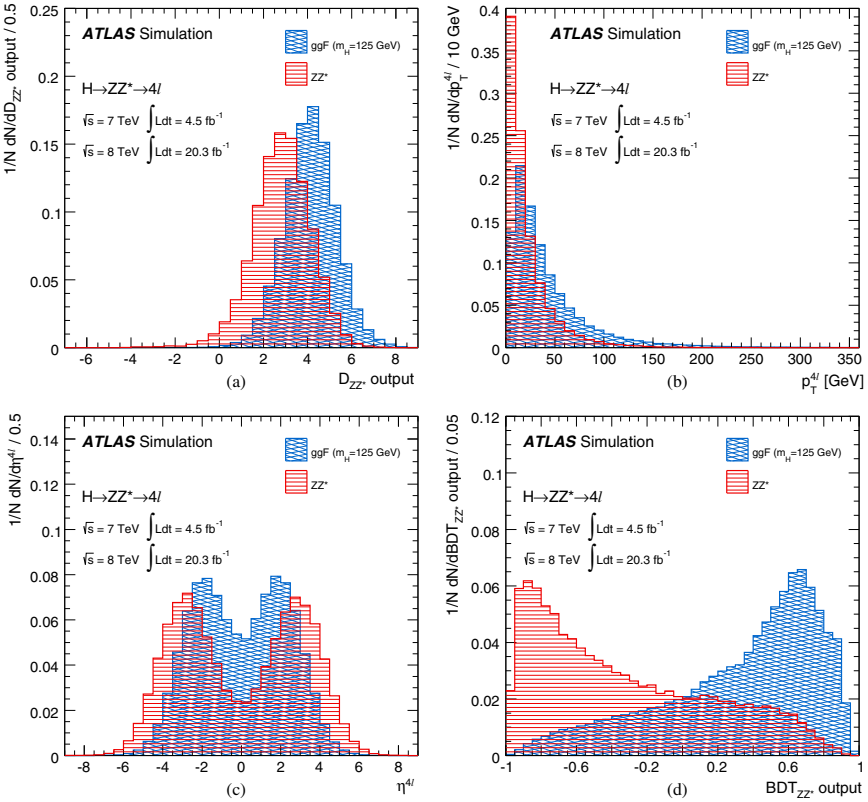

FIG. 8 (color online). Distributions for signal (blue) and ZZ^* background (red) events, showing (a) D_{ZZ^*} output, (b) $p_{\mathrm{T}}^{4\ell}$ and (c) $\eta^{4\ell}$ after the inclusive analysis selection in the mass range $115 < m_{4\ell} < 130$ GeV used for the training of the BDT_{ZZ^*} classifier. (d) BDT_{ZZ^*} output distribution for the signal (blue) and ZZ^* background (red) in the mass range $115 < m_{4\ell} < 130$ GeV. All histograms are normalized to the same area.

selection requirement for the event to be classified in the VH-hadronic enriched category, as discussed in Sec. V B. In both cases the same five discriminating variables are used. In order of decreasing separation power between the two production modes, the variables are (a) invariant mass of the dijet system, (b) pseudorapidity separation between the two jets ($|\Delta\eta_{jj}|$), (c) transverse momentum of each jet, and (d) pseudorapidity of the leading jet.

For the training of the BDT discriminant, fully simulated four-lepton Higgs boson signal events produced through ggF and VBF production and hadronically decaying vector boson events for VH production are used. The distributions of these variables for $\mathrm{BDT}_{\mathrm{VBF}}$ are presented in Figs. 9(a)–9(e), where all the expected features of the VBF production of a Higgs boson can be seen: the dijet system has a high invariant mass and the two jets are emitted in opposite high-$|\eta|$ regions with a considerable $\Delta\eta$ separation between them. The jets of ggF events, on the other hand, are more centrally produced and have a smaller invariant mass and $\Delta\eta$ separation. The separation between VBF and ggF can be seen in the output of $\mathrm{BDT}_{\mathrm{VBF}}$ in Fig. 9(f), where the separation between VBF and ZZ^* is found to be similar. The output of $\mathrm{BDT}_{\mathrm{VBF}}$ is unchanged for various mass points around the main training mass of $m_H = 125$ GeV. For variables entering the $\mathrm{BDT}_{\mathrm{VH}}$ discriminant, the invariant mass of the dijet system, which peaks at the Z mass, exhibits the most important difference between ggF and VH production modes. The other variables have less separation power. The corresponding separation for $\mathrm{BDT}_{\mathrm{VH}}$ is shown in Fig. 10. As described in Sec. V B, the VH-hadronic enriched category applies a selection on the $\mathrm{BDT}_{\mathrm{VH}}$ discriminant (< -0.4) which optimizes the signal significance.

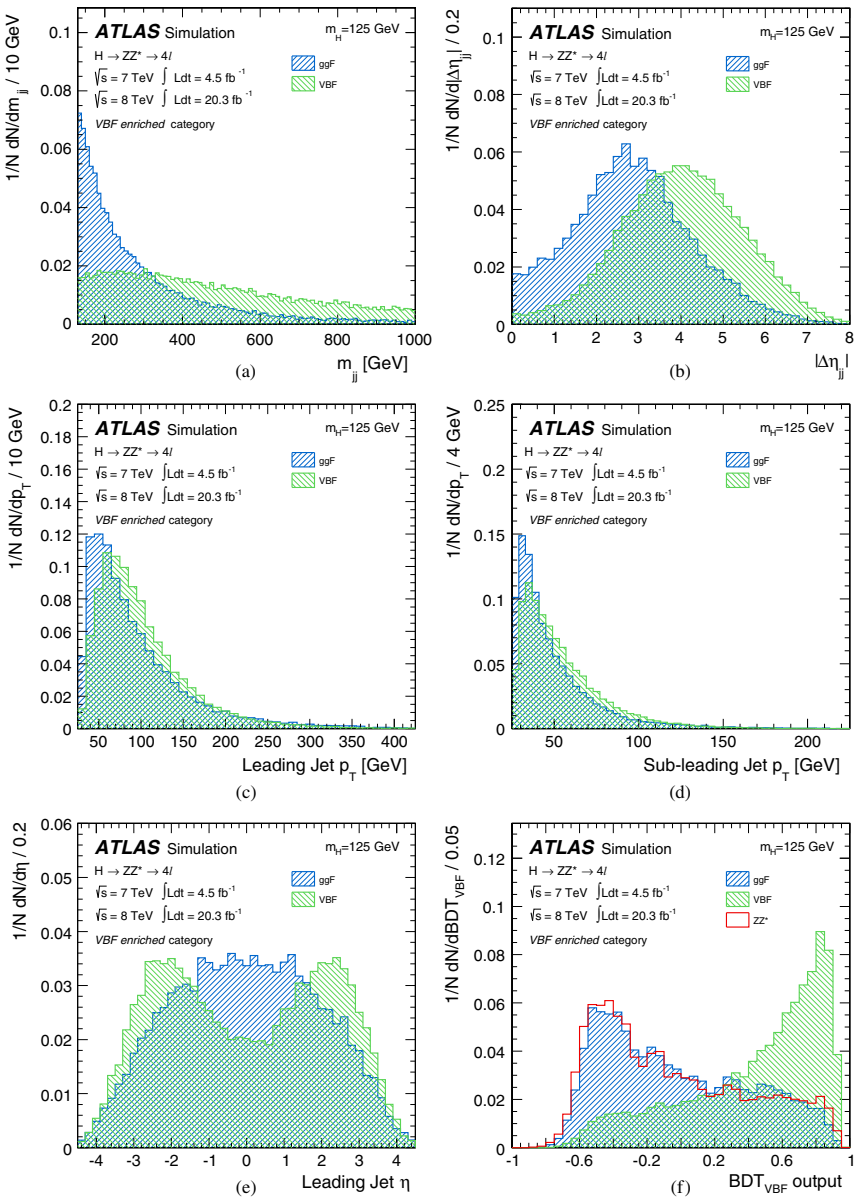

FIG. 9 (color online). Distribution of kinematic variables for signal (VBF events, green) and background (ggF events, blue) events used in the training of the VBF boosted decision tree: 9(a) dijet invariant mass, 9(b) dijet η separation, 9(c) leading jet p_{T}, 9 (d) subleading jet p_{T} and 9(e) leading jet η. 9(f) Output distributions of $\mathrm{BDT}_{\mathrm{VBF}}$ for VBF and ggF events as well as for the ZZ^* background (red). All histograms are normalized to the same area.

VIII. SIGNAL AND BACKGROUND MODELING

A. Signal and background modeling for the inclusive analysis

For the measurements of the Higgs boson mass, of its natural width and of the inclusive production rate relative to the SM expectation (the signal strength denoted as μ) in the $H \to ZZ^* \to 4\ell$ channel, three different parameterizations of the signal and background were developed as described in Ref. [9], where the Higgs boson mass measurement is reported. The baseline method is a two-dimensional (2D) fit to $m_{4\ell}$ and the BDT_{ZZ^*} output ($O_{\mathrm{BDT}_{ZZ^*}}$). This method provides the smallest expected uncertainties for both the mass and inclusive signal strength measurements. The one-dimensional (1D) fit to the $m_{4\ell}$ distribution that was used in the previous measurements [4,6] is used as a cross-check. A third method, using per-event resolution, is discussed after a description of the 1D and 2D models. The $m_{4\ell}$ range used in the fit for all of the methods is 110–140 GeV. A kernel density estimation method [97] uses fully simulated events to obtain smooth distributions for both the 1D and 2D signal models. These templates are produced using samples generated at 15 different m_H values in the range 115–130 GeV and parametrized as functions of m_H using B-spline interpolation [98]. These simulation samples at different masses are normalized to the expected SM $\sigma \times B$ [24] to derive the expected signal yields after acceptance and selection. The probability density function for the signal in the 2D fit is

$$\begin{aligned}\mathcal{P}(m_{4\ell}, O_{\mathrm{BDT}_{ZZ^*}}|m_H) &= \mathcal{P}(m_{4\ell}|O_{\mathrm{BDT}_{ZZ^*}}, m_H)\mathcal{P}(O_{\mathrm{BDT}_{ZZ^*}}|m_H) \\ &\simeq \left(\sum_{n=1}^{4} \mathcal{P}_n(m_{4\ell}|m_H)\theta_n(O_{\mathrm{BDT}_{ZZ^*}})\right)\mathcal{P}(O_{\mathrm{BDT}_{ZZ^*}}|m_H) \qquad (2)\end{aligned}$$

where θ_n defines four equal-sized bins for the value of the BDT_{ZZ^*} output, and $\mathcal{P}_n$ represents the 1D probability density function of the signal in the corresponding BDT_{ZZ^*} bin. The variation of the $m_{4\ell}$ shape is negligible within a single BDT_{ZZ^*} bin, so no bias is introduced in the mass measurement. The background model, $\mathcal{P}_{\mathrm{bkg}}(m_{4\ell}, O_{\mathrm{BDT}_{ZZ^*}})$, is described using a two-dimensional probability density. For the ZZ^* and reducible $\ell\ell + \mu\mu$ backgrounds, the two-dimensional probability density distributions are derived from simulation, where the $\ell\ell + \mu\mu$ simulation was shown to agree well with data in the control region. For the $\ell\ell + ee$ background model, the two-dimensional probability density can only be obtained from data, which is done using the $3\ell + X$ data control region weighted with the transfer factor to match the kinematics of the signal region. Figure 11 shows the probability density in the BDT_{ZZ^*}-$m_{4\ell}$ plane, for the signal with $m_H = 125$ GeV, the ZZ^* background from simulation and the reducible background from the data control region. The visible separation between the signal and the background using the BDT_{ZZ^*} discriminant is exploited in the fit. With respect to the 1D approach, there is an expected reduction of the statistical uncertainty for the mass and inclusive signal strength measurements, which is estimated from simulation to be approximately 8% for both measurements. Both the 1D and the 2D models are built using $m_{4\ell}$ after applying a Z-mass constraint to m_{12} during the fit, as described in Sec. V A. Figure 12 shows the $m_{4\ell}$ distribution for a simulated signal sample with $m_H = 125$ GeV, after applying the correction for final-state radiation and the Z-mass constraint for the 4μ, $4e$ and $2e2\mu/2\mu2e$ final states. The width of the reconstructed Higgs boson mass for $m_H = 125$ GeV ranges between 1.6 GeV (4μ final state) and 2.2 GeV ($4e$ final state) and is expected to be dominated by the experimental resolution since, for m_H of about 125 GeV, the natural width in the Standard Model is approximately 4 MeV.

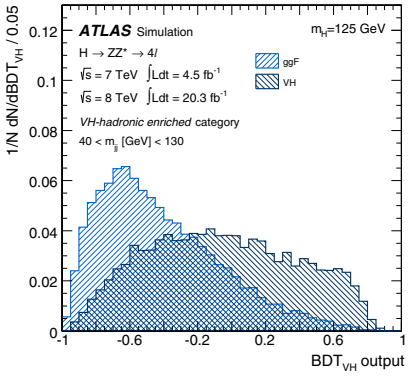

FIG. 10 (color online). Final $\mathrm{BDT}_{\mathrm{VH}}$ discriminant output for the VH-hadronic enriched category for signal (VH events, dark blue) and background (ggF events, blue) events.

In addition to the 1D and 2D fit methods described above, the signal probability density for $m_{4\ell}$ is also modeled on a per-event basis using both the BDT_{ZZ^*} information and the energy resolution of the individual leptons. This method is referred to as the per-event-resolution model and is used both as a cross-check for the mass measurement and as the baseline method to set an upper limit on the Higgs boson total width Γ_H, which is discussed elsewhere [9]. The detector-level $m_{4\ell}$ distribution for the signal is obtained for each event through the

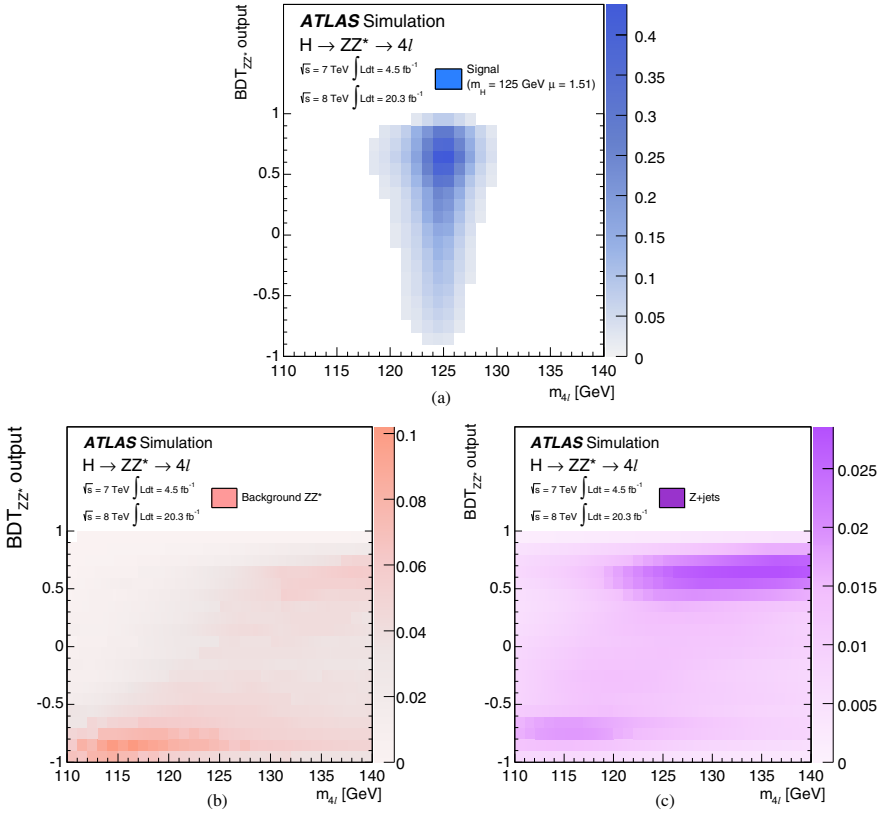

FIG. 11 (color online). Probability density for the signal and the different backgrounds normalized to the expected number of events for the 2011 and 2012 data sets, summing over all the final states: (a) $\mathcal{P}(m_{4\ell}, \mathrm{BDT}_{ZZ^*}|m_H)$ for the signal assuming $m_H = 125$ GeV, (b) probability density $\mathcal{P}(m_{4\ell}, \mathrm{BDT}_{ZZ^*})$ for the ZZ^* background and (c) $\mathcal{P}(m_{4\ell}, \mathrm{BDT}_{ZZ^*})$ for the reducible background.

convolution of an analytic description of the single-lepton detector response with a Breit-Wigner function that describes the Higgs boson mass line shape. The Z-mass constraint is not applied in this fit because this introduces a correlation between the two leptons of the leading Z which must be included in their detector response functions. The parametrization of the muon and electron response function is performed in bins of η and p_{T} of the leptons and consists of the sum of two or three normal distributions. This parametrization takes into account the tails of the single-lepton responses. A broad range of cross-checks were performed to validate all the models described above [9].

A likelihood function $\mathcal{L}$ that depends on m_H and μ is constructed using the signal and background models defined above and is defined as

$$\mathcal{L}(m_H, \mu, \boldsymbol{\theta}) = \prod_{i}^{\text{year}} \prod_{j}^{\text{final state}} \text{Poisson}(N_{ij}|\mu \cdot S_{ij}(m_H, \boldsymbol{\theta}) + B_{ij}(\boldsymbol{\theta})) \cdot \prod_{k=1}^{N_{ij}} \mathcal{F}_{ij}((m_{4\ell}, O_{\mathrm{BDT}_{ZZ^*}})_k, m_H, \mu, \boldsymbol{\theta}). \quad (3)$$

This likelihood function corresponds to the product of the Poisson probability of observing N_{ij} events in the 2011 and 2012 data sets and each of the four final states, given the expectation for the signal S_{ij} and background B_{ij}, and is multiplied with the product of the values of the probability density $\mathcal{F}_{ij}$, for $(m_{4\ell}, O_{\mathrm{BDT}_{ZZ^*}})_k$ of all events. $\mathcal{F}_{ij}$ is constructed by using both the signal and background probability density described above. The symbol $\boldsymbol{\theta}$ represents the set of nuisance parameters used to model the effect of the systematic uncertainties described in Sec. IX.

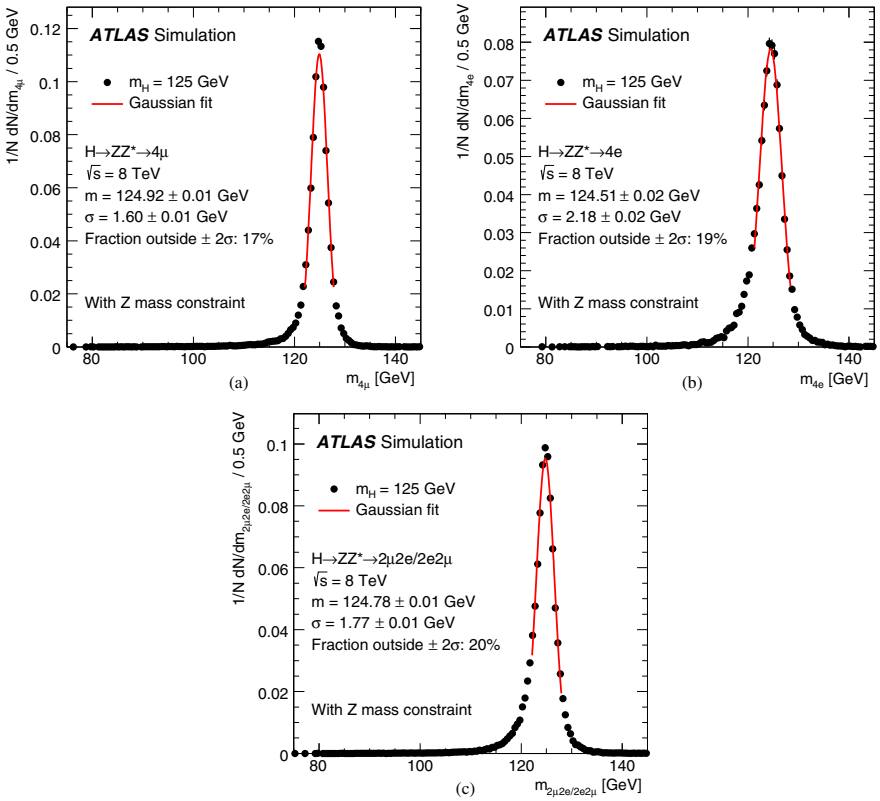

FIG. 12 (color online). Invariant mass distribution for a simulated signal sample with $m_H = 125$ GeV; superimposed is the Gaussian fit to the $m_{4\ell}$ peak after the correction for final-state radiation and the Z-mass constraint.

The statistical procedure used to interpret the data is described in Refs. [99,100]. The confidence intervals are based on the profile likelihood ratios $\Lambda(\boldsymbol{\alpha})$ that depend on one or more parameters of interest $\boldsymbol{\alpha}$ (i.e. the Higgs boson mass or the signal strength) and on the nuisance parameters $\boldsymbol{\theta}$:

$$\Lambda(\boldsymbol{\alpha}) = \frac{\mathcal{L}(\boldsymbol{\alpha}, \hat{\hat{\boldsymbol{\theta}}}(\boldsymbol{\alpha}))}{\mathcal{L}(\hat{\boldsymbol{\alpha}}, \hat{\boldsymbol{\theta}})}. \tag{4}$$

The likelihood fit to the data is then performed for the parameters of interest; $\hat{\hat{\boldsymbol{\theta}}}$ corresponds to the value of $\boldsymbol{\theta}$ which maximizes $\mathcal{L}$ for the specified $\boldsymbol{\alpha}$, and $\hat{\boldsymbol{\theta}}$ denotes the unconditional maximum likelihood estimate of the nuisance parameters, i.e. where the likelihood is maximized for both $\boldsymbol{\theta}$ and $\boldsymbol{\alpha}$. In particular, the profile likelihood ratios $\Lambda(m_H)$ and $\Lambda(\mu)$, used for the Higgs boson mass and the inclusive signal strength measurements, respectively, are

$$\Lambda(m_H) = \frac{\mathcal{L}(m_H, \hat{\hat{\mu}}(m_H), \hat{\hat{\boldsymbol{\theta}}}(m_H))}{\mathcal{L}(\hat{m}_H, \hat{\mu}, \hat{\boldsymbol{\theta}})} \quad \text{and}$$

$$\Lambda(\mu) = \frac{\mathcal{L}(\mu, \hat{\hat{\boldsymbol{\theta}}}(\mu))}{\mathcal{L}(\hat{\mu}, \hat{\boldsymbol{\theta}})}, \tag{5}$$

where the profile likelihood ratio for m_H has the signal strength treated as a parameter of interest in the fit, while that for μ is evaluated for a fixed value of m_H.

B. Signal and background modeling for the categorized analysis

The model developed for the categorized analysis allows the measurement of the signal strength for the different

production modes. Since no direct $t\bar{t}H$ and $b\bar{b}H$ production is observed, a common signal strength $\mu_{\mathrm{ggF}+t\bar{t}H+b\bar{b}H}$ is assigned to gluon fusion, $t\bar{t}H$ and $b\bar{b}H$ production. This simplification is also justified by the fact that in the SM the two production modes scale with the $q\bar{q}H$ $(q = b, t)$ coupling. Similarly, a common signal strength $\mu_{\mathrm{VBF}+\mathrm{VH}}$ is assigned to the VBF and VH production modes since in the SM they scale with the WH/ZH gauge couplings.

For the categorized analysis, all of the candidates are grouped into four separate categories to have better sensitivity to the different production mechanisms, as described in Sec. V. In the VBF enriched category, where the $\mathrm{BDT}_{\mathrm{VBF}}$ discriminant is introduced to separate the ggF-like events from VBF-like events, the two-dimensional probability density $\mathcal{P}(m_{4\ell}, \mathrm{BDT}_{\mathrm{VBF}})$ is constructed by factorizing the $\mathrm{BDT}_{\mathrm{VBF}}$ and $m_{4\ell}$ distributions. This factorization is justified by the negligible dependence of the $\mathrm{BDT}_{\mathrm{VBF}}$ on $m_{4\ell}$ for both signal and background. The $\mathrm{BDT}_{\mathrm{VBF}}$ dependence on the Higgs boson mass is negligible and is neglected in the probability density. Adding the $\mathrm{BDT}_{\mathrm{VBF}}$ in the VBF enriched category reduces the expected uncertainty on the signal strength of the VBF and VH production mechanisms $\mu_{\mathrm{VBF}+\mathrm{VH}}$ by about 25%. The improvement in the expected uncertainty on $\mu_{\mathrm{VBF}+\mathrm{VBF}+\mathrm{VH}}$ reaches approximately 35% after adding the leptonic and hadronic VH categories to the model. In these two VH categories, a simple one-dimensional fit to the $m_{4\ell}$ observable is performed, since for the VH-hadronic enriched category, a selection on the $\mathrm{BDT}_{\mathrm{VH}}$ output is included in the event selection, while for the VH-leptonic enriched category, no BDT is used. Finally, in the ggF enriched category, the 2D model defined in Eq. (2), including the BDT_{ZZ^*} trained as specified in Sec. VII A, is used. These procedures allow a further reduction of the expected uncertainty on $\mu_{\mathrm{VBF}+\mathrm{VH}}$ ($\mu_{\mathrm{ggF}+t\bar{t}H+b\bar{b}H}$) by 6% (8%).

IX. SYSTEMATIC UNCERTAINTIES

The uncertainties on the lepton reconstruction and identification efficiency, and on the lepton energy or momentum resolution and scale, are determined using samples of W, Z and J/ψ decays. The description of these systematic uncertainties, as well as of the uncertainties associated with the event categorizations, is separated into three parts. A brief overview of the systematic uncertainties that affect the mass measurement is given in Sec. IX A. The description of the systematic uncertainties related to the measurement of the signal rate and event categorizations is provided in Secs. IX B and IX C, respectively.

A. Systematic uncertainties in the mass measurement

For the $H \to ZZ^* \to 4\ell$ decay modes involving electrons, the electron energy scale uncertainty, determined from $Z \to ee$ and $J/\psi \to ee$ decays, is propagated as a function of the pseudorapidity and the transverse energy of the electrons. The precision of the energy scale is better than 0.1% for $|\eta| < 1.2$ and $1.8 < |\eta| < 2.47$, and a few per mille for $1.2 < |\eta| < 1.8$ [76]. The uncertainties on the measured Higgs boson mass due to the electron energy scale uncertainties are $\pm 0.04\%$, $\pm 0.025\%$ and $\pm 0.04\%$ for the $4e$, $2e2\mu$ and $2\mu 2e$ final states, respectively.

Similarly, for the $H \to ZZ^* \to 4\ell$ decay modes involving muons, the various components of the systematic uncertainty on the muon momentum scale are determined using large samples of $J/\psi \to \mu\mu$ and $Z \to \mu\mu$ decays and validated using $\Upsilon \to \mu\mu$, $J/\psi \to \mu\mu$ and $Z \to \mu\mu$ decays. In the muon transverse momentum range of 6–100 GeV, the systematic uncertainties on the scales are about $\pm 0.04\%$ in the barrel region and reach $\pm 0.2\%$ in the region $|\eta| > 2$ [81]. The uncertainties on the measured Higgs boson mass due to the muon energy scale uncertainties are estimated to be $\pm 0.04\%$, $\pm 0.015\%$ and $\pm 0.02\%$ for the 4μ, $2e2\mu$ and $2\mu 2e$ final states, respectively.

Uncertainties on the measured Higgs boson mass related to the background contamination and final-state QED radiation modeling are negligible compared to the other sources described above.

The weighted contributions to the uncertainty in the mass measurement, when all the final states are combined, are $\pm 0.01\%$ for the electron energy scale uncertainty and $\pm 0.03\%$ for the muon momentum scale uncertainty. The larger impact of the muon momentum scale uncertainty is due to the fact that the muon final states have a greater weight in the combined mass fit.

B. Systematic uncertainties in the inclusive signal strength measurement

The efficiencies to trigger, reconstruct and identify electrons and muons are studied using $Z \to \ell\ell$ and $J/\psi \to \ell\ell$ decays [78–81]. The expected impact from simulation of the associated systematic uncertainties on the signal yield is presented in Table IX. The impact is presented for the individual final states and for all channels combined.

The level of agreement between data and simulation for the efficiency of the isolation and impact parameter requirements of the analysis is studied using a tag-and-probe method. As a result, a small additional uncertainty on the isolation and impact parameter selection efficiency is applied for electrons with E_{T} below 15 GeV. The effect of the isolation and impact parameter uncertainties on the signal strength is given in Table IX. The corresponding uncertainty for muons is found to be negligible.

The uncertainties on the data-driven estimates of the background yields are discussed in Sec. VI and are summarized in Tables V and VII, and their impact on the signal strength is given in Table IX.

The overall uncertainty on the integrated luminosity for the complete 2011 data set is $\pm 1.8\%$ [101]. The uncertainty on the integrated luminosity for the 2012 data set is $\pm 2.8\%$; this uncertainty is derived following the methodology used

TABLE IX. The expected impact of the systematic uncertainties on the signal yield, derived from simulation, for $m_H = 125$ GeV, are summarized for each of the four final states for the combined 4.5 fb^{-1} at $\sqrt{s} = 7$ TeV and 20.3 fb^{-1} at $\sqrt{s} = 8$ TeV. The symbol "–" signifies that the systematic uncertainty does not contribute to a particular final state. The last three systematic uncertainties apply equally to all final states. All uncertainties have been symmetrized.

Source of uncertainty	4μ	$2e2\mu$	$2\mu2e$	$4e$	combined
Electron reconstruction and identification efficiencies	–	1.7%	3.3%	4.4%	1.6%
Electron isolation and impact parameter selection	–	0.07%	1.1%	1.2%	0.5%
Electron trigger efficiency	–	0.21%	0.05%	0.21%	< 0.2%
$\ell\ell + ee$ backgrounds	–	–	3.4%	3.4%	1.3%
Muon reconstruction and identification efficiencies	1.9%	1.1%	0.8%	–	1.5%
Muon trigger efficiency	0.6%	0.03%	0.6%	–	0.2%
$\ell\ell + \mu\mu$ backgrounds	1.6%	1.6%	–	–	1.2%
QCD scale uncertainty					6.5%
PDF, α_s uncertainty					6.0%
$H \to ZZ^*$ branching ratio uncertainty					4.0%

for the 2011 data set, from a preliminary calibration of the luminosity scale with beam-separation scans performed in November 2012.

The theory-related systematic uncertainty for both the signal and the ZZ^* background is discussed in Sec. III. The three most important theoretical uncertainties, which dominate the signal strength uncertainty, are given in Table IX. Uncertainties on the predicted Higgs boson p_T spectrum due to those on the PDFs and higher-order corrections are estimated to affect the signal strength by less than $\pm 1\%$. The systematic uncertainty of the ZZ^* background rate is around $\pm 4\%$ for $m_{4\ell} = 125$ GeV and increases for higher mass, averaging to around $\pm 6\%$ for the ZZ^* production above 110 GeV.

C. Systematic uncertainties in the event categorization

The systematic uncertainties on the expected yields (as in Table II) from different processes contributing to the VBF enriched, VH-hadronic enriched, VH-leptonic enriched and ggF enriched categories are reported in Table X, expressed as the fractional uncertainties on the yields. The uncertainties on the theoretical predictions for

TABLE X. Systematic uncertainties on the yields expected from various processes contributing to the VBF enriched, VH-leptonic enriched, VH-hadronic enriched and ggF enriched categories expressed as percentages of the yield. The various uncertainties are added in quadrature. Uncertainties that are negligible are denoted by a "–". All uncertainties have been symmetrized.

Process	$gg \to H, q\bar{q}/gg \to b\bar{b}H/t\bar{t}H$	$qq' \to Hqq'$	$q\bar{q} \to W/ZH$	ZZ^*
VBF enriched category				
Theoretical cross section	20.4%	4%	4%	8%
Underlying event	6.6%	1.4%	–	–
Jet energy scale	9.6%	4.8%	7.8%	9.6%
Jet energy resolution	0.9%	0.2%	1.0%	1.4%
Total	23.5%	6.4%	8.8%	12.6%
VH-hadronic enriched category				
Theoretical cross section	20.4%	4%	4%	2%
Underlying event	7.5%	3.1%	–	–
Jet energy scale	9.4%	9.3%	3.7%	12.6%
Jet energy resolution	1.0%	1.7%	0.6%	1.8%
Total	23.7%	10.7%	5.5%	12.9%
VH-leptonic enriched category				
Theoretical cross section	12%	4%	4%	5%
Leptonic VH-specific cuts	1%	1%	5%	–
Jet energy scale	8.8%	9.9%	1.7%	3.2%
Total	14.9%	10.7%	6.6%	5.9%
ggF enriched category				
Theoretical cross section	12%	4%	4%	4%
Jet energy scale	2.2%	6.6%	4.0%	1.0%
Total	12.2%	7.7%	5.7%	4.1%

TABLE XI. The number of events expected and observed for a $m_H = 125$ GeV hypothesis for the four-lepton final states in a window of $120 < m_{4\ell} < 130$ GeV. The second column shows the number of expected signal events for the full mass range, without a selection on $m_{4\ell}$. The other columns show for the 120–130 GeV mass range the number of expected signal events, the number of expected ZZ^* and reducible background events, and the signal-to-background ratio (S/B), together with the number of observed events, for 4.5 fb^{-1} at $\sqrt{s} = 7$ TeV and 20.3 fb^{-1} at $\sqrt{s} = 8$ TeV as well as for the combined sample.

Final state	Signal full mass range	Signal	ZZ^*	$Z+$jets, $t\bar{t}$	S/B	Expected	Observed
			$\sqrt{s} = 7$ TeV				
4μ	1.00 ± 0.10	0.91 ± 0.09	0.46 ± 0.02	0.10 ± 0.04	1.7	1.47 ± 0.10	2
$2e2\mu$	0.66 ± 0.06	0.58 ± 0.06	0.32 ± 0.02	0.09 ± 0.03	1.5	0.99 ± 0.07	2
$2\mu 2e$	0.50 ± 0.05	0.44 ± 0.04	0.21 ± 0.01	0.36 ± 0.08	0.8	1.01 ± 0.09	1
$4e$	0.46 ± 0.05	0.39 ± 0.04	0.19 ± 0.01	0.40 ± 0.09	0.7	0.98 ± 0.10	1
Total	2.62 ± 0.26	2.32 ± 0.23	1.17 ± 0.06	0.96 ± 0.18	1.1	4.45 ± 0.30	6
			$\sqrt{s} = 8$ TeV				
4μ	5.80 ± 0.57	5.28 ± 0.52	2.36 ± 0.12	0.69 ± 0.13	1.7	8.33 ± 0.6	12
$2e2\mu$	3.92 ± 0.39	3.45 ± 0.34	1.67 ± 0.08	0.60 ± 0.10	1.5	5.72 ± 0.37	7
$2\mu 2e$	3.06 ± 0.31	2.71 ± 0.28	1.17 ± 0.07	0.36 ± 0.08	1.8	4.23 ± 0.30	5
$4e$	2.79 ± 0.29	2.38 ± 0.25	1.03 ± 0.07	0.35 ± 0.07	1.7	3.77 ± 0.27	7
Total	15.6 ± 1.6	13.8 ± 1.4	6.24 ± 0.34	2.00 ± 0.28	1.7	22.1 ± 1.5	31
			$\sqrt{s} = 7$ TeV and $\sqrt{s} = 8$ TeV				
4μ	6.80 ± 0.67	6.20 ± 0.61	2.82 ± 0.14	0.79 ± 0.13	1.7	9.81 ± 0.64	14
$2e2\mu$	4.58 ± 0.45	4.04 ± 0.40	1.99 ± 0.10	0.69 ± 0.11	1.5	6.72 ± 0.42	9
$2\mu 2e$	3.56 ± 0.36	3.15 ± 0.32	1.38 ± 0.08	0.72 ± 0.12	1.5	5.24 ± 0.35	6
$4e$	3.25 ± 0.34	2.77 ± 0.29	1.22 ± 0.08	0.76 ± 0.11	1.4	4.75 ± 0.32	8
Total	18.2 ± 1.8	16.2 ± 1.6	7.41 ± 0.40	2.95 ± 0.33	1.6	26.5 ± 1.7	37

the cross sections for the different processes arise mainly from the requirement on the jet multiplicity used in the event categorization [102,103]. Because of event migrations, this also affects the VH-leptonic enriched and ggF enriched categories, where no explicit requirement on jets is applied. The uncertainty accounting for a potential mismodeling of the underlying event is conservatively estimated with $Z \to \mu\mu$ simulated events by applying the

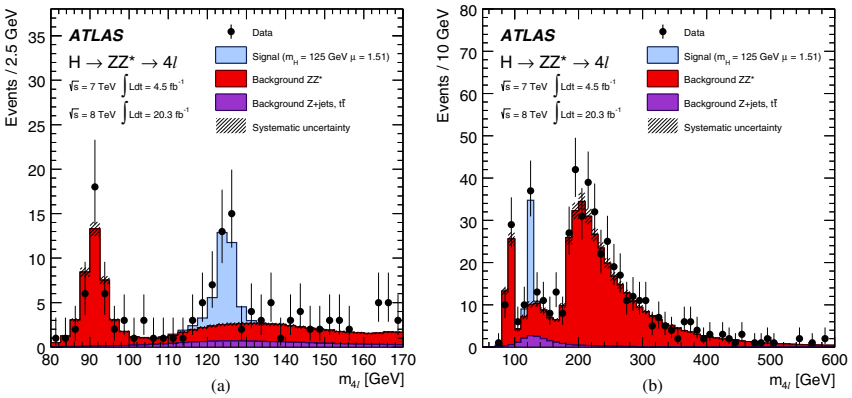

FIG. 13 (color online). The distribution of the four-lepton invariant mass, $m_{4\ell}$, for the selected candidates (filled circles) compared to the expected signal and background contributions (filled histograms) for the combined $\sqrt{s} = 7$ TeV and $\sqrt{s} = 8$ TeV data for the mass ranges: (a) 80–170 GeV, and (b) 80–600 GeV. The signal expectation shown is for a mass hypothesis of $m_H = 125$ GeV and normalized to $\mu = 1.51$ (see text). The expected backgrounds are shown separately for the ZZ^* (red histogram), and the reducible $Z+$ jets and $t\bar{t}$ backgrounds (violet histogram); the systematic uncertainty associated to the total background contribution is represented by the hatched areas.

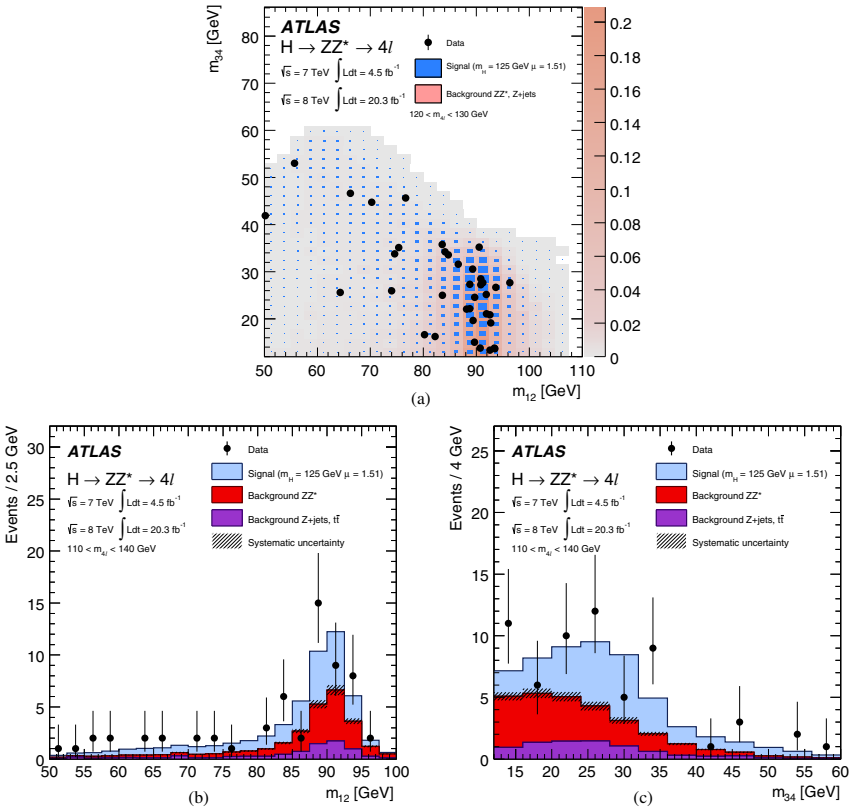

FIG. 14 (color online). Distributions of data (filled circles) and the expected signal and backgrounds events in (a) the m_{34}-m_{12} plane with the requirement of $m_{4\ell}$ in 120–130 GeV. The projected distributions for (b) m_{12} and (c) m_{34} are shown for $m_{4\ell}$ in 110–140 GeV, the fit range. The signal contribution is shown for $m_H = 125$ GeV and normalized to $\mu = 1.51$ (see text) as blue histograms in (b) and (c). The expected background contributions, ZZ^* (red histogram) and $Z+$ jets plus $t\bar{t}$ (violet histogram), are shown in (b) and (c); the systematic uncertainty associated to the total background contribution is represented by the hatched areas. The expected distributions of the Higgs signal (blue) and total background (red) are superimposed in (a), where the box size (signal) and color shading (background) represent the relative density. In every case, the combination of the 7 and 8 TeV results is shown.

selection for the VBF enriched (or VH-hadronic enriched) category and taking the difference of the efficiencies with and without multiparton interactions.

The main experimental uncertainty is related to the jet energy scale determination, including the uncertainties associated with the modeling of the absolute and relative *in situ* jet calibrations, as well as the flavor composition of the jet sample. The impact on the yields of the various categories is anticorrelated because a variation of the jet energy scale results primarily in the migration of events among the categories. The impact of the jet energy scale uncertainty results in an uncertainty of about $\pm 10\%$ for the VBF enriched category, $\pm 8\%$ for the VH-hadronic enriched category, $\pm 1.5\%$ for the VH-leptonic enriched category and $\pm 1.5\%$ for the ggF enriched category.

The uncertainty on the jet energy resolution is also taken into account, even though its impact is small compared to that of the jet energy scale uncertainty, as reported in Table X. Finally, the uncertainties associated with the additional leptons in the VH-leptonic enriched category are the same as already described in Sec. IX B for the four leptons of the Higgs boson decay.

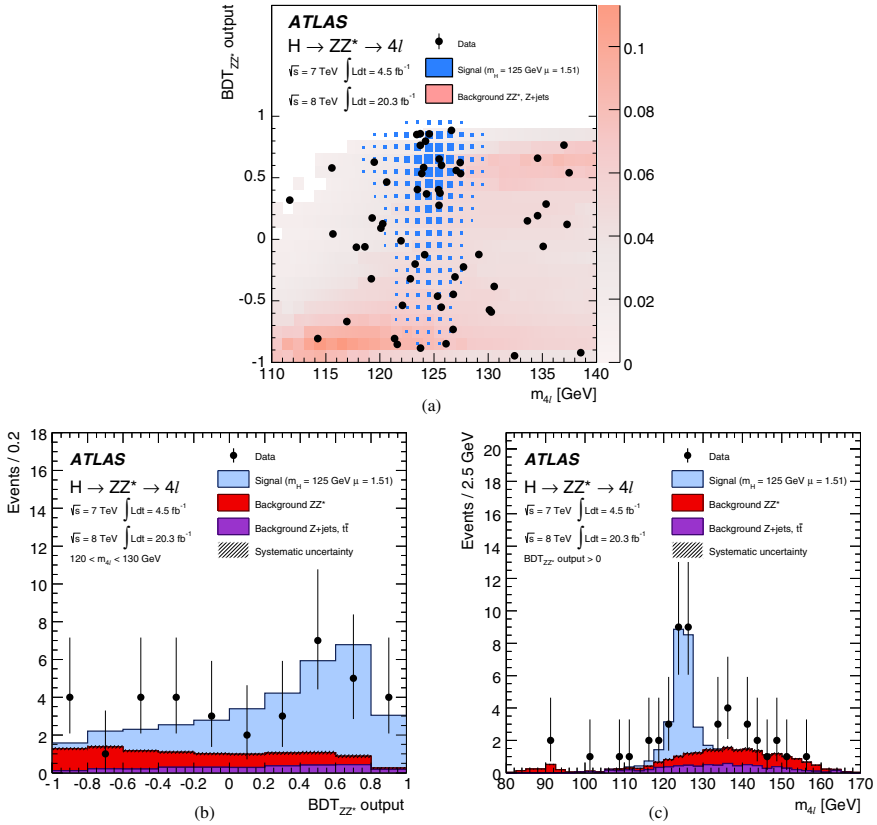

FIG. 15 (color online). Distributions of data (filled circles) and the expected signal and background events in (a) the BDT_{ZZ^*}-$m_{4\ell}$ plane, (b) BDT_{ZZ^*} with the restriction $120 < m_{4\ell} < 130$ GeV, and (c) $m_{4\ell}$ with the additional requirement that the BDT_{ZZ^*} be positive. The expected Higgs signal contribution is shown for $m_H = 125$ GeV and normalized to $\mu = 1.51$ (see text) as blue histograms in (b) and (c). The expected background contributions, ZZ^* (red histogram) and $Z +$ jets plus $t\bar{t}$ (violet histogram), are shown in (b) and (c); the systematic uncertainty associated to the total background contribution is represented by the hatched areas. The expected distributions of the Higgs signal (blue) and total background (red) are superimposed in (a), where the box size (signal) and color shading (background) represent the relative density. In every case, the combination of the 7 and 8 TeV results is shown.

X. Results

A. Results of the inclusive analysis

As described in Sec. V A, the inclusive selection is used to measure the Higgs boson mass. In addition, the inclusive signal strength measurement, described below, allows a direct comparison with the predicted total production cross section times branching ratio of the Standard Model Higgs boson at the measured mass. This inclusive analysis is the same as that used for the combined mass measurement [9]; in the following more details and new comparisons of the data and expectations are provided in view of the inclusive mass and signal strength measurements.

1. Signal and background yields

The number of observed candidate events for each of the four decay channels in a mass window of 120–130 GeV and the signal and background expectations are presented in Table XI. The signal and ZZ^* background expectations are normalized to the SM expectation while the reducible background is normalized to the data-driven estimate described in Sec. VI. Three events in the mass range

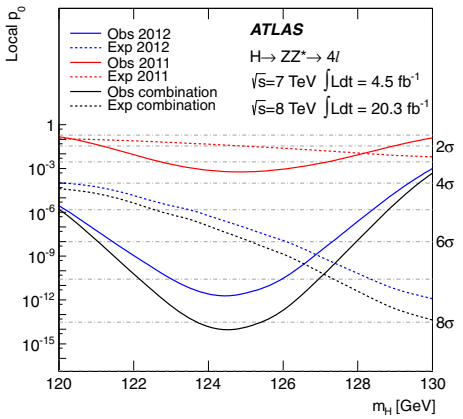

FIG. 16 (color online). The observed local p_0-value for the combination of the 2011 and 2012 data sets (solid black line) as a function of m_H; the individual results for $\sqrt{s} = 7$ TeV and 8 TeV are shown separately as red and blue solid lines, respectively. The dashed curves show the expected median of the local p_0-value for the signal hypothesis with signal strength $\mu = 1$, when evaluated at the corresponding m_H. The horizontal dot-dashed lines indicate the p_0-values corresponding to local significances of 1–8σ.

$120 < m_{4\ell} < 130$ GeV are corrected for FSR: one 4μ event and one $2\mu 2e$ are corrected for noncollinear FSR, and one $2\mu 2e$ event is corrected for collinear FSR. In the full mass spectrum, there are 8 (2) events corrected for collinear (noncollinear) FSR, in good agreement with the expected number of 11 events.

The expected $m_{4\ell}$ distribution for the backgrounds and the signal hypothesis are compared with the combined $\sqrt{s} = 7$ TeV and $\sqrt{s} = 8$ TeV data in Fig. 13 for the $m_{4\ell}$ range 80–170 GeV, and in Fig. 13(b) for the invariant mass range 80–600 GeV. In Fig. 13 one observes the single $Z \to 4\ell$ resonance [104,105], the threshold of the ZZ production above 180 GeV and a narrow peak around 125 GeV. Figure 14 shows the distribution of the m_{12} versus m_{34} invariant masses, as well as their projections, for the candidates with $m_{4\ell}$ within 120–130 GeV. The Z-mass constrained kinematic fit is not applied for these distributions. The Higgs signal is shown for $m_H = 125$ GeV with a value of $\mu = 1.51$, corresponding to the combined μ measurement for the $H \to ZZ^* \to 4\ell$ final state, discussed below in Sec. X B, scaled to this mass by the expected variation in the SM Higgs boson cross section times branching ratio.

The distribution of the BDT_{ZZ^*} output versus $m_{4\ell}$ is shown in Fig. 15(a) for the reconstructed candidates with $m_{4\ell}$ within the fitted mass range 110–140 GeV. An excess of events with high-BDT_{ZZ^*} output is present for values of $m_{4\ell}$ close to 125 GeV, compatible with the Higgs signal hypothesis at that mass. The compatibility of the data with the expectations shown in Fig. 15(a) is checked using pseudoexperiments generated according to the expected two-dimensional distribution and good agreement is found. Figure 15(b) shows the distribution of the BDT_{ZZ^*} output for the candidates in the $m_{4\ell}$ range 120–130 GeV compared with signal and background expectations. In Fig. 15(c) the distribution of the invariant mass of the four leptons is presented for candidates satisfying the requirement that the value of the BDT_{ZZ^*} output be greater than zero, which maximizes the expected significance for a SM Higgs boson with a mass of about 125 GeV.

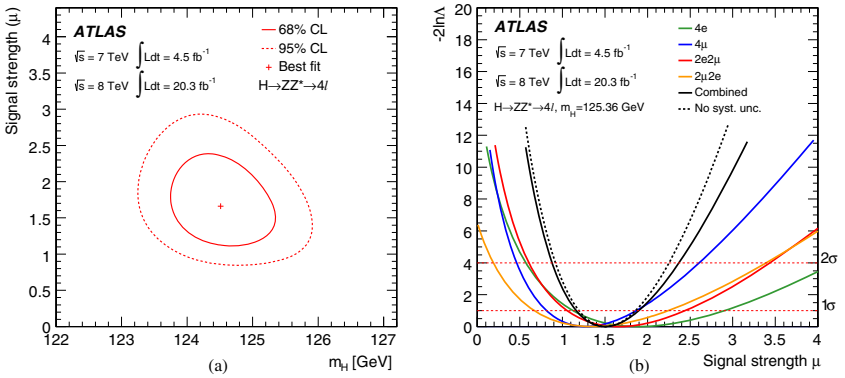

FIG. 17 (color online). (a) The 68% and 95% confidence level (CL) contours in the μ-m_H plane for the inclusive analysis. (b) The profile likelihood as a function of the inclusive signal strength μ for the individual channels ($4e$, green line; 4μ, blue line; $2e2\mu$, red line; $2\mu 2e$, yellow line) as well as for their combination (black lines); the scan for the combination of all channels is shown both with (solid line) and without (dashed line) systematic uncertainties. The value of m_H is fixed to 125.36 GeV while all the other nuisance parameters are profiled in the fit. In every case, the combination of the 7 and 8 TeV results is shown.

The local p_0-value of the observed signal, representing the significance of the excess relative to the background-only hypothesis, is obtained with the asymptotic approximation [100] using the 2D fit without any selection on BDT_{ZZ^*} and is shown as a function of m_H in Fig. 16. The local p_0-value at the measured mass for this channel, 124.51 GeV (see below), is 8.2 standard deviations. At the value of the Higgs boson mass, $m_H = 125.36$ GeV, obtained from the combination of the $H \to ZZ^* \to 4\ell$ and $H \to \gamma\gamma$ mass measurements [9], the local p_0-value decreases to 8.1 standard deviations. The expected significance at these two masses is 5.8 and 6.2 standard deviations, respectively.

2. Mass and inclusive signal strength

The models described in Sec. VIII A are used to perform the inclusive mass and signal strength measurements. The measured Higgs boson mass obtained with the baseline 2D method is $m_H = 124.51 \pm 0.52$ GeV. The signal strength at this value for m_H is $\mu = 1.66^{+0.39}_{-0.34}\,(\mathrm{stat})\,^{+0.21}_{-0.14}\,(\mathrm{syst})$. The other methods of Sec. VIII A, 1D and per-event resolution, yield similar results for the Higgs boson mass [9]. Figure 17 shows the best fit values of μ and m_H as well as the profile likelihood ratio contours in the (m_H,μ) plane corresponding to the 68% and 95% confidence level intervals. Finally, the best fit value for m_H obtained using the model developed for the categorized analysis, described in Sec. VIII B, is within 90 MeV of the value found with the inclusive 2D method.

At the combined ATLAS measured value of the Higgs boson mass, $m_H = 125.36$ GeV, the signal strength is found to be $\mu = 1.50^{+0.35}_{-0.31}\,(\mathrm{stat})\,^{+0.19}_{-0.13}\,(\mathrm{syst})$. The scan of the profile likelihood, $-2\ln\Lambda(\mu)$, as a function of the inclusive signal strength μ for each one of the four channels separately, as well as for their combination, is shown in Fig. 17(b).

B. Coupling studies

The numbers of expected and observed events in each of the categories described in Sec. V B are summarized in Table XII. The expected yield in each enriched category is given for each of the production modes, where the ggF, $b\bar{b}H$ and $t\bar{t}H$ yields are combined. The expected and observed numbers of events are given for two $m_{4\ell}$ mass ranges: 120–130 GeV and above 110 GeV. Three of the VBF candidates are found in the mass region 120–130 GeV with invariant masses of 123.2, 123.4 and 125.7 GeV. Only one VBF candidate has a $\mathrm{BDT}_{\mathrm{VBF}}$ output above zero: $m_{4\ell} = 123.4$ GeV and a $\mathrm{BDT}_{\mathrm{VBF}}$ output value of 0.7. In this mass window, the expected number of VBF candidates with $\mathrm{BDT}_{\mathrm{VBF}}$ output above zero is 1.26 ± 0.15, where half of this is expected to be from a true VBF signal, about 35% from ggF production and the rest is mostly from ZZ^* and reducible backgrounds. The distributions of $m_{4\ell}$ and the $\mathrm{BDT}_{\mathrm{VBF}}$ output for the VBF enriched category in the full mass range and in the fit range of 110–140 GeV are shown in Fig. 18. The signal purity, defined as $S/(S+B)$, as a function of the $\mathrm{BDT}_{\mathrm{VBF}}$ output is shown in Fig. 19 for Higgs events relative to the backgrounds and for VBF events relative to the other Higgs boson production mechanisms for $110 < m_{4\ell} < 140$ GeV. There is no VH candidate in the 120–130 GeV mass range for either the hadronic or leptonic categories. For the full mass range above 110 GeV all categories are dominated by ZZ^* background, and the observed number of events agrees well with the expectation as can be seen in Table XII.

In the following, measurements of the production strengths and couplings are discussed. They are all

TABLE XII. Expected and observed yields in the VBF enriched, VH-hadronic enriched, VH-leptonic enriched and ggF enriched categories. The yields are given for the different production modes and the ZZ^* and reducible background for 4.6 fb^{-1} at $\sqrt{s} = 7$ TeV and 20.3 fb^{-1} at $\sqrt{s} = 8$ TeV. The estimates are given for both the $m_{4\ell}$ mass range 120–130 GeV and the mass range above 110 GeV.

	Signal				Background			
Enriched category	$ggF + b\bar{b}H + t\bar{t}H$	VBF	VH-hadronic	VH-leptonic	ZZ^*	Z + jets, $t\bar{t}$	Total expected	Observed
				$120 < m_{4\ell} < 130$ GeV				
VBF	1.18 ± 0.37	0.75 ± 0.04	0.083 ± 0.006	0.013 ± 0.001	0.17 ± 0.03	0.25 ± 0.14	2.4 ± 0.4	3
($\mathrm{BDT}_{\mathrm{VBF}} > 0$)	0.48 ± 0.15	0.62 ± 0.04	0.023 ± 0.002	0.004 ± 0.001	0.06 ± 0.01	0.10 ± 0.05	1.26 ± 0.15	1
VH-hadronic	0.40 ± 0.12	0.034 ± 0.004	0.20 ± 0.01	0.009 ± 0.001	0.09 ± 0.01	0.09 ± 0.04	0.80 ± 0.12	0
VH-leptonic	0.013 ± 0.002	< 0.001	< 0.001	0.069 ± 0.004	0.015 ± 0.002	0.016 ± 0.019	0.11 ± 0.02	0
ggF	12.8 ± 1.3	0.57 ± 0.02	0.24 ± 0.01	0.11 ± 0.01	7.1 ± 0.2	2.7 ± 0.4	23.5 ± 1.4	34
				$m_{4\ell} > 110$ GeV				
VBF	1.4 ± 0.4	0.82 ± 0.05	0.092 ± 0.007	0.022 ± 0.002	20 ± 4	1.6 ± 0.9	$24. \pm 4.$	32
($\mathrm{BDT}_{\mathrm{VBF}} > 0$)	0.54 ± 0.17	0.68 ± 0.04	0.025 ± 0.002	0.007 ± 0.001	8.2 ± 1.6	0.6 ± 0.3	10.0 ± 1.6	12
VH-hadronic	0.46 ± 0.14	0.038 ± 0.004	0.23 ± 0.01	0.015 ± 0.001	9.0 ± 1.2	0.6 ± 0.2	10.3 ± 1.2	13
VH-leptonic	0.026 ± 0.004	< 0.002	< 0.002	0.15 ± 0.01	0.63 ± 0.04	0.11 ± 0.14	0.92 ± 0.16	1
ggF	14.1 ± 1.5	0.63 ± 0.02	0.27 ± 0.01	0.17 ± 0.01	$351. \pm 20$	16.6 ± 2.2	$383. \pm 20$	420

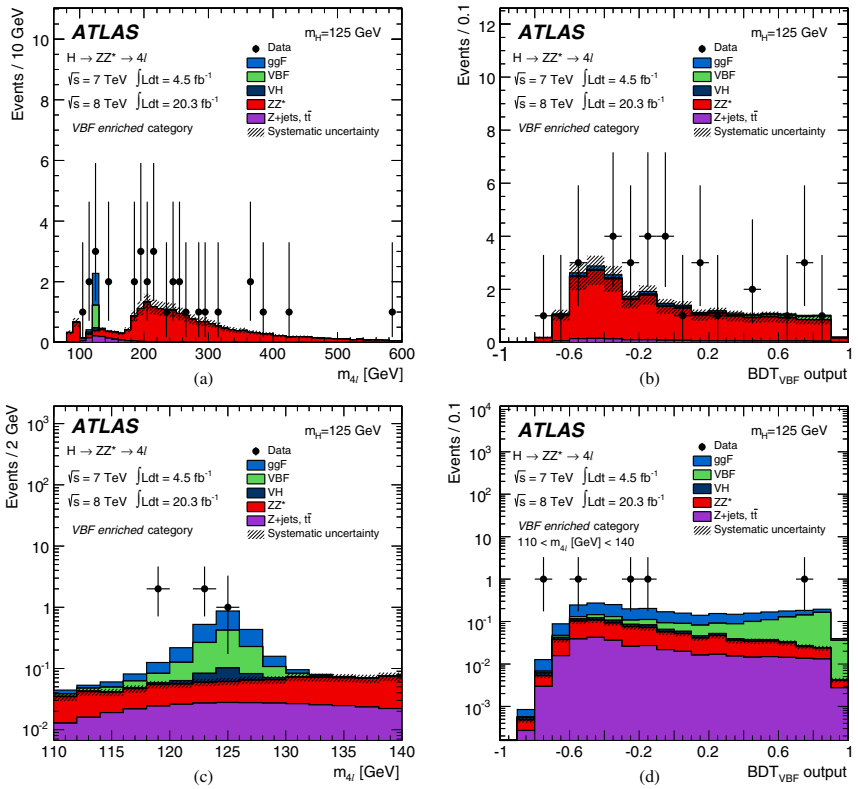

FIG. 18 (color online). Distributions of the selected events and expected signal and background yields for the VBF enriched category for (a) $m_{4\ell}$ and (b) the $\mathrm{BDT}_{\mathrm{VBF}}$ output in the full mass range, and for (c) $m_{4\ell}$ and (d) the $\mathrm{BDT}_{\mathrm{VBF}}$ output in the fit mass range $110 < m_{4\ell} < 140$ GeV. The expected Higgs signal contributions, assuming $m_H = 125$ GeV, from the ggF (blue histogram), VBF (green histogram) and VH (dark-blue histogram) production modes are included. The expected background contributions, ZZ^* (red histogram) and $Z+$ jets plus $t\bar{t}$ (violet histogram), are also shown; the systematic uncertainty associated to the total background contribution is represented by the hatched areas. In every case, the combination of the 7 and 8 TeV results is shown.

evaluated assuming the ATLAS combined mass $m_H = 125.36$ GeV. The measurement of a global signal strength factor, discussed in Sec. X A, can be extended to a measurement of the signal strength factors for specific production modes.

The production mechanisms are grouped into the "fermionic" and the "bosonic" ones. The former consists of ggF, $b\bar{b}H$ and $t\bar{t}H$, while the latter includes the VBF and VH modes. In Fig. 20 the best fit value for $\mu_{\mathrm{ggF}+b\bar{b}H+t\bar{t}H} \times B/B_{\mathrm{SM}}$ versus $\mu_{\mathrm{VBF+VH}} \times B/B_{\mathrm{SM}}$ is presented. The factor B/B_{SM}, the scale factor of the branching ratio with respect to the SM value, is included since with a single channel analysis the source of potential deviations from the SM expectation cannot be resolved between production and decay. The profile likelihood ratio contours that correspond to the 68% and 95% confidence levels are also shown. The measured values for $\mu_{\mathrm{ggF}+b\bar{b}H+t\bar{t}H} \times B/B_{\mathrm{SM}}$ and $\mu_{\mathrm{VBF+VH}} \times B/B_{\mathrm{SM}}$ are respectively

$$\mu_{\mathrm{ggF}+b\bar{b}H+t\bar{t}H} \times B/B_{\mathrm{SM}} = 1.66\,^{+0.45}_{-0.41}(\mathrm{stat})\,^{+0.25}_{-0.15}(\mathrm{syst})$$
$$\mu_{\mathrm{VBF+VH}} \times B/B_{\mathrm{SM}} = 0.26\,^{+1.60}_{-0.91}(\mathrm{stat})\,^{+0.36}_{-0.23}(\mathrm{syst}). \quad (6)$$

The rounded results, with statistical and systematic uncertainties combined, are $\mu_{\mathrm{ggF}+b\bar{b}H+t\bar{t}H} \times B/B_{\mathrm{SM}} = 1.7\,^{+0.5}_{-0.4}$ and $\mu_{\mathrm{VBF+VH}} \times B/B_{\mathrm{SM}} = 0.3\,^{+1.6}_{-0.9}$.

The fit to the categories can be constrained to extract a single overall signal strength for the $H \to ZZ^* \to 4\ell$ final state.

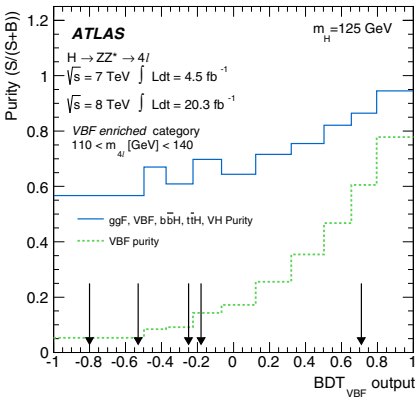

FIG. 19 (color online). Signal purity, defined as $S/(S+B)$, as a function of the $\mathrm{BDT_{VBF}}$ output. The solid blue line shows the purity for all Higgs signal production mechanisms relative to the ZZ^* and reducible backgrounds. The dashed green line shows the purity for VBF events relative to the other Higgs boson production mechanisms, for the fit region $110 < m_{4\ell} < 140$ GeV. The binning is chosen so that each bin contains 10% of the total expected signal events. The five VBF candidates observed in data in the signal region are indicated with the black arrows.

This combined $\mu \times B/B_{\mathrm{SM}}$ is $1.44^{+0.34}_{-0.31}\,(\mathrm{stat})^{+0.21}_{-0.11}\,(\mathrm{syst})$. The ambiguity between production and decay is removed in Fig. 20(b), where the ratio $\mu_{\mathrm{VBF+VH}}/\mu_{\mathrm{ggF}+b\bar{b}H+t\bar{t}H}$ is presented. The measured value of this ratio is $0.2^{+1.2}_{-0.5}$.

Following the approach and benchmarks recommended by the LHC Higgs Cross Section Working Group [103], measurements of couplings are implemented using a leading-order tree-level-motivated framework. This framework is based on the following assumptions: (a) the central value of the ATLAS combined mass measurement of $m_H = 125.36$ GeV is assumed; (b) the width of the Higgs boson is narrow, justifying the use of the zero-width approximation; and (c) only modifications of coupling strengths are considered, while the SM tensor structure is assumed, implying that the observed state is a CP-even scalar. The zero-width approximation allows the signal cross section to be decomposed in the following way: $\sigma \cdot B(i \to H \to f) = \sigma_i \cdot \Gamma_f/\Gamma_H$ where σ_i is the production cross section through the initial state i; B and Γ_f are the branching ratio and partial decay width into the final state f, respectively; and Γ_H the total width of the Higgs boson. This approach introduces scale factors applied to the Higgs boson coupling, κ_j, for particle j, which correspond to deviations from the SM Higgs coupling. For example, ggF production of the ZZ^* final state can be represented as $\sigma \cdot B(gg \to H \to ZZ^*) = \sigma_{\mathrm{SM}}(gg \to H) \cdot B_{\mathrm{SM}}(H \to ZZ^*) \cdot (\kappa_g^2 \cdot \kappa_Z^2)/\kappa_H^2$, where κ_g, κ_Z, and κ_H are the scale factors for the Higgs couplings to g and Z, and a scale factor for the total Higgs width, respectively. Results are extracted from fits to the data using the profile likelihood ratio $\Lambda(\vec{\kappa})$. In the fit, the κ_j are treated either as parameters of interest or as nuisance parameters, depending on the measurement.

One benchmark model, which simplifies the measurement of possible deviations, groups the κ_j for the electroweak vector bosons into a single scale factor, κ_{V}, and defines another coupling scale factor for all fermions, κ_{F}. The photon- and gluon-loop couplings are derived from the tree-level couplings to the massive gauge bosons and

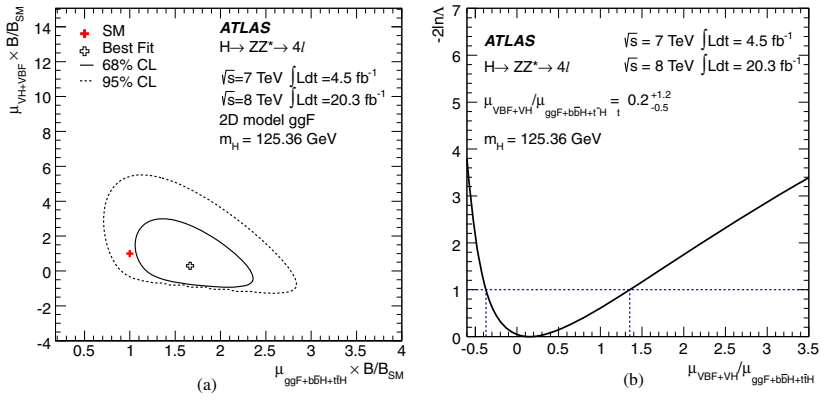

FIG. 20 (color online). (a) Likelihood contours in the $(\mu_{\mathrm{ggF}+b\bar{b}H+t\bar{t}H}, \mu_{\mathrm{VBF+VH}})$ plane including the branching ratio factor B/B_{SM}. Only the part of the plane where the expected number of signal events in each category is positive is considered. The best fit to the data (open cross) and the 68% CL (solid line) and 95% CL (dashed line) contours are also indicated, as well as the SM expectation (solid red +). (b) Results of a likelihood scan for $\mu_{\mathrm{VBF+VH}}/\mu_{\mathrm{ggF}+b\bar{b}H+t\bar{t}H}$.

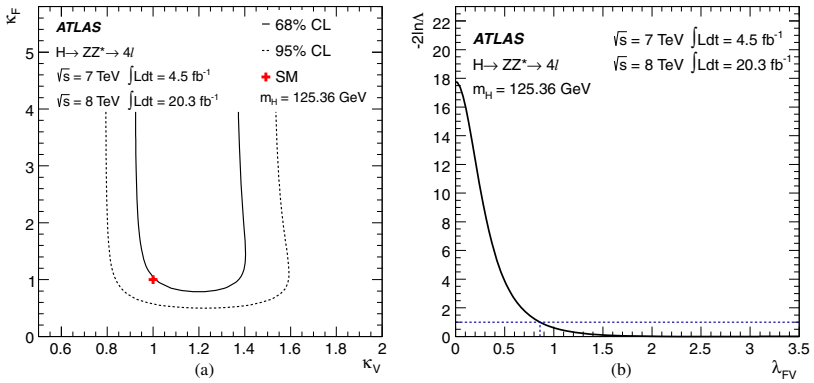

FIG. 21 (color online). (a) Likelihood contours at 68% CL (solid line) and 95% CL (dashed line) in the κ_V-κ_F plane; the SM expectation (solid red cross) is also indicated. (b) Likelihood scan as a function of the ratio $\lambda_{FV} = \kappa_F/\kappa_V$. The Higgs boson mass is assumed to be the ATLAS combined value of $m_H = 125.36$ GeV.

fermions, and it is assumed there is no non-SM contribution to the total decay width. The likelihood contours in the κ_V-κ_F plane are shown in Fig. 21. Since κ_V and κ_F are related as $\kappa_F = \kappa_V \times \mu_{ggF+b\bar{b}H+t\bar{t}H}/\mu_{VBF+VH}$, κ_F remains unbounded in Fig. 21 because the present measurement of $\mu_{VBF+VH}/\mu_{ggF+b\bar{b}H+t\bar{t}H}$ cannot exclude the value of zero, as can be seen in Fig. 20(b). The compatibility with the SM expectation is 30%. In Fig. 21(b) the likelihood scan as a function of the ratio of fermion to vector-boson coupling scale factors, $\lambda_{FV} = \kappa_F/\kappa_V$, is presented in the same benchmark model but where no assumption on the total decay width is made; the branching ratio of the Higgs boson to a pair of Z bosons cancels in the ratio. The value $\lambda_{FV} = 0$ is disfavored at the 4σ level.

XI. SUMMARY

The final Run I measurements of the Higgs boson production and couplings in the decay channel $H \to ZZ^* \to \ell^+\ell^-\ell'^+\ell'^-$ are presented. These measurements were performed using pp collision data corresponding to integrated luminosities of 4.5 fb^{-1} and 20.3 fb^{-1} at $\sqrt{s} =$ 7 TeV and $\sqrt{s} = 8$ TeV, respectively, recorded with the ATLAS detector at the LHC. The signal and background simulation, the electron and muon reconstruction and identification, the event selection and the reducible background estimations are discussed in detail. The analysis was performed both inclusively and with events separated into categories for VBF, VH and ggF production modes. Three multivariate discriminants are employed to improve the separation of the Higgs signal from the ZZ^* background, to separate VBF from ggF Higgs boson production using jet kinematics, and to distinguish hadronic decays of W and Z produced in association with a Higgs from ggF production.

For the inclusive analysis, in the m_H range 120–130 GeV, 37 events are observed while 26.5 ± 1.7 events are expected, decomposed as 16.2 ± 1.6 events for a SM Higgs signal with $m_H = 125$ GeV, 7.4 ± 0.4 ZZ^* background events and 2.9 ± 0.3 reducible background events. This excess corresponds to a $H \to ZZ^* \to 4\ell$ signal observed (expected) with a significance of 8.1 (6.2) standard deviations at the combined ATLAS measurement of the Higgs boson mass, $m_H = 125.36$ GeV [9].

For the VBF category, one event is seen with a high multivariate discriminant value and a mass of 123.4 GeV. No VH candidate is found in the m_H range 120–130 GeV with the W or Z decaying either hadronically or leptonically. The gluon fusion signal strength is found to be $1.66^{+0.45}_{-0.41}\,(\text{stat})^{+0.25}_{-0.15}\,(\text{syst})$ and the signal strength for vector-boson fusion is found to be $0.26^{+1.60}_{-0.91}\,(\text{stat})^{+0.36}_{-0.23}\,(\text{syst})$. At the combined ATLAS measurement of the Higgs boson mass, $m_H = 125.36$ GeV, the measured combined production rate relative to the SM expectation is $\mu = 1.44^{+0.34}_{-0.31}\,(\text{stat})^{+0.21}_{-0.11}\,(\text{syst})$. This measurement is based on a fit to the categories assuming a single overall signal strength. The ratio $\mu_{VBF+VH}/\mu_{ggF+b\bar{b}H+t\bar{t}H}$, which is independent of the $H \to ZZ^* \to 4\ell$ branching ratio, is found to be $0.2^{+1.2}_{-0.5}$. Finally, the observed event yields in the categories are used to quantify the compatibility with the SM predictions in terms of the Higgs coupling scale factor for weak vector bosons (κ_V) and fermions (κ_F); they are found to agree with the SM expectations.

The coupling measurements presented here for the Higgs boson decay to four leptons supersede those of the previous ATLAS study [6] and are improved with respect to the earlier results.

ACKNOWLEDGMENTS

We thank CERN for the very successful operation of the LHC, as well as the support staff from our institutions without whom ATLAS could not be operated efficiently. We acknowledge the support of ANPCyT, Argentina; YerPhI, Armenia; ARC, Australia; BMWFW and FWF, Austria; ANAS, Azerbaijan; SSTC, Belarus; CNPq and FAPESP, Brazil; NSERC, NRC and CFI, Canada; CERN; CONICYT, Chile; CAS, MOST and NSFC, China; COLCIENCIAS, Colombia; MSMT CR, MPO CR and VSC CR, Czech Republic; DNRF, DNSRC and Lundbeck Foundation, Denmark; EPLANET, ERC and NSRF, European Union; IN2P3-CNRS, CEA-DSM/IRFU, France; GNSF, Georgia; BMBF, DFG, HGF, MPG and AvH Foundation, Germany; GSRT and NSRF, Greece; ISF, MINERVA, GIF, I-CORE and Benoziyo Center, Israel; INFN, Italy; MEXT and JSPS, Japan; CNRST, Morocco; FOM and NWO, Netherlands; BRF and RCN, Norway; MNiSW and NCN, Poland; GRICES and FCT, Portugal; MNE/IFA, Romania; MES of Russia and ROSATOM, Russian Federation; JINR; MSTD, Serbia; MSSR, Slovakia; ARRS and MIZŠ, Slovenia; DST/NRF, South Africa; MINECO, Spain; SRC and Wallenberg Foundation, Sweden; SER, SNSF and Cantons of Bern and Geneva, Switzerland; NSC, Taiwan; TAEK, Turkey; STFC, the Royal Society and Leverhulme Trust, United Kingdom; DOE and NSF, United States of America. The crucial computing support from all WLCG partners is acknowledged gratefully, in particular from CERN and the ATLAS Tier-1 facilities at TRIUMF (Canada), NDGF (Denmark, Norway, Sweden), CC-IN2P3 (France), KIT/GridKA (Germany), INFN-CNAF (Italy), NL-T1 (Netherlands), PIC (Spain), ASGC (Taiwan), RAL (UK) and BNL (USA) and in the Tier-2 facilities worldwide.

[1] F. Englert and R. Brout, Phys. Rev. Lett. **13**, 321 (1964).
[2] P. W. Higgs, Phys. Rev. Lett. **13**, 508 (1964).
[3] G. S. Guralnik, C. R. Hagen, and T. W. B. Kibble, Phys. Rev. Lett. **13**, 585 (1964).
[4] ATLAS Collaboration, Phys. Lett. B **716**, 1 (2012).
[5] CMS Collaboration, Phys. Lett. B **716**, 30 (2012).
[6] ATLAS Collaboration, Phys. Lett. B **726**, 88 (2013).
[7] ATLAS Collaboration, Phys. Lett. B **726**, 120 (2013).
[8] N. Kauer and G. Passarino, J. High Energy Phys. 08 (2012) 116.
[9] ATLAS Collaboration, Phys. Rev. D **90**, 052004 (2014).
[10] CMS Collaboration, Phys. Rev. D **89**, 092007 (2014).
[11] ATLAS Collaboration, JINST **3**, S08003 (2008).
[12] P. Nason, J. High Energy Phys. 11 (2004) 040.
[13] S. Frixione, P. Nason, and C. Oleari, J. High Energy Phys. 11 (2007) 070.
[14] S. Alioli, P. Nason, C. Oleari, and E. Re, J. High Energy Phys. 06 (2010) 043.
[15] S. Alioli, P. Nason, C. Oleari, and E. Re, J. High Energy Phys. 04 (2009) 002.
[16] P. Nason and C. Oleari, J. High Energy Phys. 02 (2010) 037.
[17] D. de Florian, G. Ferrera, M. Grazzini, and D. Tommasini, J. High Energy Phys. 06 (2012) 132.
[18] M. Grazzini and H. Sargsyan, J. High Energy Phys. 09 (2013) 129.
[19] E. Bagnaschi, G. Degrassi, P. Slavich, and A. Vicini, J. High Energy Phys. 02 (2012) 088.
[20] T. Sjostrand, S. Mrenna, and P. Z. Skands, J. High Energy Phys. 05 (2006) 026.
[21] T. Sjostrand, S. Mrenna, and P. Z. Skands, Comput. Phys. Commun. **178**, 852 (2008).
[22] P. Golonka and Z. Was, Eur. Phys. J. C **45**, 97 (2006).
[23] N. Davidson, T. Przedzinski, and Z. Was, arXiv: 1011.0937.
[24] LHC Higgs Cross Section Working Group, Report No. CERN-2011-002, edited by S. Dittmaier, C. Mariotti, G. Passarino, and R. Tanaka, 2011.
[25] LHC Higgs Cross Section Working Group, Report No. CERN-2012-002, edited by S. Dittmaier, C. Mariotti, G. Passarino, and R. Tanaka, 2012.
[26] A. Djouadi, M. Spira, and P. M. Zerwas, Phys. Lett. B **264**, 440 (1991).
[27] S. Dawson, Nucl. Phys. **B359**, 283 (1991).
[28] M. Spira, A. Djouadi, D. Graudenz, and P. M. Zerwas, Nucl. Phys. **B453**, 17 (1995).
[29] R. V. Harlander and W. B. Kilgore, Phys. Rev. Lett. **88**, 201801 (2002).
[30] C. Anastasiou and K. Melnikov, Nucl. Phys. **B646**, 220 (2002).
[31] V. Ravindran, J. Smith, and W. L. van Neerven, Nucl. Phys. **B665**, 325 (2003).
[32] S. Catani, D. de Florian, M. Grazzini, and P. Nason, J. High Energy Phys. 07 (2003) 028.
[33] U. Aglietti, R. Bonciani, G. Degrassi, and A. Vicini, Phys. Lett. B **595**, 432 (2004).
[34] S. Actis, G. Passarino, C. Sturm, and S. Uccirati, Phys. Lett. B **670**, 12 (2008).
[35] D. de Florian and M. Grazzini, Phys. Lett. B **718**, 117 (2012).
[36] C. Anastasiou, S. Buehler, F. Herzog, and A. Lazopoulos, J. High Energy Phys. 04 (2012) 004.
[37] J. Baglio and A. Djouadi, J. High Energy Phys. 03 (2011) 055.
[38] M. Ciccolini, A. Denner, and S. Dittmaier, Phys. Rev. Lett. **99**, 161803 (2007).
[39] M. Ciccolini, A. Denner, and S. Dittmaier, Phys. Rev. D **77**, 013002 (2008).
[40] K. Arnold *et al.*, Comput. Phys. Commun. **180**, 1661 (2009).

[41] P. Bolzoni, F. Maltoni, S.-O. Moch, and M. Zaro, Phys. Rev. Lett. **105**, 011801 (2010).
[42] T. Han and S. Willenbrock, Phys. Lett. B **273**, 167 (1991).
[43] O. Brein, A. Djouadi, and R. Harlander, Phys. Lett. B **579**, 149 (2004).
[44] M. L. Ciccolini, S. Dittmaier, and M. Kramer, Phys. Rev. D **68**, 073003 (2003).
[45] W. Beenakker, S. Dittmaier, M. Krämer, B. Plümper, M. Spira, and P. Zerwas, Phys. Rev. Lett. **87**, 201805 (2001).
[46] W. Beenakker, S. Dittmaier, M. Krämer, B. Plümper, M. Spira, and P. Zerwas, Nucl. Phys. **B653**, 151 (2003).
[47] S. Dawson, L. Orr, L. Reina, and D. Wackeroth, Phys. Rev. D **67**, 071503 (2003).
[48] S. Dawson, C. Jackson, L. H. Orr, L. Reina, and D. Wackeroth, Phys. Rev. D **68**, 034022 (2003).
[49] S. Dawson, C. Jackson, L. Reina, and D. Wackeroth, Phys. Rev. D **69**, 074027 (2004).
[50] S. Dittmaier, M. Kramer, and M. Spira, Phys. Rev. D **70**, 074010 (2004).
[51] S. Dawson, C. Jackson, L. Reina, and D. Wackeroth, Mod. Phys. Lett. A **21**, 89 (2006).
[52] R. V. Harlander and W. B. Kilgore, Phys. Rev. D **68**, 013001 (2003).
[53] R. Harlander, M. Kramer, and M. Schumacher, arXiv:1112.3478.
[54] A. Bredenstein, A. Denner, S. Dittmaier, and M. M. Weber, Phys. Rev. D **74**, 013004 (2006).
[55] A. Bredenstein, A. Denner, S. Dittmaier, and M. M. Weber, J. High Energy Phys. 02 (2007) 080.
[56] A. Djouadi, J. Kalinowski, and M. Spira, Comput. Phys. Commun. **108**, 56 (1998).
[57] M. Botje *et al.*, arXiv:1101.0538.
[58] H.-L. Lai, M. Guzzi, J. Huston, Z. Li, P. M. Nadolsky, J. Pumplin, and C.-P. Yuan, Phys. Rev. D **82**, 074024 (2010).
[59] A. D. Martin, W. J. Stirling, R. S. Thorne, and G. Watt, Eur. Phys. J. C **63**, 189 (2009).
[60] R. D. Ball, V. Bertone, F. Cerutti, L. D. Debbio, S. Forte, A. Guffanti, J. I. Latorre, J. Rojo, and M. Ubiali, Nucl. Phys. **B849**, 296 (2011).
[61] ATLAS and CMS Collaborations, Reports No. ATL-PHYS-PUB-2011-11 and CMS-NOTE-2011-005, 2011.
[62] T. Melia, P. Nason, R. Rontsch, and G. Zanderighi, J. High Energy Phys. 11 (2011) 078.
[63] T. Binoth, N. Kauer, and P. Mertsch, arXiv:0807.0024.
[64] M. L. Mangano, M. Moretti, F. Piccinini, R. Pittau, and A. D. Polosa, J. High Energy Phys. 07 (2003) 001.
[65] M. L. Mangano, M. Moretti, F. Piccinini, and M. Treccani, J. High Energy Phys. 01 (2007) 013.
[66] K. Melnikov and F. Petriello, Phys. Rev. D **74**, 114017 (2006).
[67] C. Anastasiou, L. J. Dixon, K. Melnikov, and F. Petriello, Phys. Rev. D **69**, 094008 (2004).
[68] J. M. Campbell and R. Ellis, Nucl. Phys. B, Proc. Suppl. **205–206**, 10 (2010).
[69] J. M. Campbell and R. K. Ellis, Phys. Rev. D **62**, 114012 (2000).
[70] S. Jadach, Z. Was, R. Decker, and J. H. Kuhn, Comput. Phys. Commun. **76**, 361 (1993).
[71] P. Golonka, B. Kersevan, T. Pierzchała, E. Richter-Wąs, Z. Wąs, and M. Worek, Comput. Phys. Commun. **174**, 818 (2006).
[72] T. Gleisberg, S. Höche, F. Krauss, M. Schönherr, S. Schumann, F. Siegert, and J. Winter, J. High Energy Phys. 02 (2009) 007.
[73] ATLAS Collaboration, Eur. Phys. J. C **70**, 823 (2010).
[74] S. Agostinelli *et al.*, Nucl. Instrum. Methods Phys. Res., Sect. A **506**, 250 (2003).
[75] ATLAS Collaboration, Eur. Phys. J. C **72**, 1909 (2012).
[76] ATLAS Collaboration, Eur. Phys. J. C **74**, 3071 (2014).
[77] ATLAS Collaboration, Report No. ATLAS-CONF-2012-047, 2012.
[78] ATLAS Collaboration, Report No. ATLAS-CONF-2014-032, 2014.
[79] ATLAS Collaboration, Eur. Phys. J. C **74**, 2941 (2014).
[80] ATLAS Collaboration, Report No. ATLAS-CONF-2013-088, 2013.
[81] ATLAS Collaboration, Eur. Phys. J. C **74**, 3130 (2014).
[82] ATLAS Collaboration, Report No. ATLAS-CONF-2012-143, 2012.
[83] ATLAS Collaboration, Report No. ATLAS-CONF-2012-123, 2012.
[84] M. Cacciari and G. P. Salam, Phys. Lett. B **641**, 57 (2006).
[85] M. Cacciari, G. P. Salam, and G. Soyez, J. High Energy Phys. 04 (2008) 063.
[86] W. Lampl, S. Laplace, D. Lelas, P. Loch, H. Ma, S. Menke, S. Rajagopalan, D. Rousseau, S. Snyder, and G. Unal, Report No. ATL-LARG-PUB-2008-002, 2008.
[87] ATLAS Collaboration, Eur. Phys. J. C **73**, 2304 (2013).
[88] ATLAS Collaboration, Report No. ATLAS-CONF-2012-064, 2012.
[89] ATLAS Collaboration, arXiv:1406.0076.
[90] ATLAS Collaboration, Report No. ATLAS-CONF-2013-083, 2013.
[91] M. Cacciari and G. P. Salam, Phys. Lett. B **659**, 119 (2008).
[92] ATLAS Collaboration, Report No. ATLAS-CONF-2013-013, 2013.
[93] M. Pivk and F. Le Diberder, Nucl. Instrum. Methods Phys. Res., Sect. A **555**, 356 (2005).
[94] ATLAS Collaboration, Report No. ATLAS-CONF-2014-004, 2014.
[95] P. Speckmayer, A. Höcker, J. Stelzer, and H. Voss, J. Phys. Conf. Ser. **219**, 032057 (2010).
[96] J. Alwall, M. Herquet, F. Maltoni, O. Mattelaer, and T. Stelzer, J. High Energy Phys. 06 (2011) 128.
[97] K. S. Cranmer, Comput. Phys. Commun. **136**, 198 (2001).
[98] L. A. Piegl and W. Tiller, *The NURBS Book: Monographs in Visual Communication*, 2nd ed. (Springer, New York, 1997) Chap. 2.
[99] ATLAS Collaboration, Phys. Rev. D **86**, 032003 (2012).
[100] G. Cowan, K. Cranmer, E. Gross, and O. Vitells, Eur. Phys. J. C **71**, 1554 (2011).

[101] ATLAS Collaboration, Eur. Phys. J. C **73**, 2518 (2013).
[102] I. W. Stewart and F. J. Tackmann, Phys. Rev. D **85**, 034011 (2012).
[103] LHC Higgs Cross Section Working Group, Report No. CERN-2013-004, edited by S. Heinemeyer, C. Mariotti, G. Passarino, and R. Tanaka, CERN, Geneva, 2013.
[104] ATLAS Collaboration, Phys. Rev. Lett. **112**, 231806 (2014).
[105] CMS Collaboration, J. High Energy Phys. 12 (2012) 034.

G. Aad,[85] B. Abbott,[113] J. Abdallah,[153] S. Abdel Khalek,[117] O. Abdinov,[11] R. Aben,[107] B. Abi,[114] M. Abolins,[90] O. S. AbouZeid,[160] H. Abramowicz,[155] H. Abreu,[154] R. Abreu,[30] Y. Abulaiti,[148a,148b] B. S. Acharya,[166a,166b,b] L. Adamczyk,[38a] D. L. Adams,[25] J. Adelman,[178] S. Adomeit,[100] T. Adye,[131] T. Agatonovic-Jovin,[13a] J. A. Aguilar-Saavedra,[126a,126f] M. Agustoni,[17] S. P. Ahlen,[22] F. Ahmadov,[65,c] G. Aielli,[135a,135b] H. Akerstedt,[148a,148b] T. P. A. Åkesson,[81] G. Akimoto,[157] A. V. Akimov,[96] G. L. Alberghi,[20a,20b] J. Albert,[171] S. Albrand,[55] M. J. Alconada Verzini,[71] M. Aleksa,[30] I. N. Aleksandrov,[65] C. Alexa,[26a] G. Alexander,[155] G. Alexandre,[49] T. Alexopoulos,[10] M. Alhroob,[166a,166c] G. Alimonti,[91a] L. Alio,[85] J. Alison,[31] B. M. M. Allbrooke,[18] L. J. Allison,[72] P. P. Allport,[74] A. Aloisio,[104a,104b] A. Alonso,[36] F. Alonso,[71] C. Alpigiani,[76] A. Altheimer,[35] B. Alvarez Gonzalez,[90] M. G. Alviggi,[104a,104b] K. Amako,[66] Y. Amaral Coutinho,[24a] C. Amelung,[23] D. Amidei,[89] S. P. Amor Dos Santos,[126a,126c] A. Amorim,[126a,126b] S. Amoroso,[48] N. Amram,[155] G. Amundsen,[23] C. Anastopoulos,[141] L. S. Ancu,[49] N. Andari,[30] T. Andeen,[35] C. F. Anders,[58b] G. Anders,[30] K. J. Anderson,[31] A. Andreazza,[91a,91b] V. Andrei,[58a] X. S. Anduaga,[71] S. Angelidakis,[9] I. Angelozzi,[107] P. Anger,[44] A. Angerami,[35] F. Anghinolfi,[30] A. V. Anisenkov,[109,d] N. Anjos,[12] A. Annovi,[47] A. Antonaki,[9] M. Antonelli,[47] A. Antonov,[98] J. Antos,[146b] F. Anulli,[134a] M. Aoki,[66] L. Aperio Bella,[18] R. Apolle,[120,e] G. Arabidze,[90] I. Aracena,[145] Y. Arai,[66] J. P. Araque,[126a] A. T. H. Arce,[45] J-F. Arguin,[95] S. Argyropoulos,[42] M. Arik,[19a] A. J. Armbruster,[30] O. Arnaez,[30] V. Arnal,[82] H. Arnold,[48] M. Arratia,[28] O. Arslan,[21] A. Artamonov,[97] G. Artoni,[23] S. Asai,[157] N. Asbah,[42] A. Ashkenazi,[155] B. Åsman,[148a,148b] L. Asquith,[6] K. Assamagan,[25] R. Astalos,[146a] M. Atkinson,[167] N. B. Atlay,[143] B. Auerbach,[6] K. Augsten,[128] M. Aurousseau,[147b] G. Avolio,[30] G. Azuelos,[95,f] Y. Azuma,[157] M. A. Baak,[30] A. E. Baas,[58a] C. Bacci,[136a,136b] H. Bachacou,[138] K. Bachas,[156] M. Backes,[30] M. Backhaus,[30] J. Backus Mayes,[145] E. Badescu,[26a] P. Bagiacchi,[134a,134b] P. Bagnaia,[134a,134b] Y. Bai,[33a] T. Bain,[35] J. T. Baines,[131] O. K. Baker,[178] P. Balek,[129] F. Balli,[138] E. Banas,[39] Sw. Banerjee,[175] A. A. E. Bannoura,[177] V. Bansal,[171] H. S. Bansil,[18] L. Barak,[174] S. P. Baranov,[96] E. L. Barberio,[88] D. Barberis,[50a,50b] M. Barbero,[85] T. Barillari,[101] M. Barisonzi,[177] T. Barklow,[145] N. Barlow,[28] B. M. Barnett,[131] R. M. Barnett,[15] Z. Barnovska,[5] A. Baroncelli,[136a] G. Barone,[49] A. J. Barr,[120] F. Barreiro,[82] J. Barreiro Guimarães da Costa,[57] R. Bartoldus,[145] A. E. Barton,[72] P. Bartos,[146a] V. Bartsch,[151] A. Bassalat,[117] A. Basye,[167] R. L. Bates,[53] J. R. Batley,[28] M. Battaglia,[139] M. Battistin,[30] F. Bauer,[138] H. S. Bawa,[145,g] M. D. Beattie,[72] T. Beau,[80] P. H. Beauchemin,[163] R. Beccherle,[124a,124b] P. Bechtle,[21] H. P. Beck,[17] K. Becker,[177] S. Becker,[100] M. Beckingham,[172] C. Becot,[117] A. J. Beddall,[19c] A. Beddall,[19c] S. Bedikian,[178] V. A. Bednyakov,[65] C. P. Bee,[150] L. J. Beemster,[107] T. A. Beermann,[177] M. Begel,[25] K. Behr,[120] C. Belanger-Champagne,[87] P. J. Bell,[49] W. H. Bell,[49] G. Bella,[155] L. Bellagamba,[20a] A. Bellerive,[29] M. Bellomo,[86] K. Belotskiy,[98] O. Beltramello,[30] O. Benary,[155] D. Benchekroun,[137a] K. Bendtz,[148a,148b] N. Benekos,[167] Y. Benhammou,[155] E. Benhar Noccioli,[49] J. A. Benitez Garcia,[161b] D. P. Benjamin,[45] J. R. Bensinger,[23] K. Benslama,[132] S. Bentvelsen,[107] D. Berge,[107] E. Bergeaas Kuutmann,[168] N. Berger,[5] F. Berghaus,[171] J. Beringer,[15] C. Bernard,[22] P. Bernat,[78] C. Bernius,[79] F. U. Bernlochner,[171] T. Berry,[77] P. Berta,[129] C. Bertella,[85] G. Bertoli,[148a,148b] F. Bertolucci,[124a,124b] C. Bertsche,[113] D. Bertsche,[113] M. I. Besana,[91a] G. J. Besjes,[106] O. Bessidskaia,[148a,148b] M. Bessner,[42] N. Besson,[138] C. Betancourt,[48] S. Bethke,[101] W. Bhimji,[46] R. M. Bianchi,[125] L. Bianchini,[23] M. Bianco,[30] O. Biebel,[100] S. P. Bieniek,[78] K. Bierwagen,[54] J. Biesiada,[15] M. Biglietti,[136a] J. Bilbao De Mendizabal,[49] H. Bilokon,[47] M. Bindi,[54] S. Binet,[117] A. Bingul,[19c] C. Bini,[134a,134b] C. W. Black,[152] J. E. Black,[145] K. M. Black,[22] D. Blackburn,[140] R. E. Blair,[6] J.-B. Blanchard,[138] T. Blazek,[146a] I. Bloch,[42] C. Blocker,[23] W. Blum,[83,a] U. Blumenschein,[54] G. J. Bobbink,[107] V. S. Bobrovnikov,[109,d] S. S. Bocchetta,[81] A. Bocci,[45] C. Bock,[100] C. R. Boddy,[120] M. Boehler,[48] T. T. Boek,[177] J. A. Bogaerts,[30] A. G. Bogdanchikov,[109] A. Bogouch,[92,a] C. Bohm,[148a] J. Bohm,[127] V. Boisvert,[77] T. Bold,[38a] V. Boldea,[26a] A. S. Boldyrev,[99] M. Bomben,[80] M. Bona,[76] M. Boonekamp,[138] A. Borisov,[130] G. Borissov,[72] M. Borri,[84] S. Borroni,[42] J. Bortfeldt,[100] V. Bortolotto,[136a,136b] K. Bos,[107] D. Boscherini,[20a] M. Bosman,[12] H. Boterenbrood,[107] J. Boudreau,[125] J. Bouffard,[2] E. V. Bouhova-Thacker,[72] D. Boumediene,[34] C. Bourdarios,[117] N. Bousson,[114] S. Boutouil,[137d] A. Boveia,[31] J. Boyd,[30] I. R. Boyko,[65] I. Bozic,[13a] J. Bracinik,[18] A. Brandt,[8] G. Brandt,[15] O. Brandt,[58a] U. Bratzler,[158] B. Brau,[86] J. E. Brau,[116] H. M. Braun,[177,a]

S. F. Brazzale,[166a,166c] B. Brelier,[160] K. Brendlinger,[122] A. J. Brennan,[88] R. Brenner,[168] S. Bressler,[174] K. Bristow,[147c] T. M. Bristow,[46] D. Britton,[53] F. M. Brochu,[28] I. Brock,[21] R. Brock,[90] C. Bromberg,[90] J. Bronner,[101] G. Brooijmans,[35] T. Brooks,[77] W. K. Brooks,[32b] J. Brosamer,[15] E. Brost,[116] J. Brown,[55] P. A. Bruckman de Renstrom,[39] D. Bruncko,[146b] R. Bruneliere,[48] S. Brunet,[61] A. Bruni,[20a] G. Bruni,[20a] M. Bruschi,[20a] L. Bryngemark,[81] T. Buanes,[14] Q. Buat,[144] F. Bucci,[49] P. Buchholz,[143] R. M. Buckingham,[120] A. G. Buckley,[53] S. I. Buda,[26a] I. A. Budagov,[65] F. Buehrer,[48] L. Bugge,[119] M. K. Bugge,[119] O. Bulekov,[98] A. C. Bundock,[74] H. Burckhart,[30] S. Burdin,[74] B. Burghgrave,[108] S. Burke,[131] I. Burmeister,[43] E. Busato,[34] D. Büscher,[48] V. Büscher,[83] P. Bussey,[53] C. P. Buszello,[168] B. Butler,[57] J. M. Butler,[22] A. I. Butt,[3] C. M. Buttar,[53] J. M. Butterworth,[78] P. Butti,[107] W. Buttinger,[28] A. Buzatu,[53] M. Byszewski,[10] S. Cabrera Urbán,[169] D. Caforio,[20a,20b] O. Cakir,[4a] P. Calafiura,[15] A. Calandri,[138] G. Calderini,[80] P. Calfayan,[100] R. Calkins,[108] L. P. Caloba,[24a] D. Calvet,[34] S. Calvet,[34] R. Camacho Toro,[49] S. Camarda,[42] D. Cameron,[119] L. M. Caminada,[15] R. Caminal Armadans,[12] S. Campana,[30] M. Campanelli,[78] A. Campoverde,[150] V. Canale,[104a,104b] A. Canepa,[161a] M. Cano Bret,[76] J. Cantero,[82] R. Cantrill,[126a] T. Cao,[40] M. D. M. Capeans Garrido,[30] I. Caprini,[26a] M. Caprini,[26a] M. Capua,[37a,37b] R. Caputo,[83] R. Cardarelli,[135a] T. Carli,[30] G. Carlino,[104a] L. Carminati,[91a,91b] S. Caron,[106] E. Carquin,[32a] G. D. Carrillo-Montoya,[147c] J. R. Carter,[28] J. Carvalho,[126a,126c] D. Casadei,[78] M. P. Casado,[12] M. Casolino,[12] E. Castaneda-Miranda,[147b] A. Castelli,[107] V. Castillo Gimenez,[169] N. F. Castro,[126a] P. Catastini,[57] A. Catinaccio,[30] J. R. Catmore,[119] A. Cattai,[30] G. Cattani,[135a,135b] J. Caudron,[83] V. Cavaliere,[167] D. Cavalli,[91a] M. Cavalli-Sforza,[12] V. Cavasinni,[124a,124b] F. Ceradini,[136a,136b] B. C. Cerio,[45] K. Cerny,[129] A. S. Cerqueira,[24b] A. Cerri,[151] L. Cerrito,[76] F. Cerutti,[15] M. Cerv,[30] A. Cervelli,[17] S. A. Cetin,[19b] A. Chafaq,[137a] D. Chakraborty,[108] I. Chalupkova,[129] P. Chang,[167] B. Chapleau,[87] J. D. Chapman,[28] D. Charfeddine,[117] D. G. Charlton,[18] C. C. Chau,[160] C. A. Chavez Barajas,[151] S. Cheatham,[87] A. Chegwidden,[90] S. Chekanov,[6] S. V. Chekulaev,[161a] G. A. Chelkov,[65,h] M. A. Chelstowska,[89] C. Chen,[64] H. Chen,[25] K. Chen,[150] L. Chen,[33d,i] S. Chen,[33c] X. Chen,[33f] Y. Chen,[67] Y. Chen,[35] H. C. Cheng,[89] Y. Cheng,[31] A. Cheplakov,[65] R. Cherkaoui El Moursli,[137e] V. Chernyatin,[25,a] E. Cheu,[7] L. Chevalier,[138] V. Chiarella,[47] G. Chiefari,[104a,104b] J. T. Childers,[6] A. Chilingarov,[72] G. Chiodini,[73a] A. S. Chisholm,[18] R. T. Chislett,[78] A. Chitan,[26a] M. V. Chizhov,[65] S. Chouridou,[9] B. K. B. Chow,[100] D. Chromek-Burckhart,[30] M. L. Chu,[153] J. Chudoba,[127] J. J. Chwastowski,[39] L. Chytka,[115] G. Ciapetti,[134a,134b] A. K. Ciftci,[4a] R. Ciftci,[4a] D. Cinca,[53] V. Cindro,[75] A. Ciocio,[15] P. Cirkovic,[13b] Z. H. Citron,[174] M. Citterio,[91a] M. Ciubancan,[26a] A. Clark,[49] P. J. Clark,[46] R. N. Clarke,[15] W. Cleland,[125] J. C. Clemens,[85] C. Clement,[148a,148b] Y. Coadou,[85] M. Cobal,[166a,166c] A. Coccaro,[140] J. Cochran,[64] L. Coffey,[23] J. G. Cogan,[145] J. Coggeshall,[167] B. Cole,[35] S. Cole,[108] A. P. Colijn,[107] J. Collot,[55] T. Colombo,[58c] G. Colon,[86] G. Compostella,[101] P. Conde Muiño,[126a,126b] E. Coniavitis,[48] M. C. Conidi,[12] S. H. Connell,[147b] I. A. Connelly,[77] S. M. Consonni,[91a,91b] V. Consorti,[48] S. Constantinescu,[26a] C. Conta,[121a,121b] G. Conti,[57] F. Conventi,[104a,j] M. Cooke,[15] B. D. Cooper,[78] A. M. Cooper-Sarkar,[120] N. J. Cooper-Smith,[77] K. Copic,[15] T. Cornelissen,[177] M. Corradi,[20a] F. Corriveau,[87,k] A. Corso-Radu,[165] A. Cortes-Gonzalez,[12] G. Cortiana,[101] G. Costa,[91a] M. J. Costa,[169] D. Costanzo,[141] D. Côté,[8] G. Cottin,[28] G. Cowan,[77] B. E. Cox,[84] K. Cranmer,[110] G. Cree,[29] S. Crépé-Renaudin,[55] F. Crescioli,[80] W. A. Cribbs,[148a,148b] M. Crispin Ortuzar,[120] M. Cristinziani,[21] V. Croft,[106] G. Crosetti,[37a,37b] C.-M. Cuciuc,[26a] T. Cuhadar Donszelmann,[141] J. Cummings,[178] M. Curatolo,[47] C. Cuthbert,[152] H. Czirr,[143] P. Czodrowski,[3] Z. Czyczula,[178] S. D'Auria,[53] M. D'Onofrio,[74] M. J. Da Cunha Sargedas De Sousa,[126a,126b] C. Da Via,[84] W. Dabrowski,[38a] A. Dafinca,[120] T. Dai,[89] O. Dale,[14] F. Dallaire,[95] C. Dallapiccola,[86] M. Dam,[36] A. C. Daniells,[18] M. Dano Hoffmann,[138] V. Dao,[48] G. Darbo,[50a] S. Darmora,[8] J. A. Dassoulas,[42] A. Dattagupta,[61] W. Davey,[21] C. David,[171] T. Davidek,[129] E. Davies,[120,e] M. Davies,[155] O. Davignon,[80] A. R. Davison,[78] P. Davison,[78] Y. Davygora,[58a] E. Dawe,[144] I. Dawson,[141] R. K. Daya-Ishmukhametova,[86] K. De,[8] R. de Asmundis,[104a] S. De Castro,[20a,20b] S. De Cecco,[80] N. De Groot,[106] P. de Jong,[107] H. De la Torre,[82] F. De Lorenzi,[64] L. De Nooij,[107] D. De Pedis,[134a] A. De Salvo,[134a] U. De Sanctis,[151] A. De Santo,[151] J. B. De Vivie De Regie,[117] W. J. Dearnaley,[72] R. Debbe,[25] C. Debenedetti,[139] B. Dechenaux,[55] D. V. Dedovich,[65] I. Deigaard,[107] J. Del Peso,[82] T. Del Prete,[124a,124b] F. Deliot,[138] C. M. Delitzsch,[49] M. Deliyergiyev,[75] A. Dell'Acqua,[30] L. Dell'Asta,[22] M. Dell'Orso,[124a,124b] M. Della Pietra,[104a,j] D. della Volpe,[49] M. Delmastro,[5] P. A. Delsart,[55] C. Deluca,[107] S. Demers,[178] M. Demichev,[65] A. Demilly,[80] S. P. Denisov,[130] D. Derendarz,[39] J. E. Derkaoui,[137d] F. Derue,[80] P. Dervan,[74] K. Desch,[21] C. Deterre,[42] P. O. Deviveiros,[107] A. Dewhurst,[131] S. Dhaliwal,[107] A. Di Ciaccio,[135a,135b] L. Di Ciaccio,[5] A. Di Domenico,[134a,134b] C. Di Donato,[104a,104b] A. Di Girolamo,[30] B. Di Girolamo,[30] A. Di Mattia,[154] B. Di Micco,[136a,136b] R. Di Nardo,[47] A. Di Simone,[48] R. Di Sipio,[20a,20b] D. Di Valentino,[29] F. A. Dias,[46] M. A. Diaz,[32a] E. B. Diehl,[89] J. Dietrich,[42] T. A. Dietzsch,[58a] S. Diglio,[85] A. Dimitrievska,[13a] J. Dingfelder,[21] C. Dionisi,[134a,134b] P. Dita,[26a] S. Dita,[26a] F. Dittus,[30]

F. Djama,[85] T. Djobava,[51b] J. I. Djuvsland,[58a] M. A. B. do Vale,[24c] A. Do Valle Wemans,[126a,126g] D. Dobos,[30] C. Doglioni,[49] T. Doherty,[53] T. Dohmae,[157] J. Dolejsi,[129] Z. Dolezal,[129] B. A. Dolgoshein,[98,a] M. Donadelli,[24d] S. Donati,[124a,124b] P. Dondero,[121a,121b] J. Donini,[34] J. Dopke,[131] A. Doria,[104a] M. T. Dova,[71] A. T. Doyle,[53] M. Dris,[10] J. Dubbert,[89] S. Dube,[15] E. Dubreuil,[34] E. Duchovni,[174] G. Duckeck,[100] O. A. Ducu,[26a] D. Duda,[177] A. Dudarev,[30] F. Dudziak,[64] L. Duflot,[117] L. Duguid,[77] M. Dührssen,[30] M. Dunford,[58a] H. Duran Yildiz,[4a] M. Düren,[52] A. Durglishvili,[51b] M. Dwuznik,[38a] M. Dyndal,[38a] J. Ebke,[100] W. Edson,[2] N. C. Edwards,[46] W. Ehrenfeld,[21] T. Eifert,[145] G. Eigen,[14] K. Einsweiler,[15] T. Ekelof,[168] M. El Kacimi,[137c] M. Ellert,[168] S. Elles,[5] F. Ellinghaus,[83] N. Ellis,[30] J. Elmsheuser,[100] M. Elsing,[30] D. Emeliyanov,[131] Y. Enari,[157] O. C. Endner,[83] M. Endo,[118] R. Engelmann,[150] J. Erdmann,[178] A. Ereditato,[17] D. Eriksson,[148a] G. Ernis,[177] J. Ernst,[2] M. Ernst,[25] J. Ernwein,[138] D. Errede,[167] S. Errede,[167] E. Ertel,[83] M. Escalier,[117] H. Esch,[43] C. Escobar,[125] B. Esposito,[47] A. I. Etienvre,[138] E. Etzion,[155] H. Evans,[61] A. Ezhilov,[123] L. Fabbri,[20a,20b] G. Facini,[31] R. M. Fakhrutdinov,[130] S. Falciano,[134a] R. J. Falla,[78] J. Faltova,[129] Y. Fang,[33a] M. Fanti,[91a,91b] A. Farbin,[8] A. Farilla,[136a] T. Farooque,[12] S. Farrell,[15] S. M. Farrington,[172] P. Farthouat,[30] F. Fassi,[137e] P. Fassnacht,[30] D. Fassouliotis,[9] A. Favareto,[50a,50b] L. Fayard,[117] P. Federic,[146a] O. L. Fedin,[123,l] W. Fedorko,[170] M. Fehling-Kaschek,[48] S. Feigl,[30] L. Feligioni,[85] C. Feng,[33d] E. J. Feng,[6] H. Feng,[89] A. B. Fenyuk,[130] S. Fernandez Perez,[30] S. Ferrag,[53] J. Ferrando,[53] A. Ferrari,[168] P. Ferrari,[107] R. Ferrari,[121a] D. E. Ferreira de Lima,[53] A. Ferrer,[169] D. Ferrere,[49] C. Ferretti,[89] A. Ferretto Parodi,[50a,50b] M. Fiascaris,[31] F. Fiedler,[83] A. Filipčič,[75] M. Filipuzzi,[42] F. Filthaut,[106] M. Fincke-Keeler,[171] K. D. Finelli,[152] M. C. N. Fiolhais,[126a,126c] L. Fiorini,[169] A. Firan,[40] A. Fischer,[2] J. Fischer,[177] W. C. Fisher,[90] E. A. Fitzgerald,[23] M. Flechl,[48] I. Fleck,[143] P. Fleischmann,[89] S. Fleischmann,[177] G. T. Fletcher,[141] G. Fletcher,[76] T. Flick,[177] A. Floderus,[81] L. R. Flores Castillo,[60a] A. C. Florez Bustos,[161b] M. J. Flowerdew,[101] A. Formica,[138] A. Forti,[84] D. Fortin,[161a] D. Fournier,[117] H. Fox,[72] S. Fracchia,[12] P. Francavilla,[80] M. Franchini,[20a,20b] S. Franchino,[30] D. Francis,[30] L. Franconi,[119] M. Franklin,[57] S. Franz,[62] M. Fraternali,[121a,121b] S. T. French,[28] C. Friedrich,[42] F. Friedrich,[44] D. Froidevaux,[30] J. A. Frost,[28] C. Fukunaga,[158] E. Fullana Torregrosa,[83] B. G. Fulsom,[145] J. Fuster,[169] C. Gabaldon,[55] O. Gabizon,[177] A. Gabrielli,[20a,20b] A. Gabrielli,[134a,134b] S. Gadatsch,[107] S. Gadomski,[49] G. Gagliardi,[50a,50b] P. Gagnon,[61] C. Galea,[106] B. Galhardo,[126a,126c] E. J. Gallas,[120] V. Gallo,[17] B. J. Gallop,[131] P. Gallus,[128] G. Galster,[36] K. K. Gan,[111] J. Gao,[33b,i] Y. S. Gao,[145,g] F. M. Garay Walls,[46] F. Garberson,[178] C. García,[169] J. E. García Navarro,[169] M. Garcia-Sciveres,[15] R. W. Gardner,[31] N. Garelli,[145] V. Garonne,[30] C. Gatti,[47] G. Gaudio,[121a] B. Gaur,[143] L. Gauthier,[95] P. Gauzzi,[134a,134b] I. L. Gavrilenko,[96] C. Gay,[170] G. Gaycken,[21] E. N. Gazis,[10] P. Ge,[33d] Z. Gecse,[170] C. N. P. Gee,[131] D. A. A. Geerts,[107] Ch. Geich-Gimbel,[21] K. Gellerstedt,[148a,148b] C. Gemme,[50a] A. Gemmell,[53] M. H. Genest,[55] S. Gentile,[134a,134b] M. George,[54] S. George,[77] D. Gerbaudo,[165] A. Gershon,[155] H. Ghazlane,[137b] N. Ghodbane,[34] B. Giacobbe,[20a] S. Giagu,[134a,134b] V. Giangiobbe,[12] P. Giannetti,[124a,124b] F. Gianotti,[30] B. Gibbard,[25] S. M. Gibson,[77] M. Gilchriese,[15] T. P. S. Gillam,[28] D. Gillberg,[30] G. Gilles,[34] D. M. Gingrich,[3,f] N. Giokaris,[9] M. P. Giordani,[166a,166c] R. Giordano,[104a,104b] F. M. Giorgi,[20a] F. M. Giorgi,[16] P. F. Giraud,[138] D. Giugni,[91a] C. Giuliani,[48] M. Giulini,[58b] B. K. Gjelsten,[119] S. Gkaitatzis,[156] I. Gkialas,[156,m] L. K. Gladilin,[99] C. Glasman,[82] J. Glatzer,[30] P. C. F. Glaysher,[46] A. Glazov,[42] G. L. Glonti,[65] M. Goblirsch-Kolb,[101] J. R. Goddard,[76] J. Godlewski,[30] C. Goeringer,[83] S. Goldfarb,[89] T. Golling,[178] D. Golubkov,[130] A. Gomes,[126a,126b,126d] L. S. Gomez Fajardo,[42] R. Gonçalo,[126a] J. Goncalves Pinto Firmino Da Costa,[138] L. Gonella,[21] S. González de la Hoz,[169] G. Gonzalez Parra,[12] S. Gonzalez-Sevilla,[49] L. Goossens,[30] P. A. Gorbounov,[97] H. A. Gordon,[25] I. Gorelov,[105] B. Gorini,[30] E. Gorini,[73a,73b] A. Gorišek,[75] E. Gornicki,[39] A. T. Goshaw,[6] C. Gössling,[43] M. I. Gostkin,[65] M. Gouighri,[137a] D. Goujdami,[137c] M. P. Goulette,[49] A. G. Goussiou,[140] C. Goy,[5] S. Gozpinar,[23] H. M. X. Grabas,[138] L. Graber,[54] I. Grabowska-Bold,[38a] P. Grafström,[20a,20b] K.-J. Grahn,[42] J. Gramling,[49] E. Gramstad,[119] S. Grancagnolo,[16] V. Grassi,[150] V. Gratchev,[123] H. M. Gray,[30] E. Graziani,[136a] O. G. Grebenyuk,[123] Z. D. Greenwood,[79,n] K. Gregersen,[78] I. M. Gregor,[42] P. Grenier,[145] J. Griffiths,[8] A. A. Grillo,[139] K. Grimm,[72] S. Grinstein,[12,o] Ph. Gris,[34] Y. V. Grishkevich,[99] J.-F. Grivaz,[117] J. P. Grohs,[44] A. Grohsjean,[42] E. Gross,[174] J. Grosse-Knetter,[54] G. C. Grossi,[135a,135b] J. Groth-Jensen,[174] Z. J. Grout,[151] L. Guan,[33b] J. Guenther,[128] F. Guescini,[49] D. Guest,[178] O. Gueta,[155] C. Guicheney,[34] E. Guido,[50a,50b] T. Guillemin,[117] S. Guindon,[2] U. Gul,[53] C. Gumpert,[44] J. Guo,[35] S. Gupta,[120] P. Gutierrez,[113] N. G. Gutierrez Ortiz,[53] C. Gutschow,[78] N. Guttman,[155] C. Guyot,[138] C. Gwenlan,[120] C. B. Gwilliam,[74] A. Haas,[110] C. Haber,[15] H. K. Hadavand,[8] N. Haddad,[137e] P. Haefner,[21] S. Hageböck,[21] Z. Hajduk,[39] H. Hakobyan,[179] M. Haleem,[42] D. Hall,[120] G. Halladjian,[90] K. Hamacher,[177] P. Hamal,[115] K. Hamano,[171] M. Hamer,[54] A. Hamilton,[147a] S. Hamilton,[163] G. N. Hamity,[147c] P. G. Hamnett,[42] L. Han,[33b] K. Hanagaki,[118] K. Hanawa,[157] M. Hance,[15] P. Hanke,[58a] R. Hanna,[138] J. B. Hansen,[36] J. D. Hansen,[36] P. H. Hansen,[36] K. Hara,[162] A. S. Hard,[175] T. Harenberg,[177] F. Hariri,[117] S. Harkusha,[92] D. Harper,[89] R. D. Harrington,[46] O. M. Harris,[140] P. F. Harrison,[172] F. Hartjes,[107] M. Hasegawa,[67]

S. Hasegawa,[103] Y. Hasegawa,[142] A. Hasib,[113] S. Hassani,[138] S. Haug,[17] M. Hauschild,[30] R. Hauser,[90] M. Havranek,[127] C. M. Hawkes,[18] R. J. Hawkings,[30] A. D. Hawkins,[81] T. Hayashi,[162] D. Hayden,[90] C. P. Hays,[120] H. S. Hayward,[74] S. J. Haywood,[131] S. J. Head,[18] T. Heck,[83] V. Hedberg,[81] L. Heelan,[8] S. Heim,[122] T. Heim,[177] B. Heinemann,[15] L. Heinrich,[110] J. Hejbal,[127] L. Helary,[22] C. Heller,[100] M. Heller,[30] S. Hellman,[148a,148b] D. Hellmich,[21] C. Helsens,[30] J. Henderson,[120] R. C. W. Henderson,[72] Y. Heng,[175] C. Hengler,[42] A. Henrichs,[178] A. M. Henriques Correia,[30] S. Henrot-Versille,[117] G. H. Herbert,[16] Y. Hernández Jiménez,[169] R. Herrberg-Schubert,[16] G. Herten,[48] R. Hertenberger,[100] L. Hervas,[30] G. G. Hesketh,[78] N. P. Hessey,[107] R. Hickling,[76] E. Higón-Rodriguez,[169] E. Hill,[171] J. C. Hill,[28] K. H. Hiller,[42] S. Hillert,[21] S. J. Hillier,[18] I. Hinchliffe,[15] E. Hines,[122] M. Hirose,[159] D. Hirschbuehl,[177] J. Hobbs,[150] N. Hod,[107] M. C. Hodgkinson,[141] P. Hodgson,[141] A. Hoecker,[30] M. R. Hoeferkamp,[105] F. Hoenig,[100] J. Hoffman,[40] D. Hoffmann,[85] M. Hohlfeld,[83] T. R. Holmes,[15] T. M. Hong,[122] L. Hooft van Huysduynen,[110] W. H. Hopkins,[116] Y. Horii,[103] J-Y. Hostachy,[55] S. Hou,[153] A. Hoummada,[137a] J. Howard,[120] J. Howarth,[42] M. Hrabovsky,[115] I. Hristova,[16] J. Hrivnac,[117] T. Hryn'ova,[5] C. Hsu,[147c] P. J. Hsu,[83] S.-C. Hsu,[140] D. Hu,[35] X. Hu,[89] Y. Huang,[42] Z. Hubacek,[30] F. Hubaut,[85] F. Huegging,[21] T. B. Huffman,[120] E. W. Hughes,[35] G. Hughes,[72] M. Huhtinen,[30] T. A. Hülsing,[83] M. Hurwitz,[15] N. Huseynov,[65,c] J. Huston,[90] J. Huth,[57] G. Iacobucci,[49] G. Iakovidis,[10] I. Ibragimov,[143] L. Iconomidou-Fayard,[117] E. Ideal,[178] Z. Idrissi,[137e] P. Iengo,[104a] O. Igonkina,[107] T. Iizawa,[173] Y. Ikegami,[66] K. Ikematsu,[143] M. Ikeno,[66] Y. Ilchenko,[31,p] D. Iliadis,[156] N. Ilic,[160] Y. Inamaru,[67] T. Ince,[101] P. Ioannou,[9] M. Iodice,[136a] K. Iordanidou,[9] V. Ippolito,[57] A. Irles Quiles,[169] C. Isaksson,[168] M. Ishino,[68] M. Ishitsuka,[159] R. Ishmukhametov,[111] C. Issever,[120] S. Istin,[19a] J. M. Iturbe Ponce,[84] R. Iuppa,[135a,135b] J. Ivarsson,[81] W. Iwanski,[39] H. Iwasaki,[66] J. M. Izen,[41] V. Izzo,[104a] B. Jackson,[122] M. Jackson,[74] P. Jackson,[1] M. R. Jaekel,[30] V. Jain,[2] K. Jakobs,[48] S. Jakobsen,[30] T. Jakoubek,[127] J. Jakubek,[128] D. O. Jamin,[153] D. K. Jana,[79] E. Jansen,[78] H. Jansen,[30] J. Janssen,[21] M. Janus,[172] G. Jarlskog,[81] N. Javadov,[65,c] T. Javůrek,[48] L. Jeanty,[15] J. Jejelava,[51a,q] G.-Y. Jeng,[152] D. Jennens,[88] P. Jenni,[48,r] J. Jentzsch,[43] C. Jeske,[172] S. Jézéquel,[5] H. Ji,[175] J. Jia,[150] Y. Jiang,[33b] M. Jimenez Belenguer,[42] S. Jin,[33a] A. Jinaru,[26a] O. Jinnouchi,[159] M. D. Joergensen,[36] K. E. Johansson,[148a,148b] P. Johansson,[141] K. A. Johns,[7] K. Jon-And,[148a,148b] G. Jones,[172] R. W. L. Jones,[72] T. J. Jones,[74] J. Jongmanns,[58a] P. M. Jorge,[126a,126b] K. D. Joshi,[84] J. Jovicevic,[149] X. Ju,[175] C. A. Jung,[43] R. M. Jungst,[30] P. Jussel,[62] A. Juste Rozas,[12,o] M. Kaci,[169] A. Kaczmarska,[39] M. Kado,[117] H. Kagan,[111] M. Kagan,[145] E. Kajomovitz,[45] C. W. Kalderon,[120] S. Kama,[40] A. Kamenshchikov,[130] N. Kanaya,[157] M. Kaneda,[30] S. Kaneti,[28] V. A. Kantserov,[98] J. Kanzaki,[66] B. Kaplan,[110] A. Kapliy,[31] D. Kar,[53] K. Karakostas,[10] N. Karastathis,[10] M. J. Kareem,[54] M. Karnevskiy,[83] S. N. Karpov,[65] Z. M. Karpova,[65] K. Karthik,[110] V. Kartvelishvili,[72] A. N. Karyukhin,[130] L. Kashif,[175] G. Kasieczka,[58b] R. D. Kass,[111] A. Kastanas,[14] Y. Kataoka,[157] A. Katre,[49] J. Katzy,[42] V. Kaushik,[7] K. Kawagoe,[70] T. Kawamoto,[157] G. Kawamura,[54] S. Kazama,[157] V. F. Kazanin,[109] M. Y. Kazarinov,[65] R. Keeler,[171] R. Kehoe,[40] M. Keil,[54] J. S. Keller,[42] J. J. Kempster,[77] H. Keoshkerian,[5] O. Kepka,[127] B. P. Kerševan,[75] S. Kersten,[177] K. Kessoku,[157] J. Keung,[160] F. Khalil-zada,[11] H. Khandanyan,[148a,148b] A. Khanov,[114] A. Khodinov,[98] A. Khomich,[58a] T. J. Khoo,[28] G. Khoriauli,[21] A. Khoroshilov,[177] V. Khovanskiy,[97] E. Khramov,[65] J. Khubua,[51b] H. Y. Kim,[8] H. Kim,[148a,148b] S. H. Kim,[162] N. Kimura,[173] O. Kind,[16] B. T. King,[74] M. King,[169] R. S. B. King,[120] S. B. King,[170] J. Kirk,[131] A. E. Kiryunin,[101] T. Kishimoto,[67] D. Kisielewska,[38a] F. Kiss,[48] T. Kittelmann,[125] K. Kiuchi,[162] E. Kladiva,[146b] M. Klein,[74] U. Klein,[74] K. Kleinknecht,[83] P. Klimek,[148a,148b] A. Klimentov,[25] R. Klingenberg,[43] J. A. Klinger,[84] T. Klioutchnikova,[30] P. F. Klok,[106] E.-E. Kluge,[58a] P. Kluit,[107] S. Kluth,[101] E. Kneringer,[62] E. B. F. G. Knoops,[85] A. Knue,[53] D. Kobayashi,[159] T. Kobayashi,[157] M. Kobel,[44] M. Kocian,[145] P. Kodys,[129] P. Koevesarki,[21] T. Koffas,[29] E. Koffeman,[107] L. A. Kogan,[120] S. Kohlmann,[177] Z. Kohout,[128] T. Kohriki,[66] T. Koi,[145] H. Kolanoski,[16] I. Koletsou,[5] J. Koll,[90] A. A. Komar,[96,a] Y. Komori,[157] T. Kondo,[66] N. Kondrashova,[42] K. Köneke,[48] A. C. König,[106] S. König,[83] T. Kono,[66,s] R. Konoplich,[110,t] N. Konstantinidis,[78] R. Kopeliansky,[154] S. Koperny,[38a] L. Köpke,[83] A. K. Kopp,[48] K. Korcyl,[39] K. Kordas,[156] A. Korn,[78] A. A. Korol,[109,d] I. Korolkov,[12] E. V. Korolkova,[141] V. A. Korotkov,[130] O. Kortner,[101] S. Kortner,[101] V. V. Kostyukhin,[21] V. M. Kotov,[65] A. Kotwal,[45] C. Kourkoumelis,[9] V. Kouskoura,[156] A. Koutsman,[161a] R. Kowalewski,[171] T. Z. Kowalski,[38a] W. Kozanecki,[138] A. S. Kozhin,[130] V. Kral,[128] V. A. Kramarenko,[99] G. Kramberger,[75] D. Krasnopevtsev,[98] A. Krasznahorkay,[30] J. K. Kraus,[21] A. Kravchenko,[25] S. Kreiss,[110] M. Kretz,[58c] J. Kretzschmar,[74] K. Kreutzfeldt,[52] P. Krieger,[160] K. Kroeninger,[54] H. Kroha,[101] J. Kroll,[122] J. Kroseberg,[21] J. Krstic,[13a] U. Kruchonak,[65] H. Krüger,[21] T. Kruker,[17] N. Krumnack,[64] Z. V. Krumshteyn,[65] A. Kruse,[175] M. C. Kruse,[45] M. Kruskal,[22] T. Kubota,[88] H. Kucuk,[78] S. Kuday,[4c] S. Kuehn,[48] A. Kugel,[58c] A. Kuhl,[139] T. Kuhl,[42] V. Kukhtin,[65] Y. Kulchitsky,[92] S. Kuleshov,[32b] M. Kuna,[134a,134b] J. Kunkle,[122] A. Kupco,[127] H. Kurashige,[67] Y. A. Kurochkin,[92] R. Kurumida,[67] V. Kus,[127] E. S. Kuwertz,[149] M. Kuze,[159] J. Kvita,[115] A. La Rosa,[49] L. La Rotonda,[37a,37b] C. Lacasta,[169] F. Lacava,[134a,134b] J. Lacey,[29] H. Lacker,[16]

D. Lacour,[80] V. R. Lacuesta,[169] E. Ladygin,[65] R. Lafaye,[5] B. Laforge,[80] T. Lagouri,[178] S. Lai,[48] H. Laier,[58a] L. Lambourne,[78] S. Lammers,[61] C. L. Lampen,[7] W. Lampl,[7] E. Lançon,[138] U. Landgraf,[48] M. P. J. Landon,[76] V. S. Lang,[58a] A. J. Lankford,[165] F. Lanni,[25] K. Lantzsch,[30] S. Laplace,[80] C. Lapoire,[21] J. F. Laporte,[138] T. Lari,[91a] F. Lasagni Manghi,[20a,20b] M. Lassnig,[30] P. Laurelli,[47] W. Lavrijsen,[15] A. T. Law,[139] P. Laycock,[74] O. Le Dortz,[80] E. Le Guirriec,[85] E. Le Menedeu,[12] T. LeCompte,[6] F. Ledroit-Guillon,[55] C. A. Lee,[153] H. Lee,[107] J. S. H. Lee,[118] S. C. Lee,[153] L. Lee,[1] G. Lefebvre,[80] M. Lefebvre,[171] F. Legger,[100] C. Leggett,[15] A. Lehan,[74] M. Lehmacher,[21] G. Lehmann Miotto,[30] X. Lei,[7] W. A. Leight,[29] A. Leisos,[156] A. G. Leister,[178] M. A. L. Leite,[24d] R. Leitner,[129] D. Lellouch,[174] B. Lemmer,[54] K. J. C. Leney,[78] T. Lenz,[21] G. Lenzen,[177] B. Lenzi,[30] R. Leone,[7] S. Leone,[124a,124b] C. Leonidopoulos,[46] S. Leontsinis,[10] C. Leroy,[95] C. G. Lester,[28] C. M. Lester,[122] M. Levchenko,[123] J. Levêque,[5] D. Levin,[89] L. J. Levinson,[174] M. Levy,[18] A. Lewis,[120] G. H. Lewis,[110] A. M. Leyko,[21] M. Leyton,[41] B. Li,[33b,u] B. Li,[85] H. Li,[150] H. L. Li,[31] L. Li,[45] L. Li,[33e] S. Li,[45] Y. Li,[33c,v] Z. Liang,[139] H. Liao,[34] B. Liberti,[135a] P. Lichard,[30] K. Lie,[167] J. Liebal,[21] W. Liebig,[14] C. Limbach,[21] A. Limosani,[88] S. C. Lin,[153,w] T. H. Lin,[83] F. Linde,[107] B. E. Lindquist,[150] J. T. Linnemann,[90] E. Lipeles,[122] A. Lipniacka,[14] M. Lisovyi,[42] T. M. Liss,[167] D. Lissauer,[25] A. Lister,[170] A. M. Litke,[139] B. Liu,[153] D. Liu,[153] J. B. Liu,[33b] K. Liu,[33b,x] L. Liu,[89] M. Liu,[45] M. Liu,[33b] Y. Liu,[33b] M. Livan,[121a,121b] S. S. A. Livermore,[120] A. Lleres,[55] J. Llorente Merino,[82] S. L. Lloyd,[76] F. Lo Sterzo,[153] E. Lobodzinska,[42] P. Loch,[7] W. S. Lockman,[139] T. Loddenkoetter,[21] F. K. Loebinger,[84] A. E. Loevschall-Jensen,[36] A. Loginov,[178] T. Lohse,[16] K. Lohwasser,[42] M. Lokajicek,[127] V. P. Lombardo,[5] B. A. Long,[22] J. D. Long,[89] R. E. Long,[72] L. Lopes,[126a] D. Lopez Mateos,[57] B. Lopez Paredes,[141] I. Lopez Paz,[12] J. Lorenz,[100] N. Lorenzo Martinez,[61] M. Losada,[164] P. Loscutoff,[15] X. Lou,[41] A. Lounis,[117] J. Love,[6] P. A. Love,[72] A. J. Lowe,[145,g] F. Lu,[33a] N. Lu,[89] H. J. Lubatti,[140] C. Luci,[134a,134b] A. Lucotte,[55] F. Luehring,[61] W. Lukas,[62] L. Luminari,[134a] O. Lundberg,[148a,148b] B. Lund-Jensen,[149] M. Lungwitz,[83] D. Lynn,[25] R. Lysak,[127] E. Lytken,[81] H. Ma,[25] L. L. Ma,[33d] G. Maccarrone,[47] A. Macchiolo,[101] J. Machado Miguens,[126a,126b] D. Macina,[30] D. Madaffari,[85] R. Madar,[48] H. J. Maddocks,[72] W. F. Mader,[44] A. Madsen,[168] M. Maeno,[8] T. Maeno,[25] A. Maevskiy,[99] E. Magradze,[54] K. Mahboubi,[48] J. Mahlstedt,[107] S. Mahmoud,[74] C. Maiani,[138] C. Maidantchik,[24a] A. A. Maier,[101] A. Maio,[126a,126b,126d] S. Majewski,[116] Y. Makida,[66] N. Makovec,[117] P. Mal,[138,y] B. Malaescu,[80] Pa. Malecki,[39] V. P. Maleev,[123] F. Malek,[55] U. Mallik,[63] D. Malon,[6] C. Malone,[145] S. Maltezos,[10] V. M. Malyshev,[109] S. Malyukov,[30] J. Mamuzic,[13b] B. Mandelli,[30] L. Mandelli,[91a] I. Mandić,[75] R. Mandrysch,[63] J. Maneira,[126a,126b] A. Manfredini,[101] L. Manhaes de Andrade Filho,[24b] J. A. Manjarres Ramos,[161b] A. Mann,[100] P. M. Manning,[139] A. Manousakis-Katsikakis,[9] B. Mansoulie,[138] R. Mantifel,[87] L. Mapelli,[30] L. March,[147c] J. F. Marchand,[29] G. Marchiori,[80] M. Marcisovsky,[127] C. P. Marino,[171] M. Marjanovic,[13a] C. N. Marques,[126a] F. Marroquim,[24a] S. P. Marsden,[84] Z. Marshall,[15] L. F. Marti,[17] S. Marti-Garcia,[169] B. Martin,[30] B. Martin,[90] T. A. Martin,[172] V. J. Martin,[46] B. Martin dit Latour,[14] H. Martinez,[138] M. Martinez,[12,o] S. Martin-Haugh,[131] A. C. Martyniuk,[78] M. Marx,[140] F. Marzano,[134a] A. Marzin,[30] L. Masetti,[83] T. Mashimo,[157] R. Mashinistov,[96] J. Masik,[84] A. L. Maslennikov,[109,d] I. Massa,[20a,20b] L. Massa,[20a,20b] N. Massol,[5] P. Mastrandrea,[150] A. Mastroberardino,[37a,37b] T. Masubuchi,[157] P. Mättig,[177] J. Mattmann,[83] J. Maurer,[26a] S. J. Maxfield,[74] D. A. Maximov,[109,d] R. Mazini,[153] L. Mazzaferro,[135a,135b] G. Mc Goldrick,[160] S. P. Mc Kee,[89] A. McCarn,[89] R. L. McCarthy,[150] T. G. McCarthy,[29] N. A. McCubbin,[131] K. W. McFarlane,[56,a] J. A. Mcfayden,[78] G. Mchedlidze,[54] S. J. McMahon,[131] R. A. McPherson,[171,k] J. Mechnich,[107] M. Medinnis,[42] S. Meehan,[31] S. Mehlhase,[100] A. Mehta,[74] K. Meier,[58a] C. Meineck,[100] B. Meirose,[81] C. Melachrinos,[31] B. R. Mellado Garcia,[147c] F. Meloni,[17] A. Mengarelli,[20a,20b] S. Menke,[101] E. Meoni,[163] K. M. Mercurio,[57] S. Mergelmeyer,[21] N. Meric,[138] P. Mermod,[49] L. Merola,[104a,104b] C. Meroni,[91a] F. S. Merritt,[31] H. Merritt,[111] A. Messina,[30,z] J. Metcalfe,[25] A. S. Mete,[165] C. Meyer,[83] C. Meyer,[122] J.-P. Meyer,[138] J. Meyer,[30] R. P. Middleton,[131] S. Migas,[74] L. Mijović,[21] G. Mikenberg,[174] M. Mikestikova,[127] M. Mikuž,[75] A. Milic,[30] D. W. Miller,[31] C. Mills,[46] A. Milov,[174] D. A. Milstead,[148a,148b] D. Milstein,[174] A. A. Minaenko,[130] Y. Minami,[157] I. A. Minashvili,[65] A. I. Mincer,[110] B. Mindur,[38a] M. Mineev,[65] Y. Ming,[175] L. M. Mir,[12] G. Mirabelli,[134a] T. Mitani,[173] J. Mitrevski,[100] V. A. Mitsou,[169] S. Mitsui,[66] A. Miucci,[49] P. S. Miyagawa,[141] J. U. Mjörnmark,[81] T. Moa,[148a,148b] K. Mochizuki,[85] S. Mohapatra,[35] W. Mohr,[48] S. Molander,[148a,148b] R. Moles-Valls,[169] K. Mönig,[42] C. Monini,[55] J. Monk,[36] E. Monnier,[85] J. Montejo Berlingen,[12] F. Monticelli,[71] S. Monzani,[134a,134b] R. W. Moore,[3] N. Morange,[63] D. Moreno,[83] M. Moreno Llácer,[54] P. Morettini,[50a] M. Morgenstern,[44] M. Morii,[57] S. Moritz,[83] A. K. Morley,[149] G. Mornacchi,[30] J. D. Morris,[76] L. Morvaj,[103] H. G. Moser,[101] M. Mosidze,[51b] J. Moss,[111] K. Motohashi,[159] R. Mount,[145] E. Mountricha,[25] S. V. Mouraviev,[96,a] E. J. W. Moyse,[86] S. Muanza,[85] R. D. Mudd,[18] F. Mueller,[58a] J. Mueller,[125] K. Mueller,[21] T. Mueller,[28] T. Mueller,[83] D. Muenstermann,[49] Y. Munwes,[155] J. A. Murillo Quijada,[18] W. J. Murray,[172,131] H. Musheghyan,[54] E. Musto,[154] A. G. Myagkov,[130,aa] M. Myska,[128] O. Nackenhorst,[54] J. Nadal,[54] K. Nagai,[62] R. Nagai,[159] Y. Nagai,[85]

K. Nagano,[66] A. Nagarkar,[111] Y. Nagasaka,[59] M. Nagel,[101] A. M. Nairz,[30] Y. Nakahama,[30] K. Nakamura,[66] T. Nakamura,[157] I. Nakano,[112] H. Namasivayam,[41] G. Nanava,[21] R. Narayan,[58b] T. Nattermann,[21] T. Naumann,[42] G. Navarro,[164] R. Nayyar,[7] H. A. Neal,[89] P. Yu. Nechaeva,[96] T. J. Neep,[84] P. D. Nef,[145] A. Negri,[121a,121b] G. Negri,[30] M. Negrini,[20a] S. Nektarijevic,[49] C. Nellist,[117] A. Nelson,[165] T. K. Nelson,[145] S. Nemecek,[127] P. Nemethy,[110] A. A. Nepomuceno,[24a] M. Nessi,[30,bb] M. S. Neubauer,[167] M. Neumann,[177] R. M. Neves,[110] P. Nevski,[25] P. R. Newman,[18] D. H. Nguyen,[6] R. B. Nickerson,[120] R. Nicolaidou,[138] B. Nicquevert,[30] J. Nielsen,[139] N. Nikiforou,[35] A. Nikiforov,[16] V. Nikolaenko,[130,aa] I. Nikolic-Audit,[80] K. Nikolics,[49] K. Nikolopoulos,[18] P. Nilsson,[8] Y. Ninomiya,[157] A. Nisati,[134a] R. Nisius,[101] T. Nobe,[159] L. Nodulman,[6] M. Nomachi,[118] I. Nomidis,[29] S. Norberg,[113] M. Nordberg,[30] O. Novgorodova,[44] S. Nowak,[101] M. Nozaki,[66] L. Nozka,[115] K. Ntekas,[10] G. Nunes Hanninger,[88] T. Nunnemann,[100] E. Nurse,[78] F. Nuti,[88] B. J. O'Brien,[46] F. O'grady,[7] D. C. O'Neil,[144] V. O'Shea,[53] F. G. Oakham,[29,f] H. Oberlack,[101] T. Obermann,[21] J. Ocariz,[80] A. Ochi,[67] M. I. Ochoa,[78] S. Oda,[70] S. Odaka,[66] H. Ogren,[61] A. Oh,[84] S. H. Oh,[45] C. C. Ohm,[15] H. Ohman,[168] W. Okamura,[118] H. Okawa,[25] Y. Okumura,[31] T. Okuyama,[157] A. Olariu,[26a] A. G. Olchevski,[65] S. A. Olivares Pino,[46] D. Oliveira Damazio,[25] E. Oliver Garcia,[169] A. Olszewski,[39] J. Olszowska,[39] A. Onofre,[126a,126e] P. U. E. Onyisi,[31,p] C. J. Oram,[161a] M. J. Oreglia,[31] Y. Oren,[155] D. Orestano,[136a,136b] N. Orlando,[73a,73b] C. Oropeza Barrera,[53] R. S. Orr,[160] B. Osculati,[50a,50b] R. Ospanov,[122] G. Otero y Garzon,[27] H. Otono,[70] M. Ouchrif,[137d] E. A. Ouellette,[171] F. Ould-Saada,[119] A. Ouraou,[138] K. P. Oussoren,[107] Q. Ouyang,[33a] A. Ovcharova,[15] M. Owen,[84] V. E. Ozcan,[19a] N. Ozturk,[8] K. Pachal,[120] A. Pacheco Pages,[12] C. Padilla Aranda,[12] M. Pagáčová,[48] S. Pagan Griso,[15] E. Paganis,[141] C. Pahl,[101] F. Paige,[25] P. Pais,[86] K. Pajchel,[119] G. Palacino,[161b] S. Palestini,[30] M. Palka,[38b] D. Pallin,[34] A. Palma,[126a,126b] J. D. Palmer,[18] Y. B. Pan,[175] E. Panagiotopoulou,[10] J. G. Panduro Vazquez,[77] P. Pani,[107] N. Panikashvili,[89] S. Panitkin,[25] D. Pantea,[26a] L. Paolozzi,[135a,135b] Th. D. Papadopoulou,[10] K. Papageorgiou,[156,m] A. Paramonov,[6] D. Paredes Hernandez,[156] M. A. Parker,[28] F. Parodi,[50a,50b] J. A. Parsons,[35] U. Parzefall,[48] E. Pasqualucci,[134a] S. Passaggio,[50a] A. Passeri,[136a] F. Pastore,[136a,136b,a] Fr. Pastore,[77] G. Pásztor,[29] S. Pataraia,[177] N. D. Patel,[152] J. R. Pater,[84] S. Patricelli,[104a,104b] T. Pauly,[30] J. Pearce,[171] L. E. Pedersen,[36] M. Pedersen,[119] S. Pedraza Lopez,[169] R. Pedro,[126a,126b] S. V. Peleganchuk,[109] D. Pelikan,[168] H. Peng,[33b] B. Penning,[31] J. Penwell,[61] D. V. Perepelitsa,[25] E. Perez Codina,[161a] M. T. Pérez García-Estañ,[169] V. Perez Reale,[35] L. Perini,[91a,91b] H. Pernegger,[30] S. Perrella,[104a,104b] R. Perrino,[73a] R. Peschke,[42] V. D. Peshekhonov,[65] K. Peters,[30] R. F. Y. Peters,[84] B. A. Petersen,[30] T. C. Petersen,[36] E. Petit,[42] A. Petridis,[148a,148b] C. Petridou,[156] E. Petrolo,[134a] F. Petrucci,[136a,136b] N. E. Pettersson,[159] R. Pezoa,[32b] P. W. Phillips,[131] G. Piacquadio,[145] E. Pianori,[172] A. Picazio,[49] E. Piccaro,[76] M. Piccinini,[20a,20b] R. Piegaia,[27] D. T. Pignotti,[111] J. E. Pilcher,[31] A. D. Pilkington,[78] J. Pina,[126a,126b,126d] M. Pinamonti,[166a,166c,cc] A. Pinder,[120] J. L. Pinfold,[3] A. Pingel,[36] B. Pinto,[126a] S. Pires,[80] M. Pitt,[174] C. Pizio,[91a,91b] L. Plazak,[146a] M.-A. Pleier,[25] V. Pleskot,[129] E. Plotnikova,[65] P. Plucinski,[148a,148b] D. Pluth,[64] S. Poddar,[58a] F. Podlyski,[34] R. Poettgen,[83] L. Poggioli,[117] D. Pohl,[21] M. Pohl,[49] G. Polesello,[121a] A. Policicchio,[37a,37b] R. Polifka,[160] A. Polini,[20a] C. S. Pollard,[45] V. Polychronakos,[25] K. Pommès,[30] L. Pontecorvo,[134a] B. G. Pope,[90] G. A. Popeneciu,[26b] D. S. Popovic,[13a] A. Poppleton,[30] X. Portell Bueso,[12] S. Pospisil,[128] K. Potamianos,[15] I. N. Potrap,[65] C. J. Potter,[151] C. T. Potter,[116] G. Poulard,[30] J. Poveda,[61] V. Pozdnyakov,[65] P. Pralavorio,[85] A. Pranko,[15] S. Prasad,[30] R. Pravahan,[8] S. Prell,[64] D. Price,[84] J. Price,[74] L. E. Price,[6] D. Prieur,[125] M. Primavera,[73a] M. Proissl,[46] K. Prokofiev,[47] F. Prokoshin,[32b] E. Protopapadaki,[138] S. Protopopescu,[25] J. Proudfoot,[6] M. Przybycien,[38a] H. Przysiezniak,[5] E. Ptacek,[116] D. Puddu,[136a,136b] E. Pueschel,[86] D. Puldon,[150] M. Purohit,[25,dd] P. Puzo,[117] J. Qian,[89] G. Qin,[53] Y. Qin,[84] A. Quadt,[54] D. R. Quarrie,[15] W. B. Quayle,[166a,166b] M. Queitsch-Maitland,[84] D. Quilty,[53] A. Qureshi,[161b] V. Radeka,[25] V. Radescu,[42] S. K. Radhakrishnan,[150] P. Radloff,[116] P. Rados,[88] F. Ragusa,[91a,91b] G. Rahal,[180] S. Rajagopalan,[25] M. Rammensee,[30] A. S. Randle-Conde,[40] C. Rangel-Smith,[168] K. Rao,[165] F. Rauscher,[100] T. C. Rave,[48] T. Ravenscroft,[53] M. Raymond,[30] A. L. Read,[119] N. P. Readioff,[74] D. M. Rebuzzi,[121a,121b] A. Redelbach,[176] G. Redlinger,[25] R. Reece,[139] K. Reeves,[41] L. Rehnisch,[16] H. Reisin,[27] M. Relich,[165] C. Rembser,[30] H. Ren,[33a] Z. L. Ren,[153] A. Renaud,[117] M. Rescigno,[134a] S. Resconi,[91a] O. L. Rezanova,[109,d] P. Reznicek,[129] R. Rezvani,[95] R. Richter,[101] M. Ridel,[80] P. Rieck,[16] J. Rieger,[54] M. Rijssenbeek,[150] A. Rimoldi,[121a,121b] L. Rinaldi,[20a] E. Ritsch,[62] I. Riu,[12] F. Rizatdinova,[114] E. Rizvi,[76] S. H. Robertson,[87,k] A. Robichaud-Veronneau,[87] D. Robinson,[28] J. E. M. Robinson,[84] A. Robson,[53] C. Roda,[124a,124b] L. Rodrigues,[30] S. Roe,[30] O. Røhne,[119] S. Rolli,[163] A. Romaniouk,[98] M. Romano,[20a,20b] E. Romero Adam,[169] N. Rompotis,[140] M. Ronzani,[48] L. Roos,[80] E. Ros,[169] S. Rosati,[134a] K. Rosbach,[49] M. Rose,[77] P. Rose,[139] P. L. Rosendahl,[14] O. Rosenthal,[143] V. Rossetti,[148a,148b] E. Rossi,[104a,104b] L. P. Rossi,[50a] R. Rosten,[140] M. Rotaru,[26a] I. Roth,[174] J. Rothberg,[140] D. Rousseau,[117] C. R. Royon,[138] A. Rozanov,[85] Y. Rozen,[154] X. Ruan,[147c] F. Rubbo,[12] I. Rubinskiy,[42] V. I. Rud,[99] C. Rudolph,[44] M. S. Rudolph,[160] F. Rühr,[48] A. Ruiz-Martinez,[30] Z. Rurikova,[48] N. A. Rusakovich,[65] A. Ruschke,[100]

J. P. Rutherfoord,[7] N. Ruthmann,[48] Y. F. Ryabov,[123] M. Rybar,[129] G. Rybkin,[117] N. C. Ryder,[120] A. F. Saavedra,[152] G. Sabato,[107] S. Sacerdoti,[27] A. Saddique,[3] I. Sadeh,[155] H. F-W. Sadrozinski,[139] R. Sadykov,[65] F. Safai Tehrani,[134a] H. Sakamoto,[157] Y. Sakurai,[173] G. Salamanna,[136a,136b] A. Salamon,[135a] M. Saleem,[113] D. Salek,[107] P. H. Sales De Bruin,[140] D. Salihagic,[101] A. Salnikov,[145] J. Salt,[169] D. Salvatore,[37a,37b] F. Salvatore,[151] A. Salvucci,[106] A. Salzburger,[30] D. Sampsonidis,[156] A. Sanchez,[104a,104b] J. Sánchez,[169] V. Sanchez Martinez,[169] H. Sandaker,[14] R. L. Sandbach,[76] H. G. Sander,[83] M. P. Sanders,[100] M. Sandhoff,[177] T. Sandoval,[28] C. Sandoval,[164] R. Sandstroem,[101] D. P. C. Sankey,[131] A. Sansoni,[47] C. Santoni,[34] R. Santonico,[135a,135b] H. Santos,[126a] I. Santoyo Castillo,[151] K. Sapp,[125] A. Sapronov,[65] J. G. Saraiva,[126a,126d] B. Sarrazin,[21] G. Sartisohn,[177] O. Sasaki,[66] Y. Sasaki,[157] G. Sauvage,[5,a] E. Sauvan,[5] P. Savard,[160,f] D. O. Savu,[30] C. Sawyer,[120] L. Sawyer,[79,n] D. H. Saxon,[53] J. Saxon,[122] C. Sbarra,[20a] A. Sbrizzi,[20a,20b] T. Scanlon,[78] D. A. Scannicchio,[165] M. Scarcella,[152] V. Scarfone,[37a,37b] J. Schaarschmidt,[174] P. Schacht,[101] D. Schaefer,[30] R. Schaefer,[42] S. Schaepe,[21] S. Schaetzel,[58b] U. Schäfer,[83] A. C. Schaffer,[117] D. Schaile,[100] R. D. Schamberger,[150] V. Scharf,[58a] V. A. Schegelsky,[123] D. Scheirich,[129] M. Schernau,[165] M. I. Scherzer,[35] C. Schiavi,[50a,50b] J. Schieck,[100] C. Schillo,[48] M. Schioppa,[37a,37b] S. Schlenker,[30] E. Schmidt,[48] K. Schmieden,[30] C. Schmitt,[83] S. Schmitt,[58b] B. Schneider,[17] Y. J. Schnellbach,[74] U. Schnoor,[44] L. Schoeffel,[138] A. Schoening,[58b] B. D. Schoenrock,[90] A. L. S. Schorlemmer,[54] M. Schott,[83] D. Schouten,[161a] J. Schovancova,[25] S. Schramm,[160] M. Schreyer,[176] C. Schroeder,[83] N. Schuh,[83] M. J. Schultens,[21] H.-C. Schultz-Coulon,[58a] H. Schulz,[16] M. Schumacher,[48] B. A. Schumm,[139] Ph. Schune,[138] C. Schwanenberger,[84] A. Schwartzman,[145] T. A. Schwarz,[89] Ph. Schwegler,[101] Ph. Schwemling,[138] R. Schwienhorst,[90] J. Schwindling,[138] T. Schwindt,[21] M. Schwoerer,[5] F. G. Sciacca,[17] E. Scifo,[117] G. Sciolla,[23] W. G. Scott,[131] F. Scuri,[124a,124b] F. Scutti,[21] J. Searcy,[89] G. Sedov,[42] E. Sedykh,[123] S. C. Seidel,[105] A. Seiden,[139] F. Seifert,[128] J. M. Seixas,[24a] G. Sekhniaidze,[104a] S. J. Sekula,[40] K. E. Selbach,[46] D. M. Seliverstov,[123,a] G. Sellers,[74] N. Semprini-Cesari,[20a,20b] C. Serfon,[30] L. Serin,[117] L. Serkin,[54] T. Serre,[85] R. Seuster,[161a] H. Severini,[113] T. Sfiligoj,[75] F. Sforza,[101] A. Sfyrla,[30] E. Shabalina,[54] M. Shamim,[116] L. Y. Shan,[33a] R. Shang,[167] J. T. Shank,[22] M. Shapiro,[15] P. B. Shatalov,[97] K. Shaw,[166a,166b] C. Y. Shehu,[151] P. Sherwood,[78] L. Shi,[153,ee] S. Shimizu,[67] C. O. Shimmin,[165] M. Shimojima,[102] M. Shiyakova,[65] A. Shmeleva,[96] M. J. Shochet,[31] D. Short,[120] S. Shrestha,[64] E. Shulga,[98] M. A. Shupe,[7] S. Shushkevich,[42] P. Sicho,[127] O. Sidiropoulou,[156] D. Sidorov,[114] A. Sidoti,[134a] F. Siegert,[44] Dj. Sijacki,[13a] J. Silva,[126a,126d] Y. Silver,[155] D. Silverstein,[145] S. B. Silverstein,[148a] V. Simak,[128] O. Simard,[5] Lj. Simic,[13a] S. Simion,[117] E. Simioni,[83] B. Simmons,[78] R. Simoniello,[91a,91b] M. Simonyan,[36] P. Sinervo,[160] N. B. Sinev,[116] V. Sipica,[143] G. Siragusa,[176] A. Sircar,[79] A. N. Sisakyan,[65,a] S. Yu. Sivoklokov,[99] J. Sjölin,[148a,148b] T. B. Sjursen,[14] H. P. Skottowe,[57] K. Yu. Skovpen,[109] P. Skubic,[113] M. Slater,[18] T. Slavicek,[128] M. Slawinska,[107] K. Sliwa,[163] V. Smakhtin,[174] B. H. Smart,[46] L. Smestad,[14] S. Yu. Smirnov,[98] Y. Smirnov,[98] L. N. Smirnova,[99,ff] O. Smirnova,[81] K. M. Smith,[53] M. Smizanska,[72] K. Smolek,[128] A. A. Snesarev,[96] G. Snidero,[76] S. Snyder,[25] R. Sobie,[171,k] F. Socher,[44] A. Soffer,[155] D. A. Soh,[153,ee] C. A. Solans,[30] M. Solar,[128] J. Solc,[128] E. Yu. Soldatov,[98] U. Soldevila,[169] A. A. Solodkov,[130] A. Soloshenko,[65] O. V. Solovyanov,[130] V. Solovyev,[123] P. Sommer,[48] H. Y. Song,[33b] N. Soni,[1] A. Sood,[15] A. Sopczak,[128] B. Sopko,[128] V. Sopko,[128] V. Sorin,[12] M. Sosebee,[8] R. Soualah,[166a,166c] P. Soueid,[95] A. M. Soukharev,[109,d] D. South,[42] S. Spagnolo,[73a,73b] F. Spanò,[77] W. R. Spearman,[57] F. Spettel,[101] R. Spighi,[20a] G. Spigo,[30] L. A. Spiller,[88] M. Spousta,[129] T. Spreitzer,[160] B. Spurlock,[8] R. D. St. Denis,[53,a] S. Staerz,[44] J. Stahlman,[122] R. Stamen,[58a] S. Stamm,[16] E. Stanecka,[39] R. W. Stanek,[6] C. Stanescu,[136a] M. Stanescu-Bellu,[42] M. M. Stanitzki,[42] S. Stapnes,[119] E. A. Starchenko,[130] J. Stark,[55] P. Staroba,[127] P. Starovoitov,[42] R. Staszewski,[39] P. Stavina,[146a,a] P. Steinberg,[25] B. Stelzer,[144] H. J. Stelzer,[30] O. Stelzer-Chilton,[161a] H. Stenzel,[52] S. Stern,[101] G. A. Stewart,[53] J. A. Stillings,[21] M. C. Stockton,[87] M. Stoebe,[87] G. Stoicea,[26a] P. Stolte,[54] S. Stonjek,[101] A. R. Stradling,[8] A. Straessner,[44] M. E. Stramaglia,[17] J. Strandberg,[149] S. Strandberg,[148a,148b] A. Strandlie,[119] E. Strauss,[145] M. Strauss,[113] P. Strizenec,[146b] R. Ströhmer,[176] D. M. Strom,[116] R. Stroynowski,[40] A. Strubig,[106] S. A. Stucci,[17] B. Stugu,[14] N. A. Styles,[42] D. Su,[145] J. Su,[125] R. Subramaniam,[79] A. Succurro,[12] Y. Sugaya,[118] C. Suhr,[108] M. Suk,[128] V. V. Sulin,[96] S. Sultansoy,[4d] T. Sumida,[68] S. Sun,[57] X. Sun,[33a] J. E. Sundermann,[48] K. Suruliz,[141] G. Susinno,[37a,37b] M. R. Sutton,[151] Y. Suzuki,[66] M. Svatos,[127] S. Swedish,[170] M. Swiatlowski,[145] I. Sykora,[146a] T. Sykora,[129] D. Ta,[90] C. Taccini,[136a,136b] K. Tackmann,[42] J. Taenzer,[160] A. Taffard,[165] R. Tafirout,[161a] N. Taiblum,[155] H. Takai,[25] R. Takashima,[69] H. Takeda,[67] T. Takeshita,[142] Y. Takubo,[66] M. Talby,[85] A. A. Talyshev,[109,d] J. Y. C. Tam,[176] K. G. Tan,[88] J. Tanaka,[157] R. Tanaka,[117] S. Tanaka,[133] S. Tanaka,[66] A. J. Tanasijczuk,[144] B. B. Tannenwald,[111] N. Tannoury,[21] S. Tapprogge,[83] S. Tarem,[154] F. Tarrade,[29] G. F. Tartarelli,[91a] P. Tas,[129] M. Tasevsky,[127] T. Tashiro,[68] E. Tassi,[37a,37b] A. Tavares Delgado,[126a,126b] Y. Tayalati,[137d] F. E. Taylor,[94] G. N. Taylor,[88] W. Taylor,[161b] F. A. Teischinger,[30] M. Teixeira Dias Castanheira,[76] P. Teixeira-Dias,[77] K. K. Temming,[48] H. Ten Kate,[30] P. K. Teng,[153]

J. J. Teoh,[118] S. Terada,[66] K. Terashi,[157] J. Terron,[82] S. Terzo,[101] M. Testa,[47] R. J. Teuscher,[160,k] J. Therhaag,[21] T. Theveneaux-Pelzer,[34] J. P. Thomas,[18] J. Thomas-Wilsker,[77] E. N. Thompson,[35] P. D. Thompson,[18] P. D. Thompson,[160] R. J. Thompson,[84] A. S. Thompson,[53] L. A. Thomsen,[36] E. Thomson,[122] M. Thomson,[28] W. M. Thong,[88] R. P. Thun,[89,a] F. Tian,[35] M. J. Tibbetts,[15] V. O. Tikhomirov,[96,gg] Yu. A. Tikhonov,[109,d] S. Timoshenko,[98] E. Tiouchichine,[85] P. Tipton,[178] S. Tisserant,[85] T. Todorov,[5] S. Todorova-Nova,[129] B. Toggerson,[7] J. Tojo,[70] S. Tokár,[146a] K. Tokushuku,[66] K. Tollefson,[90] E. Tolley,[57] L. Tomlinson,[84] M. Tomoto,[103] L. Tompkins,[31] K. Toms,[105] N. D. Topilin,[65] E. Torrence,[116] H. Torres,[144] E. Torró Pastor,[169] J. Toth,[85,hh] F. Touchard,[85] D. R. Tovey,[141] H. L. Tran,[117] T. Trefzger,[176] L. Tremblet,[30] A. Tricoli,[30] I. M. Trigger,[161a] S. Trincaz-Duvoid,[80] M. F. Tripiana,[12] W. Trischuk,[160] B. Trocmé,[55] C. Troncon,[91a] M. Trottier-McDonald,[15] M. Trovatelli,[136a,136b] P. True,[90] M. Trzebinski,[39] A. Trzupek,[39] C. Tsarouchas,[30] J. C-L. Tseng,[120] P. V. Tsiareshka,[92] D. Tsionou,[138] G. Tsipolitis,[10] N. Tsirintanis,[9] S. Tsiskaridze,[12] V. Tsiskaridze,[48] E. G. Tskhadadze,[51a] I. I. Tsukerman,[97] V. Tsulaia,[15] S. Tsuno,[66] D. Tsybychev,[150] A. Tudorache,[26a] V. Tudorache,[26a] A. N. Tuna,[122] S. A. Tupputi,[20a,20b] S. Turchikhin,[99,ff] D. Turecek,[128] I. Turk Cakir,[4c] R. Turra,[91a,91b] P. M. Tuts,[35] A. Tykhonov,[49] M. Tylmad,[148a,148b] M. Tyndel,[131] K. Uchida,[21] I. Ueda,[157] R. Ueno,[29] M. Ughetto,[85] M. Ugland,[14] M. Uhlenbrock,[21] F. Ukegawa,[162] G. Unal,[30] A. Undrus,[25] G. Unel,[165] F. C. Ungaro,[48] Y. Unno,[66] C. Unverdorben,[100] D. Urbaniec,[35] P. Urquijo,[88] G. Usai,[8] A. Usanova,[62] L. Vacavant,[85] V. Vacek,[128] B. Vachon,[87] N. Valencic,[107] S. Valentinetti,[20a,20b] A. Valero,[169] L. Valery,[34] S. Valkar,[129] E. Valladolid Gallego,[169] S. Vallecorsa,[49] J. A. Valls Ferrer,[169] W. Van Den Wollenberg,[107] P. C. Van Der Deijl,[107] R. van der Geer,[107] H. van der Graaf,[107] R. Van Der Leeuw,[107] D. van der Ster,[30] N. van Eldik,[30] P. van Gemmeren,[6] J. Van Nieuwkoop,[144] I. van Vulpen,[107] M. C. van Woerden,[30] M. Vanadia,[134a,134b] W. Vandelli,[30] R. Vanguri,[122] A. Vaniachine,[6] P. Vankov,[42] F. Vannucci,[80] G. Vardanyan,[179] R. Vari,[134a] E. W. Varnes,[7] T. Varol,[86] D. Varouchas,[80] A. Vartapetian,[8] K. E. Varvell,[152] F. Vazeille,[34] T. Vazquez Schroeder,[54] J. Veatch,[7] F. Veloso,[126a,126c] S. Veneziano,[134a] A. Ventura,[73a,73b] D. Ventura,[86] M. Venturi,[171] N. Venturi,[160] A. Venturini,[23] V. Vercesi,[121a] M. Verducci,[134a,134b] W. Verkerke,[107] J. C. Vermeulen,[107] A. Vest,[44] M. C. Vetterli,[144,f] O. Viazlo,[81] I. Vichou,[167] T. Vickey,[147c,ii] O. E. Vickey Boeriu,[147c] G. H. A. Viehhauser,[120] S. Viel,[170] R. Vigne,[30] M. Villa,[20a,20b] M. Villaplana Perez,[91a,91b] E. Vilucchi,[47] M. G. Vincter,[29] V. B. Vinogradov,[65] J. Virzi,[15] I. Vivarelli,[151] F. Vives Vaque,[3] S. Vlachos,[10] D. Vladoiu,[100] M. Vlasak,[128] A. Vogel,[21] M. Vogel,[32a] P. Vokac,[128] G. Volpi,[124a,124b] M. Volpi,[88] H. von der Schmitt,[101] H. von Radziewski,[48] E. von Toerne,[21] V. Vorobel,[129] K. Vorobev,[98] M. Vos,[169] R. Voss,[30] J. H. Vossebeld,[74] N. Vranjes,[138] M. Vranjes Milosavljevic,[13a] V. Vrba,[127] M. Vreeswijk,[107] T. Vu Anh,[48] R. Vuillermet,[30] I. Vukotic,[31] Z. Vykydal,[128] P. Wagner,[21] W. Wagner,[177] H. Wahlberg,[71] S. Wahrmund,[44] J. Wakabayashi,[103] J. Walder,[72] R. Walker,[100] W. Walkowiak,[143] R. Wall,[178] P. Waller,[74] B. Walsh,[178] C. Wang,[153,jj] C. Wang,[45] F. Wang,[175] H. Wang,[15] H. Wang,[40] J. Wang,[42] J. Wang,[33a] K. Wang,[87] R. Wang,[105] S. M. Wang,[153] T. Wang,[21] X. Wang,[178] C. Wanotayaroj,[116] A. Warburton,[87] C. P. Ward,[28] D. R. Wardrope,[78] M. Warsinsky,[48] A. Washbrook,[46] C. Wasicki,[42] P. M. Watkins,[18] A. T. Watson,[18] I. J. Watson,[152] M. F. Watson,[18] G. Watts,[140] S. Watts,[84] B. M. Waugh,[78] S. Webb,[84] M. S. Weber,[17] S. W. Weber,[176] J. S. Webster,[31] A. R. Weidberg,[120] P. Weigell,[101] B. Weinert,[61] J. Weingarten,[54] C. Weiser,[48] H. Weits,[107] P. S. Wells,[30] T. Wenaus,[25] D. Wendland,[16] Z. Weng,[153,ee] T. Wengler,[30] S. Wenig,[30] N. Wermes,[21] M. Werner,[48] P. Werner,[30] M. Wessels,[58a] J. Wetter,[163] K. Whalen,[29] A. White,[8] M. J. White,[1] R. White,[32b] S. White,[124a,124b] D. Whiteson,[165] D. Wicke,[177] F. J. Wickens,[131] W. Wiedenmann,[175] M. Wielers,[131] P. Wienemann,[21] C. Wiglesworth,[36] L. A. M. Wiik-Fuchs,[21] P. A. Wijeratne,[78] A. Wildauer,[101] M. A. Wildt,[42,kk] H. G. Wilkens,[30] J. Z. Will,[100] H. H. Williams,[122] S. Williams,[28] C. Willis,[90] S. Willocq,[86] A. Wilson,[89] J. A. Wilson,[18] I. Wingerter-Seez,[5] F. Winklmeier,[116] B. T. Winter,[21] M. Wittgen,[145] T. Wittig,[43] J. Wittkowski,[100] S. J. Wollstadt,[83] M. W. Wolter,[39] H. Wolters,[126a,126c] B. K. Wosiek,[39] J. Wotschack,[30] M. J. Woudstra,[84] K. W. Wozniak,[39] M. Wright,[53] M. Wu,[55] S. L. Wu,[175] X. Wu,[49] Y. Wu,[89] E. Wulf,[35] T. R. Wyatt,[84] B. M. Wynne,[46] S. Xella,[36] M. Xiao,[138] D. Xu,[33a] L. Xu,[33b,ll] B. Yabsley,[152] S. Yacoob,[147b,mm] R. Yakabe,[67] M. Yamada,[66] H. Yamaguchi,[157] Y. Yamaguchi,[118] A. Yamamoto,[66] K. Yamamoto,[64] S. Yamamoto,[157] T. Yamamura,[157] T. Yamanaka,[157] K. Yamauchi,[103] Y. Yamazaki,[67] Z. Yan,[22] H. Yang,[33e] H. Yang,[175] U. K. Yang,[84] Y. Yang,[111] S. Yanush,[93] L. Yao,[33a] W-M. Yao,[15] Y. Yasu,[66] E. Yatsenko,[42] K. H. Yau Wong,[21] J. Ye,[40] S. Ye,[25] I. Yeletskikh,[65] A. L. Yen,[57] E. Yildirim,[42] M. Yilmaz,[4b] R. Yoosoofmiya,[125] K. Yorita,[173] R. Yoshida,[6] K. Yoshihara,[157] C. Young,[145] C. J. S. Young,[30] S. Youssef,[22] D. R. Yu,[15] J. Yu,[8] J. M. Yu,[89] J. Yu,[114] L. Yuan,[67] A. Yurkewicz,[108] I. Yusuff,[28,nn] B. Zabinski,[39] R. Zaidan,[63] A. M. Zaitsev,[130,aa] A. Zaman,[150] S. Zambito,[23] L. Zanello,[134a,134b] D. Zanzi,[88] C. Zeitnitz,[177] M. Zeman,[128] A. Zemla,[38a] K. Zengel,[23] O. Zenin,[130] T. Ženiš,[146a] D. Zerwas,[117] G. Zevi della Porta,[57] D. Zhang,[89] F. Zhang,[175] H. Zhang,[90] J. Zhang,[6] L. Zhang,[153] X. Zhang,[33d] Z. Zhang,[117] Z. Zhao,[33b] A. Zhemchugov,[65] J. Zhong,[120] B. Zhou,[89] L. Zhou,[35] N. Zhou,[165]

C. G. Zhu,[33d] H. Zhu,[33a] J. Zhu,[89] Y. Zhu,[33b] X. Zhuang,[33a] K. Zhukov,[96] A. Zibell,[176] D. Zieminska,[61] N. I. Zimine,[65] C. Zimmermann,[83] R. Zimmermann,[21] S. Zimmermann,[21] S. Zimmermann,[48] Z. Zinonos,[54] M. Ziolkowski,[143] G. Zobernig,[175] A. Zoccoli,[20a,20b] M. zur Nedden,[16] G. Zurzolo,[104a,104b] V. Zutshi[108] and L. Zwalinski[30]

(ATLAS Collaboration)

[1]*Department of Physics, University of Adelaide, Adelaide, Australia*
[2]*Physics Department, SUNY Albany, Albany, New York, USA*
[3]*Department of Physics, University of Alberta, Edmonton, AB, Canada*
[4a]*Department of Physics, Ankara University, Ankara, Turkey*
[4b]*Department of Physics, Gazi University, Ankara, Turkey*
[4c]*Istanbul Aydin University, Istanbul, Turkey*
[4d]*Division of Physics, TOBB University of Economics and Technology, Ankara, Turkey*
[5]*LAPP, CNRS/IN2P3 and Université de Savoie, Annecy-le-Vieux, France*
[6]*High Energy Physics Division, Argonne National Laboratory, Argonne, Illinois, USA*
[7]*Department of Physics, University of Arizona, Tucson, Arizona, USA*
[8]*Department of Physics, The University of Texas at Arlington, Arlington, Texas, USA*
[9]*Physics Department, University of Athens, Athens, Greece*
[10]*Physics Department, National Technical University of Athens, Zografou, Greece*
[11]*Institute of Physics, Azerbaijan Academy of Sciences, Baku, Azerbaijan*
[12]*Institut de Física d'Altes Energies and Departament de Física de la Universitat Autònoma de Barcelona, Barcelona, Spain*
[13a]*Institute of Physics, University of Belgrade, Belgrade, Serbia*
[13b]*Vinca Institute of Nuclear Sciences, University of Belgrade, Belgrade, Serbia*
[14]*Department for Physics and Technology, University of Bergen, Bergen, Norway*
[15]*Physics Division, Lawrence Berkeley National Laboratory and University of California, Berkeley, California, USA*
[16]*Department of Physics, Humboldt University, Berlin, Germany*
[17]*Albert Einstein Center for Fundamental Physics and Laboratory for High Energy Physics, University of Bern, Bern, Switzerland*
[18]*School of Physics and Astronomy, University of Birmingham, Birmingham, United Kingdom*
[19a]*Department of Physics, Bogazici University, Istanbul, Turkey*
[19b]*Department of Physics, Dogus University, Istanbul, Turkey*
[19c]*Department of Physics Engineering, Gaziantep University, Gaziantep, Turkey*
[20a]*INFN Sezione di Bologna, Italy*
[20b]*Dipartimento di Fisica e Astronomia, Università di Bologna, Bologna, Italy*
[21]*Physikalisches Institut, University of Bonn, Bonn, Germany*
[22]*Department of Physics, Boston University, Boston, Massachusetts, USA*
[23]*Department of Physics, Brandeis University, Waltham, Massachusetts, USA*
[24a]*Universidade Federal do Rio De Janeiro COPPE/EE/IF, Rio de Janeiro, Brazil*
[24b]*Federal University of Juiz de Fora (UFJF), Juiz de Fora, Brazil*
[24c]*Federal University of Sao Joao del Rei (UFSJ), Sao Joao del Rei, Brazil*
[24d]*Instituto de Fisica, Universidade de Sao Paulo, Sao Paulo, Brazil*
[25]*Physics Department, Brookhaven National Laboratory, Upton, New York, USA*
[26a]*National Institute of Physics and Nuclear Engineering, Bucharest, Romania*
[26b]*National Institute for Research and Development of Isotopic and Molecular Technologies, Physics Department, Cluj Napoca, Romania*
[26c]*University Politehnica Bucharest, Bucharest, Romania*
[26d]*West University in Timisoara, Timisoara, Romania*
[27]*Departamento de Física, Universidad de Buenos Aires, Buenos Aires, Argentina*
[28]*Cavendish Laboratory, University of Cambridge, Cambridge, United Kingdom*
[29]*Department of Physics, Carleton University, Ottawa, ON, Canada*
[30]*CERN, Geneva, Switzerland*
[31]*Enrico Fermi Institute, University of Chicago, Chicago, Illinois, USA*
[32a]*Departamento de Física, Pontificia Universidad Católica de Chile, Santiago, Chile*
[32b]*Departamento de Física, Universidad Técnica Federico Santa María, Valparaíso, Chile*
[33a]*Institute of High Energy Physics, Chinese Academy of Sciences, Beijing, China*
[33b]*Department of Modern Physics, University of Science and Technology of China, Anhui, China*
[33c]*Department of Physics, Nanjing University, Jiangsu, China*

[33d]*School of Physics, Shandong University, Shandong, China*
[33e]*Physics Department, Shanghai Jiao Tong University, Shanghai, China*
[33f]*Physics Department, Tsinghua University, Beijing 100084, China*
[34]*Laboratoire de Physique Corpusculaire, Clermont Université and Université Blaise Pascal and CNRS/IN2P3, Clermont-Ferrand, France*
[35]*Nevis Laboratory, Columbia University, Irvington, New York, USA*
[36]*Niels Bohr Institute, University of Copenhagen, Kobenhavn, Denmark*
[37a]*INFN Gruppo Collegato di Cosenza, Laboratori Nazionali di Frascati, Italy*
[37b]*Dipartimento di Fisica, Università della Calabria, Rende, Italy*
[38a]*AGH University of Science and Technology, Faculty of Physics and Applied Computer Science, Krakow, Poland*
[38b]*Marian Smoluchowski Institute of Physics, Jagiellonian University, Krakow, Poland*
[39]*The Henryk Niewodniczanski Institute of Nuclear Physics, Polish Academy of Sciences, Krakow, Poland*
[40]*Physics Department, Southern Methodist University, Dallas, Texas, USA*
[41]*Physics Department, University of Texas at Dallas, Richardson, Texas, USA*
[42]*DESY, Hamburg and Zeuthen, Germany*
[43]*Institut für Experimentelle Physik IV, Technische Universität Dortmund, Dortmund, Germany*
[44]*Institut für Kern- und Teilchenphysik, Technische Universität Dresden, Dresden, Germany*
[45]*Department of Physics, Duke University, Durham, North Carolina, USA*
[46]*SUPA - School of Physics and Astronomy, University of Edinburgh, Edinburgh, United Kingdom*
[47]*INFN Laboratori Nazionali di Frascati, Frascati, Italy*
[48]*Fakultät für Mathematik und Physik, Albert-Ludwigs-Universität, Freiburg, Germany*
[49]*Section de Physique, Université de Genève, Geneva, Switzerland*
[50a]*INFN Sezione di Genova, Genova, Italy*
[50b]*Dipartimento di Fisica, Università di Genova, Genova, Italy*
[51a]*E. Andronikashvili Institute of Physics, Iv. Javakhishvili Tbilisi State University, Tbilisi, Georgia*
[51b]*High Energy Physics Institute, Tbilisi State University, Tbilisi, Georgia*
[52]*II Physikalisches Institut, Justus-Liebig-Universität Giessen, Giessen, Germany*
[53]*SUPA - School of Physics and Astronomy, University of Glasgow, Glasgow, United Kingdom*
[54]*II Physikalisches Institut, Georg-August-Universität, Göttingen, Germany*
[55]*Laboratoire de Physique Subatomique et de Cosmologie, Université Grenoble-Alpes, CNRS/IN2P3, Grenoble, France*
[56]*Department of Physics, Hampton University, Hampton, Virginia, USA*
[57]*Laboratory for Particle Physics and Cosmology, Harvard University, Cambridge, Massachusetts, USA*
[58a]*Kirchhoff-Institut für Physik, Ruprecht-Karls-Universität Heidelberg, Heidelberg, Germany*
[58b]*Physikalisches Institut, Ruprecht-Karls-Universität Heidelberg, Heidelberg, Germany*
[58c]*ZITI Institut für technische Informatik, Ruprecht-Karls-Universität Heidelberg, Mannheim, Germany*
[59]*Faculty of Applied Information Science, Hiroshima Institute of Technology, Hiroshima, Japan*
[60a]*Department of Physics, The Chinese University of Hong Kong, Shatin, N.T., Hong Kong, China*
[60b]*Department of Physics, The University of Hong Kong, Hong Kong, China*
[60c]*Department of Physics, The Hong Kong University of Science and Technology, Clear Water Bay, Kowloon, Hong Kong, China*
[61]*Department of Physics, Indiana University, Bloomington, Indiana, USA*
[62]*Institut für Astro- und Teilchenphysik, Leopold-Franzens-Universität, Innsbruck, Austria*
[63]*University of Iowa, Iowa City, Iowa, USA*
[64]*Department of Physics and Astronomy, Iowa State University, Ames, Iowa, USA*
[65]*Joint Institute for Nuclear Research, JINR Dubna, Dubna, Russia*
[66]*KEK, High Energy Accelerator Research Organization, Tsukuba, Japan*
[67]*Graduate School of Science, Kobe University, Kobe, Japan*
[68]*Faculty of Science, Kyoto University, Kyoto, Japan*
[69]*Kyoto University of Education, Kyoto, Japan*
[70]*Department of Physics, Kyushu University, Fukuoka, Japan*
[71]*Instituto de Física La Plata, Universidad Nacional de La Plata and CONICET, La Plata, Argentina*
[72]*Physics Department, Lancaster University, Lancaster, United Kingdom*
[73a]*INFN Sezione di Lecce, Lecce, Italy*
[73b]*Dipartimento di Matematica e Fisica, Università del Salento, Lecce, Italy*
[74]*Oliver Lodge Laboratory, University of Liverpool, Liverpool, United Kingdom*
[75]*Department of Physics, Jožef Stefan Institute and University of Ljubljana, Ljubljana, Slovenia*
[76]*School of Physics and Astronomy, Queen Mary University of London, London, United Kingdom*
[77]*Department of Physics, Royal Holloway University of London, Surrey, United Kingdom*

[78]*Department of Physics and Astronomy, University College London, London, United Kingdom*
[79]*Louisiana Tech University, Ruston, Louisiana, USA*
[80]*Laboratoire de Physique Nucléaire et de Hautes Energies, UPMC and Université Paris-Diderot and CNRS/IN2P3, Paris, France*
[81]*Fysiska institutionen, Lunds universitet, Lund, Sweden*
[82]*Departamento de Fisica Teorica C-15, Universidad Autonoma de Madrid, Madrid, Spain*
[83]*Institut für Physik, Universität Mainz, Mainz, Germany*
[84]*School of Physics and Astronomy, University of Manchester, Manchester, United Kingdom*
[85]*CPPM, Aix-Marseille Université and CNRS/IN2P3, Marseille, France*
[86]*Department of Physics, University of Massachusetts, Amherst, Massachusetts, USA*
[87]*Department of Physics, McGill University, Montreal, QC, Canada*
[88]*School of Physics, University of Melbourne, Victoria, Australia*
[89]*Department of Physics, The University of Michigan, Ann Arbor, Michigan, USA*
[90]*Department of Physics and Astronomy, Michigan State University, East Lansing, Michigan, USA*
[91a]*INFN Sezione di Milano, Milano, Italy*
[91b]*Dipartimento di Fisica, Università di Milano, Milano, Italy*
[92]*B.I. Stepanov Institute of Physics, National Academy of Sciences of Belarus, Minsk, Republic of Belarus*
[93]*National Scientific and Educational Centre for Particle and High Energy Physics, Minsk, Republic of Belarus*
[94]*Department of Physics, Massachusetts Institute of Technology, Cambridge, Massachusetts, USA*
[95]*Group of Particle Physics, University of Montreal, Montreal, QC, Canada*
[96]*P.N. Lebedev Institute of Physics, Academy of Sciences, Moscow, Russia*
[97]*Institute for Theoretical and Experimental Physics (ITEP), Moscow, Russia*
[98]*National Research Nuclear University MEPhI, Moscow, Russia*
[99]*D.V. Skobeltsyn Institute of Nuclear Physics, M.V. Lomonosov Moscow State University, Moscow, Russia*
[100]*Fakultät für Physik, Ludwig-Maximilians-Universität München, München, Germany*
[101]*Max-Planck-Institut für Physik (Werner-Heisenberg-Institut), München, Germany*
[102]*Nagasaki Institute of Applied Science, Nagasaki, Japan*
[103]*Graduate School of Science and Kobayashi-Maskawa Institute, Nagoya University, Nagoya, Japan*
[104a]*INFN Sezione di Napoli, Napoli, Italy*
[104b]*Dipartimento di Fisica, Università di Napoli, Napoli, Italy*
[105]*Department of Physics and Astronomy, University of New Mexico, Albuquerque, New Mexico, USA*
[106]*Institute for Mathematics, Astrophysics and Particle Physics, Radboud University Nijmegen/Nikhef, Nijmegen, Netherlands*
[107]*Nikhef National Institute for Subatomic Physics and University of Amsterdam, Amsterdam, Netherlands*
[108]*Department of Physics, Northern Illinois University, DeKalb, Illinois, USA*
[109]*Budker Institute of Nuclear Physics, SB RAS, Novosibirsk, Russia*
[110]*Department of Physics, New York University, New York, New York, USA*
[111]*Ohio State University, Columbus, Ohio, USA*
[112]*Faculty of Science, Okayama University, Okayama, Japan*
[113]*Homer L. Dodge Department of Physics and Astronomy, University of Oklahoma, Norman, Oklahoma, USA*
[114]*Department of Physics, Oklahoma State University, Stillwater, Oklahoma, USA*
[115]*Palacký University, RCPTM, Olomouc, Czech Republic*
[116]*Center for High Energy Physics, University of Oregon, Eugene, Oregon, USA*
[117]*LAL, Université Paris-Sud and CNRS/IN2P3, Orsay, France*
[118]*Graduate School of Science, Osaka University, Osaka, Japan*
[119]*Department of Physics, University of Oslo, Oslo, Norway*
[120]*Department of Physics, Oxford University, Oxford, United Kingdom*
[121a]*INFN Sezione di Pavia, Pavia, Italy*
[121b]*Dipartimento di Fisica, Università di Pavia, Pavia, Italy*
[122]*Department of Physics, University of Pennsylvania, Philadelphia, Pennsylvania, USA*
[123]*Petersburg Nuclear Physics Institute, Gatchina, Russia*
[124a]*INFN Sezione di Pisa, Pisa, Italy*
[124b]*Dipartimento di Fisica E. Fermi, Università di Pisa, Pisa, Italy*
[125]*Department of Physics and Astronomy, University of Pittsburgh, Pittsburgh, Pennsylvania, USA*
[126a]*Laboratorio de Instrumentacao e Fisica Experimental de Particulas - LIP, Lisboa, Portugal*
[126b]*Faculdade de Ciências, Universidade de Lisboa, Lisboa, Portugal*
[126c]*Department of Physics, University of Coimbra, Coimbra, Portugal*
[126d]*Centro de Física Nuclear da Universidade de Lisboa, Lisboa, Portugal*

[126e]*Departamento de Fisica, Universidade do Minho, Braga, Portugal*
[126f]*Departamento de Fisica Teorica y del Cosmos and CAFPE, Universidad de Granada, Granada (Spain), Portugal*
[126g]*Dep Fisica and CEFITEC of Faculdade de Ciencias e Tecnologia, Universidade Nova de Lisboa, Caparica, Portugal*
[127]*Institute of Physics, Academy of Sciences of the Czech Republic, Praha, Czech Republic*
[128]*Czech Technical University in Prague, Praha, Czech Republic*
[129]*Faculty of Mathematics and Physics, Charles University in Prague, Praha, Czech Republic*
[130]*State Research Center Institute for High Energy Physics, Protvino, Russia*
[131]*Particle Physics Department, Rutherford Appleton Laboratory, Didcot, United Kingdom*
[132]*Physics Department, University of Regina, Regina, SK, Canada*
[133]*Ritsumeikan University, Kusatsu, Shiga, Japan*
[134a]*INFN Sezione di Roma, Roma, Italy*
[134b]*Dipartimento di Fisica, Sapienza Università di Roma, Roma, Italy*
[135a]*INFN Sezione di Roma Tor Vergata, Roma, Italy*
[135b]*Dipartimento di Fisica, Università di Roma Tor Vergata, Roma, Italy*
[136a]*INFN Sezione di Roma Tre, Roma, Italy*
[136b]*Dipartimento di Matematica e Fisica, Università Roma Tre, Roma, Italy*
[137a]*Faculté des Sciences Ain Chock, Réseau Universitaire de Physique des Hautes Energies - Université Hassan II, Casablanca, Morocco*
[137b]*Centre National de l'Energie des Sciences Techniques Nucleaires, Rabat, Morocco*
[137c]*Faculté des Sciences Semlalia, Université Cadi Ayyad, LPHEA-Marrakech, Morocco*
[137d]*Faculté des Sciences, Université Mohamed Premier and LPTPM, Oujda, Morocco*
[137e]*Faculté des sciences, Université Mohammed V-Agdal, Rabat, Morocco*
[138]*DSM/IRFU (Institut de Recherches sur les Lois Fondamentales de l'Univers), CEA Saclay (Commissariat à l'Energie Atomique et aux Energies Alternatives), Gif-sur-Yvette, France*
[139]*Santa Cruz Institute for Particle Physics, University of California Santa Cruz, Santa Cruz, California, USA*
[140]*Department of Physics, University of Washington, Seattle, Washington, USA*
[141]*Department of Physics and Astronomy, University of Sheffield, Sheffield, United Kingdom*
[142]*Department of Physics, Shinshu University, Nagano, Japan*
[143]*Fachbereich Physik, Universität Siegen, Siegen, Germany*
[144]*Department of Physics, Simon Fraser University, Burnaby, BC, Canada*
[145]*SLAC National Accelerator Laboratory, Stanford, California, USA*
[146a]*Faculty of Mathematics, Physics & Informatics, Comenius University, Bratislava, Slovak Republic*
[146b]*Department of Subnuclear Physics, Institute of Experimental Physics of the Slovak Academy of Sciences, Kosice, Slovak Republic*
[147a]*Department of Physics, University of Cape Town, Cape Town, South Africa*
[147b]*Department of Physics, University of Johannesburg, Johannesburg, South Africa*
[147c]*School of Physics, University of the Witwatersrand, Johannesburg, South Africa*
[148a]*Department of Physics, Stockholm University, Stockholm, Sweden*
[148b]*The Oskar Klein Centre, Stockholm, Sweden*
[149]*Physics Department, Royal Institute of Technology, Stockholm, Sweden*
[150]*Departments of Physics & Astronomy and Chemistry, Stony Brook University, Stony Brook, New York, USA*
[151]*Department of Physics and Astronomy, University of Sussex, Brighton, United Kingdom*
[152]*School of Physics, University of Sydney, Sydney, Australia*
[153]*Institute of Physics, Academia Sinica, Taipei, Taiwan*
[154]*Department of Physics, Technion: Israel Institute of Technology, Haifa, Israel*
[155]*Raymond and Beverly Sackler School of Physics and Astronomy, Tel Aviv University, Tel Aviv, Israel*
[156]*Department of Physics, Aristotle University of Thessaloniki, Thessaloniki, Greece*
[157]*International Center for Elementary Particle Physics and Department of Physics, The University of Tokyo, Tokyo, Japan*
[158]*Graduate School of Science and Technology, Tokyo Metropolitan University, Tokyo, Japan*
[159]*Department of Physics, Tokyo Institute of Technology, Tokyo, Japan*
[160]*Department of Physics, University of Toronto, Toronto, ON, Canada*
[161a]*TRIUMF, Vancouver, BC, Canada*
[161b]*Department of Physics and Astronomy, York University, Toronto, ON, Canada*
[162]*Faculty of Pure and Applied Sciences, University of Tsukuba, Tsukuba, Japan*
[163]*Department of Physics and Astronomy, Tufts University, Medford, Massachusetts, USA*
[164]*Centro de Investigaciones, Universidad Antonio Narino, Bogota, Colombia*

[165]*Department of Physics and Astronomy, University of California Irvine, Irvine, California, USA*
[166a]*INFN Gruppo Collegato di Udine, Sezione di Trieste, Udine, Italy*
[166b]*ICTP, Trieste, Italy*
[166c]*Dipartimento di Chimica, Fisica e Ambiente, Università di Udine, Udine, Italy*
[167]*Department of Physics, University of Illinois, Urbana, Illinois, USA*
[168]*Department of Physics and Astronomy, University of Uppsala, Uppsala, Sweden*
[169]*Instituto de Física Corpuscular (IFIC) and Departamento de Física Atómica, Molecular y Nuclear and Departamento de Ingeniería Electrónica and Instituto de Microelectrónica de Barcelona (IMB-CNM), University of Valencia and CSIC, Valencia, Spain*
[170]*Department of Physics, University of British Columbia, Vancouver, BC, Canada*
[171]*Department of Physics and Astronomy, University of Victoria, Victoria, BC, Canada*
[172]*Department of Physics, University of Warwick, Coventry, United Kingdom*
[173]*Waseda University, Tokyo, Japan*
[174]*Department of Particle Physics, The Weizmann Institute of Science, Rehovot, Israel*
[175]*Department of Physics, University of Wisconsin, Madison, Wisconsin, USA*
[176]*Fakultät für Physik und Astronomie, Julius-Maximilians-Universität, Würzburg, Germany*
[177]*Fachbereich C Physik, Bergische Universität Wuppertal, Wuppertal, Germany*
[178]*Department of Physics, Yale University, New Haven, Connecticut, USA*
[179]*Yerevan Physics Institute, Yerevan, Armenia*
[180]*Centre de Calcul de l'Institut National de Physique Nucléaire et de Physique des Particules (IN2P3), Villeurbanne, France*

[a]Deceased.
[b]Also at Department of Physics, King's College London, London, United Kingdom.
[c]Also at Institute of Physics, Azerbaijan Academy of Sciences, Baku, Azerbaijan.
[d]Also at Novosibirsk State University, Novosibirsk, Russia.
[e]Also at Particle Physics Department, Rutherford Appleton Laboratory, Didcot, United Kingdom.
[f]Also at TRIUMF, Vancouver, BC, Canada.
[g]Also at Department of Physics, California State University, Fresno, CA, USA.
[h]Also at Tomsk State University, Tomsk, Russia.
[i]Also at CPPM, Aix-Marseille Université and CNRS/IN2P3, Marseille, France.
[j]Also at Università di Napoli Parthenope, Napoli, Italy.
[k]Also at Institute of Particle Physics (IPP), Canada.
[l]Also at Department of Physics, St. Petersburg State Polytechnical University, St. Petersburg, Russia.
[m]Also at Department of Financial and Management Engineering, University of the Aegean, Chios, Greece.
[n]Also at Louisiana Tech University, Ruston, LA, USA.
[o]Also at Institucio Catalana de Recerca i Estudis Avancats, ICREA, Barcelona, Spain.
[p]Also at Department of Physics, The University of Texas at Austin, Austin, TX, USA.
[q]Also at Institute of Theoretical Physics, Ilia State University, Tbilisi, Georgia.
[r]Also at CERN, Geneva, Switzerland.
[s]Also at Ochadai Academic Production, Ochanomizu University, Tokyo, Japan.
[t]Also at Manhattan College, New York, NY, USA.
[u]Also at Institute of Physics, Academia Sinica, Taipei, Taiwan.
[v]Also at LAL, Université Paris-Sud and CNRS/IN2P3, Orsay, France.
[w]Also at Academia Sinica Grid Computing, Institute of Physics, Academia Sinica, Taipei, Taiwan.
[x]Also at Laboratoire de Physique Nucléaire et de Hautes Energies, UPMC and Université Paris-Diderot and CNRS/IN2P3, Paris, France.
[y]Also at School of Physical Sciences, National Institute of Science Education and Research, Bhubaneswar, India.
[z]Also at Dipartimento di Fisica, Sapienza Università di Roma, Roma, Italy.
[aa]Also at Moscow Institute of Physics and Technology State University, Dolgoprudny, Russia.
[bb]Also at Section de Physique, Université de Genève, Geneva, Switzerland.
[cc]Also at International School for Advanced Studies (SISSA), Trieste, Italy.
[dd]Also at Department of Physics and Astronomy, University of South Carolina, Columbia, SC, USA.
[ee]Also at School of Physics and Engineering, Sun Yat-sen University, Guangzhou, China.
[ff]Also at Faculty of Physics, M.V. Lomonosov Moscow State University, Moscow, Russia.
[gg]Also at National Research Nuclear University MEPhI, Moscow, Russia.
[hh]Also at Institute for Particle and Nuclear Physics, Wigner Research Centre for Physics, Budapest, Hungary.
[ii]Also at Department of Physics, Oxford University, Oxford, United Kingdom.

[jj]Also at Department of Physics, Nanjing University, Jiangsu, China.
[kk]Also at Institut für Experimentalphysik, Universität Hamburg, Hamburg, Germany.
[ll]Also at Department of Physics, The University of Michigan, Ann Arbor, MI, USA.
[mm]Also at Discipline of Physics, University of KwaZulu-Natal, Durban, South Africa.
[nn]Also at University of Malaya, Department of Physics, Kuala Lumpur, Malaysia.

Physics Letters B 738 (2014) 234–253

Contents lists available at ScienceDirect

Physics Letters B

www.elsevier.com/locate/physletb

Fiducial and differential cross sections of Higgs boson production measured in the four-lepton decay channel in pp collisions at $\sqrt{s} = 8$ TeV with the ATLAS detector

ATLAS Collaboration *

ARTICLE INFO

Article history:
Received 14 August 2014
Received in revised form 10 September 2014
Accepted 23 September 2014
Available online 28 September 2014
Editor: W.-D. Schlatter

ABSTRACT

Measurements of fiducial and differential cross sections of Higgs boson production in the $H \to ZZ^* \to 4\ell$ decay channel are presented. The cross sections are determined within a fiducial phase space and corrected for detection efficiency and resolution effects. They are based on 20.3 fb^{-1} of pp collision data, produced at $\sqrt{s} = 8$ TeV centre-of-mass energy at the LHC and recorded by the ATLAS detector. The differential measurements are performed in bins of transverse momentum and rapidity of the four-lepton system, the invariant mass of the subleading lepton pair and the decay angle of the leading lepton pair with respect to the beam line in the four-lepton rest frame, as well as the number of jets and the transverse momentum of the leading jet. The measured cross sections are compared to selected theoretical calculations of the Standard Model expectations. No significant deviation from any of the tested predictions is found.

1. Introduction

In 2012 the ATLAS and CMS Collaborations announced the discovery of a new particle [1,2] in the search for the Standard Model (SM) Higgs boson [3–8] at the CERN Large Hadron Collider (LHC) [9]. Since this discovery, the particle's mass m_H was measured by the ATLAS and CMS Collaborations [10–12]. The result of the ATLAS measurement based on 25 fb^{-1} of data collected at centre-of-mass energies of 7 TeV and 8 TeV is 125.36 ± 0.41 GeV. Tests of the couplings and spin/CP quantum numbers have been reported by both collaborations [11,13,14] and show agreement with the predicted scalar nature of the SM Higgs boson.

In this Letter, measurements of fiducial and differential production cross sections for the $H \to ZZ^* \to 4\ell$ decay channel are reported and compared to selected theoretical calculations. The event selection and the background determination are the same as in Ref. [15], where a detailed description is given. For this measurement, an integrated luminosity of 20.3 fb^{-1} of pp collisions is analyzed. The data were collected at the LHC at a centre-of-mass energy of $\sqrt{s} = 8$ TeV and recorded with the ATLAS detector [16].

The ATLAS detector covers the pseudorapidity range $|\eta| < 4.9$ and the full azimuthal angle ϕ.[1] It consists of an inner tracking detector covering the pseudorapidity range $|\eta| < 2.5$ surrounded by a superconducting solenoid, electromagnetic and hadronic calorimeters, and an external muon spectrometer with large superconducting toroidal magnets.

Fiducial cross sections are quoted to minimize the model dependence of the acceptance corrections related to the extrapolation to phase-space regions not covered by the detector. The measured fiducial cross sections are corrected for detector effects to be directly compared to theoretical calculations.

The differential measurements are performed in several observables related to the Higgs boson production and decay. These include the transverse momentum $p_{\mathrm{T},H}$ and rapidity $|y_H|$ of the Higgs boson, the invariant mass of the subleading lepton pair m_{34} (the leading and subleading lepton pairs are defined in Section 3) and the magnitude of the cosine of the decay angle of the leading lepton pair in the four-lepton rest frame with respect to the beam axis $|\cos\theta^*|$. The number of jets n_{jets} and the transverse momentum of the leading jet $p_{\mathrm{T,jet}}$ are also included. The distribution of the $p_{\mathrm{T},H}$ observable is sensitive to the Higgs boson production mechanisms as well as spin/CP quantum numbers, and can be used to test perturbative QCD predictions. This distribution

* *E-mail address:* atlas.publications@cern.ch.

[1] ATLAS uses a right-handed coordinate system with its origin at the nominal interaction point (IP) at the centre of the detector and the z-axis along the beam pipe. The x-axis points from the IP to the centre of the LHC ring, and the y-axis points upward. Cylindrical coordinates (r, ϕ) are used in the transverse plane, ϕ being the azimuthal angle around the beam pipe. The pseudorapidity is defined in terms of the polar angle θ as $\eta = -\ln[\tan(\theta/2)]$.

http://dx.doi.org/10.1016/j.physletb.2014.09.054

has been studied extensively and precise predictions exist (see e.g. Refs. [17–21]), including the effect of finite quark masses. The distribution of the $|y_H|$ observable can be used to probe the parton distribution functions (PDFs) of the proton. The distributions of the decay variables m_{34} and $|\cos\theta^*|$ are sensitive to the Lagrangian structure of Higgs boson interactions, e.g. spin/CP quantum numbers and higher-dimensional operators. The jet multiplicity and transverse momentum distributions are sensitive to QCD radiation effects and to the relative rates of Higgs boson production modes. The distribution of the transverse momentum of the leading jet probes quark and gluon radiation.

2. Theoretical predictions and simulated samples

The Higgs boson production cross sections and decay branching fractions as well as their uncertainties are taken from Refs. [21,22]. The cross sections for the gluon-fusion (ggF) process have been calculated to next-to-leading order (NLO) [23–25], and next-to-next-to-leading order (NNLO) [26–28] in QCD with additional next-to-next-to-leading logarithm (NNLL) soft-gluon resummation [29]. The cross section values have been modified to include NLO electroweak (EW) radiative corrections, assuming factorization between QCD and EW effects [30–34]. The cross sections for the vector-boson fusion (VBF) processes are calculated with full NLO QCD and EW corrections [35–37], and approximate NNLO QCD corrections are included [38]. The cross sections for the associated WH/ZH production processes (VH) are calculated at NLO [39] and at NNLO [40] in QCD, and NLO EW radiative corrections [41] are applied. The cross sections for associated Higgs boson production with a $t\bar{t}$ pair ($t\bar{t}H$) are calculated at NLO in QCD [42–45].

The Higgs boson branching fractions for decays to four-lepton final states are provided by Prophecy4f [46,47], which implements the complete NLO QCD + EW corrections and interference effects between identical final-state fermions.

The $H \to ZZ^* \to 4\ell$ signal is modelled using the Powheg Monte Carlo (MC) event generator [48–52], which calculates separately the ggF and VBF production mechanisms with matrix elements up to NLO. The description of the Higgs boson transverse momentum spectrum in the ggF process is adjusted to follow the calculation in Refs. [19,20], which includes QCD corrections up to NLO and QCD soft-gluon resummations up to NNLL, as well as finite quark masses [53]. Powheg is interfaced to Pythia8 [54] for showering and hadronization, which in turn is interfaced to Photos [55,56] to model photon radiation in the final state. Pythia8 is used to simulate VH and $t\bar{t}H$ production. The response of the ATLAS detector is modelled in a simulation [57] based on GEANT4 [58].

The measured fiducial cross-section distributions are compared to three ggF theoretical calculations: Powheg without the adjustments to the $p_{\mathrm{T},H}$ spectrum described above, Powheg interfaced to Minlo (Multi-scale improved NLO) [59] and HRes2 (v.2.2) [19,20]. Powheg with Minlo provides predictions for jet-related variables at NLO for Higgs boson production in association with one jet. The HRes2 program computes fixed-order cross sections for ggF SM Higgs boson production up to NNLO. All-order resummation of soft-gluon effects at small transverse momenta is consistently included up to NNLL, using dynamic factorization and resummation scales. The program implements top- and bottom-quark mass dependence up to NLL + NLO. At NNLL + NNLO level only the top-quark contribution is considered. HRes2 does not perform showering and QED final-state radiation effects are not included.

The contributions from the other production modes are added to the ggF predictions. At a centre-of-mass energy of 8 TeV and for a Higgs boson mass of 125.4 GeV, their relative contributions to the total cross section are 87.3% (ggF), 7.1% (VBF), 3.1% (WH), 1.9% (ZH) and 0.6% ($t\bar{t}H$), respectively.

All theoretical predictions are computed for a SM Higgs boson with mass 125.4 GeV. They are normalized to the most precise SM inclusive cross-section predictions currently available [60], corrected for the fiducial acceptance derived from the simulation.

The ZZ, WZ, $t\bar{t}$ and Z + jets background events are modelled using the simulated samples and cross sections described in Ref. [15].

3. Event selection

The detector level physics object definitions of muons, electrons, and jets, and the event selection applied in this analysis are the same as in Ref. [15], with the exception of the jet selection and the additional requirement on the four-lepton invariant mass described below. A brief overview is given in this section.

Events with at least four leptons are selected with single-lepton and dilepton triggers. The transverse momentum and transverse energy thresholds for the single-muon and single-electron triggers are 24 GeV. Two dimuon triggers are used, one with symmetric thresholds at 13 GeV and the other with asymmetric thresholds at 18 GeV and 8 GeV. For the dielectron trigger the symmetric thresholds are 12 GeV. Furthermore there is an electron–muon trigger with thresholds at 12 GeV (electron) and 8 GeV (muon).

Higgs boson candidates are formed by selecting two same-flavour opposite-sign (SFOS) lepton pairs (a lepton quadruplet). The leptons must satisfy identification, impact parameter, and track-based and calorimeter-based isolation criteria. Each muon (electron) must satisfy transverse momentum $p_{\mathrm{T}} > 6$ GeV (transverse energy $E_{\mathrm{T}} > 7$ GeV) and be in the pseudorapidity range $|\eta| < 2.7$ (2.47). The highest-p_{T} lepton in the quadruplet must satisfy $p_{\mathrm{T}} > 20$ GeV, and the second (third) lepton in p_{T} order must satisfy $p_{\mathrm{T}} > 15$ (10) GeV. The leptons are required to be separated from each other by $\Delta R \equiv \sqrt{(\Delta\eta)^2 + (\Delta\phi)^2} > 0.1$ (0.2) when having the same (different) lepton flavours.

Multiple quadruplets within a single event are possible: for four muons or four electrons there are two ways to pair the masses, and for five or more leptons there are multiple combinations. The quadruplet selection is done separately in each channel: 4μ, $2e2\mu$, $2\mu2e$, $4e$, keeping only a single quadruplet per channel. Here the first flavour index refers to the leading lepton pair, which is the pair with the invariant mass m_{12} closest to the Z boson mass [61]. The invariant mass m_{12} is required to be between 50 GeV and 106 GeV. The subleading pair of each channel is chosen as the remaining pair with mass m_{34} closest to the Z boson mass and satisfying the requirement $12 < m_{34} < 115$ GeV. Finally, if more than one channel has a quadruplet passing the selection, the channel with the highest expected signal rate is kept, in the order: 4μ, $2e2\mu$, $2\mu2e$, $4e$. A J/ψ veto is applied: $m(\ell_i, \ell_j) > 5$ GeV for SFOS lepton pairs. Only events with a four-lepton invariant mass in the range 118–129 GeV are kept. This requirement defines the signal mass window and was chosen by minimizing the expected uncertainty on the total signal yield determination, taking into account the experimental uncertainty on the Higgs boson mass.

Jets are reconstructed from topological clusters of calorimeter cells using the anti-k_t algorithm [62] with the distance parameter $R = 0.4$. In this analysis, jets [63] are selected by requiring $p_{\mathrm{T}} > 30$ GeV, $|y| < 4.4$ and, in order to avoid double counting of electrons that are also reconstructed as jets, $\Delta R(\text{jet, electron}) > 0.2$.

The events are divided into bins of the variables of interest, which are computed with the reconstructed four-momenta of the selected lepton quadruplets or from the reconstructed jets: the transverse momentum $p_{\mathrm{T},H}^{\mathrm{reco}}$ and the rapidity $|y_H^{\mathrm{reco}}|$ of the four-lepton system, the invariant mass of the subleading lepton pair

Table 1
List of selection cuts which define the fiducial region of the cross section measurement. The same flavour opposite sign lepton pairs are denoted as SFOS, the leading lepton pair mass as m_{12}, and the subleading lepton pair mass as m_{34}.

Lepton selection	
Muons:	$p_{\mathrm{T}} > 6$ GeV, $\lvert\eta\rvert < 2.7$
Electrons:	$p_{\mathrm{T}} > 7$ GeV, $\lvert\eta\rvert < 2.47$
Lepton pairing	
Leading pair:	SFOS lepton pair with smallest $\lvert m_Z - m_{\ell\ell}\rvert$
Subleading pair:	Remaining SFOS lepton pair with smallest $\lvert m_Z - m_{\ell\ell}\rvert$
Event selection	
Lepton kinematics:	$p_{\mathrm{T}} > 20, 15, 10$ GeV
Mass requirements:	$50 < m_{12} < 106$ GeV, $12 < m_{34} < 115$ GeV
Lepton separation:	$\Delta R(\ell_i, \ell_j) > 0.1$ (0.2) for same- (different-) flavour leptons
J/ψ veto:	$m(\ell_i, \ell_j) > 5$ GeV for all SFOS lepton pairs
Mass window:	$118 < m_{4\ell} < 129$ GeV

m_{34}^{reco}, the magnitude of the cosine of the decay angle of the leading lepton pair in the four-lepton rest frame with respect to the beam axis $|\cos\theta^{*\mathrm{reco}}|$, the number of jets $n_{\mathrm{jets}}^{\mathrm{reco}}$, and the transverse momentum of the leading jet $p_{\mathrm{T,jet}}^{\mathrm{reco}}$. In order to distinguish them from the unfolded variables used in the cross section bin definition, they are labelled with "reco".

4. Definition of the fiducial region

The fiducial selection, outlined in Table 1, is designed to replicate at simulation level, before applying detector effects, the analysis selection as closely as possible in order to minimize model-dependent acceptance effects on the measured cross sections.

The fiducial selection is applied to electrons and muons originating from vector-boson decays before they emit photon radiation, referred to as Born-level leptons. An alternative approach would be to correct the lepton momenta by adding final-state radiation photons within a cone of size $\Delta R < 0.1$ around each lepton (dressing). For this analysis the acceptance difference between Born and dressed-lepton definitions is less than 0.5%. Particle-level jets are reconstructed from all stable particles except muons and neutrinos using the anti-k_t algorithm with the distance parameter $R = 0.4$.

Jets are selected by requiring $p_{\mathrm{T}} > 30$ GeV, $|y| < 4.4$ and $\Delta R(\text{jet, electron}) > 0.2$. Muons (electrons) must satisfy $p_{\mathrm{T}} > 6$ (7) GeV and $|\eta| < 2.7$ (2.47). Events in which at least one of the Z bosons decays into τ leptons are removed. Quadruplets are formed from two pairs of SFOS leptons. The leptons are paired as in Section 3, including the possibility of incorrectly pairing the leptons, which happens in about 5% of the selected events for a SM Higgs boson with mass 125.4 GeV. The leading pair is defined as the SFOS lepton pair with invariant mass m_{12} closest to the Z boson mass and the subleading pair is defined as the remaining SFOS lepton pair with invariant mass m_{34} closest to the Z boson mass.

The three highest-p_{T} leptons in the quadruplet are required to have $p_{\mathrm{T}} > 20, 15, 10$ GeV, respectively, and the lepton pairs must have $50 < m_{12} < 106$ GeV and $12 < m_{34} < 115$ GeV.

The separation between the leptons is required to be $\Delta R(\ell_i, \ell_j) > 0.1$ (0.2) for same- (different-) flavour leptons. A J/ψ veto is applied: $m(\ell_i, \ell_j) > 5$ GeV for all SFOS lepton pairs. Furthermore, the mass of the four-lepton system $m_{4\ell}$ must be close to m_H, i.e. $118 < m_{4\ell} < 129$ GeV.

For a SM Higgs boson mass of 125.4 GeV, the acceptance of the fiducial selection (with respect to the full phase space of $H \to ZZ^* \to 2\ell 2\ell'$, where $\ell, \ell' = e, \mu$) is 45.7%. The number of events passing the event selection divided by the number of events passing the fiducial selection is 55.3%; about 1% of the events passing the event selection do not pass the fiducial selection.

5. Background estimate

The background estimates used in this analysis are described in detail in Ref. [15]. The irreducible ZZ and the reducible WZ background contributions are estimated using simulated samples normalized to NLO predictions. For the jet-related variables, the simulation predictions are compared to data for $m_{4\ell} > 190$ GeV where the ZZ background process is dominant; shape differences between the distributions in data and simulation are used to estimate systematic uncertainties.

The reducible Z + jets and $t\bar{t}$ background contributions are estimated with data-driven methods. Their normalizations are obtained from data control regions and extrapolated to the signal region using transfer factors. The $\ell\ell + \mu\mu$ final state is dominated by Z + heavy-flavour jets and the $\ell\ell + ee$ final state by Z + light-flavour jets. The misidentification of light-flavour jets as electrons is difficult to model in the simulation. Therefore the distributions for $\ell\ell + ee$ are taken from data control regions and extrapolated to the signal region, while the background distributions for $\ell\ell + \mu\mu$ are taken from simulated samples.

After the analysis selection about 9 background events are expected: 6.7 events from irreducible ZZ and 2.2 events from the reducible background.

The observed distributions compared to the signal and background expectations for the six reconstructed observables $p_{\mathrm{T},H}^{\mathrm{reco}}$, $|y_H^{\mathrm{reco}}|$, m_{34}^{reco}, $|\cos\theta^{*\mathrm{reco}}|$, $n_{\mathrm{jets}}^{\mathrm{reco}}$, and $p_{\mathrm{T,jet}}^{\mathrm{reco}}$ are shown in Fig. 1. The signal prediction includes VBF, ZH, WH, $t\bar{t}H$, and the Powheg ggF calculation for a Higgs boson with $m_H = 125$ GeV and is normalized to the most precise SM inclusive cross-section calculation currently available [60].

6. Observed differential yields and unfolding

The extraction of the signal yield for the measurement of the fiducial cross section is performed through a fit to the $m_{4\ell}$ distribution using shape templates for the signal and background contributions [15]. In this fit, the Higgs boson mass is fixed to 125.4 GeV and the parameter of interest is the total number of signal events. The extracted number of observed signal events in the mass window is $23.7^{+5.9}_{-5.3}(\text{stat.}) \pm 0.6(\text{syst.})$.

In the differential cross-section measurements, given the low number of signal events expected in each measured bin i, the signal yields n_i^{sig} are determined by subtracting the expected number of background events from the observed number of events. This is done within the mass window for each bin of the observable of interest. The total number of observed events in the mass window is 34 and the extracted signal yield is $25.1^{+6.3}_{-5.4}(\text{stat.})^{+0.6}_{-0.4}(\text{syst.})$ events.

The difference between the number of signal events extracted with the two methods is mainly due to fixing the Higgs boson mass to 125.4 GeV in the fit method. As reported in Ref. [10], the best fit mass in the $H \to ZZ^* \to 4\ell$ channel alone is 124.5 GeV, causing smaller weights for some events in the fit.

After subtracting the background, the measured signal yields are corrected for detector efficiency and resolution effects. This unfolding is performed using correction factors derived from simulated SM signal samples. The correction factor in the i-th bin is calculated as

$$c_i = \frac{N_i^{\mathrm{reco}}}{N_i^{\mathrm{fid}}},$$

where N_i^{reco} is the number of reconstructed events in the i-th bin of the observed distribution and N_i^{fid} is the number of events in

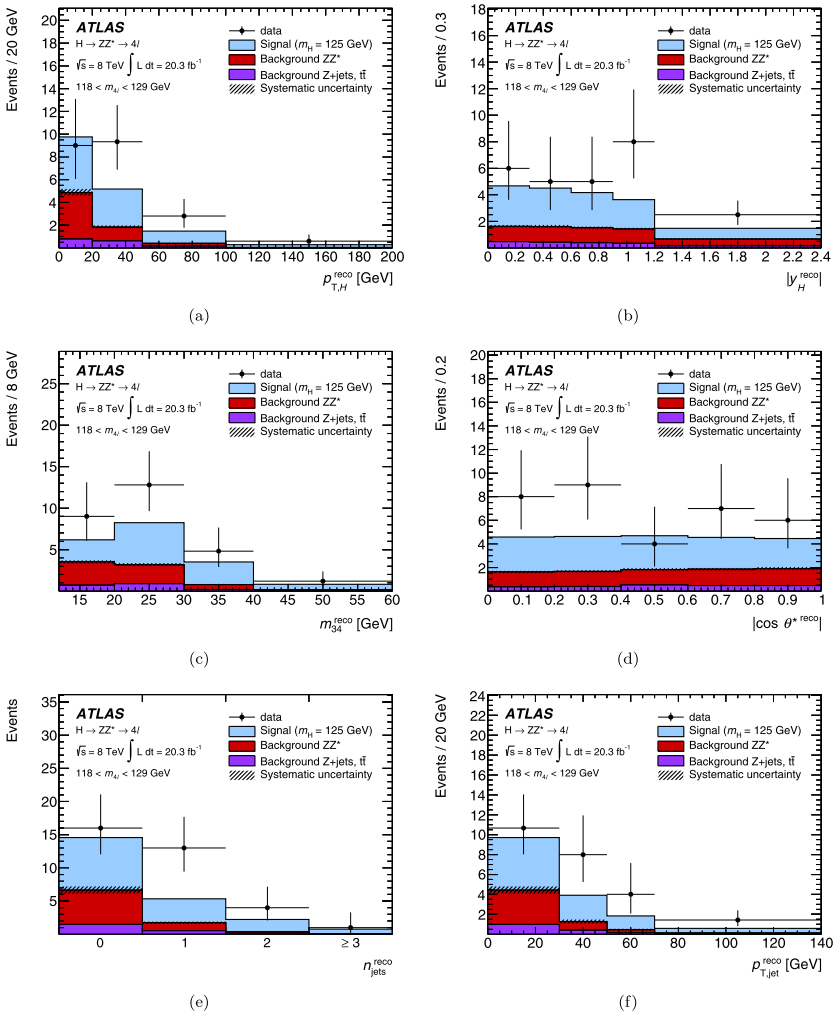

Fig. 1. Data yield distributions for the transverse momentum $p_{\mathrm{T},H}^{\mathrm{reco}}$ and the rapidity $|y_H^{\mathrm{reco}}|$ of the four-lepton system, the invariant mass of the subleading lepton pair m_{34}^{reco}, the magnitude of the cosine of the decay angle of the leading lepton pair in the four-lepton rest frame with respect to the beam axis $|\cos\theta^{*\mathrm{reco}}|$, the number of jets $n_{\mathrm{jets}}^{\mathrm{reco}}$, and the transverse momentum of the leading jet $p_{\mathrm{T,jet}}^{\mathrm{reco}}$ compared to signal and background expectations. The signal prediction includes VBF, ZH, WH, $t\bar{t}H$, and the POWHEG ggF calculation for a Higgs boson with $m_H = 125$ GeV and is normalized to the most precise SM inclusive cross-section calculation currently available [60]. The hatched areas denote the systematic uncertainties on the backgrounds. (For interpretation of the references to colour in this figure legend, the reader is referred to the web version of this article.)

the i-th bin of the particle-level distribution, within the fiducial region.

The unfolded signal yield in each bin is then converted into a differential fiducial cross section via

$$\frac{\mathrm{d}\sigma_{\mathrm{fid},i}}{\mathrm{d}x_i} = \frac{n_i^{\mathrm{sig}}}{c_i \cdot \mathcal{L}_{\mathrm{int}} \cdot \Delta x_i},$$

where Δx_i is the bin width and $\mathcal{L}_{\mathrm{int}}$ the integrated luminosity.

The correction factors used in this analysis are obtained from simulated samples for all SM Higgs production modes, using the relative rates as predicted by the SM. The inclusive correction factor is $c = 0.553 \pm 0.002(\mathrm{stat.}) \pm 0.015(\mathrm{syst.})$. The correction factors for the different production modes are 0.553 (ggF), 0.572 (VBF), 0.535 (WH), 0.551 (ZH) and 0.417 ($t\bar{t}H$). In $t\bar{t}H$ production the Higgs boson is accompanied by light- and heavy-flavour jets as well as possible additional leptons from the top-quark decays. Since lepton isolation is applied to the reconstructed but not the

Table 2
Summary of the relative systematic uncertainties on the total background contribution (top rows) and on the parameters that enter the signal extraction (bottom rows). The ranges indicate the variation across observables and bins.

Systematic uncertainties (%)	
Background	
Luminosity	1.4–2.3
Reducible background	1.6–34
Experimental, leptons	1.3–2.3
PDF/scale	3.0–24
Correction factors/conversion to σ	
Luminosity	2.8
Experimental, leptons	2.1–2.6
Experimental, jets	2.7–13
Production process	0.1–15
Higgs boson mass	0.4–2.7

fiducial objects, the correction factors for $t\bar{t}H$ differ from those for the other production modes.

For each bin, the number of expected background events, the number of observed events, the luminosity, and the correction factors are used to calculate a profile likelihood ratio [64]. The likelihood includes shape and normalization uncertainties of backgrounds and correction factors as nuisance parameters. For each variable all bins are included in the likelihood and correlations of uncertainties between the different bins and between backgrounds and correction factors are taken into account. The cross sections are extracted for each bin by minimizing twice the negative logarithm of the profile likelihood ratio $-2\ln\Lambda$. The uncertainties on the cross sections are also estimated using $-2\ln\Lambda$ by evaluating its variation as a function of the parameter of interest (the cross section value in each bin). Under the asymptotic assumption [64], $-2\ln\Lambda$ behaves as a χ^2 distribution with one degree of freedom. For some of the fitted intervals, due to the low number of events, the distribution of the profile likelihood ratio does not follow a χ^2 distribution and the uncertainties are derived using pseudo-experiments.

The compatibility between the measured cross sections and the theoretical predictions is evaluated by computing the difference between the value of $-2\ln\Lambda$ at the best-fit value and the value obtained by fixing the cross sections in all bins to the ones predicted by theory. Under the asymptotic assumption [64], this statistical observable behaves as a χ^2 with the number of degrees of freedom equal to the number of bins; it is used as a test statistic to compute the p-values quantifying the compatibility between the observed distributions and the predictions. For all measured observables the asymptotic assumption is verified with pseudo-experiments.

7. Systematic uncertainties

Systematic uncertainties are calculated for the estimated backgrounds, the correction factors, and the SM theoretical predictions; the latter only have an impact on the quantitative comparison of the measurements with different predictions. An overview of the systematic uncertainties on the total background prediction and the correction factors is shown in Table 2.

The uncertainty on the integrated luminosity is propagated in a correlated way to the backgrounds evaluated from the MC predictions and to the unfolding, where it is used when converting the estimated unfolded signal yield into a fiducial cross section. This uncertainty is derived following the same methodology as that detailed in Ref. [65] from a preliminary calibration of the luminosity scale derived from beam-separation scans performed in November 2012.

Systematic uncertainties on the data-driven estimate of the reducible backgrounds are assigned both to the normalization and the shapes of the distributions by varying the estimation methods [15].

The systematic uncertainties on the lepton trigger, reconstruction and identification efficiencies [66,67] are propagated to the signal correction factors and the ZZ^* background, taking into account correlations. For the correction factors, systematic uncertainties are assigned on the jet resolution and energy scales. The largest systematic uncertainty is due to the uncertainty in the jet flavour composition [63,68,69].

The uncertainties on the correction factors due to PDF choice as well as QCD renormalization and factorization scale variations are evaluated in signal samples using the procedure described in Ref. [15] and found to be negligible. A similar procedure is followed for most variables for the irreducible ZZ background. For the jet-related observables an uncertainty is derived instead by comparing the data with the predicted ZZ distributions for $m_{4\ell} > 190$ GeV, after normalizing the MC estimate to the observed data yield. The systematic uncertainty is estimated as the larger of the data-MC difference and the statistical uncertainty on the data. This systematic uncertainty accounts for both the theoretical and experimental uncertainties in the modelling of the ZZ jet distributions. Systematic uncertainties due to the modelling of QED final-state radiation are found to be negligible with respect to the total uncertainty.

The correction factors are calculated assuming the predicted relative cross sections of the different Higgs production modes. The corresponding systematic uncertainty is evaluated by varying these predictions within the current experimental bounds [14]. The VBF and VH fractions are varied by factors of 0.5 and 2 with respect to the SM prediction and the $t\bar{t}H$ fraction is varied by factors of 0 and 5.

The experimental uncertainty on m_H [10] is propagated to the correction factors by studying their dependence on the Higgs boson mass.

The systematic uncertainties on the theoretical predictions include the PDF and QCD scale choices as well as the uncertainty on the $H \to ZZ^*$ branching fraction [60]. The procedure described in Ref. [70] is used to evaluate the scale uncertainties of the predicted n_{jets} distribution.

The upper edges of the uncertainty ranges in Table 2 are in most cases due to the highest bins in the n_{jets} and $p_{\text{T,jet}}$ distributions. The background systematic uncertainties are large in some bins due to the limited statistics in the data control regions.

8. Results

The cross section in the fiducial region described in Table 1 is

$$\sigma_{\text{tot}}^{\text{fid}} = 2.11^{+0.53}_{-0.47}(\text{stat.}) \pm 0.08(\text{syst.})\ \text{fb}.$$

The theoretical prediction from Ref. [60] for a Higgs boson mass of 125.4 GeV is 1.30 ± 0.13 fb.

The differential cross sections as a function of $p_{\text{T},H}$, y_H, m_{34}, $|\cos\theta^*|$, n_{jets}, and $p_{\text{T,jet}}$ are shown in Fig. 2. For all variables and bins the total uncertainties on the cross-section measurements are dominated by statistical uncertainties. Powheg, Minlo and HRes2 calculations of ggF, added to VBF, ZH/WH and $t\bar{t}H$ (see Section 2), are overlaid. The HRes2 calculation was developed for modelling the Higgs kinematic variables and is only used for $p_{\text{T},H}$ and y_H. The theoretical calculations are normalized to the most precise SM inclusive cross-section predictions currently available [60].

The p-values quantifying the compatibility between data and predictions, computed with the method described in Section 6, are shown in Table 3. No significant discrepancy is observed.

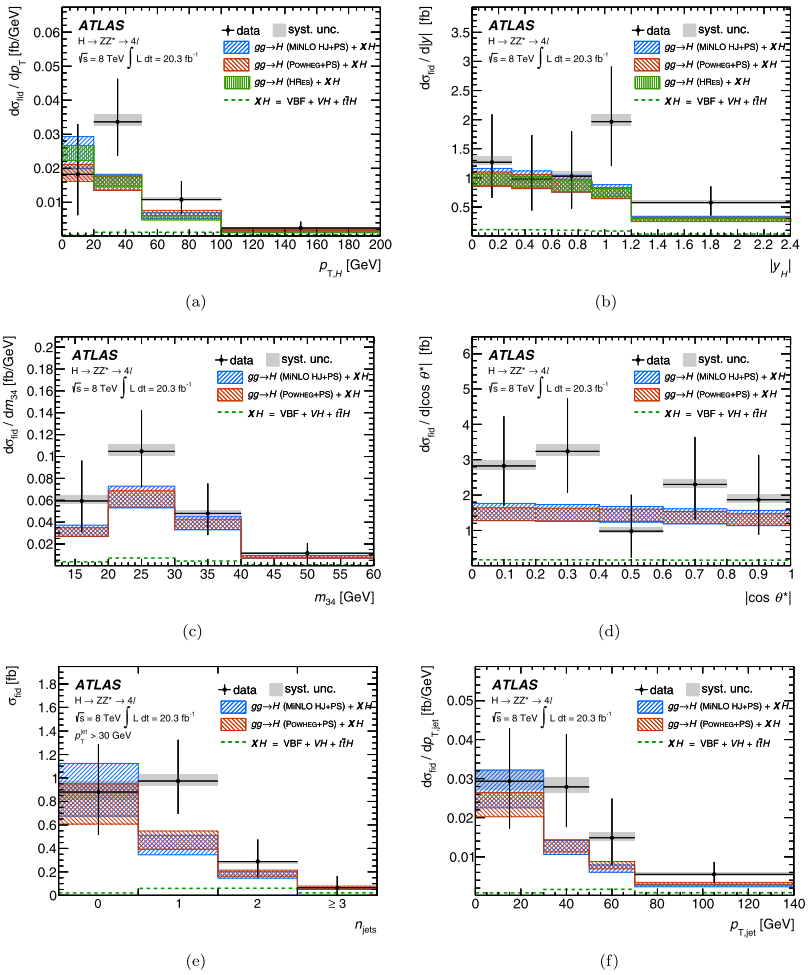

Fig. 2. Differential unfolded cross sections for the transverse momentum $p_{T,H}$ and rapidity y_H of the Higgs boson, the invariant mass of the subleading lepton pair m_{34}, the magnitude of the cosine of the decay angle of the leading lepton pair in the four-lepton rest frame with respect to the beam axis $|\cos\theta^*|$, the number of jets n_{jets}, and the transverse momentum of the leading jet $p_{\text{T,jet}}$ in the $H \to ZZ^* \to 4\ell$ decay channel compared to different theoretical calculations of the ggF process: Powheg, Minlo and HRes2. The contributions from VBF, ZH/WH and $t\bar{t}H$ are determined as described in Section 2 and added to the ggF distributions. All theoretical calculations are normalized to the most precise SM inclusive cross-section predictions currently available [60]. The error bars on the data points show the total (stat. ⊕ syst.) uncertainty, while the grey bands denote the systematic uncertainties. The bands of the theoretical prediction indicate the total uncertainty. (For interpretation of the references to colour in this figure legend, the reader is referred to the web version of this article.)

9. Conclusion

Measurements of fiducial and differential cross sections in the $H \to ZZ^* \to 4\ell$ decay channel are presented. They are based on 20.3 fb^{-1} of pp collision data, produced at $\sqrt{s} = 8$ TeV centre-of-mass energy at the LHC and recorded by the ATLAS detector. The cross sections are corrected for detector effects and compared to selected theoretical calculations. No significant deviation from the theoretical predictions is observed for any of the studied variables.

Acknowledgements

We thank CERN for the very successful operation of the LHC, as well as the support staff from our institutions without whom ATLAS could not be operated efficiently.

We acknowledge the support of ANPCyT, Argentina; YerPhI, Armenia; ARC, Australia; BMWF and FWF, Austria; ANAS, Azerbaijan; SSTC, Belarus; CNPq and FAPESP, Brazil; NSERC, NRC and CFI, Canada; CERN; CONICYT, Chile; CAS, MOST and NSFC, China; COLCIENCIAS, Colombia; MSMT CR, MPO CR and VSC CR, Czech Repub-

Table 3
Compatibility tests of data with POWHEG, MINLO and HRES2 ggF calculations of SM Higgs boson production. The compatibility p-values are obtained, as explained in the text, from the difference between $-2\ln\Lambda$ at the best-fit value and $-2\ln\Lambda$ with the cross sections fixed to the theory computations.

Variable	p-values		
	POWHEG	MINLO	HRES2
$p_{T,H}$	0.30	0.23	0.16
$\lvert y_H \rvert$	0.37	0.45	0.36
m_{34}	0.48	0.60	–
$\lvert \cos\theta^* \rvert$	0.35	0.45	–
n_{jets}	0.37	0.28	–
$p_{T,\text{jet}}$	0.33	0.26	–

lic; DNRF, DNSRC and Lundbeck Foundation, Denmark; EPLANET, ERC and NSRF, European Union; IN2P3-CNRS, CEA-DSM/IRFU, France; GNSF, Georgia; BMBF, DFG, HGF, MPG and AvH Foundation, Germany; GSRT and NSRF, Greece; ISF, MINERVA, GIF, DIP and Benoziyo Center, Israel; INFN, Italy; MEXT and JSPS, Japan; CNRST, Morocco; FOM and NWO, Netherlands; BRF and RCN, Norway; MNiSW, Poland; GRICES and FCT, Portugal; MERYS (MECTS), Romania; MES of Russia and ROSATOM, Russian Federation; JINR; MSTD, Serbia; MSSR, Slovakia; ARRS and MIZŠ, Slovenia; DST/NRF, South Africa; MICINN, Spain; SRC and Wallenberg Foundation, Sweden; SER, SNSF and Cantons of Bern and Geneva, Switzerland; NSC, Taiwan; TAEK, Turkey; STFC, the Royal Society and Leverhulme Trust, United Kingdom; DOE and NSF, United States of America.

The crucial computing support from all WLCG partners is acknowledged gratefully, in particular from CERN and the ATLAS Tier-1 facilities at TRIUMF (Canada), NDGF (Denmark, Norway, Sweden), CC-IN2P3 (France), KIT/GridKA (Germany), INFN-CNAF (Italy), NL-T1 (Netherlands), PIC (Spain), ASGC (Taiwan), RAL (UK) and BNL (USA) and in the Tier-2 facilities worldwide.

References

[1] ATLAS Collaboration, Observation of a new particle in the search for the standard model Higgs boson with the ATLAS detector at the LHC, Phys. Lett. B 716 (2012) 1–29, arXiv:1207.7214.
[2] CMS Collaboration, Observation of a new boson at a mass of 125 GeV with the CMS experiment at the LHC, Phys. Lett. B 716 (2012) 30–61, arXiv:1207.7235.
[3] F. Englert, R. Brout, Broken symmetry and the mass of gauge vector mesons, Phys. Rev. Lett. 13 (1964) 321–323.
[4] P.W. Higgs, Broken symmetries, massless particles and gauge fields, Phys. Lett. 12 (1964) 132–133.
[5] P.W. Higgs, Broken symmetries and the masses of gauge bosons, Phys. Rev. Lett. 13 (1964) 508–509.
[6] G.S. Guralnik, C.R. Hagen, T.W.B. Kibble, Global conservation laws and massless particles, Phys. Rev. Lett. 13 (1964) 585–587.
[7] P.W. Higgs, Spontaneous symmetry breakdown without massless bosons, Phys. Rev. 145 (1966) 1156–1163.
[8] T. Kibble, Symmetry breaking in non-Abelian gauge theories, Phys. Rev. 155 (1967) 1554–1561.
[9] L. Evans, P. Bryant, LHC Machine, JINST 3 (08) (2008) S08001.
[10] ATLAS Collaboration, Measurement of the Higgs boson mass from the $H \to \gamma\gamma$ and $H \to ZZ^*$ channels with the ATLAS detector using 25 fb^{-1} of pp collision data, Phys. Rev. D 90 (2014) 052004, arXiv:1406.3827.
[11] CMS Collaboration, Measurement of the properties of a Higgs boson in the four-lepton final state, Phys. Rev. D 89 (2014) 092007, arXiv:1312.5353.
[12] CMS Collaboration, Observation of the diphoton decay of the Higgs boson and measurement of its properties, arXiv:1407.0558.
[13] ATLAS Collaboration, Evidence for the spin-0 nature of the Higgs boson using ATLAS data, Phys. Lett. B 726 (2013) 120–144, arXiv:1307.1432.
[14] ATLAS Collaboration, Measurements of Higgs boson production and couplings in diboson final states with the ATLAS detector at the LHC, Phys. Lett. B 726 (2013) 88–119, arXiv:1307.1427.
[15] ATLAS Collaboration, Measurements of Higgs boson production and couplings in the four-lepton channel in pp collisions at center-of-mass energies of 7 and 8 TeV with the ATLAS detector, Phys. Rev. D (2014), submitted for publication, arXiv:1408.5191.
[16] ATLAS Collaboration, The ATLAS experiment at the CERN Large Hadron Collider, JINST 3 (2008) S08003.
[17] G. Bozzi, S. Catani, D. de Florian, M. Grazzini, Transverse-momentum resummation and the spectrum of the Higgs boson at the LHC, Nucl. Phys. B 737 (2006) 73–120, arXiv:hep-ph/0508068.
[18] D. de Florian, G. Ferrera, M. Grazzini, D. Tommasini, Transverse-momentum resummation: Higgs boson production at the Tevatron and the LHC, J. High Energy Phys. 1111 (2011) 064, arXiv:1109.2109.
[19] D. de Florian, G. Ferrera, M. Grazzini, D. Tommasini, Higgs boson production at the LHC: transverse momentum resummation effects in the $H \to 2\gamma$, $H \to WW \to l\nu l\nu$ and $H \to ZZ \to 4l$ decay modes, J. High Energy Phys. 1206 (2012) 132, arXiv:1203.6321.
[20] M. Grazzini, H. Sargsyan, Heavy-quark mass effects in Higgs boson production at the LHC, J. High Energy Phys. 1309 (2013) 129, arXiv:1306.4581.
[21] LHC Higgs Cross Section Working Group, S. Dittmaier, C. Mariotti, G. Passarino, R. Tanaka (Eds.), Handbook of LHC Higgs Cross Sections: 2. Differential Distributions, 2012 (and references therein) CERN-2012-002, arXiv:1201.3084.
[22] LHC Higgs Cross Section Working Group, S. Dittmaier, C. Mariotti, G. Passarino, R. Tanaka (Eds.), Handbook of LHC Higgs Cross Sections: 1. Inclusive Observables, 2011 (and references therein), CERN-2011-002, arXiv:1101.0593.
[23] A. Djouadi, M. Spira, P.M. Zerwas, Production of Higgs bosons in proton colliders: QCD corrections, Phys. Lett. B 264 (1991) 440–446.
[24] S. Dawson, Radiative corrections to Higgs boson production, Nucl. Phys. B 359 (1991) 283–300.
[25] M. Spira, A. Djouadi, D. Graudenz, P.M. Zerwas, Higgs boson production at the LHC, Nucl. Phys. B 453 (1995) 17–82, arXiv:hep-ph/9504378.
[26] R.V. Harlander, W.B. Kilgore, Next-to-next-to-leading order Higgs production at hadron colliders, Phys. Rev. Lett. 88 (2002) 201801, arXiv:hep-ph/0201206.
[27] C. Anastasiou, K. Melnikov, Higgs boson production at hadron colliders in NNLO QCD, Nucl. Phys. B 646 (2002) 220–256, arXiv:hep-ph/0207004.
[28] V. Ravindran, J. Smith, W.L. van Neerven, NNLO corrections to the total cross section for Higgs boson production in hadron–hadron collisions, Nucl. Phys. B 665 (2003) 325–366, arXiv:hep-ph/0302135.
[29] S. Catani, D. de Florian, M. Grazzini, P. Nason, Soft-gluon resummation for Higgs boson production at hadron colliders, J. High Energy Phys. 0307 (2003) 028, arXiv:hep-ph/0306211.
[30] U. Aglietti, R. Bonciani, G. Degrassi, A. Vicini, Two-loop light fermion contribution to Higgs production and decays, Phys. Lett. B 595 (2004) 432–441, arXiv:hep-ph/0404071.
[31] S. Actis, G. Passarino, C. Sturm, S. Uccirati, NLO electroweak corrections to Higgs Boson production at hadron colliders, Phys. Lett. B 670 (2008) 12–17, arXiv:0809.1301.
[32] D. de Florian, M. Grazzini, Higgs production at the LHC: updated cross sections at $\sqrt{s} = 8$ TeV, Phys. Lett. B 718 (2012) 117–120, arXiv:1206.4133.
[33] C. Anastasiou, S. Buehler, F. Herzog, A. Lazopoulos, Inclusive Higgs boson cross-section for the LHC at 8 TeV, J. High Energy Phys. 1204 (2012) 004, arXiv:1202.3638.
[34] J. Baglio, A. Djouadi, Higgs production at the lHC, J. High Energy Phys. 1103 (2011) 055, arXiv:1012.0530.
[35] M. Ciccolini, A. Denner, S. Dittmaier, Strong and electroweak corrections to the production of Higgs + 2 jets via weak interactions at the LHC, Phys. Rev. Lett. 99 (2007) 161803, arXiv:0707.0381.
[36] M. Ciccolini, A. Denner, S. Dittmaier, Electroweak and QCD corrections to Higgs production via vector-boson fusion at the LHC, Phys. Rev. D 77 (2008) 013002, arXiv:0710.4749.
[37] K. Arnold, et al., VBFNLO: a parton level Monte Carlo for processes with electroweak bosons, Comput. Phys. Commun. 180 (2009) 1661–1670, arXiv:0811.4559.
[38] P. Bolzoni, F. Maltoni, S.-O. Moch, M. Zaro, Higgs production via vector-boson fusion at NNLO in QCD, Phys. Rev. Lett. 105 (2010) 011801, arXiv:1003.4451.
[39] T. Han, S. Willenbrock, QCD correction to the pp → WH and ZH total cross-sections, Phys. Lett. B 273 (1991) 167–172.
[40] O. Brein, A. Djouadi, R. Harlander, NNLO QCD corrections to the Higgs-strahlung processes at hadron colliders, Phys. Lett. B 579 (2004) 149–156, arXiv:hep-ph/0307206.
[41] M.L. Ciccolini, S. Dittmaier, M. Krämer, Electroweak radiative corrections to associated WH and ZH production at hadron colliders, Phys. Rev. D 68 (2003) 073003, arXiv:hep-ph/0306234.
[42] W. Beenakker, et al., Higgs radiation off top quarks at the tevatron and the LHC, Phys. Rev. Lett. 87 (2001) 201805, arXiv:hep-ph/0107081.
[43] W. Beenakker, et al., NLO QCD corrections to $t\bar{t}$H production in hadron collisions, Nucl. Phys. B 653 (2003) 151–203, arXiv:hep-ph/0211352.
[44] S. Dawson, L. Orr, L. Reina, D. Wackeroth, Next-to-leading order QCD corrections to $pp \to t\bar{t}h$ at the CERN Large Hadron Collider, Phys. Rev. D 67 (2003) 071503, arXiv:hep-ph/0211438.
[45] S. Dawson, C. Jackson, L.H. Orr, L. Reina, D. Wackeroth, Associated Higgs production with top quarks at the Large Hadron Collider: NLO QCD corrections, Phys. Rev. D 68 (2003) 034022, arXiv:hep-ph/0305087.
[46] A. Bredenstein, A. Denner, S. Dittmaier, M.M. Weber, Precise predictions for the Higgs-boson decay $H \to WW/ZZ \to 4$ leptons, Phys. Rev. D 74 (2006) 013004, arXiv:hep-ph/0604011.

[47] A. Bredenstein, A. Denner, S. Dittmaier, M.M. Weber, Radiative corrections to the semileptonic and hadronic Higgs-boson decays $H \to WW/ZZ \to 4$ fermions, J. High Energy Phys. 0702 (2007) 080, arXiv:hep-ph/0611234.
[48] P. Nason, A new method for combining NLO QCD with shower Monte Carlo algorithms, J. High Energy Phys. 0411 (2004) 040, arXiv:hep-ph/0409146.
[49] S. Frixione, P. Nason, C. Oleari, Matching NLO QCD computations with parton shower simulations: the POWHEG method, J. High Energy Phys. 0711 (2007) 070, arXiv:0709.2092.
[50] S. Alioli, P. Nason, C. Oleari, E. Re, A general framework for implementing NLO calculations in shower Monte Carlo programs: the POWHEG BOX, J. High Energy Phys. 1006 (2010) 043, arXiv:1002.2581.
[51] S. Alioli, P. Nason, C. Oleari, E. Re, NLO Higgs boson production via gluon fusion matched with shower in POWHEG, J. High Energy Phys. 0904 (2009) 002, arXiv:0812.0578.
[52] P. Nason, C. Oleari, NLO Higgs boson production via vector-boson fusion matched with shower in POWHEG, J. High Energy Phys. 1002 (2010) 037, arXiv:0911.5299.
[53] E. Bagnaschi, G. Degrassi, P. Slavich, A. Vicini, Higgs production via gluon fusion in the POWHEG approach in the SM and in the MSSM, J. High Energy Phys. 1202 (2012) 088, arXiv:1111.2854.
[54] T. Sjostrand, S. Mrenna, P.Z. Skands, A brief introduction to PYTHIA 8.1, Comput. Phys. Commun. 178 (2008) 852–867, arXiv:0710.3820.
[55] P. Golonka, Z. Was, PHOTOS Monte, Carlo: a precision tool for QED corrections in Z and W decays, Eur. Phys. J. C 45 (2006) 97–107, arXiv:hep-ph/0506026.
[56] N. Davidson, T. Przedzinski, Z. Was, PHOTOS interface in C++: technical and physics documentation, arXiv:1011.0937.
[57] ATLAS Collaboration, The ATLAS simulation infrastructure, Eur. Phys. J. C 70 (2010) 823–874, arXiv:1005.4568.
[58] S. Agostinelli, et al., GEANT4: a simulation toolkit, Nucl. Instrum. Methods A 506 (2003) 250–303.
[59] K. Hamilton, P. Nason, G. Zanderighi, MINLO: multi-scale improved NLO, J. High Energy Phys. 1210 (2012) 155, arXiv:1206.3572.
[60] LHC Higgs Cross Section Working Group, S. Heinemeyer, C. Mariotti, G. Passarino, R. Tanaka (Eds.), Handbook of LHC Higgs Cross Sections: 3. Higgs Properties, 2013, CERN-2013-004, arXiv:1307.1347.
[61] J. Beringer, et al., Review of particle physics, Phys. Rev. D 86 (2012) 010001.
[62] M. Cacciari, G.P. Salam, G. Soyez, Anti-k_t jet clustering algorithm, J. High Energy Phys. 0804 (2008) 063, arXiv:0802.1189.
[63] ATLAS Collaboration, Jet energy measurement and its systematic uncertainty in proton–proton collisions at $\sqrt{s} = 7$ TeV with the ATLAS detector, Eur. Phys. J. C (2014), submitted for publication, arXiv:1406.0076.
[64] G. Cowan, K. Cranmer, E. Gross, O. Vitells, Asymptotic formulae for likelihood-based tests of new physics, Eur. Phys. J. C 71 (2011) 1554, arXiv:1007.1727.
[65] ATLAS Collaboration, Improved luminosity determination in pp collisions at $\sqrt{s} = 7$ TeV using the ATLAS detector at the LHC, Eur. Phys. J. C 73 (2013) 2518, arXiv:1302.4393.
[66] ATLAS Collaboration, Electron efficiency measurements with the ATLAS detector using the 2012 LHC proton–proton collision data, ATLAS-CONF-2014-032, http://cds.cern.ch/record/1706245, May 2014.
[67] ATLAS Collaboration, Measurement of the muon reconstruction performance of the ATLAS detector using 2011 and 2012 LHC proton–proton collision data, Eur. Phys. J. C (2014), submitted for publication, arXiv:1407.3935.
[68] ATLAS Collaboration, Jet energy resolution in proton–proton collisions at $\sqrt{s} = 7$ TeV recorded in 2010 with the ATLAS detector, Eur. Phys. J. C 73 (2013) 2306, arXiv:1210.6210.
[69] ATLAS Collaboration, Jet energy measurement with the ATLAS detector in proton–proton collisions at $\sqrt{s} = 7$ TeV, Eur. Phys. J. C 73 (2013) 2304, arXiv:1112.6426.
[70] I.W. Stewart, F.J. Tackmann, Theory uncertainties for Higgs and other searches using jet bins, Phys. Rev. D 85 (2012) 034011, arXiv:1107.2117.

ATLAS Collaboration

G. Aad [85], B. Abbott [113], J. Abdallah [153], S. Abdel Khalek [117], O. Abdinov [11], R. Aben [107], B. Abi [114], M. Abolins [90], O.S. AbouZeid [160], H. Abramowicz [155], H. Abreu [154], R. Abreu [30], Y. Abulaiti [148a,148b], B.S. Acharya [166a,166b,a], L. Adamczyk [38a], D.L. Adams [25], J. Adelman [178], S. Adomeit [100], T. Adye [131], T. Agatonovic-Jovin [13a], J.A. Aguilar-Saavedra [126a,126f], M. Agustoni [17], S.P. Ahlen [22], F. Ahmadov [65,b], G. Aielli [135a,135b], H. Akerstedt [148a,148b], T.P.A. Åkesson [81], G. Akimoto [157], A.V. Akimov [96], G.L. Alberghi [20a,20b], J. Albert [171], S. Albrand [55], M.J. Alconada Verzini [71], M. Aleksa [30], I.N. Aleksandrov [65], C. Alexa [26a], G. Alexander [155], G. Alexandre [49], T. Alexopoulos [10], M. Alhroob [166a,166c], G. Alimonti [91a], L. Alio [85], J. Alison [31], B.M.M. Allbrooke [18], L.J. Allison [72], P.P. Allport [74], A. Aloisio [104a,104b], A. Alonso [36], F. Alonso [71], C. Alpigiani [76], A. Altheimer [35], B. Alvarez Gonzalez [90], M.G. Alviggi [104a,104b], K. Amako [66], Y. Amaral Coutinho [24a], C. Amelung [23], D. Amidei [89], S.P. Amor Dos Santos [126a,126c], A. Amorim [126a,126b], S. Amoroso [48], N. Amram [155], G. Amundsen [23], C. Anastopoulos [141], L.S. Ancu [49], N. Andari [30], T. Andeen [35], C.F. Anders [58b], G. Anders [30], K.J. Anderson [31], A. Andreazza [91a,91b], V. Andrei [58a], X.S. Anduaga [71], S. Angelidakis [9], I. Angelozzi [107], P. Anger [44], A. Angerami [35], F. Anghinolfi [30], A.V. Anisenkov [109,c], N. Anjos [12], A. Annovi [47], A. Antonaki [9], M. Antonelli [47], A. Antonov [98], J. Antos [146b], F. Anulli [134a], M. Aoki [66], L. Aperio Bella [18], R. Apolle [120,d], G. Arabidze [90], I. Aracena [145], Y. Arai [66], J.P. Araque [126a], A.T.H. Arce [45], J-F. Arguin [95], S. Argyropoulos [42], M. Arik [19a], A.J. Armbruster [30], O. Arnaez [30], V. Arnal [82], H. Arnold [48], M. Arratia [28], O. Arslan [21], A. Artamonov [97], G. Artoni [23], S. Asai [157], N. Asbah [42], A. Ashkenazi [155], B. Åsman [148a,148b], L. Asquith [6], K. Assamagan [25], R. Astalos [146a], M. Atkinson [167], N.B. Atlay [143], B. Auerbach [6], K. Augsten [128], M. Aurousseau [147b], G. Avolio [30], G. Azuelos [95,e], Y. Azuma [157], M.A. Baak [30], A.E. Baas [58a], C. Bacci [136a,136b], H. Bachacou [138], K. Bachas [156], M. Backes [30], M. Backhaus [30], J. Backus Mayes [145], E. Badescu [26a], P. Bagiacchi [134a,134b], P. Bagnaia [134a,134b], Y. Bai [33a], T. Bain [35], J.T. Baines [131], O.K. Baker [178], P. Balek [129], F. Balli [138], E. Banas [39], Sw. Banerjee [175], A.A.E. Bannoura [177], V. Bansal [171], H.S. Bansil [18], L. Barak [174], S.P. Baranov [96], E.L. Barberio [88], D. Barberis [50a,50b], M. Barbero [85], T. Barillari [101], M. Barisonzi [177], T. Barklow [145], N. Barlow [28], B.M. Barnett [131], R.M. Barnett [15], Z. Barnovska [5], A. Baroncelli [136a], G. Barone [49], A.J. Barr [120], F. Barreiro [82], J. Barreiro Guimarães da Costa [57], R. Bartoldus [145], A.E. Barton [72], P. Bartos [146a], V. Bartsch [151], A. Bassalat [117], A. Basye [167], R.L. Bates [53], J.R. Batley [28], M. Battaglia [139], M. Battistin [30], F. Bauer [138], H.S. Bawa [145,f], M.D. Beattie [72], T. Beau [80], P.H. Beauchemin [163], R. Beccherle [124a,124b], P. Bechtle [21], H.P. Beck [17], K. Becker [177], S. Becker [100], M. Beckingham [172], C. Becot [117], A.J. Beddall [19c], A. Beddall [19c], S. Bedikian [178], V.A. Bednyakov [65], C.P. Bee [150], L.J. Beemster [107], T.A. Beermann [177], M. Begel [25],

K. Behr [120], C. Belanger-Champagne [87], P.J. Bell [49], W.H. Bell [49], G. Bella [155], L. Bellagamba [20a], A. Bellerive [29], M. Bellomo [86], K. Belotskiy [98], O. Beltramello [30], O. Benary [155], D. Benchekroun [137a], K. Bendtz [148a,148b], N. Benekos [167], Y. Benhammou [155], E. Benhar Noccioli [49], J.A. Benitez Garcia [161b], D.P. Benjamin [45], J.R. Bensinger [23], K. Benslama [132], S. Bentvelsen [107], D. Berge [107], E. Bergeaas Kuutmann [168], N. Berger [5], F. Berghaus [171], J. Beringer [15], C. Bernard [22], P. Bernat [78], C. Bernius [79], F.U. Bernlochner [171], T. Berry [77], P. Berta [129], C. Bertella [85], G. Bertoli [148a,148b], F. Bertolucci [124a,124b], C. Bertsche [113], D. Bertsche [113], M.I. Besana [91a], G.J. Besjes [106], O. Bessidskaia [148a,148b], M. Bessner [42], N. Besson [138], C. Betancourt [48], S. Bethke [101], W. Bhimji [46], R.M. Bianchi [125], L. Bianchini [23], M. Bianco [30], O. Biebel [100], S.P. Bieniek [78], K. Bierwagen [54], J. Biesiada [15], M. Biglietti [136a], J. Bilbao De Mendizabal [49], H. Bilokon [47], M. Bindi [54], S. Binet [117], A. Bingul [19c], C. Bini [134a,134b], C.W. Black [152], J.E. Black [145], K.M. Black [22], D. Blackburn [140], R.E. Blair [6], J.-B. Blanchard [138], T. Blazek [146a], I. Bloch [42], C. Blocker [23], W. Blum [83,*], U. Blumenschein [54], G.J. Bobbink [107], V.S. Bobrovnikov [109,c], S.S. Bocchetta [81], A. Bocci [45], C. Bock [100], C.R. Boddy [120], M. Boehler [48], T.T. Boek [177], J.A. Bogaerts [30], A.G. Bogdanchikov [109], A. Bogouch [92,*], C. Bohm [148a], J. Bohm [127], V. Boisvert [77], T. Bold [38a], V. Boldea [26a], A.S. Boldyrev [99], M. Bomben [80], M. Bona [76], M. Boonekamp [138], A. Borisov [130], G. Borissov [72], M. Borri [84], S. Borroni [42], J. Bortfeldt [100], V. Bortolotto [136a,136b], K. Bos [107], D. Boscherini [20a], M. Bosman [12], H. Boterenbrood [107], J. Boudreau [125], J. Bouffard [2], E.V. Bouhova-Thacker [72], D. Boumediene [34], C. Bourdarios [117], N. Bousson [114], S. Boutouil [137d], A. Boveia [31], J. Boyd [30], I.R. Boyko [65], I. Bozic [13a], J. Bracinik [18], A. Brandt [8], G. Brandt [15], O. Brandt [58a], U. Bratzler [158], B. Brau [86], J.E. Brau [116], H.M. Braun [177,*], S.F. Brazzale [166a,166c], B. Brelier [160], K. Brendlinger [122], A.J. Brennan [88], R. Brenner [168], S. Bressler [174], K. Bristow [147c], T.M. Bristow [46], D. Britton [53], F.M. Brochu [28], I. Brock [21], R. Brock [90], C. Bromberg [90], J. Bronner [101], G. Brooijmans [35], T. Brooks [77], W.K. Brooks [32b], J. Brosamer [15], E. Brost [116], J. Brown [55], P.A. Bruckman de Renstrom [39], D. Bruncko [146b], R. Bruneliere [48], S. Brunet [61], A. Bruni [20a], G. Bruni [20a], M. Bruschi [20a], L. Bryngemark [81], T. Buanes [14], Q. Buat [144], F. Bucci [49], P. Buchholz [143], R.M. Buckingham [120], A.G. Buckley [53], S.I. Buda [26a], I.A. Budagov [65], F. Buehrer [48], L. Bugge [119], M.K. Bugge [119], O. Bulekov [98], A.C. Bundock [74], H. Burckhart [30], S. Burdin [74], B. Burghgrave [108], S. Burke [131], I. Burmeister [43], E. Busato [34], D. Büscher [48], V. Büscher [83], P. Bussey [53], C.P. Buszello [168], B. Butler [57], J.M. Butler [22], A.I. Butt [3], C.M. Buttar [53], J.M. Butterworth [78], P. Butti [107], W. Buttinger [28], A. Buzatu [53], M. Byszewski [10], S. Cabrera Urbán [169], D. Caforio [20a,20b], O. Cakir [4a], P. Calafiura [15], A. Calandri [138], G. Calderini [80], P. Calfayan [100], R. Calkins [108], L.P. Caloba [24a], D. Calvet [34], S. Calvet [34], R. Camacho Toro [49], S. Camarda [42], D. Cameron [119], L.M. Caminada [15], R. Caminal Armadans [12], S. Campana [30], M. Campanelli [78], A. Campoverde [150], V. Canale [104a,104b], A. Canepa [161a], M. Cano Bret [76], J. Cantero [82], R. Cantrill [126a], T. Cao [40], M.D.M. Capeans Garrido [30], I. Caprini [26a], M. Caprini [26a], M. Capua [37a,37b], R. Caputo [83], R. Cardarelli [135a], T. Carli [30], G. Carlino [104a], L. Carminati [91a,91b], S. Caron [106], E. Carquin [32a], G.D. Carrillo-Montoya [147c], J.R. Carter [28], J. Carvalho [126a,126c], D. Casadei [78], M.P. Casado [12], M. Casolino [12], E. Castaneda-Miranda [147b], A. Castelli [107], V. Castillo Gimenez [169], N.F. Castro [126a], P. Catastini [57], A. Catinaccio [30], J.R. Catmore [119], A. Cattai [30], G. Cattani [135a,135b], J. Caudron [83], V. Cavaliere [167], D. Cavalli [91a], M. Cavalli-Sforza [12], V. Cavasinni [124a,124b], F. Ceradini [136a,136b], B.C. Cerio [45], K. Cerny [129], A.S. Cerqueira [24b], A. Cerri [151], L. Cerrito [76], F. Cerutti [15], M. Cerv [30], A. Cervelli [17], S.A. Cetin [19b], A. Chafaq [137a], D. Chakraborty [108], I. Chalupkova [129], P. Chang [167], B. Chapleau [87], J.D. Chapman [28], D. Charfeddine [117], D.G. Charlton [18], C.C. Chau [160], C.A. Chavez Barajas [151], S. Cheatham [87], A. Chegwidden [90], S. Chekanov [6], S.V. Chekulaev [161a], G.A. Chelkov [65,g], M.A. Chelstowska [89], C. Chen [64], H. Chen [25], K. Chen [150], L. Chen [33d,h], S. Chen [33c], X. Chen [33f], Y. Chen [67], Y. Chen [35], H.C. Cheng [89], Y. Cheng [31], A. Cheplakov [65], R. Cherkaoui El Moursli [137e], V. Chernyatin [25,*], E. Cheu [7], L. Chevalier [138], V. Chiarella [47], G. Chiefari [104a,104b], J.T. Childers [6], A. Chilingarov [72], G. Chiodini [73a], A.S. Chisholm [18], R.T. Chislett [78], A. Chitan [26a], M.V. Chizhov [65], S. Chouridou [9], B.K.B. Chow [100], D. Chromek-Burckhart [30], M.L. Chu [153], J. Chudoba [127], J.J. Chwastowski [39], L. Chytka [115], G. Ciapetti [134a,134b], A.K. Ciftci [4a], R. Ciftci [4a], D. Cinca [53], V. Cindro [75], A. Ciocio [15], P. Cirkovic [13b], Z.H. Citron [174], M. Citterio [91a], M. Ciubancan [26a], A. Clark [49], P.J. Clark [46], R.N. Clarke [15], W. Cleland [125], J.C. Clemens [85], C. Clement [148a,148b], Y. Coadou [85], M. Cobal [166a,166c], A. Coccaro [140], J. Cochran [64], L. Coffey [23], J.G. Cogan [145], J. Coggeshall [167], B. Cole [35], S. Cole [108], A.P. Colijn [107], J. Collot [55], T. Colombo [58c], G. Colon [86], G. Compostella [101],

P. Conde Muiño [126a,126b], E. Coniavitis [48], M.C. Conidi [12], S.H. Connell [147b], I.A. Connelly [77], S.M. Consonni [91a,91b], V. Consorti [48], S. Constantinescu [26a], C. Conta [121a,121b], G. Conti [57], F. Conventi [104a,i], M. Cooke [15], B.D. Cooper [78], A.M. Cooper-Sarkar [120], N.J. Cooper-Smith [77], K. Copic [15], T. Cornelissen [177], M. Corradi [20a], F. Corriveau [87,j], A. Corso-Radu [165], A. Cortes-Gonzalez [12], G. Cortiana [101], G. Costa [91a], M.J. Costa [169], D. Costanzo [141], D. Côté [8], G. Cottin [28], G. Cowan [77], B.E. Cox [84], K. Cranmer [110], G. Cree [29], S. Crépé-Renaudin [55], F. Crescioli [80], W.A. Cribbs [148a,148b], M. Crispin Ortuzar [120], M. Cristinziani [21], V. Croft [106], G. Crosetti [37a,37b], C.-M. Cuciuc [26a], T. Cuhadar Donszelmann [141], J. Cummings [178], M. Curatolo [47], C. Cuthbert [152], H. Czirr [143], P. Czodrowski [3], Z. Czyczula [178], S. D'Auria [53], M. D'Onofrio [74], M.J. Da Cunha Sargedas De Sousa [126a,126b], C. Da Via [84], W. Dabrowski [38a], A. Dafinca [120], T. Dai [89], O. Dale [14], F. Dallaire [95], C. Dallapiccola [86], M. Dam [36], A.C. Daniells [18], M. Dano Hoffmann [138], V. Dao [48], G. Darbo [50a], S. Darmora [8], J.A. Dassoulas [42], A. Dattagupta [61], W. Davey [21], C. David [171], T. Davidek [129], E. Davies [120,d], M. Davies [155], O. Davignon [80], A.R. Davison [78], P. Davison [78], Y. Davygora [58a], E. Dawe [144], I. Dawson [141], R.K. Daya-Ishmukhametova [86], K. De [8], R. de Asmundis [104a], S. De Castro [20a,20b], S. De Cecco [80], N. De Groot [106], P. de Jong [107], H. De la Torre [82], F. De Lorenzi [64], L. De Nooij [107], D. De Pedis [134a], A. De Salvo [134a], U. De Sanctis [151], A. De Santo [151], J.B. De Vivie De Regie [117], W.J. Dearnaley [72], R. Debbe [25], C. Debenedetti [139], B. Dechenaux [55], D.V. Dedovich [65], I. Deigaard [107], J. Del Peso [82], T. Del Prete [124a,124b], F. Deliot [138], C.M. Delitzsch [49], M. Deliyergiyev [75], A. Dell'Acqua [30], L. Dell'Asta [22], M. Dell'Orso [124a,124b], M. Della Pietra [104a,i], D. della Volpe [49], M. Delmastro [5], P.A. Delsart [55], C. Deluca [107], S. Demers [178], M. Demichev [65], A. Demilly [80], S.P. Denisov [130], D. Derendarz [39], J.E. Derkaoui [137d], F. Derue [80], P. Dervan [74], K. Desch [21], C. Deterre [42], P.O. Deviveiros [107], A. Dewhurst [131], S. Dhaliwal [107], A. Di Ciaccio [135a,135b], L. Di Ciaccio [5], A. Di Domenico [134a,134b], C. Di Donato [104a,104b], A. Di Girolamo [30], B. Di Girolamo [30], A. Di Mattia [154], B. Di Micco [136a,136b], R. Di Nardo [47], A. Di Simone [48], R. Di Sipio [20a,20b], D. Di Valentino [29], F.A. Dias [46], M.A. Diaz [32a], E.B. Diehl [89], J. Dietrich [42], T.A. Dietzsch [58a], S. Diglio [85], A. Dimitrievska [13a], J. Dingfelder [21], C. Dionisi [134a,134b], P. Dita [26a], S. Dita [26a], F. Dittus [30], F. Djama [85], T. Djobava [51b], J.I. Djuvsland [58a], M.A.B. do Vale [24c], A. Do Valle Wemans [126a,126g], D. Dobos [30], C. Doglioni [49], T. Doherty [53], T. Dohmae [157], J. Dolejsi [129], Z. Dolezal [129], B.A. Dolgoshein [98,*], M. Donadelli [24d], S. Donati [124a,124b], P. Dondero [121a,121b], J. Donini [34], J. Dopke [131], A. Doria [104a], M.T. Dova [71], A.T. Doyle [53], M. Dris [10], J. Dubbert [89], S. Dube [15], E. Dubreuil [34], E. Duchovni [174], G. Duckeck [100], O.A. Ducu [26a], D. Duda [177], A. Dudarev [30], F. Dudziak [64], L. Duflot [117], L. Duguid [77], M. Dührssen [30], M. Dunford [58a], H. Duran Yildiz [4a], M. Düren [52], A. Durglishvili [51b], M. Dwuznik [38a], M. Dyndal [38a], J. Ebke [100], W. Edson [2], N.C. Edwards [46], W. Ehrenfeld [21], T. Eifert [145], G. Eigen [14], K. Einsweiler [15], T. Ekelof [168], M. El Kacimi [137c], M. Ellert [168], S. Elles [5], F. Ellinghaus [83], N. Ellis [30], J. Elmsheuser [100], M. Elsing [30], D. Emeliyanov [131], Y. Enari [157], O.C. Endner [83], M. Endo [118], R. Engelmann [150], J. Erdmann [178], A. Ereditato [17], D. Eriksson [148a], G. Ernis [177], J. Ernst [2], M. Ernst [25], J. Ernwein [138], D. Errede [167], S. Errede [167], E. Ertel [83], M. Escalier [117], H. Esch [43], C. Escobar [125], B. Esposito [47], A.I. Etienvre [138], E. Etzion [155], H. Evans [61], A. Ezhilov [123], L. Fabbri [20a,20b], G. Facini [31], R.M. Fakhrutdinov [130], S. Falciano [134a], R.J. Falla [78], J. Faltova [129], Y. Fang [33a], M. Fanti [91a,91b], A. Farbin [8], A. Farilla [136a], T. Farooque [12], S. Farrell [15], S.M. Farrington [172], P. Farthouat [30], F. Fassi [137e], P. Fassnacht [30], D. Fassouliotis [9], A. Favareto [50a,50b], L. Fayard [117], P. Federic [146a], O.L. Fedin [123,k], W. Fedorko [170], M. Fehling-Kaschek [48], S. Feigl [30], L. Feligioni [85], C. Feng [33d], E.J. Feng [6], H. Feng [89], A.B. Fenyuk [130], S. Fernandez Perez [30], S. Ferrag [53], J. Ferrando [53], A. Ferrari [168], P. Ferrari [107], R. Ferrari [121a], D.E. Ferreira de Lima [53], A. Ferrer [169], D. Ferrere [49], C. Ferretti [89], A. Ferretto Parodi [50a,50b], M. Fiascaris [31], F. Fiedler [83], A. Filipčič [75], M. Filipuzzi [42], F. Filthaut [106], M. Fincke-Keeler [171], K.D. Finelli [152], M.C.N. Fiolhais [126a,126c], L. Fiorini [169], A. Firan [40], A. Fischer [2], J. Fischer [177], W.C. Fisher [90], E.A. Fitzgerald [23], M. Flechl [48], I. Fleck [143], P. Fleischmann [89], S. Fleischmann [177], G.T. Fletcher [141], G. Fletcher [76], T. Flick [177], A. Floderus [81], L.R. Flores Castillo [60a], A.C. Florez Bustos [161b], M.J. Flowerdew [101], A. Formica [138], A. Forti [84], D. Fortin [161a], D. Fournier [117], H. Fox [72], S. Fracchia [12], P. Francavilla [80], M. Franchini [20a,20b], S. Franchino [30], D. Francis [30], L. Franconi [119], M. Franklin [57], S. Franz [62], M. Fraternali [121a,121b], S.T. French [28], C. Friedrich [42], F. Friedrich [44], D. Froidevaux [30], J.A. Frost [28], C. Fukunaga [158], E. Fullana Torregrosa [83], B.G. Fulsom [145], J. Fuster [169], C. Gabaldon [55], O. Gabizon [177], A. Gabrielli [20a,20b], A. Gabrielli [134a,134b], S. Gadatsch [107], S. Gadomski [49], G. Gagliardi [50a,50b], P. Gagnon [61], C. Galea [106], B. Galhardo [126a,126c], E.J. Gallas [120], V. Gallo [17],

B.J. Gallop [131], P. Gallus [128], G. Galster [36], K.K. Gan [111], J. Gao [33b,h], Y.S. Gao [145,f], F.M. Garay Walls [46], F. Garberson [178], C. García [169], J.E. García Navarro [169], M. Garcia-Sciveres [15], R.W. Gardner [31], N. Garelli [145], V. Garonne [30], C. Gatti [47], G. Gaudio [121a], B. Gaur [143], L. Gauthier [95], P. Gauzzi [134a,134b], I.L. Gavrilenko [96], C. Gay [170], G. Gaycken [21], E.N. Gazis [10], P. Ge [33d], Z. Gecse [170], C.N.P. Gee [131], D.A.A. Geerts [107], Ch. Geich-Gimbel [21], K. Gellerstedt [148a,148b], C. Gemme [50a], A. Gemmell [53], M.H. Genest [55], S. Gentile [134a,134b], M. George [54], S. George [77], D. Gerbaudo [165], A. Gershon [155], H. Ghazlane [137b], N. Ghodbane [34], B. Giacobbe [20a], S. Giagu [134a,134b], V. Giangiobbe [12], P. Giannetti [124a,124b], F. Gianotti [30], B. Gibbard [25], S.M. Gibson [77], M. Gilchriese [15], T.P.S. Gillam [28], D. Gillberg [30], G. Gilles [34], D.M. Gingrich [3,e], N. Giokaris [9], M.P. Giordani [166a,166c], R. Giordano [104a,104b], F.M. Giorgi [20a], F.M. Giorgi [16], P.F. Giraud [138], D. Giugni [91a], C. Giuliani [48], M. Giulini [58b], B.K. Gjelsten [119], S. Gkaitatzis [156], I. Gkialas [156,l], L.K. Gladilin [99], C. Glasman [82], J. Glatzer [30], P.C.F. Glaysher [46], A. Glazov [42], G.L. Glonti [65], M. Goblirsch-Kolb [101], J.R. Goddard [76], J. Godlewski [30], C. Goeringer [83], S. Goldfarb [89], T. Golling [178], D. Golubkov [130], A. Gomes [126a,126b,126d], L.S. Gomez Fajardo [42], R. Gonçalo [126a], J. Goncalves Pinto Firmino Da Costa [138], L. Gonella [21], S. González de la Hoz [169], G. Gonzalez Parra [12], S. Gonzalez-Sevilla [49], L. Goossens [30], P.A. Gorbounov [97], H.A. Gordon [25], I. Gorelov [105], B. Gorini [30], E. Gorini [73a,73b], A. Gorišek [75], E. Gornicki [39], A.T. Goshaw [6], C. Gössling [43], M.I. Gostkin [65], M. Gouighri [137a], D. Goujdami [137c], M.P. Goulette [49], A.G. Goussiou [140], C. Goy [5], S. Gozpinar [23], H.M.X. Grabas [138], L. Graber [54], I. Grabowska-Bold [38a], P. Grafström [20a,20b], K-J. Grahn [42], J. Gramling [49], E. Gramstad [119], S. Grancagnolo [16], V. Grassi [150], V. Gratchev [123], H.M. Gray [30], E. Graziani [136a], O.G. Grebenyuk [123], Z.D. Greenwood [79,m], K. Gregersen [78], I.M. Gregor [42], P. Grenier [145], J. Griffiths [8], A.A. Grillo [139], K. Grimm [72], S. Grinstein [12,n], Ph. Gris [34], Y.V. Grishkevich [99], J.-F. Grivaz [117], J.P. Grohs [44], A. Grohsjean [42], E. Gross [174], J. Grosse-Knetter [54], G.C. Grossi [135a,135b], J. Groth-Jensen [174], Z.J. Grout [151], L. Guan [33b], J. Guenther [128], F. Guescini [49], D. Guest [178], O. Gueta [155], C. Guicheney [34], E. Guido [50a,50b], T. Guillemin [117], S. Guindon [2], U. Gul [53], C. Gumpert [44], J. Guo [35], S. Gupta [120], P. Gutierrez [113], N.G. Gutierrez Ortiz [53], C. Gutschow [78], N. Guttman [155], C. Guyot [138], C. Gwenlan [120], C.B. Gwilliam [74], A. Haas [110], C. Haber [15], H.K. Hadavand [8], N. Haddad [137e], P. Haefner [21], S. Hageböck [21], Z. Hajduk [39], H. Hakobyan [179], M. Haleem [42], D. Hall [120], G. Halladjian [90], K. Hamacher [177], P. Hamal [115], K. Hamano [171], M. Hamer [54], A. Hamilton [147a], S. Hamilton [163], G.N. Hamity [147c], P.G. Hamnett [42], L. Han [33b], K. Hanagaki [118], K. Hanawa [157], M. Hance [15], P. Hanke [58a], R. Hanna [138], J.B. Hansen [36], J.D. Hansen [36], P.H. Hansen [36], K. Hara [162], A.S. Hard [175], T. Harenberg [177], F. Hariri [117], S. Harkusha [92], D. Harper [89], R.D. Harrington [46], O.M. Harris [140], P.F. Harrison [172], F. Hartjes [107], M. Hasegawa [67], S. Hasegawa [103], Y. Hasegawa [142], A. Hasib [113], S. Hassani [138], S. Haug [17], M. Hauschild [30], R. Hauser [90], M. Havranek [127], C.M. Hawkes [18], R.J. Hawkings [30], A.D. Hawkins [81], T. Hayashi [162], D. Hayden [90], C.P. Hays [120], H.S. Hayward [74], S.J. Haywood [131], S.J. Head [18], T. Heck [83], V. Hedberg [81], L. Heelan [8], S. Heim [122], T. Heim [177], B. Heinemann [15], L. Heinrich [110], J. Hejbal [127], L. Helary [22], C. Heller [100], M. Heller [30], S. Hellman [148a,148b], D. Hellmich [21], C. Helsens [30], J. Henderson [120], R.C.W. Henderson [72], Y. Heng [175], C. Hengler [42], A. Henrichs [178], A.M. Henriques Correia [30], S. Henrot-Versille [117], G.H. Herbert [16], Y. Hernández Jiménez [169], R. Herrberg-Schubert [16], G. Herten [48], R. Hertenberger [100], L. Hervas [30], G.G. Hesketh [78], N.P. Hessey [107], R. Hickling [76], E. Higón-Rodriguez [169], E. Hill [171], J.C. Hill [28], K.H. Hiller [42], S. Hillert [21], S.J. Hillier [18], I. Hinchliffe [15], E. Hines [122], M. Hirose [159], D. Hirschbuehl [177], J. Hobbs [150], N. Hod [107], M.C. Hodgkinson [141], P. Hodgson [141], A. Hoecker [30], M.R. Hoeferkamp [105], F. Hoenig [100], J. Hoffman [40], D. Hoffmann [85], M. Hohlfeld [83], T.R. Holmes [15], T.M. Hong [122], L. Hooft van Huysduynen [110], W.H. Hopkins [116], Y. Horii [103], J-Y. Hostachy [55], S. Hou [153], A. Hoummada [137a], J. Howard [120], J. Howarth [42], M. Hrabovsky [115], I. Hristova [16], J. Hrivnac [117], T. Hryn'ova [5], C. Hsu [147c], P.J. Hsu [83], S.-C. Hsu [140], D. Hu [35], X. Hu [89], Y. Huang [42], Z. Hubacek [30], F. Hubaut [85], F. Huegging [21], T.B. Huffman [120], E.W. Hughes [35], G. Hughes [72], M. Huhtinen [30], T.A. Hülsing [83], M. Hurwitz [15], N. Huseynov [65,b], J. Huston [90], J. Huth [57], G. Iacobucci [49], G. Iakovidis [10], I. Ibragimov [143], L. Iconomidou-Fayard [117], E. Ideal [178], Z. Idrissi [137e], P. Iengo [104a], O. Igonkina [107], T. Iizawa [173], Y. Ikegami [66], K. Ikematsu [143], M. Ikeno [66], Y. Ilchenko [31,o], D. Iliadis [156], N. Ilic [160], Y. Inamaru [67], T. Ince [101], P. Ioannou [9], M. Iodice [136a], K. Iordanidou [9], V. Ippolito [57], A. Irles Quiles [169], C. Isaksson [168], M. Ishino [68], M. Ishitsuka [159], R. Ishmukhametov [111], C. Issever [120], S. Istin [19a], J.M. Iturbe Ponce [84], R. Iuppa [135a,135b], J. Ivarsson [81], W. Iwanski [39], H. Iwasaki [66], J.M. Izen [41], V. Izzo [104a], B. Jackson [122], M. Jackson [74], P. Jackson [1], M.R. Jaekel [30], V. Jain [2], K. Jakobs [48],

S. Jakobsen [30], T. Jakoubek [127], J. Jakubek [128], D.O. Jamin [153], D.K. Jana [79], E. Jansen [78], H. Jansen [30], J. Janssen [21], M. Janus [172], G. Jarlskog [81], N. Javadov [65,b], T. Javůrek [48], L. Jeanty [15], J. Jejelava [51a,p], G.-Y. Jeng [152], D. Jennens [88], P. Jenni [48,q], J. Jentzsch [43], C. Jeske [172], S. Jézéquel [5], H. Ji [175], J. Jia [150], Y. Jiang [33b], M. Jimenez Belenguer [42], S. Jin [33a], A. Jinaru [26a], O. Jinnouchi [159], M.D. Joergensen [36], K.E. Johansson [148a,148b], P. Johansson [141], K.A. Johns [7], K. Jon-And [148a,148b], G. Jones [172], R.W.L. Jones [72], T.J. Jones [74], J. Jongmanns [58a], P.M. Jorge [126a,126b], K.D. Joshi [84], J. Jovicevic [149], X. Ju [175], C.A. Jung [43], R.M. Jungst [30], P. Jussel [62], A. Juste Rozas [12,n], M. Kaci [169], A. Kaczmarska [39], M. Kado [117], H. Kagan [111], M. Kagan [145], E. Kajomovitz [45], C.W. Kalderon [120], S. Kama [40], A. Kamenshchikov [130], N. Kanaya [157], M. Kaneda [30], S. Kaneti [28], V.A. Kantserov [98], J. Kanzaki [66], B. Kaplan [110], A. Kapliy [31], D. Kar [53], K. Karakostas [10], N. Karastathis [10], M.J. Kareem [54], M. Karnevskiy [83], S.N. Karpov [65], Z.M. Karpova [65], K. Karthik [110], V. Kartvelishvili [72], A.N. Karyukhin [130], L. Kashif [175], G. Kasieczka [58b], R.D. Kass [111], A. Kastanas [14], Y. Kataoka [157], A. Katre [49], J. Katzy [42], V. Kaushik [7], K. Kawagoe [70], T. Kawamoto [157], G. Kawamura [54], S. Kazama [157], V.F. Kazanin [109], M.Y. Kazarinov [65], R. Keeler [171], R. Kehoe [40], M. Keil [54], J.S. Keller [42], J.J. Kempster [77], H. Keoshkerian [5], O. Kepka [127], B.P. Kerševan [75], S. Kersten [177], K. Kessoku [157], J. Keung [160], F. Khalil-zada [11], H. Khandanyan [148a,148b], A. Khanov [114], A. Khodinov [98], A. Khomich [58a], T.J. Khoo [28], G. Khoriauli [21], A. Khoroshilov [177], V. Khovanskiy [97], E. Khramov [65], J. Khubua [51b], H.Y. Kim [8], H. Kim [148a,148b], S.H. Kim [162], N. Kimura [173], O. Kind [16], B.T. King [74], M. King [169], R.S.B. King [120], S.B. King [170], J. Kirk [131], A.E. Kiryunin [101], T. Kishimoto [67], D. Kisielewska [38a], F. Kiss [48], T. Kittelmann [125], K. Kiuchi [162], E. Kladiva [146b], M. Klein [74], U. Klein [74], K. Kleinknecht [83], P. Klimek [148a,148b], A. Klimentov [25], R. Klingenberg [43], J.A. Klinger [84], T. Klioutchnikova [30], P.F. Klok [106], E.-E. Kluge [58a], P. Kluit [107], S. Kluth [101], E. Kneringer [62], E.B.F.G. Knoops [85], A. Knue [53], D. Kobayashi [159], T. Kobayashi [157], M. Kobel [44], M. Kocian [145], P. Kodys [129], P. Koevesarki [21], T. Koffas [29], E. Koffeman [107], L.A. Kogan [120], S. Kohlmann [177], Z. Kohout [128], T. Kohriki [66], T. Koi [145], H. Kolanoski [16], I. Koletsou [5], J. Koll [90], A.A. Komar [96,*], Y. Komori [157], T. Kondo [66], N. Kondrashova [42], K. Köneke [48], A.C. König [106], S. König [83], T. Kono [66,r], R. Konoplich [110,s], N. Konstantinidis [78], R. Kopeliansky [154], S. Koperny [38a], L. Köpke [83], A.K. Kopp [48], K. Korcyl [39], K. Kordas [156], A. Korn [78], A.A. Korol [109,c], I. Korolkov [12], E.V. Korolkova [141], V.A. Korotkov [130], O. Kortner [101], S. Kortner [101], V.V. Kostyukhin [21], V.M. Kotov [65], A. Kotwal [45], C. Kourkoumelis [9], V. Kouskoura [156], A. Koutsman [161a], R. Kowalewski [171], T.Z. Kowalski [38a], W. Kozanecki [138], A.S. Kozhin [130], V. Kral [128], V.A. Kramarenko [99], G. Kramberger [75], D. Krasnopevtsev [98], A. Krasznahorkay [30], J.K. Kraus [21], A. Kravchenko [25], S. Kreiss [110], M. Kretz [58c], J. Kretzschmar [74], K. Kreutzfeldt [52], P. Krieger [160], K. Kroeninger [54], H. Kroha [101], J. Kroll [122], J. Kroseberg [21], J. Krstic [13a], U. Kruchonak [65], H. Krüger [21], T. Kruker [17], N. Krumnack [64], Z.V. Krumshteyn [65], A. Kruse [175], M.C. Kruse [45], M. Kruskal [22], T. Kubota [88], H. Kucuk [78], S. Kuday [4c], S. Kuehn [48], A. Kugel [58c], A. Kuhl [139], T. Kuhl [42], V. Kukhtin [65], Y. Kulchitsky [92], S. Kuleshov [32b], M. Kuna [134a,134b], J. Kunkle [122], A. Kupco [127], H. Kurashige [67], Y.A. Kurochkin [92], R. Kurumida [67], V. Kus [127], E.S. Kuwertz [149], M. Kuze [159], J. Kvita [115], A. La Rosa [49], L. La Rotonda [37a,37b], C. Lacasta [169], F. Lacava [134a,134b], J. Lacey [29], H. Lacker [16], D. Lacour [80], V.R. Lacuesta [169], E. Ladygin [65], R. Lafaye [5], B. Laforge [80], T. Lagouri [178], S. Lai [48], H. Laier [58a], L. Lambourne [78], S. Lammers [61], C.L. Lampen [7], W. Lampl [7], E. Lançon [138], U. Landgraf [48], M.P.J. Landon [76], V.S. Lang [58a], A.J. Lankford [165], F. Lanni [25], K. Lantzsch [30], S. Laplace [80], C. Lapoire [21], J.F. Laporte [138], T. Lari [91a], F. Lasagni Manghi [20a,20b], M. Lassnig [30], P. Laurelli [47], W. Lavrijsen [15], A.T. Law [139], P. Laycock [74], O. Le Dortz [80], E. Le Guirriec [85], E. Le Menedeu [12], T. LeCompte [6], F. Ledroit-Guillon [55], C.A. Lee [153], H. Lee [107], J.S.H. Lee [118], S.C. Lee [153], L. Lee [1], G. Lefebvre [80], M. Lefebvre [171], F. Legger [100], C. Leggett [15], A. Lehan [74], M. Lehmacher [21], G. Lehmann Miotto [30], X. Lei [7], W.A. Leight [29], A. Leisos [156], A.G. Leister [178], M.A.L. Leite [24d], R. Leitner [129], D. Lellouch [174], B. Lemmer [54], K.J.C. Leney [78], T. Lenz [21], G. Lenzen [177], B. Lenzi [30], R. Leone [7], S. Leone [124a,124b], C. Leonidopoulos [46], S. Leontsinis [10], C. Leroy [95], C.G. Lester [28], C.M. Lester [122], M. Levchenko [123], J. Levêque [5], D. Levin [89], L.J. Levinson [174], M. Levy [18], A. Lewis [120], G.H. Lewis [110], A.M. Leyko [21], M. Leyton [41], B. Li [33b,t], B. Li [85], H. Li [150], H.L. Li [31], L. Li [45], L. Li [33e], S. Li [45], Y. Li [33c,u], Z. Liang [139], H. Liao [34], B. Liberti [135a], P. Lichard [30], K. Lie [167], J. Liebal [21], W. Liebig [14], C. Limbach [21], A. Limosani [88], S.C. Lin [153,v], T.H. Lin [83], F. Linde [107], B.E. Lindquist [150], J.T. Linnemann [90], E. Lipeles [122], A. Lipniacka [14], M. Lisovyi [42], T.M. Liss [167], D. Lissauer [25], A. Lister [170], A.M. Litke [139], B. Liu [153], D. Liu [153], J.B. Liu [33b], K. Liu [33b,w], L. Liu [89], M. Liu [45], M. Liu [33b], Y. Liu [33b], M. Livan [121a,121b], S.S.A. Livermore [120], A. Lleres [55], J. Llorente Merino [82], S.L. Lloyd [76], F. Lo Sterzo [153], E. Lobodzinska [42],

P. Loch [7], W.S. Lockman [139], T. Loddenkoetter [21], F.K. Loebinger [84], A.E. Loevschall-Jensen [36], A. Loginov [178], T. Lohse [16], K. Lohwasser [42], M. Lokajicek [127], V.P. Lombardo [5], B.A. Long [22], J.D. Long [89], R.E. Long [72], L. Lopes [126a], D. Lopez Mateos [57], B. Lopez Paredes [141], I. Lopez Paz [12], J. Lorenz [100], N. Lorenzo Martinez [61], M. Losada [164], P. Loscutoff [15], X. Lou [41], A. Lounis [117], J. Love [6], P.A. Love [72], A.J. Lowe [145,f], F. Lu [33a], N. Lu [89], H.J. Lubatti [140], C. Luci [134a,134b], A. Lucotte [55], F. Luehring [61], W. Lukas [62], L. Luminari [134a], O. Lundberg [148a,148b], B. Lund-Jensen [149], M. Lungwitz [83], D. Lynn [25], R. Lysak [127], E. Lytken [81], H. Ma [25], L.L. Ma [33d], G. Maccarrone [47], A. Macchiolo [101], J. Machado Miguens [126a,126b], D. Macina [30], D. Madaffari [85], R. Madar [48], H.J. Maddocks [72], W.F. Mader [44], A. Madsen [168], M. Maeno [8], T. Maeno [25], A. Maevskiy [99], E. Magradze [54], K. Mahboubi [48], J. Mahlstedt [107], S. Mahmoud [74], C. Maiani [138], C. Maidantchik [24a], A.A. Maier [101], A. Maio [126a,126b,126d], S. Majewski [116], Y. Makida [66], N. Makovec [117], P. Mal [138,x], B. Malaescu [80], Pa. Malecki [39], V.P. Maleev [123], F. Malek [55], U. Mallik [63], D. Malon [6], C. Malone [145], S. Maltezos [10], V.M. Malyshev [109], S. Malyukov [30], J. Mamuzic [13b], G. Mancini [47], B. Mandelli [30], L. Mandelli [91a], I. Mandić [75], R. Mandrysch [63], J. Maneira [126a,126b], A. Manfredini [101], L. Manhaes de Andrade Filho [24b], J.A. Manjarres Ramos [161b], A. Mann [100], P.M. Manning [139], A. Manousakis-Katsikakis [9], B. Mansoulie [138], R. Mantifel [87], L. Mapelli [30], L. March [147c], J.F. Marchand [29], G. Marchiori [80], M. Marcisovsky [127], C.P. Marino [171], M. Marjanovic [13a], C.N. Marques [126a], F. Marroquim [24a], S.P. Marsden [84], Z. Marshall [15], L.F. Marti [17], S. Marti-Garcia [169], B. Martin [30], B. Martin [90], T.A. Martin [172], V.J. Martin [46], B. Martin dit Latour [14], H. Martinez [138], M. Martinez [12,n], S. Martin-Haugh [131], A.C. Martyniuk [78], M. Marx [140], F. Marzano [134a], A. Marzin [30], L. Masetti [83], T. Mashimo [157], R. Mashinistov [96], J. Masik [84], A.L. Maslennikov [109,c], I. Massa [20a,20b], L. Massa [20a,20b], N. Massol [5], P. Mastrandrea [150], A. Mastroberardino [37a,37b], T. Masubuchi [157], P. Mättig [177], J. Mattmann [83], J. Maurer [26a], S.J. Maxfield [74], D.A. Maximov [109,c], R. Mazini [153], L. Mazzaferro [135a,135b], G. Mc Goldrick [160], S.P. Mc Kee [89], A. McCarn [89], R.L. McCarthy [150], T.G. McCarthy [29], N.A. McCubbin [131], K.W. McFarlane [56,*], J.A. Mcfayden [78], G. Mchedlidze [54], S.J. McMahon [131], R.A. McPherson [171,j], J. Mechnich [107], M. Medinnis [42], S. Meehan [31], S. Mehlhase [100], A. Mehta [74], K. Meier [58a], C. Meineck [100], B. Meirose [81], C. Melachrinos [31], B.R. Mellado Garcia [147c], F. Meloni [17], A. Mengarelli [20a,20b], S. Menke [101], E. Meoni [163], K.M. Mercurio [57], S. Mergelmeyer [21], N. Meric [138], P. Mermod [49], L. Merola [104a,104b], C. Meroni [91a], F.S. Merritt [31], H. Merritt [111], A. Messina [30,y], J. Metcalfe [25], A.S. Mete [165], C. Meyer [83], C. Meyer [122], J-P. Meyer [138], J. Meyer [30], R.P. Middleton [131], S. Migas [74], L. Mijović [21], G. Mikenberg [174], M. Mikestikova [127], M. Mikuž [75], A. Milic [30], D.W. Miller [31], C. Mills [46], A. Milov [174], D.A. Milstead [148a,148b], D. Milstein [174], A.A. Minaenko [130], Y. Minami [157], I.A. Minashvili [65], A.I. Mincer [110], B. Mindur [38a], M. Mineev [65], Y. Ming [175], L.M. Mir [12], G. Mirabelli [134a], T. Mitani [173], J. Mitrevski [100], V.A. Mitsou [169], S. Mitsui [66], A. Miucci [49], P.S. Miyagawa [141], J.U. Mjörnmark [81], T. Moa [148a,148b], K. Mochizuki [85], S. Mohapatra [35], W. Mohr [48], S. Molander [148a,148b], R. Moles-Valls [169], K. Mönig [42], C. Monini [55], J. Monk [36], E. Monnier [85], J. Montejo Berlingen [12], F. Monticelli [71], S. Monzani [134a,134b], R.W. Moore [3], N. Morange [63], D. Moreno [83], M. Moreno Llácer [54], P. Morettini [50a], M. Morgenstern [44], M. Morii [57], S. Moritz [83], A.K. Morley [149], G. Mornacchi [30], J.D. Morris [76], L. Morvaj [103], H.G. Moser [101], M. Mosidze [51b], J. Moss [111], K. Motohashi [159], R. Mount [145], E. Mountricha [25], S.V. Mouraviev [96,*], E.J.W. Moyse [86], S. Muanza [85], R.D. Mudd [18], F. Mueller [58a], J. Mueller [125], K. Mueller [21], T. Mueller [28], T. Mueller [83], D. Muenstermann [49], Y. Munwes [155], J.A. Murillo Quijada [18], W.J. Murray [172,131], H. Musheghyan [54], E. Musto [154], A.G. Myagkov [130,z], M. Myska [128], O. Nackenhorst [54], J. Nadal [54], K. Nagai [62], R. Nagai [159], Y. Nagai [85], K. Nagano [66], A. Nagarkar [111], Y. Nagasaka [59], M. Nagel [101], A.M. Nairz [30], Y. Nakahama [30], K. Nakamura [66], T. Nakamura [157], I. Nakano [112], H. Namasivayam [41], G. Nanava [21], R. Narayan [58b], T. Nattermann [21], T. Naumann [42], G. Navarro [164], R. Nayyar [7], H.A. Neal [89], P.Yu. Nechaeva [96], T.J. Neep [84], P.D. Nef [145], A. Negri [121a,121b], G. Negri [30], M. Negrini [20a], S. Nektarijevic [49], C. Nellist [117], A. Nelson [165], T.K. Nelson [145], S. Nemecek [127], P. Nemethy [110], A.A. Nepomuceno [24a], M. Nessi [30,aa], M.S. Neubauer [167], M. Neumann [177], R.M. Neves [110], P. Nevski [25], P.R. Newman [18], D.H. Nguyen [6], R.B. Nickerson [120], R. Nicolaidou [138], B. Nicquevert [30], J. Nielsen [139], N. Nikiforou [35], A. Nikiforov [16], V. Nikolaenko [130,z], I. Nikolic-Audit [80], K. Nikolics [49], K. Nikolopoulos [18], P. Nilsson [8], Y. Ninomiya [157], A. Nisati [134a], R. Nisius [101], T. Nobe [159], L. Nodulman [6], M. Nomachi [118], I. Nomidis [29], S. Norberg [113], M. Nordberg [30], O. Novgorodova [44], S. Nowak [101], M. Nozaki [66], L. Nozka [115], K. Ntekas [10], G. Nunes Hanninger [88], T. Nunnemann [100], E. Nurse [78], F. Nuti [88], B.J. O'Brien [46], F. O'grady [7], D.C. O'Neil [144], V. O'Shea [53],

F.G. Oakham [29,e], H. Oberlack [101], T. Obermann [21], J. Ocariz [80], A. Ochi [67], M.I. Ochoa [78], S. Oda [70], S. Odaka [66], H. Ogren [61], A. Oh [84], S.H. Oh [45], C.C. Ohm [15], H. Ohman [168], W. Okamura [118], H. Okawa [25], Y. Okumura [31], T. Okuyama [157], A. Olariu [26a], A.G. Olchevski [65], S.A. Olivares Pino [46], D. Oliveira Damazio [25], E. Oliver Garcia [169], A. Olszewski [39], J. Olszowska [39], A. Onofre [126a,126e], P.U.E. Onyisi [31,o], C.J. Oram [161a], M.J. Oreglia [31], Y. Oren [155], D. Orestano [136a,136b], N. Orlando [73a,73b], C. Oropeza Barrera [53], R.S. Orr [160], B. Osculati [50a,50b], R. Ospanov [122], G. Otero y Garzon [27], H. Otono [70], M. Ouchrif [137d], E.A. Ouellette [171], F. Ould-Saada [119], A. Ouraou [138], K.P. Oussoren [107], Q. Ouyang [33a], A. Ovcharova [15], M. Owen [84], V.E. Ozcan [19a], N. Ozturk [8], K. Pachal [120], A. Pacheco Pages [12], C. Padilla Aranda [12], M. Pagáčová [48], S. Pagan Griso [15], E. Paganis [141], C. Pahl [101], F. Paige [25], P. Pais [86], K. Pajchel [119], G. Palacino [161b], S. Palestini [30], M. Palka [38b], D. Pallin [34], A. Palma [126a,126b], J.D. Palmer [18], Y.B. Pan [175], E. Panagiotopoulou [10], J.G. Panduro Vazquez [77], P. Pani [107], N. Panikashvili [89], S. Panitkin [25], D. Pantea [26a], L. Paolozzi [135a,135b], Th.D. Papadopoulou [10], K. Papageorgiou [156,l], A. Paramonov [6], D. Paredes Hernandez [156], M.A. Parker [28], F. Parodi [50a,50b], J.A. Parsons [35], U. Parzefall [48], E. Pasqualucci [134a], S. Passaggio [50a], A. Passeri [136a], F. Pastore [136a,136b,*], Fr. Pastore [77], G. Pásztor [29], S. Pataraia [177], N.D. Patel [152], J.R. Pater [84], S. Patricelli [104a,104b], T. Pauly [30], J. Pearce [171], L.E. Pedersen [36], M. Pedersen [119], S. Pedraza Lopez [169], R. Pedro [126a,126b], S.V. Peleganchuk [109], D. Pelikan [168], H. Peng [33b], B. Penning [31], J. Penwell [61], D.V. Perepelitsa [25], E. Perez Codina [161a], M.T. Pérez García-Estañ [169], V. Perez Reale [35], L. Perini [91a,91b], H. Pernegger [30], S. Perrella [104a,104b], R. Perrino [73a], R. Peschke [42], V.D. Peshekhonov [65], K. Peters [30], R.F.Y. Peters [84], B.A. Petersen [30], T.C. Petersen [36], E. Petit [42], A. Petridis [148a,148b], C. Petridou [156], E. Petrolo [134a], F. Petrucci [136a,136b], N.E. Pettersson [159], R. Pezoa [32b], P.W. Phillips [131], G. Piacquadio [145], E. Pianori [172], A. Picazio [49], E. Piccaro [76], M. Piccinini [20a,20b], R. Piegaia [27], D.T. Pignotti [111], J.E. Pilcher [31], A.D. Pilkington [78], J. Pina [126a,126b,126d], M. Pinamonti [166a,166c,ab], A. Pinder [120], J.L. Pinfold [3], A. Pingel [36], B. Pinto [126a], S. Pires [80], M. Pitt [174], C. Pizio [91a,91b], L. Plazak [146a], M.-A. Pleier [25], V. Pleskot [129], E. Plotnikova [65], P. Plucinski [148a,148b], D. Pluth [64], S. Poddar [58a], F. Podlyski [34], R. Poettgen [83], L. Poggioli [117], D. Pohl [21], M. Pohl [49], G. Polesello [121a], A. Policicchio [37a,37b], R. Polifka [160], A. Polini [20a], C.S. Pollard [45], V. Polychronakos [25], K. Pommès [30], L. Pontecorvo [134a], B.G. Pope [90], G.A. Popeneciu [26b], D.S. Popovic [13a], A. Poppleton [30], X. Portell Bueso [12], S. Pospisil [128], K. Potamianos [15], I.N. Potrap [65], C.J. Potter [151], C.T. Potter [116], G. Poulard [30], J. Poveda [61], V. Pozdnyakov [65], P. Pralavorio [85], A. Pranko [15], S. Prasad [30], R. Pravahan [8], S. Prell [64], D. Price [84], J. Price [74], L.E. Price [6], D. Prieur [125], M. Primavera [73a], M. Proissl [46], K. Prokofiev [47], F. Prokoshin [32b], E. Protopapadaki [138], S. Protopopescu [25], J. Proudfoot [6], M. Przybycien [38a], H. Przysiezniak [5], E. Ptacek [116], D. Puddu [136a,136b], E. Pueschel [86], D. Puldon [150], M. Purohit [25,ac], P. Puzo [117], J. Qian [89], G. Qin [53], Y. Qin [84], A. Quadt [54], D.R. Quarrie [15], W.B. Quayle [166a,166b], M. Queitsch-Maitland [84], D. Quilty [53], A. Qureshi [161b], V. Radeka [25], V. Radescu [42], S.K. Radhakrishnan [150], P. Radloff [116], P. Rados [88], F. Ragusa [91a,91b], G. Rahal [180], S. Rajagopalan [25], M. Rammensee [30], A.S. Randle-Conde [40], C. Rangel-Smith [168], K. Rao [165], F. Rauscher [100], T.C. Rave [48], T. Ravenscroft [53], M. Raymond [30], A.L. Read [119], N.P. Readioff [74], D.M. Rebuzzi [121a,121b], A. Redelbach [176], G. Redlinger [25], R. Reece [139], K. Reeves [41], L. Rehnisch [16], H. Reisin [27], M. Relich [165], C. Rembser [30], H. Ren [33a], Z.L. Ren [153], A. Renaud [117], M. Rescigno [134a], S. Resconi [91a], O.L. Rezanova [109,c], P. Reznicek [129], R. Rezvani [95], R. Richter [101], M. Ridel [80], P. Rieck [16], J. Rieger [54], M. Rijssenbeek [150], A. Rimoldi [121a,121b], L. Rinaldi [20a], E. Ritsch [62], I. Riu [12], F. Rizatdinova [114], E. Rizvi [76], S.H. Robertson [87,j], A. Robichaud-Veronneau [87], D. Robinson [28], J.E.M. Robinson [84], A. Robson [53], C. Roda [124a,124b], L. Rodrigues [30], S. Roe [30], O. Røhne [119], S. Rolli [163], A. Romaniouk [98], M. Romano [20a,20b], E. Romero Adam [169], N. Rompotis [140], M. Ronzani [48], L. Roos [80], E. Ros [169], S. Rosati [134a], K. Rosbach [49], M. Rose [77], P. Rose [139], P.L. Rosendahl [14], O. Rosenthal [143], V. Rossetti [148a,148b], E. Rossi [104a,104b], L.P. Rossi [50a], R. Rosten [140], M. Rotaru [26a], I. Roth [174], J. Rothberg [140], D. Rousseau [117], C.R. Royon [138], A. Rozanov [85], Y. Rozen [154], X. Ruan [147c], F. Rubbo [12], I. Rubinskiy [42], V.I. Rud [99], C. Rudolph [44], M.S. Rudolph [160], F. Rühr [48], A. Ruiz-Martinez [30], Z. Rurikova [48], N.A. Rusakovich [65], A. Ruschke [100], J.P. Rutherfoord [7], N. Ruthmann [48], Y.F. Ryabov [123], M. Rybar [129], G. Rybkin [117], N.C. Ryder [120], A.F. Saavedra [152], G. Sabato [107], S. Sacerdoti [27], A. Saddique [3], I. Sadeh [155], H.F-W. Sadrozinski [139], R. Sadykov [65], F. Safai Tehrani [134a], H. Sakamoto [157], Y. Sakurai [173], G. Salamanna [136a,136b], A. Salamon [135a], M. Saleem [113], D. Salek [107], P.H. Sales De Bruin [140], D. Salihagic [101], A. Salnikov [145], J. Salt [169], D. Salvatore [37a,37b], F. Salvatore [151], A. Salvucci [106],

A. Salzburger [30], D. Sampsonidis [156], A. Sanchez [104a,104b], J. Sánchez [169], V. Sanchez Martinez [169], H. Sandaker [14], R.L. Sandbach [76], H.G. Sander [83], M.P. Sanders [100], M. Sandhoff [177], T. Sandoval [28], C. Sandoval [164], R. Sandstroem [101], D.P.C. Sankey [131], A. Sansoni [47], C. Santoni [34], R. Santonico [135a,135b], H. Santos [126a], I. Santoyo Castillo [151], K. Sapp [125], A. Sapronov [65], J.G. Saraiva [126a,126d], B. Sarrazin [21], G. Sartisohn [177], O. Sasaki [66], Y. Sasaki [157], G. Sauvage [5,*], E. Sauvan [5], P. Savard [160,e], D.O. Savu [30], C. Sawyer [120], L. Sawyer [79,m], D.H. Saxon [53], J. Saxon [122], C. Sbarra [20a], A. Sbrizzi [20a,20b], T. Scanlon [78], D.A. Scannicchio [165], M. Scarcella [152], V. Scarfone [37a,37b], J. Schaarschmidt [174], P. Schacht [101], D. Schaefer [30], R. Schaefer [42], S. Schaepe [21], S. Schaetzel [58b], U. Schäfer [83], A.C. Schaffer [117], D. Schaile [100], R.D. Schamberger [150], V. Scharf [58a], V.A. Schegelsky [123], D. Scheirich [129], M. Schernau [165], M.I. Scherzer [35], C. Schiavi [50a,50b], J. Schieck [100], C. Schillo [48], M. Schioppa [37a,37b], S. Schlenker [30], E. Schmidt [48], K. Schmieden [30], C. Schmitt [83], S. Schmitt [58b], B. Schneider [17], Y.J. Schnellbach [74], U. Schnoor [44], L. Schoeffel [138], A. Schoening [58b], B.D. Schoenrock [90], A.L.S. Schorlemmer [54], M. Schott [83], D. Schouten [161a], J. Schovancova [25], S. Schramm [160], M. Schreyer [176], C. Schroeder [83], N. Schuh [83], M.J. Schultens [21], H.-C. Schultz-Coulon [58a], H. Schulz [16], M. Schumacher [48], B.A. Schumm [139], Ph. Schune [138], C. Schwanenberger [84], A. Schwartzman [145], T.A. Schwarz [89], Ph. Schwegler [101], Ph. Schwemling [138], R. Schwienhorst [90], J. Schwindling [138], T. Schwindt [21], M. Schwoerer [5], F.G. Sciacca [17], E. Scifo [117], G. Sciolla [23], W.G. Scott [131], F. Scuri [124a,124b], F. Scutti [21], J. Searcy [89], G. Sedov [42], E. Sedykh [123], S.C. Seidel [105], A. Seiden [139], F. Seifert [128], J.M. Seixas [24a], G. Sekhniaidze [104a], S.J. Sekula [40], K.E. Selbach [46], D.M. Seliverstov [123,*], G. Sellers [74], N. Semprini-Cesari [20a,20b], C. Serfon [30], L. Serin [117], L. Serkin [54], T. Serre [85], R. Seuster [161a], H. Severini [113], T. Sfiligoj [75], F. Sforza [101], A. Sfyrla [30], E. Shabalina [54], M. Shamim [116], L.Y. Shan [33a], R. Shang [167], J.T. Shank [22], M. Shapiro [15], P.B. Shatalov [97], K. Shaw [166a,166b], C.Y. Shehu [151], P. Sherwood [78], L. Shi [153,ad], S. Shimizu [67], C.O. Shimmin [165], M. Shimojima [102], M. Shiyakova [65], A. Shmeleva [96], M.J. Shochet [31], D. Short [120], S. Shrestha [64], E. Shulga [98], M.A. Shupe [7], S. Shushkevich [42], P. Sicho [127], O. Sidiropoulou [156], D. Sidorov [114], A. Sidoti [134a], F. Siegert [44], Dj. Sijacki [13a], J. Silva [126a,126d], Y. Silver [155], D. Silverstein [145], S.B. Silverstein [148a], V. Simak [128], O. Simard [5], Lj. Simic [13a], S. Simion [117], E. Simioni [83], B. Simmons [78], R. Simoniello [91a,91b], M. Simonyan [36], P. Sinervo [160], N.B. Sinev [116], V. Sipica [143], G. Siragusa [176], A. Sircar [79], A.N. Sisakyan [65,*], S.Yu. Sivoklokov [99], J. Sjölin [148a,148b], T.B. Sjursen [14], H.P. Skottowe [57], K.Yu. Skovpen [109], P. Skubic [113], M. Slater [18], T. Slavicek [128], M. Slawinska [107], K. Sliwa [163], V. Smakhtin [174], B.H. Smart [46], L. Smestad [14], S.Yu. Smirnov [98], Y. Smirnov [98], L.N. Smirnova [99,ae], O. Smirnova [81], K.M. Smith [53], M. Smizanska [72], K. Smolek [128], A.A. Snesarev [96], G. Snidero [76], S. Snyder [25], R. Sobie [171,j], F. Socher [44], A. Soffer [155], D.A. Soh [153,ad], C.A. Solans [30], M. Solar [128], J. Solc [128], E.Yu. Soldatov [98], U. Soldevila [169], A.A. Solodkov [130], A. Soloshenko [65], O.V. Solovyanov [130], V. Solovyev [123], P. Sommer [48], H.Y. Song [33b], N. Soni [1], A. Sood [15], A. Sopczak [128], B. Sopko [128], V. Sopko [128], V. Sorin [12], M. Sosebee [8], R. Soualah [166a,166c], P. Soueid [95], A.M. Soukharev [109,c], D. South [42], S. Spagnolo [73a,73b], F. Spanò [77], W.R. Spearman [57], F. Spettel [101], R. Spighi [20a], G. Spigo [30], L.A. Spiller [88], M. Spousta [129], T. Spreitzer [160], B. Spurlock [8], R.D. St. Denis [53,*], S. Staerz [44], J. Stahlman [122], R. Stamen [58a], S. Stamm [16], E. Stanecka [39], R.W. Stanek [6], C. Stanescu [136a], M. Stanescu-Bellu [42], M.M. Stanitzki [42], S. Stapnes [119], E.A. Starchenko [130], J. Stark [55], P. Staroba [127], P. Starovoitov [42], R. Staszewski [39], P. Stavina [146a,*], P. Steinberg [25], B. Stelzer [144], H.J. Stelzer [30], O. Stelzer-Chilton [161a], H. Stenzel [52], S. Stern [101], G.A. Stewart [53], J.A. Stillings [21], M.C. Stockton [87], M. Stoebe [87], G. Stoicea [26a], P. Stolte [54], S. Stonjek [101], A.R. Stradling [8], A. Straessner [44], M.E. Stramaglia [17], J. Strandberg [149], S. Strandberg [148a,148b], A. Strandlie [119], E. Strauss [145], M. Strauss [113], P. Strizenec [146b], R. Ströhmer [176], D.M. Strom [116], R. Stroynowski [40], A. Strubig [106], S.A. Stucci [17], B. Stugu [14], N.A. Styles [42], D. Su [145], J. Su [125], R. Subramaniam [79], A. Succurro [12], Y. Sugaya [118], C. Suhr [108], M. Suk [128], V.V. Sulin [96], S. Sultansoy [4d], T. Sumida [68], S. Sun [57], X. Sun [33a], J.E. Sundermann [48], K. Suruliz [141], G. Susinno [37a,37b], M.R. Sutton [151], Y. Suzuki [66], M. Svatos [127], S. Swedish [170], M. Swiatlowski [145], I. Sykora [146a], T. Sykora [129], D. Ta [90], C. Taccini [136a,136b], K. Tackmann [42], J. Taenzer [160], A. Taffard [165], R. Tafirout [161a], N. Taiblum [155], H. Takai [25], R. Takashima [69], H. Takeda [67], T. Takeshita [142], Y. Takubo [66], M. Talby [85], A.A. Talyshev [109,c], J.Y.C. Tam [176], K.G. Tan [88], J. Tanaka [157], R. Tanaka [117], S. Tanaka [133], S. Tanaka [66], A.J. Tanasijczuk [144], B.B. Tannenwald [111], N. Tannoury [21], S. Tapprogge [83], S. Tarem [154], F. Tarrade [29], G.F. Tartarelli [91a], P. Tas [129], M. Tasevsky [127], T. Tashiro [68], E. Tassi [37a,37b], A. Tavares Delgado [126a,126b], Y. Tayalati [137d], F.E. Taylor [94], G.N. Taylor [88], W. Taylor [161b], F.A. Teischinger [30], M. Teixeira Dias Castanheira [76],

P. Teixeira-Dias [77], K.K. Temming [48], H. Ten Kate [30], P.K. Teng [153], J.J. Teoh [118], S. Terada [66], K. Terashi [157], J. Terron [82], S. Terzo [101], M. Testa [47], R.J. Teuscher [160,j], J. Therhaag [21], T. Theveneaux-Pelzer [34], J.P. Thomas [18], J. Thomas-Wilsker [77], E.N. Thompson [35], P.D. Thompson [18], P.D. Thompson [160], R.J. Thompson [84], A.S. Thompson [53], L.A. Thomsen [36], E. Thomson [122], M. Thomson [28], W.M. Thong [88], R.P. Thun [89,*], F. Tian [35], M.J. Tibbetts [15], V.O. Tikhomirov [96,af], Yu.A. Tikhonov [109,c], S. Timoshenko [98], E. Tiouchichine [85], P. Tipton [178], S. Tisserant [85], T. Todorov [5], S. Todorova-Nova [129], B. Toggerson [7], J. Tojo [70], S. Tokár [146a], K. Tokushuku [66], K. Tollefson [90], E. Tolley [57], L. Tomlinson [84], M. Tomoto [103], L. Tompkins [31], K. Toms [105], N.D. Topilin [65], E. Torrence [116], H. Torres [144], E. Torró Pastor [169], J. Toth [85,ag], F. Touchard [85], D.R. Tovey [141], H.L. Tran [117], T. Trefzger [176], L. Tremblet [30], A. Tricoli [30], I.M. Trigger [161a], S. Trincaz-Duvoid [80], M.F. Tripiana [12], W. Trischuk [160], B. Trocmé [55], C. Troncon [91a], M. Trottier-McDonald [15], M. Trovatelli [136a,136b], P. True [90], M. Trzebinski [39], A. Trzupek [39], C. Tsarouchas [30], J.C-L. Tseng [120], P.V. Tsiareshka [92], D. Tsionou [138], G. Tsipolitis [10], N. Tsirintanis [9], S. Tsiskaridze [12], V. Tsiskaridze [48], E.G. Tskhadadze [51a], I.I. Tsukerman [97], V. Tsulaia [15], S. Tsuno [66], D. Tsybychev [150], A. Tudorache [26a], V. Tudorache [26a], A.N. Tuna [122], S.A. Tupputi [20a,20b], S. Turchikhin [99,ae], D. Turecek [128], I. Turk Cakir [4c], R. Turra [91a,91b], A.J. Turvey [40], P.M. Tuts [35], A. Tykhonov [49], M. Tylmad [148a,148b], M. Tyndel [131], K. Uchida [21], I. Ueda [157], R. Ueno [29], M. Ughetto [85], M. Ugland [14], M. Uhlenbrock [21], F. Ukegawa [162], G. Unal [30], A. Undrus [25], G. Unel [165], F.C. Ungaro [48], Y. Unno [66], C. Unverdorben [100], D. Urbaniec [35], P. Urquijo [88], G. Usai [8], A. Usanova [62], L. Vacavant [85], V. Vacek [128], B. Vachon [87], N. Valencic [107], S. Valentinetti [20a,20b], A. Valero [169], L. Valery [34], S. Valkar [129], E. Valladolid Gallego [169], S. Vallecorsa [49], J.A. Valls Ferrer [169], W. Van Den Wollenberg [107], P.C. Van Der Deijl [107], R. van der Geer [107], H. van der Graaf [107], R. Van Der Leeuw [107], D. van der Ster [30], N. van Eldik [30], P. van Gemmeren [6], J. Van Nieuwkoop [144], I. van Vulpen [107], M.C. van Woerden [30], M. Vanadia [134a,134b], W. Vandelli [30], R. Vanguri [122], A. Vaniachine [6], P. Vankov [42], F. Vannucci [80], G. Vardanyan [179], R. Vari [134a], E.W. Varnes [7], T. Varol [86], D. Varouchas [80], A. Vartapetian [8], K.E. Varvell [152], F. Vazeille [34], T. Vazquez Schroeder [54], J. Veatch [7], F. Veloso [126a,126c], S. Veneziano [134a], A. Ventura [73a,73b], D. Ventura [86], M. Venturi [171], N. Venturi [160], A. Venturini [23], V. Vercesi [121a], M. Verducci [134a,134b], W. Verkerke [107], J.C. Vermeulen [107], A. Vest [44], M.C. Vetterli [144,e], O. Viazlo [81], I. Vichou [167], T. Vickey [147c,ah], O.E. Vickey Boeriu [147c], G.H.A. Viehhauser [120], S. Viel [170], R. Vigne [30], M. Villa [20a,20b], M. Villaplana Perez [91a,91b], E. Vilucchi [47], M.G. Vincter [29], V.B. Vinogradov [65], J. Virzi [15], I. Vivarelli [151], F. Vives Vaque [3], S. Vlachos [10], D. Vladoiu [100], M. Vlasak [128], A. Vogel [21], M. Vogel [32a], P. Vokac [128], G. Volpi [124a,124b], M. Volpi [88], H. von der Schmitt [101], H. von Radziewski [48], E. von Toerne [21], V. Vorobel [129], K. Vorobev [98], M. Vos [169], R. Voss [30], J.H. Vossebeld [74], N. Vranjes [138], M. Vranjes Milosavljevic [13a], V. Vrba [127], M. Vreeswijk [107], T. Vu Anh [48], R. Vuillermet [30], I. Vukotic [31], Z. Vykydal [128], P. Wagner [21], W. Wagner [177], H. Wahlberg [71], S. Wahrmund [44], J. Wakabayashi [103], J. Walder [72], R. Walker [100], W. Walkowiak [143], R. Wall [178], P. Waller [74], B. Walsh [178], C. Wang [153,ai], C. Wang [45], F. Wang [175], H. Wang [15], H. Wang [40], J. Wang [42], J. Wang [33a], K. Wang [87], R. Wang [105], S.M. Wang [153], T. Wang [21], X. Wang [178], C. Wanotayaroj [116], A. Warburton [87], C.P. Ward [28], D.R. Wardrope [78], M. Warsinsky [48], A. Washbrook [46], C. Wasicki [42], P.M. Watkins [18], A.T. Watson [18], I.J. Watson [152], M.F. Watson [18], G. Watts [140], S. Watts [84], B.M. Waugh [78], S. Webb [84], M.S. Weber [17], S.W. Weber [176], J.S. Webster [31], A.R. Weidberg [120], P. Weigell [101], B. Weinert [61], J. Weingarten [54], C. Weiser [48], H. Weits [107], P.S. Wells [30], T. Wenaus [25], D. Wendland [16], Z. Weng [153,ad], T. Wengler [30], S. Wenig [30], N. Wermes [21], M. Werner [48], P. Werner [30], M. Wessels [58a], J. Wetter [163], K. Whalen [29], A. White [8], M.J. White [1], R. White [32b], S. White [124a,124b], D. Whiteson [165], D. Wicke [177], F.J. Wickens [131], W. Wiedenmann [175], M. Wielers [131], P. Wienemann [21], C. Wiglesworth [36], L.A.M. Wiik-Fuchs [21], P.A. Wijeratne [78], A. Wildauer [101], M.A. Wildt [42,aj], H.G. Wilkens [30], J.Z. Will [100], H.H. Williams [122], S. Williams [28], C. Willis [90], S. Willocq [86], A. Wilson [89], J.A. Wilson [18], I. Wingerter-Seez [5], F. Winklmeier [116], B.T. Winter [21], M. Wittgen [145], T. Wittig [43], J. Wittkowski [100], S.J. Wollstadt [83], M.W. Wolter [39], H. Wolters [126a,126c], B.K. Wosiek [39], J. Wotschack [30], M.J. Woudstra [84], K.W. Wozniak [39], M. Wright [53], M. Wu [55], S.L. Wu [175], X. Wu [49], Y. Wu [89], E. Wulf [35], T.R. Wyatt [84], B.M. Wynne [46], S. Xella [36], M. Xiao [138], D. Xu [33a], L. Xu [33b,ak], B. Yabsley [152], S. Yacoob [147b,al], R. Yakabe [67], M. Yamada [66], H. Yamaguchi [157], Y. Yamaguchi [118], A. Yamamoto [66], K. Yamamoto [64], S. Yamamoto [157], T. Yamamura [157], T. Yamanaka [157], K. Yamauchi [103], Y. Yamazaki [67], Z. Yan [22], H. Yang [33e], H. Yang [175], U.K. Yang [84],

Y. Yang [111], S. Yanush [93], L. Yao [33a], W-M. Yao [15], Y. Yasu [66], E. Yatsenko [42], K.H. Yau Wong [21], J. Ye [40], S. Ye [25], I. Yeletskikh [65], A.L. Yen [57], E. Yildirim [42], M. Yilmaz [4b], R. Yoosoofmiya [125], K. Yorita [173], R. Yoshida [6], K. Yoshihara [157], C. Young [145], C.J.S. Young [30], S. Youssef [22], D.R. Yu [15], J. Yu [8], J.M. Yu [89], J. Yu [114], L. Yuan [67], A. Yurkewicz [108], I. Yusuff [28,am], B. Zabinski [39], R. Zaidan [63], A.M. Zaitsev [130,z], A. Zaman [150], S. Zambito [23], L. Zanello [134a,134b], D. Zanzi [88], C. Zeitnitz [177], M. Zeman [128], A. Zemla [38a], K. Zengel [23], O. Zenin [130], T. Ženiš [146a], D. Zerwas [117], G. Zevi della Porta [57], D. Zhang [89], F. Zhang [175], H. Zhang [90], J. Zhang [6], L. Zhang [153], X. Zhang [33d], Z. Zhang [117], Z. Zhao [33b], A. Zhemchugov [65], J. Zhong [120], B. Zhou [89], L. Zhou [35], N. Zhou [165], C.G. Zhu [33d], H. Zhu [33a], J. Zhu [89], Y. Zhu [33b], X. Zhuang [33a], K. Zhukov [96], A. Zibell [176], D. Zieminska [61], N.I. Zimine [65], C. Zimmermann [83], R. Zimmermann [21], S. Zimmermann [21], S. Zimmermann [48], Z. Zinonos [54], M. Ziolkowski [143], G. Zobernig [175], A. Zoccoli [20a,20b], M. zur Nedden [16], G. Zurzolo [104a,104b], V. Zutshi [108], L. Zwalinski [30]

[1] *Department of Physics, University of Adelaide, Adelaide, Australia*
[2] *Physics Department, SUNY Albany, Albany, NY, United States*
[3] *Department of Physics, University of Alberta, Edmonton, AB, Canada*
[4] [(a)] *Department of Physics, Ankara University, Ankara;* [(b)] *Department of Physics, Gazi University, Ankara;* [(c)] *Istanbul Aydin University, Istanbul;* [(d)] *Division of Physics, TOBB University of Economics and Technology, Ankara, Turkey*
[5] *LAPP, CNRS/IN2P3 and Université de Savoie, Annecy-le-Vieux, France*
[6] *High Energy Physics Division, Argonne National Laboratory, Argonne, IL, United States*
[7] *Department of Physics, University of Arizona, Tucson, AZ, United States*
[8] *Department of Physics, The University of Texas at Arlington, Arlington, TX, United States*
[9] *Physics Department, University of Athens, Athens, Greece*
[10] *Physics Department, National Technical University of Athens, Zografou, Greece*
[11] *Institute of Physics, Azerbaijan Academy of Sciences, Baku, Azerbaijan*
[12] *Institut de Física d'Altes Energies and Departament de Física de la Universitat Autònoma de Barcelona, Barcelona, Spain*
[13] [(a)] *Institute of Physics, University of Belgrade, Belgrade;* [(b)] *Vinca Institute of Nuclear Sciences, University of Belgrade, Belgrade, Serbia*
[14] *Department for Physics and Technology, University of Bergen, Bergen, Norway*
[15] *Physics Division, Lawrence Berkeley National Laboratory and University of California, Berkeley, CA, United States*
[16] *Department of Physics, Humboldt University, Berlin, Germany*
[17] *Albert Einstein Center for Fundamental Physics and Laboratory for High Energy Physics, University of Bern, Bern, Switzerland*
[18] *School of Physics and Astronomy, University of Birmingham, Birmingham, United Kingdom*
[19] [(a)] *Department of Physics, Bogazici University, Istanbul;* [(b)] *Department of Physics, Dogus University, Istanbul;* [(c)] *Department of Physics Engineering, Gaziantep University, Gaziantep, Turkey*
[20] [(a)] *INFN Sezione di Bologna;* [(b)] *Dipartimento di Fisica e Astronomia, Università di Bologna, Bologna, Italy*
[21] *Physikalisches Institut, University of Bonn, Bonn, Germany*
[22] *Department of Physics, Boston University, Boston, MA, United States*
[23] *Department of Physics, Brandeis University, Waltham, MA, United States*
[24] [(a)] *Universidade Federal do Rio De Janeiro COPPE/EE/IF, Rio de Janeiro;* [(b)] *Federal University of Juiz de Fora (UFJF), Juiz de Fora;* [(c)] *Federal University of Sao Joao del Rei (UFSJ), Sao Joao del Rei;* [(d)] *Instituto de Fisica, Universidade de Sao Paulo, Sao Paulo, Brazil*
[25] *Physics Department, Brookhaven National Laboratory, Upton, NY, United States*
[26] [(a)] *National Institute of Physics and Nuclear Engineering, Bucharest;* [(b)] *National Institute for Research and Development of Isotopic and Molecular Technologies, Physics Department, Cluj Napoca;* [(c)] *University Politehnica Bucharest, Bucharest;* [(d)] *West University in Timisoara, Timisoara, Romania*
[27] *Departamento de Física, Universidad de Buenos Aires, Buenos Aires, Argentina*
[28] *Cavendish Laboratory, University of Cambridge, Cambridge, United Kingdom*
[29] *Department of Physics, Carleton University, Ottawa, ON, Canada*
[30] *CERN, Geneva, Switzerland*
[31] *Enrico Fermi Institute, University of Chicago, Chicago, IL, United States*
[32] [(a)] *Departamento de Física, Pontificia Universidad Católica de Chile, Santiago;* [(b)] *Departamento de Física, Universidad Técnica Federico Santa María, Valparaíso, Chile*
[33] [(a)] *Institute of High Energy Physics, Chinese Academy of Sciences, Beijing;* [(b)] *Department of Modern Physics, University of Science and Technology of China, Anhui;* [(c)] *Department of Physics, Nanjing University, Jiangsu;* [(d)] *School of Physics, Shandong University, Shandong;* [(e)] *Physics Department, Shanghai Jiao Tong University, Shanghai;* [(f)] *Physics Department, Tsinghua University, Beijing 100084, China*
[34] *Laboratoire de Physique Corpusculaire, Clermont Université and Université Blaise Pascal and CNRS/IN2P3, Clermont-Ferrand, France*
[35] *Nevis Laboratory, Columbia University, Irvington, NY, United States*
[36] *Niels Bohr Institute, University of Copenhagen, Kobenhavn, Denmark*
[37] [(a)] *INFN Gruppo Collegato di Cosenza, Laboratori Nazionali di Frascati;* [(b)] *Dipartimento di Fisica, Università della Calabria, Rende, Italy*
[38] [(a)] *AGH University of Science and Technology, Faculty of Physics and Applied Computer Science, Krakow;* [(b)] *Marian Smoluchowski Institute of Physics, Jagiellonian University, Krakow, Poland*
[39] *The Henryk Niewodniczanski Institute of Nuclear Physics, Polish Academy of Sciences, Krakow, Poland*
[40] *Physics Department, Southern Methodist University, Dallas, TX, United States*
[41] *Physics Department, University of Texas at Dallas, Richardson, TX, United States*
[42] *DESY, Hamburg and Zeuthen, Germany*
[43] *Institut für Experimentelle Physik IV, Technische Universität Dortmund, Dortmund, Germany*
[44] *Institut für Kern- und Teilchenphysik, Technische Universität Dresden, Dresden, Germany*
[45] *Department of Physics, Duke University, Durham, NC, United States*
[46] *SUPA – School of Physics and Astronomy, University of Edinburgh, Edinburgh, United Kingdom*
[47] *INFN Laboratori Nazionali di Frascati, Frascati, Italy*
[48] *Fakultät für Mathematik und Physik, Albert-Ludwigs-Universität, Freiburg, Germany*
[49] *Section de Physique, Université de Genève, Geneva, Switzerland*
[50] [(a)] *INFN Sezione di Genova;* [(b)] *Dipartimento di Fisica, Università di Genova, Genova, Italy*
[51] [(a)] *E. Andronikashvili Institute of Physics, Iv. Javakhishvili Tbilisi State University, Tbilisi;* [(b)] *High Energy Physics Institute, Tbilisi State University, Tbilisi, Georgia*
[52] *II Physikalisches Institut, Justus-Liebig-Universität Giessen, Giessen, Germany*
[53] *SUPA – School of Physics and Astronomy, University of Glasgow, Glasgow, United Kingdom*
[54] *II Physikalisches Institut, Georg-August-Universität, Göttingen, Germany*
[55] *Laboratoire de Physique Subatomique et de Cosmologie, Université Grenoble-Alpes, CNRS/IN2P3, Grenoble, France*

[56] Department of Physics, Hampton University, Hampton, VA, United States
[57] Laboratory for Particle Physics and Cosmology, Harvard University, Cambridge, MA, United States
[58] [(a)] Kirchhoff-Institut für Physik, Ruprecht-Karls-Universität Heidelberg, Heidelberg; [(b)] Physikalisches Institut, Ruprecht-Karls-Universität Heidelberg, Heidelberg; [(c)] ZITI Institut für technische Informatik, Ruprecht-Karls-Universität Heidelberg, Mannheim, Germany
[59] Faculty of Applied Information Science, Hiroshima Institute of Technology, Hiroshima, Japan
[60] [(a)] Department of Physics, The Chinese University of Hong Kong, Shatin, N.T., Hong Kong; [(b)] Department of Physics, The University of Hong Kong, Hong Kong; [(c)] Department of Physics, The Hong Kong University of Science and Technology, Clear Water Bay, Kowloon, Hong Kong, China
[61] Department of Physics, Indiana University, Bloomington, IN, United States
[62] Institut für Astro- und Teilchenphysik, Leopold-Franzens-Universität, Innsbruck, Austria
[63] University of Iowa, Iowa City, IA, United States
[64] Department of Physics and Astronomy, Iowa State University, Ames, IA, United States
[65] Joint Institute for Nuclear Research, JINR Dubna, Dubna, Russia
[66] KEK, High Energy Accelerator Research Organization, Tsukuba, Japan
[67] Graduate School of Science, Kobe University, Kobe, Japan
[68] Faculty of Science, Kyoto University, Kyoto, Japan
[69] Kyoto University of Education, Kyoto, Japan
[70] Department of Physics, Kyushu University, Fukuoka, Japan
[71] Instituto de Física La Plata, Universidad Nacional de La Plata and CONICET, La Plata, Argentina
[72] Physics Department, Lancaster University, Lancaster, United Kingdom
[73] [(a)] INFN Sezione di Lecce; [(b)] Dipartimento di Matematica e Fisica, Università del Salento, Lecce, Italy
[74] Oliver Lodge Laboratory, University of Liverpool, Liverpool, United Kingdom
[75] Department of Physics, Jožef Stefan Institute and University of Ljubljana, Ljubljana, Slovenia
[76] School of Physics and Astronomy, Queen Mary University of London, London, United Kingdom
[77] Department of Physics, Royal Holloway University of London, Surrey, United Kingdom
[78] Department of Physics and Astronomy, University College London, London, United Kingdom
[79] Louisiana Tech University, Ruston, LA, United States
[80] Laboratoire de Physique Nucléaire et de Hautes Energies, UPMC and Université Paris-Diderot and CNRS/IN2P3, Paris, France
[81] Fysiska institutionen, Lunds universitet, Lund, Sweden
[82] Departamento de Fisica Teorica C-15, Universidad Autonoma de Madrid, Madrid, Spain
[83] Institut für Physik, Universität Mainz, Mainz, Germany
[84] School of Physics and Astronomy, University of Manchester, Manchester, United Kingdom
[85] CPPM, Aix-Marseille Université and CNRS/IN2P3, Marseille, France
[86] Department of Physics, University of Massachusetts, Amherst, MA, United States
[87] Department of Physics, McGill University, Montreal, QC, Canada
[88] School of Physics, University of Melbourne, Victoria, Australia
[89] Department of Physics, The University of Michigan, Ann Arbor, MI, United States
[90] Department of Physics and Astronomy, Michigan State University, East Lansing, MI, United States
[91] [(a)] INFN Sezione di Milano; [(b)] Dipartimento di Fisica, Università di Milano, Milano, Italy
[92] B.I. Stepanov Institute of Physics, National Academy of Sciences of Belarus, Minsk, Belarus
[93] National Scientific and Educational Centre for Particle and High Energy Physics, Minsk, Belarus
[94] Department of Physics, Massachusetts Institute of Technology, Cambridge, MA, United States
[95] Group of Particle Physics, University of Montreal, Montreal, QC, Canada
[96] P.N. Lebedev Institute of Physics, Academy of Sciences, Moscow, Russia
[97] Institute for Theoretical and Experimental Physics (ITEP), Moscow, Russia
[98] National Research Nuclear University MEPhI, Moscow, Russia
[99] D.V. Skobeltsyn Institute of Nuclear Physics, M.V. Lomonosov Moscow State University, Moscow, Russia
[100] Fakultät für Physik, Ludwig-Maximilians-Universität München, München, Germany
[101] Max-Planck-Institut für Physik (Werner-Heisenberg-Institut), München, Germany
[102] Nagasaki Institute of Applied Science, Nagasaki, Japan
[103] Graduate School of Science and Kobayashi-Maskawa Institute, Nagoya University, Nagoya, Japan
[104] [(a)] INFN Sezione di Napoli; [(b)] Dipartimento di Fisica, Università di Napoli, Napoli, Italy
[105] Department of Physics and Astronomy, University of New Mexico, Albuquerque, NM, United States
[106] Institute for Mathematics, Astrophysics and Particle Physics, Radboud University Nijmegen/Nikhef, Nijmegen, Netherlands
[107] Nikhef National Institute for Subatomic Physics and University of Amsterdam, Amsterdam, Netherlands
[108] Department of Physics, Northern Illinois University, DeKalb, IL, United States
[109] Budker Institute of Nuclear Physics, SB RAS, Novosibirsk, Russia
[110] Department of Physics, New York University, New York, NY, United States
[111] Ohio State University, Columbus, OH, United States
[112] Faculty of Science, Okayama University, Okayama, Japan
[113] Homer L. Dodge Department of Physics and Astronomy, University of Oklahoma, Norman, OK, United States
[114] Department of Physics, Oklahoma State University, Stillwater, OK, United States
[115] Palacký University, RCPTM, Olomouc, Czech Republic
[116] Center for High Energy Physics, University of Oregon, Eugene, OR, United States
[117] LAL, Université Paris-Sud and CNRS/IN2P3, Orsay, France
[118] Graduate School of Science, Osaka University, Osaka, Japan
[119] Department of Physics, University of Oslo, Oslo, Norway
[120] Department of Physics, Oxford University, Oxford, United Kingdom
[121] [(a)] INFN Sezione di Pavia; [(b)] Dipartimento di Fisica, Università di Pavia, Pavia, Italy
[122] Department of Physics, University of Pennsylvania, Philadelphia, PA, United States
[123] Petersburg Nuclear Physics Institute, Gatchina, Russia
[124] [(a)] INFN Sezione di Pisa; [(b)] Dipartimento di Fisica E. Fermi, Università di Pisa, Pisa, Italy
[125] Department of Physics and Astronomy, University of Pittsburgh, Pittsburgh, PA, United States
[126] [(a)] Laboratorio de Instrumentacao e Fisica Experimental de Particulas - LIP, Lisboa; [(b)] Faculdade de Ciências, Universidade de Lisboa, Lisboa; [(c)] Department of Physics, University of Coimbra, Coimbra; [(d)] Centro de Fisica Nuclear da Universidade de Lisboa, Lisboa; [(e)] Departamento de Fisica, Universidade do Minho, Braga; [(f)] Departamento de Fisica Teorica y del Cosmos and CAFPE, Universidad de Granada, Granada (Spain); [(g)] Dep Fisica and CEFITEC of Faculdade de Ciencias e Tecnologia, Universidade Nova de Lisboa, Caparica, Portugal
[127] Institute of Physics, Academy of Sciences of the Czech Republic, Praha, Czech Republic
[128] Czech Technical University in Prague, Praha, Czech Republic
[129] Faculty of Mathematics and Physics, Charles University in Prague, Praha, Czech Republic
[130] State Research Center Institute for High Energy Physics, Protvino, Russia

[131] Particle Physics Department, Rutherford Appleton Laboratory, Didcot, United Kingdom
[132] Physics Department, University of Regina, Regina, SK, Canada
[133] Ritsumeikan University, Kusatsu, Shiga, Japan
[134] [(a)] INFN Sezione di Roma; [(b)] Dipartimento di Fisica, Sapienza Università di Roma, Roma, Italy
[135] [(a)] INFN Sezione di Roma Tor Vergata; [(b)] Dipartimento di Fisica, Università di Roma Tor Vergata, Roma, Italy
[136] [(a)] INFN Sezione di Roma Tre; [(b)] Dipartimento di Matematica e Fisica, Università Roma Tre, Roma, Italy
[137] [(a)] Faculté des Sciences Ain Chock, Réseau Universitaire de Physique des Hautes Energies – Université Hassan II, Casablanca; [(b)] Centre National de l'Energie des Sciences Techniques Nucleaires, Rabat; [(c)] Faculté des Sciences Semlalia, Université Cadi Ayyad, LPHEA-Marrakech; [(d)] Faculté des Sciences, Université Mohamed Premier and LPTPM, Oujda; [(e)] Faculté des sciences, Université Mohammed V-Agdal, Rabat, Morocco
[138] DSM/IRFU (Institut de Recherches sur les Lois Fondamentales de l'Univers), CEA Saclay (Commissariat à l'Energie Atomique et aux Energies Alternatives), Gif-sur-Yvette, France
[139] Santa Cruz Institute for Particle Physics, University of California Santa Cruz, Santa Cruz, CA, United States
[140] Department of Physics, University of Washington, Seattle, WA, United States
[141] Department of Physics and Astronomy, University of Sheffield, Sheffield, United Kingdom
[142] Department of Physics, Shinshu University, Nagano, Japan
[143] Fachbereich Physik, Universität Siegen, Siegen, Germany
[144] Department of Physics, Simon Fraser University, Burnaby, BC, Canada
[145] SLAC National Accelerator Laboratory, Stanford, CA, United States
[146] [(a)] Faculty of Mathematics, Physics & Informatics, Comenius University, Bratislava; [(b)] Department of Subnuclear Physics, Institute of Experimental Physics of the Slovak Academy of Sciences, Kosice, Slovak Republic
[147] [(a)] Department of Physics, University of Cape Town, Cape Town; [(b)] Department of Physics, University of Johannesburg, Johannesburg; [(c)] School of Physics, University of the Witwatersrand, Johannesburg, South Africa
[148] [(a)] Department of Physics, Stockholm University; [(b)] The Oskar Klein Centre, Stockholm, Sweden
[149] Physics Department, Royal Institute of Technology, Stockholm, Sweden
[150] Departments of Physics & Astronomy and Chemistry, Stony Brook University, Stony Brook, NY, United States
[151] Department of Physics and Astronomy, University of Sussex, Brighton, United Kingdom
[152] School of Physics, University of Sydney, Sydney, Australia
[153] Institute of Physics, Academia Sinica, Taipei, Taiwan
[154] Department of Physics, Technion: Israel Institute of Technology, Haifa, Israel
[155] Raymond and Beverly Sackler School of Physics and Astronomy, Tel Aviv University, Tel Aviv, Israel
[156] Department of Physics, Aristotle University of Thessaloniki, Thessaloniki, Greece
[157] International Center for Elementary Particle Physics and Department of Physics, The University of Tokyo, Tokyo, Japan
[158] Graduate School of Science and Technology, Tokyo Metropolitan University, Tokyo, Japan
[159] Department of Physics, Tokyo Institute of Technology, Tokyo, Japan
[160] Department of Physics, University of Toronto, Toronto, ON, Canada
[161] [(a)] TRIUMF, Vancouver, BC; [(b)] Department of Physics and Astronomy, York University, Toronto, ON, Canada
[162] Faculty of Pure and Applied Sciences, University of Tsukuba, Tsukuba, Japan
[163] Department of Physics and Astronomy, Tufts University, Medford, MA, United States
[164] Centro de Investigaciones, Universidad Antonio Narino, Bogota, Colombia
[165] Department of Physics and Astronomy, University of California Irvine, Irvine, CA, United States
[166] [(a)] INFN Gruppo Collegato di Udine, Sezione di Trieste, Udine; [(b)] ICTP, Trieste; [(c)] Dipartimento di Chimica, Fisica e Ambiente, Università di Udine, Udine, Italy
[167] Department of Physics, University of Illinois, Urbana, IL, United States
[168] Department of Physics and Astronomy, University of Uppsala, Uppsala, Sweden
[169] Instituto de Física Corpuscular (IFIC) and Departamento de Física Atómica, Molecular y Nuclear and Departamento de Ingeniería Electrónica and Instituto de Microelectrónica de Barcelona (IMB-CNM), University of Valencia and CSIC, Valencia, Spain
[170] Department of Physics, University of British Columbia, Vancouver, BC, Canada
[171] Department of Physics and Astronomy, University of Victoria, Victoria, BC, Canada
[172] Department of Physics, University of Warwick, Coventry, United Kingdom
[173] Waseda University, Tokyo, Japan
[174] Department of Particle Physics, The Weizmann Institute of Science, Rehovot, Israel
[175] Department of Physics, University of Wisconsin, Madison, WI, United States
[176] Fakultät für Physik und Astronomie, Julius-Maximilians-Universität, Würzburg, Germany
[177] Fachbereich C Physik, Bergische Universität Wuppertal, Wuppertal, Germany
[178] Department of Physics, Yale University, New Haven, CT, United States
[179] Yerevan Physics Institute, Yerevan, Armenia
[180] Centre de Calcul de l'Institut National de Physique Nucléaire et de Physique des Particules (IN2P3), Villeurbanne, France

[a] Also at Department of Physics, King's College London, London, United Kingdom.
[b] Also at Institute of Physics, Azerbaijan Academy of Sciences, Baku, Azerbaijan.
[c] Also at Novosibirsk State University, Novosibirsk, Russia.
[d] Also at Particle Physics Department, Rutherford Appleton Laboratory, Didcot, United Kingdom.
[e] Also at TRIUMF, Vancouver, BC, Canada.
[f] Also at Department of Physics, California State University, Fresno, CA, United States.
[g] Also at Tomsk State University, Tomsk, Russia.
[h] Also at CPPM, Aix-Marseille Université and CNRS/IN2P3, Marseille, France.
[i] Also at Università di Napoli Parthenope, Napoli, Italy.
[j] Also at Institute of Particle Physics (IPP), Canada.
[k] Also at Department of Physics, St. Petersburg State Polytechnical University, St. Petersburg, Russia.
[l] Also at Department of Financial and Management Engineering, University of the Aegean, Chios, Greece.
[m] Also at Louisiana Tech University, Ruston, LA, United States.
[n] Also at Institucio Catalana de Recerca i Estudis Avancats, ICREA, Barcelona, Spain.
[o] Also at Department of Physics, The University of Texas at Austin, Austin, TX, United States.
[p] Also at Institute of Theoretical Physics, Ilia State University, Tbilisi, Georgia.
[q] Also at CERN, Geneva, Switzerland.
[r] Also at Ochadai Academic Production, Ochanomizu University, Tokyo, Japan.
[s] Also at Manhattan College, New York, NY, United States.
[t] Also at Institute of Physics, Academia Sinica, Taipei, Taiwan.
[u] Also at LAL, Université Paris-Sud and CNRS/IN2P3, Orsay, France.

[v] Also at Academia Sinica Grid Computing, Institute of Physics, Academia Sinica, Taipei, Taiwan.
[w] Also at Laboratoire de Physique Nucléaire et de Hautes Energies, UPMC and Université Paris-Diderot and CNRS/IN2P3, Paris, France.
[x] Also at School of Physical Sciences, National Institute of Science Education and Research, Bhubaneswar, India.
[y] Also at Dipartimento di Fisica, Sapienza Università di Roma, Roma, Italy.
[z] Also at Moscow Institute of Physics and Technology State University, Dolgoprudny, Russia.
[aa] Also at Section de Physique, Université de Genève, Geneva, Switzerland.
[ab] Also at International School for Advanced Studies (SISSA), Trieste, Italy.
[ac] Also at Department of Physics and Astronomy, University of South Carolina, Columbia, SC, United States.
[ad] Also at School of Physics and Engineering, Sun Yat-sen University, Guangzhou, China.
[ae] Also at Faculty of Physics, M.V.Lomonosov Moscow State University, Moscow, Russia.
[af] Also at National Research Nuclear University MEPhI, Moscow, Russia.
[ag] Also at Institute for Particle and Nuclear Physics, Wigner Research Centre for Physics, Budapest, Hungary.
[ah] Also at Department of Physics, Oxford University, Oxford, United Kingdom.
[ai] Also at Department of Physics, Nanjing University, Jiangsu, China.
[aj] Also at Institut für Experimentalphysik, Universität Hamburg, Hamburg, Germany.
[ak] Also at Department of Physics, The University of Michigan, Ann Arbor, MI, United States.
[al] Also at Discipline of Physics, University of KwaZulu-Natal, Durban, South Africa.
[am] Also at University of Malaya, Department of Physics, Kuala Lumpur, Malaysia.
[*] Deceased.

Physics Letters B 761 (2016) 350–371

Contents lists available at ScienceDirect

Physics Letters B

www.elsevier.com/locate/physletb

Measurement of the top quark mass in the $t\bar{t} \to$ dilepton channel from $\sqrt{s} = 8$ TeV ATLAS data

The ATLAS Collaboration *

ARTICLE INFO

Article history:
Received 8 June 2016
Received in revised form 21 July 2016
Accepted 8 August 2016
Available online 24 August 2016
Editor: W.-D. Schlatter

ABSTRACT

The top quark mass is measured in the $t\bar{t} \to$ dilepton channel (lepton $= e, \mu$) using ATLAS data recorded in the year 2012 at the LHC. The data were taken at a proton–proton centre-of-mass energy of $\sqrt{s} = 8$ TeV and correspond to an integrated luminosity of about 20.2 fb^{-1}. Exploiting the template method, and using the distribution of invariant masses of lepton–b-jet pairs, the top quark mass is measured to be $m_{\text{top}} = 172.99 \pm 0.41\,(\text{stat}) \pm 0.74\,(\text{syst})$ GeV, with a total uncertainty of 0.84 GeV. Finally, a combination with previous ATLAS m_{top} measurements from $\sqrt{s} = 7$ TeV data in the $t\bar{t} \to$ dilepton and $t\bar{t} \to$ lepton + jets channels results in $m_{\text{top}} = 172.84 \pm 0.34\,(\text{stat}) \pm 0.61\,(\text{syst})$ GeV, with a total uncertainty of 0.70 GeV.

1. Introduction

The mass of the top quark (m_{top}) is an important parameter of the Standard Model (SM) of particle physics. Precise measurements of m_{top} provide crucial information for global fits of electroweak parameters [1–3] which help assess the internal consistency of the SM and to probe its extensions. In addition, the value of m_{top} affects the stability of the SM Higgs potential, which has cosmological implications [4–6]. Many measurements of m_{top} have been performed by the Tevatron and LHC Collaborations. Combining a selection of those, the first Tevatron+LHC m_{top} result is $m_{\text{top}} = 173.34 \pm 0.27\,(\text{stat}) \pm 0.71\,(\text{syst})$ GeV, with a total uncertainty of 0.76 GeV [7]. Meanwhile, a number of new results have become available [8–13], some of which are more precise than the above combination. The latest ATLAS results in the $t\bar{t} \to$ lepton + jets and $t\bar{t} \to$ dilepton decay channels, both with electrons (e) and muons (μ) in the final state [14], are $m_{\text{top}} = 172.33 \pm 0.75\,(\text{stat}) \pm 1.02\,(\text{syst})$ GeV and $m_{\text{top}} = 173.79 \pm 0.54\,(\text{stat}) \pm 1.30\,(\text{syst})$ GeV, respectively.

This Letter presents a new measurement of m_{top} obtained in the $t\bar{t} \to$ dilepton decay channel using 2012 data taken at a proton–proton (pp) centre-of-mass energy of $\sqrt{s} = 8$ TeV, with an integrated luminosity of about 20.2 fb^{-1}. The analysis exploits the decay $t\bar{t} \to W^+W^-b\bar{b} \to \ell^+\ell^-\nu\bar{\nu}b\bar{b}$, which is realised when both W bosons decay into a charged lepton and its corresponding neutrino. In the analysis, the $t\bar{t}$ decay channels ee, $e\mu$ and $\mu\mu$ (including $\tau \to e, \mu$) are combined and referred to as the dilepton channel. Single-top-quark events with the same lepton final states are included in the signal. Given the larger data sample compared to Ref. [14], the event selection was optimised to achieve the smallest total uncertainty. The measurement is based on the implementation of the template method described in Ref. [14], which is calibrated using signal Monte Carlo (MC) samples. Consequently, the top quark mass measured in this way corresponds to the mass definition used in the MC program.

2. ATLAS detector

The ATLAS experiment [15] at the LHC is a multi-purpose particle detector with a forward–backward symmetric cylindrical geometry and a near 4π coverage in solid angle.[1] It consists of an inner tracking detector surrounded by a thin superconducting solenoid providing a 2 T axial magnetic field, electromagnetic and hadron calorimeters, and a muon spectrometer. The inner tracking detector covers the pseudorapidity range $|\eta| < 2.5$. It consists of silicon pixel, silicon microstrip, and transition radiation tracking detectors. Lead/liquid-argon (LAr) sampling calorimeters provide electromagnetic (EM) energy measurements with high granularity. A hadronic (steel/scintillator-tile) calorimeter covers the central pseudorapidity range ($|\eta| < 1.7$). The end-cap and forward regions are instrumented with LAr calorimeters for EM and hadronic energy mea-

[1] ATLAS uses a right-handed coordinate system with its origin at the nominal interaction point (IP) in the centre of the detector and the z-axis along the beam pipe. The x-axis points from the IP to the centre of the LHC ring, and the y-axis points upwards. Cylindrical coordinates (r, ϕ) are used in the transverse plane, ϕ being the azimuthal angle around the z-axis. The pseudorapidity is defined in terms of the polar angle θ as $\eta = -\ln\tan(\theta/2)$. Angular distance is measured in units of $\Delta R \equiv \sqrt{(\Delta\eta)^2 + (\Delta\phi)^2}$.

* *E-mail address:* atlas.publications@cern.ch.

http://dx.doi.org/10.1016/j.physletb.2016.08.042

surements up to $|\eta| = 4.9$. The muon spectrometer surrounds the calorimeters and is based on three large air–core toroid superconducting magnets with eight coils each. Its bending power is in the range from 2.0 to 7.5 T m. It includes a system of precision tracking chambers and fast detectors for triggering. A three-level trigger system is used to select events. The first-level trigger is implemented in hardware and uses a subset of the detector information to reduce the accepted event rate to at most 75 kHz. This is followed by two software-based trigger levels that together reduce the accepted rate to 400 Hz on average depending on the data-taking conditions during 2012.

3. Data and MC samples

This analysis is based on pp collision data recorded in 2012 at $\sqrt{s} = 8$ TeV. The integrated data luminosity amounts to 20.2 fb^{-1} with an uncertainty of 1.9% determined with the procedures described in Ref. [16].

The modelling of $t\bar{t}$ and single-top-quark signal events and of most background processes relies on MC simulations. For the simulation of signal events the Powheg-Box program [17–19] is used. The simulation of the top quark pair [20] and single-top-quark production in the Wt-channel [21] uses matrix elements at next-to-leading order (NLO) in the strong coupling constant α_S, with the NLO CT10 [22] parton distribution function (PDF) and the parameter $h_{\text{damp}} = \infty$. The h_{damp} parameter sets the resummation scale, which controls the transition from the matrix element to the parton shower (PS) simulation. Given that the event selection described below requires leptonic decay products of two W bosons, single-top-quark events in the s-channel and t-channel are found not to contribute to the sample.

The Pythia (v6.425) program [23] with the P2011C [24] set of tuned parameters (tune) and the corresponding CTEQ6L1 PDF [25] are employed to provide the parton shower, hadronisation and underlying-event modelling. The uncertainties due to QCD initial- and final-state radiation (ISR/FSR) modelling are estimated with samples generated with the Powheg-Box program interfaced to the Pythia program for which the parameters of the generation are varied to span the ranges compatible with the results of measurements of $t\bar{t}$ production in association with jets [26–28].

For m_{top} hypothesis testing, the $t\bar{t}$ and single-top-quark event samples are generated for five values of m_{top} in the range 167.5 to 177.5 GeV in steps of 2.5 GeV. For each m_{top} value, the MC samples are normalised according to the best available cross-section calculations, which for $m_{\text{top}} = 172.5$ GeV are $\sigma_{t\bar{t}} = 253^{+13}_{-15}$ pb [29–34] for $t\bar{t}$ production and $\sigma_{Wt} = 22.4 \pm 1.5$ pb [35] for single-top-quark production in the Wt-channel. The PDF + α_S-induced uncertainties in these cross-sections are calculated using the PDF4LHC prescription [36] with the MSTW2008 68% CL NNLO PDF [37,38], CT10 NNLO PDF [22,39] and NNPDF2.3 5f FFN PDF [40], and are added in quadrature with the uncertainties due to the choices of the factorisation and renormalisation scales.

The simulation of $W^{\pm}$ or Z boson production in association with jets is performed with the Alpgen (v2.13) program [41] interfaced to the Pythia6 program using the CTEQ6L1 PDF and the corresponding AUET2 tune [42]. Diboson production processes (WW, WZ and ZZ) are simulated using the Alpgen program interfaced to the Herwig (v6.520) program [43] with the AUET2 tune and to the Jimmy (v4.31) program [44]. All samples are simulated taking into account the effects of multiple soft pp interactions (pile-up) registered in the 2012 data. These interactions are modelled by overlaying simulated hits from events with exactly one inelastic (signal) collision per bunch crossing with hits from minimum-bias events that are produced with the Pythia (v8.160) program [45] using the A2M tune [46] and the MSTW2008 LO PDF. For this analysis, the observed values of the pile-up-related quantities $\langle\mu\rangle$, the mean number of interactions per bunch crossing, and n_{vtx}, the average number of vertices per event, are $\langle\mu\rangle = 20.7$ and $n_{\text{vtx}} = 9.2$.

Finally, the samples undergo a simulation of the ATLAS detector [47] based on Geant4 [48], and are then processed through the same reconstruction software as the data. A number of samples used to assess systematic uncertainties are produced with a faster version of the simulation which, in addition to the full simulation of the tracking, uses smearing functions and interpolates particle behaviour and calorimeter response, based on resolution functions measured in full-simulation studies, to approximate the results of the full simulation.

4. Data selection and event reconstruction

Triggers based on isolated single electrons or muons with energy or momentum thresholds of 24 GeV are used. The detector objects resulting from the top quark pair decay are electron and muon candidates, jets and missing transverse momentum ($E_{\text{T}}^{\text{miss}}$). In the following, the term lepton is used for charged leptons (excluding τ leptons) exclusively.

Electron candidates [49] are required to have a transverse energy of $E_{\text{T}} > 25$ GeV, a pseudorapidity of the corresponding EM cluster of $|\eta_{\text{cluster}}| < 2.47$, with the transition region $1.37 < |\eta_{\text{cluster}}| < 1.52$ between the barrel and the end-cap calorimeter excluded. The muon candidates [50] are required to have transverse momentum $p_{\text{T}} > 25$ GeV and $|\eta| < 2.5$. To reduce the contamination by leptons from heavy-flavour decays inside jets or from photon conversions, referred to as non-prompt (NP) leptons, strict isolation criteria are applied to the amount of activity in the vicinity of the lepton candidate [49,50].

Jets are built from topological clusters of calorimeter cells [51] with the anti-k_t jet clustering algorithm [52] using a radius parameter of $R = 0.4$. Jets are reconstructed using the local cluster weighting (LCW) and global sequential calibration (GSC) algorithms [53–55] and required to satisfy $p_{\text{T}} > 25$ GeV and $|\eta| < 2.5$. Muons reconstructed within a $\Delta R = 0.4$ cone around the axis of a jet with $p_{\text{T}} > 25$ GeV are not considered as charged-lepton candidates. In addition, jets within a $\Delta R = 0.2$ cone around an electron candidate are removed and finally electrons within a $\Delta R = 0.4$ cone around any of the remaining jets are discarded. The identification of jets containing b-hadrons, b-tagging, is used for event reconstruction and background suppression. In the following, irrespective of their origin, jets tagged by the b-tagging algorithm are referred to as b-tagged jets, whereas those not tagged are referred to as untagged jets. Similarly, whether they are tagged or not, jets originating from bottom quarks are referred to as b-jets and those from (u, d, c, s)-quarks or gluons as light jets. The working point of the neural-network-based MV1 b-tagging algorithm [56] corresponds to an average b-tagging efficiency of 70% for b-jets in simulated $t\bar{t}$ events and rejection factors of 5 for jets containing a c-hadron and 137 for jets containing only lighter-flavour hadrons. To match the b-tagging performance in the data, p_{T}- and η-dependent scale factors [56], obtained from dijet and $t\bar{t} \to$ dilepton events, are applied to MC jets depending on their true flavour. The reconstruction of the $E_{\text{T}}^{\text{miss}}$ is based on the vector sum of energy deposits in the calorimeters, projected onto the transverse plane. Muons are included in the $E_{\text{T}}^{\text{miss}}$ using their reconstructed momentum in the tracking detectors [57].

The contribution of events wrongly reconstructed as $t\bar{t} \to$ dilepton events due to the presence of objects misidentified as leptons (fake leptons), is estimated from data [58]. The technique employed uses fake-lepton and real-lepton efficiencies that depend on η and p_{T}, measured in a background-enhanced control region

Table 1
The observed numbers of events in data after the pre-selection and the final selection. In addition, the expected numbers of signal events for $m_{\text{top}} = 172.5$ GeV and background events corresponding to the integrated data luminosity are given. Two significant digits are used for the uncertainties of the predicted numbers of events explained in the text. The lower rows report the matching performance evaluated for $m_{\text{top}} = 172.5$ GeV, using one significant digit for the statistical uncertainties.

Selection	Pre-selection	Final selection
Data	36 359	9426
$t\bar{t}$ signal	$34\,300 \pm 2700$	9670 ± 770
Single-top-quark signal	1690 ± 110	363 ± 23
Fake leptons	240 ± 240	31 ± 31
Z + jets	212 ± 83	20.6 ± 8.5
$WW/WZ/ZZ$	57 ± 21	10.2 ± 3.8
Signal + background	$36\,600 \pm 2800$	$10\,100 \pm 770$
Expected background fraction	0.01 ± 0.01	0.01 ± 0.00
Data/(Signal + background)	0.99 ± 0.07	0.93 ± 0.07
Matching efficiency [%]	78.4 ± 0.2	95.3 ± 0.4
Selection purity [%]	51.6 ± 0.1	69.8 ± 0.3
Unmatched events [%]	34.2 ± 0.1	26.7 ± 0.1
Wrongly matched events [%]	14.2 ± 0.1	3.4 ± 0.0

with low $E_{\text{T}}^{\text{miss}}$ and from events with dilepton masses around the Z peak [59].

The selection from Ref. [14] is applied as a pre-selection as follows:

1. Events are required to have a signal from the single-electron or single-muon trigger and at least one primary vertex with at least five associated tracks.
2. Exactly two oppositely charged leptons are required, with at least one of them matching the reconstructed object that fired the corresponding trigger.
3. In the same-lepton-flavour channels, ee and $\mu\mu$, $E_{\text{T}}^{\text{miss}} > 60$ GeV is required. In addition, the invariant mass of the lepton pair must satisfy $m_{\ell\ell} > 15$ GeV, and must not be compatible with the Z mass within 10 GeV.
4. In the $e\mu$ channel the scalar sum of p_{T} of the two selected leptons and all jets is required to be larger than 130 GeV.
5. The presence of at least two jets with $p_{\text{T}} > 25$ GeV and $|\eta| < 2.5$ is required, and at least one of these jets has to be b-tagged.

The observed numbers of events in the data after this pre-selection, together with the expected numbers of signal and background events corresponding to the integrated data luminosity, are given in Table 1. Assuming a top quark mass of $m_{\text{top}} = 172.5$ GeV, the predicted number of events is consistent with the one observed in the data within uncertainties. For all predictions, the uncertainties are estimated as the sum in quadrature of the statistical uncertainty, a 1.9% uncertainty in the integrated luminosity, and a number of additional components. For the signal, these are a 5.4% uncertainty in the $t\bar{t}$ cross-section, or a 6.0% uncertainty in the single-top-quark cross-section, as given in Sect. 3. Finally, global 4.1%, 2.2% and 2.8% uncertainties are added, corresponding to the envelopes of the results from the eigenvector variations of the jet energy scale (JES), the relative b-to-light-jet energy scale (bJES) and the b-tagging scale factors, respectively. The background uncertainties contain jet-multiplicity-dependent uncertainties of about 40% in the normalisation of the Z + jets background and a 100% uncertainty in the normalisation of fake-lepton background.

The two jets carrying the highest MV1 weight are taken as the two b-jets originating from the decays of the two top quarks, and the two leptons are taken as the leptons from the leptonic W decays. From the two possible assignments of the two pairs, the combination leading to the lowest average invariant mass of the two lepton–b-jet pairs ($m_{\ell b}$) is retained. To estimate the performance of this algorithm in MC simulated samples, the reconstruction-level objects are matched to the closest generator-level object based on a maximum allowed ΔR, being 0.1 for leptons and 0.3 for jets. A matched object is defined as a reconstruction-level object that falls within ΔR of any generator-level object of that type, and a correct match means that this generator-level object is the one it originated from. Due to acceptance losses and reconstruction inefficiency, not all reconstruction-level objects can successfully be matched to their generator-level counterparts, resulting in unmatched events. The matching efficiency is the fraction of correctly matched events among all the matched events, and the selection purity is the fraction of correctly matched events among all events, regardless of whether they could be matched or not. The corresponding numbers for $m_{\text{top}} = 172.5$ GeV are reported in Table 1.

Starting from this pre-selection, an optimisation of the total uncertainty in m_{top} is performed. A phase-space restriction based on the average p_{T} of the two lepton–b-jet pairs ($p_{\text{T},\ell b}$) is used to obtain the smallest total uncertainty in m_{top}. The corresponding $p_{\text{T},\ell b}$ distribution is shown in Fig. 1(a). The smallest uncertainty in m_{top} corresponds to $p_{\text{T},\ell b} > 120$ GeV. The difference in shape between data and prediction is covered by the systematic uncertainty as detailed in Sect. 6. This restriction is found to also increase the fraction of correctly matched events in the $t\bar{t}$ sample, and reduces the number of unmatched or wrongly matched events.

To perform the template parameterisation described in Sect. 5, an additional selection criterion is applied, restricting the reconstructed $m_{\ell b}$ value ($m_{\ell b}^{\text{reco}}$) to the range 30 GeV $< m_{\ell b}^{\text{reco}} <$ 170 GeV. Applying both restrictions, the numbers of predicted and observed events resulting from the final selection are reported in Table 1. Using this optimisation, the matching efficiency and the sample purity are much improved as reported in the bottom rows of Table 1, while retaining about 26% of the events. Using this selection, and the objects assigned to the two lepton–b-jet pairs, the kinematic distributions in the data are well described by the predictions, as shown in Fig. 1 for the transverse momenta of b-jets and leptons, and for the $\Delta R_{\ell b}$ of the two lepton–b-jet pairs.

5. Template fit and results in the data

The implementation of the template method used in this analysis is described in Ref. [14]. For this analysis, the templates are simulated distributions of $m_{\ell b}^{\text{reco}}$, constructed for a number of discrete values of m_{top}. Appropriate functions are fitted to these templates, interpolating between different input m_{top}. The remaining parameters of the functions are fixed by a simultaneous fit to all templates, imposing linear dependences of the parameters on m_{top}. The resulting template fit function has m_{top} as the only free parameter and an unbinned likelihood maximisation gives the value of m_{top} that best describes the data. Statistically independent signal templates, comprising $t\bar{t}$ and single-top-quark events, are constructed as a function of the top quark mass used in the MC generator. Within the statistical uncertainties, the sum of a Gaussian distribution and a Landau function gives a good description of the shape of the $m_{\ell b}^{\text{reco}}$ distribution as shown in Fig. 2(a) for three values of m_{top}. With this signal choice, the background distribution is independent of m_{top}, and a Landau function is fitted to it. The sum of the signal template at $m_{\text{top}} = 172.5$ GeV and the background is compared to data in Fig. 2(b). It gives a good description of the data except for differences that can be accounted for by a different

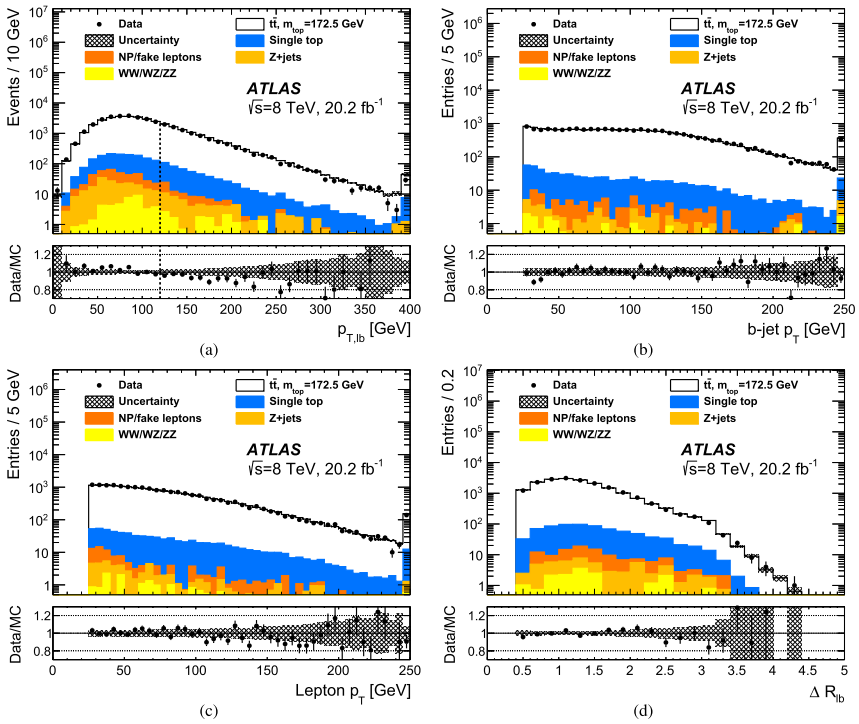

Fig. 1. Kinematic distributions obtained from the objects assigned to the two lepton–b-jet pairs for (a) the pre-selection, or (b)–(d) the final selection. The average p_{T} of the two lepton–b-jet pairs, denoted by $p_{\mathrm{T},\ell b}$, is shown in (a). The $p_{\mathrm{T},\ell b}$ requirement for the final selection is indicated by the vertical dashed line. The remaining distributions show the p_{T} of the b-jets in (b), the p_{T} of the leptons in (c), and the $\Delta R_{\ell b}$ of the lepton and the b-jet for the two lepton–b-jet pairs in (d). The rightmost bin contains the overflow, if present. For all distributions, the number of predicted events is normalised to the one observed in the data. The hatched area corresponds to the statistical uncertainties in the prediction, the uncertainty bars to the statistical uncertainties in the data. For each figure, the ratio of data and prediction is also presented.

top quark mass. In this distribution, the correctly matched events are concentrated in the central part, whereas the remainder is less peaked and accounts for most of the tails.

In this analysis the expected statistical precision as well as all systematic uncertainties are obtained from pseudo-experiments generated from MC simulated samples mimicking ATLAS data. To verify the internal consistency of the method, 1000 pseudo-experiments per mass point are performed, correcting for oversampling [60]. Within uncertainties, and for all m_{top} values, the residuals and pull means are consistent with zero and the pull widths are consistent with unity, i.e. the estimator is unbiased and uncertainties are calculated properly. The expected statistical uncertainty is obtained from the distribution of the statistical uncertainty in the fitted m_{top} of the pseudo-experiments. For $m_{\mathrm{top}} = 172.5$ GeV and the data luminosity it amounts to 0.41 ± 0.03 GeV, where the quoted precision is statistical. The $m_{\ell b}^{\mathrm{reco}}$ distribution in the data is shown in Fig. 2(c) together with the corresponding fitted probability density functions for the background alone and for the sum of signal and background. The value obtained fixing the background contribution to its prediction is $m_{\mathrm{top}} = 172.99 \pm 0.41$ (stat) GeV. The statistical uncertainty in m_{top} is taken from the parabolic approximation of the logarithm of the likelihood as shown in Fig. 2(d). The observed and predicted values of the statistical uncertainty agree.

6. Uncertainties affecting the m_{top} determination

The same systematic uncertainty sources as in Ref. [14] are investigated. Their impact on the analysis is mostly evaluated from pairs of samples expressing a particular systematic uncertainty, by constructing the corresponding templates and measuring the average difference in m_{top} of the pair from 1000 pseudo-experiments. To facilitate a combination with other results, every systematic uncertainty is assigned a statistical uncertainty, taking into account the statistical correlation of the considered samples. Following Ref. [61], the resulting uncertainty components are given in Table 2 irrespective of their statistical significance. The uncertainty sources are constructed so as to be uncorrelated with each another and thus the total uncertainty squared is calculated as the sum in quadrature of all components. The various sources of systematic uncertainties and the evaluation of their effect on m_{top} are briefly described in the following. The values are given in Table 2.

Method: The mean value of the differences between the fitted and generated m_{top} for the MC samples at various input top quark masses is assigned as the method calibration uncertainty. This also covers effects from limited numbers of MC simulated events in the templates.

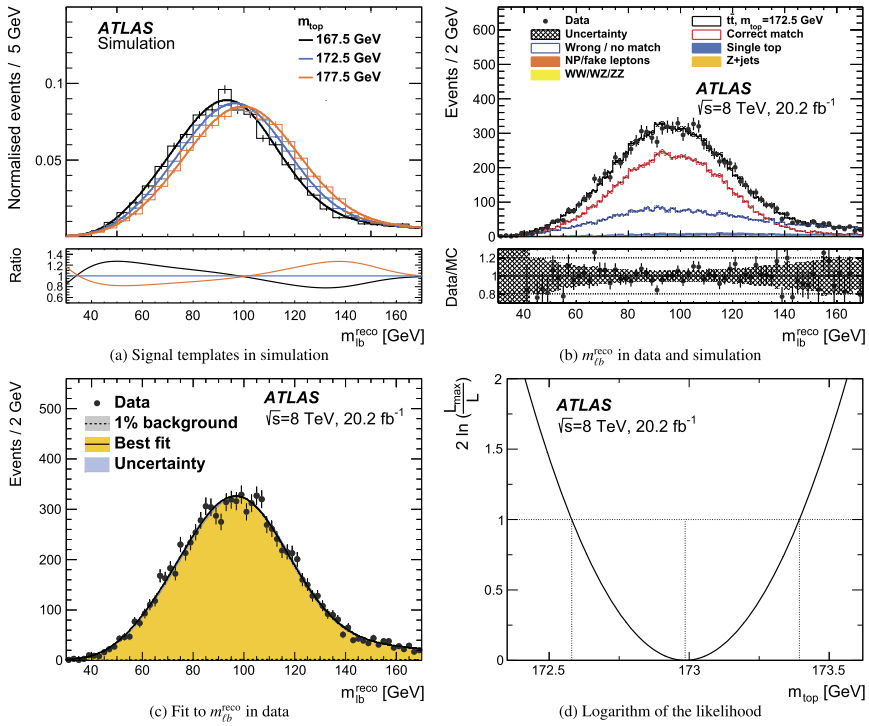

(a) Signal templates in simulation

(b) $m_{\ell b}^{\text{reco}}$ in data and simulation

(c) Fit to $m_{\ell b}^{\text{reco}}$ in data

(d) Logarithm of the likelihood

Fig. 2. Simulated signal templates (histograms) for different values of m_{top} together with the template fits (curves) are given in (a). The $m_{\ell b}^{\text{reco}}$ distribution observed in data in comparison to the prediction is shown in (b). Both figures show statistical uncertainties only. In (b) the background contributions are too small to be distinguished. The $m_{\ell b}^{\text{reco}}$ distribution is shown in (c) for data with statistical uncertainties together with the fitted probability density functions for the background alone (barely visible at the bottom of the figure) and for the sum of signal and background. The uncertainty band corresponds to the total uncertainty in m_{top}. Finally, the corresponding logarithm of the likelihood as a function of m_{top} is displayed in (d).

Signal Monte Carlo generator: The difference in m_{top} between the event sample produced with the MC@NLO program [62,63] and the default POWHEG sample, both generated at $m_{\text{top}} = 172.5$ GeV and using the HERWIG program for parton shower, hadronisation and underlying event, is quoted as a systematic uncertainty.

Hadronisation: The difference in m_{top} between samples produced with the POWHEG-BOX program and showered with either the PYTHIA6 program using the P2011C tune or the HERWIG and JIMMY programs using the ATLAS AUET2 tune [42] is quoted as a systematic uncertainty. This includes different approaches in parton-shower modelling and hadronisation, namely the Lund string model [64,65] and the cluster model [66]. The difference in shape between data and prediction observed for the $p_{\text{T},\ell b}$ distribution shown in Fig. 1(a) is much reduced when using the POWHEG+HERWIG sample and therefore covered by this uncertainty. As a check to assess the maximum possible difference in m_{top} caused by the mismodelling of the $p_{\text{T},\ell b}$ distribution, the predicted distribution is reweighted to the data distribution and the fit is repeated. The observed difference in m_{top} from the nominal sample is about 0.2 GeV, well below the statistical uncertainty in the data. Consequently, no additional uncertainty is applied. Finally, the calibration of the JES and bJES, discussed below, is also partially based on a comparison of jet energy responses in event samples produced with the Herwig++ [67] and PYTHIA6 programs. However, it was verified [68] that the amount of double-counting of JES and hadronisation effects for the $t\bar{t} \to$ lepton + jets channel is small.

Initial- and final-state QCD radiation (ISR/FSR): The uncertainty due to this effect is evaluated by comparing two dedicated samples generated with the POWHEG-BOX and PYTHIA6 programs that differ in several parameters, namely: the QCD scale Λ_{QCD}, the transverse momentum scale for space-like parton-shower evolution Q^2_{max} and the h_{damp} parameter [69]. Half the observed difference between the up variation and the down variation is quoted as a systematic uncertainty. For comparison, using the signal samples generated at $m_{\text{top}} = 172.5$ GeV, and only changing the h_{damp} parameter but using a much larger range, i.e. from ∞ to m_{top}, the measured m_{top} is lowered by 0.23 ± 0.13 GeV, where the uncertainty is statistical.

Underlying event (UE): The difference in UE modelling is assessed by comparing POWHEG samples based on the same partonic events generated with the CT10 PDFs. The difference in m_{top} for a sample with the Perugia 2012 tune (P2012) and a sample with the P2012 mpiHi tune [24] is assigned as a systematic uncertainty.

Colour reconnection (CR): This systematic uncertainty is estimated using samples with the same partonic events as for the UE uncertainty evaluation, but with the P2012 tune and the P2012 loCR tune [24] for PS and hadronisation. The difference in m_{top} is quoted as a systematic uncertainty.

Parton distribution function (PDF): The PDF systematic uncertainty is the sum in quadrature of three contributions. These are:

Table 2
The three measured values of m_{top} together with their statistical and systematic uncertainty components are shown on the left. The middle part reports the estimated correlations ρ_{ij} per pair of measurements, with 0, 1 and 2 denoting the ℓ + jets and dilepton measurements at $\sqrt{s} = 7$ TeV (from Ref. [14]) and the dilepton measurement at $\sqrt{s} = 8$ TeV, respectively. Finally, the right part lists the m_{top} results for the combinations of the two measurements at $\sqrt{s} = 7$ TeV, the two measurements in the dilepton channel and all measurements. For the individual measurements, the systematic uncertainty in m_{top} and its associated statistical uncertainty is given for each source of uncertainty. Assigned correlations are given as integer values, determined correlations as real values. The last line refers to the sum in quadrature of the statistical and systematic uncertainty components or the total correlations, respectively.

	$\sqrt{s} = 7$ TeV		$\sqrt{s} = 8$ TeV	Correlations			Combinations		
	$m_{\text{top}}^{\ell+\text{jets}}$ [GeV]	$m_{\text{top}}^{\text{dil}}$ [GeV]	$m_{\text{top}}^{\text{dil}}$ [GeV]	ρ_{01}	ρ_{02}	ρ_{12}	$m_{\text{top}}^{7\text{ TeV}}$ [GeV]	$m_{\text{top}}^{\text{dil}}$ [GeV]	$m_{\text{top}}^{\text{all}}$ [GeV]
Results	172.33	173.79	172.99				172.99	173.04	172.84
Statistics	0.75	0.54	0.41	0	0	0	0.48	0.38	0.34
Method	0.11 ± 0.10	0.09 ± 0.07	0.05 ± 0.07	0	0	0	0.07	0.05	0.05
Signal Monte Carlo generator	0.22 ± 0.21	0.26 ± 0.16	0.09 ± 0.15	+1.00	+1.00	+1.00	0.24	0.10	0.14
Hadronisation	0.18 ± 0.12	0.53 ± 0.09	0.22 ± 0.09	+1.00	+1.00	+1.00	0.34	0.24	0.23
Initial- and final-state QCD radiation	0.32 ± 0.06	0.47 ± 0.05	0.23 ± 0.07	−1.00	−1.00	+1.00	0.04	0.24	0.08
Underlying event	0.15 ± 0.07	0.05 ± 0.05	0.10 ± 0.14	−1.00	−1.00	+1.00	0.06	0.10	0.02
Colour reconnection	0.11 ± 0.07	0.14 ± 0.05	0.03 ± 0.14	−1.00	−1.00	+1.00	0.01	0.03	0.01
Parton distribution function	0.25 ± 0.00	0.11 ± 0.00	0.05 ± 0.00	+0.57	−0.29	+0.03	0.17	0.04	0.08
Background normalisation	0.10 ± 0.00	0.04 ± 0.00	0.03 ± 0.00	+1.00	+0.23	+0.23	0.07	0.03	0.04
W/Z + jets shape	0.29 ± 0.00	0.00 ± 0.00	0	0			0.16	0.00	0.09
Fake leptons shape	0.05 ± 0.00	0.01 ± 0.00	0.08 ± 0.00	+0.23	+0.20	−0.08	0.03	0.07	0.05
Jet energy scale	0.58 ± 0.11	0.75 ± 0.08	0.54 ± 0.04	−0.23	+0.06	+0.35	0.41	0.52	0.41
Relative b-to-light-jet energy scale	0.06 ± 0.03	0.68 ± 0.02	0.30 ± 0.01	+1.00	+1.00	+1.00	0.34	0.32	0.25
Jet energy resolution	0.22 ± 0.11	0.19 ± 0.04	0.09 ± 0.05	−1.00	0	0	0.03	0.08	0.08
Jet reconstruction efficiency	0.12 ± 0.00	0.07 ± 0.00	0.01 ± 0.00	+1.00	+1.00	+1.00	0.10	0.01	0.04
Jet vertex fraction	0.01 ± 0.00	0.00 ± 0.00	0.02 ± 0.00	−1.00	+1.00	−1.00	0.00	0.02	0.02
b-tagging	0.50 ± 0.00	0.07 ± 0.00	0.03 ± 0.02	−0.77	0	0	0.25	0.03	0.15
Leptons	0.04 ± 0.00	0.13 ± 0.00	0.14 ± 0.01	−0.34	−0.52	+0.96	0.05	0.14	0.09
$E_{\text{T}}^{\text{miss}}$	0.15 ± 0.04	0.04 ± 0.03	0.01 ± 0.01	−0.15	+0.25	−0.24	0.08	0.01	0.05
Pile-up	0.02 ± 0.01	0.01 ± 0.00	0.05 ± 0.01	0	0	0	0.01	0.05	0.03
Total systematic uncertainty	1.03 ± 0.31	1.31 ± 0.23	0.74 ± 0.29				0.77	0.74	0.61
Total	1.27 ± 0.33	1.41 ± 0.24	0.84 ± 0.29	−0.07	0.00	0.51	0.91	0.84	0.70

the sum in quadrature of the differences in m_{top} for the 26 eigenvector variations of the CTEQ PDF [25] and two differences in m_{top} obtained from reweighting the central CT10 PDF set to the MSTW2008 PDF [37] and the NNPDF23 PDF [40].

Background normalisation: The normalisations are varied simultaneously for the MC-based and the data-driven background estimates according to the above mentioned uncertainties.

Background shapes: Given the negligible uncertainty in the dilepton channel observed in Ref. [14], no shape uncertainty is evaluated for the MC-based background. For the data-driven background the shape uncertainty is obtained from the estimate of fake-lepton events using the matrix method [58].

Jet energy scale (JES): Mean jet energies are measured with a relative precision of about 1% to 4%, typically falling with jet p_{T} and rising with jet $|\eta|$ [70,71]. The large number of subcomponents of the total JES uncertainty are reduced by a matrix diagonalisation of the full JES covariance matrix. For each of the resulting 25 significant nuisance parameters [54] the corresponding uncertainty in m_{top} is calculated. The total JES-induced uncertainty in m_{top} is obtained by the sum in quadrature of the results for the subcomponents.

Relative *b*-to-light-jet energy scale (bJES): The bJES is an additional uncertainty for the remaining differences between b-jets and light jets after the global JES is applied and therefore the corresponding uncertainty is uncorrelated with the JES uncertainty. Jets containing b-hadrons are assigned an additional uncertainty of 0.2% to 1.2%, with lowest uncertainties for high-p_{T} b-jets [54].

Jet energy resolution (JER): The JER uncertainty is determined by the sum in quadrature of the m_{top} differences between the varied samples and the nominal sample or, where applicable, half the fitted difference between the up variation and the down variation of the components of the eigenvector decomposition.

Jet reconstruction efficiency (JRE): The JRE uncertainty is evaluated by randomly removing 2% of the jets with $p_{\text{T}} < 30$ GeV from the MC simulated events prior to the event selection to reflect the precision with which the data-to-MC JRE ratio is known [53]. The m_{top} difference with respect to the nominal sample is taken as a systematic uncertainty.

Jet vertex fraction (JVF): When summing the scalar p_{T} of all tracks in a jet, the JVF is the fraction contributed by tracks originating at the primary vertex. The uncertainty is evaluated by varying the requirement on the JVF within its uncertainty [72].

***b*-tagging**: Mismodelling of the b-tagging efficiency and mistag rate is accounted for by the application of scale factors which depend on jet p_{T} and jet η to MC simulated events [56]. The eigenvector decomposition [56,73] accounts for the uncertainties in the b-tagging, c/τ-tagging and mistagging scale factors. The final b-tagging uncertainty is the sum in quadrature of these uncorrelated components.

Lepton uncertainties: The lepton uncertainties measured in $J/\psi \to \ell\ell$ and $Z \to \ell\ell$ events are related to the electron energy or muon momentum scales and resolutions, and the trigger and identification efficiencies [49,50,74]. For each component, the corresponding uncertainty is propagated to the analysis including the recalculation of the $E_{\text{T}}^{\text{miss}}$.

Missing transverse momentum ($\boldsymbol{E_{\text{T}}^{\text{miss}}}$): The remaining contribution to the $E_{\text{T}}^{\text{miss}}$ uncertainty stems from the uncertainties in calorimeter cell energies associated with low-p_{T} jets (7 GeV $< p_{\text{T}} <$ 20 GeV), without any corresponding reconstructed physics object or from pile-up interactions. Their impact is accounted for as described in Ref. [57].

Pile-up: Besides the component treated in the JES, the residual dependence of the fitted m_{top} on the amount of pile-up activity and a possible MC mismodelling is determined. The m_{top} dependence as functions of n_{vtx} and $\langle\mu\rangle$ is found to be consistent in data and simulation. The corresponding uncertainty evaluated from the remaining difference is small.

The systematic uncertainties quoted in Table 2 carry statistical uncertainties. The statistical precision of a single sample fit is about 100 MeV. The statistical correlation of the samples is calculated from the fraction of shared events. Pairs of samples with only a change in a single parameter have high correlation and correspondingly low statistical uncertainty in the difference in m_{top}, while a pair of statistically independent samples results in a larger uncertainty.

In summary, the result in the dilepton channel at $\sqrt{s} = 8$ TeV of $m_{\text{top}} = 172.99 \pm 0.41\,(\text{stat}) \pm 0.74\,(\text{syst})$ GeV is about 40% more precise than the one obtained from the $\sqrt{s} = 7$ TeV data and the most precise single result in this decay channel to date. The increased precision is partly driven by a better knowledge of the JES and bJES. In addition, the applied optimisation procedure significantly reduces the total systematic uncertainty, mostly due to a lower impact of the JES and theory modelling uncertainties.

7. Combination with previous ATLAS measurements

The combination of the m_{top} results follows the approach developed for the combination of the $\sqrt{s} = 7$ TeV measurements in Ref. [14] including the evaluation of the correlations. For combining the measurements from data at different centre-of-mass energies a mapping of uncertainty categories is performed. Complex cases are the uncertainty components involving eigenvector decompositions such as the JES, the JER and the b-tagging scale factor uncertainties. The $\sqrt{s} = 7$ and 8 TeV measurements are treated as uncorrelated for the nuisance parameters of the JER and the b-tagging, c/τ-tagging and mistagging uncertainties. A correlated treatment of the estimators for the flavour-tagging nuisance parameters results in an insignificant change in the combination. The total JES uncertainty consists of about 20 eigenvector components, which partly differ for the analyses of $\sqrt{s} = 7$ and 8 TeV data, which make use of the EM+JES and the LCW+GSC [70] jet calibrations, respectively. For the combination, a mapping between uncertainty components at the different centre-of-mass energies is employed to identify the corresponding ones. The combination was found to be stable against variations of the assumptions for ambiguous cases.

The combination is performed using the best linear unbiased estimate (BLUE) method [75,76], implying Gaussian probability density functions for all uncertainties, using the implementation described in Ref. [77]. The central values, the list of uncertainty components and the correlations ρ of the estimators for each uncertainty component have to be provided. For the statistical, method calibration, MC-based background shape at $\sqrt{s} = 7$ TeV, and pile-up uncertainties in m_{top} the measurements are assumed to be uncorrelated. For the remaining uncertainties in m_{top}, when using $\pm 1\sigma$ variations of a systematic effect, e.g. when changing the bJES by $\pm 1\sigma$, there are two possibilities. When simultaneously applying a variation for a systematic uncertainty, e.g. $+1\sigma$ for the bJES to a pair of analyses, e.g. the dilepton measurements at $\sqrt{s} = 7$ and 8 TeV, both analyses can result in a larger or smaller m_{top} value than what is obtained for the nominal case (full correlation, $\rho = +1$), or one analysis can obtain a larger and the other a smaller value (full anti-correlation, $\rho = -1$). Consequently, an uncertainty from a source only consisting of a single variation, such as the uncertainty related to the choice of MC generator for signal events, results in a correlation of $\rho = \pm 1$. The estimator correlations for composite uncertainties are evaluated by adding the covariance terms of the subcomponents i with $\rho_i = \pm 1$ and dividing by the total uncertainties for that source. The resulting estimator

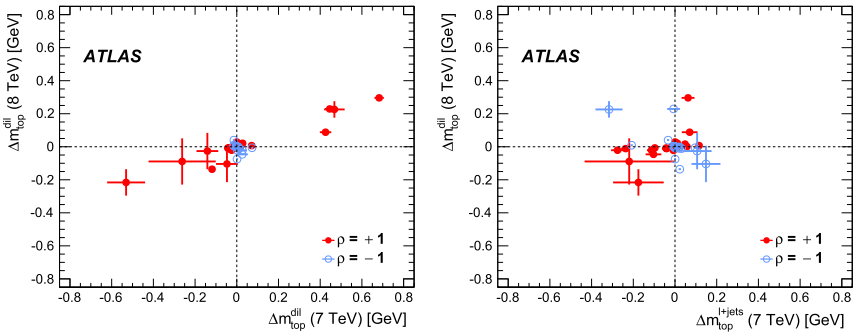

(a) $\sqrt{s}$ = 7 TeV versus $\sqrt{s}$ = 8 TeV dilepton (b) $\sqrt{s}$ = 7 TeV ℓ+jets versus $\sqrt{s}$ = 8 TeV dilepton

Fig. 3. The pairwise differences in m_{top} when simultaneously varying both analyses for a systematic uncertainty. Each cross indicates the statistical precisions of the systematic uncertainty. The red full points indicate $\rho = 1$, the blue open points $\rho = -1$.

correlation per uncertainty is quoted in Table 2 and used in the combination.

The evaluated uncertainties in m_{top} for the uncertainty components for the two dilepton analyses, denoted by Δm_{top}^{dil}, are shown in Fig. 3(a). Each point represents a systematic uncertainty together with a cross, indicating the respective statistical precision of the systematic uncertainty in the two analyses. The red full points indicate $\rho = 1$, the blue open points $\rho = -1$. Given the similarity of the analyses, a positive estimator correlation is observed for most uncertainty components of the two measurements in the dilepton channel. The corresponding distribution for the ℓ + jets measurement at $\sqrt{s} = 7$ TeV and the dilepton measurement at $\sqrt{s} = 8$ TeV is given in Fig. 3(b). In this figure, the estimates are anti-correlated for several significant uncertainties. This is caused by the in-situ measurement of the jet energy scale factor (JSF) and relative b-to-light-jet energy scale factor (bJSF) in the three-dimensional ℓ+jets analysis, detailed in Ref. [14]. The resulting total correlation for this pair is very low as shown in Table 2. The combination strongly profits from this.

The central values of the three measurements, their uncertainty components, the determined correlations per pair of measurements and the results of the combinations are given in Table 2. The pairwise differences in the three measurements are 0.75σ for the $\sqrt{s} = 7$ TeV measurements, 0.43σ for the ℓ + jets measurement at $\sqrt{s} = 7$ TeV and the dilepton measurement at $\sqrt{s} = 8$ TeV and 0.66σ for the two dilepton measurements. For all three cases σ denotes the one standard deviation of the respective m_{top} difference. The combined result in the dilepton channel alone is $m_{top}^{dil} = 173.04 \pm 0.38\,(stat) \pm 0.74\,(syst)$ GeV $= 173.04 \pm 0.84$ GeV, providing no significant improvement with respect to the more precise result at $\sqrt{s} = 8$ TeV which carries a BLUE combination weight of 0.94. This is a mere consequence of the measurement correlation of 0.51, which is close to the ratio of uncertainties (see Ref. [76]). The χ^2 probability of the combination is 51%. The stability of the combination is assessed from the results of 1000 combinations for which all input uncertainties are varied within their statistical uncertainties, which for some cases also result in different correlations (see Fig. 3). The corresponding distributions of the central values and uncertainties of the combinations are approximately Gaussian, with a width of 0.03 GeV and of 0.04 GeV, respectively.

The combination of all three measurements provides a 17% improvement with respect to the most precise single input measurement. The combined result is $m_{top}^{all} = 172.84 \pm 0.34\,(stat) \pm 0.61\,(syst)$ GeV $= 172.84 \pm 0.70$ GeV. The χ^2 probability of the combination is 73% and the BLUE combination weights of the ℓ+jets and dilepton measurements at $\sqrt{s} = 7$ TeV and the dilepton measurement at $\sqrt{s} = 8$ TeV are 0.30, 0.07 and 0.63, respectively. Again, the central value and the combined total uncertainty are both stable at the level of 0.03 GeV.

8. Conclusion

The top quark mass is measured in the $t\bar{t} \to$ dilepton channel from about 20.2 fb^{-1} of $\sqrt{s} = 8$ TeV proton–proton collision data recorded by the ATLAS detector at the LHC. Compared to the latest ATLAS measurement in this decay channel, the event selection is refined exploiting the average p_T of the lepton–b-jet pairs to enhance the fraction of correctly reconstructed events, thereby reducing the systematic uncertainties. Using the optimal point in terms of total uncertainty observed in a phase-space scan of this variable as an additional event selection criterion, the measured value of m_{top} is

$$m_{top} = 172.99 \pm 0.41\,(stat) \pm 0.74\,(syst)\,\text{GeV},$$

with a total uncertainty of 0.84 GeV. The precision is mainly limited by systematic uncertainties, mostly by the calibration of the jet energy scale, and to a lesser extent by the calibration of the relative b-to-light-jet energy scale and by the Monte Carlo modelling of signal events.

This measurement is combined with the ATLAS measurements in the $t\bar{t} \to$ lepton + jets and $t\bar{t} \to$ dilepton decay channels from $\sqrt{s} = 7$ TeV data. The correlations of the measurements are evaluated for all sources of the systematic uncertainty. Using a dedicated mapping of uncertainty categories, the combination of the three measurements results in

$$m_{top} = 172.84 \pm 0.34\,(stat) \pm 0.61\,(syst)\,\text{GeV},$$

with a total uncertainty of 0.70 GeV, i.e. a relative precision of 0.4%. The result is mostly limited by the calibration of the jet energy scales and by the Monte Carlo modelling of signal events.

Acknowledgements

We thank CERN for the very successful operation of the LHC, as well as the support staff from our institutions without whom ATLAS could not be operated efficiently.

We acknowledge the support of ANPCyT, Argentina; YerPhI, Armenia; ARC, Australia; BMWFW and FWF, Austria; ANAS, Azerbaijan; SSTC, Belarus; CNPq and FAPESP, Brazil; NSERC, NRC and CFI, Canada; CERN; CONICYT, Chile; CAS, MOST and NSFC, China; COLCIENCIAS, Colombia; MSMT CR, MPO CR and VSC CR, Czech Republic; DNRF and DNSRC, Denmark; IN2P3-CNRS, CEA-DSM/IRFU, France; GNSF, Georgia; BMBF, HGF, and MPG, Germany; GSRT, Greece; RGC, Hong Kong SAR, China; ISF, I-CORE and Benoziyo Center, Israel; INFN, Italy; MEXT and JSPS, Japan; CNRST, Morocco; FOM and NWO, Netherlands; RCN, Norway; MNiSW and NCN, Poland; FCT, Portugal; MNE/IFA, Romania; MES of Russia and NRC KI, Russian Federation; JINR; MESTD, Serbia; MSSR, Slovakia; ARRS and MIZŠ, Slovenia; DST/NRF, South Africa; MINECO, Spain; SRC and Wallenberg Foundation, Sweden; SERI, SNSF and Cantons of Bern and Geneva, Switzerland; MOST, Taiwan; TAEK, Turkey; STFC, United Kingdom; DOE and NSF, United States of America. In addition, individual groups and members have received support from BCKDF, the Canada Council, CANARIE, CRC, Compute Canada, FQRNT, and the Ontario Innovation Trust, Canada; EPLANET, ERC, FP7, Horizon 2020 and Marie Skłodowska-Curie Actions, European Union; Investissements d'Avenir Labex and Idex, ANR, Région Auvergne and Fondation Partager le Savoir, France; DFG and AvH Foundation, Germany; Herakleitos, Thales and Aristeia programmes co-financed by EU-ESF and the Greek NSRF; BSF, GIF and Minerva, Israel; BRF, Norway; Generalitat de Catalunya, Generalitat Valenciana, Spain; the Royal Society and Leverhulme Trust, United Kingdom.

The crucial computing support from all WLCG partners is acknowledged gratefully, in particular from CERN and the ATLAS Tier-1 facilities at TRIUMF (Canada), NDGF (Denmark, Norway, Sweden), CC-IN2P3 (France), KIT/GridKA (Germany), INFN-CNAF (Italy), NL-T1 (Netherlands), PIC (Spain), ASGC (Taiwan), RAL (UK) and BNL (USA) and in the Tier-2 facilities worldwide.

References

[1] ALEPH Collaboration, CDF Collaboration, D0 Collaboration, DELPHI Collaboration, L3 Collaboration, OPAL Collaboration, SLD Collaboration, The LEP Electroweak Working Group, The Tevatron Electroweak Working Group, The SLD Electroweak and Heavy Flavour Groups, arXiv:1012.2367 [hep-ex].
[2] M. Baak, et al., The global electroweak fit at NNLO and prospects for the LHC and ILC, Eur. Phys. J. C 74 (2014) 3046.
[3] K.A. Olive, et al., Particle Data Group, Review of particle physics, Chin. Phys. C 38 (2014) 090001.
[4] G. Degrassi, et al., Higgs mass and vacuum stability in the standard model at NNLO, J. High Energy Phys. 8 (2012) 98.
[5] F. Bezrukov, et al., The standard model Higgs boson as the inflaton, Phys. Lett. B 659 (2008) 703.
[6] A. De Simone, et al., Running inflation in the standard model, Phys. Lett. B 678 (2009) 1.
[7] ATLAS Collaboration, CDF Collaboration, CMS Collaboration, D0 Collaboration, First combination of Tevatron and LHC measurements of the top-quark mass, arXiv:1403.4427 [hep-ex].
[8] ATLAS Collaboration, Measurement of the top-quark mass in the fully hadronic decay channel from ATLAS data at $\sqrt{s} = 7$ TeV, Eur. Phys. J. C 75 (2015) 158.
[9] CDF Collaboration, T. Aaltonen, et al., Measurement of the top-quark mass in the $t\bar{t}$ dilepton channel using the full CDF Run II data set, Phys. Rev. D 92 (2015) 032003.
[10] CDF Collaboration, T. Aaltonen, et al., Measurement of the top-quark mass in the all-hadronic channel using the full CDF data set, Phys. Rev. D 90 (2014) 091101(R).
[11] CMS Collaboration, Measurement of the top quark mass using proton–proton data at $\sqrt{(s)} = 7$ and 8 TeV, Phys. Rev. D 93 (2016) 072004.
[12] DØ Collaboration, V.M. Abazov, et al., Precise measurement of the top quark mass in dilepton decays using optimized neutrino weighting, Phys. Lett. B 752 (2016) 18.
[13] DØ Collaboration, V.M. Abazov, et al., Precision measurement of the top quark mass in lepton + jets final states, Phys. Rev. Lett. 113 (2014) 032002.
[14] ATLAS Collaboration, Measurement of the top quark mass in the $t\bar{t} \to$ lepton + jets and $t\bar{t} \to$ dilepton channels using $\sqrt{s} = 7$ TeV ATLAS data, Eur. Phys. J. C 75 (2015) 330.
[15] ATLAS Collaboration, The ATLAS experiment at the CERN Large Hadron Collider, J. Instrum. 3 (2008) S08003.
[16] ATLAS Collaboration, Improved luminosity determination in pp collisions at $\sqrt{s} = 7$ TeV using the ATLAS detector at the LHC, Eur. Phys. J. C 73 (2013) 2518.
[17] P. Nason, A new method for combining NLO QCD with shower Monte Carlo algorithms, J. High Energy Phys. 11 (2004) 040.
[18] S. Frixione, et al., Matching NLO QCD computations with parton shower simulations: the POWHEG method, J. High Energy Phys. 11 (2007) 70.
[19] S. Alioli, P. Nason, C. Oleari, E. Re, A general framework for implementing NLO calculations in shower Monte Carlo programs: the POWHEG BOX, J. High Energy Phys. 06 (2010) 043.
[20] S. Frixione, P. Nason, G. Ridolfi, A positive-weight next-to-leading-order Monte Carlo for heavy flavour hadroproduction, J. High Energy Phys. 09 (2007) 126.
[21] E. Re, Single-top Wt-channel production matched with parton showers using the POWHEG method, Eur. Phys. J. C 71 (2011) 1547.
[22] H.L. Lai, et al., New parton distributions for collider physics, Phys. Rev. D 82 (2010) 74024.
[23] S. Mrenna, et al., PYTHIA 6.4 physics and manual, J. High Energy Phys. 05 (2006) 26.
[24] P.Z. Skands, Tuning Monte Carlo generators: the Perugia tunes, Phys. Rev. D 82 (2010) 74018.
[25] J. Pumplin, et al., New generation of parton distributions with uncertainties from global QCD analysis, J. High Energy Phys. 07 (2002) 12.
[26] ATLAS Collaboration, Measurement of $t\bar{t}$ production with a veto on additional central jet activity in pp collisions at $\sqrt{s} = 7$ TeV using the ATLAS detector, Eur. Phys. J. C 72 (2012) 2043.
[27] ATLAS Collaboration, Measurement of the $t\bar{t}$ production cross-section as a function of jet multiplicity and jet transverse momentum in 7 TeV proton–proton collisions with the ATLAS detector, J. High Energy Phys. 01 (2015) 20.
[28] ATLAS Collaboration, Comparison of Monte Carlo generator predictions to ATLAS measurements of top pair production at 7 TeV, ATL-PHYS-PUB-2015-002, 2015, http://cds.cern.ch/record/1981319.
[29] M. Cacciari, et al., Top-pair production at hadron colliders with next-to-next-to-leading logarithmic soft-gluon resummation, Phys. Lett. B 710 (2012) 612.
[30] P. Bärnreuther, et al., Percent level precision physics at the Tevatron: first genuine NNLO QCD corrections to $q\bar{q} \to t\bar{t} + X$, Phys. Rev. Lett. 109 (2012) 132001.
[31] M. Czakon, A. Mitov, NNLO corrections to top-pair production at hadron colliders: the all-fermionic scattering channels, J. High Energy Phys. 12 (2012) 54.
[32] M. Czakon, A. Mitov, NNLO corrections to top pair production at hadron colliders: the quark–gluon reaction, J. High Energy Phys. 01 (2013) 80.
[33] M. Czakon, et al., The total top quark pair production cross-section at hadron colliders through $\mathcal{O}(\alpha_S^4)$, Phys. Rev. Lett. 110 (2013) 252004.
[34] M. Czakon, A. Mitov, Top++: a program for the calculation of the top-pair cross-section at hadron colliders, Comput. Phys. Commun. 185 (2014) 2930.
[35] N. Kidonakis, Two-loop soft anomalous dimensions for single top quark associated production with a W^- or H^-, Phys. Rev. D 82 (2010) 54018.
[36] M. Botje, et al., The PDF4LHC working group interim recommendations, arXiv:1101.0538 [hep-ph].
[37] A.D. Martin, et al., Parton distributions for the LHC, Eur. Phys. J. C 63 (2009) 189.
[38] A.D. Martin, et al., Uncertainties on α_S in global PDF analyses and implications for predicted hadronic cross sections, Eur. Phys. J. C 64 (2009) 653.
[39] J. Gao, et al., The CT10 NNLO global analysis of QCD, Phys. Rev. D 89 (2014) 33009.
[40] R.D. Ball, et al., Parton distributions with LHC data, Nucl. Phys. B 867 (2013) 244.
[41] M.L. Mangano, et al., ALPGEN, a generator for hard multiparton processes in hadronic collisions, J. High Energy Phys. 07 (2003) 1.
[42] ATLAS Collaboration, New ATLAS event generator tunes to 2010 data, ATL-PHYS-PUB-2011-008, 2011, http://cds.cern.ch/record/1345343.
[43] G. Corcella, et al., HERWIG 6.5: an event generator for hadron emission reactions with interfering gluons (including supersymmetric processes), J. High Energy Phys. 01 (2001) 10.
[44] J.M. Butterworth, et al., Multiparton interactions in photoproduction at HERA, Z. Phys. C 72 (1996) 637.
[45] T. Sjöstrand, S. Mrenna, P. Skands, A brief introduction to PYTHIA 8.1, Comput. Phys. Commun. 178 (2008) 852.
[46] ATLAS Collaboration, Summary of ATLAS PYTHIA 8 tunes, ATL-PHYS-PUB-2012-003, 2012, http://cdsweb.cern.ch/record/1474107.
[47] ATLAS Collaboration, The ATLAS simulation infrastructure, Eur. Phys. J. C 70 (2010) 823.
[48] S. Agostinelli, et al., GEANT4: a simulation toolkit, Nucl. Instrum. Methods A 506 (2003) 250.
[49] ATLAS Collaboration, Electron reconstruction and identification efficiency measurements with the ATLAS detector using the 2011 LHC proton–proton collision data, Eur. Phys. J. C 74 (2014) 2941.
[50] ATLAS Collaboration, Measurement of the muon reconstruction performance of the ATLAS detector using 2011 and 2012 LHC proton–proton collision data, Eur. Phys. J. C 74 (2014) 3130.

[51] ATLAS Collaboration, Topological cell clustering in the ATLAS calorimeters and its performance in LHC Run 1, Eur. Phys. J. C (2016), in press, arXiv:1603.02934 [hep-ex].
[52] M. Cacciari, et al., The anti-k_t jet clustering algorithm, J. High Energy Phys. 04 (2008) 63.
[53] ATLAS Collaboration, Jet energy measurement with the ATLAS detector in proton–proton collisions at $\sqrt{s} = 7$ TeV, Eur. Phys. J. C 73 (2013) 2304.
[54] ATLAS Collaboration, Jet energy measurement and its systematic uncertainty in proton–proton collisions at $\sqrt{s} = 7$ TeV with the ATLAS detector, Eur. Phys. J. C 75 (2015) 17.
[55] ATLAS Collaboration, Monte Carlo calibration and combination of *in-situ* measurements of jet energy scale, jet energy resolution and jet mass in ATLAS, ATLAS-CONF-2015-037, 2015, http://cds.cern.ch/record/2044941.
[56] ATLAS Collaboration, Performance of b-jet identification in the ATLAS experiment, J. Instrum. 11 (2016) P04008.
[57] ATLAS Collaboration, Performance of missing transverse momentum reconstruction in proton–proton collisions at $\sqrt{s} = 7$ TeV with ATLAS, Eur. Phys. J. C 72 (2012) 1844.
[58] ATLAS Collaboration, Estimation of non-prompt and fake lepton backgrounds in final states with top quarks produced in proton–proton collisions at $\sqrt{s} = 8$ TeV with the ATLAS detector, ATLAS-CONF-2014-058, 2014, http://cds.cern.ch/record/1951336.
[59] ATLAS Collaboration, Measurement of the top quark-pair production cross section with ATLAS in pp collisions at $\sqrt{s} = 7$ TeV, Eur. Phys. J. C 71 (2011) 1577.
[60] R.J. Barlow, Application of the bootstrap resampling technique to particle physics experiments, http://www.hep.man.ac.uk/preprints/1999.html.
[61] R. Barlow, Systematic errors: facts and fictions, arXiv:hep-ex/0207026.
[62] S. Frixione, B.R. Webber, Matching NLO QCD computations and parton shower simulations, J. High Energy Phys. 06 (2002) 029.
[63] S. Frixione, et al., Matching NLO QCD and parton showers in heavy flavour production, J. High Energy Phys. 08 (2003) 007.
[64] B. Andersson, et al., Parton fragmentation and string dynamics, Phys. Rep. 97 (1983) 31.
[65] B. Andersson, The Lund Model, Cambridge University Press, ISBN 9780521017343, 1997.
[66] B. Webber, A QCD model for jet fragmentation including soft gluon interference, Nucl. Phys. B 238 (1984) 492.
[67] M. Bahr, et al., Herwig++ physics and manual, Eur. Phys. J. C 58 (2008) 639.
[68] ATLAS Collaboration, Impact of fragmentation modelling on the top quark mass measurement using the ATLAS detector, ATL-PHYS-PUB-2015-042, 2015, http://cds.cern.ch/record/2054420.
[69] ATLAS Collaboration, Comparison of Monte Carlo generator predictions for gap fraction and jet multiplicity observables in $t\bar{t}$ events, ATL-PHYS-PUB-2014-005, 2014, http://cds.cern.ch/record/1703034.
[70] ATLAS Collaboration, Determination of the jet energy scale and resolution at ATLAS using Z/γ-jet events in data at $\sqrt{s} = 8$ TeV, ATLAS-CONF-2015-057, 2015, http://cds.cern.ch/record/2059846.
[71] ATLAS Collaboration, Data-driven determination of the energy scale and resolution of jets reconstructed in the ATLAS calorimeters using dijet and multijet events at $\sqrt{s} = 8$ TeV, ATLAS-CONF-2015-017, 2015, http://cds.cern.ch/record/2008678.
[72] ATLAS Collaboration, Pile-up subtraction and suppression for jets in ATLAS, ATLAS-CONF-2013-083, 2013, http://cds.cern.ch/record/1570994.
[73] ATLAS Collaboration, Calibration of b-tagging using dileptonic top pair events in a combinatorial likelihood approach with the ATLAS experiment, ATLAS-CONF-2014-004, 2014, http://cdsweb.cern.ch/record/1664335.
[74] ATLAS Collaboration, Electron and photon energy calibration with the ATLAS detector using LHC Run 1 data, Eur. Phys. J. C 74 (2014) 3071.
[75] L. Lyons, et al., How to combine correlated estimates of a single physical quantity, Nucl. Instrum. Methods A 270 (1988) 110.
[76] R. Nisius, On the combination of correlated estimates of a physics observable, Eur. Phys. J. C 74 (2014) 3004.
[77] R. Nisius, A ROOT class to combine a number of correlated estimates of one or more observables using the best linear unbiased estimate method, http://blue.hepforge.org/Bluemanual.pdf.

ATLAS Collaboration

M. Aaboud [135d], G. Aad [86], B. Abbott [113], J. Abdallah [64], O. Abdinov [12], B. Abeloos [117], R. Aben [107], O.S. AbouZeid [137], N.L. Abraham [149], H. Abramowicz [153], H. Abreu [152], R. Abreu [116], Y. Abulaiti [146a,146b], B.S. Acharya [163a,163b,a], L. Adamczyk [40a], D.L. Adams [27], J. Adelman [108], S. Adomeit [100], T. Adye [131], A.A. Affolder [75], T. Agatonovic-Jovin [14], J. Agricola [56], J.A. Aguilar-Saavedra [126a,126f], S.P. Ahlen [24], F. Ahmadov [66,b], G. Aielli [133a,133b], H. Akerstedt [146a,146b], T.P.A. Åkesson [82], A.V. Akimov [96], G.L. Alberghi [22a,22b], J. Albert [168], S. Albrand [57], M.J. Alconada Verzini [72], M. Aleksa [32], I.N. Aleksandrov [66], C. Alexa [28b], G. Alexander [153], T. Alexopoulos [10], M. Alhroob [113], B. Ali [128], M. Aliev [74a,74b], G. Alimonti [92a], J. Alison [33], S.P. Alkire [37], B.M.M. Allbrooke [149], B.W. Allen [116], P.P. Allport [19], A. Aloisio [104a,104b], A. Alonso [38], F. Alonso [72], C. Alpigiani [138], M. Alstaty [86], B. Alvarez Gonzalez [32], D. Álvarez Piqueras [166], M.G. Alviggi [104a,104b], B.T. Amadio [16], K. Amako [67], Y. Amaral Coutinho [26a], C. Amelung [25], D. Amidei [90], S.P. Amor Dos Santos [126a,126c], A. Amorim [126a,126b], S. Amoroso [32], G. Amundsen [25], C. Anastopoulos [139], L.S. Ancu [51], N. Andari [19], T. Andeen [11], C.F. Anders [59b], G. Anders [32], J.K. Anders [75], K.J. Anderson [33], A. Andreazza [92a,92b], V. Andrei [59a], S. Angelidakis [9], I. Angelozzi [107], P. Anger [46], A. Angerami [37], F. Anghinolfi [32], A.V. Anisenkov [109,c], N. Anjos [13], A. Annovi [124a,124b], C. Antel [59a], M. Antonelli [49], A. Antonov [98,*], F. Anulli [132a], M. Aoki [67], L. Aperio Bella [19], G. Arabidze [91], Y. Arai [67], J.P. Araque [126a], A.T.H. Arce [47], F.A. Arduh [72], J-F. Arguin [95], S. Argyropoulos [64], M. Arik [20a], A.J. Armbruster [143], L.J. Armitage [77], O. Arnaez [32], H. Arnold [50], M. Arratia [30], O. Arslan [23], A. Artamonov [97], G. Artoni [120], S. Artz [84], S. Asai [155], N. Asbah [44], A. Ashkenazi [153], B. Åsman [146a,146b], L. Asquith [149], K. Assamagan [27], R. Astalos [144a], M. Atkinson [165], N.B. Atlay [141], K. Augsten [128], G. Avolio [32], B. Axen [16], M.K. Ayoub [117], G. Azuelos [95,d], M.A. Baak [32], A.E. Baas [59a], M.J. Baca [19], H. Bachacou [136], K. Bachas [74a,74b], M. Backes [148], M. Backhaus [32], P. Bagiacchi [132a,132b], P. Bagnaia [132a,132b], Y. Bai [35a], J.T. Baines [131], O.K. Baker [175], E.M. Baldin [109,c], P. Balek [171], T. Balestri [148], F. Balli [136], W.K. Balunas [122], E. Banas [41], Sw. Banerjee [172,e], A.A.E. Bannoura [174], L. Barak [32], E.L. Barberio [89], D. Barberis [52a,52b], M. Barbero [86], T. Barillari [101], M-S Barisits [32], T. Barklow [143], N. Barlow [30], S.L. Barnes [85], B.M. Barnett [131], R.M. Barnett [16], Z. Barnovska [5], A. Baroncelli [134a], G. Barone [25], A.J. Barr [120], L. Barranco Navarro [166], F. Barreiro [83], J. Barreiro Guimarães da Costa [35a], R. Bartoldus [143], A.E. Barton [73], P. Bartos [144a], A. Basalaev [123], A. Bassalat [117], R.L. Bates [55], S.J. Batista [158], J.R. Batley [30], M. Battaglia [137], M. Bauce [132a,132b], F. Bauer [136], H.S. Bawa [143,f], J.B. Beacham [111], M.D. Beattie [73], T. Beau [81], P.H. Beauchemin [161], P. Bechtle [23],

H.P. Beck [18,g], K. Becker [120], M. Becker [84], M. Beckingham [169], C. Becot [110], A.J. Beddall [20e], A. Beddall [20b], V.A. Bednyakov [66], M. Bedognetti [107], C.P. Bee [148], L.J. Beemster [107], T.A. Beermann [32], M. Begel [27], J.K. Behr [44], C. Belanger-Champagne [88], A.S. Bell [79], G. Bella [153], L. Bellagamba [22a], A. Bellerive [31], M. Bellomo [87], K. Belotskiy [98], O. Beltramello [32], N.L. Belyaev [98], O. Benary [153], D. Benchekroun [135a], M. Bender [100], K. Bendtz [146a,146b], N. Benekos [10], Y. Benhammou [153], E. Benhar Noccioli [175], J. Benitez [64], D.P. Benjamin [47], J.R. Bensinger [25], S. Bentvelsen [107], L. Beresford [120], M. Beretta [49], D. Berge [107], E. Bergeaas Kuutmann [164], N. Berger [5], J. Beringer [16], S. Berlendis [57], N.R. Bernard [87], C. Bernius [110], F.U. Bernlochner [23], T. Berry [78], P. Berta [129], C. Bertella [84], G. Bertoli [146a,146b], F. Bertolucci [124a,124b], I.A. Bertram [73], C. Bertsche [44], D. Bertsche [113], G.J. Besjes [38], O. Bessidskaia Bylund [146a,146b], M. Bessner [44], N. Besson [136], C. Betancourt [50], A. Bethani [57], S. Bethke [101], A.J. Bevan [77], R.M. Bianchi [125], L. Bianchini [25], M. Bianco [32], O. Biebel [100], D. Biedermann [17], R. Bielski [85], N.V. Biesuz [124a,124b], M. Biglietti [134a], J. Bilbao De Mendizabal [51], T.R.V. Billoud [95], H. Bilokon [49], M. Bindi [56], S. Binet [117], A. Bingul [20b], C. Bini [132a,132b], S. Biondi [22a,22b], D.M. Bjergaard [47], C.W. Black [150], J.E. Black [143], K.M. Black [24], D. Blackburn [138], R.E. Blair [6], J.-B. Blanchard [136], T. Blazek [144a], I. Bloch [44], C. Blocker [25], W. Blum [84,*], U. Blumenschein [56], S. Blunier [34a], G.J. Bobbink [107], V.S. Bobrovnikov [109,c], S.S. Bocchetta [82], A. Bocci [47], C. Bock [100], M. Boehler [50], D. Boerner [174], J.A. Bogaerts [32], D. Bogavac [14], A.G. Bogdanchikov [109], C. Bohm [146a], V. Boisvert [78], P. Bokan [14], T. Bold [40a], A.S. Boldyrev [163a,163c], M. Bomben [81], M. Bona [77], M. Boonekamp [136], A. Borisov [130], G. Borissov [73], J. Bortfeldt [32], D. Bortoletto [120], V. Bortolotto [61a,61b,61c], K. Bos [107], D. Boscherini [22a], M. Bosman [13], J.D. Bossio Sola [29], J. Boudreau [125], J. Bouffard [2], E.V. Bouhova-Thacker [73], D. Boumediene [36], C. Bourdarios [117], S.K. Boutle [55], A. Boveia [32], J. Boyd [32], I.R. Boyko [66], J. Bracinik [19], A. Brandt [8], G. Brandt [56], O. Brandt [59a], U. Bratzler [156], B. Brau [87], J.E. Brau [116], H.M. Braun [174,*], W.D. Breaden Madden [55], K. Brendlinger [122], A.J. Brennan [89], L. Brenner [107], R. Brenner [164], S. Bressler [171], T.M. Bristow [48], D. Britton [55], D. Britzger [44], F.M. Brochu [30], I. Brock [23], R. Brock [91], G. Brooijmans [37], T. Brooks [78], W.K. Brooks [34b], J. Brosamer [16], E. Brost [108], J.H Broughton [19], P.A. Bruckman de Renstrom [41], D. Bruncko [144b], R. Bruneliere [50], A. Bruni [22a], G. Bruni [22a], L.S. Bruni [107], BH Brunt [30], M. Bruschi [22a], N. Bruscino [23], P. Bryant [33], L. Bryngemark [82], T. Buanes [15], Q. Buat [142], P. Buchholz [141], A.G. Buckley [55], I.A. Budagov [66], F. Buehrer [50], M.K. Bugge [119], O. Bulekov [98], D. Bullock [8], H. Burckhart [32], S. Burdin [75], C.D. Burgard [50], B. Burghgrave [108], K. Burka [41], S. Burke [131], I. Burmeister [45], J.T.P. Burr [120], E. Busato [36], D. Büscher [50], V. Büscher [84], P. Bussey [55], J.M. Butler [24], C.M. Buttar [55], J.M. Butterworth [79], P. Butti [107], W. Buttinger [27], A. Buzatu [55], A.R. Buzykaev [109,c], S. Cabrera Urbán [166], D. Caforio [128], V.M. Cairo [39a,39b], O. Cakir [4a], N. Calace [51], P. Calafiura [16], A. Calandri [86], G. Calderini [81], P. Calfayan [100], G. Callea [39a,39b], L.P. Caloba [26a], S. Calvente Lopez [83], D. Calvet [36], S. Calvet [36], T.P. Calvet [86], R. Camacho Toro [33], S. Camarda [32], P. Camarri [133a,133b], D. Cameron [119], R. Caminal Armadans [165], C. Camincher [57], S. Campana [32], M. Campanelli [79], A. Camplani [92a,92b], A. Campoverde [141], V. Canale [104a,104b], A. Canepa [159a], M. Cano Bret [35e], J. Cantero [114], R. Cantrill [126a], T. Cao [42], M.D.M. Capeans Garrido [32], I. Caprini [28b], M. Caprini [28b], M. Capua [39a,39b], R. Caputo [84], R.M. Carbone [37], R. Cardarelli [133a], F. Cardillo [50], I. Carli [129], T. Carli [32], G. Carlino [104a], L. Carminati [92a,92b], S. Caron [106], E. Carquin [34b], G.D. Carrillo-Montoya [32], J.R. Carter [30], J. Carvalho [126a,126c], D. Casadei [19], M.P. Casado [13,h], M. Casolino [13], D.W. Casper [162], E. Castaneda-Miranda [145a], R. Castelijn [107], A. Castelli [107], V. Castillo Gimenez [166], N.F. Castro [126a,i], A. Catinaccio [32], J.R. Catmore [119], A. Cattai [32], J. Caudron [23], V. Cavaliere [165], E. Cavallaro [13], D. Cavalli [92a], M. Cavalli-Sforza [13], V. Cavasinni [124a,124b], F. Ceradini [134a,134b], L. Cerda Alberich [166], B.C. Cerio [47], A.S. Cerqueira [26b], A. Cerri [149], L. Cerrito [133a,133b], F. Cerutti [16], M. Cerv [32], A. Cervelli [18], S.A. Cetin [20d], A. Chafaq [135a], D. Chakraborty [108], S.K. Chan [58], Y.L. Chan [61a], P. Chang [165], J.D. Chapman [30], D.G. Charlton [19], A. Chatterjee [51], C.C. Chau [158], C.A. Chavez Barajas [149], S. Che [111], S. Cheatham [73], A. Chegwidden [91], S. Chekanov [6], S.V. Chekulaev [159a], G.A. Chelkov [66,j], M.A. Chelstowska [90], C. Chen [65], H. Chen [27], K. Chen [148], S. Chen [35c], S. Chen [155], X. Chen [35f], Y. Chen [68], H.C. Cheng [90], H.J Cheng [35a], Y. Cheng [33], A. Cheplakov [66], E. Cheremushkina [130], R. Cherkaoui El Moursli [135e], V. Chernyatin [27,*], E. Cheu [7], L. Chevalier [136], V. Chiarella [49], G. Chiarelli [124a,124b], G. Chiodini [74a], A.S. Chisholm [19], A. Chitan [28b], M.V. Chizhov [66], K. Choi [62], A.R. Chomont [36], S. Chouridou [9], B.K.B. Chow [100], V. Christodoulou [79], D. Chromek-Burckhart [32], J. Chudoba [127], A.J. Chuinard [88], J.J. Chwastowski [41], L. Chytka [115], G. Ciapetti [132a,132b], A.K. Ciftci [4a], D. Cinca [45], V. Cindro [76], I.A. Cioara [23], C. Ciocca [22a,22b], A. Ciocio [16], F. Cirotto [104a,104b], Z.H. Citron [171],

M. Citterio[92a], M. Ciubancan[28b], A. Clark[51], B.L. Clark[58], M.R. Clark[37], P.J. Clark[48], R.N. Clarke[16], C. Clement[146a,146b], Y. Coadou[86], M. Cobal[163a,163c], A. Coccaro[51], J. Cochran[65], L. Colasurdo[106], B. Cole[37], A.P. Colijn[107], J. Collot[57], T. Colombo[32], G. Compostella[101], P. Conde Muiño[126a,126b], E. Coniavitis[50], S.H. Connell[145b], I.A. Connelly[78], V. Consorti[50], S. Constantinescu[28b], G. Conti[32], F. Conventi[104a,k], M. Cooke[16], B.D. Cooper[79], A.M. Cooper-Sarkar[120], K.J.R. Cormier[158], T. Cornelissen[174], M. Corradi[132a,132b], F. Corriveau[88,l], A. Corso-Radu[162], A. Cortes-Gonzalez[32], G. Cortiana[101], G. Costa[92a], M.J. Costa[166], D. Costanzo[139], G. Cottin[30], G. Cowan[78], B.E. Cox[85], K. Cranmer[110], S.J. Crawley[55], G. Cree[31], S. Crépé-Renaudin[57], F. Crescioli[81], W.A. Cribbs[146a,146b], M. Crispin Ortuzar[120], M. Cristinziani[23], V. Croft[106], G. Crosetti[39a,39b], A. Cueto[83], T. Cuhadar Donszelmann[139], J. Cummings[175], M. Curatolo[49], J. Cúth[84], H. Czirr[141], P. Czodrowski[3], G. D'amen[22a,22b], S. D'Auria[55], M. D'Onofrio[75], M.J. Da Cunha Sargedas De Sousa[126a,126b], C. Da Via[85], W. Dabrowski[40a], T. Dado[144a], T. Dai[90], O. Dale[15], F. Dallaire[95], C. Dallapiccola[87], M. Dam[38], J.R. Dandoy[33], N.P. Dang[50], A.C. Daniells[19], N.S. Dann[85], M. Danninger[167], M. Dano Hoffmann[136], V. Dao[50], G. Darbo[52a], S. Darmora[8], J. Dassoulas[3], A. Dattagupta[62], W. Davey[23], C. David[168], T. Davidek[129], M. Davies[153], P. Davison[79], E. Dawe[89], I. Dawson[139], R.K. Daya-Ishmukhametova[87], K. De[8], R. de Asmundis[104a], A. De Benedetti[113], S. De Castro[22a,22b], S. De Cecco[81], N. De Groot[106], P. de Jong[107], H. De la Torre[83], F. De Lorenzi[65], A. De Maria[56], D. De Pedis[132a], A. De Salvo[132a], U. De Sanctis[149], A. De Santo[149], J.B. De Vivie De Regie[117], W.J. Dearnaley[73], R. Debbe[27], C. Debenedetti[137], D.V. Dedovich[66], N. Dehghanian[3], I. Deigaard[107], M. Del Gaudio[39a,39b], J. Del Peso[83], T. Del Prete[124a,124b], D. Delgove[117], F. Deliot[136], C.M. Delitzsch[51], M. Deliyergiyev[76], A. Dell'Acqua[32], L. Dell'Asta[24], M. Dell'Orso[124a,124b], M. Della Pietra[104a,k], D. della Volpe[51], M. Delmastro[5], P.A. Delsart[57], D.A. DeMarco[158], S. Demers[175], M. Demichev[66], A. Demilly[81], S.P. Denisov[130], D. Denysiuk[136], D. Derendarz[41], J.E. Derkaoui[135d], F. Derue[81], P. Dervan[75], K. Desch[23], C. Deterre[44], K. Dette[45], P.O. Deviveiros[32], A. Dewhurst[131], S. Dhaliwal[25], A. Di Ciaccio[133a,133b], L. Di Ciaccio[5], W.K. Di Clemente[122], C. Di Donato[132a,132b], A. Di Girolamo[32], B. Di Girolamo[32], B. Di Micco[134a,134b], R. Di Nardo[32], A. Di Simone[50], R. Di Sipio[158], D. Di Valentino[31], C. Diaconu[86], M. Diamond[158], F.A. Dias[48], M.A. Diaz[34a], E.B. Diehl[90], J. Dietrich[17], S. Diglio[86], A. Dimitrievska[14], J. Dingfelder[23], P. Dita[28b], S. Dita[28b], F. Dittus[32], F. Djama[86], T. Djobava[53b], J.I. Djuvsland[59a], M.A.B. do Vale[26c], D. Dobos[32], M. Dobre[28b], C. Doglioni[82], J. Dolejsi[129], Z. Dolezal[129], M. Donadelli[26d], S. Donati[124a,124b], P. Dondero[121a,121b], J. Donini[36], J. Dopke[131], A. Doria[104a], M.T. Dova[72], A.T. Doyle[55], E. Drechsler[56], M. Dris[10], Y. Du[35d], J. Duarte-Campderros[153], E. Duchovni[171], G. Duckeck[100], O.A. Ducu[95,m], D. Duda[107], A. Dudarev[32], A.Chr. Dudder[84], E.M. Duffield[16], L. Duflot[117], M. Dührssen[32], M. Dumancic[171], M. Dunford[59a], H. Duran Yildiz[4a], M. Düren[54], A. Durglishvili[53b], D. Duschinger[46], B. Dutta[44], M. Dyndal[44], C. Eckardt[44], K.M. Ecker[101], R.C. Edgar[90], N.C. Edwards[48], T. Eifert[32], G. Eigen[15], K. Einsweiler[16], T. Ekelof[164], M. El Kacimi[135c], V. Ellajosyula[86], M. Ellert[164], S. Elles[5], F. Ellinghaus[174], A.A. Elliot[168], N. Ellis[32], J. Elmsheuser[27], M. Elsing[32], D. Emeliyanov[131], Y. Enari[155], O.C. Endner[84], J.S. Ennis[169], J. Erdmann[45], A. Ereditato[18], G. Ernis[174], J. Ernst[2], M. Ernst[27], S. Errede[165], E. Ertel[84], M. Escalier[117], H. Esch[45], C. Escobar[125], B. Esposito[49], A.I. Etienvre[136], E. Etzion[153], H. Evans[62], A. Ezhilov[123], F. Fabbri[22a,22b], L. Fabbri[22a,22b], G. Facini[33], R.M. Fakhrutdinov[130], S. Falciano[132a], R.J. Falla[79], J. Faltova[129], Y. Fang[35a], M. Fanti[92a,92b], A. Farbin[8], A. Farilla[134a], C. Farina[125], E.M. Farina[121a,121b], T. Farooque[13], S. Farrell[16], S.M. Farrington[169], P. Farthouat[32], F. Fassi[135e], P. Fassnacht[32], D. Fassouliotis[9], M. Faucci Giannelli[78], A. Favareto[52a,52b], W.J. Fawcett[120], L. Fayard[117], O.L. Fedin[123,n], W. Fedorko[167], S. Feigl[119], L. Feligioni[86], C. Feng[35d], E.J. Feng[32], H. Feng[90], A.B. Fenyuk[130], L. Feremenga[8], P. Fernandez Martinez[166], S. Fernandez Perez[13], J. Ferrando[55], A. Ferrari[164], P. Ferrari[107], R. Ferrari[121a], D.E. Ferreira de Lima[59b], A. Ferrer[166], D. Ferrere[51], C. Ferretti[90], A. Ferretto Parodi[52a,52b], F. Fiedler[84], A. Filipčič[76], M. Filipuzzi[44], F. Filthaut[106], M. Fincke-Keeler[168], K.D. Finelli[150], M.C.N. Fiolhais[126a,126c], L. Fiorini[166], A. Firan[42], A. Fischer[2], C. Fischer[13], J. Fischer[174], W.C. Fisher[91], N. Flaschel[44], I. Fleck[141], P. Fleischmann[90], G.T. Fletcher[139], R.R.M. Fletcher[122], T. Flick[174], A. Floderus[82], L.R. Flores Castillo[61a], M.J. Flowerdew[101], G.T. Forcolin[85], A. Formica[136], A. Forti[85], A.G. Foster[19], D. Fournier[117], H. Fox[73], S. Fracchia[13], P. Francavilla[81], M. Franchini[22a,22b], D. Francis[32], L. Franconi[119], M. Franklin[58], M. Frate[162], M. Fraternali[121a,121b], D. Freeborn[79], S.M. Fressard-Batraneanu[32], F. Friedrich[46], D. Froidevaux[32], J.A. Frost[120], C. Fukunaga[156],

E. Fullana Torregrosa [84], T. Fusayasu [102], J. Fuster [166], C. Gabaldon [57], O. Gabizon [174], A. Gabrielli [22a,22b], A. Gabrielli [16], G.P. Gach [40a], S. Gadatsch [32], S. Gadomski [51], G. Gagliardi [52a,52b], L.G. Gagnon [95], P. Gagnon [62], C. Galea [106], B. Galhardo [126a,126c], E.J. Gallas [120], B.J. Gallop [131], P. Gallus [128], G. Galster [38], K.K. Gan [111], J. Gao [35b,86], Y. Gao [48], Y.S. Gao [143,f], F.M. Garay Walls [48], C. García [166], J.E. García Navarro [166], M. Garcia-Sciveres [16], R.W. Gardner [33], N. Garelli [143], V. Garonne [119], A. Gascon Bravo [44], K. Gasnikova [44], C. Gatti [49], A. Gaudiello [52a,52b], G. Gaudio [121a], L. Gauthier [95], I.L. Gavrilenko [96], C. Gay [167], G. Gaycken [23], E.N. Gazis [10], Z. Gecse [167], C.N.P. Gee [131], Ch. Geich-Gimbel [23], M. Geisen [84], M.P. Geisler [59a], C. Gemme [52a], M.H. Genest [57], C. Geng [35b,o], S. Gentile [132a,132b], C. Gentsos [154], S. George [78], D. Gerbaudo [13], A. Gershon [153], S. Ghasemi [141], H. Ghazlane [135b], M. Ghneimat [23], B. Giacobbe [22a], S. Giagu [132a,132b], P. Giannetti [124a,124b], B. Gibbard [27], S.M. Gibson [78], M. Gignac [167], M. Gilchriese [16], T.P.S. Gillam [30], D. Gillberg [31], G. Gilles [174], D.M. Gingrich [3,d], N. Giokaris [9], M.P. Giordani [163a,163c], F.M. Giorgi [22a], F.M. Giorgi [17], P.F. Giraud [136], P. Giromini [58], D. Giugni [92a], F. Giuli [120], C. Giuliani [101], M. Giulini [59b], B.K. Gjelsten [119], S. Gkaitatzis [154], I. Gkialas [154], E.L. Gkougkousis [117], L.K. Gladilin [99], C. Glasman [83], J. Glatzer [32], P.C.F. Glaysher [48], A. Glazov [44], M. Goblirsch-Kolb [25], J. Godlewski [41], S. Goldfarb [89], T. Golling [51], D. Golubkov [130], A. Gomes [126a,126b,126d], R. Gonçalo [126a], J. Goncalves Pinto Firmino Da Costa [136], G. Gonella [50], L. Gonella [19], A. Gongadze [66], S. González de la Hoz [166], G. Gonzalez Parra [13], S. Gonzalez-Sevilla [51], L. Goossens [32], P.A. Gorbounov [97], H.A. Gordon [27], I. Gorelov [105], B. Gorini [32], E. Gorini [74a,74b], A. Gorišek [76], E. Gornicki [41], A.T. Goshaw [47], C. Gössling [45], M.I. Gostkin [66], C.R. Goudet [117], D. Goujdami [135c], A.G. Goussiou [138], N. Govender [145b,p], E. Gozani [152], L. Graber [56], I. Grabowska-Bold [40a], P.O.J. Gradin [57], P. Grafström [22a,22b], J. Gramling [51], E. Gramstad [119], S. Grancagnolo [17], V. Gratchev [123], P.M. Gravila [28e], H.M. Gray [32], E. Graziani [134a], Z.D. Greenwood [80,q], C. Grefe [23], K. Gregersen [79], I.M. Gregor [44], P. Grenier [143], K. Grevtsov [5], J. Griffiths [8], A.A. Grillo [137], K. Grimm [73], S. Grinstein [13,r], Ph. Gris [36], J.-F. Grivaz [117], S. Groh [84], J.P. Grohs [46], E. Gross [171], J. Grosse-Knetter [56], G.C. Grossi [80], Z.J. Grout [149], L. Guan [90], W. Guan [172], J. Guenther [63], F. Guescini [51], D. Guest [162], O. Gueta [153], E. Guido [52a,52b], T. Guillemin [5], S. Guindon [2], U. Gul [55], C. Gumpert [32], J. Guo [35e], Y. Guo [35b,o], R. Gupta [42], S. Gupta [120], G. Gustavino [132a,132b], P. Gutierrez [113], N.G. Gutierrez Ortiz [79], C. Gutschow [46], C. Guyot [136], C. Gwenlan [120], C.B. Gwilliam [75], A. Haas [110], C. Haber [16], H.K. Hadavand [8], N. Haddad [135e], A. Hadef [86], S. Hageböck [23], Z. Hajduk [41], H. Hakobyan [176,*], M. Haleem [44], J. Haley [114], G. Halladjian [91], G.D. Hallewell [86], K. Hamacher [174], P. Hamal [115], K. Hamano [168], A. Hamilton [145a], G.N. Hamity [139], P.G. Hamnett [44], L. Han [35b], K. Hanagaki [67,s], K. Hanawa [155], M. Hance [137], B. Haney [122], S. Hanisch [32], P. Hanke [59a], R. Hanna [136], J.B. Hansen [38], J.D. Hansen [38], M.C. Hansen [23], P.H. Hansen [38], K. Hara [160], A.S. Hard [172], T. Harenberg [174], F. Hariri [117], S. Harkusha [93], R.D. Harrington [48], P.F. Harrison [169], F. Hartjes [107], N.M. Hartmann [100], M. Hasegawa [68], Y. Hasegawa [140], A. Hasib [113], S. Hassani [136], S. Haug [18], R. Hauser [91], L. Hauswald [46], M. Havranek [127], C.M. Hawkes [19], R.J. Hawkings [32], D. Hayakawa [157], D. Hayden [91], C.P. Hays [120], J.M. Hays [77], H.S. Hayward [75], S.J. Haywood [131], S.J. Head [19], T. Heck [84], V. Hedberg [82], L. Heelan [8], S. Heim [122], T. Heim [16], B. Heinemann [16], J.J. Heinrich [100], L. Heinrich [110], C. Heinz [54], J. Hejbal [127], L. Helary [32], S. Hellman [146a,146b], C. Helsens [32], J. Henderson [120], R.C.W. Henderson [73], Y. Heng [172], S. Henkelmann [167], A.M. Henriques Correia [32], S. Henrot-Versille [117], G.H. Herbert [17], V. Herget [173], Y. Hernández Jiménez [166], G. Herten [50], R. Hertenberger [100], L. Hervas [32], G.G. Hesketh [79], N.P. Hessey [107], J.W. Hetherly [42], R. Hickling [77], E. Higón-Rodriguez [166], E. Hill [168], J.C. Hill [30], K.H. Hiller [44], S.J. Hillier [19], I. Hinchliffe [16], E. Hines [122], R.R. Hinman [16], M. Hirose [50], D. Hirschbuehl [174], J. Hobbs [148], N. Hod [159a], M.C. Hodgkinson [139], P. Hodgson [139], A. Hoecker [32], M.R. Hoeferkamp [105], F. Hoenig [100], D. Hohn [23], T.R. Holmes [16], M. Homann [45], T.M. Hong [125], B.H. Hooberman [165], W.H. Hopkins [116], Y. Horii [103], A.J. Horton [142], J-Y. Hostachy [57], S. Hou [151], A. Hoummada [135a], J. Howarth [44], M. Hrabovsky [115], I. Hristova [17], J. Hrivnac [117], T. Hryn'ova [5], A. Hrynevich [94], C. Hsu [145c], P.J. Hsu [151,t], S.-C. Hsu [138], D. Hu [37], Q. Hu [35b], S. Hu [35e], Y. Huang [44], Z. Hubacek [128], F. Hubaut [86], F. Huegging [23], T.B. Huffman [120], E.W. Hughes [37], G. Hughes [73], M. Huhtinen [32], P. Huo [148], N. Huseynov [66,b], J. Huston [91], J. Huth [58], G. Iacobucci [51], G. Iakovidis [27], I. Ibragimov [141], L. Iconomidou-Fayard [117], E. Ideal [175], Z. Idrissi [135e], P. Iengo [32], O. Igonkina [107,u], T. Iizawa [170], Y. Ikegami [67], M. Ikeno [67], Y. Ilchenko [11,v], D. Iliadis [154], N. Ilic [143], T. Ince [101], G. Introzzi [121a,121b], P. Ioannou [9,*], M. Iodice [134a], K. Iordanidou [37], V. Ippolito [58], N. Ishijima [118], M. Ishino [155], M. Ishitsuka [157], R. Ishmukhametov [111], C. Issever [120], S. Istin [20a], F. Ito [160],

J.M. Iturbe Ponce [85], R. Iuppa [133a,133b], W. Iwanski [41], H. Iwasaki [67], J.M. Izen [43], V. Izzo [104a], S. Jabbar [3], B. Jackson [122], P. Jackson [1], V. Jain [2], K.B. Jakobi [84], K. Jakobs [50], S. Jakobsen [32], T. Jakoubek [127], D.O. Jamin [114], D.K. Jana [80], E. Jansen [79], R. Jansky [63], J. Janssen [23], M. Janus [56], G. Jarlskog [82], N. Javadov [66,b], T. Javůrek [50], F. Jeanneau [136], L. Jeanty [16], J. Jejelava [53a,w], G.-Y. Jeng [150], D. Jennens [89], P. Jenni [50,x], C. Jeske [169], S. Jézéquel [5], H. Ji [172], J. Jia [148], H. Jiang [65], Y. Jiang [35b], S. Jiggins [79], J. Jimenez Pena [166], S. Jin [35a], A. Jinaru [28b], O. Jinnouchi [157], P. Johansson [139], K.A. Johns [7], W.J. Johnson [138], K. Jon-And [146a,146b], G. Jones [169], R.W.L. Jones [73], S. Jones [7], T.J. Jones [75], J. Jongmanns [59a], P.M. Jorge [126a,126b], J. Jovicevic [159a], X. Ju [172], A. Juste Rozas [13,r], M.K. Köhler [171], A. Kaczmarska [41], M. Kado [117], H. Kagan [111], M. Kagan [143], S.J. Kahn [86], T. Kaji [170], E. Kajomovitz [47], C.W. Kalderon [120], A. Kaluza [84], S. Kama [42], A. Kamenshchikov [130], N. Kanaya [155], S. Kaneti [30], L. Kanjir [76], V.A. Kantserov [98], J. Kanzaki [67], B. Kaplan [110], L.S. Kaplan [172], A. Kapliy [33], D. Kar [145c], K. Karakostas [10], A. Karamaoun [3], N. Karastathis [10], M.J. Kareem [56], E. Karentzos [10], M. Karnevskiy [84], S.N. Karpov [66], Z.M. Karpova [66], K. Karthik [110], V. Kartvelishvili [73], A.N. Karyukhin [130], K. Kasahara [160], L. Kashif [172], R.D. Kass [111], A. Kastanas [15], Y. Kataoka [155], C. Kato [155], A. Katre [51], J. Katzy [44], K. Kawagoe [71], T. Kawamoto [155], G. Kawamura [56], V.F. Kazanin [109,c], R. Keeler [168], R. Kehoe [42], J.S. Keller [44], J.J. Kempster [78], K Kentaro [103], H. Keoshkerian [158], O. Kepka [127], B.P. Kerševan [76], S. Kersten [174], R.A. Keyes [88], M. Khader [165], F. Khalil-zada [12], A. Khanov [114], A.G. Kharlamov [109,c], T.J. Khoo [51], V. Khovanskiy [97], E. Khramov [66], J. Khubua [53b,y], S. Kido [68], C.R. Kilby [78], H.Y. Kim [8], S.H. Kim [160], Y.K. Kim [33], N. Kimura [154], O.M. Kind [17], B.T. King [75], M. King [166], S.B. King [167], J. Kirk [131], A.E. Kiryunin [101], T. Kishimoto [155], D. Kisielewska [40a], F. Kiss [50], K. Kiuchi [160], O. Kivernyk [136], E. Kladiva [144b], M.H. Klein [37], M. Klein [75], U. Klein [75], K. Kleinknecht [84], P. Klimek [108], A. Klimentov [27], R. Klingenberg [45], J.A. Klinger [139], T. Klioutchnikova [32], E.-E. Kluge [59a], P. Kluit [107], S. Kluth [101], J. Knapik [41], E. Kneringer [63], E.B.F.G. Knoops [86], A. Knue [55], A. Kobayashi [155], D. Kobayashi [157], T. Kobayashi [155], M. Kobel [46], M. Kocian [143], P. Kodys [129], N.M. Koehler [101], T. Koffas [31], E. Koffeman [107], T. Koi [143], H. Kolanoski [17], M. Kolb [59b], I. Koletsou [5], A.A. Komar [96,*], Y. Komori [155], T. Kondo [67], N. Kondrashova [44], K. Köneke [50], A.C. König [106], T. Kono [67,z], R. Konoplich [110,aa], N. Konstantinidis [79], R. Kopeliansky [62], S. Koperny [40a], L. Köpke [84], A.K. Kopp [50], K. Korcyl [41], K. Kordas [154], A. Korn [79], A.A. Korol [109,c], I. Korolkov [13], E.V. Korolkova [139], O. Kortner [101], S. Kortner [101], T. Kosek [129], V.V. Kostyukhin [23], A. Kotwal [47], A. Kourkoumeli-Charalampidi [154], C. Kourkoumelis [9], V. Kouskoura [27], A.B. Kowalewska [41], R. Kowalewski [168], T.Z. Kowalski [40a], C. Kozakai [155], W. Kozanecki [136], A.S. Kozhin [130], V.A. Kramarenko [99], G. Kramberger [76], D. Krasnopevtsev [98], M.W. Krasny [81], A. Krasznahorkay [32], A. Kravchenko [27], M. Kretz [59c], J. Kretzschmar [75], K. Kreutzfeldt [54], P. Krieger [158], K. Krizka [33], K. Kroeninger [45], H. Kroha [101], J. Kroll [122], J. Kroseberg [23], J. Krstic [14], U. Kruchonak [66], H. Krüger [23], N. Krumnack [65], A. Kruse [172], M.C. Kruse [47], M. Kruskal [24], T. Kubota [89], H. Kucuk [79], S. Kuday [4b], J.T. Kuechler [174], S. Kuehn [50], A. Kugel [59c], F. Kuger [173], A. Kuhl [137], T. Kuhl [44], V. Kukhtin [66], R. Kukla [136], Y. Kulchitsky [93], S. Kuleshov [34b], M. Kuna [132a,132b], T. Kunigo [69], A. Kupco [127], H. Kurashige [68], Y.A. Kurochkin [93], V. Kus [127], E.S. Kuwertz [168], M. Kuze [157], J. Kvita [115], T. Kwan [168], D. Kyriazopoulos [139], A. La Rosa [101], J.L. La Rosa Navarro [26d], L. La Rotonda [39a,39b], C. Lacasta [166], F. Lacava [132a,132b], J. Lacey [31], H. Lacker [17], D. Lacour [81], V.R. Lacuesta [166], E. Ladygin [66], R. Lafaye [5], B. Laforge [81], T. Lagouri [175], S. Lai [56], S. Lammers [62], W. Lampl [7], E. Lançon [136], U. Landgraf [50], M.P.J. Landon [77], M.C. Lanfermann [51], V.S. Lang [59a], J.C. Lange [13], A.J. Lankford [162], F. Lanni [27], K. Lantzsch [23], A. Lanza [121a], S. Laplace [81], C. Lapoire [32], J.F. Laporte [136], T. Lari [92a], F. Lasagni Manghi [22a,22b], M. Lassnig [32], P. Laurelli [49], W. Lavrijsen [16], A.T. Law [137], P. Laycock [75], T. Lazovich [58], M. Lazzaroni [92a,92b], B. Le [89], O. Le Dortz [81], E. Le Guirriec [86], E.P. Le Quilleuc [136], M. LeBlanc [168], T. LeCompte [6], F. Ledroit-Guillon [57], C.A. Lee [27], S.C. Lee [151], L. Lee [1], B. Lefebvre [88], G. Lefebvre [81], M. Lefebvre [168], F. Legger [100], C. Leggett [16], A. Lehan [75], G. Lehmann Miotto [32], X. Lei [7], W.A. Leight [31], A. Leisos [154,ab], A.G. Leister [175], M.A.L. Leite [26d], R. Leitner [129], D. Lellouch [171], B. Lemmer [56], K.J.C. Leney [79], T. Lenz [23], B. Lenzi [32], R. Leone [7], S. Leone [124a,124b], C. Leonidopoulos [48], S. Leontsinis [10], G. Lerner [149], C. Leroy [95], A.A.J. Lesage [136], C.G. Lester [30], M. Levchenko [123], J. Levêque [5], D. Levin [90], L.J. Levinson [171], M. Levy [19], D. Lewis [77], A.M. Leyko [23], M. Leyton [43], B. Li [35b,o], C. Li [35b], H. Li [148], H.L. Li [33], L. Li [47], L. Li [35e], Q. Li [35a], S. Li [47], X. Li [85], Y. Li [141], Z. Liang [35a], B. Liberti [133a], A. Liblong [158], P. Lichard [32], K. Lie [165], J. Liebal [23], W. Liebig [15], A. Limosani [150], S.C. Lin [151,ac], T.H. Lin [84], B.E. Lindquist [148], A.E. Lionti [51], E. Lipeles [122], A. Lipniacka [15], M. Lisovyi [59b], T.M. Liss [165], A. Lister [167],

A.M. Litke [137], B. Liu [151,ad], D. Liu [151], H. Liu [90], H. Liu [27], J. Liu [86], J.B. Liu [35b], K. Liu [86], L. Liu [165], M. Liu [47], M. Liu [35b], Y.L. Liu [35b], Y. Liu [35b], M. Livan [121a,121b], A. Lleres [57], J. Llorente Merino [35a], S.L. Lloyd [77], F. Lo Sterzo [151], E. Lobodzinska [44], P. Loch [7], W.S. Lockman [137], F.K. Loebinger [85], A.E. Loevschall-Jensen [38], K.M. Loew [25], A. Loginov [175], T. Lohse [17], K. Lohwasser [44], M. Lokajicek [127], B.A. Long [24], J.D. Long [165], R.E. Long [73], L. Longo [74a,74b], K.A. Looper [111], L. Lopes [126a], D. Lopez Mateos [58], B. Lopez Paredes [139], I. Lopez Paz [13], A. Lopez Solis [81], J. Lorenz [100], N. Lorenzo Martinez [62], M. Losada [21], P.J. Lösel [100], X. Lou [35a], A. Lounis [117], J. Love [6], P.A. Love [73], H. Lu [61a], N. Lu [90], H.J. Lubatti [138], C. Luci [132a,132b], A. Lucotte [57], C. Luedtke [50], F. Luehring [62], W. Lukas [63], L. Luminari [132a], O. Lundberg [146a,146b], B. Lund-Jensen [147], P.M. Luzi [81], D. Lynn [27], R. Lysak [127], E. Lytken [82], V. Lyubushkin [66], H. Ma [27], L.L. Ma [35d], Y. Ma [35d], G. Maccarrone [49], A. Macchiolo [101], C.M. Macdonald [139], B. Maček [76], J. Machado Miguens [122,126b], D. Madaffari [86], R. Madar [36], H.J. Maddocks [164], W.F. Mader [46], A. Madsen [44], J. Maeda [68], S. Maeland [15], T. Maeno [27], A. Maevskiy [99], E. Magradze [56], J. Mahlstedt [107], C. Maiani [117], C. Maidantchik [26a], A.A. Maier [101], T. Maier [100], A. Maio [126a,126b,126d], S. Majewski [116], Y. Makida [67], N. Makovec [117], B. Malaescu [81], Pa. Malecki [41], V.P. Maleev [123], F. Malek [57], U. Mallik [64], D. Malon [6], C. Malone [143], S. Maltezos [10], S. Malyukov [32], J. Mamuzic [166], G. Mancini [49], B. Mandelli [32], L. Mandelli [92a], I. Mandić [76], J. Maneira [126a,126b], L. Manhaes de Andrade Filho [26b], J. Manjarres Ramos [159b], A. Mann [100], A. Manousos [32], B. Mansoulie [136], J.D. Mansour [35a], R. Mantifel [88], M. Mantoani [56], S. Manzoni [92a,92b], L. Mapelli [32], G. Marceca [29], L. March [51], G. Marchiori [81], M. Marcisovsky [127], M. Marjanovic [14], D.E. Marley [90], F. Marroquim [26a], S.P. Marsden [85], Z. Marshall [16], S. Marti-Garcia [166], B. Martin [91], T.A. Martin [169], V.J. Martin [48], B. Martin dit Latour [15], M. Martinez [13,r], V.I. Martinez Outschoorn [165], S. Martin-Haugh [131], V.S. Martoiu [28b], A.C. Martyniuk [79], M. Marx [138], A. Marzin [32], L. Masetti [84], T. Mashimo [155], R. Mashinistov [96], J. Masik [85], A.L. Maslennikov [109,c], I. Massa [22a,22b], L. Massa [22a,22b], P. Mastrandrea [5], A. Mastroberardino [39a,39b], T. Masubuchi [155], P. Mättig [174], J. Mattmann [84], J. Maurer [28b], S.J. Maxfield [75], D.A. Maximov [109,c], R. Mazini [151], S.M. Mazza [92a,92b], N.C. Mc Fadden [105], G. Mc Goldrick [158], S.P. Mc Kee [90], A. McCarn [90], R.L. McCarthy [148], T.G. McCarthy [101], L.I. McClymont [79], E.F. McDonald [89], J.A. Mcfayden [79], G. Mchedlidze [56], S.J. McMahon [131], R.A. McPherson [168,l], M. Medinnis [44], S. Meehan [138], S. Mehlhase [100], A. Mehta [75], K. Meier [59a], C. Meineck [100], B. Meirose [43], D. Melini [166], B.R. Mellado Garcia [145c], M. Melo [144a], F. Meloni [18], A. Mengarelli [22a,22b], S. Menke [101], E. Meoni [161], S. Mergelmeyer [17], P. Mermod [51], L. Merola [104a,104b], C. Meroni [92a], F.S. Merritt [33], A. Messina [132a,132b], J. Metcalfe [6], A.S. Mete [162], C. Meyer [84], C. Meyer [122], J-P. Meyer [136], J. Meyer [107], H. Meyer Zu Theenhausen [59a], F. Miano [149], R.P. Middleton [131], S. Miglioranzi [52a,52b], L. Mijović [48], G. Mikenberg [171], M. Mikestikova [127], M. Mikuž [76], M. Milesi [89], A. Milic [63], D.W. Miller [33], C. Mills [48], A. Milov [171], D.A. Milstead [146a,146b], A.A. Minaenko [130], Y. Minami [155], I.A. Minashvili [66], A.I. Mincer [110], B. Mindur [40a], M. Mineev [66], Y. Ming [172], L.M. Mir [13], K.P. Mistry [122], T. Mitani [170], J. Mitrevski [100], V.A. Mitsou [166], A. Miucci [51], P.S. Miyagawa [139], J.U. Mjörnmark [82], T. Moa [146a,146b], K. Mochizuki [95], S. Mohapatra [37], S. Molander [146a,146b], R. Moles-Valls [23], R. Monden [69], M.C. Mondragon [91], K. Mönig [44], J. Monk [38], E. Monnier [86], A. Montalbano [148], J. Montejo Berlingen [32], F. Monticelli [72], S. Monzani [92a,92b], R.W. Moore [3], N. Morange [117], D. Moreno [21], M. Moreno Llácer [56], P. Morettini [52a], D. Mori [142], T. Mori [155], M. Morii [58], M. Morinaga [155], V. Morisbak [119], S. Moritz [84], A.K. Morley [150], G. Mornacchi [32], J.D. Morris [77], S.S. Mortensen [38], L. Morvaj [148], M. Mosidze [53b], J. Moss [143], K. Motohashi [157], R. Mount [143], E. Mountricha [27], S.V. Mouraviev [96,*], E.J.W. Moyse [87], S. Muanza [86], R.D. Mudd [19], F. Mueller [101], J. Mueller [125], R.S.P. Mueller [100], T. Mueller [30], D. Muenstermann [73], P. Mullen [55], G.A. Mullier [18], F.J. Munoz Sanchez [85], J.A. Murillo Quijada [19], W.J. Murray [169,131], H. Musheghyan [56], M. Muškinja [76], A.G. Myagkov [130,ae], M. Myska [128], B.P. Nachman [143], O. Nackenhorst [51], K. Nagai [120], R. Nagai [67,z], K. Nagano [67], Y. Nagasaka [60], K. Nagata [160], M. Nagel [50], E. Nagy [86], A.M. Nairz [32], Y. Nakahama [103], K. Nakamura [67], T. Nakamura [155], I. Nakano [112], H. Namasivayam [43], R.F. Naranjo Garcia [44], R. Narayan [11], D.I. Narrias Villar [59a], I. Naryshkin [123], T. Naumann [44], G. Navarro [21], R. Nayyar [7], H.A. Neal [90], P.Yu. Nechaeva [96], T.J. Neep [85], A. Negri [121a,121b], M. Negrini [22a], S. Nektarijevic [106], C. Nellist [117], A. Nelson [162], S. Nemecek [127], P. Nemethy [110], A.A. Nepomuceno [26a], M. Nessi [32,af], M.S. Neubauer [165], M. Neumann [174], R.M. Neves [110], P. Nevski [27], P.R. Newman [19], D.H. Nguyen [6], T. Nguyen Manh [95], R.B. Nickerson [120], R. Nicolaidou [136], J. Nielsen [137], A. Nikiforov [17], V. Nikolaenko [130,ae], I. Nikolic-Audit [81], K. Nikolopoulos [19], J.K. Nilsen [119], P. Nilsson [27], Y. Ninomiya [155], A. Nisati [132a], R. Nisius [101], T. Nobe [155],

M. Nomachi [118], I. Nomidis [31], T. Nooney [77], S. Norberg [113], M. Nordberg [32], N. Norjoharuddeen [120], O. Novgorodova [46], S. Nowak [101], M. Nozaki [67], L. Nozka [115], K. Ntekas [10], E. Nurse [79], F. Nuti [89], F. O'grady [7], D.C. O'Neil [142], A.A. O'Rourke [44], V. O'Shea [55], F.G. Oakham [31,d], H. Oberlack [101], T. Obermann [23], J. Ocariz [81], A. Ochi [68], I. Ochoa [37], J.P. Ochoa-Ricoux [34a], S. Oda [71], S. Odaka [67], H. Ogren [62], A. Oh [85], S.H. Oh [47], C.C. Ohm [16], H. Ohman [164], H. Oide [32], H. Okawa [160], Y. Okumura [155], T. Okuyama [67], A. Olariu [28b], L.F. Oleiro Seabra [126a], S.A. Olivares Pino [48], D. Oliveira Damazio [27], A. Olszewski [41], J. Olszowska [41], A. Onofre [126a,126e], K. Onogi [103], P.U.E. Onyisi [11,v], M.J. Oreglia [33], Y. Oren [153], D. Orestano [134a,134b], N. Orlando [61b], R.S. Orr [158], B. Osculati [52a,52b], R. Ospanov [85], G. Otero y Garzon [29], H. Otono [71], M. Ouchrif [135d], F. Ould-Saada [119], A. Ouraou [136], K.P. Oussoren [107], Q. Ouyang [35a], M. Owen [55], R.E. Owen [19], V.E. Ozcan [20a], N. Ozturk [8], K. Pachal [142], A. Pacheco Pages [13], L. Pacheco Rodriguez [136], C. Padilla Aranda [13], M. Pagáčová [50], S. Pagan Griso [16], F. Paige [27], P. Pais [87], K. Pajchel [119], G. Palacino [159b], S. Palestini [32], M. Palka [40b], D. Pallin [36], E.St. Panagiotopoulou [10], C.E. Pandini [81], J.G. Panduro Vazquez [78], P. Pani [146a,146b], S. Panitkin [27], D. Pantea [28b], L. Paolozzi [51], Th.D. Papadopoulou [10], K. Papageorgiou [154], A. Paramonov [6], D. Paredes Hernandez [175], A.J. Parker [73], M.A. Parker [30], K.A. Parker [139], F. Parodi [52a,52b], J.A. Parsons [37], U. Parzefall [50], V.R. Pascuzzi [158], E. Pasqualucci [132a], S. Passaggio [52a], Fr. Pastore [78], G. Pásztor [31,ag], S. Pataraia [174], J.R. Pater [85], T. Pauly [32], J. Pearce [168], B. Pearson [113], L.E. Pedersen [38], M. Pedersen [119], S. Pedraza Lopez [166], R. Pedro [126a,126b], S.V. Peleganchuk [109,c], O. Penc [127], C. Peng [35a], H. Peng [35b], J. Penwell [62], B.S. Peralva [26b], M.M. Perego [136], D.V. Perepelitsa [27], E. Perez Codina [159a], L. Perini [92a,92b], H. Pernegger [32], S. Perrella [104a,104b], R. Peschke [44], V.D. Peshekhonov [66], K. Peters [44], R.F.Y. Peters [85], B.A. Petersen [32], T.C. Petersen [38], E. Petit [57], A. Petridis [1], C. Petridou [154], P. Petroff [117], E. Petrolo [132a], M. Petrov [120], F. Petrucci [134a,134b], N.E. Pettersson [87], A. Peyaud [136], R. Pezoa [34b], P.W. Phillips [131], G. Piacquadio [143], E. Pianori [169], A. Picazio [87], E. Piccaro [77], M. Piccinini [22a,22b], M.A. Pickering [120], R. Piegaia [29], J.E. Pilcher [33], A.D. Pilkington [85], A.W.J. Pin [85], M. Pinamonti [163a,163c,ah], J.L. Pinfold [3], A. Pingel [38], S. Pires [81], H. Pirumov [44], M. Pitt [171], L. Plazak [144a], M.-A. Pleier [27], V. Pleskot [84], E. Plotnikova [66], P. Plucinski [91], D. Pluth [65], R. Poettgen [146a,146b], L. Poggioli [117], D. Pohl [23], G. Polesello [121a], A. Poley [44], A. Policicchio [39a,39b], R. Polifka [158], A. Polini [22a], C.S. Pollard [55], V. Polychronakos [27], K. Pommès [32], L. Pontecorvo [132a], B.G. Pope [91], G.A. Popeneciu [28c], D.S. Popovic [14], A. Poppleton [32], S. Pospisil [128], K. Potamianos [16], I.N. Potrap [66], C.J. Potter [30], C.T. Potter [116], G. Poulard [32], J. Poveda [32], V. Pozdnyakov [66], M.E. Pozo Astigarraga [32], P. Pralavorio [86], A. Pranko [16], S. Prell [65], D. Price [85], L.E. Price [6], M. Primavera [74a], S. Prince [88], K. Prokofiev [61c], F. Prokoshin [34b], S. Protopopescu [27], J. Proudfoot [6], M. Przybycien [40a], D. Puddu [134a,134b], M. Purohit [27,ai], P. Puzo [117], J. Qian [90], G. Qin [55], Y. Qin [85], A. Quadt [56], W.B. Quayle [163a,163b], M. Queitsch-Maitland [85], D. Quilty [55], S. Raddum [119], V. Radeka [27], V. Radescu [59b], S.K. Radhakrishnan [148], P. Radloff [116], P. Rados [89], F. Ragusa [92a,92b], G. Rahal [177], J.A. Raine [85], S. Rajagopalan [27], M. Rammensee [32], C. Rangel-Smith [164], M.G. Ratti [92a,92b], F. Rauscher [100], S. Rave [84], T. Ravenscroft [55], I. Ravinovich [171], M. Raymond [32], A.L. Read [119], N.P. Readioff [75], M. Reale [74a,74b], D.M. Rebuzzi [121a,121b], A. Redelbach [173], G. Redlinger [27], R. Reece [137], K. Reeves [43], L. Rehnisch [17], J. Reichert [122], H. Reisin [29], C. Rembser [32], H. Ren [35a], M. Rescigno [132a], S. Resconi [92a], O.L. Rezanova [109,c], P. Reznicek [129], R. Rezvani [95], R. Richter [101], S. Richter [79], E. Richter-Was [40b], O. Ricken [23], M. Ridel [81], P. Rieck [17], C.J. Riegel [174], J. Rieger [56], O. Rifki [113], M. Rijssenbeek [148], A. Rimoldi [121a,121b], M. Rimoldi [18], L. Rinaldi [22a], B. Ristić [51], E. Ritsch [32], I. Riu [13], F. Rizatdinova [114], E. Rizvi [77], C. Rizzi [13], S.H. Robertson [88,l], A. Robichaud-Veronneau [88], D. Robinson [30], J.E.M. Robinson [44], A. Robson [55], C. Roda [124a,124b], Y. Rodina [86], A. Rodriguez Perez [13], D. Rodriguez Rodriguez [166], S. Roe [32], C.S. Rogan [58], O. Røhne [119], A. Romaniouk [98], M. Romano [22a,22b], S.M. Romano Saez [36], E. Romero Adam [166], N. Rompotis [138], M. Ronzani [50], L. Roos [81], E. Ros [166], S. Rosati [132a], K. Rosbach [50], P. Rose [137], O. Rosenthal [141], N.-A. Rosien [56], V. Rossetti [146a,146b], E. Rossi [104a,104b], L.P. Rossi [52a], J.H.N. Rosten [30], R. Rosten [138], M. Rotaru [28b], I. Roth [171], J. Rothberg [138], D. Rousseau [117], C.R. Royon [136], A. Rozanov [86], Y. Rozen [152], X. Ruan [145c], F. Rubbo [143], M.S. Rudolph [158], F. Rühr [50], A. Ruiz-Martinez [31], Z. Rurikova [50], N.A. Rusakovich [66], A. Ruschke [100], H.L. Russell [138], J.P. Rutherfoord [7], N. Ruthmann [32], Y.F. Ryabov [123], M. Rybar [165], G. Rybkin [117], S. Ryu [6], A. Ryzhov [130], G.F. Rzehorz [56], A.F. Saavedra [150], G. Sabato [107], S. Sacerdoti [29], H.F-W. Sadrozinski [137], R. Sadykov [66], F. Safai Tehrani [132a], P. Saha [108], M. Sahinsoy [59a], M. Saimpert [136], T. Saito [155], H. Sakamoto [155], Y. Sakurai [170], G. Salamanna [134a,134b], A. Salamon [133a,133b], J.E. Salazar Loyola [34b], D. Salek [107],

P.H. Sales De Bruin [138], D. Salihagic [101], A. Salnikov [143], J. Salt [166], D. Salvatore [39a,39b], F. Salvatore [149], A. Salvucci [61a], A. Salzburger [32], D. Sammel [50], D. Sampsonidis [154], A. Sanchez [104a,104b], J. Sánchez [166], V. Sanchez Martinez [166], H. Sandaker [119], R.L. Sandbach [77], H.G. Sander [84], M. Sandhoff [174], C. Sandoval [21], R. Sandstroem [101], D.P.C. Sankey [131], M. Sannino [52a,52b], A. Sansoni [49], C. Santoni [36], R. Santonico [133a,133b], H. Santos [126a], I. Santoyo Castillo [149], K. Sapp [125], A. Sapronov [66], J.G. Saraiva [126a,126d], B. Sarrazin [23], O. Sasaki [67], Y. Sasaki [155], K. Sato [160], G. Sauvage [5,*], E. Sauvan [5], G. Savage [78], P. Savard [158,d], N. Savic [101], C. Sawyer [131], L. Sawyer [80,q], J. Saxon [33], C. Sbarra [22a], A. Sbrizzi [22a,22b], T. Scanlon [79], D.A. Scannicchio [162], M. Scarcella [150], V. Scarfone [39a,39b], J. Schaarschmidt [171], P. Schacht [101], B.M. Schachtner [100], D. Schaefer [32], R. Schaefer [44], J. Schaeffer [84], S. Schaepe [23], S. Schaetzel [59b], U. Schäfer [84], A.C. Schaffer [117], D. Schaile [100], R.D. Schamberger [148], V. Scharf [59a], V.A. Schegelsky [123], D. Scheirich [129], M. Schernau [162], C. Schiavi [52a,52b], S. Schier [137], C. Schillo [50], M. Schioppa [39a,39b], S. Schlenker [32], K.R. Schmidt-Sommerfeld [101], K. Schmieden [32], C. Schmitt [84], S. Schmitt [44], S. Schmitz [84], B. Schneider [159a], U. Schnoor [50], L. Schoeffel [136], A. Schoening [59b], B.D. Schoenrock [91], E. Schopf [23], M. Schott [84], J. Schovancova [8], S. Schramm [51], M. Schreyer [173], N. Schuh [84], A. Schulte [84], M.J. Schultens [23], H.-C. Schultz-Coulon [59a], H. Schulz [17], M. Schumacher [50], B.A. Schumm [137], Ph. Schune [136], A. Schwartzman [143], T.A. Schwarz [90], H. Schweiger [85], Ph. Schwemling [136], R. Schwienhorst [91], J. Schwindling [136], T. Schwindt [23], G. Sciolla [25], F. Scuri [124a,124b], F. Scutti [89], J. Searcy [90], P. Seema [23], S.C. Seidel [105], A. Seiden [137], F. Seifert [128], J.M. Seixas [26a], G. Sekhniaidze [104a], K. Sekhon [90], S.J. Sekula [42], D.M. Seliverstov [123,*], N. Semprini-Cesari [22a,22b], C. Serfon [119], L. Serin [117], L. Serkin [163a,163b], M. Sessa [134a,134b], R. Seuster [168], H. Severini [113], T. Sfiligoj [76], F. Sforza [32], A. Sfyrla [51], E. Shabalina [56], N.W. Shaikh [146a,146b], L.Y. Shan [35a], R. Shang [165], J.T. Shank [24], M. Shapiro [16], P.B. Shatalov [97], K. Shaw [163a,163b], S.M. Shaw [85], A. Shcherbakova [146a,146b], C.Y. Shehu [149], P. Sherwood [79], L. Shi [151,aj], S. Shimizu [68], C.O. Shimmin [162], M. Shimojima [102], M. Shiyakova [66,ak], A. Shmeleva [96], D. Shoaleh Saadi [95], M.J. Shochet [33], S. Shojaii [92a,92b], S. Shrestha [111], E. Shulga [98], M.A. Shupe [7], P. Sicho [127], A.M. Sickles [165], P.E. Sidebo [147], O. Sidiropoulou [173], D. Sidorov [114], A. Sidoti [22a,22b], F. Siegert [46], Dj. Sijacki [14], J. Silva [126a,126d], S.B. Silverstein [146a], V. Simak [128], Lj. Simic [14], S. Simion [117], E. Simioni [84], B. Simmons [79], D. Simon [36], M. Simon [84], P. Sinervo [158], N.B. Sinev [116], M. Sioli [22a,22b], G. Siragusa [173], S.Yu. Sivoklokov [99], J. Sjölin [146a,146b], M.B. Skinner [73], H.P. Skottowe [58], P. Skubic [113], M. Slater [19], T. Slavicek [128], M. Slawinska [107], K. Sliwa [161], R. Slovak [129], V. Smakhtin [171], B.H. Smart [5], L. Smestad [15], J. Smiesko [144a], S.Yu. Smirnov [98], Y. Smirnov [98], L.N. Smirnova [99,al], O. Smirnova [82], M.N.K. Smith [37], R.W. Smith [37], M. Smizanska [73], K. Smolek [128], A.A. Snesarev [96], S. Snyder [27], R. Sobie [168,l], F. Socher [46], A. Soffer [153], D.A. Soh [151], G. Sokhrannyi [76], C.A. Solans Sanchez [32], M. Solar [128], E.Yu. Soldatov [98], U. Soldevila [166], A.A. Solodkov [130], A. Soloshenko [66], O.V. Solovyanov [130], V. Solovyev [123], P. Sommer [50], H. Son [161], H.Y. Song [35b,am], A. Sood [16], A. Sopczak [128], V. Sopko [128], V. Sorin [13], D. Sosa [59b], C.L. Sotiropoulou [124a,124b], R. Soualah [163a,163c], A.M. Soukharev [109,c], D. South [44], B.C. Sowden [78], S. Spagnolo [74a,74b], M. Spalla [124a,124b], M. Spangenberg [169], F. Spanò [78], D. Sperlich [17], F. Spettel [101], R. Spighi [22a], G. Spigo [32], L.A. Spiller [89], M. Spousta [129], R.D. St. Denis [55,*], A. Stabile [92a], R. Stamen [59a], S. Stamm [17], E. Stanecka [41], R.W. Stanek [6], C. Stanescu [134a], M. Stanescu-Bellu [44], M.M. Stanitzki [44], S. Stapnes [119], E.A. Starchenko [130], G.H. Stark [33], J. Stark [57], P. Staroba [127], P. Starovoitov [59a], S. Stärz [32], R. Staszewski [41], P. Steinberg [27], B. Stelzer [142], H.J. Stelzer [32], O. Stelzer-Chilton [159a], H. Stenzel [54], G.A. Stewart [55], J.A. Stillings [23], M.C. Stockton [88], M. Stoebe [88], G. Stoicea [28b], P. Stolte [56], S. Stonjek [101], A.R. Stradling [8], A. Straessner [46], M.E. Stramaglia [18], J. Strandberg [147], S. Strandberg [146a,146b], A. Strandlie [119], M. Strauss [113], P. Strizenec [144b], R. Ströhmer [173], D.M. Strom [116], R. Stroynowski [42], A. Strubig [106], S.A. Stucci [18], B. Stugu [15], N.A. Styles [44], D. Su [143], J. Su [125], S. Suchek [59a], Y. Sugaya [118], M. Suk [128], V.V. Sulin [96], S. Sultansoy [4c], T. Sumida [69], S. Sun [58], X. Sun [35a], J.E. Sundermann [50], K. Suruliz [149], G. Susinno [39a,39b], M.R. Sutton [149], S. Suzuki [67], M. Svatos [127], M. Swiatlowski [33], I. Sykora [144a], T. Sykora [129], D. Ta [50], C. Taccini [134a,134b], K. Tackmann [44], J. Taenzer [158], A. Taffard [162], R. Tafirout [159a], N. Taiblum [153], H. Takai [27], R. Takashima [70], T. Takeshita [140], Y. Takubo [67], M. Talby [86], A.A. Talyshev [109,c], K.G. Tan [89], J. Tanaka [155], M. Tanaka [157], R. Tanaka [117], S. Tanaka [67], B.B. Tannenwald [111], S. Tapia Araya [34b], S. Tapprogge [84], S. Tarem [152], G.F. Tartarelli [92a], P. Tas [129], M. Tasevsky [127], T. Tashiro [69], E. Tassi [39a,39b], A. Tavares Delgado [126a,126b], Y. Tayalati [135e], A.C. Taylor [105], G.N. Taylor [89], P.T.E. Taylor [89], W. Taylor [159b], F.A. Teischinger [32], P. Teixeira-Dias [78], K.K. Temming [50],

D. Temple [142], H. Ten Kate [32], P.K. Teng [151], J.J. Teoh [118], F. Tepel [174], S. Terada [67], K. Terashi [155], J. Terron [83], S. Terzo [101], M. Testa [49], R.J. Teuscher [158,l], T. Theveneaux-Pelzer [86], J.P. Thomas [19], J. Thomas-Wilsker [78], E.N. Thompson [37], P.D. Thompson [19], A.S. Thompson [55], L.A. Thomsen [175], E. Thomson [122], M. Thomson [30], M.J. Tibbetts [16], R.E. Ticse Torres [86], V.O. Tikhomirov [96,an], Yu.A. Tikhonov [109,c], S. Timoshenko [98], P. Tipton [175], S. Tisserant [86], K. Todome [157], T. Todorov [5,*], S. Todorova-Nova [129], J. Tojo [71], S. Tokár [144a], K. Tokushuku [67], E. Tolley [58], L. Tomlinson [85], M. Tomoto [103], L. Tompkins [143,ao], K. Toms [105], B. Tong [58], E. Torrence [116], H. Torres [142], E. Torró Pastor [138], J. Toth [86,ap], F. Touchard [86], D.R. Tovey [139], T. Trefzger [173], A. Tricoli [27], I.M. Trigger [159a], S. Trincaz-Duvoid [81], M.F. Tripiana [13], W. Trischuk [158], B. Trocmé [57], A. Trofymov [44], C. Troncon [92a], M. Trottier-McDonald [16], M. Trovatelli [168], L. Truong [163a,163c], M. Trzebinski [41], A. Trzupek [41], J.C-L. Tseng [120], P.V. Tsiareshka [93], G. Tsipolitis [10], N. Tsirintanis [9], S. Tsiskaridze [13], V. Tsiskaridze [50], E.G. Tskhadadze [53a], K.M. Tsui [61a], I.I. Tsukerman [97], V. Tsulaia [16], S. Tsuno [67], D. Tsybychev [148], Y. Tu [61b], A. Tudorache [28b], V. Tudorache [28b], A.N. Tuna [58], S.A. Tupputi [22a,22b], S. Turchikhin [66], D. Turecek [128], D. Turgeman [171], R. Turra [92a,92b], A.J. Turvey [42], P.M. Tuts [37], M. Tyndel [131], G. Ucchielli [22a,22b], I. Ueda [155], M. Ughetto [146a,146b], F. Ukegawa [160], G. Unal [32], A. Undrus [27], G. Unel [162], F.C. Ungaro [89], Y. Unno [67], C. Unverdorben [100], J. Urban [144b], P. Urquijo [89], P. Urrejola [84], G. Usai [8], A. Usanova [63], L. Vacavant [86], V. Vacek [128], B. Vachon [88], C. Valderanis [100], E. Valdes Santurio [146a,146b], N. Valencic [107], S. Valentinetti [22a,22b], A. Valero [166], L. Valery [13], S. Valkar [129], J.A. Valls Ferrer [166], W. Van Den Wollenberg [107], P.C. Van Der Deijl [107], H. van der Graaf [107], N. van Eldik [152], P. van Gemmeren [6], J. Van Nieuwkoop [142], I. van Vulpen [107], M.C. van Woerden [32], M. Vanadia [132a,132b], W. Vandelli [32], R. Vanguri [122], A. Vaniachine [130], P. Vankov [107], G. Vardanyan [176], R. Vari [132a], E.W. Varnes [7], T. Varol [42], D. Varouchas [81], A. Vartapetian [8], K.E. Varvell [150], J.G. Vasquez [175], F. Vazeille [36], T. Vazquez Schroeder [88], J. Veatch [56], V. Veeraraghavan [7], L.M. Veloce [158], F. Veloso [126a,126c], S. Veneziano [132a], A. Ventura [74a,74b], M. Venturi [168], N. Venturi [158], A. Venturini [25], V. Vercesi [121a], M. Verducci [132a,132b], W. Verkerke [107], J.C. Vermeulen [107], A. Vest [46,aq], M.C. Vetterli [142,d], O. Viazlo [82], I. Vichou [165], T. Vickey [139], O.E. Vickey Boeriu [139], G.H.A. Viehhauser [120], S. Viel [16], L. Vigani [120], M. Villa [22a,22b], M. Villaplana Perez [92a,92b], E. Vilucchi [49], M.G. Vincter [31], V.B. Vinogradov [66], C. Vittori [22a,22b], I. Vivarelli [149], S. Vlachos [10], M. Vlasak [128], M. Vogel [174], P. Vokac [128], G. Volpi [124a,124b], M. Volpi [89], H. von der Schmitt [101], E. von Toerne [23], V. Vorobel [129], K. Vorobev [98], M. Vos [166], R. Voss [32], J.H. Vossebeld [75], N. Vranjes [14], M. Vranjes Milosavljevic [14], V. Vrba [127], M. Vreeswijk [107], R. Vuillermet [32], I. Vukotic [33], Z. Vykydal [128], P. Wagner [23], W. Wagner [174], H. Wahlberg [72], S. Wahrmund [46], J. Wakabayashi [103], J. Walder [73], R. Walker [100], W. Walkowiak [141], V. Wallangen [146a,146b], C. Wang [35c], C. Wang [35d,86], F. Wang [172], H. Wang [16], H. Wang [42], J. Wang [44], J. Wang [150], K. Wang [88], R. Wang [6], S.M. Wang [151], T. Wang [23], T. Wang [37], W. Wang [35b], X. Wang [175], C. Wanotayaroj [116], A. Warburton [88], C.P. Ward [30], D.R. Wardrope [79], A. Washbrook [48], P.M. Watkins [19], A.T. Watson [19], M.F. Watson [19], G. Watts [138], S. Watts [85], B.M. Waugh [79], S. Webb [84], M.S. Weber [18], S.W. Weber [173], J.S. Webster [6], A.R. Weidberg [120], B. Weinert [62], J. Weingarten [56], C. Weiser [50], H. Weits [107], P.S. Wells [32], T. Wenaus [27], T. Wengler [32], S. Wenig [32], N. Wermes [23], M. Werner [50], M.D. Werner [65], P. Werner [32], M. Wessels [59a], J. Wetter [161], K. Whalen [116], N.L. Whallon [138], A.M. Wharton [73], A. White [8], M.J. White [1], R. White [34b], D. Whiteson [162], F.J. Wickens [131], W. Wiedenmann [172], M. Wielers [131], P. Wienemann [23], C. Wiglesworth [38], L.A.M. Wiik-Fuchs [23], A. Wildauer [101], F. Wilk [85], H.G. Wilkens [32], H.H. Williams [122], S. Williams [107], C. Willis [91], S. Willocq [87], J.A. Wilson [19], I. Wingerter-Seez [5], F. Winklmeier [116], O.J. Winston [149], B.T. Winter [23], M. Wittgen [143], J. Wittkowski [100], T.M.H. Wolf [107], M.W. Wolter [41], H. Wolters [126a,126c], S.D. Worm [131], B.K. Wosiek [41], J. Wotschack [32], M.J. Woudstra [85], K.W. Wozniak [41], M. Wu [57], M. Wu [33], S.L. Wu [172], X. Wu [51], Y. Wu [90], T.R. Wyatt [85], B.M. Wynne [48], S. Xella [38], D. Xu [35a], L. Xu [27], B. Yabsley [150], S. Yacoob [145a], D. Yamaguchi [157], Y. Yamaguchi [118], A. Yamamoto [67], S. Yamamoto [155], T. Yamanaka [155], K. Yamauchi [103], Y. Yamazaki [68], Z. Yan [24], H. Yang [35e], H. Yang [172], Y. Yang [151], Z. Yang [15], W-M. Yao [16], Y.C. Yap [81], Y. Yasu [67], E. Yatsenko [5], K.H. Yau Wong [23], J. Ye [42], S. Ye [27], I. Yeletskikh [66], A.L. Yen [58], E. Yildirim [84], K. Yorita [170], R. Yoshida [6], K. Yoshihara [122], C. Young [143], C.J.S. Young [32], S. Youssef [24], D.R. Yu [16], J. Yu [8], J.M. Yu [90], J. Yu [65], L. Yuan [68], S.P.Y. Yuen [23], I. Yusuff [30,ar], B. Zabinski [41], R. Zaidan [35d], A.M. Zaitsev [130,ae], N. Zakharchuk [44], J. Zalieckas [15], A. Zaman [148], S. Zambito [58], L. Zanello [132a,132b], D. Zanzi [89], C. Zeitnitz [174], M. Zeman [128], A. Zemla [40a], J.C. Zeng [165], Q. Zeng [143], K. Zengel [25], O. Zenin [130], T. Ženiš [144a], D. Zerwas [117], D. Zhang [90], F. Zhang [172],

G. Zhang [35b,am], H. Zhang [35c], J. Zhang [6], L. Zhang [50], R. Zhang [23], R. Zhang [35b,as], X. Zhang [35d], Z. Zhang [117], X. Zhao [42], Y. Zhao [35d], Z. Zhao [35b], A. Zhemchugov [66], J. Zhong [120], B. Zhou [90], C. Zhou [47], L. Zhou [37], L. Zhou [42], M. Zhou [148], N. Zhou [35f], C.G. Zhu [35d], H. Zhu [35a], J. Zhu [90], Y. Zhu [35b], X. Zhuang [35a], K. Zhukov [96], A. Zibell [173], D. Zieminska [62], N.I. Zimine [66], C. Zimmermann [84], S. Zimmermann [50], Z. Zinonos [56], M. Zinser [84], M. Ziolkowski [141], L. Živković [14], G. Zobernig [172], A. Zoccoli [22a,22b], M. zur Nedden [17], L. Zwalinski [32]

[1] Department of Physics, University of Adelaide, Adelaide, Australia
[2] Physics Department, SUNY Albany, Albany NY, United States
[3] Department of Physics, University of Alberta, Edmonton AB, Canada
[4] [(a)] Department of Physics, Ankara University, Ankara; [(b)] Istanbul Aydin University, Istanbul; [(c)] Division of Physics, TOBB University of Economics and Technology, Ankara, Turkey
[5] LAPP, CNRS/IN2P3 and Université Savoie Mont Blanc, Annecy-le-Vieux, France
[6] High Energy Physics Division, Argonne National Laboratory, Argonne IL, United States
[7] Department of Physics, University of Arizona, Tucson AZ, United States
[8] Department of Physics, The University of Texas at Arlington, Arlington TX, United States
[9] Physics Department, University of Athens, Athens, Greece
[10] Physics Department, National Technical University of Athens, Zografou, Greece
[11] Department of Physics, The University of Texas at Austin, Austin TX, United States
[12] Institute of Physics, Azerbaijan Academy of Sciences, Baku, Azerbaijan
[13] Institut de Física d'Altes Energies (IFAE), The Barcelona Institute of Science and Technology, Barcelona, Spain
[14] Institute of Physics, University of Belgrade, Belgrade, Serbia
[15] Department for Physics and Technology, University of Bergen, Bergen, Norway
[16] Physics Division, Lawrence Berkeley National Laboratory and University of California, Berkeley CA, United States
[17] Department of Physics, Humboldt University, Berlin, Germany
[18] Albert Einstein Center for Fundamental Physics and Laboratory for High Energy Physics, University of Bern, Bern, Switzerland
[19] School of Physics and Astronomy, University of Birmingham, Birmingham, United Kingdom
[20] [(a)] Department of Physics, Bogazici University, Istanbul; [(b)] Department of Physics Engineering, Gaziantep University, Gaziantep; [(d)] Istanbul Bilgi University, Faculty of Engineering and Natural Sciences, Istanbul; [(e)] Bahcesehir University, Faculty of Engineering and Natural Sciences, Istanbul, Turkey
[21] Centro de Investigaciones, Universidad Antonio Narino, Bogota, Colombia
[22] [(a)] INFN Sezione di Bologna; [(b)] Dipartimento di Fisica e Astronomia, Università di Bologna, Bologna, Italy
[23] Physikalisches Institut, University of Bonn, Bonn, Germany
[24] Department of Physics, Boston University, Boston MA, United States
[25] Department of Physics, Brandeis University, Waltham MA, United States
[26] [(a)] Universidade Federal do Rio De Janeiro COPPE/EE/IF, Rio de Janeiro; [(b)] Electrical Circuits Department, Federal University of Juiz de Fora (UFJF), Juiz de Fora; [(c)] Federal University of Sao Joao del Rei (UFSJ), Sao Joao del Rei; [(d)] Instituto de Fisica, Universidade de Sao Paulo, Sao Paulo, Brazil
[27] Physics Department, Brookhaven National Laboratory, Upton NY, United States
[28] [(a)] Transilvania University of Brasov, Brasov; [(b)] National Institute of Physics and Nuclear Engineering, Bucharest; [(c)] National Institute for Research and Development of Isotopic and Molecular Technologies, Physics Department, Cluj Napoca; [(d)] University Politehnica Bucharest, Bucharest; [(e)] West University in Timisoara, Timisoara, Romania
[29] Departamento de Física, Universidad de Buenos Aires, Buenos Aires, Argentina
[30] Cavendish Laboratory, University of Cambridge, Cambridge, United Kingdom
[31] Department of Physics, Carleton University, Ottawa ON, Canada
[32] CERN, Geneva, Switzerland
[33] Enrico Fermi Institute, University of Chicago, Chicago IL, United States
[34] [(a)] Departamento de Física, Pontificia Universidad Católica de Chile, Santiago; [(b)] Departamento de Física, Universidad Técnica Federico Santa María, Valparaíso, Chile
[35] [(a)] Institute of High Energy Physics, Chinese Academy of Sciences, Beijing; [(b)] Department of Modern Physics, University of Science and Technology of China, Anhui; [(c)] Department of Physics, Nanjing University, Jiangsu; [(d)] School of Physics, Shandong University, Shandong; [(e)] Department of Physics and Astronomy, Shanghai Key Laboratory for Particle Physics and Cosmology, Shanghai Jiao Tong University, Shanghai [at]; [(f)] Physics Department, Tsinghua University, Beijing 100084, China
[36] Laboratoire de Physique Corpusculaire, Clermont Université and Université Blaise Pascal and CNRS/IN2P3, Clermont-Ferrand, France
[37] Nevis Laboratory, Columbia University, Irvington NY, United States
[38] Niels Bohr Institute, University of Copenhagen, Kobenhavn, Denmark
[39] [(a)] INFN Gruppo Collegato di Cosenza, Laboratori Nazionali di Frascati; [(b)] Dipartimento di Fisica, Università della Calabria, Rende, Italy
[40] [(a)] AGH University of Science and Technology, Faculty of Physics and Applied Computer Science, Krakow; [(b)] Marian Smoluchowski Institute of Physics, Jagiellonian University, Krakow, Poland
[41] Institute of Nuclear Physics Polish Academy of Sciences, Krakow, Poland
[42] Physics Department, Southern Methodist University, Dallas TX, United States
[43] Physics Department, University of Texas at Dallas, Richardson TX, United States
[44] DESY, Hamburg and Zeuthen, Germany
[45] Institut für Experimentelle Physik IV, Technische Universität Dortmund, Dortmund, Germany
[46] Institut für Kern- und Teilchenphysik, Technische Universität Dresden, Dresden, Germany
[47] Department of Physics, Duke University, Durham NC, United States
[48] SUPA - School of Physics and Astronomy, University of Edinburgh, Edinburgh, United Kingdom
[49] INFN Laboratori Nazionali di Frascati, Frascati, Italy
[50] Fakultät für Mathematik und Physik, Albert-Ludwigs-Universität, Freiburg, Germany
[51] Section de Physique, Université de Genève, Geneva, Switzerland
[52] [(a)] INFN Sezione di Genova; [(b)] Dipartimento di Fisica, Università di Genova, Genova, Italy
[53] [(a)] E. Andronikashvili Institute of Physics, Iv. Javakhishvili Tbilisi State University, Tbilisi; [(b)] High Energy Physics Institute, Tbilisi State University, Tbilisi, Georgia
[54] II Physikalisches Institut, Justus-Liebig-Universität Giessen, Giessen, Germany
[55] SUPA - School of Physics and Astronomy, University of Glasgow, Glasgow, United Kingdom
[56] II Physikalisches Institut, Georg-August-Universität, Göttingen, Germany
[57] Laboratoire de Physique Subatomique et de Cosmologie, Université Grenoble-Alpes, CNRS/IN2P3, Grenoble, France
[58] Laboratory for Particle Physics and Cosmology, Harvard University, Cambridge MA, United States
[59] [(a)] Kirchhoff-Institut für Physik, Ruprecht-Karls-Universität Heidelberg, Heidelberg; [(b)] Physikalisches Institut, Ruprecht-Karls-Universität Heidelberg, Heidelberg; [(c)] ZITI Institut für technische Informatik, Ruprecht-Karls-Universität Heidelberg, Mannheim, Germany
[60] Faculty of Applied Information Science, Hiroshima Institute of Technology, Hiroshima, Japan

[61] [(a)] Department of Physics, The Chinese University of Hong Kong, Shatin, N.T., Hong Kong; [(b)] Department of Physics, The University of Hong Kong, Hong Kong; [(c)] Department of Physics, The Hong Kong University of Science and Technology, Clear Water Bay, Kowloon, Hong Kong, China
[62] Department of Physics, Indiana University, Bloomington IN, United States
[63] Institut für Astro- und Teilchenphysik, Leopold-Franzens-Universität, Innsbruck, Austria
[64] University of Iowa, Iowa City IA, United States
[65] Department of Physics and Astronomy, Iowa State University, Ames IA, United States
[66] Joint Institute for Nuclear Research, JINR Dubna, Dubna, Russia
[67] KEK, High Energy Accelerator Research Organization, Tsukuba, Japan
[68] Graduate School of Science, Kobe University, Kobe, Japan
[69] Faculty of Science, Kyoto University, Kyoto, Japan
[70] Kyoto University of Education, Kyoto, Japan
[71] Department of Physics, Kyushu University, Fukuoka, Japan
[72] Instituto de Física La Plata, Universidad Nacional de La Plata and CONICET, La Plata, Argentina
[73] Physics Department, Lancaster University, Lancaster, United Kingdom
[74] [(a)] INFN Sezione di Lecce; [(b)] Dipartimento di Matematica e Fisica, Università del Salento, Lecce, Italy
[75] Oliver Lodge Laboratory, University of Liverpool, Liverpool, United Kingdom
[76] Department of Physics, Jožef Stefan Institute and University of Ljubljana, Ljubljana, Slovenia
[77] School of Physics and Astronomy, Queen Mary University of London, London, United Kingdom
[78] Department of Physics, Royal Holloway University of London, Surrey, United Kingdom
[79] Department of Physics and Astronomy, University College London, London, United Kingdom
[80] Louisiana Tech University, Ruston LA, United States
[81] Laboratoire de Physique Nucléaire et de Hautes Energies, UPMC and Université Paris-Diderot and CNRS/IN2P3, Paris, France
[82] Fysiska institutionen, Lunds universitet, Lund, Sweden
[83] Departamento de Fisica Teorica C-15, Universidad Autonoma de Madrid, Madrid, Spain
[84] Institut für Physik, Universität Mainz, Mainz, Germany
[85] School of Physics and Astronomy, University of Manchester, Manchester, United Kingdom
[86] CPPM, Aix-Marseille Université and CNRS/IN2P3, Marseille, France
[87] Department of Physics, University of Massachusetts, Amherst MA, United States
[88] Department of Physics, McGill University, Montreal QC, Canada
[89] School of Physics, University of Melbourne, Victoria, Australia
[90] Department of Physics, The University of Michigan, Ann Arbor MI, United States
[91] Department of Physics and Astronomy, Michigan State University, East Lansing MI, United States
[92] [(a)] INFN Sezione di Milano; [(b)] Dipartimento di Fisica, Università di Milano, Milano, Italy
[93] B.I. Stepanov Institute of Physics, National Academy of Sciences of Belarus, Minsk, Belarus
[94] National Scientific and Educational Centre for Particle and High Energy Physics, Minsk, Belarus
[95] Group of Particle Physics, University of Montreal, Montreal QC, Canada
[96] P.N. Lebedev Physical Institute of the Russian Academy of Sciences, Moscow, Russia
[97] Institute for Theoretical and Experimental Physics (ITEP), Moscow, Russia
[98] National Research Nuclear University MEPhI, Moscow, Russia
[99] D.V. Skobeltsyn Institute of Nuclear Physics, M.V. Lomonosov Moscow State University, Moscow, Russia
[100] Fakultät für Physik, Ludwig-Maximilians-Universität München, München, Germany
[101] Max-Planck-Institut für Physik (Werner-Heisenberg-Institut), München, Germany
[102] Nagasaki Institute of Applied Science, Nagasaki, Japan
[103] Graduate School of Science and Kobayashi-Maskawa Institute, Nagoya University, Nagoya, Japan
[104] [(a)] INFN Sezione di Napoli; [(b)] Dipartimento di Fisica, Università di Napoli, Napoli, Italy
[105] Department of Physics and Astronomy, University of New Mexico, Albuquerque NM, United States
[106] Institute for Mathematics, Astrophysics and Particle Physics, Radboud University Nijmegen/Nikhef, Nijmegen, Netherlands
[107] Nikhef National Institute for Subatomic Physics and University of Amsterdam, Amsterdam, Netherlands
[108] Department of Physics, Northern Illinois University, DeKalb IL, United States
[109] Budker Institute of Nuclear Physics, SB RAS, Novosibirsk, Russia
[110] Department of Physics, New York University, New York NY, United States
[111] Ohio State University, Columbus OH, United States
[112] Faculty of Science, Okayama University, Okayama, Japan
[113] Homer L. Dodge Department of Physics and Astronomy, University of Oklahoma, Norman OK, United States
[114] Department of Physics, Oklahoma State University, Stillwater OK, United States
[115] Palacký University, RCPTM, Olomouc, Czech Republic
[116] Center for High Energy Physics, University of Oregon, Eugene OR, United States
[117] LAL, Univ. Paris-Sud, CNRS/IN2P3, Université Paris-Saclay, Orsay, France
[118] Graduate School of Science, Osaka University, Osaka, Japan
[119] Department of Physics, University of Oslo, Oslo, Norway
[120] Department of Physics, Oxford University, Oxford, United Kingdom
[121] [(a)] INFN Sezione di Pavia; [(b)] Dipartimento di Fisica, Università di Pavia, Pavia, Italy
[122] Department of Physics, University of Pennsylvania, Philadelphia PA, United States
[123] National Research Centre "Kurchatov Institute" B.P. Konstantinov Petersburg Nuclear Physics Institute, St. Petersburg, Russia
[124] [(a)] INFN Sezione di Pisa; [(b)] Dipartimento di Fisica E. Fermi, Università di Pisa, Pisa, Italy
[125] Department of Physics and Astronomy, University of Pittsburgh, Pittsburgh PA, United States
[126] [(a)] Laboratório de Instrumentação e Física Experimental de Partículas – LIP, Lisboa; [(b)] Faculdade de Ciências, Universidade de Lisboa, Lisboa; [(c)] Department of Physics, University of Coimbra, Coimbra; [(d)] Centro de Física Nuclear da Universidade de Lisboa, Lisboa; [(e)] Departamento de Fisica, Universidade do Minho, Braga; [(f)] Departamento de Fisica Teorica y del Cosmos and CAFPE, Universidad de Granada, Granada (Spain); [(g)] Dep Fisica and CEFITEC of Faculdade de Ciencias e Tecnologia, Universidade Nova de Lisboa, Caparica, Portugal
[127] Institute of Physics, Academy of Sciences of the Czech Republic, Praha, Czech Republic
[128] Czech Technical University in Prague, Praha, Czech Republic
[129] Faculty of Mathematics and Physics, Charles University in Prague, Praha, Czech Republic
[130] State Research Center Institute for High Energy Physics (Protvino), NRC KI, Russia
[131] Particle Physics Department, Rutherford Appleton Laboratory, Didcot, United Kingdom
[132] [(a)] INFN Sezione di Roma; [(b)] Dipartimento di Fisica, Sapienza Università di Roma, Roma, Italy
[133] [(a)] INFN Sezione di Roma Tor Vergata; [(b)] Dipartimento di Fisica, Università di Roma Tor Vergata, Roma, Italy
[134] [(a)] INFN Sezione di Roma Tre; [(b)] Dipartimento di Matematica e Fisica, Università Roma Tre, Roma, Italy

[135] [(a)] Faculté des Sciences Ain Chock, Réseau Universitaire de Physique des Hautes Energies - Université Hassan II, Casablanca; [(b)] Centre National de l'Energie des Sciences Techniques Nucleaires, Rabat; [(c)] Faculté des Sciences Semlalia, Université Cadi Ayyad, LPHEA-Marrakech; [(d)] Faculté des Sciences, Université Mohamed Premier and LPTPM, Oujda; [(e)] Faculté des sciences, Université Mohammed V, Rabat, Morocco
[136] DSM/IRFU (Institut de Recherches sur les Lois Fondamentales de l'Univers), CEA Saclay (Commissariat à l'Energie Atomique et aux Energies Alternatives), Gif-sur-Yvette, France
[137] Santa Cruz Institute for Particle Physics, University of California Santa Cruz, Santa Cruz CA, United States
[138] Department of Physics, University of Washington, Seattle WA, United States
[139] Department of Physics and Astronomy, University of Sheffield, Sheffield, United Kingdom
[140] Department of Physics, Shinshu University, Nagano, Japan
[141] Fachbereich Physik, Universität Siegen, Siegen, Germany
[142] Department of Physics, Simon Fraser University, Burnaby BC, Canada
[143] SLAC National Accelerator Laboratory, Stanford CA, United States
[144] [(a)] Faculty of Mathematics, Physics & Informatics, Comenius University, Bratislava; [(b)] Department of Subnuclear Physics, Institute of Experimental Physics of the Slovak Academy of Sciences, Kosice, Slovak Republic
[145] [(a)] Department of Physics, University of Cape Town, Cape Town; [(b)] Department of Physics, University of Johannesburg, Johannesburg; [(c)] School of Physics, University of the Witwatersrand, Johannesburg, South Africa
[146] [(a)] Department of Physics, Stockholm University; [(b)] The Oskar Klein Centre, Stockholm, Sweden
[147] Physics Department, Royal Institute of Technology, Stockholm, Sweden
[148] Departments of Physics & Astronomy and Chemistry, Stony Brook University, Stony Brook NY, United States
[149] Department of Physics and Astronomy, University of Sussex, Brighton, United Kingdom
[150] School of Physics, University of Sydney, Sydney, Australia
[151] Institute of Physics, Academia Sinica, Taipei, Taiwan
[152] Department of Physics, Technion: Israel Institute of Technology, Haifa, Israel
[153] Raymond and Beverly Sackler School of Physics and Astronomy, Tel Aviv University, Tel Aviv, Israel
[154] Department of Physics, Aristotle University of Thessaloniki, Thessaloniki, Greece
[155] International Center for Elementary Particle Physics and Department of Physics, The University of Tokyo, Tokyo, Japan
[156] Graduate School of Science and Technology, Tokyo Metropolitan University, Tokyo, Japan
[157] Department of Physics, Tokyo Institute of Technology, Tokyo, Japan
[158] Department of Physics, University of Toronto, Toronto ON, Canada
[159] [(a)] TRIUMF, Vancouver BC; [(b)] Department of Physics and Astronomy, York University, Toronto ON, Canada
[160] Faculty of Pure and Applied Sciences, and Center for Integrated Research in Fundamental Science and Engineering, University of Tsukuba, Tsukuba, Japan
[161] Department of Physics and Astronomy, Tufts University, Medford MA, United States
[162] Department of Physics and Astronomy, University of California Irvine, Irvine CA, United States
[163] [(a)] INFN Gruppo Collegato di Udine, Sezione di Trieste, Udine; [(b)] ICTP, Trieste; [(c)] Dipartimento di Chimica, Fisica e Ambiente, Università di Udine, Udine, Italy
[164] Department of Physics and Astronomy, University of Uppsala, Uppsala, Sweden
[165] Department of Physics, University of Illinois, Urbana IL, United States
[166] Instituto de Fisica Corpuscular (IFIC) and Departamento de Fisica Atomica, Molecular y Nuclear and Departamento de Ingeniería Electrónica and Instituto de Microelectrónica de Barcelona (IMB-CNM), University of Valencia and CSIC, Valencia, Spain
[167] Department of Physics, University of British Columbia, Vancouver BC, Canada
[168] Department of Physics and Astronomy, University of Victoria, Victoria BC, Canada
[169] Department of Physics, University of Warwick, Coventry, United Kingdom
[170] Waseda University, Tokyo, Japan
[171] Department of Particle Physics, The Weizmann Institute of Science, Rehovot, Israel
[172] Department of Physics, University of Wisconsin, Madison WI, United States
[173] Fakultät für Physik und Astronomie, Julius-Maximilians-Universität, Würzburg, Germany
[174] Fakultät für Mathematik und Naturwissenschaften, Fachgruppe Physik, Bergische Universität Wuppertal, Wuppertal, Germany
[175] Department of Physics, Yale University, New Haven CT, United States
[176] Yerevan Physics Institute, Yerevan, Armenia
[177] Centre de Calcul de l'Institut National de Physique Nucléaire et de Physique des Particules (IN2P3), Villeurbanne, France

[a] Also at Department of Physics, King's College London, London, United Kingdom.
[b] Also at Institute of Physics, Azerbaijan Academy of Sciences, Baku, Azerbaijan.
[c] Also at Novosibirsk State University, Novosibirsk, Russia.
[d] Also at TRIUMF, Vancouver BC, Canada.
[e] Also at Department of Physics & Astronomy, University of Louisville, Louisville, KY, United States of America.
[f] Also at Department of Physics, California State University, Fresno CA, United States of America.
[g] Also at Department of Physics, University of Fribourg, Fribourg, Switzerland.
[h] Also at Departament de Fisica de la Universitat Autonoma de Barcelona, Barcelona, Spain.
[i] Also at Departamento de Fisica e Astronomia, Faculdade de Ciencias, Universidade do Porto, Portugal.
[j] Also at Tomsk State University, Tomsk, Russia.
[k] Also at Universita di Napoli Parthenope, Napoli, Italy.
[l] Also at Institute of Particle Physics (IPP), Canada.
[m] Also at National Institute of Physics and Nuclear Engineering, Bucharest, Romania.
[n] Also at Department of Physics, St. Petersburg State Polytechnical University, St. Petersburg, Russia.
[o] Also at Department of Physics, The University of Michigan, Ann Arbor MI, United States of America.
[p] Also at Centre for High Performance Computing, CSIR Campus, Rosebank, Cape Town, South Africa.
[q] Also at Louisiana Tech University, Ruston LA, United States of America.
[r] Also at Institucio Catalana de Recerca i Estudis Avancats, ICREA, Barcelona, Spain.
[s] Also at Graduate School of Science, Osaka University, Osaka, Japan.
[t] Also at Department of Physics, National Tsing Hua University, Taiwan.
[u] Also at Institute for Mathematics, Astrophysics and Particle Physics, Radboud University Nijmegen/Nikhef, Nijmegen, Netherlands.
[v] Also at Department of Physics, The University of Texas at Austin, Austin TX, United States of America.
[w] Also at Institute of Theoretical Physics, Ilia State University, Tbilisi, Georgia.
[x] Also at CERN, Geneva, Switzerland.
[y] Also at Georgian Technical University (GTU), Tbilisi, Georgia.
[z] Also at Ochadai Academic Production, Ochanomizu University, Tokyo, Japan.
[aa] Also at Manhattan College, New York NY, United States of America.
[ab] Also at Hellenic Open University, Patras, Greece.

[ac] Also at Academia Sinica Grid Computing, Institute of Physics, Academia Sinica, Taipei, Taiwan.
[ad] Also at School of Physics, Shandong University, Shandong, China.
[ae] Also at Moscow Institute of Physics and Technology State University, Dolgoprudny, Russia.
[af] Also at Section de Physique, Université de Genève, Geneva, Switzerland.
[ag] Also at Eotvos Lorand University, Budapest, Hungary.
[ah] Also at International School for Advanced Studies (SISSA), Trieste, Italy.
[ai] Also at Department of Physics and Astronomy, University of South Carolina, Columbia SC, United States of America.
[aj] Also at School of Physics and Engineering, Sun Yat-sen University, Guangzhou, China.
[ak] Also at Institute for Nuclear Research and Nuclear Energy (INRNE) of the Bulgarian Academy of Sciences, Sofia, Bulgaria.
[al] Also at Faculty of Physics, M.V. Lomonosov Moscow State University, Moscow, Russia.
[am] Also at Institute of Physics, Academia Sinica, Taipei, Taiwan.
[an] Also at National Research Nuclear University MEPhI, Moscow, Russia.
[ao] Also at Department of Physics, Stanford University, Stanford CA, United States of America.
[ap] Also at Institute for Particle and Nuclear Physics, Wigner Research Centre for Physics, Budapest, Hungary.
[aq] Also at Flensburg University of Applied Sciences, Flensburg, Germany.
[ar] Also at University of Malaya, Department of Physics, Kuala Lumpur, Malaysia.
[as] Also at CPPM, Aix-Marseille Université and CNRS/IN2P3, Marseille, France.
[at] Also affiliated with PKU-CHEP.
[*] Deceased.

Eur. Phys. J. C (2016) 76:653
DOI 10.1140/epjc/s10052-016-4466-1

THE EUROPEAN PHYSICAL JOURNAL C

Regular Article - Experimental Physics

Luminosity determination in pp collisions at $\sqrt{s} = 8$ TeV using the ATLAS detector at the LHC

ATLAS Collaboration*

CERN, 1211 Geneva 23, Switzerland

Received: 16 August 2016 / Accepted: 26 October 2016

Abstract The luminosity determination for the ATLAS detector at the LHC during pp collisions at $\sqrt{s} = 8$ TeV in 2012 is presented. The evaluation of the luminosity scale is performed using several luminometers, and comparisons between these luminosity detectors are made to assess the accuracy, consistency and long-term stability of the results. A luminosity uncertainty of $\delta\mathcal{L}/\mathcal{L} = \pm 1.9\%$ is obtained for the 22.7 fb^{-1} of pp collision data delivered to ATLAS at $\sqrt{s} = 8$ TeV in 2012.

1 Introduction

An accurate measurement of the delivered luminosity is a key component of the ATLAS [1] physics programme. For cross-section measurements, the uncertainty in the delivered luminosity is often one of the major systematic uncertainties. Searches for, and eventual discoveries of, physical phenomena beyond the Standard Model also rely on accurate information about the delivered luminosity to evaluate background levels and determine sensitivity to the signatures of new phenomena.

This paper describes the measurement of the luminosity delivered to the ATLAS detector at the LHC in pp collisions at a centre-of-mass energy of $\sqrt{s} = 8$ TeV during 2012. It is structured as follows. The strategy for measuring and calibrating the luminosity is outlined in Sect. 2, followed in Sect. 3 by a brief description of the detectors and algorithms used for luminosity determination. The absolute calibration of these algorithms by the van der Meer (*vdM*) method [2], which must be carried out under specially tailored beam conditions, is described in Sect. 4; the associated systematic uncertainties are detailed in Sect. 5. The comparison of the relative response of several independent luminometers during physics running reveals that significant time- and rate-dependent effects impacted the performance of the ATLAS bunch-by-bunch luminometers during the 2012 run (Sect. 6). Therefore this absolute *vdM* calibration cannot be invoked as is. Instead, it must be transferred, at one point in time and using an independent relative-luminosity monitor, from the low-luminosity regime of *vdM* scans to the high-luminosity conditions typical of routine physics running. Additional corrections must be applied over the course of the 2012 data-taking period to compensate for detector aging (Sect. 7). The various contributions to the systematic uncertainty affecting the integrated luminosity delivered to ATLAS in 2012 are recapitulated in Sect. 8, and the final results are summarized in Sect. 9.

* e-mail: atlas.publications@cern.ch

2 Luminosity-determination methodology

The analysis presented in this paper closely parallels, and where necessary expands, the one used to determine the luminosity in pp collisions at $\sqrt{s} = 7$ TeV [3].

The bunch luminosity $\mathcal{L}_\mathrm{b}$ produced by a single pair of colliding bunches can be expressed as

$$\mathcal{L}_\mathrm{b} = \frac{\mu f_\mathrm{r}}{\sigma_\mathrm{inel}}, \tag{1}$$

where the pile-up parameter μ is the average number of inelastic interactions per bunch crossing, f_r is the bunch revolution frequency, and σ_inel is the pp inelastic cross-section. The total instantaneous luminosity is given by

$$\mathcal{L} = \sum_{\mathrm{b}=1}^{n_\mathrm{b}} \mathcal{L}_\mathrm{b} = n_\mathrm{b} \langle \mathcal{L}_\mathrm{b} \rangle = n_\mathrm{b} \frac{\langle \mu \rangle f_\mathrm{r}}{\sigma_\mathrm{inel}}.$$

Here the sum runs over the n_b bunch pairs colliding at the interaction point (IP), $\langle \mathcal{L}_\mathrm{b} \rangle$ is the mean bunch luminosity and $\langle \mu \rangle$ is the bunch-averaged pile-up parameter. Table 1 highlights the operational conditions of the LHC during Run 1 from 2010 to 2012. Compared to previous years, operating conditions did not vary significantly during 2012, with typically 1368 bunches colliding and a peak instantaneous luminosity delivered by the LHC at the start of a fill of

Published online: 28 November 2016

Table 1 Selected LHC parameters for pp collisions at $\sqrt{s} = 7$ TeV in 2010 and 2011, and at $\sqrt{s} = 8$ TeV in 2012. Values shown are representative of the best accelerator performance during normal physics operation

Parameter	2010	2011	2012
Number of bunch pairs colliding (n_b)	348	1331	1380
Bunch spacing (ns)	150	50	50
Typical bunch population (10^{11} protons)	0.9	1.2	1.7
Peak luminosity $\mathcal{L}_{\text{peak}}$ ($10^{33}\,\text{cm}^{-2}\,\text{s}^{-1}$)	0.2	3.6	7.7
Peak number of inelastic interactions per crossing	∼5	∼20	∼40
Average number of interactions per crossing (luminosity weighted)	∼2	∼9	∼21
Total integrated luminosity delivered	$47\,\text{pb}^{-1}$	$5.5\,\text{fb}^{-1}$	$23\,\text{fb}^{-1}$

$\mathcal{L}_{\text{peak}} \approx 6\text{–}8 \times 10^{33}\,\text{cm}^{-2}\,\text{s}^{-1}$, on the average three times higher than in 2011.

ATLAS monitors the delivered luminosity by measuring μ_{vis}, the visible interaction rate per bunch crossing, with a variety of independent detectors and using several different algorithms (Sect. 3). The bunch luminosity can then be written as

$$\mathcal{L}_{\text{b}} = \frac{\mu_{\text{vis}}\, f_{\text{r}}}{\sigma_{\text{vis}}}, \tag{2}$$

where $\mu_{\text{vis}} = \varepsilon\,\mu$, ε is the efficiency of the detector and algorithm under consideration, and the visible cross-section for that same detector and algorithm is defined by $\sigma_{\text{vis}} \equiv \varepsilon\,\sigma_{\text{inel}}$. Since μ_{vis} is a directly measurable quantity, the calibration of the luminosity scale for a particular detector and algorithm amounts to determining the visible cross-section σ_{vis}. This calibration, described in detail in Sect. 4, is performed using dedicated beam-separation scans, where the absolute luminosity can be inferred from direct measurements of the beam parameters [2,4]. This known luminosity is then combined with the simultaneously measured interaction rate μ_{vis} to extract σ_{vis}.

A fundamental ingredient of the ATLAS strategy to assess and control the systematic uncertainties affecting the absolute luminosity determination is to compare the measurements of several luminometers, most of which use more than one algorithm to determine the luminosity. These multiple detectors and algorithms are characterized by significantly different acceptance, response to pile-up, and sensitivity to instrumental effects and to beam-induced backgrounds. Since the calibration of the absolute luminosity scale is carried out only two or three times per year, this calibration must either remain constant over extended periods of time and under different machine conditions, or be corrected for long-term drifts. The level of consistency across the various methods, over the full range of luminosities and beam conditions, and across many months of LHC operation, provides a direct test of the accuracy and stability of the results. A full discussion of the systematic uncertainties is presented in Sects. 5–8.

The information needed for physics analyses is the integrated luminosity for some well-defined data samples. The basic time unit for storing ATLAS luminosity information for physics use is the luminosity block (LB). The boundaries of each LB are defined by the ATLAS central trigger processor (CTP), and in general the duration of each LB is approximately one minute. Configuration changes, such as a trigger prescale adjustment, prompt a luminosity-block transition, and data are analysed assuming that each luminosity block contains data taken under uniform conditions, including luminosity. For each LB, the instantaneous luminosity from each detector and algorithm, averaged over the luminosity block, is stored in a relational database along with a variety of general ATLAS data-quality information. To define a data sample for physics, quality criteria are applied to select LBs where conditions are acceptable; then the instantaneous luminosity in that LB is multiplied by the LB duration to provide the integrated luminosity delivered in that LB. Additional corrections can be made for trigger deadtime and trigger prescale factors, which are also recorded on a per-LB basis. Adding up the integrated luminosity delivered in a specific set of luminosity blocks provides the integrated luminosity of the entire data sample.

3 Luminosity detectors and algorithms

The ATLAS detector is discussed in detail in Ref. [1]. The two primary luminometers, the BCM (Beam Conditions Monitor) and LUCID (LUminosity measurement using a Cherenkov Integrating Detector), both make deadtime-free, bunch-by-bunch luminosity measurements (Sect. 3.1). These are compared with the results of the track-counting method (Sect. 3.2), a new approach developed by ATLAS which monitors the multiplicity of charged particles produced in randomly selected colliding-bunch crossings, and is essential to assess the calibration-transfer correction from the *vdM* to the high-luminosity regime. Additional methods have been developed to disentangle the relative long-term drifts and run-to-run variations between the BCM, LUCID and track-counting measurements during high-luminosity running, thereby reducing the associated systematic uncertain-

ties to the sub-percent level. These techniques measure the total instantaneous luminosity, summed over all bunches, by monitoring detector currents sensitive to average particle fluxes through the ATLAS calorimeters, or by reporting fluences observed in radiation-monitoring equipment; they are described in Sect. 3.3.

3.1 Dedicated bunch-by-bunch luminometers

The BCM consists of four $8 \times 8\,\mathrm{mm}^2$ diamond sensors arranged around the beampipe in a cross pattern at $z = \pm 1.84\,\mathrm{m}$ on each side of the ATLAS IP.[1] If one of the sensors produces a signal over a preset threshold, a *hit* is recorded for that bunch crossing, thereby providing a low-acceptance bunch-by-bunch luminosity signal at $|\eta| = 4.2$ with sub-nanosecond time resolution. The horizontal and vertical pairs of BCM sensors are read out separately, leading to two luminosity measurements labelled BCMH and BCMV respectively. Because the thresholds, efficiencies and noise levels may exhibit small differences between BCMH and BCMV, these two measurements are treated for calibration and monitoring purposes as being produced by independent devices, although the overall response of the two devices is expected to be very similar.

LUCID is a Cherenkov detector specifically designed to measure the luminosity in ATLAS. Sixteen aluminium tubes originally filled with C_4F_{10} gas surround the beampipe on each side of the IP at a distance of 17 m, covering the pseudorapidity range $5.6 < |\eta| < 6.0$. For most of 2012, the LUCID tubes were operated under vacuum to reduce the sensitivity of the device, thereby mitigating pile-up effects and providing a wider operational dynamic range. In this configuration, Cherenkov photons are produced only in the quartz windows that separate the gas volumes from the photomultiplier tubes (PMTs) situated at the back of the detector. If one of the LUCID PMTs produces a signal over a preset threshold, that tube records a hit for that bunch crossing.

Each colliding-bunch pair is identified numerically by a bunch-crossing identifier (BCID) which labels each of the 3564 possible 25 ns slots in one full revolution of the nominal LHC fill pattern. Both BCM and LUCID are fast detectors with electronics capable of reading out the diamond-sensor and PMT hit patterns separately for each bunch crossing, thereby making full use of the available statistics. These FPGA-based front-end electronics run autonomously from the main data acquisition system, and are not affected by any deadtime imposed by the CTP.[2] They execute in real time several different online algorithms, characterized by diverse efficiencies, background sensitivities, and linearity characteristics [5].

The BCM and LUCID detectors consist of two symmetric arms placed in the forward ("A") and backward ("C") direction from the IP, which can also be treated as independent devices. The baseline luminosity algorithm is an inclusive hit requirement, known as the EventOR algorithm, which requires that at least one hit be recorded anywhere in the detector considered. Assuming that the number of interactions in a bunch crossing obeys a Poisson distribution, the probability of observing an event which satisfies the EventOR criteria can be computed as

$$P_{\text{EventOR}}\left(\mu_{\text{vis}}^{\text{OR}}\right) = N_{\text{OR}}/N_{\text{BC}} = 1 - \mathrm{e}^{-\mu_{\text{vis}}^{\text{OR}}}. \tag{3}$$

Here the raw event count N_{OR} is the number of bunch crossings, during a given time interval, in which at least one pp interaction satisfies the event-selection criteria of the OR algorithm under consideration, and N_{BC} is the total number of bunch crossings during the same interval. Solving for μ_{vis} in terms of the event-counting rate yields

$$\mu_{\text{vis}}^{\text{OR}} = -\ln\left(1 - \tfrac{N_{\text{OR}}}{N_{\text{BC}}}\right). \tag{4}$$

When $\mu_{\text{vis}} \gg 1$, event counting algorithms lose sensitivity as fewer and fewer bunch crossings in a given time interval report zero observed interactions. In the limit where $N_{\text{OR}}/N_{\text{BC}} = 1$, event counting algorithms can no longer be used to determine the interaction rate μ_{vis}: this is referred to as *saturation*. The sensitivity of the LUCID detector is high enough (even without gas in the tubes) that the LUCID_EventOR algorithm saturates in a one-minute interval at around 20 interactions per crossing, while the single-arm inclusive LUCID_EventA and LUCID_EventC algorithms can be used up to around 30 interactions per crossing. The lower acceptance of the BCM detector allowed event counting to remain viable for all of 2012.

3.2 Tracker-based luminosity algorithms

The ATLAS inner detector (ID) measures the trajectories of charged particles over the pseudorapidity range $|\eta| < 2.5$ and the full azimuth. It consists [1] of a silicon pixel detector (Pixel), a silicon micro-strip detector (SCT) and a straw-tube transition-radiation detector (TRT). Charged particles are reconstructed as tracks using an inside-out algorithm,

[1] ATLAS uses a right-handed coordinate system with its origin at the nominal interaction point in the centre of the detector, and the z-axis along the beam line. The x-axis points from the IP to the centre of the LHC ring, and the y-axis points upwards. Cylindrical coordinates (r, ϕ) are used in the transverse plane, ϕ being the azimuthal angle around the beam line. The pseudorapidity is defined in terms of the polar angle θ as $\eta = -\ln\tan(\theta/2)$.

[2] The CTP inhibits triggers (causing deadtime) for a variety of reasons, but especially for several bunch crossings after a triggered event to allow time for the detector readout to conclude. Any new triggers which occur during this time are ignored.

which starts with three-point seeds from the silicon detectors and then adds hits using a combinatoric Kalman filter [6].

The luminosity is assumed to be proportional to the number of reconstructed charged-particle tracks, with the visible interaction rate μ_{vis} taken as the number of tracks per bunch crossing averaged over a given time window (typically a luminosity block). In standard physics operation, silicon-detector data are recorded in a dedicated partial-event stream using a random trigger at a typical rate of 100 Hz, sampling each colliding-bunch pair with equal probability. Although a bunch-by-bunch luminosity measurement is possible in principle, over 1300 bunches were colliding in ATLAS for most of 2012, so that in practice only the bunch-integrated luminosity can be determined with percent-level statistical precision in a given luminosity block. During *vdM* scans, Pixel and SCT data are similarly routed to a dedicated data stream for a subset of the colliding-bunch pairs at a typical rate of 5 kHz per BCID, thereby allowing the bunch-by-bunch determination of σ_{vis}.

For the luminosity measurements presented in this paper, charged-particle track reconstruction uses hits from the silicon detectors only. Reconstructed tracks are required to have at least nine silicon hits, zero holes[3] in the Pixel detector and transverse momentum in excess of 0.9 GeV. Furthermore, the absolute transverse impact parameter with respect to the luminous centroid [7] is required to be no larger than seven times its uncertainty, as determined from the covariance matrix of the fit.

This default track selection makes no attempt to distinguish tracks originating from primary vertices from those produced in secondary interactions, as the yields of both are expected to be proportional to the luminosity. Previous studies of track reconstruction in ATLAS show that in low pile-up conditions ($\mu \leq 1$) and with a track selection looser than the above-described default, single-beam backgrounds remain well below the per-mille level [8]. However, for pile-up parameters typical of 2012 physics running, tracks formed from random hit combinations, known as *fake tracks*, can become significant [9]. The track selection above is expected to be robust against such non-linearities, as demonstrated by analysing simulated events of overlaid inelastic pp interactions produced using the PYTHIA 8 Monte Carlo event generator [10]. In the simulation, the fraction of fake tracks per event can be parameterized as a function of the true pile-up parameter, yielding a fake-track fraction of less than 0.2% at $\mu = 20$ for the default track selection. In data, this fake-track contamination is subtracted from the measured track multiplicity using the simulation-based parameterization with, as input, the $\langle\mu\rangle$ value reported by the BCMH_EventOR luminosity algorithm. An uncertainty equal to half the correction is assigned to the measured track multiplicity to account for possible systematic differences between data and simulation.

Biases in the track-counting luminosity measurement can arise from μ-dependent effects in the track reconstruction or selection requirements, which would change the reported track-counting yield per collision between the low pile-up *vdM*-calibration regime and the high-μ regime typical of physics data-taking. Short- and long-term variations in the track reconstruction and selection efficiency can also arise from changing ID conditions, for example because of temporarily disabled silicon readout modules. In general, looser track selections are less sensitive to such fluctuations in instrumental coverage; however, they typically suffer from larger fake-track contamination.

To assess the impact of such potential biases, several looser track selections, or *working points* (WP), are investigated. Most are found to be consistent with the default working point once the uncertainty affecting the simulation-based fake-track subtraction is accounted for. In the case where the Pixel-hole requirement is relaxed from zero to no more than one, a moderate difference in excess of the fake-subtraction uncertainty is observed in the data. This working point, labelled "Pixel holes $\leq$1", is used as an alternative algorithm when evaluating the systematic uncertainties associated with track-counting luminosity measurements.

In order to all but eliminate fake-track backgrounds and minimize the associated μ-dependence, another alternative is to remove the impact-parameter requirement and use the resulting superset of tracks as input to the primary-vertex reconstruction algorithm. Those tracks which, after the vertex-reconstruction fit, have a non-negligible probability of being associated to any primary vertex are counted to provide an alternative luminosity measurement. In the simulation, the performance of this "vertex-associated" working point is comparable, in terms of fake-track fraction and other residual non-linearities, to that of the default and "Pixel holes $\leq$1" track selections discussed above.

3.3 Bunch-integrating detectors

Additional algorithms, sensitive to the instantaneous luminosity summed over all bunches, provide relative-luminosity monitoring on time scales of a few seconds rather than of a bunch crossing, allowing independent checks of the linearity and long-term stability of the BCM, LUCID and track-counting algorithms. The first technique measures the particle flux from pp collisions as reflected in the current drawn by the PMTs of the hadronic calorimeter (TileCal). This flux, which is proportional to the instantaneous luminosity, is also monitored by the total ionization current flowing through a

[3] In this context, a hole is counted when a hit is expected in an active sensor located on the track trajectory between the first and the last hit associated with this track, but no such hit is found. If the corresponding sensor is known to be inactive and therefore not expected to provide a hit, no hole is counted.

well-chosen set of liquid-argon (LAr) calorimeter cells. A third technique, using Medipix radiation monitors, measures the average particle flux observed in these devices.

3.3.1 Photomultiplier currents in the central hadronic calorimeter

The TileCal [11] is constructed from plastic-tile scintillators as the active medium and from steel absorber plates. It covers the pseudorapidity range $|\eta| < 1.7$ and consists of a long central cylindrical barrel and two smaller extended barrels, one on each side of the long barrel. Each of these three cylinders is divided azimuthally into 64 modules and segmented into three radial sampling layers. Cells are defined in each layer according to a projective geometry, and each cell is connected by optical fibres to two photomultiplier tubes. The current drawn by each PMT is proportional to the total number of particles interacting in a given TileCal cell, and provides a signal proportional to the luminosity summed over all the colliding bunches. This current is monitored by an integrator system with a time constant of 10 ms and is sensitive to currents from 0.1 nA to 1.2 μA. The calibration and the monitoring of the linearity of the integrator electronics are ensured by a dedicated high-precision current-injection system.

The collision-induced PMT current depends on the pseudorapidity of the cell considered and on the radial sampling in which it is located. The cells most sensitive to luminosity variations are located near $|\eta| \approx 1.25$; at a given pseudorapidity, the current is largest in the innermost sampling layer, because the hadronic showers are progressively absorbed as they expand in the middle and outer radial layers. Long-term variations of the TileCal response are monitored, and corrected if appropriate [3], by injecting a laser pulse directly into the PMT, as well as by integrating the counting rate from a ^{137}Cs radioactive source that circulates between the calorimeter cells during calibration runs.

The TileCal luminosity measurement is not directly calibrated by the *vdM* procedure, both because its slow and asynchronous readout is not optimized to keep in step with the scan protocol, and because the luminosity is too low during the scan for many of its cells to provide accurate measurements. Instead, the TileCal luminosity calibration is performed in two steps. The PMT currents, corrected for electronics pedestals and for non-collision backgrounds[4] and averaged over the most sensitive cells, are first cross-calibrated to the absolute luminosity reported by the BCM during the April 2012 *vdM* scan session (Sect. 4). Since these high-sensitivity cells would incur radiation damage at the highest luminosities encountered during 2012, thereby requiring large calibration corrections, their luminosity scale is transferred, during an early intermediate-luminosity run and on a cell-by-cell basis, to the currents measured in the remaining cells (the sensitivities of which are insufficient under the low-luminosity conditions of *vdM* scans). The luminosity reported in any other physics run is then computed as the average, over the usable cells, of the individual cell luminosities, determined by multiplying the baseline-subtracted PMT current from that cell by the corresponding calibration constant.

3.3.2 LAr-gap currents

The electromagnetic endcap (EMEC) and forward (FCal) calorimeters are sampling devices that cover the pseudorapidity ranges of, respectively, $1.5 < |\eta| < 3.2$ and $3.2 < |\eta| < 4.9$. They are housed in the two endcap cryostats along with the hadronic endcap calorimeters.

The EMECs consist of accordion-shaped lead/stainless-steel absorbers interspersed with honeycomb-insulated electrodes that distribute the high voltage (HV) to the LAr-filled gaps where the ionization electrons drift, and that collect the associated electrical signal by capacitive coupling. In order to keep the electric field across each LAr gap constant over time, the HV supplies are regulated such that any voltage drop induced by the particle flux through a given HV sector is counterbalanced by a continuous injection of electrical current. The value of this current is proportional to the particle flux and thereby provides a relative-luminosity measurement using the EMEC HV line considered.

Both forward calorimeters are divided longitudinally into three modules. Each of these consists of a metallic absorber matrix (copper in the first module, tungsten elsewhere) containing cylindrical electrodes arranged parallel to the beam axis. The electrodes are formed by a copper (or tungsten) tube, into which a rod of slightly smaller diameter is inserted. This rod, in turn, is positioned concentrically using a helically wound radiation-hard plastic fibre, which also serves to electrically isolate the anode rod from the cathode tube. The remaining small annular gap is filled with LAr as the active medium. Only the first sampling is used for luminosity measurements. It is divided into 16 azimuthal sectors, each fed by 4 independent HV lines. As in the EMEC, the HV system provides a stable electric field across the LAr gaps and the current drawn from each line is directly proportional to the average particle flux through the corresponding FCal cells.

After correction for electronic pedestals and single-beam backgrounds, the observed currents are assumed to be proportional to the luminosity summed over all bunches; the validity of this assumption is assessed in Sect. 6. The EMEC and FCal gap currents cannot be calibrated during a *vdM* scan, because the instantaneous luminosity during these scans remains below the sensitivity of the current-measurement

[4] For each LHC fill, the currents are baseline-corrected using data recorded shortly before the LHC beams are brought into collision.

circuitry. Instead, the calibration constant associated with an individual HV line is evaluated as the ratio of the absolute luminosity reported by the baseline bunch-by-bunch luminosity algorithm (BCMH_EventOR) and integrated over one high-luminosity reference physics run, to the HV current drawn through that line, pedestal-subtracted and integrated over exactly the same time interval. This is done for each usable HV line independently. The luminosity reported in any other physics run by either the EMEC or the FCal, separately for the A and C detector arms, is then computed as the average, over the usable cells, of the individual HV-line luminosities.

3.3.3 Hit counting in the Medipix system

The Medipix (MPX) detectors are hybrid silicon pixel devices, which are distributed around the ATLAS detector [12] and are primarily used to monitor radiation conditions in the experimental hall. Each of these 12 devices consists of a 2 cm^2 silicon sensor matrix, segmented in 256×256 cells and bump-bonded to a readout chip. Each pixel in the matrix counts hits from individual particle interactions observed during a software-triggered "frame", which integrates over 5–120 s, depending upon the typical particle flux at the location of the detector considered. In order to provide calibrated luminosity measurements, the total number of pixel clusters observed in each sensor is counted and scaled to the TileCal luminosity in the same reference run as the EMEC and FCal. The six MPX detectors with the highest counting rate are analysed in this fashion for the 2012 running period; their mutual consistency is discussed in Sect. 6.

The hit-counting algorithm described above is primarily sensitive to charged particles. The MPX detectors offer the additional capability to detect thermal neutrons via $^6\mathrm{Li}(n,\alpha)^3\mathrm{H}$ reactions in a ^{6}LiF converter layer. This neutron-counting rate provides a further measure of the luminosity, which is consistent with, but statistically inferior to, the MPX hit counting measurement [12].

4 Absolute luminosity calibration by the van der Meer method

In order to use the measured interaction rate μ_{vis} as a luminosity monitor, each detector and algorithm must be calibrated by determining its visible cross-section σ_{vis}. The primary calibration technique to determine the absolute luminosity scale of each bunch-by-bunch luminosity detector and algorithm employs dedicated *vdM* scans to infer the delivered luminosity at one point in time from the measurable parameters of the colliding bunches. By comparing the known luminosity delivered in the *vdM* scan to the visible interaction rate μ_{vis}, the visible cross-section can be determined from Eq. (2).

This section is organized as follows. The formalism of the van der Meer method is recalled in Sect. 4.1, followed in Sect. 4.2 by a description of the *vdM*-calibration datasets collected during the 2012 running period. The step-by-step determination of the visible cross-section is outlined in Sect. 4.3, and each ingredient is discussed in detail in Sects. 4.4–4.10. The resulting absolute calibrations of the bunch-by-bunch luminometers, as applicable to the low-luminosity conditions of *vdM* scans, are summarized in Sect. 4.11.

4.1 Absolute luminosity from measured beam parameters

In terms of colliding-beam parameters, the bunch luminosity $\mathcal{L}_{\mathrm{b}}$ is given by

$$\mathcal{L}_{\mathrm{b}} = f_{\mathrm{r}}\, n_1 n_2 \int \hat{\rho}_1(x,y)\, \hat{\rho}_2(x,y)\, \mathrm{d}x\, \mathrm{d}y, \tag{5}$$

where the beams are assumed to collide with zero crossing angle, $n_1 n_2$ is the bunch-population product and $\hat{\rho}_{1(2)}(x,y)$ is the normalized particle density in the transverse (x–y) plane of beam 1 (2) at the IP. With the standard assumption that the particle densities can be factorized into independent horizontal and vertical component distributions, $\hat{\rho}(x,y) = \rho_x(x)\,\rho_y(y)$, Eq. (5) can be rewritten as

$$\mathcal{L}_{\mathrm{b}} = f_{\mathrm{r}}\, n_1 n_2\, \Omega_x(\rho_{x1},\rho_{x2})\, \Omega_y(\rho_{y1},\rho_{y2}), \tag{6}$$

where

$$\Omega_x(\rho_{x1},\rho_{x2}) = \int \rho_{x1}(x)\,\rho_{x2}(x)\,\mathrm{d}x$$

is the beam-overlap integral in the x direction (with an analogous definition in the y direction). In the method proposed by van der Meer [2], the overlap integral (for example in the x direction) can be calculated as

$$\Omega_x(\rho_{x1},\rho_{x2}) = \frac{R_x(0)}{\int R_x(\delta)\,\mathrm{d}\delta}, \tag{7}$$

where $R_x(\delta)$ is the luminosity (at this stage in arbitrary units) measured during a horizontal scan at the time the two beams are separated horizontally by the distance δ, and $\delta = 0$ represents the case of zero beam separation. Because the luminosity $R_x(\delta)$ is normalized to that at zero separation $R_x(0)$, any quantity proportional to the luminosity (such as μ_{vis}) can be substituted in Eq. (7) in place of R.

Defining the horizontal convolved beam size Σ_x [7,13] as

$$\Sigma_x = \frac{1}{\sqrt{2\pi}} \frac{\int R_x(\delta)\,\mathrm{d}\delta}{R_x(0)}, \tag{8}$$

and similarly for Σ_y, the bunch luminosity in Eq. (6) can be rewritten as

$$\mathcal{L}_{\mathrm{b}} = \frac{f_{\mathrm{r}} n_1 n_2}{2\pi\, \Sigma_x\, \Sigma_y}, \tag{9}$$

which allows the absolute bunch luminosity to be determined from the revolution frequency f_{r}, the bunch-population product $n_1 n_2$, and the product $\Sigma_x\, \Sigma_y$ which is measured directly during a pair of orthogonal *vdM* (beam-separation) scans. In the case where the luminosity curve $R_x(\delta)$ is Gaussian, Σ_x coincides with the standard deviation of that distribution. It is important to note that the *vdM* method does not rely on any particular functional form of $R_x(\delta)$: the quantities Σ_x and Σ_y can be determined for any observed luminosity curve from Eq. (8) and used with Eq. (9) to determine the absolute luminosity at $\delta = 0$.

In the more general case where the factorization assumption breaks down, i.e. when the particle densities [or more precisely the dependence of the luminosity on the beam separation (δ_x, δ_y)] cannot be factorized into a product of uncorrelated x and y components, the formalism can be extended to yield [4]

$$\Sigma_x\, \Sigma_y = \frac{1}{2\pi} \frac{\int R_{x,y}(\delta_x, \delta_y)\, \mathrm{d}\delta_x\, \mathrm{d}\delta_y}{R_{x,y}(0,0)}, \tag{10}$$

with Eq. (9) remaining formally unaffected. Luminosity calibration in the presence of non-factorizable bunch-density distributions is discussed extensively in Sect. 4.8.

The measured product of the transverse convolved beam sizes $\Sigma_x\, \Sigma_y$ is directly related to the reference specific luminosity:[5]

$$\mathcal{L}_{\mathrm{spec}} \equiv \frac{\mathcal{L}_{\mathrm{b}}}{n_1 n_2} = \frac{f_{\mathrm{r}}}{2\pi\, \Sigma_x\, \Sigma_y}$$

which, together with the bunch currents, determines the absolute luminosity scale. To calibrate a given luminosity algorithm, one can equate the absolute luminosity computed from beam parameters using Eq. (9) to that measured according to Eq. (2) to get

$$\sigma_{\mathrm{vis}} = \mu_{\mathrm{vis}}^{\mathrm{MAX}} \frac{2\pi\ \Sigma_x\, \Sigma_y}{n_1 n_2}, \tag{11}$$

where $\mu_{\mathrm{vis}}^{\mathrm{MAX}}$ is the visible interaction rate per bunch crossing reported at the peak of the scan curve by that particular algorithm. Equation (11) provides a direct calibration of the visible cross-section σ_{vis} for each algorithm in terms of the peak visible interaction rate $\mu_{\mathrm{vis}}^{\mathrm{MAX}}$, the product of the convolved beam widths $\Sigma_x\, \Sigma_y$, and the bunch-population product $n_1 n_2$.

In the presence of a significant crossing angle in one of the scan planes, the formalism becomes considerably more involved [14], but the conclusions remain unaltered and Eqs. (8)–(11) remain valid. The non-zero vertical crossing angle in some scan sessions widens the luminosity curve by a factor that depends on the bunch length, the transverse beam size and the crossing angle, but reduces the peak luminosity by the same factor. The corresponding increase in the measured value of Σ_y is exactly compensated by the decrease in $\mu_{\mathrm{vis}}^{\mathrm{MAX}}$, so that no correction for the crossing angle is needed in the determination of σ_{vis}.

4.2 Luminosity-scan datasets

The beam conditions during *vdM* scans are different from those in normal physics operation, with lower bunch intensities and only a few tens of widely spaced bunches circulating. These conditions are optimized to reduce various systematic uncertainties in the calibration procedure [7]. Three scan sessions were performed during 2012: in April, July, and November (Table 2). The April scans were performed with nominal collision optics ($\beta^\star = 0.6$ m), which minimizes the accelerator set-up time but yields conditions which are inadequate for achieving the best possible calibration accuracy.[6] The July and November scans were performed using dedicated *vdM*-scan optics with $\beta^\star = 11$ m, in order to increase the transverse beam sizes while retaining a sufficiently high collision rate even in the tails of the scans. This strategy limits the impact of the vertex-position resolution on the non-factorization analysis, which is detailed in Sect. 4.8, and also reduces potential μ-dependent calibration biases. In addition, the observation of large non-factorization effects in the April and July scan data motivated, for the November scan, a dedicated set-up of the LHC injector chain [16] to produce more Gaussian and less correlated transverse beam profiles.

Since the luminosity can be different for each colliding-bunch pair, both because the beam sizes differ from bunch to bunch and because the bunch populations n_1 and n_2 can each vary by up to $\pm 10\%$, the determination of Σ_x and Σ_y and the measurement of $\mu_{\mathrm{vis}}^{\mathrm{MAX}}$ are performed independently for each colliding-bunch pair. As a result, and taking the November session as an example, each scan set provides 29 independent measurements of σ_{vis}, allowing detailed consistency checks.

[5] The specific luminosity is defined as the luminosity per bunch and per unit bunch-population product [7].

[6] The β function describes the single-particle motion and determines the variation of the beam envelope along the beam trajectory. It is calculated from the focusing properties of the magnetic lattice (see for example Ref. [15]). The symbol $\beta^\star$ denotes the value of the β function at the IP.

Table 2 Summary of the main characteristics of the 2012 *vdM* scans performed at the ATLAS interaction point. The nominal tranverse beam size is computed using the nominal LHC emittance ($\epsilon_N = 3.75$ μm-radians). The actual transverse emittance and single-beam size are estimated by combining the convolved transverse widths measured in the first scan of each session with the nominal IP β-function. The values of the luminosity/bunch and of μ are given for zero beam separation during the first scan. The specific luminosity decreases by 6–17% over the duration of a given scan session

Scan labels	I–III	IV–IX	X–XV
Date	16 April 2012	19 July 2012	22, 24 November 2012
LHC fill number	2520	2855, 2856	3311, 3316
Total number of bunches per beam	48	48	39
Number of bunches colliding in ATLAS	35	35	29
Typical number of protons per bunch $n_{1,2}$	0.6×10^{11}	0.9×10^{11}	0.9×10^{11}
Nominal β-function at the IP ($\beta^\star$) (m)	0.6	11	11
Nominal transverse single-beam size σ_b^{nom} (μm)	23	98	98
Actual transverse emittance ϵ_N (μm-radians)	2.3	3.2	3.1
Actual transverse single-beam size σ_b (μm)	18	91	89
Actual transverse luminous size $\sigma_{\mathcal{L}}$ ($\approx \sigma_b/\sqrt{2}$) ($\mu$m)	13	65	63
Nominal vertical half crossing-angle (μrad)	$\pm$145	0	0
Typical luminosity/bunch ($\mu b^{-1}\,s^{-1}$)	0.8	0.09	0.09
Pile-up parameter μ (interactions/crossing)	5.2	0.6	0.6
Scan sequence	3 sets of centred $x + y$ scans (I–III)	4 sets of centred $x + y$ scans (IV–VI, VIII) plus 2 sets of $x + y$ off-axis scans (VII, IX)	4 sets of centred $x + y$ scans (X, XI, XIV, XV) plus 2 sets of $x + y$ off-axis scans (XII, XIII)
Total scan steps per plane	25	25 (sets IV–VII) 17 (sets VIII–IX)	25
Maximum beam separation	$\pm 6\sigma_b^{nom}$	$\pm 6\sigma_b^{nom}$	$\pm 6\sigma_b^{nom}$
Scan duration per step (s)	20	30	30

To further test the reproducibility of the calibration procedure, multiple centred-scan[7] sets, each consisting of one horizontal scan and one vertical scan, are executed in the same scan session. In November for instance, two sets of centred scans (X and XI) were performed in quick succession, followed by two sets of off-axis scans (XII and XIII), where the beams were separated by 340 and 200 μm respectively in the non-scanning direction. A third set of centred scans (XIV) was then performed as a reproducibility check. A fourth centred scan set (XV) was carried out approximately one day later in a different LHC fill.

The variation of the calibration results between individual scan sets in a given scan session is used to quantify the reproducibility of the optimal relative beam position, the convolved beam sizes, and the visible cross-sections. The reproducibility and consistency of the visible cross-section results across the April, July and November scan sessions provide a measure of the long-term stability of the response of each detector, and are used to assess potential systematic biases in the *vdM*-calibration technique under different accelerator conditions.

[7] A *centred* (or *on-axis*) beam-separation scan is one where the beams are kept centred on each other in the transverse direction orthogonal to the scan axis. An *offset* (or *off-axis*) scan is one where the beams are partially separated in the non-scanning direction.

4.3 *vdM*-scan analysis methodology

The 2012 *vdM* scans were used to derive calibrations for the LUCID_EventOR, BCM_EventOR and track-counting algorithms. Since there are two distinct BCM readouts, calibrations are determined separately for the horizontal (BCMH) and vertical (BCMV) detector pairs. Similarly, the fully inclusive (EventOR) and single-arm inclusive (EventA, EventC) algorithms are calibrated independently. For the April scan session, the dedicated track-counting event stream (Sect. 3.2) used the same random trigger as during physics operation. For the July and November sessions, where the typical event rate was lower by an order of magnitude, track counting was performed on events triggered by the ATLAS Minimum Bias Trigger Scintillator (MBTS) [1]. Corrections for MBTS trigger inefficiency and for CTP-induced deadtime are applied, at each scan step separately, when calculating the average number of tracks per event.

For each individual algorithm, the *vdM* data are analysed in the same manner. The specific visible interaction rate

$\mu_{\rm vis}/(n_1 n_2)$ is measured, for each colliding-bunch pair, as a function of the nominal beam separation (i.e. the separation specified by the LHC control system) in two orthogonal scan directions (x and y). The value of $\mu_{\rm vis}$ is determined from the raw counting rate using the formalism described in Sect. 3.1 or 3.2. The specific interaction rate is used so that the calculation of Σ_x and Σ_y properly takes into account the bunch-current variation during the scan; the measurement of the bunch-population product $n_1 n_2$ is detailed in Sect. 4.10.

Figure 1 shows examples of horizontal-scan curves measured for a single BCID using two different algorithms. At each scan step, the visible interaction rate $\mu_{\rm vis}$ is first corrected for afterglow, instrumental noise and beam-halo backgrounds as described in Sect. 4.4, and the nominal beam separation is rescaled using the calibrated beam-separation scale (Sect. 4.5). The impact of orbit drifts is addressed in Sect. 4.6, and that of beam–beam deflections and of the dynamic-β effect is discussed in Sect. 4.7. For each BCID and each scan independently, a characteristic function is fitted to the corrected data; the peak of the fitted function provides a measurement of $\mu_{\rm vis}^{\rm MAX}$, while the convolved width Σ is computed from the integral of the function using Eq. (8). Depending on the beam conditions, this function can be a single-Gaussian function plus a constant term, a double-Gaussian function plus a constant term, a Gaussian function times a polynomial (plus a constant term), or other variations. As described in Sect. 5, the differences between the results extracted using different characteristic functions are taken into account as a systematic uncertainty in the calibration result.

The combination of one horizontal (x) scan and one vertical (y) scan is the minimum needed to perform a measurement of $\sigma_{\rm vis}$. In principle, while the $\mu_{\rm vis}^{\rm MAX}$parameter is detector- and algorithm-specific, the convolved widths Σ_x and Σ_y, which together specify the head-on reference luminosity, do not need to be determined using that same detector and algorithm. In practice, it is convenient to extract all the parameters associated with a given algorithm consistently from a single set of scan curves, and the average value of $\mu_{\rm vis}^{\rm MAX}$ between the two scan planes is used. The correlations between the fitted values of $\mu_{\rm vis}^{\rm MAX}$, Σ_x and Σ_y are taken into account when evaluating the statistical uncertainty affecting $\sigma_{\rm vis}$.

Each BCID should yield the same measured $\sigma_{\rm vis}$ value, and so the average over all BCIDs is taken as the $\sigma_{\rm vis}$ measurement for the scan set under consideration. The bunch-to-bunch consistency of the visible cross-section for a given luminosity algorithm, as well as the level of agreement between Σ values measured by different detectors and algorithms in a given scan set, are discussed in Sect. 5 as part of the systematic uncertainty.

Once visible cross-sections have been determined from each scan set as described above, two beam-dynamical effects must be considered (and if appropriate corrected for), both associated with the shape of the colliding bunches in transverse phase space: non-factorization and emittance growth. These are discussed in Sects. 4.8 and 4.9 respectively.

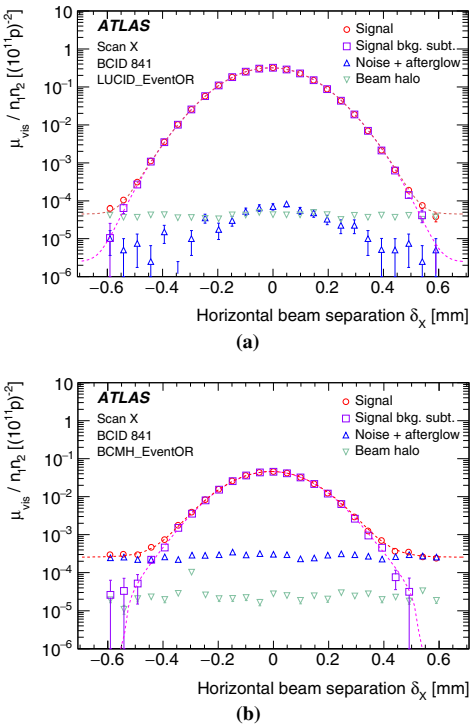

Fig. 1 Beam-separation dependence of the specific visible interaction rate measured using the **a** LUCID_EventOR and **b** BCMH_EventOR algorithms during horizontal scan X, before (*red circles*) and after (*purple squares*) afterglow, noise and single-beam background subtraction. The subtracted contributions are shown as triangles. The scan curves are fitted to a Gaussian function multiplied by a sixth-order polynomial, plus a constant

4.4 Background subtraction

The *vdM* calibration procedure is affected by three distinct background contributions to the luminosity signal: afterglow, instrumental noise, and single-beam backgrounds.

As detailed in Refs. [3,5], both the LUCID and BCM detectors observe some small activity in the BCIDs immediately following a collision, which in later BCIDs decays to a baseline value with several different time constants. This afterglow is most likely caused by photons from nuclear de-excitation, which in turn is induced by the hadronic cascades initiated by pp collision products. For a given bunch pat-

tern, the afterglow level is observed to be proportional to the luminosity in the colliding-bunch slots. During *vdM* scans, it lies three to four orders of magnitude below the luminosity signal, but reaches a few tenths of a percent during physics running because of the much denser bunch pattern.

Instrumental noise is, under normal circumstances, a few times smaller than the single-beam backgrounds, and remains negligible except at the largest beam separations. However, during a one-month period in late 2012 that includes the November *vdM* scans, the A arm of both BCM detectors was affected by high-rate electronic noise corresponding to about 0.5% (1%) of the visible interaction rate, at the peak of the scan, in the BCMH (BCMV) diamond sensors (Fig. 1b). This temporary perturbation, the cause of which could not be identified, disappeared a few days after the scan session. Nonetheless, it was large enough that a careful subtraction procedure had to be implemented in order for this noise not to bias the fit of the BCM luminosity-scan curves.

Since afterglow and instrumental noise both induce random hits at a rate that varies slowly from one BCID to the next, they are subtracted together from the raw visible interaction rate μ_{vis} in each colliding-bunch slot. Their combined magnitude is estimated using the rate measured in the immediately preceding bunch slot, assuming that the variation of the afterglow level from one bunch slot to the next can be neglected.

A third background contribution arises from activity correlated with the passage of a single beam through the detector. This activity is attributed to a combination of shower debris from beam–gas interactions and from beam-tail particles that populate the beam halo and impinge on the luminosity detectors in time with the circulating bunch. It is observed to be proportional to the bunch population, can differ slightly between beams 1 and 2, but is otherwise uniform for all bunches in a given beam. The total single-beam background in a colliding-bunch slot is estimated by measuring the single-beam rates in unpaired bunches (after subtracting the afterglow and noise as done for colliding-bunch slots), separately for beam 1 and beam 2, rescaling them by the ratio of the bunch populations in the unpaired and colliding bunches, and summing the contributions from the two beams. This background typically amounts to 2×10^{-4} (8×10^{-4}) of the luminosity at the peak of the scan for the LUCID (BCM) EventOR algorithms. Because it depends neither on the luminosity nor on the beam separation, it can become comparable to the actual luminosity in the tails of the scans.

4.5 Determination of the absolute beam-separation scale

Another key input to the *vdM* scan technique is the knowledge of the beam separation at each scan step. The ability to measure Σ depends upon knowing the absolute distance by which the beams are separated during the *vdM* scan, which is controlled by a set of closed orbit bumps[8] applied locally near the ATLAS IP. To determine this beam-separation scale, dedicated calibration measurements were performed close in time to the April and July scan sessions using the same optical configuration at the interaction point. Such length-scale scans are performed by displacing both beams transversely by five steps over a range of up to $\pm 3\sigma_{\mathrm{b}}^{\mathrm{nom}}$, at each step keeping the beams well centred on each other in the scanning plane. The actual displacement of the luminous region can then be measured with high accuracy using the primary-vertex position reconstructed by the ATLAS tracking detectors. Since each of the four bump amplitudes (two beams in two transverse directions) depends on different magnet and lattice functions, the length-scale calibration scans are performed so that each of these four calibration constants can be extracted independently. The July 2012 calibration data for the horizontal bump of beam 2 are presented in Fig. 2. The scale factor which relates the nominal beam displacement to the measured displacement of the luminous centroid is given by the slope of the fitted straight line; the intercept is irrelevant.

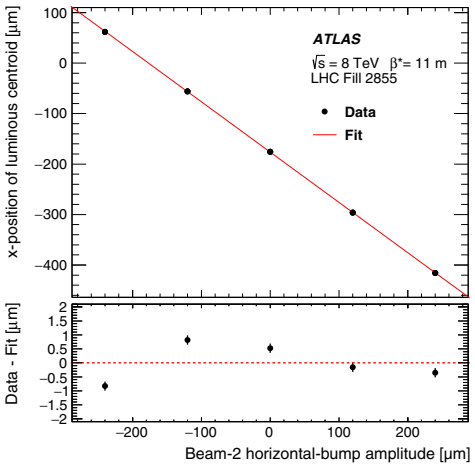

Fig. 2 Length-scale calibration scan for the x direction of beam 2. Shown is the measured displacement of the luminous centroid as a function of the expected displacement based on the corrector bump amplitude. The *line* is a linear fit to the data, and the residual is shown in the *bottom panel*. *Error bars* are statistical only

Since the coefficients relating magnet currents to beam displacements depend on the interaction-region optics, the absolute length scale depends on the $\beta^\star$ setting and must

[8] A closed orbit bump is a local distortion of the beam orbit that is implemented using pairs of steering dipoles located on either side of the affected region. In this particular case, these bumps are tuned to offset the trajectory of either beam parallel to itself at the IP, in either the horizontal or the vertical direction.

Table 3 Length-scale calibrations at the ATLAS interaction point at $\sqrt{s} = 8$ TeV. Values shown are the ratio of the beam displacement measured by ATLAS using the average primary-vertex position, to the nominal displacement entered into the accelerator control system. Ratios are shown for each individual beam in both planes, as well as for the beam-separation scale that determines that of the convolved beam sizes in the *vdM* scan. The uncertainties are statistical only

Calibration session(s)	April 2012		July 2012 (applicable to November)	
$\beta^\star$	0.6 m		11 m	
	Horizontal	Vertical	Horizontal	Vertical
Displacement scale				
Beam 1	0.9882 ± 0.0008	0.9881 ± 0.0008	0.9970 ± 0.0004	0.9961 ± 0.0006
Beam 2	0.9822 ± 0.0008	0.9897 ± 0.0009	0.9964 ± 0.0004	0.9951 ± 0.0004
Separation scale	0.9852 ± 0.0006	0.9889 ± 0.0006	0.9967 ± 0.0003	0.9956 ± 0.0004

be recalibrated when the latter changes. The results of the 2012 length-scale calibrations are summarized in Table 3. Because the beam-separation scans discussed in Sect. 4.2 are performed by displacing the two beams symmetrically in opposite directions, the relevant scale factor in the determination of Σ is the average of the scale factors for beam 1 and beam 2 in each plane. A total correction of -2.57% (-0.77%) is applied to the convolved-width product $\Sigma_x \Sigma_y$ and to the visible cross-sections measured during the April (July and November) 2012 *vdM* scans.

4.6 Orbit-drift corrections

Transverse drifts of the individual beam orbits at the IP during a scan session can distort the luminosity-scan curves and, if large enough, bias the determination of the overlap integrals and/or of the peak interaction rate. Such effects are monitored by extrapolating to the IP beam-orbit segments measured using beam-position monitors (BPMs) located in the LHC arcs [17], where the beam trajectories should remain unaffected by the *vdM* closed-orbit bumps across the IP. This procedure is applied to each beam separately and provides measurements of the relative drift of the two beams during the scan session, which are used to correct the beam separation at each scan step as well as between the x and y scans. The resulting impact on the visible cross-section varies from one scan set to the next; it does not exceed $\pm 0.6\%$ in any 2012 scan set, except for scan set X where the orbits drifted rapidly enough for the correction to reach $+1.1\%$.

4.7 Beam–beam corrections

When charged-particle bunches collide, the electromagnetic field generated by a bunch in beam 1 distorts the individual particle trajectories in the corresponding bunch of beam 2 (and vice-versa). This so-called *beam–beam interaction* affects the scan data in two ways.

First, when the bunches are not exactly centred on each other in the x–y plane, their electromagnetic repulsion induces a mutual angular kick [18] of a fraction of a microradian and modulates the actual transverse separation at the IP in a manner that depends on the separation itself. The phenomenon is well known from e^+e^- colliders and has been observed at the LHC at a level consistent with predictions [17]. If left unaccounted for, these *beam–beam deflections* would bias the measurement of the overlap integrals in a manner that depends on the bunch parameters.

The second phenomenon, called *dynamic* β [19], arises from the mutual defocusing of the two colliding bunches: this effect is conceptually analogous to inserting a small quadrupole at the collision point. The resulting fractional change in $\beta^\star$, or equivalently the optical demagnification between the LHC arcs and the collision point, varies with the transverse beam separation, slightly modifying, at each scan step, the effective beam separation in both planes (and thereby also the collision rate), and resulting in a distortion of the shape of the *vdM* scan curves.

The amplitude and the beam-separation dependence of both effects depend similarly on the beam energy, the tunes[9] and the unperturbed β-functions, as well as on the bunch intensities and transverse beam sizes. The beam–beam deflections and associated orbit distortions are calculated analytically [13] assuming elliptical Gaussian beams that collide in ATLAS only. For a typical bunch, the peak angular kick during the November 2012 scans is about $\pm 0.25\,\mu$rad, and the corresponding peak increase in relative beam separation amounts to $\pm 1.7\,\mu$m. The MAD-X optics code [20] is used to validate this analytical calculation, and to verify that higher-order dynamical effects (such as the orbit shifts induced at other collision points by beam–beam deflections at the ATLAS IP) result in negligible corrections to the analytical prediction.

The dynamic evolution of $\beta^\star$ during the scan is modelled using the MAD-X simulation assuming bunch parameters representative of the May 2011 *vdM* scan [3], and then scaled

[9] The tune of a storage ring is defined as the betatron phase advance per turn, or equivalently as the number of betatron oscillations over one full ring circumference.

using the beam energies, the $\beta^\star$ settings, as well as the measured intensities and convolved beam sizes of each colliding-bunch pair. The correction function is intrinsically independent of whether the bunches collide in ATLAS only, or also at other LHC interaction points [19]. For the November session, the peak-to-peak $\beta^\star$ variation during a scan is about 1.1%.

At each scan step, the predicted deflection-induced change in beam separation is added to the nominal beam separation, and the dynamic-β effect is accounted for by rescaling both the effective beam separation and the measured visible interaction rate to reflect the beam-separation dependence of the IP β-functions. Comparing the results of the 2012 scan analysis without and with beam–beam corrections, it is found that the visible cross-sections are increased by 1.2–1.8% by the deflection correction, and reduced by 0.2–0.3% by the dynamic-β correction. The net combined effect of these beam–beam corrections is a 0.9–1.5% increase of the visible cross-sections, depending on the scan set considered.

4.8 Non-factorization effects

The original *vdM* formalism [2] explicitly assumes that the particle densities in each bunch can be factorized into independent horizontal and vertical components, such that the term $1/2\pi\,\Sigma_x\,\Sigma_y$ in Eq. (9) fully describes the overlap integral of the two beams. If this factorization assumption is violated, the horizontal (vertical) convolved beam width Σ_x (Σ_y) is no longer independent of the vertical (horizontal) beam separation δ_y (δ_x); similarly, the transverse luminous size [7] in one plane ($\sigma_{x\mathcal{L}}$ or $\sigma_{y\mathcal{L}}$), as extracted from the spatial distribution of reconstructed collision vertices, depends on the separation in the other plane. The generalized *vdM* formalism summarized by Eq. (10) correctly handles such two-dimensional luminosity distributions, provided the dependence of these distributions on the beam separation in the transverse plane is known with sufficient accuracy.

Non-factorization effects are unambiguously observed in some of the 2012 scan sessions, both from significant differences in Σ_x (Σ_y) between a standard scan and an off-axis scan, during which the beams are partially separated in the non-scanning plane (Sect. 4.8.1), and from the δ_x (δ_y) dependence of $\sigma_{y\mathcal{L}}$ ($\sigma_{x\mathcal{L}}$) during a standard horizontal (vertical) scan (Sect. 4.8.2). Non-factorization effects can also be quantified, albeit with more restrictive assumptions, by performing a simultaneous fit to horizontal and vertical *vdM* scan curves using a non-factorizable function to describe the simultaneous dependence of the luminosity on the x and y beam separation (Sect. 4.8.3).

A large part of the scan-to-scan irreproducibility observed during the April and July scan sessions can be attributed to non-factorization effects, as discussed for ATLAS in Sect. 4.8.4 below and as independently reported by the LHCb Collaboration [21]. The strength of the effect varies widely across *vdM* scan sessions, differs somewhat from one bunch to the next and evolves with time within one LHC fill. Overall, the body of available observations can be explained neither by residual linear x–y coupling in the LHC optics [3,22], nor by crossing-angle or beam–beam effects; instead, it points to non-linear transverse correlations in the phase space of the individual bunches. This phenomenon was never envisaged at previous colliders, and was considered for the first time at the LHC [3] as a possible source of systematic uncertainty in the absolute luminosity scale. More recently, the non-factorizability of individual bunch density distributions was demonstrated directly by an LHCb beam–gas imaging analysis [21].

4.8.1 *Off-axis* vdM *scans*

An unambiguous signature of non-factorization can be provided by comparing the transverse convolved width measured during centred (or on-axis) *vdM* scans with the same quantity extracted from an offset (or off-axis) scan, i.e. one where the two beams are significantly separated in the direction orthogonal to that of the scan. This is illustrated in Fig. 3a. The beams remained vertically centred on each other during the first three horizontal scans (the first horizontal scan) of LHC fill 2855 (fill 2856), and were separated vertically by approximately 340 μm (roughly $4\sigma_b$) during the last horizontal scan in each fill. In both fills, the horizontal convolved beam size is significantly larger when the beams are vertically separated, demonstrating that the horizontal luminosity distribution depends on the vertical beam separation, i.e. that the horizontal and vertical luminosity distributions do not factorize.

The same measurement was carried out during the November scan session: the beams remained vertically centred on each other during the first, second and last scans (Fig. 3b), and were separated vertically by about 340 (200) μm during the third (fourth) scan. The horizontal convolved beam size increases with time at an approximately constant rate, reflecting transverse-emittance growth. No significant deviation from this trend is observed when the beams are separated vertically, suggesting that the horizontal luminosity distribution is independent of the vertical beam separation, i.e. that during the November scan session the horizontal and vertical luminosity distributions approximately factorize.

4.8.2 *Determination of single-beam parameters from luminous-region and luminosity-scan data*

While a single off-axis scan can provide convincing evidence for non-factorization, it samples only one thin slice in the (δ_x, δ_y) beam-separation space and is therefore insufficient to fully determine the two-dimensional luminosity distribution. Characterizing the latter by performing an x–

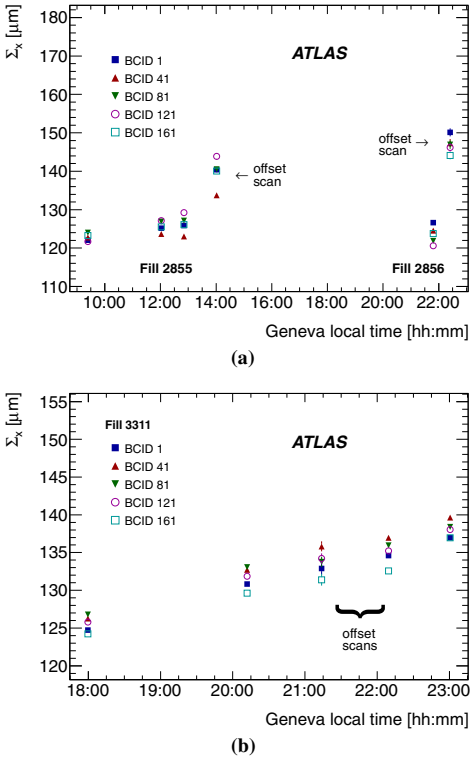

Fig. 3 Time evolution of the horizontal convolved beam size Σ_x for five different colliding-bunch pairs (BCIDs), measured using the LUCID_EventOR luminosity algorithm during the **a** July and **b** November 2012 *vdM*-scan sessions

y grid scan (rather than two one-dimensional x and y scans) would be prohibitively expensive in terms of beam time, as well as limited by potential emittance-growth biases. The strategy, therefore, is to retain the standard *vdM* technique (which assumes factorization) as the baseline calibration method, and to use the data to constrain possible non-factorization biases. In the absence of input from beam–gas imaging (which requires a vertex-position resolution within the reach of LHCb only), the most powerful approach so far has been the modelling of the simultaneous beam-separation-dependence of the luminosity and of the luminous-region geometry. In this procedure, the parameters describing the transverse proton-density distribution of individual bunches are determined by fitting the evolution, during *vdM* scans, not only of the luminosity itself but also of the position, orientation and shape of its spatial distribution, as reflected by that of reconstructed pp-collision vertices [23]. Luminosity profiles are then generated for simulated *vdM* scans using these fitted single-beam parameters, and analysed in the same fashion as real *vdM* scan data. The impact of non-factorization on the absolute luminosity scale is quantified by the ratio R_{NF} of the "measured" luminosity extracted from the one-dimensional simulated luminosity profiles using the standard *vdM* method, to the "true" luminosity from the computed four-dimensional (x, y, z, t) overlap integral [7] of the single-bunch distributions at zero beam separation. This technique is closely related to beam–beam imaging [7,24,25], with the notable difference that it is much less sensitive to the vertex-position resolution because it is used only to estimate a small fractional correction to the overlap integral, rather than its full value.

The luminous region is modelled by a three-dimensional (3D) ellipsoid [7]. Its parameters are extracted, at each scan step, from an unbinned maximum-likelihood fit of a 3D Gaussian function to the spatial distribution of the reconstructed primary vertices that were collected, at the corresponding beam separation, from the limited subset of colliding-bunch pairs monitored by the high-rate, dedicated ID-only data stream (Sect. 3.2). The vertex-position resolution, which is somewhat larger (smaller) than the transverse luminous size during scan sets I–III (scan sets IV–XV), is determined from the data as part of the fitting procedure [23]. It potentially impacts the reported horizontal and vertical luminous sizes, but not the measured position, orientation nor length of the luminous ellipsoid.

The single-bunch proton-density distributions $\rho_B(x, y, z)$ are parameterized, independently for each beam B ($B = 1$, 2), as the non-factorizable sum of up to three 3D Gaussian or super-Gaussian [26] distributions ($G_{\mathrm{a}}, G_{\mathrm{b}}, G_{\mathrm{c}}$) with arbitrary widths and orientations [27,28]:

$$\rho_B = w_{\mathrm{a}B}\times G_{\mathrm{a}B}+(1-w_{\mathrm{a}B})[w_{\mathrm{b}B}\times G_{\mathrm{b}B}+(1-w_{\mathrm{b}B})\times G_{\mathrm{c}B}]\,,$$

where the weights $w_{\mathrm{a(b)}B}$, $(1-w_{\mathrm{a(b)}B})$ add up to one by construction. The overlap integral of these density distributions, which allows for a crossing angle in both planes, is evaluated at each scan step to predict the produced luminosity and the geometry of the luminous region for a given set of bunch parameters. This calculation takes into account the impact, on the relevant observables, of the luminosity backgrounds, orbit drifts and beam–beam corrections. The bunch parameters are then adjusted, by means of a χ^2-minimization procedure, to provide the best possible description of the centroid position, the orientation and the resolution-corrected widths of the luminous region measured at each step of a given set of on-axis x and y scans. Such a fit is illustrated in Fig. 4 for one of the horizontal scans in the July 2012 session. The goodness of fit is satisfactory ($\chi^2 = 1.3$ per degree of freedom), even if some systematic deviations are apparent in the tails of the scan. The strong horizontal-separation dependence of the

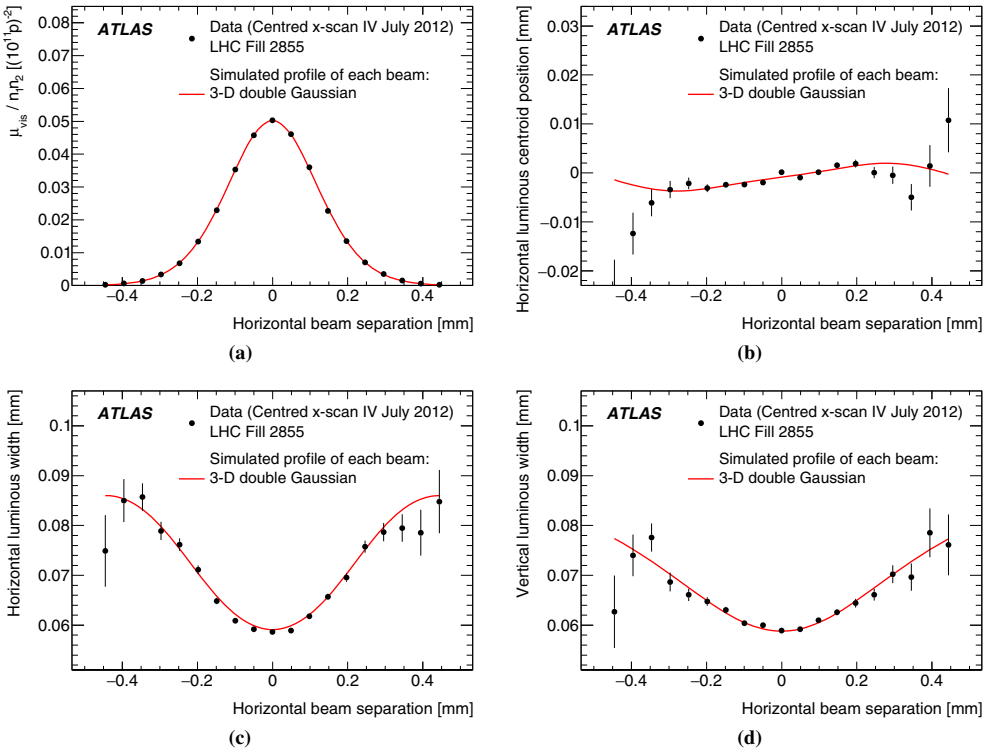

Fig. 4 Beam-separation dependence of the luminosity and of a subset of luminous-region parameters during horizontal *vdM* scan IV. The *points* represent **a** the specific visible interaction rate (or equivalently the specific luminosity), **b** the *horizontal* position of the luminous centroid, **c**, **d** the *horizontal* and *vertical* luminous widths $\sigma_{x\mathcal{L}}$ and $\sigma_{y\mathcal{L}}$. The *red line* is the result of the fit described in the text

vertical luminous size (Fig. 4d) confirms the presence of significant non-factorization effects, as already established from the off-axis luminosity data for that scan session (Fig. 3a).

This procedure is applied to all 2012 *vdM* scan sets, and the results are summarized in Fig. 5. The luminosity extracted from the standard *vdM* analysis with the assumption that factorization is valid, is larger than that computed from the reconstructed single-bunch parameters. This implies that neglecting non-factorization effects in the *vdM* calibration leads to overestimating the absolute luminosity scale (or equivalently underestimating the visible cross-section) by up to 3% (4.5%) in the April (July) scan session. Non-factorization biases remain below 0.8% in the November scans, thanks to bunch-tailoring in the LHC injector chain [16]. These observations are consistent, in terms both of absolute magnitude and of time evolution within a scan session, with those reported by LHCb [21] and CMS [29,30] in the same fills.

4.8.3 *Non-factorizable* vdM *fits to luminosity-scan data*

A second approach, which does not use luminous-region data, performs a combined fit of the measured beam-separation dependence of the specific visible interaction rate to horizontal- and vertical-scan data simultaneously, in order to determine the overlap integral(s) defined by either Eq. (8) or Eq. (10). Considered fit functions include factorizable or non-factorizable combinations of two-dimensional Gaussian or other functions (super-Gaussian, Gaussian times polynomial) where the (non-)factorizability between the two scan directions is imposed by construction.

The fractional difference between σ_{vis} values extracted from such factorizable and non-factorizable fits, i.e. the multiplicative correction factor to be applied to visible cross-sections extracted from a standard *vdM* analysis, is consistent with the equivalent ratio R_{NF} extracted from the analysis of Sect. 4.8.2 within 0.5% or less for all scan sets. Com-

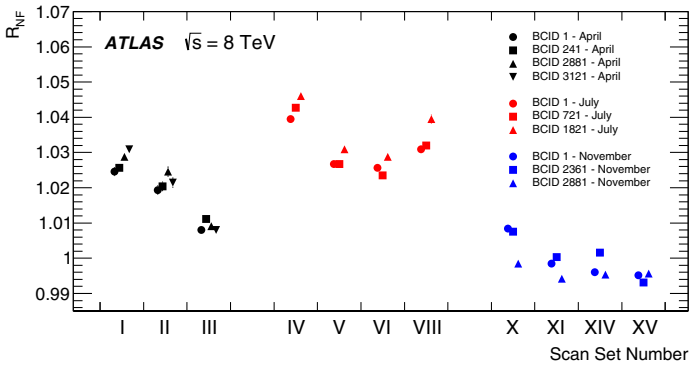

Fig. 5 Ratio R_{NF} of the luminosity determined by the *vdM* method assuming factorization, to that evaluated from the overlap integral of the reconstructed single-bunch profiles at the peak of each scan set. The results are *colour-coded* by scan session. *Each point* corresponds to one colliding-bunch pair in the dedicated ID-only stream. The statistical errors are smaller than the symbols

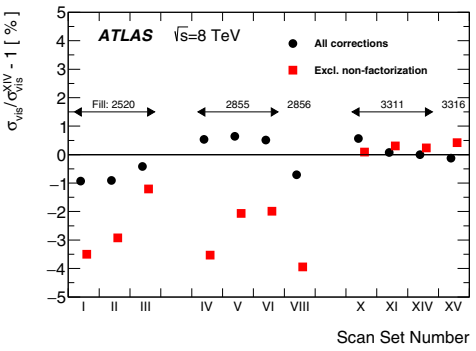

Fig. 6 Comparison of *vdM*-calibrated visible cross-sections for the default track-counting algorithm, with all corrections applied (*black circles*) and with all corrections except for non-factorization (*red squares*). Shown is the fractional difference between the visible cross-section from a given scan set, and the fully corrected visible cross-section from scan set XIV. The LHC fill numbers corresponding to each scan set are indicated

bined with the results of the off-axis scans, this confirms that while the April and July *vdM* analyses require substantial non-factorization corrections, non-factorization biases during the November scan session remain small.

4.8.4 Non-factorization corrections and scan-to-scan consistency

Non-factorization corrections significantly improve the reproducibility of the calibration results (Fig. 6). Within a given LHC fill and in the absence of non-factorization corrections, the visible cross-section increases with time, as also observed at other IPs in the same fills [21,29], suggesting that the underlying non-linear correlations evolve over time. Applying the non-factorization corrections extracted from the luminous-region analysis dramatically improves the scan-to-scan consistency within the April and July scan sessions, as well as from one session to the next. The 1.0–1.4% inconsistency between the fully corrected cross-sections (black circles) in scan sets I–III and in later scans, as well as the difference between fills 2855 and 2856 in the July session, are discussed in Sect. 4.11.

4.9 Emittance-growth correction

The *vdM* scan formalism assumes that both convolved beam sizes Σ_x, Σ_y (and therefore the transverse emittances of each beam) remain constant, both during a single x or y scan and in the interval between the horizontal scan and the associated vertical scan.

Emittance growth within a scan would manifest itself by a slight distortion of the scan curve. The associated systematic uncertainty, determined from pseudo-scans simulated with the observed level of emittance growth, was found to be negligible.

Emittance growth between scans manifests itself by a slight increase of the measured value of Σ from one scan to the next, and by a simultaneous decrease in specific luminosity. Each scan set requires 40–60 min, during which time the convolved beam sizes each grow by 1–2%, and the peak specific interaction rate decreases accordingly as $1/(\Sigma_x \Sigma_y)$. This is illustrated in Fig. 7, which displays the Σ_x and $\mu_{\mathrm{vis}}^{\mathrm{MAX}}/(n_1 n_2)$ values measured by the BCMH_EventOR algorithm during scan sets XI, XIV and XV. For each BCID, the convolved beam sizes increase, and the peak specific interaction rate decreases, from scan XI to scan XIV; since scan XV took place very early in the following fill, the corresponding transverse beam sizes (specific rates) are smaller (larger) than for the previous scan sets.

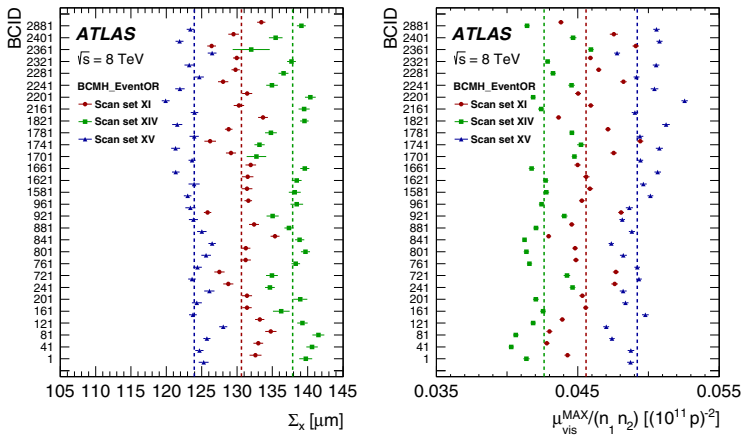

Fig. 7 Bunch-by-bunch **a** horizontal convolved beam size and **b** peak specific interaction rate measured in scan sets XI, XIV, and XV for the BCMH_EventOR algorithm. The *vertical lines* represent the weighted average over colliding-bunch pairs for each scan set separately. The *error bars* are statistical only, and are approximately the size of the marker

If the horizontal and vertical emittances grow at identical rates, the procedure described in Sect. 4.3 remains valid without any need for correction, provided that the decrease in peak rate is fully accounted for by the increase in $(\Sigma_x \Sigma_y)$, and that the peak specific interaction rate in Eq. (11) is computed as the average of the specific rates at the peak of the horizontal and the vertical scan:

$$\mu_{\mathrm{vis}}^{\mathrm{MAX}}/n_1 n_2 = \frac{(\mu_{\mathrm{vis}}^{\mathrm{MAX}}/n_1 n_2)_x + (\mu_{\mathrm{vis}}^{\mathrm{MAX}}/n_1 n_2)_y}{2} .$$

The horizontal-emittance growth rate is measured from the bunch-by-bunch difference in fitted convolved width between two consecutive horizontal scans in the same LHC fill, and similarly for the vertical emittance. For LHC fill 3311 (scan sets X–XIV), these measurements reveal that the horizontal convolved width grew 1.5–2 times faster than the vertical width. The potential bias associated with unequal horizontal and vertical growth rates can be corrected for by interpolating the measured values of Σ_x, Σ_y and $\mu_{\mathrm{vis}}^{\mathrm{MAX}}$ to a common reference time, assuming that all three observables evolve linearly with time. This reference time is in principle arbitrary: it can be, for instance, the peak of the x scan (in which case only Σ_y needs to be interpolated), or the peak of the y scan, or any other value. The visible cross-section, computed from Eq. (11) using measured values projected to a common reference time, should be independent of the reference time chosen.

Applying this procedure to the November scan session results in fractional corrections to σ_{vis} of 1.38, 0.22 and 0.04% for scan sets X, XI and XIV, respectively. The correction for scan set X is exceptionally large because operational difficulties forced an abnormally long delay (almost two hours) between the horizontal scan and the vertical scan, exacerbating the impact of the unequal horizontal and vertical growth rates; its magnitude is validated by the noticeable improvement it brings to the scan-to-scan reproducibility of σ_{vis}.

No correction is available for scan set XV, as no other scans were performed in LHC fill 3316. However, in that case the delay between the x and y scans was short enough, and the consistency of the resulting σ_{vis} values with those in scan sets XI and XIV sufficiently good (Fig. 6), that this missing correction is small enough to be covered by the systematic uncertainties discussed in Sects. 5.2.6 and 5.2.8.

Applying the same procedure to the July scan session yields emittance-growth corrections below 0.3% in all cases. However, the above-described correction procedure is, strictly speaking, applicable only when non-factorization effects are small enough to be neglected. When the factorization hypothesis no longer holds, the very concept of separating horizontal and vertical emittance growth is ill-defined. In addition, the time evolution of the fitted one-dimensional convolved widths and of the associated peak specific rates is presumably more influenced by the progressive dilution, over time, of the non-factorization effects discussed in Sect. 4.8 above. Therefore, and given that the non-factorization cor-

Table 4 Systematic uncertainties affecting the bunch-population product $n_1 n_2$ during the 2012 *vdM* scans

Scan set number	I–III	IV–VII	VIII–IX	X–XIV	XV
LHC fill number	2520	2855	2856	3311	3316
Fractional systematic uncertainty (%)					
Total intensity scale (DCCT)	0.26	0.21	0.21	0.22	0.23
Bunch-by-bunch fraction (FBCT)	0.03	0.04	0.04	0.04	0.04
Ghost charge (LHCb beam–gas)	0.04	0.03	0.04	0.04	0.02
Satellites (longitudinal density monitor)	0.07	0.02	0.03	0.01	<0.01
Total	0.27	0.22	0.22	0.24	0.23

rections applied to scan sets I–VIII (Fig. 5) are up to ten times larger than a typical emittance-growth correction, no such correction is applied to the April and July scan results; an appropriately conservative systematic uncertainty must be assigned instead.

4.10 Bunch-population determination

The bunch-population measurements are performed by the LHC Bunch-Current Normalization Working Group and have been described in detail in Refs. [21,27,31–33]. A brief summary of the analysis is presented here. The fractional uncertainties affecting the bunch-population product ($n_1 n_2$) are summarized in Table 4.

The LHC bunch currents are determined in a multi-step process due to the different capabilities of the available instrumentation. First, the total intensity of each beam is monitored by two identical and redundant DC current transformers (DCCT), which are high-accuracy devices but have no ability to distinguish individual bunch populations. Each beam is also monitored by two fast beam-current transformers (FBCT), which measure relative bunch currents individually for each of the 3564 nominal 25 ns slots in each beam; these fractional bunch populations are converted into absolute bunch currents using the overall current scale provided by the DCCT. Finally, corrections are applied to account for out-of-time charge present in a given BCID but not colliding at the interaction point.

A precision current source with a relative accuracy of 0.05% is used to calibrate the DCCT at regular intervals. An exhaustive analysis of the various sources of systematic uncertainty in the absolute scale of the DCCT, including in particular residual non-linearities, long-term stability and dependence on beam conditions, is documented in Ref. [31]. In practice, the uncertainty depends on the beam intensity and the acquisition conditions, and must be evaluated on a fill-by-fill basis; it typically translates into a 0.2–0.3% uncertainty in the absolute luminosity scale.

Because of the highly demanding bandwidth specifications dictated by single-bunch current measurements, the FBCT response is potentially sensitive to the frequency spectrum radiated by the circulating bunches, timing adjustments with respect to the RF phase, and bunch-to-bunch intensity or length variations. Dedicated laboratory measurements and beam experiments, comparisons with the response of other bunch-aware beam instrumentation (such as the ATLAS beam pick-up timing system), as well as the imposition of constraints on the bunch-to-bunch consistency of the measured visible cross-sections, resulted in a <0.04% systematic luminosity-calibration uncertainty in the luminosity scale arising from the relative-intensity measurements [27,32].

Additional corrections to the bunch-by-bunch population are made to correct for *ghost charge* and *satellite bunches*. Ghost charge refers to protons that are present in nominally empty bunch slots at a level below the FBCT threshold (and hence invisible), but which still contribute to the current measured by the more accurate DCCT. Highly precise measurements of these tiny currents (normally at most a few per mille of the total intensity) have been achieved [27] by comparing the number of beam–gas vertices reconstructed by LHCb in nominally empty bunch slots, to that in non-colliding bunches whose current is easily measurable. For the 2012 luminosity-calibration fills, the ghost-charge correction to the bunch-population product ranges from −0.21 to −0.65%; its systematic uncertainty is dominated by that affecting the LHCb trigger efficiency for beam–gas events.

Satellite bunches describe out-of-time protons present in collision bunch slots that are measured by the FBCT, but that remain captured in an RF bucket at least one period (2.5 ns) away from the nominally filled LHC bucket. As such, they experience at most long-range encounters with the nominally filled bunches in the other beam. The best measurements are obtained using the longitudinal density monitor. This instrument uses avalanche photodiodes with 90 ps timing resolution to compare the number of infrared synchrotron-radiation photons originating from satellite RF buckets, to that from the nominally filled buckets. The corrections to the bunch-population product range from −0.03 to −0.65%, with the lowest satellite fraction achieved in scans X–XV. The measurement techniques, as well as the associ-

ated corrections and systematic uncertainties, are detailed in Ref. [33].

4.11 Calibration results

4.11.1 Summary of calibration corrections

With the exception of the noise and single-beam background subtractions (which depend on the location, geometry and instrumental response of individual subdetectors), all the above corrections to the *vdM*-calibrated visible cross-sections are intrinsically independent of the luminometer and luminosity algorithm considered. The beam-separation scale, as well as the orbit-drift and beam–beam corrections, impact the effective beam separation at each scan step; the non-factorization and emittance-growth corrections depend on the properties of each colliding bunch-pair and on their time evolution over the course of a fill; and corrections to the bunch-population product translate into an overall scale factor that is common to all scan sets within a given LHC fill. The mutual consistency of these corrections was explicitly verified for the LUCID_EventOR and BCM_EventOR visible cross-sections, for which independently determined corrections are in excellent agreement. As the other algorithms (in particular track counting) are statistically less precise during *vdM* scans, their visible cross-sections are corrected using scale factors extracted from the LUCID_EventOR scan analysis.

The dominant correction in scan sets I–VIII (Fig. 8) is associated with non-factorization; it is also the most uncertain, because it is sensitive to the vertex-position resolution, especially in scan sets I–III where the transverse luminous size is significantly smaller than the resolution. In contrast, non-factorization corrections are moderate in scan sets X–XV, suggesting a correspondingly minor contribution to the systematic uncertainty for the November scan session.

The next largest correction in scan sets I–III is that of the beam-separation scale, which, because of different $\beta^\star$ settings, is uncorrelated between the April session and the other two sessions, and fully correlated across scan sets IV–XV (Sect. 5.1.3). The correction to the bunch-population product is equally shared among FBCT, ghost-charge and satellite corrections in scan sets I–III, and dominated by the ghost-charge subtraction in scans IV–XV. This correction is uncorrelated between scan sessions, but fully correlated between scan sets in the same fill.

Of comparable magnitude across all scan sets, and partially correlated between them, is the beam–beam correction; its systematic uncertainty is moderate and can be calculated reliably (Sect. 5.2.3). The uncertainties associated with orbit drifts (Sect. 5.2.1) and emittance growth (Sect. 5.2.6) are small, except for scan set X where these corrections are largest.

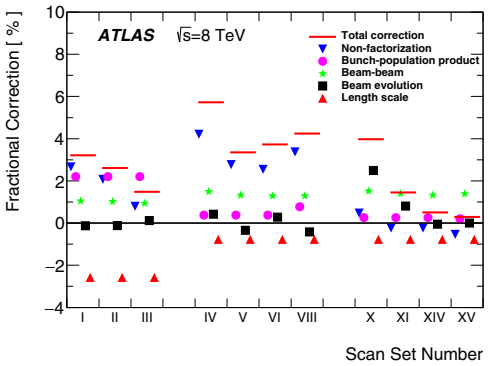

Fig. 8 Luminometer-independent corrections to the visible cross-sections calibrated by the van der Meer method, averaged over all colliding bunches and displayed separately for each scan set. The length–scale, beam–beam, non-factorization and bunch–population corrections are discussed in Sects. 4.5, 4.7, 4.8 and 4.10, respectively. The orbit–drift (Sect. 4.6) and emittance–growth (Sect. 4.9) corrections are combined for clarity, and their cumulative effect is displayed as "beam evolution". The sum of all corrections is shown, for each scan set, by the red line

4.11.2 Consistency of vdM *calibrations across 2012 scan sessions*

The relative stability of *vdM* calibrations, across scan sets within a scan session and from one scan session to the next, can be quantified by the ratio $S^k_{\text{calib},\,j}$ of the visible cross-section for luminosity algorithm k (k = BCMH_EventOR, BCMV_EventOR, LUCID_EventA,…) in a given scan set j to that in a reference scan set, arbitrarily chosen as scan set XIV:

$$S^k_{\text{calib},\,j} = \sigma^k_{\text{vis},\,j} / \sigma^k_{\text{vis, XIV}} \,.$$

The ratio $S^k_{\text{calib},\,j}$ is presented in Fig. 9a for a subset of BCM, LUCID and track-counting algorithms. Several features are apparent.

- The visible cross-section associated with the LUCID_EventA algorithm drops significantly between the April and July scan sessions, and then again between July and November.
- For each algorithm separately, the σ_{vis} variation across scan sets within a given LHC fill (scan sets I–III, IV–VI and X–XIV) remains below 0.5%, except for scan set X which stands out by 1%.
- The absolute calibrations of the BCMH_EventOR and track-counting algorithms are stable to better than ±0.8% across scan sets IV–VI and X–XV, with the inconsistency being again dominated by scan set X.

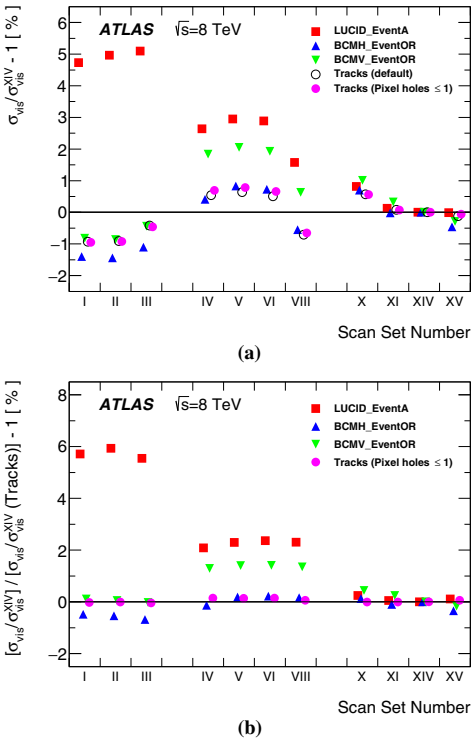

Fig. 9 **a** Stability of absolutely calibrated visible cross-sections across scan sets, as quantified by the ratio of the visible cross-section in a given scan set to that of the same luminosity algorithm in scan set XIV. **b** Relative instrumental stability of different luminosity algorithms across scan sets, as quantified by the ratio shown in **a** for a given algorithm, divided by the same ratio for the default track-counting algorithm

- Between scan sets IV–VI and X–XV, the calibrations of the track counting, BCMH_EventOR and BCMV_EventOR algorithms drop on the average by 0.5, 0.6 and 1.7% respectively.
- The calibrations of the BCM_EventOR (track-counting) algorithm in scan sets I–III and VIII are lower by up to 1.4% (2%) compared to the other scan sets. This structure, which is best visible in Fig. 6, is highly correlated across all algorithms. Since the corresponding luminosity detectors use very different technologies, this particular feature cannot be caused by luminometer instrumental effects.

In order to separate purely instrumental drifts in the ATLAS luminometers from *vdM*-calibration inconsistencies linked to other sources (such as accelerator parameters or beam conditions), Fig. 9b shows the variation, across scan sets j, of the double ratio

$$S^k_{\text{instr},j} = S^k_{\text{calib},j} / S^{\text{track counting}}_{\text{calib},j} = \frac{\sigma^k_{\text{vis},j}/\sigma^k_{\text{vis, XIV}}}{\sigma^{\text{track counting}}_{\text{vis},j}/\sigma^{\text{track counting}}_{\text{vis, XIV}}},$$

which quantifies the stability of algorithm k relative to that of the default track-counting algorithm. Track counting is chosen as the reference here because it is the bunch-by-bunch algorithm whose absolute calibration is the most stable over time (Figs. 6 and 9a), and that displays the best stability relative to all bunch-integrating luminosity algorithms during physics running across the entire 2012 running period (this is demonstrated in Sect. 6.1). By construction, the instrumental-stability parameter $S^k_{\text{instr},j}$ is sensitive only to instrumental effects, because the corrections described in Sects. 4.5–4.10 are intrinsically independent of the luminosity algorithm considered. The following features emerge.

- For each algorithm individually, the instrumental stability is typically better than 0.5% within each scan session.
- The instrumental stability of both the "Pixel holes $\leq$1" selection and the vertex-associated track selection (not shown) is better than 0.2% across all scan sets.
- Relative to track counting, the LUCID efficiency drops by 3.5% between the April and July scan sessions, and by an additional 2.2% between July and November. This degradation is understood to be caused by PMT aging.
- The BCMH_EventOR efficiency increases by about 0.7% with respect to that of track counting between the April and July sessions, and then remains stable to within 0.2–0.4% across the July and November sessions. In contrast, the efficiency of the BCMV_EventOR algorithm compared to that of track counting increases by about 1.3% from April to July, and drops back to its original level by the November session. These long-term variations in the response of various subsets of diamond sensors in the low-luminosity regime of *vdM* scans are possibly related to subtle solid-state physics effects arising from the combination of radiation damage during physics running [3,34] and of partial annealing during beam-off and low-luminosity periods. Aging effects of comparable magnitude are observed at high luminosity (Sect. 6).
- Given the 0.7% relative stability, between scan sets I–III and IV–VI, of the track-counting and BCMH_EventOR calibrations (Fig. 9b), the 1.4–2.0% discrepancy, between the April and July *vdM*-scan sessions, that affects the absolute calibrations of both the BCMH_EventOR and the track-counting algorithms (Fig. 9a) cannot be primarily instrumental in nature. The actual cause could not be identified with certainty. Since the transverse luminous size $\sigma_{\mathcal{L}}$ in the April session (Table 2) is approximately three times smaller than the vertex-position resolution, a plausible scenario is that a small error in the estimated resolution biases the reconstructed luminous size in such

a way as to underestimate the non-factorization corrections R_{NF}, and thereby the visible cross-sections, in scan sets I–III.

- Similarly, the 1.3% discrepancy, between scan sets IV–VI and scan set VIII, of the absolute calibrations of all algorithms (Fig. 9a) cannot be instrumental either. Here however, the luminous size is 1.5 times larger than the resolution: resolution biases (if any) should be noticeably smaller than in the April scan session. But as scan sets IV–VIII were carried out in two consecutive LHC fills under very similar beam conditions, such biases should impact scan sets IV–VI and VIII in the same manner.

4.11.3 Final visible cross-sections for bunch-by-bunch luminosity algorithms

The percent-level inconsistencies of the absolute calibrations between April and July and within the July session itself, as well as the excellent internal consistency of the November results for all algorithms (Fig. 9a), suggest that the November calibrations are the most reliable. In addition, the calibrations extracted from scan sets I–VIII are affected by several large adjustments that in some cases partially cancel (Fig. 8); of these the most uncertain are the non-factorization corrections, which affect the November scans much less. The cumulated magnitude of the corrections is also smallest for scan sets XI–XV (scan set X suffers from larger orbit-drift and emittance-growth corrections because of the long delay between the x and y scans).

The combination of these arguments suggests that the visible cross-sections, averaged over all colliding bunches in each scan set and then averaged over scan sets XI–XV, should be adopted as the best estimate $\overline{\sigma}_{\mathrm{vis}}$ of the absolute luminosity scale at the time of, and applicable to the beam conditions during, the November 2012 *vdM* session. Table 5 lists the $\overline{\sigma}_{\mathrm{vis}}$ values for the main luminosity algorithms considered in this paper; the associated systematic uncertainties are detailed in Sect. 5. Transferring the BCM and LUCID calibrations to the high-luminosity regime of routine physics operation, and accounting for time-dependent variations in luminometer response over the course of the 2012 running period, is addressed in Sect. 7.3.

5 van der Meer calibration uncertainties

This section details the systematic uncertainties affecting the visible cross-sections reported in Table 5. The contributions from instrumental effects (Sect. 5.1) are comparable in magnitude to those associated with beam conditions (Sect. 5.2), while those from the bunch-population product (Sect. 5.3) are about three times smaller. A summary is presented in Table 6.

Table 5 Visible cross-sections averaged over scan sets XI–XV

Luminosity algorithm	$\overline{\sigma}_{\mathrm{vis}}$ (mb)	Statistical uncertainty (%)
BCMH_EventOR	5.0541	0.05
BCMV_EventOR	5.0202	0.06
LUCID_EventOR	35.316	0.02
LUCID_EventA	23.073	0.02
LUCID_EventC	20.422	0.02
Track counting (Pixel holes $\leq$1)	243.19	0.14
Track counting (default)	241.27	0.14
Track counting (vertex-associated)	226.24	0.14

Table 6 Fractional systematic uncertainties affecting the visible cross-section $\overline{\sigma}_{\mathrm{vis}}$ averaged over *vdM* scan sets XI–XV (November 2012)

Source	Uncertainty (%)
Reference specific luminosity	0.50
Noise and background subtraction	0.30
Length-scale calibration	0.40
Absolute ID length scale	0.30
Subtotal, instrumental effects	0.77
Orbit drifts	0.10
Beam-position jitter	0.20
Beam–beam corrections	0.28
Fit model	0.50
Non-factorization correction	0.50
Emittance-growth correction	0.10
Bunch-by-bunch σ_{vis} consistency	0.23
Scan-to-scan consistency	0.31
Subtotal, beam conditions	0.89
Bunch-population product	0.24
Total	1.20

5.1 Instrumental effects

5.1.1 Reference specific luminosity

For simplicity, the visible cross-section extracted from *vdM* scans for a given luminometer utilizes the specific luminosity measured by that same luminometer. Since this quantity depends only on the convolved beam sizes, consistent results should be reported by all detectors and algorithms for a given scan set.

Figure 10 compares the $\mathcal{L}_{\mathrm{spec}}$ values measured by two independent luminosity algorithms in three consecutive scan sets. Bunch-to-bunch variations of the specific luminosity are typically 5–10% (Fig. 10a), reflecting bunch-to-bunch differ-

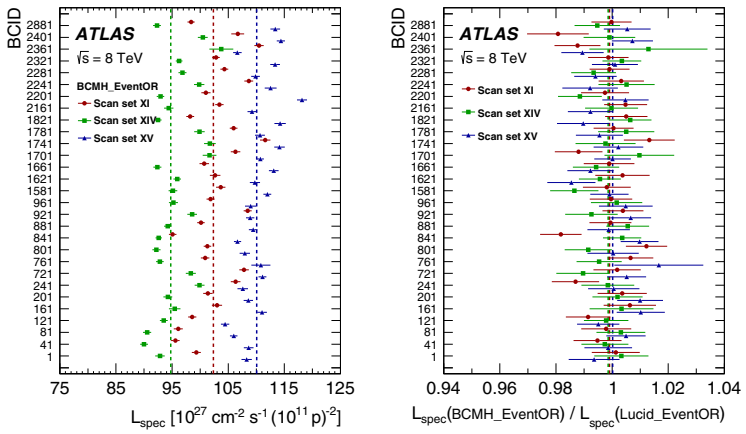

Fig. 10 **a** Bunch-by-bunch specific luminosity for scan sets XI, XIV and XV determined using the BCMH_EventOR algorithm. **b** Bunch-by-bunch ratio of the $\mathcal{L}_{\text{spec}}$ values reported by the BCMH_EventOR and LUCID_EventOR algorithms. The *vertical lines* indicate the weighted average over BCIDs for the three scan sets separately. The *error bars* represent statistical uncertainties only

ences in transverse emittance also seen during normal physics fills. A systematic reduction in $\mathcal{L}_{\text{spec}}$ can be observed from scan XI to scan XIV, caused by emittance growth over the duration of the fill. Although the two algorithms appear statistically consistent for each bunch pair separately (Fig. 10b), their bunch-averaged ratio systematically differs from unity by a small amount. The largest such discrepancy in scan sets XI–XV among the BCM, LUCID and track-counting algorithms amounts to 0.5% and is adopted as the systematic uncertainty associated with the choice of reference specific-luminosity value.

5.1.2 Noise and background subtraction

To assess possible uncertainties in the default subtraction scheme, an alternative fit is performed to data without applying the background-correction procedure of Sect. 4.4, but interpreting the constant (i.e. separation-independent) term in the fitting function as the sum of instrumental noise and single-beam backgrounds. The maximum difference observed between these two background treatments, averaged over scan sets XI–XV, amounts to less than 0.3% (0.02%) for the BCMH_EventOR (LUCID_EventOR) algorithm. A systematic uncertainty of ±0.3% is thus assigned to the background-subtraction procedure during *vdM* scans.

5.1.3 Length-scale calibration

The length scale of each scan step enters the extraction of $\Sigma_{x,y}$ and hence directly affects the absolute luminosity scale. The corresponding calibration procedure is described in Sect. 4.5. Combining in quadrature the statistical errors in the horizontal and vertical beam-separation scales (Table 3) yields a statistical uncertainty of ±0.08% in the length-scale product.

The residual non-linearity visible in Fig. 2, and also observed in length-scale calibration scans performed in 2011, could be caused either by the power converters that drive the steering correctors forming the closed-orbit bumps, by the response of the steering correctors themselves, or by magnetic imperfections (higher multipole components) at large betatron amplitudes in the quadrupoles located within those orbit bumps. The potential impact of such a non-linearity on the luminosity calibration is estimated to be less than 0.05%.

Another potential source of bias is associated with orbit drifts. These were monitored during each of the four length-scale scans using the method outlined in Sect. 4.6, revealing no significant drift. Small inconsistencies in the transverse beam positions extrapolated to the IP from the BPMs in the left and right arcs are used to set an upper limit on the potential orbit drift, during each scan, of the beam being calibrated, resulting in an overall ±0.4% uncertainty in the length-scale product and therefore in the visible cross-section.

5.1.4 Absolute length scale of the inner detector

The determination of the beam-separation scale is based on comparing the scan step requested by the LHC control system with the actual transverse displacement of the luminous centroid measured by ATLAS. This measurement relies on

the length scale of the ATLAS inner detector tracking system (primarily the Pixel detector) being correct in measuring displacements of vertex positions away from the centre of the detector. The determination of the uncertainty in this absolute length scale is described in Ref. [3]; its impact amounts to a systematic uncertainty of ±0.3% in the visible cross-section.

5.2 Beam conditions

5.2.1 *Orbit drifts during* vdM *scans*

The systematic uncertainty associated with orbit drifts is taken as half of the correction described in Sect. 4.6, averaged over scan sets XI–XV. It translates into a ±0.1% systematic uncertainty in $\overline{\sigma}_{\text{vis}}$. Because the sign and amplitude of the orbit drifts vary over time, this uncertainty is uncorrelated with that affecting the length-scale calibration.

5.2.2 *Beam-position jitter*

At each step of a scan, the actual beam separation may be affected by random deviations of the beam positions from their nominal settings, which in turn induce fluctuations in the luminosity measured at each scan point. The magnitude of this potential jitter was evaluated from the variation between consecutive measurements, a few seconds apart, of the relative beam separation at the IP extracted from single-beam orbits measured by BPMs in the nearby LHC arcs and extrapolated to the IP (Sect. 4.6). The typical jitter in transverse beam separation observed during the November scan session amounts to 0.75 μm RMS. The resulting systematic uncertainty in σ_{vis} is obtained by random Gaussian smearing of the nominal separation by this amount, independently at each scan step, in a series of simulated scans. The RMS of the resulting fluctuations in fitted visible cross-section yields a ±0.2% systematic uncertainty associated with beam-position jitter.

5.2.3 *Beam–beam corrections*

For given values of the bunch intensity and transverse convolved beam sizes, which are precisely measured, the deflection-induced orbit distortion and the relative variation of $\beta^\star$ are both proportional to $\beta^\star$ itself; they also depend on the fractional tune. Assigning a ±20% uncertainty to each β-function value at the IP and a ±0.01 upper limit to each tune variation results in a ±0.28% uncertainty in σ_{vis}. This uncertainty is computed with the conservative assumption that β-function and tune uncertainties are correlated between the horizontal and vertical planes, but uncorrelated between the two LHC rings.

5.2.4 *Fit model*

The choice of the fit function is arbitrary, but guided by the requirement that the fit provides faithful measurements of the integral under the luminosity-scan curve and of the rate at zero beam separation. The choice of functional form therefore depends on the underlying shapes of the colliding bunches, as manifested in the beam-separation dependence of the luminosity. Scan sets I–VIII are best modelled using a double Gaussian function plus a constant. The beam shapes are different in scan sets X–XV [16]: here the best fit is obtained using a Gaussian function multiplied by a sixth-order polynomial. Additional fits are performed with different model assumptions: a super-Gaussian function, and a Gaussian function multiplied by a fourth-order polynomial (plus a constant term in all cases). The maximum fractional difference between the results of these different fits, across scan sets XI–XV and across the BCM, LUCID and track-counting algorithms, amounts to 0.5%. This value is assigned as the uncertainty associated with the fit model.

5.2.5 *Non-factorization correction*

The non-factorization corrections extracted from the luminous-region analysis (Sect. 4.8.2) and the non-factorizable *vdM* fits (Sect. 4.8.3), are consistent to within 0.5% or less in all scan sets. This value is chosen as the systematic uncertainty associated with non-factorization biases in the November scans.

5.2.6 *Emittance-growth correction*

The uncertainty in the correction described in Sect. 4.9 is estimated as the largest difference in the scan-averaged correction for extreme choices of reference times, and amounts to ±0.1% in $\overline{\sigma}_{\text{vis}}$.

5.2.7 *Consistency of bunch-by-bunch visible cross-sections*

The calibrated σ_{vis} value associated with a given luminometer and algorithm should be a universal scale factor independent of beam conditions or BCID. The variation in σ_{vis} across colliding-bunch pairs in a given scan set, as well as between scan sets, is used to quantify the reproducibility and stability of the calibration procedure during a scan session.

The comparison of Fig. 11a, b for scan sets XI, XIV and XV suggests that some of the σ_{vis} variation from one bunch pair to the next is not statistical in nature, but rather correlated across bunch slots. The non-statistical component of this variation, i.e. the difference in quadrature between the RMS bunch-by-bunch variation of σ_{vis} within a given scan set and the average statistical uncertainty affecting a single-BCID σ_{vis} measurement, is taken as a systematic uncertainty in the calibration technique. The largest such difference across scan

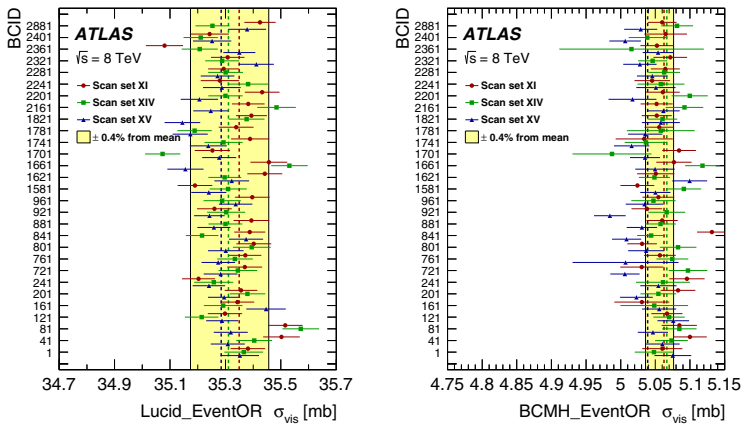

Fig. 11 Bunch-by-bunch σ_{vis} values measured in scan sets XI, XIV, and XV for the **a** LUCID_EventOR and **b** BCMH_EventOR algorithm. The *error bars* are statistical only. The *vertical lines* represent the weighted average over colliding-bunch pairs, separately for each scan set. The *shaded band* indicates a ±0.4% variation from the average, which is the sum in quadrature of the systematic uncertainties associated with bunch-by-bunch and scan-to-scan σ_{vis} consistency

sets XI–XV, evaluated using the measured LUCID_EventOR visible cross-section, amounts to 0.23%. The RMS bunch-by-bunch fluctuation of the BCM cross-sections is, in all cases but one, slightly smaller than the corresponding bunch-averaged statistical uncertainty, indicating that the statistical sensitivity of the BCM algorithms is insufficient to provide a reliable estimate of this uncertainty; the LUCID result is therefore adopted as a measure of the σ_{vis} bunch-by-bunch consistency.

5.2.8 *Scan-to-scan reproducibility*

The reproducibility of the visible cross-sections across the selected November scan sets, as illustrated in Fig. 9a, is used as a measure of the residual inconsistencies potentially associated with imperfect correction procedures and unidentified sources of non-reproducibility. The largest such difference in visible cross-section between scan sets XI–XV, as reported by any of the BCM_EventOR, LUCID_EventOR or track-counting algorithms, amounts to ±0.31%.

5.3 Bunch-population product

The determination of this uncertainty (±0.24%) is discussed in Sect. 4.10 and summarized in Table 4.

5.4 Summary of van der Meer calibration uncertainties

The systematic uncertainties affecting the November 2012 *vdM* calibration are summarized in Table 6; they apply equally to all *vdM*-calibrated luminosity algorithms. The statistical uncertainties, in contrast, are algorithm dependent (Table 5), but small by comparison.

The uncertainties affecting the April and July 2012 calibrations have not been evaluated in detail. Most of them would be of comparable magnitude to their November counterparts, except for additional sizeable contributions from the non-factorization effects and scan-to-scan inconsistencies discussed in Sect. 4.11.

6 Consistency of relative-luminosity measurements during physics running

The calibration of $\overline{\sigma}_{\text{vis}}$ was performed at only a few points in time (Table 2), and at values of μ low compared to the pile-up levels routinely encountered during physics operation (Fig. 12). In this section, the stability of the luminosity measurement over the 2012 high-luminosity data sample is characterized from two distinct viewpoints: time stability of the relative response of various luminosity algorithms across the entire running period (Sect. 6.1), and linearity of the calibrated luminosity values with respect to the actual pile-up parameter μ (Sect. 6.2). The relative con-

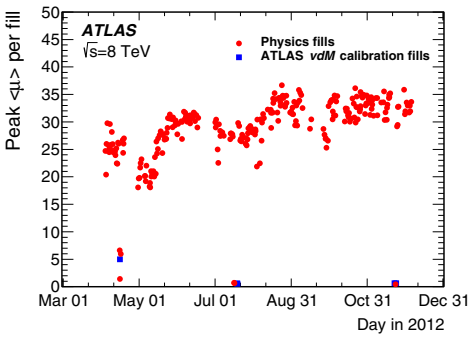

Fig. 12 History of the peak bunch-averaged pile-up parameter $\langle\mu\rangle$ during 2012, restricted to stable-beam periods

sistency across all available luminosity detectors and algorithms is used to assess the robustness of the results and to quantify systematic variations in the response of the various luminometers.

6.1 Relative stability of luminosity measurements over time

6.1.1 Consistency within individual luminometer subsystems

Figure 13a illustrates the internal consistency of the luminosity values reported by independent bunch-by-bunch algorithms during the 2012 running period, noise- and afterglow-subtracted as described in Sect. 4.4, then summed over all colliding bunches and integrated over the stable-beam period in each ATLAS run. In order to better illustrate their relative time evolution, these run-integrated luminosity ratios are shown *anchored*, i.e. normalized to the corresponding ratio in a high-luminosity run close in time to the November *vdM*-scan session.

During most of 2012, the ratio of the luminosity values reported by the horizontal and vertical pairs of BCM sensors is stable within a $\pm 0.4\%$ envelope, with the notable exception of a sharp -0.6% step, lasting approximately one month, during which the BCM was affected by electronic noise (Sect. 4.4). While during physics operation the noise itself has a negligible impact on the measured luminosity, its onset was accompanied by step changes in the response of individual diamond sensors; similar efficiency shifts in the opposite direction were observed when the noise disappeared, a few days after the November *vdM* session.

The history of the luminosity ratio between the A and C arms of LUCID exhibits two distinct bands, each with a peak-to-peak scatter of up to $\pm 0.8\%$ and separated by 1.5% on the average. The step change in late June 2012 is associated with turning off two PMTs in the C arm, which were drawing excessive current. To mitigate the impact of this operational change on the LUCID performance, the LUCID luminosity before (after) this step change is determined using the April (November) 2012 *vdM* calibrations.

While relative efficiency variations among individual BCM sensors, or between the two LUCID arms, can be monitored using such internal luminosity ratios, quantifying the associated shifts in their absolute calibration requires an external reference. This can be provided, for instance, by the calorimeter- or MPX-based hit-counting luminosity algorithms presented in Sect. 3.3. Among these, the best internal performance is offered by the EMEC and the TileCal: in the high-luminosity regime, both achieve an arm-to-arm consistency better than $\pm 0.4\%$ across the 2012 running period (Fig. 13b). The two FCal arms display a relative drift of about 1% which is highly correlated among all channels in each arm. The run-to-run spread of the MPX luminosity ratios (Fig. 13c) lies in the 2% range.

While calorimeter algorithms lack sensitivity in the *vdM*-calibration regime, the track-counting method can be absolutely calibrated with a precision comparable to that of the BCM and LUCID algorithms (Table 5). As demonstrated below, it also offers competitive precision for the run-integrated luminosity[10] during physics operation, thereby providing additional constraints on the performance of the other bunch-by-bunch algorithms.

Figure 14 displays the history of the luminosity reported by the two alternative track-counting working points introduced in Sect. 3.2, normalized to that from the default WP. In contrast to what is presented in Fig. 13, these ratios are not anchored, but directly reflect the relative response of the three algorithms as calibrated in the November 2012 *vdM*-scan session. While the three working points are consistent within 0.2% at the very beginning of the 2012 running period (which corresponds to the April *vdM*-scan session), counting vertex-associated tracks results, during most of the year, in a luminosity value lower by about 1.3% compared to the other two WPs. Comparison with the history of the mean pile-up parameter (Fig. 12) suggests that this inconsistency is not time-related but μ-dependent, as further discussed in Sect. 6.2.

6.1.2 Consistency between luminometer subsystems

Figure 15 shows the ratio of the integrated luminosity per ATLAS run as measured by a variety of luminosity algo-

[10] Except for *vdM*-scan sessions, track–counting-based luminosity measurements on shorter time scales (a few luminosity blocks), or on a bunch-by-bunch basis, are statistically limited by the available data-acquisition bandwidth.

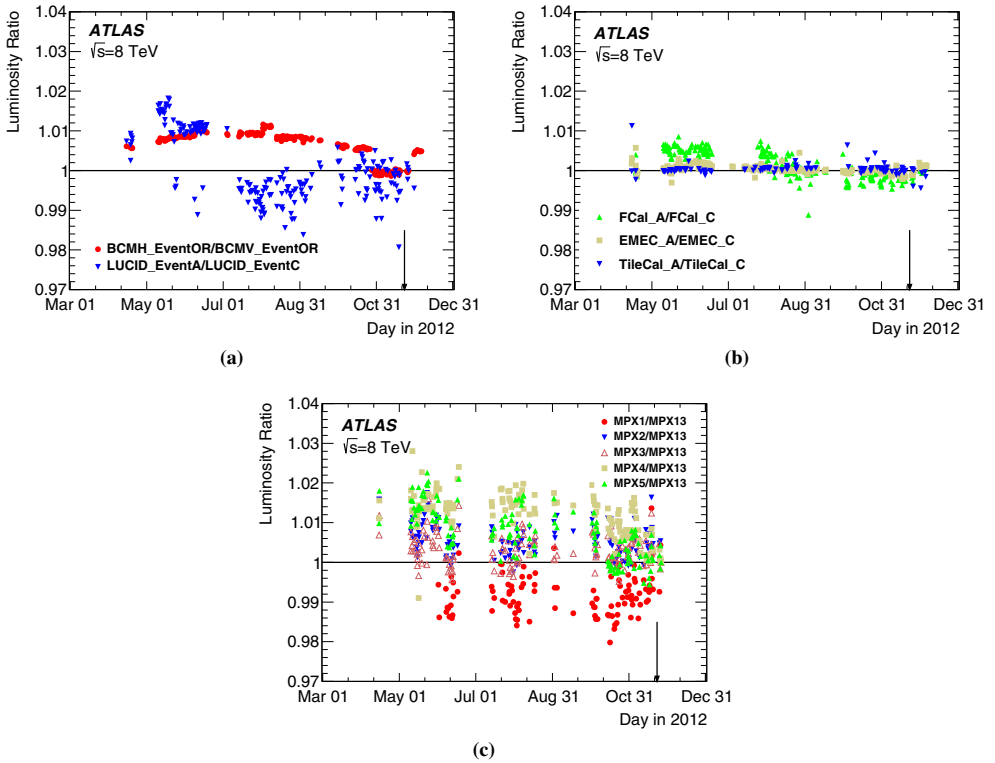

Fig. 13 **a** History of the ratio of the integrated luminosities per run reported by the BCM inclusive–OR algorithms (BCMV_EventOR/BCMH_EventOR) and by the LUCID single-arm algorithms (LUCID_EventA/LUCID_EventC), during routine physics operation at high luminosity. **b** History of the ratio of the integrated luminosities per run reported by the A and C arms of the electromagnetic endcap (EMEC), hadronic (TileCal) and forward (FCal) calorimeters. **c** History of the ratio of the integrated luminosities per run reported by five of the six individual MPX sensors, to that reported by the sixth sensor in the same run. In all figures, *each point* shows the ratio for a single run relative to that in a reference run taken on November 25, 2012 (LHC fill 3323). Statistical uncertainties are negligible. The *vertical arrows* indicate the time of the November 2012 *vdM* scan session

rithms, to that reported by the TileCal. Even though a systematic trend between the LAr and TileCal measurements is apparent, the calorimeter algorithms are consistent to better than ±0.7%. The TileCal luminosity is consistent with that from the default track-counting algorithm to within ±0.4% or less.

In contrast, both BCM and LUCID exhibit significant variations in response over the course of 2012, which vary from channel to channel and are attributed to, respectively, radiation-induced lattice defects and PMT aging. Among these, the BCMH_EventOR algorithm exhibits the least severe deviation from its response at the time of the November *vdM*-scan session. Its long-term drift is, however, large enough to warrant a time-dependent response correction that is based on one of the more stable relative-luminosity monitors shown in Fig. 15, and that is described in Sect. 7.3.2.

6.2 μ dependence

As the pile-up response of a given luminosity algorithm is determined by the instrumental characteristics of the luminometer considered, the BCMH_EventOR and BCMV_EventOR algorithms are expected to exhibit little μ-dependence with respect to each other, even if both may be affected by a common non-linearity with respect to the actual instantaneous luminosity. The same applies to ratios of luminosity values reported independently by the A and C arms of FCal, EMEC, LUCID and TileCal.

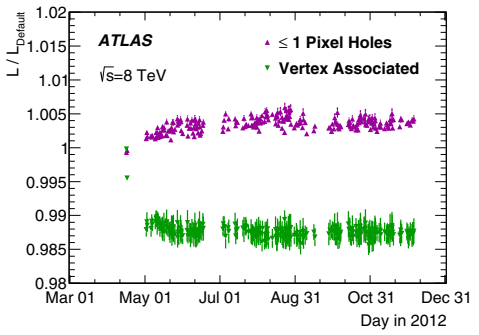

Fig. 14 History of the integrated-luminosity values reported by the two alternative track-counting methods, normalized to that from the default track selection, each as absolutely calibrated by the *vdM* method. *Each point* represents the mean over a single ATLAS run. The *error bars* reflect the systematic uncertainty associated with the simulation-based fake-track subtraction. No track-counting data are available prior to the first *vdM*-scan session (16 April 2012)

In contrast, the track-counting luminosities obtained using the three track selections defined in Sect. 3.2 exhibit a noticeable relative non-linearity (Fig. 16a). The pattern is consistent with that observed in Fig. 14. At very low μ, the three working points are fully consistent, as expected from having been *vdM*-calibrated at $\mu \sim 0.5$. As μ increases, loosening the pixel-hole requirement on the selected tracks results, after fake-track subtraction, in a residual positive non-linearity of at most 0.7% in the reported $\langle\mu\rangle$ value. In contrast, the vertex-associated track count exhibits, also after fake-track correction, a negative non-linearity with respect to the default WP, which peaks at -1.3% and then decreases in magnitude. Even though the simulation should account for the pile-up dependence of the fake-track fraction and of the track- and vertex-reconstruction efficiencies, it fails to explain the relative μ-dependence observed in the data between the three track-counting selections. The onset of the discrepancies appears to lie in the range $2 < \mu < 10$. However, only very limited data, all from a single run with a small number of isolated bunches, are available in that μ range, so that no firm conclusions can be drawn. A conservative approach is therefore adopted: the observed discrepancy between track-counting WPs is used as a data-driven upper limit on a potential bias affecting the absolute track-based luminosity scale in the high-μ regime. The impact of this systematic uncertainty is discussed in Sect. 7.3.1.

In the absence of any absolute linearity reference, potential pile–up-dependent biases in the high-μ regime can be constrained by the relative μ-dependence of the luminosity values reported by luminometers based on very different technologies (Fig. 16b). The relative non-linearity between the BCMH_EventOR and the TileCal (the default track-counting) algorithm does not exceed $\pm 0.3\%$ ($\pm 0.5\%$) over the $\langle\mu\rangle$ range accessible in this run; the root causes of the relative μ-dependence between these three luminometers remain under investigation. An extensive analysis of the more severe LUCID non-linearity indicates that under typical physics operating conditions, the large currents drawn by the LUCID PMTs significantly distort their response.

The run-averaged pile-up parameter changes from one run to the next, because of variations both in the initial luminosity and in the duration of LHC fills. Therefore, the larger the relative μ-dependence between two algorithms, the larger the fill-to-fill fluctuations in the ratio of the run-integrated luminosities reported by these two algorithms. This effect contributes significantly to the point-to-point scatter that is apparent in Fig. 15.

7 Luminosity determination during physics running

To determine the integrated luminosity used in ATLAS physics analyses, a single bunch-by-bunch algorithm is selected as the baseline to provide the central value for a certain time range (Sect. 7.1). The corresponding *vdM*-calibrated luminosity values are first background-subtracted (Sect. 7.2), and then corrected for rate- and time-dependent biases that impact high-luminosity operation (Sect. 7.3). The consistency of the various ATLAS luminosity measurements after all corrections is quantified in Sect. 7.4, together with the associated systematic uncertainty.

7.1 Baseline luminosity algorithm

The choice of algorithm is determined in part by the reproducibility and long-term stability of its absolute calibration. Figure 9 shows that in this respect, the BCMH_EventOR and track-counting algorithms perform noticeably better than BCMV_EventOR and LUCID. Studies of relative stability during physics running (Fig. 15) and of μ dependence (Fig. 16b) lead to the same conclusion. As track counting is active only during stable-beam operation and is statistically marginal at the luminosity-block level, it is not suitable for use as a baseline algorithm, but it is retained as a reference method to assess systematic biases. The BCMH_EventOR algorithm supplies the absolute luminosity during most of the 2012 running period; it is supplemented by the LUCID_EventA algorithm during the few runs where the BCM is not available, and which represent less than 1% of the 2012 integrated luminosity.

7.2 Background subtraction

During high-luminosity physics running, instrumental noise and single-beam backgrounds become negligible by com-

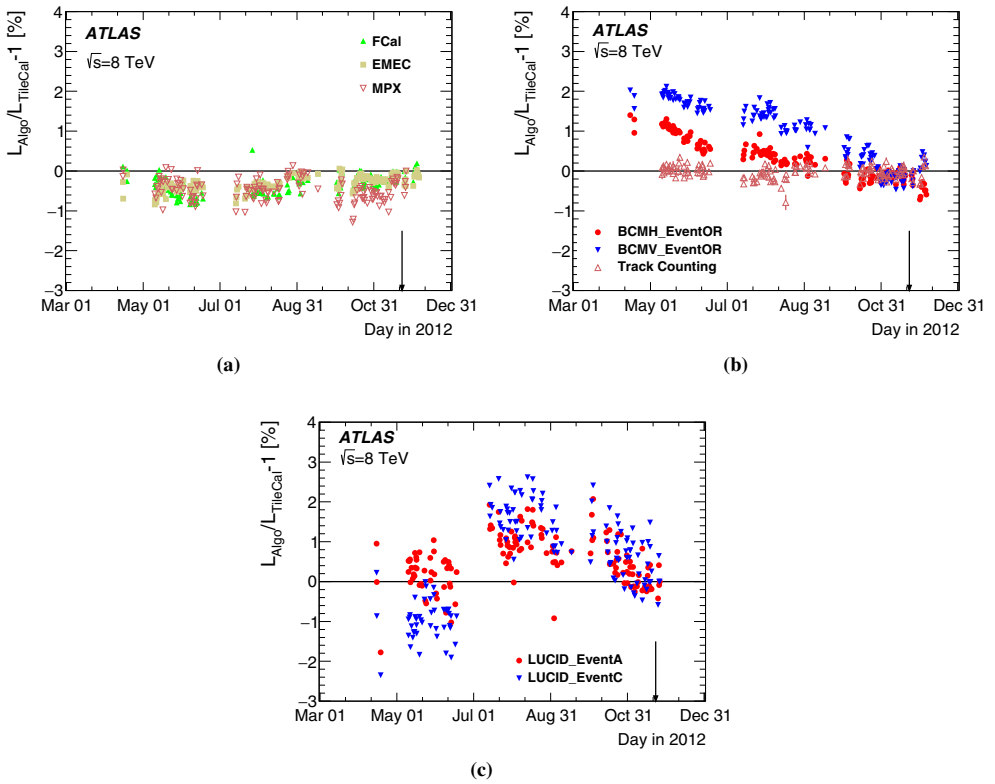

Fig. 15 History of the luminosity per run, compared to the value measured by TileCal, for **a** bunch-integrating, **b** BCM and track-counting, and **c** LUCID algorithms, during routine physics operation at high luminosity. *Each point* shows for a single run the mean deviation from a reference run taken on November 25, 2012 (LHC fill 3323). The EMEC, FCal and TileCal values are computed using the average of the luminosities reported by the A and C arms of the corresponding calorimeter; the MPX values reflect the average over the six sensors. The step in LUCID response is moderate thanks to the use of the April calibration for the LUCID data recorded before July. The *vertical arrows* indicate the time of the November *vdM* scan session

parison to the luminosity; only afterglow remains as a significant background. With a 2012 bunch spacing of 50 ns and typically over 1000 colliding bunches, it reaches a fairly stable equilibrium after the first few bunches in a train. It is observed to scale with the instantaneous luminosity and typically amounts to 0.2–0.5% of the luminosity signal.

The bunch-by-bunch noise- and afterglow-subtraction procedure described in Sect. 4.4 is applied to all BCM and LUCID luminosity determinations. Since the afterglow level in the BCID immediately following a colliding-bunch slot may differ from that in the second BCID after this slot (i.e. in the next colliding-bunch slot), BCIDs at the end of a bunch train were used to evaluate a possible bias in the method. This study suggests that the subtraction over-corrects the BCMH_EventOR luminosity by approximately 0.2%. A systematic uncertainty of ±0.2% is therefore assigned to the afterglow correction.

7.3 Corrections to the absolute calibration in the high-luminosity regime

Extrapolating the curves of Fig. 16b to very low $\langle\mu\rangle$ suggests that for some algorithms, the *vdM*-based luminosity scale may not be directly applicable in the pile-up regime typical of physics operation. Percent-level corrections are indeed required (Sect. 7.3.1) to transfer, at one point in time, the absolute calibration of BCM and LUCID from the low-luminosity regime of *vdM* scans ($\mu \sim 0.5$, $\mathcal{L} \sim$

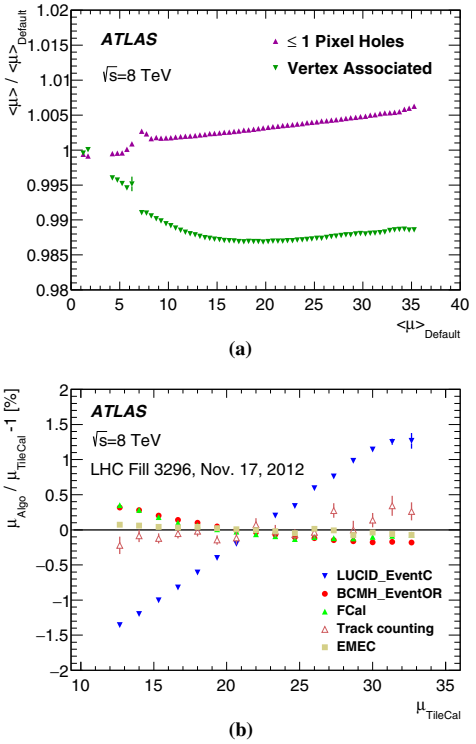

Fig. 16 **a** Ratio of the bunch-averaged pile-up parameter $\langle\mu\rangle$ reported using different track-counting working points, to that from the default WP, as a function of the $\langle\mu\rangle$ value obtained using the default WP. The data are averaged over all stable-beam runs. **b** Fractional deviation of the bunch-averaged pile-up parameter $\langle\mu\rangle$, obtained using different algorithms, from the TileCal value, as a function of $\langle\mu\rangle_{\text{TileCal}}$, during a physics run selected to cover the widest possible $\langle\mu\rangle$ range. The data are normalized such that all algorithms yield the same integrated luminosity in the run considered

2×10^{30} cm^{-2}s^{-1}) to that of routine physics operation ($\mu\sim$ 20–25, $\mathcal{L}>10^{33}$ cm^{-2}s^{-1}). In addition, a time-dependent correction (Sect. 7.3.2) must be applied to the luminosity of the baseline algorithm to compensate for the long-term drifts apparent in Fig. 15.

7.3.1 *Calibration transfer from the* vdM *regime to physics conditions*

The history of the instantaneous-luminosity values reported during part of the November *vdM*-scan session by the track-counting and LUCID_EventA algorithms, relative to the BCMH_EventOR algorithm and using the calibrations listed in Table 5, is presented in Fig. 17a. The ratio of the default track-counting (LUCID) luminosity integrated over several hours immediately before and after scan set XV, to that from the BCMH_EventOR algorithm, is consistent with unity within 0.5% (0.4%). The run-integrated luminosity values associated, in that same fill, with the other two track selections (not shown) are consistent with the default track selection within less than one per mille.

However, at high luminosity these ratios differ from unity by several percent (Fig. 17b), with all BCM (LUCID) algorithms reporting a lower (higher) luminosity compared to the track-counting method. In addition, the vertex-associated track selection is no longer consistent with the other two, as discussed in Sect. 6.

To provide consistent luminosity measurements, all algorithms must be corrected to some common absolute scale in the high-luminosity regime. As calorimeter-based luminometers lack sensitivity in the *vdM*-scan regime, only track counting remains to quantify the relative shifts in response of the BCM and LUCID algorithms between the *vdM*-scan and high-luminosity regimes. First, the run-to-run fluctuations in Fig. 17b are smoothed by parameterizing the luminosity ratios as a linear function of the cumulative integrated-luminosity fraction, used here as a proxy for calendar time. Then, for each BCM algorithm and for a given track selection, the difference between the fitted ratio in the high-luminosity reference fill where the calibration transfer is performed (LHC fill 3323), and the corresponding run-integrated luminosity ratio under *vdM* conditions (LHC fill 3316), quantifies the shift in the BCM luminosity scale with respect to track counting. The same procedure is applied to LUCID.

The results are summarized in Table 7 for the default track selection. The BCMH_EventOR efficiency drops by 2.5% with respect to track counting. Naively extrapolating the relative μ-dependence of these two algorithms from the high-μ regime (Fig. 16b) to $\mu\sim0.5$ predicts a shift of 1.3%, about half of the effect observed.[11] Similarly, the μ-dependence of LUCID_EventC predicts a 3% increase in response when going from the *vdM*-scan regime to the high-luminosity regime, while the measured step amounts to +3.9%. These observations suggest that while the measured relative μ-dependence of the three algorithms is consistent with the signs of the calibration shifts and appears to account for a large fraction of their magnitude, other effects also play a role. For instance, studies of the CMS diamond sensors [34] suggest that the response of the BCM may depend on the

[11] Since the mechanisms driving the μ-dependence are neither well characterized nor understood, and in the absence of sufficient data linking the μ range in routine physics operation (Fig. 16b) to that in the *vdM*-scan regime ($\mu\sim0.5$), such an extrapolation is indicative only: it cannot be relied upon for a quantitative evaluation of the calibration-transfer correction.

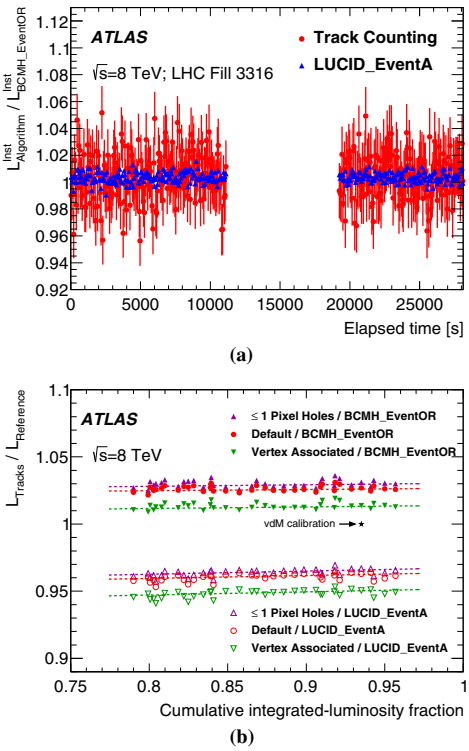

Fig. 17 **a** History of the ratio of the instantaneous luminosity reported by the default track-counting and LUCID_EventA algorithms to that from the BCMH_EventOR algorithm under *vdM*-scan conditions, during LHC fill 3316. The gap corresponds to scan set XV. The *error bars* are statistical. **b** Evolution of the ratio of the integrated luminosity per run reported by the three track-counting algorithms to that from the BCMH_EventOR and LUCID_EventA algorithms, in the few weeks in late 2012 during which the BCM response is approximately constant, as a function of the cumulative delivered luminosity (normalized to the 2012 total). Each point shows the ratio for a single high-luminosity run. The *dashed lines* are *straight-line* fits to the data. The reference run (LHC fill 3323) took place the day following the November *vdM*-scan session, which is indicated by the *star*

total instantaneous collision rate (i.e. on the product of $\langle\mu\rangle$ and the total number of colliding bunches) through a polarization mechanism associated with radiation-induced lattice defects.

The track-counting results lie between BCM and LUCID, and using the track scale as a proxy for the true scale is consistent to within 0.5% with taking the average scale from all the algorithms listed in Table 7. The choice of which track selection to use as reference is somewhat arbitrary. The default working point appears as the natural choice given that

Table 7 Measured fractional shift in luminosity scale between the *vdM*-scan regime (LHC fill 3316) and a nearby high-luminosity ATLAS run (LHC fill 3323), using the default track-counting algorithm as the reference. The errors shown are statistical only; they are dominated by track-counting statistics in the *vdM*-scan fill, and are therefore fully correlated across the four ratios

Luminosity algorithm	Calibration shift w.r.t. track counting (%)
BCMH_eventOR	-2.5 ± 0.1
BCMV_eventOR	-2.9 ± 0.1
LUCID_eventA	$+3.5 \pm 0.1$
LUCID_eventC	$+3.9 \pm 0.1$

it exhibits the smallest relative μ-dependence with respect to TileCal, suffers from the smallest uncertainty arising from the simulation-based fake-track subtraction, and lies between the extremes of the three track selections.

The systematic uncertainty in the calibration-transfer corrections of Table 7 is estimated to be $\pm 1.4\%$. It is dominated by the 1.3% inconsistency (Figs. 16a, 17b) between the default and the vertex-associated track selections. Additional contributions arise from the small inconsistency between the BCM-based and track-based luminosity measurements during the *vdM*-scan fill (0.5%), from a small deadtime correction that affects the *vdM*-scan track-counting data only (0.2%), and from the track-counting statistics during the *vdM*-scan fill (0.1%). The slight integrated-luminosity (or time) dependence of the BCM to track-counting luminosity ratio visible in Fig. 17b is accounted for as part of the long-term drift correction, discussed next.

7.3.2 *Long-term drift correction*

The second step in transferring the *vdM*-based calibrations to an arbitrary high-luminosity physics run consists in correcting for the long-term drifts apparent in Fig. 15, using one of the more stable monitors (EMEC, FCal, TileCal or track counting) as a reference. The absolute luminosity scale of the selected reference monitor is first anchored to that of BCM (or LUCID) in the high-luminosity reference run where the calibration transfer is performed (LHC fill 3323). The run-by-run luminosity ratio of the considered bunch-by-bunch algorithm to the chosen reference is then parameterized as a function of the cumulative integrated-luminosity fraction. This choice of variable, instead of calendar time, is inspired by (but not dependent upon) the assumption that detector aging increases smoothly with integrated radiation dose; it also simplifies the analysis by eliminating the gaps between running periods (Fig. 15). A two-segment, piece-wise linear fit is used to smooth the run-to-run fluctuations, with one segment covering the entire year except for the BCM

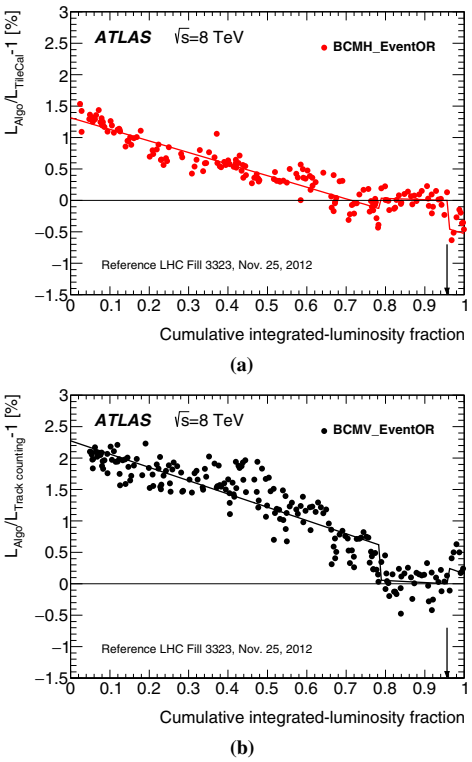

Fig. 18 History of the fractional difference in integrated luminosity per run **a** between the BCMH_EventOR and the TileCal algorithm, and **b** between the BCMV_EventOR and the default track-counting algorithm. *Each point* shows the mean difference for a single run compared to that in the reference run (LHC fill 3323) in which the calibration transfer is performed. The *lines* represent the fit discussed in the text. The *vertical arrow* indicates the time of the reference run

noise period, and the second, shorter segment accounting for the gain shift during that same noise period (Fig. 18). This empirical parameterization yields a satisfactory description of the entire data set. It provides a run-by-run correction to the instantaneous luminosity reported by each BCM or LUCID algorithm: a positive (negative) value of the fit function in a given ATLAS run results in a downwards (upwards) luminosity adjustment for every luminosity block in that run. This implies that the absolute luminosity scale in each LHC fill is effectively carried by the reference monitor, while the time- and BCID-dependence of the luminosity during that same fill continues to be provided by the bunch-by-bunch algorithm considered.

The net impact of this procedure on the integrated luminosity for the entire 2012 running period is documented in Table 8. The TileCal- and track–counting-based corrections are effectively indistinguishable; the former is chosen for the central value because of the slightly smaller run-to-run scatter of the BCM/TileCal luminosity ratio. The largest difference between reference monitors amounts to 0.3%, and reflects the relative slope between the FCal and TileCal algorithms in Fig. 15a. This value is taken as the systematic uncertainty in the long-term drift correction.

7.4 Consistency of ATLAS luminosity measurements after all corrections

A global check of the consistency of the corrections described in Sects. 7.2 and 7.3 is provided by the comparison of the 2012 integrated-luminosity values reported by different bunch-by-bunch algorithms. For high-luminosity runs ($\beta^\star = 0.6$ m and at least 1050 colliding bunches) under stable-beam conditions, after background subtraction, calibration transfer and long-term drift correction of the BCM and LUCID data, the integrated luminosity reported by BCMV_EventOR agrees with that from the BCMH_EventOR baseline within 0.01%. For the subset of such runs where both LUCID and BCM deliver valid luminosity data, which corresponds to about 91% of the 2012 integrated luminosity, both single-arm LUCID algorithms agree with the BCMH_EventOR baseline within 0.5%. It should be stressed, however, that these BCM- and LUCID-based luminosity determinations are correlated, because they were all drift-corrected to the same reference.

The internal consistency of the absolute luminosity measurements at $\sqrt{s} = 8$ TeV in the high-luminosity regime is illustrated in Fig. 19. The run-to-run fluctuations reflect the combined impact of the relative μ-dependence of the various algorithms, of imperfectly corrected medium-term drifts and of other sources of non-reproducibility. With the exception of some of the LUCID data, they remain within a $\pm 0.5\%$ band, which provides a measure of the systematic uncertainty associated with the run-to-run consistency of independent luminosity measurements.

8 Total luminosity uncertainty for the 2012 *pp* run

Table 9 regroups the contributions to the total uncertainty in the luminosity values provided for physics analyses. The *vdM*-calibration uncertainties are detailed in Tables 5 and 6. The afterglow subtraction, the calibration transfer from the *vdM*-scan to the high-luminosity regime and the long-term drift correction applied to the bunch-by-bunch luminometers are described in Sects. 7.2, 7.3.1 and 7.3.2 respectively. The run-to-run consistency of the ATLAS luminosity measurements is assessed in Sect. 7.4. The resulting total uncertainty amounts to $\pm 1.9\%$.

Table 8 Impact of the long-term drift correction on the 2012 integrated luminosity

Reference algorithm	Fractional change in integrated luminosity [%]			
	BCMH_EventOR	BCMV_EventOR	LUCID_EventA	LUCID_EventC
EMEC	−0.59	−1.26	−0.70	−0.49
FCal	−0.70	−1.36	−0.68	−0.52
TileCal	−0.44	−1.09	−0.54	−0.26
Track counting	−0.45	−1.12	−0.57	−0.34

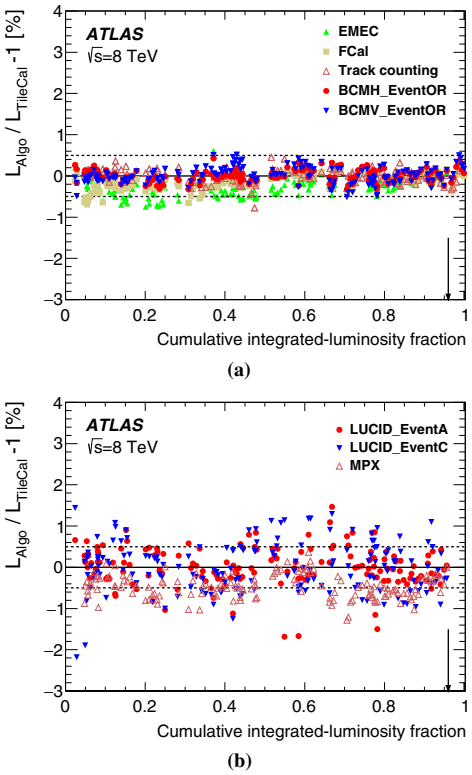

Fig. 19 History of the fractional difference in run-integrated luminosity between the TileCal algorithm and the drift-corrected **a** BCM and **b** LUCID and MPX algorithms. The results of the other possible reference monitors (EMEC, FCal and track counting) are taken from Fig. 15 and included here for comparison. *Each point* shows the mean difference for a single run compared to that in the reference fill indicated by the arrow. The *dashed horizontal lines* delimit a ±0.5% window around zero

9 Summary

The ATLAS luminosity scale for the 2012 LHC run has been calibrated using data from dedicated beam-separation scans, also known as van der Meer scans. The *vdM*-calibration uncertainty is smaller than for the 2011 data set [3], thanks to improved control of beam-dynamical effects (beam–beam deflections, dynamic β, non-factorization) and to a refined analysis of the non-reproducibility of beam conditions (orbit drift, emittance growth). The total systematic uncertainty in the delivered luminosity is no longer dominated by *vdM*-calibration uncertainties. The largest contribution arises from instrumental effects that require the transfer of the absolute luminosity scale from the low-rate *vdM*-scan regime to the high-luminosity conditions of routine physics operation; residual run-to-run and long-term inconsistencies between independent luminosity measurements also contribute significantly.

Table 9 Relative uncertainty in the calibrated luminosity scale, broken down by source

Uncertainty source	$\delta\mathcal{L}/\mathcal{L}$ [%]
van der Meer calibration	1.2
Afterglow subtraction	0.2
Calibration transfer from *vdM*-scan to high-luminosity regime	1.4
Long-term drift correction	0.3
Run-to-run consistency	0.5
Total	1.9

The combination of these systematic uncertainties results in a final uncertainty of $\delta\mathcal{L}/\mathcal{L} = \pm 1.9\%$ in the luminosity measured by ATLAS during pp collisions at $\sqrt{s} = 8$ TeV for the 22.7 fb^{-1} of data delivered to ATLAS in 2012. This uncertainty applies to the high-luminosity data sample and any subset thereof, but not necessarily to a few special runs taken under very low pile-up conditions, such as those dedicated to elastic-scattering measurements: the latter require a separate analysis tailored to their specific experimental conditions.

Acknowledgements We thank CERN for the very successful operation of the LHC, as well as the support staff from our institutions without whom ATLAS could not be operated efficiently. We acknowledge the support of ANPCyT, Argentina; YerPhI, Armenia; ARC, Australia; BMWFW and FWF, Austria; ANAS, Azerbaijan; SSTC, Belarus; CNPq and FAPESP, Brazil; NSERC, NRC and CFI, Canada; CERN; CONICYT, Chile; CAS, MOST and NSFC, China; COLCIENCIAS, Colombia; MSMT CR, MPO CR and VSC CR, Czech Republic; DNRF and

DNSRC, Denmark; IN2P3-CNRS, CEA-DSM/IRFU, France; GNSF, Georgia; BMBF, HGF, and MPG, Germany; GSRT, Greece; RGC, Hong Kong SAR, China; ISF, I-CORE and Benoziyo Center, Israel; INFN, Italy; MEXT and JSPS, Japan; CNRST, Morocco; FOM and NWO, Netherlands; RCN, Norway; MNiSW and NCN, Poland; FCT, Portugal; MNE/IFA, Romania; MES of Russia and NRC KI, Russian Federation; JINR; MESTD, Serbia; MSSR, Slovakia; ARRS and MIZŠ, Slovenia; DST/NRF, South Africa; MINECO, Spain; SRC and Wallenberg Foundation, Sweden; SERI, SNSF and Cantons of Bern and Geneva, Switzerland; MOST, Taiwan; TAEK, Turkey; STFC, United Kingdom; DOE and NSF, United States of America. In addition, individual groups and members have received support from BCKDF, the Canada Council, CANARIE, CRC, Compute Canada, FQRNT, and the Ontario Innovation Trust, Canada; EPLANET, ERC, FP7, Horizon 2020 and Marie Skłodowska-Curie Actions, European Union; Investissements d'Avenir Labex and Idex, ANR, Région Auvergne and Fondation Partager le Savoir, France; DFG and AvH Foundation, Germany; Herakleitos, Thales and Aristeia programmes co-financed by EU-ESF and the Greek NSRF; BSF, GIF and Minerva, Israel; BRF, Norway; Generalitat de Catalunya, Generalitat Valenciana, Spain; the Royal Society and Leverhulme Trust, United Kingdom. The crucial computing support from all WLCG partners is acknowledged gratefully, in particular from CERN, the ATLAS Tier-1 facilities at TRIUMF (Canada), NDGF (Denmark, Norway, Sweden), CC-IN2P3 (France), KIT/GridKA (Germany), INFN-CNAF (Italy), NL-T1 (Netherlands), PIC (Spain), ASGC (Taiwan), RAL (UK) and BNL (USA), the Tier-2 facilities worldwide and large non-WLCG resource providers. Major contributors of computing resources are listed in Ref. [35].

Funded by SCOAP[3].

References

1. ATLAS Collaboration, The ATLAS Experiment at the CERN Large Hadron Collider. JINST **3**, S08003 (2008). doi:10.1088/1748-0221/3/08/S08003
2. S. van der Meer, Calibration of the effective beam height in the ISR. CERN-ISR-PO-68-31 (1968). http://cds.cern.ch/record/296752
3. ATLAS Collaboration, Improved luminosity determination in pp collisions at $\sqrt{s} = 7$ TeV using the ATLAS detector at the LHC. Eur. Phys. J. C **73**, 2518 (2013). doi:10.1140/epjc/s10052-013-2518-3, arXiv:1302.4393 [hep-ex]
4. C. Rubbia, Measurement of the luminosity of $p\bar{p}$ collider with a (generalized) van der Meer Method. CERN-$p\bar{p}$-Note-38 (1977). http://cds.cern.ch/record/1025746
5. ATLAS Collaboration, Luminosity determination in pp collisions at $\sqrt{s} = 7$ TeV using the ATLAS detector at the LHC. Eur. Phys. J. C **71** 1630 (2011). doi:10.1140/epjc/s10052-011-1630-5, arXiv:1101.2185 [hep-ex]
6. ATLAS Collaboration, Concepts, design and implementation of the ATLAS new tracking (NEWT). ATL-SOFT-PUB-2007-007 (2007). http://cds.cern.ch/record/1020106
7. P. Grafström, W. Kozanecki, Luminosity determination at proton colliders. Progr. Part. Nucl. Phys. **81**, 97–148 (2015). doi:10.1016/j.ppnp.2014.11.002
8. ATLAS Collaboration, Charged-particle multiplicities in pp interactions measured with the ATLAS detector at the LHC. New J. Phys. **13** 053033 (2011). doi:10.1088/1367-2630/13/5/053033, arXiv:1012.5104 [hep-ex]
9. ATLAS Collaboration, Performance of the atlas inner detector track and vertex reconstruction in the high pile-up LHC environment. ATLAS-CONF-2012-042 (2012). http://cdsweb.cern.ch/record/1435196
10. T. Sjöstrand, S. Mrenna, P. Skands, A brief introduction to PYTHIA 8.1. Comput. Phys. Commun. **178**, 852 (2008). doi:10.1016/j.cpc.2008.01.036. arXiv:0710.3820 [hep-ph]
11. Tile Calorimeter Collaboration, Tile calorimeter technical design report. CERN-LHCC-96-042 (1996). http://cds.cern.ch/record/331062
12. A. Sopczak et al., MPX detectors as LHC luminosity monitor. IEEE Trans. Nucl. Sci. **62**, 3225 (2015). http://ieeexplore.ieee.org/stamp/stamp.jsp?arnumber=7349015
13. M. Venturini, W. Kozanecki, Out-of-plane deflections as a diagnostic tool and application to PEP-II. SLAC-PUB-8700 (2001). http://slac.stanford.edu/pubs/slacpubs/8500/slac-pub-8700.pdf
14. W. Herr, B. Muratori, Concept of luminosity. Yellow Report CERN 2006-002 (2006). http://cds.cern.ch/record/941318
15. H. Wiedemann, Particle accelerator physics, graduate texts in physics. Springer, ISBN 9783319183169, 9783319183176 (2015). http://www.springer.com/us/book/9783319183169?wt_mc=ThirdParty.SpringerLink.3.EPR653.About_eBook
16. H. Bartosik, G. Rumolo, Production of the single bunch for Van der Meer scans in the LHC injector chain. CERN-ACC-NOTE-2013-0008 (2013). http://cds.cern.ch/record/1590405
17. W. Kozanecki, T. Pieloni, J. Wenninger, Observation of beam-beam deflections with LHC orbit data. CERN-ACC-NOTE-2013-0006 (2013). http://cds.cern.ch/record/1581723
18. P. Bambade et al., Observation of beam-beam deflections at the interaction point of the SLAC linear collider. Phys. Rev. Lett. **62**, 2949 (1989). doi:10.1103/PhysRevLett.62.2949
19. W. Herr, Beam-beam effects and dynamic β^*. Proc. LHC Lumi Days (2012). http://indico.cern.ch/event/162948/contributions/1417430/attachments/191879/269237/S3_WH.pdf
20. CERN Accelerator Beam Physics Group, MAD–Methodical Accelerator Design. http://mad.web.cern.ch/mad/
21. LHCb Collaboration, R. Aaij et al., Precision luminosity measurements at LHCb. JINST **9**, P12005 (2014). doi:10.1088/1748-0221/9/12/P12005, arXiv:1410.0149 [hep-ex]
22. S.M. White, Determination of the absolute luminosity at the LHC. CERN-THESIS-2010-139 (2010). http://cds.cern.ch/record/1308187
23. ATLAS Collaboration, Characterization of interaction-point beam parameters using the pp event-vertex distribution reconstructed in the ATLAS detector at the LHC. ATLAS-CONF-2010-027 (2010). http://cdsweb.cern.ch/record/1277659
24. V. Balagura, Notes on van der Meer scan for absolute luminosity measurement. Nucl. Instrum. Methods A **654**, 634–638 (2011). doi:10.1016/j.nima.2011.06.007, arXiv:1103.1129 [physics.ins-det]
25. LHCb Collaboration, R. Aaij et al., Absolute luminosity measurements with the LHCb detector at the LHC. JINST **7**, P01010 (2012). doi:10.1088/1748-0221/7/01/P01010, arXiv:1110.2866 [hep-ex]
26. F.J. Decker, Beam distributions beyond RMS. SLAC-PUB-95-6684 (1994). http://www.slac.stanford.edu/cgi-wrap/getdoc/slac-pub-6841.pdf
27. C. Barschel, Precision luminosity measurement at LHCb with beam-gas imaging. CERN-THESIS-2013-301 (2014). http://cds.cern.ch/record/1693671

28. S.N. Webb, Factorisation of beams in van der Meer scans and measurements of the ϕ_η^* distribution of $Z \to e^+e^-$ events in pp collisions at $\sqrt{s} = 8$ TeV with the ATLAS detector. CERN-THESIS-2015-054 (2015). http://cds.cern.ch/record/2020875
29. CMS Collaboration, CMS luminosity based on pixel cluster counting—summer 2012 update. CMS-PAS-LUM-12-001 (2012). http://cds.cern.ch/record/1482193
30. CMS Collaboration, CMS luminosity based on pixel cluster counting—summer 2013 update. CMS-PAS-LUM-13-001 (2013). http://cds.cern.ch/record/1598864
31. C. Barschel et al., Results of the LHC DCCT calibration studies. CERN-ATS-Note-2012-026 PERF (2012). http://cdsweb.cern.ch/record/1425904
32. G. Anders et al., Study of the Relative Bunch Populations for Luminosity Calibration, CERN-ATS-Note-2012-028 PERF (2012). http://cdsweb.cern.ch/record/1427726
33. A Boccardi et al., LHC luminosity calibration using the longitudinal density monitor. CERN-ATS-Note-2013-034 TECH (2013). http://cds.cern.ch/record/1556087
34. M. Guthoff et al., Radiation damage in the diamond based beam condition monitors of the CMS experiment at the Large Hadron Collider (LHC) at CERN. Nucl. Instrum. Methods. A **730** 168–173 (2013). doi:10.1016/j.nima.2013.05.041
35. ATLAS Collaboration, ATLAS computing acknowledgements 2016–2017. ATL-GEN-PUB-2016-002 (2016). http://cds.cern.ch/record/2202407

ATLAS Collaboration

M. Aaboud[136d], G. Aad[87], B. Abbott[114], J. Abdallah[65], O. Abdinov[12], B. Abeloos[118], R. Aben[108], O. S. AbouZeid[138], N. L. Abraham[150], H. Abramowicz[154], H. Abreu[153], R. Abreu[117], Y. Abulaiti[147a,147b], B. S. Acharya[164a,164b,a], L. Adamczyk[40a], D. L. Adams[27], J. Adelman[109], S. Adomeit[101], T. Adye[132], A. A. Affolder[76], T. Agatonovic-Jovin[14], J. Agricola[56], J. A. Aguilar-Saavedra[127a,127f], S. P. Ahlen[24], F. Ahmadov[67,b], G. Aielli[134a,134b], H. Akerstedt[147a,147b], T. P. A. Åkesson[83], A. V. Akimov[97], G. L. Alberghi[22a,22b], J. Albert[169], S. Albrand[57], M. J. Alconada Verzini[73], M. Aleksa[32], I. N. Aleksandrov[67], C. Alexa[28b], G. Alexander[154], T. Alexopoulos[10], M. Alhroob[114], M. Aliev[75a,75b], G. Alimonti[93a], J. Alison[33], S. P. Alkire[37], B. M. M. Allbrooke[150], B. W. Allen[117], P. P. Allport[19], A. Aloisio[105a,105b], A. Alonso[38], F. Alonso[73], C. Alpigiani[139], M. Alstaty[87], B. Alvarez Gonzalez[32], D. Álvarez Piqueras[167], M. G. Alviggi[105a,105b], B. T. Amadio[16], K. Amako[68], Y. Amaral Coutinho[26a], C. Amelung[25], D. Amidei[91], S. P. Amor Dos Santos[127a,127c], A. Amorim[127a,127b], S. Amoroso[32], G. Amundsen[25], C. Anastopoulos[140], L. S. Ancu[51], N. Andari[109], T. Andeen[11], C. F. Anders[60b], G. Anders[32], J. K. Anders[76], K. J. Anderson[33], A. Andreazza[93a,93b], V. Andrei[60a], S. Angelidakis[9], I. Angelozzi[108], P. Anger[46], A. Angerami[37], F. Anghinolfi[32], A. V. Anisenkov[110,c], N. Anjos[13], A. Annovi[125a,125b], M. Antonelli[49], A. Antonov[99,*], F. Anulli[133a], M. Aoki[68], L. Aperio Bella[19], G. Arabidze[92], Y. Arai[68], J. P. Araque[127a], A. T. H. Arce[47], F. A. Arduh[73], J.-F. Arguin[96], S. Argyropoulos[65], M. Arik[20a], A. J. Armbruster[144], L. J. Armitage[78], O. Arnaez[32], H. Arnold[50], M. Arratia[30], O. Arslan[23], A. Artamonov[98], G. Artoni[121], S. Artz[85], S. Asai[156], N. Asbah[44], A. Ashkenazi[154], B. Åsman[147a,147b], L. Asquith[150], K. Assamagan[27], R. Astalos[145a], M. Atkinson[166], N. B. Atlay[142], K. Augsten[129], G. Avolio[32], B. Axen[16], M. K. Ayoub[118], G. Azuelos[96,d], M. A. Baak[32], A. E. Baas[60a], M. J. Baca[19], H. Bachacou[137], K. Bachas[75a,75b], M. Backes[32], M. Backhaus[32], P. Bagiacchi[133a,133b], P. Bagnaia[133a,133b], Y. Bai[35a], J. T. Baines[132], O. K. Baker[176], E. M. Baldin[110,c], P. Balek[130], T. Balestri[149], F. Balli[137], W. K. Balunas[123], E. Banas[41], Sw. Banerjee[173,e], A. A. E. Bannoura[175], L. Barak[32], E. L. Barberio[90], D. Barberis[52a,52b], M. Barbero[87], T. Barillari[102], T. Barklow[144], N. Barlow[30], S. L. Barnes[86], B. M. Barnett[132], R. M. Barnett[16], Z. Barnovska[5], A. Baroncelli[135a], G. Barone[25], A. J. Barr[121], L. Barranco Navarro[167], F. Barreiro[84], J. Barreiro Guimarães da Costa[35a], R. Bartoldus[144], A. E. Barton[74], P. Bartos[145a], A. Basalaev[124], A. Bassalat[118], R. L. Bates[55], S. J. Batista[159], J. R. Batley[30], M. Battaglia[138], M. Bauce[133a,133b], F. Bauer[137], H. S. Bawa[144,f], J. B. Beacham[112], M. D. Beattie[74], T. Beau[82], P. H. Beauchemin[162], P. Bechtle[23], H. P. Beck[18,g], K. Becker[121], M. Becker[85], M. Beckingham[170], C. Becot[111], A. J. Beddall[20d], A. Beddall[20b], V. A. Bednyakov[67], M. Bedognetti[108], C. P. Bee[149], L. J. Beemster[108], T. A. Beermann[32], M. Begel[27], J. K. Behr[44], C. Belanger-Champagne[89], A. S. Bell[80], G. Bella[154], L. Bellagamba[22a], A. Bellerive[31], M. Bellomo[88], K. Belotskiy[99], O. Beltramello[32], N. L. Belyaev[99], O. Benary[154], D. Benchekroun[136a], M. Bender[101], K. Bendtz[147a,147b], N. Benekos[10], Y. Benhammou[154], E. Benhar Noccioli[176], J. Benitez[65], D. P. Benjamin[47], J. R. Bensinger[25], S. Bentvelsen[108], L. Beresford[121], M. Beretta[49], D. Berge[108], E. Bergeaas Kuutmann[165], N. Berger[5], J. Beringer[16], S. Berlendis[57], N. R. Bernard[88], C. Bernius[111], F. U. Bernlochner[23], T. Berry[79], P. Berta[130], C. Bertella[85], G. Bertoli[147a,147b], F. Bertolucci[125a,125b], I. A. Bertram[74], C. Bertsche[44], D. Bertsche[114], G. J. Besjes[38], O. Bessidskaia Bylund[147a,147b], M. Bessner[44], N. Besson[137], C. Betancourt[50], S. Bethke[102], A. J. Bevan[78], W. Bhimji[16], R. M. Bianchi[126], L. Bianchini[25], M. Bianco[32], O. Biebel[101], D. Biedermann[17], R. Bielski[86], N. V. Biesuz[125a,125b], M. Biglietti[135a], J. Bilbao De Mendizabal[51], H. Bilokon[49], M. Bindi[56], S. Binet[118], A. Bingul[20b], C. Bini[133a,133b], S. Biondi[22a,22b], D. M. Bjergaard[47], C. W. Black[151], J. E. Black[144], K. M. Black[24], D. Blackburn[139], R. E. Blair[6], J.-B. Blanchard[137], J. E. Blanco[79], T. Blazek[145a], I. Bloch[44], C. Blocker[25], W. Blum[85,*], U. Blumenschein[56], S. Blunier[34a], G. J. Bobbink[108], V. S. Bobrovnikov[110,c], S. S. Bocchetta[83], A. Bocci[47], C. Bock[101], M. Boehler[50],

D. Boerner[175], J. A. Bogaerts[32], D. Bogavac[14], A. G. Bogdanchikov[110], C. Bohm[147a], V. Boisvert[79], P. Bokan[14], T. Bold[40a], A. S. Boldyrev[164a,164c], M. Bomben[82], M. Bona[78], M. Boonekamp[137], A. Borisov[131], G. Borissov[74], J. Bortfeldt[101], D. Bortoletto[121], V. Bortolotto[62a,62b,62c], K. Bos[108], D. Boscherini[22a], M. Bosman[13], J. D. Bossio Sola[29], J. Boudreau[126], J. Bouffard[2], E. V. Bouhova-Thacker[74], D. Boumediene[36], C. Bourdarios[118], S. K. Boutle[55], A. Boveia[32], J. Boyd[32], I. R. Boyko[67], J. Bracinik[19], A. Brandt[8], G. Brandt[56], O. Brandt[60a], U. Bratzler[157], B. Brau[88], J. E. Brau[117], H. M. Braun[175,*], W. D. Breaden Madden[55], K. Brendlinger[123], A. J. Brennan[90], L. Brenner[108], R. Brenner[165], S. Bressler[172], T. M. Bristow[48], D. Britton[55], D. Britzger[44], F. M. Brochu[30], I. Brock[23], R. Brock[92], G. Brooijmans[37], T. Brooks[79], W. K. Brooks[34b], J. Brosamer[16], E. Brost[117], J. H Broughton[19], P. A. Bruckman de Renstrom[41], D. Bruncko[145b], R. Bruneliere[50], A. Bruni[22a], G. Bruni[22a], L. S. Bruni[108], BH Brunt[30], M. Bruschi[22a], N. Bruscino[23], P. Bryant[33], L. Bryngemark[83], T. Buanes[15], Q. Buat[143], P. Buchholz[142], A. G. Buckley[55], I. A. Budagov[67], F. Buehrer[50], M. K. Bugge[120], O. Bulekov[99], D. Bullock[8], H. Burckhart[32], S. Burdin[76], C. D. Burgard[50], B. Burghgrave[109], K. Burka[41], S. Burke[132], I. Burmeister[45], E. Busato[36], D. Büscher[50], V. Büscher[85], P. Bussey[55], J. M. Butler[24], C. M. Buttar[55], J. M. Butterworth[80], P. Butti[108], W. Buttinger[27], A. Buzatu[55], A. R. Buzykaev[110,c], S. Cabrera Urbán[167], D. Caforio[129], V. M. Cairo[39a,39b], O. Cakir[4a], N. Calace[51], P. Calafiura[16], A. Calandri[87], G. Calderini[82], P. Calfayan[101], L. P. Caloba[26a], D. Calvet[36], S. Calvet[36], T. P. Calvet[87], R. Camacho Toro[33], S. Camarda[32], P. Camarri[134a,134b], D. Cameron[120], R. Caminal Armadans[166], C. Camincher[57], S. Campana[32], M. Campanelli[80], A. Camplani[93a,93b], A. Campoverde[142], V. Canale[105a,105b], A. Canepa[160a], M. Cano Bret[35e], J. Cantero[115], R. Cantrill[127a], T. Cao[42], M. D. M. Capeans Garrido[32], I. Caprini[28b], M. Caprini[28b], M. Capua[39a,39b], R. Caputo[85], R. M. Carbone[37], R. Cardarelli[134a], F. Cardillo[50], I. Carli[130], T. Carli[32], G. Carlino[105a], L. Carminati[93a,93b], S. Caron[107], E. Carquin[34b], G. D. Carrillo-Montoya[32], J. R. Carter[30], J. Carvalho[127a,127c], D. Casadei[19], M. P. Casado[13,h], M. Casolino[13], D. W. Casper[163], E. Castaneda-Miranda[146a], R. Castelijn[108], A. Castelli[108], V. Castillo Gimenez[167], N. F. Castro[127a,i], A. Catinaccio[32], J. R. Catmore[120], A. Cattai[32], J. Caudron[85], V. Cavaliere[166], E. Cavallaro[13], D. Cavalli[93a], M. Cavalli-Sforza[13], V. Cavasinni[125a,125b], F. Ceradini[135a,135b], L. Cerda Alberich[167], B. C. Cerio[47], A. S. Cerqueira[26b], A. Cerri[150], L. Cerrito[78], F. Cerutti[16], M. Cerv[32], A. Cervelli[18], S. A. Cetin[20c], A. Chafaq[136a], D. Chakraborty[109], S. K. Chan[59], Y. L. Chan[62a], P. Chang[166], J. D. Chapman[30], D. G. Charlton[19], A. Chatterjee[51], C. C. Chau[159], C. A. Chavez Barajas[150], S. Che[112], S. Cheatham[74], A. Chegwidden[92], S. Chekanov[6], S. V. Chekulaev[160a], G. A. Chelkov[67,j], M. A. Chelstowska[91], C. Chen[66], H. Chen[27], K. Chen[149], S. Chen[35c], S. Chen[156], X. Chen[35f], Y. Chen[69], H. C. Cheng[91], H. J Cheng[35a], Y. Cheng[33], A. Cheplakov[67], E. Cheremushkina[131], R. Cherkaoui El Moursli[136e], V. Chernyatin[27,*], E. Cheu[7], L. Chevalier[137], V. Chiarella[49], G. Chiarelli[125a,125b], G. Chiodini[75a], A. S. Chisholm[19], A. Chitan[28b], M. V. Chizhov[67], K. Choi[63], A. R. Chomont[36], S. Chouridou[9], B. K. B. Chow[101], V. Christodoulou[80], D. Chromek-Burckhart[32], J. Chudoba[128], A. J. Chuinard[89], J. J. Chwastowski[41], L. Chytka[116], G. Ciapetti[133a,133b], A. K. Ciftci[4a], D. Cinca[55], V. Cindro[77], I. A. Cioara[23], A. Ciocio[16], F. Cirotto[105a,105b], Z. H. Citron[172], M. Citterio[93a], M. Ciubancan[28b], A. Clark[51], B. L. Clark[59], M. R. Clark[37], P. J. Clark[48], R. N. Clarke[16], C. Clement[147a,147b], Y. Coadou[87], M. Cobal[164a,164c], A. Coccaro[51], J. Cochran[66], L. Coffey[25], L. Colasurdo[107], B. Cole[37], A. P. Colijn[108], J. Collot[57], T. Colombo[32], G. Compostella[102], P. Conde Muiño[127a,127b], E. Coniavitis[50], S. H. Connell[146b], I. A. Connelly[79], V. Consorti[50], S. Constantinescu[28b], G. Conti[32], F. Conventi[105a,k], M. Cooke[16], B. D. Cooper[80], A. M. Cooper-Sarkar[121], K. J. R. Cormier[159], T. Cornelissen[175], M. Corradi[133a,133b], F. Corriveau[89,l], A. Corso-Radu[163], A. Cortes-Gonzalez[13], G. Cortiana[102], G. Costa[93a], M. J. Costa[167], D. Costanzo[140], G. Cottin[30], G. Cowan[79], B. E. Cox[86], K. Cranmer[111], S. J. Crawley[55], G. Cree[31], S. Crépé-Renaudin[57], F. Crescioli[82], W. A. Cribbs[147a,147b], M. Crispin Ortuzar[121], M. Cristinziani[23], V. Croft[107], G. Crosetti[39a,39b], T. Cuhadar Donszelmann[140], J. Cummings[176], M. Curatolo[49], J. Cúth[85], C. Cuthbert[151], H. Czirr[142], P. Czodrowski[3], G. D'amen[22a,22b], S. D'Auria[55], M. D'Onofrio[76], M. J. Da Cunha Sargedas De Sousa[127a,127b], C. Da Via[86], W. Dabrowski[40a], T. Dado[145a], T. Dai[91], O. Dale[15], F. Dallaire[96], C. Dallapiccola[88], M. Dam[38], J. R. Dandoy[33], N. P. Dang[50], A. C. Daniells[19], N. S. Dann[86], M. Danninger[168], M. Dano Hoffmann[137], V. Dao[50], G. Darbo[52a], S. Darmora[8], J. Dassoulas[3], A. Dattagupta[63], W. Davey[23], C. David[169], T. Davidek[130], M. Davies[154], P. Davison[80], E. Dawe[90], I. Dawson[140], R. K. Daya-Ishmukhametova[88], K. De[8], R. de Asmundis[105a], A. De Benedetti[114], S. De Castro[22a,22b], S. De Cecco[82], N. De Groot[107], P. de Jong[108], H. De la Torre[84], F. De Lorenzi[66], A. De Maria[56], D. De Pedis[133a], A. De Salvo[133a], U. De Sanctis[150], A. De Santo[150], J. B. De Vivie De Regie[118], W. J. Dearnaley[74], R. Debbe[27], C. Debenedetti[138], D. V. Dedovich[67], N. Dehghanian[3], I. Deigaard[108], M. Del Gaudio[39a,39b], J. Del Peso[84], T. Del Prete[125a,125b], D. Delgove[118], F. Deliot[137], C. M. Delitzsch[51], M. Deliyergiyev[77], A. Dell'Acqua[32], L. Dell'Asta[24], M. Dell'Orso[125a,125b], M. Della Pietra[105a,k], D. della Volpe[51], M. Delmastro[5], P. A. Delsart[57], C. Deluca[108], D. A. DeMarco[159], S. Demers[176], M. Demichev[67], A. Demilly[82], S. P. Denisov[131], D. Denysiuk[137], D. Derendarz[41], J. E. Derkaoui[136d], F. Derue[82], P. Dervan[76], K. Desch[23], C. Deterre[44], K. Dette[45], P. O. Deviveiros[32], A. Dewhurst[132], S. Dhaliwal[25], A. Di Ciaccio[134a,134b], L. Di Ciaccio[5], W. K. Di Clemente[123], C. Di Donato[133a,133b], A. Di Girolamo[32], B. Di Girolamo[32], B. Di Micco[135a,135b], R. Di Nardo[32], A. Di Simone[50],

R. Di Sipio[159], D. Di Valentino[31], C. Diaconu[87], M. Diamond[159], F. A. Dias[48], M. A. Diaz[34a], E. B. Diehl[91], J. Dietrich[17], S. Diglio[87], A. Dimitrievska[14], J. Dingfelder[23], P. Dita[28b], S. Dita[28b], F. Dittus[32], F. Djama[87], T. Djobava[53b], J. I. Djuvsland[60a], M. A. B. do Vale[26c], D. Dobos[32], M. Dobre[28b], C. Doglioni[83], T. Dohmae[156], J. Dolejsi[130], Z. Dolezal[130], B. A. Dolgoshein[99,*], M. Donadelli[26d], S. Donati[125a,125b], P. Dondero[122a,122b], J. Donini[36], J. Dopke[132], A. Doria[105a], M. T. Dova[73], A. T. Doyle[55], E. Drechsler[56], M. Dris[10], Y. Du[35d], J. Duarte-Campderros[154], E. Duchovni[172], G. Duckeck[101], O. A. Ducu[96,m], D. Duda[108], A. Dudarev[32], E. M. Duffield[16], L. Duflot[118], L. Duguid[79], M. Dührssen[32], M. Dumancic[172], M. Dunford[60a], H. Duran Yildiz[4a], M. Düren[54], A. Durglishvili[53b], D. Duschinger[46], B. Dutta[44], M. Dyndal[44], C. Eckardt[44], K. M. Ecker[102], R. C. Edgar[91], N. C. Edwards[48], T. Eifert[32], G. Eigen[15], K. Einsweiler[16], T. Ekelof[165], M. El Kacimi[136c], V. Ellajosyula[87], M. Ellert[165], S. Elles[5], F. Ellinghaus[175], A. A. Elliot[169], N. Ellis[32], J. Elmsheuser[27], M. Elsing[32], D. Emeliyanov[132], Y. Enari[156], O. C. Endner[85], M. Endo[119], J. S. Ennis[170], J. Erdmann[45], A. Ereditato[18], G. Ernis[175], J. Ernst[2], M. Ernst[27], S. Errede[166], E. Ertel[85], M. Escalier[118], H. Esch[45], C. Escobar[126], B. Esposito[49], A. I. Etienvre[137], E. Etzion[154], H. Evans[63], A. Ezhilov[124], F. Fabbri[22a,22b], L. Fabbri[22a,22b], G. Facini[33], R. M. Fakhrutdinov[131], S. Falciano[133a], R. J. Falla[80], J. Faltova[32], Y. Fang[35a], M. Fanti[93a,93b], A. Farbin[8], A. Farilla[135a], C. Farina[126], T. Farooque[13], S. Farrell[16], S. M. Farrington[170], P. Farthouat[32], F. Fassi[136e], P. Fassnacht[32], D. Fassouliotis[9], M. Faucci Giannelli[79], A. Favareto[52a,52b], W. J. Fawcett[121], L. Fayard[118], O. L. Fedin[124,n], W. Fedorko[168], S. Feigl[120], L. Feligioni[87], C. Feng[35d], E. J. Feng[32], H. Feng[91], A. B. Fenyuk[131], L. Feremenga[8], P. Fernandez Martinez[167], S. Fernandez Perez[13], J. Ferrando[55], A. Ferrari[165], P. Ferrari[108], R. Ferrari[122a], D. E. Ferreira de Lima[60b], A. Ferrer[167], D. Ferrere[51], C. Ferretti[91], A. Ferretto Parodi[52a,52b], F. Fiedler[85], A. Filipčič[77], M. Filipuzzi[44], F. Filthaut[107], M. Fincke-Keeler[169], K. D. Finelli[151], M. C. N. Fiolhais[127a,127c], L. Fiorini[167], A. Firan[42], A. Fischer[2], C. Fischer[13], J. Fischer[175], W. C. Fisher[92], N. Flaschel[44], I. Fleck[142], P. Fleischmann[91], G. T. Fletcher[140], R. R. M. Fletcher[123], T. Flick[175], A. Floderus[83], L. R. Flores Castillo[62a], M. J. Flowerdew[102], G. T. Forcolin[86], A. Formica[137], A. Forti[86], A. G. Foster[19], D. Fournier[118], H. Fox[74], S. Fracchia[13], P. Francavilla[82], M. Franchini[22a,22b], D. Francis[32], L. Franconi[120], M. Franklin[59], M. Frate[163], M. Fraternali[122a,122b], D. Freeborn[80], S. M. Fressard-Batraneanu[32], F. Friedrich[46], D. Froidevaux[32], J. A. Frost[121], C. Fukunaga[157], E. Fullana Torregrosa[85], T. Fusayasu[103], J. Fuster[167], C. Gabaldon[57], O. Gabizon[175], A. Gabrielli[22a,22b], A. Gabrielli[16], G. P. Gach[40a], S. Gadatsch[32], S. Gadomski[51], G. Gagliardi[52a,52b], L. G. Gagnon[96], P. Gagnon[63], C. Galea[107], B. Galhardo[127a,127c], E. J. Gallas[121], B. J. Gallop[132], P. Gallus[129], G. Galster[38], K. K. Gan[112], J. Gao[35b,87], Y. Gao[48], Y. S. Gao[144,f], F. M. Garay Walls[48], C. García[167], J. E. García Navarro[167], M. Garcia-Sciveres[16], R. W. Gardner[33], N. Garelli[144], V. Garonne[120], A. Gascon Bravo[44], C. Gatti[49], A. Gaudiello[52a,52b], G. Gaudio[122a], B. Gaur[142], L. Gauthier[96], I. L. Gavrilenko[97], C. Gay[168], G. Gaycken[23], E. N. Gazis[10], Z. Gecse[168], C. N. P. Gee[132], Ch. Geich-Gimbel[23], M. Geisen[85], M. P. Geisler[60a], C. Gemme[52a], M. H. Genest[57], C. Geng[35b,o], S. Gentile[133a,133b], S. George[79], D. Gerbaudo[13], A. Gershon[154], S. Ghasemi[142], H. Ghazlane[136b], M. Ghneimat[23], B. Giacobbe[22a], S. Giagu[133a,133b], P. Giannetti[125a,125b], B. Gibbard[27], S. M. Gibson[79], M. Gignac[168], M. Gilchriese[16], T. P. S. Gillam[30], D. Gillberg[31], G. Gilles[175], D. M. Gingrich[3,d], N. Giokaris[9], M. P. Giordani[164a,164c], F. M. Giorgi[22a], F. M. Giorgi[17], P. F. Giraud[137], P. Giromini[59], D. Giugni[93a], F. Giuli[121], C. Giuliani[102], M. Giulini[60b], B. K. Gjelsten[120], S. Gkaitatzis[155], I. Gkialas[155], E. L. Gkougkousis[118], L. K. Gladilin[100], C. Glasman[84], J. Glatzer[50], P. C. F. Glaysher[48], A. Glazov[44], M. Goblirsch-Kolb[102], J. Godlewski[41], S. Goldfarb[91], T. Golling[51], D. Golubkov[131], A. Gomes[127a,127b,127d], R. Gonçalo[127a], J. Goncalves Pinto Firmino Da Costa[137], G. Gonella[50], L. Gonella[19], A. Gongadze[67], S. González de la Hoz[167], G. Gonzalez Parra[13], S. Gonzalez-Sevilla[51], L. Goossens[32], P. A. Gorbounov[98], H. A. Gordon[27], I. Gorelov[106], B. Gorini[32], E. Gorini[75a,75b], A. Gorišek[77], E. Gornicki[41], A. T. Goshaw[47], C. Gössling[45], M. I. Gostkin[67], C. R. Goudet[118], D. Goujdami[136c], A. G. Goussiou[139], N. Govender[146b,p], E. Gozani[153], L. Graber[56], I. Grabowska-Bold[40a], P. O. J. Gradin[57], P. Grafström[22a,22b], J. Gramling[51], E. Gramstad[120], S. Grancagnolo[17], V. Gratchev[124], P. M. Gravila[28e], H. M. Gray[32], E. Graziani[135a], Z. D. Greenwood[81,q], C. Grefe[23], K. Gregersen[80], I. M. Gregor[44], P. Grenier[144], K. Grevtsov[5], J. Griffiths[8], A. A. Grillo[138], K. Grimm[74], S. Grinstein[13,r], Ph. Gris[36], J. -F. Grivaz[118], S. Groh[85], J. P. Grohs[46], E. Gross[172], J. Grosse-Knetter[56], G. C. Grossi[81], Z. J. Grout[150], L. Guan[91], W. Guan[173], J. Guenther[129], F. Guescini[51], D. Guest[163], O. Gueta[154], E. Guido[52a,52b], T. Guillemin[5], S. Guindon[2], U. Gul[55], C. Gumpert[32], J. Guo[35e], Y. Guo[35b,o], S. Gupta[121], G. Gustavino[133a,133b], P. Gutierrez[114], N. G. Gutierrez Ortiz[80], C. Gutschow[46], C. Guyot[137], C. Gwenlan[121], C. B. Gwilliam[76], A. Haas[111], C. Haber[16], H. K. Hadavand[8], N. Haddad[136e], A. Hadef[87], P. Haefner[23], S. Hageböck[23], Z. Hajduk[41], H. Hakobyan[177,*], M. Haleem[44], J. Haley[115], G. Halladjian[92], G. D. Hallewell[87], K. Hamacher[175], P. Hamal[116], K. Hamano[169], A. Hamilton[146a], G. N. Hamity[140], P. G. Hamnett[44], L. Han[35b], K. Hanagaki[68,s], K. Hanawa[156], M. Hance[138], B. Haney[123], P. Hanke[60a], R. Hanna[137], J. B. Hansen[38], J. D. Hansen[38], M. C. Hansen[23], P. H. Hansen[38], K. Hara[161], A. S. Hard[173], T. Harenberg[175], F. Hariri[118], S. Harkusha[94], R. D. Harrington[48], P. F. Harrison[170], F. Hartjes[108], N. M. Hartmann[101], M. Hasegawa[69], Y. Hasegawa[141], A. Hasib[114], S. Hassani[137], S. Haug[18], R. Hauser[92], L. Hauswald[46], M. Havranek[128], C. M. Hawkes[19],

R. J. Hawkings[32], D. Hayden[92], C. P. Hays[121], J. M. Hays[78], H. S. Hayward[76], S. J. Haywood[132], S. J. Head[19], T. Heck[85], V. Hedberg[83], L. Heelan[8], S. Heim[123], T. Heim[16], B. Heinemann[16], J. J. Heinrich[101], L. Heinrich[111], C. Heinz[54], J. Hejbal[128], L. Helary[24], S. Hellman[147a,147b], C. Helsens[32], J. Henderson[121], R. C. W. Henderson[74], Y. Heng[173], S. Henkelmann[168], A. M. Henriques Correia[32], S. Henrot-Versille[118], G. H. Herbert[17], Y. Hernández Jiménez[167], G. Herten[50], R. Hertenberger[101], L. Hervas[32], G. G. Hesketh[80], N. P. Hessey[108], J. W. Hetherly[42], R. Hickling[78], E. Higón-Rodriguez[167], E. Hill[169], J. C. Hill[30], K. H. Hiller[44], S. J. Hillier[19], I. Hinchliffe[16], E. Hines[123], R. R. Hinman[16], M. Hirose[158], D. Hirschbuehl[175], J. Hobbs[149], N. Hod[160a], M. C. Hodgkinson[140], P. Hodgson[140], A. Hoecker[32], M. R. Hoeferkamp[106], F. Hoenig[101], D. Hohn[23], T. R. Holmes[16], M. Homann[45], T. M. Hong[126], B. H. Hooberman[166], W. H. Hopkins[117], Y. Horii[104], A. J. Horton[143], J-Y. Hostachy[57], S. Hou[152], A. Hoummada[136a], J. Howarth[44], M. Hrabovsky[116], I. Hristova[17], J. Hrivnac[118], T. Hryn'ova[5], A. Hrynevich[95], C. Hsu[146c], P. J. Hsu[152,t], S. -C. Hsu[139], D. Hu[37], Q. Hu[35b], Y. Huang[44], Z. Hubacek[129], F. Hubaut[87], F. Huegging[23], T. B. Huffman[121], E. W. Hughes[37], G. Hughes[74], M. Huhtinen[32], T. A. Hülsing[85], P. Huo[149], N. Huseynov[67,b], J. Huston[92], J. Huth[59], G. Iacobucci[51], G. Iakovidis[27], I. Ibragimov[142], L. Iconomidou-Fayard[118], E. Ideal[176], Z. Idrissi[136e], P. Iengo[32], O. Igonkina[108,u], T. Iizawa[171], Y. Ikegami[68], M. Ikeno[68], Y. Ilchenko[11,v], D. Iliadis[155], N. Ilic[144], T. Ince[102], G. Introzzi[122a,122b], P. Ioannou[9,*], M. Iodice[135a], K. Iordanidou[37], V. Ippolito[59], M. Ishino[70], M. Ishitsuka[158], R. Ishmukhametov[112], C. Issever[121], S. Istin[20a], F. Ito[161], J. M. Iturbe Ponce[86], R. Iuppa[134a,134b], W. Iwanski[41], H. Iwasaki[68], J. M. Izen[43], V. Izzo[105a], S. Jabbar[3], B. Jackson[123], M. Jackson[76], P. Jackson[1], V. Jain[2], K. B. Jakobi[85], K. Jakobs[50], S. Jakobsen[32], T. Jakoubek[128], D. O. Jamin[115], D. K. Jana[81], E. Jansen[80], R. Jansky[64], J. Janssen[23], M. Janus[56], G. Jarlskog[83], N. Javadov[67,b], T. Javůrek[50], F. Jeanneau[137], L. Jeanty[16], J. Jejelava[53a,w], G. -Y. Jeng[151], D. Jennens[90], P. Jenni[50,x], J. Jentzsch[45], C. Jeske[170], S. Jézéquel[5], H. Ji[173], J. Jia[149], H. Jiang[66], Y. Jiang[35b], S. Jiggins[80], J. Jimenez Pena[167], S. Jin[35a], A. Jinaru[28b], O. Jinnouchi[158], P. Johansson[140], K. A. Johns[7], W. J. Johnson[139], K. Jon-And[147a,147b], G. Jones[170], R. W. L. Jones[74], S. Jones[7], T. J. Jones[76], J. Jongmanns[60a], P. M. Jorge[127a,127b], J. Jovicevic[160a], X. Ju[173], A. Juste Rozas[13,r], M. K. Köhler[172], A. Kaczmarska[41], M. Kado[118], H. Kagan[112], M. Kagan[144], S. J. Kahn[87], E. Kajomovitz[47], C. W. Kalderon[121], A. Kaluza[85], S. Kama[42], A. Kamenshchikov[131], N. Kanaya[156], S. Kaneti[30], L. Kanjir[77], V. A. Kantserov[99], J. Kanzaki[68], B. Kaplan[111], L. S. Kaplan[173], A. Kapliy[33], D. Kar[146c], K. Karakostas[10], A. Karamaoun[3], N. Karastathis[10], M. J. Kareem[56], E. Karentzos[10], M. Karnevskiy[85], S. N. Karpov[67], Z. M. Karpova[67], K. Karthik[111], V. Kartvelishvili[74], A. N. Karyukhin[131], K. Kasahara[161], L. Kashif[173], R. D. Kass[112], A. Kastanas[15], Y. Kataoka[156], C. Kato[156], A. Katre[51], J. Katzy[44], K. Kawagoe[72], T. Kawamoto[156], G. Kawamura[56], S. Kazama[156], V. F. Kazanin[110,c], R. Keeler[169], R. Kehoe[42], J. S. Keller[44], J. J. Kempster[79], K. Kawade[104], H. Keoshkerian[159], O. Kepka[128], B. P. Kerševan[77], S. Kersten[175], R. A. Keyes[89], F. Khalil-zada[12], A. Khanov[115], A. G. Kharlamov[110,c], T. J. Khoo[51], V. Khovanskiy[98], E. Khramov[67], J. Khubua[53b,y], S. Kido[69], H. Y. Kim[8], S. H. Kim[161], Y. K. Kim[33], N. Kimura[155], O. M. Kind[17], B. T. King[76], M. King[167], S. B. King[168], J. Kirk[132], A. E. Kiryunin[102], T. Kishimoto[69], D. Kisielewska[40a], F. Kiss[50], K. Kiuchi[161], O. Kivernyk[137], E. Kladiva[145b], M. H. Klein[37], M. Klein[76], U. Klein[76], K. Kleinknecht[85], P. Klimek[147a,147b], A. Klimentov[27], R. Klingenberg[45], J. A. Klinger[140], T. Klioutchnikova[32], E. -E. Kluge[60a], P. Kluit[108], S. Kluth[102], J. Knapik[41], E. Kneringer[64], E. B. F. G. Knoops[87], A. Knue[55], A. Kobayashi[156], D. Kobayashi[158], T. Kobayashi[156], M. Kobel[46], M. Kocian[144], P. Kodys[130], T. Koffas[31], E. Koffeman[108], T. Koi[144], H. Kolanoski[17], M. Kolb[60b], I. Koletsou[5], A. A. Komar[97,*], Y. Komori[156], T. Kondo[68], N. Kondrashova[44], K. Köneke[50], A. C. König[107], T. Kono[68,z], R. Konoplich[111,aa], N. Konstantinidis[80], R. Kopeliansky[63], S. Koperny[40a], L. Köpke[85], A. K. Kopp[50], K. Korcyl[41], K. Kordas[155], A. Korn[80], A. A. Korol[110,c], I. Korolkov[13], E. V. Korolkova[140], O. Kortner[102], S. Kortner[102], T. Kosek[130], V. V. Kostyukhin[23], A. Kotwal[47], A. Kourkoumeli-Charalampidi[155], C. Kourkoumelis[9], V. Kouskoura[27], A. B. Kowalewska[41], R. Kowalewski[169], T. Z. Kowalski[40a], C. Kozakai[156], W. Kozanecki[137], A. S. Kozhin[131], V. A. Kramarenko[100], G. Kramberger[77], D. Krasnopevtsev[99], M. W. Krasny[82], A. Krasznahorkay[32], J. K. Kraus[23], A. Kravchenko[27], M. Kretz[60c], J. Kretzschmar[76], K. Kreutzfeldt[54], P. Krieger[159], K. Krizka[33], K. Kroeninger[45], H. Kroha[102], J. Kroll[123], J. Kroseberg[23], J. Krstic[14], U. Kruchonak[67], H. Krüger[23], N. Krumnack[66], A. Kruse[173], M. C. Kruse[47], M. Kruskal[24], T. Kubota[90], H. Kucuk[80], S. Kuday[4b], J. T. Kuechler[175], S. Kuehn[50], A. Kugel[60c], F. Kuger[174], A. Kuhl[138], T. Kuhl[44], V. Kukhtin[67], R. Kukla[137], Y. Kulchitsky[94], S. Kuleshov[34b], M. Kuna[133a,133b], T. Kunigo[70], A. Kupco[128], H. Kurashige[69], Y. A. Kurochkin[94], V. Kus[128], E. S. Kuwertz[169], M. Kuze[158], J. Kvita[116], T. Kwan[169], D. Kyriazopoulos[140], A. La Rosa[102], J. L. La Rosa Navarro[26d], L. La Rotonda[39a,39b], C. Lacasta[167], F. Lacava[133a,133b], J. Lacey[31], H. Lacker[17], D. Lacour[82], V. R. Lacuesta[167], E. Ladygin[67], R. Lafaye[5], B. Laforge[82], T. Lagouri[176], S. Lai[56], S. Lammers[63], W. Lampl[7], E. Lançon[137], U. Landgraf[50], M. P. J. Landon[78], V. S. Lang[60a], J. C. Lange[13], A. J. Lankford[163], F. Lanni[27], K. Lantzsch[23], A. Lanza[122a], S. Laplace[82], C. Lapoire[32], J. F. Laporte[137], T. Lari[93a], F. Lasagni Manghi[22a,22b], M. Lassnig[32], P. Laurelli[49], W. Lavrijsen[16], A. T. Law[138], P. Laycock[76], T. Lazovich[59], M. Lazzaroni[93a,93b], B. Le[90], O. Le Dortz[82], E. Le Guirriec[87], E. P. Le Quilleuc[137], M. LeBlanc[169], T. LeCompte[6], F. Ledroit-Guillon[57], C. A. Lee[27],

S. C. Lee[152], L. Lee[1], G. Lefebvre[82], M. Lefebvre[169], F. Legger[101], C. Leggett[16], A. Lehan[76], G. Lehmann Miotto[32], X. Lei[7], W. A. Leight[31], A. Leisos[155,ab], A. G. Leister[176], M. A. L. Leite[26d], R. Leitner[130], D. Lellouch[172], B. Lemmer[56], K. J. C. Leney[80], T. Lenz[23], B. Lenzi[32], R. Leone[7], S. Leone[125a,125b], C. Leonidopoulos[48], S. Leontsinis[10], G. Lerner[150], C. Leroy[96], A. A. J. Lesage[137], C. G. Lester[30], M. Levchenko[124], J. Levêque[5], D. Levin[91], L. J. Levinson[172], M. Levy[19], D. Lewis[78], A. M. Leyko[23], M. Leyton[43], B. Li[35b,o], H. Li[149], H. L. Li[33], L. Li[47], L. Li[35e], Q. Li[35a], S. Li[47], X. Li[86], Y. Li[142], Z. Liang[35a], B. Liberti[134a], A. Liblong[159], P. Lichard[32], K. Lie[166], J. Liebal[23], W. Liebig[15], A. Limosani[151], S. C. Lin[152,ac], T. H. Lin[85], B. E. Lindquist[149], A. E. Lionti[51], E. Lipeles[123], A. Lipniacka[15], M. Lisovyi[60b], T. M. Liss[166], A. Lister[168], A. M. Litke[138], B. Liu[152,ad], D. Liu[152], H. Liu[91], H. Liu[27], J. Liu[87], J. B. Liu[35b], K. Liu[87], L. Liu[166], M. Liu[47], M. Liu[35b], Y. L. Liu[35b], Y. Liu[35b], M. Livan[122a,122b], A. Lleres[57], J. Llorente Merino[35a], S. L. Lloyd[78], F. Lo Sterzo[152], E. Lobodzinska[44], P. Loch[7], W. S. Lockman[138], F. K. Loebinger[86], A. E. Loevschall-Jensen[38], K. M. Loew[25], A. Loginov[176,*], T. Lohse[17], K. Lohwasser[44], M. Lokajicek[128], B. A. Long[24], J. D. Long[166], R. E. Long[74], L. Longo[75a,75b], K. A. Looper[112], L. Lopes[127a], D. Lopez Mateos[59], B. Lopez Paredes[140], I. Lopez Paz[13], A. Lopez Solis[82], J. Lorenz[101], N. Lorenzo Martinez[63], M. Losada[21], P. J. Lösel[101], X. Lou[35a], A. Lounis[118], J. Love[6], P. A. Love[74], H. Lu[62a], N. Lu[91], H. J. Lubatti[139], C. Luci[133a,133b], A. Lucotte[57], C. Luedtke[50], F. Luehring[63], W. Lukas[64], L. Luminari[133a], O. Lundberg[147a,147b], B. Lund-Jensen[148], P. M. Luzi[82], D. Lynn[27], R. Lysak[128], E. Lytken[83], V. Lyubushkin[67], H. Ma[27], L. L. Ma[35d], Y. Ma[35d], G. Maccarrone[49], A. Macchiolo[102], C. M. Macdonald[140], B. Maček[77], J. Machado Miguens[123,127b], D. Madaffari[87], R. Madar[36], H. J. Maddocks[165], W. F. Mader[46], A. Madsen[44], J. Maeda[69], S. Maeland[15], T. Maeno[27], A. Maevskiy[100], E. Magradze[56], J. Mahlstedt[108], C. Maiani[118], C. Maidantchik[26a], A. A. Maier[102], T. Maier[101], A. Maio[127a,127b,127d], S. Majewski[117], Y. Makida[68], N. Makovec[118], B. Malaescu[82], Pa. Malecki[41], V. P. Maleev[124], F. Malek[57], U. Mallik[65], D. Malon[6], C. Malone[144], S. Maltezos[10], S. Malyukov[32], J. Mamuzic[167], G. Mancini[49], B. Mandelli[32], L. Mandelli[93a], I. Mandić[77], J. Maneira[127a,127b], L. Manhaes de Andrade Filho[26b], J. Manjarres Ramos[160b], A. Mann[101], A. Manousos[32], B. Mansoulie[137], J. D. Mansour[35a], R. Mantifel[89], M. Mantoani[56], S. Manzoni[93a,93b], L. Mapelli[32], G. Marceca[29], L. March[51], G. Marchiori[82], M. Marcisovsky[128], M. Marjanovic[14], D. E. Marley[91], F. Marroquim[26a], S. P. Marsden[86], Z. Marshall[16], S. Marti-Garcia[167], B. Martin[92], T. A. Martin[170], V. J. Martin[48], B. Martin dit Latour[15], M. Martinez[13,r], S. Martin-Haugh[132], V. S. Martoiu[28b], A. C. Martyniuk[80], M. Marx[139], A. Marzin[32], L. Masetti[85], T. Mashimo[156], R. Mashinistov[97], J. Masik[86], A. L. Maslennikov[110,c], I. Massa[22a,22b], L. Massa[22a,22b], P. Mastrandrea[5], A. Mastroberardino[39a,39b], T. Masubuchi[156], P. Mättig[175], J. Mattmann[85], J. Maurer[28b], S. J. Maxfield[76], D. A. Maximov[110,c], R. Mazini[152], S. M. Mazza[93a,93b], N. C. Mc Fadden[106], G. Mc Goldrick[159], S. P. Mc Kee[91], A. McCarn[91], R. L. McCarthy[149], T. G. McCarthy[102], L. I. McClymont[80], E. F. McDonald[90], K. W. McFarlane[58,*], J. A. Mcfayden[80], G. Mchedlidze[56], S. J. McMahon[132], R. A. McPherson[169,l], M. Medinnis[44], S. Meehan[139], S. Mehlhase[101], A. Mehta[76], K. Meier[60a], C. Meineck[101], B. Meirose[43], D. Melini[167], B. R. Mellado Garcia[146c], M. Melo[145a], F. Meloni[18], S. B. Menary[86], A. Mengarelli[22a,22b], S. Menke[102], E. Meoni[162], S. Mergelmeyer[17], P. Mermod[51], L. Merola[105a,105b], C. Meroni[93a], F. S. Merritt[33], A. Messina[133a,133b], J. Metcalfe[6], A. S. Mete[163], C. Meyer[85], C. Meyer[123], J-P. Meyer[137], J. Meyer[108], H. Meyer Zu Theenhausen[60a], F. Miano[150], R. P. Middleton[132], S. Miglioranzi[52a,52b], L. Mijović[23], G. Mikenberg[172], M. Mikestikova[128], M. Mikuž[77], M. Milesi[90], A. Milic[64], D. W. Miller[33], C. Mills[48], A. Milov[172], D. A. Milstead[147a,147b], A. A. Minaenko[131], Y. Minami[156], I. A. Minashvili[67], A. I. Mincer[111], B. Mindur[40a], M. Mineev[67], Y. Ming[173], L. M. Mir[13], K. P. Mistry[123], T. Mitani[171], J. Mitrevski[101], V. A. Mitsou[167], A. Miucci[51], P. S. Miyagawa[140], J. U. Mjörnmark[83], T. Moa[147a,147b], K. Mochizuki[96], S. Mohapatra[37], S. Molander[147a,147b], R. Moles-Valls[23], R. Monden[70], M. C. Mondragon[92], K. Mönig[44], J. Monk[38], E. Monnier[87], A. Montalbano[149], J. Montejo Berlingen[32], F. Monticelli[73], S. Monzani[93a,93b], R. W. Moore[3], N. Morange[118], D. Moreno[21], M. Moreno Llácer[56], P. Morettini[52a], D. Mori[143], T. Mori[156], M. Morii[59], M. Morinaga[156], V. Morisbak[120], S. Moritz[85], A. K. Morley[151], G. Mornacchi[32], J. D. Morris[78], S. S. Mortensen[38], L. Morvaj[149], M. Mosidze[53b], J. Moss[144], K. Motohashi[158], R. Mount[144], E. Mountricha[27], S. V. Mouraviev[97,*], E. J. W. Moyse[88], S. Muanza[87], R. D. Mudd[19], F. Mueller[102], J. Mueller[126], R. S. P. Mueller[101], T. Mueller[30], D. Muenstermann[74], P. Mullen[55], G. A. Mullier[18], F. J. Munoz Sanchez[86], J. A. Murillo Quijada[19], W. J. Murray[170,132], H. Musheghyan[56], M. Muškinja[77], A. G. Myagkov[131,ae], M. Myska[129], B. P. Nachman[144], O. Nackenhorst[51], K. Nagai[121], R. Nagai[68,z], K. Nagano[68], Y. Nagasaka[61], K. Nagata[161], M. Nagel[50], E. Nagy[87], A. M. Nairz[32], Y. Nakahama[32], K. Nakamura[68], T. Nakamura[156], I. Nakano[113], H. Namasivayam[43], R. F. Naranjo Garcia[44], R. Narayan[11], D. I. Narrias Villar[60a], I. Naryshkin[124], T. Naumann[44], G. Navarro[21], R. Nayyar[7], H. A. Neal[91], P. Yu. Nechaeva[97], T. J. Neep[86], P. D. Nef[144], A. Negri[122a,122b], M. Negrini[22a], S. Nektarijevic[107], C. Nellist[118], A. Nelson[163], S. Nemecek[128], P. Nemethy[111], A. A. Nepomuceno[26a], M. Nessi[32,af], M. S. Neubauer[166], M. Neumann[175], R. M. Neves[111], P. Nevski[27], P. R. Newman[19], D. H. Nguyen[6], T. Nguyen Manh[96], R. B. Nickerson[121], R. Nicolaidou[137], J. Nielsen[138], A. Nikiforov[17], V. Nikolaenko[131,ae], I. Nikolic-Audit[82], K. Nikolopoulos[19], J. K. Nilsen[120],

P. Nilsson[27], Y. Ninomiya[156], A. Nisati[133a], R. Nisius[102], T. Nobe[156], L. Nodulman[6], M. Nomachi[119], I. Nomidis[31], T. Nooney[78], S. Norberg[114], M. Nordberg[32], N. Norjoharuddeen[121], O. Novgorodova[46], S. Nowak[102], M. Nozaki[68], L. Nozka[116], K. Ntekas[10], E. Nurse[80], F. Nuti[90], F. O'grady[7], D. C. O'Neil[143], A. A. O'Rourke[44], V. O'Shea[55], F. G. Oakham[31,d], H. Oberlack[102], T. Obermann[23], J. Ocariz[82], A. Ochi[69], I. Ochoa[37], J. P. Ochoa-Ricoux[34a], S. Oda[72], S. Odaka[68], H. Ogren[63], A. Oh[86], S. H. Oh[47], C. C. Ohm[16], H. Ohman[165], H. Oide[32], H. Okawa[161], Y. Okumura[33], T. Okuyama[68], A. Olariu[28b], L. F. Oleiro Seabra[127a], S. A. Olivares Pino[48], D. Oliveira Damazio[27], A. Olszewski[41], J. Olszowska[41], A. Onofre[127a,127e], K. Onogi[104], P. U. E. Onyisi[11,v], M. J. Oreglia[33], Y. Oren[154], D. Orestano[135a,135b], N. Orlando[62b], R. S. Orr[159], B. Osculati[52a,52b], R. Ospanov[86], G. Otero y Garzon[29], H. Otono[72], M. Ouchrif[136d], F. Ould-Saada[120], A. Ouraou[137], K. P. Oussoren[108], Q. Ouyang[35a], M. Owen[55], R. E. Owen[19], V. E. Ozcan[20a], N. Ozturk[8], K. Pachal[143], A. Pacheco Pages[13], C. Padilla Aranda[13], M. Pagáčová[50], S. Pagan Griso[16], F. Paige[27], P. Pais[88], K. Pajchel[120], G. Palacino[160b], S. Palestini[32], M. Palka[40b], D. Pallin[36], A. Palma[127a,127b], E. St. Panagiotopoulou[10], C. E. Pandini[82], J. G. Panduro Vazquez[79], P. Pani[147a,147b], S. Panitkin[27], D. Pantea[28b], L. Paolozzi[51], Th. D. Papadopoulou[10], K. Papageorgiou[155], A. Paramonov[6], D. Paredes Hernandez[176], A. J. Parker[74], M. A. Parker[30], K. A. Parker[140], F. Parodi[52a,52b], J. A. Parsons[37], U. Parzefall[50], V. R. Pascuzzi[159], E. Pasqualucci[133a], S. Passaggio[52a], Fr. Pastore[79], G. Pásztor[31,ag], S. Pataraia[175], J. R. Pater[86], T. Pauly[32], J. Pearce[169], B. Pearson[114], L. E. Pedersen[38], M. Pedersen[120], S. Pedraza Lopez[167], R. Pedro[127a,127b], S. V. Peleganchuk[110,c], D. Pelikan[165], O. Penc[128], C. Peng[35a], H. Peng[35b], J. Penwell[63], B. S. Peralva[26b], M. M. Perego[137], D. V. Perepelitsa[27], E. Perez Codina[160a], L. Perini[93a,93b], H. Pernegger[32], S. Perrella[105a,105b], R. Peschke[44], V. D. Peshekhonov[67], K. Peters[44], R. F. Y. Peters[86], B. A. Petersen[32], T. C. Petersen[38], E. Petit[57], A. Petridis[1], C. Petridou[155], P. Petroff[118], E. Petrolo[133a], M. Petrov[121], F. Petrucci[135a,135b], N. E. Pettersson[88], A. Peyaud[137], R. Pezoa[34b], P. W. Phillips[132], G. Piacquadio[144,ah], E. Pianori[170], A. Picazio[88], E. Piccaro[78], M. Piccinini[22a,22b], M. A. Pickering[121], R. Piegaia[29], J. E. Pilcher[33], A. D. Pilkington[86], A. W. J. Pin[86], M. Pinamonti[164a164c,ai], J. L. Pinfold[3], A. Pingel[38], S. Pires[82], H. Pirumov[44], M. Pitt[172], L. Plazak[145a], M.-A. Pleier[27], V. Pleskot[85], E. Plotnikova[67], P. Plucinski[92], D. Pluth[66], R. Poettgen[147a,147b], L. Poggioli[118], D. Pohl[23], G. Polesello[122a], A. Poley[44], A. Policicchio[39a,39b], R. Polifka[159], A. Polini[22a], C. S. Pollard[55], V. Polychronakos[27], K. Pommès[32], L. Pontecorvo[133a], B. G. Pope[92], G. A. Popeneciu[28c], D. S. Popovic[14], A. Poppleton[32], S. Pospisil[129], K. Potamianos[16], I. N. Potrap[67], C. J. Potter[30], C. T. Potter[117], G. Poulard[32], J. Poveda[32], V. Pozdnyakov[67], M. E. Pozo Astigarraga[32], P. Pralavorio[87], A. Pranko[16], S. Prell[66], D. Price[86], L. E. Price[6], M. Primavera[75a], S. Prince[89], M. Proissl[48], K. Prokofiev[62c], F. Prokoshin[34b], S. Protopopescu[27], J. Proudfoot[6], M. Przybycien[40a], D. Puddu[135a,135b], M. Purohit[27,aj], P. Puzo[118], J. Qian[91], G. Qin[55], Y. Qin[86], A. Quadt[56], W. B. Quayle[164a,164b], M. Queitsch-Maitland[86], D. Quilty[55], S. Raddum[120], V. Radeka[27], V. Radescu[60b], S. K. Radhakrishnan[149], P. Radloff[117], P. Rados[90], F. Ragusa[93a,93b], G. Rahal[178], J. A. Raine[86], S. Rajagopalan[27], M. Rammensee[32], C. Rangel-Smith[165], M. G. Ratti[93a,93b], F. Rauscher[101], S. Rave[85], T. Ravenscroft[55], I. Ravinovich[172], M. Raymond[32], A. L. Read[120], N. P. Readioff[76], M. Reale[75a,75b], D. M. Rebuzzi[122a,122b], A. Redelbach[174], G. Redlinger[27], R. Reece[138], K. Reeves[43], L. Rehnisch[17], J. Reichert[123], H. Reisin[29], C. Rembser[32], H. Ren[35a], M. Rescigno[133a], S. Resconi[93a], O. L. Rezanova[110,c], P. Reznicek[130], R. Rezvani[96], R. Richter[102], S. Richter[80], E. Richter-Was[40b], O. Ricken[23], M. Ridel[82], P. Rieck[17], C. J. Riegel[175], J. Rieger[56], O. Rifki[114], M. Rijssenbeek[149], A. Rimoldi[122a,122b], M. Rimoldi[18], L. Rinaldi[22a], B. Ristić[51], E. Ritsch[32], I. Riu[13], F. Rizatdinova[115], E. Rizvi[78], C. Rizzi[13], S. H. Robertson[89,l], A. Robichaud-Veronneau[89], D. Robinson[30], J. E. M. Robinson[44], A. Robson[55], C. Roda[125a,125b], Y. Rodina[87], A. Rodriguez Perez[13], D. Rodriguez Rodriguez[167], S. Roe[32], C. S. Rogan[59], O. Røhne[120], A. Romaniouk[99], M. Romano[22a,22b], S. M. Romano Saez[36], E. Romero Adam[167], N. Rompotis[139], M. Ronzani[50], L. Roos[82], E. Ros[167], S. Rosati[133a], K. Rosbach[50], P. Rose[138], O. Rosenthal[142], N. -A. Rosien[56], V. Rossetti[147a,147b], E. Rossi[105a,105b], L. P. Rossi[52a], J. H. N. Rosten[30], R. Rosten[139], M. Rotaru[28b], I. Roth[172], J. Rothberg[139], D. Rousseau[118], C. R. Royon[137], A. Rozanov[87], Y. Rozen[153], X. Ruan[146c], F. Rubbo[144], M. S. Rudolph[159], F. Rühr[50], A. Ruiz-Martinez[31], Z. Rurikova[50], N. A. Rusakovich[67], A. Ruschke[101], H. L. Russell[139], J. P. Rutherfoord[7], N. Ruthmann[32], Y. F. Ryabov[124], M. Rybar[166], G. Rybkin[118], S. Ryu[6], A. Ryzhov[131], G. F. Rzehorz[56], A. F. Saavedra[151], G. Sabato[108], S. Sacerdoti[29], H. F.-W. Sadrozinski[138], R. Sadykov[67], F. Safai Tehrani[133a], P. Saha[109], M. Sahinsoy[60a], M. Saimpert[137], T. Saito[156], H. Sakamoto[156], Y. Sakurai[171], G. Salamanna[135a,135b], A. Salamon[134a,134b], J. E. Salazar Loyola[34b], D. Salek[108], P. H. Sales De Bruin[139], D. Salihagic[102], A. Salnikov[144], J. Salt[167], D. Salvatore[39a,39b], F. Salvatore[150], A. Salvucci[62a], A. Salzburger[32], D. Sammel[50], D. Sampsonidis[155], A. Sanchez[105a,105b], J. Sánchez[167], V. Sanchez Martinez[167], H. Sandaker[120], R. L. Sandbach[78], H. G. Sander[85], M. Sandhoff[175], C. Sandoval[21], R. Sandstroem[102], D. P. C. Sankey[132], M. Sannino[52a,52b], A. Sansoni[49], C. Santoni[36], R. Santonico[134a,134b], H. Santos[127a], I. Santoyo Castillo[150], K. Sapp[126], A. Sapronov[67], J. G. Saraiva[127a,127d], B. Sarrazin[23], O. Sasaki[68], Y. Sasaki[156], K. Sato[161], G. Sauvage[5,*], E. Sauvan[5], G. Savage[79], P. Savard[159,d], C. Sawyer[132], L. Sawyer[81,q], J. Saxon[33], C. Sbarra[22a], A. Sbrizzi[22a,22b], T. Scanlon[80], D. A. Scannicchio[163], M. Scarcella[151], V. Scarfone[39a,39b], J. Schaarschmidt[172], P. Schacht[102], B. M. Schachtner[101],

D. Schaefer[32], R. Schaefer[44], J. Schaeffer[85], S. Schaepe[23], S. Schaetzel[60b], U. Schäfer[85], A. C. Schaffer[118], D. Schaile[101], R. D. Schamberger[149], V. Scharf[60a], V. A. Schegelsky[124], D. Scheirich[130], M. Schernau[163], C. Schiavi[52a,52b], S. Schier[138], C. Schillo[50], M. Schioppa[39a,39b], S. Schlenker[32], K. R. Schmidt-Sommerfeld[102], K. Schmieden[32], C. Schmitt[85], S. Schmitt[44], S. Schmitz[85], B. Schneider[160a], U. Schnoor[50], L. Schoeffel[137], A. Schoening[60b], B. D. Schoenrock[92], E. Schopf[23], M. Schott[85], J. Schovancova[8], S. Schramm[51], M. Schreyer[174], N. Schuh[85], M. J. Schultens[23], H. -C. Schultz-Coulon[60a], H. Schulz[17], M. Schumacher[50], B. A. Schumm[138], Ph. Schune[137], A. Schwartzman[144], T. A. Schwarz[91], Ph. Schwegler[102], H. Schweiger[86], Ph. Schwemling[137], R. Schwienhorst[92], J. Schwindling[137], T. Schwindt[23], G. Sciolla[25], F. Scuri[125a,125b], F. Scutti[90], J. Searcy[91], P. Seema[23], S. C. Seidel[106], A. Seiden[138], F. Seifert[129], J. M. Seixas[26a], G. Sekhniaidze[105a], K. Sekhon[91], S. J. Sekula[42], D. M. Seliverstov[124,*], N. Semprini-Cesari[22a,22b], C. Serfon[120], L. Serin[118], L. Serkin[164a,164b], M. Sessa[135a,135b], R. Seuster[169], H. Severini[114], T. Sfiligoj[77], F. Sforza[32], A. Sfyrla[51], E. Shabalina[56], N. W. Shaikh[147a,147b], L. Y. Shan[35a], R. Shang[166], J. T. Shank[24], M. Shapiro[16], P. B. Shatalov[98], K. Shaw[164a,164b], S. M. Shaw[86], A. Shcherbakova[147a,147b], C. Y. Shehu[150], P. Sherwood[80], L. Shi[152,ak], S. Shimizu[69], C. O. Shimmin[163], M. Shimojima[103], M. Shiyakova[67,al], A. Shmeleva[97], D. Shoaleh Saadi[96], M. J. Shochet[33], S. Shojaii[93a,93b], S. Shrestha[112], E. Shulga[99], M. A. Shupe[7], P. Sicho[128], A. M. Sickles[166], P. E. Sidebo[148], O. Sidiropoulou[174], D. Sidorov[115], A. Sidoti[22a,22b], F. Siegert[46], Dj. Sijacki[14], J. Silva[127a,127d], S. B. Silverstein[147a], V. Simak[129], O. Simard[5], Lj. Simic[14], S. Simion[118], E. Simioni[85], B. Simmons[80], D. Simon[36], M. Simon[85], P. Sinervo[159], N. B. Sinev[117], M. Sioli[22a,22b], G. Siragusa[174], S. Yu. Sivoklokov[100], J. Sjölin[147a,147b], T. B. Sjursen[15], M. B. Skinner[74], H. P. Skottowe[59], P. Skubic[114], M. Slater[19], T. Slavicek[129], M. Slawinska[108], K. Sliwa[162], R. Slovak[130], V. Smakhtin[172], B. H. Smart[5], L. Smestad[15], J. Smiesko[145a], S. Yu. Smirnov[99], Y. Smirnov[99], L. N. Smirnova[100,am], O. Smirnova[83], M. N. K. Smith[37], R. W. Smith[37], M. Smizanska[74], K. Smolek[129], A. A. Snesarev[97], S. Snyder[27], R. Sobie[169,l], F. Socher[46], A. Soffer[154], D. A. Soh[152], G. Sokhrannyi[77], C. A. Solans Sanchez[32], M. Solar[129], E. Yu. Soldatov[99], U. Soldevila[167], A. A. Solodkov[131], A. Soloshenko[67], O. V. Solovyanov[131], V. Solovyev[124], P. Sommer[50], H. Son[162], H. Y. Song[35b,an], A. Sood[16], A. Sopczak[129], V. Sopko[129], V. Sorin[13], D. Sosa[60b], C. L. Sotiropoulou[125a,125b], R. Soualah[164a,164c], A. M. Soukharev[110,c], D. South[44], B. C. Sowden[79], S. Spagnolo[75a,75b], M. Spalla[125a,125b], M. Spangenberg[170], F. Spanò[79], D. Sperlich[17], F. Spettel[102], R. Spighi[22a], G. Spigo[32], L. A. Spiller[90], M. Spousta[130], R. D. St. Denis[55,*], A. Stabile[93a], R. Stamen[60a], S. Stamm[17], E. Stanecka[41], R. W. Stanek[6], C. Stanescu[135a], M. Stanescu-Bellu[44], M. M. Stanitzki[44], S. Stapnes[120], E. A. Starchenko[131], G. H. Stark[33], J. Stark[57], P. Staroba[128], P. Starovoitov[60a], S. Stärz[32], R. Staszewski[41], P. Steinberg[27], B. Stelzer[143], H. J. Stelzer[32], O. Stelzer-Chilton[160a], H. Stenzel[54], G. A. Stewart[55], J. A. Stillings[23], M. C. Stockton[89], M. Stoebe[89], G. Stoicea[28b], P. Stolte[56], S. Stonjek[102], A. R. Stradling[8], A. Straessner[46], M. E. Stramaglia[18], J. Strandberg[148], S. Strandberg[147a,147b], A. Strandlie[120], M. Strauss[114], P. Strizenec[145b], R. Ströhmer[174], D. M. Strom[117], R. Stroynowski[42], A. Strubig[107], S. A. Stucci[18], B. Stugu[15], N. A. Styles[44], D. Su[144], J. Su[126], R. Subramaniam[81], S. Suchek[60a], Y. Sugaya[119], M. Suk[129], V. V. Sulin[97], S. Sultansoy[4c], T. Sumida[70], S. Sun[59], X. Sun[35a], J. E. Sundermann[50], K. Suruliz[150], G. Susinno[39a,39b], M. R. Sutton[150], S. Suzuki[68], M. Svatos[128], M. Swiatlowski[33], I. Sykora[145a], T. Sykora[130], D. Ta[50], C. Taccini[135a,135b], K. Tackmann[44], J. Taenzer[159], A. Taffard[163], R. Tafirout[160a], N. Taiblum[154], H. Takai[27], R. Takashima[71], T. Takeshita[141], Y. Takubo[68], M. Talby[87], A. A. Talyshev[110,c], K. G. Tan[90], J. Tanaka[156], R. Tanaka[118], S. Tanaka[68], B. B. Tannenwald[112], S. Tapia Araya[34b], S. Tapprogge[85], S. Tarem[153], G. F. Tartarelli[93a], P. Tas[130], M. Tasevsky[128], T. Tashiro[70], E. Tassi[39a,39b], A. Tavares Delgado[127a,127b], Y. Tayalati[136d], A. C. Taylor[106], G. N. Taylor[90], P. T. E. Taylor[90], W. Taylor[160b], F. A. Teischinger[32], P. Teixeira-Dias[79], K. K. Temming[50], D. Temple[143], H. Ten Kate[32], P. K. Teng[152], J. J. Teoh[119], F. Tepel[175], S. Terada[68], K. Terashi[156], J. Terron[84], S. Terzo[102], M. Testa[49], R. J. Teuscher[159,l], T. Theveneaux-Pelzer[87], J. P. Thomas[19], J. Thomas-Wilsker[79], E. N. Thompson[37], P. D. Thompson[19], A. S. Thompson[55], L. A. Thomsen[176], E. Thomson[123], M. Thomson[30], M. J. Tibbetts[16], R. E. Ticse Torres[87], V. O. Tikhomirov[97,ao], Yu. A. Tikhonov[110,c], S. Timoshenko[99], P. Tipton[176], S. Tisserant[87], K. Todome[158], T. Todorov[5,*], S. Todorova-Nova[130], J. Tojo[72], S. Tokár[145a], K. Tokushuku[68], E. Tolley[59], L. Tomlinson[86], M. Tomoto[104], L. Tompkins[144,ap], K. Toms[106], B. Tong[59], E. Torrence[117], H. Torres[143], E. Torró Pastor[139], J. Toth[87,aq], F. Touchard[87], D. R. Tovey[140], T. Trefzger[174], A. Tricoli[27], I. M. Trigger[160a], S. Trincaz-Duvoid[82], M. F. Tripiana[13], W. Trischuk[159], B. Trocmé[57], A. Trofymov[44], C. Troncon[93a], M. Trottier-McDonald[16], M. Trovatelli[169], L. Truong[164a,164c], M. Trzebinski[41], A. Trzupek[41], J. C.-L. Tseng[121], P. V. Tsiareshka[94], G. Tsipolitis[10], N. Tsirintanis[9], S. Tsiskaridze[13], V. Tsiskaridze[50], E. G. Tskhadadze[53a], K. M. Tsui[62a], I. I. Tsukerman[98], V. Tsulaia[16], S. Tsuno[68], D. Tsybychev[149], A. Tudorache[28b], V. Tudorache[28b], A. N. Tuna[59], S. A. Tupputi[22a,22b], S. Turchikhin[100,am], D. Turecek[129], D. Turgeman[172], R. Turra[93a,93b], A. J. Turvey[42], P. M. Tuts[37], M. Tyndel[132], G. Ucchielli[22a,22b], I. Ueda[156], R. Ueno[31], M. Ughetto[147a,147b], F. Ukegawa[161], G. Unal[32], A. Undrus[27], G. Unel[163], F. C. Ungaro[90], Y. Unno[68], C. Unverdorben[101], J. Urban[145b], P. Urquijo[90], P. Urrejola[85], G. Usai[8], A. Usanova[64], L. Vacavant[87], V. Vacek[129], B. Vachon[89], C. Valderanis[101], E. Valdes Santurio[147a,147b], N. Valencic[108], S. Valentinetti[22a,22b], A. Valero[167],

L. Valery[13], S. Valkar[130], S. Vallecorsa[51], J. A. Valls Ferrer[167], W. Van Den Wollenberg[108], P. C. Van Der Deijl[108], R. van der Geer[108], H. van der Graaf[108], N. van Eldik[153], P. van Gemmeren[6], J. Van Nieuwkoop[143], I. van Vulpen[108], M. C. van Woerden[32], M. Vanadia[133a,133b], W. Vandelli[32], R. Vanguri[123], A. Vaniachine[131], P. Vankov[108], G. Vardanyan[177], R. Vari[133a], E. W. Varnes[7], T. Varol[42], D. Varouchas[82], A. Vartapetian[8], K. E. Varvell[151], J. G. Vasquez[176], F. Vazeille[36], T. Vazquez Schroeder[89], J. Veatch[56], L. M. Veloce[159], F. Veloso[127a,127c], S. Veneziano[133a], A. Ventura[75a,75b], M. Venturi[169], N. Venturi[159], A. Venturini[25], V. Vercesi[122a], M. Verducci[133a,133b], W. Verkerke[108], J. C. Vermeulen[108], A. Vest[46,ar], M. C. Vetterli[143,d], O. Viazlo[83], I. Vichou[166,*], T. Vickey[140], O. E. Vickey Boeriu[140], G. H. A. Viehhauser[121], S. Viel[16], L. Vigani[121], R. Vigne[64], M. Villa[22a,22b], M. Villaplana Perez[93a,93b], E. Vilucchi[49], M. G. Vincter[31], V. B. Vinogradov[67], C. Vittori[22a,22b], I. Vivarelli[150], S. Vlachos[10], M. Vlasak[129], M. Vogel[175], P. Vokac[129], G. Volpi[125a,125b], M. Volpi[90], H. von der Schmitt[102], E. von Toerne[23], V. Vorobel[130], K. Vorobev[99], M. Vos[167], R. Voss[32], J. H. Vossebeld[76], N. Vranjes[14], M. Vranjes Milosavljevic[14], V. Vrba[128], M. Vreeswijk[108], R. Vuillermet[32], I. Vukotic[33], Z. Vykydal[129], P. Wagner[23], W. Wagner[175], H. Wahlberg[73], S. Wahrmund[46], J. Wakabayashi[104], J. Walder[74], R. Walker[101], W. Walkowiak[142], V. Wallangen[147a,147b], C. Wang[35c], C. Wang[35d,87], F. Wang[173], H. Wang[16], H. Wang[42], J. Wang[44], J. Wang[151], K. Wang[89], R. Wang[6], S. M. Wang[152], T. Wang[23], T. Wang[37], W. Wang[35b], X. Wang[176], C. Wanotayaroj[117], A. Warburton[89], C. P. Ward[30], D. R. Wardrope[80], A. Washbrook[48], P. M. Watkins[19], A. T. Watson[19], M. F. Watson[19], G. Watts[139], S. Watts[86], B. M. Waugh[80], S. Webb[85], M. S. Weber[18], S. W. Weber[174], J. S. Webster[6], A. R. Weidberg[121], B. Weinert[63], J. Weingarten[56], C. Weiser[50], H. Weits[108], P. S. Wells[32], T. Wenaus[27], T. Wengler[32], S. Wenig[32], N. Wermes[23], M. Werner[50], M. D. Werner[66], P. Werner[32], M. Wessels[60a], J. Wetter[162], K. Whalen[117], N. L. Whallon[139], A. M. Wharton[74], A. White[8], M. J. White[1], R. White[34b], D. Whiteson[163], F. J. Wickens[132], W. Wiedenmann[173], M. Wielers[132], P. Wienemann[23], C. Wiglesworth[38], L. A. M. Wiik-Fuchs[23], A. Wildauer[102], F. Wilk[86], H. G. Wilkens[32], H. H. Williams[123], S. Williams[108], C. Willis[92], S. Willocq[88], J. A. Wilson[19], I. Wingerter-Seez[5], F. Winklmeier[117], O. J. Winston[150], B. T. Winter[23], M. Wittgen[144], J. Wittkowski[101], S. J. Wollstadt[85], M. W. Wolter[41], H. Wolters[127a,127c], B. K. Wosiek[41], J. Wotschack[32], M. J. Woudstra[86], K. W. Wozniak[41], M. Wu[57], M. Wu[33], S. L. Wu[173], X. Wu[51], Y. Wu[91], T. R. Wyatt[86], B. M. Wynne[48], S. Xella[38], D. Xu[35a], L. Xu[27], B. Yabsley[151], S. Yacoob[146a], R. Yakabe[69], D. Yamaguchi[158], Y. Yamaguchi[119], A. Yamamoto[68], S. Yamamoto[156], T. Yamanaka[156], K. Yamauchi[104], Y. Yamazaki[69], Z. Yan[24], H. Yang[35e], H. Yang[173], Y. Yang[152], Z. Yang[15], W.-M. Yao[16], Y. C. Yap[82], Y. Yasu[68], E. Yatsenko[5], K. H. Yau Wong[23], J. Ye[42], S. Ye[27], I. Yeletskikh[67], A. L. Yen[59], E. Yildirim[85], K. Yorita[171], R. Yoshida[6], K. Yoshihara[123], C. Young[144], C. J. S. Young[32], S. Youssef[24], D. R. Yu[16], J. Yu[8], J. M. Yu[91], J. Yu[66], L. Yuan[69], S. P. Y. Yuen[23], I. Yusuff[30,as], B. Zabinski[41], R. Zaidan[35d], A. M. Zaitsev[131,ae], N. Zakharchuk[44], J. Zalieckas[15], A. Zaman[149], S. Zambito[59], L. Zanello[133a,133b], D. Zanzi[90], C. Zeitnitz[175], M. Zeman[129], A. Zemla[40a], J. C. Zeng[166], Q. Zeng[144], K. Zengel[25], O. Zenin[131], T. Ženiš[145a], D. Zerwas[118], D. Zhang[91], F. Zhang[173], G. Zhang[35b,an], H. Zhang[35c], J. Zhang[6], L. Zhang[50], R. Zhang[23], R. Zhang[35b,at], X. Zhang[35d], Z. Zhang[118], X. Zhao[42], Y. Zhao[35d], Z. Zhao[35b], A. Zhemchugov[67], J. Zhong[121], B. Zhou[91], C. Zhou[47], L. Zhou[37], L. Zhou[42], M. Zhou[149], N. Zhou[35f], C. G. Zhu[35d], H. Zhu[35a], J. Zhu[91], Y. Zhu[35b], X. Zhuang[35a], K. Zhukov[97], A. Zibell[174], D. Zieminska[63], N. I. Zimine[67], C. Zimmermann[85], S. Zimmermann[50], Z. Zinonos[56], M. Zinser[85], M. Ziolkowski[142], L. Živković[14], G. Zobernig[173], A. Zoccoli[22a,22b], M. zur Nedden[17], G. Zurzolo[105a,105b], L. Zwalinski[32]

[1] Department of Physics, University of Adelaide, Adelaide, Australia
[2] Physics Department, SUNY Albany, Albany, NY, USA
[3] Department of Physics, University of Alberta, Edmonton, AB, Canada
[4] [(a)]Department of Physics, Ankara University, Ankara, Turkey; [(b)]Istanbul Aydin University, Istanbul, Turkey; [(c)]Division of Physics, TOBB University of Economics and Technology, Ankara, Turkey
[5] LAPP, CNRS/IN2P3 and Université Savoie Mont Blanc, Annecy-le-Vieux, France
[6] High Energy Physics Division, Argonne National Laboratory, Argonne, IL, USA
[7] Department of Physics, University of Arizona, Tucson, AZ, USA
[8] Department of Physics, The University of Texas at Arlington, Arlington, TX, USA
[9] Physics Department, University of Athens, Athens, Greece
[10] Physics Department, National Technical University of Athens, Zografou, Greece
[11] Department of Physics, The University of Texas at Austin, Austin, TX, USA
[12] Institute of Physics, Azerbaijan Academy of Sciences, Baku, Azerbaijan
[13] Institut de Física d'Altes Energies (IFAE), The Barcelona Institute of Science and Technology, Barcelona, Spain
[14] Institute of Physics, University of Belgrade, Belgrade, Serbia
[15] Department for Physics and Technology, University of Bergen, Bergen, Norway
[16] Physics Division, Lawrence Berkeley National Laboratory, University of California, Berkeley, CA, USA

[17] Department of Physics, Humboldt University, Berlin, Germany
[18] Albert Einstein Center for Fundamental Physics and Laboratory for High Energy Physics, University of Bern, Bern, Switzerland
[19] School of Physics and Astronomy, University of Birmingham, Birmingham, UK
[20] [(a)]Department of Physics, Bogazici University, Istanbul, Turkey; [(b)]Department of Physics Engineering, Gaziantep University, Gaziantep, Turkey; [(c)]Faculty of Engineering and Natural Sciences, Istanbul Bilgi University, Istanbul, Turkey; [(d)]Faculty of Engineering and Natural Sciences, Bahcesehir University, Istanbul, Turkey
[21] Centro de Investigaciones, Universidad Antonio Narino, Bogotá, Colombia
[22] [(a)]INFN Sezione di Bologna, Bologna, Italy; [(b)]Dipartimento di Fisica e Astronomia, Università di Bologna, Bologna, Italy
[23] Physikalisches Institut, University of Bonn, Bonn, Germany
[24] Department of Physics, Boston University, Boston, MA, USA
[25] Department of Physics, Brandeis University, Waltham, MA, USA
[26] [(a)]Universidade Federal do Rio De Janeiro COPPE/EE/IF, Rio de Janeiro, Brazil; [(b)]Electrical Circuits Department, Federal University of Juiz de Fora (UFJF), Juiz de Fora, Brazil; [(c)]Federal University of Sao Joao del Rei (UFSJ), São João del Rei, Brazil; [(d)]Instituto de Fisica, Universidade de Sao Paulo, São Paulo, Brazil
[27] Physics Department, Brookhaven National Laboratory, Upton, NY, USA
[28] [(a)]Transilvania University of Brasov, Brasov, Romania; [(b)]National Institute of Physics and Nuclear Engineering, Bucharest, Romania; [(c)]Physics Department, National Institute for Research and Development of Isotopic and Molecular Technologies, Cluj-Napoca, Romania; [(d)]University Politehnica Bucharest, Bucharest, Romania; [(e)]West University in Timisoara, Timisoara, Romania
[29] Departamento de Física, Universidad de Buenos Aires, Buenos Aires, Argentina
[30] Cavendish Laboratory, University of Cambridge, Cambridge, UK
[31] Department of Physics, Carleton University, Ottawa, ON, Canada
[32] CERN, Geneva, Switzerland
[33] Enrico Fermi Institute, University of Chicago, Chicago, IL, USA
[34] [(a)]Departamento de Física, Pontificia Universidad Católica de Chile, Santiago, Chile; [(b)]Departamento de Física, Universidad Técnica Federico Santa María, Valparaíso, Chile
[35] [(a)]Institute of High Energy Physics, Chinese Academy of Sciences, Beijing, China; [(b)]Department of Modern Physics, University of Science and Technology of China, Anhui, China; [(c)]Department of Physics, Nanjing University, Jiangsu, China; [(d)]School of Physics, Shandong University, Shandong, China; [(e)]Department of Physics and Astronomy, Shanghai Key Laboratory for Particle Physics and Cosmology, Shanghai Jiao Tong University (also affiliated with PKU-CHEP), Shanghai, China; [(f)]Physics Department, Tsinghua University, Beijing 100084, China
[36] Laboratoire de Physique Corpusculaire, Clermont Université and Université Blaise Pascal and CNRS/IN2P3, Clermont-Ferrand, France
[37] Nevis Laboratory, Columbia University, Irvington, NY, USA
[38] Niels Bohr Institute, University of Copenhagen, Copenhagen, Denmark
[39] [(a)]INFN Gruppo Collegato di Cosenza, Laboratori Nazionali di Frascati, Cosenza, Italy; [(b)]Dipartimento di Fisica, Università della Calabria, Rende, Italy
[40] [(a)]AGH University of Science and Technology, Faculty of Physics and Applied Computer Science, Kraków, Poland; [(b)]Marian Smoluchowski Institute of Physics, Jagiellonian University, Kraków, Poland
[41] Institute of Nuclear Physics, Polish Academy of Sciences, Kraków, Poland
[42] Physics Department, Southern Methodist University, Dallas, TX, USA
[43] Physics Department, University of Texas at Dallas, Richardson, TX, USA
[44] DESY, Hamburg and Zeuthen, Germany
[45] Lehrstuhl für Experimentelle Physik IV, Technische Universität Dortmund, Dortmund, Germany
[46] Institut für Kern–und Teilchenphysik, Technische Universität Dresden, Dresden, Germany
[47] Department of Physics, Duke University, Durham, NC, USA
[48] SUPA-School of Physics and Astronomy, University of Edinburgh, Edinburgh, UK
[49] INFN Laboratori Nazionali di Frascati, Frascati, Italy
[50] Fakultät für Mathematik und Physik, Albert-Ludwigs-Universität, Freiburg, Germany
[51] Section de Physique, Université de Genève, Geneva, Switzerland
[52] [(a)]INFN Sezione di Genova, Genoa, Italy; [(b)]Dipartimento di Fisica, Università di Genova, Genoa, Italy

[53] [(a)]E. Andronikashvili Institute of Physics, Iv. Javakhishvili Tbilisi State University, Tbilisi, Georgia; [(b)]High Energy Physics Institute, Tbilisi State University, Tbilisi, Georgia
[54] II Physikalisches Institut, Justus-Liebig-Universität Giessen, Giessen, Germany
[55] SUPA-School of Physics and Astronomy, University of Glasgow, Glasgow, UK
[56] II Physikalisches Institut, Georg-August-Universität, Göttingen, Germany
[57] Laboratoire de Physique Subatomique et de Cosmologie, Université Grenoble-Alpes, CNRS/IN2P3, Grenoble, France
[58] Department of Physics, Hampton University, Hampton, VA, USA
[59] Laboratory for Particle Physics and Cosmology, Harvard University, Cambridge, MA, USA
[60] [(a)]Kirchhoff-Institut für Physik, Ruprecht-Karls-Universität Heidelberg, Heidelberg, Germany; [(b)]Physikalisches Institut, Ruprecht-Karls-Universität Heidelberg, Heidelberg, Germany; [(c)]ZITI Institut für technische Informatik, Ruprecht-Karls-Universität Heidelberg, Mannheim, Germany
[61] Faculty of Applied Information Science, Hiroshima Institute of Technology, Hiroshima, Japan
[62] [(a)]Department of Physics, The Chinese University of Hong Kong, Shatin, NT, Hong Kong; [(b)]Department of Physics, The University of Hong Kong, Pokfulam, Hong Kong; [(c)]Department of Physics, The Hong Kong University of Science and Technology, Clear Water Bay, Kowloon, Hong Kong, China
[63] Department of Physics, Indiana University, Bloomington, IN, USA
[64] Institut für Astro–und Teilchenphysik, Leopold-Franzens-Universität, Innsbruck, Austria
[65] University of Iowa, Iowa City, IA, USA
[66] Department of Physics and Astronomy, Iowa State University, Ames, IA, USA
[67] Joint Institute for Nuclear Research, JINR Dubna, Dubna, Russia
[68] KEK, High Energy Accelerator Research Organization, Tsukuba, Japan
[69] Graduate School of Science, Kobe University, Kobe, Japan
[70] Faculty of Science, Kyoto University, Kyoto, Japan
[71] Kyoto University of Education, Kyoto, Japan
[72] Department of Physics, Kyushu University, Fukuoka, Japan
[73] Instituto de Física La Plata, Universidad Nacional de La Plata and CONICET, La Plata, Argentina
[74] Physics Department, Lancaster University, Lancaster, UK
[75] [(a)]INFN Sezione di Lecce, Lecce, Italy; [(b)]Dipartimento di Matematica e Fisica, Università del Salento, Lecce, Italy
[76] Oliver Lodge Laboratory, University of Liverpool, Liverpool, UK
[77] Department of Physics, Jožef Stefan Institute, University of Ljubljana, Ljubljana, Slovenia
[78] School of Physics and Astronomy, Queen Mary University of London, London, UK
[79] Department of Physics, Royal Holloway University of London, Surrey, UK
[80] Department of Physics and Astronomy, University College London, London, UK
[81] Louisiana Tech University, Ruston, LA, USA
[82] Laboratoire de Physique Nucléaire et de Hautes Energies, UPMC and Université Paris-Diderot and CNRS/IN2P3, Paris, France
[83] Fysiska institutionen, Lunds universitet, Lund, Sweden
[84] Departamento de Fisica Teorica C-15, Universidad Autonoma de Madrid, Madrid, Spain
[85] Institut für Physik, Universität Mainz, Mainz, Germany
[86] School of Physics and Astronomy, University of Manchester, Manchester, UK
[87] CPPM, Aix-Marseille Université and CNRS/IN2P3, Marseille, France
[88] Department of Physics, University of Massachusetts, Amherst, MA, USA
[89] Department of Physics, McGill University, Montreal, QC, Canada
[90] School of Physics, University of Melbourne, Victoria, Australia
[91] Department of Physics, The University of Michigan, Ann Arbor, MI, USA
[92] Department of Physics and Astronomy, Michigan State University, East Lansing, MI, USA
[93] [(a)]INFN Sezione di Milano, Milan, Italy; [(b)]Dipartimento di Fisica, Università di Milano, Milan, Italy
[94] B.I. Stepanov Institute of Physics, National Academy of Sciences of Belarus, Minsk, Republic of Belarus
[95] National Scientific and Educational Centre for Particle and High Energy Physics, Minsk, Republic of Belarus
[96] Group of Particle Physics, University of Montreal, Montreal, QC, Canada
[97] P.N. Lebedev Physical Institute of the Russian, Academy of Sciences, Moscow, Russia
[98] Institute for Theoretical and Experimental Physics (ITEP), Moscow, Russia
[99] National Research Nuclear University MEPhI, Moscow, Russia

[100] D.V. Skobeltsyn Institute of Nuclear Physics, M.V. Lomonosov Moscow State University, Moscow, Russia
[101] Fakultät für Physik, Ludwig-Maximilians-Universität München, Munich, Germany
[102] Max-Planck-Institut für Physik (Werner-Heisenberg-Institut), Munich, Germany
[103] Nagasaki Institute of Applied Science, Nagasaki, Japan
[104] Graduate School of Science and Kobayashi-Maskawa Institute, Nagoya University, Nagoya, Japan
[105] [(a)]INFN Sezione di Napoli, Naples, Italy; [(b)]Dipartimento di Fisica, Università di Napoli, Naples, Italy
[106] Department of Physics and Astronomy, University of New Mexico, Albuquerque, NM, USA
[107] Institute for Mathematics Astrophysics and Particle Physics, Radboud University Nijmegen/Nikhef, Nijmegen, The Netherlands
[108] Nikhef National Institute for Subatomic Physics and University of Amsterdam, Amsterdam, The Netherlands
[109] Department of Physics, Northern Illinois University, DeKalb, IL, USA
[110] Budker Institute of Nuclear Physics, SB RAS, Novosibirsk, Russia
[111] Department of Physics, New York University, New York, NY, USA
[112] Ohio State University, Columbus, OH, USA
[113] Faculty of Science, Okayama University, Okayama, Japan
[114] Homer L. Dodge Department of Physics and Astronomy, University of Oklahoma, Norman, OK, USA
[115] Department of Physics, Oklahoma State University, Stillwater, OK, USA
[116] Palacký University, RCPTM, Olomouc, Czech Republic
[117] Center for High Energy Physics, University of Oregon, Eugene, OR, USA
[118] LAL, Univ. Paris-Sud, CNRS/IN2P3, Université Paris-Saclay, Orsay, France
[119] Graduate School of Science, Osaka University, Osaka, Japan
[120] Department of Physics, University of Oslo, Oslo, Norway
[121] Department of Physics, Oxford University, Oxford, UK
[122] [(a)]INFN Sezione di Pavia, Pavia, Italy; [(b)]Dipartimento di Fisica, Università di Pavia, Pavia, Italy
[123] Department of Physics, University of Pennsylvania, Philadelphia, PA, USA
[124] National Research Centre "Kurchatov Institute" B.P. Konstantinov Petersburg Nuclear Physics Institute, St. Petersburg, Russia
[125] [(a)]INFN Sezione di Pisa, Pisa, Italy; [(b)]Dipartimento di Fisica E. Fermi, Università di Pisa, Pisa, Italy
[126] Department of Physics and Astronomy, University of Pittsburgh, Pittsburgh, PA, USA
[127] [(a)]Laboratório de Instrumentação e Física Experimental de Partículas-LIP, Lisbon, Portugal; [(b)]Faculdade de Ciências, Universidade de Lisboa, Lisbon, Portugal; [(c)]Department of Physics, University of Coimbra, Coimbra, Portugal; [(d)]Centro de Física Nuclear da Universidade de Lisboa, Lisbon, Portugal; [(e)]Departamento de Fisica, Universidade do Minho, Braga, Portugal; [(f)]Departamento de Fisica Teorica y del Cosmos and CAFPE, Universidad de Granada, Granada, Spain; [(g)]Dep Fisica and CEFITEC of Faculdade de Ciencias e Tecnologia, Universidade Nova de Lisboa, Caparica, Portugal
[128] Institute of Physics, Academy of Sciences of the Czech Republic, Prague, Czech Republic
[129] Czech Technical University in Prague, Prague, Czech Republic
[130] Faculty of Mathematics and Physics, Charles University in Prague, Prague, Czech Republic
[131] State Research Center Institute for High Energy Physics (Protvino), NRC KI, Moscow, Russia
[132] Particle Physics Department, Rutherford Appleton Laboratory, Didcot, UK
[133] [(a)]INFN Sezione di Roma, Rome, Italy; [(b)]Dipartimento di Fisica, Sapienza Università di Roma, Rome, Italy
[134] [(a)]INFN Sezione di Roma Tor Vergata, Rome, Italy; [(b)]Dipartimento di Fisica, Università di Roma Tor Vergata, Rome, Italy
[135] [(a)]INFN Sezione di Roma Tre, Rome, Italy; [(b)]Dipartimento di Matematica e Fisica, Università Roma Tre, Rome, Italy
[136] [(a)]Faculté des Sciences Ain Chock, Réseau Universitaire de Physique des Hautes Energies-Université Hassan II, Casablanca, Morocco; [(b)]Centre National de l'Energie des Sciences Techniques Nucleaires, Rabat, Morocco; [(c)]Faculté des Sciences Semlalia, Université Cadi Ayyad, LPHEA-Marrakech, Marrakesh, Morocco; [(d)]Faculté des Sciences, Université Mohamed Premier and LPTPM, Oujda, Morocco; [(e)]Faculté des , Sciences, Université Mohammed V, Rabat, Morocco
[137] DSM/IRFU (Institut de Recherches sur les Lois Fondamentales de l'Univers), CEA Saclay (Commissariat à l'Energie Atomique et aux Energies Alternatives), Gif-sur-Yvette, France
[138] Santa Cruz Institute for Particle Physics, University of California Santa Cruz, Santa Cruz, CA, USA
[139] Department of Physics, University of Washington, Seattle, WA, USA

[140] Department of Physics and Astronomy, University of Sheffield, Sheffield, UK
[141] Department of Physics, Shinshu University, Nagano, Japan
[142] Fachbereich Physik, Universität Siegen, Siegen, Germany
[143] Department of Physics, Simon Fraser University, Burnaby, BC, Canada
[144] SLAC National Accelerator Laboratory, Stanford, CA, USA
[145] [(a)]Faculty of Mathematics, Physics and Informatics, Comenius University, Bratislava, Slovakia; [(b)]Department of Subnuclear Physics, Institute of Experimental Physics of the Slovak Academy of Sciences, Kosice, Slovak Republic
[146] [(a)]Department of Physics, University of Cape Town, Cape Town, South Africa; [(b)]Department of Physics, University of Johannesburg, Johannesburg, South Africa; [(c)]School of Physics, University of the Witwatersrand, Johannesburg, South Africa
[147] [(a)]Department of Physics, Stockholm University, Stockholm, Sweden; [(b)]The Oskar Klein Centre, Stockholm, Sweden
[148] Physics Department, Royal Institute of Technology, Stockholm, Sweden
[149] Departments of Physics and Astronomy and Chemistry, Stony Brook University, Stony Brook, NY, USA
[150] Department of Physics and Astronomy, University of Sussex, Brighton, UK
[151] School of Physics, University of Sydney, Sydney, Australia
[152] Institute of Physics, Academia Sinica, Taipei, Taiwan
[153] Department of Physics, Technion: Israel Institute of Technology, Haifa, Israel
[154] Raymond and Beverly Sackler School of Physics and Astronomy, Tel Aviv University, Tel Aviv, Israel
[155] Department of Physics, Aristotle University of Thessaloniki, Thessaloniki, Greece
[156] International Center for Elementary Particle Physics and Department of Physics, The University of Tokyo, Tokyo, Japan
[157] Graduate School of Science and Technology, Tokyo Metropolitan University, Tokyo, Japan
[158] Department of Physics, Tokyo Institute of Technology, Tokyo, Japan
[159] Department of Physics, University of Toronto, Toronto, ON, Canada
[160] [(a)]TRIUMF, Vancouver, BC, Canada; [(b)]Department of Physics and Astronomy, York University, Toronto, ON, Canada
[161] Faculty of Pure and Applied Sciences, and Center for Integrated Research in Fundamental Science and Engineering, University of Tsukuba, Tsukuba, Japan
[162] Department of Physics and Astronomy, Tufts University, Medford, MA, United States of America
[163] Department of Physics and Astronomy, University of California Irvine, Irvine, CA, USA
[164] [(a)]INFN Gruppo Collegato di Udine, Sezione di Trieste, Udine, Italy; [(b)]ICTP, Trieste, Italy; [(c)]Dipartimento di Chimica, Fisica e Ambiente, Università di Udine, Udine, Italy
[165] Department of Physics and Astronomy, University of Uppsala, Uppsala, Sweden
[166] Department of Physics, University of Illinois, Urbana, IL, USA
[167] Instituto de Fisica Corpuscular (IFIC) and Departamento de Fisica Atomica, Molecular y Nuclear and Departamento de Ingeniería Electrónica and Instituto de Microelectrónica de Barcelona (IMB-CNM), University of Valencia and CSIC, Valencia, Spain
[168] Department of Physics, University of British Columbia, Vancouver, BC, Canada
[169] Department of Physics and Astronomy, University of Victoria, Victoria, BC, Canada
[170] Department of Physics, University of Warwick, Coventry, UK
[171] Waseda University, Tokyo, Japan
[172] Department of Particle Physics, The Weizmann Institute of Science, Rehovot, Israel
[173] Department of Physics, University of Wisconsin, Madison, WI, USA
[174] Fakultät für Physik und Astronomie, Julius-Maximilians-Universität, Würzburg, Germany
[175] Fakultät für Mathematik und Naturwissenschaften, Fachgruppe Physik, Bergische Universität Wuppertal, Wuppertal, Germany
[176] Department of Physics, Yale University, New Haven, CT, USA
[177] Yerevan Physics Institute, Yerevan, Armenia
[178] Centre de Calcul de l'Institut National de Physique Nucléaire et de Physique des Particules (IN2P3), Villeurbanne, France

[a] Also at Department of Physics, King's College London, London, UK
[b] Also at Institute of Physics, Azerbaijan Academy of Sciences, Baku, Azerbaijan
[c] Also at Novosibirsk State University, Novosibirsk, Russia
[d] Also at TRIUMF, Vancouver, BC, Canada
[e] Also at Department of Physics & Astronomy, University of Louisville, Louisville, KY, USA

[f] Also at Department of Physics, California State University, Fresno, CA, USA
[g] Also at Department of Physics, University of Fribourg, Fribourg, Switzerland
[h] Also at Departament de Fisica de la Universitat Autonoma de Barcelona, Barcelona, Spain
[i] Also at Departamento de Fisica e Astronomia, Faculdade de Ciencias, Universidade do Porto, Portugal
[j] Also at Tomsk State University, Tomsk, Russia
[k] Also at Universita di Napoli Parthenope, Napoli, Italy
[l] Also at Institute of Particle Physics (IPP), Canada
[m] Also at National Institute of Physics and Nuclear Engineering, Bucharest, Romania
[n] Also at Department of Physics, St. Petersburg State Polytechnical University, St. Petersburg, Russia
[o] Also at Department of Physics, The University of Michigan, Ann Arbor, MI, USA
[p] Also at Centre for High Performance Computing, CSIR Campus, Rosebank, Cape Town, South Africa
[q] Also at Louisiana Tech University, Ruston, LA, USA
[r] Also at Institucio Catalana de Recerca i Estudis Avancats, ICREA, Barcelona, Spain
[s] Also at Graduate School of Science, Osaka University, Osaka, Japan
[t] Also at Department of Physics, National Tsing Hua University, Taiwan
[u] Also at Institute for Mathematics, Astrophysics and Particle Physics, Radboud University Nijmegen/Nikhef, Nijmegen, Netherlands
[v] Also at Department of Physics, The University of Texas at Austin, Austin, TX, USA
[w] Also at Institute of Theoretical Physics, Ilia State University, Tbilisi, Georgia
[x] Also at CERN, Geneva, Switzerland
[y] Also at Georgian Technical University (GTU),Tbilisi, Georgia
[z] Also at Ochadai Academic Production, Ochanomizu University, Tokyo, Japan
[aa] Also at Manhattan College, New York, NY, USA
[ab] Also at Hellenic Open University, Patras, Greece
[ac] Also at Academia Sinica Grid Computing, Institute of Physics, Academia Sinica, Taipei, Taiwan
[ad] Also at School of Physics, Shandong University, Shandong, China
[ae] Also at Moscow Institute of Physics and Technology State University, Dolgoprudny, Russia
[af] Also at Section de Physique, Université de Genève, Geneva, Switzerland
[ag] Also at Eotvos Lorand University, Budapest, Hungary
[ah] Also at Departments of Physics & Astronomy and Chemistry, Stony Brook University, Stony Brook, NY, USA
[ai] Also at International School for Advanced Studies (SISSA), Trieste, Italy
[aj] Also at Department of Physics and Astronomy, University of South Carolina, Columbia, SC, USA
[ak] Also at School of Physics and Engineering, Sun Yat-sen University, Guangzhou, China
[al] Also at Institute for Nuclear Research and Nuclear Energy (INRNE) of the Bulgarian Academy of Sciences, Sofia, Bulgaria
[am] Also at Faculty of Physics, M.V. Lomonosov Moscow State University, Moscow, Russia
[an] Also at Institute of Physics, Academia Sinica, Taipei, Taiwan
[ao] Also at National Research Nuclear University MEPhI, Moscow, Russia
[ap] Also at Department of Physics, Stanford University, Stanford, CA, USA
[aq] Also at Institute for Particle and Nuclear Physics, Wigner Research Centre for Physics, Budapest, Hungary
[ar] Also at Flensburg University of Applied Sciences, Flensburg, Germany
[as] Also at University of Malaya, Department of Physics, Kuala Lumpur, Malaysia
[at] Also at CPPM, Aix-Marseille Université and CNRS/IN2P3, Marseille, France
[*] Deceased

Eur. Phys. J. C (2014) 74:3130
DOI 10.1140/epjc/s10052-014-3130-x

THE EUROPEAN PHYSICAL JOURNAL C

Regular Article - Experimental Physics

Measurement of the muon reconstruction performance of the ATLAS detector using 2011 and 2012 LHC proton–proton collision data

ATLAS Collaboration[⋆]

CERN, 1211 Geneva 23, Switzerland

Received: 16 July 2014 / Accepted: 14 October 2014 / Published online: 26 November 2014

Abstract This paper presents the performance of the ATLAS muon reconstruction during the LHC run with pp collisions at $\sqrt{s} = 7$–8 TeV in 2011–2012, focusing mainly on data collected in 2012. Measurements of the reconstruction efficiency and of the momentum scale and resolution, based on large reference samples of $J/\psi \to \mu\mu$, $Z \to \mu\mu$ and $\Upsilon \to \mu\mu$ decays, are presented and compared to Monte Carlo simulations. Corrections to the simulation, to be used in physics analysis, are provided. Over most of the covered phase space (muon $|\eta| < 2.7$ and $5 \lesssim p_{\mathrm{T}} \lesssim 100$ GeV) the efficiency is above 99 % and is measured with per-mille precision. The momentum resolution ranges from 1.7 % at central rapidity and for transverse momentum $p_{\mathrm{T}} \simeq 10$ GeV, to 4 % at large rapidity and $p_{\mathrm{T}} \simeq 100$ GeV. The momentum scale is known with an uncertainty of 0.05 % to 0.2 % depending on rapidity. A method for the recovery of final state radiation from the muons is also presented.

1 Introduction

The efficient identification of muons and the accurate measurement of their momenta are two of the main features of the ATLAS detector [1] at the LHC. These characteristics are often crucial in physics analysis, as for example in precise measurements of Standard Model processes [2–4], in the discovery of the Higgs boson, in the determination of its mass [5,6], and in searches for physics beyond the Standard Model [7,8]. This publication presents the performance of the ATLAS muon reconstruction during the LHC run at $\sqrt{s} = 7$–8 TeV, focusing mainly on data collected in 2012. The performance of the ATLAS muon reconstruction has already been presented in a recent publication [9] based on 2010 data. The results presented here are based on an integrated luminosity ≈500 times larger, which allows a large reduction of the uncertainties. The measurements of the efficiency, of the momentum scale and resolution are discussed with a particular emphasis on the comparison between data and Monte Carlo (MC) simulation, on the corrections used in the physics analyses and on the associated systematic uncertainties. Muons with very large transverse momentum,[1] $p_{\mathrm{T}} > 120$ GeV, are not treated here as they will be the subject of a forthcoming publication on the alignment of the ATLAS muon spectrometer and its high-p_{T} performance.

This publication is structured as follows: Sect. 2 gives a short description of muon detection in ATLAS and Sect. 3 describes the real and simulated data samples used in the performance analysis. The measurement of the reconstruction efficiency is described in Sect. 4 while Sect. 5 reports the momentum scale and resolution. A method for including photons from final-state radiation in the reconstruction of the muon kinematics, is described in Sect. 6. Conclusions are given in Sect. 7.

2 Muon identification and reconstruction

A detailed description of the ATLAS detector can be found elsewhere [1]. The ATLAS experiment uses the information from the muon spectrometer (MS) and from the inner detector (ID) and, to a lesser extent, from the calorimeter, to identify and precisely reconstruct muons produced in the pp collisions.

⋆ e-mail: atlas.publications@cern.ch

[1] ATLAS uses a right-handed coordinate system with its origin at the nominal interaction point (IP) in the centre of the detector and the z-axis along the beam pipe. The x-axis points from the IP to the centre of the LHC ring, and the y-axis points upward. Cylindrical coordinates (r, ϕ) are used in the transverse plane, ϕ being the azimuthal angle around the beam pipe. The pseudorapidity and the transverse momentum are defined in terms of the polar angle θ as $\eta = -\ln\tan(\theta/2)$ and $p_{\mathrm{T}} = p\sin\theta$, respectively. The $\eta-\phi$ distance between two particles is defined as $\Delta R = \sqrt{\Delta\eta^2 + \Delta\phi^2}$.

The MS is the outermost of the ATLAS sub-detectors: it is designed to detect charged particles in the pseudorapidity region up to $|\eta| = 2.7$, and to provide momentum measurement with a relative resolution better than 3 % over a wide p_{T} range and up to 10 % at $p_{\mathrm{T}} \approx 1$ TeV. The MS consists of one barrel part (for $|\eta| < 1.05$) and two end-cap sections. A system of three large superconducting air-core toroid magnets provides a magnetic field with a bending integral of about 2.5 Tm in the barrel and up to 6 Tm in the end-caps. Triggering and η, ϕ position measurements, with typical spatial resolution of 5–10 mm, are provided by the Resistive Plate Chambers (RPC, three doublet layers for $|\eta| < 1.05$) and by the Thin Gap Chambers (TGC, three triplet and doublet layers for $1.0 < |\eta| < 2.4$). Precise muon momentum measurement is possible up to $|\eta| = 2.7$ and it is provided by three layers of Monitored Drift Tube Chambers (MDT), each chamber providing six to eight η measurements along the muon track. For $|\eta| > 2$ the inner layer is instrumented with a quadruplet of Cathode Strip Chambers (CSC) instead of MDTs. The single hit resolution in the bending plane for the MDT and the CSC is about 80 μm and 60 μm, respectively. Tracks in the MS are reconstructed in two steps: first local track segments are sought within each layer of chambers and then local track segments from different layers are combined into full MS tracks.

The ID provides an independent measurement of the muon track close to the interaction point. It consists of three sub-detectors: the Silicon Pixels and the Semi-Conductor Tracker (SCT) detectors for $|\eta| < 2.5$ and the Transition Radiation Tracker (TRT) covering $|\eta| < 2.0$. They provide high-resolution coordinate measurements for track reconstruction inside an axial magnetic field of 2 T. A track in the barrel region has typically 3 Pixel hits, 8 SCT hits, and approximately 30 TRT hits.

The material between the interaction point and the MS ranges approximately from 100 to 190 radiation lengths, depending on η, and consists mostly of calorimeters. The sampling liquid-argon (LAr) electromagnetic calorimeter covers $|\eta| < 3.2$ and is surrounded by hadronic calorimeters based on iron and scintillator tiles for $|\eta| \lesssim 1.5$ and on LAr for larger values of $|\eta|$.

Muon identification is performed according to several reconstruction criteria (leading to different muon "types"), according to the available information from the ID, the MS, and the calorimeter sub-detector systems. The different types are:

- Stand-Alone (SA) muons: the muon trajectory is reconstructed only in the MS. The parameters of the muon track at the interaction point are determined by extrapolating the track back to the point of closest approach to the beam line, taking into account the estimated energy loss of the muon in the calorimeters. In general the muon has to traverse at least two layers of MS chambers to provide a track measurement. SA muons are mainly used to extend the acceptance to the range $2.5 < |\eta| < 2.7$ which is not covered by the ID;
- Combined (CB) muon: track reconstruction is performed independently in the ID and MS, and a combined track is formed from the successful combination of a MS track with an ID track. This is the main type of reconstructed muons;
- Segment-tagged (ST) muons: a track in the ID is classified as a muon if, once extrapolated to the MS, it is associated with at least one local track segment in the MDT or CSC chambers. ST muons can be used to increase the acceptance in cases in which the muon crossed only one layer of MS chambers, either because of its low p_{T} or because it falls in regions with reduced MS acceptance;
- Calorimeter-tagged (CaloTag) muons: a track in the ID is identified as a muon if it could be associated to an energy deposit in the calorimeter compatible with a minimum ionizing particle. This type has the lowest purity of all the muon types but it recovers acceptance in the uninstrumented regions of the MS. The identification criteria of this muon type are optimized for a region of $|\eta| < 0.1$ and a momentum range of $25 \lesssim p_{\mathrm{T}} \lesssim 100$ GeV.

CB candidates have the highest muon purity. The reconstruction of tracks in the spectrometer, and as a consequence the SA and CB muons, is affected by acceptance losses mainly in two regions: at $\eta \approx 0$, where the MS is only partially equipped with muon chambers in order to provide space for the services for the ID and the calorimeters, and in the region $(1.1 < \eta < 1.3)$ between the barrel and the positive η end-cap, where there are regions in ϕ with only one layer of chambers traversed by muons in the MS, due to the fact that some of the chambers of that region were not yet installed.[2]

The reconstruction of the SA, CB and ST muons (all using the MS information) has been performed using two independent reconstruction software packages, implementing different strategies [10] (named "Chains") both for the reconstruction of muons in the MS and for the ID-MS combination. For the ID-MS combination, the first chain ("Chain 1") performs a statistical combination of the track parameters of the SA and ID muon tracks using the corresponding covariance matrices. The second ("Chain 2") performs a global refit of the muon track using the hits from both the ID and MS sub-detectors. The use of two independent codes provided redundancy and robustness in the ATLAS commissioning phase. A unified reconstruction programme ("Chain 3") has been developed to incorporate the best features of the two chains and has been used, in parallel to the other two, for the reconstruction

[2] The installation of all the muon chambers in this region has been completed during the 2013–2014 LHC shutdown.

of 2012 data. It is planned to use only Chain 3 for future data taking. So far, the first two chains were used in all ATLAS publications. As the three chains have similar performance, only results for "Chain 1" are shown in the present publication. A summary of the results for the other two chains is reported in Appendix A.

The following quality requirements are applied to the ID tracks used for CB, ST or CaloTag muons:

- at least 1 Pixel hit;
- at least 5 SCT hits;
- at most 2 active Pixel or SCT sensors traversed by the track but without hits;
- in the region of full TRT acceptance, $0.1 < |\eta| < 1.9$, at least 9 TRT hits.

The number of hits required in the first two points is reduced by one if the track traverses a sensor known to be inefficient according to a time-dependent database. The above requirements are dropped in the region $|\eta| > 2.5$, where short ID track segments can be matched to SA muons to form a CB muon.

3 Data and Monte Carlo samples

3.1 Data samples

The results presented in this article are mostly obtained from the analysis of $\sqrt{s} = 8$ TeV pp collision events corresponding to an integrated luminosity of 20.3 fb^{-1} collected by the ATLAS detector in 2012. Results from pp collisions at $\sqrt{s} = 7$ TeV, collected in 2011, are presented in Appendix B. Events are accepted only if the ID, the MS and the calorimeter detectors were operational and both solenoid and toroid magnet systems were on.

The online event selection was performed by a three-level trigger system described in Ref. [11]. The performance of the ATLAS muon trigger during the 2012 data taking period is reported in Ref. [12]. The $Z \to \mu\mu$ candidates have been selected online by requiring at least one muon candidate with $p_{\mathrm{T}} > 24$ GeV, isolated from other activity in the ID. The $J/\psi \to \mu\mu$ and the $\Upsilon \to \mu\mu$ samples used for momentum scale and resolution studies have been selected online with two dedicated dimuon triggers that require two opposite-charge muons compatible with the same vertex, with transverse momentum $p_{\mathrm{T}} > 6$ GeV, and the dimuon invariant mass in the range 2.5–4.5 GeV for the J/ψ and 8–11 GeV for the Υ trigger. The $J/\psi \to \mu\mu$ sample used for the efficiency measurement was instead selected using a mix of single-muon triggers and a dedicated trigger requiring a muon with $p_{\mathrm{T}} > 6$ GeV and an ID track with $p_{\mathrm{T}} > 3.5$ GeV, such that the invariant mass of the muon+track pair, under a muon mass hypothesis, is in the window 2.7–3.5 GeV. This dedicated trigger operated during the whole data taking period with a prescaled rate of $\approx$1 Hz.

3.2 Monte Carlo samples

Monte Carlo samples for the process $pp \to (Z/\gamma^*)X \to \mu^+\mu^- X$, called $Z \to \mu\mu$ in the following, were generated using POWHEG [13] interfaced to PYTHIA8 [14]. The CT10 [15] parton density functions (PDFs) have been used. The PHOTOS [16] package has been used to simulate final state photon radiation (FSR), using the exponentiated mode that leads to multi-photon emission taking into account γ^* interference in Z decays. To improve the description of the dimuon invariant mass distribution, the generated lineshape was reweighted using an improved Born approximation with a running-width definition of the Z lineshape parameters. The ALPGEN [17] generator, interfaced with PYTHIA6 [18], was also used to generate alternative $Z \to \mu\mu$ samples.

Samples of prompt $J/\psi \to \mu\mu$ and of $\Upsilon \to \mu\mu$ were generated using PYTHIA8, complemented with PHOTOS to simulate the effects of final state radiation. The samples were generated requiring each muon to have $p_{\mathrm{T}} > 6.5(6)$ GeV for J/ψ (Υ). The J/ψ distribution in rapidity and transverse momentum has been reweighted in the simulated samples to match the distribution observed in the data. The samples used for the simulation of the backgrounds to $Z \to \mu\mu$ are described in detail in [19], they include $Z \to \tau\tau$, $W \to \mu\nu$ and $W \to \tau\nu$, generated with POWHEG, WW, ZZ and WZ generated with SHERPA [20], $t\bar{t}$ samples generated with MC@NLO [21] and $b\bar{b}$ as well as $c\bar{c}$ samples generated with PYTHIA6.

All the generated samples were passed through the simulation of the ATLAS detector based on GEANT4 [22,23] and were reconstructed with the same programs used for the data. The ID and the MS were simulated with an ideal geometry without any misalignment. To emulate the effect of the misalignments of the MS chambers in real data, the reconstruction of the muon tracks in the simulated samples was performed using a random set of MS alignment constants. The amount of random smearing applied to these alignment constants was derived from an early assessment of the precision of the alignment, performed with special runs in which the toroidal magnetic field was off. The knowledge of the alignment constants improved with time. In particular the alignment constants used for the reconstruction of the data were more precise than those used to define the random smearing applied in the simulation, resulting in some cases in a worse MS resolution in MC than in data.

4 Efficiency

The availability of two independent detectors to reconstruct the muons (the ID and the MS) enables a precise determination of the muon reconstruction efficiency in the region $|\eta| < 2.5$. This is obtained with the so called tag-and-probe method described in the next section. A different methodology, described in Sect. 4.2, is used in the region $2.5 < |\eta| < 2.7$ in which only one detector (the MS) is available.

4.1 Muon reconstruction efficiency in the region $|\eta| < 2.5$

The tag-and-probe method is employed to measure the reconstruction efficiencies of all muon types within the acceptance of the ID ($|\eta| < 2.5$). The conditional probability that a muon reconstructed by the ID is also reconstructed using the MS as a particular muon type, $P(\text{Type}|\text{ID})$, with Type = (CB, ST), can be measured using ID probes. Conversely, the conditional probability that a muon reconstructed by the MS is also reconstructed in the ID, $P(\text{ID}|\text{MS})$, is measured using MS tracks as probes.

For each muon type, the total reconstruction efficiency is given by:

$$\varepsilon(\text{Type}) = \varepsilon(\text{Type}|\text{ID}) \cdot \varepsilon(\text{ID}), \tag{1}$$

where $\varepsilon(\text{ID})$ is the probability that a muon is reconstructed as an ID track. The quantity $\varepsilon(\text{ID})$ cannot be measured directly and is replaced by $\varepsilon(\text{ID}|\text{MS})$ to give the tag-and-probe approximation:

$$\varepsilon(\text{Type}) \simeq \varepsilon(\text{Type}|\text{ID}) \cdot \varepsilon(\text{ID}|\text{MS}). \tag{2}$$

The level of agreement of the measured efficiency, $\varepsilon^{\text{Data}}(\text{Type})$, with the efficiency measured with the same method in MC, $\varepsilon^{\text{MC}}(\text{Type})$, is expressed as the ratio between these two numbers, called "efficiency scale factor" or SF:

$$SF = \frac{\varepsilon^{\text{Data}}(\text{Type})}{\varepsilon^{\text{MC}}(\text{Type})}. \tag{3}$$

Possible biases introduced by the tag-and-probe approximation and other systematic effects on the efficiency measurement, which appear both in data and in MC, cancel in the SF. The SF is therefore used to correct the simulation in physics analysis.

4.1.1 The tag-and-probe method with $Z \to \mu\mu$ events

For $Z \to \mu\mu$ decays, events are selected by requiring two oppositely charged isolated muons[3] with transverse momenta of at least $p_{\text{T}} > 25$ and 10 GeV respectively and a dimuon invariant mass within 10 GeV of the Z-boson mass. The muons are required to be back to back in the transverse plane ($\Delta\phi > 2$). One of the muons is required to be a CB muon, and to have triggered the readout of the event. This muon is called the "tag". The other muon, the so-called "probe", is required to be a MS track (i.e. a SA or a CB muon) when $\varepsilon(\text{ID}|\text{MS})$ is to be measured. The probe is required to be a CaloTag muon for the measurement of $\varepsilon(\text{Type}|\text{ID})$. The use of CaloTag muons as the ID probes reduces the background in the $Z \to \mu\mu$ sample by an order of magnitude without biasing the efficiency measurement. The MS probes are also used to measure the efficiency of CaloTag muons. After selecting all tag-probe pairs, an attempt is made to match the probe to a reconstructed muon: a match is successful when the muon and the probe are close in the $\eta - \phi$ plane ($\Delta R < 0.01$ for CaloTag probes to be matched with CB or ST muons and $\Delta R < 0.05$ for MS probes to be matched to ID or CaloTag muons).

4.1.2 Background treatment in $Z \to \mu\mu$ events

Apart from $Z \to \mu\mu$ events, a small fraction of the selected tag-probe pairs may come from other sources. For a precise efficiency measurement, these backgrounds have to be estimated and subtracted. Contributions from $Z \to \tau\tau$ and $t\bar{t}$ decays are estimated using MC simulation. Additionally, QCD multijet events and $W \to \mu\nu$ decays in association with jet activity (W+jets) can yield tag-probe pairs through secondary muons from heavy- or light-hadron decays. As these backgrounds are approximately charge-symmetric, they are estimated from the data using same-charge (SC) tag-probe pairs. This leads to the following estimate of the opposite-charge (OC) background for each region of the kinematic phase-space:

$$N(\text{Bkg}) = N_{\text{OC}}^{Z,t\bar{t}\ \text{MC}} + T \cdot (N_{\text{SC}}^{\text{Data}} - N_{\text{SC}}^{Z,t\bar{t}\ \text{MC}}) \tag{4}$$

where $N_{OC}^{Z,t\bar{t}\ \text{MC}}$ is the contribution from $Z \to \tau\tau$ and $t\bar{t}$ decays, $N_{\text{SC}}^{\text{Data}}$ is the number of SC pairs measured in data and $N_{\text{SC}}^{Z,t\bar{t}\ \text{MC}}$ is the estimated contribution of the $Z \to \mu\mu$, $Z \to \tau\tau$ and $t\bar{t}$ processes to the SC sample. T is a global transfer factor that takes into account the residual charge asymmetry of the QCD multijet and W+jets samples, estimated using the simulation:

$$T = 1 + \theta; \qquad \theta = \frac{N_{\text{OC}}^{\text{QCD+W MC}} - N_{\text{SC}}^{\text{QCD+W MC}}}{N_{\text{SC}}^{\text{Data}}}. \tag{5}$$

For the kinematic region covered by the measurement, the transfer factor is $T = 1.15$ for CaloTag probes. For the MS probes the misidentification rate is low and the residual QCD

[3] Here a muon is considered to be isolated when the sum of the momenta of the other tracks with $p_{\text{T}} > 1$ GeV in a cone of $\Delta R = 0.4$ around the muon track is less than 0.15 times the muon momentum itself. Different cone sizes and cuts on the momentum fraction are used in other parts of this paper.

multijet background has a large contribution from oppositely charged muon pairs in $b\bar{b}$ decays, leading to $T = 2.6$. The efficiency for finding a muon of type A given a probe of type B, corrected for the effect of background, can then be computed as:

$$\varepsilon(\mathrm{A}|\mathrm{B}) = \frac{N^{\mathrm{Match}}_{\mathrm{Probes}}(\mathrm{Data}) - N^{\mathrm{Match}}_{\mathrm{Probes}}(\mathrm{Bkg})}{N^{\mathrm{All}}_{\mathrm{Probes}}(\mathrm{Data}) - N^{\mathrm{All}}_{\mathrm{Probes}}(\mathrm{Bkg})}, \tag{6}$$

where $N^{\mathrm{All}}_{\mathrm{Probes}}$ stands for the total number of probes considered and $N^{\mathrm{Match}}_{\mathrm{Probes}}$ is the number of probes successfully matched to a reconstructed muon of type A. According to the background estimate reported above, the sample of selected CaloTag probes is more than 99.5 % pure in $Z \to \mu\mu$ decays, as shown in Fig. 1. The $Z \to \mu\mu$ purity is maximal for muon $p_{\mathrm{T}} \simeq 40$ GeV and decreases to 98.5 % (97 %) for $p_{\mathrm{T}} = 10$ (100) GeV. The $Z \to \mu\mu$ purity has a weak dependence on the average number of inelastic pp interactions per bunch crossing, $\langle\mu\rangle$, decreasing from 99.8 % at $\langle\mu\rangle = 10$ to 99.5 % at $\langle\mu\rangle = 34$. A purity above 99.8 % is obtained in the selection of MS probes, with weaker dependence on p_{T} and $\langle\mu\rangle$.

4.1.3 Low p_{T} efficiencies from $J/\psi \to \mu\mu$ decays

The efficiencies extracted from $Z \to \mu\mu$ decays are complemented at low p_{T} with results derived from a sample of $J/\psi \to \mu\mu$ events. In 2012 ATLAS collected approximately 2M $J/\psi \to \mu\mu$ decays which were not biased by dimuon triggers requirements, using a combination of single muon triggers (isolated and non-isolated) and the dedicated "muon + track" trigger described in Sect. 3.1.

The analysis proceeds in a similar manner to the $Z \to \mu\mu$ with some modifications due to the different kinematics of the J/ψ. Tags are required to be CB muons with $p_{\mathrm{T}} > 4$ GeV and $|\eta| < 2.5$. As with the Z, the tag must have triggered the read-out of the event. Probes are sought from amongst the ID tracks and must have $p_{\mathrm{T}} > 2.5$ GeV and $|\eta| < 2.5$, opposite charge to the tag muon, and must form with the tag an invariant mass in the window 2.7–3.5 GeV. Finally the tag-probe pairs must fit to a common vertex with a very loose quality cut of $\chi^2 < 200$ for one degree of freedom, which removes tracks from different vertices, without any significant efficiency loss. Muon reconstruction efficiencies are then derived by binning in small cells of p_{T} and η of the probe tracks. Invariant mass distributions are built in each cell for two samples: (a) all tag-probe pairs and (b) tag-probe pairs in which the probe failed to be reconstructed in the MS. The invariant mass distributions are fitted with a signal plus background model to obtain the number of J/ψ signal events in the two samples, called $N_a(p_{\mathrm{T}}, \eta)$ and $N_b(p_{\mathrm{T}}, \eta)$, respectively. The fit model is a Gaussian plus a second order polynomial for the background. The two samples are fitted simultaneously using the same mean and width to describe the signal. The MS reconstruction efficiency in a given (p_{T}, η) cell is then defined as:

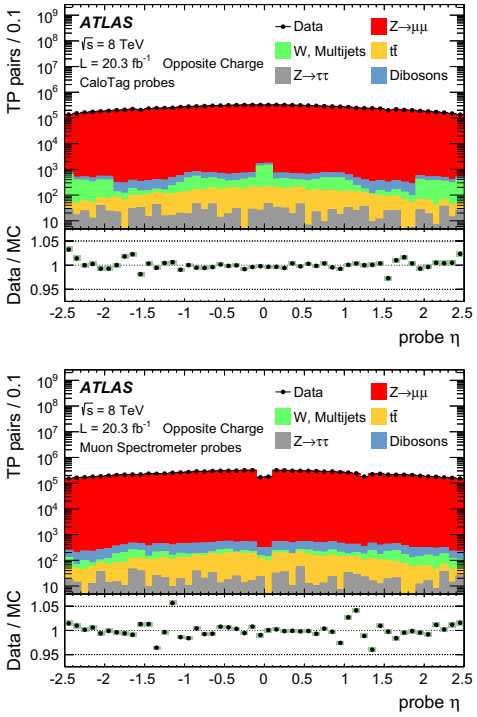

Fig. 1 Pseudorapidity distribution of the CaloTag (*top*) or MS (*bottom*) probes used in the tag-and-probe analysis. The *bottom panel* shows the ratio between observed and expected counts. The sum of the MC samples is normalized to the number of events in the data. The *green band* represents the statistical uncertainty

$$\varepsilon_{p_{\mathrm{T}},\eta}(\mathrm{Type}|\mathrm{ID}) = 1 - \frac{N_b(p_{\mathrm{T}}, \eta)}{N_a(p_{\mathrm{T}}, \eta)}. \tag{7}$$

The largest contribution to the systematic uncertainty originates from the model used in the fit. This uncertainty was estimated by changing the background model to a first or a third order polynomial and by relaxing the constraint that the mass and the width of the J/ψ signal are the same between the two samples. The resulting variations in the efficiency are added in quadrature to the statistical uncertainty to give the total uncertainty on the efficiency. The efficiency integrated over the full η region is obtained as an average of the efficiencies of the different η cells. This method ensures a reduced dependency on local variations of background

and resolution, and on the kinematic distribution of the probes.

4.1.4 Systematic uncertainties

The main contributions to the systematic uncertainty on the measurement of the efficiency SFs are shown in Fig. 2, as a function of η and p_{T}, and are discussed below (the labels in parenthesis refer to the legend of Fig. 2):

- (Bkg) the uncertainty on the data-driven background estimate is evaluated by varying the charge-asymmetry parameter θ of Eq. (5) by $\pm 100\,\%$. This results in an uncertainty of the efficiency measurement below 0.1 % in a large momentum range, reaching up to 0.2 % for low muon momenta where the contribution of the background is most significant.
- (dR) the choice of the cone size used for matching reconstructed muons to probe objects has been optimized to minimize the amount of matches with wrong tracks while keeping the maximum match efficiency for correct tracks. A systematic uncertainty is evaluated by varying the cone size by $\pm 50\,\%$. This yields an uncertainty of $\approx 0.1\,\%$.
- (TP approximation) possible biases in the tag-and-probe method, for example due to different distributions between MS probes and "true" muons or due to correlation between ID and MS efficiencies, are investigated. The simulation is used to compare the efficiency measured with the tag-and-probe method with the "true" MC efficiency calculated as the fraction of generator-level muons that are successfully reconstructed. Agreement within less than 0.1 % is observed, with the exception of the region $|\eta| < 0.1$. In the extraction of the data/MC scale factors, the difference between the measured and the "true" efficiency cancels to first order. To take into account possible imperfection of the simulation, half the observed difference is used as an additional systematic uncertainty on the SF.
- (Probes) the scale factor maps may be sensitive to disagreements between data and simulation in the kinematic distributions of the probes. The corresponding systematic uncertainty is estimated by reweighting the distribution of the probes in the simulation to bring it into agreement with the data. The resulting effect on the efficiency is below 0.1 % over most of the phase space.
- (Low p_{T}) for $4 < p_{\mathrm{T}} < 10$ GeV the systematic uncertainties are obtained from the analysis performed with the $J/\psi \to \mu\mu$ sample, as discussed in Sect. 4.1.3 (not shown in Fig. 2). The resulting uncertainty on the low-p_{T} SFs ranges between 0.5 % and 2 %, depending on p_{T} and η and is dominated by the uncertainty on the background model.
- (High p_{T}) no significant dependence of the measured SFs with p_{T} was observed in the momentum range considered.

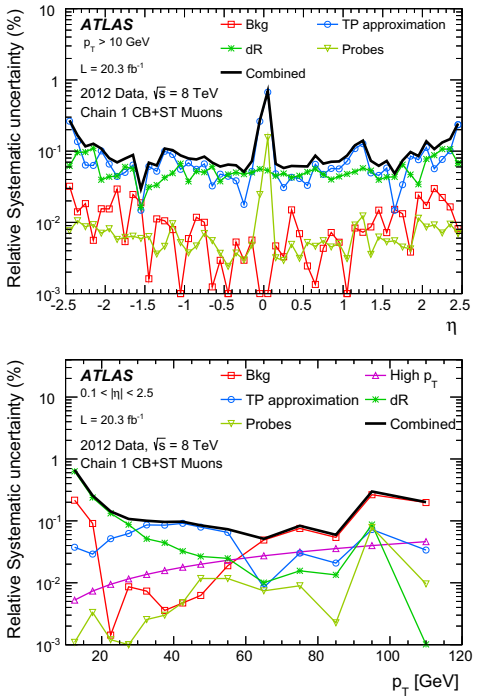

Fig. 2 Systematic uncertainty on the efficiency scale factor for CB+ST muons, obtained from $Z \to \mu\mu$ data, as a function of η (*top*) and p_{T} (*bottom*) for muons with $p_{\mathrm{T}} > 10$ GeV. The background systematic uncertainty in the last two bins of the *bottom plot* is affected by a large statistical uncertainty. The combined systematic uncertainty is the sum in quadrature of the individual contributions

An upper limit on the SF variation for large muon momenta has been extracted by using a MC simulation with built-in imperfections, including a realistic residual misalignment of the detector components or a 10 % variation of the muon energy loss. On the basis of this, a systematic uncertainty of $\pm 0.42\,\% \times (p_{\mathrm{T}}/1\ \mathrm{TeV})$ is obtained.

4.1.5 Results

Figure 3 shows the muon reconstruction efficiency ε(Type) as a function of η as measured from $Z \to \mu\mu$ events. The combination of all the muon reconstruction types (for CB, ST, and CaloTag muons) gives a uniform muon reconstruction efficiency of about 99 % over most the detector regions. The use of ST muons allows the recovery of efficiency especially in the region $1.1 < \eta < 1.3$ (from 85 % to 99 %) in which

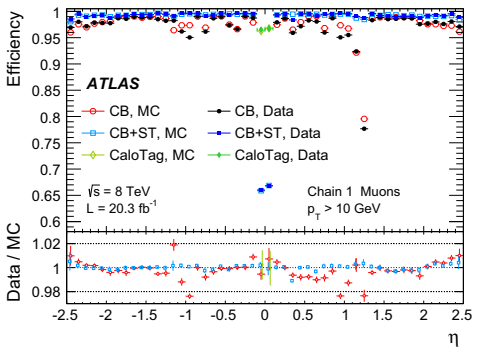

Fig. 3 Muon reconstruction efficiency as a function of η measured in $Z \to \mu\mu$ events for muons with $p_{\mathrm{T}} > 10$ GeV and different muon reconstruction types. CaloTag muons are only shown in the region $|\eta| < 0.1$, where they are used in physics analyses. The *error bars* on the efficiencies indicate the statistical uncertainty. The *panel at the bottom* shows the ratio between the measured and predicted efficiencies. The *error bars* on the ratios are the combination of statistical and systematic uncertainties

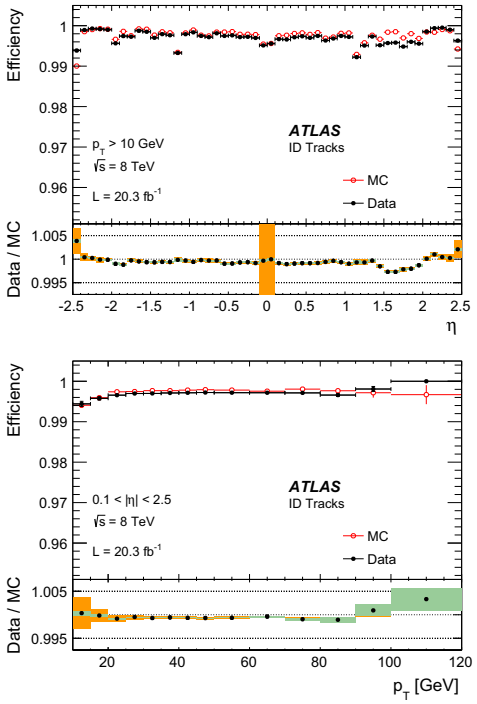

Fig. 4 ID muon reconstruction efficiency as a function of η (*top*) and p_{T} (*bottom*) measured in $Z \to \mu\mu$ events for muons with $p_{\mathrm{T}} > 10$ GeV. The *error bars* on the efficiencies indicate the statistical uncertainty. The *panel at the bottom* shows the ratio between the measured and predicted efficiencies. The *green areas* depict the pure statistical uncertainty, while the *orange areas* also include systematic uncertainties

part of the MS chambers were not installed, as discussed in Sect. 2. The remaining inefficiency of the combination of CB or ST muons (CB+ST) at $|\eta| < 0.1$ (66 %) is almost fully recovered by the use of CaloTag muons (97 %).

The efficiencies measured in experimental and simulated data are in good agreement, in general well within 1 %. The largest differences are observed in the CB muons. To reconstruct an MS track, the Chain 1 reconstruction requires track segments in at least two layers of precision chambers (MDT or CSC) and at least one measurement of the ϕ coordinate from trigger chambers (RPC or TGC). These requirements introduce some dependency on detector conditions and on the details of the simulation in the regions in which only two layers of precision chambers or only one layer of trigger chambers are crossed by the muons. This results in a reduction of efficiency in data with respect to MC of approximately 1 % in the region of $\eta \sim 0.5$ due the RPC detector conditions and to local deviations up to about 2 % at $0.9 < |\eta| < 1.3$ related to imperfections in the simulation of the barrel-endcap transition region. For the CB+ST muons the agreement between data and MC is very good, with the only exception of a low-efficiency region in data at $\eta = 0.3$–0.4 related to an inactive portion of an MDT chamber (not included in MC) in a region with reduced coverage due to the supporting structure of the ATLAS detector.[4]

The ID muon reconstruction efficiency, $\varepsilon(\mathrm{ID}|\mathrm{MS})$, for $p_{\mathrm{T}} > 10$ GeV as a function of η and p_T is shown in Fig. 4. The efficiency is greater than 0.99 and there is very good agreement between data and MC. The small efficiency reduction in the region $1.5 < \eta < 2$ is related to temporary hardware problems in the silicon detectors. The larger uncertainty at $|\eta| < 0.1$ is related to the limited MS coverage in that region.

Figure 5 shows the reconstruction efficiencies for CB and for CB+ST muons as a function of the transverse momentum, including results from $Z \to \mu\mu$ and $J/\psi \to \mu\mu$. A steep increase of the efficiency is observed at low p_{T}, in particular for the CB reconstruction, since a minimum momentum of approximately 3 GeV is required for a muon to traverse the calorimeter material and cross at least two layers of MS stations before being bent back by the magnetic field. Above $p_{\mathrm{T}} \approx 20$ GeV, the reconstruction efficiency for both CB and CB+ST muons is expected to be independent of the transverse momentum. This is confirmed within 0.5 % by the $Z \to \mu\mu$ data. The drop in efficiency observed in the J/ψ data at $p_{\mathrm{T}} > 15$ GeV is due to the inefficiency of the MS

[4] This effect is also visible in Fig. 9 at $\phi \simeq -1$.

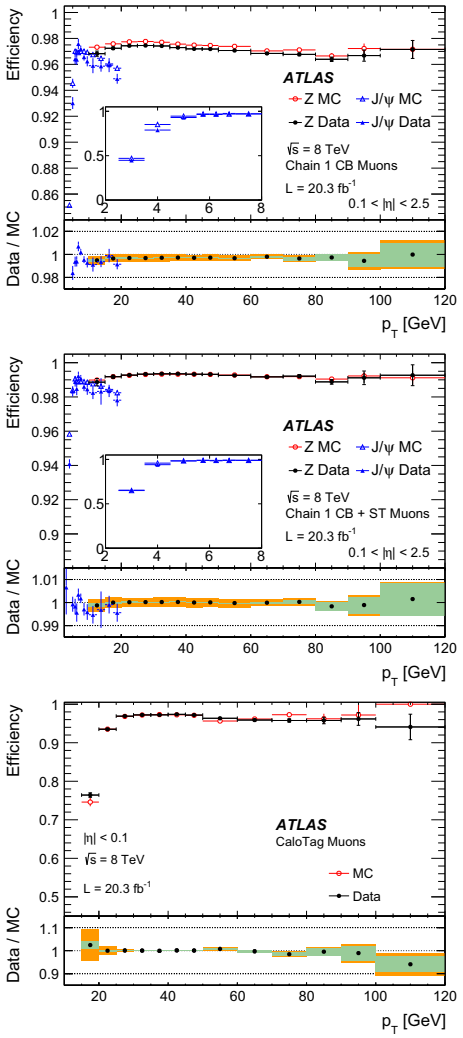

Fig. 5 Reconstruction efficiency for CB (*top*), CB+ST (*middle*) and CaloTag (*bottom*) muons as a function of the p_{T} of the muon, for muons with $0.1 < |\eta| < 2.5$ for CB and CB+ST muons and for $|\eta| < 0.1$ for CaloTag muons. The *upper two plots* also show the result obtained with $Z \to \mu\mu$ and $J/\psi \to \mu\mu$ events. The *insets on the upper plots* show the detail of the efficiency as a function of p_{T} in the low p_{T} region. The CaloTag muon efficiency (*bottom*) is only measured with $Z \to \mu\mu$ events. The *error bars* on the efficiencies indicate the statistical uncertainty for $Z \to \mu\mu$ and include also the fit model uncertainty for $J/\psi \to \mu\mu$. The *panel at the bottom* shows the ratio between the measured and predicted efficiencies. The *green areas* show the pure statistical uncertainty, while the *orange areas* also include systematic uncertainties

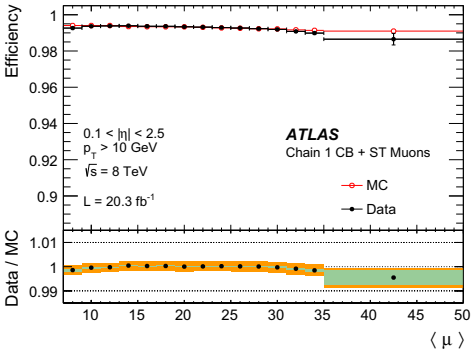

Fig. 6 Measured CB+ST muon reconstruction efficiency for muons with $p_{\mathrm{T}} > 10$ GeV as a function of the average number of inelastic pp collisions per bunch crossing $\langle\mu\rangle$. The *error bars* on the efficiencies indicate the statistical uncertainty. The *panel at the bottom* shows the ratio between the measured and predicted efficiencies. The *green areas* depict the pure statistical uncertainty, while the *orange areas* also include systematic uncertainties

reconstruction for muon pairs with small angular separation as in the case of highly boosted J/ψ. This effect is well reproduced by MC and the SF of the $J/\psi \to \mu\mu$ analysis are in good agreement with those from $Z \to \mu\mu$ in the overlap region. The CaloTag muon efficiency reaches a plateau of approximately 0.97 above $p_{\mathrm{T}} \gtrsim 30$ GeV, where it is well predicted by the MC.

Figure 6 shows the reconstruction efficiency for CB+ST muons as a function of $\langle\mu\rangle$, showing a high value (on average above 0.99) and remarkable stability. A small efficiency drop of about 1 % is only observed for $\langle\mu\rangle \gtrsim 35$. This is mainly caused by limitations of the MDT readout electronics in the high-rate regions close to the beam lines. These limitations are being addressed in view of the next LHC run.

4.2 Muon reconstruction efficiency for $|\eta| > 2.5$

As described in the previous sections, the CB muon reconstruction is limited by the ID acceptance which covers the pseudo-rapidity region $|\eta| < 2.5$. Above $|\eta| = 2.5$, SA muons are the only muon type that provides large efficiency. A measurement of the efficiency SF for muons in the range $2.5 < |\eta| < 2.7$, hereafter called high-η, is needed for the physics analyses that exploit the full MS acceptance.

A comparison with the Standard Model calculations for $Z \to \mu\mu$ events is used to measure the reconstruction efficiency SF in the high-η region. To reduce the theoretical and experimental uncertainties, the efficiency SF is calculated from the double ratio

$$\mathrm{SF} = \frac{\frac{N^{\mathrm{Data}}(2.5<|\eta_{\mathrm{fwd}}|<2.7)}{N^{\mathrm{MC}}(2.5<|\eta_{\mathrm{fwd}}|<2.7)}}{\frac{N^{\mathrm{Data}}(2.2<|\eta_{\mathrm{fwd}}|<2.5)}{N^{\mathrm{MC}}(2.2<|\eta_{\mathrm{fwd}}|<2.5)}}, \tag{8}$$

where the numerator is the ratio of the number of $Z \to \mu\mu$ candidates in data and in MC for which one of the muons, called the *forward* muon, is required to be in the high-η region $2.5 < |\eta_{\mathrm{fwd}}| < 2.7$ while the other muon from the Z decay, called the *central* muon, is required to have $|\eta| < 2.5$. The denominator is the ratio of $Z \to \mu\mu$ candidates in data over MC with the forward muon lying in the control region $2.2 < |\eta_{\mathrm{fwd}}| < 2.5$ and the central muon in the region $|\eta| < 2.2$. In both the numerator and denominator the central muon is required to be a CB muon while the forward muon can either be a CB or SA muon. The simulation of muons with $|\eta| < 2.5$ is corrected using the standard SF described in the previous section.

The selection of the central muon is similar to that of the tag muon in the tag-and-probe method. It is required to have triggered the event readout, to be isolated and to have transverse momentum $p_{\mathrm{T}} > 25$ GeV. The requirements for the forward muon include calorimeter-based isolation, requiring the transverse energy E_T measured in the calorimeter in a cone of $\Delta R = 0.2$ (excluding the energy lost by the muon itself) around the muon track, to be less than 10 % of the muon p_{T}. The central and forward muons are required to have opposite charge, a dimuon invariant mass within 10 GeV of the Z mass, and a separation in (η, ϕ) space of $\Delta R > 0.2$.

Different sources of systematic uncertainties have been considered: a first group is obtained by varying the p_{T} and isolation cuts on the central muons and the dimuon mass window. These variations produce effects of less than 0.3 % in the efficiency SF for the p_{T} range 20–60 GeV. The effect of the calorimetric isolation on the efficiency SF yields an uncertainty of less than 1 %, which is estimated by comparing the nominal SF values with the ones extracted when no calorimetric isolation is applied on the forward muons and by studying the dependence of this cut on the number of pp interactions. The contribution from the background processes, mainly dimuons from b and $\bar{b}$ decays, has been studied using MC background samples and found to be negligible.

The theoretical uncertainty from higher-order corrections is estimated by varying the renormalization and factorization scales in the POWHEG NLO calculation at the generator level and is found to produce a negligible effect on the ratio of Eq. (8). The uncertainty from the knowledge of the parton densities is estimated by reweighting the PDFs used in the MC samples from CT10 to MSTW2008NLO [24] and by studying, at the generator level, the effect of the uncertainty associated to the MSTW2008 PDF set on the double ratio of Eq. (8), obtaining an overall theoretical uncertainty of less than 0.55 %.

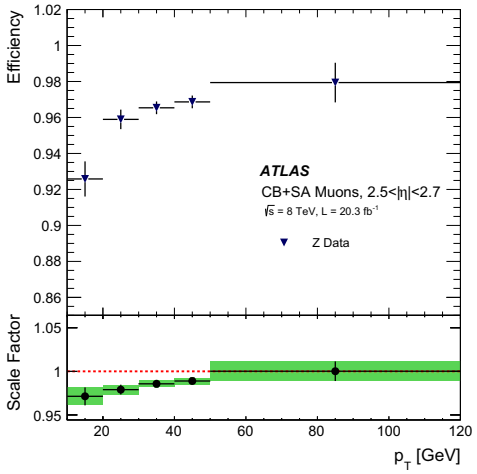

Fig. 7 Reconstruction efficiency for muons within $2.5 < |\eta| < 2.7$ from $Z \to \mu\mu$ events. The *upper plot* shows the efficiency obtained as the product of scale factor (Eq. 8) and the MC efficiency. The *lower plot* shows the scale factor. The *error bars* correspond to the statistical uncertainty while the *green shaded band* corresponds to the statistical and systematic uncertainty added in quadrature

The efficiency in this region is obtained as the product of the SF and the "true" MC efficiency, calculated as the fraction of generator-level muons that are successfully reconstructed. The reconstruction efficiency and the SF for muons in the high-η region is shown in Fig. 7 as a function of the muon p_{T}.

4.3 Scale factor maps

The standard approach used in ATLAS for physics analysis is to correct the muon reconstruction efficiency in the simulation using efficiency scale factors (SFs). The SFs are obtained with the tag-and-probe method using $Z \to \mu\mu$ events, as described above, and are provided to the analyses in the form of η–ϕ maps. Since no significant p_{T} dependence of the SF has been observed, no p_{T} binning is used in the SF maps. Different maps are produced for different data taking sub-periods with homogeneous detector conditions. The whole 2012 dataset is divided into 10 sub-periods. For each analysis, the final map is obtained as an average of the maps for all sub-periods, weighted by the periods' contribution to the integrated luminosity under study.

Figures 8 and 9 show the maps of the efficiencies measured using the data in the η–ϕ plane and the corresponding Scale Factors. The large data sample allows for a precise resolution of localized efficiency losses, for example in the

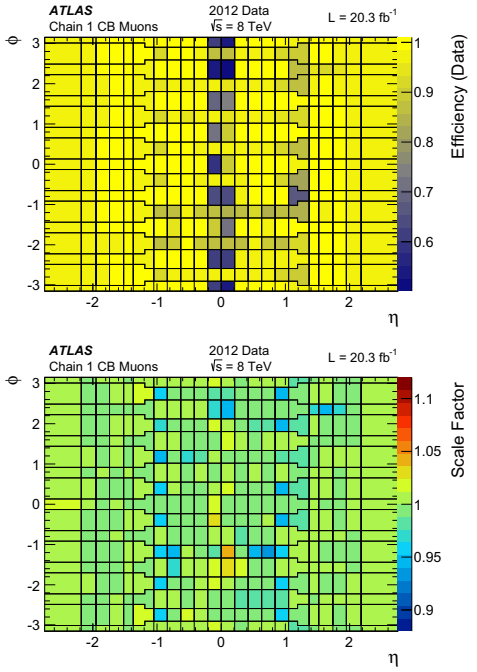

Fig. 8 Reconstruction efficiency measured in the experimental data (*top*), and the data/MC efficiency scale factor (*bottom*) for CB muons as a function of η and ϕ for muons with $p_{\mathrm{T}} > 10$ GeV

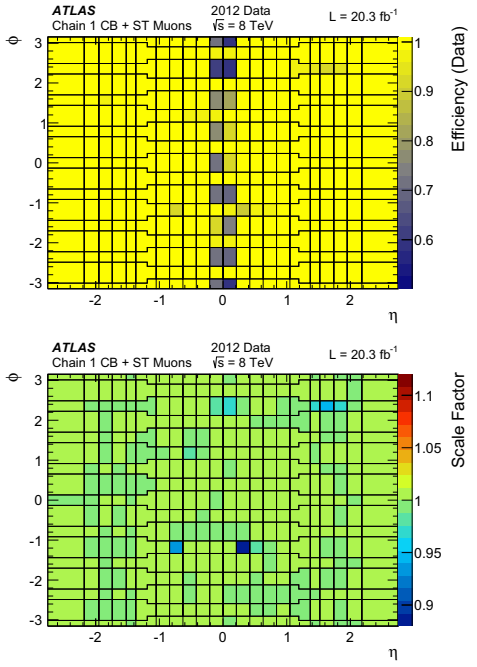

Fig. 9 Reconstruction efficiency measured in the experimental data (*top*) and the data/MC efficiency scale factor (*bottom*) for CB+ST muons as a function of η and ϕ for muons with $p_{\mathrm{T}} > 10$ GeV

muon spectrometer for $|\eta| \sim 0$ due to limited coverage. The SF maps show local differences between data and MC related to detector conditions as discussed in Sect. 4.1.5.

5 Momentum scale and resolution

The large samples of $J/\psi \to \mu\mu$, $\Upsilon \to \mu\mu$ and $Z \to \mu\mu$ decays collected by ATLAS are used to study in detail the muon momentum scale and resolution. The ATLAS simulation includes the best knowledge of the detector geometry, material distribution, and physics model of the muon interaction at the time of the MC events were generated. Additional corrections are needed to reproduce the muon momentum resolution and scale of experimental data at the level of precision that can be obtained using high-statistics samples of dimuon resonances. Section 5.1 describes the methodology used to extract the corrections to be applied to the MC simulation. In Sect. 5.2, the muon momentum scale and resolution is studied in the data and in MC samples with and without corrections.

5.1 Corrections to the muon momentum in MC

Similarly to Ref. [9], the simulated muon transverse momenta reconstructed in the ID and in the MS sub-detectors, $p_{\mathrm{T}}^{\mathrm{MC,Det}}$, where Det = ID, MS, are corrected using the following equation:

$$p_{\mathrm{T}}^{\mathrm{Cor,Det}} = \frac{p_{\mathrm{T}}^{\mathrm{MC,Det}} + \sum_{n=0}^{1} s_n^{\mathrm{Det}}(\eta,\phi)(p_{\mathrm{T}}^{\mathrm{MC,Det}})^n}{1 + \sum_{m=0}^{2} \Delta r_m^{\mathrm{Det}}(\eta,\phi)(p_{\mathrm{T}}^{\mathrm{MC,Det}})^{m-1} g_m} \quad (\text{with } s_0^{\mathrm{ID}} = 0 \text{ and } \Delta r_0^{\mathrm{ID}} = 0), \tag{9}$$

where g_m are normally distributed random variables with mean 0 and width 1 and the terms $\Delta r_m^{\mathrm{Det}}(\eta,\phi)$ and $s_n^{\mathrm{Det}}(\eta,\phi)$ describe, respectively, the momentum resolution smearing and the scale corrections applied in a specific η, ϕ detector region. The motivations for Eq. (9) are the following:

– corrections are defined in $\eta - \phi$ detector regions such that in each region the variation of momentum resolution and scale, and therefore of their possible corrections, are

expected to be small. In particular the nominal muon identification acceptance region (up to $|\eta| = 2.7$) is divided in 18 η sectors of size $\Delta\eta$ between 0.2 and 0.4, for both the MS and the ID. In addition, the MS is divided into two types of ϕ sectors of approximate size of $\pi/8$, exploiting the octagonal symmetry of the magnetic system : the sectors that include the magnet coils (called "small sectors") and the sectors between two coils (called "large sectors").

– The $\Delta r_m^{\mathrm{Det}}(\eta, \phi)$ correction terms introduce a p_{T} dependent momentum smearing that effectively increases the relative momentum resolution, $\frac{\sigma(p_{\mathrm{T}})}{p_{\mathrm{T}}}$, when underestimated by the simulation. The $\Delta r_m^{\mathrm{Det}}(\eta, \phi)$ terms can be related to different sources of experimental resolution by comparing the coefficient of the p_{T} powers in the denominator of Eq. (9) to the following empirical parametrization of the muon momentum resolution (see for example [25]):

$$\frac{\sigma(p_{\mathrm{T}})}{p_{\mathrm{T}}} = r_0/p_{\mathrm{T}} \oplus r_1 \oplus r_2 \cdot p_{\mathrm{T}}, \tag{10}$$

where $\oplus$ denotes a sum in quadrature. The first term (proportional to $1/p_{\mathrm{T}}$) accounts for fluctuations of the energy loss in the traversed material. Multiple scattering, local magnetic field inhomogeneities and local radial displacements are responsible for the second term (constant in p_{T}). The third term (proportional to p_{T}) describes intrinsic resolution effects caused by the spatial resolution of the hit measurements and by residual misalignment. Energy loss fluctuations are relevant for muons traversing the calorimeter in front of the MS but they are negligible in the ID measurement. For this reason Δr_0^{ID} is set to zero in Eq. (9).

– Imperfect knowledge of the magnetic field integral and of the radial dimension of the detector are reflected in the multiplicative momentum scale difference s_1^{Det} between data and simulation. In addition, the $s_0^{\mathrm{MS}}(\eta, \phi)$ term is necessary to model the p_{T} scale dependence observed in the MS momentum reconstruction due to differences between data and MC in the energy loss of muons passing through the calorimeter and other materials between the interaction point and the MS. As the energy loss between the interaction point and the ID is negligible, $s_0^{\mathrm{ID}}(\eta)$ is set to zero.

The separate correction of ID and MS momentum reconstruction allows a direct understanding of the sources of the corrections. In a second step the corrections are propagated to the CB momentum reconstruction, $p_{\mathrm{T}}^{\mathrm{Cor,CB}}$, using a weighted average:

$$p_{\mathrm{T}}^{\mathrm{Cor,CB}} = f \cdot p_{\mathrm{T}}^{\mathrm{Cor,ID}} + (1 - f) \cdot p_{\mathrm{T}}^{\mathrm{Cor,MS}}, \tag{11}$$

with the weight f derived for each muon by expressing the CB transverse momentum before corrections, $p_{\mathrm{T}}^{\mathrm{MC,CB}}$, as a linear combination of $p_{\mathrm{T}}^{\mathrm{MC,ID}}$ and $p_{\mathrm{T}}^{\mathrm{MC,MS}}$:

$$p_{\mathrm{T}}^{\mathrm{MC,CB}} = f \cdot p_{\mathrm{T}}^{\mathrm{MC,ID}} + (1 - f) \cdot p_{\mathrm{T}}^{\mathrm{MC,MS}} \tag{12}$$

and solving the corresponding linear equation.

5.1.1 *Correction extraction using a template fit to $J/\psi \to \mu\mu$ and $Z \to \mu\mu$ events*

The MS and ID correction parameters contained in Eq. (9) need to be extracted from data. For this purpose, a MC template maximum likelihood fit is used to compare the simulation to the data for $J/\psi \to \mu\mu$ and $Z \to \mu\mu$ candidate events: this gives sensitivity to reconstructed muon momenta in the p_{T} range from a few GeV to ≈ 100 GeV. The dataset used for the correction extraction consists of 6M $J/\psi \to \mu\mu$ and 9M $Z \to \mu\mu$ candidates passing the final selection.

The $J/\psi \to \mu\mu$ and $Z \to \mu\mu$ candidates have been selected online according to the requirements described in Sect. 3.1 and, offline, by requiring two CB muons. For the correction extraction in a specific $\eta - \phi$ Region Of Fit (ROF), the ID and MS reconstructed momenta are considered individually. All the events with at least one of the two muons in the ROF contribute to the correction extraction fit. The angles from the CB reconstruction are used to define the ROF and to calculate the invariant mass distributions.

The ID corrections are extracted using the distribution of the ID dimuon invariant mass, $m_{\mu\mu}^{\mathrm{ID}}$. Events with $m_{\mu\mu}^{\mathrm{ID}}$ in the window 2.76–3.6 GeV and $p_{\mathrm{T}}^{\mathrm{ID}}$ in the range 8–17 GeV are selected as $J/\psi \to \mu\mu$ candidate decays; events with $m_{\mu\mu}^{\mathrm{ID}}$ between 76 and 96 GeV and the leading (sub-leading) muons with $26 < p_{\mathrm{T}}^{\mathrm{ID}} < 300$ GeV ($15 < p_{\mathrm{T}}^{\mathrm{ID}} < 300$ GeV) are selected as $Z \to \mu\mu$ candidate decays. To enhance the sensitivity to the p_{T} dependent correction effects, the $m_{\mu\mu}^{\mathrm{ID}}$ is classified according to the p_{T} of the muons: for $J/\psi \to \mu\mu$ candidates the $p_{\mathrm{T}}^{\mathrm{ID}}$ of the sub-leading muon defines three bins with lower thresholds at $p_{\mathrm{T}}^{\mathrm{ID}} = 8, 9, 11$ GeV, for $Z \to \mu\mu$ candidates the $p_{\mathrm{T}}^{\mathrm{ID}}$ of the leading muon defines three bins with lower thresholds at $p_{\mathrm{T}}^{\mathrm{ID}} = 26, 47, 70$ GeV.

Similarly, the MS corrections are extracted using the distribution of the MS reconstructed dimuon invariant mass, $m_{\mu\mu}^{\mathrm{MS}}$, in the same way as for the ID. However, as in the MS part of Eq. (9) more correction parameters and more ROFs are present, an additional variable sensitive to the momentum scale and resolution is added to the MS fit. The variable, used only in $Z \to \mu\mu$ candidate events, is defined by the following equation:

$$\rho = \frac{p_{\mathrm{T}}^{\mathrm{MS}} - p_{\mathrm{T}}^{\mathrm{ID}}}{p_{\mathrm{T}}^{\mathrm{ID}}}, \tag{13}$$

representing a measurement of the p_{T} imbalance between the measurement in the ID and in the MS. The ρ variable is binned according to $p_{\mathrm{T}}^{\mathrm{MS}}$ of the muon in the ROF: the lower thresholds are $p_{\mathrm{T}}^{\mathrm{MS}} = 20, 30, 35, 40, 45, 55, 70$ GeV.

In order to compare the simulation to the data distributions, the corresponding templates of $m_{\mu\mu}^{\mathrm{ID}}$, $m_{\mu\mu}^{\mathrm{MS}}$, and ρ are built using the MC samples of the $J/\psi \to \mu\mu$ and $Z \to \mu\mu$ signals. The background in the $Z \to \mu\mu$ mass region is added to the templates using the simulation and corresponds to approximately 0.1 % of the $Z \to \mu\mu$ candidates. The non-resonant background to $J/\psi \to \mu\mu$, coming from decays of light and heavy hadrons and from Drell–Yan production, accounts for about 15 % of the selected $J/\psi \to \mu\mu$ candidates. As it is not possible to accurately simulate it, a data driven approach is used to evaluate it: an analytic model of the background plus the J/ψ signal is fitted to the dimuon mass spectrum of the $J/\psi \to \mu\mu$ candidates in a mass range 2.7–4.0 GeV, then the background model and its normalization are used in the template fit from which the momentum correction are extracted. The analytic fit is performed independently on the ID and MS event candidates. The non-resonant dimuon background is parametrized with an exponential function, while the J/ψ and ψ^{2S} resonances are parametrized by a Crystal-Ball function [26] in the ID fits, or by a Gaussian distribution convoluted with a Landau in the MS fits, where energy loss effects due to the calorimeter material are larger.

The template fit machinery involves several steps: first a binned likelihood function $\mathcal{L}$ is built to compare the data to the MC templates of signal plus background. Then modified templates are generated by varying the correction parameters in Eq. (9) and applying them to the muon momentum of the simulated signal events. The $-2\ln\mathcal{L}$ between data and the modified template is then minimized using MINUIT [27]. The procedure is iterated across all the ROFs: the first fit is performed using only events with both muons in the ROF, the following fits allow also one of the muons in a previously analysed ROF and one in the ROF under investigation. After all the detector ROFs have been analysed, the fit procedure is iterated twice in order to improve the stability of the results. The correction extraction is performed first for the ID and then for the MS, such that the ID transverse momentum present in Eq. (13) can be kept constant during the MS correction extraction.

Although the use of p_{T} bins for the construction of the templates gives a good sensitivity to the p_{T} dependence of the scale corrections, the fit is not very sensitive to the resolution correction terms $\Delta r_0^{\mathrm{MS}}(\eta,\phi)$ and $\Delta r_2^{\mathrm{MS}}(\eta,\phi)$ of Eq. (9). The reasons for this are, at low p_{T}, the $p_{\mathrm{T}} > 8$ GeV selection cut applied to the J/ψ data sample, which limits the sensitivity to $\Delta r_0^{\mathrm{MS}}(\eta,\phi)$, and, at high p_{T}, the limited statistics of the $Z \to \mu\mu$ data sample with $p_{\mathrm{T}}^{\mathrm{MS}} > 100$ GeV, which limits the sensitivity to $\Delta r_2^{\mathrm{MS}}(\eta,\phi)$. As the energy loss fluctuations do not show significant disagreement between data and MC for $|\eta| > 0.8$, the parameter $\Delta r_0^{\mathrm{MS}}(\eta,\phi)$ has been fixed to zero in this region. The effect of the misalignment of MS chambers in real data, which is expected to be the largest contribution to $\Delta r_2^{\mathrm{MS}}(\eta,\phi)$, is already taken into account in the simulation as described in Sect. 3.2. Therefore the $\Delta r_2^{\mathrm{MS}}(\eta,\phi)$ term is also fixed to zero in the MS correction extraction. Two of the systematic uncertainties described in Sect. 5.1.2 are used to cover possible deviations from zero of these two terms.

5.1.2 Systematic uncertainties

Systematic uncertainties cover imperfections in the model used for the muon momentum correction and in the fit procedure used for the extraction of the correction terms. In particular the correction extraction procedure has been repeated using the following different configurations:

- variation of ± 5 GeV in the dimuon mass window used for the $Z \to \mu\mu$ event selection. This is intended to cover resolution differences between data and MC that are beyond a simple Gaussian smearing. This results in one of the largest systematic uncertainties on the resolution corrections, with an average effect of ≈ 10 % on the Δr_1^{ID}, Δr_2^{ID}, and Δr_1^{MS} parameters.
- Two variations of the J/ψ templates used in the fit. The first concerns the J/ψ background parametrization: new $m_{\mu\mu}^{\mathrm{MS}}$ and $m_{\mu\mu}^{\mathrm{ID}}$ background templates are generated using a linear model, for the MS fits, and a linear-times-exponential model, for the ID fits. The second variation concerns the J/ψ event selection: the minimum muon $p_{\mathrm{T}}^{MS,ID}$ cut is raised from 8 to 10 GeV, thus reducing the weight of low-p_{T} muons on the corrections. The resulting variations on the resolution correction parameters are ≈ 10 % of Δr_1^{ID} and Δr_1^{MS}. The effect is also relevant for the MS scale corrections with a variation of ≈ 0.01 GeV on s_0^{MS} and of $\approx 4 \times 10^{-4}$ on s_1^{MS}.
- The ID correction extraction is repeated using $J/\psi \to \mu\mu$ events only or $Z \to \mu\mu$ events only. Since such configurations have a reduced statistical power, only the s_1^{ID} correction parameter is left free in the fit, while the resolution correction terms are fixed to nominal values. The resulting uncertainty on s_1^{ID}, ranging from 0.01 % to 0.05 % from the central to the forward region of the ID, accounts for non-linear effects on the ID scale.
- The parameter Δr_0^{MS} of Eq. (9) is left free in all the regions, instead of fixing it to zero for $|\eta| > 0.8$. The largest variation of 0.08 GeV is applied as an additional systematic uncertainty on the parameter.
- The MS correction is extracted using a special $Z \to \mu\mu$ MC sample with ideal geometry, i.e. where no simulation of the misalignment of the MS chambers is applied. This is needed because the standard simulation has a too pessimistic resolution in the $|\eta| < 1.25$ region, forcing the

Δr_1^{MS} parameter to values compatible with zero. The template fit performed with the ideal-geometry $Z \to \mu\mu$ MC sample gives $\Delta r_1^{\mathrm{MS}} > 0$ in the region $0.4 < |\eta| < 1.25$. The largest variation of Δr_1^{MS}, corresponding to 0.012, is applied as an additional systematic uncertainty for this region.
- Variation of the normalization of the MC samples used in $Z \to \mu\mu$ background estimate by factors of two and one half. The resulting systematic uncertainty is small except for the detector regions with $|\eta| > 2.0$, where the effect is comparable to the other uncertainties.

Independently from the fit procedure, the following studies are used to derive additional systematic uncertainties:

- The simulation of the ID includes an excess of material for $|\eta| > 2.3$ resulting in a muon momentum resolution with is too pessimistic. Such imperfection is covered by adding a systematic uncertainties of 2×10^{-3} on the s_1^{ID} parameter, and of 0.01 on the Δr_1^{ID} parameter, both for $|\eta| > 2.3$. These are the largest systematic uncertainties on the ID correction parameters.
- The position of the mass peak in the $Z \to \mu\mu$ sample is studied in finer η bins than those used to extract the corrections, using the fit that will be discussed in Sect. 5.2 as an alternative to the template fitting method. An additional uncertainty of 2×10^{-4} on the $s_1^{\mathrm{ID}}(\eta)$ parameter is found to cover all the observed deviations between data and corrected MC.
- The effect of the measurement of the angle of the muon tracks has been checked by using the J/ψ MC and conservatively increasing the track angular resolution by $\approx 40\,\%$. The maximum effect is an increase of the resolution correction Δr_1^{ID} of 0.001, which is added to the systematic uncertainties.
- Special runs with the toroidal magnetic field off have been used to evaluate the quality of the MS chamber alignment. These results are compared to the chamber misalignments in the simulation to define the systematic uncertainty on the $\Delta r_2^{\mathrm{MS}}(\eta, \phi)$ resolution correction parameter.

The final uncertainty on each of the eight muon momentum correction parameters is derived from the sum in quadrature of all the listed uncertainty sources. This is simplified for use in standard physics analyses, for which only four systematic variations are provided: global upper and lower scale variations and independent resolution variations for the ID and the MS. The upper and lower scale variations are obtained by a simultaneous variation of all the ID and MS scale correction parameters by 1σ. The resolution variation for ID (MS) is obtained by the simultaneous variation of all the ID (MS) correction parameters.

Table 1 Summary of ID muon momentum resolution and scale corrections used in Eq. (9), averaged over three main detector regions. The corrections are derived in 18 η detector regions, as described in Sect. 5.1.1, and averaged according to the η width of each region. The uncertainties are the result of the sum in quadrature of the statistical and systematic uncertainties. Only upper uncertainties are reported for the Δr parameters; lower uncertainties are evaluated by symmetrization, as described in Sect. 5.1.2

Region	Δr_1^{ID}	Δr_2^{ID} [TeV^{-1}]	s_1^{ID}
$\lvert\eta\rvert < 1.05$	$0.0068^{+0.0010}$	$0.146^{+0.039}$	$-0.92^{+0.26}_{-0.22} \times 10^{-3}$
$1.05 \le \lvert\eta\rvert < 2.0$	$0.0105^{+0.0018}$	$0.302^{+0.046}$	$-0.86^{+0.30}_{-0.35} \times 10^{-3}$
$\lvert\eta\rvert \ge 2.0$	$0.0069^{+0.0121}$	$0.088^{+0.084}$	$-0.49^{+1.17}_{-1.63} \times 10^{-3}$

The MC-smearing approach of Eq. (9) cannot be used to correct the MC when the resolution in real data is better than in the simulation. To deal with these cases, the amount of resolution that should be subtracted in quadrature from the simulation to reproduce the data is included in the positive ID and MS resolution variations. Then the prescription for physics analysis is to symmetrize the effect of the positive variation of resolution parameters around the nominal value of the physical observables under study.

5.1.3 *Result of the muon momentum scale and resolution corrections*

The ID and MS correction parameters used in Eq. (9) are shown in Tables 1 and 2, averaged over three η regions. The scale correction to the simulated ID track reconstruction is always below 0.1 % with an uncertainty ranging from ≈ 0.02 %, for $|\eta| < 1.0$, to 0.2 %, for $|\eta| > 2.3$. The correction to the MS scale is $\lesssim 0.1$ % except for the large MS sectors in the barrel region of the detector, where a correction of $\approx$0.3 % is needed, and for specific MS regions with $1.25 < |\eta| < 1.5$ where a correction of about -0.4 % is needed. An energy loss correction of approximately 30 MeV is visible for low values of p_{T} in the MS reconstruction. This correction corresponds to about 1 % of the total energy loss in the calorimeter and in the dead material in front of the spectrometer and is compatible with the accuracy of the material budget used in the simulation. Depending on the considered p_{T} range, total resolution smearing corrections below 10 % and below 15 % are needed for the simulated ID and MS track reconstructions.

5.2 Measurement of the dimuon mass scale and resolution

The collected samples of $J/\psi \to \mu\mu$, $\Upsilon \to \mu\mu$ and $Z \to \mu\mu$ decays have been used to study the muon momentum resolution and to validate the momentum corrections obtained with the template fit method described in the previous section with a different methodology. In addition the Υ sample, not

Table 2 Summary of MS momentum resolution and scale corrections for small and large MS sectors, averaged over three main detector regions. The corrections for large and small MS sectors are derived in 18 η detector regions, as described in Sect. 5.1.1, and averaged according to the η width of each region. The parameters Δr_0^{MS}, for $|\eta| > 1.05$, and Δr_2^{MS}, for the full η range, are fixed to zero. The uncertainties are the result of the sum in quadrature of the statistical and systematic uncertainties. Only upper uncertainties are reported for the Δr parameters; lower uncertainties are evaluated by symmetrization, as described in Sect. 5.1.2

Region	Δr_0^{MS} [GeV]	Δr_1^{MS}	Δr_2^{MS} [TeV^{-1}]	s_0^{MS} [GeV]	s_1^{MS}
$\lvert\eta\rvert < 1.05$ (small)	$0.115^{+0.083}$	$0.0030^{+0.0079}$	$0^{+0.21}$	$-0.035^{+0.017}_{-0.011}$	$+3.57^{+0.38}_{-0.60} \times 10^{-3}$
$\lvert\eta\rvert < 1.05$ (large)	$0.101^{+0.090}$	$0.0034^{+0.0081}$	$0^{+0.11}$	$-0.022^{+0.007}_{-0.014}$	$-0.22^{+0.37}_{-0.24} \times 10^{-3}$
$1.05 \leq \lvert\eta\rvert < 2.0$ (small)	$0^{+0.080}$	$0.0171^{+0.0059}$	$0^{+0.22}$	$-0.032^{+0.017}_{-0.016}$	$-1.07^{+0.77}_{-0.93} \times 10^{-3}$
$1.05 \leq \lvert\eta\rvert < 2.0$ (large)	$0^{+0.080}$	$0.0190^{+0.0047}$	$0^{+0.17}$	$-0.026^{+0.009}_{-0.017}$	$-1.46^{+0.45}_{-0.57} \times 10^{-3}$
$\lvert\eta\rvert \geq 2.0$ (small)	$0^{+0.080}$	$0.0022^{+0.0075}$	$0^{+0.06}$	$-0.031^{+0.029}_{-0.031}$	$-0.91^{+1.63}_{-0.91} \times 10^{-3}$
$\lvert\eta\rvert \geq 2.0$ (large)	$0^{+0.080}$	$0.0171^{+0.0052}$	$0^{+0.29}$	$-0.057^{+0.019}_{-0.021}$	$+0.40^{+1.22}_{-0.50} \times 10^{-3}$

used in the extraction of the corrections, provides an independent validation.

Neglecting angular effects, the invariant mass resolution $\sigma(m_{\mu\mu})$ is related to the momentum resolution by

$$\frac{\sigma(m_{\mu\mu})}{m_{\mu\mu}} = \frac{1}{2}\frac{\sigma(p_1)}{p_1} \oplus \frac{1}{2}\frac{\sigma(p_2)}{p_2}, \tag{14}$$

where p_1 and p_2 are the momenta of the two muons. If the momentum resolution is similar for the two muons then the relative mass resolution is proportional to the relative momentum resolution:

$$\frac{\sigma(m_{\mu\mu})}{m_{\mu\mu}} = \frac{1}{\sqrt{2}}\frac{\sigma(p)}{p}. \tag{15}$$

The mass resolution has been obtained by fitting the width of the invariant mass peaks. In the $J/\psi \to \mu\mu$ and $\Upsilon \to \mu\mu$ decays, the intrinsic width of the resonance is negligible with respect to the experimental resolution. In the $Z \to \mu\mu$ case the fits have been performed using a convolution of the true line-shape obtained from the MC simulation with an experimental resolution function. The momentum scale was obtained by comparing the mass peak position in data and in MC. Details of the event selection and of the invariant mass fits are given below.

5.2.1 *Event selection and mass fitting*

The J/ψ and Υ events are selected online by the dedicated dimuon triggers described in Sect. 3.1. The offline event selection requires in addition that both muons are reconstructed as CB muons and have $p_{\mathrm{T}} > 7$ GeV. The trigger acceptance limits the muons to the region $|\eta| < 2.4$. The resulting data samples consist of 17M and 4.7M candidates for J/ψ and Υ, respectively. The $Z \to \mu\mu$ sample was selected online with the single-muon trigger described in Sect. 4.1. One of the two muons can be outside the trigger acceptance, allowing coverage of the full range $|\eta| < 2.7$. The offline selection requires two opposite-charge muons, one with $p_{\mathrm{T}} > 25$ GeV and one with $p_{\mathrm{T}} > 20$ GeV. The two muons are required to be isolated, to have opposite charges and to be compatible with the primary interaction vertex.

The invariant mass distribution of the $J/\psi \to \mu\mu$, $\Upsilon \to \mu\mu$ and $Z \to \mu\mu$ samples are shown in Fig. 10 and compared with uncorrected and corrected MC. With the uncorrected MC the signal peaks have smaller width and are slightly shifted with respect to data. After correction, the lineshapes of the three resonances agree very well with the data. For a detailed study, the position $\langle m_{\mu\mu}\rangle$ and the width $\sigma(m_{\mu\mu})$ of the mass peaks are extracted in bins of η and p_{T} from fits of the invariant mass distributions of the three resonances.

In the J/ψ case, for each bin, the background is obtained from a fit of two sideband regions outside the J/ψ mass peak ($2.55 < m_{\mu\mu} < 2.9$ and $3.3 < m_{\mu\mu} < 4.0$ GeV) using a second order polynomial. The background is then subtracted from the signal mass window. The parameters $\langle m_{\mu\mu}\rangle$ and $\sigma(m_{\mu\mu})$ of the background subtracted signal distribution are obtained with a Gaussian fit in the range $\langle m_{\mu\mu}\rangle \pm 1.5\sigma(m_{\mu\mu})$, obtained using an iterative procedure. Systematic uncertainties associated to the fit are evaluated by repeating the fit using a third order polynomial as the background model and by varying the fit range to $\pm 1\times$ and $\pm 2 \times \sigma(m_{\mu\mu})$.

As shown in Fig. 10, the three Υ resonances (1S, 2S, 3S) partially overlap. Moreover in the Υ case the mass window imposed by the trigger limits considerably the size of the sidebands available for fixing the background level. Therefore a different fit strategy is adopted in this case. For each bin, the whole invariant mass distribution in the range $8.5 < m_{\mu\mu} < 11.5$ GeV is fitted with a linear background plus three Crystal-Ball functions representing the three resonances. The α and n parameters that fix the tail of the Crystal-Ball function are fixed to the values obtained from a fit of the signal MC mass distribution. The relative mass shifts of

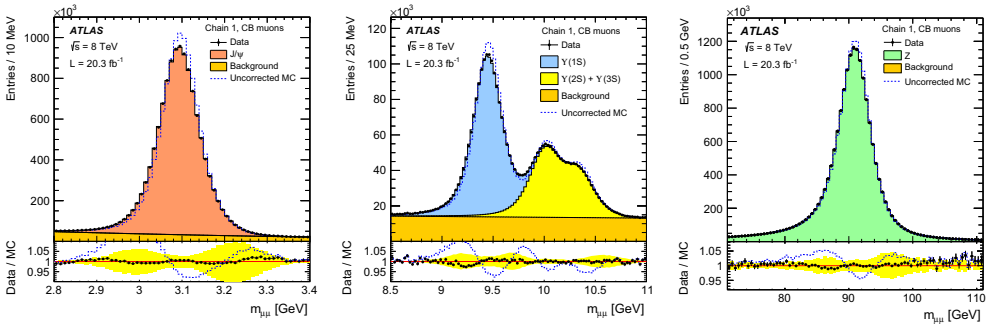

Fig. 10 Dimuon invariant mass distribution of $J/\psi \to \mu\mu$ (*left*), $\Upsilon \to \mu\mu$ (*center*) and $Z \to \mu\mu$ (*right*) candidate events reconstructed with CB muons. The *upper panels* show the invariant mass distribution for data and for the signal MC simulation plus the background estimate. The *points* show the data, the *filled histograms* show the simulation with the MC momentum corrections applied and the *dashed histogram* shows the simulation when no correction is applied. Background estimates are added to the signal simulation. The *lower panels* show the Data/MC ratios. The *band* represents the effect of the systematic uncertainties on the MC momentum corrections. In the J/ψ case the background was fitted in a sideband region as described in the text. In the Υ case a simultaneous fit of the normalization of the three simulated $\Upsilon \to \mu\mu$ distributions and of a linear background was performed. In the Z case, the MC background samples are added to the signal sample according to their expected cross sections. The sum of background and signal MC is normalized to the data

the three signal peaks are fixed using the PDG masses of the three resonances, while the widths of the three peaks, divided by the corresponding PDG masses, are constrained to be equal. The remaining free parameters in the fit are the mass scale, the width $\sigma(m_{\mu\mu})$ of the $\Upsilon(1S)$, the relative normalizations of the $\Upsilon(2S)$ and $\Upsilon(3S)$ distributions with respect to $\Upsilon(1S)$ and two parameters for the linear background. A similar fit is performed on the MC simulation of the invariant mass distribution obtained by adding the three signal peaks and a flat background distribution. The fit systematic uncertainties have been evaluated by chaining the fit range to $8.25 < m_{\mu\mu} < 11.75$ and $8.75 < m_{\mu\mu} < 11.0$ GeV and by varying the α and n parameters in the range allowed by fits to the simulation.

In the $Z \to \mu\mu$ case, for each bin, the true lineshape predicted by the MC simulation is parametrized with a Breit–Wigner function. The measured dimuon mass spectrum is fitted with a Crystal-Ball function, representing the experimental resolution effects, convoluted with the Breit–Wigner parametrization of the true lineshape. The fit is repeated in different ranges around the mass peak (corresponding approximately to one to two standard deviations) and the spread of the results is used to evaluate the systematic uncertainty of the fit.

5.2.2 Mass scale results

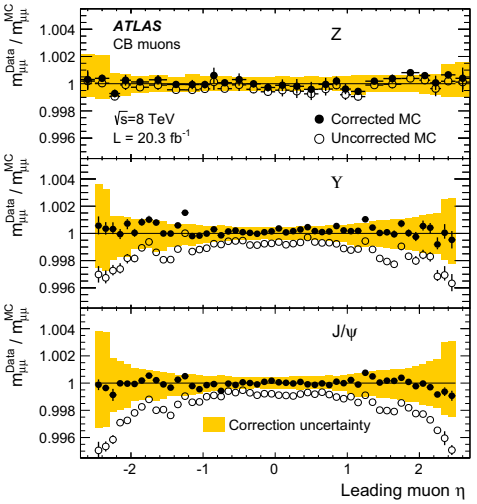

Fig. 11 Ratio of the fitted mean mass, $\langle m_{\mu\mu} \rangle$, for data and corrected MC from Z (*top*), Υ (*middle*), and J/ψ (*bottom*) events as a function of the pseudorapidity of the highest-p_{T} muon. The ratio is shown for corrected MC (*filled symbols*) and uncorrected MC (*empty symbols*). The *error bars* represent the statistical and the systematic uncertainty on the mass fits added in quadrature. The *bands* show the uncertainty on the MC corrections calculated separately for the three samples

Figure 11 shows the Data/MC ratio of the mean mass $\langle m_{\mu\mu} \rangle$ obtained from the fits to the Z, J/ψ, Υ samples described above, as a function of the pseudorapidity of the highest-p_{T} muon for pairs of CB muons. For the uncorrected MC, the ratio deviates from unity in the large $|\eta|$ region of the J/ψ and Υ cases by up to 5 %. This is mainly due to imperfections

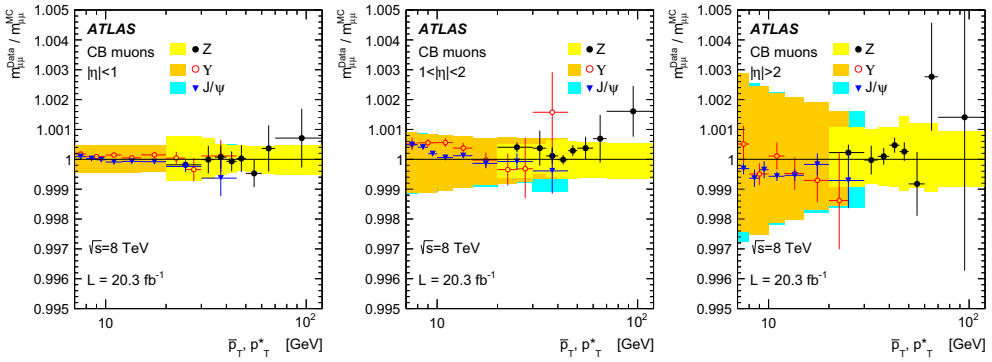

Fig. 12 Ratio of the fitted mean mass, $\langle m_{\mu\mu}\rangle$, for data and corrected MC from J/ψ, Υ and Z events as a function of the average transverse momentum in three $|\eta|$ ranges. Both muons are required to be in the same $|\eta|$ range. The J/ψ and Υ data are shown as a function of the $\bar{p}_{\mathrm{T}} = \frac{1}{2}(p_{\mathrm{T},1} + p_{\mathrm{T},2})$ while for Z data are plotted as a function of p_{T}^{*} as defined in Eq. (16). The *error bars* represent the statistical uncertainty and the systematic uncertainty on the fit added in quadrature. The *bands* show the uncertainty on the MC corrections calculated separately for the three samples

in the simulation of the muon energy loss that have a larger effect at low p_{T} and in the forward η region where the MS measurement has a larger weight in the MS-ID combination. The corrected MC is in very good agreement with the data, well within the scale systematics that are $\approx 0.035\,\%$ in the barrel region and increase with $|\eta|$ to reach $\sim 0.2\,\%$ in the region $|\eta| > 2$ for the $Z \to \mu\mu$ case.

Figure 12 shows the data/MC ratio for $\langle m_{\mu\mu}\rangle$ as a function of the transverse momentum $\langle p_{\mathrm{T}}\rangle$ for muons in three different pseudorapidity regions.

For the J/ψ and Υ cases, $\langle p_{\mathrm{T}}\rangle$ is defined as the average momentum $\bar{p}_T = \frac{1}{2}(p_{\mathrm{T},1} + p_{\mathrm{T},2})$ while in the Z case it is defined as

$$p_{\mathrm{T}}^{*} = m_Z \sqrt{\frac{\sin\theta_1 \sin\theta_2}{2(1-\cos\alpha_{12})}}, \tag{16}$$

where m_Z is the Z pole mass [28], θ_1, θ_2 are the polar angles of the two muons and α_{12} is the opening angle of the muon pair. This definition, based on angular variables only, removes the correlation between the measurement of the dimuon mass and of the average p_{T} that is particularly relevant around the Jacobian peak at $p_{\mathrm{T}} = m_Z/2$ in the distribution of muons from Z decays.

The data from the three resonances span from $\langle p_{\mathrm{T}}\rangle = 7$ GeV to $\langle p_{\mathrm{T}}\rangle = 120$ GeV and show that the momentum scale is well known and within the assigned systematic uncertainties in the whole p_{T} range.

5.2.3 Resolution results

The dimuon mass width $\sigma(m_{\mu\mu})$ for CB muons is shown as a function of the leading-muon η in Fig. 13 for the three resonances. The width of the uncorrected MC is 5–10 % smaller than that of the data. After correction the MC reproduces the width of the data well within the correction uncertainties.

At a given η, the relative dimuon mass resolution $\sigma(m_{\mu\mu})/m_{\mu\mu}$ depends approximately on $\langle p_{\mathrm{T}}\rangle$ (Eq. 15). This allows a direct comparison of the momentum resolution using different resonances. This is shown in Fig. 14, where the relative mass resolution from $J/\psi \to \mu\mu$, $\Upsilon \to \mu\mu$ and $Z \to \mu\mu$ events is compared in three regions of $|\eta|$. The $J/\psi \to \mu\mu$ and $\Upsilon \to \mu\mu$ resolutions are in good agreement.

In the $Z \to \mu\mu$ sample, due to the decay kinematics, below $\langle p_{\mathrm{T}}\rangle = m_Z/2$ there is a strong correlation between $\langle p_{\mathrm{T}}\rangle$ and the pseudorapidity of the muons, in such a way that the lower is the $\langle p_{\mathrm{T}}\rangle$, the larger is the $|\eta|$ of the muons. Above $\langle p_{\mathrm{T}}\rangle = m_Z/2$, the correlation effect is strongly reduced and the Z measurements are well aligned with those from the lighter resonances. In the barrel region, $|\eta| < 1$, the mass resolution increases from $\sigma(m_{\mu\mu})/m_{\mu\mu} \approx 1.2\,\%$ at $p_{\mathrm{T}} < 10$ GeV to $\sigma(m_{\mu\mu})/m_{\mu\mu} \approx 2\,\%$ at $p_{\mathrm{T}} = 100$ GeV. For $|\eta| > 1$ it goes from $\sigma(m_{\mu\mu})/m_{\mu\mu} \approx 2\,\%$ to $\approx 3\,\%$ in the same p_{T} range. This behavior is very well reproduced by the corrected MC. Following Eq. (15), it is possible to scale $\sigma(m_{\mu\mu})/m_{\mu\mu}$ by $\sqrt{2}$ to extract a measurement of the relative momentum resolution $\sigma(p)/p$, which ranges from $\approx 1.7\,\%$ in the central region and at low p_{T} to $\approx 4\,\%$ at large η and $p_{\mathrm{T}} = 100$ GeV.

To understand better the p_{T} dependence of the momentum resolution of CB muons, it is useful to study separately the resolution of the ID and of the MS measurements, as shown in Figs. 15 and 16. The ID measurement has a better resolution than the MS in the p_{T} range under study for $|\eta| < 2$ while

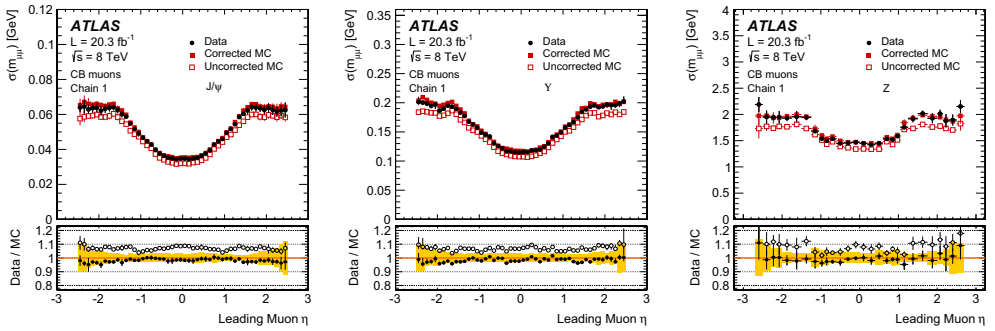

Fig. 13 Dimuon invariant mass resolution for CB muons for $J/\psi \to \mu\mu$ (**a**), $\Upsilon \to \mu\mu$ (**b**) and $Z \to \mu\mu$ (**c**) events for data and for uncorrected and corrected MC as a function of the pseudorapidity of the highest-p_T muon. The *upper plots* show the fitted resolution parameter for data, uncorrected MC and corrected MC. The *lower panels* show the data/MC ratio, using uncorrected and corrected MC. The *error bars* represent the statistical uncertainty and the systematic uncertainty on the fit added in quadrature. The *bands in the lower panels* represent the systematic uncertainty on the correction

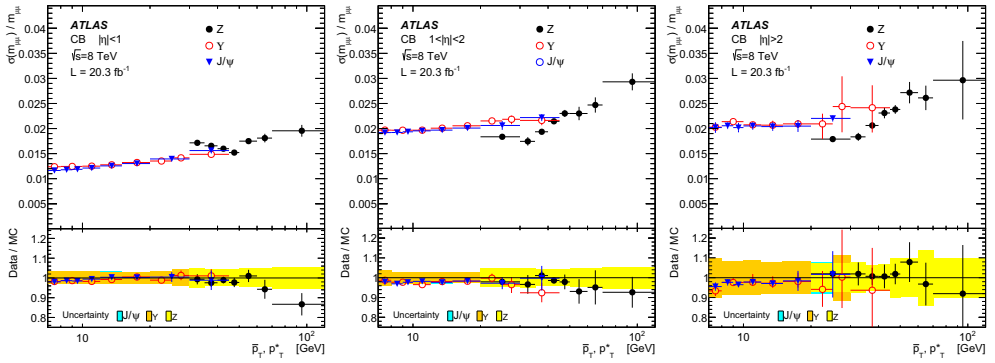

Fig. 14 Dimuon invariant mass resolution for CB muons measured from J/ψ, Υ and Z events as a function of the average transverse momentum in three $|\eta|$ ranges. Both muons are required to be in the same $|\eta|$ range. The J/ψ and Υ data are plotted as a function of $\bar{p}_T = \frac{1}{2}(p_{T,1} + p_{T,2})$ while for Z data are plotted as a function of p_T^* as defined in Eq. (16). The *error bars* represent statistical and systematic errors added in quadrature. The *lower panel* shows the ratio between data and the corrected MC, with *bands* representing the uncertainty on the MC corrections for the three calibration samples

the MS has a better resolution at larger $|\eta|$. The resolution of the CB muons is significantly better than the ID or the MS measurements taken separately in the whole $|\eta|$ range. The ID resolution has an approximately linear increases with p_T, corresponding to a non-zero r_2 term in Eq. (10). The MS resolution is largest in the region $1 < |\eta| < 2$ which contains the areas with the lowest magnetic field integral. In the region $|\eta| < 1$ there is a visible increase at low p_T that corresponds to the presence of a non-zero r_0 term in Eq. (10). The p_T dependence of the resolutions for both the ID and the MS measurements is well reproduced by the corrected MC. According to studies based on MC, the MS measurement is expected to dominate over the ID in the whole $|\eta|$ range for sufficiently large p_T.

6 Final state radiation recovery

The invariant mass distributions of resonances that decay into muons, such as $Z \to \mu\mu$ and $H \to ZZ \to 4\ell$, is affected by QED final state radiation of photons, causing the mass reconstructed using muons to be shifted to lower values.

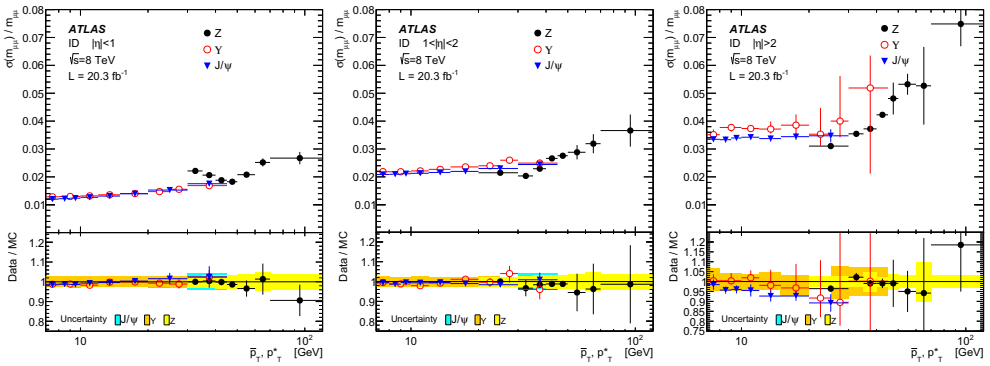

Fig. 15 Dimuon invariant mass resolution for muons reconstructed with the ID only, measured from J/ψ, Υ and Z events as a function of the average transverse momentum in three $|\eta|$ ranges. Other details as in Fig. 14

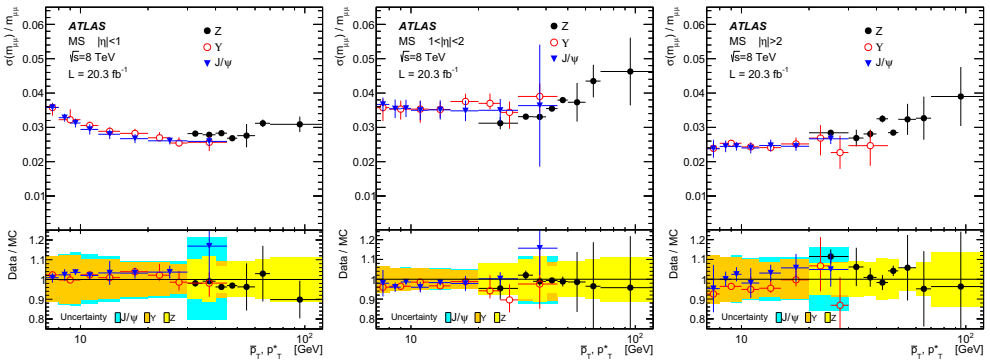

Fig. 16 Dimuon invariant mass resolution for muons reconstructed with the MS only, measured from J/ψ, Υ and Z events as a function of the average transverse momentum in three $|\eta|$ ranges. Other details as in Fig. 14

In this section, a dedicated method to include FSR photons in the reconstruction of resonances decaying into muons is introduced and tested with $Z \to \mu\mu$ data. This method has been used in several ATLAS publications [6,29].

Final state radiation photons emitted collinearly to muons can be reconstructed with the LAr calorimeter: electromagnetic clusters are searched for within a narrow cone around the axis defined by the muon momentum direction at the interaction point (i.e. the direction which would be followed by an uncharged particle). The longitudinal segmentation of the LAr calorimeter is exploited to reduce fake photon clusters produced by muon energy losses in the calorimeter. This is achieved by using as a discriminant the fraction f_1 of the cluster energy deposited in the first segment of the calorimeter divided by the total cluster energy. Collinear FSR photon candidates are required to have $E_T > 1.5$ GeV, $\Delta R_{\text{cluster},\mu} < 0.15$ and $f_1 > 0.1$. In addition, non-collinear FSR photons are recovered using the standard ATLAS photon reconstruction, selecting isolated photons emitted with $\Delta R_{\text{cluster},\mu} > 0.15$ and with $E_T > 10$ GeV [30].

The effect of adding a collinear or non-collinear FSR photon to the $Z \to \mu\mu$ invariant mass in data is studied in a sample obtained with a dedicated selection of $Z \to \mu\mu$ candidates plus at least one radiated photon candidate.

The correction for collinear FSR is applied for events in the mass window 66 GeV$< m_{\mu\mu} <$ 89 GeV while the correction for non-collinear FSR photons is applied only if the collinear search has failed and the dimuon mass satisfies $m_{\mu\mu} < 81$ GeV.

In Fig. 17 the invariant mass distributions for the sample of $Z \to \mu\mu$ events with a FSR photon candidate are shown before and after the addition of collinear and non-collinear FSR photons. A good agreement between data and MC is observed for the corrected $Z \to \mu\mu$ events. According to

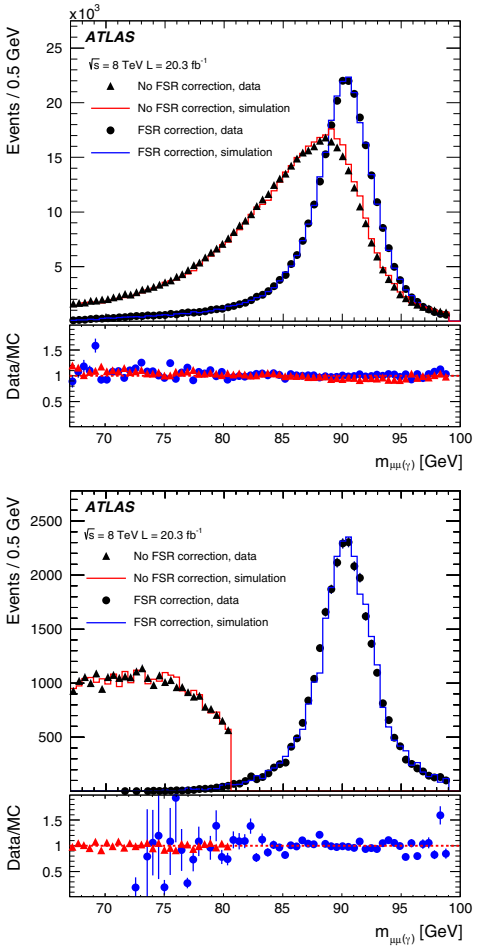

Fig. 17 Invariant mass distribution of $Z \to \mu\mu$ events with identified FSR in data before (*filled triangles*) and after (*filled circles*) FSR correction, for collinear (*top*) and non-collinear (*bottom*) FSR. The MC prediction is shown before correction (*red histogram*) and after correction (*blue histogram*)

MC studies, the collinear FSR selection has an efficiency of 70 ± 4 % for FSR photons emitted with $E_T > 1.5$ GeV and $\Delta R_{\gamma,\mu} < 0.15$ in the fiducial region defined requiring $|\eta| < 2.37$ and excluding the calorimeter crack region $1.37 < |\eta| < 1.52$. About 85 % of the corrected events have genuine FSR photons, with the remaining photons coming from muon bremsstrahlung or ionization or from random matching with energy depositions from other sources. The fraction of all $Z \to \mu\mu$ events corrected with a collinear FSR photon is $\simeq 4$ %. The non-collinear FSR selection has an efficiency of 60 ± 3 % in the fiducial region and a purity of ≥ 95 %. The fraction of $Z \to \mu\mu$ events corrected with a non-collinear FSR photon is $\simeq 1$ %.

The FSR correction may introduce systematic variations in the invariant mass scale and resolution. To study these effects, a Gaussian fit of the $Z \to \mu\mu$ distribution has been performed in the mass range 91.18 ± 3.00 GeV. The FSR correction induces a mass shift of $+40 \pm 3$ MeV and an improvement of the resolution of 3 ± 1 % in the full $Z \to \mu\mu$ sample. The effects observed in the data are well reproduced by the MC. The systematic uncertainty introduced by the FSR recovery on the inclusive Z mass scale can be understood by considering a 0.5 % photon energy scale uncertainty, the fact that only 5 % of the Z events are corrected, and that the fraction of energy carried by the photons is a few %. This leads to a systematic uncertainty smaller than 2 MeV.

The effect of pile up on the FSR correction has been estimated by dividing the data and the MC into three categories based on the average number of interactions per bunch crossing: $\langle\mu\rangle = 0$–17, 17–23, 23–40. A comparison of the fitted Z mass between data and MC has been performed in the three categories and no dependence on $\langle\mu\rangle$ was observed. Good agreement between data and MC within the statistical uncertainties was found.

7 Conclusions

The performance of the ATLAS muon reconstruction has been measured using data from LHC pp collisions at $\sqrt{s} =$ 7–8 TeV. The muon reconstruction efficiency is close to 99 % over most of the pseudorapidity range of $|\eta| < 2.5$ and for $p_{\mathrm{T}} > 10$ GeV. The large collected sample of 9M $Z \to \mu\mu$ decays allows the measurement of the efficiency over the full acceptance of $|\eta| < 2.7$, and with a precision at the 1 per-mille level for $|\eta| < 2.5$. By including $J/\psi \to \mu\mu$ decays, the efficiency measurement has been extended over the transverse momentum range from $p_{\mathrm{T}} \approx 4$ GeV to $p_{\mathrm{T}} \approx$ 100 GeV.

The muon momentum scale and resolution has been studied in detail using large calibration samples of $J/\psi \to \mu\mu$, $\Upsilon \to \mu\mu$ and $Z \to \mu\mu$ decays. These studies have been used to correct the MC simulation to improve the data-MC agreement and to minimize the uncertainties in physics analyses. The momentum scale for combined muons is known with an uncertainty of ± 0.05 % for $|\eta| < 1$, which increases to $\lesssim 0.2$ % for $|\eta| > 2.3$ for $Z \to \mu\mu$ events. The dimuon mass resolution is ≈ 1.2 % (2 %) at low-p_{T} increasing to ≈ 2 % (3 %) at $p_{\mathrm{T}} \approx 100$ GeV for $|\eta| < 1$ ($|\eta| > 1$). The resolution is reproduced by the corrected simulation within relative uncertainties of 3 % to 10 % depending on η and p_{T}.

The mass resolution for the $Z \to \mu\mu$ resonance was found to improve when photons from QED final state radiation are recovered. The FSR recovery allows to recover $\approx 4\,\%$ of the events from the low-mass tail to the peak region, improving the dimuon mass resolution by $\approx 3\,\%$.

Acknowledgments We thank CERN for the very successful operation of the LHC, as well as the support staff from our institutions without whom ATLAS could not be operated efficiently. We acknowledge the support of ANPCyT, Argentina; YerPhI, Armenia; ARC, Australia; BMWF and FWF, Austria; ANAS, Azerbaijan; SSTC, Belarus; CNPq and FAPESP, Brazil; NSERC, NRC and CFI, Canada; CERN; CONICYT, Chile; CAS, MOST and NSFC, China; COLCIENCIAS, Colombia; MSMT CR, MPO CR and VSC CR, Czech Republic; DNRF, DNSRC and Lundbeck Foundation, Denmark; EPLANET, ERC and NSRF, European Union; IN2P3-CNRS, CEA-DSM/IRFU, France; GNSF, Georgia; BMBF, DFG, HGF, MPG and AvH Foundation, Germany; GSRT and NSRF, Greece; ISF, MINERVA, GIF, I-CORE and Benoziyo Center, Israel; INFN, Italy; MEXT and JSPS, Japan; CNRST, Morocco; FOM and NWO, The Netherlands; BRF and RCN, Norway; MNiSW and NCN, Poland; GRICES and FCT, Portugal; MNE/IFA, Romania; MES of Russia and ROSATOM, Russian Federation; JINR; MSTD, Serbia; MSSR, Slovakia; ARRS and MIZŠ, Slovenia; DST/NRF, South Africa; MINECO, Spain; SRC and Wallenberg Foundation, Sweden; SER, SNSF and Cantons of Bern and Geneva, Switzerland; NSC, Taiwan; TAEK, Turkey; STFC, the Royal Society and Leverhulme Trust, UK; DOE and NSF, USA. The crucial computing support from all WLCG partners is acknowledged gratefully, in particular from CERN and the ATLAS Tier-1 facilities at TRIUMF (Canada), NDGF (Denmark, Norway, Sweden), CC-IN2P3 (France), KIT/GridKA (Germany), INFN-CNAF (Italy), NL-T1 (The Netherlands), PIC (Spain), ASGC (Taiwan), RAL (UK) and BNL (USA) and in the Tier-2 facilities worldwide.

Appendix A: Results with different reconstruction "Chains"

This appendix reports the main results obtained with the other two muon reconstruction software packages used to process 2012 data, Chain 2 and the unified reconstruction programme Chain-3. Figure 18 shows the efficiency as a function of η for Chain 2 and Chain 3 and is similar to Fig. 3 for Chain 1.

The efficiency drop that is observed in Chain 1 for CB muons at $|\eta| \simeq 1.2$ is not present in the other two packages due to the less strict selection on the number of measurements in the MS. These relaxed requirements also improve the data/MC agreement. In Chain 2 the CB+ST efficiency is higher than the CB efficiency alone, similarly to Chain 1. For Chain 3, the distinction between CB and ST muons is not applicable anymore since a ID-MS combined momentum fit is performed also in the case of muons that traversed only one MS chamber, a category that is assigned to ST muons in Chain 1 and (with some exceptions) in Chain 2. Therefore only one type of Chain 3 muons is considered, which was tuned to provide a purity similar to that of the CB muons of Chain 1.

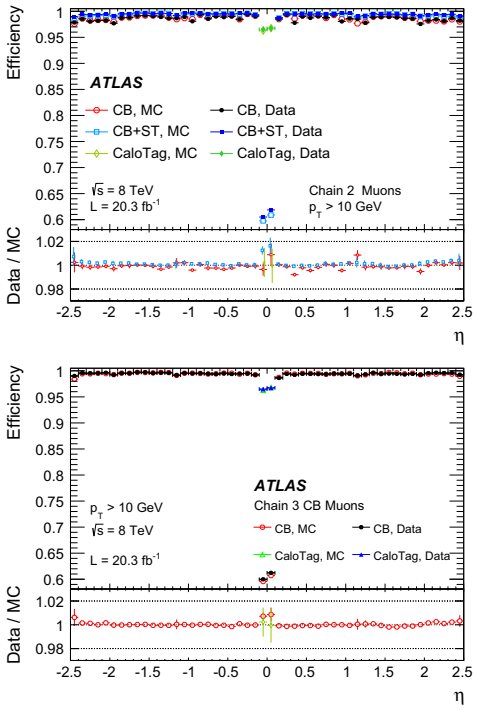

Fig. 18 Muon reconstruction efficiency as a function of η, measured using $Z \to \mu\mu$ events, for muons reconstructed with Chain-2 (*top*) and Chain-3 (*bottom*), for different muon reconstruction types. CaloTag muons are shown in the region $|\eta| < 0.1$, where they are used in physics analyses. The *error bars* shown for the efficiencies represent the statistical uncertainty. The *panel at the bottom* shows the ratio between the measured and predicted efficiencies. The *error bars* show statistical and systematic uncertainties added in quadrature

The momentum resolution of the three chains is very similar, with Chain 3 having approximately 2 % better resolution than Chain 1. The data/MC agreement and the amount of correction applied to the simulation is compatible among the three packages.

Appendix B: Results on 2011 data

During the 2011 data taking period, the LHC delivered pp collisions at a center of mass energy of $\sqrt{s} = 7$ TeV. A sample corresponding to an integrated luminosity of 4.5 fb^{-1}

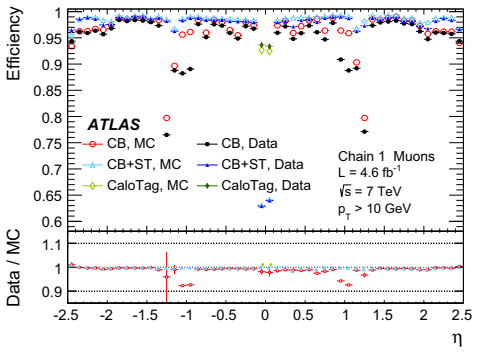

Fig. 19 Muon reconstruction efficiency as a function of η measured in $Z \to \mu\mu$ events in the 2011 data sample for different muon reconstruction types. CaloTag muons are only shown in the region $|\eta| < 0.1$, where they are used in physics analyses. For the efficiency, the *error bars* indicate the statistical uncertainty. The *panel at the bottom* shows the ratio between the measured and MC efficiencies. The *error bars on the ratios* show the combination of statistical and systematic uncertainties. The lower efficiency of CB muons at $|\eta| \approx 1.2$ is due to the fact that some of the MS chambers were not yet installed

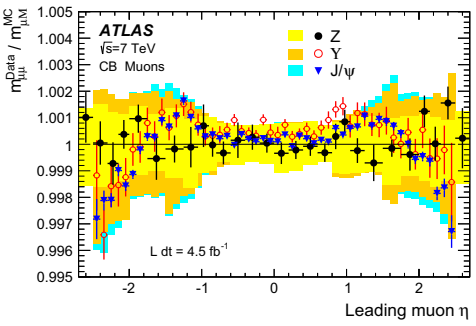

Fig. 20 Ratio of the fitted mean mass, $\langle m_{\mu\mu} \rangle$, for data and corrected MC in the 2011 data samples. Measurements from J/ψ, Υ and Z events are shown as a function of η of the highest-p_{T} muon. The *bands* show the uncertainty on the MC corrections extracted for the three calibration samples

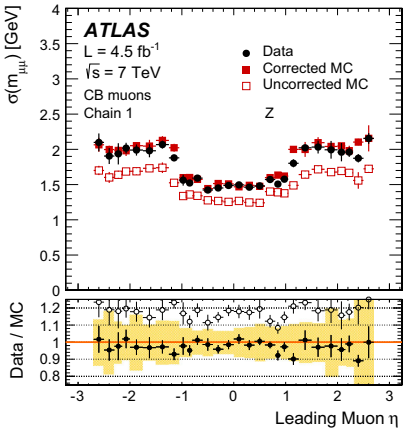

Fig. 21 Dimuon mass resolution $\sigma(m_{\mu\mu})$ reconstructed with Chain 1 CB muons for $Z \to \mu\mu$ events recorded in 2011 for data and for uncorrected and corrected MC, as a function of the pseudorapidity of the highest-p_{T} muon. The *lower panel* shows the data/MC ratio and the band shows the systematic uncertainty from the momentum corrections

has been used to measure the muon reconstruction performance with 2011 data. The ID and MS configurations were the same in 2011 as in 2012, with the exception of additional MDT chambers installed between the two periods to increase the number of MS layers from one to two at $\eta = -1.2$ and in part of the region at $\eta = 1.2$. The trigger thresholds were in general lower in 2011. The reconstruction programs used for 2011 data were similar to those used in 2012, although several improvements have been introduced between the two periods. Tighter requirements on the ID tracks associated to the muon track were applied in 2011. Similar MC samples as those used for the study of 2012 data have been generated at $\sqrt{s} = 7$ TeV for the study of muon performance in 2011, using the same simulation based on GEANT4. The reconstruction of the 2011 simulated data was performed with ideal alignment in the MS.

The efficiency, calculated with the "tag and probe" method as in 2012, is presented in Fig. 19 for Chain 1 muons. The main difference with respect to 2012 is the lower efficiency of CB muons at $|\eta| \simeq 1.2$, in which a layer of MDT chambers was missing, and the inefficiency introduced by the tighter ID selection.

The momentum corrections have been derived for the 2011 MC in the same way as for the 2012 MC. After correction, the mass scales of data and MC are in good agreement as shown in Fig. 20. Due to the smaller data sample, the momentum corrections have larger uncertainties than in 2012. The resolution for CB muons obtained with Z events is presented in Fig. 21. The resolution of the uncorrected MC is $\approx 20\,\%$ smaller than data, significantly worse than in the 2012 case. This is due to the improvements introduced in the reconstruction of 2012 data, including a better knowledge of the ID and MS alignments, and to the use of the ideal MS alignment in the 2011 simulation.

References

1. ATLAS Collaboration, JINST **3**, S08003 (2008)
2. ATLAS Collaboration, Phys. Rev. D **85**, 072004 (2012). arXiv:1109.5141 [hep-ex]

3. ATLAS Collaboration, JHEP **1405**, 068 (2014). arXiv:1402.6263 [hep-ex]
4. ATLAS Collaboration, JHEP **1406**, 112 (2014). arXiv:1404.1212 [hep-ex]
5. ATLAS Collaboration, Phys. Lett. B **716**, 1–29 (2012). arXiv:1207.7214 [hep-ex]
6. ATLAS Collaboration, Phys. Rev. D **90**, 052004 (2014). arXiv:1406.3827 [hep-ex]
7. ATLAS Collaboration, Phys. Rev. D **87**, 015010 (2013). arXiv:1211.1150 [hep-ex]
8. ATLAS Collaboration, Phys. Rev. D **88**, 072001 (2013). arXiv:1308.4075 [hep-ex]
9. ATLAS Collaboration, Eur. Phys. J. C **74**, 3034 (2014). arXiv:1404.4562 [hep-ex]
10. ATLAS Collaboration, Expected performance of the ATLAS experiment–detector, trigger and physics. CERN, Geneva (2009). arXiv:0901.0512 [hep-ex]
11. ATLAS Collaboration, Eur. Phys. J. C **72**, 1849 (2012). arXiv:1110.1530 [hep-ex]
12. ATLAS Collaboration, submitted to Eur. Phys. J. C (2014). arXiv:1408.3179 [hep-ex]
13. S. Alioli, P. Nason, C. Oleari, E. Re, JHEP **1006**, 043 (2010). arXiv:1002.2581 [hep-ph]
14. T. Sjöstrand, S. Mrenna, P. Skands, Comput. Phys. Commun. **178**, 852 (2008). arXiv:0710.3820 [hep-ph]
15. H.-L. Lai et al., Phys. Rev. D **82**, 074024 (2010). arXiv:1007.2241 [hep-ph]
16. P. Golonka, Z. Was, Eur. Phys. J. C **45**, 97 (2006). arXiv:0506026 [hep-ph]
17. M. L. Mangano et al., JHEP **0307**, 001 (2003). arXiv:0206293 [hep-ph]
18. T. Sjöstrand, S. Mrenna, P. Skands, JHEP **0605**, 026 (2006). arXiv:0603175 [hep-ph]
19. ATLAS Collaboration, Phys. Rev. D **85**, 092002 (2012). arXiv:1201.1276 [hep-ex]
20. T. Gleisberg et al., JHEP **0902**, 007 (2009). arXiv:0811.4622 [hep-ph]
21. S. Frixione, B. R. Webber, JHEP **0206**, 029 (2002). arXiv:0204244 [hep-ph]
22. ATLAS Collaboration, Eur. Phys. J. C **70**, 823 (2010). arXiv:1005.4568 [physics.ins-det]
23. S. Agostinelli et al., Nucl. Instrum. Method A **506**, 250 (2003)
24. A. Martin, W. Stirling, R. Thorne, G. Watt, Eur. Phys. J. C **63**, 189 (2009). arXiv:0901.0002 [hep-ph]
25. C. Grupen, B. Shwartz, Particle Detectors, 2nd edn. Cambridge University Press, Cambridge (2008)
26. M. Oreglia, SLAC-R-0236 (1980) (appendix D)
27. F. James, M. Roos, Comput. Phys. Commun. **10**, 343–367 (1975)
28. Particle Data Group, J. Beringer et al. Phys. Rev. D **86**, 010001 (2012)
29. ATLAS Collaboration, Phys. Lett. B **732**, 8–27 (2014). arXiv:1402.3051 [hep-ex]
30. ATLAS Collaboration, Phys. Rev. D **89**, 052004 (2014). arXiv:1311.1440 [hep-ex]

ATLAS Collaboration

G. Aad[84], B. Abbott[112], J. Abdallah[152], S. Abdel Khalek[116], O. Abdinov[11], R. Aben[106], B. Abi[113], M. Abolins[89], O. S. AbouZeid[159], H. Abramowicz[154], H. Abreu[153], R. Abreu[30], Y. Abulaiti[147a,147b], B. S. Acharya[165a,165b,a], L. Adamczyk[38a], D. L. Adams[25], J. Adelman[177], S. Adomeit[99], T. Adye[130], T. Agatonovic-Jovin[13a], J. A. Aguilar-Saavedra[125a,125f], M. Agustoni[17], S. P. Ahlen[22], F. Ahmadov[64,b], G. Aielli[134a,134b], H. Akerstedt[147a,147b], T. P. A. Åkesson[80], G. Akimoto[156], A. V. Akimov[95], G. L. Alberghi[20a,20b], J. Albert[170], S. Albrand[55], M. J. Alconada Verzini[70], M. Aleksa[30], I. N. Aleksandrov[64], C. Alexa[26a], G. Alexander[154], G. Alexandre[49], T. Alexopoulos[10], M. Alhroob[165a,165b], G. Alimonti[90a], L. Alio[84], J. Alison[31], B. M. M. Allbrooke[18], L. J. Allison[71], P. P. Allport[73], J. Almond[83], A. Aloisio[103a,103b], A. Alonso[36], F. Alonso[70], C. Alpigiani[75], A. Altheimer[35], B. Alvarez Gonzalez[89], M. G. Alviggi[103a,103b], K. Amako[65], Y. Amaral Coutinho[24a], C. Amelung[23], D. Amidei[88], S. P. Amor Dos Santos[125a,125c], A. Amorim[125a,125b], S. Amoroso[48], N. Amram[154], G. Amundsen[23], C. Anastopoulos[140], L. S. Ancu[49], N. Andari[30], T. Andeen[35], C. F. Anders[58b], G. Anders[30], K. J. Anderson[31], A. Andreazza[90a,90b], V. Andrei[58a], X. S. Anduaga[70], S. Angelidakis[9], I. Angelozzi[106], P. Anger[44], A. Angerami[35], F. Anghinolfi[30], A. V. Anisenkov[108], N. Anjos[125a], A. Annovi[47], A. Antonaki[9], M. Antonelli[47], A. Antonov[97], J. Antos[145b], F. Anulli[133a], M. Aoki[65], L. Aperio Bella[18], R. Apolle[119,c], G. Arabidze[89], I. Aracena[144], Y. Arai[65], J. P. Araque[125a], A. T. H. Arce[45], J.-F. Arguin[94], S. Argyropoulos[42], M. Arik[19a], A. J. Armbruster[30], O. Arnaez[30], V. Arnal[81], H. Arnold[48], M. Arratia[28], O. Arslan[21], A. Artamonov[96], G. Artoni[23], S. Asai[156], N. Asbah[42], A. Ashkenazi[154], B. Åsman[147a,147b], L. Asquith[6], K. Assamagan[25], R. Astalos[145a], M. Atkinson[166], N. B. Atlay[142], B. Auerbach[6], K. Augsten[127], M. Aurousseau[146b], G. Avolio[30], G. Azuelos[94,d], Y. Azuma[156], M. A. Baak[30], A. Baas[58a], C. Bacci[135a,135b], H. Bachacou[137], K. Bachas[155], M. Backes[30], M. Backhaus[30], J. Backus Mayes[144], E. Badescu[26a], P. Bagiacchi[133a,133b], P. Bagnaia[133a,133b], Y. Bai[33a], T. Bain[35], J. T. Baines[130], O. K. Baker[177], P. Balek[128], F. Balli[137], E. Banas[39], Sw. Banerjee[174], A. A. E. Bannoura[176], V. Bansal[170], H. S. Bansil[18], L. Barak[173], S. P. Baranov[95], E. L. Barberio[87], D. Barberis[50a,50b], M. Barbero[84], T. Barillari[100], M. Barisonzi[176], T. Barklow[144], N. Barlow[28], B. M. Barnett[130], R. M. Barnett[15], Z. Barnovska[5], A. Baroncelli[135a], G. Barone[49], A. J. Barr[119], F. Barreiro[81], J. Barreiro Guimarães da Costa[57], R. Bartoldus[144], A. E. Barton[71], P. Bartos[145a], V. Bartsch[150], A. Bassalat[116], A. Basye[166], R. L. Bates[53], J. R. Batley[28], M. Battaglia[138], M. Battistin[30], F. Bauer[137], H. S. Bawa[144,e], M. D. Beattie[71], T. Beau[79], P. H. Beauchemin[162], R. Beccherle[123a,123b],

P. Bechtle[21], H. P. Beck[17], K. Becker[176], S. Becker[99], M. Beckingham[171], C. Becot[116], A. J. Beddall[19c], A. Beddall[19c], S. Bedikian[177], V. A. Bednyakov[64], C. P. Bee[149], L. J. Beemster[106], T. A. Beermann[176], M. Begel[25], K. Behr[119], C. Belanger-Champagne[86], P. J. Bell[49], W. H. Bell[49], G. Bella[154], L. Bellagamba[20a], A. Bellerive[29], M. Bellomo[85], K. Belotskiy[97], O. Beltramello[30], O. Benary[154], D. Benchekroun[136a], K. Bendtz[147a,147b], N. Benekos[166], Y. Benhammou[154], E. Benhar Noccioli[49], J. A. Benitez Garcia[160b], D. P. Benjamin[45], J. R. Bensinger[23], K. Benslama[131], S. Bentvelsen[106], D. Berge[106], E. Bergeaas Kuutmann[16], N. Berger[5], F. Berghaus[170], J. Beringer[15], C. Bernard[22], P. Bernat[77], C. Bernius[78], F. U. Bernlochner[170], T. Berry[76], P. Berta[128], C. Bertella[84], G. Bertoli[147a,147b], F. Bertolucci[123a,123b], C. Bertsche[112], D. Bertsche[112], M. Bessner[42], M. I. Besana[90a], G. J. Besjes[105], O. Bessidskaia[147a,147b], N. Besson[137], C. Betancourt[48], S. Bethke[100], W. Bhimji[46], R. M. Bianchi[124], L. Bianchini[23], M. Bianco[30], O. Biebel[99], S. P. Bieniek[77], K. Bierwagen[54], J. Biesiada[15], M. Biglietti[135a], J. Bilbao De Mendizabal[49], H. Bilokon[47], M. Bindi[54], S. Binet[116], A. Bingul[19c], C. Bini[133a,133b], C. W. Black[151], J. E. Black[144], K. M. Black[22], D. Blackburn[139], R. E. Blair[6], J.-B. Blanchard[137], T. Blazek[145a], I. Bloch[42], C. Blocker[23], W. Blum[82,*], U. Blumenschein[54], G. J. Bobbink[106], V. S. Bobrovnikov[108], S. S. Bocchetta[80], A. Bocci[45], C. Bock[99], C. R. Boddy[119], M. Boehler[48], T. T. Boek[176], J. A. Bogaerts[30], A. G. Bogdanchikov[108], A. Bogouch[91,*], C. Bohm[147a], J. Bohm[126], V. Boisvert[76], T. Bold[38a], V. Boldea[26a], A. S. Boldyrev[98], M. Bomben[79], M. Bona[75], M. Boonekamp[137], A. Borisov[129], G. Borissov[71], M. Borri[83], S. Borroni[42], J. Bortfeldt[99], V. Bortolotto[135a,135b], K. Bos[106], D. Boscherini[20a], M. Bosman[12], H. Boterenbrood[106], J. Boudreau[124], J. Bouffard[2], E. V. Bouhova-Thacker[71], D. Boumediene[34], C. Bourdarios[116], N. Bousson[113], S. Boutouil[136d], A. Boveia[31], J. Boyd[30], I. R. Boyko[64], J. Bracinik[18], A. Brandt[8], G. Brandt[15], O. Brandt[58a], U. Bratzler[157], B. Brau[85], J. E. Brau[115], H. M. Braun[176,*], S. F. Brazzale[165a,165c], B. Brelier[159], K. Brendlinger[121], A. J. Brennan[87], R. Brenner[167], S. Bressler[173], K. Bristow[146c], T. M. Bristow[46], D. Britton[53], F. M. Brochu[28], I. Brock[21], R. Brock[89], C. Bromberg[89], J. Bronner[100], G. Brooijmans[35], T. Brooks[76], W. K. Brooks[32b], J. Brosamer[15], E. Brost[115], J. Brown[55], P. A. Bruckman de Renstrom[39], D. Bruncko[145b], R. Bruneliere[48], S. Brunet[60], A. Bruni[20a], G. Bruni[20a], M. Bruschi[20a], L. Bryngemark[80], T. Buanes[14], Q. Buat[143], F. Bucci[49], P. Buchholz[142], R. M. Buckingham[119], A. G. Buckley[53], S. I. Buda[26a], I. A. Budagov[64], F. Buehrer[48], L. Bugge[118], M. K. Bugge[118], O. Bulekov[97], A. C. Bundock[73], H. Burckhart[30], S. Burdin[73], B. Burghgrave[107], S. Burke[130], I. Burmeister[43], E. Busato[34], D. Büscher[48], V. Büscher[82], P. Bussey[53], C. P. Buszello[167], B. Butler[57], J. M. Butler[22], A. I. Butt[3], C. M. Buttar[53], J. M. Butterworth[77], P. Butti[106], W. Buttinger[28], A. Buzatu[53], M. Byszewski[10], S. Cabrera Urbán[168], D. Caforio[20a,20b], O. Cakir[4a], P. Calafiura[15], A. Calandri[137], G. Calderini[79], P. Calfayan[99], R. Calkins[107], L. P. Caloba[24a], D. Calvet[34], S. Calvet[34], R. Camacho Toro[49], S. Camarda[42], D. Cameron[118], L. M. Caminada[15], R. Caminal Armadans[12], S. Campana[30], M. Campanelli[77], A. Campoverde[149], V. Canale[103a,103b], A. Canepa[160a], M. Cano Bret[75], J. Cantero[81], R. Cantrill[125a], T. Cao[40], M. D. M. Capeans Garrido[30], I. Caprini[26a], M. Caprini[26a], M. Capua[37a,37b], R. Caputo[82], R. Cardarelli[134a], T. Carli[30], G. Carlino[103a], L. Carminati[90a,90b], S. Caron[105], E. Carquin[32a], G. D. Carrillo-Montoya[146c], J. R. Carter[28], J. Carvalho[125a,125c], D. Casadei[77], M. P. Casado[12], M. Casolino[12], E. Castaneda-Miranda[146b], A. Castelli[106], V. Castillo Gimenez[168], N. F. Castro[125a], P. Catastini[57], A. Catinaccio[30], J. R. Catmore[118], A. Cattai[30], G. Cattani[134a,134b], S. Caughron[89], V. Cavaliere[166], D. Cavalli[90a], M. Cavalli-Sforza[12], V. Cavasinni[123a,123c], F. Ceradini[135a,135b], B. Cerio[45], K. Cerny[128], A. S. Cerqueira[24b], A. Cerri[150], L. Cerrito[75], F. Cerutti[15], M. Cerv[30], A. Cervelli[17], S. A. Cetin[19b], A. Chafaq[136a], D. Chakraborty[107], I. Chalupkova[128], P. Chang[166], B. Chapleau[86], J. D. Chapman[28], D. Charfeddine[116], D. G. Charlton[18], C. C. Chau[159], C. A. Chavez Barajas[150], S. Cheatham[86], A. Chegwidden[89], S. Chekanov[6], S. V. Chekulaev[160a], G. A. Chelkov[64,f], M. A. Chelstowska[88], C. Chen[63], H. Chen[25], K. Chen[149], L. Chen[33d,g], S. Chen[33c], X. Chen[146c], Y. Chen[66], Y. Chen[35], H. C. Cheng[88], Y. Cheng[31], A. Cheplakov[64], R. Cherkaoui El Moursli[136e], V. Chernyatin[25,*], E. Cheu[7], L. Chevalier[137], V. Chiarella[47], G. Chiefari[103a,103b], J. T. Childers[6], A. Chilingarov[71], G. Chiodini[72a], A. S. Chisholm[18], R. T. Chislett[77], A. Chitan[26a], M. V. Chizhov[64], S. Chouridou[9], B. K. B. Chow[99], D. Chromek-Burckhart[30], M. L. Chu[152], J. Chudoba[126], J. J. Chwastowski[39], L. Chytka[114], G. Ciapetti[133a,133b], A. K. Ciftci[4a], R. Ciftci[4a], D. Cinca[53], V. Cindro[74], A. Ciocio[15], P. Cirkovic[13b], Z. H. Citron[173], M. Citterio[90a], M. Ciubancan[26a], A. Clark[49], P. J. Clark[46], R. N. Clarke[15], W. Cleland[124], J. C. Clemens[84], C. Clement[147a,147b], Y. Coadou[84], M. Cobal[165a,165c], A. Coccaro[139], J. Cochran[63], L. Coffey[23], J. G. Cogan[144], J. Coggeshall[166], B. Cole[35], S. Cole[107], A. P. Colijn[106], J. Collot[55], T. Colombo[58c], G. Colon[85], G. Compostella[100], P. Conde Muiño[125a,125b], E. Coniavitis[48], M. C. Conidi[12], S. H. Connell[146b], I. A. Connelly[76], S. M. Consonni[90a,90b], V. Consorti[48], S. Constantinescu[26a], C. Conta[120a,120b], G. Conti[57], F. Conventi[103a,h], M. Cooke[15], B. D. Cooper[77], A. M. Cooper-Sarkar[119], N. J. Cooper-Smith[76], K. Copic[15], T. Cornelissen[176], M. Corradi[20a], F. Corriveau[86,i], A. Corso-Radu[164], A. Cortes-Gonzalez[12], G. Cortiana[100], G. Costa[90a], M. J. Costa[168], D. Costanzo[140], D. Côté[8], G. Cottin[28], G. Cowan[76], B. E. Cox[83], K. Cranmer[109], G. Cree[29], S. Crépé-Renaudin[55], F. Crescioli[79], W. A. Cribbs[147a,147b], M. Crispin Ortuzar[119], M. Cristinziani[21], V. Croft[105], G. Crosetti[37a,37b], C.-M. Cuciuc[26a], T. Cuhadar Donszelmann[140], J. Cummings[177], M. Curatolo[47], C. Cuthbert[151], H. Czirr[142], P. Czodrowski[3], Z. Czyczula[177], S. D'Auria[53],

M. D'Onofrio[73], M. J. Da Cunha Sargedas De Sousa[125a,125b], C. Da Via[83], W. Dabrowski[38a], A. Dafinca[119], T. Dai[88], O. Dale[14], F. Dallaire[94], C. Dallapiccola[85], M. Dam[36], A. C. Daniells[18], M. Dano Hoffmann[137], V. Dao[48], G. Darbo[50a], S. Darmora[8], J. A. Dassoulas[42], A. Dattagupta[60], W. Davey[21], C. David[170], T. Davidek[128], E. Davies[119,c], M. Davies[154], O. Davignon[79], A. R. Davison[77], P. Davison[77], Y. Davygora[58a], E. Dawe[143], I. Dawson[140], R. K. Daya-Ishmukhametova[85], K. De[8], R. de Asmundis[103a], S. De Castro[20a,20b], S. De Cecco[79], N. De Groot[105], P. de Jong[106], H. De la Torre[81], F. De Lorenzi[63], L. De Nooij[106], D. De Pedis[133a], A. De Salvo[133a], U. De Sanctis[165a,165b], A. De Santo[150], J. B. De Vivie De Regie[116], W. J. Dearnaley[71], R. Debbe[25], C. Debenedetti[138], B. Dechenaux[55], D. V. Dedovich[64], I. Deigaard[106], J. Del Peso[81], T. Del Prete[123a,123b], F. Deliot[137], C. M. Delitzsch[49], M. Deliyergiyev[74], A. Dell'Acqua[30], L. Dell'Asta[22], M. Dell'Orso[123a,123b], M. Della Pietra[103a,h], D. della Volpe[49], M. Delmastro[5], P. A. Delsart[55], C. Deluca[106], S. Demers[177], M. Demichev[64], A. Demilly[79], S. P. Denisov[129], D. Derendarz[39], J. E. Derkaoui[136d], F. Derue[79], P. Dervan[73], K. Desch[21], C. Deterre[42], P. O. Deviveiros[106], A. Dewhurst[130], S. Dhaliwal[106], A. Di Ciaccio[134a,134b], L. Di Ciaccio[5], A. Di Domenico[133a,133b], C. Di Donato[103a,103b], A. Di Girolamo[30], B. Di Girolamo[30], A. Di Mattia[153], B. Di Micco[135a,135b], R. Di Nardo[47], A. Di Simone[48], R. Di Sipio[20a,20b], D. Di Valentino[29], F. A. Dias[46], M. A. Diaz[32a], E. B. Diehl[88], J. Dietrich[42], T. A. Dietzsch[58a], S. Diglio[84], A. Dimitrievska[13a], J. Dingfelder[21], C. Dionisi[133a,133b], P. Dita[26a], S. Dita[26a], F. Dittus[30], F. Djama[84], T. Djobava[51b], M. A. B. do Vale[24c], A. Do Valle Wemans[125a,125g], T. K. O. Doan[5], D. Dobos[30], C. Doglioni[49], T. Doherty[53], T. Dohmae[156], J. Dolejsi[128], Z. Dolezal[128], B. A. Dolgoshein[97,*], M. Donadelli[24d], S. Donati[123a,123b], P. Dondero[120a,120b], J. Donini[34], J. Dopke[130], A. Doria[103a], M. T. Dova[70], A. T. Doyle[53], M. Dris[10], J. Dubbert[88], S. Dube[15], E. Dubreuil[34], E. Duchovni[173], G. Duckeck[99], O. A. Ducu[26a], D. Duda[176], A. Dudarev[30], F. Dudziak[63], L. Duflot[116], L. Duguid[76], M. Dührssen[30], M. Dunford[58a], H. Duran Yildiz[4a], M. Düren[52], A. Durglishvili[51b], M. Dwuznik[38a], M. Dyndal[38a], J. Ebke[99], W. Edson[2], N. C. Edwards[46], W. Ehrenfeld[21], T. Eifert[144], G. Eigen[14], K. Einsweiler[15], T. Ekelof[167], M. El Kacimi[136c], M. Ellert[167], S. Elles[5], F. Ellinghaus[82], N. Ellis[30], J. Elmsheuser[99], M. Elsing[30], D. Emeliyanov[130], Y. Enari[156], O. C. Endner[82], M. Endo[117], R. Engelmann[149], J. Erdmann[177], A. Ereditato[17], D. Eriksson[147a], G. Ernis[176], J. Ernst[2], M. Ernst[25], J. Ernwein[137], D. Errede[166], S. Errede[166], E. Ertel[82], M. Escalier[116], H. Esch[43], C. Escobar[124], B. Esposito[47], A. I. Etienvre[137], E. Etzion[154], H. Evans[60], A. Ezhilov[122], L. Fabbri[20a,20b], G. Facini[31], R. M. Fakhrutdinov[129], S. Falciano[133a], R. J. Falla[77], J. Faltova[128], Y. Fang[33a], M. Fanti[90a,90b], A. Farbin[8], A. Farilla[135a], T. Farooque[12], S. Farrell[15], S. M. Farrington[171], P. Farthouat[30], F. Fassi[136e], P. Fassnacht[30], D. Fassouliotis[9], A. Favareto[50a,50b], L. Fayard[116], P. Federic[145a], O. L. Fedin[122,j], W. Fedorko[169], M. Fehling-Kaschek[48], S. Feigl[30], L. Feligioni[84], C. Feng[33d], E. J. Feng[6], H. Feng[88], A. B. Fenyuk[129], S. Fernandez Perez[30], S. Ferrag[53], J. Ferrando[53], A. Ferrari[167], P. Ferrari[106], R. Ferrari[120a], D. E. Ferreira de Lima[53], A. Ferrer[168], D. Ferrere[49], C. Ferretti[88], A. Ferretto Parodi[50a,50b], M. Fiascaris[31], F. Fiedler[82], A. Filipčič[74], M. Filipuzzi[42], F. Filthaut[105], M. Fincke-Keeler[170], K. D. Finelli[151], M. C. N. Fiolhais[125a,125c], L. Fiorini[168], A. Firan[40], A. Fischer[2], J. Fischer[176], W. C. Fisher[89], E. A. Fitzgerald[23], M. Flechl[48], I. Fleck[142], P. Fleischmann[88], S. Fleischmann[176], G. T. Fletcher[140], G. Fletcher[75], T. Flick[176], A. Floderus[80], L. R. Flores Castillo[174k], A. C. Florez Bustos[160b], M. J. Flowerdew[100], A. Formica[137], A. Forti[83], D. Fortin[160a], D. Fournier[116], H. Fox[71], S. Fracchia[12], P. Francavilla[79], M. Franchini[20a,20b], S. Franchino[30], D. Francis[30], L. Franconi[118], M. Franklin[57], S. Franz[61], M. Fraternali[120a,120b], S. T. French[28], C. Friedrich[42], F. Friedrich[44], D. Froidevaux[30], J. A. Frost[28], C. Fukunaga[157], E. Fullana Torregrosa[82], B. G. Fulsom[144], J. Fuster[168], C. Gabaldon[55], O. Gabizon[173], A. Gabrielli[20a,20b], A. Gabrielli[133a,133b], S. Gadatsch[106], S. Gadomski[49], G. Gagliardi[50a,50b], P. Gagnon[60], C. Galea[105], B. Galhardo[125a,125c], E. J. Gallas[119], V. Gallo[17], B. J. Gallop[130], P. Gallus[127], G. Galster[36], K. K. Gan[110], J. Gao[33b,g], Y. S. Gao[144,e], F. M. Garay Walls[46], F. Garberson[177], C. García[168], J. E. García Navarro[168], M. Garcia-Sciveres[15], R. W. Gardner[31], N. Garelli[144], V. Garonne[30], C. Gatti[47], G. Gaudio[120a], B. Gaur[142], L. Gauthier[94], P. Gauzzi[133a,133b], I. L. Gavrilenko[95], C. Gay[169], G. Gaycken[21], E. N. Gazis[10], P. Ge[33d], Z. Gecse[169], C. N. P. Gee[130], D. A. A. Geerts[106], Ch. Geich-Gimbel[21], K. Gellerstedt[147a,147b], C. Gemme[50a], A. Gemmell[53], M. H. Genest[55], S. Gentile[133a,133b], M. George[54], S. George[76], D. Gerbaudo[164], A. Gershon[154], H. Ghazlane[136b], N. Ghodbane[34], B. Giacobbe[20a], S. Giagu[133a,133b], V. Giangiobbe[12], P. Giannetti[123a,123b], F. Gianotti[30], B. Gibbard[25], S. M. Gibson[76], M. Gilchriese[15], T. P. S. Gillam[28], D. Gillberg[30], G. Gilles[34], D. M. Gingrich[3,d], N. Giokaris[9], M. P. Giordani[165a,165c], R. Giordano[103a,103b], F. M. Giorgi[20a], F. M. Giorgi[16], P. F. Giraud[137], D. Giugni[90a], C. Giuliani[48], M. Giulini[58b], B. K. Gjelsten[118], S. Gkaitatzis[155], I. Gkialas[155,l], L. K. Gladilin[98], C. Glasman[81], J. Glatzer[30], P. C. F. Glaysher[46], A. Glazov[42], G. L. Glonti[64], M. Goblirsch-Kolb[100], J. R. Goddard[75], J. Godfrey[143], J. Godlewski[30], C. Goeringer[82], S. Goldfarb[88], T. Golling[177], D. Golubkov[129], A. Gomes[125a,125b,125d], L. S. Gomez Fajardo[42], R. Gonçalo[125a], J. Goncalves Pinto Firmino Da Costa[137], L. Gonella[21], S. González de la Hoz[168], G. Gonzalez Parra[12], S. Gonzalez-Sevilla[49], L. Goossens[30], P. A. Gorbounov[96], H. A. Gordon[25], I. Gorelov[104], B. Gorini[30], E. Gorini[72a,72b], A. Gorišek[74], E. Gornicki[39], A. T. Goshaw[6], C. Gössling[43], M. I. Gostkin[64], M. Gouighri[136a], D. Goujdami[136c], M. P. Goulette[49], A. G. Goussiou[139], C. Goy[5], S. Gozpinar[23], H. M. X. Grabas[137], L. Graber[54], I. Grabowska-Bold[38a],

P. Grafström[20a,20b], K.-J. Grahn[42], J. Gramling[49], E. Gramstad[118], S. Grancagnolo[16], V. Grassi[149], V. Gratchev[122], H. M. Gray[30], E. Graziani[135a], O. G. Grebenyuk[122], Z. D. Greenwood[78,m], K. Gregersen[77], I. M. Gregor[42], P. Grenier[144], J. Griffiths[8], A. A. Grillo[138], K. Grimm[71], S. Grinstein[12,n], Ph. Gris[34], Y. V. Grishkevich[98], J.-F. Grivaz[116], J. P. Grohs[44], A. Grohsjean[42], E. Gross[173], J. Grosse-Knetter[54], G. C. Grossi[134a,134b], J. Groth-Jensen[173], Z. J. Grout[150], L. Guan[33b], F. Guescini[49], D. Guest[177], O. Gueta[154], C. Guicheney[34], E. Guido[50a,50b], T. Guillemin[116], S. Guindon[2], U. Gul[53], C. Gumpert[44], J. Gunther[127], J. Guo[35], S. Gupta[119], P. Gutierrez[112], N. G. Gutierrez Ortiz[53], C. Gutschow[77], N. Guttman[154], C. Guyot[137], C. Gwenlan[119], C. B. Gwilliam[73], A. Haas[109], C. Haber[15], H. K. Hadavand[8], N. Haddad[136e], P. Haefner[21], S. Hageböeck[21], Z. Hajduk[39], H. Hakobyan[178], M. Haleem[42], D. Hall[119], G. Halladjian[89], K. Hamacher[176], P. Hamal[114], K. Hamano[170], M. Hamer[54], A. Hamilton[146a], S. Hamilton[162], G. N. Hamity[146c], P. G. Hamnett[42], L. Han[33b], K. Hanagaki[117], K. Hanawa[156], M. Hance[15], P. Hanke[58a], R. Hann[137], J. B. Hansen[36], J. D. Hansen[36], P. H. Hansen[36], K. Hara[161], A. S. Hard[174], T. Harenberg[176], F. Hariri[116], S. Harkusha[91], D. Harper[88], R. D. Harrington[46], O. M. Harris[139], P. F. Harrison[171], F. Hartjes[106], M. Hasegawa[66], S. Hasegawa[102], Y. Hasegawa[141], A. Hasib[112], S. Hassani[137], S. Haug[17], M. Hauschild[30], R. Hauser[89], M. Havranek[126], C. M. Hawkes[18], R. J. Hawkings[30], A. D. Hawkins[80], T. Hayashi[161], D. Hayden[89], C. P. Hays[119], H. S. Hayward[73], S. J. Haywood[130], S. J. Head[18], T. Heck[82], V. Hedberg[80], L. Heelan[8], S. Heim[121], T. Heim[176], B. Heinemann[15], L. Heinrich[109], J. Hejbal[126], L. Helary[22], C. Heller[99], M. Heller[30], S. Hellman[147a,147b], D. Hellmich[21], C. Helsens[30], J. Henderson[119], R. C. W. Henderson[71], Y. Heng[174], C. Hengler[42], A. Henrichs[177], A. M. Henriques Correia[30], S. Henrot-Versille[116], C. Hensel[54], G. H. Herbert[16], Y. Hernández Jiménez[168], R. Herrberg-Schubert[16], G. Herten[48], R. Hertenberger[99], L. Hervas[30], G. G. Hesketh[77], N. P. Hessey[106], R. Hickling[75], E. Higón-Rodriguez[168], E. Hill[170], J. C. Hill[28], K. H. Hiller[42], S. Hillert[21], S. J. Hillier[18], I. Hinchliffe[15], E. Hines[121], M. Hirose[158], D. Hirschbuehl[176], J. Hobbs[149], N. Hod[106], M. C. Hodgkinson[140], P. Hodgson[140], A. Hoecker[30], M. R. Hoeferkamp[104], F. Hoenig[99], J. Hoffman[40], D. Hoffmann[84], J. I. Hofmann[58a], M. Hohlfeld[82], T. R. Holmes[15], T. M. Hong[121], L. Hooft van Huysduynen[109], Y. Horii[102], J.-Y. Hostachy[55], S. Hou[152], A. Hoummada[136a], J. Howard[119], J. Howarth[42], M. Hrabovsky[114], I. Hristova[16], J. Hrivnac[116], T. Hryn'ova[5], C. Hsu[146c], P. J. Hsu[82], S.-C. Hsu[139], D. Hu[35], X. Hu[25], Y. Huang[42], Z. Hubacek[30], F. Hubaut[84], F. Huegging[21], T. B. Huffman[119], E. W. Hughes[35], G. Hughes[71], M. Huhtinen[30], T. A. Hülsing[82], M. Hurwitz[15], N. Huseynov[64,b], J. Huston[89], J. Huth[57], G. Iacobucci[49], G. Iakovidis[10], I. Ibragimov[142], L. Iconomidou-Fayard[116], E. Ideal[177], P. Iengo[103a], O. Igonkina[106], T. Iizawa[172], Y. Ikegami[65], K. Ikematsu[142], M. Ikeno[65], Y. Ilchenko[31,o], D. Iliadis[155], N. Ilic[159], Y. Inamaru[66], T. Ince[100], P. Ioannou[9], M. Iodice[135a], K. Iordanidou[9], V. Ippolito[57], A. Irles Quiles[168], C. Isaksson[167], M. Ishino[67], M. Ishitsuka[158], R. Ishmukhametov[110], C. Issever[119], S. Istin[19a], J. M. Iturbe Ponce[83], R. Iuppa[134a,134b], J. Ivarsson[80], W. Iwanski[39], H. Iwasaki[65], J. M. Izen[41], V. Izzo[103a], B. Jackson[121], M. Jackson[73], P. Jackson[1], M. R. Jaekel[30], V. Jain[2], K. Jakobs[48], S. Jakobsen[30], T. Jakoubek[126], J. Jakubek[127], D. O. Jamin[152], D. K. Jana[78], E. Jansen[77], H. Jansen[30], J. Janssen[21], M. Janus[171], G. Jarlskog[80], N. Javadov[64,b], T. Javůrek[48], L. Jeanty[15], J. Jejelava[51a,p], G.-Y. Jeng[151], D. Jennens[87], P. Jenni[48,q], J. Jentzsch[43], C. Jeske[171], S. Jézéquel[5], H. Ji[174], J. Jia[149], Y. Jiang[33b], M. Jimenez Belenguer[42], S. Jin[33a], A. Jinaru[26a], O. Jinnouchi[158], M. D. Joergensen[36], K. E. Johansson[147a,147b], P. Johansson[140], K. A. Johns[7], K. Jon-And[147a,147b], G. Jones[171], R. W. L. Jones[71], T. J. Jones[73], J. Jongmanns[58a], P. M. Jorge[125a,125b], K. D. Joshi[83], J. Jovicevic[148], X. Ju[174], C. A. Jung[43], R. M. Jungst[30], P. Jussel[61], A. Juste Rozas[12,n], M. Kaci[168], A. Kaczmarska[39], M. Kado[116], H. Kagan[110], M. Kagan[144], E. Kajomovitz[45], C. W. Kalderon[119], S. Kama[40], A. Kamenshchikov[129], N. Kanaya[156], M. Kaneda[30], S. Kaneti[28], V. A. Kantserov[97], J. Kanzaki[65], B. Kaplan[109], A. Kapliy[31], D. Kar[53], K. Karakostas[10], N. Karastathis[10], M. Karnevskiy[82], S. N. Karpov[64], Z. M. Karpova[64], K. Karthik[109], V. Kartvelishvili[71], A. N. Karyukhin[129], L. Kashif[174], G. Kasieczka[58b], R. D. Kass[110], A. Kastanas[14], Y. Kataoka[156], A. Katre[49], J. Katzy[42], V. Kaushik[7], K. Kawagoe[69], T. Kawamoto[156], G. Kawamura[54], S. Kazama[156], V. F. Kazanin[108], M. Y. Kazarinov[64], R. Keeler[170], R. Kehoe[40], M. Keil[54], J. S. Keller[42], J. J. Kempster[76], H. Keoshkerian[5], O. Kepka[126], B. P. Kerševan[74], S. Kersten[176], K. Kessoku[156], J. Keung[159], F. Khalil-zada[11], H. Khandanyan[147a,147b], A. Khanov[113], A. Khodinov[97], A. Khomich[58a], T. J. Khoo[28], G. Khoriauli[21], A. Khoroshilov[176], V. Khovanskiy[96], E. Khramov[64], J. Khubua[51b], H. Y. Kim[8], H. Kim[147a,147b], S. H. Kim[161], N. Kimura[172], O. Kind[16], B. T. King[73], M. King[168], R. S. B. King[119], S. B. King[169], J. Kirk[130], A. E. Kiryunin[100], T. Kishimoto[66], D. Kisielewska[38a], F. Kiss[48], T. Kittelmann[124], K. Kiuchi[161], E. Kladiva[145b], M. Klein[73], U. Klein[73], K. Kleinknecht[82], P. Klimek[147a,147b], A. Klimentov[25], R. Klingenberg[43], J. A. Klinger[83], T. Klioutchnikova[30], P. F. Klok[105], E.-E. Kluge[58a], P. Kluit[106], S. Kluth[100], E. Kneringer[61], E. B. F. G. Knoops[84], A. Knue[53], D. Kobayashi[158], T. Kobayashi[156], M. Kobel[44], M. Kocian[144], P. Kodys[128], P. Koevesarki[21], T. Koffas[29], E. Koffeman[106], L. A. Kogan[119], S. Kohlmann[176], Z. Kohout[127], T. Kohriki[65], T. Koi[144], H. Kolanoski[16], I. Koletsou[5], J. Koll[89], A. A. Komar[95,*], Y. Komori[156], T. Kondo[65], N. Kondrashova[42], K. Köneke[48], A. C. König[105], S. König[82], T. Kono[65,r], R. Konoplich[109,s], N. Konstantinidis[77], R. Kopeliansky[153], S. Koperny[38a], L. Köpke[82], A. K. Kopp[48], K. Korcyl[39], K. Kordas[155], A. Korn[77], A. A. Korol[108,t], I. Korolkov[12], E. V. Korolkova[140], V. A. Korotkov[129],

O. Kortner[100], S. Kortner[100], V. V. Kostyukhin[21], V. M. Kotov[64], A. Kotwal[45], C. Kourkoumelis[9], V. Kouskoura[155], A. Koutsman[160a], R. Kowalewski[170], T. Z. Kowalski[38a], W. Kozanecki[137], A. S. Kozhin[129], V. Kral[127], V. A. Kramarenko[98], G. Kramberger[74], D. Krasnopevtsev[97], M. W. Krasny[79], A. Krasznahorkay[30], J. K. Kraus[21], A. Kravchenko[25], S. Kreiss[109], M. Kretz[58c], J. Kretzschmar[73], K. Kreutzfeldt[52], P. Krieger[159], K. Kroeninger[54], H. Kroha[100], J. Kroll[121], J. Kroseberg[21], J. Krstic[13a], U. Kruchonak[64], H. Krüger[21], T. Kruker[17], N. Krumnack[63], Z. V. Krumshteyn[64], A. Kruse[174], M. C. Kruse[45], M. Kruskal[22], T. Kubota[87], S. Kuday[4a], S. Kuehn[48], A. Kugel[58c], A. Kuhl[138], T. Kuhl[42], V. Kukhtin[64], Y. Kulchitsky[91], S. Kuleshov[32b], M. Kuna[133a,133b], J. Kunkle[121], A. Kupco[126], H. Kurashige[66], Y. A. Kurochkin[91], R. Kurumida[66], V. Kus[126], E. S. Kuwertz[148], M. Kuze[158], J. Kvita[114], A. La Rosa[49], L. La Rotonda[37a,37b], C. Lacasta[168], F. Lacava[133a,133b], J. Lacey[29], H. Lacker[16], D. Lacour[79], V. R. Lacuesta[168], E. Ladygin[64], R. Lafaye[5], B. Laforge[79], T. Lagouri[177], S. Lai[48], H. Laier[58a], L. Lambourne[77], S. Lammers[60], C. L. Lampen[7], W. Lampl[7], E. Lançon[137], U. Landgraf[48], M. P. J. Landon[75], V. S. Lang[58a], A. J. Lankford[164], F. Lanni[25], K. Lantzsch[30], S. Laplace[79], C. Lapoire[21], J. F. Laporte[137], T. Lari[90a], M. Lassnig[30], P. Laurelli[47], W. Lavrijsen[15], A. T. Law[138], P. Laycock[73], O. Le Dortz[79], E. Le Guirriec[84], E. Le Menedeu[12], T. LeCompte[6], F. Ledroit-Guillon[55], C. A. Lee[152], H. Lee[106], J. S. H. Lee[117], S. C. Lee[152], L. Lee[1], G. Lefebvre[79], M. Lefebvre[170], F. Legger[99], C. Leggett[15], A. Lehan[73], M. Lehmacher[21], G. Lehmann Miotto[30], X. Lei[7], W. A. Leight[29], A. Leisos[155], A. G. Leister[177], M. A. L. Leite[24d], R. Leitner[128], D. Lellouch[173], B. Lemmer[54], K. J. C. Leney[77], T. Lenz[21], G. Lenzen[176], B. Lenzi[30], R. Leone[7], S. Leone[123a,123b], K. Leonhardt[44], C. Leonidopoulos[46], S. Leontsinis[10], C. Leroy[94], C. G. Lester[28], C. M. Lester[121], M. Levchenko[122], J. Levêque[5], D. Levin[88], L. J. Levinson[173], M. Levy[18], A. Lewis[119], G. H. Lewis[109], A. M. Leyko[21], M. Leyton[41], B. Li[33b,u], B. Li[84], H. Li[149], H. L. Li[31], L. Li[45], L. Li[33e], S. Li[45], Y. Li[33c,v], Z. Liang[138], H. Liao[34], B. Liberti[134a], P. Lichard[30], K. Lie[166], J. Liebal[21], W. Liebig[14], C. Limbach[21], A. Limosani[87], S. C. Lin[152,w], T. H. Lin[82], F. Linde[106], B. E. Lindquist[149], J. T. Linnemann[89], E. Lipeles[121], A. Lipniacka[14], M. Lisovyi[42], T. M. Liss[166], D. Lissauer[25], A. Lister[169], A. M. Litke[138], B. Liu[152], D. Liu[152], J. B. Liu[33b], K. Liu[33b,x], L. Liu[88], M. Liu[45], M. Liu[33b], Y. Liu[33b], M. Livan[120a,120b], S. S. A. Livermore[119], A. Lleres[55], J. Llorente Merino[81], S. L. Lloyd[75], F. Lo Sterzo[152], E. Lobodzinska[42], P. Loch[7], W. S. Lockman[138], T. Loddenkoetter[21], F. K. Loebinger[83], A. E. Loevschall-Jensen[36], A. Loginov[177], T. Lohse[16], K. Lohwasser[42], M. Lokajicek[126], V. P. Lombardo[5], B. A. Long[22], J. D. Long[88], R. E. Long[71], L. Lopes[125a], D. Lopez Mateos[57], B. Lopez Paredes[140], I. Lopez Paz[12], J. Lorenz[99], N. Lorenzo Martinez[60], M. Losada[163], P. Loscutoff[15], X. Lou[41], A. Lounis[116], J. Love[6], P. A. Love[71], A. J. Lowe[144,e], F. Lu[33a], N. Lu[88], H. J. Lubatti[139], C. Luci[133a,133b], A. Lucotte[55], F. Luehring[60], W. Lukas[61], L. Luminari[133a], O. Lundberg[147a,147b], B. Lund-Jensen[148], M. Lungwitz[82], D. Lynn[25], R. Lysak[126], E. Lytken[80], H. Ma[25], L. L. Ma[33d], G. Maccarrone[47], A. Macchiolo[100], J. Machado Miguens[125a,125b], D. Macina[30], D. Madaffari[84], R. Madar[48], H. J. Maddocks[71], W. F. Mader[44], A. Madsen[167], M. Maeno[8], T. Maeno[25], E. Magradze[54], K. Mahboubi[48], J. Mahlstedt[106], S. Mahmoud[73], C. Maiani[137], C. Maidantchik[24a], A. A. Maier[100], A. Maio[125a,125b,125d], S. Majewski[115], Y. Makida[65], N. Makovec[116], P. Mal[137,y], B. Malaescu[79], Pa. Malecki[39], V. P. Maleev[122], F. Malek[55], U. Mallik[62], D. Malon[6], C. Malone[144], S. Maltezos[10], V. M. Malyshev[108], S. Malyukov[30], J. Mamuzic[13b], B. Mandelli[30], L. Mandelli[90a], I. Mandić[74], R. Mandrysch[62], J. Maneira[125a,125b], A. Manfredini[100], L. Manhaes de Andrade Filho[24b], J. A. Manjarres Ramos[160b], A. Mann[99], P. M. Manning[138], A. Manousakis-Katsikakis[9], B. Mansoulie[137], R. Mantifel[86], L. Mapelli[30], L. March[168], J. F. Marchand[29], G. Marchiori[79], M. Marcisovsky[126], C. P. Marino[170], M. Marjanovic[13a], C. N. Marques[125a], F. Marroquim[24a], S. P. Marsden[83], Z. Marshall[15], L. F. Marti[17], S. Marti-Garcia[168], B. Martin[30], B. Martin[89], T. A. Martin[171], V. J. Martin[46], B. Martin dit Latour[14], H. Martinez[137], M. Martinez[12,n], S. Martin-Haugh[130], A. C. Martyniuk[77], M. Marx[139], F. Marzano[133a], A. Marzin[30], L. Masetti[82], T. Mashimo[156], R. Mashinistov[95], J. Masik[83], A. L. Maslennikov[108], I. Massa[20a,20b], L. Massa[20a,20b], N. Massol[5], P. Mastrandrea[149], A. Mastroberardino[37a,37b], T. Masubuchi[156], P. Mättig[176], J. Mattmann[82], J. Maurer[26a], S. J. Maxfield[73], D. A. Maximov[108,t], R. Mazini[152], L. Mazzaferro[134a,134b], G. Mc Goldrick[159], S. P. Mc Kee[88], A. McCarn[88], R. L. McCarthy[149], T. G. McCarthy[29], N. A. McCubbin[130], K. W. McFarlane[56,*], J. A. Mcfayden[77], G. Mchedlidze[54], S. J. McMahon[130], R. A. McPherson[170,i], A. Meade[85], J. Mechnich[106], M. Medinnis[42], S. Meehan[31], S. Mehlhase[99], A. Mehta[73], K. Meier[58a], C. Meineck[99], B. Meirose[80], C. Melachrinos[31], B. R. Mellado Garcia[146c], F. Meloni[17], A. Mengarelli[20a,20b], S. Menke[100], E. Meoni[162], K. M. Mercurio[57], S. Mergelmeyer[21], N. Meric[137], P. Mermod[49], L. Merola[103a,103b], C. Meroni[90a], F. S. Merritt[31], H. Merritt[110], A. Messina[30,z], J. Metcalfe[25], A. S. Mete[164], C. Meyer[82], C. Meyer[121], J.-P. Meyer[137], J. Meyer[30], R. P. Middleton[130], S. Migas[73], L. Mijović[21], G. Mikenberg[173], M. Mikestikova[126], M. Mikuž[74], A. Milic[30], D. W. Miller[31], C. Mills[46], A. Milov[173], D. A. Milstead[147a,147b], D. Milstein[173], A. A. Minaenko[129], I. A. Minashvili[64], A. I. Mincer[109], B. Mindur[38a], M. Mineev[64], Y. Ming[174], L. M. Mir[12], G. Mirabelli[133a], T. Mitani[172], J. Mitrevski[99], V. A. Mitsou[168], S. Mitsui[65], A. Miucci[49], P. S. Miyagawa[140], J. U. Mjörnmark[80], T. Moa[147a,147b], K. Mochizuki[84], S. Mohapatra[35], W. Mohr[48], S. Molander[147a,147b], R. Moles-Valls[168], K. Mönig[42], C. Monini[55], J. Monk[36], E. Monnier[84], J. Montejo Berlingen[12], F. Monticelli[70], S. Monzani[133a,133b], R. W. Moore[3], N. Morange[62], D. Moreno[82],

M. Moreno Llácer[54], P. Morettini[50a], M. Morgenstern[44], M. Morii[57], S. Moritz[82], A. K. Morley[148], G. Mornacchi[30], J. D. Morris[75], L. Morvaj[102], H. G. Moser[100], M. Mosidze[51b], J. Moss[110], K. Motohashi[158], R. Mount[144], E. Mountricha[25], S. V. Mouraviev[95,*], E. J. W. Moyse[85], S. Muanza[84], R. D. Mudd[18], F. Mueller[58a], J. Mueller[124], K. Mueller[21], T. Mueller[28], T. Mueller[82], D. Muenstermann[49], Y. Munwes[154], J. A. Murillo Quijada[18], W. J. Murray[171,130], H. Musheghyan[54], E. Musto[153], A. G. Myagkov[129,aa], M. Myska[127], O. Nackenhorst[54], J. Nadal[54], K. Nagai[61], R. Nagai[158], Y. Nagai[84], K. Nagano[65], A. Nagarkar[110], Y. Nagasaka[59], M. Nagel[100], A. M. Nairz[30], Y. Nakahama[30], K. Nakamura[65], T. Nakamura[156], I. Nakano[111], H. Namasivayam[41], G. Nanava[21], R. Narayan[58b], T. Nattermann[21], T. Naumann[42], G. Navarro[163], R. Nayyar[7], H. A. Neal[88], P. Yu. Nechaeva[95], T. J. Neep[83], P. D. Nef[144], A. Negri[120a,120b], G. Negri[30], M. Negrini[20a], S. Nektarijevic[49], A. Nelson[164], T. K. Nelson[144], S. Nemecek[126], P. Nemethy[109], A. A. Nepomuceno[24a], M. Nessi[30,ab], M. S. Neubauer[166], M. Neumann[176], R. M. Neves[109], P. Nevski[25], P. R. Newman[18], D. H. Nguyen[6], R. B. Nickerson[119], R. Nicolaidou[137], B. Nicquevert[30], J. Nielsen[138], N. Nikiforou[35], A. Nikiforov[16], V. Nikolaenko[129,aa], I. Nikolic-Audit[79], K. Nikolics[49], K. Nikolopoulos[18], P. Nilsson[8], Y. Ninomiya[156], A. Nisati[133a], R. Nisius[100], T. Nobe[158], L. Nodulman[6], M. Nomachi[117], I. Nomidis[29], S. Norberg[112], M. Nordberg[30], O. Novgorodova[44], S. Nowak[100], M. Nozaki[65], L. Nozka[114], K. Ntekas[10], G. Nunes Hanninger[87], T. Nunnemann[99], E. Nurse[77], F. Nuti[87], B. J. O'Brien[46], F. O'grady[7], D. C. O'Neil[143], V. O'Shea[53], F. G. Oakham[29,d], H. Oberlack[100], T. Obermann[21], J. Ocariz[79], A. Ochi[66], M. I. Ochoa[77], S. Oda[69], S. Odaka[65], H. Ogren[60], A. Oh[83], S. H. Oh[45], C. C. Ohm[15], H. Ohman[167], W. Okamura[117], H. Okawa[25], Y. Okumura[31], T. Okuyama[156], A. Olariu[26a], A. G. Olchevski[64], S. A. Olivares Pino[46], D. Oliveira Damazio[25], E. Oliver Garcia[168], A. Olszewski[39], J. Olszowska[39], A. Onofre[125a,125e], P. U. E. Onyisi[31,o], C. J. Oram[160a], M. J. Oreglia[31], Y. Oren[154], D. Orestano[135a,135b], N. Orlando[72a,72b], C. Oropeza Barrera[53], R. S. Orr[159], B. Osculati[50a,50b], R. Ospanov[121], G. Otero y Garzon[27], H. Otono[69], M. Ouchrif[136d], E. A. Ouellette[170], F. Ould-Saada[118], A. Ouraou[137], K. P. Oussoren[106], Q. Ouyang[33a], A. Ovcharova[15], M. Owen[83], V. E. Ozcan[19a], N. Ozturk[8], K. Pachal[119], A. Pacheco Pages[12], C. Padilla Aranda[12], M. Pagáčová[48], S. Pagan Griso[15], E. Paganis[140], C. Pahl[100], F. Paige[25], P. Pais[85], K. Pajchel[118], G. Palacino[160b], S. Palestini[30], M. Palka[38b], D. Pallin[34], A. Palma[125a,125b], J. D. Palmer[18], Y. B. Pan[174], E. Panagiotopoulou[10], J. G. Panduro Vazquez[76], P. Pani[106], N. Panikashvili[88], S. Panitkin[25], D. Pantea[26a], L. Paolozzi[134a,134b], Th. D. Papadopoulou[10], K. Papageorgiou[155,l], A. Paramonov[6], D. Paredes Hernandez[34], M. A. Parker[28], F. Parodi[50a,50b], J. A. Parsons[35], U. Parzefall[48], E. Pasqualucci[133a], S. Passaggio[50a], A. Passeri[135a], F. Pastore[135a,135b,*], Fr. Pastore[76], G. Pásztor[29], S. Pataraia[176], N. D. Patel[151], J. R. Pater[83], S. Patricelli[103a,103b], T. Pauly[30], J. Pearce[170], L. E. Pedersen[36], M. Pedersen[118], S. Pedraza Lopez[168], R. Pedro[125a,125b], S. V. Peleganchuk[108], D. Pelikan[167], H. Peng[33b], B. Penning[31], J. Penwell[60], D. V. Perepelitsa[25], E. Perez Codina[160a], M. T. Pérez García-Estañ[168], V. Perez Reale[35], L. Perini[90a,90b], H. Pernegger[30], R. Perrino[72a], R. Peschke[42], V. D. Peshekhonov[64], K. Peters[30], R. F. Y. Peters[83], B. A. Petersen[30], T. C. Petersen[36], E. Petit[42], A. Petridis[147a,147b], C. Petridou[155], E. Petrolo[133a], F. Petrucci[135a,135b], N. E. Pettersson[158], R. Pezoa[32b], P. W. Phillips[130], G. Piacquadio[144], E. Pianori[171], A. Picazio[49], E. Piccaro[75], M. Piccinini[20a,20b], R. Piegaia[27], D. T. Pignotti[110], J. E. Pilcher[31], A. D. Pilkington[77], J. Pina[125a,125b,125d], M. Pinamonti[165a,165c,ac], A. Pinder[119], J. L. Pinfold[3], A. Pingel[36], B. Pinto[125a], S. Pires[79], M. Pitt[173], C. Pizio[90a,90b], L. Plazak[145a], M.-A. Pleier[25], V. Pleskot[128], E. Plotnikova[64], P. Plucinski[147a,147b], S. Poddar[58a], F. Podlyski[34], R. Poettgen[82], L. Poggioli[116], D. Pohl[21], M. Pohl[49], G. Polesello[120a], A. Policicchio[37a,37b], R. Polifka[159], A. Polini[20a], C. S. Pollard[45], V. Polychronakos[25], K. Pommès[30], L. Pontecorvo[133a], B. G. Pope[89], G. A. Popeneciu[26b], D. S. Popovic[13a], A. Poppleton[30], X. Portell Bueso[12], S. Pospisil[127], K. Potamianos[15], I. N. Potrap[64], C. J. Potter[150], C. T. Potter[115], G. Poulard[30], J. Poveda[60], V. Pozdnyakov[64], P. Pralavorio[84], A. Pranko[15], S. Prasad[30], R. Pravahan[8], S. Prell[63], D. Price[83], J. Price[73], L. E. Price[6], D. Prieur[124], M. Primavera[72a], M. Proissl[46], K. Prokofiev[47], F. Prokoshin[32b], E. Protopapadaki[137], S. Protopopescu[25], J. Proudfoot[6], M. Przybycien[38a], H. Przysiezniak[5], E. Ptacek[115], D. Puddu[135a,135b], E. Pueschel[85], D. Puldon[149], M. Purohit[25,ad], P. Puzo[116], J. Qian[88], G. Qin[53], Y. Qin[83], A. Quadt[54], D. R. Quarrie[15], W. B. Quayle[165a,165b], M. Queitsch-Maitland[83], D. Quilty[53], A. Qureshi[160b], V. Radeka[25], V. Radescu[42], S. K. Radhakrishnan[149], P. Radloff[115], P. Rados[87], F. Ragusa[90a,90b], G. Rahal[179], S. Rajagopalan[25], M. Rammensee[30], A. S. Randle-Conde[40], C. Rangel-Smith[167], K. Rao[164], F. Rauscher[99], T. C. Rave[48], T. Ravenscroft[53], M. Raymond[30], A. L. Read[118], N. P. Readioff[73], D. M. Rebuzzi[120a,120b], A. Redelbach[175], G. Redlinger[25], R. Reece[138], K. Reeves[41], L. Rehnisch[16], H. Reisin[27], M. Relich[164], C. Rembser[30], H. Ren[33a], Z. L. Ren[152], A. Renaud[116], M. Rescigno[133a], S. Resconi[90a], O. L. Rezanova[108,t], P. Reznicek[128], R. Rezvani[94], R. Richter[100], M. Ridel[79], P. Rieck[16], J. Rieger[54], M. Rijssenbeek[149], A. Rimoldi[120a,120b], L. Rinaldi[20a], E. Ritsch[61], I. Riu[12], F. Rizatdinova[113], E. Rizvi[75], S. H. Robertson[86,i], A. Robichaud-Veronneau[86], D. Robinson[28], J. E. M. Robinson[83], A. Robson[53], C. Roda[123a,123b], L. Rodrigues[30], S. Roe[30], O. Røhne[118], S. Rolli[162], A. Romaniouk[97], M. Romano[20a,20b], E. Romero Adam[168], N. Rompotis[139], M. Ronzani[48], L. Roos[79], E. Ros[168], S. Rosati[133a], K. Rosbach[49], M. Rose[76], P. Rose[138], P. L. Rosendahl[14], O. Rosenthal[142], V. Rossetti[147a,147b], E. Rossi[103a,103b], L. P. Rossi[50a], R. Rosten[139], M. Rotaru[26a], I. Roth[173], J. Rothberg[139], D. Rousseau[116], C. R. Royon[137], A. Rozanov[84], Y. Rozen[153], X. Ruan[146c], F. Rubbo[12], I. Rubinskiy[42],

V. I. Rud[98], C. Rudolph[44], M. S. Rudolph[159], F. Rühr[48], A. Ruiz-Martinez[30], Z. Rurikova[48], N. A. Rusakovich[64], A. Ruschke[99], J. P. Rutherfoord[7], N. Ruthmann[48], Y. F. Ryabov[122], M. Rybar[128], G. Rybkin[116], N. C. Ryder[119], A. F. Saavedra[151], S. Sacerdoti[27], A. Saddique[3], I. Sadeh[154], H. F.-W. Sadrozinski[138], R. Sadykov[64], F. Safai Tehrani[133a], H. Sakamoto[156], Y. Sakurai[172], G. Salamanna[135a,135b], A. Salamon[134a], M. Saleem[112], D. Salek[106], P. H. Sales De Bruin[139], D. Salihagic[100], A. Salnikov[144], J. Salt[168], D. Salvatore[37a,37b], F. Salvatore[150], A. Salvucci[105], A. Salzburger[30], D. Sampsonidis[155], A. Sanchez[103a,103b], J. Sánchez[168], V. Sanchez Martinez[168], H. Sandaker[14], R. L. Sandbach[75], H. G. Sander[82], M. P. Sanders[99], M. Sandhoff[176], T. Sandoval[28], C. Sandoval[163], R. Sandstroem[100], D. P. C. Sankey[130], A. Sansoni[47], C. Santoni[34], R. Santonico[134a,134b], H. Santos[125a], I. Santoyo Castillo[150], K. Sapp[124], A. Sapronov[64], J. G. Saraiva[125a,125d], B. Sarrazin[21], G. Sartisohn[176], O. Sasaki[65], Y. Sasaki[156], G. Sauvage[5,*], E. Sauvan[5], P. Savard[159,d], D. O. Savu[30], C. Sawyer[119], L. Sawyer[78,m], D. H. Saxon[53], J. Saxon[121], C. Sbarra[20a], A. Sbrizzi[3], T. Scanlon[77], D. A. Scannicchio[164], M. Scarcella[151], V. Scarfone[37a,37b], J. Schaarschmidt[173], P. Schacht[100], D. Schaefer[30], R. Schaefer[42], S. Schaepe[21], S. Schaetzel[58b], U. Schäfer[82], A. C. Schaffer[116], D. Schaile[99], R. D. Schamberger[149], V. Scharf[58a], V. A. Schegelsky[122], D. Scheirich[128], M. Schernau[164], M. I. Scherzer[35], C. Schiavi[50a,50b], J. Schieck[99], C. Schillo[48], M. Schioppa[37a,37b], S. Schlenker[30], E. Schmidt[48], K. Schmieden[30], C. Schmitt[82], S. Schmitt[58b], B. Schneider[17], Y. J. Schnellbach[73], U. Schnoor[44], L. Schoeffel[137], A. Schoening[58b], B. D. Schoenrock[89], A. L. S. Schorlemmer[54], M. Schott[82], D. Schouten[160a], J. Schovancova[25], S. Schramm[159], M. Schreyer[175], C. Schroeder[82], N. Schuh[82], M. J. Schultens[21], H.-C. Schultz-Coulon[58a], H. Schulz[16], M. Schumacher[48], B. A. Schumm[138], Ph. Schune[137], C. Schwanenberger[83], A. Schwartzman[144], Ph. Schwegler[100], Ph. Schwemling[137], R. Schwienhorst[89], J. Schwindling[137], T. Schwindt[21], M. Schwoerer[5], F. G. Sciacca[17], E. Scifo[116], G. Sciolla[23], W. G. Scott[130], F. Scuri[123a,123b], F. Scutti[21], J. Searcy[88], G. Sedov[42], E. Sedykh[122], S. C. Seidel[104], A. Seiden[138], F. Seifert[127], J. M. Seixas[24a], G. Sekhniaidze[103a], S. J. Sekula[40], K. E. Selbach[46], D. M. Seliverstov[122,*], G. Sellers[73], N. Semprini-Cesari[20a,20b], C. Serfon[30], L. Serin[116], L. Serkin[54], T. Serre[84], R. Seuster[160a], H. Severini[112], T. Sfiligoj[74], F. Sforza[100], A. Sfyrla[30], E. Shabalina[54], M. Shamim[115], L. Y. Shan[33a], R. Shang[166], J. T. Shank[22], M. Shapiro[15], P. B. Shatalov[96], K. Shaw[165a,165b], C. Y. Shehu[150], P. Sherwood[77], L. Shi[152,ae], S. Shimizu[66], C. O. Shimmin[164], M. Shimojima[101], M. Shiyakova[64], A. Shmeleva[95], M. J. Shochet[31], D. Short[119], S. Shrestha[63], E. Shulga[97], M. A. Shupe[7], S. Shushkevich[42], P. Sicho[126], O. Sidiropoulou[155], D. Sidorov[113], A. Sidoti[133a], F. Siegert[44], Dj. Sijacki[13a], J. Silva[125a,125d], Y. Silver[154], D. Silverstein[144], S. B. Silverstein[147a], V. Simak[127], O. Simard[5], Lj. Simic[13a], S. Simion[116], E. Simioni[82], B. Simmons[77], R. Simoniello[90a,90b], M. Simonyan[36], P. Sinervo[159], N. B. Sinev[115], V. Sipica[142], G. Siragusa[175], A. Sircar[78], A. N. Sisakyan[64,*], S. Yu. Sivoklokov[98], J. Sjölin[147a,147b], T. B. Sjursen[14], H. P. Skottowe[57], K. Yu. Skovpen[108], P. Skubic[112], M. Slater[18], T. Slavicek[127], K. Sliwa[162], V. Smakhtin[173], B. H. Smart[46], L. Smestad[14], S. Yu. Smirnov[97], Y. Smirnov[97], L. N. Smirnova[98,af], O. Smirnova[80], K. M. Smith[53], M. Smizanska[71], K. Smolek[127], A. A. Snesarev[95], G. Snidero[75], S. Snyder[25], R. Sobie[170,i], F. Socher[44], A. Soffer[154], D. A. Soh[152,ae], C. A. Solans[30], M. Solar[127], J. Solc[127], E. Yu. Soldatov[97], U. Soldevila[168], A. A. Solodkov[129], A. Soloshenko[64], O. V. Solovyanov[129], V. Solovyev[122], P. Sommer[48], H. Y. Song[33b], N. Soni[1], A. Sood[15], A. Sopczak[127], B. Sopko[127], V. Sopko[127], V. Sorin[12], M. Sosebee[8], R. Soualah[165a,165c], P. Soueid[94], A. M. Soukharev[108], D. South[42], S. Spagnolo[72a,72b], F. Spanò[76], W. R. Spearman[57], F. Spettel[100], R. Spighi[20a], G. Spigo[30], L. A. Spiller[87], M. Spousta[128], T. Spreitzer[159], B. Spurlock[8], R. D. St. Denis[53,*], S. Staerz[44], J. Stahlman[121], R. Stamen[58a], S. Stamm[16], E. Stanecka[39], R. W. Stanek[6], C. Stanescu[135a], M. Stanescu-Bellu[42], M. M. Stanitzki[42], S. Stapnes[118], E. A. Starchenko[129], J. Stark[55], P. Staroba[126], P. Starovoitov[42], R. Staszewski[39], P. Stavina[145a,*], P. Steinberg[25], B. Stelzer[143], H. J. Stelzer[30], O. Stelzer-Chilton[160a], H. Stenzel[52], S. Stern[100], G. A. Stewart[53], J. A. Stillings[21], M. C. Stockton[86], M. Stoebe[86], G. Stoicea[26a], P. Stolte[54], S. Stonjek[100], A. R. Stradling[8], A. Straessner[44], M. E. Stramaglia[17], J. Strandberg[148], S. Strandberg[147a,147b], A. Strandlie[118], E. Strauss[144], M. Strauss[112], P. Strizenec[145b], R. Ströhmer[175], D. M. Strom[115], R. Stroynowski[40], A. Struebig[105], S. A. Stucci[17], B. Stugu[14], N. A. Styles[42], D. Su[144], J. Su[124], R. Subramaniam[78], A. Succurro[12], Y. Sugaya[117], C. Suhr[107], M. Suk[127], V. V. Sulin[95], S. Sultansoy[4c], T. Sumida[67], S. Sun[57], X. Sun[33a], J. E. Sundermann[48], K. Suruliz[140], G. Susinno[37a,37b], M. R. Sutton[150], Y. Suzuki[65], M. Svatos[126], S. Swedish[169], M. Swiatlowski[144], I. Sykora[145a], T. Sykora[128], D. Ta[89], C. Taccini[135a,135b], K. Tackmann[42], J. Taenzer[159], A. Taffard[164], R. Tafirout[160a], N. Taiblum[154], H. Takai[25], R. Takashima[68], H. Takeda[66], T. Takeshita[141], Y. Takubo[65], M. Talby[84], A. A. Talyshev[108,t], J. Y. C. Tam[175], K. G. Tan[87], J. Tanaka[156], R. Tanaka[116], S. Tanaka[132], S. Tanaka[65], A. J. Tanasijczuk[143], B. B. Tannenwald[110], N. Tannoury[21], S. Tapprogge[82], S. Tarem[153], F. Tarrade[29], G. F. Tartarelli[90a], P. Tas[128], M. Tasevsky[126], T. Tashiro[67], E. Tassi[37a,37b], A. Tavares Delgado[125a,125b], Y. Tayalati[136d], F. E. Taylor[93], G. N. Taylor[87], W. Taylor[160b], F. A. Teischinger[30], M. Teixeira Dias Castanheira[75], P. Teixeira-Dias[76], K. K. Temming[48], H. Ten Kate[30], P. K. Teng[152], J. J. Teoh[117], S. Terada[65], K. Terashi[156], J. Terron[81], S. Terzo[100], M. Testa[47], R. J. Teuscher[159,i], J. Therhaag[21], T. Theveneaux-Pelzer[34], J. P. Thomas[18], J. Thomas-Wilsker[76], E. N. Thompson[35], P. D. Thompson[18], P. D. Thompson[159], R. J. Thompson[83], A. S. Thompson[53], L. A. Thomsen[36], E. Thomson[121],

M. Thomson[28], W. M. Thong[87], R. P. Thun[88,*], F. Tian[35], M. J. Tibbetts[15], V. O. Tikhomirov[95,ag], Yu. A. Tikhonov[108,t], S. Timoshenko[97], E. Tiouchichine[84], P. Tipton[177], S. Tisserant[84], T. Todorov[5], S. Todorova-Nova[128], B. Toggerson[7], J. Tojo[69], S. Tokár[145a], K. Tokushuku[65], K. Tollefson[89], L. Tomlinson[83], M. Tomoto[102], L. Tompkins[31], K. Toms[104], N. D. Topilin[64], E. Torrence[115], H. Torres[143], E. Torró Pastor[168], J. Toth[84,ah], F. Touchard[84], D. R. Tovey[140], H. L. Tran[116], T. Trefzger[175], L. Tremblet[30], A. Tricoli[30], I. M. Trigger[160a], S. Trincaz-Duvoid[79], M. F. Tripiana[12], W. Trischuk[159], B. Trocmé[55], C. Troncon[90a], M. Trottier-McDonald[143], M. Trovatelli[135a,135b], P. True[89], M. Trzebinski[39], A. Trzupek[39], C. Tsarouchas[30], J. C.-L. Tseng[119], P. V. Tsiareshka[91], D. Tsionou[137], G. Tsipolitis[10], N. Tsirintanis[9], S. Tsiskaridze[12], V. Tsiskaridze[48], E. G. Tskhadadze[51a], I. I. Tsukerman[96], V. Tsulaia[15], S. Tsuno[65], D. Tsybychev[149], A. Tudorache[26a], V. Tudorache[26a], A. N. Tuna[121], S. A. Tupputi[20a,20b], S. Turchikhin[98,af], D. Turecek[127], I. Turk Cakir[4d], R. Turra[90a,90b], P. M. Tuts[35], A. Tykhonov[49], M. Tylmad[147a,147b], M. Tyndel[130], K. Uchida[21], I. Ueda[156], R. Ueno[29], M. Ughetto[84], M. Ugland[14], M. Uhlenbrock[21], F. Ukegawa[161], G. Unal[30], A. Undrus[25], G. Unel[164], F. C. Ungaro[48], Y. Unno[65], C. Unverdorben[99], D. Urbaniec[35], P. Urquijo[87], G. Usai[8], A. Usanova[61], L. Vacavant[84], V. Vacek[127], B. Vachon[86], N. Valencic[106], S. Valentinetti[20a,20b], A. Valero[168], L. Valery[34], S. Valkar[128], E. Valladolid Gallego[168], S. Vallecorsa[49], J. A. Valls Ferrer[168], W. Van Den Wollenberg[106], P. C. Van Der Deijl[106], R. van der Geer[106], H. van der Graaf[106], R. Van Der Leeuw[106], D. van der Ster[30], N. van Eldik[30], P. van Gemmeren[6], J. Van Nieuwkoop[143], I. van Vulpen[106], M. C. van Woerden[30], M. Vanadia[133a,133b], W. Vandelli[30], R. Vanguri[121], A. Vaniachine[6], P. Vankov[42], F. Vannucci[79], G. Vardanyan[178], R. Vari[133a], E. W. Varnes[7], T. Varol[85], D. Varouchas[79], A. Vartapetian[8], K. E. Varvell[151], F. Vazeille[34], T. Vazquez Schroeder[54], J. Veatch[7], F. Veloso[125a,125c], S. Veneziano[133a], A. Ventura[72a,72b], D. Ventura[85], M. Venturi[170], N. Venturi[159], A. Venturini[23], V. Vercesi[120a], M. Verducci[133a,133b], W. Verkerke[106], J. C. Vermeulen[106], A. Vest[44], M. C. Vetterli[143,d], O. Viazlo[80], I. Vichou[166], T. Vickey[146c,ai], O. E. Vickey Boeriu[146c], G. H. A. Viehhauser[119], S. Viel[169], R. Vigne[30], M. Villa[20a,20b], M. Villaplana Perez[90a,90b], E. Vilucchi[47], M. G. Vincter[29], V. B. Vinogradov[64], J. Virzi[15], I. Vivarelli[150], F. Vives Vaque[3], S. Vlachos[10], D. Vladoiu[99], M. Vlasak[127], A. Vogel[21], M. Vogel[32a], P. Vokac[127], G. Volpi[123a,123b], M. Volpi[87], H. von der Schmitt[100], H. von Radziewski[48], E. von Toerne[21], V. Vorobel[128], K. Vorobev[97], M. Vos[168], R. Voss[30], J. H. Vossebeld[73], N. Vranjes[137], M. Vranjes Milosavljevic[13a], V. Vrba[126], M. Vreeswijk[106], T. Vu Anh[48], R. Vuillermet[30], I. Vukotic[31], Z. Vykydal[127], P. Wagner[21], W. Wagner[176], H. Wahlberg[70], S. Wahrmund[44], J. Wakabayashi[102], J. Walder[71], R. Walker[99], W. Walkowiak[142], R. Wall[177], P. Waller[73], B. Walsh[177], C. Wang[152,aj], C. Wang[45], F. Wang[174], H. Wang[15], H. Wang[40], J. Wang[42], J. Wang[33a], K. Wang[86], R. Wang[104], S. M. Wang[152], T. Wang[21], X. Wang[177], C. Wanotayaroj[115], A. Warburton[86], C. P. Ward[28], D. R. Wardrope[77], M. Warsinsky[48], A. Washbrook[46], C. Wasicki[42], P. M. Watkins[18], A. T. Watson[18], I. J. Watson[151], M. F. Watson[18], G. Watts[139], S. Watts[83], B. M. Waugh[77], S. Webb[83], M. S. Weber[17], S. W. Weber[175], J. S. Webster[31], A. R. Weidberg[119], P. Weigell[100], B. Weinert[60], J. Weingarten[54], C. Weiser[48], H. Weits[106], P. S. Wells[30], T. Wenaus[25], D. Wendland[16], Z. Weng[152,ae], T. Wengler[30], S. Wenig[30], N. Wermes[21], M. Werner[48], P. Werner[30], M. Wessels[58a], J. Wetter[162], K. Whalen[29], A. White[8], M. J. White[1], R. White[32b], S. White[123a,123b], D. Whiteson[164], D. Wicke[176], F. J. Wickens[130], W. Wiedenmann[174], M. Wielers[130], P. Wienemann[21], C. Wiglesworth[36], L. A. M. Wiik-Fuchs[21], P. A. Wijeratne[77], A. Wildauer[100], M. A. Wildt[42,ak], H. G. Wilkens[30], J. Z. Will[99], H. H. Williams[121], S. Williams[28], C. Willis[89], S. Willocq[85], A. Wilson[88], J. A. Wilson[18], I. Wingerter-Seez[5], F. Winklmeier[115], B. T. Winter[21], M. Wittgen[144], T. Wittig[43], J. Wittkowski[99], S. J. Wollstadt[82], M. W. Wolter[39], H. Wolters[125a,125c], B. K. Wosiek[39], J. Wotschack[30], M. J. Woudstra[83], K. W. Wozniak[39], M. Wright[53], M. Wu[55], S. L. Wu[174], X. Wu[49], Y. Wu[88], E. Wulf[35], T. R. Wyatt[83], B. M. Wynne[46], S. Xella[36], M. Xiao[137], D. Xu[33a], L. Xu[33b,al], B. Yabsley[151], S. Yacoob[146b,am], R. Yakabe[66], M. Yamada[65], H. Yamaguchi[156], Y. Yamaguchi[117], A. Yamamoto[65], K. Yamamoto[63], S. Yamamoto[156], T. Yamamura[156], T. Yamanaka[156], K. Yamauchi[102], Y. Yamazaki[66], Z. Yan[22], H. Yang[33e], H. Yang[174], U. K. Yang[83], Y. Yang[110], S. Yanush[92], L. Yao[33a], W.-M. Yao[15], Y. Yasu[65], E. Yatsenko[42], K. H. Yau Wong[21], J. Ye[40], S. Ye[25], I. Yeletskikh[64], A. L. Yen[57], E. Yildirim[42], M. Yilmaz[4b], R. Yoosoofmiya[124], K. Yorita[172], R. Yoshida[6], K. Yoshihara[156], C. Young[144], C. J. S. Young[30], S. Youssef[22], D. R. Yu[15], J. Yu[8], J. M. Yu[88], J. Yu[113], L. Yuan[66], A. Yurkewicz[107], I. Yusuff[28,an], B. Zabinski[39], R. Zaidan[62], A. M. Zaitsev[129,aa], A. Zaman[149], S. Zambito[23], L. Zanello[133a,133b], D. Zanzi[100], C. Zeitnitz[176], M. Zeman[127], A. Zemla[38a], K. Zengel[23], O. Zenin[129], T. Ženiš[145a], D. Zerwas[116], G. Zevi della Porta[57], D. Zhang[88], F. Zhang[174], H. Zhang[89], J. Zhang[6], L. Zhang[152], X. Zhang[33d], Z. Zhang[116], Z. Zhao[33b], A. Zhemchugov[64], J. Zhong[119], B. Zhou[88], L. Zhou[35], N. Zhou[164], C. G. Zhu[33d], H. Zhu[33a], J. Zhu[88], Y. Zhu[33b], X. Zhuang[33a], K. Zhukov[95], A. Zibell[175], D. Zieminska[60], N. I. Zimine[64], C. Zimmermann[82], R. Zimmermann[21], S. Zimmermann[21], S. Zimmermann[48], Z. Zinonos[54], M. Ziolkowski[142], G. Zobernig[174], A. Zoccoli[20a,20b], M. zur Nedden[16], G. Zurzolo[103a,103b], V. Zutshi[107], L. Zwalinski[30]

[1] Department of Physics, University of Adelaide, Adelaide, Australia
[2] Physics Department, SUNY Albany, Albany, NY, USA

[3] Department of Physics, University of Alberta, Edmonton, AB, Canada
[4] [(a)] Department of Physics, Ankara University, Ankara, Turkey; [(b)] Department of Physics, Gazi University, Ankara, Turkey; [(c)] Division of Physics, TOBB University of Economics and Technology, Ankara, Turkey; [(d)] Turkish Atomic Energy Authority, Ankara, Turkey
[5] LAPP, CNRS/IN2P3 and Université de Savoie, Annecy-le-Vieux, France
[6] High Energy Physics Division, Argonne National Laboratory, Argonne, IL, USA
[7] Department of Physics, University of Arizona, Tucson, AZ, USA
[8] Department of Physics, The University of Texas at Arlington, Arlington, TX, USA
[9] Physics Department, University of Athens, Athens, Greece
[10] Physics Department, National Technical University of Athens, Zografou, Greece
[11] Institute of Physics, Azerbaijan Academy of Sciences, Baku, Azerbaijan
[12] Institut de Física d'Altes Energies and Departament de Física de la Universitat Autònoma de Barcelona, Barcelona, Spain
[13] [(a)] Institute of Physics, University of Belgrade, Belgrade, Serbia; [(b)] Vinca Institute of Nuclear Sciences, University of Belgrade, Belgrade, Serbia
[14] Department for Physics and Technology, University of Bergen, Bergen, Norway
[15] Physics Division, Lawrence Berkeley National Laboratory and University of California, Berkeley, CA, USA
[16] Department of Physics, Humboldt University, Berlin, Germany
[17] Albert Einstein Center for Fundamental Physics and Laboratory for High Energy Physics, University of Bern, Bern, Switzerland
[18] School of Physics and Astronomy, University of Birmingham, Birmingham, UK
[19] [(a)] Department of Physics, Bogazici University, Istanbul, Turkey; [(b)] Department of Physics, Dogus University, Istanbul, Turkey; [(c)] Department of Physics Engineering, Gaziantep University, Gaziantep, Turkey
[20] [(a)] INFN Sezione di Bologna, Bologna, Italy; [(b)] Dipartimento di Fisica e Astronomia, Università di Bologna, Bologna, Italy
[21] Physikalisches Institut, University of Bonn, Bonn, Germany
[22] Department of Physics, Boston University, Boston, MA, USA
[23] Department of Physics, Brandeis University, Waltham, MA, USA
[24] [(a)] Universidade Federal do Rio De Janeiro COPPE/EE/IF, Rio de Janeiro, Brazil; [(b)] Federal University of Juiz de Fora (UFJF), Juiz de Fora, Brazil; [(c)] Federal University of Sao Joao del Rei (UFSJ), Sao Joao del Rei, Brazil; [(d)] Instituto de Fisica, Universidade de Sao Paulo, São Paulo, Brazil
[25] Physics Department, Brookhaven National Laboratory, Upton, NY, USA
[26] [(a)] National Institute of Physics and Nuclear Engineering, Bucharest, Romania; [(b)] Physics Department, National Institute for Research and Development of Isotopic and Molecular Technologies, Cluj Napoca, Romania; [(c)] University Politehnica Bucharest, Bucharest, Romania; [(d)] West University in Timisoara, Timisoara, Romania
[27] Departamento de Física, Universidad de Buenos Aires, Buenos Aires, Argentina
[28] Cavendish Laboratory, University of Cambridge, Cambridge, UK
[29] Department of Physics, Carleton University, Ottawa, ON, Canada
[30] CERN, Geneva, Switzerland
[31] Enrico Fermi Institute, University of Chicago, Chicago, IL, USA
[32] [(a)] Departamento de Física, Pontificia Universidad Católica de Chile, Santiago, Chile; [(b)] Departamento de Física, Universidad Técnica Federico Santa María, Valparaiso, Chile
[33] [(a)] Institute of High Energy Physics, Chinese Academy of Sciences, Beijing, China; [(b)] Department of Modern Physics, University of Science and Technology of China, Hefei, Anhui, China; [(c)] Department of Physics, Nanjing University, Nanjing, Jiangsu, China; [(d)] School of Physics, Shandong University, Jinan, Shandong, China; [(e)] Physics Department,, Shanghai Jiao Tong University, Shanghai, China
[34] Laboratoire de Physique Corpusculaire, Clermont Université and Université Blaise Pascal and CNRS/IN2P3, Clermont-Ferrand, France
[35] Nevis Laboratory, Columbia University, Irvington, NY, USA
[36] Niels Bohr Institute, University of Copenhagen, Copenhagen, Denmark
[37] [(a)] INFN Gruppo Collegato di Cosenza, Laboratori Nazionali di Frascati, Frascati, Italy; [(b)] Dipartimento di Fisica, Università della Calabria, Rende, Italy
[38] [(a)] Faculty of Physics and Applied Computer Science, AGH University of Science and Technology, Kraków, Poland;

[b] Marian Smoluchowski Institute of Physics, Jagiellonian University, Kraków, Poland
[39] The Henryk Niewodniczanski Institute of Nuclear Physics, Polish Academy of Sciences, Kraków, Poland
[40] Physics Department, Southern Methodist University, Dallas, TX, USA
[41] Physics Department, University of Texas at Dallas, Richardson, TX, USA
[42] DESY, Hamburg and Zeuthen, Germany
[43] Institut für Experimentelle Physik IV, Technische Universität Dortmund, Dortmund, Germany
[44] Institut für Kern- und Teilchenphysik, Technische Universität Dresden, Dresden, Germany
[45] Department of Physics, Duke University, Durham, NC, USA
[46] SUPA-School of Physics and Astronomy, University of Edinburgh, Edinburgh, UK
[47] INFN Laboratori Nazionali di Frascati, Frascati, Italy
[48] Fakultät für Mathematik und Physik, Albert-Ludwigs-Universität, Freiburg, Germany
[49] Section de Physique, Université de Genève, Geneva, Switzerland
[50] [a] INFN Sezione di Genova, Genoa, Italy; [b] Dipartimento di Fisica, Università di Genova, Genova, Italy
[51] [a] E. Andronikashvili Institute of Physics, Iv. Javakhishvili Tbilisi State University, Tbilisi, Georgia; [b] High Energy Physics Institute, Tbilisi State University, Tbilisi, Georgia
[52] II Physikalisches Institut, Justus-Liebig-Universität Giessen, Giessen, Germany
[53] SUPA-School of Physics and Astronomy, University of Glasgow, Glasgow, UK
[54] II Physikalisches Institut, Georg-August-Universität, Göttingen, Germany
[55] Laboratoire de Physique Subatomique et de Cosmologie, Université Grenoble-Alpes, CNRS/IN2P3, Grenoble, France
[56] Department of Physics, Hampton University, Hampton, VA, USA
[57] Laboratory for Particle Physics and Cosmology, Harvard University, Cambridge, MA, USA
[58] [a] Kirchhoff-Institut für Physik, Ruprecht-Karls-Universität Heidelberg, Heidelberg, Germany; [b] Physikalisches Institut, Ruprecht-Karls-Universität Heidelberg, Heidelberg, Germany; [c] ZITI Institut für technische Informatik, Ruprecht-Karls-Universität Heidelberg, Mannheim, Germany
[59] Faculty of Applied Information Science, Hiroshima Institute of Technology, Hiroshima, Japan
[60] Department of Physics, Indiana University, Bloomington, IN, USA
[61] Institut für Astro- und Teilchenphysik, Leopold-Franzens-Universität, Innsbruck, Austria
[62] University of Iowa, Iowa City, IA, USA
[63] Department of Physics and Astronomy, Iowa State University, Ames, IA, USA
[64] Joint Institute for Nuclear Research, JINR Dubna, Dubna, Russia
[65] KEK, High Energy Accelerator Research Organization, Tsukuba, Japan
[66] Graduate School of Science, Kobe University, Kobe, Japan
[67] Faculty of Science, Kyoto University, Kyoto, Japan
[68] Kyoto University of Education, Kyoto, Japan
[69] Department of Physics, Kyushu University, Fukuoka, Japan
[70] Instituto de Física La Plata, Universidad Nacional de La Plata and CONICET, La Plata, Argentina
[71] Physics Department, Lancaster University, Lancaster, UK
[72] [a] INFN Sezione di Lecce, Lecce, Italy; [b] Dipartimento di Matematica e Fisica, Università del Salento, Lecce, Italy
[73] Oliver Lodge Laboratory, University of Liverpool, Liverpool, UK
[74] Department of Physics, Jožef Stefan Institute and University of Ljubljana, Ljubljana, Slovenia
[75] School of Physics and Astronomy, Queen Mary University of London, London, UK
[76] Department of Physics, Royal Holloway University of London, Surrey, UK
[77] Department of Physics and Astronomy, University College London, London, UK
[78] Louisiana Tech University, Ruston, LA, USA
[79] Laboratoire de Physique Nucléaire et de Hautes Energies, UPMC and Université Paris-Diderot and CNRS/IN2P3, Paris, France
[80] Fysiska institutionen, Lunds universitet, Lund, Sweden
[81] Departamento de Fisica Teorica C-15, Universidad Autonoma de Madrid, Madrid, Spain
[82] Institut für Physik, Universität Mainz, Mainz, Germany
[83] School of Physics and Astronomy, University of Manchester, Manchester, UK
[84] CPPM, Aix-Marseille Université and CNRS/IN2P3, Marseille, France
[85] Department of Physics, University of Massachusetts, Amherst, MA, USA
[86] Department of Physics, McGill University, Montreal, QC, Canada

[87] School of Physics, University of Melbourne, Parkville, VIC, Australia
[88] Department of Physics, The University of Michigan, Ann Arbor, MI, USA
[89] Department of Physics and Astronomy, Michigan State University, East Lansing, MI, USA
[90] [(a)] INFN Sezione di Milano, Milan, Italy; [(b)] Dipartimento di Fisica, Università di Milano, Milan, Italy
[91] B.I. Stepanov Institute of Physics, National Academy of Sciences of Belarus, Minsk, Republic of Belarus
[92] National Scientific and Educational Centre for Particle and High Energy Physics, Minsk, Republic of Belarus
[93] Department of Physics, Massachusetts Institute of Technology, Cambridge, MA, USA
[94] Group of Particle Physics, University of Montreal, Montreal, QC, Canada
[95] P.N. Lebedev Institute of Physics, Academy of Sciences, Moscow, Russia
[96] Institute for Theoretical and Experimental Physics (ITEP), Moscow, Russia
[97] Moscow Engineering and Physics Institute (MEPhI), Moscow, Russia
[98] D.V. Skobeltsyn Institute of Nuclear Physics, M.V. Lomonosov Moscow State University, Moscow, Russia
[99] Fakultät für Physik, Ludwig-Maximilians-Universität München, Munich, Germany
[100] Max-Planck-Institut für Physik (Werner-Heisenberg-Institut), Munich, Germany
[101] Nagasaki Institute of Applied Science, Nagasaki, Japan
[102] Graduate School of Science and Kobayashi-Maskawa Institute, Nagoya University, Nagoya, Japan
[103] [(a)] INFN Sezione di Napoli, Naples, Italy; [(b)] Dipartimento di Fisica, Università di Napoli, Naples, Italy
[104] Department of Physics and Astronomy, University of New Mexico, Albuquerque, NM, USA
[105] Institute for Mathematics, Astrophysics and Particle Physics, Radboud University Nijmegen/Nikhef, Nijmegen, The Netherlands
[106] Nikhef National Institute for Subatomic Physics and University of Amsterdam, Amsterdam, The Netherlands
[107] Department of Physics, Northern Illinois University, DeKalb, IL, USA
[108] Budker Institute of Nuclear Physics, SB RAS, Novosibirsk, Russia
[109] Department of Physics, New York University, New York, NY, USA
[110] Ohio State University, Columbus, OH, USA
[111] Faculty of Science, Okayama University, Okayama, Japan
[112] Homer L. Dodge Department of Physics and Astronomy, University of Oklahoma, Norman, OK, USA
[113] Department of Physics, Oklahoma State University, Stillwater, OK, USA
[114] Palacký University, RCPTM, Olomouc, Czech Republic
[115] Center for High Energy Physics, University of Oregon, Eugene, OR, USA
[116] LAL, Université Paris-Sud and CNRS/IN2P3, Orsay, France
[117] Graduate School of Science, Osaka University, Osaka, Japan
[118] Department of Physics, University of Oslo, Oslo, Norway
[119] Department of Physics, Oxford University, Oxford, UK
[120] [(a)] INFN Sezione di Pavia, Pavia, Italy; [(b)] Dipartimento di Fisica, Università di Pavia, Pavia, Italy
[121] Department of Physics, University of Pennsylvania, Philadelphia, PA, USA
[122] Petersburg Nuclear Physics Institute, Gatchina, Russia
[123] [(a)] INFN Sezione di Pisa, Pisa, Italy; [(b)] Dipartimento di Fisica E. Fermi, Università di Pisa, Pisa, Italy
[124] Department of Physics and Astronomy, University of Pittsburgh, Pittsburgh, PA, USA
[125] [(a)] Laboratorio de Instrumentacao e Fisica Experimental de Particulas-LIP, Lisbon, Portugal; [(b)] Faculdade de Ciências, Universidade de Lisboa, Lisbon, Portugal; [(c)] Department of Physics, University of Coimbra, Coimbra, Portugal; [(d)] Centro de Física Nuclear da Universidade de Lisboa, Lisbon, Portugal; [(e)] Departamento de Fisica, Universidade do Minho, Braga, Portugal; [(f)] Departamento de Fisica Teorica y del Cosmos and CAFPE, Universidad de Granada, Granada, Spain; [(g)] Dep Fisica and CEFITEC of Faculdade de Ciencias e Tecnologia, Universidade Nova de Lisboa, Caparica, Portugal
[126] Institute of Physics, Academy of Sciences of the Czech Republic, Prague, Czech Republic
[127] Czech Technical University in Prague, Prague, Czech Republic
[128] Faculty of Mathematics and Physics, Charles University in Prague, Prague, Czech Republic
[129] State Research Center Institute for High Energy Physics, Protvino, Russia
[130] Particle Physics Department, Rutherford Appleton Laboratory, Didcot, UK
[131] Physics Department, University of Regina, Regina, SK, Canada
[132] Ritsumeikan University, Kusatsu, Shiga, Japan
[133] [(a)] INFN Sezione di Roma, Rome, Italy; [(b)] Dipartimento di Fisica, Sapienza Università di Roma, Rome, Italy

[134] [(a)] INFN Sezione di Roma Tor Vergata, Rome, Italy; [(b)] Dipartimento di Fisica, Università di Roma Tor Vergata, Rome, Italy
[135] [(a)] INFN Sezione di Roma Tre, Rome, Italy; [(b)] Dipartimento di Matematica e Fisica, Università Roma Tre, Rome, Italy
[136] [(a)] Faculté des Sciences Ain Chock, Réseau Universitaire de Physique des Hautes Energies-Université Hassan II, Casablanca, Morocco; [(b)] Centre National de l'Energie des Sciences Techniques Nucleaires, Rabat, Morocco; [(c)] Faculté des Sciences Semlalia, Université Cadi Ayyad, LPHEA-Marrakech, Marrakech, Morocco; [(d)] Faculté des Sciences, Université Mohamed Premier and LPTPM, Oujda, Morocco; [(e)] Faculté des Sciences, Université Mohammed V-Agdal, Rabat, Morocco
[137] DSM/IRFU (Institut de Recherches sur les Lois Fondamentales de l'Univers), CEA Saclay (Commissariat à l'Energie Atomique et aux Energies Alternatives), Gif-sur-Yvette, France
[138] Santa Cruz Institute for Particle Physics, University of California Santa Cruz, Santa Cruz, CA, USA
[139] Department of Physics, University of Washington, Seattle, WA, USA
[140] Department of Physics and Astronomy, University of Sheffield, Sheffield, UK
[141] Department of Physics, Shinshu University, Nagano, Japan
[142] Fachbereich Physik, Universität Siegen, Siegen, Germany
[143] Department of Physics, Simon Fraser University, Burnaby, BC, Canada
[144] SLAC National Accelerator Laboratory, Stanford, CA, USA
[145] [(a)] Faculty of Mathematics, Physics and Informatics, Comenius University, Bratislava, Slovak Republic; [(b)] Department of Subnuclear Physics, Institute of Experimental Physics of the Slovak Academy of Sciences, Kosice, Slovak Republic
[146] [(a)] Department of Physics, University of Cape Town, Cape Town, South Africa; [(b)] Department of Physics, University of Johannesburg, Johannesburg, South Africa; [(c)] School of Physics, University of the Witwatersrand, Johannesburg, South Africa
[147] [(a)] Department of Physics, Stockholm University, Stockholm, Sweden; [(b)] The Oskar Klein Centre, Stockholm, Sweden
[148] Physics Department, Royal Institute of Technology, Stockholm, Sweden
[149] Departments of Physics and Astronomy and Chemistry, Stony Brook University, Stony Brook, NY, USA
[150] Department of Physics and Astronomy, University of Sussex, Brighton, UK
[151] School of Physics, University of Sydney, Sydney, Australia
[152] Institute of Physics, Academia Sinica, Taipei, Taiwan
[153] Department of Physics, Technion, Israel Institute of Technology, Haifa, Israel
[154] Raymond and Beverly Sackler School of Physics and Astronomy, Tel Aviv University, Tel Aviv, Israel
[155] Department of Physics, Aristotle University of Thessaloniki, Thessaloniki, Greece
[156] International Center for Elementary Particle Physics and Department of Physics, The University of Tokyo, Tokyo, Japan
[157] Graduate School of Science and Technology, Tokyo Metropolitan University, Tokyo, Japan
[158] Department of Physics, Tokyo Institute of Technology, Tokyo, Japan
[159] Department of Physics, University of Toronto, Toronto, ON, Canada
[160] [(a)] TRIUMF, Vancouver, BC, Canada; [(b)] Department of Physics and Astronomy, York University, Toronto, ON, Canada
[161] Faculty of Pure and Applied Sciences, University of Tsukuba, Tsukuba, Japan
[162] Department of Physics and Astronomy, Tufts University, Medford, MA, USA
[163] Centro de Investigaciones, Universidad Antonio Narino, Bogota, Colombia
[164] Department of Physics and Astronomy, University of California Irvine, Irvine, CA, USA
[165] [(a)] INFN Gruppo Collegato di Udine, Sezione di Trieste, Udine, Italy; [(b)] ICTP, Trieste, Italy; [(c)] Dipartimento di Chimica, Fisica e Ambiente, Università di Udine, Udine, Italy
[166] Department of Physics, University of Illinois, Urbana, IL, USA
[167] Department of Physics and Astronomy, University of Uppsala, Uppsala, Sweden
[168] Instituto de Física Corpuscular (IFIC) and Departamento de Física Atómica, Molecular y Nuclear and Departamento de Ingeniería Electrónica and Instituto de Microelectrónica de Barcelona (IMB-CNM), University of Valencia and CSIC, Valencia, Spain
[169] Department of Physics, University of British Columbia, Vancouver, BC, Canada
[170] Department of Physics and Astronomy, University of Victoria, Victoria, BC, Canada
[171] Department of Physics, University of Warwick, Coventry, UK
[172] Waseda University, Tokyo, Japan
[173] Department of Particle Physics, The Weizmann Institute of Science, Rehovot, Israel
[174] Department of Physics, University of Wisconsin, Madison, WI, USA

[175] Fakultät für Physik und Astronomie, Julius-Maximilians-Universität, Würzburg, Germany
[176] Fachbereich C Physik, Bergische Universität Wuppertal, Wuppertal, Germany
[177] Department of Physics, Yale University, New Haven, CT, USA
[178] Yerevan Physics Institute, Yerevan, Armenia
[179] Centre de Calcul de l'Institut National de Physique Nucléaire et de Physique des Particules (IN2P3), Villeurbanne, France

[a] Also at Department of Physics, King's College London, London, UK
[b] Also at Institute of Physics, Azerbaijan Academy of Sciences, Baku, Azerbaijan
[c] Also at Particle Physics Department, Rutherford Appleton Laboratory, Didcot, UK
[d] Also at TRIUMF, Vancouver, BC, Canada
[e] Also at Department of Physics, California State University, Fresno, CA, USA
[f] Also at Tomsk State University, Tomsk, Russia
[g] Also at CPPM, Aix-Marseille Université and CNRS/IN2P3, Marseille, France
[h] Also at Università di Napoli Parthenope, Naples, Italy
[i] Also at Institute of Particle Physics (IPP), Victoria, Canada
[j] Also at Department of Physics, St. Petersburg State Polytechnical University, St. Petersburg, Russia
[k] Also at Chinese University of Hong Kong, Hong Kong, China
[l] Also at Department of Financial and Management Engineering, University of the Aegean, Chios, Greece
[m] Also at Louisiana Tech University, Ruston, LA, USA
[n] Also at Institucio Catalana de Recerca i Estudis Avancats, ICREA, Barcelona, Spain
[o] Also at Department of Physics, The University of Texas at Austin, Austin, TX, USA
[p] Also at Institute of Theoretical Physics, Ilia State University, Tbilisi, Georgia
[q] Also at CERN, Geneva, Switzerland
[r] Also at Ochadai Academic Production, Ochanomizu University, Tokyo, Japan
[s] Also at Manhattan College, New York, NY, USA
[t] Also at Novosibirsk State University, Novosibirsk, Russia
[u] Also at Institute of Physics, Academia Sinica, Taipei, Taiwan
[v] Also at LAL, Université Paris-Sud and CNRS/IN2P3, Orsay, France
[w] Also at Academia Sinica Grid Computing, Institute of Physics, Academia Sinica, Taipei, Taiwan
[x] Also at Laboratoire de Physique Nucléaire et de Hautes Energies, UPMC and Université Paris-Diderot and CNRS/IN2P3, Paris, France
[y] Also at School of Physical Sciences, National Institute of Science Education and Research, Bhubaneswar, India
[z] Also at Dipartimento di Fisica, Sapienza Università di Roma, Rome, Italy
[aa] Also at Moscow Institute of Physics and Technology State University, Dolgoprudny, Russia
[ab] Also at Section de Physique, Université de Genève, Geneva, Switzerland
[ac] Also at International School for Advanced Studies (SISSA), Trieste, Italy
[ad] Also at Department of Physics and Astronomy, University of South Carolina, Columbia, SC, USA
[ae] Also at School of Physics and Engineering, Sun Yat-sen University, Guangzhou, China
[af] Also at Faculty of Physics, M.V. Lomonosov Moscow State University, Moscow, Russia
[ag] Also at Moscow Engineering and Physics Institute (MEPhI), Moscow, Russia
[ah] Also at Institute for Particle and Nuclear Physics, Wigner Research Centre for Physics, Budapest, Hungary
[ai] Also at Department of Physics, Oxford University, Oxford, UK
[aj] Also at Department of Physics, Nanjing University, Jiangsu, China
[ak] Also at Institut für Experimentalphysik, Universität Hamburg, Hamburg, Germany
[al] Also at Department of Physics, The University of Michigan, Ann Arbor, MI, USA
[am] Also at Discipline of Physics, University of KwaZulu-Natal, Durban, South Africa
[an] Also at University of Malaya, Department of Physics, Kuala Lumpur, Malaysia
* Deceased

Eur. Phys. J. C (2012) 72:2241
DOI 10.1140/epjc/s10052-012-2241-5

THE EUROPEAN PHYSICAL JOURNAL C

Letter

ATLAS search for a heavy gauge boson decaying to a charged lepton and a neutrino in pp collisions at $\sqrt{s} = 7$ TeV

The ATLAS Collaboration[⋆]
CERN, Geneva, Switzerland

Received: 20 September 2012 / Revised: 18 October 2012 / Published online: 8 December 2012

Abstract The ATLAS detector at the LHC is used to search for high-mass states, such as heavy charged gauge bosons (W'), decaying to a charged lepton (electron or muon) and a neutrino. Results are presented based on the analysis of pp collisions at a center-of-mass energy of 7 TeV corresponding to an integrated luminosity of 4.7 fb^{-1}. No excess beyond Standard Model expectations is observed. A W' with Sequential Standard Model couplings is excluded at the 95 % credibility level for masses up to 2.55 TeV. Excited chiral bosons (W^*) with equivalent coupling strength are excluded for masses up to 2.42 TeV.

1 Introduction

High-energy collisions at the CERN Large Hadron Collider provide the opportunity to search unexplored regions for physics beyond the Standard Model (SM) of strong and electroweak interactions. One extension common to many models is the existence of additional heavy gauge bosons, the charged ones commonly denoted W'. Such particles are most easily searched for in their decay to a charged lepton (electron or muon) and a neutrino.

This letter describes such a search performed using 7 TeV pp collision data collected with the ATLAS detector during 2011 corresponding to a total integrated luminosity of 4.7 fb^{-1}. The data are used to extend current limits [1–4] on σB (cross section times branching fraction) for $W' \to \ell\nu$ ($\ell = e$ or μ) as a function of W' mass. Limits are evaluated in the context of the Sequential Standard Model (SSM), i.e. the extended gauge model of Ref. [5] with the W' coupling to WZ set to zero. In this model, the W' has the same couplings to fermions as the SM W boson and a width which increases linearly with the W' mass. A previous letter [4] described a similar search with a subset (1.0 fb^{-1}) of the data used in this study. Here the mass range of the search is extended and the limits in the previously covered region are significantly improved because of the fivefold increase in integrated luminosity. An improved lower mass limit assuming SSM coupling strength is also reported.

A search is also performed for the charged partners, denoted W^*, of the chiral boson excitations described in Ref. [6] with theoretical motivation in Ref. [7]. The anomalous (magnetic-moment type) coupling of the W^* leads to kinematic distributions significantly different from those of the W'. The previous search for this resonance [3] was performed using data acquired in 2010 with an integrated luminosity less than 1 % of that used here. The search region is expanded to both lower and higher masses and the limits are considerably improved in the region covered by the previous search. A lower mass limit is evaluated by fixing the W^* coupling strengths to give the same partial decay widths as the SSM W'.

The analysis presented here identifies event candidates in the electron and muon channels, sets separate limits for $W'/W^* \to e\nu$ and $W'/W^* \to \mu\nu$, and then combines these assuming a common branching fraction for the two channels. The kinematic variable used to identify the W'/W^* is the transverse mass

$$m_{\mathrm{T}} = \sqrt{2 p_{\mathrm{T}} E_{\mathrm{T}}^{\mathrm{miss}} (1 - \cos\varphi_{\ell\nu})}, \tag{1}$$

whose distribution has a Jacobian peak and falls sharply above the resonance mass. Here p_{T} is the lepton transverse momentum, $E_{\mathrm{T}}^{\mathrm{miss}}$ is the magnitude of the missing transverse momentum (missing E_{T}), and $\varphi_{\ell\nu}$ is the angle between the p_{T} and missing E_{T} vectors. Throughout this letter, transverse refers to the plane perpendicular to the colliding beams, longitudinal means parallel to the beams, θ and φ are the polar and azimuthal angles with respect to the longitudinal direction, and pseudorapidity is defined as $\eta = -\ln(\tan(\theta/2))$.

Figure 1 shows the electron η and the m_{T} spectra for $W' \to e\nu$ and $W^* \to e\nu$, with $m_{W'} = m_{W^*} = 2.0$ TeV, from

⋆ e-mail: atlas.publications@cern.ch

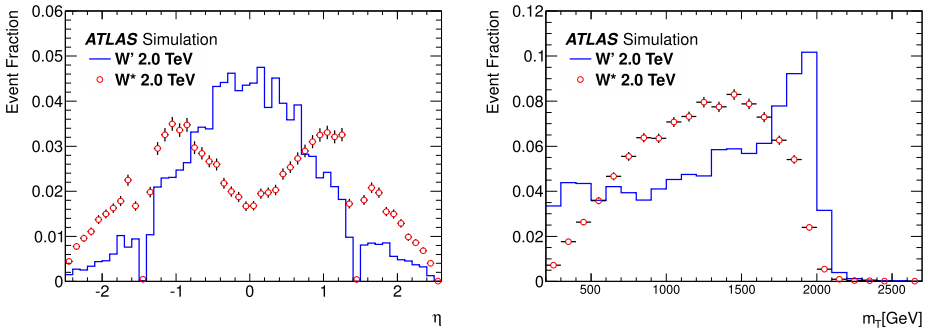

Fig. 1 Reconstructed electron η (*left*) and m_{T} (*right*) distributions for $W' \to e\nu$ and $W^* \to e\nu$ with $m_{W'} = m_{W^*} = 2.0$ TeV. All distributions are normalised to unit area

the event generation, detector simulation and reconstruction described below. The difference in kinematic shape is evident: the W' is more central in pseudorapidity and has a sharper m_{T} spectrum.

The main background to the $W'/W^* \to \ell\nu$ signal comes from the high-m_{T} tail of SM W boson decay to the same final state. Other backgrounds are Z bosons decaying into two leptons where one lepton is not reconstructed, W or Z decaying to τ leptons where a τ subsequently decays to an electron or muon, and diboson production. These are collectively referred to as the electroweak (EW) background. In addition, there is a background contribution from $t\bar{t}$ and single-top production which is most important for the lowest W' masses considered here, where it constitutes about 15 % of the background after event selection. Other strong-interaction background sources, where a light or heavy hadron decays semileptonically or a jet is misidentified as an electron, are estimated to be at most 10 % of the total background in the electron channel and a negligible fraction in the muon channel. These are called QCD background in the following.

2 Detector, trigger and reconstruction

The ATLAS detector [8] has three major components: the inner tracking detector, the calorimeter and the muon spectrometer. Charged particle tracks and vertices are reconstructed with silicon pixel and silicon strip detectors covering $|\eta| < 2.5$ and straw-tube transition radiation detectors covering $|\eta| < 2.0$, all immersed in a homogeneous 2 T magnetic field provided by a superconducting solenoid. This tracking detector is surrounded by a finely segmented, hermetic calorimeter system that covers $|\eta| < 4.9$ and provides three-dimensional reconstruction of particle showers. It uses liquid argon for the inner EM (electromagnetic) compartment followed by a hadronic compartment based on scintillating tiles in the central region ($|\eta| < 1.7$) and liquid argon for higher $|\eta|$. Outside the calorimeter, there is a muon spectrometer with air-core toroids providing a magnetic field, whose integral averages about 3 Tm. The deflection of the muons in the magnetic field is measured with three layers of precision drift-tube chambers for $|\eta| < 2.0$ and one layer of cathode-strip chambers followed by two layers of drift-tube chambers for $2.0 < |\eta| < 2.7$. Additional resistive-plate and thin-gap chambers provide muon triggering capability and measurement of the φ coordinate.

The data used in the electron channel are recorded with a trigger requiring the presence of an EM cluster (i.e. an energy cluster in the EM compartment of the calorimeter) with energy corresponding to an electron with $p_{\mathrm{T}} > 80$ GeV. This substantial increase over the p_{T} threshold used in the previous analysis [4] is required to maintain high efficiency (above 99 %) and keep the trigger rate at a tolerable level for the high luminosity used to acquire the bulk of the data. For the muon channel, matching tracks in the muon spectrometer and inner detector with combined $p_{\mathrm{T}} > 22$ GeV are used to select events. Events are also recorded if a muon with $p_{\mathrm{T}} > 40$ GeV is found in the muon spectrometer. These are the same p_{T} thresholds used in the previous analysis and, despite stricter hit requirements imposed for the higher-luminosity data, the muon trigger efficiency remains 80–90 % in the regions of interest.

Each EM cluster with $E_{\mathrm{T}} > 85$ GeV and $|\eta| < 1.37$ or $1.52 < |\eta| < 2.47$ is considered as an electron candidate if it matches an inner detector track. The electron direction is defined as that of the reconstructed track and its energy as that of the cluster, with a small η-dependent energy scale correction. The energy resolution is 2 % for $E_{\mathrm{T}} \approx 50$ GeV and approaches 1 % in the high-E_{T} range relevant to this analysis. To discriminate against hadronic jets, requirements are

imposed on the lateral shower shapes in the first two layers of the EM compartment of the calorimeter and on the fraction of energy leaking into the hadronic compartment. A hit in the first pixel layer is required to reduce background from photon conversions in the inner detector material. These requirements result in about 90 % identification efficiency for electrons with $E_{\mathrm{T}} > 85$ GeV and a 2×10^{-4} probability to falsely identify jets as electrons before isolation requirements are imposed [9].

Muons are required to have $p_{\mathrm{T}} > 25$ GeV, where the momentum of the muon is obtained by combining the inner detector and muon spectrometer measurements. The p_{T} threshold allows the high trigger efficiency. To ensure precise measurement of the momentum, muons are required to have hits in all three muon layers and are restricted to those η-ranges where the muon spectrometer alignment is best understood: approximately $|\eta| < 1.0$ and $1.3 < |\eta| < 2.0$. The average momentum resolution is about 15 % at $p_{\mathrm{T}} = 1$ TeV. About 80 % of the muons in these η-ranges are reconstructed, with most of the loss coming from regions with limited detector coverage.

The missing E_{T} in each event is evaluated by summing over energy-calibrated physics objects (jets, photons and leptons) and adding corrections for calorimeter deposits away from these objects [10]. This is an improvement over the previous analysis which did not include the energy calibration.

This analysis makes use of all the $\sqrt{s} = 7$ TeV data collected in 2011 for which the relevant detector systems were operating properly. The integrated luminosity for the data used in this study is 4.7 fb^{-1} in both the electron and muon decay channels. The uncertainty on this measurement is 3.9 % [11, 12].

3 Simulation

Except for the QCD background, which is measured with data, expected signal and background levels are evaluated using simulated samples, normalised with calculated cross sections and the integrated luminosity of the data.

The W' signal and the W/Z boson backgrounds are generated with PYTHIA 6.421 [13] using the modified leading-order (LO) parton distribution functions (PDFs) of Ref. [14]. PYTHIA is also used for the $W^* \to \ell\nu$ event generation, but with initial kinematics generated at LO with COMPHEP [15] using the CTEQ6L1 PDFs [16]. The $t\bar{t}$ background is generated with MC@NLO 3.41 [17] using the CTEQ6.6 [18] PDFs. For all samples, final-state photon radiation is handled by PHOTOS [19]. The ATLAS full detector simulation [20] based on GEANT4 [21] is used to propagate the particles and account for the response of the detector.

The PYTHIA signal model for W' has $V-A$ SM couplings to fermions but does not include interference between W and W'. For both W' and W^*, decays to channels other than $e\nu$ and $\mu\nu$, including $\tau\nu$, ud, sc and tb, are included in the calculation of the widths but are not explicitly included as signal or background. At high mass ($m_{W'} > 1$ TeV), the branching fraction to each of the lepton decay channels is 8.2 %.

The $W \to \ell\nu$ events are reweighted to have the NNLO (next-to-next-to-leading-order) QCD mass dependence of ZWPROD [22] following the G_μ scheme [23] and using the MSTW2008 PDFs [24]. Higher-order electroweak corrections (in addition to the photon radiation included in the simulation) are calculated using HORACE [23, 25]. In the high-mass region of interest, the electroweak corrections reduce the cross sections by 11 % at $m_{\ell\nu} = 1$ TeV and by 18 % at $m_{\ell\nu} = 2$ TeV.

The $W \to \ell\nu$ and $Z \to \ell\ell$ cross sections are calculated at NNLO using FEWZ [26, 27] with the same PDFs, scheme and electroweak corrections used in the ZWPROD event reweighting. The $W' \to \ell\nu$ cross sections are calculated in the same way, except the electroweak corrections beyond final-state radiation are not included because the calculation for the SM W cannot be applied directly. The $t\bar{t}$ cross section is calculated at approximate-NNLO [28–30] assuming a top-quark mass of 172.5 GeV. The $W^* \to \ell\nu$ cross-section evaluation is performed with COMPHEP using the CTEQ6L1 PDFs (i.e. same as the event generation). The signal and most important background cross sections are listed in Table 1.

Cross-section uncertainties for $W' \to \ell\nu$ and the W/Z [9] and $t\bar{t}$ [31] backgrounds are estimated from the MSTW2008 PDF error sets, the difference between the MSTW2008 and CTEQ6.6 PDFs, and variation of renormalization and factorization scales by a factor of two. The estimates from the three sources are combined in quadrature. Most of the net uncertainty comes from the PDF error sets and the MSTW-CTEQ difference, in roughly equal proportion. The $W^* \to \ell\nu$ cross-section uncertainties are evaluated with the CTEQ61 [16] PDF error sets.

4 Event selection

The primary vertex for each event is required to have at least three tracks with $p_{\mathrm{T}} > 0.4$ GeV and to have a longitudinal distance less than 200 mm from the center of the collision region. Due to the high luminosity, there are an average of more than ten additional interactions per event in the data used for this analysis. The primary vertex is defined to be the one with the highest summed track p_{T}^2. Spurious tails in missing E_{T}, arising from calorimeter noise and other detector problems are suppressed by checking the quality of

Table 1 Calculated values of σB for $W' \to \ell\nu$, $W^* \to \ell\nu$ and the leading backgrounds. The value for $t\bar{t} \to \ell X$ includes all final states with at least one lepton (e, μ or τ). The others are exclusive and are used for both $\ell = e$ and $\ell = \mu$. All calculations are NNLO except W^* which is LO and $t\bar{t}$ which is approximate-NNLO

Process	Mass [GeV]	σB [pb]
$W' \to \ell\nu$	300	130.5
	400	41.6
	500	17.25
	600	8.27
	750	3.20
	1000	0.837
	1250	0.261
	1500	0.0887
	1750	0.0325
	2000	0.0126
	2250	0.00526
	2500	0.00235
	2750	0.001156
	3000	0.000643
$W^* \to \ell\nu$	400	29.6
	500	12.6
	750	2.34
	1000	0.610
	1250	0.188
	1500	0.0636
	1750	0.0226
	2000	0.00819
	2250	0.00299
	2500	0.000109
	2750	0.000391
	3000	0.000138
$W \to \ell\nu$		10460
$Z/\gamma^* \to \ell\ell$ ($m_{Z/\gamma^*} > 60$ GeV)		989
$t\bar{t} \to \ell X$		89.4

each reconstructed jet and discarding events where any jet has a shape indicating such problems, following Ref. [32]. In addition, the inner detector track associated with the electron or muon is required to be compatible with originating from the primary vertex, specifically to have transverse distance of closest approach $|d_0| < 1$ mm and longitudinal distance at this point $|z_0| < 5$ mm in the electron channel. For the muon channel, the requirements are $|d_0| < 0.2$ mm and $|z_0| < 1$ mm. Events are required to have exactly one candidate electron or one candidate muon satisfying these requirements.

To suppress the QCD background, the lepton is required to be isolated. In the electron channel, the isolation energy is measured with the calorimeter in a cone $\Delta R < 0.4$ ($\Delta R \equiv \sqrt{(\Delta\eta)^2 + (\Delta\varphi)^2}$) around the electron track, and the requirement is $\sum E_{\mathrm{T}} < 9$ GeV, where the sum includes all calorimeter energy clusters in the cone excluding the core energy deposited by the electron. The sum is corrected to account for additional interactions and leakage of the electron energy outside this core. In the muon channel, the isolation energy is measured using inner detector tracks with $p_{\mathrm{T}}^{\mathrm{trk}} > 1$ GeV in a cone $\Delta R < 0.3$ around the muon track. The isolation requirement is $\sum p_{\mathrm{T}}^{\mathrm{trk}} < 0.05\ p_{\mathrm{T}}$, where the muon track is excluded from the sum. The scaling of the threshold with the muon p_{T} reduces efficiency losses due to radiation from the muon at high p_{T}.

Table 2 Expected numbers of events from the various background sources in each decay channel for $m_{\mathrm{T}} > 794$ GeV, the region used to search for a W' with a mass of 1000 GeV in the electron and muon channels. The $W \to \ell\nu$ and $Z \to \ell\ell$ entries include the expected contributions from the τ-lepton. The uncertainties are those from the Monte Carlo statistics

	$e\nu$	$\mu\nu$
$W \to \ell\nu$	14.2±0.5	11.2±0.5
$Z \to \ell\ell$	0.022±0.001	0.76±0.01
diboson	1.2±0.2	0.71±0.15
$t\bar{t}$	0.24±0.11	0.09±0.05
QCD	0.8±0.3	–
Total	16.5±0.6	12.8±0.5

Missing E_{T} thresholds are imposed to further suppress the background from QCD and W+jets (events where the SM W recoils against hadronic jets). In both channels, the threshold used for the charged lepton p_{T} is also applied to the missing E_{T}: $E_{\mathrm{T}}^{\mathrm{miss}} > 85$ GeV for the electron channel and $E_{\mathrm{T}}^{\mathrm{miss}} > 25$ GeV for the muon channel.

The above constitute the event preselection requirements. An m_{T} threshold varying with W' or W^* mass and decay channel is applied after preselection to establish the final event counts.

In the electron channel, the QCD background is estimated from data using the *ABCD* technique [33] with the isolation energy and missing E_{T} serving as discriminants. Consistent results are obtained using the *inverted isolation* technique described in Ref. [3].

The QCD background for the muon channel is evaluated using the *matrix method* [31]. This background is less than 1 % of the total background, and so it is neglected in the following.

The same reconstruction and event selection are applied to both data and simulated samples. Figure 2 shows the charged lepton p_{T}, missing E_{T}, and m_{T} spectra for events with $m_{\mathrm{T}} > 200$ GeV in each channel after event preselection. The data, the expected background, and three examples of W' signals at different masses are shown. The m_{T} threshold, which is below that used in all of the final selections, discriminates against the W+jets and QCD backgrounds.

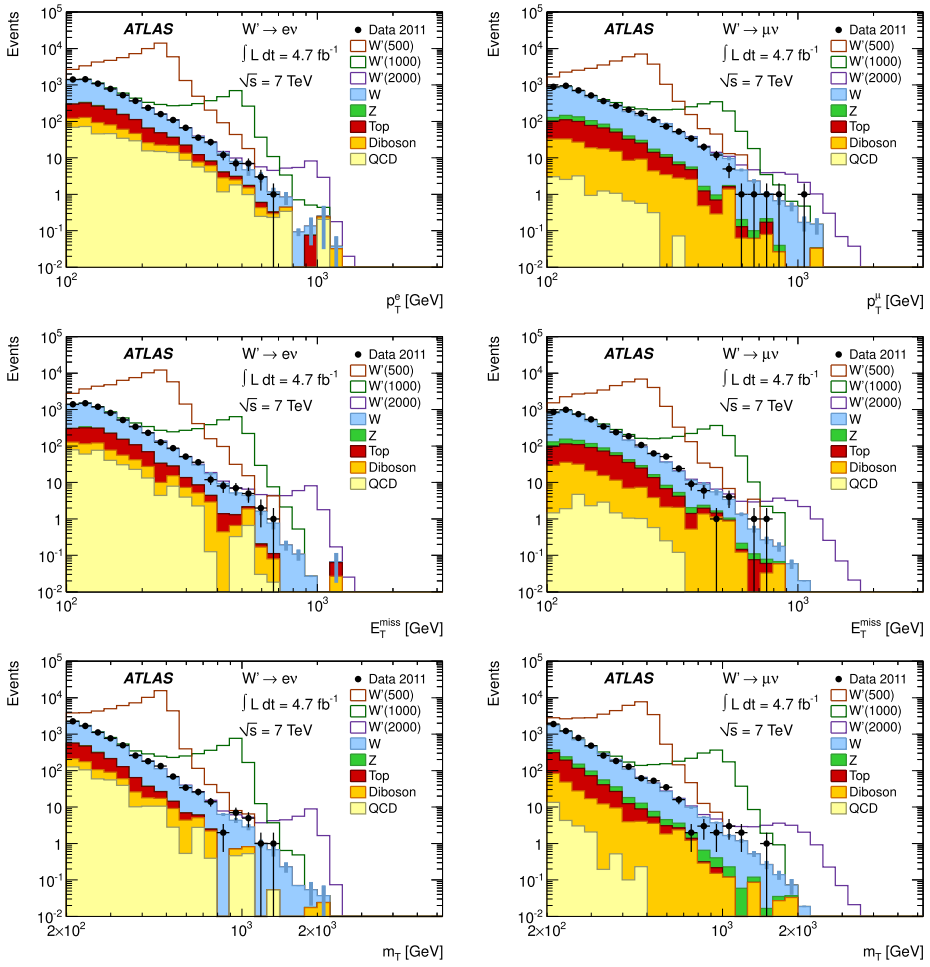

Fig. 2 Spectra of charged lepton p_{T} (*top*), missing E_{T} (*center*) and m_{T} (*bottom*) for the electron (*left*) and muon (*right*) channels for events with $m_{\mathrm{T}} > 200$ GeV after event preselection. The points represent data and the filled histograms show the stacked backgrounds. Open histograms are $W' \to \ell\nu$ signals added to the background with masses in GeV indicated in parentheses in the legend. The QCD backgrounds estimated from data are also shown. The signal and other background samples are normalised using the integrated luminosity of the data and the NNLO (approximate-NNLO for $t\bar{t}$) cross sections listed in Table 1. The error bars on the data and background sums are statistical, i.e. the latter do not include the systematic uncertainties used in the statistical analysis

The m_{T} spectra for the data and expected background are consistent within statistical and systematic uncertainties.

Table 2 shows the contributions to the background for $m_{\mathrm{T}} > 794$ GeV, the region used to search for a W' with a mass of 1000 GeV. The $W \to \ell\nu$ background dominates and the background for the electron channel is higher than that for muons because of the difference in acceptance.

5 Statistical analysis and systematics

Discovery significance and σB limits are evaluated independently for W' and W^* following the same procedure as for the previous analysis [4]. The observed number of events N_{obs} is the count after final selection including the requirement $m_{\mathrm{T}} > m_{\mathrm{T_{min}}}$, with that threshold chosen sepa-

Table 3 Event selection efficiencies for the $W' \to e\nu$ and $W' \to \mu\nu$ searches. The first three columns are the W' mass, m_{T} threshold and decay channel. The next two are the signal selection efficiency, $\varepsilon_{\mathrm{sig}}$, and the prediction for the number of signal events, N_{sig}, obtained with this efficiency. The uncertainty on N_{sig} includes contributions from the uncertainty on the cross sections but not from that on the integrated luminosity

$m_{W'}$ [GeV]	$m_{\mathrm{T_{min}}}$ [GeV]		$\varepsilon_{\mathrm{sig}}$	N_{sig}
300	251	$e\nu$	0.288 ± 0.023	176000±19000
		$\mu\nu$	0.186 ± 0.016	114000±13000
400	355	$e\nu$	0.237 ± 0.023	46200±5600
		$\mu\nu$	0.153 ± 0.018	30000±4100
500	447	$e\nu$	0.237 ± 0.023	19200±2300
		$\mu\nu$	0.145 ± 0.019	11700±1800
600	501	$e\nu$	0.307 ± 0.024	11900±1300
		$\mu\nu$	0.195 ± 0.017	7600±900
750	631	$e\nu$	0.297 ± 0.023	4470±470
		$\mu\nu$	0.189 ± 0.016	2840±320
1000	794	$e\nu$	0.339 ± 0.023	1330±130
		$\mu\nu$	0.223 ± 0.015	877±90
1250	1000	$e\nu$	0.323 ± 0.024	395±47
		$\mu\nu$	0.212 ± 0.019	259±34
1500	1122	$e\nu$	0.351 ± 0.026	146±20
		$\mu\nu$	0.237 ± 0.021	99±14
1750	1413	$e\nu$	0.280 ± 0.024	42.7±6.8
		$\mu\nu$	0.179 ± 0.024	27.3±5.2
2000	1413	$e\nu$	0.317 ± 0.025	18.8±3.2
		$\mu\nu$	0.215 ± 0.022	12.7±2.3
2250	1413	$e\nu$	0.315 ± 0.022	7.8±1.5
		$\mu\nu$	0.218 ± 0.017	5.4±1.0
2500	1413	$e\nu$	0.276 ± 0.024	3.1±1.4
		$\mu\nu$	0.184 ± 0.024	2.0±1.0
2750	1413	$e\nu$	0.217 ± 0.020	1.18±0.59
		$\mu\nu$	0.149 ± 0.020	0.81±0.41
3000	1413	$e\nu$	0.143 ± 0.027	0.43±0.25
		$\mu\nu$	0.106 ± 0.031	0.32±0.20

Table 4 Event selection efficiencies for the $W^* \to e\nu$ and $W^* \to \mu\nu$ searches. The first three columns are the W^* mass, m_{T} threshold and decay channel. The next two are the signal selection efficiency, $\varepsilon_{\mathrm{sig}}$, and the prediction for the number of signal events, N_{sig}, obtained with this efficiency. The uncertainty on N_{sig} includes contributions from the uncertainty on the cross sections but not from that on the integrated luminosity

m_{W^*} [GeV]	$m_{\mathrm{T_{min}}}$ [GeV]		$\varepsilon_{\mathrm{sig}}$	N_{sig}
400	316	$e\nu$	0.189 ± 0.021	26300±3200
		$\mu\nu$	0.118 ± 0.020	16400±2900
500	398	$e\nu$	0.182 ± 0.020	10800±1300
		$\mu\nu$	0.114 ± 0.021	6740±1300
750	562	$e\nu$	0.224 ± 0.021	2460±270
		$\mu\nu$	0.143 ± 0.019	1570±230
1000	708	$e\nu$	0.267 ± 0.022	766±83
		$\mu\nu$	0.172 ± 0.017	493±60
1250	891	$e\nu$	0.254 ± 0.021	225±26
	794	$\mu\nu$	0.216 ± 0.015	192±21
1500	1122	$e\nu$	0.212 ± 0.021	63.5±9.0
	1000	$\mu\nu$	0.192 ± 0.016	57.5±7.5
1750	1122	$e\nu$	0.330 ± 0.023	35.0±5.0
		$\mu\nu$	0.208 ± 0.016	22.1±3.2
2000	1413	$e\nu$	0.258 ± 0.021	9.9±1.7
		$\mu\nu$	0.156 ± 0.018	6.0±1.2
2250	1413	$e\nu$	0.338 ± 0.024	4.8±1.0
		$\mu\nu$	0.211 ± 0.016	2.97±0.63
2500	1413	$e\nu$	0.397 ± 0.025	2.03±0.53
		$\mu\nu$	0.241 ± 0.016	1.23±0.32
2750	1413	$e\nu$	0.449 ± 0.027	0.83±0.28
		$\mu\nu$	0.260 ± 0.016	0.48±0.16
3000	1413	$e\nu$	0.475 ± 0.029	0.31±0.13
		$\mu\nu$	0.276 ± 0.016	0.179±0.077

rately for each mass and decay channel to maximize sensitivity. A Bayesian posterior probability distribution for the signal σB is evaluated with a Poisson likelihood at each mass for each decay channel and for the combination of the two channels. A positive, flat prior is used for the signal σB, and Gaussian distributions are used for the three nuisance parameters: $\varepsilon_{\mathrm{sig}}$, the efficiency to select signal events, N_{bg}, the expected number of background events and L_{int}, the integrated luminosity. For each observed posterior, an ensemble of expected posteriors is generated assuming no signal and the same prior distributions for N_{bg} and L_{int}.

Each of the observed posteriors is used to evaluate an observed limit on σB, and the ensemble of expected posteriors provides the corresponding expected limit distribution. All limits are at 95 % CL (credibility level). Discovery significance is assessed from the fraction of the expected posteriors that are more signal-like than the observation.

The values and uncertainties for $\varepsilon_{\mathrm{sig}}$ are presented in Tables 3 and 4, and those for N_{bg} and N_{obs} in Table 5. The $\varepsilon_{\mathrm{sig}}$ tables also give the predicted numbers of signal events, N_{sig}, with their uncertainties accounting for the uncertainties in both $\varepsilon_{\mathrm{sig}}$ and the cross-section calculations.

The maximum value for the $W' \to \ell\nu$ signal selection efficiency is at $m_{W'} = 1500$ GeV. For lower masses, the efficiency falls because the relative m_{T} threshold, $m_{\mathrm{T_{min}}}/m_{W'}$, is increased to reduce the background level. For higher masses, the efficiency falls because a large fraction of the cross section goes via off-shell production with $m_{\ell\nu} \ll m_{W'}$. This effect is not seen for $W^* \to \ell\nu$ because its derivative couplings [6] suppress off-shell production at low mass.

The fraction of fully simulated signal events that pass the event selection and are above the m_{T} threshold provides the initial estimate of $\varepsilon_{\mathrm{sig}}$ for each channel and mass. For W',

Table 5 Background levels and observed counts for the $W' \to \ell\nu$ and $W^* \to \ell\nu$ searches in both the electron and muon channels. The first two columns are the m_{T} threshold and decay channel, followed by the expected number of background events, N_{bg}, and the number of events observed in data, N_{obs}. The uncertainty on N_{bg} includes contributions from the uncertainties on the cross sections but not from that on the integrated luminosity

$m_{\mathrm{T_{min}}}$ [GeV]		N_{bg}	N_{obs}
251	$e\nu$	3190±260	3105
	$\mu\nu$	1950±190	2023
316	$e\nu$	1240±100	1229
	$\mu\nu$	773±72	750
355	$e\nu$	761±64	734
	$\mu\nu$	492±44	491
398	$e\nu$	467±39	474
	$\mu\nu$	285±26	307
447	$e\nu$	277±24	293
	$\mu\nu$	178±15	179
501	$e\nu$	164±14	159
	$\mu\nu$	113±10	117
562	$e\nu$	95.8±8.4	90
	$\mu\nu$	66.2±5.8	64
631	$e\nu$	54.5±5.2	56
	$\mu\nu$	40.0±3.7	29
708	$e\nu$	30.7±3.0	30
	$\mu\nu$	22.7±2.2	13
794	$e\nu$	16.5±1.7	16
	$\mu\nu$	12.8±1.4	11
891	$e\nu$	9.0±1.0	14
1000	$e\nu$	5.15±0.69	7
	$\mu\nu$	3.86±0.58	6
1122	$e\nu$	2.57±0.42	2
	$\mu\nu$	2.21±0.34	3
1413	$e\nu$	0.64±0.18	0
	$\mu\nu$	0.51±0.12	1

small corrections are then made to account for the difference in acceptance at NNLO (obtained from FEWZ) and that in the LO simulation. These vary from a 10 % increase for $m_{W'} = 500$ GeV to an 11 % decrease for $m_{W'} = 2500$ GeV. Contributions from $W' \to \tau\nu$ with the τ-lepton decaying leptonically have been neglected. These would increase the W' signal strength by 3–4 % for the highest masses. The background level is estimated for each mass by summing the EW and $t\bar{t}$ event counts from simulation, and adding the small QCD contribution in the electron channel.

The uncertainties on $\varepsilon_{\mathrm{sig}}$, N_{bg} and L_{int} account for experimental and theoretical systematic effects as well as the statistics of the simulation samples. The uncertainty on L_{int} is included separately to allow for the correlation between signal and background. The experimental systematic uncertainties include efficiencies for the electron or muon trigger, reconstruction and selection. Lepton momentum and missing E_{T} response, characterised by scale and resolution, are also included. Most of these performance metrics are measured at relatively low p_{T} and their values are extrapolated to the high-p_{T} regime relevant to this analysis. The uncertainties in these extrapolations are included but their contributions are small compared to the total uncertainty on $\varepsilon_{\mathrm{sig}}$ or N_{bg}. The uncertainty on the QCD background estimate also contributes to the background-level uncertainties for the electron channel. Theoretical uncertainties include those from the cross-section calculations (see Sect. 3) and from the W' acceptance corrections. The values for the uncertainties are similar to those obtained in the previous analysis. Table 6 summarizes the uncertainties on the event selection efficiencies and background levels for the $W' \to \ell\nu$ signal with $m_{W'} = 1500$ GeV using $m_{\mathrm{T}} > 1122$ GeV.

Table 6 Relative uncertainties on the event selection efficiency and background level for a W' with a mass of 1500 GeV. The efficiency uncertainties include contributions from the trigger, reconstruction and event selection. The cross-section uncertainty for $\varepsilon_{\mathrm{sig}}$ is that assigned to the acceptance correction described in the text. The cross-section uncertainty on N_{bg} is that from the cross-section calculations. The last row gives the total uncertainties

Source	$\varepsilon_{\mathrm{sig}}$		N_{bg}	
	$e\nu$	$\mu\nu$	$e\nu$	$\mu\nu$
Efficiency	5 %	2 %	4 %	2 %
Energy/momentum resolution	–	1 %	3 %	–
Energy/momentum scale	2 %	–	4 %	–
Missing E_{T}	–	–	2 %	4 %
QCD background	–	–	4 %	–
Monte Carlo statistics	5 %	9 %	10 %	9 %
Cross section (shape/level)	3 %	3 %	12 %	12 %
Total	7 %	9 %	17 %	16 %

6 Results

None of the observations for any mass point in either channel or their combination shows an excess with significance above three sigma, so there is no evidence for the observation of $W' \to \ell\nu$ or $W^* \to \ell\nu$. Tables 7 and 8 and Fig. 3 present the 95 % CL observed limits on σB for both $W' \to \ell\nu$ and $W^* \to \ell\nu$ in the electron channel, the muon channel and their combination. The tables also give the limits obtained without systematic uncertainties and with various subsets. The uncertainties on the signal efficiency have very little effect on the final limits, and the background-level and luminosity uncertainties are important only for the lowest masses. The figure also shows the expected limits and the

Table 7 Observed upper limits on σB for $W' \to e\nu$, $W' \to \mu\nu$ and the combination of the two. The *first two columns* are the W' mass and decay channel. The *following columns* are the 95 % CL limits with headers indicating the nuisance parameters for which uncertainties are included: S for the event selection efficiency ($\varepsilon_{\mathrm{sig}}$), B for the background level (N_{bg}), and L for the integrated luminosity (L_{int}). These values neglect correlations between the two channels for the combined limit. The only important correlation, that from the background cross section, is included in the column $\mathrm{SB_cL}$. The last column in each row (SBL for e and μ and $\mathrm{SB_cL}$ for $e\mu$) is the final limit (including all systematic uncertainties) for the mass listed in the first column. These are the limits shown in Fig. 3 (left)

$m_{W'}$ [GeV]		95 % CL limit on σB [fb]				
		none	S	SB	SBL	$\mathrm{SB_cL}$
300	e	50	51	356	500	
	μ	173	179	514	557	
	$e\mu$	61	62	295	329	389
400	e	36	37	111	124	
	μ	62	65	140	153	
	$e\mu$	30	30	84	92	110
500	e	43	44	65	70	
	μ	42	44	64	69	
	$e\mu$	32	32	47	50	56
600	e	16	17	25	27	
	μ	28	29	36	39	
	$e\mu$	14	14	21	22	24
750	e	12	13	15	15	
	μ	9.0	9.2	11	11	
	$e\mu$	6.8	6.8	8.1	8.4	9.2
1000	e	5.6	6.0	6.3	6.5	
	μ	7.1	7.2	7.5	7.7	
	$e\mu$	4.1	4.1	4.4	4.4	4.6
1250	e	5.5	5.5	5.6	5.7	
	μ	8.2	8.4	8.5	8.6	
	$e\mu$	4.7	4.7	4.8	4.9	4.9
1500	e	2.8	2.8	2.9	2.9	
	μ	5.2	5.4	5.4	5.4	
	$e\mu$	2.3	2.3	2.3	2.4	2.4
1750	e	2.3	2.3	2.3	2.3	
	μ	5.2	5.5	5.5	5.5	
	$e\mu$	1.9	1.9	1.9	1.9	1.9
2000	e	2.0	2.0	2.0	2.1	
	μ	4.3	4.4	4.5	4.5	
	$e\mu$	1.6	1.6	1.6	1.6	1.6
2250	e	2.0	2.1	2.1	2.1	
	μ	4.2	4.3	4.3	4.4	
	$e\mu$	1.6	1.6	1.6	1.6	1.6
2500	e	2.3	2.4	2.4	2.4	
	μ	5.0	5.3	5.3	5.3	
	$e\mu$	1.9	1.9	1.9	1.9	1.9
2750	e	2.9	3.0	3.0	3.0	
	μ	6.2	6.6	6.6	6.7	
	$e\mu$	2.3	2.4	2.4	2.4	2.4
3000	e	4.5	5.0	5.0	5.0	
	μ	8.7	15	15	15	
	$e\mu$	3.5	3.7	3.7	3.7	3.7

Table 8 Observed upper limits on σB for $W^* \to e\nu$, $W^* \to \mu\nu$ and the combination of the two. The columns are as for Table 7. The final (rightmost) limits are shown in Fig. 3 (right)

m_{W^*} [GeV]		95 % CL limit on σB [fb]				
		none	S	SB	SBL	$\mathrm{SB_cL}$
400	e	68	71	236	264	
	μ	68	75	263	289	
	$e\mu$	47	48	167	186	222
500	e	57	60	114	125	
	μ	93	106	160	171	
	$e\mu$	57	58	96	104	116
750	e	16	17	22	24	
	μ	23	25	30	31	
	$e\mu$	13	13	17	18	19
1000	e	10	10	11	11	
	μ	7.0	7.2	7.8	8.1	
	$e\mu$	5.0	5.1	5.6	5.8	6.2
1250	e	11	11	11	11	
	μ	7.3	7.4	7.8	7.9	
	$e\mu$	6.7	6.7	6.9	7.0	7.2
1500	e	4.6	4.7	4.8	4.8	
	μ	9.0	9.2	9.3	9.4	
	$e\mu$	4.2	4.3	4.3	4.3	4.4
1750	e	3.0	3.0	3.0	3.0	
	μ	6.0	6.1	6.1	6.2	
	$e\mu$	2.5	2.5	2.6	2.6	2.6
2000	e	2.5	2.5	2.5	2.5	
	μ	5.9	6.2	6.2	6.2	
	$e\mu$	2.1	2.1	2.1	2.1	2.1
2250	e	1.9	1.9	1.9	1.9	
	μ	4.4	4.5	4.5	4.5	
	$e\mu$	1.6	1.6	1.6	1.6	1.6
2500	e	1.5	1.5	1.5	1.5	
	μ	3.8	3.9	3.9	3.9	
	$e\mu$	1.3	1.3	1.3	1.4	1.4
2750	e	1.4	1.4	1.4	1.4	
	μ	3.6	3.6	3.6	3.6	
	$e\mu$	1.2	1.2	1.2	1.2	1.2
3000	e	1.3	1.4	1.4	1.4	
	μ	3.4	3.4	3.4	3.4	
	$e\mu$	1.1	1.1	1.1	1.1	1.1

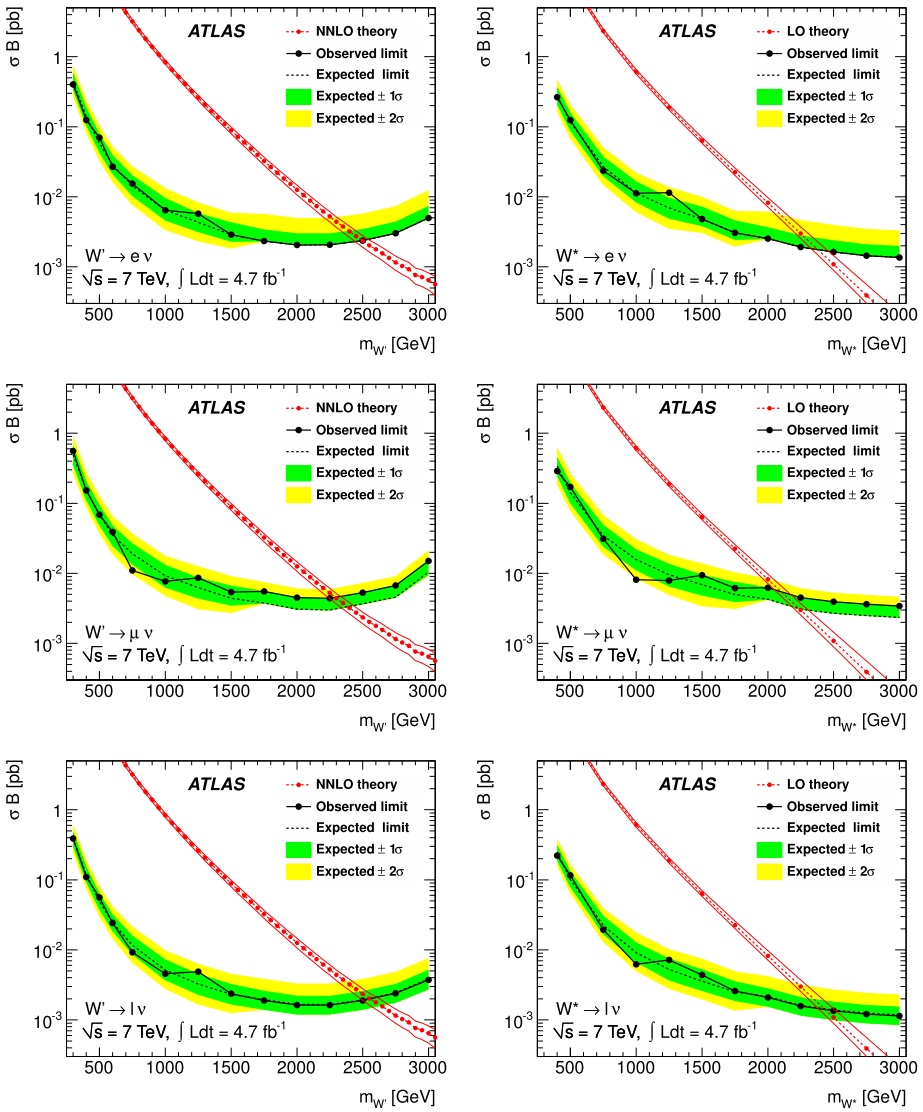

Fig. 3 Expected and observed limits on σB for $W' \to \ell\nu$ (*left*) and $W^* \to \ell\nu$ (*right*) in the electron channel (*top*), muon channel (*center*) and combined (*bottom*) assuming the same branching fraction for both channels. The calculated values for σB (NNLO for W' and LO for W^*) and their uncertainties are also shown

theoretical σB for an SSM W' and for a W^* with quark and gluon coupling strengths normalised to reproduce the W' width.

The intersection between the central theoretical prediction and the observed limits provides the 95 % CL lower limits on the mass. Table 9 presents the expected and ob-

Table 9 W' and W^* mass limits for the electron and muon decay channels and their combination. The first column is the decay channel and the following give the expected (Exp.) and observed (Obs.) mass limits for the SSM W' and for the W^* with equivalent couplings (i.e. chosen to produce the same decay width as the SSM W'). Masses below the reported limit are excluded by this search

	Mass limit [TeV]			
	W'		W^*	
	Exp.	Obs.	Exp.	Obs.
e	2.50	2.50	2.38	2.38
μ	2.38	2.28	2.25	2.09
$e\mu$	2.55	2.55	2.42	2.42

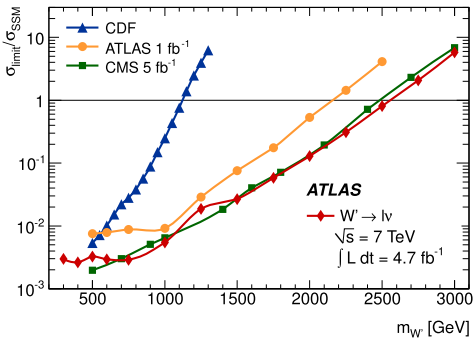

Fig. 4 Normalised cross-section limits ($\sigma_{\text{limit}}/\sigma_{\text{SSM}}$) for $W' \to \ell\nu$ as a function of mass for this measurement and from CDF, CMS and the previous ATLAS search. The cross-section calculations assume the W' has the same couplings as the SM W boson. The region above each curve is excluded at the 95 % CL

served W' and W^* mass limits for the electron and muon decay channels and their combination.

The limits presented here are a significant improvement over those reported in previous ATLAS analyses. Figure 4 shows the new and previous ATLAS σB limits for $W' \to \ell\nu$ along with the most recent results from CMS [2] and CDF [1]. Compared with the previous ATLAS results, the limits presented here cover a wider mass range and are about a factor of five lower at the upper end of the range where they overlap. Limits from CMS based on data from the same LHC run period are similar.

7 Conclusions

The ATLAS detector has been used to search for new high-mass states decaying to a lepton plus missing E_{T} in pp collisions at $\sqrt{s} = 7$ TeV using 4.7 fb^{-1} of integrated luminosity. No excess beyond SM expectations is observed. Bayesian limits on σB are shown in Figs. 3 and 4. A W' with SSM couplings is excluded for $m_{W'} < 2.55$ TeV at the 95 % CL and a W^* with equivalent couplings for $m_{W^*} < 2.42$ TeV.

Acknowledgements We thank CERN for the very successful operation of the LHC, as well as the support staff from our institutions without whom ATLAS could not be operated efficiently.

We acknowledge the support of ANPCyT, Argentina; YerPhI, Armenia; ARC, Australia; BMWF, Austria; ANAS, Azerbaijan; SSTC, Belarus; CNPq and FAPESP, Brazil; NSERC, NRC and CFI, Canada; CERN; CONICYT, Chile; CAS, MOST and NSFC, China; COLCIENCIAS, Colombia; MSMT CR, MPO CR and VSC CR, Czech Republic; DNRF, DNSRC and Lundbeck Foundation, Denmark; EPLANET and ERC, European Union; IN2P3-CNRS, CEA-DSM/IRFU, France; GNAS, Georgia; BMBF, DFG, HGF, MPG and AvH Foundation, Germany; GSRT, Greece; ISF, MINERVA, GIF, DIP and Benoziyo Center, Israel; INFN, Italy; MEXT and JSPS, Japan; CNRST, Morocco; FOM and NWO, Netherlands; RCN, Norway; MNiSW, Poland; GRICES and FCT, Portugal; MERYS (MECTS), Romania; MES of Russia and ROSATOM, Russian Federation; JINR; MSTD, Serbia; MSSR, Slovakia; ARRS and MVZT, Slovenia; DST/NRF, South Africa; MICINN, Spain; SRC and Wallenberg Foundation, Sweden; SER, SNSF and Cantons of Bern and Geneva, Switzerland; NSC, Taiwan; TAEK, Turkey; STFC, the Royal Society and Leverhulme Trust, United Kingdom; DOE and NSF, United States of America.

The crucial computing support from all WLCG partners is acknowledged gratefully, in particular from CERN and the ATLAS Tier-1 facilities at TRIUMF (Canada), NDGF (Denmark, Norway, Sweden), CC-IN2P3 (France), KIT/GridKA (Germany), INFN-CNAF (Italy), NL-T1 (Netherlands), PIC (Spain), ASGC (Taiwan), RAL (UK) and BNL (USA) and in the Tier-2 facilities worldwide.

References

1. T. Aaltonen et al. (CDF Collaboration), Phys. Rev. D **83**, 031102 (2011). arXiv:1012.5145
2. CMS Collaboration, J. High Energy Phys. (2012). doi:10.1007/JHEP08(2012)023 arXiv:1204.4764
3. ATLAS Collaboration, Phys. Lett. B **701**, 50 (2011). arXiv:1103.1391
4. ATLAS Collaboration, Phys. Lett. B **705**, 28 (2011). arXiv:1108.1316
5. G. Altarelli, B. Mele, M. Ruiz-Altaba, Z. Phys. C **45**, 109 (1989)
6. M.V. Chizhov, V.A. Bednyakov, J.A. Budagov, Phys. At. Nucl. **71**, 2096 (2008)
7. M. Chizhov, G. Dvali, Phys. Lett. B **703**, 593 (2011). arXiv:0908.0924
8. ATLAS Collaboration, J. Instrum. **3**, S08003 (2008)
9. ATLAS Collaboration, J. High Energy Phys. **1012**, 060 (2010). arXiv:1010.2130
10. ATLAS Collaboration, Eur. Phys. J. C **72**, 1844 (2012). arXiv:1108.5602
11. ATLAS Collaboration, Eur. Phys. J. C **71**, 1630 (2011). arXiv:1101.2185
12. ATLAS Collaboration, ATLAS-CONF-2011-116 (2011). http://cdsweb.cern.ch/record/1376384
13. T. Sjostrand, S. Mrenna, P. Skands, J. High Energy Phys. **0605**, 026 (2006)
14. A. Sherstnev, R.S. Thorne, Eur. Phys. J. C **55**, 553 (2008). arXiv:0711.2473

15. E. Boos et al. (CompHEP Collaboration), Nucl. Instrum. Methods A **534**, 250 (2004). arXiv:hep-ph/0403113
16. J. Pumplin, D. Stump, J. Huston et al., J. High Energy Phys. **0207**, 012 (2002). arXiv:hep-ph/0201195
17. S. Frixione, B.R. Webber, J. High Energy Phys. **0206**, 029 (2002). arXiv:hep-ph/0204244
18. P.M. Nadolsky et al., Phys. Rev. D **78**, 013004 (2008). arXiv:0802.0007
19. P. Golonka, Z. Was, Eur. Phys. J. C **45**, 97 (2006). arXiv:hep-ph/0506026
20. ATLAS Collaboration, Eur. Phys. J. C **70**, 823 (2010). arXiv:1005.4568 [physics.ins-det]
21. S. Agostinelli et al. (GEANT4 Collaboration), Nucl. Instrum. Methods A **506**, 250 (2003)
22. R. Hamberg, W.L. van Neerven, T. Matsuura, Nucl. Phys. B **359**, 343 (1991)
23. C. Carloni Calame, G. Montagna, O. Nicrosini et al., J. High Energy Phys. **0612**, 016 (2006). arXiv:hep-ph/0609170
24. A. Martin, W. Stirling, R. Thorne et al., Eur. Phys. J. C **63**, 189 (2009). arXiv:0901.0002
25. C.M. Carloni Calame, G. Montagna, O. Nicrosini et al., J. High Energy Phys. **0710**, 109 (2007). arXiv:0710.1722
26. K. Melnikov, F. Petriello, Phys. Rev. D **74**, 114017 (2006). arXiv:hep-ph/0609070
27. R. Gavin, Y. Li, F. Petriello et al., Comput. Phys. Commun. **182**, 2388 (2011). arXiv:1011.3540
28. S. Moch, P. Uwer, Phys. Rev. D **78**, 034003 (2008). arXiv:0804.1476
29. U. Langenfeld, S. Moch, P. Uwer, arXiv:0907.2527 (2009)
30. M. Aliev et al., Comput. Phys. Commun. **182**, 1034 (2010). arXiv:1007.1327
31. ATLAS Collaboration, Eur. Phys. J. C **71**, 1577 (2011). arXiv:1012.1792
32. ATLAS Collaboration, ATLAS-CONF-2010-038 (2010). http://cdsweb.cern.ch/record/1277678
33. ATLAS Collaboration, Phys. Rev. D **83**, 052005 (2011). arXiv:1012.4389

The ATLAS Collaboration

G. Aad[48], T. Abajyan[21], B. Abbott[111], J. Abdallah[12], S. Abdel Khalek[115], A.A. Abdelalim[49], O. Abdinov[11], R. Aben[105], B. Abi[112], M. Abolins[88], O.S. AbouZeid[158], H. Abramowicz[153], H. Abreu[136], B.S. Acharya[164a,164b], L. Adamczyk[38], D.L. Adams[25], T.N. Addy[56], J. Adelman[176], S. Adomeit[98], P. Adragna[75], T. Adye[129], S. Aefsky[23], J.A. Aguilar-Saavedra[124b,a], M. Agustoni[17], M. Aharrouche[81], S.P. Ahlen[22], F. Ahles[48], A. Ahmad[148], M. Ahsan[41], G. Aielli[133a,133b], T. Akdogan[19a], T.P.A. Åkesson[79], G. Akimoto[155], A.V. Akimov[94], M.S. Alam[2], M.A. Alam[76], J. Albert[169], S. Albrand[55], M. Aleksa[30], I.N. Aleksandrov[64], F. Alessandria[89a], C. Alexa[26a], G. Alexander[153], G. Alexandre[49], T. Alexopoulos[10], M. Alhroob[164a,164c], M. Aliev[16], G. Alimonti[89a], J. Alison[120], B.M.M. Allbrooke[18], P.P. Allport[73], S.E. Allwood-Spiers[53], J. Almond[82], A. Aloisio[102a,102b], R. Alon[172], A. Alonso[79], F. Alonso[70], A. Altheimer[35], B. Alvarez Gonzalez[88], M.G. Alviggi[102a,102b], K. Amako[65], C. Amelung[23], V.V. Ammosov[128,*], S.P. Amor Dos Santos[124a], A. Amorim[124a,b], N. Amram[153], C. Anastopoulos[30], L.S. Ancu[17], N. Andari[115], T. Andeen[35], C.F. Anders[58b], G. Anders[58a], K.J. Anderson[31], A. Andreazza[89a,89b], V. Andrei[58a], M-L. Andrieux[55], X.S. Anduaga[70], P. Anger[44], A. Angerami[35], F. Anghinolfi[30], A. Anisenkov[107], N. Anjos[124a], A. Annovi[47], A. Antonaki[9], M. Antonelli[47], A. Antonov[96], J. Antos[144b], F. Anulli[132a], M. Aoki[101], S. Aoun[83], L. Aperio Bella[5], R. Apolle[118,c], G. Arabidze[88], I. Aracena[143], Y. Arai[65], A.T.H. Arce[45], S. Arfaoui[148], J-F. Arguin[15], E. Arik[19a,*], M. Arik[19a], A.J. Armbruster[87], O. Arnaez[81], V. Arnal[80], C. Arnault[115], A. Artamonov[95], G. Artoni[132a,132b], D. Arutinov[21], S. Asai[155], R. Asfandiyarov[173], S. Ask[28], B. Åsman[146a,146b], L. Asquith[6], K. Assamagan[25], A. Astbury[169], M. Atkinson[165], B. Aubert[5], E. Auge[115], K. Augsten[127], M. Aurousseau[145a], G. Avolio[163], R. Avramidou[10], D. Axen[168], G. Azuelos[93,d], Y. Azuma[155], M.A. Baak[30], G. Baccaglioni[89a], C. Bacci[134a,134b], A.M. Bach[15], H. Bachacou[136], K. Bachas[30], M. Backes[49], M. Backhaus[21], E. Badescu[26a], P. Bagnaia[132a,132b], S. Bahinipati[3], Y. Bai[33a], D.C. Bailey[158], T. Bain[158], J.T. Baines[129], O.K. Baker[176], M.D. Baker[25], S. Baker[77], E. Banas[39], P. Banerjee[93], Sw. Banerjee[173], D. Banfi[30], A. Bangert[150], V. Bansal[169], H.S. Bansil[18], L. Barak[172], S.P. Baranov[94], A. Barbaro Galtieri[15], T. Barber[48], E.L. Barberio[86], D. Barberis[50a,50b], M. Barbero[21], D.Y. Bardin[64], T. Barillari[99], M. Barisonzi[175], T. Barklow[143], N. Barlow[28], B.M. Barnett[129], R.M. Barnett[15], A. Baroncelli[134a], G. Barone[49], A.J. Barr[118], F. Barreiro[80], J. Barreiro Guimarães da Costa[57], P. Barrillon[115], R. Bartoldus[143], A.E. Barton[71], V. Bartsch[149], A. Basye[165], R.L. Bates[53], L. Batkova[144a], J.R. Batley[28], A. Battaglia[17], M. Battistin[30], F. Bauer[136], H.S. Bawa[143,e], S. Beale[98], T. Beau[78], P.H. Beauchemin[161], R. Beccherle[50a], P. Bechtle[21], H.P. Beck[17], A.K. Becker[175], S. Becker[98], M. Beckingham[138], K.H. Becks[175], A.J. Beddall[19c], A. Beddall[19c], S. Bedikian[176], V.A. Bednyakov[64], C.P. Bee[83], L.J. Beemster[105], M. Begel[25], S. Behar Harpaz[152], P.K. Behera[62], M. Beimforde[99], C. Belanger-Champagne[85], P.J. Bell[49], W.H. Bell[49], G. Bella[153], L. Bellagamba[20a], F. Bellina[30], M. Bellomo[30], A. Belloni[57], O. Beloborodova[107,f], K. Belotskiy[96], O. Beltramello[30], O. Benary[153], D. Benchekroun[135a], K. Bendtz[146a,146b], N. Benekos[165], Y. Benhammou[153], E. Benhar Noccioli[49], J.A. Benitez Garcia[159b], D.P. Benjamin[45], M. Benoit[115], J.R. Bensinger[23], K. Benslama[130], S. Bentvelsen[105], D. Berge[30], E. Bergeaas Kuutmann[42], N. Berger[5], F. Berghaus[169], E. Berglund[105], J. Beringer[15], P. Bernat[77], R. Bernhard[48], C. Bernius[25], T. Berry[76], C. Bertella[83],

A. Bertin[20a,20b], F. Bertolucci[122a,122b], M.I. Besana[89a,89b], G.J. Besjes[104], N. Besson[136], S. Bethke[99], W. Bhimji[46], R.M. Bianchi[30], M. Bianco[72a,72b], O. Biebel[98], S.P. Bieniek[77], K. Bierwagen[54], J. Biesiada[15], M. Biglietti[134a], H. Bilokon[47], M. Bindi[20a,20b], S. Binet[115], A. Bingul[19c], C. Bini[132a,132b], C. Biscarat[178], B. Bittner[99], K.M. Black[22], R.E. Blair[6], J.-B. Blanchard[136], G. Blanchot[30], T. Blazek[144a], I. Bloch[42], C. Blocker[23], J. Blocki[39], A. Blondel[49], W. Blum[81], U. Blumenschein[54], G.J. Bobbink[105], V.B. Bobrovnikov[107], S.S. Bocchetta[79], A. Bocci[45], C.R. Boddy[118], M. Boehler[48], J. Boek[175], N. Boelaert[36], J.A. Bogaerts[30], A. Bogdanchikov[107], A. Bogouch[90,*], C. Bohm[146a], J. Bohm[125], V. Boisvert[76], T. Bold[38], V. Boldea[26a], N.M. Bolnet[136], M. Bomben[78], M. Bona[75], M. Boonekamp[136], S. Bordoni[78], C. Borer[17], A. Borisov[128], G. Borissov[71], I. Borjanovic[13a], M. Borri[82], S. Borroni[87], V. Bortolotto[134a,134b], K. Bos[105], D. Boscherini[20a], M. Bosman[12], H. Boterenbrood[105], J. Bouchami[93], J. Boudreau[123], E.V. Bouhova-Thacker[71], D. Boumediene[34], C. Bourdarios[115], N. Bousson[83], A. Boveia[31], J. Boyd[30], I.R. Boyko[64], I. Bozovic-Jelisavcic[13b], J. Bracinik[18], P. Branchini[134a], G.W. Brandenburg[57], A. Brandt[8], G. Brandt[118], O. Brandt[54], U. Bratzler[156], B. Brau[84], J.E. Brau[114], H.M. Braun[175,*], S.F. Brazzale[164a,164c], B. Brelier[158], J. Bremer[30], K. Brendlinger[120], R. Brenner[166], S. Bressler[172], D. Britton[53], F.M. Brochu[28], I. Brock[21], R. Brock[88], F. Broggi[89a], C. Bromberg[88], J. Bronner[99], G. Brooijmans[35], T. Brooks[76], W.K. Brooks[32b], G. Brown[82], H. Brown[8], P.A. Bruckman de Renstrom[39], D. Bruncko[144b], R. Bruneliere[48], S. Brunet[60], A. Bruni[20a], G. Bruni[20a], M. Bruschi[20a], T. Buanes[14], Q. Buat[55], F. Bucci[49], J. Buchanan[118], P. Buchholz[141], R.M. Buckingham[118], A.G. Buckley[46], S.I. Buda[26a], I.A. Budagov[64], B. Budick[108], V. Büscher[81], L. Bugge[117], M.K. Bugge[117], O. Bulekov[96], A.C. Bundock[73], M. Bunse[43], T. Buran[117], H. Burckhart[30], S. Burdin[73], T. Burgess[14], S. Burke[129], E. Busato[34], P. Bussey[53], C.P. Buszello[166], B. Butler[143], J.M. Butler[22], C.M. Buttar[53], J.M. Butterworth[77], W. Buttinger[28], S. Cabrera Urbán[167], D. Caforio[20a,20b], O. Cakir[4a], P. Calafiura[15], G. Calderini[78], P. Calfayan[98], R. Calkins[106], L.P. Caloba[24a], R. Caloi[132a,132b], D. Calvet[34], S. Calvet[34], R. Camacho Toro[34], P. Camarri[133a,133b], D. Cameron[117], L.M. Caminada[15], R. Caminal Armadans[12], S. Campana[30], M. Campanelli[77], V. Canale[102a,102b], F. Canelli[31,g], A. Canepa[159a], J. Cantero[80], R. Cantrill[76], L. Capasso[102a,102b], M.D.M. Capeans Garrido[30], I. Caprini[26a], M. Caprini[26a], D. Capriotti[99], M. Capua[37a,37b], R. Caputo[81], R. Cardarelli[133a], T. Carli[30], G. Carlino[102a], L. Carminati[89a,89b], B. Caron[85], S. Caron[104], E. Carquin[32b], G.D. Carrillo Montoya[173], A.A. Carter[75], J.R. Carter[28], J. Carvalho[124a,h], D. Casadei[108], M.P. Casado[12], M. Cascella[122a,122b], C. Caso[50a,50b,*], A.M. Castaneda Hernandez[173,i], E. Castaneda-Miranda[173], V. Castillo Gimenez[167], N.F. Castro[124a], G. Cataldi[72a], P. Catastini[57], A. Catinaccio[30], J.R. Catmore[30], A. Cattai[30], G. Cattani[133a,133b], S. Caughron[88], V. Cavaliere[165], P. Cavalleri[78], D. Cavalli[89a], M. Cavalli-Sforza[12], V. Cavasinni[122a,122b], F. Ceradini[134a,134b], A.S. Cerqueira[24b], A. Cerri[30], L. Cerrito[75], F. Cerutti[47], S.A. Cetin[19b], A. Chafaq[135a], D. Chakraborty[106], I. Chalupkova[126], K. Chan[3], P. Chang[165], B. Chapleau[85], J.D. Chapman[28], J.W. Chapman[87], E. Chareyre[78], D.G. Charlton[18], V. Chavda[82], C.A. Chavez Barajas[30], S. Cheatham[85], S. Chekanov[6], S.V. Chekulaev[159a], G.A. Chelkov[64], M.A. Chelstowska[104], C. Chen[63], H. Chen[25], S. Chen[33c], X. Chen[173], Y. Chen[35], A. Cheplakov[64], R. Cherkaoui El Moursli[135e], V. Chernyatin[25], E. Cheu[7], S.L. Cheung[158], L. Chevalier[136], G. Chiefari[102a,102b], L. Chikovani[51a,*], J.T. Childers[30], A. Chilingarov[71], G. Chiodini[72a], A.S. Chisholm[18], R.T. Chislett[77], A. Chitan[26a], M.V. Chizhov[64], G. Choudalakis[31], S. Chouridou[137], I.A. Christidi[77], A. Christov[48], D. Chromek-Burckhart[30], M.L. Chu[151], J. Chudoba[125], G. Ciapetti[132a,132b], A.K. Ciftci[4a], R. Ciftci[4a], D. Cinca[34], V. Cindro[74], C. Ciocca[20a,20b], A. Ciocio[15], M. Cirilli[87], P. Cirkovic[13b], Z.H. Citron[172], M. Citterio[89a], M. Ciubancan[26a], A. Clark[49], P.J. Clark[46], R.N. Clarke[15], W. Cleland[123], J.C. Clemens[83], B. Clement[55], C. Clement[146a,146b], Y. Coadou[83], M. Cobal[164a,164c], A. Coccaro[138], J. Cochran[63], L. Coffey[23], J.G. Cogan[143], J. Coggeshall[165], E. Cogneras[178], J. Colas[5], S. Cole[106], A.P. Colijn[105], N.J. Collins[18], C. Collins-Tooth[53], J. Collot[55], T. Colombo[119a,119b], G. Colon[84], P. Conde Muiño[124a], E. Coniavitis[118], M.C. Conidi[12], S.M. Consonni[89a,89b], V. Consorti[48], S. Constantinescu[26a], C. Conta[119a,119b], G. Conti[57], F. Conventi[102a,j], M. Cooke[15], B.D. Cooper[77], A.M. Cooper-Sarkar[118], K. Copic[15], T. Cornelissen[175], M. Corradi[20a], F. Corriveau[85,k], A. Cortes-Gonzalez[165], G. Cortiana[99], G. Costa[89a], M.J. Costa[167], D. Costanzo[139], D. Côté[30], L. Courneyea[169], G. Cowan[76], C. Cowden[28], B.E. Cox[82], K. Cranmer[108], F. Crescioli[122a,122b], M. Cristinziani[21], G. Crosetti[37a,37b], S. Crépé-Renaudin[55], C.-M. Cuciuc[26a], C. Cuenca Almenar[176], T. Cuhadar Donszelmann[139], M. Curatolo[47], C.J. Curtis[18], C. Cuthbert[150], P. Cwetanski[60], H. Czirr[141], P. Czodrowski[44], Z. Czyczula[176], S. D'Auria[53], M. D'Onofrio[73], A. D'Orazio[132a,132b], M.J. Da Cunha Sargedas De Sousa[124a], C. Da Via[82], W. Dabrowski[38], A. Dafinca[118], T. Dai[87], C. Dallapiccola[84], M. Dam[36], M. Dameri[50a,50b], D.S. Damiani[137], H.O. Danielsson[30], V. Dao[49], G. Darbo[50a], G.L. Darlea[26b], J.A. Dassoulas[42], W. Davey[21], T. Davidek[126], N. Davidson[86], R. Davidson[71], E. Davies[118,c], M. Davies[93], O. Davignon[78], A.R. Davison[77], Y. Davygora[58a], E. Dawe[142], I. Dawson[139], R.K. Daya-Ishmukhametova[23], K. De[8], R. de Asmundis[102a], S. De Castro[20a,20b], S. De Cecco[78], J. de Graat[98], N. De Groot[104], P. de Jong[105], C. De La Taille[115], H. De la Torre[80], F. De Lorenzi[63], L. de Mora[71], L. De Nooij[105], D. De Pedis[132a], A. De Salvo[132a], U. De Sanctis[164a,164c], A. De Santo[149], J.B. De Vivie De Regie[115], G. De Zorzi[132a,132b], W.J. Dearnaley[71], R. Debbe[25], C. Debenedetti[46], B. Dechenaux[55], D.V. Dedovich[64], J. Degenhardt[120], C. Del Papa[164a,164c], J. Del Peso[80], T. Del Prete[122a,122b], T. Delemontex[55], M. Deliyergiyev[74], A. Dell'Acqua[30], L. Dell'Asta[22], M. Della Pietra[102a,j], D. della Volpe[102a,102b], M. Delmastro[5], P.A. Delsart[55], C. Deluca[105],

S. Demers[176], M. Demichev[64], B. Demirkoz[12,l], J. Deng[163], S.P. Denisov[128], D. Derendarz[39], J.E. Derkaoui[135d], F. Derue[78], P. Dervan[73], K. Desch[21], E. Devetak[148], P.O. Deviveiros[105], A. Dewhurst[129], B. DeWilde[148], S. Dhaliwal[158], R. Dhullipudi[25,m], A. Di Ciaccio[133a,133b], L. Di Ciaccio[5], A. Di Girolamo[30], B. Di Girolamo[30], S. Di Luise[134a,134b], A. Di Mattia[173], B. Di Micco[30], R. Di Nardo[47], A. Di Simone[133a,133b], R. Di Sipio[20a,20b], M.A. Diaz[32a], E.B. Diehl[87], J. Dietrich[42], T.A. Dietzsch[58a], S. Diglio[86], K. Dindar Yagci[40], J. Dingfelder[21], F. Dinut[26a], C. Dionisi[132a,132b], P. Dita[26a], S. Dita[26a], F. Dittus[30], F. Djama[83], T. Djobava[51b], M.A.B. do Vale[24c], A. Do Valle Wemans[124a,n], T.K.O. Doan[5], M. Dobbs[85], R. Dobinson[30,*], D. Dobos[30], E. Dobson[30,o], J. Dodd[35], C. Doglioni[49], T. Doherty[53], Y. Doi[65,*], J. Dolejsi[126], I. Dolenc[74], Z. Dolezal[126], B.A. Dolgoshein[96,*], T. Dohmae[155], M. Donadelli[24d], J. Donini[34], J. Dopke[30], A. Doria[102a], A. Dos Anjos[173], A. Dotti[122a,122b], M.T. Dova[70], A.D. Doxiadis[105], A.T. Doyle[53], N. Dressnandt[120], M. Dris[10], J. Dubbert[99], S. Dube[15], E. Duchovni[172], G. Duckeck[98], D. Duda[175], A. Dudarev[30], F. Dudziak[63], M. Dührssen[30], I.P. Duerdoth[82], L. Duflot[115], M-A. Dufour[85], L. Duguid[76], M. Dunford[30], H. Duran Yildiz[4a], R. Duxfield[139], M. Dwuznik[38], F. Dydak[30], M. Düren[52], W.L. Ebenstein[45], J. Ebke[98], S. Eckweiler[81], K. Edmonds[81], W. Edson[2], C.A. Edwards[76], N.C. Edwards[53], W. Ehrenfeld[42], T. Eifert[143], G. Eigen[14], K. Einsweiler[15], E. Eisenhandler[75], T. Ekelof[166], M. El Kacimi[135c], M. Ellert[166], S. Elles[5], F. Ellinghaus[81], K. Ellis[75], N. Ellis[30], J. Elmsheuser[98], M. Elsing[30], D. Emeliyanov[129], R. Engelmann[148], A. Engl[98], B. Epp[61], J. Erdmann[54], A. Ereditato[17], D. Eriksson[146a], J. Ernst[2], M. Ernst[25], J. Ernwein[136], D. Errede[165], S. Errede[165], E. Ertel[81], M. Escalier[115], H. Esch[43], C. Escobar[123], X. Espinal Curull[12], B. Esposito[47], F. Etienne[83], A.I. Etienvre[136], E. Etzion[153], D. Evangelakou[54], H. Evans[60], L. Fabbri[20a,20b], C. Fabre[30], R.M. Fakhrutdinov[128], S. Falciano[132a], Y. Fang[173], M. Fanti[89a,89b], A. Farbin[8], A. Farilla[134a], J. Farley[148], T. Farooque[158], S. Farrell[163], S.M. Farrington[170], P. Farthouat[30], F. Fassi[167], P. Fassnacht[30], D. Fassouliotis[9], B. Fatholahzadeh[158], A. Favareto[89a,89b], L. Fayard[115], S. Fazio[37a,37b], R. Febbraro[34], P. Federic[144a], O.L. Fedin[121], W. Fedorko[88], M. Fehling-Kaschek[48], L. Feligioni[83], D. Fellmann[6], C. Feng[33d], E.J. Feng[6], A.B. Fenyuk[128], J. Ferencei[144b], W. Fernando[6], S. Ferrag[53], J. Ferrando[53], V. Ferrara[42], A. Ferrari[166], P. Ferrari[105], R. Ferrari[119a], D.E. Ferreira de Lima[53], A. Ferrer[167], D. Ferrere[49], C. Ferretti[87], A. Ferretto Parodi[50a,50b], M. Fiascaris[31], F. Fiedler[81], A. Filipčič[74], F. Filthaut[104], M. Fincke-Keeler[169], M.C.N. Fiolhais[124a,h], L. Fiorini[167], A. Firan[40], G. Fischer[42], M.J. Fisher[109], M. Flechl[48], I. Fleck[141], J. Fleckner[81], P. Fleischmann[174], S. Fleischmann[175], T. Flick[175], A. Floderus[79], L.R. Flores Castillo[173], M.J. Flowerdew[99], T. Fonseca Martin[17], A. Formica[136], A. Forti[82], D. Fortin[159a], D. Fournier[115], A.J. Fowler[45], H. Fox[71], P. Francavilla[12], M. Franchini[20a,20b], S. Franchino[119a,119b], D. Francis[30], T. Frank[172], S. Franz[30], M. Fraternali[119a,119b], S. Fratina[120], S.T. French[28], C. Friedrich[42], F. Friedrich[44], R. Froeschl[30], D. Froidevaux[30], J.A. Frost[28], C. Fukunaga[156], E. Fullana Torregrosa[30], B.G. Fulsom[143], J. Fuster[167], C. Gabaldon[30], O. Gabizon[172], T. Gadfort[25], S. Gadomski[49], G. Gagliardi[50a,50b], P. Gagnon[60], C. Galea[98], B. Galhardo[124a], E.J. Gallas[118], V. Gallo[17], B.J. Gallop[129], P. Gallus[125], K.K. Gan[109], Y.S. Gao[143,e], A. Gaponenko[15], F. Garberson[176], M. Garcia-Sciveres[15], C. García[167], J.E. García Navarro[167], R.W. Gardner[31], N. Garelli[30], H. Garitaonandia[105], V. Garonne[30], C. Gatti[47], G. Gaudio[119a], B. Gaur[141], L. Gauthier[136], P. Gauzzi[132a,132b], I.L. Gavrilenko[94], C. Gay[168], G. Gaycken[21], E.N. Gazis[10], P. Ge[33d], Z. Gecse[168], C.N.P. Gee[129], D.A.A. Geerts[105], Ch. Geich-Gimbel[21], K. Gellerstedt[146a,146b], C. Gemme[50a], A. Gemmell[53], M.H. Genest[55], S. Gentile[132a,132b], M. George[54], S. George[76], P. Gerlach[175], A. Gershon[153], C. Geweniger[58a], H. Ghazlane[135b], N. Ghodbane[34], B. Giacobbe[20a], S. Giagu[132a,132b], V. Giakoumopoulou[9], V. Giangiobbe[12], F. Gianotti[30], B. Gibbard[25], A. Gibson[158], S.M. Gibson[30], M. Gilchriese[15], D. Gillberg[29], A.R. Gillman[129], D.M. Gingrich[3,d], J. Ginzburg[153], N. Giokaris[9], M.P. Giordani[164c], R. Giordano[102a,102b], F.M. Giorgi[16], P. Giovannini[99], P.F. Giraud[136], D. Giugni[89a], M. Giunta[93], P. Giusti[20a], B.K. Gjelsten[117], L.K. Gladilin[97], C. Glasman[80], J. Glatzer[48], A. Glazov[42], K.W. Glitza[175], G.L. Glonti[64], J.R. Goddard[75], J. Godfrey[142], J. Godlewski[30], M. Goebel[42], T. Göpfert[44], C. Goeringer[81], C. Gössling[43], S. Goldfarb[87], T. Golling[176], A. Gomes[124a,b], L.S. Gomez Fajardo[42], R. Gonçalo[76], J. Goncalves Pinto Firmino Da Costa[42], L. Gonella[21], S. González de la Hoz[167], G. Gonzalez Parra[12], M.L. Gonzalez Silva[27], S. Gonzalez-Sevilla[49], J.J. Goodson[148], L. Goossens[30], P.A. Gorbounov[95], H.A. Gordon[25], I. Gorelov[103], G. Gorfine[175], B. Gorini[30], E. Gorini[72a,72b], A. Gorišek[74], E. Gornicki[39], B. Gosdzik[42], A.T. Goshaw[6], M. Gosselink[105], M.I. Gostkin[64], I. Gough Eschrich[163], M. Gouighri[135a], D. Goujdami[135c], M.P. Goulette[49], A.G. Goussiou[138], C. Goy[5], S. Gozpinar[23], I. Grabowska-Bold[38], P. Grafström[20a,20b], K-J. Grahn[42], F. Grancagnolo[72a], S. Grancagnolo[16], V. Grassi[148], V. Gratchev[121], N. Grau[35], H.M. Gray[30], J.A. Gray[148], E. Graziani[134a], O.G. Grebenyuk[121], T. Greenshaw[73], Z.D. Greenwood[25,m], K. Gregersen[36], I.M. Gregor[42], P. Grenier[143], J. Griffiths[8], N. Grigalashvili[64], A.A. Grillo[137], S. Grinstein[12], Ph. Gris[34], Y.V. Grishkevich[97], J.-F. Grivaz[115], E. Gross[172], J. Grosse-Knetter[54], J. Groth-Jensen[172], K. Grybel[141], D. Guest[176], C. Guicheney[34], S. Guindon[54], U. Gul[53], H. Guler[85,p], J. Gunther[125], B. Guo[158], J. Guo[35], P. Gutierrez[111], N. Guttman[153], O. Gutzwiller[173], C. Guyot[136], C. Gwenlan[118], C.B. Gwilliam[73], A. Haas[143], S. Haas[30], C. Haber[15], H.K. Hadavand[40], D.R. Hadley[18], P. Haefner[21], F. Hahn[30], S. Haider[30], Z. Hajduk[39], H. Hakobyan[177], D. Hall[118], J. Haller[54], K. Hamacher[175], P. Hamal[113], K. Hamano[86], M. Hamer[54], A. Hamilton[145b,q], S. Hamilton[161], L. Han[33b], K. Hanagaki[116], K. Hanawa[160], M. Hance[15], C. Handel[81], P. Hanke[58a], J.R. Hansen[36], J.B. Hansen[36], J.D. Hansen[36], P.H. Hansen[36], P. Hansson[143],

K. Hara[160], G.A. Hare[137], T. Harenberg[175], S. Harkusha[90], D. Harper[87], R.D. Harrington[46], O.M. Harris[138], J. Hartert[48], F. Hartjes[105], T. Haruyama[65], A. Harvey[56], S. Hasegawa[101], Y. Hasegawa[140], S. Hassani[136], S. Haug[17], M. Hauschild[30], R. Hauser[88], M. Havranek[21], C.M. Hawkes[18], R.J. Hawkings[30], A.D. Hawkins[79], T. Hayakawa[66], T. Hayashi[160], D. Hayden[76], C.P. Hays[118], H.S. Hayward[73], S.J. Haywood[129], S.J. Head[18], V. Hedberg[79], L. Heelan[8], S. Heim[88], B. Heinemann[15], S. Heisterkamp[36], L. Helary[22], C. Heller[98], M. Heller[30], S. Hellman[146a,146b], D. Hellmich[21], C. Helsens[12], R.C.W. Henderson[71], M. Henke[58a], A. Henrichs[54], A.M. Henriques Correia[30], S. Henrot-Versille[115], C. Hensel[54], T. Henß[175], C.M. Hernandez[8], Y. Hernández Jiménez[167], R. Herrberg[16], G. Herten[48], R. Hertenberger[98], L. Hervas[30], G.G. Hesketh[77], N.P. Hessey[105], E. Higón-Rodriguez[167], J.C. Hill[28], K.H. Hiller[42], S. Hillert[21], S.J. Hillier[18], I. Hinchliffe[15], E. Hines[120], M. Hirose[116], F. Hirsch[43], D. Hirschbuehl[175], J. Hobbs[148], N. Hod[153], M.C. Hodgkinson[139], P. Hodgson[139], A. Hoecker[30], M.R. Hoeferkamp[103], J. Hoffman[40], D. Hoffmann[83], M. Hohlfeld[81], M. Holder[141], S.O. Holmgren[146a], T. Holy[127], J.L. Holzbauer[88], T.M. Hong[120], L. Hooft van Huysduynen[108], S. Horner[48], J-Y. Hostachy[55], S. Hou[151], A. Hoummada[135a], J. Howard[118], J. Howarth[82], I. Hristova[16], J. Hrivnac[115], T. Hryn'ova[5], P.J. Hsu[81], S.-C. Hsu[15], D. Hu[35], Z. Hubacek[127], F. Hubaut[83], F. Huegging[21], A. Huettmann[42], T.B. Huffman[118], E.W. Hughes[35], G. Hughes[71], M. Huhtinen[30], M. Hurwitz[15], U. Husemann[42], N. Huseynov[64,r], J. Huston[88], J. Huth[57], G. Iacobucci[49], G. Iakovidis[10], M. Ibbotson[82], I. Ibragimov[141], L. Iconomidou-Fayard[115], J. Idarraga[115], P. Iengo[102a], O. Igonkina[105], Y. Ikegami[65], M. Ikeno[65], D. Iliadis[154], N. Ilic[158], T. Ince[21], J. Inigo-Golfin[30], P. Ioannou[9], M. Iodice[134a], K. Iordanidou[9], V. Ippolito[132a,132b], A. Irles Quiles[167], C. Isaksson[166], M. Ishino[67], M. Ishitsuka[157], R. Ishmukhametov[40], C. Issever[118], S. Istin[19a], A.V. Ivashin[128], W. Iwanski[39], H. Iwasaki[65], J.M. Izen[41], V. Izzo[102a], B. Jackson[120], J.N. Jackson[73], P. Jackson[1], M.R. Jaekel[30], V. Jain[60], K. Jakobs[48], S. Jakobsen[36], T. Jakoubek[125], J. Jakubek[127], D.K. Jana[111], E. Jansen[77], H. Jansen[30], A. Jantsch[99], M. Janus[48], G. Jarlskog[79], L. Jeanty[57], I. Jen-La Plante[31], D. Jennens[86], P. Jenni[30], A.E. Loevschall-Jensen[36], P. Ježo[36], S. Jézéquel[5], M.K. Jha[20a], H. Ji[173], W. Ji[81], J. Jia[148], Y. Jiang[33b], M. Jimenez Belenguer[42], S. Jin[33a], O. Jinnouchi[157], M.D. Joergensen[36], D. Joffe[40], M. Johansen[146a,146b], K.E. Johansson[146a], P. Johansson[139], S. Johnert[42], K.A. Johns[7], K. Jon-And[146a,146b], G. Jones[170], R.W.L. Jones[71], T.J. Jones[73], C. Joram[30], P.M. Jorge[124a], K.D. Joshi[82], J. Jovicevic[147], T. Jovin[13b], X. Ju[173], C.A. Jung[43], R.M. Jungst[30], V. Juranek[125], P. Jussel[61], A. Juste Rozas[12], S. Kabana[17], M. Kaci[167], A. Kaczmarska[39], P. Kadlecik[36], M. Kado[115], H. Kagan[109], M. Kagan[57], E. Kajomovitz[152], S. Kalinin[175], L.V. Kalinovskaya[64], S. Kama[40], N. Kanaya[155], M. Kaneda[30], S. Kaneti[28], T. Kanno[157], V.A. Kantserov[96], J. Kanzaki[65], B. Kaplan[108], A. Kapliy[31], J. Kaplon[30], D. Kar[53], M. Karagounis[21], K. Karakostas[10], M. Karnevskiy[42], V. Kartvelishvili[71], A.N. Karyukhin[128], L. Kashif[173], G. Kasieczka[58b], R.D. Kass[109], A. Kastanas[14], M. Kataoka[5], Y. Kataoka[155], E. Katsoufis[10], J. Katzy[42], V. Kaushik[7], K. Kawagoe[69], T. Kawamoto[155], G. Kawamura[81], M.S. Kayl[105], S. Kazama[155], V.A. Kazanin[107], M.Y. Kazarinov[64], R. Keeler[169], P.T. Keener[120], R. Kehoe[40], M. Keil[54], G.D. Kekelidze[64], J.S. Keller[138], M. Kenyon[53], O. Kepka[125], N. Kerschen[30], B.P. Kerševan[74], S. Kersten[175], K. Kessoku[155], J. Keung[158], F. Khalil-zada[11], H. Khandanyan[146a,146b], A. Khanov[112], D. Kharchenko[64], A. Khodinov[96], A. Khomich[58a], T.J. Khoo[28], G. Khoriauli[21], A. Khoroshilov[175], V. Khovanskiy[95], E. Khramov[64], J. Khubua[51b], H. Kim[146a,146b], S.H. Kim[160], N. Kimura[171], O. Kind[16], B.T. King[73], M. King[66], R.S.B. King[118], J. Kirk[129], A.E. Kiryunin[99], T. Kishimoto[66], D. Kisielewska[38], T. Kitamura[66], T. Kittelmann[123], K. Kiuchi[160], E. Kladiva[144b], M. Klein[73], U. Klein[73], K. Kleinknecht[81], M. Klemetti[85], A. Klier[172], P. Klimek[146a,146b], A. Klimentov[25], R. Klingenberg[43], J.A. Klinger[82], E.B. Klinkby[36], T. Klioutchnikova[30], P.F. Klok[104], S. Klous[105], E.-E. Kluge[58a], T. Kluge[73], P. Kluit[105], S. Kluth[99], N.S. Knecht[158], E. Kneringer[61], E.B.F.G. Knoops[83], A. Knue[54], B.R. Ko[45], T. Kobayashi[155], M. Kobel[44], M. Kocian[143], P. Kodys[126], K. Köneke[30], A.C. König[104], S. Koenig[81], L. Köpke[81], F. Koetsveld[104], P. Koevesarki[21], T. Koffas[29], E. Koffeman[105], L.A. Kogan[118], S. Kohlmann[175], F. Kohn[54], Z. Kohout[127], T. Kohriki[65], T. Koi[143], G.M. Kolachev[107,*], H. Kolanoski[16], V. Kolesnikov[64], I. Koletsou[89a], J. Koll[88], A.A. Komar[94], Y. Komori[155], T. Kondo[65], T. Kono[42,s], A.I. Kononov[48], R. Konoplich[108,t], N. Konstantinidis[77], S. Koperny[38], K. Korcyl[39], K. Kordas[154], A. Korn[118], A. Korol[107], I. Korolkov[12], E.V. Korolkova[139], V.A. Korotkov[128], O. Kortner[99], S. Kortner[99], V.V. Kostyukhin[21], S. Kotov[99], V.M. Kotov[64], A. Kotwal[45], C. Kourkoumelis[9], V. Kouskoura[154], A. Koutsman[159a], R. Kowalewski[169], T.Z. Kowalski[38], W. Kozanecki[136], A.S. Kozhin[128], V. Kral[127], V.A. Kramarenko[97], G. Kramberger[74], M.W. Krasny[78], A. Krasznahorkay[108], J.K. Kraus[21], S. Kreiss[108], F. Krejci[127], J. Kretzschmar[73], N. Krieger[54], P. Krieger[158], K. Kroeninger[54], H. Kroha[99], J. Kroll[120], J. Kroseberg[21], J. Krstic[13a], U. Kruchonak[64], H. Krüger[21], T. Kruker[17], N. Krumnack[63], Z.V. Krumshteyn[64], T. Kubota[86], S. Kuday[4a], S. Kuehn[48], A. Kugel[58c], T. Kuhl[42], D. Kuhn[61], V. Kukhtin[64], Y. Kulchitsky[90], S. Kuleshov[32b], C. Kummer[98], M. Kuna[78], J. Kunkle[120], A. Kupco[125], H. Kurashige[66], M. Kurata[160], Y.A. Kurochkin[90], V. Kus[125], E.S. Kuwertz[147], M. Kuze[157], J. Kvita[142], R. Kwee[16], A. La Rosa[49], L. La Rotonda[37a,37b], L. Labarga[80], J. Labbe[5], S. Lablak[135a], C. Lacasta[167], F. Lacava[132a,132b], H. Lacker[16], D. Lacour[78], V.R. Lacuesta[167], E. Ladygin[64], R. Lafaye[5], B. Laforge[78], T. Lagouri[176], S. Lai[48], E. Laisne[55], M. Lamanna[30], L. Lambourne[77], C.L. Lampen[7], W. Lampl[7], E. Lancon[136], U. Landgraf[48], M.P.J. Landon[75], J.L. Lane[82], V.S. Lang[58a], C. Lange[42], A.J. Lankford[163], F. Lanni[25], K. Lantzsch[175], S. Laplace[78], C. Lapoire[21], J.F. Laporte[136], T. Lari[89a], A. Larner[118], M. Lassnig[30], P. Laurelli[47], V. Lavorini[37a,37b], W. Lavrijsen[15], P. Laycock[73], O. Le Dortz[78], E. Le Guirriec[83], E. Le Menedeu[12],

T. LeCompte[6], F. Ledroit-Guillon[55], H. Lee[105], J.S.H. Lee[116], S.C. Lee[151], L. Lee[176], M. Lefebvre[169], M. Legendre[136], F. Legger[98], C. Leggett[15], M. Lehmacher[21], G. Lehmann Miotto[30], X. Lei[7], M.A.L. Leite[24d], R. Leitner[126], D. Lellouch[172], B. Lemmer[54], V. Lendermann[58a], K.J.C. Leney[145b], T. Lenz[105], G. Lenzen[175], B. Lenzi[30], K. Leonhardt[44], S. Leontsinis[10], F. Lepold[58a], C. Leroy[93], J-R. Lessard[169], C.G. Lester[28], C.M. Lester[120], J. Levêque[5], D. Levin[87], L.J. Levinson[172], A. Lewis[118], G.H. Lewis[108], A.M. Leyko[21], M. Leyton[16], B. Li[83], H. Li[173,u], S. Li[33b,v], X. Li[87], Z. Liang[118,w], H. Liao[34], B. Liberti[133a], P. Lichard[30], M. Lichtnecker[98], K. Lie[165], W. Liebig[14], C. Limbach[21], A. Limosani[86], M. Limper[62], S.C. Lin[151,x], F. Linde[105], J.T. Linnemann[88], E. Lipeles[120], A. Lipniacka[14], T.M. Liss[165], D. Lissauer[25], A. Lister[49], A.M. Litke[137], C. Liu[29], D. Liu[151], H. Liu[87], J.B. Liu[87], L. Liu[87], M. Liu[33b], Y. Liu[33b], M. Livan[119a,119b], S.S.A. Livermore[118], A. Lleres[55], J. Llorente Merino[80], S.L. Lloyd[75], E. Lobodzinska[42], P. Loch[7], W.S. Lockman[137], T. Loddenkoetter[21], F.K. Loebinger[82], A. Loginov[176], C.W. Loh[168], T. Lohse[16], K. Lohwasser[48], M. Lokajicek[125], V.P. Lombardo[5], R.E. Long[71], L. Lopes[124a], D. Lopez Mateos[57], J. Lorenz[98], N. Lorenzo Martinez[115], M. Losada[162], P. Loscutoff[15], F. Lo Sterzo[132a,132b], M.J. Losty[159a,*], X. Lou[41], A. Lounis[115], K.F. Loureiro[162], J. Love[6], P.A. Love[71], A.J. Lowe[143,e], F. Lu[33a], H.J. Lubatti[138], C. Luci[132a,132b], A. Lucotte[55], A. Ludwig[44], D. Ludwig[42], I. Ludwig[48], J. Ludwig[48], F. Luehring[60], G. Luijckx[105], W. Lukas[61], L. Luminari[132a], E. Lund[117], B. Lund-Jensen[147], B. Lundberg[79], J. Lundberg[146a,146b], O. Lundberg[146a,146b], J. Lundquist[36], M. Lungwitz[81], D. Lynn[25], E. Lytken[79], H. Ma[25], L.L. Ma[173], G. Maccarrone[47], A. Macchiolo[99], B. Maček[74], J. Machado Miguens[124a], R. Mackeprang[36], R.J. Madaras[15], H.J. Maddocks[71], W.F. Mader[44], R. Maenner[58c], T. Maeno[25], P. Mättig[175], S. Mättig[81], L. Magnoni[163], E. Magradze[54], K. Mahboubi[48], J. Mahlstedt[105], S. Mahmoud[73], G. Mahout[18], C. Maiani[136], C. Maidantchik[24a], A. Maio[124a,b], S. Majewski[25], Y. Makida[65], N. Makovec[115], P. Mal[136], B. Malaescu[30], Pa. Malecki[39], P. Malecki[39], V.P. Maleev[121], F. Malek[55], U. Mallik[62], D. Malon[6], C. Malone[143], S. Maltezos[10], V. Malyshev[107], S. Malyukov[30], R. Mameghani[98], J. Mamuzic[13b], A. Manabe[65], L. Mandelli[89a], I. Mandić[74], R. Mandrysch[16], J. Maneira[124a], A. Manfredini[99], P.S. Mangeard[88], L. Manhaes de Andrade Filho[24b], J.A. Manjarres Ramos[136], A. Mann[54], P.M. Manning[137], A. Manousakis-Katsikakis[9], B. Mansoulie[136], A. Mapelli[30], L. Mapelli[30], L. March[80], J.F. Marchand[29], F. Marchese[133a,133b], G. Marchiori[78], M. Marcisovsky[125], C.P. Marino[169], F. Marroquim[24a], Z. Marshall[30], F.K. Martens[158], L.F. Marti[17], S. Marti-Garcia[167], B. Martin[30], B. Martin[88], J.P. Martin[93], T.A. Martin[18], V.J. Martin[46], B. Martin dit Latour[49], S. Martin-Haugh[149], M. Martinez[12], V. Martinez Outschoorn[57], A.C. Martyniuk[169], M. Marx[82], F. Marzano[132a], A. Marzin[111], L. Masetti[81], T. Mashimo[155], R. Mashinistov[94], J. Masik[82], A.L. Maslennikov[107], I. Massa[20a,20b], G. Massaro[105], N. Massol[5], P. Mastrandrea[148], A. Mastroberardino[37a,37b], T. Masubuchi[155], P. Matricon[115], H. Matsunaga[155], T. Matsushita[66], C. Mattravers[118,c], J. Maurer[83], S.J. Maxfield[73], A. Mayne[139], R. Mazini[151], M. Mazur[21], L. Mazzaferro[133a,133b], M. Mazzanti[89a], J. Mc Donald[85], S.P. Mc Kee[87], A. McCarn[165], R.L. McCarthy[148], T.G. McCarthy[29], N.A. McCubbin[129], K.W. McFarlane[56,*], J.A. Mcfayden[139], G. Mchedlidze[51b], T. Mclaughlan[18], S.J. McMahon[129], R.A. McPherson[169,k], A. Meade[84], J. Mechnich[105], M. Mechtel[175], M. Medinnis[42], R. Meera-Lebbai[111], T. Meguro[116], R. Mehdiyev[93], S. Mehlhase[36], A. Mehta[73], K. Meier[58a], B. Meirose[79], C. Melachrinos[31], B.R. Mellado Garcia[173], F. Meloni[89a,89b], L. Mendoza Navas[162], Z. Meng[151,u], A. Mengarelli[20a,20b], S. Menke[99], E. Meoni[161], K.M. Mercurio[57], P. Mermod[49], L. Merola[102a,102b], C. Meroni[89a], F.S. Merritt[31], H. Merritt[109], A. Messina[30,y], J. Metcalfe[25], A.S. Mete[163], C. Meyer[81], C. Meyer[31], J-P. Meyer[136], J. Meyer[174], J. Meyer[54], T.C. Meyer[30], J. Miao[33d], S. Michal[30], L. Micu[26a], R.P. Middleton[129], S. Migas[73], L. Mijović[136], G. Mikenberg[172], M. Mikestikova[125], M. Mikuž[74], D.W. Miller[31], R.J. Miller[88], W.J. Mills[168], C. Mills[57], A. Milov[172], D.A. Milstead[146a,146b], D. Milstein[172], A.A. Minaenko[128], M. Miñano Moya[167], I.A. Minashvili[64], A.I. Mincer[108], B. Mindur[38], M. Mineev[64], Y. Ming[173], L.M. Mir[12], G. Mirabelli[132a], J. Mitrevski[137], V.A. Mitsou[167], S. Mitsui[65], P.S. Miyagawa[139], J.U. Mjörnmark[79], T. Moa[146a,146b], V. Moeller[28], K. Mönig[42], N. Möser[21], S. Mohapatra[148], W. Mohr[48], R. Moles-Valls[167], A. Molfetas[30], J. Monk[77], E. Monnier[83], J. Montejo Berlingen[12], F. Monticelli[70], S. Monzani[20a,20b], R.W. Moore[3], G.F. Moorhead[86], C. Mora Herrera[49], A. Moraes[53], N. Morange[136], J. Morel[54], G. Morello[37a,37b], D. Moreno[81], M. Moreno Llácer[167], P. Morettini[50a], M. Morgenstern[44], M. Morii[57], A.K. Morley[30], G. Mornacchi[30], J.D. Morris[75], L. Morvaj[101], H.G. Moser[99], M. Mosidze[51b], J. Moss[109], R. Mount[143], E. Mountricha[10,z], S.V. Mouraviev[94,*], E.J.W. Moyse[84], F. Mueller[58a], J. Mueller[123], K. Mueller[21], T.A. Müller[98], T. Mueller[81], D. Muenstermann[30], Y. Munwes[153], W.J. Murray[129], I. Mussche[105], E. Musto[102a,102b], A.G. Myagkov[128], M. Myska[125], J. Nadal[12], K. Nagai[160], R. Nagai[157], K. Nagano[65], A. Nagarkar[109], Y. Nagasaka[59], M. Nagel[99], A.M. Nairz[30], Y. Nakahama[30], K. Nakamura[155], T. Nakamura[155], I. Nakano[110], G. Nanava[21], A. Napier[161], R. Narayan[58b], M. Nash[77,c], T. Nattermann[21], T. Naumann[42], G. Navarro[162], H.A. Neal[87], P.Yu. Nechaeva[94], T.J. Neep[82], A. Negri[119a,119b], G. Negri[30], M. Negrini[20a], S. Nektarijevic[49], A. Nelson[163], T.K. Nelson[143], S. Nemecek[125], P. Nemethy[108], A.A. Nepomuceno[24a], M. Nessi[30,aa], M.S. Neubauer[165], M. Neumann[175], A. Neusiedl[81], R.M. Neves[108], P. Nevski[25], F.M. Newcomer[120], P.R. Newman[18], V. Nguyen Thi Hong[136], R.B. Nickerson[118], R. Nicolaidou[136], B. Nicquevert[30], F. Niedercorn[115], J. Nielsen[137], N. Nikiforou[35], A. Nikiforov[16], V. Nikolaenko[128], I. Nikolic-Audit[78], K. Nikolics[49], K. Nikolopoulos[18], H. Nilsen[48], P. Nilsson[8], Y. Ninomiya[155], A. Nisati[132a], R. Nisius[99], T. Nobe[157], L. Nodulman[6], M. Nomachi[116], I. Nomidis[154], S. Nor-

berg[111], M. Nordberg[30], P.R. Norton[129], J. Novakova[126], M. Nozaki[65], L. Nozka[113], I.M. Nugent[159a], A.-E. Nuncio-Quiroz[21], G. Nunes Hanninger[86], T. Nunnemann[98], E. Nurse[77], B.J. O'Brien[46], D.C. O'Neil[142], V. O'Shea[53], L.B. Oakes[98], F.G. Oakham[29,d], H. Oberlack[99], J. Ocariz[78], A. Ochi[66], S. Oda[69], S. Odaka[65], J. Odier[83], H. Ogren[60], A. Oh[82], S.H. Oh[45], C.C. Ohm[30], T. Ohshima[101], H. Okawa[25], Y. Okumura[31], T. Okuyama[155], A. Olariu[26a], A.G. Olchevski[64], S.A. Olivares Pino[32a], M. Oliveira[124a,h], D. Oliveira Damazio[25], E. Oliver Garcia[167], D. Olivito[120], A. Olszewski[39], J. Olszowska[39], A. Onofre[124a,ab], P.U.E. Onyisi[31], C.J. Oram[159a], M.J. Oreglia[31], Y. Oren[153], D. Orestano[134a,134b], N. Orlando[72a,72b], I. Orlov[107], C. Oropeza Barrera[53], R.S. Orr[158], B. Osculati[50a,50b], R. Ospanov[120], C. Osuna[12], G. Otero y Garzon[27], J.P. Ottersbach[105], M. Ouchrif[135d], E.A. Ouellette[169], F. Ould-Saada[117], A. Ouraou[136], Q. Ouyang[33a], A. Ovcharova[15], M. Owen[82], S. Owen[139], V.E. Ozcan[19a], N. Ozturk[8], A. Pacheco Pages[12], C. Padilla Aranda[12], S. Pagan Griso[15], E. Paganis[139], C. Pahl[99], F. Paige[25], P. Pais[84], K. Pajchel[117], G. Palacino[159b], C.P. Paleari[7], S. Palestini[30], D. Pallin[34], A. Palma[124a], J.D. Palmer[18], Y.B. Pan[173], E. Panagiotopoulou[10], P. Pani[105], N. Panikashvili[87], S. Panitkin[25], D. Pantea[26a], A. Papadelis[146a], Th.D. Papadopoulou[10], A. Paramonov[6], D. Paredes Hernandez[34], W. Park[25,ac], M.A. Parker[28], F. Parodi[50a,50b], J.A. Parsons[35], U. Parzefall[48], S. Pashapour[54], E. Pasqualucci[132a], S. Passaggio[50a], A. Passeri[134a], F. Pastore[134a,134b,*], Fr. Pastore[76], G. Pásztor[49,ad], S. Pataraia[175], N. Patel[150], J.R. Pater[82], S. Patricelli[102a,102b], T. Pauly[30], M. Pecsy[144a], S. Pedraza Lopez[167], M.I. Pedraza Morales[173], S.V. Peleganchuk[107], D. Pelikan[166], H. Peng[33b], B. Penning[31], A. Penson[35], J. Penwell[60], M. Perantoni[24a], K. Perez[35,ae], T. Perez Cavalcanti[42], E. Perez Codina[159a], M.T. Pérez García-Estañ[167], V. Perez Reale[35], L. Perini[89a,89b], H. Pernegger[30], R. Perrino[72a], P. Perrodo[5], V.D. Peshekhonov[64], K. Peters[30], B.A. Petersen[30], J. Petersen[30], T.C. Petersen[36], E. Petit[5], A. Petridis[154], C. Petridou[154], E. Petrolo[132a], F. Petrucci[134a,134b], D. Petschull[42], M. Petteni[142], R. Pezoa[32b], A. Phan[86], P.W. Phillips[129], G. Piacquadio[30], A. Picazio[49], E. Piccaro[75], M. Piccinini[20a,20b], S.M. Piec[42], R. Piegaia[27], D.T. Pignotti[109], J.E. Pilcher[31], A.D. Pilkington[82], J. Pina[124a,b], M. Pinamonti[164a,164c], A. Pinder[118], J.L. Pinfold[3], B. Pinto[124a], C. Pizio[89a,89b], M. Plamondon[169], M.-A. Pleier[25], E. Plotnikova[64], A. Poblaguev[25], S. Poddar[58a], F. Podlyski[34], L. Poggioli[115], D. Pohl[21], M. Pohl[49], G. Polesello[119a], A. Policicchio[37a,37b], A. Polini[20a], J. Poll[75], V. Polychronakos[25], D. Pomeroy[23], K. Pommès[30], L. Pontecorvo[132a], B.G. Pope[88], G.A. Popeneciu[26a], D.S. Popovic[13a], A. Poppleton[30], X. Portell Bueso[30], G.E. Pospelov[99], S. Pospisil[127], I.N. Potrap[99], C.J. Potter[149], C.T. Potter[114], G. Poulard[30], J. Poveda[60], V. Pozdnyakov[64], R. Prabhu[77], P. Pralavorio[83], A. Pranko[15], S. Prasad[30], R. Pravahan[25], S. Prell[63], K. Pretzl[17], D. Price[60], J. Price[73], L.E. Price[6], D. Prieur[123], M. Primavera[72a], K. Prokofiev[108], F. Prokoshin[32b], S. Protopopescu[25], J. Proudfoot[6], X. Prudent[44], M. Przybycien[38], H. Przysiezniak[5], S. Psoroulas[21], E. Ptacek[114], E. Pueschel[84], J. Purdham[87], M. Purohit[25,ac], P. Puzo[115], Y. Pylypchenko[62], J. Qian[87], A. Quadt[54], D.R. Quarrie[15], W.B. Quayle[173], F. Quinonez[32a], M. Raas[104], V. Radeka[25], V. Radescu[42], P. Radloff[114], T. Rador[19a], F. Ragusa[89a,89b], G. Rahal[178], A.M. Rahimi[109], D. Rahm[25], S. Rajagopalan[25], M. Rammensee[48], M. Rammes[141], A.S. Randle-Conde[40], K. Randrianarivony[29], F. Rauscher[98], T.C. Rave[48], M. Raymond[30], A.L. Read[117], D.M. Rebuzzi[119a,119b], A. Redelbach[174], G. Redlinger[25], R. Reece[120], K. Reeves[41], E. Reinherz-Aronis[153], A. Reinsch[114], I. Reisinger[43], C. Rembser[30], Z.L. Ren[151], A. Renaud[115], M. Rescigno[132a], S. Resconi[89a], B. Resende[136], P. Reznicek[98], R. Rezvani[158], R. Richter[99], E. Richter-Was[5,af], M. Ridel[78], M. Rijpstra[105], M. Rijssenbeek[148], A. Rimoldi[119a,119b], L. Rinaldi[20a], R.R. Rios[40], I. Riu[12], G. Rivoltella[89a,89b], F. Rizatdinova[112], E. Rizvi[75], S.H. Robertson[85,k], A. Robichaud-Veronneau[118], D. Robinson[28], J.E.M. Robinson[82], A. Robson[53], J.G. Rocha de Lima[106], C. Roda[122a,122b], D. Roda Dos Santos[30], A. Roe[54], S. Roe[30], O. Røhne[117], S. Rolli[161], A. Romaniouk[96], M. Romano[20a,20b], G. Romeo[27], E. Romero Adam[167], N. Rompotis[138], L. Roos[78], E. Ros[167], S. Rosati[132a], K. Rosbach[49], A. Rose[149], M. Rose[76], G.A. Rosenbaum[158], E.I. Rosenberg[63], P.L. Rosendahl[14], O. Rosenthal[141], L. Rosselet[49], V. Rossetti[12], E. Rossi[132a,132b], L.P. Rossi[50a], M. Rotaru[26a], I. Roth[172], J. Rothberg[138], D. Rousseau[115], C.R. Royon[136], A. Rozanov[83], Y. Rozen[152], X. Ruan[33a,ag], F. Rubbo[12], I. Rubinskiy[42], N. Ruckstuhl[105], V.I. Rud[97], C. Rudolph[44], G. Rudolph[61], F. Rühr[7], A. Ruiz-Martinez[63], L. Rumyantsev[64], Z. Rurikova[48], N.A. Rusakovich[64], J.P. Rutherfoord[7], C. Ruwiedel[15,*], P. Ruzicka[125], Y.F. Ryabov[121], M. Rybar[126], G. Rybkin[115], N.C. Ryder[118], A.F. Saavedra[150], I. Sadeh[153], H.F-W. Sadrozinski[137], R. Sadykov[64], F. Safai Tehrani[132a], H. Sakamoto[155], G. Salamanna[75], A. Salamon[133a], M. Saleem[111], D. Salek[30], D. Salihagic[99], A. Salnikov[143], J. Salt[167], B.M. Salvachua Ferrando[6], D. Salvatore[37a,37b], F. Salvatore[149], A. Salvucci[104], A. Salzburger[30], D. Sampsonidis[154], B.H. Samset[117], A. Sanchez[102a,102b], V. Sanchez Martinez[167], H. Sandaker[14], H.G. Sander[81], M.P. Sanders[98], M. Sandhoff[175], T. Sandoval[28], C. Sandoval[162], R. Sandstroem[99], D.P.C. Sankey[129], A. Sansoni[47], C. Santamarina Rios[85], C. Santoni[34], R. Santonico[133a,133b], H. Santos[124a], J.G. Saraiva[124a], T. Sarangi[173], E. Sarkisyan-Grinbaum[8], F. Sarri[122a,122b], G. Sartisohn[175], O. Sasaki[65], Y. Sasaki[155], N. Sasao[67], I. Satsounkevitch[90], G. Sauvage[5,*], E. Sauvan[5], J.B. Sauvan[115], P. Savard[158,d], V. Savinov[123], D.O. Savu[30], L. Sawyer[25,m], D.H. Saxon[53], J. Saxon[120], C. Sbarra[20a], A. Sbrizzi[20a,20b], D.A. Scannicchio[163], M. Scarcella[150], J. Schaarschmidt[115], P. Schacht[99], D. Schaefer[120], U. Schäfer[81], S. Schaepe[21], S. Schaetzel[58b], A.C. Schaffer[115], D. Schaile[98], R.D. Schamberger[148], A.G. Schamov[107], V. Scharf[58a], V.A. Schegelsky[121], D. Scheirich[87], M. Schernau[163], M.I. Scherzer[35], C. Schiavi[50a,50b], J. Schieck[98], M. Schioppa[37a,37b], S. Schlenker[30], E. Schmidt[48], K. Schmieden[21], C. Schmitt[81], S. Schmitt[58b],

M. Schmitz[21], B. Schneider[17], U. Schnoor[44], A. Schoening[58b], A.L.S. Schorlemmer[54], M. Schott[30], D. Schouten[159a], J. Schovancova[125], M. Schram[85], C. Schroeder[81], N. Schroer[58c], M.J. Schultens[21], J. Schultes[175], H.-C. Schultz-Coulon[58a], H. Schulz[16], M. Schumacher[48], B.A. Schumm[137], Ph. Schune[136], C. Schwanenberger[82], A. Schwartzman[143], Ph. Schwegler[99], Ph. Schwemling[78], R. Schwienhorst[88], R. Schwierz[44], J. Schwindling[136], T. Schwindt[21], M. Schwoerer[5], G. Sciolla[23], W.G. Scott[129], J. Searcy[114], G. Sedov[42], E. Sedykh[121], S.C. Seidel[103], A. Seiden[137], F. Seifert[44], J.M. Seixas[24a], G. Sekhniaidze[102a], S.J. Sekula[40], K.E. Selbach[46], D.M. Seliverstov[121], B. Sellden[146a], G. Sellers[73], M. Seman[144b], N. Semprini-Cesari[20a,20b], C. Serfon[98], L. Serin[115], L. Serkin[54], R. Seuster[99], H. Severini[111], A. Sfyrla[30], E. Shabalina[54], M. Shamim[114], L.Y. Shan[33a], J.T. Shank[22], Q.T. Shao[86], M. Shapiro[15], P.B. Shatalov[95], K. Shaw[164a,164c], D. Sherman[176], P. Sherwood[77], S. Shimizu[101], M. Shimojima[100], T. Shin[56], M. Shiyakova[64], A. Shmeleva[94], M.J. Shochet[31], D. Short[118], S. Shrestha[63], E. Shulga[96], M.A. Shupe[7], P. Sicho[125], A. Sidoti[132a], F. Siegert[48], Dj. Sijacki[13a], O. Silbert[172], J. Silva[124a], Y. Silver[153], D. Silverstein[143], S.B. Silverstein[146a], V. Simak[127], O. Simard[136], Lj. Simic[13a], S. Simion[115], E. Simioni[81], B. Simmons[77], R. Simoniello[89a,89b], M. Simonyan[36], P. Sinervo[158], N.B. Sinev[114], V. Sipica[141], G. Siragusa[174], A. Sircar[25], A.N. Sisakyan[64,*], S.Yu. Sivoklokov[97], J. Sjölin[146a,146b], T.B. Sjursen[14], L.A. Skinnari[15], H.P. Skottowe[57], K. Skovpen[107], P. Skubic[111], M. Slater[18], T. Slavicek[127], K. Sliwa[161], V. Smakhtin[172], B.H. Smart[46], L. Smestad[117], S.Yu. Smirnov[96], Y. Smirnov[96], L.N. Smirnova[97], O. Smirnova[79], B.C. Smith[57], D. Smith[143], K.M. Smith[53], M. Smizanska[71], K. Smolek[127], A.A. Snesarev[94], S.W. Snow[82], J. Snow[111], S. Snyder[25], R. Sobie[169,k], J. Sodomka[127], A. Soffer[153], C.A. Solans[167], M. Solar[127], J. Solc[127], E.Yu. Soldatov[96], U. Soldevila[167], E. Solfaroli Camillocci[132a,132b], A.A. Solodkov[128], O.V. Solovyanov[128], V. Solovyev[121], N. Soni[1], V. Sopko[127], B. Sopko[127], M. Sosebee[8], R. Soualah[164a,164c], A. Soukharev[107], S. Spagnolo[72a,72b], F. Spanò[76], R. Spighi[20a], G. Spigo[30], R. Spiwoks[30], M. Spousta[126,ah], T. Spreitzer[158], B. Spurlock[8], R.D. St. Denis[53], J. Stahlman[120], R. Stamen[58a], E. Stanecka[39], R.W. Stanek[6], C. Stanescu[134a], M. Stanescu-Bellu[42], M.M. Stanitzki[42], S. Stapnes[117], E.A. Starchenko[128], J. Stark[55], P. Staroba[125], P. Starovoitov[42], R. Staszewski[39], A. Staude[98], P. Stavina[144a,*], G. Steele[53], P. Steinbach[44], P. Steinberg[25], I. Stekl[127], B. Stelzer[142], H.J. Stelzer[88], O. Stelzer-Chilton[159a], H. Stenzel[52], S. Stern[99], G.A. Stewart[30], J.A. Stillings[21], M.C. Stockton[85], K. Stoerig[48], G. Stoicea[26a], S. Stonjek[99], P. Strachota[126], A.R. Stradling[8], A. Straessner[44], J. Strandberg[147], S. Strandberg[146a,146b], A. Strandlie[117], M. Strang[109], E. Strauss[143], M. Strauss[111], P. Strizenec[144b], R. Ströhmer[174], D.M. Strom[114], J.A. Strong[76,*], R. Stroynowski[40], J. Strube[129], B. Stugu[14], I. Stumer[25,*], J. Stupak[148], P. Sturm[175], N.A. Styles[42], D.A. Soh[151,w], D. Su[143], HS. Subramania[3], A. Succurro[12], Y. Sugaya[116], C. Suhr[106], M. Suk[126], V.V. Sulin[94], S. Sultansoy[4d], T. Sumida[67], X. Sun[55], J.E. Sundermann[48], K. Suruliz[139], G. Susinno[37a,37b], M.R. Sutton[149], Y. Suzuki[65], Y. Suzuki[66], M. Svatos[125], S. Swedish[168], I. Sykora[144a], T. Sykora[126], J. Sánchez[167], D. Ta[105], K. Tackmann[42], A. Taffard[163], R. Tafirout[159a], N. Taiblum[153], Y. Takahashi[101], H. Takai[25], R. Takashima[68], H. Takeda[66], T. Takeshita[140], Y. Takubo[65], M. Talby[83], A. Talyshev[107,f], M.C. Tamsett[25], K.G. Tan[86], J. Tanaka[155], R. Tanaka[115], S. Tanaka[131], S. Tanaka[65], A.J. Tanasijczuk[142], K. Tani[66], N. Tannoury[83], S. Tapprogge[81], D. Tardif[158], S. Tarem[152], F. Tarrade[29], G.F. Tartarelli[89a], P. Tas[126], M. Tasevsky[125], E. Tassi[37a,37b], M. Tatarkhanov[15], Y. Tayalati[135d], C. Taylor[77], F.E. Taylor[92], G.N. Taylor[86], W. Taylor[159b], M. Teinturier[115], F.A. Teischinger[30], M. Teixeira Dias Castanheira[75], P. Teixeira-Dias[76], K.K. Temming[48], H. Ten Kate[30], P.K. Teng[151], S. Terada[65], K. Terashi[155], J. Teron[80], M. Testa[47], R.J. Teuscher[158,k], J. Therhaag[21], T. Theveneaux-Pelzer[78], S. Thoma[48], J.P. Thomas[18], E.N. Thompson[35], P.D. Thompson[18], P.D. Thompson[158], A.S. Thompson[53], L.A. Thomsen[36], E. Thomson[120], M. Thomson[28], W.M. Thong[86], R.P. Thun[87], F. Tian[35], M.J. Tibbetts[15], T. Tic[125], V.O. Tikhomirov[94], Y.A. Tikhonov[107,f], S. Timoshenko[96], P. Tipton[176], S. Tisserant[83], T. Todorov[5], S. Todorova-Nova[161], B. Toggerson[163], J. Tojo[69], S. Tokár[144a], K. Tokushuku[65], K. Tollefson[88], M. Tomoto[101], L. Tompkins[31], K. Toms[103], A. Tonoyan[14], C. Topfel[17], N.D. Topilin[64], I. Torchiani[30], E. Torrence[114], H. Torres[78], E. Torró Pastor[167], J. Toth[83,ad], F. Touchard[83], D.R. Tovey[139], T. Trefzger[174], L. Tremblet[30], A. Tricoli[30], I.M. Trigger[159a], S. Trincaz-Duvoid[78], M.F. Tripiana[70], N. Triplett[25], W. Trischuk[158], B. Trocmé[55], C. Troncon[89a], M. Trottier-McDonald[142], M. Trzebinski[39], A. Trzupek[39], C. Tsarouchas[30], J.C-L. Tseng[118], M. Tsiakiris[105], P.V. Tsiareshka[90], D. Tsionou[5,ai], G. Tsipolitis[10], S. Tsiskaridze[12], V. Tsiskaridze[48], E.G. Tskhadadze[51a], I.I. Tsukerman[95], V. Tsulaia[15], J.-W. Tsung[21], S. Tsuno[65], D. Tsybychev[148], A. Tua[139], A. Tudorache[26a], V. Tudorache[26a], J.M. Tuggle[31], M. Turala[39], D. Turecek[127], I. Turk Cakir[4e], E. Turlay[105], R. Turra[89a,89b], P.M. Tuts[35], A. Tykhonov[74], M. Tylmad[146a,146b], M. Tyndel[129], G. Tzanakos[9], K. Uchida[21], I. Ueda[155], R. Ueno[29], M. Ugland[14], M. Uhlenbrock[21], M. Uhrmacher[54], F. Ukegawa[160], G. Unal[30], A. Undrus[25], G. Unel[163], Y. Unno[65], D. Urbaniec[35], P. Urquijo[21], G. Usai[8], M. Uslenghi[119a,119b], L. Vacavant[83], V. Vacek[127], B. Vachon[85], S. Vahsen[15], J. Valenta[125], S. Valentinetti[20a,20b], A. Valero[167], S. Valkar[126], E. Valladolid Gallego[167], S. Vallecorsa[152], J.A. Valls Ferrer[167], R. Van Berg[120], P.C. Van Der Deijl[105], R. van der Geer[105], H. van der Graaf[105], R. Van Der Leeuw[105], E. van der Poel[105], D. van der Ster[30], N. van Eldik[30], P. van Gemmeren[6], I. van Vulpen[105], M. Vanadia[99], W. Vandelli[30], A. Vaniachine[6], P. Vankov[42], F. Vannucci[78], R. Vari[132a], T. Varol[84], D. Varouchas[15], A. Vartapetian[8], K.E. Varvell[150], V.I. Vassilakopoulos[56], F. Vazeille[34], T. Vazquez Schroeder[54], G. Vegni[89a,89b], J.J. Veillet[115], F. Veloso[124a], R. Veness[30], S. Veneziano[132a], A. Ventura[72a,72b], D. Ventura[84], M. Venturi[48], N. Venturi[158], V. Vercesi[119a],

M. Verducci[138], W. Verkerke[105], J.C. Vermeulen[105], A. Vest[44], M.C. Vetterli[142,d], I. Vichou[165], T. Vickey[145b,aj], O.E. Vickey Boeriu[145b], G.H.A. Viehhauser[118], S. Viel[168], M. Villa[20a,20b], M. Villaplana Perez[167], E. Vilucchi[47], M.G. Vincter[29], E. Vinek[30], V.B. Vinogradov[64], M. Virchaux[136,*], J. Virzi[15], O. Vitells[172], M. Viti[42], I. Vivarelli[48], F. Vives Vaque[3], S. Vlachos[10], D. Vladoiu[98], M. Vlasak[127], A. Vogel[21], P. Vokac[127], G. Volpi[47], M. Volpi[86], G. Volpini[89a], H. von der Schmitt[99], H. von Radziewski[48], E. von Toerne[21], V. Vorobel[126], V. Vorwerk[12], M. Vos[167], R. Voss[30], T.T. Voss[175], J.H. Vossebeld[73], N. Vranjes[136], M. Vranjes Milosavljevic[105], V. Vrba[125], M. Vreeswijk[105], T. Vu Anh[48], R. Vuillermet[30], I. Vukotic[31], W. Wagner[175], P. Wagner[120], H. Wahlen[175], S. Wahrmund[44], J. Wakabayashi[101], S. Walch[87], J. Walder[71], R. Walker[98], W. Walkowiak[141], R. Wall[176], P. Waller[73], B. Walsh[176], C. Wang[45], H. Wang[173], H. Wang[33b,ak], J. Wang[151], J. Wang[55], R. Wang[103], S.M. Wang[151], T. Wang[21], A. Warburton[85], C.P. Ward[28], M. Warsinsky[48], A. Washbrook[46], C. Wasicki[42], I. Watanabe[66], P.M. Watkins[18], A.T. Watson[18], I.J. Watson[150], M.F. Watson[18], G. Watts[138], S. Watts[82], A.T. Waugh[150], B.M. Waugh[77], M.S. Weber[17], P. Weber[54], A.R. Weidberg[118], P. Weigell[99], J. Weingarten[54], C. Weiser[48], P.S. Wells[30], T. Wenaus[25], D. Wendland[16], Z. Weng[151,w], T. Wengler[30], S. Wenig[30], N. Wermes[21], M. Werner[48], P. Werner[30], M. Werth[163], M. Wessels[58a], J. Wetter[161], C. Weydert[55], K. Whalen[29], S.J. Wheeler-Ellis[163], A. White[8], M.J. White[86], S. White[122a,122b], S.R. Whitehead[118], D. Whiteson[163], D. Whittington[60], F. Wicek[115], D. Wicke[175], F.J. Wickens[129], W. Wiedenmann[173], M. Wielers[129], P. Wienemann[21], C. Wiglesworth[75], L.A.M. Wiik-Fuchs[48], P.A. Wijeratne[77], A. Wildauer[99], M.A. Wildt[42,s], I. Wilhelm[126], H.G. Wilkens[30], J.Z. Will[98], E. Williams[35], H.H. Williams[120], W. Willis[35], S. Willocq[84], J.A. Wilson[18], M.G. Wilson[143], A. Wilson[87], I. Wingerter-Seez[5], S. Winkelmann[48], F. Winklmeier[30], M. Wittgen[143], S.J. Wollstadt[81], M.W. Wolter[39], H. Wolters[124a,h], W.C. Wong[41], G. Wooden[87], B.K. Wosiek[39], J. Wotschack[30], M.J. Woudstra[82], K.W. Wozniak[39], K. Wraight[53], M. Wright[53], B. Wrona[73], S.L. Wu[173], X. Wu[49], Y. Wu[33b,al], E. Wulf[35], B.M. Wynne[46], S. Xella[36], M. Xiao[136], S. Xie[48], C. Xu[33b,z], D. Xu[139], B. Yabsley[150], S. Yacoob[145a,am], M. Yamada[65], H. Yamaguchi[155], A. Yamamoto[65], K. Yamamoto[63], S. Yamamoto[155], T. Yamamura[155], T. Yamanaka[155], J. Yamaoka[45], T. Yamazaki[155], Y. Yamazaki[66], Z. Yan[22], H. Yang[87], U.K. Yang[82], Y. Yang[109], Z. Yang[146a,146b], S. Yanush[91], L. Yao[33a], Y. Yao[15], Y. Yasu[65], G.V. Ybeles Smit[130], J. Ye[40], S. Ye[25], M. Yilmaz[4c], R. Yoosoofmiya[123], K. Yorita[171], R. Yoshida[6], C. Young[143], C.J. Young[118], S. Youssef[22], D. Yu[25], J. Yu[8], J. Yu[112], L. Yuan[66], A. Yurkewicz[106], M. Byszewski[30], B. Zabinski[39], R. Zaidan[62], A.M. Zaitsev[128], Z. Zajacova[30], L. Zanello[132a,132b], D. Zanzi[99], A. Zaytsev[25], C. Zeitnitz[175], M. Zeman[125], A. Zemla[39], C. Zendler[21], O. Zenin[128], T. Ženiš[144a], Z. Zinonos[122a,122b], S. Zenz[15], D. Zerwas[115], G. Zevi della Porta[57], Z. Zhan[33d], D. Zhang[33b,ak], H. Zhang[88], J. Zhang[6], X. Zhang[33d], Z. Zhang[115], L. Zhao[108], T. Zhao[138], Z. Zhao[33b], A. Zhemchugov[64], J. Zhong[118], B. Zhou[87], N. Zhou[163], Y. Zhou[151], C.G. Zhu[33d], H. Zhu[42], J. Zhu[87], Y. Zhu[33b], X. Zhuang[98], V. Zhuravlov[99], D. Zieminska[60], N.I. Zimin[64], R. Zimmermann[21], S. Zimmermann[21], S. Zimmermann[48], M. Ziolkowski[141], R. Zitoun[5], L. Živković[35], V.V. Zmouchko[128,*], G. Zobernig[173], A. Zoccoli[20a,20b], M. zur Nedden[16], V. Zutshi[106], L. Zwalinski[30]

[1]School of Chemistry and Physics, University of Adelaide, Adelaide, Australia
[2]Physics Department, SUNY Albany, Albany NY, United States of America
[3]Department of Physics, University of Alberta, Edmonton AB, Canada
[4(a)]Department of Physics, Ankara University, Ankara; [(b)]Department of Physics, Dumlupinar University, Kutahya; [(c)]Department of Physics, Gazi University, Ankara; [(d)]Division of Physics, TOBB University of Economics and Technology, Ankara; [(e)]Turkish Atomic Energy Authority, Ankara, Turkey
[5]LAPP, CNRS/IN2P3 and Université de Savoie, Annecy-le-Vieux, France
[6]High Energy Physics Division, Argonne National Laboratory, Argonne IL, United States of America
[7]Department of Physics, University of Arizona, Tucson AZ, United States of America
[8]Department of Physics, The University of Texas at Arlington, Arlington TX, United States of America
[9]Physics Department, University of Athens, Athens, Greece
[10]Physics Department, National Technical University of Athens, Zografou, Greece
[11]Institute of Physics, Azerbaijan Academy of Sciences, Baku, Azerbaijan
[12]Institut de Física d'Altes Energies and Departament de Física de la Universitat Autònoma de Barcelona and ICREA, Barcelona, Spain
[13(a)]Institute of Physics, University of Belgrade, Belgrade; [(b)]Vinca Institute of Nuclear Sciences, University of Belgrade, Belgrade, Serbia
[14]Department for Physics and Technology, University of Bergen, Bergen, Norway
[15]Physics Division, Lawrence Berkeley National Laboratory and University of California, Berkeley CA, United States of America
[16]Department of Physics, Humboldt University, Berlin, Germany

[17]Albert Einstein Center for Fundamental Physics and Laboratory for High Energy Physics, University of Bern, Bern, Switzerland
[18]School of Physics and Astronomy, University of Birmingham, Birmingham, United Kingdom
[19(a)]Department of Physics, Bogazici University, Istanbul; [(b)]Division of Physics, Dogus University, Istanbul; [(c)]Department of Physics Engineering, Gaziantep University, Gaziantep; [(d)]Department of Physics, Istanbul Technical University, Istanbul, Turkey
[20(a)]INFN Sezione di Bologna; [(b)]Dipartimento di Fisica, Università di Bologna, Bologna, Italy
[21]Physikalisches Institut, University of Bonn, Bonn, Germany
[22]Department of Physics, Boston University, Boston MA, United States of America
[23]Department of Physics, Brandeis University, Waltham MA, United States of America
[24(a)]Universidade Federal do Rio De Janeiro COPPE/EE/IF, Rio de Janeiro; [(b)]Federal University of Juiz de Fora (UFJF), Juiz de Fora; [(c)]Federal University of Sao Joao del Rei (UFSJ), Sao Joao del Rei; [(d)]Instituto de Fisica, Universidade de Sao Paulo, Sao Paulo, Brazil
[25]Physics Department, Brookhaven National Laboratory, Upton NY, United States of America
[26(a)]National Institute of Physics and Nuclear Engineering, Bucharest; [(b)]University Politehnica Bucharest, Bucharest; [(c)]West University in Timisoara, Timisoara, Romania
[27]Departamento de Física, Universidad de Buenos Aires, Buenos Aires, Argentina
[28]Cavendish Laboratory, University of Cambridge, Cambridge, United Kingdom
[29]Department of Physics, Carleton University, Ottawa ON, Canada
[30]CERN, Geneva, Switzerland
[31]Enrico Fermi Institute, University of Chicago, Chicago IL, United States of America
[32(a)]Departamento de Física, Pontificia Universidad Católica de Chile, Santiago; [(b)]Departamento de Física, Universidad Técnica Federico Santa María, Valparaíso, Chile
[33(a)]Institute of High Energy Physics, Chinese Academy of Sciences, Beijing; [(b)]Department of Modern Physics, University of Science and Technology of China, Anhui; [(c)]Department of Physics, Nanjing University, Jiangsu; [(d)]School of Physics, Shandong University, Shandong, China
[34]Laboratoire de Physique Corpusculaire, Clermont Université and Université Blaise Pascal and CNRS/IN2P3, Clermont-Ferrand, France
[35]Nevis Laboratory, Columbia University, Irvington NY, United States of America
[36]Niels Bohr Institute, University of Copenhagen, Kobenhavn, Denmark
[37(a)]INFN Gruppo Collegato di Cosenza; [(b)]Dipartimento di Fisica, Università della Calabria, Arcavata di Rende, Italy
[38]AGH University of Science and Technology, Faculty of Physics and Applied Computer Science, Krakow, Poland
[39]The Henryk Niewodniczanski Institute of Nuclear Physics, Polish Academy of Sciences, Krakow, Poland
[40]Physics Department, Southern Methodist University, Dallas TX, United States of America
[41]Physics Department, University of Texas at Dallas, Richardson TX, United States of America
[42]DESY, Hamburg and Zeuthen, Germany
[43]Institut für Experimentelle Physik IV, Technische Universität Dortmund, Dortmund, Germany
[44]Institut für Kern- und Teilchenphysik, Technical University Dresden, Dresden, Germany
[45]Department of Physics, Duke University, Durham NC, United States of America
[46]SUPA - School of Physics and Astronomy, University of Edinburgh, Edinburgh, United Kingdom
[47]INFN Laboratori Nazionali di Frascati, Frascati, Italy
[48]Fakultät für Mathematik und Physik, Albert-Ludwigs-Universität, Freiburg, Germany
[49]Section de Physique, Université de Genève, Geneva, Switzerland
[50(a)]INFN Sezione di Genova; [(b)]Dipartimento di Fisica, Università di Genova, Genova, Italy
[51(a)]E. Andronikashvili Institute of Physics, Tbilisi State University, Tbilisi; [(b)]High Energy Physics Institute, Tbilisi State University, Tbilisi, Georgia
[52]II Physikalisches Institut, Justus-Liebig-Universität Giessen, Giessen, Germany
[53]SUPA - School of Physics and Astronomy, University of Glasgow, Glasgow, United Kingdom
[54]II Physikalisches Institut, Georg-August-Universität, Göttingen, Germany
[55]Laboratoire de Physique Subatomique et de Cosmologie, Université Joseph Fourier and CNRS/IN2P3 and Institut National Polytechnique de Grenoble, Grenoble, France
[56]Department of Physics, Hampton University, Hampton VA, United States of America
[57]Laboratory for Particle Physics and Cosmology, Harvard University, Cambridge MA, United States of America

[58(a)]Kirchhoff-Institut für Physik, Ruprecht-Karls-Universität Heidelberg, Heidelberg; [(b)]Physikalisches Institut, Ruprecht-Karls-Universität Heidelberg, Heidelberg; [(c)]ZITI Institut für technische Informatik, Ruprecht-Karls-Universität Heidelberg, Mannheim, Germany
[59]Faculty of Applied Information Science, Hiroshima Institute of Technology, Hiroshima, Japan
[60]Department of Physics, Indiana University, Bloomington IN, United States of America
[61]Institut für Astro- und Teilchenphysik, Leopold-Franzens-Universität, Innsbruck, Austria
[62]University of Iowa, Iowa City IA, United States of America
[63]Department of Physics and Astronomy, Iowa State University, Ames IA, United States of America
[64]Joint Institute for Nuclear Research, JINR Dubna, Dubna, Russia
[65]KEK, High Energy Accelerator Research Organization, Tsukuba, Japan
[66]Graduate School of Science, Kobe University, Kobe, Japan
[67]Faculty of Science, Kyoto University, Kyoto, Japan
[68]Kyoto University of Education, Kyoto, Japan
[69]Department of Physics, Kyushu University, Fukuoka, Japan
[70]Instituto de Física La Plata, Universidad Nacional de La Plata and CONICET, La Plata, Argentina
[71]Physics Department, Lancaster University, Lancaster, United Kingdom
[72(a)]INFN Sezione di Lecce; [(b)]Dipartimento di Matematica e Fisica, Università del Salento, Lecce, Italy
[73]Oliver Lodge Laboratory, University of Liverpool, Liverpool, United Kingdom
[74]Department of Physics, Jožef Stefan Institute and University of Ljubljana, Ljubljana, Slovenia
[75]School of Physics and Astronomy, Queen Mary University of London, London, United Kingdom
[76]Department of Physics, Royal Holloway University of London, Surrey, United Kingdom
[77]Department of Physics and Astronomy, University College London, London, United Kingdom
[78]Laboratoire de Physique Nucléaire et de Hautes Energies, UPMC and Université Paris-Diderot and CNRS/IN2P3, Paris, France
[79]Fysiska institutionen, Lunds universitet, Lund, Sweden
[80]Departamento de Fisica Teorica C-15, Universidad Autonoma de Madrid, Madrid, Spain
[81]Institut für Physik, Universität Mainz, Mainz, Germany
[82]School of Physics and Astronomy, University of Manchester, Manchester, United Kingdom
[83]CPPM, Aix-Marseille Université and CNRS/IN2P3, Marseille, France
[84]Department of Physics, University of Massachusetts, Amherst MA, United States of America
[85]Department of Physics, McGill University, Montreal QC, Canada
[86]School of Physics, University of Melbourne, Victoria, Australia
[87]Department of Physics, The University of Michigan, Ann Arbor MI, United States of America
[88]Department of Physics and Astronomy, Michigan State University, East Lansing MI, United States of America
[89(a)]INFN Sezione di Milano; [(b)]Dipartimento di Fisica, Università di Milano, Milano, Italy
[90]B.I. Stepanov Institute of Physics, National Academy of Sciences of Belarus, Minsk, Republic of Belarus
[91]National Scientific and Educational Centre for Particle and High Energy Physics, Minsk, Republic of Belarus
[92]Department of Physics, Massachusetts Institute of Technology, Cambridge MA, United States of America
[93]Group of Particle Physics, University of Montreal, Montreal QC, Canada
[94]P.N. Lebedev Institute of Physics, Academy of Sciences, Moscow, Russia
[95]Institute for Theoretical and Experimental Physics (ITEP), Moscow, Russia
[96]Moscow Engineering and Physics Institute (MEPhI), Moscow, Russia
[97]Skobeltsyn Institute of Nuclear Physics, Lomonosov Moscow State University, Moscow, Russia
[98]Fakultät für Physik, Ludwig-Maximilians-Universität München, München, Germany
[99]Max-Planck-Institut für Physik (Werner-Heisenberg-Institut), München, Germany
[100]Nagasaki Institute of Applied Science, Nagasaki, Japan
[101]Graduate School of Science and Kobayashi–Maskawa Institute, Nagoya University, Nagoya, Japan
[102(a)]INFN Sezione di Napoli; [(b)]Dipartimento di Scienze Fisiche, Università di Napoli, Napoli, Italy
[103]Department of Physics and Astronomy, University of New Mexico, Albuquerque NM, United States of America
[104]Institute for Mathematics, Astrophysics and Particle Physics, Radboud University Nijmegen/Nikhef, Nijmegen, Netherlands
[105]Nikhef National Institute for Subatomic Physics and University of Amsterdam, Amsterdam, Netherlands
[106]Department of Physics, Northern Illinois University, DeKalb IL, United States of America

[107]Budker Institute of Nuclear Physics, SB RAS, Novosibirsk, Russia
[108]Department of Physics, New York University, New York NY, United States of America
[109]Ohio State University, Columbus OH, United States of America
[110]Faculty of Science, Okayama University, Okayama, Japan
[111]Homer L. Dodge Department of Physics and Astronomy, University of Oklahoma, Norman OK, United States of America
[112]Department of Physics, Oklahoma State University, Stillwater OK, United States of America
[113]Palacký University, RCPTM, Olomouc, Czech Republic
[114]Center for High Energy Physics, University of Oregon, Eugene OR, United States of America
[115]LAL, Université Paris-Sud and CNRS/IN2P3, Orsay, France
[116]Graduate School of Science, Osaka University, Osaka, Japan
[117]Department of Physics, University of Oslo, Oslo, Norway
[118]Department of Physics, Oxford University, Oxford, United Kingdom
[119(a)]INFN Sezione di Pavia; [(b)]Dipartimento di Fisica, Università di Pavia, Pavia, Italy
[120]Department of Physics, University of Pennsylvania, Philadelphia PA, United States of America
[121]Petersburg Nuclear Physics Institute, Gatchina, Russia
[122(a)]INFN Sezione di Pisa; [(b)]Dipartimento di Fisica E. Fermi, Università di Pisa, Pisa, Italy
[123]Department of Physics and Astronomy, University of Pittsburgh, Pittsburgh PA, United States of America
[124(a)]Laboratorio de Instrumentacao e Fisica Experimental de Particulas - LIP, Lisboa, Portugal; [(b)]Departamento de Fisica Teorica y del Cosmos and CAFPE, Universidad de Granada, Granada, Spain
[125]Institute of Physics, Academy of Sciences of the Czech Republic, Praha, Czech Republic
[126]Faculty of Mathematics and Physics, Charles University in Prague, Praha, Czech Republic
[127]Czech Technical University in Prague, Praha, Czech Republic
[128]State Research Center Institute for High Energy Physics, Protvino, Russia
[129]Particle Physics Department, Rutherford Appleton Laboratory, Didcot, United Kingdom
[130]Physics Department, University of Regina, Regina SK, Canada
[131]Ritsumeikan University, Kusatsu, Shiga, Japan
[132(a)]INFN Sezione di Roma I; [(b)]Dipartimento di Fisica, Università La Sapienza, Roma, Italy
[133(a)]INFN Sezione di Roma Tor Vergata; [(b)]Dipartimento di Fisica, Università di Roma Tor Vergata, Roma, Italy
[134(a)]INFN Sezione di Roma Tre; [(b)]Dipartimento di Fisica, Università Roma Tre, Roma, Italy
[135(a)]Faculté des Sciences Ain Chock, Réseau Universitaire de Physique des Hautes Energies - Université Hassan II, Casablanca; [(b)]Centre National de l'Energie des Sciences Techniques Nucleaires, Rabat; [(c)]Faculté des Sciences Semlalia, Université Cadi Ayyad, LPHEA, Marrakech; [(d)]Faculté des Sciences, Université Mohamed Premier and LPTPM, Oujda; [(e)]Faculté des sciences, Université Mohammed V-Agdal, Rabat, Morocco
[136]DSM/IRFU (Institut de Recherches sur les Lois Fondamentales de l'Univers), CEA Saclay (Commissariat a l'Energie Atomique), Gif-sur-Yvette, France
[137]Santa Cruz Institute for Particle Physics, University of California Santa Cruz, Santa Cruz CA, United States of America
[138]Department of Physics, University of Washington, Seattle WA, United States of America
[139]Department of Physics and Astronomy, University of Sheffield, Sheffield, United Kingdom
[140]Department of Physics, Shinshu University, Nagano, Japan
[141]Fachbereich Physik, Universität Siegen, Siegen, Germany
[142]Department of Physics, Simon Fraser University, Burnaby BC, Canada
[143]SLAC National Accelerator Laboratory, Stanford CA, United States of America
[144(a)]Faculty of Mathematics, Physics & Informatics, Comenius University, Bratislava; [(b)]Department of Subnuclear Physics, Institute of Experimental Physics of the Slovak Academy of Sciences, Kosice, Slovak Republic
[145(a)]Department of Physics, University of Johannesburg, Johannesburg; [(b)]School of Physics, University of the Witwatersrand, Johannesburg, South Africa
[146(a)]Department of Physics, Stockholm University; [(b)]The Oskar Klein Centre, Stockholm, Sweden
[147]Physics Department, Royal Institute of Technology, Stockholm, Sweden
[148]Departments of Physics & Astronomy and Chemistry, Stony Brook University, Stony Brook NY, United States of America
[149]Department of Physics and Astronomy, University of Sussex, Brighton, United Kingdom
[150]School of Physics, University of Sydney, Sydney, Australia

[151]Institute of Physics, Academia Sinica, Taipei, Taiwan
[152]Department of Physics, Technion: Israel Institute of Technology, Haifa, Israel
[153]Raymond and Beverly Sackler School of Physics and Astronomy, Tel Aviv University, Tel Aviv, Israel
[154]Department of Physics, Aristotle University of Thessaloniki, Thessaloniki, Greece
[155]International Center for Elementary Particle Physics and Department of Physics, The University of Tokyo, Tokyo, Japan
[156]Graduate School of Science and Technology, Tokyo Metropolitan University, Tokyo, Japan
[157]Department of Physics, Tokyo Institute of Technology, Tokyo, Japan
[158]Department of Physics, University of Toronto, Toronto ON, Canada
[159(a)]TRIUMF, Vancouver BC; [(b)]Department of Physics and Astronomy, York University, Toronto ON, Canada
[160]Faculty of Pure and Applied Sciences, University of Tsukuba, Tsukuba, Japan
[161]Department of Physics and Astronomy, Tufts University, Medford MA, United States of America
[162]Centro de Investigaciones, Universidad Antonio Narino, Bogota, Colombia
[163]Department of Physics and Astronomy, University of California Irvine, Irvine CA, United States of America
[164(a)]INFN Gruppo Collegato di Udine, Udine; [(b)]ICTP, Trieste; [(c)]Dipartimento di Chimica, Fisica e Ambiente, Università di Udine, Udine, Italy
[165]Department of Physics, University of Illinois, Urbana IL, United States of America
[166]Department of Physics and Astronomy, University of Uppsala, Uppsala, Sweden
[167]Instituto de Física Corpuscular (IFIC) and Departamento de Física Atómica, Molecular y Nuclear and Departamento de Ingeniería Electrónica and Instituto de Microelectrónica de Barcelona (IMB-CNM), University of Valencia and CSIC, Valencia, Spain
[168]Department of Physics, University of British Columbia, Vancouver BC, Canada
[169]Department of Physics and Astronomy, University of Victoria, Victoria BC, Canada
[170]Department of Physics, University of Warwick, Coventry, United Kingdom
[171]Waseda University, Tokyo, Japan
[172]Department of Particle Physics, The Weizmann Institute of Science, Rehovot, Israel
[173]Department of Physics, University of Wisconsin, Madison WI, United States of America
[174]Fakultät für Physik und Astronomie, Julius-Maximilians-Universität, Würzburg, Germany
[175]Fachbereich C Physik, Bergische Universität Wuppertal, Wuppertal, Germany
[176]Department of Physics, Yale University, New Haven CT, United States of America
[177]Yerevan Physics Institute, Yerevan, Armenia
[178]Centre de Calcul de l'Institut National de Physique Nucléaire et de Physique des Particules (IN2P3), Villeurbanne, France
[a]Also at Laboratorio de Instrumentacao e Fisica Experimental de Particulas - LIP, Lisboa, Portugal
[b]Also at Faculdade de Ciencias and CFNUL, Universidade de Lisboa, Lisboa, Portugal
[c]Also at Particle Physics Department, Rutherford Appleton Laboratory, Didcot, United Kingdom
[d]Also at TRIUMF, Vancouver BC, Canada
[e]Also at Department of Physics, California State University, Fresno CA, United States of America
[f]Also at Novosibirsk State University, Novosibirsk, Russia
[g]Also at Fermilab, Batavia IL, United States of America
[h]Also at Department of Physics, University of Coimbra, Coimbra, Portugal
[i]Also at Department of Physics, UASLP, San Luis Potosi, Mexico
[j]Also at Università di Napoli Parthenope, Napoli, Italy
[k]Also at Institute of Particle Physics (IPP), Canada
[l]Also at Department of Physics, Middle East Technical University, Ankara, Turkey
[m]Also at Louisiana Tech University, Ruston LA, United States of America
[n]Also at Dep Fisica and CEFITEC of Faculdade de Ciencias e Tecnologia, Universidade Nova de Lisboa, Caparica, Portugal
[o]Also at Department of Physics and Astronomy, University College London, London, United Kingdom
[p]Also at Group of Particle Physics, University of Montreal, Montreal QC, Canada
[q]Also at Department of Physics, University of Cape Town, Cape Town, South Africa
[r]Also at Institute of Physics, Azerbaijan Academy of Sciences, Baku, Azerbaijan
[s]Also at Institut für Experimentalphysik, Universität Hamburg, Hamburg, Germany
[t]Also at Manhattan College, New York NY, United States of America

[u] Also at School of Physics, Shandong University, Shandong, China
[v] Also at CPPM, Aix-Marseille Université and CNRS/IN2P3, Marseille, France
[w] Also at School of Physics and Engineering, Sun Yat-sen University, Guanzhou, China
[x] Also at Academia Sinica Grid Computing, Institute of Physics, Academia Sinica, Taipei, Taiwan
[y] Also at Dipartimento di Fisica, Università La Sapienza, Roma, Italy
[z] Also at DSM/IRFU (Institut de Recherches sur les Lois Fondamentales de l'Univers), CEA Saclay (Commissariat a l'Energie Atomique), Gif-sur-Yvette, France
[aa] Also at Section de Physique, Université de Genève, Geneva, Switzerland
[ab] Also at Departamento de Fisica, Universidade de Minho, Braga, Portugal
[ac] Also at Department of Physics and Astronomy, University of South Carolina, Columbia SC, United States of America
[ad] Also at Institute for Particle and Nuclear Physics, Wigner Research Centre for Physics, Budapest, Hungary
[ae] Also at California Institute of Technology, Pasadena CA, United States of America
[af] Also at Institute of Physics, Jagiellonian University, Krakow, Poland
[ag] Also at LAL, Université Paris-Sud and CNRS/IN2P3, Orsay, France
[ah] Also at Nevis Laboratory, Columbia University, Irvington NY, United States of America
[ai] Also at Department of Physics and Astronomy, University of Sheffield, Sheffield, United Kingdom
[aj] Also at Department of Physics, Oxford University, Oxford, United Kingdom
[ak] Also at Institute of Physics, Academia Sinica, Taipei, Taiwan
[al] Also at Department of Physics, The University of Michigan, Ann Arbor MI, United States of America
[am] Also at Discipline of Physics, University of KwaZulu-Natal, Durban, South Africa
[*] Deceased

Published for SISSA by Springer

Received: *July 29, 2014*
Accepted: *August 13, 2014*
Published: *September 5, 2014*

Search for new particles in events with one lepton and missing transverse momentum in pp collisions at $\sqrt{s} = 8$ TeV with the ATLAS detector

The ATLAS collaboration

E-mail: atlas.publications@cern.ch

Abstract: This paper presents a search for new particles in events with one lepton (electron or muon) and missing transverse momentum using 20.3 fb^{-1} of proton-proton collision data at $\sqrt{s} = 8$ TeV recorded by the ATLAS experiment at the Large Hadron Collider. No significant excess beyond Standard Model expectations is observed. A W' with Sequential Standard Model couplings is excluded at the 95% confidence level for masses up to 3.24 TeV. Excited chiral bosons (W^*) with equivalent coupling strengths are excluded for masses up to 3.21 TeV. In the framework of an effective field theory limits are also set on the dark matter-nucleon scattering cross-section as well as the mass scale M_* of the unknown mediating interaction for dark matter pair production in association with a leptonically decaying W.

Keywords: Hadron-Hadron Scattering, Beyond Standard Model

ArXiv ePrint: 1407.7494

doi:10.1007/JHEP09(2014)037

Contents

JHEP09(2014)037

1 Introduction

High-energy collisions at CERN's Large Hadron Collider (LHC) provide new opportunities to search for physics beyond the Standard Model (SM). This paper describes such a search in events containing a lepton (electron or muon) and missing transverse momentum using 8 TeV pp collision data collected with the ATLAS detector during 2012, corresponding to a total integrated luminosity of 20.3 fb^{-1}.

The first new-physics scenario that is considered in this paper is the Sequential Standard Model (SSM), the extended gauge model of ref. [1]. This model proposes the existence of additional heavy gauge bosons, of which the charged ones are commonly denoted W'. The W' has the same couplings to fermions as the SM W boson and a width that increases linearly with the W' mass. The coupling of the W' to WZ is set to zero. Similar searches [2–7] have been performed using $\sqrt{s} = 1.96$ TeV $p\bar{p}$ collision data by the CDF Collaboration, $\sqrt{s} = 7$ TeV pp collision data by the ATLAS Collaboration as well as $\sqrt{s} = 7$ TeV and $\sqrt{s} = 8$ TeV data by the CMS Collaboration.

The second new-physics scenario that is considered originates from ref. [8] and proposes the existence of charged partners, denoted W^*, of the chiral boson excitations described in ref. [9]. The anomalous (magnetic-moment type) coupling of the W^* leads to kinematic distributions significantly different from those of the W' as demonstrated in the previous ATLAS search [7] that was performed using 7 TeV pp collision data collected in 2011 corresponding to an integrated luminosity of 4.7 fb^{-1}. In the analysis presented in this

paper the search region is expanded to higher masses and the sensitivity is considerably improved in the region covered by the previous search.

The third new-physics scenario considered is of direct production of weakly interacting candidate dark matter (DM) particles. These particles can be pair-produced at the LHC, $pp \to \chi\bar{\chi}$, via a new intermediate state. Since DM particles do not interact with the detector material, these events can be detected if there is associated initial-state radiation of a SM particle [10–13]. The Tevatron and LHC collaborations have reported limits on the cross-section of $p\bar{p}/pp \to \chi\bar{\chi} + X$ where X is a hadronic jet [14–16], a photon [17, 18], a hadronically decaying W or Z boson [19] or a leptonically decaying Z boson [20]. Previous LHC results have also been reinterpreted to set limits on the scenario where X is a leptonically decaying W boson [21]. This analysis is the first direct ATLAS search for this case. Limits are reported for the DM-nucleon scattering cross-section as well as the mass scale, M_*, of a new SM-DM interaction expressed in an effective field theory (EFT) as a four-point contact interaction [22–27]. As discussed in the literature, e.g. refs. [28, 29], the EFT formalism is not always an appropriate approximation but this issue is not addressed any further in this paper. Four effective operators are used as a representative set based on the definitions in ref. [13]: D1 scalar, D5 vector (both constructive and destructive interference cases are considered, the former denoted by D5c and the latter by D5d) and D9 tensor.

The analysis presented here identifies event candidates in the electron and muon channels, sets separate limits and then combines these assuming a common branching fraction for the two final states. The kinematic variable used to identify the signal is the transverse mass

$$m_{\mathrm{T}} = \sqrt{2p_{\mathrm{T}}E_{\mathrm{T}}^{\mathrm{miss}}(1 - \cos\varphi_{\ell\nu})}, \tag{1.1}$$

where p_{T} is the lepton transverse momentum, $E_{\mathrm{T}}^{\mathrm{miss}}$ is the magnitude of the missing transverse momentum vector and $\varphi_{\ell\nu}$ is the angle between the p_{T} and $E_{\mathrm{T}}^{\mathrm{miss}}$ vectors.[1]

The main background to the W', W^* and DM signals comes from the tail of the m_{T} distribution from SM W boson production with decays to the same final state. Other relevant backgrounds are Z boson production with decays into two leptons where one lepton is not reconstructed, W or Z production with decays to τ leptons where a τ subsequently decays to either an electron or a muon, and diboson production. These are collectively referred to as the electroweak (EW) background. There is also a contribution to the background from $t\bar{t}$ and single-top production, collectively referred to as the top background, which is most important for the lowest W'/W^* masses considered here, where it constitutes about 10% of the background after event selection in the electron channel and 15% in the muon channel. Other relevant strong-interaction background sources occur when a light or heavy hadron decays semileptonically or when a jet is misidentified as an electron or muon. These are referred to as the multi-jet background in this paper.

[1] ATLAS uses a right-handed coordinate system with its origin at the nominal interaction point in the centre of the detector and the z-axis along the beam pipe. Cylindrical coordinates (r, φ) are used in the transverse plane, φ being the azimuthal angle around the beam pipe. The pseudorapidity η is defined in terms of the polar angle θ by $\eta = -\ln\tan(\theta/2)$.

JHEP09(2014)037

2 The ATLAS detector

The ATLAS detector [30] is a multi-purpose particle physics detector with a forward-backward symmetric cylindrical geometry and nearly 4π coverage in solid angle. The ATLAS detector has three major components: the inner tracking detector (ID), the calorimeter and the muon spectrometer (MS). Tracks and vertices of charged particles are reconstructed with silicon pixel and silicon microstrip detectors covering $|\eta| < 2.5$ and straw-tube transition radiation detectors covering $|\eta| < 2.0$, all immersed in a homogeneous 2 T magnetic field provided by a superconducting solenoid. The ID is surrounded by a hermetic calorimeter that covers $|\eta| < 4.9$ and provides three-dimensional reconstruction of particle showers. The electromagnetic calorimeter is a liquid argon (LAr) sampling calorimeter, which uses lead absorbers for $|\eta| < 3.2$ and copper absorbers in the very forward region. The hadronic sampling calorimeter uses plastic scintillator tiles as the active material and iron absorbers in the region $|\eta| < 1.7$. In the region $1.5 < |\eta| < 4.9$, liquid argon is used as the active material, with copper and/or tungsten absorbers. The MS surrounds the calorimeters and consists of three large superconducting toroid systems (each with eight coils) together with multiple layers of trigger chambers up to $|\eta| < 2.4$ and tracking chambers, providing precision track measurements, up to $|\eta| < 2.7$.

3 Trigger and reconstruction

The data used in the electron channel were recorded with a trigger requiring the presence of an energy cluster in the EM compartment of the calorimeter (EM cluster) with $E_{\mathrm{T}} > 120\,\mathrm{GeV}$. For the muon channel, matching tracks in the MS and ID with combined $p_{\mathrm{T}} > 36\,\mathrm{GeV}$ are used to select events. In order to compensate for the small loss in the selection efficiency at high p_{T} due to this matching, events are also recorded if a muon with $p_{\mathrm{T}} > 40\,\mathrm{GeV}$ and $|\eta| < 1.05$ is found in the MS. The average trigger efficiency (measured with respect to reconstructed objects) is above 99% in the electron channel and 80%–90% in the muon channel for the region of interest in this analysis.

Each EM cluster with $E_{\mathrm{T}} > 125\,\mathrm{GeV}$ and $|\eta| < 1.37$ or $1.52 < |\eta| < 2.47$ is considered as an electron candidate if it is matched to an ID track. The region $1.37 \leq |\eta| \leq 1.52$ exhibits degraded energy resolution due to the transition from the central region to the forward regions of the calorimeters and is therefore excluded. The track and the cluster must satisfy a set of identification criteria that are optimised for the conditions of many proton-proton collisions in the same or nearby beam bunch crossings (in-time or out-of-time pile-up, respectively) [31]. These criteria require the shower profiles to be consistent with those expected for electrons and impose a minimum requirement on the amount of transition radiation that is present. In addition, to suppress background from photon conversions, a hit in the first layer of the pixel detector is required if an active pixel sensor is traversed. The electron's energy is obtained from the calorimeter measurements while its direction is obtained from the associated track. In the high-E_{T} range relevant for this analysis, the electromagnetic calorimeter energy resolution is measured in data to be 1.2%

JHEP09(2014)037

in the central region and 1.8% in the forward region [32]. These requirements result in about a 90% identification efficiency for electrons with $E_{\mathrm{T}} > 125\,\mathrm{GeV}$.

Muons are required to have a $p_{\mathrm{T}} > 45\,\mathrm{GeV}$, where the momentum of the muon is obtained by combining the ID and MS measurements. To ensure an accurate measurement of the momentum, muons are required to have hits in three MS layers and are restricted to the ranges $|\eta| < 1.0$ and $1.3 < |\eta| < 2.0$. Some of the chambers in the region $1.0 < |\eta| < 1.3$ were not yet installed, hence the momentum resolution of MS tracks is degraded in this region. Including the muon candidates with an η-range $2.0 < |\eta| < 2.5$ would lead to an increase in the signal selection efficiency of up to 12% for lower W' masses and of up to 3% for a W' mass of 3 TeV. However, the background levels in the signal region would increase by more than 15%. Therefore, the previously stated η restrictions are retained. For the final selection of good muon candidates, the individual ID and MS momentum measurements are required to be in agreement within 5 standard deviations. The average momentum resolution is about 15%–20% at $p_{\mathrm{T}} = 1\,\mathrm{TeV}$. About 80% of the muons in the η-range considered are reconstructed, with most of the loss coming from regions without three MS layers.

The $E_{\mathrm{T}}^{\mathrm{miss}}$ in each event is evaluated by summing over energy-calibrated physics objects (jets, photons and leptons) and adding corrections for calorimeter deposits not associated with these objects [33].

This analysis makes use of all of the $\sqrt{s} = 8\,\mathrm{TeV}$ data collected in 2012 for which the relevant detector systems were operating properly and all data quality requirements were satisfied. The integrated luminosity of the data used in this study is $20.3\,\mathrm{fb}^{-1}$ for both the electron and muon decay channels. The uncertainty on this measurement is 2.8%, which is derived following the methodology detailed in ref. [34].

4 Monte Carlo simulation

With the exception of the multi-jet background, which is estimated from data, expected signals and backgrounds are evaluated using simulated Monte Carlo samples and normalised using the calculated cross-sections and the integrated luminosity of the data.

The W' signal events are generated at leading order (LO) with Pythia v8.165 [35, 36] using the MSTW2008 LO [37] parton distribution functions (PDFs). Pythia is also used for the fragmentation and hadronisation of $W^* \to \ell\nu$ events that are generated at LO with CalcHEP v3.3.6 [38] using the CTEQ6L1 PDFs [39]. DM signal samples are generated at LO with Madgraph5 v1.4.5 [40] using the MSTW2008 LO PDFs, interfaced to Pythia v8.165.

The W/Z boson and $t\bar{t}$ backgrounds are generated at next-to-leading order (NLO) with Powheg-Box r1556 [41] using the CT10 NLO [42] PDFs. For the W/Z backgrounds, fragmentation and hadronisation is performed with Pythia v8.165, while for $t\bar{t}$ Pythia v6.426 is used. The single-top background is generated at NLO with MC@NLO v4.06 [43] using the CT10 NLO PDFs for the Wt- and s-channels, and with AcerMC v3.8 [44] using the CTEQ6L1 PDFs for the t-channel. Fragmentation and hadronisation for the MC@NLO samples are performed with Herwig v6.520 [45], using Jimmy v4.31 [46] for the underlying event, whereas Pythia v6.426 is used for the AcerMC samples. The WW, WZ and ZZ

JHEP09(2014)037

diboson backgrounds are generated at LO with Sherpa v1.4.1 [47] using the CT10 NLO PDFs.

The Pythia signal model for W' has $V-A$ SM couplings to fermions but does not include interference between the W and W'. For both W' and W^*, decay channels beside $e\nu$ and $\mu\nu$, notably $\tau\nu$, ud, sc and tb, are included in the calculation of the widths but are not explicitly included as signal or background. At high mass ($m_{W'} > 1\,\text{TeV}$), the total width is about 3.5 % of the pole mass, and the branching fraction to each of the lepton decay channels is 8.2%.

For all samples, final-state photon radiation from leptons is handled by Photos [48]. The ATLAS full detector simulation [49] based on Geant4 [50] is used to propagate the particles and account for the response of the detector. For the underlying event, the ATLAS tune AUET2B [51] is used for Pythia 6 and AU2 [52] is used for Pythia 8, while AUET2 [53] is used for the Herwig with Jimmy. The effect of pile-up is incorporated into the simulation by overlaying additional minimum-bias events generated with Pythia onto the generated hard-scatter events. Simulated events are weighted to match the distribution of the number of interactions per bunch crossing observed in data, but are otherwise reconstructed in the same manner as data.

The $W \to \ell\nu$ and $Z \to \ell\ell$ cross-sections are calculated at next-to-next-to-leading order (NNLO) in QCD with ZWPROD [54] using MSTW2008 NNLO PDFs. Consistent results are obtained using VRAP v0.9 [55] and FEWZ v3.1b2 [56, 57]. Higher-order electroweak corrections are calculated with MCSANC [58]. Mass-dependent K-factors obtained from the ratios of the calculated higher-order cross-sections to the cross-sections of the generated samples are used to scale W^+, W^- and Z backgrounds separately. The $W' \to \ell\nu$ cross-sections are calculated in the same way, except that the electroweak corrections beyond final-state radiation are not included because the calculation for the SM W cannot be applied directly. Cross sections for $W^* \to \ell\nu$ are kept at LO due to the non-renormalisability of the model at higher orders in QCD. The $t\bar{t}$ cross-section is also calculated at NNLO including resummation of next-to-next-to-leading logarithmic (NNLL) soft gluon terms obtained with Top++ v2.0 [59–64] for a top quark mass of 172.5 GeV. The W', W^*, and DM particle signal cross-sections are listed in tables 1 and 2. The most important background cross-sections are listed in table 3.

Uncertainties on the W' cross-section and the W/Z background cross-sections are estimated from variations of the renormalisation and factorisation scales, PDF+α_s variations and PDF choice. The scale uncertainties are estimated by varying both the renormalisation and factorisation scales simultaneously up or down by a factor of two. The resulting maximum variation from the two fluctuations is taken as the symmetric scale uncertainty. The PDF+α_s uncertainty is evaluated using 90% confidence level (CL) eigenvector and 90% CL α_s variations of the nominal MSTW2008 NNLO PDF set and combined with the scale uncertainty in quadrature. The PDF choice uncertainty is evaluated by comparing the central values of the MSTW2008 NNLO, CT10 NNLO, NNPDF 2.3 NNLO [65], ABM11 5N NNLO [66] and HERAPDF 1.5 NNLO [67] PDF sets. The envelope of the PDF central value comparisons and the combination of the scale and PDF+α_s uncertainties is taken as the total uncertainty on the differential cross-section as a function of the invariant mass of

JHEP09(2014)037

Mass [GeV]	$W' \to \ell\nu$ σB [pb]	$W^* \to \ell\nu$ σB [pb]
300	149.0	
400	50.2	37.6
500	21.4	16.2
600	10.4	7.95
750	4.16	3.17
1000	1.16	0.882
1250	0.389	0.294
1500	0.146	0.108
1750	0.0581	0.0423
2000	0.0244	0.0171
2250	0.0108	0.00700
2500	0.00509	0.00290
2750	0.00258	0.00120
3000	0.00144	4.9×10^{-4}
3250	8.9×10^{-4}	2.0×10^{-4}
3500	5.9×10^{-4}	8.0×10^{-5}
3750	4.2×10^{-4}	3.2×10^{-5}
4000	3.1×10^{-4}	1.3×10^{-5}

Table 1. Predicted values of the cross-section times branching fraction (σB) for $W' \to \ell\nu$ and $W^* \to \ell\nu$. The σB for $W' \to \ell\nu$ are at NNLO while those for $W^* \to \ell\nu$ are at LO. The values are given per channel, with $\ell = e$ or μ.

the lepton-neutrino system ($m_{\ell\nu}$). The PDF and α_s uncertainties on the $t\bar{t}$ cross-section are calculated using the PDF4LHC prescription [68] with the MSTW2008 68% CL NNLO, CT10 NNLO and NNPDF2.3 5f FFN PDF error sets added in quadrature to the scale uncertainty. The systematic uncertainty arising from the variation of the top mass by ± 1 GeV is also added in quadrature.

An additional uncertainty on the differential cross-section due to the beam energy uncertainty is calculated as function of $m_{\ell\nu}$ for the charged-current Drell-Yan process with VRAP at NNLO using CT10 NNLO PDFs by taking a 0.66% uncertainty on the energy of each 4 TeV proton beam as determined in ref. [69]. The size of this uncertainty is observed to be about 2% (6%) at $m_{\ell\nu} = 2$ (3) TeV. The calculated uncertainties are propagated to both the W and W'/W^* processes in order to derive uncertainties on the background levels as well as the signal selection efficiencies in each signal region.

Uncertainties are not reported on the cross-sections for the W^* due to the breakdown of higher-order corrections for non-renormalisable models. However, uncertainties on the

JHEP09(2014)037

m_χ [GeV]	DM production σB [pb] D1 $M_* = 10\,\text{GeV}$	D5d $M_* = 100\,\text{GeV}$	D5c $M_* = 1\,\text{TeV}$	D9 $M_* = 1\,\text{TeV}$
1	439	72.2	0.0608	0.0966
100	332	70.8	0.0575	0.0870
200	201	58.8	0.0488	0.0695
400	64.6	32.9	0.0279	0.0365
1000	1.60	2.37	0.00192	0.00227
1300	0.213	0.454	0.000351	0.000412

Table 2. Predicted values of σB for DM signal with different mass values, m_χ. The values of M_* used in the calculation for a given operator are also shown. The cross-sections are at LO, and the values are given for the sum of three lepton flavours $\ell = e, \mu, \tau$.

Process	σB [pb]
$W \to \ell\nu$	12190
$Z/\gamma^* \to \ell\ell$ ($m_{Z/\gamma^*} > 60\,\text{GeV}$)	1120
$t\bar{t} \to \ell X$	137.3

Table 3. Predicted values of σB for the leading backgrounds. The value for $t\bar{t} \to \ell X$ includes all final states with at least one lepton (e, μ or τ). The others are exclusive and are used for both $\ell = e$ and $\ell = \mu$. All cross-sections are at NNLO.

signal selection efficiency for the W^* are evaluated using the same relative differential cross-section uncertainty as for the W'. Uncertainties on DM production are evaluated using 68% confidence level eigenvector variations of the nominal MSTW2008 LO PDF set as in [19].

5 Event selection

The primary vertex for each event is required to have at least three tracks with $p_\text{T} > 0.4\,\text{GeV}$ and to have a longitudinal distance less than 200 mm from the centre of the collision region. There are on average 20.7 interactions per event in the data used for this analysis. The primary vertex is defined to be the one with the highest summed track p_T^2. Spurious tails in the E_T^miss distribution, arising from calorimeter noise and other detector problems are suppressed by checking the quality of each reconstructed jet and discarding events containing reconstructed jets of poor quality, following the description given in ref. [70]. In addition, the ID track associated with the electron or muon is required to be compatible with originating from the primary vertex by requiring that the transverse distance of closest approach, d_0, satisfies $|d_0| < 1$ (0.2) mm and longitudinal distance, z_0, satisfies $|z_0| < 5$ (1) mm for the electron (muon). Events are required to have exactly one electron candidate with $E_\text{T} > 125\,\text{GeV}$ or one muon candidate with $p_\text{T} > 45\,\text{GeV}$

JHEP09(2014)037

satisfying these requirements and the identification criteria described in section 3. In the electron channel, events having additional electrons with $E_{\mathrm{T}} > 20\,\mathrm{GeV}$, passing all electron identification criteria, are discarded. Similarly, in the muon channel, events having additional muon candidates with a p_{T} threshold of 20 GeV are discarded.

To suppress the multi-jet background, the lepton is required to be isolated. In the electron channel, the isolation energy is measured with the calorimeter in a cone $\Delta R = \sqrt{(\Delta\eta)^2 + (\Delta\varphi)^2} = 0.2$ around the electron track, and the requirement is $\Sigma E_{\mathrm{T}}^{\mathrm{calo}} < 0.007 \times E_{\mathrm{T}} + 5\,\mathrm{GeV}$, where the sum includes all calorimeter energy clusters in the cone excluding those that are attributed to the electron. The scaling of the isolation requirement with the electron E_{T} reduces the efficiency loss due to radiation from the electron at high E_{T}. In the muon channel, the isolation energy is measured using ID tracks with $p_{\mathrm{T}}^{\mathrm{trk}} > 1$ GeV in a cone $\Delta R = 0.3$ around the muon track. The isolation requirement is $\sum p_{\mathrm{T}}^{\mathrm{trk}} < 0.05 \times p_{\mathrm{T}}$, where the muon track is excluded from the sum. As in the electron channel, the scaling of the isolation requirement with the muon p_{T} reduces the efficiency loss due to radiation from the muon at high p_{T}.

An $E_{\mathrm{T}}^{\mathrm{miss}}$ requirement is imposed to select signal events and to further suppress the contributions from the multi-jet and SM W backgrounds. In both channels, the requirement placed on the charged lepton p_{T} is also applied to the $E_{\mathrm{T}}^{\mathrm{miss}}$: $E_{\mathrm{T}}^{\mathrm{miss}} > 125\,\mathrm{GeV}$ for the electron channel and $E_{\mathrm{T}}^{\mathrm{miss}} > 45\,\mathrm{GeV}$ for the muon channel.

The multi-jet background around the Jacobian peak of the m_{T} distribution is evaluated using the *matrix method* as described in ref. [71] in both the electron and muon channels. The high-mass tail of the distribution is then fitted by a power-law function in order to determine the level of the multi-jet background in the region used to search for new physics. In the electron channel, the multi-jet background constitutes about 2%–4% of the total background at high m_{T}. Consistent results are obtained using the *inverted isolation* technique described in ref. [5]. In the muon channel, the multi-jet background constitutes about 1%–3% of the total background at high m_{T}. The uncertainty of the multi-jet background is determined by varying the selection requirements used to define the control region and by varying the m_{T} threshold of the fitting range used in the extrapolation to high m_{T}.

The same reconstruction criteria and event selection are applied to both the data and simulated samples. Figure 1 shows the p_{T}, $E_{\mathrm{T}}^{\mathrm{miss}}$, and m_{T} spectra for each channel after event selection for the data, the expected background and three examples of W' signals at different masses. Prior to investigating if there is evidence for a signal, the agreement between the data and the predicted background is established for events with $m_{\mathrm{T}} < 252\,\mathrm{GeV}$, the lowest m_{T} threshold used to search for new physics. The optimisation of the m_{T} thresholds for event selection is described below. The agreement between the data and expected background is good. Table 4 shows an example of how different sources contribute to the background for $m_{\mathrm{T}} > 1500\,\mathrm{GeV}$, the region used to search for a W' with a mass of 2000 GeV. The $W \to \ell\nu$ background is the dominant contribution for both the electron and muon channels. The $Z \to \ell\ell$ background in the electron channel is smaller than in the muon channel due to calorimeters having larger η coverage than the MS, and the electron energy resolution being better than the muon momentum resolution at high p_{T}.

JHEP09(2014)037

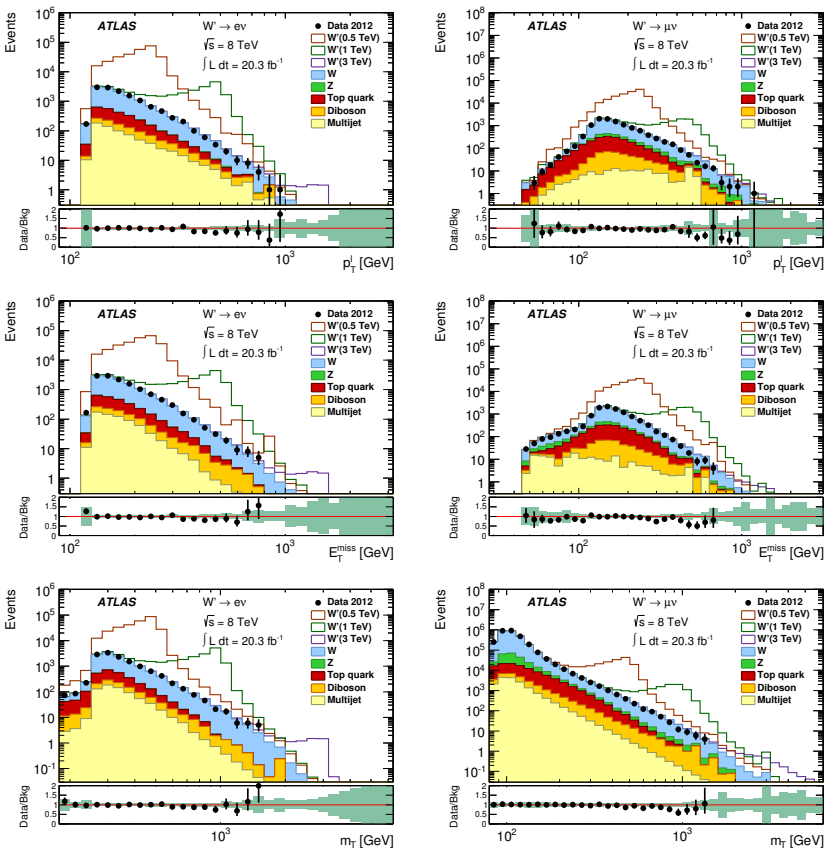

Figure 1. Spectra of lepton p_{T} (top), $E_{\mathrm{T}}^{\mathrm{miss}}$ (centre) and m_{T} (bottom) for the electron (left) and muon (right) channels after the event selection. The spectra of p_{T} and $E_{\mathrm{T}}^{\mathrm{miss}}$ are shown with the requirement $m_{\mathrm{T}} > 252\,\mathrm{GeV}$. The points represent data and the filled, stacked histograms show the predicted backgrounds. Open histograms are $W' \to \ell\nu$ signals added to the background with their masses in GeV indicated in parentheses in the legend. The signal and background samples are normalised using the integrated luminosity of the data and the NNLO cross-sections listed in tables 1 and 3, except for the multi-jet background which is estimated from data. The error bars on the data points are statistical. The ratio of the data to the total background prediction is shown below each of the distributions. The bands represent the systematic uncertainties on the background including the ones arising from the statistical uncertainty of the simulated samples.

JHEP09(2014)037

	$e\nu$		$\mu\nu$	
$W \to \ell\nu$	2.65	$\pm$ 0.10	2.28	$\pm$ 0.21
$Z \to \ell\ell$	0.00163	$\pm$ 0.00022	0.232	$\pm$ 0.005
Diboson	0.27	$\pm$ 0.23	0.46	$\pm$ 0.23
Top	0.0056	$\pm$ 0.0009	0.0017	$\pm$ 0.0001
Multi-jet	0.066	$\pm$ 0.020	0.046	$\pm$ 0.039
Total	2.99	$\pm$ 0.25	3.01	$\pm$ 0.31

Table 4. Expected numbers of events from the various background sources in each decay channel for $m_{\mathrm{T}} > 1500\,\mathrm{GeV}$, the region used to search for a W' with a mass of 2000 GeV. The $W \to \ell\nu$ and $Z \to \ell\ell$ rows include the expected contributions from the τ-lepton. The uncertainties are statistical.

JHEP09(2014)037

6 Statistical analysis and systematic uncertainties

A Bayesian analysis is performed to set limits on the studied processes. For each candidate mass and decay channel, events are counted above an m_{T} threshold. The optimisation of m_{Tmin} is done separately for $W' \to \ell\nu$ and $W^* \to \ell\nu$. For each candidate mass, the m_{Tmin} values that minimise the expected cross-section limits are obtained in the electron and muon channels separately, but for simplicity the lower value is used in both channels since this has a negligible impact on the final results. A similar optimisation is performed when setting the limits on DM production, and in this case a single m_{Tmin} is chosen for each operator. The expected number of events in each channel is

$$N_{\mathrm{exp}} = \varepsilon_{\mathrm{sig}} L_{\mathrm{int}} \sigma B + N_{\mathrm{bkg}}, \tag{6.1}$$

where L_{int} is the integrated luminosity of the data sample, $\varepsilon_{\mathrm{sig}}$ is the signal selection efficiency defined as the fraction of signal events that satisfy the event selection criteria as well as $m_{\mathrm{T}} > m_{\mathrm{Tmin}}$, N_{bkg} is the expected number of background events, and σB is the cross-section times branching fraction. Using Poisson statistics, the likelihood to observe N_{obs} events is

$$\mathcal{L}(N_{\mathrm{obs}}|\sigma B) = \frac{(L_{\mathrm{int}}\varepsilon_{\mathrm{sig}}\sigma B + N_{\mathrm{bkg}})^{N_{\mathrm{obs}}} \mathrm{e}^{-(L_{\mathrm{int}}\varepsilon_{\mathrm{sig}}\sigma B + N_{\mathrm{bkg}})}}{N_{\mathrm{obs}}!}. \tag{6.2}$$

Uncertainties are included by introducing nuisance parameters θ_i, each with a probability density function $g_i(\theta_i)$, and integrating the product of the Poisson likelihood with the probability density function. The integrated likelihood is

$$\mathcal{L}_B(N_{\mathrm{obs}}|\sigma B) = \int \mathcal{L}(N_{\mathrm{obs}}|\sigma B) \prod g_i(\theta_i) d\theta_i, \tag{6.3}$$

where a log-normal distribution is used for the $g_i(\theta_i)$. The nuisance parameters are taken to be: L_{int}, $\varepsilon_{\mathrm{sig}}$ and N_{bkg}, with the appropriate correlation accounted for between the first and the third parameters.

The measurements in the two decay channels are combined assuming the same branching fraction for each. Equation (6.3) remains valid with the Poisson likelihood replaced by the product of the Poisson likelihoods for the two channels. The integrated luminosities for the electron and muon channels are fully correlated. For $W'/W^* \to \ell\nu$ the signal selection efficiencies and background levels are partly correlated with each other and between the two channels due to the full correlation of the cross-section uncertainties. If these correlations were not included, the observed σB limits would improve by 25%–30% for the lowest mass points, a few percent for the intermediate mass points and by about 10% for the highest mass points.

Bayes' theorem gives the posterior probability that the signal has signal strength σB:

$$P_{\text{post}}(\sigma B|N_{\text{obs}}) = N\mathcal{L}_B(N_{\text{obs}}|\sigma B)\, P_{\text{prior}}(\sigma B) \tag{6.4}$$

where $P_{\text{prior}}(\sigma B)$ is the assumed prior probability, here chosen to be flat in σB, for $\sigma B > 0$. The constant factor N normalises the total probability to one. The posterior probability is evaluated for each mass and decay channel as well as for their combination, and then used to set a limit on σB.

The inputs for the evaluation of $\mathcal{L}_B$ (and hence P_{post}) are L_{int}, ε_{sig}, N_{bkg}, N_{obs} and the uncertainties on the first three. The uncertainties on ε_{sig} and N_{bkg} account for experimental and theoretical systematic effects as well as the statistics of the simulated samples. The experimental systematic uncertainties include those on the efficiencies of the electron or muon trigger, reconstruction and event/object selection. Uncertainties in the lepton energy/momentum and $E_{\text{T}}^{\text{miss}}$, characterised by scale and resolution uncertainties, are also included. Performance metrics are obtained in-situ using well-known processes such as $Z \to \ell\ell$ [31, 72, 73]. Since most of these performance metrics are measured at relatively low p_{T} their values are extrapolated to the high-p_{T} regime relevant to this analysis using MC simulation. The uncertainties in these extrapolations are included but are too small to significantly affect the results. Table 5 summarises the uncertainties on the event selection efficiencies and the expected number of background events for the $W' \to \ell\nu$ signal with $m_{W'} = 2000\,\text{GeV}$ using $m_{\text{T}} > 1500\,\text{GeV}$, and W^* signal with $m_{W^*} = 2000\,\text{GeV}$ using $m_{\text{T}} > 1337\,\text{GeV}$.

7 Results

The inputs for the evaluation of $\mathcal{L}_B$ are listed in tables 6, 7 and 8. The uncertainties on ε_{sig} and N_{bkg} account for all relevant experimental and theoretical effects except for the uncertainty on the integrated luminosity. The latter is included separately and is correlated between signal and background. The tables also list the predicted numbers of signal events, N_{sig}, with their uncertainties accounting for the uncertainties in both ε_{sig} and the cross-section calculation. The maximum value for the signal selection efficiency is at $m_{W'} = 2000\,\text{GeV}$. For lower masses, the efficiency falls because the relative m_{T} threshold, $m_{\text{Tmin}}/m_{W'}$, increases in order to reduce the background level. The contribution from $W' \to \tau\nu$ with a leptonically decaying τ is neglected. It would increase the signal yield

JHEP09(2014)037

Source	ε_{sig}		N_{bkg}	
	$e\nu$	$\mu\nu$	$e\nu$	$\mu\nu$
$W' \to \ell\nu$				
Reconstruction and trigger efficiency	2.5%	4.1%	2.7%	4.1%
Lepton energy/momentum resolution	0.2%	1.4%	1.9%	18%
Lepton energy/momentum scale	1.2%	1.8%	3.5%	1.5%
$E_{\text{T}}^{\text{miss}}$ scale and resolution	0.1%	0.1%	1.2%	0.5%
Beam energy	0.5%	0.5%	2.8%	2.1%
Multi-jet background	-	-	2.2%	3.4%
Monte Carlo statistics	0.9%	1.3%	8.5%	10%
Cross-section (shape/level)	2.9%	2.8%	18%	15%
Total	4.2%	5.6%	21%	27%
$W^* \to \ell\nu$				
Reconstruction and trigger efficiency	2.7%	4.1%	2.6%	4.0%
Lepton energy/momentum resolution	0.4%	0.9%	3.0%	17%
Lepton energy/momentum scale	2.4%	2.4%	3.1%	1.5%
$E_{\text{T}}^{\text{miss}}$ scale and resolution	0.1%	0.4%	3.1%	0.6%
Beam energy	0.1%	0.1%	2.5%	1.9%
Multi-jet background	-	-	1.8%	2.6%
Monte Carlo statistics	1.2%	1.8%	6.7%	8.6%
Cross-section (shape/level)	0.2%	0.2%	17%	15%
Total	3.9%	5.1%	19%	25%

Table 5. Relative uncertainties on the selection efficiency ε_{sig} and expected number of background events N_{bkg} for a W' (upper part of the table) and W^* (lower part of the table) with a mass of 2000 GeV. The efficiency uncertainties include contributions from the trigger, reconstruction and event selection. The last row gives the total relative uncertainties.

by 2%–3% for the highest masses. The background level is estimated for each mass by summing over all of the background sources.

The number of observed events is generally in good agreement with the expected number of background events for all mass bins. None of the observations for any mass point in either channel or their combination show a significant excess above background, so there is no evidence for the observation of either $W' \to \ell\nu$ or $W^* \to \ell\nu$. A deficit in the number of observed events with respect to the expected number of background events is observed in the muon channel. This deficit has at most a 2.2σ local significance.

Tables 9 and 10 and figure 2 present the 95% confidence level (CL) observed limits on σB for both $W' \to \ell\nu$ and $W^* \to \ell\nu$ in the electron channel, the muon channel and their combination. The tables also give the limits obtained without systematic uncertainties.

JHEP09(2014)037

$m_{W'}$ [GeV]	m_{Tmin} [GeV]	Channel	$\varepsilon_{\mathrm{sig}}$	N_{sig}	N_{bkg}	N_{obs}
300	252	$e\nu$	0.228 ± 0.009	688000 ± 28000	12900 ± 820	12717
		$\mu\nu$	0.184 ± 0.007	555000 ± 21000	11300 ± 770	10927
400	336	$e\nu$	0.319 ± 0.012	325000 ± 12000	5280 ± 360	5176
		$\mu\nu$	0.193 ± 0.007	196000 ± 7500	3490 ± 250	3317
500	423	$e\nu$	0.325 ± 0.013	141000 ± 5700	2070 ± 150	2017
		$\mu\nu$	0.186 ± 0.007	80900 ± 3200	1370 ± 100	1219
600	474	$e\nu$	0.397 ± 0.014	83800 ± 2900	1260 ± 96	1214
		$\mu\nu$	0.229 ± 0.009	48200 ± 1900	827 ± 64	719
750	597	$e\nu$	0.393 ± 0.013	33200 ± 1100	456 ± 45	414
		$\mu\nu$	0.226 ± 0.009	19100 ± 750	305 ± 30	255
1000	796	$e\nu$	0.386 ± 0.012	9080 ± 290	116 ± 15	101
		$\mu\nu$	0.219 ± 0.009	5160 ± 220	84 ± 10	58
1250	1002	$e\nu$	0.378 ± 0.012	2980 ± 98	35.3 ± 5.8	34
		$\mu\nu$	0.210 ± 0.009	1650 ± 73	28.3 ± 4.6	19
1500	1191	$e\nu$	0.376 ± 0.014	1110 ± 40	13.2 ± 2.5	14
		$\mu\nu$	0.206 ± 0.010	610 ± 30	10.9 ± 2.3	6
1750	1416	$e\nu$	0.336 ± 0.013	396 ± 16	4.56 ± 0.92	5
		$\mu\nu$	0.182 ± 0.010	214 ± 12	4.3 ± 1.1	0
2000	1500	$e\nu$	0.370 ± 0.015	183.0 ± 7.7	2.99 ± 0.61	3
		$\mu\nu$	0.198 ± 0.011	98.0 ± 5.5	3.01 ± 0.80	0
2250	1683	$e\nu$	0.327 ± 0.015	71.5 ± 3.3	1.38 ± 0.33	0
		$\mu\nu$	0.173 ± 0.011	37.9 ± 2.3	1.44 ± 0.33	0
2500	1888	$e\nu$	0.262 ± 0.018	27.1 ± 1.8	0.432 ± 0.091	0
		$\mu\nu$	0.140 ± 0.012	14.4 ± 1.2	0.61 ± 0.15	0
2750	1888	$e\nu$	0.235 ± 0.024	12.3 ± 1.3	0.432 ± 0.091	0
		$\mu\nu$	0.127 ± 0.014	6.64 ± 0.74	0.61 ± 0.15	0
3000	1888	$e\nu$	0.183 ± 0.029	5.33 ± 0.86	0.432 ± 0.091	0
		$\mu\nu$	0.100 ± 0.016	2.93 ± 0.48	0.61 ± 0.15	0
3250	1888	$e\nu$	0.124 ± 0.033	2.22 ± 0.59	0.432 ± 0.091	0
		$\mu\nu$	0.069 ± 0.018	1.24 ± 0.32	0.61 ± 0.15	0
3500	1888	$e\nu$	0.077 ± 0.031	0.92 ± 0.36	0.432 ± 0.091	0
		$\mu\nu$	0.044 ± 0.017	0.52 ± 0.20	0.61 ± 0.15	0
3750	1888	$e\nu$	0.047 ± 0.024	0.40 ± 0.21	0.432 ± 0.091	0
		$\mu\nu$	0.028 ± 0.013	0.24 ± 0.11	0.61 ± 0.15	0
4000	1888	$e\nu$	0.031 ± 0.018	0.20 ± 0.11	0.432 ± 0.091	0
		$\mu\nu$	0.019 ± 0.010	0.121 ± 0.061	0.61 ± 0.15	0

Table 6. Inputs for the $W' \to \ell\nu$ σB limit calculations. The first three columns are the W' mass, m_{T} threshold and decay channel. The next two are the signal selection efficiency, $\varepsilon_{\mathrm{sig}}$, and the prediction for the number of signal events, N_{sig}, obtained with this efficiency. The last two columns are the expected number of background events, N_{bkg}, and the number of events observed in data, N_{obs}. The uncertainties on N_{sig} and N_{bkg} include contributions from the uncertainties on the cross-sections but not from that on the integrated luminosity.

JHEP09(2014)037

m_{W^*} [GeV]	m_{Tmin} [GeV]	Channel	$\varepsilon_{\mathrm{sig}}$	N_{sig}	N_{bkg}	N_{obs}
400	317	$e\nu$	0.196 ± 0.010	149000 ± 7400	6630 ± 440	6448
		$\mu\nu$	0.111 ± 0.005	84900 ± 3700	4420 ± 310	4230
500	377	$e\nu$	0.246 ± 0.011	80900 ± 3500	3320 ± 220	3275
		$\mu\nu$	0.140 ± 0.006	45900 ± 1900	2210 ± 160	2008
600	448	$e\nu$	0.257 ± 0.011	41400 ± 1800	1630 ± 120	1582
		$\mu\nu$	0.144 ± 0.006	23200 ± 960	1080 ± 79	938
750	564	$e\nu$	0.248 ± 0.011	15900 ± 680	593 ± 54	524
		$\mu\nu$	0.143 ± 0.006	9200 ± 400	388 ± 35	321
1000	710	$e\nu$	0.302 ± 0.013	5390 ± 230	203 ± 24	177
		$\mu\nu$	0.174 ± 0.007	3100 ± 130	143 ± 17	109
1250	843	$e\nu$	0.337 ± 0.013	2010 ± 79	86 ± 12	79
		$\mu\nu$	0.191 ± 0.008	1140 ± 50	65.5 ± 8.5	40
1500	1062	$e\nu$	0.296 ± 0.011	648 ± 25	25.8 ± 4.4	26
		$\mu\nu$	0.164 ± 0.007	360 ± 16	20.9 ± 3.8	12
1750	1191	$e\nu$	0.324 ± 0.013	278 ± 11	13.2 ± 2.5	14
		$\mu\nu$	0.182 ± 0.009	156.0 ± 7.6	10.9 ± 2.3	6
2000	1337	$e\nu$	0.341 ± 0.013	118.0 ± 4.6	6.8 ± 1.3	9
		$\mu\nu$	0.186 ± 0.010	64.6 ± 3.3	5.8 ± 1.4	3
2250	1416	$e\nu$	0.391 ± 0.014	55.5 ± 2.0	4.56 ± 0.92	5
		$\mu\nu$	0.204 ± 0.010	28.9 ± 1.5	4.3 ± 1.1	0
2500	1683	$e\nu$	0.337 ± 0.013	19.80 ± 0.76	1.38 ± 0.33	0
		$\mu\nu$	0.179 ± 0.010	10.50 ± 0.57	1.44 ± 0.33	0
2750	1888	$e\nu$	0.322 ± 0.013	7.84 ± 0.31	0.432 ± 0.091	0
		$\mu\nu$	0.161 ± 0.011	3.92 ± 0.27	0.61 ± 0.15	0
3000	1888	$e\nu$	0.382 ± 0.015	3.80 ± 0.15	0.432 ± 0.091	0
		$\mu\nu$	0.185 ± 0.011	1.84 ± 0.11	0.61 ± 0.15	0
3250	1888	$e\nu$	0.437 ± 0.018	1.770 ± 0.073	0.432 ± 0.091	0
		$\mu\nu$	0.218 ± 0.014	0.880 ± 0.056	0.61 ± 0.15	0
3500	1888	$e\nu$	0.474 ± 0.025	0.766 ± 0.040	0.432 ± 0.091	0
		$\mu\nu$	0.229 ± 0.016	0.371 ± 0.027	0.61 ± 0.15	0
3750	1888	$e\nu$	0.498 ± 0.055	0.320 ± 0.035	0.432 ± 0.091	0
		$\mu\nu$	0.244 ± 0.029	0.157 ± 0.019	0.61 ± 0.15	0
4000	1888	$e\nu$	0.487 ± 0.150	0.124 ± 0.038	0.432 ± 0.091	0
		$\mu\nu$	0.242 ± 0.073	0.062 ± 0.019	0.61 ± 0.15	0

Table 7. Inputs for the $W^* \to \ell\nu$ σB limit calculations. The columns are the same as in table 6.

JHEP09(2014)037

m_χ [GeV]	m_{Tmin} [GeV]	Channel	$\varepsilon_{\mathrm{sig}}$	N_{sig}	N_{bkg}		N_{obs}
D1 Operator							
1	796	$e\nu$	0.0294 ± 0.0044	87000 ± 13000	$e\nu$	116 ± 15	101
		$\mu\nu$	0.0177 ± 0.0023	52500 ± 7000	$\mu\nu$	84 ± 10	58
100		$e\nu$	0.0396 ± 0.0052	89000 ± 12000			
		$\mu\nu$	0.0252 ± 0.0033	56600 ± 7500			
200		$e\nu$	0.0484 ± 0.0057	65800 ± 7700			
		$\mu\nu$	0.0293 ± 0.0034	39900 ± 4600			
400		$e\nu$	0.0709 ± 0.0071	30900 ± 3100			
		$\mu\nu$	0.0398 ± 0.0041	17300 ± 1800			
1000		$e\nu$	0.0989 ± 0.0100	1070 ± 110			
		$\mu\nu$	0.0621 ± 0.0068	673 ± 73			
1300		$e\nu$	0.0964 ± 0.0095	138 ± 14			
		$\mu\nu$	0.0522 ± 0.0048	75.1 ± 6.9			
D5d Operator							
1	597	$e\nu$	0.0148 ± 0.0016	7230 ± 800	$e\nu$	456 ± 45	414
		$\mu\nu$	0.0080 ± 0.0011	3890 ± 530	$\mu\nu$	305 ± 30	255
100		$e\nu$	0.0158 ± 0.0018	7580 ± 850			
		$\mu\nu$	0.0096 ± 0.0012	4600 ± 580			
200		$e\nu$	0.0147 ± 0.0015	5850 ± 610			
		$\mu\nu$	0.0086 ± 0.0011	3420 ± 430			
400		$e\nu$	0.0190 ± 0.0020	4220 ± 440			
		$\mu\nu$	0.0113 ± 0.0013	2500 ± 300			
1000		$e\nu$	0.0281 ± 0.0025	450 ± 41			
		$\mu\nu$	0.0177 ± 0.0019	283 ± 30			
1300		$e\nu$	0.0291 ± 0.0028	89.3 ± 8.5			
		$\mu\nu$	0.0167 ± 0.0018	51.1 ± 5.4			
D5c Operator							
1	843	$e\nu$	0.0737 ± 0.0047	30.3 ± 1.9	$e\nu$	86 ± 12	79
		$\mu\nu$	0.0435 ± 0.0034	17.9 ± 1.4	$\mu\nu$	65.5 ± 8.5	40
100		$e\nu$	0.0798 ± 0.0050	31.0 ± 1.9			
		$\mu\nu$	0.0437 ± 0.0034	17.0 ± 1.3			
200		$e\nu$	0.0762 ± 0.0049	25.1 ± 1.6			
		$\mu\nu$	0.0461 ± 0.0034	15.2 ± 1.1			
400		$e\nu$	0.0857 ± 0.0055	16.2 ± 1.0			
		$\mu\nu$	0.0532 ± 0.0040	10.0 ± 0.8			
1000		$e\nu$	0.0987 ± 0.0091	1.28 ± 0.12			
		$\mu\nu$	0.0636 ± 0.0057	0.824 ± 0.074			
1300		$e\nu$	0.1010 ± 0.0095	0.240 ± 0.023			
		$\mu\nu$	0.0589 ± 0.0057	0.140 ± 0.014			
D9 Operator							
1	843	$e\nu$	0.0851 ± 0.0053	55.5 ± 3.5	$e\nu$	86 ± 12	79
		$\mu\nu$	0.0517 ± 0.0035	33.8 ± 2.3	$\mu\nu$	65.5 ± 8.5	40
100		$e\nu$	0.0950 ± 0.0056	55.8 ± 3.3			
		$\mu\nu$	0.0529 ± 0.0038	31.1 ± 2.3			
200		$e\nu$	0.1040 ± 0.0062	48.9 ± 2.9			
		$\mu\nu$	0.0553 ± 0.0039	26.0 ± 1.8			
400		$e\nu$	0.1030 ± 0.0067	25.5 ± 1.6			
		$\mu\nu$	0.0578 ± 0.0042	14.3 ± 1.0			
1000		$e\nu$	0.1070 ± 0.0092	1.63 ± 0.14			
		$\mu\nu$	0.0615 ± 0.0055	0.944 ± 0.084			
1300		$e\nu$	0.1020 ± 0.0100	0.285 ± 0.029			
		$\mu\nu$	0.0573 ± 0.0056	0.160 ± 0.016			

Table 8. Inputs to the limit calculations on the pair production of DM particles for the operators D1, D5d, D5c and D9. Expected number of signal events for each operator is calculated for a different value of the mass scale, notably $M_* = 10\,\mathrm{GeV}$ for D1, $M_* = 100\,\mathrm{GeV}$ for D5d, and $M_* = 1\,\mathrm{TeV}$ for operators D9 and D5c. The columns are the same as in table 6.

JHEP09(2014)037

Limits with various subsets of the systematic uncertainties are shown for $W' \to \ell\nu$ as a representative case. The uncertainties on the signal selection efficiency have very little effect on the final limits, and the background-level and luminosity uncertainties are important only for the lowest masses. Figure 2 also shows the expected limits and the theoretical σB for a W' and for a W^*. Limits are evaluated by fixing the W^* coupling strengths to give the same partial decay widths as the W'. The off-shell production of W' degrades the acceptance at high mass, worsening the limits. As discussed in section 1, W^* has different couplings with respect to W', enhancing the production at the pole. Since the off-shell production is reduced with respect to W', the W^* limits do not show the same behaviour at high mass.

In figure 2 the intersection between the central theoretical prediction and the observed limits provides the 95% CL lower limits on the mass. The expected and observed W' and W^* mass limits for the electron and muon decay channels as well as their combination are listed in table 11. The difference between the expected and observed combined mass limits originate from the slight data deficit in each decay channel that are individually not significant. The band around the theoretical prediction in figure 2 indicates the total theory uncertainty as described earlier in the text. The mass limit for the W' decreases by 50 GeV if the intersection between the lower theoretical prediction and the observed limit is used. The uncertainties on $\varepsilon_{\mathrm{sig}}$, N_{bkg} and L_{int} affect the derived mass limits by a similar amount. Limits are also evaluated following the $\mathrm{CL_s}$ prescription [74] using the profile likelihood ratio as the test statistic including all uncertainties. The cross-section limits are found to agree within 10% across the entire mass range, with only marginal impact on the mass limit. The mass limits presented here are a significant improvement over those reported in previous ATLAS and CMS searches [4–7].

The results of the search for pair production of DM particles in association with a leptonically decaying W boson are shown in figures 3 and 4. The former shows the observed limits on M_*, the mass scale of the unknown mediating interaction for the DM particle pair production, whereas the latter shows the observed limits on the DM-nucleon scattering cross-section. Both are shown as a function of the DM particle mass, m_χ, and presented at 90% CL. Results of the previous ATLAS searches for hadronically decaying W/Z [19], leptonically decaying Z [20], and $j + \chi\chi$ [15] are also shown. The observed limits on M_* as a function of m_χ are by a factor $\sim$1.5 stronger in the search for DM production in association with hadronically decaying W with respect the ones presented in this paper.

8 Conclusions

A search is presented for new high-mass states decaying to a lepton (electron or muon) plus missing transverse momentum using 20.3 fb^{-1} of proton-proton collision data at $\sqrt{s} =$ 8 TeV recorded with the ATLAS experiment at the Large Hadron Collider. No significant excess beyond SM expectations is observed. Limits on σB are presented. A W' with SSM couplings is excluded for masses below 3.24 TeV at 95% CL. The exclusion for W^* with equivalent couplings is 3.21 TeV. For the pair production of weakly interacting DM particles in events with a leptonically decaying W, limits are set on the mass scale, M_*, of the unknown mediating interaction as well as on the DM-nucleon scattering cross-section.

JHEP09(2014)037

m_{W'/W^*} [GeV]	Channel	95% CL limit on σB [fb]							
		W'						W^*	
		none	S	SB	SBL	SB_c	SB_cL	none	SB_cL
300	$e\nu$	29.0	29.1	304	342	305	343		
	$\mu\nu$	22.4	22.4	327	363	327	363		
	both	14.2	14.2	219	269	290	331		
400	$e\nu$	14.1	14.1	94.8	105	95.0	105	20.7	204
	$\mu\nu$	12.6	12.6	91.3	102	91.4	102	25.1	233
	both	7.55	7.56	63.4	77.0	83.2	94.7	12.6	197
500	$e\nu$	9.14	9.18	38.7	42.2	38.8	42.4	17.3	87.5
	$\mu\nu$	6.42	6.44	30.6	34.0	30.7	34.1	10.5	77.9
	both	4.26	4.26	22.3	27.0	29.8	33.9	7.54	77.7
600	$e\nu$	5.67	5.68	19.5	21.2	19.7	21.4	10.4	43.9
	$\mu\nu$	4.38	4.40	15.5	17.0	15.6	17.1	7.11	32.8
	both	2.78	2.78	11.1	13.2	15.5	17.4	4.75	33.9
750	$e\nu$	2.95	2.95	8.25	8.71	8.35	8.81	4.23	14.9
	$\mu\nu$	3.33	3.34	7.89	8.35	7.97	8.43	5.23	14.7
	both	1.73	1.73	5.06	5.63	7.01	7.52	2.51	12.8
1000	$e\nu$	1.84	1.85	3.25	3.34	3.29	3.38	2.69	6.01
	$\mu\nu$	1.86	1.87	2.87	2.95	2.92	3.00	3.02	5.88
	both	1.03	1.04	1.86	1.96	2.48	2.58	1.57	4.94
1250	$e\nu$	1.63	1.64	2.06	2.09	2.09	2.12	2.29	3.65
	$\mu\nu$	1.62	1.62	2.01	2.04	2.04	2.07	1.78	2.60
	both	0.990	0.991	1.30	1.34	1.54	1.57	1.16	2.53
1500	$e\nu$	1.27	1.28	1.40	1.41	1.42	1.43	1.99	2.39
	$\mu\nu$	1.21	1.22	1.35	1.36	1.37	1.38	1.71	2.06
	both	0.775	0.777	0.879	0.890	0.967	0.979	1.14	1.63
1750	$e\nu$	0.964	0.967	0.993	0.997	1.01	1.01	1.48	1.64
	$\mu\nu$	0.813	0.818	0.818	0.821	0.827	0.831	1.37	1.54
	both	0.521	0.522	0.533	0.537	0.563	0.567	0.889	1.10
2000	$e\nu$	0.721	0.724	0.735	0.738	0.743	0.746	1.34	1.40
	$\mu\nu$	0.747	0.751	0.751	0.754	0.760	0.762	1.18	1.26
	both	0.415	0.416	0.422	0.424	0.439	0.441	0.831	0.922

Table 9. Observed upper limits on σB for W' and W^* with masses up to 2000 GeV. The first column is the W'/W^* mass and the following columns refer to the 95% CL limits for the W' with headers indicating the nuisance parameters for which uncertainties are included: S for the event selection efficiency (ε_{sig}), B for the background level (N_{bkg}), and L for the integrated luminosity (L_{int}). The column labelled SBL includes all uncertainties neglecting correlations. Results are also presented when including the correlation of the signal and background cross-section uncertainties, as well as the correlation of the background cross-section uncertainties for the combined limits (SB_c, SB_cL). The last two columns show the limits for the W^* without nuisance parameters and when including all nuisance parameters with correlations.

JHEP09(2014)037

m_{W'/W^*} [GeV]	Channel	95% CL limit on σB [fb]							
		W'						W^*	
		none	S	SB	SBL	SB_c	SB_cL	none	SB_cL
2250	$e\nu$	0.453	0.455	0.455	0.456	0.458	0.459	0.830	0.859
	$\mu\nu$	0.853	0.859	0.859	0.862	0.866	0.869	0.726	0.734
	both	0.296	0.297	0.297	0.298	0.301	0.303	0.457	0.488
2500	$e\nu$	0.564	0.569	0.569	0.570	0.572	0.573	0.438	0.441
	$\mu\nu$	1.06	1.07	1.07	1.08	1.08	1.08	0.828	0.837
	both	0.368	0.370	0.370	0.371	0.376	0.377	0.287	0.289
2750	$e\nu$	0.629	0.643	0.643	0.644	0.648	0.649	0.459	0.462
	$\mu\nu$	1.16	1.19	1.19	1.20	1.21	1.21	0.917	0.928
	both	0.409	0.413	0.413	0.414	0.425	0.426	0.306	0.308
3000	$e\nu$	0.809	0.852	0.852	0.853	0.863	0.865	0.387	0.389
	$\mu\nu$	1.47	1.55	1.55	1.56	1.58	1.58	0.798	0.807
	both	0.523	0.534	0.534	0.536	0.566	0.567	0.261	0.263
3250	$e\nu$	1.20	1.37	1.37	1.37	1.40	1.40	0.338	0.340
	$\mu\nu$	2.14	2.45	2.45	2.45	2.52	2.52	0.678	0.687
	both	0.768	0.815	0.815	0.816	0.919	0.920	0.226	0.228
3500	$e\nu$	1.92	2.56	2.56	2.56	2.64	2.64	0.312	0.315
	$\mu\nu$	3.37	4.38	4.38	4.39	4.56	4.57	0.645	0.655
	both	1.22	1.38	1.38	1.38	1.72	1.73	0.210	0.213
3750	$e\nu$	3.12	4.90	4.90	4.90	5.07	5.08	0.297	0.307
	$\mu\nu$	5.32	7.85	7.85	7.86	8.22	8.24	0.605	0.630
	both	1.97	2.37	2.37	2.38	3.26	3.27	0.199	0.208
4000	$e\nu$	4.76	8.07	8.07	8.09	8.38	8.40	0.304	0.372
	$\mu\nu$	7.75	12.0	12.0	12.0	12.6	12.6	0.613	0.749
	both	2.95	3.66	3.66	3.66	5.24	5.24	0.203	0.255

Table 10. Observed upper limits on σB for W' and W^* with masses above 2000 GeV. The columns are the same as in table 9.

	$m_{W'}$ [TeV]		m_{W^*} [TeV]	
Decay	Exp.	Obs.	Exp.	Obs.
$e\nu$	3.13	3.13	3.08	3.08
$\mu\nu$	2.97	2.97	2.83	2.83
Both	3.17	3.24	3.12	3.21

Table 11. Lower limits on the W' and W^* masses. The first column is the decay channel ($e\nu$, $\mu\nu$ or both combined) and the following give the expected (Exp.) and observed (Obs.) mass limits.

JHEP09(2014)037

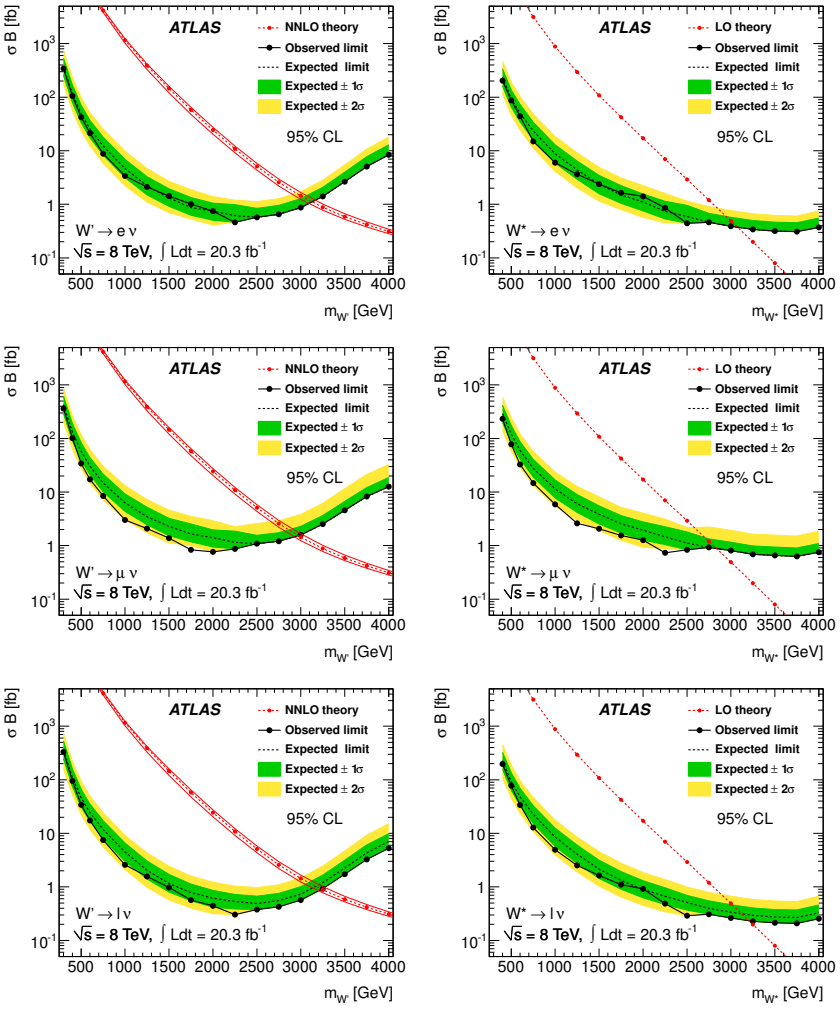

Figure 2. Observed and expected limits on σB for W' (left) and W^* (right) at 95% CL in the electron channel (top), muon channel (centre) and the combination (bottom) assuming the same branching fraction for both channels. The predicted values for σB and their uncertainties (except for W^*) are also shown. The calculation of uncertainties on the W' cross-sections is explained in section 4.

JHEP09(2014)037

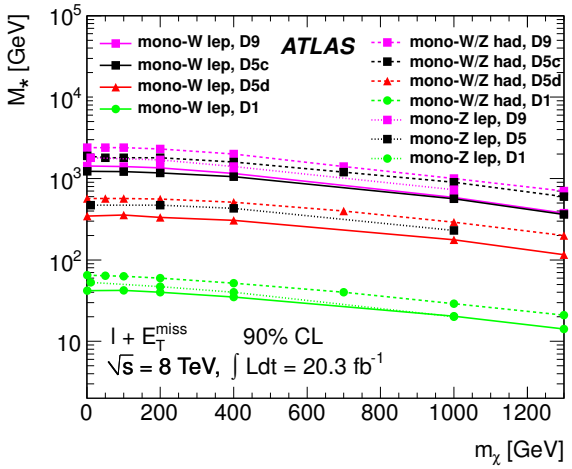

Figure 3. Observed limits on M_* as a function of the DM particle mass (m_χ) at 90% CL for the combination of the electron and muon channel, for various operators as described in the text. For each operator, the values below the corresponding line are excluded. No signal samples are generated for masses below 1 GeV but the limits are expected to be stable down to arbitrarily small values. Results of the previous ATLAS searches for hadronically decaying W/Z [19] and leptonically decaying Z [20] are also shown.

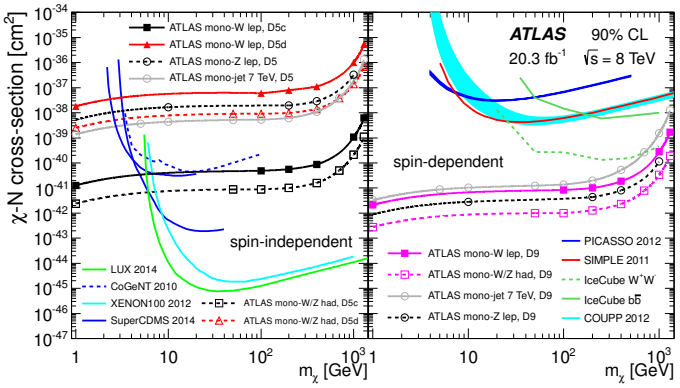

Figure 4. Observed limits on the DM-nucleon scattering cross-section as a function of m_χ at 90% CL for spin-independent (left) and spin-dependent (right) operators in the EFT. Results are compared with the previous ATLAS searches for hadronically decaying W/Z [19], leptonically decaying Z [20], and $j + \chi\chi$ [15], and with direct detection searches by CoGeNT [75], XENON100 [76], CDMS [77, 78], LUX [79], COUPP [80], SIMPLE [81], PICASSO [82] and IceCube [83]. The comparison between direct detection and ATLAS results is only possible within the limits of the validity of the EFT [84].

JHEP09(2014)037

Acknowledgments

We thank CERN for the very successful operation of the LHC, as well as the support staff from our institutions without whom ATLAS could not be operated efficiently.

We acknowledge the support of ANPCyT, Argentina; YerPhI, Armenia; ARC, Australia; BMWF and FWF, Austria; ANAS, Azerbaijan; SSTC, Belarus; CNPq and FAPESP, Brazil; NSERC, NRC and CFI, Canada; CERN; CONICYT, Chile; CAS, MOST and NSFC, China; COLCIENCIAS, Colombia; MSMT CR, MPO CR and VSC CR, Czech Republic; DNRF, DNSRC and Lundbeck Foundation, Denmark; EPLANET, ERC and NSRF, European Union; IN2P3-CNRS, CEA-DSM/IRFU, France; GNSF, Georgia; BMBF, DFG, HGF, MPG and AvH Foundation, Germany; GSRT and NSRF, Greece; ISF, MINERVA, GIF, I-CORE and Benoziyo Center, Israel; INFN, Italy; MEXT and JSPS, Japan; CNRST, Morocco; FOM and NWO, Netherlands; BRF and RCN, Norway; MNiSW and NCN, Poland; GRICES and FCT, Portugal; MNE/IFA, Romania; MES of Russia and ROSATOM, Russian Federation; JINR; MSTD, Serbia; MSSR, Slovakia; ARRS and MIZŠ, Slovenia; DST/NRF, South Africa; MINECO, Spain; SRC and Wallenberg Foundation, Sweden; SER, SNSF and Cantons of Bern and Geneva, Switzerland; NSC, Taiwan; TAEK, Turkey; STFC, the Royal Society and Leverhulme Trust, United Kingdom; DOE and NSF, United States of America.

The crucial computing support from all WLCG partners is acknowledged gratefully, in particular from CERN and the ATLAS Tier-1 facilities at TRIUMF (Canada), NDGF (Denmark, Norway, Sweden), CC-IN2P3 (France), KIT/GridKA (Germany), INFN-CNAF (Italy), NL-T1 (Netherlands), PIC (Spain), ASGC (Taiwan), RAL (U.K.) and BNL (U.S.A.) and in the Tier-2 facilities worldwide.

JHEP09(2014)037

References

[1] G. Altarelli, B. Mele and M. Ruiz-Altaba, *Searching for new heavy vector bosons in $p\bar{p}$ colliders*, *Z. Phys.* **C 45** (1989) 109 [*Erratum ibid.* **C 47** (1990) 676] [INSPIRE].

[2] CDF collaboration, T. Aaltonen et al., *Search for a new heavy gauge boson W' with electron + missing E_T event signature in $p\bar{p}$ collisions at $\sqrt{s} = 1.96$ TeV*, *Phys. Rev.* **D 83** (2011) 031102 [arXiv:1012.5145] [INSPIRE].

[3] CMS collaboration, *Search for leptonic decays of W' bosons in pp collisions at $\sqrt{s} = 7$ TeV*, *JHEP* **08** (2012) 023 [arXiv:1204.4764] [INSPIRE].

[4] CMS collaboration, *Search for new physics in final states with a lepton and missing transverse energy in pp collisions at the LHC*, *Phys. Rev.* **D 87** (2013) 072005 [arXiv:1302.2812] [INSPIRE].

[5] ATLAS collaboration, *Search for high-mass states with one lepton plus missing transverse momentum in proton-proton collisions at $\sqrt{s} = 7$ TeV with the ATLAS detector*, *Phys. Lett.* **B 701** (2011) 50 [arXiv:1103.1391] [INSPIRE].

[6] ATLAS collaboration, *Search for a heavy gauge boson decaying to a charged lepton and a neutrino in* $1\,\text{fb}^{-1}$ *of pp collisions at* $\sqrt{s} = 7$ *TeV using the ATLAS detector*, *Phys. Lett.* **B 705** (2011) 28 [arXiv:1108.1316] [INSPIRE].

[7] ATLAS collaboration, *ATLAS search for a heavy gauge boson decaying to a charged lepton and a neutrino in pp collisions at* $\sqrt{s} = 7$ *TeV*, *Eur. Phys. J.* **C 72** (2012) 2241 [arXiv:1209.4446] [INSPIRE].

[8] M.V. Chizhov and G. Dvali, *Origin and phenomenology of weak-doublet spin-1 bosons*, *Phys. Lett.* **B 703** (2011) 593 [arXiv:0908.0924] [INSPIRE].

[9] M.V. Chizhov, V.A. Bednyakov and J.A. Budagov, *Proposal for chiral bosons search at LHC via their unique new signature*, *Phys. Atom. Nucl.* **71** (2008) 2096 [arXiv:0801.4235] [INSPIRE].

[10] A. Birkedal, K. Matchev and M. Perelstein, *Dark matter at colliders: a model independent approach*, *Phys. Rev.* **D 70** (2004) 077701 [hep-ph/0403004] [INSPIRE].

[11] J. Goodman et al., *Constraints on light Majorana dark matter from colliders*, *Phys. Lett.* **B 695** (2011) 185 [arXiv:1005.1286] [INSPIRE].

[12] Y. Bai, P.J. Fox and R. Harnik, *The Tevatron at the frontier of dark matter direct detection*, *JHEP* **12** (2010) 048 [arXiv:1005.3797] [INSPIRE].

[13] J. Goodman et al., *Constraints on dark matter from colliders*, *Phys. Rev.* **D 82** (2010) 116010 [arXiv:1008.1783] [INSPIRE].

[14] CDF collaboration, T. Aaltonen et al., *A search for dark matter in events with one jet and missing transverse energy in* $p\bar{p}$ *collisions at* $\sqrt{s} = 1.96$ *TeV*, *Phys. Rev. Lett.* **108** (2012) 211804 [arXiv:1203.0742] [INSPIRE].

[15] ATLAS collaboration, *Search for dark matter candidates and large extra dimensions in events with a jet and missing transverse momentum with the ATLAS detector*, *JHEP* **04** (2013) 075 [arXiv:1210.4491] [INSPIRE].

[16] CMS collaboration, *Search for dark matter and large extra dimensions in monojet events in pp collisions at* $\sqrt{s} = 7$ *TeV*, *JHEP* **09** (2012) 094 [arXiv:1206.5663] [INSPIRE].

[17] ATLAS collaboration, *Search for dark matter candidates and large extra dimensions in events with a photon and missing transverse momentum in pp collision data at* $\sqrt{s} = 7$ *TeV with the ATLAS detector*, *Phys. Rev. Lett.* **110** (2013) 011802 [arXiv:1209.4625] [INSPIRE].

[18] CMS collaboration, *Search for dark matter and large extra dimensions in pp collisions yielding a photon and missing transverse energy*, *Phys. Rev. Lett.* **108** (2012) 261803 [arXiv:1204.0821] [INSPIRE].

[19] ATLAS collaboration, *Search for dark matter in events with a hadronically decaying* W *or* Z *boson and missing transverse momentum in pp collisions at* $\sqrt{s} = 8$ *TeV with the ATLAS detector*, *Phys. Rev. Lett.* **112** (2014) 041802 [arXiv:1309.4017] [INSPIRE].

[20] ATLAS collaboration, *Search for dark matter in events with a* Z *boson and missing transverse momentum in pp collisions at* $\sqrt{s} = 8$ *TeV with the ATLAS detector*, *Phys. Rev.* **D 90** (2014) 012004 [arXiv:1404.0051] [INSPIRE].

[21] Y. Bai and T.M.P. Tait, *Searches with mono-leptons*, *Phys. Lett.* **B 723** (2013) 384 [arXiv:1208.4361] [INSPIRE].

JHEP09(2014)037

[22] M. Beltrán, D. Hooper, E.W. Kolb, Z.A.C. Krusberg and T.M.P. Tait, *Maverick dark matter at colliders*, *JHEP* **09** (2010) 037 [arXiv:1002.4137] [INSPIRE].

[23] Q.-H. Cao, C.-R. Chen, C.S. Li and H. Zhang, *Effective dark matter model: relic density, CDMS II, Fermi LAT and LHC*, *JHEP* **08** (2011) 018 [arXiv:0912.4511] [INSPIRE].

[24] A. Rajaraman, W. Shepherd, T.M.P. Tait and A.M. Wijangco, *LHC bounds on interactions of dark matter*, *Phys. Rev.* **D 84** (2011) 095013 [arXiv:1108.1196] [INSPIRE].

[25] P.J. Fox, R. Harnik, J. Kopp and Y. Tsai, *Missing energy signatures of dark matter at the LHC*, *Phys. Rev.* **D 85** (2012) 056011 [arXiv:1109.4398] [INSPIRE].

[26] K. Cheung, P.-Y. Tseng, Y.-L.S. Tsai and T.-C. Yuan, *Global constraints on effective dark matter interactions: relic density, direct detection, indirect detection and collider*, *JCAP* **05** (2012) 001 [arXiv:1201.3402] [INSPIRE].

[27] R.C. Cotta, J.L. Hewett, M.P. Le and T.G. Rizzo, *Bounds on dark matter interactions with electroweak gauge bosons*, *Phys. Rev.* **D 88** (2013) 116009 [arXiv:1210.0525] [INSPIRE].

[28] O. Buchmueller, M.J. Dolan and C. McCabe, *Beyond effective field theory for dark matter searches at the LHC*, *JHEP* **01** (2014) 025 [arXiv:1308.6799] [INSPIRE].

[29] G. Busoni, A. De Simone, E. Morgante and A. Riotto, *On the validity of the effective field theory for dark matter searches at the LHC*, *Phys. Lett.* **B 728** (2014) 412 [arXiv:1307.2253] [INSPIRE].

[30] ATLAS collaboration, *The ATLAS experiment at the CERN Large Hadron Collider*, 2008 *JINST* **3** S08003 [INSPIRE].

[31] ATLAS collaboration, *Electron reconstruction and identification efficiency measurements with the ATLAS detector using the* 2011 *LHC proton-proton collision data*, *Eur. Phys. J.* **C 74** (2014) 2941 [arXiv:1404.2240] [INSPIRE].

[32] ATLAS collaboration, *Electron performance measurements with the ATLAS detector using the* 2010 *LHC proton-proton collision data*, *Eur. Phys. J.* **C 72** (2012) 1909 [arXiv:1110.3174] [INSPIRE].

[33] ATLAS collaboration, *Performance of missing transverse momentum reconstruction in proton-proton collisions at* 7 *TeV with ATLAS*, *Eur. Phys. J.* **C 72** (2012) 1844 [arXiv:1108.5602] [INSPIRE].

[34] ATLAS collaboration, *Improved luminosity determination in pp collisions at* $\sqrt{s} = 7$ *TeV using the ATLAS detector at the LHC*, *Eur. Phys. J.* **C 73** (2013) 2518 [arXiv:1302.4393] [INSPIRE].

[35] T. Sjöstrand, S. Mrenna and P.Z. Skands, *PYTHIA* 6.4 *physics and manual*, *JHEP* **05** (2006) 026 [hep-ph/0603175] [INSPIRE].

[36] T. Sjöstrand, S. Mrenna and P.Z. Skands, *A brief introduction to PYTHIA* 8.1, *Comput. Phys. Commun.* **178** (2008) 852 [arXiv:0710.3820] [INSPIRE].

[37] A.D. Martin, W.J. Stirling, R.S. Thorne and G. Watt, *Parton distributions for the LHC*, *Eur. Phys. J.* **C 63** (2009) 189 [arXiv:0901.0002] [INSPIRE].

[38] A. Belyaev, N.D. Christensen and A. Pukhov, *CalcHEP* 3.4 *for collider physics within and beyond the Standard Model*, *Comput. Phys. Commun.* **184** (2013) 1729 [arXiv:1207.6082] [INSPIRE].

JHEP09(2014)037

[39] J. Pumplin et al., *New generation of parton distributions with uncertainties from global QCD analysis*, *JHEP* **07** (2002) 012 [hep-ph/0201195] [INSPIRE].

[40] J. Alwall, M. Herquet, F. Maltoni, O. Mattelaer and T. Stelzer, *MadGraph 5: going beyond*, *JHEP* **06** (2011) 128 [arXiv:1106.0522] [INSPIRE].

[41] S. Frixione, P. Nason and C. Oleari, *Matching NLO QCD computations with parton shower simulations: the POWHEG method*, *JHEP* **11** (2007) 070 [arXiv:0709.2092] [INSPIRE].

[42] H.-L. Lai et al., *New parton distributions for collider physics*, *Phys. Rev.* **D 82** (2010) 074024 [arXiv:1007.2241] [INSPIRE].

[43] S. Frixione and B.R. Webber, *Matching NLO QCD computations and parton shower simulations*, *JHEP* **06** (2002) 029 [hep-ph/0204244] [INSPIRE].

[44] B.P. Kersevan and E. Richter-Was, *The Monte Carlo event generator AcerMC versions* 2.0 *to* 3.8 *with interfaces to PYTHIA* 6.4*, HERWIG* 6.5 *and ARIADNE* 4.1, *Comput. Phys. Commun.* **184** (2013) 919 [hep-ph/0405247] [INSPIRE].

[45] G. Corcella et al., *HERWIG* 6*: an event generator for hadron emission reactions with interfering gluons (including supersymmetric processes)*, *JHEP* **01** (2001) 010 [hep-ph/0011363] [INSPIRE].

[46] J.M. Butterworth and M.H. Seymour, *Multi-parton interactions in Herwig for the LHC*, http://projects.hepforge.org/jimmy, (2007).

[47] T. Gleisberg et al., *Event generation with SHERPA* 1.1, *JHEP* **02** (2009) 007 [arXiv:0811.4622] [INSPIRE].

[48] P. Golonka and Z. Was, *PHOTOS Monte Carlo: a precision tool for QED corrections in Z and W decays*, *Eur. Phys. J.* **C 45** (2006) 97 [hep-ph/0506026] [INSPIRE].

[49] ATLAS collaboration, *The ATLAS simulation infrastructure*, *Eur. Phys. J.* **C 70** (2010) 823 [arXiv:1005.4568] [INSPIRE].

[50] GEANT4 collaboration, S. Agostinelli et al., *GEANT4: a simulation toolkit*, *Nucl. Instrum. Meth.* **A 506** (2003) 250 [INSPIRE].

[51] ATLAS collaboration, *ATLAS tunes of PYTHIA* 6 *and PYTHIA* 8 *for MC*11, ATL-PHYS-PUB-2011-009, CERN, Geneva Switzerland (2011).

[52] ATLAS collaboration, *Summary of ATLAS PYTHIA* 8 *tunes*, ATL-PHYS-PUB-2012-003, CERN, Geneva Switzerland (2012).

[53] ATLAS collaboration, *New ATLAS event generator tunes to* 2010 *data*, ATL-PHYS-PUB-2011-008, CERN, Geneva Switzerland (2011).

[54] R. Hamberg, W.L. van Neerven and T. Matsuura, *A complete calculation of the order α_S^2 correction to the Drell-Yan K factor*, *Nucl. Phys.* **B 359** (1991) 343 [*Erratum ibid.* **B 644** (2002) 403] [INSPIRE].

[55] C. Anastasiou, L.J. Dixon, K. Melnikov and F. Petriello, *High precision QCD at hadron colliders: electroweak gauge boson rapidity distributions at NNLO*, *Phys. Rev.* **D 69** (2004) 094008 [hep-ph/0312266] [INSPIRE].

[56] K. Melnikov and F. Petriello, *Electroweak gauge boson production at hadron colliders through $O(\alpha_S^2)$*, *Phys. Rev.* **D 74** (2006) 114017 [hep-ph/0609070] [INSPIRE].

JHEP09(2014)037

[57] R. Gavin, Y. Li, F. Petriello and S. Quackenbush, *FEWZ 2.0: a code for hadronic Z production at next-to-next-to-leading order*, *Comput. Phys. Commun.* **182** (2011) 2388 [arXiv:1011.3540] [INSPIRE].

[58] S.G. Bondarenko and A.A. Sapronov, *NLO EW and QCD proton-proton cross section calculations with mcsanc-v1.01*, *Comput. Phys. Commun.* **184** (2013) 2343 [arXiv:1301.3687] [INSPIRE].

[59] M. Cacciari, M. Czakon, M. Mangano, A. Mitov and P. Nason, *Top-pair production at hadron colliders with next-to-next-to-leading logarithmic soft-gluon resummation*, *Phys. Lett.* **B 710** (2012) 612 [arXiv:1111.5869] [INSPIRE].

[60] P. Bärnreuther, M. Czakon and A. Mitov, *Percent level precision physics at the Tevatron: first genuine NNLO QCD corrections to $q\bar{q} \to t\bar{t} + X$*, *Phys. Rev. Lett.* **109** (2012) 132001 [arXiv:1204.5201] [INSPIRE].

[61] M. Czakon and A. Mitov, *NNLO corrections to top-pair production at hadron colliders: the all-fermionic scattering channels*, *JHEP* **12** (2012) 054 [arXiv:1207.0236] [INSPIRE].

[62] M. Czakon and A. Mitov, *NNLO corrections to top pair production at hadron colliders: the quark-gluon reaction*, *JHEP* **01** (2013) 080 [arXiv:1210.6832] [INSPIRE].

[63] M. Czakon, P. Fiedler and A. Mitov, *Total top-quark pair-production cross section at hadron colliders through $O(\alpha_S^4)$*, *Phys. Rev. Lett.* **110** (2013) 252004 [arXiv:1303.6254] [INSPIRE].

[64] M. Czakon and A. Mitov, *Top++: a program for the calculation of the top-pair cross-section at hadron colliders*, *Comput. Phys. Commun.* **185** (2014) 2930 [arXiv:1112.5675] [INSPIRE].

[65] R.D. Ball et al., *Parton distributions with LHC data*, *Nucl. Phys.* **B 867** (2013) 244 [arXiv:1207.1303] [INSPIRE].

[66] S. Alekhin, J. Blumlein and S. Moch, *Parton distribution functions and benchmark cross sections at NNLO*, *Phys. Rev.* **D 86** (2012) 054009 [arXiv:1202.2281] [INSPIRE].

[67] H1 and ZEUS collaborations, V. Radescu, *HERA precision measurements and impact for LHC predictions*, in *Proceedings of Moriond QCD* 2011, La Thuile Italy (2011) [H1prelim-11-042] [ZEUS-prel-11-002] [arXiv:1107.4193] [INSPIRE].

[68] S. Alekhin et al., *The PDF4LHC working group interim report*, arXiv:1101.0536 [INSPIRE].

[69] J. Wenninger, *Energy calibration of the LHC beams at 4 TeV*, CERN-ATS-2013-040, CERN, Geneva Switzerland (2013).

[70] ATLAS collaboration, *Selection of jets produced in proton-proton collisions with the ATLAS detector using 2011 data*, ATLAS-CONF-2012-020, CERN, Geneva Switzerland (2012).

[71] ATLAS collaboration, *Measurement of the top quark-pair production cross section with ATLAS in pp collisions at $\sqrt{s} = 7$ TeV*, *Eur. Phys. J.* **C 71** (2011) 1577 [arXiv:1012.1792] [INSPIRE].

[72] ATLAS collaboration, *Measurement of the muon reconstruction performance of the ATLAS detector using 2011 and 2012 LHC proton-proton collision data*, arXiv:1407.3935 [INSPIRE].

[73] ATLAS collaboration, *Performance of missing transverse momentum reconstruction in ATLAS studied in proton-proton collisions recorded in 2012 at 8 TeV*, ATLAS-CONF-2013-082, CERN, Geneva Switzerland (2013).

[74] A.L. Read, *Modified frequentist analysis of search results (the CL_s method)*, CERN-OPEN-2000-205, CERN, Geneva Switzerland (2000).

JHEP09(2014)037

[75] CoGeNT collaboration, C.E. Aalseth et al., *Results from a search for light-mass dark matter with a P-type point contact germanium detector*, *Phys. Rev. Lett.* **106** (2011) 131301 [arXiv:1002.4703] [INSPIRE].

[76] XENON100 collaboration, E. Aprile et al., *Dark matter results from* 225 *live days of XENON*100 *data*, *Phys. Rev. Lett.* **109** (2012) 181301 [arXiv:1207.5988] [INSPIRE].

[77] SuperCDMS collaboration, R. Agnese et al., *Search for low-mass weakly interacting massive particles using voltage-assisted calorimetric ionization detection in the SuperCDMS experiment*, *Phys. Rev. Lett.* **112** (2014) 041302 [arXiv:1309.3259] [INSPIRE].

[78] SuperCDMS collaboration, R. Agnese et al., *Search for low-mass WIMPs with SuperCDMS*, *Phys. Rev. Lett.* **112** (2014) 241302 [arXiv:1402.7137] [INSPIRE].

[79] LUX collaboration, D.S. Akerib et al., *First results from the LUX dark matter experiment at the Sanford Underground Research Facility*, *Phys. Rev. Lett.* **112** (2014) 091303 [arXiv:1310.8214] [INSPIRE].

[80] COUPP collaboration, E. Behnke et al., *First dark matter search results from a* 4 *kg* CF_3I *bubble chamber operated in a deep underground site*, *Phys. Rev.* **D 86** (2012) 052001 [arXiv:1204.3094] [INSPIRE].

[81] M. Felizardo et al., *Final analysis and results of the phase II SIMPLE dark matter search*, *Phys. Rev. Lett.* **108** (2012) 201302 [arXiv:1106.3014] [INSPIRE].

[82] PICASSO collaboration, S. Archambault et al., *Constraints on low-mass WIMP interactions on* ^{19}F *from PICASSO*, *Phys. Lett.* **B 711** (2012) 153 [arXiv:1202.1240] [INSPIRE].

[83] IceCube collaboration, M.G. Aartsen et al., *Search for dark matter annihilations in the sun with the* 79*-string IceCube detector*, *Phys. Rev. Lett.* **110** (2013) 131302 [arXiv:1212.4097] [INSPIRE].

[84] ATLAS collaboration, *Sensitivity to WIMP dark matter in the final states containing jets and missing transverse momentum with the ATLAS detector at* 14 *TeV LHC*, ATL-PHYS-PUB-2014-007, CERN, Geneva Switzerland (2014).

JHEP09(2014)037

The ATLAS collaboration

G. Aad[84], B. Abbott[112], J. Abdallah[152], S. Abdel Khalek[116], O. Abdinov[11], R. Aben[106], B. Abi[113], M. Abolins[89], O.S. AbouZeid[159], H. Abramowicz[154], H. Abreu[153], R. Abreu[30], Y. Abulaiti[147a,147b], B.S. Acharya[165a,165b,a], L. Adamczyk[38a], D.L. Adams[25], J. Adelman[177], S. Adomeit[99], T. Adye[130], T. Agatonovic-Jovin[13a], J.A. Aguilar-Saavedra[125a,125f], M. Agustoni[17], S.P. Ahlen[22], F. Ahmadov[64,b], G. Aielli[134a,134b], H. Akerstedt[147a,147b], T.P.A. Åkesson[80], G. Akimoto[156], A.V. Akimov[95], G.L. Alberghi[20a,20b], J. Albert[170], S. Albrand[55], M.J. Alconada Verzini[70], M. Aleksa[30], I.N. Aleksandrov[64], C. Alexa[26a], G. Alexander[154], G. Alexandre[49], T. Alexopoulos[10], M. Alhroob[165a,165c], G. Alimonti[90a], L. Alio[84], J. Alison[31], B.M.M. Allbrooke[18], L.J. Allison[71], P.P. Allport[73], J. Almond[83], A. Aloisio[103a,103b], A. Alonso[36], F. Alonso[70], C. Alpigiani[75], A. Altheimer[35], B. Alvarez Gonzalez[89], M.G. Alviggi[103a,103b], K. Amako[65], Y. Amaral Coutinho[24a], C. Amelung[23], D. Amidei[88], S.P. Amor Dos Santos[125a,125c], A. Amorim[125a,125b], S. Amoroso[48], N. Amram[154], G. Amundsen[23], C. Anastopoulos[140], L.S. Ancu[49], N. Andari[30], T. Andeen[35], C.F. Anders[58b], G. Anders[30], K.J. Anderson[31], A. Andreazza[90a,90b], V. Andrei[58a], X.S. Anduaga[70], S. Angelidakis[9], I. Angelozzi[106], P. Anger[44], A. Angerami[35], F. Anghinolfi[30], A.V. Anisenkov[108], N. Anjos[125a], A. Annovi[47], A. Antonaki[9], M. Antonelli[47], A. Antonov[97], J. Antos[145b], F. Anulli[133a], M. Aoki[65], L. Aperio Bella[18], R. Apolle[119,c], G. Arabidze[89], I. Aracena[144], Y. Arai[65], J.P. Araque[125a], A.T.H. Arce[45], J-F. Arguin[94], S. Argyropoulos[42], M. Arik[19a], A.J. Armbruster[30], O. Arnaez[30], V. Arnal[81], H. Arnold[48], M. Arratia[28], O. Arslan[21], A. Artamonov[96], G. Artoni[23], S. Asai[156], N. Asbah[42], A. Ashkenazi[154], B. Åsman[147a,147b], L. Asquith[6], K. Assamagan[25], R. Astalos[145a], M. Atkinson[166], N.B. Atlay[142], B. Auerbach[6], K. Augsten[127], M. Aurousseau[146b], G. Avolio[30], G. Azuelos[94,d], Y. Azuma[156], M.A. Baak[30], C. Bacci[135a,135b], H. Bachacou[137], K. Bachas[155], M. Backes[30], M. Backhaus[30], J. Backus Mayes[144], E. Badescu[26a], P. Bagiacchi[133a,133b], P. Bagnaia[133a,133b], Y. Bai[33a], T. Bain[35], J.T. Baines[130], O.K. Baker[177], S. Baker[77], P. Balek[128], F. Balli[137], E. Banas[39], Sw. Banerjee[174], A.A.E. Bannoura[176], V. Bansal[170], H.S. Bansil[18], L. Barak[173], S.P. Baranov[95], E.L. Barberio[87], D. Barberis[50a,50b], M. Barbero[84], T. Barillari[100], M. Barisonzi[176], T. Barklow[144], N. Barlow[28], B.M. Barnett[130], R.M. Barnett[15], Z. Barnovska[5], A. Baroncelli[135a], G. Barone[49], A.J. Barr[119], F. Barreiro[81], J. Barreiro Guimarães da Costa[57], R. Bartoldus[144], A.E. Barton[71], P. Bartos[145a], V. Bartsch[150], A. Bassalat[116], A. Basye[166], R.L. Bates[53], L. Batkova[145a], J.R. Batley[28], M. Battaglia[138], M. Battistin[30], F. Bauer[137], H.S. Bawa[144,e], T. Beau[79], P.H. Beauchemin[162], R. Beccherle[123a,123b], P. Bechtle[21], H.P. Beck[17], K. Becker[176], M. Becker[82], S. Becker[99], M. Beckingham[139], C. Becot[116], A.J. Beddall[19c], A. Beddall[19c], S. Bedikian[177], V.A. Bednyakov[64], C.P. Bee[149], L.J. Beemster[106], T.A. Beermann[176], M. Begel[25], K. Behr[119], C. Belanger-Champagne[86], P.J. Bell[49], W.H. Bell[49], G. Bella[154], L. Bellagamba[20a], A. Bellerive[29], M. Bellomo[85], K. Belotskiy[97], O. Beltramello[30], O. Benary[154], D. Benchekroun[136a], K. Bendtz[147a,147b], N. Benekos[166], Y. Benhammou[154], E. Benhar Noccioli[49], J.A. Benitez Garcia[160b], D.P. Benjamin[45], J.R. Bensinger[23], K. Benslama[131], S. Bentvelsen[106], D. Berge[106], E. Bergeaas Kuutmann[16], N. Berger[5], F. Berghaus[170], E. Berglund[106], J. Beringer[15], C. Bernard[22], P. Bernat[77], C. Bernius[78], F.U. Bernlochner[170], T. Berry[76], P. Berta[128], C. Bertella[84], G. Bertoli[147a,147b], F. Bertolucci[123a,123b], D. Bertsche[112], M.I. Besana[90a], G.J. Besjes[105], O. Bessidskaia[147a,147b], M. Bessner[42], N. Besson[137], C. Betancourt[48], S. Bethke[100], W. Bhimji[46], R.M. Bianchi[124], L. Bianchini[23], M. Bianco[30], O. Biebel[99], S.P. Bieniek[77], K. Bierwagen[54], J. Biesiada[15], M. Biglietti[135a], J. Bilbao De Mendizabal[49], H. Bilokon[47], M. Bindi[54], S. Binet[116], A. Bingul[19c], C. Bini[133a,133b], C.W. Black[151], J.E. Black[144], K.M. Black[22], D. Blackburn[139], R.E. Blair[6], J.-B. Blanchard[137], T. Blazek[145a], I. Bloch[42], C. Blocker[23], W. Blum[82,*], U. Blumenschein[54], G.J. Bobbink[106], V.S. Bobrovnikov[108], S.S. Bocchetta[80], A. Bocci[45], C. Bock[99], C.R. Boddy[119], M. Boehler[48], J. Boek[176], T.T. Boek[176], J.A. Bogaerts[30], A.G. Bogdanchikov[108], A. Bogouch[91,*],

JHEP09(2014)037

C. Bohm[147a], J. Bohm[126], V. Boisvert[76], T. Bold[38a], V. Boldea[26a], A.S. Boldyrev[98], M. Bomben[79], M. Bona[75], M. Boonekamp[137], A. Borisov[129], G. Borissov[71], M. Borri[83], S. Borroni[42], J. Bortfeldt[99], V. Bortolotto[135a,135b], K. Bos[106], D. Boscherini[20a], M. Bosman[12], H. Boterenbrood[106], J. Boudreau[124], J. Bouffard[2], E.V. Bouhova-Thacker[71], D. Boumediene[34], C. Bourdarios[116], N. Bousson[113], S. Boutouil[136d], A. Boveia[31], J. Boyd[30], I.R. Boyko[64], I. Bozovic-Jelisavcic[13b], J. Bracinik[18], A. Brandt[8], G. Brandt[15], O. Brandt[58a], U. Bratzler[157], B. Brau[85], J.E. Brau[115], H.M. Braun[176,*], S.F. Brazzale[165a,165c], B. Brelier[159], K. Brendlinger[121], A.J. Brennan[87], R. Brenner[167], S. Bressler[173], K. Bristow[146c], T.M. Bristow[46], D. Britton[53], F.M. Brochu[28], I. Brock[21], R. Brock[89], C. Bromberg[89], J. Bronner[100], G. Brooijmans[35], T. Brooks[76], W.K. Brooks[32b], J. Brosamer[15], E. Brost[115], G. Brown[83], J. Brown[55], P.A. Bruckman de Renstrom[39], D. Bruncko[145b], R. Bruneliere[48], S. Brunet[60], A. Bruni[20a], G. Bruni[20a], M. Bruschi[20a], L. Bryngemark[80], T. Buanes[14], Q. Buat[143], F. Bucci[49], P. Buchholz[142], R.M. Buckingham[119], A.G. Buckley[53], S.I. Buda[26a], I.A. Budagov[64], F. Buehrer[48], L. Bugge[118], M.K. Bugge[118], O. Bulekov[97], A.C. Bundock[73], H. Burckhart[30], S. Burdin[73], B. Burghgrave[107], S. Burke[130], I. Burmeister[43], E. Busato[34], D. Büscher[48], V. Büscher[82], P. Bussey[53], C.P. Buszello[167], B. Butler[57], J.M. Butler[22], A.I. Butt[3], C.M. Buttar[53], J.M. Butterworth[77], P. Butti[106], W. Buttinger[28], A. Buzatu[53], M. Byszewski[10], S. Cabrera Urbán[168], D. Caforio[20a,20b], O. Cakir[4a], P. Calafiura[15], A. Calandri[137], G. Calderini[79], P. Calfayan[99], R. Calkins[107], L.P. Caloba[24a], D. Calvet[34], S. Calvet[34], R. Camacho Toro[49], S. Camarda[42], D. Cameron[118], L.M. Caminada[15], R. Caminal Armadans[12], S. Campana[30], M. Campanelli[77], A. Campoverde[149], V. Canale[103a,103b], A. Canepa[160a], M. Cano Bret[75], J. Cantero[81], R. Cantrill[76], T. Cao[40], M.D.M. Capeans Garrido[30], I. Caprini[26a], M. Caprini[26a], M. Capua[37a,37b], R. Caputo[82], R. Cardarelli[134a], T. Carli[30], G. Carlino[103a], L. Carminati[90a,90b], S. Caron[105], E. Carquin[32a], G.D. Carrillo-Montoya[146c], J.R. Carter[28], J. Carvalho[125a,125c], D. Casadei[77], M.P. Casado[12], M. Casolino[12], E. Castaneda-Miranda[146b], A. Castelli[106], V. Castillo Gimenez[168], N.F. Castro[125a], P. Catastini[57], A. Catinaccio[30], J.R. Catmore[118], A. Cattai[30], G. Cattani[134a,134b], S. Caughron[89], V. Cavaliere[166], D. Cavalli[90a], M. Cavalli-Sforza[12], V. Cavasinni[123a,123b], F. Ceradini[135a,135b], B. Cerio[45], K. Cerny[128], A.S. Cerqueira[24b], A. Cerri[150], L. Cerrito[75], F. Cerutti[15], M. Cerv[30], A. Cervelli[17], S.A. Cetin[19b], A. Chafaq[136a], D. Chakraborty[107], I. Chalupkova[128], K. Chan[3], P. Chang[166], B. Chapleau[86], J.D. Chapman[28], D. Charfeddine[116], D.G. Charlton[18], C.C. Chau[159], C.A. Chavez Barajas[150], S. Cheatham[86], A. Chegwidden[89], S. Chekanov[6], S.V. Chekulaev[160a], G.A. Chelkov[64,f], M.A. Chelstowska[88], C. Chen[63], H. Chen[25], K. Chen[149], L. Chen[33d,g], S. Chen[33c], X. Chen[146c], Y. Chen[35], H.C. Cheng[88], Y. Cheng[31], A. Cheplakov[64], R. Cherkaoui El Moursli[136e], V. Chernyatin[25,*], E. Cheu[7], L. Chevalier[137], V. Chiarella[47], G. Chiefari[103a,103b], J.T. Childers[6], A. Chilingarov[71], G. Chiodini[72a], A.S. Chisholm[18], R.T. Chislett[77], A. Chitan[26a], M.V. Chizhov[64], S. Chouridou[9], B.K.B. Chow[99], D. Chromek-Burckhart[30], M.L. Chu[152], J. Chudoba[126], J.J. Chwastowski[39], L. Chytka[114], G. Ciapetti[133a,133b], A.K. Ciftci[4a], R. Ciftci[4a], D. Cinca[62], V. Cindro[74], A. Ciocio[15], P. Cirkovic[13b], Z.H. Citron[173], M. Citterio[90a], M. Ciubancan[26a], A. Clark[49], P.J. Clark[46], R.N. Clarke[15], W. Cleland[124], J.C. Clemens[84], C. Clement[147a,147b], Y. Coadou[84], M. Cobal[165a,165c], A. Coccaro[139], J. Cochran[63], L. Coffey[23], J.G. Cogan[144], J. Coggeshall[166], B. Cole[35], S. Cole[107], A.P. Colijn[106], J. Collot[55], T. Colombo[58c], G. Colon[85], G. Compostella[100], P. Conde Muiño[125a,125b], E. Coniavitis[167], M.C. Conidi[12], S.H. Connell[146b], I.A. Connelly[76], S.M. Consonni[90a,90b], V. Consorti[48], S. Constantinescu[26a], C. Conta[120a,120b], G. Conti[57], F. Conventi[103a,h], M. Cooke[15], B.D. Cooper[77], A.M. Cooper-Sarkar[119], N.J. Cooper-Smith[76], K. Copic[15], T. Cornelissen[176], M. Corradi[20a], F. Corriveau[86,i], A. Corso-Radu[164], A. Cortes-Gonzalez[12], G. Cortiana[100], G. Costa[90a], M.J. Costa[168], D. Costanzo[140], D. Côté[8], G. Cottin[28], G. Cowan[76], B.E. Cox[83], K. Cranmer[109],

JHEP09(2014)037

G. Cree[29], S. Crépé-Renaudin[55], F. Crescioli[79], W.A. Cribbs[147a,147b], M. Crispin Ortuzar[119], M. Cristinziani[21], V. Croft[105], G. Crosetti[37a,37b], C.-M. Cuciuc[26a], T. Cuhadar Donszelmann[140], J. Cummings[177], M. Curatolo[47], C. Cuthbert[151], H. Czirr[142], P. Czodrowski[3], Z. Czyczula[177], S. D'Auria[53], M. D'Onofrio[73], M.J. Da Cunha Sargedas De Sousa[125a,125b], C. Da Via[83], W. Dabrowski[38a], A. Dafinca[119], T. Dai[88], O. Dale[14], F. Dallaire[94], C. Dallapiccola[85], M. Dam[36], A.C. Daniells[18], M. Dano Hoffmann[137], V. Dao[105], G. Darbo[50a], S. Darmora[8], J.A. Dassoulas[42], A. Dattagupta[60], W. Davey[21], C. David[170], T. Davidek[128], E. Davies[119,c], M. Davies[154], O. Davignon[79], A.R. Davison[77], P. Davison[77], Y. Davygora[58a], E. Dawe[143], I. Dawson[140], R.K. Daya-Ishmukhametova[85], K. De[8], R. de Asmundis[103a], S. De Castro[20a,20b], S. De Cecco[79], N. De Groot[105], P. de Jong[106], H. De la Torre[81], F. De Lorenzi[63], L. De Nooij[106], D. De Pedis[133a], A. De Salvo[133a], U. De Sanctis[165a,165b], A. De Santo[150], J.B. De Vivie De Regie[116], W.J. Dearnaley[71], R. Debbe[25], C. Debenedetti[46], B. Dechenaux[55], D.V. Dedovich[64], I. Deigaard[106], J. Del Peso[81], T. Del Prete[123a,123b], F. Deliot[137], C.M. Delitzsch[49], M. Deliyergiyev[74], A. Dell'Acqua[30], L. Dell'Asta[22], M. Dell'Orso[123a,123b], M. Della Pietra[103a,h], D. della Volpe[49], M. Delmastro[5], P.A. Delsart[55], C. Deluca[106], S. Demers[177], M. Demichev[64], A. Demilly[79], S.P. Denisov[129], D. Derendarz[39], J.E. Derkaoui[136d], F. Derue[79], P. Dervan[73], K. Desch[21], C. Deterre[42], P.O. Deviveiros[106], A. Dewhurst[130], S. Dhaliwal[106], A. Di Ciaccio[134a,134b], L. Di Ciaccio[5], A. Di Domenico[133a,133b], C. Di Donato[103a,103b], A. Di Girolamo[30], B. Di Girolamo[30], A. Di Mattia[153], B. Di Micco[135a,135b], R. Di Nardo[47], A. Di Simone[48], R. Di Sipio[20a,20b], D. Di Valentino[29], M.A. Diaz[32a], E.B. Diehl[88], J. Dietrich[42], T.A. Dietzsch[58a], S. Diglio[84], A. Dimitrievska[13a], J. Dingfelder[21], C. Dionisi[133a,133b], P. Dita[26a], S. Dita[26a], F. Dittus[30], F. Djama[84], T. Djobava[51b], M.A.B. do Vale[24c], A. Do Valle Wemans[125a,125g], T.K.O. Doan[5], D. Dobos[30], C. Doglioni[49], T. Doherty[53], T. Dohmae[156], J. Dolejsi[128], Z. Dolezal[128], B.A. Dolgoshein[97,*], M. Donadelli[24d], S. Donati[123a,123b], P. Dondero[120a,120b], J. Donini[34], J. Dopke[30], A. Doria[103a], M.T. Dova[70], A.T. Doyle[53], M. Dris[10], J. Dubbert[88], S. Dube[15], E. Dubreuil[34], E. Duchovni[173], G. Duckeck[99], O.A. Ducu[26a], D. Duda[176], A. Dudarev[30], F. Dudziak[63], L. Duflot[116], L. Duguid[76], M. Dührssen[30], M. Dunford[58a], H. Duran Yildiz[4a], M. Düren[52], A. Durglishvili[51b], M. Dwuznik[38a], M. Dyndal[38a], J. Ebke[99], W. Edson[2], N.C. Edwards[46], W. Ehrenfeld[21], T. Eifert[144], G. Eigen[14], K. Einsweiler[15], T. Ekelof[167], M. El Kacimi[136c], M. Ellert[167], S. Elles[5], F. Ellinghaus[82], N. Ellis[30], J. Elmsheuser[99], M. Elsing[30], D. Emeliyanov[130], Y. Enari[156], O.C. Endner[82], M. Endo[117], R. Engelmann[149], J. Erdmann[177], A. Ereditato[17], D. Eriksson[147a], G. Ernis[176], J. Ernst[2], M. Ernst[25], J. Ernwein[137], D. Errede[166], S. Errede[166], E. Ertel[82], M. Escalier[116], H. Esch[43], C. Escobar[124], B. Esposito[47], A.I. Etienvre[137], E. Etzion[154], H. Evans[60], A. Ezhilov[122], L. Fabbri[20a,20b], G. Facini[31], R.M. Fakhrutdinov[129], S. Falciano[133a], R.J. Falla[77], J. Faltova[128], Y. Fang[33a], M. Fanti[90a,90b], A. Farbin[8], A. Farilla[135a], T. Farooque[12], S. Farrell[164], S.M. Farrington[171], P. Farthouat[30], F. Fassi[136e], P. Fassnacht[30], D. Fassouliotis[9], A. Favareto[50a,50b], L. Fayard[116], P. Federic[145a], O.L. Fedin[122,j], W. Fedorko[169], M. Fehling-Kaschek[48], S. Feigl[30], L. Feligioni[84], C. Feng[33d], E.J. Feng[6], H. Feng[88], A.B. Fenyuk[129], S. Fernandez Perez[30], S. Ferrag[53], J. Ferrando[53], A. Ferrari[167], P. Ferrari[106], R. Ferrari[120a], D.E. Ferreira de Lima[53], A. Ferrer[168], D. Ferrere[49], C. Ferretti[88], A. Ferretto Parodi[50a,50b], M. Fiascaris[31], F. Fiedler[82], A. Filipčič[74], M. Filipuzzi[42], F. Filthaut[105], M. Fincke-Keeler[170], K.D. Finelli[151], M.C.N. Fiolhais[125a,125c], L. Fiorini[168], A. Firan[40], J. Fischer[176], W.C. Fisher[89], E.A. Fitzgerald[23], M. Flechl[48], I. Fleck[142], P. Fleischmann[88], S. Fleischmann[176], G.T. Fletcher[140], G. Fletcher[75], T. Flick[176], A. Floderus[80], L.R. Flores Castillo[174,k], A.C. Florez Bustos[160b], M.J. Flowerdew[100], A. Formica[137], A. Forti[83], D. Fortin[160a], D. Fournier[116], H. Fox[71], S. Fracchia[12], P. Francavilla[79], M. Franchini[20a,20b], S. Franchino[30], D. Francis[30], M. Franklin[57], S. Franz[61], M. Fraternali[120a,120b], S.T. French[28],

JHEP09(2014)037

C. Friedrich[42], F. Friedrich[44], D. Froidevaux[30], J.A. Frost[28], C. Fukunaga[157], E. Fullana Torregrosa[82], B.G. Fulsom[144], J. Fuster[168], C. Gabaldon[55], O. Gabizon[173], A. Gabrielli[20a,20b], A. Gabrielli[133a,133b], S. Gadatsch[106], S. Gadomski[49], G. Gagliardi[50a,50b], P. Gagnon[60], C. Galea[105], B. Galhardo[125a,125c], E.J. Gallas[119], V. Gallo[17], B.J. Gallop[130], P. Gallus[127], G. Galster[36], K.K. Gan[110], R.P. Gandrajula[62], J. Gao[33b,g], Y.S. Gao[144,e], F.M. Garay Walls[46], F. Garberson[177], C. García[168], J.E. García Navarro[168], M. Garcia-Sciveres[15], R.W. Gardner[31], N. Garelli[144], V. Garonne[30], C. Gatti[47], G. Gaudio[120a], B. Gaur[142], L. Gauthier[94], P. Gauzzi[133a,133b], I.L. Gavrilenko[95], C. Gay[169], G. Gaycken[21], E.N. Gazis[10], P. Ge[33d], Z. Gecse[169], C.N.P. Gee[130], D.A.A. Geerts[106], Ch. Geich-Gimbel[21], K. Gellerstedt[147a,147b], C. Gemme[50a], A. Gemmell[53], M.H. Genest[55], S. Gentile[133a,133b], M. George[54], S. George[76], D. Gerbaudo[164], A. Gershon[154], H. Ghazlane[136b], N. Ghodbane[34], B. Giacobbe[20a], S. Giagu[133a,133b], V. Giangiobbe[12], P. Giannetti[123a,123b], F. Gianotti[30], B. Gibbard[25], S.M. Gibson[76], M. Gilchriese[15], T.P.S. Gillam[28], D. Gillberg[30], G. Gilles[34], D.M. Gingrich[3,d], N. Giokaris[9], M.P. Giordani[165a,165c], R. Giordano[103a,103b], F.M. Giorgi[20a], F.M. Giorgi[16], P.F. Giraud[137], D. Giugni[90a], C. Giuliani[48], M. Giulini[58b], B.K. Gjelsten[118], S. Gkaitatzis[155], I. Gkialas[155,l], L.K. Gladilin[98], C. Glasman[81], J. Glatzer[30], P.C.F. Glaysher[46], A. Glazov[42], G.L. Glonti[64], M. Goblirsch-Kolb[100], J.R. Goddard[75], J. Godfrey[143], J. Godlewski[30], C. Goeringer[82], S. Goldfarb[88], T. Golling[177], D. Golubkov[129], A. Gomes[125a,125b,125d], L.S. Gomez Fajardo[42], R. Gonçalo[125a], J. Goncalves Pinto Firmino Da Costa[137], L. Gonella[21], S. González de la Hoz[168], G. Gonzalez Parra[12], M.L. Gonzalez Silva[27], S. Gonzalez-Sevilla[49], L. Goossens[30], P.A. Gorbounov[96], H.A. Gordon[25], I. Gorelov[104], B. Gorini[30], E. Gorini[72a,72b], A. Gorišek[74], E. Gornicki[39], A.T. Goshaw[6], C. Gössling[43], M.I. Gostkin[64], M. Gouighri[136a], D. Goujdami[136c], M.P. Goulette[49], A.G. Goussiou[139], C. Goy[5], S. Gozpinar[23], H.M.X. Grabas[137], L. Graber[54], I. Grabowska-Bold[38a], P. Grafström[20a,20b], K-J. Grahn[42], J. Gramling[49], E. Gramstad[118], S. Grancagnolo[16], V. Grassi[149], V. Gratchev[122], H.M. Gray[30], E. Graziani[135a], O.G. Grebenyuk[122], Z.D. Greenwood[78,m], K. Gregersen[77], I.M. Gregor[42], P. Grenier[144], J. Griffiths[8], A.A. Grillo[138], K. Grimm[71], S. Grinstein[12,n], Ph. Gris[34], Y.V. Grishkevich[98], J.-F. Grivaz[116], J.P. Grohs[44], A. Grohsjean[42], E. Gross[173], J. Grosse-Knetter[54], G.C. Grossi[134a,134b], J. Groth-Jensen[173], Z.J. Grout[150], L. Guan[33b], F. Guescini[49], D. Guest[177], O. Gueta[154], C. Guicheney[34], E. Guido[50a,50b], T. Guillemin[116], S. Guindon[2], U. Gul[53], C. Gumpert[44], J. Gunther[127], J. Guo[35], S. Gupta[119], P. Gutierrez[112], N.G. Gutierrez Ortiz[53], C. Gutschow[77], N. Guttman[154], C. Guyot[137], C. Gwenlan[119], C.B. Gwilliam[73], A. Haas[109], C. Haber[15], H.K. Hadavand[8], N. Haddad[136e], P. Haefner[21], S. Hageböck[21], Z. Hajduk[39], H. Hakobyan[178], M. Haleem[42], D. Hall[119], G. Halladjian[89], K. Hamacher[176], P. Hamal[114], K. Hamano[170], M. Hamer[54], A. Hamilton[146a], S. Hamilton[162], P.G. Hamnett[42], L. Han[33b], K. Hanagaki[117], K. Hanawa[156], M. Hance[15], P. Hanke[58a], R. Hanna[137], J.B. Hansen[36], J.D. Hansen[36], P.H. Hansen[36], K. Hara[161], A.S. Hard[174], T. Harenberg[176], F. Hariri[116], S. Harkusha[91], D. Harper[88], R.D. Harrington[46], O.M. Harris[139], P.F. Harrison[171], F. Hartjes[106], S. Hasegawa[102], Y. Hasegawa[141], A. Hasib[112], S. Hassani[137], S. Haug[17], M. Hauschild[30], R. Hauser[89], M. Havranek[126], C.M. Hawkes[18], R.J. Hawkings[30], A.D. Hawkins[80], T. Hayashi[161], D. Hayden[89], C.P. Hays[119], H.S. Hayward[73], S.J. Haywood[130], S.J. Head[18], T. Heck[82], V. Hedberg[80], L. Heelan[8], S. Heim[121], T. Heim[176], B. Heinemann[15], L. Heinrich[109], S. Heisterkamp[36], J. Hejbal[126], L. Helary[22], C. Heller[99], M. Heller[30], S. Hellman[147a,147b], D. Hellmich[21], C. Helsens[30], J. Henderson[119], R.C.W. Henderson[71], C. Hengler[42], A. Henrichs[177], A.M. Henriques Correia[30], S. Henrot-Versille[116], C. Hensel[54], G.H. Herbert[16], Y. Hernández Jiménez[168], R. Herrberg-Schubert[16], G. Herten[48], R. Hertenberger[99], L. Hervas[30], G.G. Hesketh[77], N.P. Hessey[106], R. Hickling[75], E. Higón-Rodriguez[168], E. Hill[170], J.C. Hill[28], K.H. Hiller[42], S. Hillert[21], S.J. Hillier[18], I. Hinchliffe[15], E. Hines[121], M. Hirose[158],

JHEP09(2014)037

D. Hirschbuehl[176], J. Hobbs[149], N. Hod[106], M.C. Hodgkinson[140], P. Hodgson[140], A. Hoecker[30], M.R. Hoeferkamp[104], J. Hoffman[40], D. Hoffmann[84], J.I. Hofmann[58a], M. Hohlfeld[82], T.R. Holmes[15], T.M. Hong[121], L. Hooft van Huysduynen[109], J-Y. Hostachy[55], S. Hou[152], A. Hoummada[136a], J. Howard[119], J. Howarth[42], M. Hrabovsky[114], I. Hristova[16], J. Hrivnac[116], T. Hryn'ova[5], P.J. Hsu[82], S.-C. Hsu[139], D. Hu[35], X. Hu[25], Y. Huang[42], Z. Hubacek[30], F. Hubaut[84], F. Huegging[21], T.B. Huffman[119], E.W. Hughes[35], G. Hughes[71], M. Huhtinen[30], T.A. Hülsing[82], M. Hurwitz[15], N. Huseynov[64,b], J. Huston[89], J. Huth[57], G. Iacobucci[49], G. Iakovidis[10], I. Ibragimov[142], L. Iconomidou-Fayard[116], E. Ideal[177], P. Iengo[103a], O. Igonkina[106], T. Iizawa[172], Y. Ikegami[65], K. Ikematsu[142], M. Ikeno[65], Y. Ilchenko[31,ab], D. Iliadis[155], N. Ilic[159], Y. Inamaru[66], T. Ince[100], P. Ioannou[9], M. Iodice[135a], K. Iordanidou[9], V. Ippolito[57], A. Irles Quiles[168], C. Isaksson[167], M. Ishino[67], M. Ishitsuka[158], R. Ishmukhametov[110], C. Issever[119], S. Istin[19a], J.M. Iturbe Ponce[83], R. Iuppa[134a,134b], J. Ivarsson[80], W. Iwanski[39], H. Iwasaki[65], J.M. Izen[41], V. Izzo[103a], B. Jackson[121], M. Jackson[73], P. Jackson[1], M.R. Jaekel[30], V. Jain[2], K. Jakobs[48], S. Jakobsen[30], T. Jakoubek[126], J. Jakubek[127], D.O. Jamin[152], D.K. Jana[78], E. Jansen[77], H. Jansen[30], J. Janssen[21], M. Janus[171], G. Jarlskog[80], N. Javadov[64,b], T. Javůrek[48], L. Jeanty[15], J. Jejelava[51a,o], G.-Y. Jeng[151], D. Jennens[87], P. Jenni[48,p], J. Jentzsch[43], C. Jeske[171], S. Jézéquel[5], H. Ji[174], W. Ji[82], J. Jia[149], Y. Jiang[33b], M. Jimenez Belenguer[42], S. Jin[33a], A. Jinaru[26a], O. Jinnouchi[158], M.D. Joergensen[36], K.E. Johansson[147a], P. Johansson[140], K.A. Johns[7], K. Jon-And[147a,147b], G. Jones[171], R.W.L. Jones[71], T.J. Jones[73], J. Jongmanns[58a], P.M. Jorge[125a,125b], K.D. Joshi[83], J. Jovicevic[148], X. Ju[174], C.A. Jung[43], R.M. Jungst[30], P. Jussel[61], A. Juste Rozas[12,n], M. Kaci[168], A. Kaczmarska[39], M. Kado[116], H. Kagan[110], M. Kagan[144], E. Kajomovitz[45], C.W. Kalderon[119], S. Kama[40], N. Kanaya[156], M. Kaneda[30], S. Kaneti[28], T. Kanno[158], V.A. Kantserov[97], J. Kanzaki[65], B. Kaplan[109], A. Kapliy[31], D. Kar[53], K. Karakostas[10], N. Karastathis[10], M. Karnevskiy[82], S.N. Karpov[64], Z.M. Karpova[64], K. Karthik[109], V. Kartvelishvili[71], A.N. Karyukhin[129], L. Kashif[174], G. Kasieczka[58b], R.D. Kass[110], A. Kastanas[14], Y. Kataoka[156], A. Katre[49], J. Katzy[42], V. Kaushik[7], K. Kawagoe[69], T. Kawamoto[156], G. Kawamura[54], S. Kazama[156], V.F. Kazanin[108], M.Y. Kazarinov[64], R. Keeler[170], R. Kehoe[40], M. Keil[54], J.S. Keller[42], J.J. Kempster[76], H. Keoshkerian[5], O. Kepka[126], B.P. Kerševan[74], S. Kersten[176], K. Kessoku[156], J. Keung[159], F. Khalil-zada[11], H. Khandanyan[147a,147b], A. Khanov[113], A. Khodinov[97], A. Khomich[58a], T.J. Khoo[28], G. Khoriauli[21], A. Khoroshilov[176], V. Khovanskiy[96], E. Khramov[64], J. Khubua[51b], H.Y. Kim[8], H. Kim[147a,147b], S.H. Kim[161], N. Kimura[172], O. Kind[16], B.T. King[73], M. King[168], R.S.B. King[119], S.B. King[169], J. Kirk[130], A.E. Kiryunin[100], T. Kishimoto[66], D. Kisielewska[38a], F. Kiss[48], T. Kitamura[66], T. Kittelmann[124], K. Kiuchi[161], E. Kladiva[145b], M. Klein[73], U. Klein[73], K. Kleinknecht[82], P. Klimek[147a,147b], A. Klimentov[25], R. Klingenberg[43], J.A. Klinger[83], T. Klioutchnikova[30], P.F. Klok[105], E.-E. Kluge[58a], P. Kluit[106], S. Kluth[100], E. Kneringer[61], E.B.F.G. Knoops[84], A. Knue[53], T. Kobayashi[156], M. Kobel[44], M. Kocian[144], P. Kodys[128], P. Koevesarki[21], T. Koffas[29], E. Koffeman[106], L.A. Kogan[119], S. Kohlmann[176], Z. Kohout[127], T. Kohriki[65], T. Koi[144], H. Kolanoski[16], I. Koletsou[5], J. Koll[89], A.A. Komar[95,*], Y. Komori[156], T. Kondo[65], N. Kondrashova[42], K. Köneke[48], A.C. König[105], S. König[82], T. Kono[65,q], R. Konoplich[109,r], N. Konstantinidis[77], R. Kopeliansky[153], S. Koperny[38a], L. Köpke[82], A.K. Kopp[48], K. Korcyl[39], K. Kordas[155], A. Korn[77], A.A. Korol[108,s], I. Korolkov[12], E.V. Korolkova[140], V.A. Korotkov[129], O. Kortner[100], S. Kortner[100], V.V. Kostyukhin[21], V.M. Kotov[64], A. Kotwal[45], C. Kourkoumelis[9], V. Kouskoura[155], A. Koutsman[160a], R. Kowalewski[170], T.Z. Kowalski[38a], W. Kozanecki[137], A.S. Kozhin[129], V. Kral[127], V.A. Kramarenko[98], G. Kramberger[74], D. Krasnopevtsev[97], M.W. Krasny[79], A. Krasznahorkay[30], J.K. Kraus[21], A. Kravchenko[25], S. Kreiss[109], M. Kretz[58c], J. Kretzschmar[73], K. Kreutzfeldt[52], P. Krieger[159], K. Kroeninger[54], H. Kroha[100], J. Kroll[121], J. Kroseberg[21], J. Krstic[13a],

JHEP09(2014)037

U. Kruchonak[64], H. Krüger[21], T. Kruker[17], N. Krumnack[63], Z.V. Krumshteyn[64], A. Kruse[174], M.C. Kruse[45], M. Kruskal[22], T. Kubota[87], S. Kuday[4a], S. Kuehn[48], A. Kugel[58c], A. Kuhl[138], T. Kuhl[42], V. Kukhtin[64], Y. Kulchitsky[91], S. Kuleshov[32b], M. Kuna[133a,133b], J. Kunkle[121], A. Kupco[126], H. Kurashige[66], Y.A. Kurochkin[91], R. Kurumida[66], V. Kus[126], E.S. Kuwertz[148], M. Kuze[158], J. Kvita[114], A. La Rosa[49], L. La Rotonda[37a,37b], C. Lacasta[168], F. Lacava[133a,133b], J. Lacey[29], H. Lacker[16], D. Lacour[79], V.R. Lacuesta[168], E. Ladygin[64], R. Lafaye[5], B. Laforge[79], T. Lagouri[177], S. Lai[48], H. Laier[58a], L. Lambourne[77], S. Lammers[60], C.L. Lampen[7], W. Lampl[7], E. Lançon[137], U. Landgraf[48], M.P.J. Landon[75], V.S. Lang[58a], C. Lange[42], A.J. Lankford[164], F. Lanni[25], K. Lantzsch[30], S. Laplace[79], C. Lapoire[21], J.F. Laporte[137], T. Lari[90a], M. Lassnig[30], P. Laurelli[47], W. Lavrijsen[15], A.T. Law[138], P. Laycock[73], B.T. Le[55], O. Le Dortz[79], E. Le Guirriec[84], E. Le Menedeu[12], T. LeCompte[6], F. Ledroit-Guillon[55], C.A. Lee[152], H. Lee[106], J.S.H. Lee[117], S.C. Lee[152], L. Lee[177], G. Lefebvre[79], M. Lefebvre[170], F. Legger[99], C. Leggett[15], A. Lehan[73], M. Lehmacher[21], G. Lehmann Miotto[30], X. Lei[7], W.A. Leight[29], A. Leisos[155], A.G. Leister[177], M.A.L. Leite[24d], R. Leitner[128], D. Lellouch[173], B. Lemmer[54], K.J.C. Leney[77], T. Lenz[106], G. Lenzen[176], B. Lenzi[30], R. Leone[7], K. Leonhardt[44], S. Leontsinis[10], C. Leroy[94], C.G. Lester[28], C.M. Lester[121], M. Levchenko[122], J. Levêque[5], D. Levin[88], L.J. Levinson[173], M. Levy[18], A. Lewis[119], G.H. Lewis[109], A.M. Leyko[21], M. Leyton[41], B. Li[33b,t], B. Li[84], H. Li[149], H.L. Li[31], L. Li[45], L. Li[33e], S. Li[45], Y. Li[33c,u], Z. Liang[138], H. Liao[34], B. Liberti[134a], P. Lichard[30], K. Lie[166], J. Liebal[21], W. Liebig[14], C. Limbach[21], A. Limosani[87], S.C. Lin[152,v], T.H. Lin[82], F. Linde[106], B.E. Lindquist[149], J.T. Linnemann[89], E. Lipeles[121], A. Lipniacka[14], M. Lisovyi[42], T.M. Liss[166], D. Lissauer[25], A. Lister[169], A.M. Litke[138], B. Liu[152], D. Liu[152], J.B. Liu[33b], K. Liu[33b,w], L. Liu[88], M. Liu[45], M. Liu[33b], Y. Liu[33b], M. Livan[120a,120b], S.S.A. Livermore[119], A. Lleres[55], J. Llorente Merino[81], S.L. Lloyd[75], F. Lo Sterzo[152], E. Lobodzinska[42], P. Loch[7], W.S. Lockman[138], T. Loddenkoetter[21], F.K. Loebinger[83], A.E. Loevschall-Jensen[36], A. Loginov[177], C.W. Loh[169], T. Lohse[16], K. Lohwasser[42], M. Lokajicek[126], V.P. Lombardo[5], B.A. Long[22], J.D. Long[88], R.E. Long[71], L. Lopes[125a], D. Lopez Mateos[57], B. Lopez Paredes[140], I. Lopez Paz[12], J. Lorenz[99], N. Lorenzo Martinez[60], M. Losada[163], P. Loscutoff[15], X. Lou[41], A. Lounis[116], J. Love[6], P.A. Love[71], A.J. Lowe[144,e], F. Lu[33a], H.J. Lubatti[139], C. Luci[133a,133b], A. Lucotte[55], F. Luehring[60], W. Lukas[61], L. Luminari[133a], O. Lundberg[147a,147b], B. Lund-Jensen[148], M. Lungwitz[82], D. Lynn[25], R. Lysak[126], E. Lytken[80], H. Ma[25], L.L. Ma[33d], G. Maccarrone[47], A. Macchiolo[100], J. Machado Miguens[125a,125b], D. Macina[30], D. Madaffari[84], R. Madar[48], H.J. Maddocks[71], W.F. Mader[44], A. Madsen[167], M. Maeno[8], T. Maeno[25], E. Magradze[54], K. Mahboubi[48], J. Mahlstedt[106], S. Mahmoud[73], C. Maiani[137], C. Maidantchik[24a], A. Maio[125a,125b,125d], S. Majewski[115], Y. Makida[65], N. Makovec[116], P. Mal[137,x], B. Malaescu[79], Pa. Malecki[39], V.P. Maleev[122], F. Malek[55], U. Mallik[62], D. Malon[6], C. Malone[144], S. Maltezos[10], V.M. Malyshev[108], S. Malyukov[30], J. Mamuzic[13b], B. Mandelli[30], L. Mandelli[90a], I. Mandić[74], R. Mandrysch[62], J. Maneira[125a,125b], A. Manfredini[100], L. Manhaes de Andrade Filho[24b], J.A. Manjarres Ramos[160b], A. Mann[99], P.M. Manning[138], A. Manousakis-Katsikakis[9], B. Mansoulie[137], R. Mantifel[86], L. Mapelli[30], L. March[168], J.F. Marchand[29], G. Marchiori[79], M. Marcisovsky[126], C.P. Marino[170], M. Marjanovic[13a], C.N. Marques[125a], F. Marroquim[24a], S.P. Marsden[83], Z. Marshall[15], L.F. Marti[17], S. Marti-Garcia[168], B. Martin[30], B. Martin[89], T.A. Martin[171], V.J. Martin[46], B. Martin dit Latour[14], H. Martinez[137], M. Martinez[12,n], S. Martin-Haugh[130], A.C. Martyniuk[77], M. Marx[139], F. Marzano[133a], A. Marzin[30], L. Masetti[82], T. Mashimo[156], R. Mashinistov[95], J. Masik[83], A.L. Maslennikov[108], I. Massa[20a,20b], N. Massol[5], P. Mastrandrea[149], A. Mastroberardino[37a,37b], T. Masubuchi[156], T. Matsushita[66], P. Mättig[176], J. Mattmann[82], J. Maurer[26a], S.J. Maxfield[73], D.A. Maximov[108,s], R. Mazini[152], L. Mazzaferro[134a,134b], G. Mc Goldrick[159], S.P. Mc Kee[88], A. McCarn[88], R.L. McCarthy[149], T.G. McCarthy[29], N.A. McCubbin[130], K.W. McFarlane[56,*], J.A. Mcfayden[77], G. Mchedlidze[54],

JHEP09(2014)037

S.J. McMahon[130], R.A. McPherson[170,i], A. Meade[85], J. Mechnich[106], M. Medinnis[42], S. Meehan[31], S. Mehlhase[36], A. Mehta[73], K. Meier[58a], C. Meineck[99], B. Meirose[80], C. Melachrinos[31], B.R. Mellado Garcia[146c], F. Meloni[90a,90b], A. Mengarelli[20a,20b], S. Menke[100], E. Meoni[162], K.M. Mercurio[57], S. Mergelmeyer[21], N. Meric[137], P. Mermod[49], L. Merola[103a,103b], C. Meroni[90a], F.S. Merritt[31], H. Merritt[110], A. Messina[30,y], J. Metcalfe[25], A.S. Mete[164], C. Meyer[82], C. Meyer[31], J-P. Meyer[137], J. Meyer[30], R.P. Middleton[130], S. Migas[73], L. Mijović[21], G. Mikenberg[173], M. Mikestikova[126], M. Mikuž[74], A. Milic[30], D.W. Miller[31], C. Mills[46], A. Milov[173], D.A. Milstead[147a,147b], D. Milstein[173], A.A. Minaenko[129], I.A. Minashvili[64], A.I. Mincer[109], B. Mindur[38a], M. Mineev[64], Y. Ming[174], L.M. Mir[12], G. Mirabelli[133a], T. Mitani[172], J. Mitrevski[99], V.A. Mitsou[168], S. Mitsui[65], A. Miucci[49], P.S. Miyagawa[140], J.U. Mjörnmark[80], T. Moa[147a,147b], K. Mochizuki[84], V. Moeller[28], S. Mohapatra[35], W. Mohr[48], S. Molander[147a,147b], R. Moles-Valls[168], K. Mönig[42], C. Monini[55], J. Monk[36], E. Monnier[84], J. Montejo Berlingen[12], F. Monticelli[70], S. Monzani[133a,133b], R.W. Moore[3], A. Moraes[53], N. Morange[62], D. Moreno[82], M. Moreno Llácer[54], P. Morettini[50a], M. Morgenstern[44], M. Morii[57], S. Moritz[82], A.K. Morley[148], G. Mornacchi[30], J.D. Morris[75], L. Morvaj[102], H.G. Moser[100], M. Mosidze[51b], J. Moss[110], R. Mount[144], E. Mountricha[25], S.V. Mouraviev[95,*], E.J.W. Moyse[85], S. Muanza[84], R.D. Mudd[18], F. Mueller[58a], J. Mueller[124], K. Mueller[21], T. Mueller[28], T. Mueller[82], D. Muenstermann[49], Y. Munwes[154], J.A. Murillo Quijada[18], W.J. Murray[171,130], H. Musheghyan[54], E. Musto[153], A.G. Myagkov[129,z], M. Myska[127], O. Nackenhorst[54], J. Nadal[54], K. Nagai[61], R. Nagai[158], Y. Nagai[84], K. Nagano[65], A. Nagarkar[110], Y. Nagasaka[59], M. Nagel[100], A.M. Nairz[30], Y. Nakahama[30], K. Nakamura[65], T. Nakamura[156], I. Nakano[111], H. Namasivayam[41], G. Nanava[21], R. Narayan[58b], T. Nattermann[21], T. Naumann[42], G. Navarro[163], R. Nayyar[7], H.A. Neal[88], P.Yu. Nechaeva[95], T.J. Neep[83], A. Negri[120a,120b], G. Negri[30], M. Negrini[20a], S. Nektarijevic[49], A. Nelson[164], T.K. Nelson[144], S. Nemecek[126], P. Nemethy[109], A.A. Nepomuceno[24a], M. Nessi[30,aa], M.S. Neubauer[166], M. Neumann[176], R.M. Neves[109], P. Nevski[25], P.R. Newman[18], D.H. Nguyen[6], R.B. Nickerson[119], R. Nicolaidou[137], B. Nicquevert[30], J. Nielsen[138], N. Nikiforou[35], A. Nikiforov[16], V. Nikolaenko[129,z], I. Nikolic-Audit[79], K. Nikolics[49], K. Nikolopoulos[18], P. Nilsson[8], Y. Ninomiya[156], A. Nisati[133a], R. Nisius[100], T. Nobe[158], L. Nodulman[6], M. Nomachi[117], I. Nomidis[155], S. Norberg[112], M. Nordberg[30], S. Nowak[100], M. Nozaki[65], L. Nozka[114], K. Ntekas[10], G. Nunes Hanninger[87], T. Nunnemann[99], E. Nurse[77], F. Nuti[87], B.J. O'Brien[46], F. O'grady[7], D.C. O'Neil[143], V. O'Shea[53], F.G. Oakham[29,d], H. Oberlack[100], T. Obermann[21], J. Ocariz[79], A. Ochi[66], M.I. Ochoa[77], S. Oda[69], S. Odaka[65], H. Ogren[60], A. Oh[83], S.H. Oh[45], C.C. Ohm[30], H. Ohman[167], T. Ohshima[102], W. Okamura[117], H. Okawa[25], Y. Okumura[31], T. Okuyama[156], A. Olariu[26a], A.G. Olchevski[64], S.A. Olivares Pino[46], D. Oliveira Damazio[25], E. Oliver Garcia[168], A. Olszewski[39], J. Olszowska[39], A. Onofre[125a,125e], P.U.E. Onyisi[31,ab], C.J. Oram[160a], M.J. Oreglia[31], Y. Oren[154], D. Orestano[135a,135b], N. Orlando[72a,72b], C. Oropeza Barrera[53], R.S. Orr[159], B. Osculati[50a,50b], R. Ospanov[121], G. Otero y Garzon[27], H. Otono[69], M. Ouchrif[136d], E.A. Ouellette[170], F. Ould-Saada[118], A. Ouraou[137], K.P. Oussoren[106], Q. Ouyang[33a], A. Ovcharova[15], M. Owen[83], V.E. Ozcan[19a], N. Ozturk[8], K. Pachal[119], A. Pacheco Pages[12], C. Padilla Aranda[12], M. Pagáčová[48], S. Pagan Griso[15], E. Paganis[140], C. Pahl[100], F. Paige[25], P. Pais[85], K. Pajchel[118], G. Palacino[160b], S. Palestini[30], M. Palka[38b], D. Pallin[34], A. Palma[125a,125b], J.D. Palmer[18], Y.B. Pan[174], E. Panagiotopoulou[10], J.G. Panduro Vazquez[76], P. Pani[106], N. Panikashvili[88], S. Panitkin[25], D. Pantea[26a], L. Paolozzi[134a,134b], Th.D. Papadopoulou[10], K. Papageorgiou[155,l], A. Paramonov[6], D. Paredes Hernandez[34], M.A. Parker[28], F. Parodi[50a,50b], J.A. Parsons[35], U. Parzefall[48], E. Pasqualucci[133a], S. Passaggio[50a], A. Passeri[135a], F. Pastore[135a,135b,*], Fr. Pastore[76], G. Pásztor[29], S. Pataraia[176], N.D. Patel[151], J.R. Pater[83], S. Patricelli[103a,103b], T. Pauly[30], J. Pearce[170], M. Pedersen[118],

JHEP09(2014)037

S. Pedraza Lopez[168], R. Pedro[125a,125b], S.V. Peleganchuk[108], D. Pelikan[167], H. Peng[33b], B. Penning[31], J. Penwell[60], D.V. Perepelitsa[25], E. Perez Codina[160a], M.T. Pérez García-Estañ[168], V. Perez Reale[35], L. Perini[90a,90b], H. Pernegger[30], R. Perrino[72a], R. Peschke[42], V.D. Peshekhonov[64], K. Peters[30], R.F.Y. Peters[83], B.A. Petersen[30], T.C. Petersen[36], E. Petit[42], A. Petridis[147a,147b], C. Petridou[155], E. Petrolo[133a], F. Petrucci[135a,135b], M. Petteni[143], N.E. Pettersson[158], R. Pezoa[32b], P.W. Phillips[130], G. Piacquadio[144], E. Pianori[171], A. Picazio[49], E. Piccaro[75], M. Piccinini[20a,20b], R. Piegaia[27], D.T. Pignotti[110], J.E. Pilcher[31], A.D. Pilkington[77], J. Pina[125a,125b,125d], M. Pinamonti[165a,165c,ac], A. Pinder[119], J.L. Pinfold[3], A. Pingel[36], B. Pinto[125a], S. Pires[79], M. Pitt[173], C. Pizio[90a,90b], L. Plazak[145a], M.-A. Pleier[25], V. Pleskot[128], E. Plotnikova[64], P. Plucinski[147a,147b], S. Poddar[58a], F. Podlyski[34], R. Poettgen[82], L. Poggioli[116], D. Pohl[21], M. Pohl[49], G. Polesello[120a], A. Policicchio[37a,37b], R. Polifka[159], A. Polini[20a], C.S. Pollard[45], V. Polychronakos[25], K. Pommès[30], L. Pontecorvo[133a], B.G. Pope[89], G.A. Popeneciu[26b], D.S. Popovic[13a], A. Poppleton[30], X. Portell Bueso[12], G.E. Pospelov[100], S. Pospisil[127], K. Potamianos[15], I.N. Potrap[64], C.J. Potter[150], C.T. Potter[115], G. Poulard[30], J. Poveda[60], V. Pozdnyakov[64], P. Pralavorio[84], A. Pranko[15], S. Prasad[30], R. Pravahan[8], S. Prell[63], D. Price[83], J. Price[73], L.E. Price[6], D. Prieur[124], M. Primavera[72a], M. Proissl[46], K. Prokofiev[47], F. Prokoshin[32b], E. Protopapadaki[137], S. Protopopescu[25], J. Proudfoot[6], M. Przybycien[38a], H. Przysiezniak[5], E. Ptacek[115], E. Pueschel[85], D. Puldon[149], M. Purohit[25,ad], P. Puzo[116], J. Qian[88], G. Qin[53], Y. Qin[83], A. Quadt[54], D.R. Quarrie[15], W.B. Quayle[165a,165b], M. Queitsch-Maitland[83], D. Quilty[53], A. Qureshi[160b], V. Radeka[25], V. Radescu[42], S.K. Radhakrishnan[149], P. Radloff[115], P. Rados[87], F. Ragusa[90a,90b], G. Rahal[179], S. Rajagopalan[25], M. Rammensee[30], A.S. Randle-Conde[40], C. Rangel-Smith[167], K. Rao[164], F. Rauscher[99], T.C. Rave[48], T. Ravenscroft[53], M. Raymond[30], A.L. Read[118], N.P. Readioff[73], D.M. Rebuzzi[120a,120b], A. Redelbach[175], G. Redlinger[25], R. Reece[138], K. Reeves[41], L. Rehnisch[16], H. Reisin[27], M. Relich[164], C. Rembser[30], H. Ren[33a], Z.L. Ren[152], A. Renaud[116], M. Rescigno[133a], S. Resconi[90a], O.L. Rezanova[108,s], P. Reznicek[128], R. Rezvani[94], R. Richter[100], M. Ridel[79], P. Rieck[16], J. Rieger[54], M. Rijssenbeek[149], A. Rimoldi[120a,120b], L. Rinaldi[20a], E. Ritsch[61], I. Riu[12], F. Rizatdinova[113], E. Rizvi[75], S.H. Robertson[86,i], A. Robichaud-Veronneau[86], D. Robinson[28], J.E.M. Robinson[83], A. Robson[53], C. Roda[123a,123b], L. Rodrigues[30], S. Roe[30], O. Røhne[118], S. Rolli[162], A. Romaniouk[97], M. Romano[20a,20b], G. Romeo[27], E. Romero Adam[168], N. Rompotis[139], L. Roos[79], E. Ros[168], S. Rosati[133a], K. Rosbach[49], M. Rose[76], P.L. Rosendahl[14], O. Rosenthal[142], V. Rossetti[147a,147b], E. Rossi[103a,103b], L.P. Rossi[50a], R. Rosten[139], M. Rotaru[26a], I. Roth[173], J. Rothberg[139], D. Rousseau[116], C.R. Royon[137], A. Rozanov[84], Y. Rozen[153], X. Ruan[146c], F. Rubbo[12], I. Rubinskiy[42], V.I. Rud[98], C. Rudolph[44], M.S. Rudolph[159], F. Rühr[48], A. Ruiz-Martinez[30], Z. Rurikova[48], N.A. Rusakovich[64], A. Ruschke[99], J.P. Rutherfoord[7], N. Ruthmann[48], Y.F. Ryabov[122], M. Rybar[128], G. Rybkin[116], N.C. Ryder[119], A.F. Saavedra[151], S. Sacerdoti[27], A. Saddique[3], I. Sadeh[154], H.F-W. Sadrozinski[138], R. Sadykov[64], F. Safai Tehrani[133a], H. Sakamoto[156], Y. Sakurai[172], G. Salamanna[75], A. Salamon[134a], M. Saleem[112], D. Salek[106], P.H. Sales De Bruin[139], D. Salihagic[100], A. Salnikov[144], J. Salt[168], B.M. Salvachua Ferrando[6], D. Salvatore[37a,37b], F. Salvatore[150], A. Salvucci[105], A. Salzburger[30], D. Sampsonidis[155], A. Sanchez[103a,103b], J. Sánchez[168], V. Sanchez Martinez[168], H. Sandaker[14], R.L. Sandbach[75], H.G. Sander[82], M.P. Sanders[99], M. Sandhoff[176], T. Sandoval[28], C. Sandoval[163], R. Sandstroem[100], D.P.C. Sankey[130], A. Sansoni[47], C. Santoni[34], R. Santonico[134a,134b], H. Santos[125a], I. Santoyo Castillo[150], K. Sapp[124], A. Sapronov[64], J.G. Saraiva[125a,125d], B. Sarrazin[21], G. Sartisohn[176], O. Sasaki[65], Y. Sasaki[156], G. Sauvage[5,*], E. Sauvan[5], P. Savard[159,d], D.O. Savu[30], C. Sawyer[119], L. Sawyer[78,m], D.H. Saxon[53], J. Saxon[121], C. Sbarra[20a], A. Sbrizzi[3], T. Scanlon[77], D.A. Scannicchio[164], M. Scarcella[151], J. Schaarschmidt[173], P. Schacht[100], D. Schaefer[121], R. Schaefer[42], S. Schaepe[21], S. Schaetzel[58b], U. Schäfer[82],

JHEP09(2014)037

A.C. Schaffer[116], D. Schaile[99], R.D. Schamberger[149], V. Scharf[58a], V.A. Schegelsky[122], D. Scheirich[128], M. Schernau[164], M.I. Scherzer[35], C. Schiavi[50a,50b], J. Schieck[99], C. Schillo[48], M. Schioppa[37a,37b], S. Schlenker[30], E. Schmidt[48], K. Schmieden[30], C. Schmitt[82], S. Schmitt[58b], B. Schneider[17], Y.J. Schnellbach[73], U. Schnoor[44], L. Schoeffel[137], A. Schoening[58b], B.D. Schoenrock[89], A.L.S. Schorlemmer[54], M. Schott[82], D. Schouten[160a], J. Schovancova[25], S. Schramm[159], M. Schreyer[175], C. Schroeder[82], N. Schuh[82], M.J. Schultens[21], H.-C. Schultz-Coulon[58a], H. Schulz[16], M. Schumacher[48], B.A. Schumm[138], Ph. Schune[137], C. Schwanenberger[83], A. Schwartzman[144], Ph. Schwegler[100], Ph. Schwemling[137], R. Schwienhorst[89], J. Schwindling[137], T. Schwindt[21], M. Schwoerer[5], F.G. Sciacca[17], E. Scifo[116], G. Sciolla[23], W.G. Scott[130], F. Scuri[123a,123b], F. Scutti[21], J. Searcy[88], G. Sedov[42], E. Sedykh[122], S.C. Seidel[104], A. Seiden[138], F. Seifert[127], J.M. Seixas[24a], G. Sekhniaidze[103a], S.J. Sekula[40], K.E. Selbach[46], D.M. Seliverstov[122,*], G. Sellers[73], N. Semprini-Cesari[20a,20b], C. Serfon[30], L. Serin[116], L. Serkin[54], T. Serre[84], R. Seuster[160a], H. Severini[112], F. Sforza[100], A. Sfyrla[30], E. Shabalina[54], M. Shamim[115], L.Y. Shan[33a], R. Shang[166], J.T. Shank[22], Q.T. Shao[87], M. Shapiro[15], P.B. Shatalov[96], K. Shaw[165a,165b], C.Y. Shehu[150], P. Sherwood[77], L. Shi[152,ae], S. Shimizu[66], C.O. Shimmin[164], M. Shimojima[101], M. Shiyakova[64], A. Shmeleva[95], M.J. Shochet[31], D. Short[119], S. Shrestha[63], E. Shulga[97], M.A. Shupe[7], S. Shushkevich[42], P. Sicho[126], O. Sidiropoulou[155], D. Sidorov[113], A. Sidoti[133a], F. Siegert[44], Dj. Sijacki[13a], J. Silva[125a,125d], Y. Silver[154], D. Silverstein[144], S.B. Silverstein[147a], V. Simak[127], O. Simard[5], Lj. Simic[13a], S. Simion[116], E. Simioni[82], B. Simmons[77], R. Simoniello[90a,90b], M. Simonyan[36], P. Sinervo[159], N.B. Sinev[115], V. Sipica[142], G. Siragusa[175], A. Sircar[78], A.N. Sisakyan[64,*], S.Yu. Sivoklokov[98], J. Sjölin[147a,147b], T.B. Sjursen[14], H.P. Skottowe[57], K.Yu. Skovpen[108], P. Skubic[112], M. Slater[18], T. Slavicek[127], K. Sliwa[162], V. Smakhtin[173], B.H. Smart[46], L. Smestad[14], S.Yu. Smirnov[97], Y. Smirnov[97], L.N. Smirnova[98,af], O. Smirnova[80], K.M. Smith[53], M. Smizanska[71], K. Smolek[127], A.A. Snesarev[95], G. Snidero[75], S. Snyder[25], R. Sobie[170,i], F. Socher[44], A. Soffer[154], D.A. Soh[152,ae], C.A. Solans[30], M. Solar[127], J. Solc[127], E.Yu. Soldatov[97], U. Soldevila[168], E. Solfaroli Camillocci[133a,133b], A.A. Solodkov[129], A. Soloshenko[64], O.V. Solovyanov[129], V. Solovyev[122], P. Sommer[48], H.Y. Song[33b], N. Soni[1], A. Sood[15], A. Sopczak[127], B. Sopko[127], V. Sopko[127], V. Sorin[12], M. Sosebee[8], R. Soualah[165a,165c], P. Soueid[94], A.M. Soukharev[108], D. South[42], S. Spagnolo[72a,72b], F. Spanò[76], W.R. Spearman[57], R. Spighi[20a], G. Spigo[30], M. Spousta[128], T. Spreitzer[159], B. Spurlock[8], R.D. St. Denis[53,*], S. Staerz[44], J. Stahlman[121], R. Stamen[58a], E. Stanecka[39], R.W. Stanek[6], C. Stanescu[135a], M. Stanescu-Bellu[42], M.M. Stanitzki[42], S. Stapnes[118], E.A. Starchenko[129], J. Stark[55], P. Staroba[126], P. Starovoitov[42], R. Staszewski[39], P. Stavina[145a,*], P. Steinberg[25], B. Stelzer[143], H.J. Stelzer[30], O. Stelzer-Chilton[160a], H. Stenzel[52], S. Stern[100], G.A. Stewart[53], J.A. Stillings[21], M.C. Stockton[86], M. Stoebe[86], G. Stoicea[26a], P. Stolte[54], S. Stonjek[100], A.R. Stradling[8], A. Straessner[44], M.E. Stramaglia[17], J. Strandberg[148], S. Strandberg[147a,147b], A. Strandlie[118], E. Strauss[144], M. Strauss[112], P. Strizenec[145b], R. Ströhmer[175], D.M. Strom[115], R. Stroynowski[40], S.A. Stucci[17], B. Stugu[14], N.A. Styles[42], D. Su[144], J. Su[124], HS. Subramania[3], R. Subramaniam[78], A. Succurro[12], Y. Sugaya[117], C. Suhr[107], M. Suk[127], V.V. Sulin[95], S. Sultansoy[4c], T. Sumida[67], X. Sun[33a], J.E. Sundermann[48], K. Suruliz[140], G. Susinno[37a,37b], M.R. Sutton[150], Y. Suzuki[65], M. Svatos[126], S. Swedish[169], M. Swiatlowski[144], I. Sykora[145a], T. Sykora[128], D. Ta[89], K. Tackmann[42], J. Taenzer[159], A. Taffard[164], R. Tafirout[160a], N. Taiblum[154], Y. Takahashi[102], H. Takai[25], R. Takashima[68], H. Takeda[66], T. Takeshita[141], Y. Takubo[65], M. Talby[84], A.A. Talyshev[108,s], J.Y.C. Tam[175], K.G. Tan[87], J. Tanaka[156], R. Tanaka[116], S. Tanaka[132], S. Tanaka[65], A.J. Tanasijczuk[143], K. Tani[66], N. Tannoury[21], S. Tapprogge[82], S. Tarem[153], F. Tarrade[29], G.F. Tartarelli[90a], P. Tas[128], M. Tasevsky[126], T. Tashiro[67], E. Tassi[37a,37b], A. Tavares Delgado[125a,125b], Y. Tayalati[136d], F.E. Taylor[93], G.N. Taylor[87], W. Taylor[160b],

JHEP09(2014)037

F.A. Teischinger[30], M. Teixeira Dias Castanheira[75], P. Teixeira-Dias[76], K.K. Temming[48], H. Ten Kate[30], P.K. Teng[152], J.J. Teoh[117], S. Terada[65], K. Terashi[156], J. Terron[81], S. Terzo[100], M. Testa[47], R.J. Teuscher[159,i], J. Therhaag[21], T. Theveneaux-Pelzer[34], J.P. Thomas[18], J. Thomas-Wilsker[76], E.N. Thompson[35], P.D. Thompson[18], P.D. Thompson[159], A.S. Thompson[53], L.A. Thomsen[36], E. Thomson[121], M. Thomson[28], W.M. Thong[87], R.P. Thun[88,*], F. Tian[35], M.J. Tibbetts[15], V.O. Tikhomirov[95,ag], Yu.A. Tikhonov[108,s], S. Timoshenko[97], E. Tiouchichine[84], P. Tipton[177], S. Tisserant[84], T. Todorov[5], S. Todorova-Nova[128], B. Toggerson[7], J. Tojo[69], S. Tokár[145a], K. Tokushuku[65], K. Tollefson[89], L. Tomlinson[83], M. Tomoto[102], L. Tompkins[31], K. Toms[104], N.D. Topilin[64], E. Torrence[115], H. Torres[143], E. Torró Pastor[168], J. Toth[84,ah], F. Touchard[84], D.R. Tovey[140], H.L. Tran[116], T. Trefzger[175], L. Tremblet[30], A. Tricoli[30], I.M. Trigger[160a], S. Trincaz-Duvoid[79], M.F. Tripiana[70], N. Triplett[25], W. Trischuk[159], B. Trocmé[55], C. Troncon[90a], M. Trottier-McDonald[143], M. Trovatelli[135a,135b], P. True[89], M. Trzebinski[39], A. Trzupek[39], C. Tsarouchas[30], J.C-L. Tseng[119], P.V. Tsiareshka[91], D. Tsionou[137], G. Tsipolitis[10], N. Tsirintanis[9], S. Tsiskaridze[12], V. Tsiskaridze[48], E.G. Tskhadadze[51a], I.I. Tsukerman[96], V. Tsulaia[15], S. Tsuno[65], D. Tsybychev[149], A. Tudorache[26a], V. Tudorache[26a], A.N. Tuna[121], S.A. Tupputi[20a,20b], S. Turchikhin[98,af], D. Turecek[127], I. Turk Cakir[4d], R. Turra[90a,90b], P.M. Tuts[35], A. Tykhonov[74], M. Tylmad[147a,147b], M. Tyndel[130], K. Uchida[21], I. Ueda[156], R. Ueno[29], M. Ughetto[84], M. Ugland[14], M. Uhlenbrock[21], F. Ukegawa[161], G. Unal[30], A. Undrus[25], G. Unel[164], F.C. Ungaro[48], Y. Unno[65], C. Unverdorben[99], D. Urbaniec[35], P. Urquijo[87], G. Usai[8], A. Usanova[61], L. Vacavant[84], V. Vacek[127], B. Vachon[86], N. Valencic[106], S. Valentinetti[20a,20b], A. Valero[168], L. Valery[34], S. Valkar[128], E. Valladolid Gallego[168], S. Vallecorsa[49], J.A. Valls Ferrer[168], P.C. Van Der Deijl[106], R. van der Geer[106], H. van der Graaf[106], R. Van Der Leeuw[106], D. van der Ster[30], N. van Eldik[30], P. van Gemmeren[6], J. Van Nieuwkoop[143], I. van Vulpen[106], M.C. van Woerden[30], M. Vanadia[133a,133b], W. Vandelli[30], R. Vanguri[121], A. Vaniachine[6], P. Vankov[42], F. Vannucci[79], G. Vardanyan[178], R. Vari[133a], E.W. Varnes[7], T. Varol[85], D. Varouchas[79], A. Vartapetian[8], K.E. Varvell[151], F. Vazeille[34], T. Vazquez Schroeder[54], J. Veatch[7], F. Veloso[125a,125c], S. Veneziano[133a], A. Ventura[72a,72b], D. Ventura[85], M. Venturi[170], N. Venturi[159], A. Venturini[23], V. Vercesi[120a], M. Verducci[139], W. Verkerke[106], J.C. Vermeulen[106], A. Vest[44], M.C. Vetterli[143,d], O. Viazlo[80], I. Vichou[166], T. Vickey[146c,ai], O.E. Vickey Boeriu[146c], G.H.A. Viehhauser[119], S. Viel[169], R. Vigne[30], M. Villa[20a,20b], M. Villaplana Perez[90a,90b], E. Vilucchi[47], M.G. Vincter[29], V.B. Vinogradov[64], J. Virzi[15], I. Vivarelli[150], F. Vives Vaque[3], S. Vlachos[10], D. Vladoiu[99], M. Vlasak[127], A. Vogel[21], M. Vogel[32a], P. Vokac[127], G. Volpi[123a,123b], M. Volpi[87], H. von der Schmitt[100], H. von Radziewski[48], E. von Toerne[21], V. Vorobel[128], K. Vorobev[97], M. Vos[168], R. Voss[30], J.H. Vossebeld[73], N. Vranjes[137], M. Vranjes Milosavljevic[106], V. Vrba[126], M. Vreeswijk[106], T. Vu Anh[48], R. Vuillermet[30], I. Vukotic[31], Z. Vykydal[127], P. Wagner[21], W. Wagner[176], H. Wahlberg[70], S. Wahrmund[44], J. Wakabayashi[102], J. Walder[71], R. Walker[99], W. Walkowiak[142], R. Wall[177], P. Waller[73], B. Walsh[177], C. Wang[152,aj], C. Wang[45], F. Wang[174], H. Wang[15], H. Wang[40], J. Wang[42], J. Wang[33a], K. Wang[86], R. Wang[104], S.M. Wang[152], T. Wang[21], X. Wang[177], C. Wanotayaroj[115], A. Warburton[86], C.P. Ward[28], D.R. Wardrope[77], M. Warsinsky[48], A. Washbrook[46], C. Wasicki[42], I. Watanabe[66], P.M. Watkins[18], A.T. Watson[18], I.J. Watson[151], M.F. Watson[18], G. Watts[139], S. Watts[83], B.M. Waugh[77], S. Webb[83], M.S. Weber[17], S.W. Weber[175], J.S. Webster[31], A.R. Weidberg[119], P. Weigell[100], B. Weinert[60], J. Weingarten[54], C. Weiser[48], H. Weits[106], P.S. Wells[30], T. Wenaus[25], D. Wendland[16], Z. Weng[152,ae], T. Wengler[30], S. Wenig[30], N. Wermes[21], M. Werner[48], P. Werner[30], M. Wessels[58a], J. Wetter[162], K. Whalen[29], A. White[8], M.J. White[1], R. White[32b], S. White[123a,123b], D. Whiteson[164], D. Wicke[176], F.J. Wickens[130], W. Wiedenmann[174], M. Wielers[130], P. Wienemann[21], C. Wiglesworth[36], L.A.M. Wiik-Fuchs[21], P.A. Wijeratne[77], A. Wildauer[100],

JHEP09(2014)037

M.A. Wildt[42,ak], H.G. Wilkens[30], J.Z. Will[99], H.H. Williams[121], S. Williams[28], C. Willis[89], S. Willocq[85], A. Wilson[88], J.A. Wilson[18], I. Wingerter-Seez[5], F. Winklmeier[115], B.T. Winter[21], M. Wittgen[144], T. Wittig[43], J. Wittkowski[99], S.J. Wollstadt[82], M.W. Wolter[39], H. Wolters[125a,125c], B.K. Wosiek[39], J. Wotschack[30], M.J. Woudstra[83], K.W. Wozniak[39], M. Wright[53], M. Wu[55], S.L. Wu[174], X. Wu[49], Y. Wu[88], E. Wulf[35], T.R. Wyatt[83], B.M. Wynne[46], S. Xella[36], M. Xiao[137], D. Xu[33a], L. Xu[33b,al], B. Yabsley[151], S. Yacoob[146b,am], M. Yamada[65], H. Yamaguchi[156], Y. Yamaguchi[156], A. Yamamoto[65], K. Yamamoto[63], S. Yamamoto[156], T. Yamamura[156], T. Yamanaka[156], K. Yamauchi[102], Y. Yamazaki[66], Z. Yan[22], H. Yang[33e], H. Yang[174], U.K. Yang[83], Y. Yang[110], S. Yanush[92], L. Yao[33a], W-M. Yao[15], Y. Yasu[65], E. Yatsenko[42], K.H. Yau Wong[21], J. Ye[40], S. Ye[25], A.L. Yen[57], E. Yildirim[42], M. Yilmaz[4b], R. Yoosoofmiya[124], K. Yorita[172], R. Yoshida[6], K. Yoshihara[156], C. Young[144], C.J.S. Young[30], S. Youssef[22], D.R. Yu[15], J. Yu[8], J.M. Yu[88], J. Yu[113], L. Yuan[66], A. Yurkewicz[107], B. Zabinski[39], R. Zaidan[62], A.M. Zaitsev[129,z], A. Zaman[149], S. Zambito[23], L. Zanello[133a,133b], D. Zanzi[100], C. Zeitnitz[176], M. Zeman[127], A. Zemla[38a], K. Zengel[23], O. Zenin[129], T. Ženiš[145a], D. Zerwas[116], G. Zevi della Porta[57], D. Zhang[88], F. Zhang[174], H. Zhang[89], J. Zhang[6], L. Zhang[152], X. Zhang[33d], Z. Zhang[116], Z. Zhao[33b], A. Zhemchugov[64], J. Zhong[119], B. Zhou[88], L. Zhou[35], N. Zhou[164], C.G. Zhu[33d], H. Zhu[33a], J. Zhu[88], Y. Zhu[33b], X. Zhuang[33a], K. Zhukov[95], A. Zibell[175], D. Zieminska[60], N.I. Zimine[64], C. Zimmermann[82], R. Zimmermann[21], S. Zimmermann[21], S. Zimmermann[48], Z. Zinonos[54], M. Ziolkowski[142], G. Zobernig[174], A. Zoccoli[20a,20b], M. zur Nedden[16], G. Zurzolo[103a,103b], V. Zutshi[107] and L. Zwalinski[30].

[1] *Department of Physics, University of Adelaide, Adelaide, Australia*
[2] *Physics Department, SUNY Albany, Albany NY, United States of America*
[3] *Department of Physics, University of Alberta, Edmonton AB, Canada*
[4] [(a)] *Department of Physics, Ankara University, Ankara;* [(b)] *Department of Physics, Gazi University, Ankara;* [(c)] *Division of Physics, TOBB University of Economics and Technology, Ankara;* [(d)] *Turkish Atomic Energy Authority, Ankara, Turkey*
[5] *LAPP, CNRS/IN2P3 and Université de Savoie, Annecy-le-Vieux, France*
[6] *High Energy Physics Division, Argonne National Laboratory, Argonne IL, United States of America*
[7] *Department of Physics, University of Arizona, Tucson AZ, United States of America*
[8] *Department of Physics, The University of Texas at Arlington, Arlington TX, United States of America*
[9] *Physics Department, University of Athens, Athens, Greece*
[10] *Physics Department, National Technical University of Athens, Zografou, Greece*
[11] *Institute of Physics, Azerbaijan Academy of Sciences, Baku, Azerbaijan*
[12] *Institut de Física d'Altes Energies and Departament de Física de la Universitat Autònoma de Barcelona, Barcelona, Spain*
[13] [(a)] *Institute of Physics, University of Belgrade, Belgrade;* [(b)] *Vinca Institute of Nuclear Sciences, University of Belgrade, Belgrade, Serbia*
[14] *Department for Physics and Technology, University of Bergen, Bergen, Norway*
[15] *Physics Division, Lawrence Berkeley National Laboratory and University of California, Berkeley CA, United States of America*
[16] *Department of Physics, Humboldt University, Berlin, Germany*
[17] *Albert Einstein Center for Fundamental Physics and Laboratory for High Energy Physics, University of Bern, Bern, Switzerland*
[18] *School of Physics and Astronomy, University of Birmingham, Birmingham, United Kingdom*
[19] [(a)] *Department of Physics, Bogazici University, Istanbul;* [(b)] *Department of Physics, Dogus University, Istanbul;* [(c)] *Department of Physics Engineering, Gaziantep University, Gaziantep, Turkey*
[20] [(a)] *INFN Sezione di Bologna;* [(b)] *Dipartimento di Fisica e Astronomia, Università di Bologna, Bologna, Italy*
[21] *Physikalisches Institut, University of Bonn, Bonn, Germany*

JHEP09(2014)037

[22] Department of Physics, Boston University, Boston MA, United States of America
[23] Department of Physics, Brandeis University, Waltham MA, United States of America
[24] [(a)] Universidade Federal do Rio De Janeiro COPPE/EE/IF, Rio de Janeiro; [(b)] Federal University of Juiz de Fora (UFJF), Juiz de Fora; [(c)] Federal University of Sao Joao del Rei (UFSJ), Sao Joao del Rei; [(d)] Instituto de Fisica, Universidade de Sao Paulo, Sao Paulo, Brazil
[25] Physics Department, Brookhaven National Laboratory, Upton NY, United States of America
[26] [(a)] National Institute of Physics and Nuclear Engineering, Bucharest; [(b)] National Institute for Research and Development of Isotopic and Molecular Technologies, Physics Department, Cluj Napoca; [(c)] University Politehnica Bucharest, Bucharest; [(d)] West University in Timisoara, Timisoara, Romania
[27] Departamento de Física, Universidad de Buenos Aires, Buenos Aires, Argentina
[28] Cavendish Laboratory, University of Cambridge, Cambridge, United Kingdom
[29] Department of Physics, Carleton University, Ottawa ON, Canada
[30] CERN, Geneva, Switzerland
[31] Enrico Fermi Institute, University of Chicago, Chicago IL, United States of America
[32] [(a)] Departamento de Física, Pontificia Universidad Católica de Chile, Santiago; [(b)] Departamento de Física, Universidad Técnica Federico Santa María, Valparaíso, Chile
[33] [(a)] Institute of High Energy Physics, Chinese Academy of Sciences, Beijing; [(b)] Department of Modern Physics, University of Science and Technology of China, Anhui; [(c)] Department of Physics, Nanjing University, Jiangsu; [(d)] School of Physics, Shandong University, Shandong; [(e)] Physics Department, Shanghai Jiao Tong University, Shanghai, China
[34] Laboratoire de Physique Corpusculaire, Clermont Université and Université Blaise Pascal and CNRS/IN2P3, Clermont-Ferrand, France
[35] Nevis Laboratory, Columbia University, Irvington NY, United States of America
[36] Niels Bohr Institute, University of Copenhagen, Kobenhavn, Denmark
[37] [(a)] INFN Gruppo Collegato di Cosenza, Laboratori Nazionali di Frascati; [(b)] Dipartimento di Fisica, Università della Calabria, Rende, Italy
[38] [(a)] AGH University of Science and Technology, Faculty of Physics and Applied Computer Science, Krakow; [(b)] Marian Smoluchowski Institute of Physics, Jagiellonian University, Krakow, Poland
[39] The Henryk Niewodniczanski Institute of Nuclear Physics, Polish Academy of Sciences, Krakow, Poland
[40] Physics Department, Southern Methodist University, Dallas TX, United States of America
[41] Physics Department, University of Texas at Dallas, Richardson TX, United States of America
[42] DESY, Hamburg and Zeuthen, Germany
[43] Institut für Experimentelle Physik IV, Technische Universität Dortmund, Dortmund, Germany
[44] Institut für Kern- und Teilchenphysik, Technische Universität Dresden, Dresden, Germany
[45] Department of Physics, Duke University, Durham NC, United States of America
[46] SUPA - School of Physics and Astronomy, University of Edinburgh, Edinburgh, United Kingdom
[47] INFN Laboratori Nazionali di Frascati, Frascati, Italy
[48] Fakultät für Mathematik und Physik, Albert-Ludwigs-Universität, Freiburg, Germany
[49] Section de Physique, Université de Genève, Geneva, Switzerland
[50] [(a)] INFN Sezione di Genova; [(b)] Dipartimento di Fisica, Università di Genova, Genova, Italy
[51] [(a)] E. Andronikashvili Institute of Physics, Iv. Javakhishvili Tbilisi State University, Tbilisi; [(b)] High Energy Physics Institute, Tbilisi State University, Tbilisi, Georgia
[52] II Physikalisches Institut, Justus-Liebig-Universität Giessen, Giessen, Germany
[53] SUPA - School of Physics and Astronomy, University of Glasgow, Glasgow, United Kingdom
[54] II Physikalisches Institut, Georg-August-Universität, Göttingen, Germany
[55] Laboratoire de Physique Subatomique et de Cosmologie, Université Grenoble-Alpes, CNRS/IN2P3, Grenoble, France
[56] Department of Physics, Hampton University, Hampton VA, United States of America
[57] Laboratory for Particle Physics and Cosmology, Harvard University, Cambridge MA, United States of America

JHEP09(2014)037

[58] [(a)] Kirchhoff-Institut für Physik, Ruprecht-Karls-Universität Heidelberg, Heidelberg; [(b)] Physikalisches Institut, Ruprecht-Karls-Universität Heidelberg, Heidelberg; [(c)] ZITI Institut für technische Informatik, Ruprecht-Karls-Universität Heidelberg, Mannheim, Germany
[59] Faculty of Applied Information Science, Hiroshima Institute of Technology, Hiroshima, Japan
[60] Department of Physics, Indiana University, Bloomington IN, United States of America
[61] Institut für Astro- und Teilchenphysik, Leopold-Franzens-Universität, Innsbruck, Austria
[62] University of Iowa, Iowa City IA, United States of America
[63] Department of Physics and Astronomy, Iowa State University, Ames IA, United States of America
[64] Joint Institute for Nuclear Research, JINR Dubna, Dubna, Russia
[65] KEK, High Energy Accelerator Research Organization, Tsukuba, Japan
[66] Graduate School of Science, Kobe University, Kobe, Japan
[67] Faculty of Science, Kyoto University, Kyoto, Japan
[68] Kyoto University of Education, Kyoto, Japan
[69] Department of Physics, Kyushu University, Fukuoka, Japan
[70] Instituto de Física La Plata, Universidad Nacional de La Plata and CONICET, La Plata, Argentina
[71] Physics Department, Lancaster University, Lancaster, United Kingdom
[72] [(a)] INFN Sezione di Lecce; [(b)] Dipartimento di Matematica e Fisica, Università del Salento, Lecce, Italy
[73] Oliver Lodge Laboratory, University of Liverpool, Liverpool, United Kingdom
[74] Department of Physics, Jožef Stefan Institute and University of Ljubljana, Ljubljana, Slovenia
[75] School of Physics and Astronomy, Queen Mary University of London, London, United Kingdom
[76] Department of Physics, Royal Holloway University of London, Surrey, United Kingdom
[77] Department of Physics and Astronomy, University College London, London, United Kingdom
[78] Louisiana Tech University, Ruston LA, United States of America
[79] Laboratoire de Physique Nucléaire et de Hautes Energies, UPMC and Université Paris-Diderot and CNRS/IN2P3, Paris, France
[80] Fysiska institutionen, Lunds universitet, Lund, Sweden
[81] Departamento de Fisica Teorica C-15, Universidad Autonoma de Madrid, Madrid, Spain
[82] Institut für Physik, Universität Mainz, Mainz, Germany
[83] School of Physics and Astronomy, University of Manchester, Manchester, United Kingdom
[84] CPPM, Aix-Marseille Université and CNRS/IN2P3, Marseille, France
[85] Department of Physics, University of Massachusetts, Amherst MA, United States of America
[86] Department of Physics, McGill University, Montreal QC, Canada
[87] School of Physics, University of Melbourne, Victoria, Australia
[88] Department of Physics, The University of Michigan, Ann Arbor MI, United States of America
[89] Department of Physics and Astronomy, Michigan State University, East Lansing MI, United States of America
[90] [(a)] INFN Sezione di Milano; [(b)] Dipartimento di Fisica, Università di Milano, Milano, Italy
[91] B.I. Stepanov Institute of Physics, National Academy of Sciences of Belarus, Minsk, Republic of Belarus
[92] National Scientific and Educational Centre for Particle and High Energy Physics, Minsk, Republic of Belarus
[93] Department of Physics, Massachusetts Institute of Technology, Cambridge MA, United States of America
[94] Group of Particle Physics, University of Montreal, Montreal QC, Canada
[95] P.N. Lebedev Institute of Physics, Academy of Sciences, Moscow, Russia
[96] Institute for Theoretical and Experimental Physics (ITEP), Moscow, Russia
[97] Moscow Engineering and Physics Institute (MEPhI), Moscow, Russia
[98] D.V.Skobeltsyn Institute of Nuclear Physics, M.V.Lomonosov Moscow State University, Moscow, Russia
[99] Fakultät für Physik, Ludwig-Maximilians-Universität München, München, Germany
[100] Max-Planck-Institut für Physik (Werner-Heisenberg-Institut), München, Germany

JHEP09(2014)037

[101] Nagasaki Institute of Applied Science, Nagasaki, Japan
[102] Graduate School of Science and Kobayashi-Maskawa Institute, Nagoya University, Nagoya, Japan
[103] [(a)] INFN Sezione di Napoli; [(b)] Dipartimento di Fisica, Università di Napoli, Napoli, Italy
[104] Department of Physics and Astronomy, University of New Mexico, Albuquerque NM, United States of America
[105] Institute for Mathematics, Astrophysics and Particle Physics, Radboud University Nijmegen/Nikhef, Nijmegen, Netherlands
[106] Nikhef National Institute for Subatomic Physics and University of Amsterdam, Amsterdam, Netherlands
[107] Department of Physics, Northern Illinois University, DeKalb IL, United States of America
[108] Budker Institute of Nuclear Physics, SB RAS, Novosibirsk, Russia
[109] Department of Physics, New York University, New York NY, United States of America
[110] Ohio State University, Columbus OH, United States of America
[111] Faculty of Science, Okayama University, Okayama, Japan
[112] Homer L. Dodge Department of Physics and Astronomy, University of Oklahoma, Norman OK, United States of America
[113] Department of Physics, Oklahoma State University, Stillwater OK, United States of America
[114] Palacký University, RCPTM, Olomouc, Czech Republic
[115] Center for High Energy Physics, University of Oregon, Eugene OR, United States of America
[116] LAL, Université Paris-Sud and CNRS/IN2P3, Orsay, France
[117] Graduate School of Science, Osaka University, Osaka, Japan
[118] Department of Physics, University of Oslo, Oslo, Norway
[119] Department of Physics, Oxford University, Oxford, United Kingdom
[120] [(a)] INFN Sezione di Pavia; [(b)] Dipartimento di Fisica, Università di Pavia, Pavia, Italy
[121] Department of Physics, University of Pennsylvania, Philadelphia PA, United States of America
[122] Petersburg Nuclear Physics Institute, Gatchina, Russia
[123] [(a)] INFN Sezione di Pisa; [(b)] Dipartimento di Fisica E. Fermi, Università di Pisa, Pisa, Italy
[124] Department of Physics and Astronomy, University of Pittsburgh, Pittsburgh PA, United States of America
[125] [(a)] Laboratorio de Instrumentacao e Fisica Experimental de Particulas - LIP, Lisboa; [(b)] Faculdade de Ciências, Universidade de Lisboa, Lisboa; [(c)] Department of Physics, University of Coimbra, Coimbra; [(d)] Centro de Física Nuclear da Universidade de Lisboa, Lisboa; [(e)] Departamento de Fisica, Universidade do Minho, Braga; [(f)] Departamento de Fisica Teorica y del Cosmos and CAFPE, Universidad de Granada, Granada (Spain); [(g)] Dep Fisica and CEFITEC of Faculdade de Ciencias e Tecnologia, Universidade Nova de Lisboa, Caparica, Portugal
[126] Institute of Physics, Academy of Sciences of the Czech Republic, Praha, Czech Republic
[127] Czech Technical University in Prague, Praha, Czech Republic
[128] Faculty of Mathematics and Physics, Charles University in Prague, Praha, Czech Republic
[129] State Research Center Institute for High Energy Physics, Protvino, Russia
[130] Particle Physics Department, Rutherford Appleton Laboratory, Didcot, United Kingdom
[131] Physics Department, University of Regina, Regina SK, Canada
[132] Ritsumeikan University, Kusatsu, Shiga, Japan
[133] [(a)] INFN Sezione di Roma; [(b)] Dipartimento di Fisica, Sapienza Università di Roma, Roma, Italy
[134] [(a)] INFN Sezione di Roma Tor Vergata; [(b)] Dipartimento di Fisica, Università di Roma Tor Vergata, Roma, Italy
[135] [(a)] INFN Sezione di Roma Tre; [(b)] Dipartimento di Matematica e Fisica, Università Roma Tre, Roma, Italy
[136] [(a)] Faculté des Sciences Ain Chock, Réseau Universitaire de Physique des Hautes Energies - Université Hassan II, Casablanca; [(b)] Centre National de l'Energie des Sciences Techniques Nucleaires, Rabat; [(c)] Faculté des Sciences Semlalia, Université Cadi Ayyad, LPHEA-Marrakech; [(d)] Faculté des Sciences, Université Mohamed Premier and LPTPM, Oujda; [(e)] Faculté des sciences, Université Mohammed V-Agdal, Rabat, Morocco

JHEP09(2014)037

[137] DSM/IRFU (Institut de Recherches sur les Lois Fondamentales de l'Univers), CEA Saclay (Commissariat à l'Energie Atomique et aux Energies Alternatives), Gif-sur-Yvette, France
[138] Santa Cruz Institute for Particle Physics, University of California Santa Cruz, Santa Cruz CA, United States of America
[139] Department of Physics, University of Washington, Seattle WA, United States of America
[140] Department of Physics and Astronomy, University of Sheffield, Sheffield, United Kingdom
[141] Department of Physics, Shinshu University, Nagano, Japan
[142] Fachbereich Physik, Universität Siegen, Siegen, Germany
[143] Department of Physics, Simon Fraser University, Burnaby BC, Canada
[144] SLAC National Accelerator Laboratory, Stanford CA, United States of America
[145] [(a)] Faculty of Mathematics, Physics & Informatics, Comenius University, Bratislava; [(b)] Department of Subnuclear Physics, Institute of Experimental Physics of the Slovak Academy of Sciences, Kosice, Slovak Republic
[146] [(a)] Department of Physics, University of Cape Town, Cape Town; [(b)] Department of Physics, University of Johannesburg, Johannesburg; [(c)] School of Physics, University of the Witwatersrand, Johannesburg, South Africa
[147] [(a)] Department of Physics, Stockholm University; [(b)] The Oskar Klein Centre, Stockholm, Sweden
[148] Physics Department, Royal Institute of Technology, Stockholm, Sweden
[149] Departments of Physics & Astronomy and Chemistry, Stony Brook University, Stony Brook NY, United States of America
[150] Department of Physics and Astronomy, University of Sussex, Brighton, United Kingdom
[151] School of Physics, University of Sydney, Sydney, Australia
[152] Institute of Physics, Academia Sinica, Taipei, Taiwan
[153] Department of Physics, Technion: Israel Institute of Technology, Haifa, Israel
[154] Raymond and Beverly Sackler School of Physics and Astronomy, Tel Aviv University, Tel Aviv, Israel
[155] Department of Physics, Aristotle University of Thessaloniki, Thessaloniki, Greece
[156] International Center for Elementary Particle Physics and Department of Physics, The University of Tokyo, Tokyo, Japan
[157] Graduate School of Science and Technology, Tokyo Metropolitan University, Tokyo, Japan
[158] Department of Physics, Tokyo Institute of Technology, Tokyo, Japan
[159] Department of Physics, University of Toronto, Toronto ON, Canada
[160] [(a)] TRIUMF, Vancouver BC; [(b)] Department of Physics and Astronomy, York University, Toronto ON, Canada
[161] Faculty of Pure and Applied Sciences, University of Tsukuba, Tsukuba, Japan
[162] Department of Physics and Astronomy, Tufts University, Medford MA, United States of America
[163] Centro de Investigaciones, Universidad Antonio Narino, Bogota, Colombia
[164] Department of Physics and Astronomy, University of California Irvine, Irvine CA, United States of America
[165] [(a)] INFN Gruppo Collegato di Udine, Sezione di Trieste, Udine; [(b)] ICTP, Trieste; [(c)] Dipartimento di Chimica, Fisica e Ambiente, Università di Udine, Udine, Italy
[166] Department of Physics, University of Illinois, Urbana IL, United States of America
[167] Department of Physics and Astronomy, University of Uppsala, Uppsala, Sweden
[168] Instituto de Física Corpuscular (IFIC) and Departamento de Física Atómica, Molecular y Nuclear and Departamento de Ingeniería Electrónica and Instituto de Microelectrónica de Barcelona (IMB-CNM), University of Valencia and CSIC, Valencia, Spain
[169] Department of Physics, University of British Columbia, Vancouver BC, Canada
[170] Department of Physics and Astronomy, University of Victoria, Victoria BC, Canada
[171] Department of Physics, University of Warwick, Coventry, United Kingdom
[172] Waseda University, Tokyo, Japan
[173] Department of Particle Physics, The Weizmann Institute of Science, Rehovot, Israel
[174] Department of Physics, University of Wisconsin, Madison WI, United States of America

JHEP09(2014)037

[175] Fakultät für Physik und Astronomie, Julius-Maximilians-Universität, Würzburg, Germany
[176] Fachbereich C Physik, Bergische Universität Wuppertal, Wuppertal, Germany
[177] Department of Physics, Yale University, New Haven CT, United States of America
[178] Yerevan Physics Institute, Yerevan, Armenia
[179] Centre de Calcul de l'Institut National de Physique Nucléaire et de Physique des Particules (IN2P3), Villeurbanne, France
[a] Also at Department of Physics, King's College London, London, United Kingdom
[b] Also at Institute of Physics, Azerbaijan Academy of Sciences, Baku, Azerbaijan
[c] Also at Particle Physics Department, Rutherford Appleton Laboratory, Didcot, United Kingdom
[d] Also at TRIUMF, Vancouver BC, Canada
[e] Also at Department of Physics, California State University, Fresno CA, United States of America
[f] Also at Tomsk State University, Tomsk, Russia
[g] Also at CPPM, Aix-Marseille Université and CNRS/IN2P3, Marseille, France
[h] Also at Università di Napoli Parthenope, Napoli, Italy
[i] Also at Institute of Particle Physics (IPP), Canada
[j] Also at Department of Physics, St. Petersburg State Polytechnical University, St. Petersburg, Russia
[k] Also at Chinese University of Hong Kong, China
[l] Also at Department of Financial and Management Engineering, University of the Aegean, Chios, Greece
[m] Also at Louisiana Tech University, Ruston LA, United States of America
[n] Also at Institucio Catalana de Recerca i Estudis Avancats, ICREA, Barcelona, Spain
[o] Also at Institute of Theoretical Physics, Ilia State University, Tbilisi, Georgia
[p] Also at CERN, Geneva, Switzerland
[q] Also at Ochadai Academic Production, Ochanomizu University, Tokyo, Japan
[r] Also at Manhattan College, New York NY, United States of America
[s] Also at Novosibirsk State University, Novosibirsk, Russia
[t] Also at Institute of Physics, Academia Sinica, Taipei, Taiwan
[u] Also at LAL, Université Paris-Sud and CNRS/IN2P3, Orsay, France
[v] Also at Academia Sinica Grid Computing, Institute of Physics, Academia Sinica, Taipei, Taiwan
[w] Also at Laboratoire de Physique Nucléaire et de Hautes Energies, UPMC and Université Paris-Diderot and CNRS/IN2P3, Paris, France
[x] Also at School of Physical Sciences, National Institute of Science Education and Research, Bhubaneswar, India
[y] Also at Dipartimento di Fisica, Sapienza Università di Roma, Roma, Italy
[z] Also at Moscow Institute of Physics and Technology State University, Dolgoprudny, Russia
[aa] Also at section de Physique, Université de Genève, Geneva, Switzerland
[ab] Also at Department of Physics, The University of Texas at Austin, Austin TX, United States of America
[ac] Also at International School for Advanced Studies (SISSA), Trieste, Italy
[ad] Also at Department of Physics and Astronomy, University of South Carolina, Columbia SC, United States of America
[ae] Also at School of Physics and Engineering, Sun Yat-sen University, Guangzhou, China
[af] Also at Faculty of Physics, M.V.Lomonosov Moscow State University, Moscow, Russia
[ag] Also at Moscow Engineering and Physics Institute (MEPhI), Moscow, Russia
[ah] Also at Institute for Particle and Nuclear Physics, Wigner Research Centre for Physics, Budapest, Hungary
[ai] Also at Department of Physics, Oxford University, Oxford, United Kingdom
[aj] Also at Department of Physics, Nanjing University, Jiangsu, China
[ak] Also at Institut für Experimentalphysik, Universität Hamburg, Hamburg, Germany
[al] Also at Department of Physics, The University of Michigan, Ann Arbor MI, United States of America
[am] Also at Discipline of Physics, University of KwaZulu-Natal, Durban, South Africa
[*] Deceased

JHEP09(2014)037

PROCEEDINGS OF SCIENCE

Challenges in W mass measurements with ATLAS and CMS

Nenad Vranjes[*†]
Institute of Physics, Belgrade, Serbia
E-mail: nenad.vranjes@cern.ch

The mass of the W boson is an important parameter of the Standard Model of particle physics. In this proceedings experimental and theoretical challenges that need to be faced in order to achieve precision of the order of 10 MeV are discussed. The status of various experimental studies related to this measurement are presented.

Fourth Annual Large Hadron Collider Physics
13-18 June 2016
Lund, Sweden

[*]Speaker.
[†]on behalf of the ATLAS and CMS collaborations

http://pos.sissa.it/

PoS(LHCP2016)053

1. Introduction

The Standard Model (SM) [1, 2, 3] with radiative corrections [4] provides a predictive theoretical framework in which the fundamental parameters (particle masses and couplings) are interconnected via an overconstrained set of relations. At lowest order, the W boson mass, m_W, can be written as a function of the Z boson mass, m_Z, the fine-structure constant, α, and the Fermi constant, G_F. Higher order corrections introduce additional dependence of m_W on the gauge couplings and the masses of the heavy particles of the SM. The relation between the parameters is the following:

$$m_W^2\left(1-\frac{m_W^2}{m_Z^2}\right)=\frac{\pi\alpha}{\sqrt{2}G_F}(1+\Delta r), \tag{1.1}$$

where Δr incorporates the effect of higher-order corrections [5, 6]. The Δr term depends strongly on the top and bottom quark masses, m_t and m_b, and logarithmically on the mass of the Higgs boson, m_H. In Beyond standard model (BSM) theories, Δr also receives contributions from additional particles, and the comparison of the measured and predicted values of m_W allows to probe for BSM physics. In the context of global fits of the SM parameters, constraints on BSM physics are currently dominated by the experimental uncertainty on the W boson mass [7].

Previous measurements of m_W were performed at the SPS collider with the UA1 and UA2 experiments [8, 9], at the LEP collider by the ALEPH, DELPHI, L3, and OPAL experiments [10], and at the Tevatron collider by the CDF and D0 experiments [11, 12, 13]. The current world average value of $m_W = 80385 \pm 15$ MeV [14] is dominated by the CDF and D0 measurements performed with $p\bar{p}$ collision data collected and a center-of -mass energy of $\sqrt{s} = 1.96$ TeV [15, 16, 17]. For these results only about 20% (50%) of the total data collected by CDF (D0) is used.

Given the precisely measured values of α, G_F and m_Z, and taking $m_t = 173.34 \pm 0.76$ GeV [18] and $m_H = 125.09 \pm 0.24$ GeV [19] as inputs, the SM prediction of m_W leads to the uncertainty of $\delta m_W = 8$ MeV. The latest most precise measurement of m_t with uncertainty of 0.66 GeV [20] pushes δm_W further to 6 MeV which represents a target for the accuracy of present and future measurements of the W boson mass. Therefore improving the accuracy of the experimental measurements of m_W is of prime importance for testing the overall consistency of the SM. Both Large Hadron Collider (LHC) general purpose experiments, ATLAS [21] and CMS [22], are pursuing the efforts that would lead to the m_W measurement with best possible precision. The ultimate combined precision at the LHC is estimated to be $\delta m_W = 5$ MeV [23].

2. Measurement of m_W at hadron colliders

At hadron colliders, m_W is measured using leptonic decays of the W boson: $W \to \ell\nu$, $\ell = e, \mu$. These represent clean final states with best possible experimental control (in terms of experimental uncertainties). Due to the presence of the neutrino in the final state, m_W is extracted from the kinematic variables measured in the plane perpendicular to the beam direction. Sensitive observables are the transverse momentum of the charged lepton, p_T^ℓ, the transverse momentum of the neutrino, p_T^ν, and the transverse mass of the W boson, $m_T^W = \sqrt{2p_T^\ell p_T^\nu(1-\cos\varphi)}$, where φ is the opening angle between the charged lepton and neutrino momenta in the plane transverse to the

beam. The magnitude and direction of p_T^ν are inferred from the missing transverse momentum vector, E_T^{miss}, which corresponds to the momentum imbalance in the transverse plane and defined as $\overrightarrow{E_T}^{miss} = -(\overrightarrow{pT}^{\ell} + \overrightarrow{u})$. Here u is referred to as the hadronic recoil and corresponds to the measured transverse momentum of the W boson.

The transverse momentum of the charged lepton and the transverse momentum of the neutrino show a Jacobian peak at a value corresponding to $m_W/2$, whereas the transverse mass distribution peaks at the value of m_W. Typically, m_W is determined by comparing the expected final state distributions (templates), predicted with simulated samples for different values of m_W to the measured distribution. Hence the sensitivity to m_W, reflects all the physics aspects of the W boson production and decay processes, as well as the response of the detector. Experimentally, the p_T^ℓ and m_T^W distributions are affected by the lepton energy calibration. The m_T^W distribution is also affected by the calibration of the recoil response. The p_T^ℓ and m_T^W distributions are broadened by the transverse momentum distribution of the W boson, p_T^W, and are sensitive to the W boson helicity states, which are determined by the proton density functions (PDFs) [24]. Compared to p_T^ℓ and m_T, the E_T^{miss} distribution has smaller sensitivity to such physics modeling effects, but larger uncertainties due to the recoil calibration.

With typical selection requirements $30 < p_T^\ell < 55$ GeV, $30 < E_T^{miss} < 55$ GeV, $60 < m_T^W < 100$ GeV, $u < 15$ GeV [25], order of several 10^7 $W \to \ell\nu$ candidates are collected per experiment during the LHC Run-1. The available statistics leads to the statistical precision of m_W of O(2 MeV) per experiment, which sets the target scale for the systematic uncertainties. Beside W events, order of 10 milion of $Z \to \ell\ell$ events is collected, which can be used to constrained experimental as well as uncertainties arising from the production and decay of the W boson.

3. Constraining experimental uncertainties

The first major goal in constraining experimental uncertainties is the calibration of the electron energy and muon momentum. The analysed final states of W and Z bosons are dominated by the leptons, the rest of the event consisting of mostly soft hadronic activity. This hadronic activity is considered as a global quantity recoiling against the decaying boson.

After the completion of the Run 1, the LHC experiments have finalised their calibrations and published an extensive set of results on electron, muon and recoil performance [26, 27, 28]. Due to to the large statistics of the collected calibration samples, notably events from low-mass resonances (J/ψ, Υ), as well as leptonic W and Z events, the quality of the modeling of the data by the simulation has been vastly improved compared to the initial performance. However further improvements are desirable for the m_W measurements. For example, the improved muon calibration is derived using the J/ψ and $\Upsilon(1S)$ dimuon decays at CMS for the exercise of an m_Z measurement in the $W-like$ $Z \to \mu\mu$ events [25] , which will be described later. Since the momentum range of the J/ψ and Υ samples is very different from the W and Z ones, the challenge is to find a physically motivated model that describes the detector well in the whole range where the muon momentum measurement precision is dominated by the inner tracker measurement. Three effects are accounted for in the muon momentum calibration to correct the curvature of the muon ($k = 1/p_T$): (i) small variations of the magnetic field, (ii) residual misalignment effects, (iii) imperfect modeling of the material resulting in different energy loss. The magnetic field is a multiplicative factor to the cur-

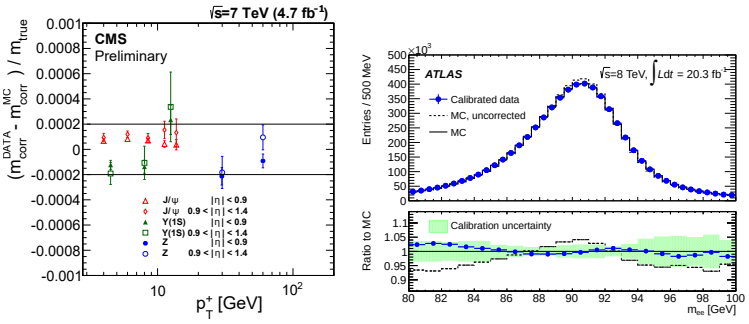

Figure 1: Left: Closure of the calibration of the relative scale (data with respect to MC) for J/ψ, $\Upsilon(1S)$, and Z dimuons, as a function of p_T of the positive muon, after applying the calibration corrections measured with the J/ψ and $\Upsilon(1S)$samples, [25]. Right: Electron pair invariant mass distribution for $Z \to ee$ decays in data and improved simulation. Energy scale corrections are applied to the data. The improved simulation is shown before and after energy resolution corrections, [28].

vature (A) while the misalignment is an additive factor (M) with opposite sign for opposite muon charge. The energy loss correction is an additive term (ε) to the muon momentum (p) resulting in a term that includes angular dependence. The corrected curvature, k^c, is given with:

$$k^c = (A-1)k + qM + \frac{k}{1+k\varepsilon sin\theta}, \tag{3.1}$$

where θ and q are the polar angle and the charge of the muon. The calibration is implemented using a Kalman filter, and its event-by-event uncertainty is estimated by propagating the uncertainties of the two tracks using their full covariance matrices. Corrections are derived for both data and simulation, with values that are found to be typically small: A differs from unity by less than 0.0005, M is less than 10^{-4} GeV^{-1}, and ε is of the order of 4 MeV. The muon momentum resolution is also corrected for. To estimate the closure of the calibration technique, an independent fit is implemented using the J/ψ, $\Upsilon(1S)$, and Z resonances, to measure the difference between the dimuon mass scales obtained in data and in simulation (Fig. 1). Agreement at the 0.2 per-mil level is achieved for the J/ψ and $\Upsilon(1S)$ and Z events, which is the systematic uncertainty of the method.

In the electron channel, J/ψ events are not collected as efficiently, so the Z sample constitutes the main handle on the EM calorimeter energy scale. In the case of electrons, a major difficulty is to understand the calorimeter intercalibration, and the passive detector material upstream of it, before the $Z \to e^+e^-$ peak position can reliably be interpreted in terms of the calorimeter energy scale and used as a reference applying to the W production. The electron calibration closure in $Z \to ee$ events is demonstrated in Fig. 1.

The E_T^{miss} is estimated from the lepton momentum and the measured hadronic recoil. In principle, the hadronic recoil directly reflects the hadronic activity balancing the boson p_T. In practice, however, this quantity is also influenced by other effects, such as the underlying event, multiple parton interactions, and pileup collisions. To reach an accurate control of the E_T^{miss} a precise and

reliably-calibrated measurement of the hadronic recoil is needed, with a required precision of half a percent to match δm_W of 10–20 MeV.

For the reconstruction of the hadronic recoil, ATLAS uses a dedicated recoil algorithm exploited in p_T^W measurement [29]. The calculation is based on the sum over calorimeter cells excluding the cells associated to the lepton. Energy of low-p_T particles is removed along the lepton direction is compensated from the measured underlying event. CMS exploits its Particle flow algorithm [30] ('pfMET') with reconstruction and identification of each particle with an optimised combination of all subdetector information. Similar resolution of $u_\parallel$ is obtained between ATLAS and CMS for the given algorithm. In order to improve the performance of the reconstruction of the hadronic recoil for the m_W measurement CMS uses track-based definition ('tkMET'), where recoil is calculated as a vectorial sum of the p_T of a charged hadron with δz <0.1 cm from the primary vertex. While this definition has the drawback of only retaining 40% of the hadronic recoil probed with the more widely used pfMET, it has the advantages of exhibiting a better data-MC agreement and of being essentially insensitive to pileup. More importantly, it provides, in the presence of pileup, the best discriminating power for the transverse mass Jacobian peak (Fig. 2).

In both experiments, recoil calibration is performed exploiting $Z \to \ell\ell$ events, after lepton calibration is applied. In addition, since the decay is fully measured, momentum balance in the transverse plane can be exploited to determine the response and resolution of the hadronic recoil. To effectively study the properties of the hadronic recoil and partially disentangle the hadronic activity recoiling against the boson p_T from the other effects, the recoil vector is projected along the directions parallel ($u_\parallel$) and perpendicular ($u_\perp$) to the boson p_T direction. Here $u_\parallel$ should be proportional to the boson p_T, the proportionality coefficient depending on the E_T^{miss} definition; $u_\perp$ is expected to be distributed around zero. In CMS $u_\parallel$ and $u_\perp$ are modeled empirically by a sum of three Gaussians, whose parameters are polynomial functions of $p_T^{\mu\mu}$. The calibration is performed in rapidity bins, to minimise uncertainty arising from the vector boson modeling. The models obtained from fitting the different (data and simulated) event samples are used to derive corrections that can be used to transform the original recoil values of a source event sample into corrected values matching the distribution of a target event sample (Fig. 2).

4. Modeling of the W boson production and decay

Measurements of m_W at the LHC are affected by significant complexity related to the strong interaction. In particular, at the LHC centre-of-mass energies and in proton-proton collisions, approximately 25% of the inclusive W production rate is induced by at least one second generation quark (s, c) in the initial state. The amount of heavy-quark-initiated production has implications on the p_T^W distribution, and, as a consequence, the measurement of the m_W is sensitive to the strange and charm quark PDFs. In contrast, second generation quarks contribute only to approximately 5% of the overall W boson production rate at the Tevatron. The most relevant proton PDF constraints are obtained from measurements of the inclusive W^+ , W^- and Z inclusive cross section and rapidity distributions. These observables and their ratios allow, together with slightly more complex final states such $W + c$, a full flavour decomposition of the proton PDFs and a mapping of their Bjorken x dependence. When colliding, the initial state partons radiate a large number of mostly soft gluons, as a result of their mutual interactions. This initial state "parton shower" contributes to

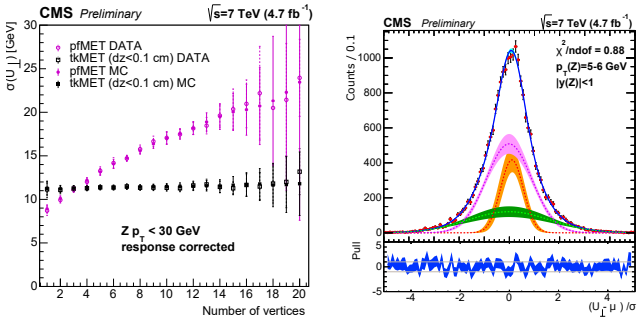

Figure 2: Left: Recoil resolution from Z events as a function of the number of vertices for pfMET (circles) and tkMET (squares), after response correction, from simulated and data samples. Right: Example of the fit to calibration data events using the sum of three Gaussians to the $u_{\parallel}$ distribution, [25].

the transverse momentum distribution of the W and Z. The details of these processes are not fully predictable and are modelled in a semi-phenomenological way tuned via $Z \to \ell\ell$ events. The LHC experiments perform an extensive measurement program that aims at constraining the QCD parameters describing these effects. Strong experimental constraints on the PDFs come from the W cross sections, measured differentially in lepton η. In particular the η-dependent W charge asymmetry is specifically sensitive to the u and d quark valence ratio. These measurements have been pursued by ATLAS and CMS [31]. Z cross section measurements are also performed [32, 33]. In conjunction with the W cross section, this provides information on the strange density [34]. The strange density can also be probed directly, via measurements of $W + c$ production [35]. The non-perturbative parameters are most accurately probed through measurements of the Z boson transverse momentum measurements [36], or of the angular correlations of its decay products [37, 38]. Some results are demonstrated in Fig. 3. The measurements of the correlation of the angular distributions with the lepton transverse momentum distributions, are an important ingredient in m_W measurement. Alternatively constraining p_T^W can be achieved by means of the direct measurement of this observable. However, longer dedicated runs with low pileup would be needed.

Another important aspect for the measurement of m_W is the theoretical description of electroweak corrections, and in particular the modeling of photon radiation from the W and Z boson decay leptons.

5. Z boson mass measurement in $W-like$ events

This analysis performed by CMS [25] consist of a measurement of the Z boson mass using a sample of so-called $W-like$ events, i.e. $Z \to \mu\mu$ events where one of the two muons is removed to mimic the $W \to \mu\nu$ event topology. The analysis is based on the 7 TeV pp data sample collected in 2011, using a single-muon trigger. The sample already provides statistical uncertainties similar to those of the Tevatron m_W results. This exercise represents a proof of principle, showing that the

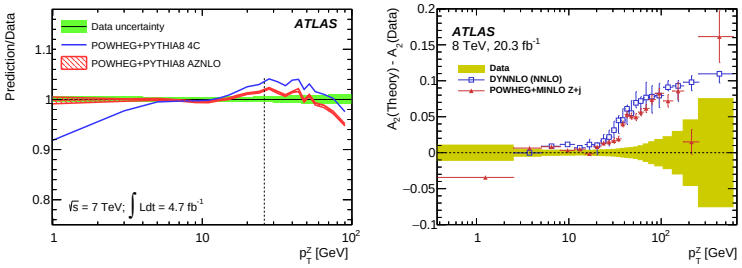

Figure 3: Left: Comparison of tuned predictions to the p_T^Z differential cross sections, for dressed kinematics and in the full rapidity range. Comparison of the POWHEG+PYTHIA8 set-up with the 4C and AZNLO tunes to the same data. The vertical dashed lines show the upper limit of the tuning range [36]. Right: Distributions of the angular coefficients $A2$ as a function of p_T^Z [38].

analysis procedure is reliable and thereby validating the tools and techniques that will be applied in the W boson mass measurement. The Z boson leptonic decays can be triggered and selected at the LHC with high purity. They are used for calibration purposes and their differential cross sections provide precise information about PDFs and the production processes. The transverse momentum distribution of the Z boson can be accurately measured and used to tune non-perturbative parameters in the Monte Carlo generators.

The signal samples are generated with POWHEG [39, 40, 41, 42] linked to PYTHIA8 [43] with tune 4C, interfaced with NLO PDF set NNPDF 2.3 [44]. As this setup does not describe well the boson transverse momentum, p_T^Z is reweighted to data, in bins of 0.5 GeV, to the measured distribution in Z data events. In addition, the default settings of the POWHEG program show discrepancies when compared to the measured angular coefficients of Drell-Yan events, so the $\cos\theta^*$ defined in the Collins-Soper frame is reweighted to data, as a function of the Z rapidity. Since the boson p_T and angular coefficient reweightings are performed in the final fit phase space at reconstruction level, no systematic uncertainty is assigned.

The selected events are required to pass the single trigger requirement and the two muons must have opposite sign with the invariant mass above 50 GeV. The selection of Z events requires both muons to be of high quality, isolated, and have a distance of closest approach between the muon and the beam line $d_{xy} < 0.2$ cm. An event enters in the positive (negative) $W-like$ sample if the $\mu^+(\mu^-)$ is matched to the trigger and fulfills the acceptance conditions $|\eta| < 0.9$, $p_T^\mu > 30$ GeV, while the $\mu^-(\mu^+)$ is only required to have $p_T^\mu > 10$ GeV and $|\eta| < 2.1$. In view of measuring the mass, the analysis only uses the transverse recoil of the boson and the Z transverse component of the muon momentum. A narrow kinematic region, defined to mimic the phase space expected to be selected in the W mass analysis, selects the final sample of $W-like$ events: $30 < p_T^\mu < 55$ GeV, $30 < E_T^{miss} < 55$ GeV, $60 < m_T < 100$ GeV, $u < 15$ GeV, $p_T^{\mu\mu} < 30$ GeV. The background contamination is at the per-mil level, evaluated from MC simulation.

The fits of the sensitive observables are performed in the ranges 32–45 GeV (lepton p_T and E_T^{miss}) and 65–100 GeV (m_T), scaled by the ratio of m_Z^{PDG}/m_W^{PDG} =1.134 to retain a phase space

similar to that intended for the W mass fits. All the fits involving mass measurements are performed with a binned-template likelihood-ratio fitting procedure. Three distributions are independently fitted fixing the normalization of the sum to the number of data events. The statistical correlation has been estimated confirming that m_T^W is highly correlated with both p_T^ℓ and E_T^{miss}, while lepton p_T and E_T^{miss} are practically uncorrelated.

The systematic uncertainty associated with the modeling of the muon efficiencies is evaluated assuming uncorrelated bin-by-bin statistical uncertainties and 1% systematic uncertainties of the "Tag and Probe" methodology. Two sources of systematic uncertainties are considered for the calibration of the lepton momentum scale and resolution: the deviation from perfect closure, and the statistical uncertainty of the calibration sample. Two sources of systematic uncertainties for the mass fits dominated the recoil corrections as well: propagation of the statistical uncertainty of the recoil fits due to the limited statistical accuracy of the calibration sample, and the deviation from the perfect closure of the calibration fits estimated with an alternative model based on an adaptive kernel probability density function. The associated PDF uncertainties are evaluated with the NNPDF 2.3 at NLO set, through a MC-like approach: all 100 NNPDF are tested members and compute the standard deviation. The systematic uncertainty associated with the QED modeling is evaluated by comparing the templates obtained by reweighting the invariant mass distributions with different configurations at generator level, in the full phase space, after final state radiation. The central choice is POWHEG NLO EW+QCD interfaced to PYTHIA 8 for both QCD and QED showers, while the alternative configuration is obtained by switching off the NLO EW contribution. The expected uncertainties are collected in Table 1, symmetrising the largest value between the $\pm 1\sigma$ variations. The results of the fits to the data are shown in Fig. 4, with experimental uncertainties quoted separately from the others.

	m_Z^{W-like}, μ^+			m_Z^{W-like}, μ^-		
Uncertainty	p_T	E_T^{miss}	m_T	p_T	E_T^{miss}	m_T
Muon efficiency	1	1	1	1	1	1
Muon calibration	14	13	14	12	15	14
Recoil calibration	0	9	13	0	9	14
Total exp.	14	17	19	12	18	19
Alternative data rwgt.	5	4	5	14	11	11
PDF	6	5	5	6	5	5
QED	22	23	24	23	23	24
MC Statistics MC	7	6	8	7	6	8
Total other.	24	25	27	24	25	27
Total syst.	28	30	32	30	32	34
Data stat.	40	36	46	39	35	45
Overal	49	47	56	50	48	57

Table 1: Uncertainties on m_Z in $W-like$ events separated by the muon charge [25]. Results are in MeV.

The systematic uncertainties on the lepton momentum and recoil calibrations reflect the present status of the calibrations and may improve in the future by refining the calibration models. The un-

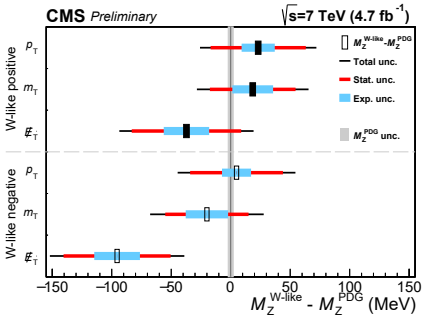

Figure 4: Difference between the fitted mass and Z mass from the PDG, obtained with each of the three observables, together with the corresponding uncertainties [25]. Each of the six measurements can only be considered individually.

certainty related to PDF reflects the knowledge of the parton densities relevant for Z production, that benefits from precise measurements of the p_T^Z and y^Z. This uncertainty will be different and expected to be larger in W events, with the W polarization and charm-initiated processes as the most relevant [24]. On the other hand, when performing the measurement of the W boson mass, the modeling of such aspects will require an extrapolation from the measurements with the Z boson to the expectations for the W boson. The major difficulty arises from correlations among PDF, boson p_T and polarization, and the underlying event, which imply correlated systematic uncertainties in the evaluation of the PDF uncertainties, the systematics of the matrix element, the resummed parts of the calculations, and the parton shower model. In this analysis the largest systematic uncertainty arises from the QED modeling, which is evaluated very conservatively switching on and off the NLO EW contributions in POWHEG. For the m_W analysis this uncertainty needs to be refined which is expected to decrease significantly. Background uncertainty, however, will increase due to larger background level (especially of the hard-to-model multijet background) in the W events.

Special care will be needed for all the systematic constrains performed on Z events when ported to the W, not only to the modeling uncertainties, but also to the experimental ones. For example, recoil response may show some differences in Z and W events, hence systematics due to the calibration performed solely on the Z needs to be addressed.

6. Summary

In short, the detector calibration is at the level required for a first competitive measurement of the m_W at the LHC. The physics modeling of the W boson production and decay represents a major challenge. Ancillary measurements help to constrain physics model and analysis strategy to minimise model dependence and tune state of the art MC. A deep understanding of Drell-Yan production at the LHC is crucial.

Author is supported by Serbian Ministry of Education, Science and Technological development project 171004.

References

[1] S. L. Glashow, Nucl. Phys. **22**, 579 (1961).

[2] A. Salam, Conf. Proc. C **680519**, 367 (1968).

[3] S. Weinberg, Phys. Rev. Lett. **19**, 1264 (1967).

[4] D. Y. Bardin, P. Christova, M. Jack, L. Kalinovskaya, A. Olchevski, S. Riemann and T. Riemann, Comput. Phys. Commun. **133**, 229 (2001) [hep-ph/9908433].

[5] M. Awramik, M. Czakon, A. Freitas and G. Weiglein, Phys. Rev. D **69**, 053006 (2004) [hep-ph/0311148].

[6] A. Sirlin, Phys. Rev. D **22**, 971 (1980).

[7] M. Baak *et al.* [Gfitter Group Collaboration], Eur. Phys. J. C **74**, 3046 (2014) [arXiv:1407.3792 [hep-ph]].

[8] G. Arnison *et al.* [UA1 Collaboration], Europhys. Lett. **1**, 327 (1986).

[9] J. Alitti *et al.* [UA2 Collaboration], Phys. Lett. B **276**, 354 (1992).

[10] S. Schael *et al.* [ALEPH and DELPHI and L3 and OPAL and LEP Electroweak Collaborations], Phys. Rept. **532**, 119 (2013) [arXiv:1302.3415 [hep-ex]].

[11] T. Affolder *et al.* [CDF Collaboration], Phys. Rev. D **64**, 052001 (2001) [hep-ex/0007044].

[12] V. M. Abazov *et al.* [D0 Collaboration], Phys. Rev. D **66**, 012001 (2002) [hep-ex/0204014].

[13] V. M. Abazov *et al.* [CDF and D0 Collaborations], Phys. Rev. D **70**, 092008 (2004) [hep-ex/0311039].

[14] K. A. Olive *et al.* [Particle Data Group Collaboration], Chin. Phys. C **38**, 090001 (2014).

[15] T. Aaltonen *et al.* [CDF Collaboration], Phys. Rev. Lett. **108**, 151803 (2012) [arXiv:1203.0275 [hep-ex]].

[16] V. M. Abazov *et al.* [D0 Collaboration], Phys. Rev. Lett. **108**, 151804 (2012) [arXiv:1203.0293 [hep-ex]].

[17] T. A. Aaltonen *et al.* [CDF and D0 Collaborations], Phys. Rev. D **88**, no. 5, 052018 (2013) [arXiv:1307.7627 [hep-ex]].

[18] ATLAS and CDF and CMS and D0 Collaborations, arXiv:1403.4427 [hep-ex].

[19] ATLAS and CMS Collaborations, Phys. Rev. Lett. **114**, 191803 (2015) [arXiv:1503.07589 [hep-ex]].

[20] CMS Collaboration, CMS-PAS-TOP-14-015.

[21] ATLAS Collaboration, JINST **3**, S08003 (2008).

[22] CMS Collaboration, JINST **3**, S08004 (2008).

[23] M. Baak *et al.*, arXiv:1310.6708 [hep-ph].

[24] ATLAS Collaboration, ATL-PHYS-PUB-2014-015.

[25] CMS Collaboration, CMS-PAS-SMP-14-007.

[26] ATLAS Collaboration, Eur. Phys. J. C **74**, no. 11, 3130 (2014) [arXiv:1407.3935 [hep-ex]].

[27] CMS Collaboration, JINST **10**, no. 02, P02006 (2015) [arXiv:1411.0511 [physics.ins-det]].

[28] ATLAS Collaboration, Eur. Phys. J. C **74**, no. 10, 3071 (2014) [arXiv:1407.5063 [hep-ex]].

[29] ATLAS Collaboration, Phys. Rev. D **85**, 012005 (2012) [arXiv:1108.6308 [hep-ex]].

[30] CMS Collaboration, CMS-PAS-PFT-09-001.

[31] CMS Collaboration, Eur. Phys. J. C **76**, no. 8, 469 (2016) [arXiv:1603.01803 [hep-ex]].

[32] CMS Collaboration, Phys. Lett. B **749**, 187 (2015) [arXiv:1504.03511 [hep-ex]].

[33] ATLAS Collaboration, Phys. Rev. D **85**, 072004 (2012) [arXiv:1109.5141 [hep-ex]].

[34] ATLAS Collaboration, Phys. Rev. Lett. **109**, 012001 (2012) [arXiv:1203.4051 [hep-ex]].

[35] CMS Collaboration, JHEP **1402**, 013 (2014) [arXiv:1310.1138 [hep-ex]].

[36] ATLAS Collaboration, JHEP **1409**, 145 (2014) [arXiv:1406.3660 [hep-ex]].

[37] CMS Collaboration, Phys. Lett. B **750**, 154 (2015) [arXiv:1504.03512 [hep-ex]].

[38] ATLAS Collaboration, arXiv:1606.00689 [hep-ex].

[39] P. Nason, JHEP **0411**, 040 (2004) [hep-ph/0409146].

[40] S. Frixione, P. Nason and C. Oleari, JHEP **0711**, 070 (2007) [arXiv:0709.2092 [hep-ph]].

[41] S. Alioli, P. Nason, C. Oleari and E. Re, JHEP **1006**, 043 (2010) [arXiv:1002.2581 [hep-ph]].

[42] L. Barze, G. Montagna, P. Nason, O. Nicrosini, F. Piccinini and A. Vicini, Eur. Phys. J. C **73**, no. 6, 2474 (2013) [arXiv:1302.4606 [hep-ph]].

[43] T. Sjostrand, S. Mrenna and P. Z. Skands, Comput. Phys. Commun. **178**, 852 (2008) [arXiv:0710.3820 [hep-ph]].

[44] R. D. Ball *et al.*, Nucl. Phys. B **867**, 244 (2013) [arXiv:1207.1303 [hep-ph]].

ELECTROWEAK TESTS AT THE LHC

N. VRANJEŠ, On behalf of ATLAS and CMS Collaborations
DSM/IRFU (Institut de Recherches sur les Lois Fondamentales de l' Univers), CEA Saclay (Commissariat à l' Energie Atomique et aux Energies Alternatives), Gif-sur-Yvette, France

Some recent electroweak physics results obtained with the ATLAS and CMS experiments are reviewed. The Z boson transverse momentum, W+charm and W boson charge asymmetry are presented in the context of the W boson mass measurement The topics covered include also measurements of anomalous triple gauge couplings probed with the diboson production, and the studies of vector boson fusion and vector boson scattering using measurements of the electroweak components of Zjj and $W^{\pm}W^{\pm}jj$ production.

ATL-PHYS-PROC-2014-139
17 September 2014

1 Introduction

Measurements in the electroweak sector of the Standard Model (SM) constitute a vital part of the physics program that is carried out at the Large Hadron Collider (LHC) by ATLAS [1] and CMS [2] experiments CERN. High statistics of the collected data and unprecedented energy regime put SM to a new test. While waiting for the first measurement of the W boson mass at the LHC, already many important results are obtained and in some cases of gauge boson couplings most stringent constrains are set.

2 Measurement of W boson mass

While expecting the first measurement of the W boson mass from the LHC experiments, one can briefly review the current situation for Blois 2014 conference. The Tevatron experiments measured the W boson mass [3] with the combined precision of 16 MeV, dominating the world average $M_W = 80385 \pm 15$ MeV. Measurements from the Tevatron may eventually reach combined uncertainty of 10 MeV, the uncertainty that is now obtained from the global electroweak fit using the Higgs boson mass as an input [4]. This sets the target precision that would be desirable to achieve by the LHC in the near future. Giving the $W \to \ell\nu$ production cross section of about 10.5 nb and 12 nb at the LHC collision energies of 7 TeV and 8 TeV respectively, the statistical uncertainty of a few MeV per experiment for the dataset that has been collected up to now is expected. High collision energy at the LHC leads not only to the small statistical uncertainty of the W mass, but also to the increase of the size of the calibration samples such as $J/\psi \to \ell\ell$ and $Z/\gamma^* \to \ell\ell$ with respect to the Tevatron, hence the experimental uncertainties on the lepton momentum scale and resolution, as well as the hadronic recoil resolution uncertainty, could be at the level (or better) reached at the Tevatron. Here, the uncertainties arising from the limited knowledge of parton distribution functions (PDFs) and the modelling of the lepton transverse momentum are highlighted. In this context, we briefly discuss the measurement of the Z boson transverse momentum by ATLAS [5], performed also by CMS collaboration [6], and W charge asymmetry, as well as W+charm measurement by the CMS [7] and ATLAS [8]. Most of

these measurements are performed with proton-proton collision data collected at $\sqrt{s} = 7$ TeV, and integrated luminosity of 4.7 fb^{-1}.

Measurements of the $Z \to \ell\ell$ transverse momentum (p_T^Z) and ϕ^* spectra [9] offer the insight into the dynamical effects of the strong interaction, namely, perturbative predictions and PDF (in the high-p_T/low-ϕ^* range), and resummation and the parton shower models (low-p_T/high-ϕ^* range). Based on most precise independent single measurements, the p_T^Z in the muon channel and ϕ^* in the electron channel, the parton shower tunes are performed in order to determine the sensitivity of the measured p_T^Z cross sections to the parton shower model parameters in state-of-the-art MC generators, and to constrain the models by trying to achieve precise predictions of vector boson production. The final tunes referred to as AZNLO applied to `Powheg+Pythia8` leads to the agreement with the data to better than 2% in the range used for the tuning, and for $p_T^Z < 50$ GeV, as demonstrated in Fig. 1.

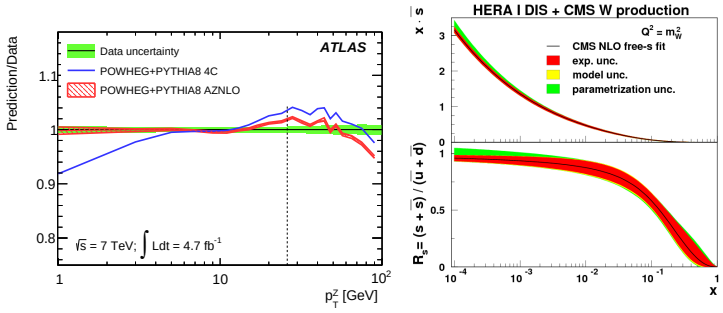

Figure 1 – *Left*: Comparison of tuned predictions for `Powheg+Pythia8` obtained from the p_T^Z and ϕ^* differential cross section measurements [5,9].The vertical dashed lines show the upper limit of the tuning range. The previous default tune (4C) used in ATLAS is also presented in the figure. *Right*: Antistrange-quark distribution and the ratio, obtained in the QCD analysis of the HERA and CMS data, shown as functions of x at the scale $Q^2 = m_W^2$. The bands represents the total and separate uncertainties arising from different sources [7].

Measurements of the vector bosons in association with heavy flavor, such as W+c production, have a unique sensitivity to the flavour decomposition of the proton, especially the strange density. In the analysis performed by ATLAS [8], W+c production is studied in events in which a W decays to an electron or muon, and the charm quark is tagged either by its semileptonic decay to a muon or by the presence of a charmed meson. The total and differential cross sections as a function of the pseudorapidity of the lepton from the W boson decay are measured and compared to the predictions of NLO QCD calculations obtained from various PDF parameterisations. Within uncertainties, the data are consistent with a wide range of PDFs, but show a preference for PDFs with an $SU(3)$-symmetric light-quark sea. The ratio of the strange-to-down sea quark distributions is determined to be $0.96+0.26$ at $Q^2 = 1.9$ GeV^2. Measurements of the muon charge asymmetry in inclusive $W \to \mu\nu$ production performed by CMS [7] provides additional constraints on the PDFs of the proton in the range of the x from 10^{-3} to 10^{-1}. These measurements and the recent CMS measurement of associated $W + c$ production are used together with the cross sections for inclusive DIS data from HERA in an NLO QCD analysis. The determination of the valence quark distributions is improved, and the strange-quark distribution is probed directly through the leading-order process $g + s \to W + c$. Since the per-bin total experimental uncertainties are significantly smaller than the uncertainty in the current PDF parametrizations, this measurement can be used to constrain PDFs in the next generation of PDF sets. The strange quark distribution and the ratio strange-to-valence are illustrated in Fig. 1.

3 Anomalous gauge boson couplings

Self interactions of gauge bosons manifest themselves as couplings of three of four gauge bosons: WWZ, $WW\gamma$, $WWZ\gamma$, $WW\gamma\gamma$, $WWZZ$, and $WWWW$. Structure of these couplings is completely determined by $SU(2)_L \times U(1)_Y$ symmetry and their precision measurement can either confirm SM or indicate presence of Beyond Standard Model (BSM) physics at the higher mass scale through the discovery of anomalous triple (aTGC) and quartic (aQGC) gauge boson couplings. The existence of anomalous couplings can be tested at the LHC through the studies of multiboson (W, Z, γ) production or through studies of vector boson fusion (VBF) and vector boson scattering (VBS) processes.

Charged TGCs refer to couplings with vertices containing charged gauge bosons. BSM physics can be modelled by effective Lagrangian with aTGC parameters ($\lambda_{\gamma,Z}, \Delta\kappa_{\gamma,Z}, g_1^Z$), whose values are zero in the SM. Processes that are used to probe charged aTGCs are WZ, $W\gamma$ and WW production through the leptonic decays of the W and Z bosons. Both, ATLAS and CMS published results [10,11,12,13,14,15] using the full dataset collected at 7 TeV corresponding to about 5 fb^{-1}, while 8 TeV data are yet to be fully analysed. Neutral TGC (forbidden in the SM at the tree level) can be probed by studying ZZ and $Z\gamma$ production in the final states with leptonic decays of Z boson (including neutrino decays). Both collaborations published results with 7 TeV datasets [15,16,17,18], and CMS also completed 8 TeV $ZZ \to \ell\ell\ell\ell, \ell\ell\nu\nu$ analyses [19,20]. The measurements of the mentioned processes are used to set limits on aTGC parameters $f_{\gamma,Z}^{4,5}$ and $h_{\gamma,Z}^{3,4}$ for the neutral ZZZ and γZZ vertices. All measured values of the aTGC parameters are consistent with the values predicted by the SM, with the precision that supersedes the one reached at the Tevatron as shown [21] in Fig 2. While for the most stringent limits on charged aTGC come from LEP, the neutral aTGC LHC measurements improve the combined LEP results by a large factor (typically 5-10). Further increase in precision can be achieved by completing analysis of 8 TeV datasets and channel combination as it has been done by CMS for the results obtained with $Z\gamma \to \nu\nu\gamma$ and $Z\gamma \to \ell\ell\gamma$ channels [16].

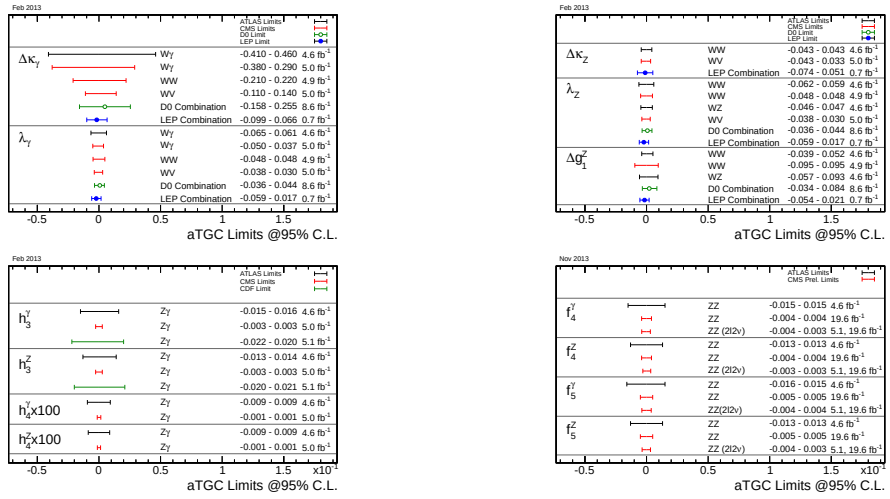

Figure 2 – Limits (95% CL) on charged aTGC $WW\gamma$ (*top left*) and WWZ (*top right*) couplings, neutral aTGC $Z\gamma\gamma$ and $ZZ\gamma$ couplings (*bottom left*) and $ZZ\gamma$ and ZZZ couplings (*bottom right*). The presence of a possible charged aTGC contribution is parameterized in the so called LEP parametrization. Limits on neutral aTGC are placed on the anomalous parameters h_3, h_4, f_4 and f_5.

The electroweak production of two jets in association with a Z/γ^* boson (Zjj) has been recently observed by ATLAS and CMS [22,23], while the observation of $W^{\pm}W^{\pm}jj$ is reported by ATLAS [24]. The results are obtained using 20.3 fb^{-1} of data collected at $\sqrt{s}$ = 8 TeV. The first observation of electroweak Zjj production contributes to the investigation of electroweak symmetry breaking, being the first observation of a VBF process, and the measurement is used to constrain aTGCs. For Zjj, the strong production dominates, making extremely challenging the measurement and study of the purely electroweak component, which can be enhanced in appropriate phase spaces. A detector-corrected fiducial cross section for electroweak production measured by ATLAS is $\sigma_{ewk}^{fid} = 54.7 \pm 4.6(stat.)^{+9.8}_{-10.4}(syst.) \pm 1.5(lumi)$ fb, in agreement with SM. Similar result is obtained by CMS. The first evidence for electroweak $W^{\pm}W^{\pm}jj$ processes represents a milestone in the investigation of the electroweak symmetry breaking since the scattering of two longitudinally polarized W bosons violates unitarity without delicate cancellations from the Higgs boson. The strong production does not dominate, making this channel an ideal choice for the study of electroweak production in the VBS. Evidences of inclusive and electroweak production are observed with 4.6 and 3.6σ, respectively. The measured electroweak cross section is found to be in agreement with the SM setting the limits on aQGCs in terms of parameters α_4, α_5: $-0.14 < \alpha_4 < 0.16$ and $-0.23 < \alpha_5 < 0.24$ (for $\alpha_{5,4} = 0$ respectively).

4 Summary

Prospects for the first measurement of the W boson mass at the LHC and some relevant measurements are briefly discussed. Anomalous coupling parameters of three and four gauge bosons are measured in different processes and all are in the agreement with SM.

References

1. ATLAS Collaboration, JINST **3** (2008) S08003.
2. CMS Collaboration, JINST **3** (2008) S08004.
3. CDF and D0 Collaborations, T. A. Aaltonen *et al.*, Phys. Rev. D **88**, 052018 (2013) [arXiv:1307.7627 [hep-ex]].
4. M.Baak *et al*, arXiv:1407.3792 [hep-ph].
5. ATLAS Collaboration, arXiv:1406.3660 [hep-ex].
6. CMS Collaboration, Phys. Rev. D **85**, 032002 (2012), [arXiv:1110.4973 [hep-ex]].
7. CMS Collaboration, Phys. Rev. D **90**, 032004 (2014), arXiv:1312.6283 [hep-ex].
8. ATLAS Collaboration, JHEP **1405**, 068 (2014) [arXiv:1402.6263 [hep-ex]].
9. ATLAS Collaboration, Phys. Lett. B **720**, 32 (2013), arXiv:1211.6899 [hep-ex].
10. ATLAS Collaboration, Phys. Rev. D **87**, no. 11, 112001 (2013).
11. CMS Collaboration, Eur. Phys. J. C **73**, 2610 (2013) [arXiv:1306.1126 [hep-ex]].
12. ATLAS Collaboration, Eur. Phys. J. C **72**, 2173 (2012) [arXiv:1208.1390 [hep-ex]].
13. CMS Collaboration, CMS-PAS-SMP-12-006, `https://cds.cern.ch/record/1564318`
14. ATLAS Collaboration, Phys. Rev. D **87**, no. 11, 112003 (2013) [arXiv:1302.1283 [hep-ex]].
15. CMS Collaboration, Phys. Rev. D **89**, 092005 (2014) [arXiv:1308.6832 [hep-ex]].
16. CMS Collaboration, JHEP **1310**, 164 (2013) [arXiv:1309.1117 [hep-ex]].
17. ATLAS Collaboration, ATLAS-CONF-2013-020, `https://cds.cern.ch/record/1525555`
18. ATLAS Collaboration, JHEP **1303**, 128 (2013) [arXiv:1211.6096 [hep-ex]].
19. CMS Collaboration, CMS-PAS-SMP-13-005, `https://cds.cern.ch/record/1706050`
20. CMS Collaboration, CMS-PAS-SMP-12-016, `http://cds.cern.ch/record/1633371`
21. CMS Collaboration, `twiki.cern.ch/twiki/bin/view/CMSPublic/PhysicsResultsSMPaTGC`
22. ATLAS Collaboration, JHEP **1404**, 031 (2014) [arXiv:1401.7610 [hep-ex]].
23. CMS Collaboration, CMS-PAS-FSQ-12-035, `https://cds.cern.ch/record/1601549`
24. ATLAS Collaboration, arXiv:1405.6241 [hep-ex].

Our calculations of electronic properties of HCCNTs are in support of this res
although we adopt a bit different structural model. Within the proposed mod
construction of a particular HCCNT is in one-to-one correspondence with the tri
connected graph of pentagons, hexagons and heptagons, conventionally defined
$(n_6,n_7,n_7,n_5,(\boldsymbol{b}_1,\boldsymbol{b}_2))$, where $(\boldsymbol{b}_1,\boldsymbol{b}_2)$, are the super-cell vectors, while the tiling pattern
given by the first four parameters. Here, we present technique of construction of
metallic HCCNTs introducing particular types of graphs and showing that
metallic characteristics are governed by a specific distribution of pentagons [13].

Also, effect of uniaxial strain on the electronic band structure and opti
absorption spectra is analyzed. It is shown that strain can generate the gap closing
the SC tubes and also substantial changes in the optical conductivity over wide ene
range [14]. In particular, absorption spectra of the semi-metallic and narrow band g
SC coils are extremely sensitive to the uniaxial strain. Thus, rather wide spectrum
to the highest optical frequencies can be absorbed by an ensemble of the HC
having only slightly different coil parameters. These startling properties of HC
imply their potential applications as electromagnetic absorbers and optically
tactile sensors with highly sensitive discriminatory abilities.

ACKNOWLEDGMENT

Funding of Serbian Ministry of Science (ON171035) and Swiss National
Foundation (SCOPES IZ73Z0-128037/1) is acknowledged.

LITERATURE

[1] S. Ihara, S. Itoh and J. Kitakami, Phys. Rev.B **48**, 5634 (1993).
[2] B. I. Dunlap, Phys. Rev. B **46**, 1933 (1992).
[3] X.B. Zhang et al., , Europhys. Lett. **27**, 141 (1994).
[4] S. Amelinckx et al. Science **265**, 635 (1994).
[5] D. Fejes, L. Forro and K. Hernadi, Phys. Status Solidi B **247**, 2713 (2010).
[6] D. Fejes and K. Hernadi, Materials **3**, 2618 (2010).
[7] I. Milosevic; et al, Phys. Status Solidi B, **249**, 2442 (2012).
[8] I. Laszlo and A. Rassat, J. Chem. Inf. Comput. Sci. **43**, 519 (2003).
[9] M.Damnjanovic and I. Milosevic, *Line Goups in Physics*, Springer-Verlag Berlin 2010.
[10] D. Fejes, et al., ECS Solid State Lett. **2** (2013).
[11] Z.P.Popovic et al., XXVII Int. Winterschool on Electronic Properties of Novel M
Molecular Nanostrucutres, Kirchberg in Tirol, Austria, 2013.
[12] K. Akagi et al., Phys. Rev. Lett. **74**, 2307 (1995).
[13] S.Dmitrovic et al., XXVII Int. Winterschool on Electronic Properties of Novel M
Molecular Nanostrucutres, Kirchberg in Tirol, Austria, 2013.
[14] S. Dmitrovic et al., Jour. of Nanoelectron.and Optoelectron. **8**, (2013).

ПОСЛЕДЊИ РЕЗУЛТАТИ ЕКСПЕРИМЕНТА АТЛАС

Н. Врањеш

Институт за физику и CEA-Saclay
e-mail: nenad.vranjes@cern.ch

Експеримент АТЛАС на Великом сударачу хадрона у ЦЕРН-у има веома
истраживачки програм који између осталог обухвата прецизна мерења параметара
Стандардног модела (СМ), физику Хигсовог бозона, као и потрагу за новим честицама
које представљају теорије изван Стандардног модела. У овом раду приказан је део
резултата добијених анализом података из протон-протон судара на енергији
центра масе $\sqrt{s}$=7 TeV и $\sqrt{s}$=8 TeV.

1. УВОД

АТЛАС [1] је један од четири главна детектора на Великом сударачу хадрона
. Детектор има цилиндричну геометрију, његова висина је 22 m,
44 m, а укупна маса уграђеног материјала износи преко 7000 тона.
састоји од неколико поддетектора: унутрашњег детектора за мерење
наелектрисаних честица, електромагнетног и хадронског калориметра и
спектрометра. Унутрашњи детектор се налази у хомогеном магнетном
генерише соленоидни магнет јачине 2T, док суперпроводни тороидни
генеришу магнето поље спектрометра. Детектор и његове главне
су приказане на Сл.1. Комбиновање информација из различитих
омогућава реконструкцију енергије (или имуплса) и положаја
фотона, тау-лептона, хадронских џетова, као и селекцију
џетова из тешких кваркова, и мерење недостајућег трансверзалног
Систем за тригеровање омогућава ефикасну преселекцију догађаја и
смањивање до 400 релевантних догађаја у секунди. Дистрибуција,
и анализа података заснивају се на компјутерском систему и
мрежи за симулацију и обраду података која се ослања на ресурсе
LHC Computing Grid-a [2].

Сакупљање података из протон-протон судара започело је крајем 2009. године,
енергији судара од 900 GeV, да би затим било настављено на енергији
2010. и 2011. У периоду од априла до децембра 2012. протонски
су снимани на енергији 8 TeV, а током неколико недеља 2011. и 2013.
снимани из судара јона олова на енергији 2.76 TeV/нуклеону. Током
2011. године Велики сударач хадрона је испоручио АТЛАС-у податке
са интегралној луминозности 5.6 fb^{-1} односно 23.3 fb^{-1}, како је
приказано на Сл.2. Средња ефикасност узимања података је износила 93%, а

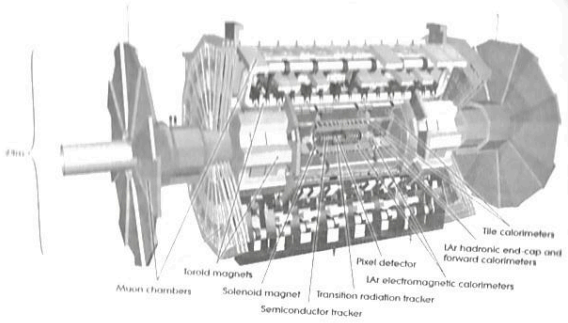

СЛИКА 1. Приказ АТЛАС детектора.

већањем средњег броја интеракција приликом укрштања протонских снопова, 2. Највећа достигнута луминозност у протон-протон сударим измерена на ТЛАС детектору је $7.7 \cdot 10^{33}$ $cm^{-2}s^{-1}$, што одговара око 37 додатних *minimum bias* ерakција (процеси ниског предатог импулса). Сигнал који потиче од онизавања ових додатних интеракција у истом и временски суседним ишталима протонских снопова најчешће се назива *pileup*, и представља ћени изазов за тригеровање и реконструкцију објеката као и за компјутерски тем.

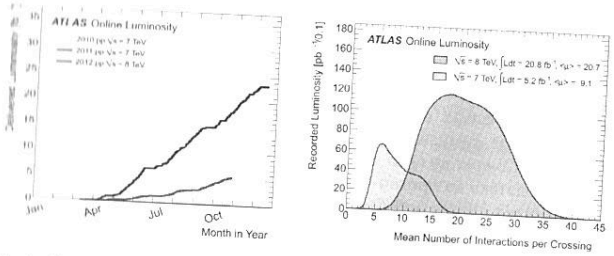

СЛ. 2. Лево: Кумулативна интегрална луминозност у зависности од месеца у току ерске године. Десно: интегрална луминозност у зависности од средњег броја протон-интеракција при укрштању снопова.

3. ТЕСТОВИ СТАНДАРДНОГ МОДЕЛА

Мерења тоталног и диференцијалних пресека за продукцију градијентних [illegible] и фотона γ), као и парова градијентних бозона (WW, $W\gamma$, WZ, ZZ, $Z\gamma$) [illegible] поређење са теоријским предвиђањима представља значајан тест [illegible] модела. Маса топ кварка је један од основних параметара у СМ-у и [illegible] прецизно мерење заједно са прецизним мерењима других параметара у [illegible] сектору, пре свега масе W и Хигсовог бозона, омогућава [illegible] конзистентности модела.

Продукција градијентних бозона

Резултати мерења тоталног пресека за продукцију градијентних бозона [illegible] са теоријским предвиђањима приказани су на Сл.3. Пресеци за [illegible] продукцију W и Z бозона у њиховим лептонским каналима распада [illegible] су коришћењем 35 pb^{-1} података сакупљених током 2010. године [3], [illegible] детаљна мерења добијена коришћењем података из 2011. и 2012. [illegible] Приказане грешке мерења узимају у обзир статистичке и систематске [illegible] неодређености, као и неодређеност у мерењу луминозности. Теоријски пресеци [illegible] израчунати укључујући квантнохромодинамичке корекције вишег реда у [illegible] на Борнов ниво. Добијени резултати демонстрирају сјајан успех [illegible] израчунавања и добар ниво тренутног познавања партонских [illegible] функција протона.

Важан тест електрослабог сектора СМ-а представља и мерење троструких и [illegible] спрезања градијентних бозона. Постојање, тип и јачина ових [illegible] потпуно су одређени неабеловом структуром $SU(2)_L \& U(1)_Y$ групе [illegible], тако да би аномална спрезања индиректно указала на постојање [illegible] феномена на енергетској скали која се не може директно тестирати на [illegible] сударачу. Трострука спрезања се могу директно тестирати мерењем [illegible] и диференцијалних пресека за продукцију парова градијентних бозона. Мерење тоталних пресека за WW, WZ и ZZ процесе у њиховим чисто лептонским [illegible] распада сумаризовани су на Сл.3. Пресеци за продукцију $W\gamma$ и $Z\gamma$ [illegible] до сада на целокупном скупу података на енергији 7 TeV и резултати [illegible] у сагласју са предвиђањима заснованим на СМ-у [4]. Мерења диференцијалних [illegible] у свим дибозонским каналима су искоришћена како би се поставила [illegible] ограничења на аномална трострука спрезања градијентних бозона. Никакво [illegible] одступање од СМ-а није уочено и сва добијена ограничења (95% C.L.) су [illegible] у односу на вредности измерене на Теватрону. Већа статистика [illegible] прецизније мерење аномалних спрезања на АТЛАС-у од [illegible] лимита са колајдера ЛЕП. Резултати лимита на аномална

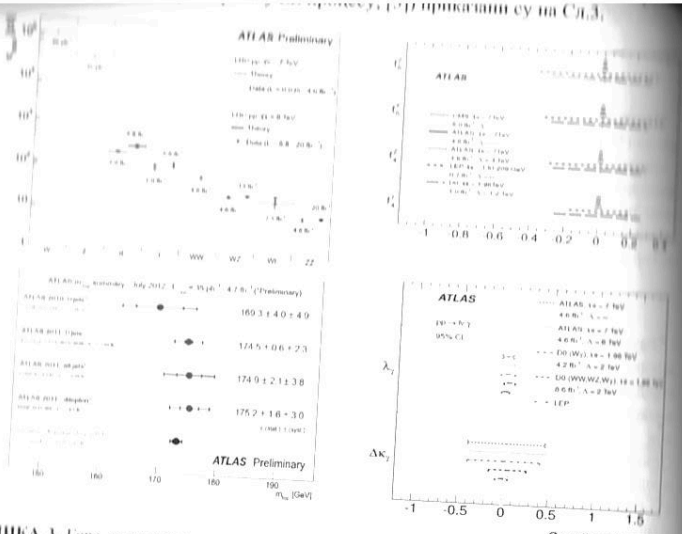

СЛИКА 3. Горе лево: измерени тотални пресеци за неколико процеса означених на графику. Доле лево: Измерена маса топ кварка у неколико канала распада. Црвена хоризонтална линија представља статистичку, а плава статистичку и систематску грешку мерења заједно. Приказано је поређење са комбинованим резултатом са колајдера Теватрон. Десно: 95% C.L. на троструке аномалне спрезања на АТЛАС-у, Теватрону и ЛЕП-у.

Маса топ кварка

Експерименти на Теватрону су начинили импресиван напредак у физици топ кварка у погледу мерења његових особина као што су маса, ширина, наелектрисање, спин и поларизација [6,7]. Последњи комбиновани резултат за масу топ кварка на Теватрону износи $m_{top} = 173.20 \pm 0.51$ (stat) $\pm$ 0.71 (syst) GeV, постављајући АТЛАС и ЦМС експериментима као циљ мерење са прецизношћу бољом од 1 GeV. На АТЛАС-у маса топ кварка је до сада измерена у сва три канала распада: семилептонском, дилептонском и чисто хадронском, Сл.3. Најбоља прецизност је постигнута у семилептонском каналу [8] са резултатом $m_{top} = 174.5 \pm 2.4$ GeV. У грешци мерења доминира систематска неодређеност, док је статистичка неодређеност упоредива са статистичком неодређеношћу на Теватрону. Главна компонента у систематској неодређености произилази из

коначни резултат АТЛАС и ЦМС експеримената је [9]:

$m_{top} = 173.3 \pm 0.5$ (stat) $\pm$ 1.3 (syst) GeV.

2. ХИГС

Откриће новог скаларног бозона

Према Стандардном моделу елементарне честице добијају масу кроз механизам спонтаног нарушења електрослабе симетрије. Последица таквог механизма је постојање скаларног бозона познатог под називом Хигсов бозон [10,11,12]. СМ не предвиђа директно масу Хигсовог бозона. Са друге стране сирина Хигсовог бозона и јачина спрезања са другим честицама (фермионима и калибрационим бозонима) зависе од његове масе и масе честице са којом се спрежу. Због тога је феноменологија Хигсовог бозона заправо одређена његовом масом.

У јулу 2012. колаборације АТЛАС и ЦМС су независно потврдиле откриће нове честице чије особине би могле бити конзистентне са Хигсовим бозоном у Стандардном моделу [13,14]. На хадронском сударачу Хигсов бозон се доминантно производи кроз процес глуон-глуон фузије (са топ или ботом кварком као интермедијарном честицом), а ређе кроз процесе фузије векторских бозона (*W* или *Z*), или заједно са *W* или *Z* бозоном, или паром топ и антитоп кварка. За откриће нове честице комбиновано је пет канала распада Хигсовог бозона (који одговарају истом броју експерименталних сигнатура). Ти канали су $H \to ZZ^* \to 4\ell$, $H \to \gamma\gamma$, $H \to WW^* \to \ell\nu\ell\nu$, $H \to \tau^+\tau^-$ и $H \to bb$ (ℓ означава електрон или мион, τ тау лептон, b означава ботом кварк, а ν неутрино). Анализирани су подаци који одговарају интегралној луминозности 4.8 fb^{-1} односно 5.8 fb^{-1} сакупљених на енергији 7 TeV односно 8 TeV за канале $H \to ZZ^* \to 4\ell$, $H \to \gamma\gamma$, $H \to WW^* \to \ell\nu\ell\nu$, док су за $\tau^+\tau^-$ и bb канале коришћени само подаци из 2011. године. Због високог *pileup*–а који погоршава мерење недостајућег трансверзалног импулса, за канал у коме се Хигс распада на два *W* бозона анализирано је само финално стање у коме је фон узрокован лошом резолуцијом недостајућег трансверзалног импулса најмањи. Постојање СМ Хигсовог бозона је искључено на нивоу поверења 95% у масеном опсегу 111-559 GeV, осим у региону 122-131 GeV. У овом масеном опсегу забележено је одступање од очекиваног фона са статистичким значајем од 5.9 стандардних девијација, док је у целом истраживаном масеном опсегу 110-600 GeV статистички значај одступања износио 5.1 стандардну девијацију. Измерена маса нове честице је 126.0 $\pm$ 0.4 (stat) $\pm$ 0.4 (syst) GeV, а јачина сигнала 1.4 $\pm$ 0.3 конзистентна је са вредношћу 1.0 очекиваним за СМ Хигс бозон дате масе. Распад на $\gamma\gamma$ искључује могућност да је спин новог бозона једнак јединици.

одговарају интегралној луминозности 21 fb^{-1} [15,16,17]. Резултати потврђ
постојање новог скаларног бозона, са статистичким значајем сигнала од
стандардних девијација. Расподеле инваријантне масе у $H \to ZZ^* \to 4\ell$ и $H \to \gamma\gamma$
приказане на Сл.4. У даљем тексту овог рада нови скаларни бозон ће бити
називан Хигсов бозон.

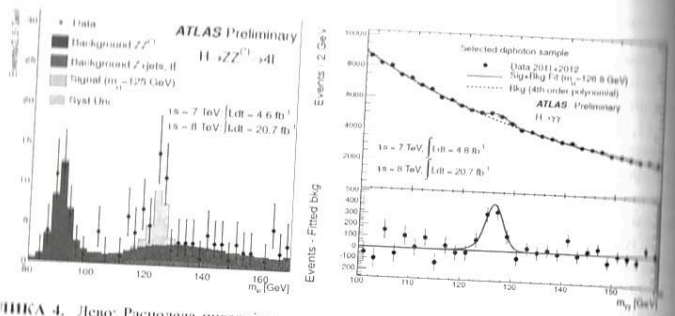

СЛИКА 4. Лево: Расподела инваријантне масе четири лептона у догађајима прикупљеним на енергији 8 TeV и 7 TeV . На графику су приказани и очекивани фон и сигнал који би потицао од СМ Хигсовог бозона масе 125 GeV. Десно: инваријантна маса два фотона у догађајима на енергији 8 TeV и 7 TeV. Црвена линија представља фит података функцијом у којој је суперпониран сигнал који би потицао од СМ Хигсовог бозона масе 126.8 GeV и фона описаног Бернштајновим полиномом четвртог реда. Доњи хистограм представља разлику између реалних података и фитованог фона.

Мерење масе, спина и парности

Откриће Хигсовог бозона представља важан корак у разумевању механизма нарушења симетрије електрослабог сектора СМ. У наредном периоду један од главних задатака на АТЛАС-у биће мерење масе, спина, парности и јачине спрезања новог бозона са фермионима и градијентним бозонима, као и јачине самоспрезања. АТЛАС колаборација је недавно објавила низ прелиминарних резултата који се односе на мерење масе [18], спина и парности [17,19,20], као и јачина спрезања са градијентним бозонима и фермионима [21].

Маса новог бозона је измерена користећи све податке скупљене током 2012. у каналима са најбољом масеном резолуцијом, $H \to ZZ^* \to 4\ell$ и $H \to \gamma\gamma$. Измерена маса у каналу са четири лептона износи $m_H = 124.3^{+0.6}_{-0.5}(stat)^{+0.5}_{-0.3}(syst)$ GeV. Масе у каналима у којима доминирају миони (4μ, 2μ2e) се у оквиру грешке слажу са добијеним вредностима масе у каналима у којима доминирају електрони (4e, 2e2μ). У двофотонском каналу измерена маса је 126.8±0.2(*stat*)±0.7(*syst*) GeV. У

канала износи $2.3^{+0.6}_{-0.5}(stat)^{+0.5}_{-0.3}(syst)$ GeV, односно 2.4 стандардне
претпостављајући да су систематске неодређености дистрибуиране по
расподели. Комбинујући мерења у $H \to ZZ^* \to 4\ell$ и $H \to \gamma\gamma$ каналу измерена
Хигсовог бозона износи:

$$m_H = 125.5 \pm 0.2(stat)^{+0.5}_{-0.6}(syst) \text{ GeV}.$$

Парност спина Хигсовог бозона у $H \to ZZ^* \to 4\ell$, $H \to \gamma\gamma$ и $H \to WW^* \to \ell\nu\ell\nu$ каналима
и јачине парности у $H \to ZZ^* \to 4\ell$ и $H \to WW^* \to \ell\nu\ell\nu$ обављено је кроз мерење
својстава (углова и импулса) продукованих честица. Тестиране су различите
хипотезе за спин и парност Хигсовог бозона $J^P = 0^+, 0^-, 2^+, 2^-$. Вредност спина 2 је
у свим анализираним каналима искључена на нивоу поверења најмање 95%. У
четворолептонском каналу негативна парност Хигсовог бозона са спином 0 је
искључена на нивоу поверења 97.8%.

Спрезања са градијентним бозонима и фермионима

У мерење масе измерена је и јачина сигнала за пет анализираних канала
распада Хигсовог бозона. Јачина сигнала се дефинише као однос између
опсервираног пресека за продукцију Хигсовог бозона у датом каналу распада и
пресека који предвиђа Стандардни модел за дату масу Хигса: $\mu_i = \sigma_i/\sigma_{i,SM}$.
Сличан параметар се може увести за факторе гранања $\mu_j = B_j/B_{j,SM}$, па се под
јачином сигнала овде подразумева један глобални фактор $\mu = \mu_i\mu_j$. На Сл.5
приказане су јачине спрезања у анализираним каналима, као и измерене масе у
четворолептонском и двофотонском каналу у зависности од измерених
вредности њихових јачина сигнала. Глобална јачина сигнала добијена
комбинацијом свих анализираних канала износи $\mu = 1.30 \pm 0.13$ (stat) ± 0.14 (syst)
за масу Хигса од 125.5 GeV. Добијена јачина веома слабо зависи од масе
Хигсовог бозона, до 4% за m_H у интервалу 124.5-126.5 GeV. Поред мерења
јачине сигнала у различитим каналима распада измерена је и релативна јачина за
различите механизме продукције Хигсовог бозона $\mu_{ggF+ttH}/\mu_{VBF+VH}$, где су
механизми продукције груписани према константама спрезања. Измерена
вредност $\mu_{ggF+ttH}/\mu_{VBF+VH} = 1.2^{+0.7}_{-0.5}$ је конзистентна са СМ. Такође, измерене су
вредности релативних фактора гранања за три канала распада $\gamma\gamma/ZZ$, $\gamma\gamma/WW$ и
ZZ/WW и све добијене вредности су конзистентне са СМ у оквиру статистичке
прецизности. У овим мерењима као претпоставка је узето да сви опсервирани
сигнали потичу од распада једног СМ Хигс бозона. За конзистентно мерење
константи спрезања Хигсовог бозона механизми продукције и канали распада се
не могу разматрати независно. Једноставни модели у најнижој апроксимацији
[22] су коришћени да би се тестирале корелације између продукције и распада
Хигсовог бозона у различитим финалним стањима. Претпоставка ових модела је

спрезања мења, док је тензорска структура спрезања као у СМ. Сва мер
спрезања су конзистентна са СМ, а грешком мерења доминира статис
неодређеност чија вредност износи 20-50% у зависности од мерене ком
спрезања и разматраног финалног стања.

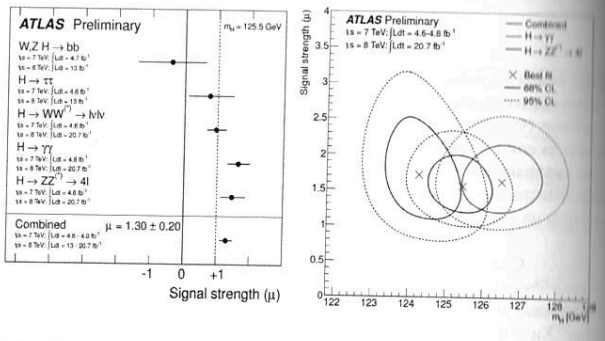

СЛИКА 5. Лево: Јачина сигнала μ за масу СМ Хиговог бозона m_H =125.5 GeV. Десно: интервали нивоа поверења у (μ, m_H) равни за $H \to ZZ^* \to 4\ell$ и $H \to \gamma\gamma$ канале. На оба графика приказани су и комбиновани резултати.

3. ПОТРАГА ЗА ЧЕСТИЦАМА ИЗВАН СТАНДАРДНОГ МОДЕЛА

Паралелно са прецизним мерењима параметара Стандардног модела и прва мерењима масе и спрезања Хигсовог бозона, на АТЛАС експерименту се одвија директна потрага за честицама чије постојање предвиђају теорије изван СМ. Разлози за проширење СМ-а су добро познати и многобројни [23]. Многе теорије и модели који покушавају да одговоре на нека од отворених питања предвиђају да би нове честице могле имати масе ~TeV, и самим тим могле бити продуковане и детектоване на Великом сударачу хадрона.

Суперсиметрија (*SUSY*) је највише мотивисана теорија изван Стандардног модела. Трагања за *SUSY* сигналима најчешће подразумевају издвајање догађаја са великим недостајућим трансверзалним импулсом који потиче од слабоинтерагујуће најлакше суперсиметричне честице код модела са очувањем *R*-парности, или од неутрина продукованих у распадима најлакше суперсиметричне честица код модела у којима је *R*-парност нарушена. Због тога је селекција догађаја заснована на великом недостајућем импулсу, великом броју џетова из доминантних распада *SUSY* честица, могућим лептонима, фотонима или помереним вертексима дугоживећих честица. Измереном масом Хигсовог

партнере градијентних бозона са масама ~200 GeV. Велики
на ATLAS-у посвећен је овим трагањима. Нажалост до сада није
тврђен значајно одступање од предвиђања СМ, што је за последицу
ало ограничења на параметре различитих *SUSY* модела, [24].
ена на масе суперсиметричних честица приказане су на Сл.6.
ATLAS експерименту се трага и за честицама чије постојање предвиђају
ије које нису засноване на суперсиметрији. Нови феномени би се
ифестовати кроз различите експерименталне сигнатуре, на пример као
ронске или двофотонске резонанце, нерезонантну продукцију два
или два хадронска џета, или спектакуларне сигнатуре са великим бројем
џетова као сто је то случај у теоријама у којима би квантна
ија јако интерогавала на енергетској скали од ~TeV. Одступање од СМ-
ено. Преглед резултата може се наћи у [25].

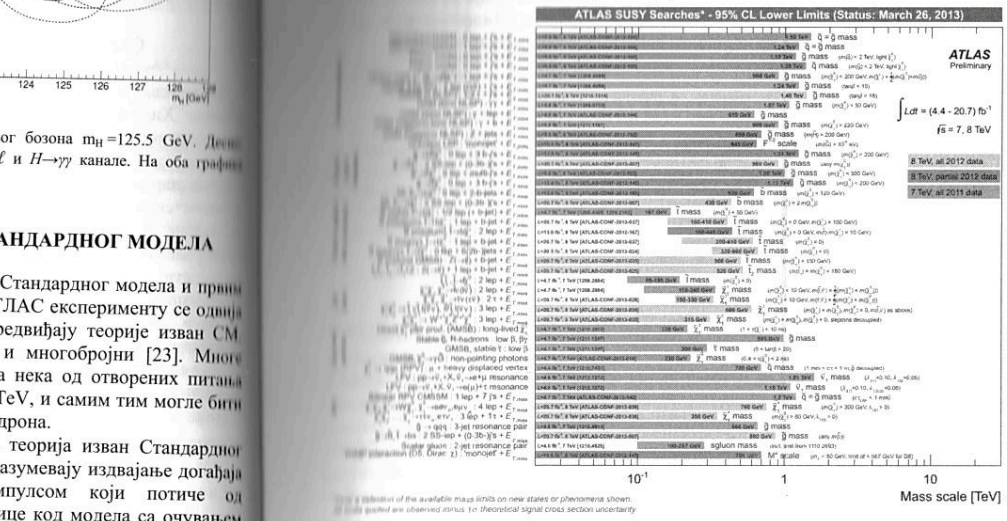

СЛИКА 6. Доња ограничења на масе суперсиметричних честица према последњим резултатима АТЛАС експеримента.

...мионима сакупљеним до сада. Сви досадашњи резултати су конзистентни с предвиђањима Стандардног модела.

Потрага за Хигсовим бозоном резултирала је открићем скаларног бозона у јулу 2012. године. Према прелиминарним резултатима добијеним анализом података који одговарају интегралној луминозности ~25 fb^{-1} измерена маса скаларног бозона је ~125.5 GeV, а спин и парност $J^P=0^+$. Измерена спрезања са градијентним бозонима и фермионима су конзистентна са предвиђањима Стандардног модела. Већа количина података је неопходна за боље разумевање природе нове честице и прецизније мерење њених особина.

ЗАХВАЛНИЦА

Захваљујем се организаторима XII конгреса физичара Србије на позиву за ово предавање. Захваљујем се др Љ. Симић, др М. Врањеш Милосављевић, др Д Поповић и др Ђ. Шијачком на корисним саветима везаним за текст.

ЛИТЕРАТУРА

[1] ATLAS Collaboration, JINST 3 , S08003 (2008).
[2] ATLAS Collaboration, Eur. Phys. J. C 70 (2010) 823–874.
[3] ATLAS Collaboration, Phys. Rev. D 85, 072004 (2012) [39 pp].
[4] ATLAS Collaboration, arXiv:1302.1283 [hep-ex].
[5] ATLAS Collaboration, JHEP03(2013)128, arXiv:1211.6096 [hep-ex].
[6] CDF Collaboration, http://www-cdf.fnal.gov/physics/new/top/public_tprop.html
[7] D0 Collaboration, http://www-d0.fnal.gov/Run2Physics/WWW/results/top.htm
[8] ATLAS Collaboration, Eur. Phys. J. C 72 (2011) 20-46.
[9] ATLAS Collaboration, ATLAS-CONF-2013-033.
[10] F. Englert and R. Brout, Phys. Rev. Lett. (1964) 321–323.
[11] P. W. Higgs, Phys. Rev. Lett. 13 (1964) 508–509.
[12] G. S. Guralnik, C. R. Hagen, and T. W. B. Kibble, Phys. Rev. Lett. 13 (1964) 585–587.
[13] ATLAS Collaboration, Phys. Lett. B716 (2012) 1-29, arXiv:1207.7214 [hep-ex].
[14] CMS Collaboration, Phys. Lett. B716 (2012) 30-61, arXiv:1207.7235 [hep-ex].
[15] ATLAS Collaboration, ATLAS-CONF-2013-030.
[16] ATLAS Collaboration, ATLAS-CONF-2013-012.
[17] ATLAS Collaboration, ATLAS-CONF-2013-013.
[18] ATLAS Collaboration, ATLAS-CONF-2013-014.
[19] ATLAS Collaboration, ATLAS-CONF-2013-031.
[20] ATLAS Collaboration, ATLAS-CONF-2013-029.
[21] ATLAS Collaboration, ATLAS-CONF-2013-034.
[22] LHC Higgs Cross Section Working Group, CERN-2012-002, arXiv:1201.3084 [hep-ph].
[23] John Ellis, arXiv:1102.5009v1 [hep-ph], CERN-PH-TH/2011-003.
[24] https://twiki.cern.ch/twiki/bin/view/AtlasPublic/SupersymmetryPublicResults
[25] https://twiki.cern.ch/twiki/bin/view/AtlasPublic/ExoticsPublicResults

ЕКСПЕРИМЕНТ CMS НА LHC-У И РЕЗУЛТАТИ СРПСКЕ ГРУПЕ ИСТРАЖИВАЧА И ИНЖЕЊЕРА

М. Ђорђевић[1], Ј. Милошевић[1], Н. Миленовић[1*], Д. Деветак[1], Н. Смиљковић[4*], Д. Јовановић[2] и П. Адзић[2]

[1] Универзитет у Београду - Институт за нуклеарне науке "Винча", Мике Петров Алаша 12-14, п. фах 522, 11001 Београд
[2] Универзитет у Београду - Физички факултет, Студентски трг 12, 11000 Београ
[3] University of Florida - The Institute for High Energy Physics and AstroPhysics, P.O. 118440, Gainesville, FL, U.S.A. (* и И.Н.Н. "Винча")
[4] The European Organization for Nuclear Research (CERN) - Route de Meyrin 385 1217 Meyrin, Switzerland (* и И.Н.Н. "Винча")
e-mail: mdjordjevic@vinca.rs

Апстракт. Приказани су резултати активности српске групе на експерименту CMS у LHC-у. Представљена су делови резултата који се односе на: потрагу за Хигс бозоном каналима распада γγ и ZZ, што је довело до открића тешког бозона, затим резултат мерења пресека за продукцију стања Zγ, као и резултати потраге за аномалним ZZγ и Zγ спрезањима. У оквиру програма судара тешких јона, анализиране су азимутална анизотропије и особине млазева честица. Изложене су активности групе у области хардвера, које укључују рад на конструкцији и одржавању два значајна система у контролу електромагнетског калориметра ECAL, једног од четири под-система детектора CMS. На крају, дат је приказ инжењерског ангажовања српске групе на дизајну, моделовању и конструкцији детектора CMS.

1. УВОД

Изузетно добро функционисање Великог хадронског сударача (LHC) у CE у, почев од његовог пуштања у рад у новембру 2009. године, па све до данас, и високе перформансе свих детектора на овом акцелератору, премашили су очекивања. То је резултирало великом количином изузетно квалитет података који су прикупљени у сударима протона и тешких јона олов рекордним енергијама. Анализа ових података довела је до низа значај резултата од којих је свакако најважније откриће тешког бозона, компатибил са Хигс бозоном којег предвиђа Стандардни Модел (СМ). Према СМ Хигс бо се распада и на дволептонска и двобозонска финална стања: ττ, μμ, γγ, ZZ, W Zγ. Најновији подаци прикупљени детектором CMS омогућују мер ефикасног пресека за продукцију двобозонских финалних стања на до недостижним енергијама, затим потрагу за Хигсим бозоном у неко предвиђених канала распада, као и евентуално регистровање феномена одговарају новој физици изван СМ.

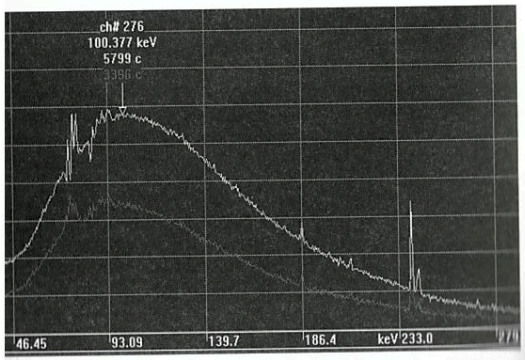

нструментални спектри фонског зрачења континуираног спектра које долази
е, у површинској лабораторији (горњи) и у подземној лабораторији на
тралне брзине бројања у њима су око 21 и 12 cps респективно.

лне ситуације које резултују у оваквим фонским спектрима
имулиране програмским пакетима GEANT4 и CORSIKA
је то зрачење континуираног спектра двојаког порекла – једно
едставља расејано и деградирано зрачење електромагнетне
мичког зрачења, док другим делом представља од целокупне
о зрачење терестријалног порекла, често познатог под називом
ion" [1]. И поред велике сличности збирног спектра на
е да је релативни удео ове две компоненте веома различит на
ције, и тај релативни удео још треба одредити.

ЗАХВАЛНИЦА

реализован уз подршку Министарства за просвету, науку
вој Републике Србије, у оквиру пројекта ОИ 171002.

ЛИТЕРАТУРА

Nucl. Instr. and Meth. in Phys. Res. **A591** 470-475 2008
Instr. and Meth. **172** 559-566 1980

КАРАКТЕРИСТИКЕ РЕКОНСТРУКЦИЈЕ МИОНА НИСКОГ ИМПУЛСА НА АТЛАС ДЕТЕКТОРУ

А. Димитриевска[1)] и Н. Врањеш[2)]

1) Универзитет у Београду – Институт за физику, Прегревица 118, 11000 Београд
2) CEA-Saclay
e-mail: adimitrievska@ipb.ac.rs

Апстракт. Испитиване су карактеристике реконструкције миона ниског импулса на АТЛАС детектору коришћењем миона из распада J/ψ мезона. Како је маса J/ψ мезона веома прецизно измерена на претходним експериментима, и како је природна ширина занемарива према инструменталној ширини, те како се J/ψ мезони обилно производе на Великом хадронском сударачу, они представљају одлично оруђе за калибрацију импулса миона у опсегу компатибилном са опсегом импулса миона из распада Z бозона.

1. УВОД

АТЛАС детектор [1] је један од четири експеримената који су постављени на LHC-у. Он је, по димензијама, највећи конструисани детектор, има цилиндричну симетрију дужине 44 m, са пречником 25 m и масом око 7000 t.

АТЛАС детектор има слојевиту структуру и састоји се од четири система, унутрашњег детектора, калориметарског система, мионског спектрометра и магнетног система. Унутрашњи детектор се налази најближе вакуумској цеви кроз коју пролазе протони. Основна функција унутрашњег детектора је одређивање трајекторија наелектрисаних честица, мерење импулса честица, као и за реконструкцију вертекса. Калориметерски систем се састоји од електромагнетног и хадронског калориметра. Електромагнетни калориметар је смештен око соленоида који окружује унутрашњи детектор. Основни циљ калориметара је мерење енергије електрона, фотона и хадронских џетова. Мионски спектрометар [2] окружује хадронски калориметар и омогућава идентификацију и веома прецизно мерење импулса миона. Магнетни систем АТЛАС детектора се састоји од суперпроводног соленоидног магнета који се налази у средини детектора, да би се створило константно магнетно поље, и три торусна магнета у облику торуса који стварају магнетно поље у мионском спектрометру.

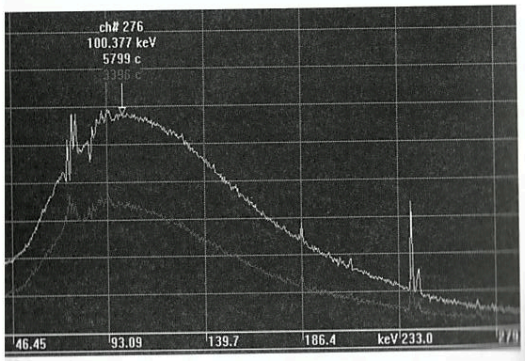

нструментални спектри фонског зрачења континуираног спектра које долази
е, у површинској лабораторији (горњи) и у подземној лабораторији на
тралне брзине бројања у њима су око 21 и 12 cps респективно.

лне ситуације које резултују у оваквим фонским спектрима
имулиране програмским пакетима GEANT4 и CORSIKA
је то зрачење континуираног спектра двојаког порекла – једно
едставља расејано и деградирано зрачење електромагнетне
мичког зрачења, док другим делом представља од целокупне
о зрачење терестријалног порекла, често познатог под називом
ion" [1]. И поред велике сличности збирног спектра на
е да је релативни удео ове две компоненте веома различит на
ције, и тај релативни удео још треба одредити.

ЗАХВАЛНИЦА

реализован уз подршку Министарства за просвету, науку
вој Републике Србије, у оквиру пројекта ОИ 171002.

ЛИТЕРАТУРА

Nucl. Instr. and Meth. in Phys. Res. **A591** 470-475 2008
Instr. and Meth. **172** 559-566 1980

КАРАКТЕРИСТИКЕ РЕКОНСТРУКЦИЈЕ МИОНА НИСКОГ ИМПУЛСА НА АТЛАС ДЕТЕКТОРУ

А. Димитриевска[1)] и Н. Врањеш[2)]

1) Универзитет у Београду – Институт за физику, Прегревица 118, 11000 Београд
2) CEA-Saclay
e-mail: adimitrievska@ipb.ac.rs

Апстракт. Испитиване су карактеристике реконструкције миона ниског импулса на АТЛАС детектору коришћењем миона из распада J/ψ мезона. Како је маса J/ψ мезона веома прецизно измерена на претходним експериментима, и како је природна ширина занемарива према инструменталној ширини, те како се J/ψ мезони обилно производе на Великом хадронском сударачу, они представљају одлично оруђе за калибрацију импулса миона у опсегу компатибилном са опсегом импулса миона из распада Z бозона.

1. УВОД

АТЛАС детектор [1] је један од четири експеримената који су постављени на LHC-у. Он је, по димензијама, највећи конструисани детектор, има цилиндричну симетрију дужине 44 m, са пречником 25 m и масом око 7000 t.

АТЛАС детектор има слојевиту структуру и састоји се од четири система, унутрашњег детектора, калориметарског система, мионског спектрометра и магнетног система. Унутрашњи детектор се налази најближе вакуумској цеви кроз коју пролазе протони. Основна функција унутрашњег детектора је одређивање трајекторија наелектрисаних честица, мерење импулса честица, као и за реконструкцију вертекса. Калориметерски систем се састоји од електромагнетног и хадронског калориметра. Електромагнетни калориметар је постављен око соленоида који окружује унутрашњи детектор. Основни циљ калориметара је мерење енергије електрона, фотона и хадронских џетова. Мионски спектрометар [2] окружује хадронски калориметар и омогућава идентификацију и веома прецизно мерење импулса миона. Магнетни систем АТЛАС детектора се састоји од суперпроводног соленоидног магнета који се налази у средини детектора, да би се створило константно магнетно поље, и три суперпроводна магнета у облику торуса који стварају магнетно поље у мионском спектрометру.

2. РЕКОНСТРУКЦИЈА МИОНА

ти од начина реконструкције разликујемо неколико типова миона тектору [3]:

ed су миони који су реконструисани на основу статистичке нације импулса и пложаја из мионског спектрометра и унутрашњег ора. Енергетски губици миона приликом проласка кроз иметре су урачунати коришћењем параметризоване функције која у обзир расподелу материјала испред мионског система;

ılone су миони који су реконструисани само у мионском ометру, уз пропагацију положаја миона до тачке интеракције и навање енертегских губитака кроз калориметар;

nt-tagged су миони чији је импулс потпуно реконструисан у ашњеном детектору. Идентификација миона извршена је пањем трага у унутрашњем детектору и сегемента реконструисаног ској комори најближој калориметру;

gged су попут *segment-tagged* потпуно реконструисани у ашњем детектору. али се за њихову идентификацију користи ована енергија у калориметру.

трукцију миона утичу непрецизно познавање мапе магнетног поља губитак енергије миона при проласку кроз калориметре, недовољно оравнање мионских комора, као и неодређености у моделовању расејања миона при проласку кроз детектор.

3. РЕЗУЛТАТИ И ДИСКУСИЈА

у реконструкције миона који су настали распадом J/ψ мезона инваријантна маса ова два миона у зависности од рапидитета. Услови они треба да испуне је да се налазе у малом просторном углу да имају трансверзални импулс већи од 6 GeV. Селектовани су ови иони. На основу података прикупљених током 2012. године при 8 TeV реконструисано је око 30 милиона кандидата J/ψ мезона. ој прикупљених J/ψ мезона омогућава прецизно испитивање ика Мионског спектрометра.

иказује инваријантну масу два миона реконструисана на три начина од рапидитета. Инваријантна маса је израчуната користећи импулс она и угао између њих:

$$M_{\mu\mu} = \sqrt{p_1^{\mu} p_2^{\mu} (1 - \cos_{12})},$$

на маса је израчуната на три начина: користећи импулс измерен и детектору, користећи импулс измерен у мионском спектрометру, и комбиновани импулс.

Са Сл.1. се види да је инваријантна маса добиејена коришћењем импулса измереног у унутрашњем детектору веома блиска табличној вредности 3096.916±0.011 MeV, што указује на добру калибрацију имулса у унутрашњем детектору. Инваријантна маса израчуната коришћењем импулса из мионског спектрометра одступа од табличне вредности у централној области (|η|<1) у средњем за око 20 MeV, односно ~0.6%. Вредност масе добијене из комбинованог импулса је ближа табличној вредности, пошто у статистичкој комбинацији за мионе ниског импулса доминира информација из унутрашњег детектора. Ипак одступање од табличне вредности износи око ~0.1% под утицајем спектрометра.

Како је проверено да одступање не зависи од импулса миона, узето је да енергијски губици миона у калориметрима већи од параметризованих вредности које се урачунавају при реконструкцији миона у мионском спектрометру. Корекција за појединачне мионе је добијена фитовањем разлике импулса миона у спектрометру и унутрашњем детектору у функцији рапидитета. После примене оваквих корекција на импулс миона у спектрометру добијено је много боље слагање са табличном вредношћу масе J/ψ користећи спектрометраски и последично комбиновани импулса миона.

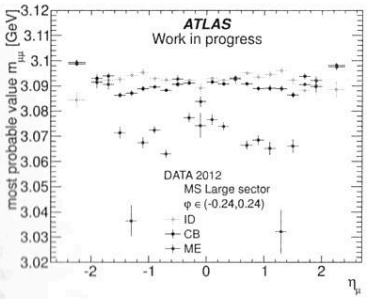

Инваријантна маса два миона у зависности од рапидитета. Инваријантна маса је ја у три начина: користећи импулс измерен у унутрашњем детектору, користећи измерен у мионском спектрометру са урачунатим емертегтским губицима, као и ани импулс. У сва тру случаја угао је измерен у унутрашњем детекору

ЗАХВАЛНИЦА

рад је спроведен уз подршку Министарства за просвету, науку и

SPISAK CITATA BEZ AUTOCITATA PREMA BAZI INSPIRE-HEP

1. Aaboud, M., ... ,Vranjes N., *et al.* [ATLAS Collaboration], *Measurement of the top quark mass in the $t\bar{t} \to$ dilepton channel from $\sqrt{s} = 8$ TeV ATLAS data*, Phys.Lett. B761 (2016) 350-371, arXiv:1606.02179 [hep-ex].

    1. M. Butenschoen, B. Dehnadi, A. Hoang, V. Mateu, M. Preisser and I. W. Stewart, PoS DIS **2016** (2016) 153.
    2. A. O. M. Iorio, S. Bifani and M. Franchini, PoS PP **@LHC2016** (2016) 019.
    3. M. Butenschoen, B. Dehnadi, A. H. Hoang, V. Mateu, M. Preisser and I. W. Stewart, PoS LL **2016** (2016) 066.
    4. CMS Collaboration [CMS Collaboration], CMS-PAS-TOP-15-015.
    5. K. Kawana, arXiv:1609.00513 [hep-th].
    6. M. J. Boland *et al.* [CLIC and CLICdp Collaborations], arXiv:1608.07537 [physics.acc-ph].
    7. N. Haba, N. Okada and T. Yamada, Phys. Rev. D **94** (2016) no.7, 071701 [arXiv:1608.04065 [hep-ph]].
    8. CMS Collaboration [CMS Collaboration], CMS-PAS-TOP-15-008.
    9. M. Butenschoen, B. Dehnadi, A. H. Hoang, V. Mateu, M. Preisser and I. W. Stewart, Phys. Rev. Lett. **117** (2016) no.23, 232001 [arXiv:1608.01318 [hep-ph]].
    10. W. E. East, J. Kearney, B. Shakya, H. Yoo and K. M. Zurek, [arXiv:1607.00381 [hep-ph]].
    11. G. Bevilacqua, PoS DIS **2016** (2016) 151 [arXiv:1606.09501 [hep-ph]].

2. Aad, G., ... ,Vranjes N., *et al.* [ATLAS Collaboration], *Fiducial and differential cross sections of Higgs boson production measured in the four-lepton decay channel in pp collisions at $\sqrt{s}$=8 TeV with the ATLAS detector*, Phys.Lett. B738 (2014) 234-253, arXiv:1408.3226 [hep-ex].

    1. M. Grazzini, A. Ilnicka, M. Spira and M. Wiesemann, arXiv:1612.00283 [hep-ph].
    2. M. A. Ebert and F. J. Tackmann, arXiv:1611.08610 [hep-ph].
    3. V. S. Rawoot, R. Islam and M. Kumar, arXiv:1610.09940 [hep-ph].
    4. D. de Florian *et al.* [LHC Higgs Cross Section Working Group Collaboration], arXiv:1610.07922 [hep-ph].
    5. T. Neumann and C. Williams, PoS LL **2016** (2016) 027.
    6. T. Neumann and C. Williams, arXiv:1609.00367 [hep-ph].
    7. M. Kumar *et al.*, arXiv:1608.03466 [hep-ph].
    8. W. Adam, J. Pradler, J. Schieck, C. Schwanda and W. Waltenberger, arXiv:1607.01212 [hep-ph].
    9. R. Contino *et al.*, arXiv:1606.09408 [hep-ph].

10. F. Bishara, U. Haisch, P. F. Monni and E. Re, arXiv:1606.09253 [hep-ph].
11. Y. Soreq, H. X. Zhu and J. Zupan, arXiv:1606.09621 [hep-ph].
12. V. Khachatryan *et al.* [CMS Collaboration], [arXiv:1606.01522 [hep-ex]].
13. A. Arbey, S. Fichet, F. Mahmoudi and G. Moreau, JHEP **1611** (2016) 097 [arXiv:1606.00455 [hep-ph]].
14. P. Sun, C.-P. Yuan and F. Yuan, Phys. Lett. B **762** (2016) 47 [arXiv:1605.00063 [hep-ph]].
15. C. Gao, M. A. Luty, M. Mulhearn, N. A. Neill and Z. Wang, arXiv:1604.03108 [hep-ph].
16. R. Frederix, S. Frixione, E. Vryonidou and M. Wiesemann, JHEP **1608** (2016) 006 [arXiv:1604.03017 [hep-ph]].
17. M. Bonvini, S. Marzani, C. Muselli and L. Rottoli, JHEP **1608** (2016) 105 [arXiv:1603.08000 [hep-ph]].
18. J. Bernon, A. Goudelis, S. Kraml, K. Mawatari and D. Sengupta, JHEP **1605** (2016) 128 [arXiv:1603.03421 [hep-ph]].
19. P. Sun, J. Isaacson, C.-P. Yuan and F. Yuan, arXiv:1602.08133 [hep-ph].
20. V. Khachatryan *et al.* [CMS Collaboration], JHEP **1604** (2016) 005 [arXiv:1512.08377 [hep-ex]].
21. CMS Collaboration [CMS Collaboration], CMS-PAS-HIG-15-010.
22. M. Grazzini, A. Ilnicka, M. Spira and M. Wiesemann, PoS EPS **-HEP2015** (2015) 144 [arXiv:1511.08059 [hep-ph]].
23. S. Marzani, Phys. Rev. D **93** (2016) no.5, 054047 [arXiv:1511.06039 [hep-ph]].
24. S. von Buddenbrock, J. Phys. Conf. Ser. **645** (2015) no.1, 012017.
25. D. Gossman, J. Phys. Conf. Ser. **645** (2015) no.1, 012010.
26. CMS Collaboration [CMS Collaboration], CMS-PAS-HIG-15-002.
27. S. Fichet and G. Moreau, Nucl. Phys. B **905** (2016) 391 [arXiv:1509.00472 [hep-ph]].
28. V. Khachatryan *et al.* [CMS Collaboration], Eur. Phys. J. C **76** (2016) no.1, 13 [arXiv:1508.07819 [hep-ex]].
29. CMS Collaboration [CMS Collaboration], CMS-PAS-HIG-14-028.
30. S. von Buddenbrock *et al.*, arXiv:1506.00612 [hep-ph].
31. G. Moortgat-Pick *et al.*, Eur. Phys. J. C **75** (2015) no.8, 371 [arXiv:1504.01726 [hep-ph]].
32. S. Boselli, C. M. Carloni Calame, G. Montagna, O. Nicrosini and F. Piccinini, JHEP **1506** (2015) 023 [arXiv:1503.07394 [hep-ph]].
33. P. Checchia, Int. J. Mod. Phys. A **30** (2015) no.07, 1530003.
34. K. Hamilton, P. Nason and G. Zanderighi, JHEP **1505** (2015) 140 [arXiv:1501.04637 [hep-ph]].

35. V. Khachatryan *et al.* [CMS Collaboration], Eur. Phys. J. C **75** (2015) no.5, 212 [arXiv:1412.8662 [hep-ex]].
36. B. Grzadkowski, O. M. Ogreid and P. Osland, JHEP **1411** (2014) 084 [arXiv:1409.7265 [hep-ph]].
37. A. David, J. Heikkil and G. Petrucciani, Eur. Phys. J. C **75** (2015) no.2, 49 [arXiv:1409.6132 [hep-ph]].

3. Aad, G., ... ,Vranjes N., *et al.* [ATLAS Collaboration], *Measurement of the Higgs boson mass from the $H \to \gamma\gamma$ and $H \to ZZ^* \to 4\ell$ channels with the ATLAS detector using 25 fb^{-1} of pp collision data*, Phys.Rev. D90 (2014) no.5, 052004, arXiv:1406.3827 [hep-ex].

1. M. Dubinin and E. Petrova, arXiv:1612.03655 [hep-ph].
2. C. Han, K. i. Hikasa, L. Wu, J. M. Yang and Y. Zhang, arXiv:1612.02296 [hep-ph].
3. C. Mariotti and G. Passarino, arXiv:1612.00269 [hep-ph].
4. Z. Heng and H. Zhou, Chin. J. Phys. **52** (2016) no.2, 308.
5. B. Courbon [CMS Collaboration], PoS DIS **2016** (2016) 098.
6. V. Khachatryan *et al.* [CMS Collaboration], [arXiv:1610.08066 [hep-ex]].
7. D. de Florian *et al.* [LHC Higgs Cross Section Working Group Collaboration], arXiv:1610.07922 [hep-ph].
8. S. Y. Ho, G. Faisel and J. Tandean, PoS DSU **2015** (2016) 068.
9. F. Yu, arXiv:1609.06592 [hep-ph].
10. A. Donini and S. G. Marimn, arXiv:1609.05654 [hep-ph].
11. S. Bhattacharya and S. Jain, Pramana **87** (2016) no.3, 35.
12. J. Garay Garca, doi:10.3204/PUBDB-2016-03304
13. M. N. Dubinin and E. Y. Petrova, Phys. Atom. Nucl. **79** (2016) no.4, 488 [Yad. Fiz. **79** (2016) no.4, 302].
14. CMS Collaboration [CMS Collaboration], CMS-PAS-HIG-16-023.
15. P. Bandyopadhyay, C. Coriano, A. Costantini and L. Delle Rose, JHEP **1609** (2016) 084 [arXiv:1607.01933 [hep-ph]].
16. W. Adam, J. Pradler, J. Schieck, C. Schwanda and W. Waltenberger, arXiv:1607.01212 [hep-ph].
17. F. Bishara, U. Haisch, P. F. Monni and E. Re, arXiv:1606.09253 [hep-ph].
18. L. Wang, S. Yang and X. F. Han, arXiv:1606.04408 [hep-ph].
19. T. Hahn, S. Heinemeyer, W. Hollik, H. Rzehak and G. Weiglein, Nucl. Part. Phys. Proc. **273-275** (2016) 794.
20. A. Arhrib, R. Benbrik, C. H. Chen, M. Gomez-Bock and S. Semlali, Nucl. Part. Phys. Proc. **273-275** (2016) 2430.
21. C. Grojean, Nucl. Part. Phys. Proc. **273-275** (2016) 11.

22. V. Khachatryan *et al.* [CMS Collaboration], JHEP **1608** (2016) 122 [arXiv:1605.04608 [hep-ex]].
23. T. Cohen, G. D. Kribs, A. E. Nelson and B. Ostdiek, Phys. Rev. D **94** (2016) no.1, 015031 [arXiv:1605.04308 [hep-ph]].
24. R. Deen, B. A. Ovrut and A. Purves, JHEP **1607** (2016) 043 [arXiv:1604.08588 [hep-ph]].
25. CMS Collaboration [CMS Collaboration], CMS-PAS-B2G-16-003.
26. V. Khachatryan *et al.* [CMS Collaboration], Eur. Phys. J. C **76** (2016) no.8, 460 [arXiv:1603.00765 [hep-ex]].
27. L. Zarate, JHEP **1607** (2016) 102 [arXiv:1601.05946 [hep-ph]].
28. T. S. Virdee, Annalen Phys. **528** (2016) 35.
29. A. Ahriche, S. M. Boucenna and S. Nasri, Phys. Rev. D **93** (2016) no.7, 075036 [arXiv:1601.04336 [hep-ph]].
30. C. Grojean, Nucl. Part. Phys. Proc. **267-269** (2015) 15.
31. S. Furui, PoS FPCP **2015** (2015) 087.
32. K. Endo, K. Ishiwata and Y. Sumino, Phys. Rev. D **94** (2016) no.7, 075007 [arXiv:1601.00696 [hep-ph]].
33. P. Bandyopadhyay, K. Huitu and S. Niyogi, JHEP **1607** (2016) 015 [arXiv:1512.09241 [hep-ph]].
34. P. Bandyopadhyay, C. Corian and A. Costantini, Phys. Rev. D **94** (2016) no.5, 055030 [arXiv:1512.08651 [hep-ph]].
35. J. K. Behr, D. Bortoletto, J. A. Frost, N. P. Hartland, C. Issever and J. Rojo, Eur. Phys. J. C **76** (2016) no.7, 386 [arXiv:1512.08928 [hep-ph]].
36. A. Donini, arXiv:1512.03978 [hep-ph].
37. V. Khachatryan *et al.* [CMS Collaboration], Phys. Lett. B **758** (2016) 296 [arXiv:1511.03610 [hep-ex]].
38. M. Quiros, M. Garcia-Pepin and A. Delgado, PoS PLANCK **2015** (2015) 109 [arXiv:1511.03254 [hep-ph]].
39. M. D. Goodsell, K. Nickel and F. Staub, Phys. Lett. B **758** (2016) 18 [arXiv:1511.01904 [hep-ph]].
40. A. Belyaev, V. Sanz and M. Thomas, JHEP **1601** (2016) 102 [arXiv:1510.07688 [hep-ph]].
41. V. Khachatryan *et al.* [CMS Collaboration], JHEP **1601** (2016) 079 [arXiv:1510.06534 [hep-ex]].
42. P. Bandyopadhyay, C. Coriano and A. Costantini, JHEP **1512** (2015) 127 [arXiv:1510.06309 [hep-ph]].
43. A. Szczurek, PoS EPS **-HEP2015** (2015) 145 [arXiv:1510.03731 [hep-ph]].
44. S. H. Hendi, B. Eslam Panah, M. Momennia and S. Panahiyan, Eur. Phys. J. C **75** (2015) no.9, 457 [arXiv:1509.03081 [hep-th]].

45. X. F. Han, L. Wang and J. M. Yang, Mod. Phys. Lett. A **31** (2016) no.31, 1650178 [arXiv:1509.02453 [hep-ph]].
46. S. Gori, J. Gu and L. T. Wang, JHEP **1604** (2016) 062 [arXiv:1508.07010 [hep-ph]].
47. H. L. Li, P. C. Lu, Z. G. Si and Y. Wang, Chin. Phys. C **40** (2016) no.6, 063102 [arXiv:1508.06416 [hep-ph]].
48. G. Mittag, doi:10.3204/DESY-THESIS-2015-029
49. K. Harigaya, arXiv:1508.04811 [hep-ph].
50. T. Kitahara, arXiv:1508.04810 [hep-ph].
51. K. Azizi, A. T. Olgun and Z. Tavuko?lu, Phys. Rev. D **92** (2015) no.11, 115025 [arXiv:1508.03980 [hep-ph]].
52. CMS Collaboration [CMS Collaboration], CMS-PAS-SUS-13-023.
53. G. Lee and C. E. M. Wagner, Phys. Rev. D **92** (2015) no.7, 075032 [arXiv:1508.00576 [hep-ph]].
54. V. Khachatryan *et al.* [CMS Collaboration], Phys. Rev. D **92** (2015) no.7, 072010 [arXiv:1507.06656 [hep-ex]].
55. S. Chang, S. K. Kang, J. P. Lee and J. Song, Phys. Rev. D **92** (2015) no.7, 075023 [arXiv:1507.03618 [hep-ph]].
56. N. Aghanim *et al.* [Planck Collaboration], Astron. Astrophys. **594** (2016) A11 [arXiv:1507.02704 [astro-ph.CO]].
57. M. Verzetti, CERN-THESIS-2014-263, CMS-TS-2015-003.
58. C. Elsasser, CERN-THESIS-2015-020.
59. J. Webster, CERN-THESIS-2015-087.
60. K. Harigaya, M. Ibe, M. Kawasaki and T. T. Yanagida, JCAP **1511** (2015) no.11, 003 [arXiv:1507.00119 [hep-ph]].
61. F. Coradeschi, D. de Florian, N. Fidanza and J. Mazzitelli, Nucl. Part. Phys. Proc. **258-259** (2015) 253.
62. M. Yang, arXiv:1506.06804 [hep-ex].
63. D. Fontes, J. C. Romo, R. Santos and J. P. Silva, Phys. Rev. D **92** (2015) no.5, 055014 [arXiv:1506.06755 [hep-ph]].
64. L. A. Anchordoqui, V. Barger, H. Goldberg, X. Huang, D. Marfatia, L. H. M. da Silva and T. J. Weiler, Phys. Rev. D **92** (2015) no.6, 063504 [arXiv:1506.04702 [hep-ph]].
65. P. Bandyopadhyay, C. Coriano and A. Costantini, JHEP **1509** (2015) 045 [arXiv:1506.03634 [hep-ph]].
66. V. Khachatryan *et al.* [CMS Collaboration], Phys. Rev. D **93** (2016) no.1, 012001 [arXiv:1506.03062 [hep-ex]].
67. J. R. Espinosa and C. Grojean, Comptes Rendus Physique **16** (2015) 394.
68. N. Greiner, S. Hche, G. Luisoni, M. Schnherr, J. C. Winter and V. Yundin, JHEP **1601** (2016) 169 [arXiv:1506.01016 [hep-ph]].

69. D. Fontes, J. C. Romo, J. P. Silva and R. Santos, arXiv:1506.00860 [hep-ph].
70. K. Harigaya, M. Ibe, K. Schmitz and T. T. Yanagida, Phys. Lett. B **749** (2015) 298 [arXiv:1506.00426 [hep-ph]].
71. S. Sukhoruchkin, Nucl. Part. Phys. Proc. **258-259** (2015) 268.
72. K. Harigaya, M. Ibe and M. Suzuki, JHEP **1509** (2015) 155 [arXiv:1505.05024 [hep-ph]].
73. N. Karagiannakis, G. Lazarides and C. Pallis, PoS CORFU **2014** (2015) 115 [arXiv:1505.04144 [hep-ph]].
74. A. Liu, FERMILAB-THESIS-2015-04.
75. K. Harigaya, T. T. Yanagida and N. Yokozaki, Phys. Rev. D **92** (2015) no.3, 035011 [arXiv:1505.01987 [hep-ph]].
76. S. Zheng, Eur. Phys. J. C **75** (2015) no.10, 489 [arXiv:1504.08093 [hep-ph]].
77. S. Oda, N. Okada and D. s. Takahashi, Phys. Rev. D **92** (2015) no.1, 015026 [arXiv:1504.06291 [hep-ph]].
78. F. Coradeschi, D. de Florian, L. J. Dixon, N. Fidanza, S. Hche, H. Ita, Y. Li and J. Mazzitelli, Phys. Rev. D **92** (2015) no.1, 013004 [arXiv:1504.05215 [hep-ph]].
79. N. Blinov, J. Kozaczuk, D. E. Morrissey and C. Tamarit, Phys. Rev. D **92** (2015) no.3, 035012 [arXiv:1504.05195 [hep-ph]].
80. V. Khachatryan *et al.* [CMS Collaboration], Phys. Lett. B **748** (2015) 221 [arXiv:1504.04710 [hep-ex]].
81. B. Bhattacherjee, A. Chakraborty and A. Choudhury, Phys. Rev. D **92** (2015) no.9, 093007 [arXiv:1504.04308 [hep-ph]].
82. A. Randle-Conde, arXiv:1504.04302 [hep-ex].
83. S. Furui, arXiv:1504.03795 [hep-ph].
84. C. Alvarado, A. Delgado, A. Martin and B. Ostdiek, Phys. Rev. D **92** (2015) no.3, 035009 [arXiv:1504.03683 [hep-ph]].
85. J. Ellis, Nucl. Part. Phys. Proc. **267-269** (2015) 3 [arXiv:1504.03654 [hep-ph]].
86. G. Moortgat-Pick *et al.*, Eur. Phys. J. C **75** (2015) no.8, 371 [arXiv:1504.01726 [hep-ph]].
87. V. Khachatryan *et al.* [CMS Collaboration], JHEP **1510** (2015) 144 [arXiv:1504.00936 [hep-ex]].
88. J. Hisano, K. Ishiwata and N. Nagata, JHEP **1506** (2015) 097 d [arXiv:1504.00915 [hep-ph]].
89. P. S. B. Dev and A. Pilaftsis, J. Phys. Conf. Ser. **631** (2015) no.1, 012030 [arXiv:1503.09140 [hep-ph]].
90. S. Choudhury, EPJ Web Conf. **90** (2015) 05002.
91. N. A. Ky and N. T. H. Van, arXiv:1503.08630 [hep-ph].
92. J. M. Cline, G. Dupuis, Z. Liu and W. Xue, Phys. Rev. D **91** (2015) no.11, 115010 [arXiv:1503.08213 [hep-ph]].

93. A. Chakraborty, D. K. Ghosh, S. Mondal, S. Poddar and D. Sengupta, Phys. Rev. D **91** (2015) 115018 [arXiv:1503.07592 [hep-ph]].

94. S. Boselli, C. M. Carloni Calame, G. Montagna, O. Nicrosini and F. Piccinini, JHEP **1506** (2015) 023 [arXiv:1503.07394 [hep-ph]].

95. G. Abbas, A. Celis, X. Q. Li, J. Lu and A. Pich, JHEP **1506** (2015) 005 [arXiv:1503.06423 [hep-ph]].

96. N. Karagiannakis, G. Lazarides and C. Pallis, Phys. Rev. D **92** (2015) no.8, 085018 [arXiv:1503.06186 [hep-ph]].

97. CMS Collaboration [CMS Collaboration], CMS-PAS-HIG-14-030.

98. T. A. Aaltonen *et al.* [CDF and D0 Collaborations], Phys. Rev. Lett. **115** (2015) no.15, 152003 [arXiv:1503.05027 [hep-ex]].

99. N. E. Bomark, S. Moretti and L. Roszkowski, J. Phys. G **43** (2016) no.10, 105003 [arXiv:1503.04228 [hep-ph]].

100. S. P. Martin, Phys. Rev. D **91** (2015) no.11, 114003 [arXiv:1503.03782 [hep-ph]].

101. H. Beauchesne, K. Earl and T. Grgoire, JHEP **1508** (2015) 117 [arXiv:1503.03099 [hep-ph]].

102. B. A. Ovrut, A. Purves and S. Spinner, JHEP **1506** (2015) 182 [arXiv:1503.01473 [hep-ph]].

103. P. Checchia, Int. J. Mod. Phys. A **30** (2015) no.07, 1530003.

104. O. L. Trinhammer, H. G. Bohr and M. S. Jensen, Int. J. Mod. Phys. A **30** (2015) no.14, 1550078 [arXiv:1503.00620 [physics.gen-ph]].

105. G. Perez, Y. Soreq, E. Stamou and K. Tobioka, Phys. Rev. D **92** (2015) no.3, 033016 [arXiv:1503.00290 [hep-ph]].

106. G. von Gersdorff, E. Pontn and R. Rosenfeld, JHEP **1506** (2015) 119 [arXiv:1502.07340 [hep-ph]].

107. I. Masina, G. Nardini and M. Quiros, Phys. Rev. D **92** (2015) no.3, 035003 [arXiv:1502.06525 [hep-ph]].

108. A. Achterberg, S. Amoroso, S. Caron, L. Hendriks, R. Ruiz de Austri and C. Weniger, JCAP **1508** (2015) no.08, 006 [arXiv:1502.05703 [hep-ph]].

109. V. Khachatryan *et al.* [CMS Collaboration], Eur. Phys. J. C **75** (2015) no.7, 325 [arXiv:1502.02522 [hep-ex]].

110. D. Fontes, J. C. Romo, R. Santos and J. P. Silva, JHEP **1506** (2015) 060 [arXiv:1502.01720 [hep-ph]].

111. C. Bonilla, J. W. F. Valle and J. C. Romo, Phys. Rev. D **91** (2015) no.11, 113015 [arXiv:1502.01649 [hep-ph]].

112. T. Aaltonen *et al.* [CDF and D0 Collaborations], Phys. Rev. Lett. **114** (2015) no.15, 151802 [arXiv:1502.00967 [hep-ex]].

113. L. Anderlini, arXiv:1502.00932 [stat.AP].

114. K. Harigaya, T. T. Yanagida and N. Yokozaki, Phys. Rev. D **91** (2015) no.7, 075010 [arXiv:1501.07447 [hep-ph]].

115. L. N. Mihaila and M. Steinhauser, Nucl. Part. Phys. Proc. **261-262** (2015) 443 [arXiv:1501.07128 [hep-ph]].

116. A. Ahriche, G. Faisel, S. Y. Ho, S. Nasri and J. Tandean, Phys. Rev. D **92** (2015) no.3, 035020 [arXiv:1501.06605 [hep-ph]].

117. S. Fichet, B. Herrmann and Y. Stoll, JHEP **1505** (2015) 091 [arXiv:1501.05307 [hep-ph]].

118. J. Ellis, J. Phys. Conf. Ser. **631** (2015) no.1, 012001 [arXiv:1501.05418 [hep-ph]].

119. N. Okada and Q. Shafi, Phys. Lett. B **747** (2015) 223 [arXiv:1501.05375 [hep-ph]].

120. J. Saxon, CERN-THESIS-2014-084.

121. C. Vernieri, CERN-THESIS-2014-161, CMS-TS-2014-035.

122. Y. Chen, CERN-THESIS-2014-201, CMS-TS-2014-044, FERMILAB-THESIS-2014-27.

123. P. Schwegler, CERN-THESIS-2014-091, MPP-2014-302.

124. V. Martn Lozano, J. M. Moreno and C. B. Park, JHEP **1508** (2015) 004 [arXiv:1501.03799 [hep-ph]].

125. K. Cheung, J. S. Lee and P. Y. Tseng, Phys. Rev. D **92** (2015) no.9, 095004 [arXiv:1501.03552 [hep-ph]].

126. F. Boudjema, R. M. Godbole, D. Guadagnoli and K. A. Mohan, Phys. Rev. D **92** (2015) no.1, 015019 [arXiv:1501.03157 [hep-ph]].

127. M. E. Gomez, S. Heinemeyer and M. Rehman, Eur. Phys. J. C **75** (2015) no.9, 434 [arXiv:1501.02258 [hep-ph]].

128. T. Robens and T. Stefaniak, Eur. Phys. J. C **75** (2015) 104 [arXiv:1501.02234 [hep-ph]].

129. J. de Blas, M. Chala, M. Perez-Victoria and J. Santiago, JHEP **1504** (2015) 078 [arXiv:1412.8480 [hep-ph]].

130. V. Khachatryan *et al.* [CMS Collaboration], Eur. Phys. J. C **75** (2015) no.5, 212 [arXiv:1412.8662 [hep-ex]].

131. M. Szleper, arXiv:1412.8367 [hep-ph].

132. A. Fedynitch, M. W. Krasny and W. P?aczek, Acta Phys. Polon. B **46** (2015) no.5, 983 [arXiv:1412.6681 [hep-ph]].

133. L. Wang and X. F. Han, JHEP **1505** (2015) 039 [arXiv:1412.4874 [hep-ph]].

134. J. W. van Holten, Ned. Tijdschr. v. Natk. 81 (2015),12 [arXiv:1412.4226 [hep-ph]].

135. F. Jegerlehner, M. Y. Kalmykov and B. A. Kniehl, J. Phys. Conf. Ser. **608** (2015) no.1, 012074 [arXiv:1412.4215 [hep-ph]].

136. T. Goto, Y. Okada, T. Shindou, M. Tanaka and R. Watanabe, Phys. Rev. D **91** (2015) no.3, 033007 [arXiv:1412.2530 [hep-ph]].

137. J. Ellis, PoS Beauty **2014** (2015) 056 [arXiv:1412.2666 [hep-ph]].

138. K. Cheung, R. Huo, J. S. Lee and Y. L. Sming Tsai, JHEP **1504** (2015) 151 [arXiv:1411.7329 [hep-ph]].

139. X. G. He, C. J. Lee, J. Tandean and Y. J. Zheng, Phys. Rev. D **91** (2015) no.7, 076008 [arXiv:1411.6612 [hep-ph]].

140. K. O. Astapov and S. V. Demidov, JHEP **1501** (2015) 136 [arXiv:1411.6222 [hep-ph]].

141. M. Tonini, DESY-THESIS-2014-038.

142. A. Arhrib, R. Benbrik, G. Moultaka and L. Rahili, arXiv:1411.5645 [hep-ph].

143. CMS Collaboration [CMS Collaboration], CMS-PAS-HIG-14-011.

144. H. K. Dreiner, K. Nickel and F. Staub, Phys. Lett. B **742** (2015) 261 [arXiv:1411.3731 [hep-ph]].

145. L. S. Kisslinger and D. Das, Int. J. Mod. Phys. A **31** (2016) no.07, 1630010 [arXiv:1411.3680 [hep-ph]].

146. B. Dumont, doi:10.1007/978-3-319-44956-2 arXiv:1411.3465 [hep-ph].

147. V. Khachatryan *et al.* [CMS Collaboration], Phys. Rev. D **92** (2015) no.1, 012004 [arXiv:1411.3441 [hep-ex]].

148. A. Bartl, H. Eberl, E. Ginina, K. Hidaka and W. Majerotto, Phys. Rev. D **91** (2015) no.1, 015007 d [arXiv:1411.2840 [hep-ph]].

149. M. de Vries, doi:10.3204/DESY-THESIS-2014-035

150. M. Badziak, Z. Lalak, M. Lewicki, M. Olechowski and S. Pokorski, JHEP **1503** (2015) 003 [arXiv:1411.1450 [hep-ph]].

151. T. Abe, R. Kitano and R. Sato, Phys. Rev. D **91** (2015) no.9, 095004 [arXiv:1411.1335 [hep-ph]].

152. J. Fan, M. Reece and L. T. Wang, JHEP **1509** (2015) 196 [arXiv:1411.1054 [hep-ph]].

153. M. Ciuchini, E. Franco, S. Mishima, M. Pierini, L. Reina and L. Silvestrini, arXiv:1410.6940 [hep-ph].

154. C. J. Lee and J. Tandean, JHEP **1504** (2015) 174 [arXiv:1410.6803 [hep-ph]].

155. A. Thamm, doi:10.5075/epfl-thesis-6346

156. A. Parolini, "The Higgs as a Supersymmetric Nambu-Goldstone Boson," CITATION = INSPIRE-1322174;

157. J. Hisano, D. Kobayashi, N. Mori and E. Senaha, Phys. Lett. B **742** (2015) 80 [arXiv:1410.3569 [hep-ph]].

158. G. Degrassi, S. Di Vita and P. Slavich, Eur. Phys. J. C **75** (2015) no.2, 61 [arXiv:1410.3432 [hep-ph]].

159. A. Efrati, E. Kuflik, S. Nussinov, Y. Soreq and T. Volansky, Phys. Rev. D **91** (2015) no.5, 055034 [arXiv:1410.2225 [hep-ph]].

160. M. Gouzevitch, A. Kaczmarska, M. Mhlleitner and K. Turzynski, PoS DIS **2014** (2014) 003.

161. J. Cao, D. Li, L. Shang, P. Wu and Y. Zhang, JHEP **1412** (2014) 026 [arXiv:1409.8431 [hep-ph]].

162. Y. B. Liu and Z. J. Xiao, J. Phys. G **42** (2015) no.5, 055004 [arXiv:1409.8000 [hep-ph]].

163. A. David, J. Heikkil and G. Petrucciani, Eur. Phys. J. C **75** (2015) no.2, 49 [arXiv:1409.6132 [hep-ph]].

164. V. I. Telnov, JINST **9** (2014) C09029 [arXiv:1409.5577 [physics.acc-ph]].

165. S. Furui, arXiv:1409.3761 [hep-ph].

166. J. Harz, B. Herrmann, M. Klasen and K. Kovarik, Phys. Rev. D **91** (2015) no.3, 034028 [arXiv:1409.2898 [hep-ph]].

167. G. Faisel, S. Y. Ho and J. Tandean, Phys. Lett. B **738** (2014) 380 [arXiv:1408.5887 [hep-ph]].

168. J. Harz, B. Herrmann, M. Klasen, K. Kovarik, M. Meinecke and P. Steppeler, arXiv:1408.4960 [hep-ph].

169. R. Grber, M. M. Mhlleitner, E. Popenda and A. Wlotzka, Eur. Phys. J. C **75** (2015) 420 [arXiv:1408.4662 [hep-ph]].

170. P. S. Bhupal Dev and A. Pilaftsis, JHEP **1412** (2014) 024 Erratum: [JHEP **1511** (2015) 147] [arXiv:1408.3405 [hep-ph]].

171. M. Frank and S. Mondal, Phys. Rev. D **90** (2014) no.7, 075013 [arXiv:1408.2223 [hep-ph]].

172. S. A. R. Ellis, G. L. Kane and B. Zheng, JHEP **1507** (2015) 081 [arXiv:1408.1961 [hep-ph]].

173. A. Alves, A. G. Dias and R. da Silva, Physica **420** (2015) 1 [arXiv:1408.0827 [hep-ph]].

174. A. Andreassen, W. Frost and M. D. Schwartz, Phys. Rev. Lett. **113** (2014) no.24, 241801 [arXiv:1408.0292 [hep-ph]].

175. K. Cheung, J. S. Lee and P. Y. Tseng, Phys. Rev. D **90** (2014) 095009 [arXiv:1407.8236 [hep-ph]].

176. V. Keus, S. F. King, S. Moretti and D. Sokolowska, JHEP **1411** (2014) 016 [arXiv:1407.7859 [hep-ph]].

177. J. A. Casas, J. M. Moreno, S. Robles, K. Rolbiecki and B. Zaldvar, JHEP **1506** (2015) 070 [arXiv:1407.6966 [hep-ph]].

178. A. Ahriche, A. Arhrib and S. Nasri, Phys. Lett. B **743** (2015) 279 [arXiv:1407.5283 [hep-ph]].

179. S. P. Martin and D. G. Robertson, Phys. Rev. D **90** (2014) no.7, 073010 [arXiv:1407.4336 [hep-ph]].

180. A. Szczurek, M. Luszczak and R. Maciula, Phys. Rev. D **90** (2014) no.9, 094023 [arXiv:1407.4243 [hep-ph]].

181. E. Bagnaschi, G. F. Giudice, P. Slavich and A. Strumia, JHEP **1409** (2014) 092 [arXiv:1407.4081 [hep-ph]].

182. N. Chakrabarty, U. K. Dey and B. Mukhopadhyaya, JHEP **1412** (2014) 166 [arXiv:1407.2145 [hep-ph]].
183. CMS Collaboration [CMS Collaboration], CMS-PAS-HIG-14-009.
184. G. Moortgat-Pick, S. Porto and K. Rolbiecki, JHEP **1409** (2014) 002 [arXiv:1406.7701 [hep-ph]].
185. R. Dermisek, A. Raval and S. Shin, Phys. Rev. D **90** (2014) no.3, 034023 [arXiv:1406.7018 [hep-ph]].
186. E. L. Berger, S. B. Giddings, H. Wang and H. Zhang, Phys. Rev. D **90** (2014) no.7, 076004 [arXiv:1406.6054 [hep-ph]].
187. I. Moult and I. W. Stewart, JHEP **1409** (2014) 129 [arXiv:1405.5534 [hep-ph]].
188. A. Alves, E. Ramirez Barreto and A. G. Dias, arXiv:1312.5333 [hep-ph].
189. G. Cottin, M. A. Diaz, S. Olivares and N. Rojas, arXiv:1211.1000 [hep-ph].

4. Aad, G., ... ,Vranjes N., *et al.* [ATLAS Collaboration], *Measurements of Higgs boson production and couplings in the four-lepton channel in pp collisions at center-of-mass energies of 7 and 8 TeV with the ATLAS detector*, Phys.Rev. D91 (2015) no.1, 012006, arXiv:1408.5191 [hep-ex].

    1. R. C. Malm, "Five-dimensional perspective on Higgs physics and the b?s? transition in a warped extra dimension," CITATION = INSPIRE-1501832;
    2. C. Mariotti and G. Passarino, arXiv:1612.00269 [hep-ph].
    3. M. Ciuchini, J. de Blas, E. Franco, D. Ghosh, S. Mishima, M. Pierini, L. Reina and L. Silvestrini, PoS LeptonPhoton **2015** (2016) 013.
    4. N. Orlando and O. B. O. T. A. Collaboration, PoS LeptonPhoton **2015** (2016) 085.
    5. S. Wertz, J. Phys. Conf. Ser. **762** (2016) no.1, 012053.
    6. B. Biedermann, A. Denner, S. Dittmaier, L. Hofer and B. Jager, arXiv:1611.05338 [hep-ph].
    7. S. Demidov and I. Sobolev, EPJ Web Conf. **125** (2016) 02017.
    8. A. Donini and S. G. Marimn, arXiv:1609.05654 [hep-ph].
    9. J. de Blas, M. Ciuchini, E. Franco, S. Mishima, M. Pierini, L. Reina and L. Silvestrini, arXiv:1608.01509 [hep-ph].
    10. P. Bechtle, H. E. Haber, S. Heinemeyer, O. Stl, T. Stefaniak, G. Weiglein and L. Zeune, arXiv:1608.00638 [hep-ph].
    11. F. Maltoni, E. Vryonidou and C. Zhang, JHEP **1610** (2016) 123 [arXiv:1607.05330 [hep-ph]].
    12. N. Chen and Z. Liu, arXiv:1607.02154 [hep-ph].
    13. P. Bandyopadhyay, C. Coriano, A. Costantini and L. Delle Rose, JHEP **1609** (2016) 084 [arXiv:1607.01933 [hep-ph]].
    14. A. Karam and K. Tamvakis, Phys. Rev. D **94** (2016) no.5, 055004 [arXiv:1607.01001 [hep-ph]].

15. S. von Buddenbrock *et al.*, Eur. Phys. J. C **76** (2016) no.10, 580 [arXiv:1606.01674 [hep-ph]].
16. V. Khachatryan *et al.* [CMS Collaboration], [arXiv:1606.01522 [hep-ex]].
17. A. Arbey, S. Fichet, F. Mahmoudi and G. Moreau, JHEP **1611** (2016) 097 [arXiv:1606.00455 [hep-ph]].
18. S. V. Demidov and I. V. Sobolev, JHEP **1608** (2016) 030 [arXiv:1605.08220 [hep-ph]].
19. B. Yang, Z. Liu, J. Han and G. Yang, Adv. High Energy Phys. **2016** (2016) 2613187 [arXiv:1605.00877 [hep-ph]].
20. G. Dupuis, JHEP **1607** (2016) 008 [arXiv:1604.04552 [hep-ph]].
21. CMS Collaboration [CMS Collaboration], CMS-PAS-HIG-16-007.
22. A. Karam and K. Tamvakis, PoS CORFU **2015** (2016) 073 [arXiv:1603.08470 [hep-ph]].
23. H. E. Herde, PoS EPS **-HEP2015** (2015) 285.
24. L. Reina, J. de Blas, M. Ciuchini, E. Franco, D. Ghosh, S. Mishima, M. Pierini and L. Silvestrini, PoS EPS **-HEP2015** (2015) 187.
25. A. R. Drger, doi:10.3204/DESY-THESIS-2016-005
26. J. Nakamura and J. Baglio, arXiv:1603.02315 [hep-ph].
27. J. Fumagalli and M. Postma, JHEP **1605** (2016) 049 [arXiv:1602.07234 [hep-ph]].
28. S. De Curtis, S. Moretti, K. Yagyu and E. Yildirim, Phys. Rev. D **94** (2016) 055017 [arXiv:1602.06437 [hep-ph]].
29. B. Biedermann, A. Denner, S. Dittmaier, L. Hofer and B. Jger, Phys. Rev. Lett. **116** (2016) no.16, 161803 [arXiv:1601.07787 [hep-ph]].
30. T. S. Virdee, Annalen Phys. **528** (2016) 35.
31. H. Okada and K. Yagyu, Phys. Lett. B **756** (2016) 337 [arXiv:1601.05038 [hep-ph]].
32. G. C. Dorsch, S. J. Huber, K. Mimasu and J. M. No, Phys. Rev. D **93** (2016) no.11, 115033 [arXiv:1601.04545 [hep-ph]].
33. J. C. Sanabria [ATLAS and CMS Collaborations], Nucl. Part. Phys. Proc. **267-269** (2015) 25. doi:10.1016/j.nuclphysbps.2015.10.078
34. P. Bandyopadhyay, K. Huitu and S. Niyogi, JHEP **1607** (2016) 015 [arXiv:1512.09241 [hep-ph]].
35. S. Liebler, S. Profumo and T. Stefaniak, JHEP **1604** (2016) 143 [arXiv:1512.09172 [hep-ph]].
36. S. Kanemura, K. Nishiwaki, H. Okada, Y. Orikasa, S. C. Park and R. Watanabe, arXiv:1512.09048 [hep-ph].
37. P. Bandyopadhyay, C. Corian and A. Costantini, Phys. Rev. D **94** (2016) no.5, 055030 [arXiv:1512.08651 [hep-ph]].
38. S. Moretti and K. Yagyu, Phys. Rev. D **93** (2016) no.5, 055043 [arXiv:1512.07462 [hep-ph]].

39. J. Baglio, Phys. Rev. D **93** (2016) no.5, 054010 [arXiv:1512.05787 [hep-ph]].
40. CMS Collaboration [CMS Collaboration], CMS-PAS-HIG-15-010.
41. A. Donini, arXiv:1512.03978 [hep-ph].
42. H. Castilla-Valdez, A. Moyotl, M. A. Perez and C. G. Honorato, Phys. Rev. D **93** (2016) no.5, 055001 [arXiv:1512.03872 [hep-ph]].
43. F. Caola, K. Melnikov, R. Rntsch and L. Tancredi, Phys. Lett. B **754** (2016) 275 [arXiv:1511.08617 [hep-ph]].
44. N. Oshimo, Phys. Rev. D **93** (2016) no.9, 095017 [arXiv:1511.06846 [hep-ph]].
45. T. Nobe, doi:10.1007/978-981-10-0003-4
46. S. Kanemura, M. Kikuchi and K. Yagyu, Nucl. Phys. B **907** (2016) 286 [arXiv:1511.06211 [hep-ph]].
47. C. Englert, R. Kogler, H. Schulz and M. Spannowsky, Eur. Phys. J. C **76** (2016) no.7, 393 [arXiv:1511.05170 [hep-ph]].
48. T. Han, S. K. Kang and J. Sayre, JHEP **1602** (2016) 097 [arXiv:1511.05162 [hep-ph]].
49. O. A. Ducu, CPPM-T-2015-06.
50. V. Khachatryan *et al.* [CMS Collaboration], JHEP **1601** (2016) 079 [arXiv:1510.06534 [hep-ex]].
51. P. Bandyopadhyay, C. Coriano and A. Costantini, JHEP **1512** (2015) 127 [arXiv:1510.06309 [hep-ph]].
52. H. Okada, Y. Orikasa and K. Yagyu, arXiv:1510.00799 [hep-ph].
53. Y. T. Chien, V. Cirigliano, W. Dekens, J. de Vries and E. Mereghetti, JHEP **1602** (2016) 011 [arXiv:1510.00725 [hep-ph]].
54. R. C. Lane, "Searches for neutral Higgs bosons in the $\tau\tau$ final state with the CMS detector," CITATION = INSPIRE-1395771;of 17 Dec 2016
55. S. Kanemura and K. Yagyu, Phys. Lett. B **751** (2015) 289 [arXiv:1509.06060 [hep-ph]].
56. CMS Collaboration [CMS Collaboration], CMS-PAS-HIG-15-002.
57. D. A. Camargo, arXiv:1509.04263 [hep-ph].
58. S. Fichet and G. Moreau, Nucl. Phys. B **905** (2016) 391 [arXiv:1509.00472 [hep-ph]].
59. A. Karam and K. Tamvakis, Phys. Rev. D **92** (2015) no.7, 075010 [arXiv:1508.03031 [hep-ph]].
60. M. R. Buckley and D. Feld, Phys. Rev. D **92** (2015) no.7, 075024 [arXiv:1508.00908 [hep-ph]].
61. A. Falkowski, M. Gonzalez-Alonso, A. Greljo and D. Marzocca, Phys. Rev. Lett. **116** (2016) no.1, 011801 [arXiv:1508.00581 [hep-ph]].
62. K. Kainulainen, K. Tuominen and V. Vaskonen, Phys. Rev. D **93** (2016) no.1, 015016 [arXiv:1507.04931 [hep-ph]].

63. D. Croon, V. Sanz and E. R. M. Tarrant, Phys. Rev. D **94** (2016) no.4, 045010 [arXiv:1507.04653 [hep-ph]].

64. K. Nishiwaki, H. Okada and Y. Orikasa, Phys. Rev. D **92** (2015) no.9, 093013 [arXiv:1507.02412 [hep-ph]].

65. K. M. Mercurio, CERN-THESIS-2014-227.

66. A. Pich, Nucl. Instrum. Meth. A **824** (2016) 43 [arXiv:1507.01250 [hep-ph]].

67. J. Bernon, J. F. Gunion, H. E. Haber, Y. Jiang and S. Kraml, Phys. Rev. D **92** (2015) no.7, 075004 [arXiv:1507.00933 [hep-ph]].

68. N. A. K? and N. T. H. Vn, J. Phys. Conf. Ser. **627** (2015) no.1, 012011.

69. P. Bandyopadhyay, C. Coriano and A. Costantini, JHEP **1509** (2015) 045 [arXiv:1506.03634 [hep-ph]].

70. M. Bauer, M. Carena and K. Gemmler, JHEP **1511** (2015) 016 [arXiv:1506.01719 [hep-ph]].

71. N. Greiner, S. Hche, G. Luisoni, M. Schnherr, J. C. Winter and V. Yundin, JHEP **1601** (2016) 169 [arXiv:1506.01016 [hep-ph]].

72. G. Belanger, D. Ghosh, R. Godbole and S. Kulkarni, JHEP **1509** (2015) 214 [arXiv:1506.00665 [hep-ph]].

73. B. Altunkaynak, W. S. Hou, C. Kao, M. Kohda and B. McCoy, Phys. Lett. B **751** (2015) 135 [arXiv:1506.00651 [hep-ph]].

74. K. Yagyu, arXiv:1505.06886 [hep-ph].

75. S. Dwivedi, D. K. Ghosh, B. Mukhopadhyaya and A. Shivaji, Phys. Rev. D **92** (2015) no.9, 095015 [arXiv:1505.05844 [hep-ph]].

76. T. Corbett, O. J. P. Eboli, D. Goncalves, J. Gonzalez-Fraile, T. Plehn and M. Rauch, JHEP **1508** (2015) 156 [arXiv:1505.05516 [hep-ph]].

77. X. Shou-Jian, M. Wen-Gan, G. Lei, Z. Ren-You, C. Chong and S. Mao, J. Phys. G **42** (2015) no.6, 065006 [arXiv:1505.03226 [hep-ph]].

78. A. Pich, arXiv:1505.01813 [hep-ph].

79. A. Falkowski, Pramana **87** (2016) no.3, 39 [arXiv:1505.00046 [hep-ph]].

80. J. B. Flament, arXiv:1504.07919 [hep-ph].

81. S. Moretti, D. Rojas and K. Yagyu, JHEP **1508** (2015) 116 [arXiv:1504.06432 [hep-ph]].

82. N. Craig, F. D'Eramo, P. Draper, S. Thomas and H. Zhang, JHEP **1506** (2015) 137 [arXiv:1504.04630 [hep-ph]].

83. B. Bhattacherjee, A. Chakraborty and A. Choudhury, Phys. Rev. D **92** (2015) no.9, 093007 [arXiv:1504.04308 [hep-ph]].

84. G. Moortgat-Pick *et al.*, Eur. Phys. J. C **75** (2015) no.8, 371 [arXiv:1504.01726 [hep-ph]].

85. N. A. Ky and N. T. H. Van, arXiv:1503.08630 [hep-ph].

86. J. M. Cline, G. Dupuis, Z. Liu and W. Xue, Phys. Rev. D **91** (2015) no.11, 115010 [arXiv:1503.08213 [hep-ph]].
87. A. Chakraborty, D. K. Ghosh, S. Mondal, S. Poddar and D. Sengupta, Phys. Rev. D **91** (2015) 115018 [arXiv:1503.07592 [hep-ph]].
88. S. Boselli, C. M. Carloni Calame, G. Montagna, O. Nicrosini and F. Piccinini, JHEP **1506** (2015) 023 [arXiv:1503.07394 [hep-ph]].
89. N. E. Bomark, S. Moretti and L. Roszkowski, J. Phys. G **43** (2016) no.10, 105003 [arXiv:1503.04228 [hep-ph]].
90. P. Checchia, Int. J. Mod. Phys. A **30** (2015) no.07, 1530003.
91. G. Aad *et al.* [ATLAS Collaboration], Eur. Phys. J. C **75** (2015) no.7, 335 [arXiv:1503.01060 [hep-ex]].
92. M. Flechl [ATLAS and CMS Collaborations], J. Phys. Conf. Ser. **631** (2015) no.1, 012028 [arXiv:1503.00632 [hep-ex]].
93. G. Perez, Y. Soreq, E. Stamou and K. Tobioka, Phys. Rev. D **92** (2015) no.3, 033016 [arXiv:1503.00290 [hep-ph]].
94. S. Kanemura, M. Kikuchi and K. Yagyu, Nucl. Phys. B **896** (2015) 80 [arXiv:1502.07716 [hep-ph]].
95. M. Gorbahn, J. M. No and V. Sanz, JHEP **1510** (2015) 036 [arXiv:1502.07352 [hep-ph]].
96. K. Goebel,
97. A. Arbey, G. Cacciapaglia, H. Cai, A. Deandrea, S. Le Corre and F. Sannino, arXiv:1502.04718 [hep-ph].
98. J. Bernon and B. Dumont, Eur. Phys. J. C **75** (2015) no.9, 440 [arXiv:1502.04138 [hep-ph]].
99. Z. X. Heng, D. W. Li and H. J. Zhou, Commun. Theor. Phys. **63** (2015) no.2, 188.
100. B. Li and C. E. M. Wagner, Phys. Rev. D **91** (2015) 095019 [arXiv:1502.02210 [hep-ph]].
101. A. Falkowski, C. Gross and O. Lebedev, JHEP **1505** (2015) 057 [arXiv:1502.01361 [hep-ph]].
102. K. Blum, R. T. D'Agnolo and J. Fan, JHEP **1503** (2015) 166 [arXiv:1502.01045 [hep-ph]].
103. T. Aaltonen *et al.* [CDF and D0 Collaborations], Phys. Rev. Lett. **114** (2015) no.15, 151802 [arXiv:1502.00967 [hep-ex]].
104. P. Ko, Y. Omura and C. Yu, JHEP **1506** (2015) 034 [arXiv:1502.00262 [hep-ph]].
105. N. Craig, A. Katz, M. Strassler and R. Sundrum, JHEP **1507** (2015) 105 [arXiv:1501.05310 [hep-ph]].
106. F. Boudjema, R. M. Godbole, D. Guadagnoli and K. A. Mohan, Phys. Rev. D **92** (2015) no.1, 015019 [arXiv:1501.03157 [hep-ph]].

107. A. Askew, P. Jaiswal, T. Okui, H. B. Prosper and N. Sato, Phys. Rev. D **91** (2015) no.7, 075014 [arXiv:1501.03156 [hep-ph]].

108. T. Robens and T. Stefaniak, Eur. Phys. J. C **75** (2015) 104 [arXiv:1501.02234 [hep-ph]].

109. C. Bonilla, D. Sokolowska, N. Darvishi, J. L. Diaz-Cruz and M. Krawczyk, J. Phys. G **43** (2016) no.6, 065001 [arXiv:1412.8730 [hep-ph]].

110. V. Khachatryan *et al.* [CMS Collaboration], Eur. Phys. J. C **75** (2015) no.5, 212 [arXiv:1412.8662 [hep-ex]].

111. M. Szleper, arXiv:1412.8367 [hep-ph].

112. L. Bian, T. Liu and J. Shu, Phys. Rev. Lett. **115** (2015) 021801 [arXiv:1411.6695 [hep-ph]].

113. A. Efrati, E. Kuflik, S. Nussinov, Y. Soreq and T. Volansky, Phys. Rev. D **91** (2015) no.5, 055034 [arXiv:1410.2225 [hep-ph]].

114. P. Ghosh, D. E. Lopez-Fogliani, V. A. Mitsou, C. Munoz and R. Ruiz de Austri, JHEP **1411** (2014) 102 [arXiv:1410.2070 [hep-ph], arXiv:1410.2070].

115. J. Cao, D. Li, L. Shang, P. Wu and Y. Zhang, JHEP **1412** (2014) 026 [arXiv:1409.8431 [hep-ph]].

116. Y. n. Mao and S. h. Zhu, Phys. Rev. D **90** (2014) no.11, 115024 [arXiv:1409.6844 [hep-ph]].

117. A. David, J. Heikkil and G. Petrucciani, Eur. Phys. J. C **75** (2015) no.2, 49 [arXiv:1409.6132 [hep-ph]].

118. J. Bernon, B. Dumont and S. Kraml, Phys. Rev. D **90** (2014) 071301 [arXiv:1409.1588 [hep-ph]].

119. B. Bhattacherjee and A. Choudhury, Phys. Rev. D **91** (2015) 073015 [arXiv:1407.6866 [hep-ph]].

120. R. Enberg, J. Rathsman and G. Wouda, Phys. Rev. D **91** (2015) no.9, 095002 [arXiv:1311.4367 [hep-ph]].

5. Aad, G., ... ,Vranjes N., *et al.* [ATLAS Collaboration], *Measurement of the muon reconstruction performance of the ATLAS detector using 2011 and 2012 LHC proton–proton collision data*, Eur.Phys.J. C74 (2014) no.11, 3130, arXiv:1407.3935 [hep-ex].

1. N. Filipovic, CERN-THESIS-2015-344.

2. N. Chen and Z. Liu, arXiv:1607.02154 [hep-ph].

3. CMS Collaboration [CMS Collaboration], CMS-PAS-TOP-15-019.

4. T. Nobe, doi:10.1007/978-981-10-0003-4

5. K. Pedersen and Z. Sullivan, Phys. Rev. D **93** (2016) no.1, 014014 [arXiv:1511.05990 [hep-ph]].

6. A. Gupta, R. Primulando and P. Saraswat, JHEP **1509** (2015) 079 [arXiv:1504.01385 [hep-ph]].

6. Aad, G., ... ,Vranjes N., *et al.* [ATLAS Collaboration], *Search for new particles in events with one lepton and missing transverse momentum in pp collisions at* $\sqrt{s}$ *=8 TeV with the ATLAS detector*, JHEP 1409 (2014) 037, arXiv:1407.7494 [hep-ex].

    1. S. Funatsu, H. Hatanaka, Y. Hosotani and Y. Orikasa, arXiv:1612.03378 [hep-ph].
    2. S. P. Liew, M. Papucci, A. Vichi and K. M. Zurek, arXiv:1612.00219 [hep-ph].
    3. M. Farina, G. Panico, D. Pappadopulo, J. T. Ruderman, R. Torre and A. Wulzer, arXiv:1609.08157 [hep-ph].
    4. S. Fichet, arXiv:1609.01762 [hep-ph].
    5. K. Ghorbani and L. Khalkhali, arXiv:1608.04559 [hep-ph].
    6. J. L. Feng, B. Fornal, I. Galon, S. Gardner, J. Smolinsky, T. M. P. Tait and P. Tanedo, arXiv:1608.03591 [hep-ph].
    7. CMS Collaboration [CMS Collaboration], CMS-PAS-EXO-16-038.
    8. CMS Collaboration [CMS Collaboration], CMS-PAS-EXO-16-010.
    9. V. Khachatryan *et al.* [CMS Collaboration], [arXiv:1607.05764 [hep-ex]].
    10. A. Dedes, D. Karamitros and V. C. Spanos, Phys. Rev. D **94** (2016) no.9, 095008 [arXiv:1607.05040 [hep-ph]].
    11. T. Abe and R. Nagai, arXiv:1607.03706 [hep-ph].
    12. S. Mehlhase [ATLAS Collaboration], AIP Conf. Proc. **1743** (2016) 050011.
    13. T. Bhattacharya, V. Cirigliano, S. Cohen, R. Gupta, H. W. Lin and B. Yoon, Phys. Rev. D **94** (2016) no.5, 054508 [arXiv:1606.07049 [hep-lat]].
    14. S. Lowette, J. Phys. Conf. Ser. **718** (2016) no.2, 022011.
    15. P. Ko, A. Natale, M. Park and H. Yokoya, arXiv:1605.07058 [hep-ph].
    16. CMS Collaboration [CMS Collaboration], CMS-PAS-B2G-16-007.
    17. V. Khachatryan *et al.* [CMS Collaboration], [arXiv:1603.08914 [hep-ex]].
    18. M. Sigamani [CMS Collaboration], arXiv:1603.08434 [hep-ex].
    19. A. De Simone and T. Jacques, Eur. Phys. J. C **76** (2016) no.7, 367 [arXiv:1603.08002 [hep-ph]].
    20. U. Haisch, F. Kahlhoefer and T. M. P. Tait, Phys. Lett. B **760** (2016) 207 [arXiv:1603.01267 [hep-ph]].
    21. J. Ren and J. H. Yu, arXiv:1602.07708 [hep-ph].
    22. V. Khachatryan *et al.* [CMS Collaboration], Eur. Phys. J. C **76** (2016) no.5, 237 [arXiv:1601.06431 [hep-ex]].
    23. H. S. Bawa [ATLAS and CMS Collaborations], Nucl. Part. Phys. Proc. **267-269** (2015) 277.
    24. H. Hatanaka, arXiv:1512.06595 [hep-ph].
    25. L. Basso, JHEP **1604** (2016) 087 [arXiv:1512.06381 [hep-ph]].
    26. CMS Collaboration [CMS Collaboration], CMS-PAS-EXO-15-006.

27. S. Knapen, T. Melia, M. Papucci and K. Zurek, Phys. Rev. D **93** (2016) no.7, 075020 [arXiv:1512.04928 [hep-ph]].
28. T. Pook, arXiv:1512.02371 [hep-ex].
29. N. F. Bell, Y. Cai and R. K. Leane, JCAP **1601** (2016) no.01, 051 [arXiv:1512.00476 [hep-ph]].
30. V. Khachatryan *et al.* [CMS Collaboration], Phys. Rev. D **93** (2016) no.5, 052011 [arXiv:1511.09375 [hep-ex]].
31. T. Appelquist, Y. Bai, J. Ingoldby and M. Piai, JHEP **1601** (2016) 109 [arXiv:1511.05473 [hep-ph]].
32. A. Sajjad, Phys. Rev. D **93** (2016) no.5, 055028 [arXiv:1511.02244 [hep-ph]].
33. H. S. Fukano, S. Matsuzaki, K. Terashi and K. Yamawaki, Nucl. Phys. B **904** (2016) 400 [arXiv:1510.08184 [hep-ph]].
34. M. J. Baker *et al.*, JHEP **1512** (2015) 120 [arXiv:1510.03434 [hep-ph]].
35. A. de Cosa [CMS and ATLAS Collaborations], arXiv:1510.01516 [hep-ex].
36. T. Mondal, U. K. Dey and P. Konar, Phys. Rev. D **92** (2015) no.9, 096005 [arXiv:1508.04960 [hep-ph]].
37. V. Khachatryan *et al.* [CMS Collaboration], Phys. Lett. B **755** (2016) 196 [arXiv:1508.04308 [hep-ex]].
38. E. Izaguirre, G. Krnjaic and B. Shuve, Phys. Rev. D **93** (2016) no.6, 063523 [arXiv:1508.03050 [hep-ph]].
39. M. Low, A. Tesi and L. T. Wang, Phys. Rev. D **92** (2015) no.8, 085019 [arXiv:1507.07557 [hep-ph]].
40. L. Bian, D. Liu and J. Shu, arXiv:1507.06018 [hep-ph].
41. C. H. Chen and T. Nomura, Phys. Lett. B **749** (2015) 464 [arXiv:1507.04431 [hep-ph]].
42. C. W. Chiang, H. Fukuda, K. Harigaya, M. Ibe and T. T. Yanagida, JHEP **1511** (2015) 015 [arXiv:1507.02483 [hep-ph]].
43. A. Carmona, A. Delgado, M. Quirs and J. Santiago, JHEP **1509** (2015) 186 [arXiv:1507.01914 [hep-ph]].
44. T. Abe, T. Kitahara and M. M. Nojiri, JHEP **1602** (2016) 084 [arXiv:1507.01681 [hep-ph]].
45. T. Abe, R. Nagai, S. Okawa and M. Tanabashi, Phys. Rev. D **92** (2015) no.5, 055016 [arXiv:1507.01185 [hep-ph]].
46. Q. H. Cao, B. Yan and D. M. Zhang, Phys. Rev. D **92** (2015) no.9, 095025 [arXiv:1507.00268 [hep-ph]].
47. A. Thamm, R. Torre and A. Wulzer, Phys. Rev. Lett. **115** (2015) no.22, 221802 [arXiv:1506.08688 [hep-ph]].
48. Y. Gao, T. Ghosh, K. Sinha and J. H. Yu, Phys. Rev. D **92** (2015) no.5, 055030 [arXiv:1506.07511 [hep-ph]].

49. K. Cheung, W. Y. Keung, P. Y. Tseng and T. C. Yuan, Phys. Lett. B **751** (2015) 188 [arXiv:1506.06064 [hep-ph]].
50. J. Hisano, N. Nagata and Y. Omura, Phys. Rev. D **92** (2015) no.5, 055001 [arXiv:1506.03931 [hep-ph]].
51. H. S. Fukano, M. Kurachi, S. Matsuzaki, K. Terashi and K. Yamawaki, Phys. Lett. B **750** (2015) 259 [arXiv:1506.03751 [hep-ph]].
52. A. Greljo, G. Isidori and D. Marzocca, JHEP **1507** (2015) 142 [arXiv:1506.01705 [hep-ph]].
53. G. Belanger, D. Ghosh, R. Godbole and S. Kulkarni, JHEP **1509** (2015) 214 [arXiv:1506.00665 [hep-ph]].
54. B. Zaldivar, arXiv:1505.04579 [hep-ph].
55. V. A. Bednyakov, arXiv:1505.04380 [hep-ph].
56. M. Autran, K. Bauer, T. Lin and D. Whiteson, Phys. Rev. D **92** (2015) no.3, 035007 [arXiv:1504.01386 [hep-ph]].
57. A. Gupta, R. Primulando and P. Saraswat, JHEP **1509** (2015) 079 [arXiv:1504.01385 [hep-ph]].
58. N. F. Bell, Y. Cai, J. B. Dent, R. K. Leane and T. J. Weiler, Phys. Rev. D **92** (2015) no.5, 053008 [arXiv:1503.07874 [hep-ph]].
59. CMS Collaboration [CMS Collaboration], CMS-PAS-EXO-14-010.
60. CMS Collaboration [CMS Collaboration], CMS-PAS-EXO-12-011.
61. C. Arina, M. E. C. Catalan, S. Kraml, S. Kulkarni and U. Laa, JHEP **1505** (2015) 142 [arXiv:1503.02960 [hep-ph]].
62. F. Maltoni, A. Martini, K. Mawatari and B. Oexl, JHEP **1504** (2015) 021 [arXiv:1502.01637 [hep-ph]].
63. M. Cahill-Rowley, S. El Hedri, W. Shepherd and D. G. E. Walker, arXiv:1501.03153 [hep-ph].
64. A. Crivellin, U. Haisch and A. Hibbs, Phys. Rev. D **91** (2015) 074028 [arXiv:1501.00907 [hep-ph]].
65. S. El Hedri, W. Shepherd and D. G. E. Walker, arXiv:1412.5660 [hep-ph].
66. S. Chang, J. Galloway, M. Luty, E. Salvioni and Y. Tsai, JHEP **1503** (2015) 017 [arXiv:1411.6023 [hep-ph]].
67. D. S. M. Alves, J. Galloway, J. T. Ruderman and J. R. Walsh, JHEP **1502** (2015) 007 [arXiv:1410.6810 [hep-ph]].
68. D. Becciolini, D. Buarque Franzosi, R. Foadi, M. T. Frandsen, T. Hapola and F. Sannino, Phys. Rev. D **92** (2015) no.1, 015013 Addendum: [Phys. Rev. D **92** (2015) no.7, 079904] [arXiv:1410.6492 [hep-ph]].
69. T. Jezo, M. Klasen, D. R. Lamprea, F. Lyonnet and I. Schienbein, JHEP **1412** (2014) 092 [arXiv:1410.4692 [hep-ph]].

70. G. Aad *et al.* [ATLAS Collaboration], Eur. Phys. J. C **75** (2015) no.2, 92 [arXiv:1410.4031 [hep-ex]].
71. H. Baer, A. Mustafayev and X. Tata, Phys. Rev. D **90** (2014) no.11, 115007 [arXiv:1409.7058 [hep-ph]].
72. A. Crivellin and U. Haisch, Phys. Rev. D **90** (2014) 115011 [arXiv:1408.5046 [hep-ph]].

7. Aad, G., ... ,Vranjes N., *et al.* [ATLAS Collaboration], *ATLAS search for a heavy gauge boson decaying to a charged lepton and a neutrino in pp collisions at* $\sqrt{s}$*=7 TeV*, Eur.Phys.J. C72 (2012) 2241, arXiv:1209.4446 [hep-ex].

1. L. A. Anchordoqui, I. Antoniadis, H. Goldberg, X. Huang, D. Lust and T. R. Taylor, arXiv:1611.09785 [hep-ph].
2. C. Niehoff, P. Stangl and D. M. Straub, arXiv:1611.09356 [hep-ph].
3. CMS Collaboration [CMS Collaboration], CMS-PAS-B2G-16-009.
4. T. E. Balestri, CERN-THESIS-2015-249.
5. A. Doff and C. Siqueira, Phys. Lett. B **754** (2016) 294 [arXiv:1512.03256 [hep-ph]].
6. V. Khachatryan *et al.* [CMS Collaboration], JHEP **1602** (2016) 122 [arXiv:1509.06051 [hep-ex]].
7. K. K. Vos, H. W. Wilschut and R. G. E. Timmermans, Rev. Mod. Phys. **87** (2015) 1483 [arXiv:1509.04007 [hep-ph]].
8. T. Mondal, U. K. Dey and P. Konar, Phys. Rev. D **92** (2015) no.9, 096005 [arXiv:1508.04960 [hep-ph]].
9. C. Niehoff, P. Stangl and D. M. Straub, JHEP **1601** (2016) 119 [arXiv:1508.00569 [hep-ph]].
10. J. Hetzel, arXiv:1504.06739 [hep-ph].
11. J. Hetzel and B. Stech, Phys. Rev. D **91** (2015) 055026 [arXiv:1502.00919 [hep-ph]].
12. D. Sperka, CERN-THESIS-2014-062.
13. D. S. M. Alves, J. Galloway, J. T. Ruderman and J. R. Walsh, JHEP **1502** (2015) 007 [arXiv:1410.6810 [hep-ph]].
14. T. Jezo, M. Klasen, D. R. Lamprea, F. Lyonnet and I. Schienbein, JHEP **1412** (2014) 092 [arXiv:1410.4692 [hep-ph]].
15. V. Khachatryan *et al.* [CMS Collaboration], Phys. Rev. D **91** (2015) no.9, 092005 [arXiv:1408.2745 [hep-ex]].
16. V. Khachatryan *et al.* [CMS Collaboration], Phys. Lett. B **740** (2015) 83 [arXiv:1407.3476 [hep-ex]].
17. Y. G. Kim and K. Y. Lee, Phys. Rev. D **90** (2014) 117702 [arXiv:1405.7762 [hep-ph]].
18. Q. G. Zeng, S. Yang, C. X. Yue and Y. Yu, Europhys. Lett. **107** (2014) 41002 [arXiv:1403.3144 [hep-ph]].
19. X. Gong, H. L. Li, C. F. Qiao, Z. G. Si and Z. J. Yang, Phys. Rev. D **89** (2014) no.5, 055022 [arXiv:1403.0347 [hep-ph]].

20. D. Cogollo, A. X. Gonzalez-Morales, F. S. Queiroz and P. R. Teles, JCAP **1411** (2014) no.11, 002 [arXiv:1402.3271 [hep-ph]].
21. S. Chatrchyan *et al.* [CMS Collaboration], JHEP **1405** (2014) 108 [arXiv:1402.2176 [hep-ex]].
22. T. Je?o, M. Klasen, F. Lyonnet, F. Montanet, I. Schienbein and M. Tartare, Phys. Rev. D **89** (2014) no.7, 077702 [arXiv:1401.6012 [hep-ph]].
23. E. Accomando, D. Becciolini, A. Belyaev, S. De Curtis, D. Dominici, S. F. King, S. Moretti and C. Shepherd-Themistocleous, PoS DIS **2013** (2013) 125.
24. A. Roitgrund, G. Eilam and S. Bar-Shalom, Comput. Phys. Commun. **203** (2016) 18 [arXiv:1401.3345 [hep-ph]].
25. G. Bambhaniya, J. Chakrabortty, J. Gluza, M. Kordiaczy?ska and R. Szafron, JHEP **1405** (2014) 033 [arXiv:1311.4144 [hep-ph]].
26. S. Profumo and F. S. Queiroz, Eur. Phys. J. C **74** (2014) no.7, 2960 [arXiv:1307.7802 [hep-ph]].
27. A. Freitas, K. Hagiwara, S. Heinemeyer, P. Langacker, K. Moenig, M. Tanabashi and G. W. Wilson, arXiv:1307.3962 [hep-ph].
28. E. Kou, C. D. L and F. S. Yu, JHEP **1312** (2013) 102 [arXiv:1305.3173 [hep-ph]].
29. T. Abe and R. Kitano, Phys. Rev. D **88** (2013) no.1, 015019 [arXiv:1305.2047 [hep-ph]].
30. E. Accomando, D. Becciolini, A. Belyaev, S. Moretti and C. Shepherd-Themistocleous, JHEP **1310** (2013) 153 [arXiv:1304.6700 [hep-ph]].
31. T. Abe, N. Chen and H. J. He, arXiv:1304.5085 [hep-ph].
32. X. F. Wang, C. Du and H. J. He, Phys. Lett. B **723** (2013) 314 [arXiv:1304.2257 [hep-ph]].
33. S. Chatrchyan *et al.* [CMS Collaboration], Phys. Rev. D **87** (2013) no.7, 072005 [arXiv:1302.2812 [hep-ex]].
34. I. T. Cakir, A. Senol and A. T. Tasci, Acta Phys. Polon. B **44** (2013) 203 [arXiv:1212.2357 [hep-ph]].
35. M. Chala, JHEP **1301** (2013) 122 [arXiv:1210.6208 [hep-ph]].
36. V. Cirigliano, M. Gonzalez-Alonso and M. L. Graesser, JHEP **1302** (2013) 046 [arXiv:1210.4553 [hep-ph]].